

Transmission Lines and Maxwell's Equations

Phil Lucht

Rimrock Digital Technology, Salt Lake City, Utah 84103

last update: Oct 20, 2014

rimrock@xmission.com

Maple code is available upon request. Comments and errata are welcome.

The material in this document is copyrighted by the author.

The graphics look ratty in Windows Adobe PDF viewers when not scaled up, but look just fine in this excellent freeware viewer: <http://www.tracker-software.com/pdf-xchange-products-comparison-chart>.

The table of contents has live links. Most PDF viewers provide these links as bookmarks on the left.

Overview and Summary	8
Chapter Summaries.....	10
Appendix Summaries.....	11
Symbols used in this document.....	14
Chapter 1: Basic Equations	19
1.1 Maxwell's Equations in a Conducting Dielectric Medium	19
(a) Notes on Maxwell's Equations	19
(b) Integral Forms of Maxwell's Equations and Continuity.....	24
(c) Rules for behavior of fields and potentials at a boundary	27
1.2 The Field Wave Equations.....	32
1.3 The Potential Wave Equations.....	33
(a) The Potential Wave Equations in the Lorenz gauge.....	33
(b) Special Relativity Note.....	35
(c) The Potential Wave Equations in the King and Lorenz Gauges with Conductors	37
1.4 Retarded Solutions in the Lorenz gauge: Propagators	46
1.5 The Wave Equations in the Frequency Domain	49
(a) The Transformed Wave Equations	49
(b) The Helmholtz Integrals in the King Gauge.....	51
(c) King's leading factor ($1/4\pi\epsilon$) and the final Helmholtz Integrals.....	52
(d) Frequency domain wave equations for fields and potentials in the Lorenz Gauge.....	60
(e) Self Consistency of Helmholtz Integral Solutions.....	61
1.6 Reinterpretation of all equations in terms of complex functions	63
(a) Complex Functions.....	63
(b) Monochrome time	64
(c) Why complex fields: The Fourier Transform	65
(d) Monochrome E and B fields.....	66
(e) The Line Strength	67
(f) Overloaded Notation and Maxwell's Equations in ω space	68
Chapter 2: The Round Wire and the Skin Effect	69
2.1 The Implicit Wave Context, Helmholtz Equations and the Skin Effect	69
2.2 Derivation of E(r), B(r) and J(r) for a round wire	72

2.3 A study of the solution of a round wire	79
(a) Kelvin Functions	79
(b) Plots of $ E(r)/E(a) $ for various δ values	80
(c) Review of the round wire solution	84
(d) Plots of the round wire solution for Belden 8281 at 5 MHz.....	86
2.4 The Surface Impedance $Z_s(\omega)$ of a Round Wire.....	88
(a) Expressions for Surface Impedance.....	89
(b) Low frequency limit of $Z_s(\omega)$	90
(c) High frequency limit of $Z_s(\omega)$	91
(d) Plots of $Z_s(\omega)$ versus skin depth δ	92
2.5 Surface Impedance for a Transmission Line.....	95
Chapter 3: Transmission Line Preliminaries	98
3.1 Why is there no free charge inside a conductor or a dielectric?	98
3.2 How thick is the surface charge layer on a conductor?.....	100
3.3 How does loss tangent affect dielectric conductivity?	101
3.4 Size of E fields in conductor and dielectric; conservation of total current at a boundary.....	104
3.5 The TEM mode fields and currents for an <i>ideal</i> transmission line	107
3.6 The TEM mode fields and currents for a <i>practical</i> transmission line.....	110
3.7 The general shape of fields, charges, and currents on a transmission line.....	112
(a) E_θ at a conductor surface vanishes	112
(b) The transverse vector potential components are small	113
(c) The scalar potential ϕ on a conductor surface	113
(d) B and A_z on a conductor surface.....	117
A Counter Example and Comments on the Low Frequency Regime	119
(e) Observations about the E and B field lines in a transmission line dielectric	121
(f) Drawings of the fields.....	123
(g) More on the field and current structure	125
(h) Estimate of the ratio J_r/J_z	127
3.8 Review of Transmission Line Preliminaries.....	129
Chapter 4: Transmission Line Equations	132
4.1 Computation of potential ϕ due to one conductor of a transmission line	132
4.2 Computation of potential ϕ due to both conductors of a transmission line	134
4.3 The Transmission Line Limit.....	135
4.4 General Calculation of $V(z)$	138
4.5 Example: Transmission line with widely-spaced round wires of unequal diameters	144
Power Transmission Lines (also Telephone and Telegraph)	148
4.6 Example: A coaxial cable	150
4.7 Computation of A_z due to one conductor of a transmission line	154
Comments regarding μ	155
4.8 Computation of potential A_z due to both conductors of a transmission line	158
4.9 Transmission Line Limit Revisited.....	158
4.10 General Calculation of $W(z)$	159
4.11 Relations involving C and G and the charges and currents in a transmission line	162
4.12 The Classical Transmission Line Equations	165
(a) Initial Processing	165

(b) Averaging Repair and the Transmission Line Equations	166
(c) An example of $K = K_L$	171
(d) Summary of Results	174
(e) Time domain equations (telegraph equations).....	176
4.13 Modifications to account for $\mu_d \neq \mu_1 \neq \mu_2$	177
Chapter 5: The Transverse Problem.....	182
5.1 Separation of ϕ	182
5.2 Separation of A_z	184
5.3 Development of the Transverse Problem.....	186
(a) $k_\phi = k_A$ and the transverse equations.....	186
(b) The scaling boundary condition on $\phi_\tau(x)$	188
(c) Energy Conservation in a Transmission Line.....	190
5.4 The Low-Loss Approximation.....	191
(a) Transverse Equations for a Low-Loss transmission line.....	191
(b) The scaling boundary condition (5.3.13) revisited.....	194
5.5 The Capacitor Problem: How to Find K	195
5.6 What happens if low-loss is not assumed?.....	201
Chapter 6: Two Cylindrical Conductors	204
6.1 A candidate transverse potential ϕ_τ	204
6.2 Ancient Greece circa 230 BC.....	204
6.3 Back to the Future: Calculation of K	207
6.4 Summary of Line Parameter Results	214
6.5. The Proximity Effect for a Transmission Line made of Two Round Wires	215
(a) The surface charge density and its moments	215
(b) The Proximity Effect.....	218
(c) Plots of the Proximity and Skin Effects.....	219
(d) The relationship between $J_z(a,\theta)$ and $n(\theta)$ obtained from $\text{div } E = 0$	224
(e) The Proximity Effect At Low Frequencies.....	226
(f) Active perimeter p and Z_s for a two-cylinder transmission line.....	227
(g) The Proximity Effect For Currents in the Same Direction.....	230
Chapter 7: The Low Frequency Limit of the Theory	231
7.1 A Review of Appendix D.....	231
(a) The Four Equations	231
(b) The Two Boundary Conditions	231
(c) The e^{-jkz} Ansatz.....	232
(d) The Appendix D E-field Solutions.....	233
7.2 First Sign of Trouble: J_z Asymmetry at DC.....	234
7.3 A proof that J_z must be uniform at DC	236
7.4 Second Sign of Trouble: Infinite B fields as $\omega \rightarrow 0$	242
7.5 What is the cause of the Trouble as $\omega \rightarrow 0$?	246
Appendix A: Gauge Invariance	250
A.0 The Poisson Equation and its Solution.....	250
A.1 Existence of A such that $B = \text{curl } A$ and $\text{div } A = 0$	253
A.2 Existence of A' such that $B = \text{curl } A'$ and $\text{div } A' = f$	255

A.3 Existence of ϕ such that $E = -\text{grad } \phi$	255
A.4 Existence of A' and ϕ' such that $B = \text{curl } A'$, $E = -\text{grad } \phi' - \partial_t A'$, and $\text{div } A' = f$	256
A.5 Gauge Invariance	257
A.6 The Lorenz Gauge and QED.....	258
A.7 Finding the gauge function Λ for the Lorenz Gauge: time-domain propagators	260
Appendix B: Magnetization Surface Currents on a Conductor	263
B.1 Relationship between surface current K and the field H at a conductor boundary	263
B.2 Calculation of H from the current J in a conductor	268
(a) An expression for H in terms of J	268
(b) An alternative derivation using the vector potential A	269
(c) Boundary conditions.....	271
(d) The Biot-Savart Law in 3D and 2D.....	271
B.3 General Method for computing the surface current J_m on a wire.....	273
B.4 Surface current on a round wire with uniform J	273
B.5 Computing H_θ for a round wire using the General Method of B.3	274
B.6 Modification of King's Helmholtz integral solution when $\mu_1 \neq \mu_2$	278
(a) General Discussion	278
(b) Statement and Proof of the J_m Lemma.....	279
(c) Statement and Proof of the J_m Theorem.....	286
B.7 Application of the J_m Lemma to a round wire with uniform J_z	290
(a) The $A_z^{(c)}$ term.....	291
(b) The $A_z^{(m)}$ term	293
(c) Adding the two terms and checking boundary conditions.....	293
(d) Plots of A_z and B_θ and H_θ	295
Appendix C: DC Properties of a Wire	297
C.1 The DC resistance of a wire	297
C.2 The DC surface impedance of a wire	297
C.3 The DC internal and external inductance of a round wire.....	298
C.4 The DC internal inductance of a wire of rectangular cross section.....	301
C.5 The DC internal inductance of a thin flat wire	310
C.6 The DC internal inductance of a hollow round wire	315
Appendix D: The General E and B Fields Inside an Infinite Straight Round Wire	320
D.1 Partial Wave Expansion	321
(a) The General Method.....	321
(b) Partial Wave Expansions.....	323
(c) The Vector Laplacian in Cylindrical Coordinates.....	324
(d) The three Helmholtz equations and $\text{div } E = 0$ (in partial waves)	325
D.2 Solutions for E_z , E_r and E_θ	329
(a) The E_z Solution	329
(b) The E_r Solution	330
(c) The E_θ Solution	332
(d) The Charge Pumping Boundary Condition	336
(e) Application of the Boundary Conditions.....	337
Second summary of the E field solutions.....	340

D.3 What about the E_θ Helmholtz Equation ?	343
D.4 Computation of the B fields in the round wire.....	344
D.5 Verification that the E and B fields satisfy the Maxwell equations	348
D.6 The exact E and B fields for the $m=0$ partial wave.....	349
D.7 What about the E fields <i>outside</i> the round wire?	351
D.8 About the boundary condition $E_\theta(a,m) = 0$	353
(a) The Quasi-Static Argument	354
(b) An Ansatz Argument.....	356
D.9 About the boundary condition $E_r(a,\theta) = (j\omega/\sigma) n(\theta)$	357
(a) The notion of Debye Surface Currents	357
(b) The role of Debye Surface Currents in the boundary condition.....	359
(c) Where does surface charge $n(\theta)$ come from?	361
(d) Modifications for a Conducting Dielectric.....	364
D.10 High frequency limit of the round wire E fields	371
(a) Symmetry of e_m, f_m, g_m and h_m and expansions for $E_i(r,\theta)$	371
(b) High frequency evaluation of e_m, f_m, g_m and h_m and the E fields	372
D.11 Low frequency limit of the round wire E fields	378
(a) A High Level Review of Appendix D and its Accuracy	378
(b) Low frequency values for β'	379
(c) Low frequency evaluation of e_m, f_m, g_m and h_m	380
(d) Low frequency E fields	382
Appendix E: How Thick is Surface Charge on a Metal Conductor?	386
Appendix F: Waveguides.....	390
F.1 Discussion.....	390
F.2 The TE waveguide modes for a parallel-plate transmission line	390
F.3 A waveguide interpretation.....	394
Appendix G: The DC vector potential of a round wire carrying a uniform current.....	396
G.1 Setup and Assumptions	396
G.2 Direct solution for $A_z(r)$ from the differential equation.....	397
G.3 Instant solution for A using Ampere's Law, and computation of J_m	400
The Magnetization Current	401
G.4 Solution for A_z using the 2D Helmholtz Integral	402
G.5 Comments on the low frequency solution for A_z	405
Appendix H: Laplace and Helmholtz Propagators in 3D.....	407
Appendix I: Laplace and Helmholtz Propagators in 2D	412
Appendix J: The 3D→2D Propagator Transition.....	420
Appendix K: The Network Model: Comparison of Network and Maxwell Views	426
(a) The Network Model	426
(b) Network Model Characteristic Impedance.....	427
(c) Network Model Transmission Line Equations.....	429
(d) Network Model Parameters obtained from Maxwell's Equations.....	430
(e) Low frequency case for round conductors (no skin effect)	431
(f) High frequency case for round conductors (strong skin effect)	432

Appendix L: Point and Line Charges in Dielectrics	434
L.1 The potential of a point charge inside a thick dielectric spherical shell	434
L.2 Limits of the Previous Problem	439
(a) Point charge in a spherical cavity in a dielectric	439
(b) Point charge embedded in a dielectric sphere	440
(c) Point charge embedded in an infinite dielectric medium	441
L.3 The potential of a line charge inside a thick dielectric cylindrical shell.....	442
L.4 Limits of the Previous Problem	445
(a) Line charge in an infinite cylindrical hole in a dielectric	445
(b) Line charge embedded in an infinite dielectric cylinder	446
(c) Line charge embedded in an infinite dielectric medium	446
Appendix M: Why the transverse vector potential A_{\perp} is small for a transmission line.....	448
Appendix N: Drude, Magnetic Ohm's Law, Regular Hall Effect, Radial Hall Effect	456
N.1 The Drude Model of Conduction	456
N.2 A Theory of the Hall Effect	458
N.3 The Cyclotron Frequency.....	462
N.4 Steady-state Electron Motion with E and B fields: Magnetic Ohm's Law.....	463
N.5 Theory of the Hall Effect Revisited	466
N.6 Theory of the Hall Effect with Multiple Carrier Types	467
N.7 The Radial Hall Effect in a Round Wire.....	470
N.8 Magnetic Ohm's Law for Arbitrary B	477
Appendix O: How to plot 2D magnetic field lines.....	480
(a) Statement of the Problem	480
(b) The Brute Force Method	480
(c) The ODE Method	481
Example: Magnetic field lines for a two-cylinder transmission line	482
(d) The Analytic Method	487
Appendix P: Eddy Currents and the Proximity Effect.....	489
P.1 Eddy Current Analysis.....	490
P.2 Eddy currents in a thin round plate in a uniform B field	493
P.3 Eddy currents in a thin round plate in a <i>non</i> -uniform B field	497
(a) The stream function method in Cartesian Coordinates.....	498
(b) The stream function method in Cylindrical Coordinates	499
(c) Using the stream function method to solve the plate problem	500
P.4 Self-induced eddy currents in a round wire	504
P.5 Eddy currents induced in a quiet round-wire by an external B field	509
P.6 Eddy currents induced in an current-carrying wire by an external B field	512
P.7 Summary of Round Wire Examples	513
P.8 Eddy currents in Transmission Lines: The Proximity Effect.....	514
P.9 Quantitative Evaluation of Eddy Currents and The Proximity Effect	518
P.10 Influence of Proximity and Skin Effects on Wire Resistance.....	519
Appendix Q: Properties of the functions $k(\omega)$ and $Z_0(\omega)$; plots for Belden 8281 cable	521
Q.1 A Simple Model for R, L, G and C	522
Q.2 Real and Imaginary parts of $k(\omega)$	529
Q.3 Large ω limit of $k(\omega)$	530

Q.4 Small ω limit of $k(\omega)$	534
Q.5 The general appearance of $\text{Re}(k)$ and $\text{Im}(k)$ for Belden 8281 cable	539
Q.6 Real and Imaginary parts of $Z_0(\omega)$	545
Q.7 Large ω limit of $Z_0(\omega)$	547
Q.8 Small ω limit of $Z_0(\omega)$	551
Q.9 The general appearance of $\text{Re}(Z_0)$ and $\text{Im}(Z_0)$ for Belden 8281 cable	555
Appendix R: Belden 8281 Coaxial Cable, a Case Study	561
(a) Geometry of the cable.....	561
(b) Capacitance C	562
(c) Conductance G	563
(d) External inductance L_e	564
(e) Total DC Inductance.....	564
(f) High Frequency Inductance and Resistance	566
(g) The Tinning Correction	567
(h) Characteristic Impedance	570
(i) Phase Velocity and Attenuation	572
Appendix S: Details of the Chapter 4 Averaging Procedure	577
References	582

Overview and Summary

This monograph uses the Maxwell and associated potential equations to determine the behavior of infinitely-long straight transmission lines. The presentation is loosely based on R.W.P. King's book *Transmission-Line Theory*. No attempt is made to address non-straight geometries, bends, stubs and many other practical applications described by King. There is no discussion of discontinuities, reflections, standing wave ratios, Smith charts, or any of the traditional topics associated with transmission lines (see, for example, Pozar 2012). The emphasis is more on how one derives the transmission line parameters R, L, G, C directly from electromagnetic theory, and what approximations are made in doing so. A key requirement is that the wavelength of a transmission line wave be significantly larger than the line's transverse dimensions, something we refer to as the "transmission line limit". Although the discussion generally concerns transmission lines with two conductors, comments here and there show how the conclusions can be extended to transmission lines with more than two conductors.

Unlike waveguides, low-loss TEM transmission lines are most easily analyzed using potentials rather than fields due to the nature of the boundary conditions. This then brings up the can of worms known as "the gauge condition". We show how a variant of the Lorenz gauge which we call "the King gauge" (since King uses it) serves to clarify the meaning of the Helmholtz integrals for the scalar and vector potentials over the surface and interior of the transmission line conductors. This subject is somewhat glossed over in King's highly compressed theoretical summary, and we could not find clarification in his many other books on the subject. By the way, most books on "transmission lines" are concerned with the practical aspects of electrical power distribution and King's book is somewhat of a rarity, though there are other good books on the subject. It is true that a waveguide is in fact a transmission line, but we use the term "transmission line" to imply the TEM mode of transmission.

An ancillary topic receiving much attention in this document is the description of the fields, potentials and currents *inside* a transmission line conductor operating at angular frequency ω . Mainly the discussion concerns round wires. A uniform round wire seems a simple physical object, yet the analysis is quite complicated and involves the so-called Kelvin functions. The skin effect and surface impedance of such a wire are considered in detail, and then later the proximity effect enters the picture.

There are very few "it can be shown" phrases in this document. Almost everything is derived in detail and the results verified against external sources. Simple examples are always presented and calculations for these examples are fully displayed, perhaps to a level of detail the reader will find annoying. Our view is that a piece of theory is useless if one cannot apply it to a simple case and get a reasonable result.

The reader is assumed to have some knowledge of ordinary and partial differential equations and associated calculus. Green's Functions (which we call propagators) appear frequently, since these are useful in solving differential equations, and details are provided for readers not familiar with this subject. In particular, our first major waypoint is the derivation of the transmission line potentials in the form of King's Helmholtz integrals as shown in box (1.5.23). The propagators in these integrals are the 3D Helmholtz free-space fundamental solutions $e^{-j\beta R}/R$. This subject is fully laid out for the interested reader in Appendices H and I for the 3D and 2D Helmholtz partial differential equations which are the frequency domain Fourier transforms of the more familiar 3D and 2D wave equations.

The document consists of seven Chapters which are followed at the end by Appendices A through S. The latter deal with issues thought too detailed or perhaps too peripheral to the main topic to appear in the main text, but which we nevertheless felt were worth including. Many of the appendices are stand-alone monographs in their own right, addressing some related topic (eddy currents, gauge invariance, field line plotting methods, Hall effects, network model, fields inside a round wire, etc.) The final section contains a list of References.

Maple is used as needed to compute analytic integrals, solve equations, do unpleasant algebra, and make graphs. The reader need not be a Maple expert to read and understand the presented Maple code.

To reduce clutter, derivatives that would normally be written $\frac{\partial f}{\partial x}$ or $\partial f/\partial x$ are written as $\partial_x f$. Symbols $\text{div } \mathbf{F}$, $\text{curl } \mathbf{F}$ and $\text{grad } \psi$ are generally used instead of $\nabla \cdot \mathbf{F}$, $\nabla \times \mathbf{F}$ and $\nabla \psi$. The scalar Laplacian is always ∇^2 . Symbol σ is used for conductivity, so surface charge is relegated to symbol n , which is also used to indicate a derivative normal to a surface $\partial_n f$.

Rather than use exotic script fonts or decorations to distinguish various forms of the electric field E , we use an "overloaded" notation where the argument list or context determines which E function is implied.

When an equation is repeated after its first occurrence, the equation number is put in italics.

A fairly complete list of the symbols used in this document is presented after the summaries below.

Chapter Summaries

Chapter 1 states Maxwell's Equations and associated equations which extend Maxwell's theory from the vacuum to conducting dielectric and magnetic media. After some comments, many of these equations are restated in integral form using the divergence theorem and Stokes's theorem, and then the behavior of field components at boundaries is obtained. Wave equations for both the fields and potentials are described, and the subject of gauges is dealt with. Starting with Section 1.5 the wave equations are transformed to the frequency domain and Helmholtz equations with parameter β^2 appear. King's Helmholtz integral solutions of these equations are then derived using what we call the King gauge. Finally, Section 1.6 clarifies the reasons for using complex fields when physical \mathbf{E} and \mathbf{B} fields are real.

Chapter 2 derives expressions for the \mathbf{E} and \mathbf{B} fields (and current $\mathbf{J} = \sigma\mathbf{E}$) inside a round wire which is assumed to have an axially symmetric current flow. The resulting fields are rather complicated and reveal the skin effect. The surface impedance is defined and various quantities are plotted. Assumptions are made about the vector directional nature of the \mathbf{E} and \mathbf{B} fields in this analysis. The same problem is treated without these assumptions and for an arbitrary transverse current distribution in Appendix D. The main results of that lengthy appendix appear in box (D.9.39).

Chapter 3 first discusses odd topics such as the dielectric loss tangent, the thickness of surface charge, and why there is no free charge inside a conductor or a dielectric. The chapter then presents a qualitative description of the \mathbf{E} and \mathbf{B} fields of a TEM mode transmission line, with some sketches of the fields. Finally, various Facts about such a transmission line are stated.

Chapter 4 uses the Helmholtz integral form of the potentials to derive the well-known transmission line equations which are these,

$$\partial_z V(z) = -z i(z) \qquad \partial_z i(z) = -y V(z) \qquad (4.12.15)$$

$$z = R + j\omega L \qquad y = G + j\omega C \quad . \qquad (4.12.16)$$

In this process, the "transmission line limit" is assumed. It says that the wavelength on the line is much longer than the transverse dimensions of the line. The analysis then yields precise meanings for the parameters R , L , G and C . L is in fact the sum of external and internal inductance contributions $L_e + L_i$ and it turns out that L_e , C and G are all related to each other in terms of a certain dimensionless real parameter K as shown in (4.12.24). Parameters R and L_i are the real and imaginary parts of the sum of the conductor surface impedances $Z_{s1} + Z_{s2}$. For closely spaced conductors, it is shown how quantities like Z_{s1} are interpreted as perimeter averages. This chapter's analysis is first carried out assuming that the conductors and dielectric all have the same magnetic permeability μ , but then Section 4.13 shows how to generalize the results for arbitrary magnetic conductors and dielectric.

At this point, the transmission line parameters are clarified and are related to each other, but they are not "known" due to the fact that their solutions involve integral equations over the transmission line geometry. This is the typical chicken-and-egg problem one encounters in all real-world electromagnetic problems. Apart from simple cases (such as very thin transmission line conductors), further approximation must be made.

Chapter 5 describes the required approximation. It is basically a continuation of the "transmission line limit" mentioned earlier, along with a notion of "low loss", which then allows the transmission line problem to be reformulated as a 2D potential theory problem which we call "the transverse problem". It is then basically a "capacitor problem" and then any transmission line geometry can be solved at least numerically. Basically the assumption that the conductors are very *good* conductors transforms the transverse Helmholtz equation into the 2D Laplace equation which is the basis of 2D potential theory.

Chapter 6 then gives a complete discussion of the exact solution, within the assumptions just mentioned, for transmission lines consisting of two parallel solid cylindrical conductors of arbitrary diameter and arbitrary relative (but not intersecting) position. This includes twin-lead lines with equal and unequal conductor diameters as well as on- and off-centered coaxial lines. Since an infinite radius cylinder is a plane, this discussion also obtains the exact solution for a transmission line consisting of a round wire over a ground plane. Then the proximity and skin effects are analytically calculated for this transmission line and the current density J_z is plotted over the wire cross section for various wire sizes, locations, and frequencies. It is shown that J_z tracks the charge density $n(\theta)$ around the wire perimeter of each wire. At low ω the entire model is uncertain, and it is shown why the limit $\omega \rightarrow 0$ cannot be interpreted in the way one might think. The active perimeter p and average surface impedance Z_s and are then computed. The final section comments on the proximity effect for conductors in which currents flow in the same direction.

Chapter 7 demonstrates that the theory of Chapters 4-6 (and Appendix D for the round wire) has definite problems at low frequencies, and explains why these problems are to be expected. It also presents a derivation of the fact that current density J_z is uniform in a round wire at DC.

Appendix Summaries

Appendix A discusses **gauge invariance** and proves the existence of gauges in which $\text{div } \mathbf{A}$ can be set to any arbitrary (but reasonable) scalar function, \mathbf{A} being the vector potential appearing in $\mathbf{B} = \text{curl } \mathbf{A}$. The notion of a Green's function or "propagator" is introduced, along with the tool of **parts integration** in multiple dimensions. A few passing comments are added regarding the connection to special relativity, covariance and quantum field theory.

Appendix B analyzes the situation in which the transmission line dielectric and conductors have different magnetic permeability μ , a situation not treated in King's TLT book. This causes a bound **magnetization** current density \mathbf{J}_m to appear both at boundaries (as a surface current) and in the bulk conductors (as a volume current). It is shown ("the \mathbf{J}_m theorem") that the theory of Chapter 4 with its Helmholtz integrals for the potentials can be "rescued" by adding just the surface component of the magnetization current \mathbf{J}_m to the true conduction current in the vector potential integrand. A general method is given for computing this surface current \mathbf{J}_m from the conduction current distribution \mathbf{J} in the conductor, using the \mathbf{H} field as an intermediary. As usual, the round wire serves as a calculational example.

Appendix C concerns the seemingly mundane subject: **DC properties of wires**. The main issue here is the DC inductance of wires which are treated from a stored energy viewpoint. Internal inductances are computed for a round wire and a hollow round pipe. It is shown that even for a simple rectangular cross section (including square), the internal inductance cannot be expressed analytically (at least using our

method) and a numerical calculation is required. That calculation has been done recently (2009) by Holloway and Kuester.

Appendix D computes the **E and B fields inside a round wire** which is assumed to be one conductor of a transmission line down which a traveling wave propagates at frequency ω . The solution is obtained using azimuthal partial wave analysis. The **E** field Helmholtz equations are directly solved in cylindrical coordinates, and the **B** field is then computed from Maxwell's curl **E** equation. Boundary conditions at the wire surface are discussed. The results (D.4.13) are expressed in terms of the surface charge moment η_m in each partial wave. The results for the $m=0$ partial wave are compared with the results of Chapter 2 which assumed a symmetric current distribution. A passing glance is taken at the corresponding fields outside the wire, then the two boundary conditions are examined more closely, including consideration of Debye surface currents. The source of the surface charge $n(\theta)$ is pondered. The dielectric is initially assumed to be non-conducting, but then this restriction is removed. Finally the high ω and low ω limits of the **E** and **B** fields are calculated. It is noted that the entire model is not meaningful very close to $\omega = 0$.

Appendix E ponders the **thickness of the surface charge** on a conductor. It is shown that the charge layer thickness is about 1/3 the radius of a copper atom for a copper conductor, and that this is 4000 times smaller than the skin depth at 100 GHz.

Appendix F is an elementary discussion of the **waveguide modes** of a parallel plate transmission line. It shows why there is a cutoff frequency below which no waveguide modes can operate, whereas the "transmission line (TEM) mode" on the same structure operates all the way down to very low ω .

Appendix G computes the DC vector **potential A_z inside and outside a round wire** carrying uniform current. The computation is done three ways, the most difficult using the Helmholtz (Laplace) integral. When the dielectric surrounding the wire has a μ different from that of the wire, a homogeneous solution must be added to the Helmholtz particular integral solution. It is this homogeneous solution that is synthesized by adding the surface magnetization current discussed in Appendix B.

Appendices H and I derive the **Laplace and Helmholtz Green's Functions** for the 3D and 2D Laplace and Helmholtz differential equations. These play a major role in the entire document.

Appendix J shows how the transmission line transverse analysis replaces 3D propagators with 2D propagators of the Helmholtz and Laplace equations. Results obtained blindly in the main document are interpreted in terms of these Green's function propagators.

Appendix K presents the standard **network model** of a transmission line as the limit of a set of lumped circuit components. By computing the characteristic impedance Z_0 both from this network model and from Maxwell's equations, it is shown that the R,L,G,C parameters of both models have the same meaning, and this makes the connection between these network-model parameters and those obtained in Chapter 4 from the Maxwell equations.

Appendix L considers a **point charge** located at the center of the cavity of a thick spherical dielectric shell. The electrostatic problem is solved and limiting cases are obtained. The solution provides an interpretation of how bound charge is accounted for by the dielectric constant ϵ in $E_{\mathbf{x}} = (1/4\pi\epsilon)(q/r)$. This 3D analysis is then repeated in 2D for a **line charge** in the cavity of an infinite cylindrical shell.

Appendix M shows qualitatively that, in the King gauge, the vector potential transverse components \mathbf{A}_t are much **smaller** than the longitudinal component A_z for all frequencies of transmission line interest.

Appendix N describes some subtle aspects of current flow in the presence of magnetic fields. The regular Hall effect is treated, the notion of **magnetic Ohm's law** is derived, and the **Hall effect** is reconsidered in light of this law. After dealing with multiple carrier types and magnetoresistance, we show that in a static round wire carrying a current I , the longitudinal current density J_z is uniform, and there exists a **radial Hall effect** inside the wire. There is a small radial electric field E_r and a small free charge density ρ inside the wire which is balanced by a small surface charge on the wire surface. The cyclotron frequency ω_c plays a major role in this discussion.

Appendix O reviews three methods for generating **2D field line plots**. The first method is brute force tracking iteration, while the second method makes use of Maple's ability to numerically solve a pair of coupled differential equations. The third analytic method works in some cases. An example of each method is presented.

Appendix P discusses the **eddy current** interpretation of the skin and proximity effects. A perturbation expansion is developed and for small ω and the first term of this expansion is used to compute the eddy currents in some simple cases. A thin round plate is treated analytically for a uniform then for a non-uniform external B field. Then a series of qualitative examples leads to an explanation of the skin and proximity effects in a transmission line as well as in generic parallel wires with same or oppositely directed currents. It is shown why there is current crowding, and why such wires attract or repel.

Appendix Q computes the real and imaginary parts of $k(\omega) = -j \sqrt{(R+j\omega L)(G+j\omega C)}$ and then evaluates the limits for large and small ω . This task is then repeated for $Z_0(\omega) = \sqrt{\frac{R+j\omega L}{G+j\omega C}}$. The general appearance of $k(\omega)$ and $Z_0(\omega)$ over a very wide range of ω is shown for Belden 8281 cable as a prototype.

Appendix R applies the theory developed in this document to a case study: **Belden 8281** coaxial cable.

Appendix S shows that the conclusions of Chapter 4 are maintained for closely spaced conductors when the various parameters of the theory are averaged over the perimeters of the conductors.

Symbols used in this document

Symbols are listed "alphabetically" in four groups. Some symbols have multiple meanings separated by semicolons. The list shows the first use location of unusual symbols. The reader seeking entertainment might compare these choices to his or her favorites. The sheer *number* of symbols is an indication of the complexity hidden within a simple infinite straight transmission line.

Operators and Special Symbols

\equiv	is defined as (\approx approx. equal, \sim ballpark equal)
$\mathbf{A} \bullet \mathbf{B}$	3D dot product
$a^{\mathbf{n}} b_{\mathbf{p}}$	implied summation, see for example (1.3.11)
$a * b$	regular multiplication
a^*	complex conjugation
aka	also known as
a/b	space (and effort) saving version of $\frac{a}{b}$. Examples: $\partial F/\partial t = \frac{\partial F}{\partial t}$, $\sin(x)/(3ab\sigma) = \frac{\sin(x)}{3ab\sigma}$ (except where expressions are very confusing with the slash notation).
∂_t	partial time derivative $\partial/\partial t$, so then $\partial F/\partial t = \partial_t F$
$\partial_{\mathbf{x}}$	partial spatial derivative $\partial/\partial \mathbf{x}$ (similarly $\partial_{\mathbf{y}}$, $\partial_{\mathbf{z}}$, $\partial_{\boldsymbol{\theta}}$, $\partial_{\mathbf{r}}$, etc.)
∂_i	partial spatial derivative $\partial/\partial x_i$
∂'_i	partial spatial derivative $\partial/\partial x'_i$
M^T	transpose of matrix M
QED	thus it is proved
RHS	right hand side, LHS is left hand side
$\Sigma_{i=1}^3$	budget summation notation (fits on a single line)
$\dot{\mathbf{v}}$	same as $d\mathbf{v}/dt$
\square	d'Alembertian = the 4D version of $-\nabla^2$. $\square = (1/c)^2 \partial_t^2 - \nabla^2$, see (1.3.11)
\star	Moon and Spencer notation for the <i>vector</i> Laplacian (also written ∇^2) (D.1.10)
E^\wedge	Fourier Transform of E; this \wedge notation is used only in Section 1.6
$\hat{\mathbf{x}}$	unit vector indicator
\oint	closed line integral, usually $\oint ds$

Capital Latin

A	vector potential (1.3.1); $A_{\mathbf{z}\mathbf{t}}$ is transverse vector potential, see (5.2.1)
A	a surface area, dA = a differential piece of this area (often dS); A = Angstrom = 10^{-10} m
B	magnetic field, see (1.1.5) (sometimes called magnetic induction)
B	a bipolar coordinate used in Ch 6 (often called ξ elsewhere)
\mathcal{B}	$\mathcal{B} \equiv (\xi_{\mathbf{d}}/\epsilon_{\mathbf{d}})$ CVR $_{\mathbf{d}\mathbf{c}}$, a combination of App D symbols, introduced in (D.9.36)
C	generic constant name (also A,B,C,D...); conductor name such as C_1 and C_2
C	capacitance (often per unit length of a transmission line)
C'	complex capacitance, see (4.11.9) $C'/C = q_{\mathbf{c}}/q_{\mathbf{s}} = (\xi/\epsilon)$
D	diffusion constant, see App E and (3.1.1); generic transverse dimension of a transmission line
D	electric displacement, see comment (5) below (1.1.18)

E	electric field, but see Section 1.6 (f) about our heavily overloaded notations
G	conductance per unit length between conductors of a transmission line
H	magnetic field, see (1.1.5); $H^{(1)}(z)$ = Hankel function
I	$I = i(0)$, first used in (D.2.31) (total current in a wire at $z = 0$)
J, J_i	current density and component thereof
J_c	conduction current (as opposed to displacement current or polarization current)
J_m	magnetization current, see (1.1.20)
J_{po1}	polarization current, see (1.1.10)
J_m(z)	Bessel function
J^μ	contravariant 4-vector (related objects $F^{\mu\nu}$, ∂^μ , ∂_μ , A^μ , see App A.6 and Sec 1.3 (b))
K	surface current; constant appearing in transmission line parameter calculations, see (4.4.8)
K_z	surface current component in the z direction
K_L	see (4.10.9)
K_m	coefficient appearing in Appendix D
L	inductance; sometimes a differential operator (such as $L_{\mathbf{x}} = \partial_{\mathbf{x}}^2$ or $L_{\mathbf{r}}$)
L_e	external inductance of a transmission line (does not include energy storage inside conductors)
L_i	internal inductance of a conductor (does not include energy storage outside the conductor)
M	magnetization, see (1.1.21)
M_v(z)	$J_v(e^{j3\pi/4}z) = M_v(z) e^{j\theta_v(z)}$ for real z
N_m	moment of charge density $n(\theta)$ on a round wire, see (D.1.5)
P	electric polarization, see (1.1.12)
P	power, $P = IV$, see (C.3.3); total conductor perimeter
Q	total charge on something
R	resistance, often per unit length; distance between two 3D points ($R = \mathbf{x} - \mathbf{x}' $)
R_{dc}	DC resistance of a conductor (per length). For a round wire of radius a, $R_{dc} = 1/(\sigma\pi a^2)$.
R_H	Hall coefficient, see (N.2.4)
S	a surface area, $dS =$ a differential piece of this area, $d\mathbf{S} = dS \hat{\mathbf{n}}$; sign of $-\text{Im}(Z_0)$ in (Q.6.1)
T_z	stream function (also T); T is the current vector potential, see (P.3.7) and text above
T	thickness; temperature; $T_F =$ Fermi temperature
U	energy stored in an inductor, $U = (1/2)L I^2$, see (C.3.4)
V	voltage; sometimes volume, differential dV . When mixed, volume is \mathcal{V} or $d\mathcal{V}$
V_H	Hall voltage, see (N.2.6)
V(z)	$\Delta\phi$ between transmission line conductors at some z, see (4.4.1)
W(z)	ΔA_z between conductors at some z, see (4.10.1)
W	width of something
X	reactance $X_C = 1/(\omega C)$, $X_L \equiv \omega L_e$, see (4.12.24)
Z_s	surface impedance, see Section 2.4
Z₀	characteristic impedance of a transmission line, see (4.4.12) and (K.4)
Z_m	intrinsic impedance of a medium $= \sqrt{\mu/\epsilon}$, see (4.4.14)
Z_{fs}	impedance of free space (377Ω), see (1.1.29)
Z_m	complex intrinsic impedance of a medium $= \sqrt{\mu/\xi}$, see end of Section 4.4 (not used)

Lower Case Latin:

a	radius of a round wire (a_1 and a_2 if there are two round wires)
a_m	coefficient appearing in Appendix D
b	distance between centers of a transmission line made of two round wires
$b(x,y)$	transverse current density in a conductor, normalized to 1
$ber_n(z)$	Kelvin function [also $bei_n(z)$], $J_\nu(e^{j3\pi/4}z) = ber_\nu(z) + j bei_\nu(z)$ for real z , see (2.3.1)
c	speed of light in vacuum
ch	cosh
cof	cofactor matrix (as in $c^{-1} = \text{cof}(c^T)/\det(c)$ for matrix c)
curl	curl (sometimes written as $\nabla \times$)
d	diameter of a round wire (d_1 and d_2 if there are two round wires); bipolar focal distance
dS	differential vector Surface area (scalar is dS , but sometimes written as dA) (\mathbf{A} = vector potential)
ds	differential distance along a curve (written elsewhere as $d\ell$) ; scalar distance is ds
dS_ξ	local Stakgold surface area element in n dimensions with ξ the normal direction
dV	differential volume ; differential voltage
det	determinant of a matrix
div	divergence (sometimes written as $\nabla \cdot$)
e	electron charge, $e = - e $; $e = 2.71$
e_m	a combination of Bessel functions, see (D.4.9)
$\exp(z)$	e^z
f	frequency; generic function name
f_m	a combination of Bessel functions, see (D.2.33)
g_m	a combination of Bessel functions, see (D.2.33)
grad	gradient (sometimes written as ∇)
$g(x x')$	Green's function (aka a Green function or propagator); sometimes written $g(\mathbf{x},\mathbf{x}')$ or $g(\mathbf{x},t; \mathbf{x}',t')$
h_m	a combination of Bessel functions, see (D.2.33)
h	height of something, like wire center line above a plane; Planck's constant
$i(z)$	total current in a conductor at location z , first used in (4.7.3) and (4.7.5); $i(0) = I$ in App D.
j	$\sqrt{-1}$, see comment above (D.1.3)
k	sometimes used for a wavenumber (k_ϕ , k_A , k in App D, etc.); Boltzmann's constant
$k(x,x')$	kernel in an integral equation or integral expression
m	meter; partial wave label in Appendix D; mass of particle (an electron)
n	surface charge density; normal vector (\mathbf{n}); normal component (E_n); electron density (n_e)
$n(\theta)$	surface charge density on a round conductor which is part of a transmission line
n	surface charge per unit perimeter distance of a conductor (Cou/m); sometimes per angle
n_{free}	free surface charge (does not include any polarization charge)
n_s	same as n_{free}
n_c	transport surface charge density, see (1.5.17): $n_c = (\xi/\epsilon)n_s$
p	active perimeter length; momentum
q	generic point charge
$q(z)$	total charge per unit length on a conductor at location z , first used in (4.1.2) and (4.1.4)
r	radial variable for cylindrical coordinates (ρ is charge density) ; sometimes spherical r
$s(\mathbf{x})$	generic source function, see for example (H.1.8)
sh	sinh

$s_{i,j}$	a 2D distance between points i and j
t	time; thickness of something
t	as subscript means either tangential (E_t) or transverse (E_\perp)
\tan_L	loss tangent see (3.3.2) (appears as $\tan\delta$ in other sources, aka dissipation factor)
th	tanh
u	energy density in a magnetic field, $u = (1/2) \mathbf{B} \cdot \mathbf{H}$, see (C.3.1) ; generic function name
v_d	speed of light in a dielectric (sometimes just v)
v	drift velocity of electrons in a conductor, see App N; sometimes $\mathbf{v} =$ generic velocity
w	width of something (sometimes means ω in Maple programs)
x, x_a	$x = \beta'r$, $x_a = \beta'a$, see (D.2.33)
\mathbf{x}, \mathbf{x}'	generic points in 3D space (sometimes written \mathbf{r}, \mathbf{r}')
\hat{x}	unit vector in the x direction (similarly \hat{y} , $\hat{\theta}$, \hat{n} etc.)
y	admittance per unit length of a transmission line see (4.12.15)
z	impedance per unit length of a transmission line see (4.12.15)
z	longitudinal dimension of a transmission line or round wire; generic Bessel Function argument

Greek

// pseudo-alphabetical

$\alpha(x,y)$	transverse charge density in a conductor, normalized to 1 (is delta function on surface)
β	wavenumber inside a transmission line conductor, see (1.5.1c)
β_d	wavenumber for dielectric surrounding transmission line conductors, see (1.5.1a)
β_{d0}	wavenumber for non-conducting dielectric, see (1.5.1b)
β'	$\beta'^2 \equiv \beta^2 - k^2$ see (D.2.2)
∂	partial derivative (see operator list above)
$\delta(x)$	Dirac delta function; $\delta(\mathbf{r}) =$ 3D delta function
δ	skin depth, see (2.2.20)
$\delta_{i,j}$	Kronecker delta
ϵ	absolute electric permeability ($\epsilon = \epsilon_0$ in vacuum), $\epsilon = \epsilon' - j\epsilon''$; a small real quantity $\epsilon > 0$
ϵ_{rel}	ϵ/ϵ_0
ϵ_{ijk}	permutation tensor
ξ	complex electric permeability (1.5.1) ($\xi = \epsilon - \sigma/j\omega$); ξ = a bipolar coordinate called B in Ch. 6
ξ	Stakgold n-1 dimensional coordinate of a point on a surface σ
ϕ	scalar potential, see (1.3.1); ϕ_\perp is the transverse scalar potential, see (5.1.1)
κ	$= 1/\mu$, inverse mobility, see (N.8.1)
λ	wavelength
λ_D	Debye length, see Appendix E
Λ	generic gauge function (Appendix A.2); arbitrary large cutoff value, see (J.10)
η_m	normalized moment of charge density on a round wire, see (D.2.30)
π	3.14 (= Pi in Maple V)
ρ	charge density (Coul/m ³); resistivity $\rho = 1/\sigma$ (ohm-m);
ρ_{free}	free charge density
ρ_{pol}	polarization charge density, see (1.1.11)
σ	conductivity (surface charge therefore is n, not σ) ; standard deviation; Stakgold surface label
σ_{eff}	effective conductivity see (3.3.4)
θ	azimuthal angle for cylindrical coordinates (ϕ is scalar potential)

- $\theta_\nu(z)$ $J_\nu(e^{j3\pi/4}z) = M_\nu(z) e^{j\theta_\nu(z)}$ for real z
- $\theta(a>b)$ Heaviside step function, normally written $\theta(a-b)$ or $H(a-b)$: $\theta(a>b>c) = \theta(a>b) \theta(b>c)$
- τ collision time, see Appendix N
- μ absolute magnetic permeability ($\mu=\mu_0$ in vac) ; carrier mobility in App N; mean value; microns
- ω angular frequency
- ω_c cyclotron frequency, see (N.3.1)
- χ_e, χ_m electric and magnetic susceptibility

Chapter 1: Basic Equations

In this chapter we state the basic equations to be used later in the calculation of transmission line parameters and in the exploration of transmission line behavior.

1.1 Maxwell's Equations in a Conducting Dielectric Medium

Our working set of equations is the following:

$$\text{curl } \mathbf{H} = \partial_t \mathbf{D} + \mathbf{J} \quad \text{Maxwell curl H equation } (\mathbf{J} = \mathbf{J}_c) \quad (1.1.1)$$

$$\text{curl } \mathbf{E} = -\partial_t \mathbf{B} \quad \text{Maxwell curl E equation} \quad (1.1.2)$$

$$\text{div } \mathbf{D} = \rho \quad \text{Maxwell div D equation } (\rho = \rho_{\text{free}}) \quad (1.1.3)$$

$$\text{div } \mathbf{B} = 0 \quad \text{Maxwell div B equation} \quad (1.1.4)$$

$$\mathbf{B} = \mu \mathbf{H} \quad \text{magnetic permeability } \mu \quad (1.1.5)$$

$$\mathbf{D} = \epsilon \mathbf{E} \quad \text{electric permeability } \epsilon \text{ (dielectric constant)} \quad (1.1.6)$$

$$\mathbf{J} = \sigma \mathbf{E} \quad \text{Ohm's Law } (\sigma = \text{conductivity}) \quad (1.1.7)$$

$$\text{div } \mathbf{J} = -\partial_t \rho \quad \text{Equation of Continuity (see item 7 below)} \quad (1.1.8)$$

(a) Notes on Maxwell's Equations

Although Maxwell's equations ("the Maxwell equations") provide a concise overview of classical electrodynamics, there is a lot going on "under the hood" and clarification of the meaning of certain symbols seems useful, hence the following set of notes.

0. It is understood that, in a medium other than the vacuum (that is, a "ponderable" medium), all the mathematical fields shown above like \mathbf{E} , \mathbf{D} , \mathbf{B} , \mathbf{H} , \mathbf{J} , ρ (and later \mathbf{A} and ϕ) are average fields in the sense discussed in Jackson Sections 4.3 and 6.6. The partial differential equations are meaningful for differential volumes, areas and distances which are very small but still contain enough atoms or molecules (perhaps at least 1000) so that averaging makes sense. We shall refer to the various electric and magnetic fields as "fields" to distinguish them from "potentials" like \mathbf{A} and ϕ , though all these quantities are mathematical fields.

1. The equations above are all expressed in SI units. The connection with cgs/Gaussian units is explained in an Appendix present in all three of the Jackson *Classical Electrodynamics* editions. The above equations appear in Jackson's third edition at these locations,

(1.1.1) through (1.14):	p 2 (I.1a)	Maxwell's Equations
(1.1.5) and (1.16):	p 296 top line	permeability constitutive relations
(1.1.7)	p 219 (5.159)	Ohm's Law constitutive relation $\mathbf{J} = \sigma \mathbf{E}$
(1.1.8)	p 3 (I.2)	equation of continuity

2. All media (conductors, dielectrics between conductors) are assumed to be homogeneous and isotropic so that the quantities σ , ϵ and μ are constant scalars in space (not tensors) for a given medium. In the vacuum these constants take the values $\sigma = 0$, $\epsilon = \epsilon_0$ and $\mu = \mu_0$. An implication of σ , μ and ϵ being constants in space is that they pass through the div , curl , grad and ∇^2 operators just as would any constant like π . One must be a little careful at a boundary between homogenous media since these constants can be different in the two media. In principle, all three quantities can vary in time, and when transformed to the frequency domain, $\sigma(\omega)$, $\epsilon(\omega)$ and $\mu(\omega)$ can (and do) vary with ω . However, we shall assume that for our frequencies of interest, these quantities are constant in ω and are therefore also constant in time so they pass through ∂_t .

3. The difference between ϵ and ϵ_0 is caused by polarization of bound charge in a medium. Equations dealing with polarization are these [see Jackson pp 153-4 or Panofsky & Phillips pp 28-30 and p 129-130 on the polarization current] :

$$\mathbf{p}dV = \text{electric dipole moment contained in volume } dV \text{ of a dielectric} \quad (1.1.9)$$

$$\mathbf{J}_{\text{pol}} \equiv \partial_t \mathbf{P} = \text{polarization current density} \quad (1.1.10)$$

$$\rho_{\text{pol}} = -\text{div } \mathbf{P} = \text{polarization charge density} \quad (1.1.11)$$

$$\mathbf{P} = \epsilon_0 \chi_e \mathbf{E} \quad // \text{ polarization assumed proportional to the polarizing } \mathbf{E} \text{ field} \quad (1.1.12)$$

$$\mathbf{D} = \epsilon_0 \mathbf{E} + \mathbf{P} = \epsilon_0(1 + \chi_e) \mathbf{E} = \epsilon \mathbf{E} = \text{"the electric displacement"} \quad (1.1.13)$$

$$\epsilon = \epsilon_0(1 + \chi_e) \quad // \epsilon = \text{dielectric constant, } \chi_e = \text{electric susceptibility} \quad (1.1.14)$$

$$\text{div } \mathbf{E} = (1/\epsilon_0)(\text{div } \mathbf{D} - \text{div } \mathbf{P}) = (1/\epsilon_0)(\rho_{\text{free}} + \rho_{\text{pol}}) \quad \text{"E sees all charges"} \quad (1.1.15)$$

The \mathbf{E} field causes polarization \mathbf{P} either by causing existing tiny dipole objects (e.g., molecules) in a medium to "line up", or by causing tiny non-dipole objects (e.g., atoms) to have dipole moments and then those get lined up. See for example Bleaney & Bleaney Chapter 10 " Dielectrics".

Comment: Since $\mathbf{D} = \epsilon_0 \mathbf{E} + \mathbf{P}$, the \mathbf{D} and \mathbf{E} fields are scaled differently. It might have been better had the \mathbf{D} field been replaced by $\mathbf{D} = \epsilon_0 \mathbf{D}'$ in which case $\mathbf{D}' = \mathbf{E} + \mathbf{P}/\epsilon_0$; then one can make clearer statements about \mathbf{D}' versus \mathbf{E} . For example, in a dielectric capacitor with fixed conductor charges ($Q, -Q$) there exist both \mathbf{D}' and \mathbf{E} fields, and $\mathbf{D}' = (\epsilon/\epsilon_0) \mathbf{E} > \mathbf{E}$. The \mathbf{D}' field can be interpreted as the \mathbf{E} field that *would* be present were the dielectric replaced by empty space. The dielectric in effect shields the charge, reducing \mathbf{E} and hence V , does not change Q , and, since $Q = CV$, it increases capacitance C by (ϵ/ϵ_0) for fixed Q .

4. As noted in (1.1.3), the ρ in $\text{div } \mathbf{D} = \rho$ is the free charge density ρ_{free} and does not include possible polarization charge density. In contrast, the \mathbf{E} field "sees" both free charge ρ_{free} and polarization charge ρ_{pol} , as derived above in (1.1.15) from (1.1.13),

$$\text{div } \mathbf{E} = (1/\epsilon_0) (\rho_{\text{free}} + \rho_{\text{pol}}) = (1/\epsilon) \rho_{\text{free}} . \quad (1.1.16)$$

In the rightmost expression, the polarization charge is incorporated into the $1/\epsilon$ factor. Appendix L shows how this works physically in the case of point and line charges embedded in a dielectric.

5. The \mathbf{J} in $\text{curl } \mathbf{H} = \partial_t \mathbf{D} + \mathbf{J}$ is the conduction current \mathbf{J}_c . If polarization current \mathbf{J}_{pol} is present, it is included in the "displacement current" term $\partial_t \mathbf{D}$ along with the Maxwell "vacuum polarization current" $\mathbf{J}_{\text{vac}} = \epsilon_0 \partial_t \mathbf{E}$. That is,

$$\mathbf{J}_d \equiv \partial_t \mathbf{D} = \partial_t [\epsilon_0 \mathbf{E} + \mathbf{P}] = \partial_t \mathbf{P} + \epsilon_0 \partial_t \mathbf{E} = \mathbf{J}_{\text{pol}} + \mathbf{J}_{\text{vac}} \quad \rho_{\text{pol}} = -\text{div } \mathbf{P} . \quad (1.1.17)$$

The \mathbf{J}_{vac} term $\epsilon_0 \partial_t \mathbf{E}$ was "added" by Maxwell to the curl \mathbf{H} equation (Ampere's Law) to make it self-consistent. Since $\text{div } \text{curl } \mathbf{H} = 0$, and since $\text{curl } \mathbf{H} = \mathbf{J}_d + \mathbf{J}_c$, one must have $\text{div } [\mathbf{J}_d + \mathbf{J}_c] = 0$:

$$\begin{aligned} \text{div } [\mathbf{J}_d + \mathbf{J}_c] &= \text{div } [\partial_t \mathbf{P} + \epsilon_0 \partial_t \mathbf{E}] + \text{div } [\mathbf{J}_c] = \partial_t [\text{div } \mathbf{P} + \epsilon_0 \text{div } \mathbf{E}] - \partial_t \rho_{\text{free}} \\ &= \partial_t (-\rho_{\text{pol}}) + \partial_t (\rho_{\text{free}} + \rho_{\text{pol}}) - \partial_t \rho_{\text{free}} = 0 \end{aligned} \quad (1.1.18)$$

where we have used continuity $\text{div } \mathbf{J}_c = -\partial_t \rho_{\text{free}}$, see item 7 below.

Comment on "Displacement": In the case of polar molecule polarization, the polarization charge and current can be viewed as being caused by a "displacement of bound charge" as suggested by this very symbolic picture of a parallel plate capacitor

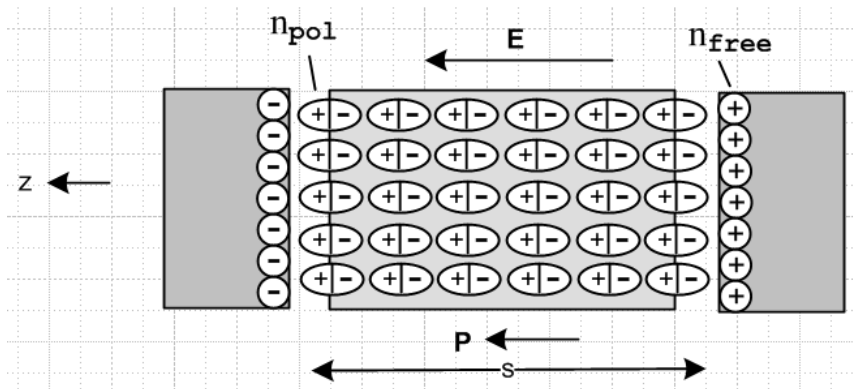


Fig 1.1

The applied \mathbf{E} field of the plates lines up the polar molecules and thus causes a polarization charge density n_{pol} to appear on the side faces of the dielectric, as if it were an "electret" object. One can imagine that, with an AC plate voltage, as the applied \mathbf{E} field changes to the other polarity, the polar molecules rotate in place 180 degrees putting the positive bound charge on the opposite plate, and as this happens, there is a polarization current $\mathbf{J}_{\text{pol}} = \partial_t \mathbf{P}$ inside the dielectric. In reality, the molecules are close

to randomly oriented and the above effect is obtained for the "average" molecule. In any event, the \mathbf{E} field causes surface polarization charge densities n_{po1} at the faces of the dielectric, and one then thinks of the normally neutral-everywhere bound charge distribution as being "displaced" such that one face has positive charge and the other negative. It is in this sense that Maxwell started using the word "displacement". Before the \mathbf{J}_{vac} term was added, Maxwell had $\mathbf{J}_{\text{d}} \equiv \partial_{\text{t}}\mathbf{D} = \mathbf{J}_{\text{po1}}$ and this associated $\partial_{\text{t}}\mathbf{D}$ entirely with \mathbf{J}_{po1} and thus with the displacement of the dielectric bound charge, and so Maxwell referred to \mathbf{D} as the "electric displacement" and $\partial_{\text{t}}\mathbf{D}$ as the "displacement current".

Fig 1.1 shows how the polarization charge acts to shield the free charge, so $n_{\text{tot}} = n_{\text{free}} - n_{\text{po1}}$.

6. If there is any magnetization current $\mathbf{J}_{\text{m}} = \text{curl } \mathbf{M}$, it is absorbed into the distinction between \mathbf{B} and \mathbf{H} and therefore does not appear on the right side of $\text{curl } \mathbf{H} = \partial_{\text{t}}\mathbf{D} + \mathbf{J}_{\text{c}}$. The current \mathbf{J}_{m} is discussed for example in Panofsky & Phillips, Sections 7-12, 7-13 and 8-1. The basic equations are as follows,

$$\mathbf{M}dV = \text{magnetic dipole moment contained in volume } dV \text{ of a medium} \quad (1.1.19)$$

$$\mathbf{J}_{\text{m}} = \text{curl } \mathbf{M} = \text{magnetization current density} \quad (\Rightarrow \text{div } \mathbf{J}_{\text{m}} = 0) \quad (1.1.20)$$

$$\mathbf{M} = \chi_{\text{m}} \mathbf{H} = \text{magnetization} \quad // = [\mu/\mu_0 - 1] \mathbf{H} \text{ from (1.1.23)} \quad (1.1.21)$$

$$\mathbf{B} = \mu_0(\mathbf{H} + \mathbf{M}) = \mu_0(1 + \chi_{\text{m}})\mathbf{H} = \mu\mathbf{H} = \text{"magnetic induction"} \text{ (informally, magnetic field)} \quad (1.1.22)$$

$$\mu = \mu_0(1 + \chi_{\text{m}}) \quad // \mu = \text{magnetic permeability, } \chi_{\text{m}} = \text{magnetic susceptibility} \quad (1.1.23)$$

$$\begin{aligned} \text{curl } \mathbf{B} &= \mu_0(\text{curl } \mathbf{H} + \text{curl } \mathbf{M}) = \mu_0(\partial_{\text{t}}\mathbf{D} + \mathbf{J}_{\text{c}}) + \mu_0\mathbf{J}_{\text{m}} \\ &= \mu_0(\partial_{\text{t}}\mathbf{D} + \mathbf{J}_{\text{c}} + \mathbf{J}_{\text{m}}) \quad . \quad \text{" } \mathbf{B} \text{ sees all currents"} \end{aligned} \quad (1.1.24)$$

7. The "equation of continuity" (1.1.8) expresses the fact that charge cannot be created or destroyed. Barring ionization of a dielectric, free charge and bound charge (polarization charge) cannot be converted into each other and are therefore separately conserved. Thus we have several different equations of continuity: [see for example Haus and Melcher, Section 6.2, equations (10) and (13)]

$$\text{div } \mathbf{J}_{\text{c}} = -\partial_{\text{t}}\rho_{\text{free}} \quad // \text{conservation of free charge (aka true or unpaired charge)} \quad (1.1.25)$$

$$\text{div } \mathbf{J}_{\text{p}} = -\partial_{\text{t}}\rho_{\text{po1}} \quad // \text{conservation of polarization charge (aka bound or paired charge)} \quad (1.1.26)$$

$$\text{div } [\mathbf{J}_{\text{c}} + \mathbf{J}_{\text{p}}] = -\partial_{\text{t}}[\rho_{\text{free}} + \rho_{\text{po1}}] = -\partial_{\text{t}}\rho_{\text{tot}} \quad // \text{sum of above two equations} \quad (1.1.27)$$

$$\text{div } [\mathbf{J}_{\text{c}} + \mathbf{J}_{\text{d}}] = 0 \neq -\partial_{\text{t}}\rho_{\text{tot}} \quad // \text{reminder of item 5 above} \quad (1.1.18)$$

8. Ohm's Law $\mathbf{J} = \sigma\mathbf{E}$ is assumed to be a valid constitutive relation for our media of interest. One should keep in mind that this is an approximation, whereas the Maxwell equations and the continuity equations are not. Just under the surface charge on a conductor, Ohm's Law is violated as discussed in Appendix E due to a diffusion current generated by charges piled up at the surface. Ohm's Law is also violated in the

presence of very strong magnetic fields as shown in (N.4.10). In this case one can say that Ohm's Law is still valid, but σ is a tensor instead of a scalar.

9. As will be shown in Section 3.1, inside a medium such as a dielectric or a conductor, and at frequencies of interest to us, there can exist no net charge densities, so $\rho_{\text{free}} = 0$. In a dielectric there are no available free charges, while in a conductor, any departure from neutrality would be instantly restored. All free charge densities for our application reside on the *surfaces* of conductors only. If we were interested in the behavior of a transmission line embedded in a charged plasma, things would be different.

10. As noted in item 1, all our equations are expressed in Système Internationale (SI) units. In this system, formerly known as "rationalized m.k.s.", the speed of light is concealed in the symbols μ_0 and ϵ_0 . Here are the usual historical names given to the symbols appearing in our equations, along with one or more expressions of the SI units for each symbol:

$$\begin{aligned}
 \mathbf{E} &= \text{electric field (volts/m)} \\
 \mathbf{H} &= \text{magnetic field (amp/m)} \\
 \mathbf{D} &= \text{electric displacement (coulomb/m}^2\text{, same units as surface charge)} \\
 \mathbf{B} &= \text{magnetic field (tesla = amp-henry/m}^2\text{ = volt-sec/m}^2\text{ = weber/m}^2\text{)} & 1 \text{ tesla} = 10,000 \text{ gauss} \\
 \mathbf{J} &= \text{current density (amps/m}^2\text{)} \\
 \rho &= \text{charge density (coulombs/m}^3\text{)} \\
 \sigma &= \text{conductivity of the medium (mho/m = ohm}^{-1}\text{/m)} \\
 \mu/\mu_0 &= \text{relative magnetic permeability of the medium (dimensionless)} \\
 \epsilon/\epsilon_0 &= \text{relative electric permittivity = relative dielectric constant (dimensionless)} \\
 \mu_0 &= \text{permeability of free space} = 4\pi \times 10^{-7} \text{ henry/m} \\
 \epsilon_0 &= \text{permittivity of free space} = 8.8541877 \times 10^{-12} \text{ farad/m} & (1.1.28)
 \end{aligned}$$

Here are some unit relations obtainable from $Q = CV$, $V = IR$, $LC = 1/\omega^2$, $\tau = RC = L/R$, $I = dQ/dt$:

$$\begin{aligned}
 \text{coulomb} &= \text{farad-volt} & \text{volt} &= \text{ampere-ohm} & \text{henry-farad} &= \text{sec}^2 \\
 \text{farad} &= \text{sec/ohm} & \text{henry} &= \text{ohm-sec} & \text{henry / farad} &= \text{ohm}^2 \\
 \text{ampere} &= \text{coulomb/sec} & \text{mho} &= \text{ohm}^{-1} & \text{mho/F} &= \text{sec}^{-1} \\
 \text{newton} &= \text{coulomb-volt/m} = \text{kg-m/sec}^2 & // \text{ F} &= \text{qE} = \text{ma} & \text{amp-henry} &= \text{volt-sec} \\
 \\
 c &= 1/\sqrt{\mu_0 \epsilon_0} = 2.9979246 \times 10^8 \text{ m/sec} & & = \text{speed of light} & & \\
 \\
 Z_{\text{fs}} &= \sqrt{\mu_0/\epsilon_0} = 376.73032 \text{ ohms} & & = \text{"impedance of free space"} & & \\
 \\
 \sigma &= 5.81 \times 10^7 \text{ mho/m for copper} & & & & (1.1.29)
 \end{aligned}$$

Notice how the names of eight people have become forever embedded into the SI unit system.

Comment: Inevitably, any given author will at some point refer to both \mathbf{B} and \mathbf{H} as "the magnetic field". We shall do that throughout, using the historical symbols \mathbf{B} or \mathbf{H} to indicate which "kind" of magnetic

field we are talking about. Some authors refer to \mathbf{B} as the magnetic flux density or the magnetic induction to distinguish \mathbf{B} from \mathbf{H} .

(b) Integral Forms of Maxwell's Equations and Continuity

The equations above involving the divergence and curl operators have integral forms thanks to these two fundamental mathematical theorems which have nothing to do with electromagnetism in particular,

$$\int_V \operatorname{div} \mathbf{F} \, dV = \int_S \mathbf{F} \cdot d\mathbf{S} \quad // \text{"the divergence theorem"} \quad \text{Spiegel 22.59} \quad (1.1.30)$$

$$\int_S \operatorname{curl} \mathbf{F} \cdot d\mathbf{S} = \oint_C \mathbf{F} \cdot d\mathbf{s} \quad // \text{"Stokes's theorem"} \quad \text{Spiegel 22.60} \quad (1.1.31)$$

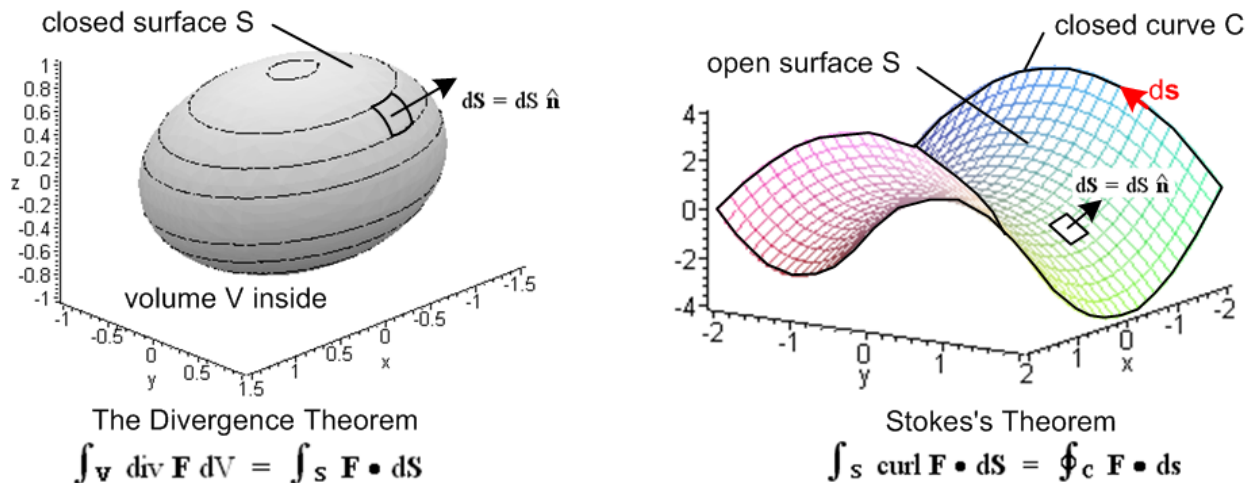


Fig 1.2

The first theorem involves a closed boundary surface S which encloses a volume V and says that the volume integral of $\operatorname{div} \mathbf{F}$ over V equals the surface integral of \mathbf{F} over S . The second involves a closed bounding curve C (possibly non-planar) which bounds an arbitrary open surface S (also possibly non-planar) and says that the line integral of \mathbf{F} around C equals the surface integral of $\operatorname{curl} \mathbf{F}$ over S . In the divergence theorem, $d\mathbf{S}$ points "out" from the volume, and in Stokes's Theorem, the direction of $d\mathbf{S}$ and $d\mathbf{s}$ are related by the right-hand rule where fingers fit the boundary curve and the thumb gives the direction of $d\mathbf{S}$. In both theorems the differential vector area patch is $d\mathbf{S} = dS \hat{\mathbf{n}}$ where $\hat{\mathbf{n}}$ is normal to the surface.

Both theorems have meanings in n -dimensional space, but our interest is mainly $n = 3$. Both theorems are not hard to derive and this is done in textbooks usually by breaking up the surface into tiny squares and the volume into tiny cubes. Once one sees these derivations, the theorems become less mysterious.

In general terms, the divergence theorem says that $\operatorname{div} \mathbf{F}$ is somehow a source of the field \mathbf{F} and the amount of \mathbf{F} flowing out through a closed bounding surface equals the amount of \mathbf{F} that is generated inside the volume. When \mathbf{F} is the electric field \mathbf{E} , the divergence theorem is called **Gauss's Law** and says

that the total electric flux "flowing out" [that is to say, $\int_{\mathbf{S}} \mathbf{E} \cdot d\mathbf{S}$] equals the total of the source inside the volume [$(1/\epsilon) \int_{\mathbf{V}} \rho \, dV$], usually called "the total charge enclosed". Thus,

$$\operatorname{div} \mathbf{D} = \rho \quad \Leftrightarrow \quad \int_{\mathbf{V}} \rho \, dV = \int_{\mathbf{S}} \mathbf{D} \cdot d\mathbf{S} \quad (1.1.32)$$

$$\operatorname{div} \mathbf{E} = \rho/\epsilon \quad \Leftrightarrow \quad \int_{\mathbf{V}} \rho \, dV = \int_{\mathbf{S}} \epsilon \mathbf{E} \cdot d\mathbf{S} \quad (1.1.33)$$

Since the magnetic field has no corresponding charge, one always has $\int_{\mathbf{S}} \mathbf{B} \cdot d\mathbf{S} = 0$, a theorem which seems to have no name,

$$\operatorname{div} \mathbf{B} = 0 \quad \Leftrightarrow \quad \int_{\mathbf{S}} \mathbf{B} \cdot d\mathbf{S} = 0 \quad . \quad \text{S is any closed surface} \quad (1.1.34)$$

The surface integral of an \mathbf{E} or \mathbf{B} field is often referred to as the total electric or magnetic "flux" passing through the surface, even though nothing is really flowing in a mechanical sense.

The divergence operator also occurs in the equation of continuity (1.1.8) so we have

$$\operatorname{div} \mathbf{J} = -\partial_t \rho \quad \Leftrightarrow \quad -\partial_t \left[\int_{\mathbf{V}} \rho \, dV \right] = \int_{\mathbf{S}} \mathbf{J} \cdot d\mathbf{S} \quad (1.1.35)$$

This is the prototype application of the divergence theorem in that it is easily understandable: the total electric current flowing out through some closed surface S must equal the rate at which the total charge inside the surface is decreasing. One can write a similar statement for mass flowing out from a volume in which ρ would be the mass density and $\mathbf{J} = \rho \mathbf{v}$ the mass current, \mathbf{v} being the velocity field.

The Stokes theorem is a bit more mysterious. Since this theorem is associated with George Stokes, it is called Stokes's theorem, but is sometimes called Stokes' theorem (one would not say Gauss' theorem). The curl of a vector field is associated with the amount of "rotation" the field has at some point in space, and in fact curl is sometimes written Rot. If one considers a tiny patch and finds that the line integral of the field around the boundary of that patch is non-zero, then the vector field has a non-zero curl at that point in the direction normal to the patch. At any point where a fluid has a vortex, the curl is non-zero, for example. When Stokes's theorem is applied to the electric field, one has

$$\operatorname{curl} \mathbf{E} = -\partial_t \mathbf{B} \quad \Leftrightarrow \quad \oint_{\mathbf{C}} \mathbf{E} \cdot d\mathbf{s} = -\partial_t \left[\int_{\mathbf{S}} \mathbf{B} \cdot d\mathbf{S} \right] \quad (1.1.36)$$

This says that the voltage induced around a closed loop (the "electromotive force") is proportional to the rate of change of the magnetic flux through that loop, a principle known as **Faraday's Law of Induction**. If water power rotates a wire loop in the presence of some magnets, one has an electric generator.

On the other hand, when Stokes's theorem is applied to the magnetic field, one gets

$$\text{curl } \mathbf{H} = \partial_t \mathbf{D} + \mathbf{J} \quad \Leftrightarrow \quad \oint_C \mathbf{H} \cdot d\mathbf{s} = \int_S [\partial_t \mathbf{D} + \mathbf{J}] \cdot d\mathbf{S} \quad (1.1.37)$$

$$\text{curl } \mathbf{B} = \mu \varepsilon \partial_t \mathbf{E} + \mu \mathbf{J} \quad \Leftrightarrow \quad \oint_C \mathbf{B} \cdot d\mathbf{s} = \mu \int_S [\varepsilon \partial_t \mathbf{E} + \mathbf{J}] \cdot d\mathbf{S} \quad (1.1.38)$$

μ constant in space, ε constant in time

When the situation is static, one has $\oint_C \mathbf{H} \cdot d\mathbf{s} = \int_S d\mathbf{S} \cdot \mathbf{J}$ which says the line integral of the magnetic field \mathbf{H} around some loop equals the total current passing through any open surface whose boundary is that loop (the "current enclosed"), a principle known as **Ampere's Law**.

Later we shall encounter a certain "vector potential \mathbf{A} " which is related to the \mathbf{B} field by $\mathbf{B} = \text{curl } \mathbf{A}$. Since we are writing out "integral forms" of differential relationships, we can then add this to the list,

$$\text{curl } \mathbf{A} = \mathbf{B} \quad \Leftrightarrow \quad \oint_C \mathbf{A} \cdot d\mathbf{s} = \int_S \mathbf{B} \cdot d\mathbf{S} . \quad (1.1.39)$$

If the bounding curve C were a wire carrying a current I which creates both \mathbf{A} and \mathbf{B} , then both sides of the above integral form will be proportional to I , and the constant of proportionality is by definition the **self-inductance** L of the loop,

$$\oint_C \mathbf{A} \cdot d\mathbf{s} = \int_S \mathbf{B} \cdot d\mathbf{S} = [\text{magnetic flux through surface } S] = L I \quad . \quad (1.1.40)$$

There are of course many surfaces S which span a given curve C , and (1.1.39) says that all such surfaces give exactly the same $\int_S \mathbf{B} \cdot d\mathbf{S}$ and thus the same L , so L is really a geometric property of the curve C .

We shall be using *all* these integral forms in the document below.

(c) Rules for behavior of fields and potentials at a boundary

Consider the boundary between two different media called 1 and 2. Consider a tiny red "math loop" of width L and height $2s$ which straddles the media boundary which here is seen edge on,

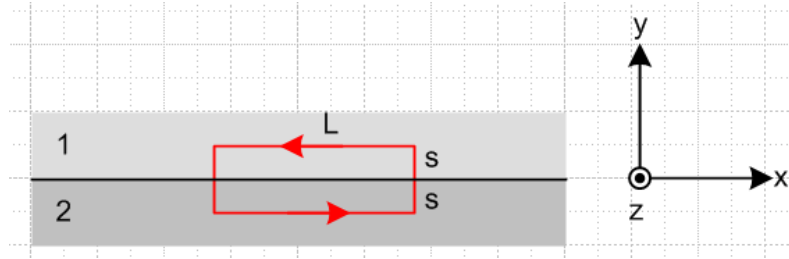


Fig 1.3

For the electric field we have from above (for our loop, $d\mathbf{S} = dS \hat{\mathbf{z}}$)

$$\text{curl } \mathbf{E} = -\partial_t \mathbf{B} \quad \Leftrightarrow \quad \oint \mathbf{E} \cdot d\mathbf{s} = - \left[\int_s (\partial_t \mathbf{B}) \cdot d\mathbf{S} \right]. \quad (1.1.36)$$

Since the loop is tiny and since the fields are assumed to be non-singular, we can regard \mathbf{E} and \mathbf{B} as a constant everywhere on each half of the loop (for our purposes here). The line integral around the loop is then (start at lower left corner)

$$\begin{aligned} \oint \mathbf{E} \cdot d\mathbf{s} &= LE_{\mathbf{x}}^{(2)} + s E_{\mathbf{y}}^{(2)} + s E_{\mathbf{y}}^{(1)} - LE_{\mathbf{x}}^{(1)} - s E_{\mathbf{y}}^{(1)} - s E_{\mathbf{y}}^{(2)} \\ &= L [E_{\mathbf{x}}^{(2)} - E_{\mathbf{x}}^{(1)}] . \end{aligned}$$

The area integral on the right side of (1.1.36) is

$$-\int_s (\partial_t \mathbf{B}) \cdot d\mathbf{S} = -\partial_t B_z^{(1)} sL - \partial_t B_z^{(2)} sL = -sL [\partial_t B_z^{(1)} + \partial_t B_z^{(2)}]$$

so the integral form in (1.1.36) says

$$[E_{\mathbf{x}}^{(2)} - E_{\mathbf{x}}^{(1)}] L = -sL [\partial_t B_z^{(1)} + \partial_t B_z^{(2)}] .$$

As long as $\partial_t B_z$ is finite at the surface, as $s \rightarrow 0$ the right side vanishes and we conclude that

$$[E_{\mathbf{x}}^{(2)} - E_{\mathbf{x}}^{(1)}] = 0 .$$

We then summarize for both the x and z directions by saying (t means tangential to boundary)

$$E_{t1} = E_{t2} \quad \text{or} \quad (1/\epsilon_1)D_{t1} = (1/\epsilon_2)D_{t2} \quad (1.1.41)$$

so the tangential (parallel) components of the electric field is continuous through a boundary.

A similar analysis using the curl \mathbf{H} equation,

$$\text{curl } \mathbf{H} = \partial_t \mathbf{D} + \mathbf{J} \quad \Leftrightarrow \quad \oint \mathbf{H} \cdot d\mathbf{s} = \int_S [\partial_t \mathbf{D} + \mathbf{J}] \cdot d\mathbf{S} \quad (1.1.37)$$

leads to

$$[H_x^{(2)} - H_x^{(1)}] L = \int_S L [\partial_t D_z^{(1)} + J_z^{(1)} + \partial_t D_z^{(2)} + J_z^{(2)}] \cdot \hat{\mathbf{z}} \cdot d\mathbf{S}$$

As long as $\partial_t D_x$ and J_x are finite (non-singular) at the surface, we conclude from $s \rightarrow 0$ that

$$H_{t1} = H_{t2} \quad \text{or} \quad (1/\mu_1)B_{t1} = (1/\mu_2)B_{t2} \quad (1.1.42)$$

However, it is possible to have \mathbf{J} be singular at the surface in the form of a surface current \mathbf{K} where

$$\mathbf{J} = \mathbf{K} \delta(y) \quad J = \text{amp/m}^2 \quad K = \text{amp/m} \quad (1.1.43)$$

and in this case we find that

$$[H_x^{(2)} - H_x^{(1)}] L = \int_S [\mathbf{J}] \cdot d\mathbf{S} = \int_S \mathbf{K} \delta(y) \cdot d\mathbf{S} \hat{\mathbf{z}} = \int_S K_x \delta(y) dx dy = \int_S K_x dx \approx K_x L$$

Were we to rotate the Fig 1.3 red loop -90° about the y axis, we would instead get

$$[H_z^{(2)} - H_z^{(1)}] L = \int_S [\mathbf{J}] \cdot d\mathbf{S} = \int_S \mathbf{K} \delta(y) \cdot d\mathbf{S} [-\hat{\mathbf{x}}] = - \int_S K_x \delta(y) dx dy = - \int_S K_x dx \approx -K_x L$$

where a minus sign appears on the right. Letting x or z be the transverse direction t , we can combine the above equations into the single statement

$$H_{t2}^{(2)} - H_{t1}^{(1)} = \mathbf{K}^{\text{free}} \cdot [\hat{\mathbf{t}} \times \hat{\mathbf{n}}] = \mathbf{K}^{\text{free}} \cdot \hat{\boldsymbol{\tau}} \equiv K_{\boldsymbol{\tau}}^{\text{free}} \quad \hat{\boldsymbol{\tau}} \equiv \hat{\mathbf{t}} \times \hat{\mathbf{n}}$$

where unit vector $\hat{\boldsymbol{\tau}} \equiv \hat{\mathbf{t}} \times \hat{\mathbf{n}}$ is "the other" transverse unit vector relative to $\hat{\mathbf{t}}$. As usual, $\hat{\mathbf{n}}$ is a normal unit vector pointing from medium 2 into medium 1 ($\hat{\mathbf{y}}$ in Fig 1.3). To summarize, we have shown that

$$H_{t2} - H_{t1} = K_{\boldsymbol{\tau}}^{\text{free}} \quad \text{or} \quad (1/\mu_2)B_{t2} - (1/\mu_1)B_{t1} = K_{\boldsymbol{\tau}}^{\text{free}} \quad (1.1.44)$$

Notice that this $K_{\boldsymbol{\tau}}$ is a "free" surface current, and not a bound magnetization surface current since such a magnetization current is not "seen" by \mathbf{H} .

Because $\text{div } \mathbf{B} = 0$, \mathbf{B} can be written as $\mathbf{B} = \text{curl } \mathbf{A}$ where \mathbf{A} is the so-called vector potential discussed below in (1.3.1). In the special case that $\mathbf{A} = A_z(x,y) \hat{\mathbf{z}}$, one finds that

$$\begin{aligned} \mathbf{B} = \text{curl } \mathbf{A} &= \hat{\mathbf{x}} (\partial_y A_z - \partial_z A_y) + \hat{\mathbf{y}} (\partial_z A_x - \partial_x A_z) + \hat{\mathbf{z}} (\partial_x A_y - \partial_y A_x) = \hat{\mathbf{x}} (\partial_y A_z) - \hat{\mathbf{y}} (\partial_x A_z) \\ \Rightarrow \quad B_x &= (\partial_y A_z) \quad B_y = -\hat{\mathbf{y}} (\partial_x A_z) \quad B_z = 0 \quad (1.1.45) \end{aligned}$$

According to (1.1.44) one has,

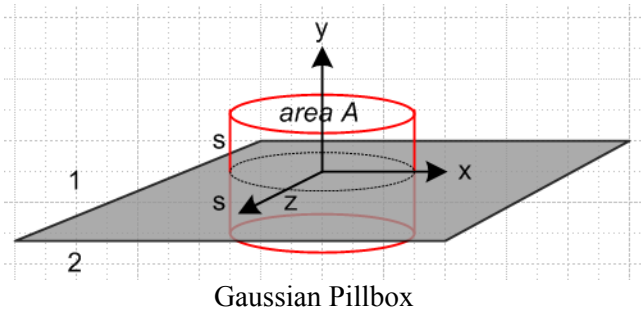
$$\begin{aligned} (1/\mu_2)B_{x2} - (1/\mu_1)B_{x1} &= K_z^{\text{free}} \\ (1/\mu_2)B_{z2} - (1/\mu_1)B_{z1} &= -K_x^{\text{free}} \end{aligned}$$

For our special case $\mathbf{A} = A_z \hat{\mathbf{z}}$ the second equation says $K_x^{\text{free}} = 0$ since $B_{z1} = B_{z2} = 0$. The first equation may be written

$$(1/\mu_2) (\partial_n A_{z2}) - (1/\mu_1) (\partial_n A_{z1}) = K_z^{\text{free}} \tag{1.1.46}$$

where $\hat{\mathbf{n}}$ (here $\hat{\mathbf{y}}$) is the usual normal vector (pointing into medium 1) and z is the direction in which \mathbf{A} points. If $\mu_1 = \mu_2 = \mu_0$, we have $(\partial_n A_z)_2 - (\partial_n A_z)_1 = \mu_0 K_z$ and K_z is then proportional to the normal slope jump in A_z at the boundary surface. As earlier, K_z is a "free" surface current.

Next, we put a tiny "Gaussian pillbox" straddling the two media. Area A and height $2s$ are both very small.



a pill box circa 1830

Fig 1.4

For the electric displacement \mathbf{D} we consider

$$\text{div } \mathbf{D} = \rho_{\text{free}} \quad \Leftrightarrow \quad \int_V \rho_{\text{free}} dV = \int_S \mathbf{D} \cdot d\mathbf{S} \tag{1.1.13}$$

where volume V is of the box shown. The surface integral is

$$\int_S \mathbf{D} \cdot d\mathbf{S} = D_y^{(1)} A - D_y^{(2)} A + \text{contributions from the sides of the box} .$$

Since we assume \mathbf{D} is non-singular, the side contributions vanish as $s \rightarrow 0$ since the side area vanishes. Assuming a charge density n_{free} exists on the boundary between the two media, the volume integral is $n_{\text{free}} A$ and then the conclusion, generalized to the perpendicular field component, is

$$D_{n1} - D_{n2} = n_{\text{free}} \quad \text{or} \quad [\epsilon_1 E_{1n} - \epsilon_2 E_{2n}] = n_{\text{free}} \tag{1.1.47}$$

where $\hat{\mathbf{n}}$ points into medium 1. If the two media are conducting dielectrics with Ohm's law $\mathbf{J}_c = \sigma \mathbf{E}$, we can apply continuity (1.1.25) to the Gaussian box to find that

$$\operatorname{div} \mathbf{J}_c = -\partial_t \rho_{\text{free}} \quad \Leftrightarrow \quad -\partial_t \left[\int_V \rho_{\text{free}} dV \right] = \int_S \mathbf{J}_c \cdot d\mathbf{S} \quad (1.1.35)$$

so that

$$-\partial_t n_{\text{free}} = [J_{n1} - J_{n2}] = \sigma_1 E_{n1} - \sigma_2 E_{n2}$$

or for monochrome time dependence (coming soon, along with notation explanation),

$$-j\omega n_{\text{free}} = \sigma_1 E_{n1} - \sigma_2 E_{n2} \quad // \text{ frequency domain}$$

Recall now from (1.1.47) that

$$n_{\text{free}} = \varepsilon_1 E_{n1} - \varepsilon_2 E_{n2} \quad (1.1.47)$$

Adding the last equation to $1/j\omega$ times the previous equation gives

$$0 = [\varepsilon_1 + \sigma_1/j\omega] E_{n1} - [\varepsilon_2 + \sigma_2/j\omega] E_{n2} \quad .$$

In terms of the **complex dielectric constants** $\xi_i \equiv \varepsilon_i + \sigma_i/j\omega$ this says that $0 = \xi_1 E_{n1} - \xi_2 E_{n2}$ so that

$$\xi_1 E_{n1} = \xi_2 E_{n2} \quad // \text{ frequency domain} \quad (1.1.48)$$

In the limit that, say, medium 2 becomes a perfect conductor, $\xi_2 \approx \sigma_2/j\omega \rightarrow \infty$ and $E_{n2} \rightarrow 0$, but the product is maintained equal to $\xi_1 E_{n1}$.

Returning again to the special case in which vector potential $\mathbf{A} = A_z \hat{\mathbf{z}}$, since $\mathbf{E} = -\nabla\phi - \partial_t \mathbf{A}$ (as shown in (1.3.1)), we have $E_y = -\partial_y \phi$ since $A_y = 0$. In terms of Fig 1.3 where y is the direction normal to the surface, one has $E_n = -\partial_n \phi$ and then (1.1.47) may be written

$$\varepsilon_2 (\partial_n \phi)_2 - \varepsilon_1 (\partial_n \phi)_1 = n_{\text{free}} \quad (1.1.49)$$

which can be compared to (1.1.46). If $\varepsilon_1 = \varepsilon_2 = \varepsilon_0$, we have $(\partial_n \phi)_2 - (\partial_n \phi)_1 = n_{\text{free}}/\varepsilon_0$ and then n_{free} is proportional to the normal slope jump in ϕ at the boundary surface.

Finally, the other divergence equation

$$\operatorname{div} \mathbf{B} = 0 \quad \Leftrightarrow \quad \int_S \mathbf{B} \cdot d\mathbf{S} = 0 \quad \text{S is any closed surface} \quad (1.1.34)$$

leads to the conclusion that

$$B_{n1} = B_{n2} \quad \text{or} \quad \mu_1 H_{n1} = \mu_2 H_{n2} \quad (1.1.50)$$

We now summarize these rules in a box, always assuming that there is no singularity in some quantity to invalidate the claims:

Rules for continuity of normal and tangential fields at a boundary:		(1.1.51)
The fields here are either $\mathbf{F}(x,t)$ or $\mathbf{F}(x,\omega)$, except (1.1.48) which is only for $\mathbf{E}(x,\omega)$:		
$t = \text{tangential} = \text{parallel} = \parallel$: $\hat{\boldsymbol{\tau}} \equiv \hat{\mathbf{t}} \times \hat{\mathbf{n}}$		
$E_{t1} = E_{t2}$	or	$(1/\epsilon_1)D_{t1} = (1/\epsilon_2)D_{t2}$ (1.1.41)
$H_{t2} - H_{t1} = K_{\boldsymbol{\tau}}^{\text{free}}$	or	$(1/\mu_2)B_{t2} - (1/\mu_1)B_{t1} = K_{\boldsymbol{\tau}}^{\text{free}}$ (1.1.44)
Special case $\mathbf{A} = A_z(x,y) \hat{\mathbf{z}}$:		$(1/\mu_2) (\partial_n A_z)_2 - (1/\mu_1) (\partial_n A_z)_1 = K_z^{\text{free}}$ (1.1.46)
$n = \text{normal} = \text{perpendicular} = \perp$: (symbol n is also used for surface charge density)		
$B_{n1} = B_{n2}$	or	$\mu_1 H_{n1} = \mu_2 H_{n2}$ (1.1.50)
$D_{n1} - D_{n2} = n_{\text{free}}$	or	$[\epsilon_1 E_{n1} - \epsilon_2 E_{n2}] = n_{\text{free}}$ (1.1.47)
and for monochrome time dependence:		$\xi_1 E_{n1} = \xi_2 E_{n2}$ where $\xi = \epsilon + \sigma/j\omega$ (1.1.48)
Special case $\mathbf{A} = A_z \hat{\mathbf{z}}$:		$\epsilon_2 (\partial_n \phi)_2 - \epsilon_1 (\partial_n \phi)_1 = n_{\text{free}}$ (1.1.49)

Tangential and normal boundary conditions can always be written in the following manner,

$$\begin{aligned} \mathbf{F}_{t1} = \mathbf{F}_{t2} & \Leftrightarrow \mathbf{n} \times \mathbf{F}_1 = \mathbf{n} \times \mathbf{F}_2 \\ \mathbf{F}_{n1} = \mathbf{F}_{n2} & \Leftrightarrow \mathbf{n} \cdot \mathbf{F}_1 = \mathbf{n} \cdot \mathbf{F}_2 \end{aligned} \quad (1.1.52)$$

as can be seen by expanding $\mathbf{F} = F_n \hat{\mathbf{n}} + F_t \hat{\mathbf{t}}$ and noting that $\hat{\mathbf{n}} \times \hat{\mathbf{t}} = 0$ and $\hat{\mathbf{n}} \cdot \hat{\mathbf{n}} = 1$. The E and B boundary conditions in the above table appear as follows in King (1945), page 204 (obtained from the University of Utah's robotic automated retrieval center ARC),

$\xi_1(\hat{n}_1, \mathbf{E}_1) + \xi_2(\hat{n}_2, \mathbf{E}_2) = 0$	(31a)	$\xi_1 E_{n1} = \xi_2 E_{n2}$
$[\hat{n}_1, \mathbf{E}_1] + [\hat{n}_2, \mathbf{E}_2] = 0$	(31b)	$E_{t1} = E_{t2}$
$v_1[\hat{n}_1, \mathbf{B}_1] + v_2[\hat{n}_2, \mathbf{B}_2] = 0$	(31c)	$(1/\mu_2)B_{t2} = (1/\mu_1)B_{t1}$
$(\hat{n}_1, \mathbf{B}_1) + (\hat{n}_2, \mathbf{B}_2) = 0$	(31d)	$B_{n1} = B_{n2}$

where $\hat{\mathbf{n}}_1 = -\hat{\mathbf{n}}_2$, $(\mathbf{n}, \mathbf{F}) = \mathbf{n} \cdot \mathbf{F}$, $[\mathbf{n}, \mathbf{F}] = \mathbf{n} \times \mathbf{F}$, and $v = 1/\mu$.

1.2 The Field Wave Equations

In the following, quantities μ and ϵ are treated as constants, independent of space and time.

The \mathbf{E} wave equation may be derived using these steps :

$$\begin{aligned} \text{curl } \mathbf{E} &= -\partial_t \mathbf{B} && // \text{Maxwell (1.1.2)} \\ \text{curl curl } \mathbf{E} &= -\partial_t \text{curl } \mathbf{B} = -\mu \partial_t [\text{curl } \mathbf{H}] = -\mu \partial_t [\partial_t \mathbf{D} + \mathbf{J}] && // \text{curl both sides and Maxwell (1.1.1)} \\ \text{grad div } \mathbf{E} - \nabla^2 \mathbf{E} &= -\mu \partial_t [\partial_t [\epsilon \mathbf{E}] + \mathbf{J}] && // \text{vector identity on left and } \mathbf{D} = \epsilon \mathbf{E} \\ (\nabla^2 - \mu \epsilon \partial_t^2) \mathbf{E} &= \mu \partial_t \mathbf{J} + (1/\epsilon) \text{grad } \rho . && // \text{div } \mathbf{E} = \rho/\epsilon \end{aligned}$$

The \mathbf{B} wave equation uses these steps :

$$\begin{aligned} \text{curl } \mathbf{H} &= \partial_t \mathbf{D} + \mathbf{J} && // \text{Maxwell (1.1.1)} \\ \text{curl curl } \mathbf{H} &= \text{curl } [\partial_t \mathbf{D}] + \text{curl } \mathbf{J} && // \text{curl both sides} \\ \text{grad div } \mathbf{H} - \nabla^2 \mathbf{H} &= \epsilon \partial_t (\text{curl } \mathbf{E}) + \text{curl } \mathbf{J} && // \text{vector identity on left and } \mathbf{D} = \epsilon \mathbf{E} \\ (1/\mu) \text{grad div } \mathbf{B} - \nabla^2 \mathbf{H} &= \epsilon \mu \partial_t (-\partial_t \mathbf{H}) + \text{curl } \mathbf{J} && // \text{Maxwell (1.1.2) and } \mathbf{B} = \mu \mathbf{H} \text{ twice} \\ (\nabla^2 - \mu \epsilon \partial_t^2) \mathbf{H} &= -\text{curl } \mathbf{J} && // \text{since div } \mathbf{B} = 0 \text{ (1.1.4)} \end{aligned}$$

The two results are then

$$(\nabla^2 - \mu \epsilon \partial_t^2) \mathbf{E} = \mu \partial_t \mathbf{J} + (1/\epsilon) \text{grad } \rho \quad (1.2.1)$$

$$(\nabla^2 - \mu \epsilon \partial_t^2) \mathbf{B} = -\mu \text{curl } \mathbf{J} \quad (1.2.2)$$

which agree with Jackson p 246 (6.49) and (6.50). Recall that $\mu \epsilon = 1/v^2$ where v is the speed of light in the medium of interest. These two equations are undamped driven wave equations.

1.3 The Potential Wave Equations

(a) The Potential Wave Equations in the Lorenz gauge

It is possible to work with the scalar and vector potentials ϕ and \mathbf{A} instead of the fields \mathbf{E} and \mathbf{B} . If ϕ and \mathbf{A} can be determined, then \mathbf{E} and \mathbf{B} are fully determined by (1.3.1) below. However, in the other direction, if \mathbf{E} and \mathbf{B} are known, then ϕ and \mathbf{A} are determined only up to a certain "gauge transformation" degree of freedom, a subject discussed in Appendix A. The fields \mathbf{E} and \mathbf{B} are physically observable quantities while the potentials ϕ and \mathbf{A} in general are not and should be regarded as intermediate "helper" functions. In SI units, the \mathbf{E} and \mathbf{B} fields are obtained from ϕ and \mathbf{A} in this manner : [Jackson p 239 (6.7) and (6.9)]

$$\mathbf{B} = \text{curl } \mathbf{A} \quad \mathbf{E} = -\text{grad } \phi - \partial_t \mathbf{A} \quad . \quad (1.3.1)$$

$$\begin{aligned} \mathbf{A} &= \text{vector potential (tesla-m = amp-henry/m = volt-sec/m)} & \mathbf{E} &= \text{volt/m} \\ \phi &= \text{scalar potential (volts)} & \mathbf{B} &= \text{tesla} \quad . \end{aligned}$$

Appendix A (Fact 4) shows that there is a continuum of possible choices (ϕ, \mathbf{A}) all of which give the same physical fields (\mathbf{E}, \mathbf{B}) according to (1.3.1). It turns out that, along this continuum, $\text{div } \mathbf{A}$ takes different functional forms. Fact 4 shows that there always exists a choice (ϕ, \mathbf{A}) for which $\text{div } \mathbf{A} = \text{any function one wants!}$ Selecting $f(x)$ for $\text{div } \mathbf{A} = f(x)$ is called "making a gauge choice". Different gauge choices just result in different (ϕ, \mathbf{A}) potentials, but always the same (\mathbf{E}, \mathbf{B}) . In the following derivations of the wave equations for \mathbf{A} and ϕ , we shall be making a certain gauge choice as indicated.

The following steps are used to develop the ϕ wave equation. In the vacuum one has $\mu = \mu_0$ and $\epsilon = \epsilon_0$ and $\mu\epsilon = 1/c^2$ and these are the parameters one sees in the Jackson equation references below.

$$\begin{aligned} \mathbf{E} &= -\text{grad } \phi - \partial_t \mathbf{A} & // (1.3.1) [= Jackson (6.9)] \\ \text{div } \mathbf{E} &= -\text{div grad } \phi - \partial_t (\text{div } \mathbf{A}) & // \text{take div of both sides} \\ \nabla^2 \phi + \partial_t [\text{div } \mathbf{A}] &= -\rho/\epsilon & // \text{div } \mathbf{E} = \rho/\epsilon \quad [= Jackson (6.10)] & (1.3.2) \\ (\nabla^2 - \mu\epsilon \partial_t^2)\phi &= -(1/\epsilon)\rho \quad . & // \text{apply gauge choice } \text{div } \mathbf{A} = -\mu\epsilon \partial_t \phi \end{aligned}$$

And the following steps are used to develop the \mathbf{A} wave equation:

$$\begin{aligned} \text{curl } \mathbf{H} &= \partial_t \mathbf{D} + \mathbf{J} & // \text{Maxwell (1.1.1)} \\ (1/\mu) \text{curl curl } \mathbf{A} &= \mu\epsilon \partial_t \mathbf{E} + \mathbf{J} & // \mathbf{H} = \mathbf{B}/\mu, \mathbf{B} = \text{curl } \mathbf{A} \text{ from (1.3.1), and } \mathbf{D} = \epsilon\mathbf{E} \\ \text{grad div } \mathbf{A} - \nabla^2 \mathbf{A} &= \mu\epsilon \partial_t [-\text{grad } \phi - \partial_t \mathbf{A}] + \mu\mathbf{J} & // \text{vector identity and (1.3.1) } \mathbf{E} = -\text{grad } \phi - \partial_t \mathbf{A} \\ (\nabla^2 - \mu\epsilon \partial_t^2) \mathbf{A} &= \text{grad } [\mu\epsilon \partial_t \phi + \text{div } \mathbf{A}] - \mu\mathbf{J} & // [= Jackson (6.11)] & (1.3.3) \\ (\nabla^2 - \mu\epsilon \partial_t^2) \mathbf{A} &= -\mu\mathbf{J} \quad . & // \text{apply same gauge choice } \text{div } \mathbf{A} = -\mu\epsilon \partial_t \phi \end{aligned}$$

The results are then

$$(\nabla^2 - \mu\epsilon \partial_t^2)\phi = - (1/\epsilon)\rho \quad [= \text{Jackson (6.15)}] \quad (1.3.4)$$

$$(\nabla^2 - \mu\epsilon \partial_t^2)\mathbf{A} = - \mu\mathbf{J} \quad [= \text{Jackson (6.16)}] \quad (1.3.5)$$

$$\text{div}\mathbf{A} = - \mu\epsilon \partial_t\phi . \quad [= \text{Jackson (6.14)}] \quad // \text{ Lorenz Gauge} \quad (1.3.6)$$

As discussed in the comment below, this gauge choice is now called the Lorenz Gauge. One should notice how the gauge choice decouples the two wave equations (1.3.2) and (1.3.3) so one resulting equation only involves ϕ and ρ , while the other involves only \mathbf{A} and \mathbf{J} . We end up then with undamped driven wave equations with simple driving terms. Note that $\rho = \rho_{\text{free}}$ (does not include polarization charge ρ_{pol}) and that $\mathbf{J} = \mathbf{J}_c$ (does not include magnetization current \mathbf{J}_m). In effect, ρ_{pol} and \mathbf{J}_m are incorporated into the constants ϵ and μ .

Comment 1: For perhaps 100 years pretty much all (non-Danish) papers and textbooks (including Jackson's first two editions in 1962 and 1975 and the initial six printings of his 1998 third edition) referred to the Lorenz gauge as the Lorentz gauge, and it was then convenient to say that the Lorentz gauge condition is Lorentz invariant since it transforms as a scalar equation under Lorentz transformations. Now we have to say that the Lorenz gauge is Lorentz invariant because Lorentz was mistakenly credited for first using this gauge condition, see Jackson's note p 294 added in his 7th printing. Although the Dane Ludvig Lorenz (1829-1891) was 24 years older than the Dutchman Hendrick Lorentz (1853 –1928), they were contemporary though independent workers at the time (1867) that Lorenz first published the use of his now-eponymous gauge condition. Lorentz will just have to be content with his transformations, his invariance, his contraction and his force law which says $\mathbf{F} = q(\mathbf{E} + \mathbf{v} \times \mathbf{B})$. For more on Lorenz and Lorentz, see Nevels and Shin.

Comment 2: We speak of (1.3.6) as "the Lorenz gauge" and $\text{div}\mathbf{A} = 0$ as "the Coulomb gauge". These gauges are really *conditions* on \mathbf{A} and do not fully specify \mathbf{A} since many vector fields \mathbf{A} can have the same divergence. So a gauge specifies a class of possible \mathbf{A} fields, not a particular one.

(b) Special Relativity Note

At first encounter, one is amazed at how similar the two equations (1.3.4) and (1.3.5) appear. Here we shall show why that is so. We now assume the medium is the vacuum so $\mu\epsilon = \mu_0\epsilon_0 = 1/c^2$. Then the two equations may be written,

$$(\nabla^2 - \frac{1}{c^2} \partial_t^2)\phi = -(1/\epsilon_0)\rho \quad (1.3.7)$$

$$(\nabla^2 - \frac{1}{c^2} \partial_t^2)\mathbf{A} = -\mu_0\mathbf{J} \quad (1.3.8)$$

As shown in Appendix A.6, one can construct Lorentz 4-vectors $A^\mu = (\frac{1}{c}\phi, \mathbf{A})$ and $J^\mu = (c\rho, \mathbf{J})$ with the identification of $A^0 \equiv \phi/c$ and $J^0 \equiv c\rho$. The above equations can then be written, using proper tensor notation where common vectors are contravariant with an upper index,

$$(\nabla^2 - \frac{1}{c^2} \partial_t^2)[cA^0] = -(1/\epsilon_0)[J^0/c] = -(1/\epsilon_0)[J^0/c] (c^2\mu_0\epsilon_0) = -\mu_0 cJ^0 \quad (1.3.9)$$

$$(\nabla^2 - \frac{1}{c^2} \partial_t^2)A^i = -\mu_0 J^i \quad (1.3.10)$$

Cancelling the c's in the first equation allows both equations to be written as a single 4-vector equation

$$(\nabla^2 - \frac{1}{c^2} \partial_t^2)A^\mu = -\mu_0 J^\mu$$

or

$$\square A^\mu = \mu_0 J^\mu \quad \text{where} \quad \square \equiv \partial_\mu \partial^\mu = \frac{1}{c^2} \partial_t^2 - \nabla^2 \quad (1.3.11)$$

This equation is covariant because both sides transform as a Lorentz 4-vector (the operator \square transforms as a Lorentz scalar). Special relativity requires that all equations of physics be covariant under Lorentz transformations. This is similar to Newton's Law $\mathbf{F} = m\mathbf{a}$ being covariant under rotations, where both sides transform as 3-vectors. If we start with the correct law of physics (1.3.11) and work backwards through the equation pairs above, where we add a medium with μ and ϵ , we end up with our starting point (1.3.4) and (1.3.5) and the similarity of these two equations is then explained as being a requirement of special relativity.

Recall the Lorenz gauge choice (1.3.6) which was required to decouple things above,

$$\text{div}\mathbf{A} = -\mu_0\epsilon_0 \partial_t\phi = -\frac{1}{c^2} \partial_t\phi \quad (1.3.6)$$

As shown in Appendix A.6, this Lorenz gauge condition can be expressed in covariant form as

$$\partial_\mu A^\mu = 0 \quad \Leftrightarrow \quad \text{div}\mathbf{A} = -\frac{1}{c^2} \partial_t\phi \quad (1.3.12)$$

while the equation of continuity states

$$\partial_{\mu} J^{\mu} = 0 \quad \Leftrightarrow \quad \text{div} \mathbf{J} = -\partial_t \rho \quad . \quad (1.3.13)$$

Both sides of these last two tensor-notation equations transform as a rank-0 tensor (scalar) so the equations are covariant (0 is a scalar). As one changes frames of reference doing Lorentz transformations (rotations and "boosts"), the potential wave equation, the gauge condition, and the continuity relation always maintain the same tensor form.

In closing this relativity note, we must mention that the four Maxwell equations (with $\varepsilon = \varepsilon_0$ and $\mu = \mu_0$ and $\mu_0 \varepsilon_0 = 1/c^2$) can also be stated in covariant notation. One first defines the following antisymmetric rank-2 tensor (see Appendix A.5 concerning up and down indices etc.)

$$F^{\mu\nu} \equiv \partial^{\mu} A^{\nu} - \partial^{\nu} A^{\mu} \quad A^{\mu} = \left(\frac{1}{c} \phi, \mathbf{A} \right) \quad \mathbf{J}^{\mu} = (c\rho, \mathbf{J}) \quad \partial^{\mu} = (\partial^0, \partial^{\mathbf{i}}) = (\partial_0, -\partial_{\mathbf{i}}) \quad (1.3.14)$$

where obviously $F^{\mu\nu} = -F^{\nu\mu}$ and $F^{\mu\mu} = 0$ for diagonal elements. Then the two Maxwell homogeneous (no sources) equations appear as

$$\begin{aligned} \partial^{\alpha} F^{\mu\nu} + \partial^{\nu} F^{\alpha\mu} + \partial^{\mu} F^{\nu\alpha} &= 0 & // \text{ both sides transform as a rank-3 tensor so covariant} \\ \Leftrightarrow \quad \text{curl } \mathbf{E} + \partial_t \mathbf{B} &= 0 \quad \text{and} \quad \text{div } \mathbf{B} = 0 & (1.1.2) \text{ and } (1.1.4) \end{aligned} \quad (1.3.15)$$

while the two Maxwell inhomogeneous equations are (implied sum on μ)

$$\begin{aligned} \partial_{\mu} F^{\mu\nu} &= \mu_0 J^{\nu} & // \text{ both sides transform as a rank-1 tensor (4-vector) so covariant} \\ \Leftrightarrow \quad \text{curl } \mathbf{B} - \mu_0 \varepsilon_0 \partial_t \mathbf{E} &= \mu_0 \mathbf{J} \quad \text{and} \quad \text{div } \mathbf{E} = \rho / \varepsilon_0 & (1.1.24) \text{ and } (1.1.15) \end{aligned} \quad (1.3.16)$$

The fields are given by (ε is the permutation tensor),

$$\begin{aligned} B_1 &= -F^{23} & E_1 &= cF^{10} & \text{or} & B_{\mathbf{i}} &= -(1/2)\varepsilon_{\mathbf{i}jk} F^{jk} & \text{and} & E_{\mathbf{i}} &= cF^{\mathbf{i}0} \\ B_2 &= -F^{31} & E_2 &= cF^{20} & & & & & & \\ B_3 &= -F^{12} & E_3 &= cF^{30} & & & & & & \end{aligned} \quad (1.3.17)$$

The \mathbf{E} and \mathbf{B} fields are part of the tensor $F^{\mu\nu}$ and so do not transform as four vectors like A^{μ} . That is to say, there are no 4-vectors of the form E^{μ} or B^{ν} , so there is no up and down index on a field, so the index is just written down. Jackson states the above facts (but in Gaussian units) in his Section 11.9 along with a description of the notion of covariance.

Example: $\mu_0 J^2 = \partial_{\mu} F^{\mu 2} = \partial_0 F^{02} + \partial_1 F^{12} + \partial_2 F^{22} + \partial_3 F^{32} = (1/c)\partial_t(-1/cE_2) + \partial_1(-B_3) + 0 + \partial_3(+B_1)$

$$= -(1/c^2)\partial_t E_2 + [\text{curl } \mathbf{B}]_2 \quad \Rightarrow \quad \mu_0 \mathbf{J} = \text{curl} \mathbf{B} - \mu_0 \varepsilon_0 \partial_t \mathbf{E} \quad \text{in the 2 component}$$

(c) The Potential Wave Equations in the King and Lorenz Gauges with Conductors

We refer to a certain gauge condition below as "the King gauge" because King (see Refs.) made extensive use of this condition in his books and papers at least as early as 1945. Perhaps this gauge has some official name, but we are not aware of it.

We start with this King gauge and treat \mathbf{A} and then ϕ . Then we do the Lorenz gauge case for \mathbf{A} and ϕ , and finally we look at the wave equations for \mathbf{E} and \mathbf{B} . The motivation for using the King gauge is explained.

Unlike most sources on this subject, we allow for the possibility that the conductors' μ_i might differ from that of the dielectric.

KING GAUGE

Wave equation for \mathbf{A}

Consider the following general cross section of a transmission line which happens to be of coaxial cable type,

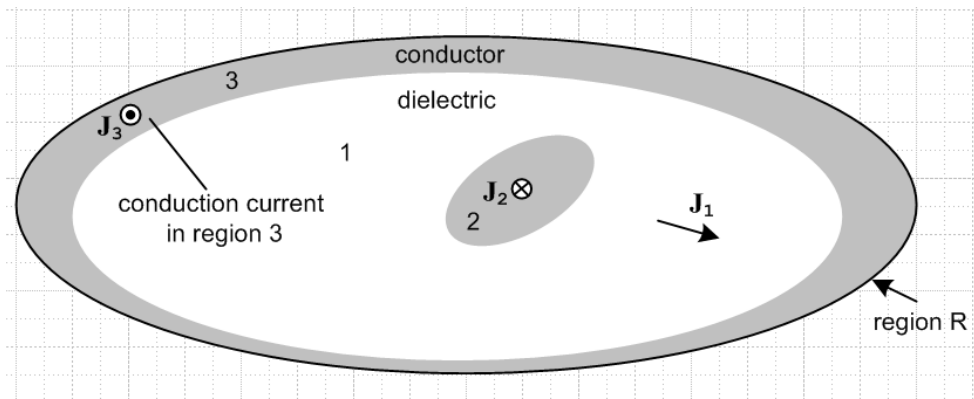


Fig 1.5

The gray regions 2 and 3 are conductors, while the white region 1 is the (possibly conducting) dielectric. Currents \mathbf{J}_1 , \mathbf{J}_2 and \mathbf{J}_3 are conduction currents.

We start by selecting the **King gauge for region 1** and we apply it to all three regions,

$$\text{div } \mathbf{A} = -\mu_1 \epsilon_1 \partial_t \phi - \mu_1 \sigma_1 \phi \quad // \equiv \text{King gauge, applied to all of } R \quad (1.3.18)$$

We first obtain the wave equation for \mathbf{A} in **region 1**. Start with (1.3.3) which gives the wave equation for \mathbf{A} before any gauge choice is made,

$$(\nabla^2 - \mu_1 \epsilon_1 \partial_t^2) \mathbf{A} = \text{grad} [\mu_1 \epsilon_1 \partial_t \phi + \text{div} \mathbf{A}] - \mu_1 \mathbf{J} \quad // \text{region 1} \quad (1.3.3)$$

Now insert the King gauge (1.3.18) to get

$$\begin{aligned}
(\nabla^2 - \mu_1 \epsilon_1 \partial_t^2) \mathbf{A} &= \text{grad} [\mu_1 \epsilon_1 \partial_t \phi + (-\mu_1 \epsilon_1 \partial_t \phi - \mu_1 \sigma_1 \phi)] - \mu_1 \mathbf{J} \\
&= -\mu_1 \sigma_1 \text{grad} \phi - \mu_1 \mathbf{J} \\
&= -\mu_1 \sigma_1 (-\mathbf{E} - \partial_t \mathbf{A}) - \mu_1 (\sigma_1 \mathbf{E}) . \quad // \text{ from (1.3.1) and } \mathbf{J} = \sigma_1 \mathbf{E} \\
&= -\mu_1 \sigma_1 (-\partial_t \mathbf{A}) .
\end{aligned}$$

Thus the wave equation for \mathbf{A} in region 1 is

$$(\nabla^2 - \mu_1 \epsilon_1 \partial_t^2 - \mu_1 \sigma_1 \partial_t) \mathbf{A} = 0 \quad // \text{ region 1} \quad (1.3.19)$$

This is a damped wave equation with no driving source; the equation is homogeneous.

Now we start over with (1.3.3) for **region 2**:

$$(\nabla^2 - \mu_2 \epsilon_2 \partial_t^2) \mathbf{A} = \text{grad} [\mu_2 \epsilon_2 \partial_t \phi + \text{div} \mathbf{A}] - \mu_2 \mathbf{J}_2 \quad // \text{ region 2} \quad (1.3.3)$$

As before, we insert the region-1 King gauge expression (1.3.18) for $\text{div} \mathbf{A}$, even though we are now working in region 2, and we make an assumption that conductor 2 is a "very good conductor".

$$\begin{aligned}
(\nabla^2 - \mu_2 \epsilon_2 \partial_t^2) \mathbf{A} &= \text{grad} [\mu_2 \epsilon_2 \partial_t \phi + (-\mu_1 \epsilon_1 \partial_t \phi - \mu_1 \sigma_1 \phi)] - \mu_2 \mathbf{J}_2 \\
&= [\mu_2 \epsilon_2 \partial_t + (-\mu_1 \epsilon_1 \partial_t - \mu_1 \sigma_1)] \text{grad} \phi - \mu_2 \mathbf{J}_2 \\
&= [(\mu_2 \epsilon_2 - \mu_1 \epsilon_1) \partial_t - \mu_1 \sigma_1] \text{grad} \phi - \mu_2 \mathbf{J}_2 \\
&= [(\mu_2 \epsilon_2 - \mu_1 \epsilon_1) \partial_t - \mu_1 \sigma_1] (-\mathbf{E} - \partial_t \mathbf{A}) - \mu_2 \mathbf{J}_2 \quad // \text{ using (1.3.1)} \\
&= [(\mu_2 \epsilon_2 - \mu_1 \epsilon_1) \partial_t - \mu_1 \sigma_1] (-\mathbf{J}_2 / \sigma_2 - \partial_t \mathbf{A}) - \mu_2 \mathbf{J}_2 \quad // \mathbf{J}_2 = \sigma_2 \mathbf{E} \\
&\approx [(\mu_2 \epsilon_2 - \mu_1 \epsilon_1) \partial_t - \mu_1 \sigma_1] (-\partial_t \mathbf{A}) - \mu_2 \mathbf{J}_2 \quad // \text{ since } \sigma_2 \text{ is very large in conductor 2} \\
&= -[(\mu_2 \epsilon_2 - \mu_1 \epsilon_1) \partial_t^2 - \mu_1 \sigma_1 \partial_t] \mathbf{A} - \mu_2 \mathbf{J}_2 .
\end{aligned}$$

The "large σ_2 " assumption made two lines above is discussed at the end of this section. It puts a lower limit on the value ω for which the \mathbf{A} wave equation is valid, but this limit is quite low relative to the normal use of a transmission line so it does not affect our analysis.

Notice that we have chosen *not* to set $\mathbf{J}_2 = \sigma_2 \mathbf{E}$ in region 2 for the last term, we just leave it as \mathbf{J}_2 . Moving the first term on the right to the left one gets

$$(\nabla^2 - \mu_2 \varepsilon_2 \partial_t^2 + [(\mu_2 \varepsilon_2 - \mu_1 \varepsilon_1) \partial_t^2 - \mu_1 \sigma_1 \partial_t]) \mathbf{A} = -\mu_2 \mathbf{J}_2$$

or

$$(\nabla^2 - \mu_1 \varepsilon_1 \partial_t^2 - \mu_1 \sigma_1 \partial_t) \mathbf{A} = -\mu_2 \mathbf{J}_2 \quad // \text{ region 2} \quad (1.3.20)$$

On the left side we see the same region-1 damped wave operator although we are in region 2, and \mathbf{J}_2 is the conduction current density in region 2. A similar result applies for region 3. Thus we have shown that

$$\begin{aligned} (\nabla^2 - \mu_1 \varepsilon_1 \partial_t^2 - \mu_1 \sigma_1 \partial_t) \mathbf{A} &= 0 && \text{region 1} \\ (\nabla^2 - \mu_1 \varepsilon_1 \partial_t^2 - \mu_1 \sigma_1 \partial_t) \mathbf{A} &= -\mu_2 \mathbf{J}_2 && \text{region 2} \\ (\nabla^2 - \mu_1 \varepsilon_1 \partial_t^2 - \mu_1 \sigma_1 \partial_t) \mathbf{A} &= -\mu_3 \mathbf{J}_3 && \text{region 3} \end{aligned} \quad (1.3.21)$$

We combine these into a single equation which is then valid over all of region R,

$$(\nabla^2 - \mu_1 \varepsilon_1 \partial_t^2 - \mu_1 \sigma_1) \mathbf{A} = -\mu_2 \mathbf{J}_2 - \mu_3 \mathbf{J}_3 \quad \text{all of region R} \quad (1.3.22)$$

with the understanding that the conduction current in region 1 has already been accounted for and \mathbf{J}_i represents conduction currents in conductor i . We could generalize this result for a region R containing any number N of conductors labeled $i = 2, 3, \dots, N+1$

$$(\nabla^2 - \mu_1 \varepsilon_1 \partial_t^2 - \mu_1 \sigma_1) \mathbf{A} = -\sum_{i=2}^{N+1} \mu_i \mathbf{J}_i \quad \text{all of region R} \quad (1.3.23)$$

Wave equation for ϕ

We first obtain the wave equation for ϕ in region 1. Start with (1.3.2) which gives the wave equation for ϕ before any gauge choice is made,

$$\nabla^2 \phi + \partial_t [\text{div } \mathbf{A}] = -\rho / \varepsilon_1 \quad (1.3.2)$$

Now use the same global region-R King gauge (1.3.18) for $\text{div } \mathbf{A}$,

$$\begin{aligned} \nabla^2 \phi + \partial_t [-\mu_1 \varepsilon_1 \partial_t \phi - \mu_1 \sigma_1 \phi] &= -\rho_1 / \varepsilon_1 \\ (\nabla^2 - \mu_1 \varepsilon_1 \partial_t^2 - \mu_1 \sigma_1 \partial_t) \phi &= -(1/\varepsilon_1) \rho_1 \quad // \text{ region 1} \end{aligned} \quad (1.3.24)$$

Again the same damped region-1 wave operator appears on the left side. Since the King gauge is the same in all three regions, we can write

$$\begin{aligned} (\nabla^2 - \mu_1 \varepsilon_1 \partial_t^2 - \mu_1 \sigma_1 \partial_t) \phi &= -(1/\varepsilon_1) \rho^{(1)} && // \text{ region 1} \\ (\nabla^2 - \mu_1 \varepsilon_1 \partial_t^2 - \mu_1 \sigma_1 \partial_t) \phi &= -(1/\varepsilon_2) \rho^{(2)} && // \text{ region 2} \\ (\nabla^2 - \mu_1 \varepsilon_1 \partial_t^2 - \mu_1 \sigma_1 \partial_t) \phi &= -(1/\varepsilon_3) \rho^{(3)} && // \text{ region 3} \end{aligned} \quad (1.3.25)$$

where ρ always means free charge. The three equations are basically the same because the pre-gauge equation (1.3.2) has no region-specific parameters apart from ε_1 , in contrast with (1.3.3) quoted above.

Now the only actual free charge present is the surface charge on the outside surfaces of the conductors and we shall regard all these charge densities as residing in region 1, the dielectric (just inside the boundaries of region 1). Thus, write

$$\begin{aligned} \rho^{(1)} &= \rho_2 + \rho_3 & // = \sum_{i=2}^{N+1} \rho_i \\ \rho^{(2)} &= 0 \\ \rho^{(3)} &= 0 \end{aligned} \tag{1.3.26}$$

where ρ_i is the surface charge density on conductor i. Then combine the above three equations into a single equation for all of region R

$$(\nabla^2 - \mu_1 \epsilon_1 \partial_t^2 - \mu_1 \sigma_1 \partial_t) \phi = - (1/\epsilon_1) \sum_{i=2}^{N+1} \rho_i \quad \text{all of region R} \tag{1.3.27}$$

Conclusion for wave equations in the King gauge

Here then are the wave equations for ϕ and \mathbf{A} in region R using the region-1 King gauge:

Potential Wave Equations in the King Gauge (1.3.28)

$$\begin{aligned} (\nabla^2 - \mu_1 \epsilon_1 \partial_t^2 - \mu_1 \sigma_1 \partial_t) \phi &= - (1/\epsilon_1) \sum_{i=2}^{N+1} \rho_i & \text{all of region R} & (1.3.27) \\ (\nabla^2 - \mu_1 \epsilon_1 \partial_t^2 - \mu_1 \sigma_1 \partial_t) \mathbf{A} &= - \sum_{i=2}^{N+1} \mu_i \mathbf{J}_i & \text{all of region R} & (1.3.23) \\ \text{div } \mathbf{A} &= - \mu_1 \epsilon_1 \partial_t \phi - \mu_1 \sigma_1 \phi & \text{King gauge} & (1.3.18) \end{aligned}$$

1 = dielectric 2,3,4,... N+1 = conductors (there are N conductors)
 ρ_i = free surface charge density on conductor i
 \mathbf{J}_i = free current density in conductor i (\mathbf{J}_1 in the dielectric exists but does not appear in $\sum_i \mu_i \mathbf{J}_i$)

To be consistent with later sections, we put subscript d on dielectric properties, and we renumber the conductors 1 to N instead of 2 to N+1. The above box then becomes

Potential Wave Equations in the King Gauge (1.3.29)

$$\begin{aligned} (\nabla^2 - \mu_d \epsilon_d \partial_t^2 - \mu_d \sigma_d \partial_t) \phi &= - (1/\epsilon_d) \sum_i \rho_i & \text{all of region R} \\ (\nabla^2 - \mu_d \epsilon_d \partial_t^2 - \mu_d \sigma_d \partial_t) \mathbf{A} &= - \sum_i \mu_i \mathbf{J}_i & \text{all of region R} \\ \text{div } \mathbf{A} &= - \mu_d \epsilon_d \partial_t \phi - \mu_d \sigma_d \phi & \text{King gauge} \end{aligned}$$

$\mu_d, \epsilon_d, \sigma_d$ = dielectric 1,3,4,... N = conductors $\sum_i = \sum_{i=1}^N$ μ_i = for conductor i
 ρ_i = free surface charge density on conductor i
 \mathbf{J}_i = free current density in conductor i (\mathbf{J} in the dielectric exists but does not appear in $\sum_i \mu_i \mathbf{J}_i$)

The word "free" is used above to emphasize the fact that possible polarization charge densities and magnetization current densities are *not* included in these ρ_{i} and \mathbf{J}_{i} .

King never writes these wave equations in his transmission-line theory book, so it is difficult to find verification of our logic pathway in his book. However, Panofsky and Phillips *do* show the equations and we quote the relevant section from p 241 of their book:

14-1] THE WAVE EQUATION FOR THE POTENTIALS 241

We obtain the symmetrical set of equations:

$$\nabla^2 \mathbf{A} - \mu\epsilon \frac{\partial^2 \mathbf{A}}{\partial t^2} - \mu\sigma \frac{\partial \mathbf{A}}{\partial t} = -\mu \mathbf{j}', \quad (14-4)$$

$$\nabla^2 \phi - \mu\epsilon \frac{\partial^2 \phi}{\partial t^2} - \mu\sigma \frac{\partial \phi}{\partial t} = -\rho/\epsilon. \quad (14-5)$$

Here \mathbf{j}' represents a current given by $\mathbf{j}' = \sigma \mathbf{E}'$, that part of the current density that is produced by the external electromotive forces. It does not contain any part of the current induced by the electric fields in conducting media and represented by the last term on the left side of Eq. (14-4).

Their last sentence says that $\mathbf{J} = \sigma \mathbf{E}$ in the conducting dielectric has been incorporated into the $-\mu\sigma \partial_t \mathbf{A}$ term in their first equation, just as we have done above. These authors have assumed that the μ 's of the dielectric and the conductors are all the same (normally $\mu = \mu_0$). In order to obtain the above equations, Panofsky and Phillips use the King gauge (1.3.18) but they refer to this gauge simply as "the Lorentz condition" (illustrating Comments 1 and 2 above). From their page 240,

within an additive arbitrary function of position. Let us define the divergence of \mathbf{A} by what is called the Lorentz condition,

$$\nabla \cdot \mathbf{A} + \mu\epsilon \frac{\partial \phi}{\partial t} + \mu\sigma \phi = 0, \quad (14-2)$$

which in free space becomes

$$\nabla \cdot \mathbf{A} + \frac{1}{c^2} \frac{\partial \phi}{\partial t} = 0. \quad (14-3)$$

LORENTZ GAUGE

If we carry out the exact same program with respect to Fig 1.5 using a region-1 (dielectric) global Lorenz gauge for all of R,

$$\text{div} \mathbf{A} = -\mu_1 \epsilon_1 \partial_t \phi, \quad (1.3.30)$$

we obtain these results for \mathbf{A} , where in region 1 the conduction current is *not* absorbed into a damping term on the left side,

$$\begin{aligned}
(\nabla^2 - \mu_1 \epsilon_1 \partial_t^2) \mathbf{A} &= -\mu_1 \mathbf{J}_1 && \text{region 1} \\
(\nabla^2 - \mu_1 \epsilon_1 \partial_t^2) \mathbf{A} &= -\mu_2 \mathbf{J}_2 && \text{region 2} \\
(\nabla^2 - \mu_1 \epsilon_1 \partial_t^2) \mathbf{A} &= -\mu_3 \mathbf{J}_3 && \text{region 3}
\end{aligned}$$

As before, all three equations have the same wave operator on the left side. Again assuming N conductors, we combine these into a single equation as follows

$$(\nabla^2 - \mu_1 \epsilon_1 \partial_t^2) \mathbf{A} = -\sum_{i=1}^{N+1} \mu_i \mathbf{J}_i \quad \text{all of region R} \quad (1.3.31)$$

Meanwhile, the results for ϕ are

$$\begin{aligned}
(\nabla^2 - \mu_1 \epsilon_1 \partial_t^2) \phi &= -\rho^{(1)}/\epsilon_1 && \text{region 1} \\
(\nabla^2 - \mu_1 \epsilon_1 \partial_t^2) \phi &= -\rho^{(2)}/\epsilon_2 && \text{region 2} \\
(\nabla^2 - \mu_1 \epsilon_1 \partial_t^2) \phi &= -\rho^{(3)}/\epsilon_3 && \text{region 3}
\end{aligned}$$

so that with the same comments made earlier in (1.3.26) this becomes

$$(\nabla^2 - \mu_1 \epsilon_1 \partial_t^2) \phi = -(1/\epsilon_1) \sum_{i=2}^{N+1} \rho_i \quad \text{all of region R} \quad (1.3.32)$$

We then make the same notational change made above to get these Lorenz-gauge results:

$$(\nabla^2 - \mu_d \epsilon_d \partial_t^2) \phi = -(1/\epsilon) \sum_{i=1}^N \rho_i \quad \text{all of region R} \quad (1.3.33)$$

$$(\nabla^2 - \mu_d \epsilon_d \partial_t^2) \mathbf{A} = -\sum_{i=1}^N \mu_i \mathbf{J}_i - \mu_d \mathbf{J} \quad \text{all of region R} \quad (1.3.34)$$

Notice that no conductivities appear in these equations.

COMPARISON

We can now do a side-by-side comparison, where \sum_i is a sum over the conductors $i = 1, 2, \dots, N$

King Gauge:

$$(\nabla^2 - \mu_d \epsilon_d \partial_t^2 - \mu_d \sigma_d \partial_t) \phi = -(1/\epsilon_d) \sum_i \rho_i \quad \text{all of region R} \quad (1.3.29)$$

$$(\nabla^2 - \mu_d \epsilon_d \partial_t^2 - \mu_d \sigma_d \partial_t) \mathbf{A} = -\sum_i \mu_i \mathbf{J}_i \quad \text{all of region R} \quad (1.3.29)$$

$$\text{div } \mathbf{A} = -\mu_d \epsilon_d \partial_t \phi - \mu_d \sigma_d \phi \quad \text{King gauge} \quad (1.3.29)$$

Lorenz Gauge:

$$(\nabla^2 - \mu_d \epsilon_d \partial_t^2) \phi = -(1/\epsilon_d) \sum_i \rho_i \quad \text{all of region R} \quad (1.3.33)$$

$$(\nabla^2 - \mu_d \epsilon_d \partial_t^2) \mathbf{A} = -\sum_i \mu_i \mathbf{J}_i - \mu_d \mathbf{J} \quad \text{all of region R} \quad (1.3.34)$$

$$\text{div } \mathbf{A} = -\mu_d \epsilon_d \partial_t \phi \quad \text{Lorenz gauge} \quad (1.3.30)$$

In the Lorenz gauge, we get undamped wave operators, but the sum on the right of the \mathbf{A} equation includes the current \mathbf{J} in the dielectric, whereas this is not the case in the King gauge. In a situation where we have prescribed currents \mathbf{J}_i in the conductors, it is inconvenient to have to worry about the dielectric conduction current \mathbf{J} which complicates the solution of the problem. In the King gauge, we get damped

wave operators but we have to include only the current in the conductors since the current in the dielectric has been incorporated into the damping term. When we transform to the frequency domain and write the Helmholtz equation for \mathbf{A} and its Helmholtz Integral solution, we need only integrate over the conductors which makes life easier. This then is the motivation for the King gauge. For a non-conducting dielectric both gauge conditions are the same since $\sigma = 0$.

E AND B WAVE EQUATIONS

Meanwhile, the \mathbf{E} and \mathbf{B} *field* wave equations of course don't know anything about gauges and from (1.2.1) and (1.2.2) we have, with respect to Fig 1.5, ($\rho_s = \rho_2 + \rho_3 = \sum_{i=2}^{N+1} \rho_i$, 1 = dielectric)

$$\begin{aligned}
 (\nabla^2 - \mu_1 \varepsilon_1 \partial_t^2) \mathbf{E} &= \mu_1 \partial_t \mathbf{J}_1 + (1/\varepsilon_1) \text{grad } \rho^{(1)} = \mu_1 \partial_t \mathbf{J}_1 + (1/\varepsilon_1) \text{grad } \rho_s & // \text{ region 1} \\
 (\nabla^2 - \mu_2 \varepsilon_2 \partial_t^2) \mathbf{E} &= \mu_2 \partial_t \mathbf{J}_2 + (1/\varepsilon_2) \text{grad } \rho^{(2)} = \mu_2 \partial_t \mathbf{J}_2 & // \text{ region 2} \\
 (\nabla^2 - \mu_3 \varepsilon_3 \partial_t^2) \mathbf{E} &= \mu_3 \partial_t \mathbf{J}_3 + (1/\varepsilon_3) \text{grad } \rho^{(3)} = \mu_3 \partial_t \mathbf{J}_3 & // \text{ region 3} \\
 (\nabla^2 - \mu_1 \varepsilon_1 \partial_t^2) \mathbf{B} &= -\mu_1 \text{curl } \mathbf{J}_1 & // \text{ region 1} \\
 (\nabla^2 - \mu_2 \varepsilon_2 \partial_t^2) \mathbf{B} &= -\mu_2 \text{curl } \mathbf{J}_2 & // \text{ region 2} \\
 (\nabla^2 - \mu_3 \varepsilon_3 \partial_t^2) \mathbf{B} &= -\mu_3 \text{curl } \mathbf{J}_3 & // \text{ region 3}
 \end{aligned} \tag{1.3.35}$$

where $\mathbf{J}_i = \sigma_i \mathbf{E}$. We cannot unify each group of three equations into a single region R equation as we could in the potential case since the wave operators are different in each region. Using $\mathbf{J}_i = \sigma_i \mathbf{E}$ and $\text{curl } \mathbf{E} = -\partial_t \mathbf{B}$ and (1.3.26) the above equations can be rewritten as,

$$\begin{aligned}
 (\nabla^2 - \mu_1 \varepsilon_1 \partial_t^2 - \mu_1 \sigma_1 \partial_t) \mathbf{E} &= (1/\varepsilon_1) \sum_{i=2}^{N+1} \text{grad } \rho_i & // \text{ region 1} \\
 (\nabla^2 - \mu_2 \varepsilon_2 \partial_t^2 - \mu_2 \sigma_2 \partial_t) \mathbf{E} &= 0 & // \text{ region 2} \\
 (\nabla^2 - \mu_3 \varepsilon_3 \partial_t^2 - \mu_3 \sigma_3 \partial_t) \mathbf{E} &= 0 & // \text{ region 3} \\
 (\nabla^2 - \mu_1 \varepsilon_1 \partial_t^2 - \mu_1 \sigma_1 \partial_t) \mathbf{B} &= 0 & // \text{ region 1} \\
 (\nabla^2 - \mu_2 \varepsilon_2 \partial_t^2 - \mu_2 \sigma_2 \partial_t) \mathbf{B} &= 0 & // \text{ region 2} \\
 (\nabla^2 - \mu_3 \varepsilon_3 \partial_t^2 - \mu_3 \sigma_3 \partial_t) \mathbf{B} &= 0 & // \text{ region 3}
 \end{aligned} \tag{1.3.36}$$

Again the three damped wave operators are different. The solution of these equations requires solving the first equation for the "particular" solution in region 1, finding all possible homogenous solutions to all 6 equations in their regions using appropriate harmonic forms with "constants to be determined", then matching these conditions at the two boundaries to evaluate the constants. In contrast, in the *potential* problem of (1.3.28),

$$\begin{aligned}
 (\nabla^2 - \mu_1 \varepsilon_1 \partial_t^2 - \mu_1 \sigma_1 \partial_t) \varphi &= -(1/\varepsilon_1) \sum_{i=2}^{N+1} \rho_i & \text{all of region R} & (1.3.26) \\
 (\nabla^2 - \mu_1 \varepsilon_1 \partial_t^2 - \mu_1 \sigma_1 \partial_t) \mathbf{A} &= -\sum_{i=2}^N \mu_i \mathbf{J}_i & \text{all of region R} & (1.3.23) \\
 \text{div } \mathbf{A} &= -\mu_1 \varepsilon_1 \partial_t \varphi - \mu_1 \sigma_1 \varphi & \text{King gauge} & (1.3.18) \tag{1.3.28}
 \end{aligned}$$

one worries about a single unified region R and there is only one damped wave operator. The method of solution is to find the particular solutions of the φ and \mathbf{A} equations, add in homogenous solutions and match boundary conditions.

The "large σ_2 " assumption. This assumption was used above in the development of the region 2 damped wave equation (1.3.20) for \mathbf{A} . Looking back at the development one sees that the approximation made was in fact $|\mathbf{E}| \ll |\partial_t \mathbf{A}|$ inside the conductor. An estimation of the validity of this inequality requires material that appears in later chapters, so we assume that material in what follows. It will turn out that we only care about the z component of the \mathbf{A} wave equation which involves A_z , because the transverse components of \mathbf{A} are so small that they can be neglected (Appendix M and self-consistency). Thus, we want to show that $|E_z| \ll |\omega A_z|$ where E_z and A_z are now in the frequency domain. From the study of "the transverse problem" in Chapter 5, we can make a ballpark estimate that $A_{z\mathbf{t}}(x,y) \sim K$, where $A_{z\mathbf{t}}$ is a certain transverse version of A_z , and where K is a certain dimensionless constant arising in the theory. This estimate for $A_{z\mathbf{t}}$ arises from the boundary conditions on $A_{z\mathbf{t}}$ shown in (5.3.11). The connection between A_z and $A_{z\mathbf{t}}$ is given in (5.2.1)

$$A_z(x,y,z) = \frac{\mu_d}{4\pi} i(z) A_{z\mathbf{t}}(x,y) \quad (5.2.1)$$

so we then have $A_z \sim (\mu_d/4\pi) i(z) K = (\mu_d/4\pi) I K$ where $i(z) = I$ is the current in a conductor. For a round wire of radius a we can estimate $J_z = I/(\pi a^2)$. Then from $J_z = \sigma E_z$ we have $E_z \sim I/(\pi a^2 \sigma)$. The inequality in question is then

$$|E_z| \ll |\omega A_z|$$

$$I/(\pi a^2 \sigma) \ll \omega (\mu_d/4\pi) I K$$

$$1/(a^2 \sigma) \ll \omega (\mu_d K/4)$$

$$\omega \gg \frac{1}{a^2} \frac{4}{\sigma \mu K} \quad // \text{ assume } \mu_d = \mu = \mu_0$$

or

$$f \gg \frac{1}{a^2} \frac{2}{\pi} \frac{1}{K} \frac{1}{\mu \sigma} \quad (1.3.37)$$

For a copper conductor, $\mu \sigma \approx 4\pi * 5.81 = 73.0 \text{ sec/m}^2$ so then

$$f \gg \frac{1}{a^2} \frac{2}{\pi} \frac{1}{K} \frac{1}{73} = .0087/(a^2 K) \quad (1.3.38)$$

In order to justify our "large σ_2 " assumption, we require that the operating frequency be significantly larger than $.0087/(a^2 K)$. We will show in the following two examples that this is quite a low frequency and one always operates above this lower limit in a practical application.

Example 1: Belden 8281 coaxial cable is treated as a case study in Appendix R. For the central conductor, $a = 394 \mu$ and the cable has $K = 3.7$. Our condition is then $f \gg 15 \text{ KHz}$,

```

a := 394e-6:
K := 3.7:
f := .0087/(a^2*K);

```

$f = 15146.94627$

Since 15 KHz is an audio frequency, while Belden 8281 coaxial cable is used for RF signals, this lower limit is not an issue. That is to say, the A_z wave equation (1.3.20) is valid for ω of practical use.

Example 2: At the end of Section 4.6 below we consider a power distribution transmission line which has two conductors with $a = 1/2$ " and $K = 17.5$. For such a transmission line, our condition is $f \gg 3$ Hz,

```

a := (2.54e-2)/2:
K := 17.5:
f := .0087/(a^2*K);

```

$f = 3.082291879$

Since power systems operate at 50 or 60 Hz, this lower bound of 3 Hz is well surpassed.

1.4 Retarded Solutions in the Lorenz gauge: Propagators

In a medium where μ and ϵ are time-independent, the Lorenz gauge equations (1.3.4) and (1.3.5) apply,

$$(\nabla^2 - \mu\epsilon \partial_t^2)\phi = -(1/\epsilon)\rho \quad (1.3.4)$$

$$(\nabla^2 - \mu\epsilon \partial_t^2)\mathbf{A} = -\mu\mathbf{J} . \quad (1.3.5)$$

One approach to solving these equations for \mathbf{A} and ϕ is the method of retarded solutions. We seek to solve an equation of this form

$$(\nabla^2 - \mu\epsilon \partial_t^2) u = -f , \quad (1.4.1)$$

where for example in (1.3.4) $u = \phi$ and $f = \rho/\epsilon$. Since $\mu\epsilon = 1/v^2$ where v is the wave velocity in the medium, write (1.4.1) as

$$(\partial_t^2 - v^2\nabla^2) u = v^2f$$

or

$$\square u = f \quad \text{where} \quad \square \equiv \frac{1}{v^2} \partial_t^2 - \nabla^2 . \quad (1.4.2)$$

This last equation is similar to (A.7.2) of Appendix A and can be solved in the same manner. Define a Green's function g as the solution of

$$v^2 \square g(\mathbf{x},t; \mathbf{x}',t') = \delta(\mathbf{x}-\mathbf{x}')\delta(t-t') \quad \text{with } g = 0 \text{ when } |\mathbf{x}-\mathbf{x}'| \rightarrow \infty . \quad (1.4.3)$$

This is just (A.7.3) with $c = v$. As (A.7.4) shows, the solution is given by

$$v^2 g(\mathbf{x},t; \mathbf{x}',t') = (1/4\pi R)\delta(t-t'-R/v) \quad \text{with } R = |\mathbf{x}-\mathbf{x}'| . \quad (1.4.4)$$

The delta function only gets a hit if $t = t'+R/v$, so there is never a hit if $t < t'$. In other words, $g = 0$ for $t < t'$, and g is often referred to as a "causal" Green's function. Jackson (6.41) and (6.44) uses $G^{(+)} = 4\pi v^2 g$ with $v = c$ and refers to the solution as a "retarded Green function". See also Stakgold references in Appendix A. The solution to (1.4.1) is then

$$u(\mathbf{x},t) = \int d^3x' \int dt' v^2 g(\mathbf{x},t; \mathbf{x}',t') f(\mathbf{x}',t') \quad (1.4.5)$$

as can be verified by applying \square to both sides and making use of (1.4.3). The Green's Function $g(\mathbf{x},t; \mathbf{x}',t')$ is the free-space fundamental solution (propagator) of the wave equation. Insert (1.4.4) into (1.4.5) to get,

$$\begin{aligned} u(\mathbf{x},t) &= \int d^3x' \int dt' (1/4\pi R)\delta(t-t'-R/v) f(\mathbf{x}',t') = \int d^3x' (1/4\pi R) f(\mathbf{x}', t-R/v) \\ &= \frac{1}{4\pi} \int d^3x' \frac{f(\mathbf{x}',t-R/v)}{R} . \end{aligned} \quad (1.4.6)$$

Thus, the solutions to (1.3.2) and (1.3.3) are (Lorenz gauge) :

$$\varphi(\mathbf{x},t) = \frac{1}{4\pi\epsilon} \int d^3x' \frac{\rho(\mathbf{x}',t-R/v)}{R} \quad (1.4.7)$$

$$\mathbf{A}(\mathbf{x},t) = \frac{\mu}{4\pi} \int d^3x' \frac{\mathbf{J}(\mathbf{x}',t-R/v)}{R} \quad R = |\mathbf{x}-\mathbf{x}'| \quad (1.4.8)$$

The potentials at time t are generated by the values the sources *had* at time $t - R/v$ since the influence of the sources travels at finite velocity v through the medium. These last equations agree with Jackson p 246 (6.48). Note that $1/4\pi R$ is the free-space propagator of the Laplace equation. It describes how a source at location \mathbf{x}' and earlier time $t-R/v$ propagates its influence into the potential at observation point \mathbf{x} and current time t . Compare (1.4.6) to (A.0.2) which is the solution to the electrostatic Poisson equation, where the source has no time dependence (it is static).

Jumping the gun slightly, it is interesting now to Fourier Transform the above equations. First, write

$$\rho(\mathbf{x}',t-R/v) = \int_{-\infty}^{\infty} dt' \delta(t'-[t-R/v]) \rho(\mathbf{x}',t') \quad (1.4.9)$$

Then using the Fourier Integral Transform (1.6.8),

$$\begin{aligned} \varphi(\mathbf{x},\omega) &= \int_{-\infty}^{\infty} dt \varphi(\mathbf{x},t) e^{-j\omega t} && // (1.6.8a) \\ &= \int_{-\infty}^{\infty} dt \left[\frac{1}{4\pi\epsilon} \int d^3x' \frac{\rho(\mathbf{x}',t-R/v)}{R} \right] e^{-j\omega t} && // \text{insert } \varphi \text{ from (1.4.7)} \\ &= \frac{1}{4\pi\epsilon} \int_{-\infty}^{\infty} dt \int d^3x' \frac{1}{R} \int_{-\infty}^{\infty} dt' \delta(t'-[t-R/v]) \rho(\mathbf{x}',t') e^{-j\omega t} && // \text{insert } \rho(\mathbf{x}',t-R/v) \text{ from (1.4.9)} \\ &= \frac{1}{4\pi\epsilon} \int d^3x' \frac{1}{R} \int_{-\infty}^{\infty} dt' \rho(\mathbf{x}',t') e^{-j\omega[t'+R/v]} && // \text{do the } dt \text{ integration} \\ &= \frac{1}{4\pi\epsilon} \int d^3x' \frac{e^{-j\beta R}}{R} \int_{-\infty}^{\infty} dt' \rho(\mathbf{x}',t') e^{-j\omega t'} && // \text{let } \beta \equiv \omega/v \\ &= \frac{1}{4\pi\epsilon} \int d^3x' \frac{e^{-j\beta R}}{R} \rho(\mathbf{x}',\omega) \quad (1.6.8a) \end{aligned}$$

Thus, in the frequency domain the retarded potential solutions appear as

$$\varphi(\mathbf{x}, \omega) = \frac{1}{4\pi\epsilon} \int d^3x' \frac{e^{-j\beta R}}{R} \rho(\mathbf{x}', \omega) \quad (1.4.10)$$

$$\mathbf{A}(\mathbf{x}, \omega) = \frac{\mu}{4\pi} \int d^3x' \frac{e^{-j\beta R}}{R} \mathbf{J}(\mathbf{x}', \omega) . \quad R = |\mathbf{x} - \mathbf{x}'| \quad \beta = \omega/v \quad (1.4.11)$$

These are the single-region expressions of the Helmholtz integrals we shall obtain in the next section by a somewhat different path using a different gauge. These integrals then are the ω -domain versions of the retarded potential solutions in the time domain. The factor $e^{-j\beta R}/R$ is the ω -space 3D Helmholtz propagator discussed below and in Appendix H. It describes how the ω -domain source (ρ or \mathbf{J}) at location \mathbf{x}' propagates to its potential at location \mathbf{x} .

These last two equations have the general form

$$f_1(\mathbf{x}) = \int k(\mathbf{x}, \mathbf{x}') f_2(\mathbf{x}') d^3x' \quad (1.4.12)$$

and the propagator $k(\mathbf{x}, \mathbf{x}')$ is sometimes called "the kernel" and defines an integral operator K . Then the above equation is written $f_1 = Kf_2$ which is a mapping from one function to another in a Hilbert Space of functions. Similarly, equation (1.4.5) has the form

$$f_1(\mathbf{x}, t) = \int \int k(\mathbf{x}, t; \mathbf{x}', t') f_2(\mathbf{x}', t') d^3x' dt' \quad (1.4.13)$$

where now the kernel $k(\mathbf{x}, t; \mathbf{x}', t')$ is a spacetime propagator describing how f_2 at \mathbf{x}' and t' contributes to f_1 at \mathbf{x} and t . The total function f_1 is the sum of all these propagated contributions. For the particular propagator shown in (1.4.5), $f_1(\mathbf{x}, t)$ would only get contributions from $f_2(\mathbf{x}', t')$ at past times t' , so that k is a causal propagator. The same notion of $f_1 = Kf_2$ applies.

Comment: The word "propagator" is commonly used in quantum mechanics where the entity being propagated is a probability amplitude, and the total amplitude for some "event" is the sum of all the propagated contributions. This viewpoint was promoted by Richard Feynman, and the graphical representation of equations like (1.4.12) is called a Feynman Diagram :

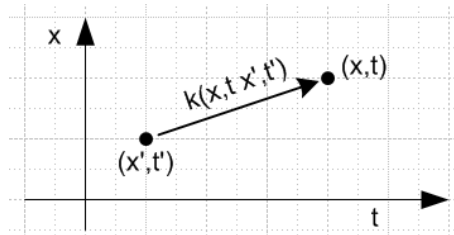


Fig 1.6

1.5 The Wave Equations in the Frequency Domain

(a) The Transformed Wave Equations

A standard method of solving wave equations involves transforming the equations from the time domain to the frequency ω domain using the Fourier Integral Transform, assuming that the μ , ϵ and σ are constants (possibly complex). As an example, we start with the ϕ equation in box (1.3.29) and expand $\phi(\mathbf{x},t)$ and $\rho_s(\mathbf{x},t)$ onto their Fourier components using (1.6.8). The overloaded notation is explained in Section 1.6 (f).

$$(\nabla^2 - \mu_d \epsilon_d \partial_t^2 - \mu_d \sigma_d \partial_t) \phi(\mathbf{x},t) = - (1/\epsilon_d) \sum_i \rho_i(\mathbf{x},t) \quad (1.3.29)$$

$$(\nabla^2 - \mu_d \epsilon_d \partial_t^2 - \mu_d \sigma_d \partial_t) \left[(1/2\pi) \int_{-\infty}^{\infty} d\omega e^{+j\omega t} \phi(\mathbf{x},\omega) \right] = - (1/\epsilon_d) \left[(1/2\pi) \int_{-\infty}^{\infty} d\omega e^{+j\omega t} \sum_i \rho_i(\mathbf{x},\omega) \right]$$

$$\int_{-\infty}^{\infty} d\omega (\nabla^2 - \mu_d \epsilon_d \partial_t^2 - \mu_d \sigma_d \partial_t) e^{+j\omega t} \phi(\mathbf{x},\omega) = - (1/\epsilon_d) \int_{-\infty}^{\infty} d\omega e^{+j\omega t} \sum_i \rho_i(\mathbf{x},\omega)$$

$$\int_{-\infty}^{\infty} d\omega (\nabla^2 + \mu_d \epsilon_d \omega^2 - j\omega \mu_d \sigma_d) e^{+j\omega t} \phi(\mathbf{x},\omega) = - (1/\epsilon_d) \int_{-\infty}^{\infty} d\omega e^{+j\omega t} \sum_i \rho_i(\mathbf{x},\omega)$$

$$\int_{-\infty}^{\infty} d\omega e^{+j\omega t} \left[(\nabla^2 + \mu_d \epsilon_d \omega^2 - j\omega \mu_d \sigma_d) \phi(\mathbf{x},\omega) \right] = \int_{-\infty}^{\infty} d\omega e^{+j\omega t} \left[- (1/\epsilon_d) \sum_i \rho_i(\mathbf{x},\omega) \right] .$$

At this point we invoke the completeness of the set of functions $\{e^{j\omega t}\}$ on the interval $(-\infty, \infty)$ to claim that the integrands must be equal, giving (1.3.29) transformed to the frequency domain,

$$(\nabla^2 + \mu_d \epsilon_d \omega^2 - j\omega \mu_d \sigma_d) \phi(\mathbf{x},\omega) = - (1/\epsilon_d) \sum_i \rho_i(\mathbf{x},\omega) .$$

or

$$(\nabla^2 + \beta_d^2) \phi(\mathbf{x},\omega) = - (1/\epsilon_d) \sum_i \rho_i(\mathbf{x},\omega)$$

where β_d^2 is the following complex "Helmholtz parameter" [of Helmholtz operator $(\nabla^2 + \beta_d^2)$],

$$\beta_d^2 = \mu_d \epsilon_d \omega^2 - j\omega \mu_d \sigma_d = \omega^2 \mu_d (\epsilon_d - j\sigma_d/\omega) = \omega^2 \mu_d \xi_d \quad \xi_d \equiv \epsilon_d - j\sigma_d/\omega . \quad (1.5.1a)$$

$$\beta_{d0}^2 = \omega^2 \mu_d \epsilon_d \quad \text{when } \sigma_d = 0 \text{ (non-conducting dielectric)} \quad (1.5.1b)$$

Here $\xi_d(\omega)$ is the "complex dielectric constant", nothing more or less than the expression shown.

We shall have occasion (mainly in Appendix D) to use the damped wave equation for the \mathbf{E} field inside a transmission line conductor. We referred to such conductors as region 2 or region 3 in the discussion above, but here we shall use no subscript to denote parameters inside a conductor. Looking at (1.3.36), such a wave equation when converted to the frequency domain becomes,

$$(\nabla^2 + \beta^2) \mathbf{E}(\mathbf{x},\omega) = 0 \quad (1.5.27)$$

where

$$\beta^2 = \mu\epsilon\omega^2 - j\omega\mu\sigma = \omega^2\mu(\epsilon - j\sigma/\omega) = \omega^2\mu\xi \quad \xi \equiv \epsilon - j\sigma/\omega \quad (1.5.1c)$$

and all parameters here refer to the conductor. This has the same form as (1.5.1a) but with no dielectric subscripts. For copper, we show later in (2.2.3) that for $f \ll 10^{18}$ Hz, one can neglect the ϵ term in the above expression for β^2 which then gives

$$\beta^2 = -j\omega\mu\sigma \quad (1.5.1d)$$

Note: Hermann von Helmholtz (1821-1894) was an early electromagnetic researcher and equations of the form $(\nabla^2 + k^2)f = g$ bear his name. As we have just seen, his equation arises from a temporal Fourier or Laplace transform of a wave equation. Since k will have another meaning in Chapter 5, and to be consistent with King p 10 (15a,b,c), we define the quantities in (1.5.1) as β^2 instead of k^2 . King bolds parameters when they are complex, but we do not, so we have β^2 instead of $\boldsymbol{\beta}^2$.

Examination of the above transformation shows that any equation can be transformed from the time domain to the frequency domain using these simple rules,

$$\partial_t \rightarrow +j\omega \quad \partial_t^2 \rightarrow -\omega^2 \quad F(\mathbf{x},t) \rightarrow F(\mathbf{x},\omega) \quad (1.5.2)$$

where it is understood (Section 1.6) that $F(\mathbf{x},t)$ and $F(\mathbf{x},\omega)$ are different functions.

Thus, the frequency-domain representations of the King-gauge potential wave equations shown in (1.3.29) are:

Potential Wave Equations in the King Gauge (ω domain)

$$(\nabla^2 + \beta_d^2)\phi = - (1/\epsilon_d) \sum_i \rho_i \quad \text{all of region R} \quad (1.5.3)$$

$$(\nabla^2 + \beta_d^2)\mathbf{A} = - \sum_i \mu_i \mathbf{J}_i \quad \text{all of region R} \quad (1.5.4)$$

$$\text{div } \mathbf{A} = - \mu_d \epsilon_d j\omega\phi - \mu_d \sigma_d \phi = -j\omega\mu_d(\epsilon_d + \sigma_d/j\omega)\phi = -j\omega\mu_d \xi_d \phi = -j(\beta_d^2/\omega)\phi \quad \text{King gauge} \quad (1.5.5)$$

$$\beta_d^2 = \mu_d \epsilon_d \omega^2 - j\omega\mu_d \sigma_d = \omega^2\mu_d(\epsilon_d - j\sigma_d/\omega) = \omega^2\mu_d \xi_d \quad \xi_d \equiv \epsilon_d - j\sigma_d/\omega \quad (1.5.1a)$$

$$\mu_d, \epsilon_d, \sigma_d = \text{dielectric} \quad 1,3,4,\dots \quad N = \text{conductors} \quad \sum_i = \sum_{i=1}^N \quad \mu_i = \text{for conductor } i$$

ρ_i = free surface charge density on conductor i

\mathbf{J}_i = free current density in conductor i (\mathbf{J} in the dielectric exists but does not appear in $\sum_i \mu_i \mathbf{J}_i$)

In these equations, all mathematical fields ϕ , \mathbf{A} , ρ_i , \mathbf{J}_i are functions of \mathbf{x} and ω . Note from (1.5.5) that in the ω domain, the King gauge is the Lorenz gauge with $\epsilon_d \rightarrow \xi_d$.

(b) The Helmholtz Integrals in the King Gauge

The next step is to solve the above equations for φ and \mathbf{A} . The method was demonstrated in Appendix A.0 and is applied again here. We first define the free-space Green's Function g by this boundary value problem,

$$-(\nabla^2 + \beta_d^2)g(\mathbf{x}, \mathbf{x}') = \delta(\mathbf{x} - \mathbf{x}') \quad \text{where} \quad \lim_{|\mathbf{x}| \rightarrow \infty} g(\mathbf{x}, \mathbf{x}') = 0 \quad . \quad (1.5.6)$$

As shown in (H.1.5), the solution to problem (1.5.6) is

$$g(\mathbf{x}, \mathbf{x}') = \frac{1}{4\pi} \frac{e^{-j\beta_d R}}{R} \quad R = |\mathbf{x} - \mathbf{x}'| \quad . \quad (1.5.7)$$

As (1.5.1a) shows, in a conducting dielectric β_d^2 has a small negative phase, so β_d has half this negative phase and β_d then has a small negative imaginary part. Then $e^{-j\beta_d R} \rightarrow 0$ for large R , as required by the condition of problem (1.5.6). This is why $e^{+j\beta_d R}/R$ is a rejected solution.

The Helmholtz equations (1.5.3) and (1.5.4) have the following particular solutions ($dV' = d^3x'$),

$$\varphi(\mathbf{x}, \omega) = \frac{1}{4\pi\epsilon} \sum_i \int \rho_i(\mathbf{x}', \omega) \frac{e^{-j\beta_d R}}{R} dV' \quad R = |\mathbf{x} - \mathbf{x}'| \quad (1.5.8)$$

$$\mathbf{A}(\mathbf{x}, \omega) = \frac{1}{4\pi} \sum_i \int \mu_i \mathbf{J}_i(\mathbf{x}', \omega) \frac{e^{-j\beta_d R}}{R} dV' \quad R = |\mathbf{x} - \mathbf{x}'| \quad . \quad (1.5.9)$$

In these equations, β_d is a function of ω , namely $\beta_d = \omega^2 \mu_d \epsilon_d$ as in (1.5.1a), and $\sum_i = \sum_{i=1}^N$ is over the conductors. Since $(\nabla^2 + \beta_d^2)$ is the Helmholtz operator, solutions of the form (1.5.8) and (1.5.9) are sometimes called "Helmholtz integrals".

To verify that the φ of (1.5.8) solves (1.5.3) we use (1.5.7) to write,

$$\varphi(\mathbf{x}, \omega) = \int [\sum_i \rho_i(\mathbf{x}', \omega)/\epsilon] g(\mathbf{x}, \mathbf{x}') dV'$$

so that,

$$\begin{aligned} -(\nabla^2 + \beta_d^2) \varphi(\mathbf{x}, \omega) &= \int [\sum_i \rho_i(\mathbf{x}', \omega)/\epsilon] \{ -(\nabla^2 + \beta_d^2)g(\mathbf{x}, \mathbf{x}') \} dV' \\ &= \int [\sum_i \rho_i(\mathbf{x}', \omega)/\epsilon] \{ \delta(\mathbf{x} - \mathbf{x}') \} d^3x' = \sum_i \rho_i(\mathbf{x}, \omega)/\epsilon \quad . \end{aligned}$$

In the limit $\omega \rightarrow 0$ we find from (1.5.1a) that $\beta_d(\omega) \rightarrow 0$ and then (1.5.9) is the same as (A.0.2) obtained from electrostatics and Poisson's Equation.

In (1.5.8) the *volume* density function $\rho_{\mathbf{s}}(\mathbf{x}',\omega) \equiv \Sigma_{\mathbf{i}}\rho_{\mathbf{i}}(\mathbf{x}',\omega)$ represents a surface charge density, so it is convenient to represent ϕ as a surface integral over the corresponding *surface* charge density $n_{\mathbf{s}}(\mathbf{x}',\omega)$,

$$\phi(\mathbf{x},\omega) = \frac{1}{4\pi\epsilon} \int n_{\mathbf{s}}(\mathbf{x}',\omega) \frac{e^{-j\beta_{\mathbf{d}}R}}{R} dS' \quad R = |\mathbf{x} - \mathbf{x}'| \quad (1.5.10)$$

Comments on n , σ and Dirichlet: Usually one uses σ for a surface charge, but σ is already used for conductivity so we use n . To further complicate things, in his potential theory discussion of Chapter 6, Stakgold uses σ to represent our surface S enclosing a volume V (his region R) as in our Fig 1.2. Stakgold uses n to indicate a normal derivative, as in this Dirichlet problem solution of the Poisson equation $-\nabla^2\phi(\mathbf{x}) = q(\mathbf{x})$,

$$\phi(\mathbf{x}) = \int_{\mathbf{R}} d\mathbf{x}' g(\mathbf{x}|\mathbf{x}') q(\mathbf{x}') - \int_{\sigma} dS_{\xi} f(\xi) \partial_{\xi n} g(\mathbf{x}|\xi) \quad // \text{ Stakgold (6.81)} \quad (1.5.11)$$

Here $\partial_{\xi n} = \partial/\partial n_{\xi}$ where n_{ξ} is a local coordinate on the surface σ at point ξ which is normal to the surface. In this equation, $q(\mathbf{x})$ is the Poisson source (think $\rho(\mathbf{x})/\epsilon_0$), $g(\mathbf{x}|\xi)$ is the *full* Green's function, meaning $g = 0$ on boundary σ , and $f(\xi)$ is the Dirichlet prescribed potential on the enclosing boundary σ . Stakgold also uses n for number of dimensions and his work is always done in n spatial dimensions.

In (1.5.11), the first term is the particular solution, like our Helmholtz integral, while the second term is a homogenous solution to $-\nabla^2\phi(\mathbf{x}) = 0$ which, when added in, makes things work at boundaries. Our Helmholtz integral, however, uses the *free-space* Green's Function, so we cannot just add on Stakgold's Dirichlet term to get a solution.

The above Poisson Dirichlet solution (1.5.11) seems mysterious at first viewing, but is easily derived using $-\nabla^2 g(\mathbf{x}|\mathbf{x}') = \delta(\mathbf{x}-\mathbf{x}')$, $-\nabla^2\phi(\mathbf{x}) = q(\mathbf{x})$ [$= \rho(\mathbf{x})/\epsilon$], and the famous Green's 2nd "symmetric" identity, where $\partial\phi/\partial n = \hat{\mathbf{n}} \cdot \nabla\phi =$ the same normal derivative $\partial_{\xi n}$ discussed above,

$$\begin{aligned} \int_{\mathbf{V}} dV \psi \nabla^2\phi &= \int_{\mathbf{S}} dS \psi (\partial\phi/\partial n) - \int_{\mathbf{V}} dV (\nabla\psi \cdot \nabla\phi) && \text{Green \#1} \\ \int_{\mathbf{V}} dV [\psi \nabla^2\phi - \phi \nabla^2\psi] &= \int_{\mathbf{S}} dS [\psi (\partial\phi/\partial n) - \phi (\partial\psi/\partial n)] \quad . && \text{Green \#2} \end{aligned} \quad (1.5.12)$$

Here #2 = #1(ψ,ϕ) - #1(ϕ,ψ) and #1 is derived from the divergence theorem (1.1.30) with $\mathbf{F} = \psi\nabla\phi$ and vector identity $\nabla \cdot (\psi\nabla\phi) = \nabla\psi \cdot \nabla\phi + \psi \nabla^2\phi$ and $d\mathbf{S} = dS \hat{\mathbf{n}}$. Green was a busy man. Equation (1.5.11) is then obtained by setting $\psi = g$ in (1.5.12), recalling that $g = 0$ on σ .

Since Green #2 is also valid if we replace $\nabla^2 \rightarrow (\nabla^2 + k^2)$, (1.5.11) is also formally valid for a Helmholtz Dirichlet problem where then g is the full Helmholtz Green's function.

(c) King's leading factor ($1/4\pi\xi$) and the final Helmholtz Integrals

This is a somewhat subtle point and something that King never discusses much in his transmission-line theory book. The issue is that there are two different entities $n_{\mathbf{s}}$ and $n_{\mathbf{c}}$ which have units charge/area, and they are related by $n_{\mathbf{s}} = (\epsilon_{\mathbf{d}}/\xi_{\mathbf{d}}) n_{\mathbf{c}}$ where $\xi_{\mathbf{d}} = \epsilon_{\mathbf{d}} + \sigma_{\mathbf{d}}/j\omega$ is the complex dielectric constant (in the dielectric) which incorporates the effect of possible dielectric conductivity. In a transmission line

problem, it is n_c that is specified by the boundary conditions and not n_s (which is the actual surface charge density). For that reason, one replaces (1.5.10) with,

$$\varphi(\mathbf{x}, \omega) = \frac{1}{4\pi\epsilon_d} \int n_c(\mathbf{x}', \omega) \frac{e^{-j\beta_d R}}{R} dS' \quad R = |\mathbf{x} - \mathbf{x}'| \quad (1.5.13)$$

which explains the leading factor $\frac{1}{4\pi\epsilon}$ which appears every time King writes down the Helmholtz integral for φ in his books. In the discussion below we describe n_c and its relation to n_s , and then we show how this relation works in the simple example of a parallel plate capacitor.

Consider the situation at a general boundary between dielectric (region 1) and conductor (region 2) where there exists a surface charge density n_s :

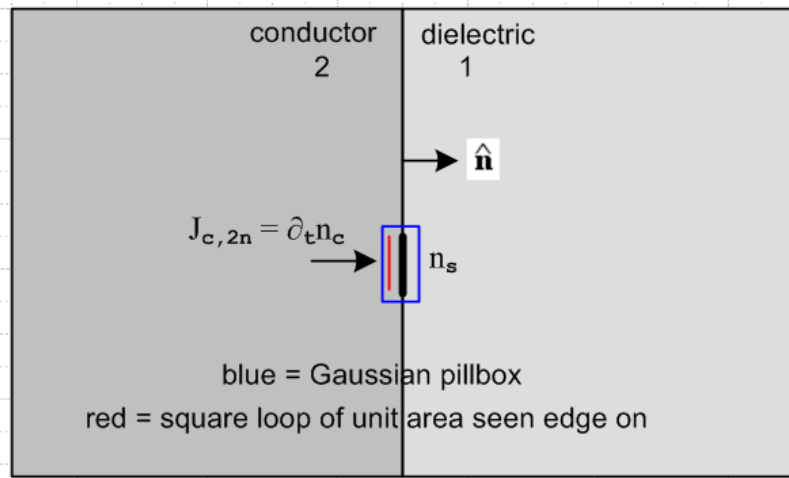


Fig 1.7

In (1.1.18) it was shown that $\text{div} [\mathbf{J}_d + \mathbf{J}_c] = 0$ where $\mathbf{J}_c = \sigma\mathbf{E}$ is the conduction current and \mathbf{J}_d the displacement current $\partial_t\mathbf{D} = \epsilon\partial_t\mathbf{E}$. The divergence theorem (1.1.30) then says

$$0 = \int_V \text{div} [\mathbf{J}_d + \mathbf{J}_c] dV = \int_S [\mathbf{J}_d + \mathbf{J}_c] \cdot d\mathbf{S} .$$

Applied to the blue pillbox which straddles the boundary in the figure, we find

$$J_{d1n} + J_{c1n} = J_{d2n} + J_{c2n}$$

where n means normal component. Writing this out,

$$\epsilon_1\partial_t E_{1n} + \sigma_1 E_{1n} = \epsilon_2\partial_t E_{2n} + \sigma_2 E_{2n} \approx \sigma_2 E_{2n} = J_{c2n}$$

since σ_2 is huge inside the conductor. Therefore,

$$J_{c2n} = \sigma_1 E_{1n} + \varepsilon_1 \partial_t E_{1n} . \quad (1.5.14)$$

Meanwhile, Gauss's Law (1.1.32) with (1.1.6) states that

$$\text{div}(\varepsilon \mathbf{E}) = \rho \quad \Leftrightarrow \quad \int_V \rho \, dV = \int_S \varepsilon \mathbf{E} \cdot d\mathbf{S} . \quad (1.1.33)$$

Applied to the same blue pillbox we find

$$\mathbf{n}_s = \varepsilon_1 E_{n1} - \varepsilon_2 E_{n2} \approx \varepsilon_1 E_{n1}$$

since $E_{n2} \approx 0$ inside the conductor. Thus,

$$E_{n1} = n_s / \varepsilon_1 \quad \text{and then} \quad J_{cn1} = \sigma_1 E_{n1} = n_s (\sigma_1 / \varepsilon_1) . \quad (1.5.15)$$

Then (1.5.14) can be written as

$$J_{c2n} = \sigma_1 E_{1n} + \varepsilon_1 \partial_t E_{1n} = (\sigma_1 + \varepsilon_1 \partial_t) E_{1n} = (1/\varepsilon_1)(\sigma_1 + \varepsilon_1 \partial_t) n_s$$

or, writing out the arguments,

$$J_{c2n}(\mathbf{x}, t) = (1/\varepsilon_1)(\sigma_1 + \varepsilon_1 \partial_t) n_s(\mathbf{x}, t) . \quad (1)$$

In the frequency domain with rules (1.5.2) this becomes

$$\begin{aligned} J_{c2n}(\mathbf{x}, \omega) &= (1/\varepsilon_1)(\sigma_1 + \varepsilon_1 j\omega) n_s(\mathbf{x}, \omega) \\ &= (1/\varepsilon_1) (j\omega)(\varepsilon_1 + \sigma_1/j\omega) n_s(\mathbf{x}, \omega) \\ &= (\xi_1/\varepsilon_1) (j\omega) n_s(\mathbf{x}, \omega) . \quad \xi_1 \equiv \varepsilon_1 + \sigma_1/j\omega = \text{complex dielectric constant} \end{aligned} \quad (1.5.16)$$

If we observe the conduction current J_{c2n} in the conductor just below the surface and flowing through a unit-area loop (red in Fig 1.7), we can write $J_{c2n} = \partial_t n_c$ where $n_c(t)$ is the total amount of conduction charge flowing through that unit-area loop from some initial time t_0 to the current time t (one could take t_0 to be 1 time unit before t , for example),

$$J_{c2n}(\mathbf{x}, t) = \partial_t n_c(\mathbf{x}, t) \quad n_c(\mathbf{x}, t) = \int_{t_0}^t dt' J_{c2n}(\mathbf{x}, t') . \quad (2)$$

or

$$J_{c2n}(\mathbf{x}, \omega) = j\omega n_c(\mathbf{x}, \omega) . \quad (3)$$

Thus we have,

$$\partial_t n_c(\mathbf{x}, t) = (1/\varepsilon_1)(\sigma_1 + \varepsilon_1 \partial_t) n_s(\mathbf{x}, t) \quad // \text{ from (1) and (2)}$$

or

$$j\omega n_c(\mathbf{x},\omega) = (\xi_1/\varepsilon_1) (j\omega) n_s(\mathbf{x},\omega) \quad // \text{ from (3) and (1.5.16)}$$

or

$$n_c(\mathbf{x},\omega) = (\xi_1/\varepsilon_1) n_s(\mathbf{x},\omega) . \quad // \text{ divide by } j\omega \quad (1.5.17)$$

where is our result claimed at the start that $n_s = (\varepsilon_d/\xi_d) n_c$. Note that:

- The quantity n_s is the amount of free charge per unit area on the conductor surface.
- The quantity n_c does not represent any kind of surface charge anywhere (free or otherwise).

n_c is related to the transport of conduction charge carriers through the charge-neutral interior of the conductor just below the surface. There is no unit-area surface which holds n_c amount of charge, but both n_s and n_c have the dimensions of charge/area so both could be called "surface charge".

These two areal charge densities are different simply because the dielectric leaks charge off the surface. We are now going to rederive (1.5.17) a different way. We can write, using the blue pillbox of Fig 1.7 and continuity relation (1.1.25),

$$\text{div } \mathbf{J}_c = -\partial_t \rho_{free} \quad \Leftrightarrow \quad -\partial_t \left[\int_V \rho_{free} dV \right] = \int_S \mathbf{J}_c \cdot d\mathbf{S} . \quad (1.1.25)$$

$$\Rightarrow -\partial_t \left[\int_V n_s dS \right] = \int_S \mathbf{J}_c \cdot d\mathbf{S}$$

$$\Rightarrow -\partial_t n_s = J_{cn1} - J_{cn2} = \sigma_1(n_s/\varepsilon_1) - \partial_t n_c \quad // \text{ see above: } J_{cn1} = \sigma_1(n_s/\varepsilon_1), J_{cn2} = \partial_t n_c$$

so

$$\partial_t n_s = \partial_t n_c - \sigma_1(n_s/\varepsilon_1) \quad // \text{ change in } n_s = \text{flow in} - \text{flow out}$$

or

$$j\omega n_s = j\omega n_c - \sigma_1 n_s / \varepsilon_1 \quad \Rightarrow \quad (j\omega + \sigma_1/\varepsilon_1) n_s = j\omega n_c \quad \Rightarrow \quad (j\omega \varepsilon_1 + \sigma_1) n_s = j\omega \varepsilon_1 n_c$$

$$\Rightarrow (\varepsilon_1 + \sigma_1/j\omega) n_s = \varepsilon_1 n_c \quad \Rightarrow \quad \xi_1 n_s = \varepsilon_1 n_c \quad \Rightarrow \quad n_c = (\xi_1/\varepsilon_1) n_s$$

which is the same as (1.5.17). Note that if surface charge n_s is real, n_c is complex.

It is useful at this point to examine the simple case of a parallel plate capacitor to see the meaning of n_s and n_c . The plate separation s is meant to be very small compared to the transverse dimensions of the plates, so the picture is distorted. We drop the subscript 1 on dielectric properties.

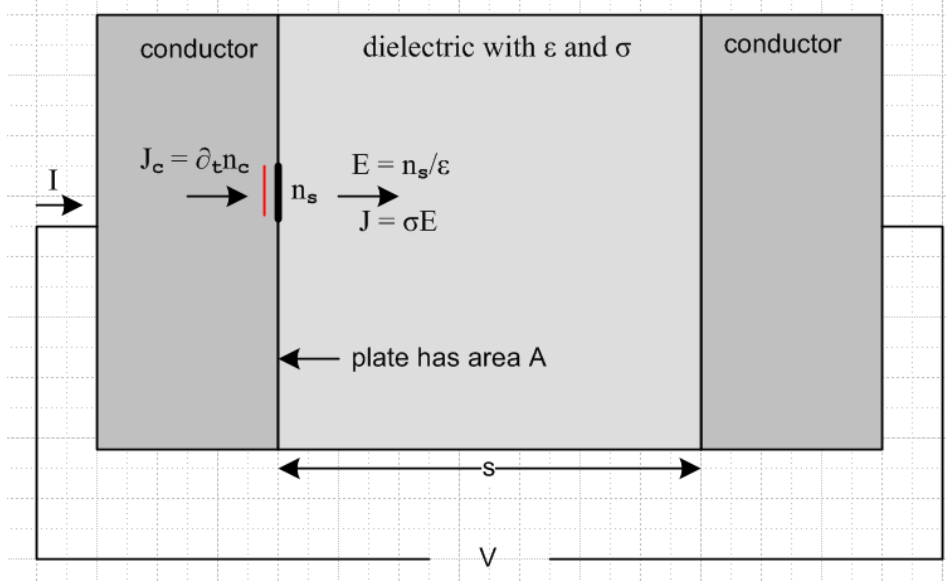


Fig 1.8

First off, a DC analysis of the above device shows that the capacitor has resistance R ,

$$R = \frac{V}{I} = \frac{V}{JA} = \frac{Es}{\sigma_d EA} = (s/\sigma_d A) . \quad (1.5.18)$$

Now we assume an AC voltage V . The total current entering the conducting capacitor is $I = J_c A$. If we think of $I = \partial_t Q$ then Q is the amount of charge passing through the external wire per unit time. Q is *not* the total charge on the left plate surface which in fact is $Q_s = n_s A$. Since $I = J_c A$ we have $\partial_t Q = (\partial_t n_c) A$ and therefore $Q = n_c A$.

Meanwhile, the voltage V between the plates is $V = Es$, and we know that $E = n_s/\epsilon_d$ from Gauss's law (ignoring E inside the conductor). Thus $V = (s/\epsilon_d)n_s$.

If we define the (complex) capacitance by $Q = C'V$, then

$$C' = \frac{Q}{V} = \frac{n_c A}{(s/\epsilon_d)n_s} = \frac{n_c}{n_s} (A\epsilon_d/s) = (\xi_d/\epsilon_d) (A\epsilon_d/s) = (\xi_d/\epsilon_d) C = (A\xi_d/s) . \quad (1.5.19)$$

The capacitance C' is complex because it accounts for both the capacitance and conductance of the dielectric,

$$C' = \frac{\epsilon_d + \sigma_d/j\omega}{\epsilon_d} (A\epsilon_d/s) = (A\epsilon_d/s) + (\sigma_d A/s)/(j\omega) = C + 1/(j\omega R) \quad (1.5.20)$$

or

$$j\omega C' = j\omega C + 1/R = j\omega C + G \quad G = \text{conductance} = 1/R = (\sigma_d A/s) = (A\epsilon_d/s)(\sigma_d/\epsilon_d) = C (\sigma_d/\epsilon_d)$$

or

$$\frac{1}{Z} = \frac{1}{X_c} + \frac{1}{R} \quad Z = X_c' = \frac{1}{j\omega C'} \quad X_c = \frac{1}{j\omega C} \quad (1.5.21)$$

which is the rule for computing an impedance Z for a capacitor and resistor in parallel

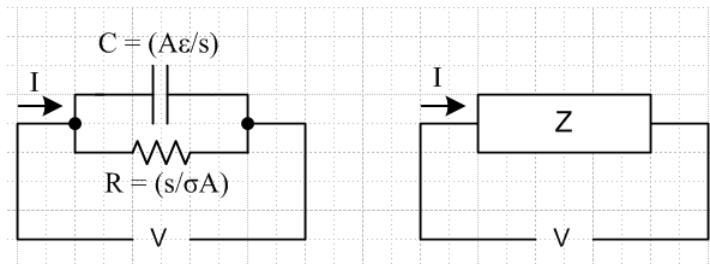


Fig 1.9

Looking back at this example, it is clear that if one wants to compute the complete impedance of the conducting capacitor, one uses $C' = Q/V$ where $Q = An_c$. The ratio Q_s/V gives only the capacitance C .

$$\frac{Q_s}{V} = \frac{n_s A}{(s/\epsilon_d)n_s} = (A\epsilon_d/s) = C . \quad (1.5.22)$$

In this conducting capacitor problem, the boundary conditions are the voltage V or the total current I . Specification of the current $I = \partial_\epsilon(n_c A)$ is really a specification of n_c since in the frequency domain we then have $I = j\omega An_c$. In analyzing the problem in full, we are thus interested in working with n_c and not n_s .

So recalling now the King gauge Helmholtz integral for φ ,

$$\varphi(\mathbf{x}, \omega) = \frac{1}{4\pi\epsilon} \int n_s(\mathbf{x}', \omega) \frac{e^{-j\beta_d R}}{R} dS' \quad R = |\mathbf{x} - \mathbf{x}'| , \quad (1.5.10)$$

since it will be more convenient to have n_c in the integrand, we use (1.5.17) that $n_s = (\epsilon_d/\xi) n_c$ to rewrite the above expression as

$$\varphi(\mathbf{x}, \omega) = \frac{1}{4\pi\xi_d} \int n_c(\mathbf{x}', \omega) \frac{e^{-j\beta_d R}}{R} dS' \quad R = |\mathbf{x} - \mathbf{x}'| \quad (1.5.13)$$

which is just (1.5.13) stated earlier.

So here are our final forms of the Helmholtz integrals of interest, where now write $n_c = \sum_i n_{ci}$,

$$\varphi(\mathbf{x}, \omega) = \frac{1}{4\pi\xi_d} \sum_i \int n_{ci}(\mathbf{x}', \omega) \frac{e^{-j\beta_d R}}{R} dS' \quad R = |\mathbf{x} - \mathbf{x}'| \quad (1.5.13)$$

$$\mathbf{A}(\mathbf{x}, \omega) = \frac{1}{4\pi} \sum_i \int \mu_i \mathbf{J}_i(\mathbf{x}', \omega) \frac{e^{-j\beta_d R}}{R} dV' \quad R = |\mathbf{x} - \mathbf{x}'| \quad (1.5.9)$$

$$\beta_d^2 = \mu_d \epsilon_d \omega^2 - j\omega \mu_d \sigma_d = \omega^2 \mu_d (\epsilon_d - j\sigma_d/\omega) = \omega^2 \mu_d \xi_d \quad \xi_d \equiv \epsilon_d - j\sigma_d/\omega \quad (1.5.1)$$

where the sum \sum_i is over all conductors. If all conductor have the same $\mu_i = \mu_c$, (1.5.9) simplifies to

$$\mathbf{A}(\mathbf{x}, \omega) = \frac{\mu_c}{4\pi} \sum_i \int \mathbf{J}_i(\mathbf{x}', \omega) \frac{e^{-j\beta_d R}}{R} dV' \quad R = |\mathbf{x} - \mathbf{x}'| \quad (1.5.9)'$$

We now quote directly from King's *Transmission-Line Theory* book to show how he presents the Helmholtz integrals for ϕ and \mathbf{A} . What we call the King gauge appears as (2b). His symbols σ , ϵ , μ , ξ and β apply to the dielectric.

$$-\text{grad } \phi = \mathbf{E} + \frac{\partial \mathbf{A}}{\partial t} \quad (1)$$

$$\text{curl } \mathbf{A} = \mathbf{B} \quad (2a)$$

$$\text{div } \mathbf{A} = -\sigma \mu \phi - \epsilon \mu \frac{\partial \phi}{\partial t} \quad (2b)$$

// page 8

$$\beta^2 \equiv \omega^2 \mu \xi \quad (10)$$

// page 9

$$\phi = \frac{1}{4\pi\xi} \iint \mathbf{n}' \frac{e^{-j\beta R}}{R} dS' \quad (23)$$

$$\mathbf{A} = \frac{1}{4\pi\mathbf{v}} \iiint \mathbf{i}' \frac{e^{-j\beta R}}{R} dV' \quad (24)$$

where \mathbf{n}' is the charge density on the surface element dS' of the conduc-

// page 11

Comments:

(1) King's (23) and (24) are for one conductor, while our (1.5.13) and (1.5.9) are for several conductors.

(2) Due to time lag effects, ϵ and σ may be complex, so $\epsilon = \epsilon' - j\epsilon''$ and $\sigma = \sigma' - j\sigma''$. In this case

$$\xi_d \equiv \epsilon_d - j\sigma_d/\omega = (\epsilon'_d - j\epsilon''_d) - j(\sigma'_d - j\sigma''_d)/\omega = [\epsilon'_d - \sigma''_d/\omega] - j[\sigma'_d + \omega\epsilon''_d]/\omega = \epsilon_{eff} - j\sigma_{eff}/\omega$$

so one would replace $\epsilon_d \rightarrow \epsilon_{eff}$ and $\sigma_d \rightarrow \sigma_{eff}$ in all equations (see King p 9 footnote).

(3) In the same way, time lag effects can cause $\mu = \mu' - j\mu''$ (hysteresis) [generic μ]

(4) King uses bold font for vectors *and* for quantities which are complex. For example his ξ of $\xi = \epsilon - j\sigma/\omega$ is bolded. Similarly, our (1.5.1) that $\beta^2 = \omega^2 \mu \xi$ becomes his equation (10) above, $\beta^2 = \omega^2 \boldsymbol{\mu} \boldsymbol{\xi}$. He does not use d subscripts on dielectric parameters as we do.

(5) King assumes that all conductors *and* the dielectric have the same μ , something we did not assume. In order to make (23) and (24) look as similar as possible, he defines $\mathbf{v} \equiv 1/\mu$. Since these parameters can both be complex, he writes them as $\boldsymbol{\mu}$ and \mathbf{v} . This then explains the factor $1/(4\pi\mathbf{v})$ appearing in his (24) which then agrees with our (1.5.9)'.

(6) He shows his equation (23) charge density \mathbf{n}' in bold, indicating it is complex. His \mathbf{n}' is our n_c , also complex. He refers to \mathbf{n}' as "charge density on the surface" but he really means it to be n_c as we have discussed at length above, and this is how he uses it in his calculations.

King uses these Helmholtz integrals (23) and (24) for φ and \mathbf{A} extensively in his book to compute the parameters of various complicated transmission line geometries and interfaces. We shall pursue this subject more in Chapter 4 for some simple cases.

We should point out that King makes no attempt to derive his equations (23) and (24) and more or less just pulls them out of a hat. We spent some time perusing several of King's other 11 books looking for some kind of derivation but were unsuccessful. The equations do appear in more or less the same form in his earliest book *Electromagnetic Engineering* (1945). So in some sense, we have spent the first 40 pages of this Chapter deriving his equations (23) and (24). For that reason, it is worth gathering up the results in a summary box:

Potential Solutions for φ and \mathbf{A} in the King Gauge	(ω space)	(1.5.23)
$\varphi(\mathbf{x}, \omega) = \frac{1}{4\pi\zeta_d} \sum_i \int n_{ci}(\mathbf{x}', \omega) \frac{e^{-j\beta_d R}}{R} dS'$	$R = \mathbf{x} - \mathbf{x}' $	(1.5.13)
$\varphi(\mathbf{x}, \omega) = \frac{1}{4\pi\zeta_d} \sum_i \int \rho_{ci}(\mathbf{x}', \omega) \frac{e^{-j\beta_d R}}{R} dV'$	// using volume charge representation $\rho_c dV' = n_c dS'$	
$\mathbf{A}(\mathbf{x}, \omega) = \frac{1}{4\pi} \sum_i \int \mu_i \mathbf{J}_i(\mathbf{x}', \omega) \frac{e^{-j\beta_d R}}{R} dV'$		(1.5.9)
$\mathbf{A}(\mathbf{x}, \omega) = \frac{\mu}{4\pi} \sum_i \int \mathbf{J}_i(\mathbf{x}', \omega) \frac{e^{-j\beta_d R}}{R} dV'$	// if all $\mu_i = \mu$	(1.5.9)'
$\mu_d, \epsilon_d, \sigma_d =$ dielectric; $\mu_i =$ inside conductor i ;		
$\beta_d^2 = \mu_d \epsilon_d \omega^2 - j\omega \mu_d \sigma_d = \omega^2 \mu_d (\epsilon_d - j\sigma_d/\omega) = \omega^2 \mu_d \zeta_d$	$\zeta_d \equiv \epsilon_d - j\sigma_d/\omega$	(1.5.1a)
$\text{div } \mathbf{A} = -\mu_d \epsilon_d j\omega \varphi - \mu_d \sigma_d \varphi = -j\omega \mu_d (\epsilon_d + \sigma_d/j\omega) \varphi = -j\omega \mu_d \zeta_d \varphi$	// King gauge	(1.5.5)
$\mathbf{B} = \text{curl } \mathbf{A}$	$\mathbf{E} = -\text{grad } \varphi - \partial_t \mathbf{A}$	(1.3.1)

The Helmholtz integrals are just "particular solutions" to the potential wave equations. In order to solve a problem, one must add to these particular solutions whatever homogeneous solutions are necessary in order to match all boundary conditions.

(d) Frequency domain wave equations for fields and potentials in the Lorenz Gauge

We now use the earlier notation with reference to Fig 1.5 where dielectric = 1 and conductors = 2,3...N+1 for N conductors. The Lorenz gauge condition is given by (1.3.30) transformed to the ω domain,

$$\text{div} \mathbf{A} = -\mu_1 \epsilon_1 j \omega \phi . \quad (1.5.24)$$

Undamped Lorenz-gauge *potential* wave equations (1.3.32) and (1.3.31) : $k_1^2 = \omega^2 \mu_1 \epsilon_1$

$$\begin{aligned} (\nabla^2 + k_1^2) \phi &= - (1/\epsilon_1) \sum_{i=2}^{N+1} \rho_i && \text{all of region R} \\ (\nabla^2 + k_1^2) \mathbf{A} &= - \sum_{i=1}^{N+1} \mu_i \mathbf{J}_i && \text{all of region R} \end{aligned} \quad (1.5.25)$$

In the Lorenz gauge, the potential wave equations don't have damped operator versions. However, for the field wave equations (which know nothing of gauge) we can write both undamped and damped versions:

Undamped *field* wave equations (1.3.35) : $k_i^2 = \omega^2 \mu_i \epsilon_i$

$$\begin{aligned} (\nabla^2 + k_1^2) \mathbf{E} &= \mu_1 j \omega \mathbf{J}_1 + (1/\epsilon_1) \sum_{i=2}^{N+1} \text{grad } \rho_i && (\nabla^2 + k_1^2) \mathbf{B} = -\mu_1 \text{curl } \mathbf{J}_1 && // \text{ region 1} \\ (\nabla^2 + k_2^2) \mathbf{E} &= \mu_2 j \omega \mathbf{J}_2 && (\nabla^2 + k_2^2) \mathbf{B} = -\mu_2 \text{curl } \mathbf{J}_2 && // \text{ region 2} \\ (\nabla^2 + k_3^2) \mathbf{E} &= \mu_3 j \omega \mathbf{J}_3 && (\nabla^2 + k_3^2) \mathbf{B} = -\mu_3 \text{curl } \mathbf{J}_3 && // \text{ region 3} \end{aligned} \quad (1.5.26)$$

Damped *field* wave equations (1.3.36) : $\beta_i^2 = \omega^2 \mu_i \xi_i$

$$\begin{aligned} (\nabla^2 + \beta_1^2) \mathbf{E} &= (1/\epsilon_1) \sum_{i=2}^{N+1} \text{grad } \rho_i && (\nabla^2 + \beta_1^2) \mathbf{B} = 0 && // \text{ region 1} \\ (\nabla^2 + \beta_2^2) \mathbf{E} &= 0 && (\nabla^2 + \beta_2^2) \mathbf{B} = 0 && // \text{ region 2} \\ (\nabla^2 + \beta_3^2) \mathbf{E} &= 0 && (\nabla^2 + \beta_3^2) \mathbf{B} = 0 && // \text{ region 3} \end{aligned} \quad (1.5.27)$$

These last equations follow from the previous set using $\mathbf{J}_i = \sigma_i \mathbf{E}$ and $\text{curl } \mathbf{J}_i = \sigma_i \text{curl } \mathbf{E} = -j \omega \sigma_i \mathbf{B}$.

The solution method was outlined earlier: for each inhomogeneous equation compute the particular solution as a Helmholtz integral, then for all equations identify generic homogeneous solutions with unknown constants, and finally determine those constants using boundary conditions from box (1.1.51). The potential approach has the advantage of a single wave operator and only two equations, while the damped field approach has the advantage of not involving any currents, but the disadvantage of having three times more equations and requiring computation of $\text{grad } \rho_i$. There is a lot more to keep track of. These are all of course *vector* Helmholtz equations.

In a problem having only a single region (having μ, ϵ, σ) containing current density \mathbf{J} and charge density ρ (perhaps inside the region, perhaps just on the surface), the Lorenz-gauge potential wave equations above in (1.5.25) may be written

$$\begin{aligned} (\nabla^2 + k^2) \phi &= - (1/\epsilon) \rho && k^2 = \omega^2 \mu \epsilon && \text{all of region R} \\ (\nabla^2 + k^2) \mathbf{A} &= - \mu \mathbf{J} && k^2 = \omega^2 \mu \epsilon && \text{all of region R} \end{aligned} \quad (1.5.28)$$

These equations may be derived directly from the single-region field wave equations (1.2.1) and (1.2.2) converted to the frequency domain,

$$\begin{aligned} (\nabla^2 + k^2)\mathbf{E} &= j\omega\mu\mathbf{J} + (1/\varepsilon)\text{grad } \rho & k^2 &= \omega^2\mu\varepsilon \\ (\nabla^2 + k^2)\mathbf{B} &= -\mu\text{curl } \mathbf{J} \end{aligned} \quad (1.5.29)$$

Each of these last four equations has its own Helmholtz integral,

$$\begin{aligned} \varphi(\mathbf{x},\omega) &= \frac{1}{4\pi\varepsilon} \int \rho(\mathbf{x}',\omega) \frac{e^{-jkR}}{R} dV' & R &= |\mathbf{x} - \mathbf{x}'| & k^2 &= \omega^2\mu\varepsilon \\ \mathbf{A}(\mathbf{x},\omega) &= \frac{\mu}{4\pi} \int \mathbf{J}(\mathbf{x}',\omega) \frac{e^{-jkR}}{R} dV' \end{aligned} \quad (1.5.30)$$

$$\begin{aligned} \mathbf{E}(\mathbf{x},\omega) &= -\frac{1}{4\pi} \int [j\omega\mu\mathbf{J}(\mathbf{x}',\omega) + (1/\varepsilon)\text{grad } \rho(\mathbf{x}',\omega)] \frac{e^{-jkR}}{R} dV' \\ \mathbf{B}(\mathbf{x},\omega) &= \frac{\mu}{4\pi} \int [\text{curl } \mathbf{J}(\mathbf{x}',\omega)] \frac{e^{-jkR}}{R} dV' \end{aligned} \quad (1.5.31)$$

The $\mathbf{A}(\mathbf{x},\omega)$ Helmholtz integral (1.5.30) appears on Jackson p 408, Eq. (9.3), with $j \rightarrow -i$ and $\mu \rightarrow \mu_0$.

For this same single-region problem, the damped wave equation (1.5.27) becomes

$$\begin{aligned} (\nabla^2 + \beta^2)\mathbf{E} &= (1/\varepsilon)\text{grad } \rho & \beta^2 &= \omega^2\mu\xi \\ (\nabla^2 + \beta^2)\mathbf{B} &= 0 \end{aligned} \quad (1.5.32)$$

where again ρ might be in the volume and/or on the surface of the volume. This follows directly from (1.5.29) using the methods above.

(e) Self Consistency of Helmholtz Integral Solutions

The various Helmholtz partial differential equations encountered in the previous sections have solutions expressed as "Helmholtz integrals". In particular, our King gauge Helmholtz integrals for the potentials have this form,

$$\varphi(\mathbf{x},\omega) = \frac{1}{4\pi\varepsilon_d} \sum_i \int n_{ci}(\mathbf{x}',\omega) \frac{e^{-j\beta_d R}}{R} dS' \quad R = |\mathbf{x} - \mathbf{x}'| \quad (1.5.13)$$

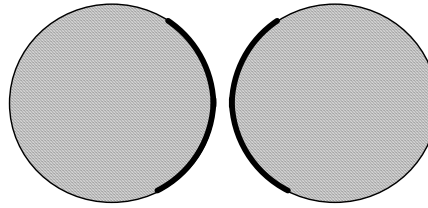
$$\mathbf{A}(\mathbf{x},\omega) = \frac{1}{4\pi} \sum_i \int \mu_i \mathbf{J}_i(\mathbf{x}',\omega) \frac{e^{-j\beta_d R}}{R} dV' \quad (1.5.9)$$

These equations sometimes give the impression that one can willy-nilly specify an arbitrary charge distribution n_{ci} and an arbitrary current distribution \mathbf{J}_i for a set of transmission line conductors and then these Helmholtz integrals will generate the correct potentials \mathbf{A} and φ from which the correct fields \mathbf{E} and \mathbf{B} may be obtained using (1.3.1),

$$\mathbf{B} = \text{curl } \mathbf{A} \quad \mathbf{E} = -\text{grad } \varphi - j\omega\mathbf{A} \quad (1.3.1)$$

This is a false impression for one to infer from the discussion of the previous sections.

For example, in a "fat twinlead" transmission line of the kind to be mentioned in Section 2.5 below,



Fat twinlead

Fig 2.16

the charge and current densities are extremely non-uniform. One cannot arbitrarily specify for this problem a uniform n and J_z distribution in each conductor and expect the resultant \mathbf{E} and \mathbf{B} fields to be correct.

The issue here is that solutions have to be self-consistent. Suppose one *were* to specify for the above fat twin-lead problem a uniform n and J_z . That is to say, one specifies that surface charge n is uniform around each circular cross section perimeter, and J_z is uniform across each disk area. The Helmholtz integrals shown above would then yield some \mathbf{A} and φ and that in turn would yield some \mathbf{E} and \mathbf{B} for the fields in the dielectric between the conductors. One could then compute from the \mathbf{E} field the value of surface charge n on each conductor using (1.1.47) $n = \epsilon_d E_n$, where E_n is the normal \mathbf{E} field just above the conductor surface. Similarly, one could compute conduction currents in the conductors perhaps from $\mathbf{J} = (1/\mu)\text{curl } \mathbf{B} - j\omega\epsilon\mathbf{E}$ which is Maxwell (1.1.1). One would find, unfortunately, that the resulting n and \mathbf{J} did not agree with the initially assumed values of n and \mathbf{J} . Such a "solution" is then meaningless because it is not self-consistent.

All real-world Maxwell equation problems tend to have this circular aspect which makes solutions more difficult than the solution of idealized problems. A problem mentioned elsewhere in this document is that of a radiating dipole antenna. One can assume a certain sine shaped current pattern in the antenna, compute from it the potentials and fields, and one will find when the antenna current is back-computed from those fields that the pattern is not quite a sine pattern unless the wire is infinitely thin.

There are then two useful conclusions to be drawn here.

First, if transmission line conductors *are* very thin relative to their spacing, it is just fine to assume a uniform charge and current distribution in those wires, since the actual non-uniformity will have only a small effect on the solutions.

Second, a general method of solution is to start with some charge and current distributions that seem reasonable based on one's general analysis of a problem. One can then find the back-computed charges and currents, and adjust the input model accordingly. This would be the basis of either an analytic iterative procedure, where the model has some adjustable parameters, or of a numerical procedure where the model is the set of values that comprise the charge and current distribution and some kind of iterative "relaxation" method then produces self-consistent solutions.

We note that the exact solution of the "fat twin lead" transmission line is derived in Chapter 6 by a method which bypasses this iterative process, and which works only due to the simple nature of the geometry.

1.6 Reinterpretation of all equations in terms of complex functions

It seemed useful to defer the topics of this section to avoid cluttering up the preceding five sections. The Fourier Transform has already been used in the previous two sections, and here we discuss it more formally as a motivating factor in changing our point of view from real to complex functions. The general nature of the Fourier Transform of complex monochrome ($e^{j\omega t}$) fields sets the stage for the analysis of the round wire in Chapter 2.

(a) Complex Functions

Up to this point, we have been regarding the following fields as representing real physical quantities,

$$\begin{array}{cccc} \mathbf{H}(\mathbf{x},t) & \mathbf{D}(\mathbf{x},t) & \mathbf{J}(\mathbf{x},t) & \mathbf{A}(\mathbf{x},t) \\ \mathbf{B}(\mathbf{x},t) & \mathbf{E}(\mathbf{x},t) & \rho(\mathbf{x},t) & \varphi(\mathbf{x},t) \end{array} \quad (1.6.1)$$

The fields, potentials and sources exist in the real physical world and are related by equations involving real operators like curl and $\partial/\partial t$. We can represent such an equation as $L_{\mathbf{x},t}f(\mathbf{x},t) = g(\mathbf{x},t)$ where $L_{\mathbf{x},t}$ is some real differential operator and f and g are real fields.

One can extend f and g such that f and g are either both the real or both the imaginary parts of complex functions F and G . Then the equation $L_{\mathbf{x},t}F(\mathbf{x},t) = G(\mathbf{x},t)$ represents two distinct physical equations which we can write as

$$\begin{array}{l} L_{\mathbf{x},t}F(\mathbf{x},t) = G(\mathbf{x},t) \quad \Rightarrow \quad L_{\mathbf{x},t}[f(\mathbf{x},t) + jf'(\mathbf{x},t)] = [g(\mathbf{x},t) + jg'(\mathbf{x},t)] \quad \Rightarrow \\ L_{\mathbf{x},t}f(\mathbf{x},t) = g(\mathbf{x},t) \quad \quad \quad F(\mathbf{x},t) = f(\mathbf{x},t) + jf'(\mathbf{x},t) \\ L_{\mathbf{x},t}f'(\mathbf{x},t) = g'(\mathbf{x},t) \quad \quad \quad G(\mathbf{x},t) = g(\mathbf{x},t) + jg'(\mathbf{x},t) \end{array} \quad (1.6.2)$$

It is convenient to regard all the mathematical fields listed above in (1.6.1) as complex fields like F and G . For example, we might write the Maxwell curl \mathbf{E} equation (1.1.2) in this manner

$$\begin{array}{l} \text{curl } \mathbf{E}(\mathbf{x},t) = -\partial \mathbf{B}(\mathbf{x},t)/\partial t \quad \quad \quad \mathbf{E}(\mathbf{x},t) = \mathbf{e}(\mathbf{x},t) + j \mathbf{e}'(\mathbf{x},t) \\ \quad \quad \quad \quad \quad \quad \quad \quad \quad \quad \quad \quad \quad \quad \quad \mathbf{B}(\mathbf{x},t) = \mathbf{b}(\mathbf{x},t) + j \mathbf{b}'(\mathbf{x},t) \end{array} \quad (1.6.3)$$

where $\mathbf{e} = \text{Re}(\mathbf{E})$ and $\mathbf{e}' = \text{Im}(\mathbf{E})$ and similarly for the \mathbf{B} field.

The single left equation of (1.6.3) then represents these two different physical equations with real fields

$$\begin{array}{l} \text{curl } \mathbf{e}(\mathbf{x},t) = -\partial \mathbf{b}(\mathbf{x},t)/\partial t \\ \text{curl } \mathbf{e}'(\mathbf{x},t) = -\partial \mathbf{b}'(\mathbf{x},t)/\partial t \end{array} \quad (1.6.4)$$

Thus, one can regard one's physical fields as either the real or imaginary parts of the complex fields.

(b) Monochrome time

The classic application of this idea is the assumption that some complex field is "monochrome" (monochromatic) in its time dependence, meaning for example,

$$E_i(\mathbf{x}, t) = e^{j[\omega_1 t + \varphi_i(\mathbf{x}, \omega_1)]} E_i(\mathbf{x}, \omega_1) = e^{j\omega_1 t} e^{j\varphi_i(\mathbf{x}, \omega_1)} E_i(\mathbf{x}, \omega_1) , \quad (1.6.5)$$

where $E_i(\mathbf{x}, \omega_1) = |E_i(\mathbf{x}, t)|$ is real. Index i denotes a field component in an arbitrary coordinate system, not just Cartesian coordinates. All time dependence is in the $e^{j\omega_1 t}$ factor and all spatial dependence is in the factor $[e^{j\varphi_i(\mathbf{x}, \omega_1)} E_i(\mathbf{x}, \omega_1)]$ -- separation of variables. This monochrome field might be regarded as a probe or driver of some system and the solution fields $E_i(\mathbf{x}, t)$ and phases $\varphi_i(\mathbf{x}, \omega_1)$ might depend parametrically on the probe frequency ω_1 as well as on position \mathbf{x} .

For (1.6.5) the corresponding physical field assumption is either of these equations,

$$\begin{aligned} e_i(\mathbf{x}, t) &= \text{Re}\{E_i(\mathbf{x}, t)\} = \cos[\omega_1 t + \varphi_i(\mathbf{x}, \omega_1)] E_i(\mathbf{x}, \omega_1) \\ e'_i(\mathbf{x}, t) &= \text{Im}\{E_i(\mathbf{x}, t)\} = \sin[\omega_1 t + \varphi_i(\mathbf{x}, \omega_1)] E_i(\mathbf{x}, \omega_1) . \end{aligned} \quad (1.6.6)$$

We stress again that the phase $\varphi_i(\mathbf{x}, \omega_1)$ might depend on both \mathbf{x} and ω_1 . A good prototype 1D example for the ω_1 dependence of phase $\varphi_1(\mathbf{x}, \omega_1)$ is a damped harmonic oscillator with resonant frequency ω_0 which is driven at frequency ω_1 , $\ddot{x} + (1/\tau)\dot{x} + \omega_0^2 x = k \sin(\omega_1 t)$. The solution is,

$$x(t) = x(0) \sin[\omega_1 t + \varphi(\omega_1)] \quad \tan \varphi(\omega_1) = -(\omega_1/\tau)/(\omega_0^2 - \omega_1^2) .$$

Of course the solution function $x(t)$ is not a field over \mathbb{R}^3 , so in this case the phase φ has no \mathbf{x} dependence.

Comments:

1. The assumed form (1.6.5) is the most general form one can have for a monochrome field. One can always assume a more restrictive form for a certain type of problem and see where it leads. Such a restricted form is an "ansatz" form meaning that one assumes that restricted form and then one tries to find the solution to a specific problem with the \mathbf{E} field so restricted. If a solution is found which satisfies Maxwell's equations, then the ansatz form is justified. For example, one might use the more restrictive ansatz where $\varphi_i(\mathbf{x}, \omega) = \varphi_i(\omega)$, or even more restrictive with $\varphi_i(\mathbf{x}, \omega) = \varphi_i$, a constant.

2. For a wave problem, one might try the following ansatz form which is a restriction of (1.6.5),

$$E_i(x, y, z, t) = e^{j(\omega_1 t - \mathbf{kz})} e^{j\varphi_i(\mathbf{x}, \mathbf{y}, \omega_1)} E_i(x, y, \omega_1) \quad (1.6.7)$$

where $E_i(x, y, \omega_1)$ is real. In this form the entire dependence on t and z is exposed in the first factor, so the solution then represents a wave traveling in the z direction.

3. Note in (1.6.5) that the phase function $\varphi_i(\mathbf{x}, \omega_1)$ can be different for different components $E_i(\mathbf{x}, t)$. Appendix D studies the fields inside a round wire and the three field components E_z , E_r and E_θ do indeed have different phases for that problem.

(c) Why complex fields: The Fourier Transform

The reason for using a complex field like $\mathbf{E}(\mathbf{x}, t)$ instead of the real field $\mathbf{e}(\mathbf{x}, t)$ has to do with the Fourier Transform (or the Laplace Transform). This transform is almost always needed to solve a non-trivial problem involving Maxwell's equations, and we saw it in action in Section 1.5. With the convention that the $(1/2\pi)$ goes in the expansion formula along with $e^{+j\omega t}$, we write the **Fourier Integral Transform** as :
[for want of a better notation, $f^\wedge(\omega)$ is the transform of $f(t)$]

$$\mathbf{E}^\wedge(\mathbf{x}, \omega) = \int_{-\infty}^{\infty} dt \mathbf{E}(\mathbf{x}, t) e^{-j\omega t} \quad \text{projection = transform} \quad (1.6.8a)$$

$$\mathbf{E}(\mathbf{x}, t) = (1/2\pi) \int_{-\infty}^{\infty} d\omega \mathbf{E}^\wedge(\mathbf{x}, \omega) e^{+j\omega t} \quad \text{expansion = inverse transform = recovery} \quad (1.6.8b)$$

Here $\mathbf{E}(\mathbf{x}, t)$ is the original complex field whose real and imaginary parts are physical fields as in (1.6.3) or (1.6.6), while $\mathbf{E}^\wedge(\mathbf{x}, \omega)$ is the Fourier Transform of $\mathbf{E}(\mathbf{x}, t)$.

As (1.6.8) shows, the dimensional units of the temporal Fourier transform of some quantity have an extra sec factor. For example, since $\dim[\mathbf{E}(\mathbf{x}, t)] = \text{volt/m}$, it follows that $\dim[\mathbf{E}^\wedge(\mathbf{x}, \omega)] = \text{volt-sec/m}$.

An obvious property of the Fourier Transform is this:

$$\partial_t \mathbf{E}(\mathbf{x}, t) = (1/2\pi) \int_{-\infty}^{\infty} d\omega \mathbf{E}^\wedge(\mathbf{x}, \omega) \partial_t e^{+j\omega t} = (1/2\pi) \int_{-\infty}^{\infty} d\omega [j\omega \mathbf{E}^\wedge(\mathbf{x}, \omega)] e^{+j\omega t}$$

which we can write as (symbol \leftrightarrow means "corresponds to")

$$\mathbf{E}(\mathbf{x}, t) \leftrightarrow \mathbf{E}^\wedge(\mathbf{x}, \omega) \quad \Leftrightarrow \quad \partial_t \mathbf{E}(\mathbf{x}, t) \leftrightarrow j\omega \mathbf{E}^\wedge(\mathbf{x}, \omega) \quad (1.6.9)$$

which is just another way to state our rule (1.5.2).

In the case of assumed monochrome time dependence of the form (1.6.5) (reflected in (1.6.6)) one finds that

$$E_i(\mathbf{x}, t) = e^{j[\omega_1 t + \varphi_i(\mathbf{x}, \omega_1)]} E_i(\mathbf{x}, \omega_1) \quad (1.6.5)$$

$$\begin{aligned} E_i^\wedge(\mathbf{x}, \omega) &= \int_{-\infty}^{\infty} dt [e^{j\omega_1 t} e^{j\varphi_i(\mathbf{x}, \omega_1)} E_i(\mathbf{x}, \omega_1)] e^{-j\omega t} = E_i(\mathbf{x}, \omega_1) e^{j\varphi_i(\mathbf{x}, \omega_1)} \int_{-\infty}^{\infty} dt e^{j(\omega_1 - \omega) t} \\ &= [E_i(\mathbf{x}, \omega_1) e^{j\varphi_i(\mathbf{x}, \omega_1)}] 2\pi\delta(\omega - \omega_1) \end{aligned} \quad (1.6.10)$$

or

$$\mathbf{E}^\wedge(\mathbf{x}, \omega) = \mathbf{E}(\mathbf{x}, 0) 2\pi\delta(\omega - \omega_1) . \quad (1.6.11)$$

It is this very simple single- δ -function form that motivates the use of complex fields as carriers of the real physical fields. One can of course Fourier-transform the monochrome *physical* field directly, but the result is clumsy to deal with. For example,

$$\begin{aligned} \mathbf{e}_i(\mathbf{x}, t) &= \text{Re} \{ E_i(\mathbf{x}, t) \} = \cos[\omega_1 t + \varphi_i(\mathbf{x}, \omega_1)] E_i(\mathbf{x}, \omega_1) \\ \mathbf{e}'_i(\mathbf{x}, t) &= \text{Im} \{ E_i(\mathbf{x}, t) \} = \sin[\omega_1 t + \varphi_i(\mathbf{x}, \omega_1)] E_i(\mathbf{x}, \omega_1) \end{aligned} \quad (1.6.6)$$

$$\begin{aligned} \hat{e}_i(\mathbf{x}, \omega) &= \int_{-\infty}^{\infty} dt \{ \cos[\omega_1 t + \varphi_i(\mathbf{x}, \omega_1)] E_i(\mathbf{x}, \omega_1) \} e^{-j\omega t} \\ &= E_i(\mathbf{x}, \omega_1) (1/2) \int_{-\infty}^{\infty} dt \{ e^{j[\omega_1 t + \varphi_i(\mathbf{x}, \omega_1)]} + e^{-j[\omega_1 t + \varphi_i(\mathbf{x}, \omega_1)]} \} e^{-j\omega t} \\ &= E_i(\mathbf{x}, \omega_1) [e^{j\varphi_i(\mathbf{x}, \omega_1)} \pi \delta(\omega - \omega_1) + e^{-j\varphi_i(\mathbf{x}, \omega_1)} \pi \delta(\omega + \omega_1)] \end{aligned} \quad (1.6.12)$$

or

$$\hat{e}(\mathbf{x}, \omega) = [\mathbf{e}(\mathbf{x}, 0) + j\mathbf{e}'(\mathbf{x}, 0)] \pi \delta(\omega - \omega_1) + [\mathbf{e}(\mathbf{x}, 0) - j\mathbf{e}'(\mathbf{x}, 0)] \pi \delta(\omega + \omega_1) \quad (1.6.13)$$

This lacks the friendliness of (1.6.11) in that the real and imaginary parts of $\mathbf{E}(\mathbf{x}, 0)$ both appear on the right, and two different ω -space delta functions are required. One could by fiat set $\mathbf{e}' = 0$, for example, but the two delta functions still remain.

A directly related benefit of using the complex function approach is the fact that math with exponentials is so much simpler than the corresponding math with trig functions, as for example

$$e^{j(\omega t + \varphi)} e^{-j(\omega' t + \varphi')} = e^{j(\omega - \omega') t} e^{j(\varphi - \varphi')} \quad // \text{dependence on } t \text{ isolated to one factor}$$

versus

$$\cos(\omega t + \varphi) \cos(\omega' t + \varphi') = (1/2) \{ \cos[(\omega - \omega') t + (\varphi - \varphi')] + \cos[(\omega + \omega') t + (\varphi + \varphi')] \} .$$

Comment: Using the real cosine form shown as the first line of (1.6.6) along with the Fourier Cosine Transform is not viable because $\cos[\omega_1 t + \varphi_i(\mathbf{x}, \omega_1)] E_i(\mathbf{x}, \omega_1)$ is not an even function of t .

(d) Monochrome \mathbf{E} and \mathbf{B} fields

One might seek to solve a system using monochrome fields of the form (1.6.5) for both the electric and magnetic fields. Those forms would be (\mathbf{E} and \mathbf{B} are real)

$$\begin{aligned} E_i(\mathbf{x}, t) &= e^{j[\omega_1 t + \varphi_{ei}(\mathbf{x}, \omega_1)]} E_i(\mathbf{x}, \omega_1) \\ B_i(\mathbf{x}, t) &= e^{j[\omega_1 t + \varphi_{bi}(\mathbf{x}, \omega_1)]} B_i(\mathbf{x}, \omega_1) \end{aligned} \quad (1.6.14)$$

where we assume the same frequency ω_1 for both fields, but allow the fields to have different phase functions φ_{ei} and φ_{bi} . In this case (1.6.10) becomes

$$\begin{aligned} \hat{E}_i(\mathbf{x}, \omega) &= E_i(\mathbf{x}, \omega_1) e^{j\varphi_{ei}(\mathbf{x}, \omega_1)} 2\pi \delta(\omega - \omega_1) \\ \hat{B}_i(\mathbf{x}, \omega) &= B_i(\mathbf{x}, \omega_1) e^{j\varphi_{bi}(\mathbf{x}, \omega_1)} 2\pi \delta(\omega - \omega_1) \end{aligned} \quad (1.6.15)$$

The ratio of E_i over B_j is then given by

$$\frac{\hat{E}_i(\mathbf{x}, \omega)}{\hat{B}_j(\mathbf{x}, \omega)} = \frac{E_i(\mathbf{x}, \omega_1)}{B_j(\mathbf{x}, \omega_1)} e^{j[\varphi_{ei}(\mathbf{x}, \omega_1) - \varphi_{bj}(\mathbf{x}, \omega_1)]} \quad (1.6.16)$$

Since E_i and B_j are real, the phase of the ratio E_i/B_j is determined by the last factor and will in general be a function of both position \mathbf{x} and frequency ω_1 . We shall see this situation arise in Chapter 2 where we calculate the fields inside a conducting round wire.

(e) The Line Strength

In the discussion above we have already defined many kinds of electric fields:

$E_i(\mathbf{x},t)$	general complex electric field (component i)	(1.6.17)
$e_i(\mathbf{x},t)$	$\text{Re}[E_i(\mathbf{x},t)]$ = candidate physical field	
$e'_i(\mathbf{x},t)$	$\text{Im}[E_i(\mathbf{x},t)]$ = candidate physical field	
$E_i^{\wedge}(\mathbf{x},\omega)$	Fourier Integral Transform of $E_i(\mathbf{x},t)$	
$E_i(\mathbf{x},\omega)$	magnitude of a monochrome field with frequency ω	
$\varphi_i(\mathbf{x},\omega)$	phase of a monochrome field with frequency ω	
$\mathcal{E}_i(\mathbf{x},\omega)$	line strength of a monochromatic field with frequency ω	

The last item is new. It has been added to make the above list complete, and we define it right here. Recall the form of the Fourier Transform of a monochrome field given in (1.6.1),

$$E_i^{\wedge}(\mathbf{x},\omega) = [E_i(\mathbf{x},\omega_1) e^{j\varphi_i(\mathbf{x},\omega_1)}] 2\pi\delta(\omega-\omega_1) . \quad (1.6.10)$$

The factor [...] which multiplies $2\pi\delta(\omega-\omega_1)$ we shall refer to as the **line strength** of the monochromatic electric field component, and we shall use this notation,

$$\mathcal{E}_i(\mathbf{x},\omega_1) \equiv [E_i(\mathbf{x},\omega_1) e^{j\varphi_i(\mathbf{x},\omega_1)}] \quad // \quad E_i(\mathbf{x},\omega_1) = |\mathcal{E}_i(\mathbf{x},\omega_1)| \quad (1.6.18)$$

and then

$$E_i^{\wedge}(\mathbf{x},\omega) = \mathcal{E}_i(\mathbf{x},\omega_1) 2\pi\delta(\omega-\omega_1) . \quad \mathcal{E}_i(\mathbf{x},\omega_1) = \text{line strength} \quad (1.6.19)$$

Since we shall normally refer to a monochrome frequency as ω (rather than ω_1) with dependence $e^{j\omega t}$, we can rewrite the last three equations as

$$E_i^{\wedge}(\mathbf{x},\omega') = [E_i(\mathbf{x},\omega) e^{j\varphi_i(\mathbf{x},\omega)}] 2\pi\delta(\omega'-\omega) \quad (1.6.20)$$

$$\mathcal{E}_i(\mathbf{x},\omega) \equiv [E_i(\mathbf{x},\omega) e^{j\varphi_i(\mathbf{x},\omega)}] \quad // \quad E_i(\mathbf{x},\omega) = |\mathcal{E}_i(\mathbf{x},\omega)| \quad (1.6.21)$$

$$E_i^{\wedge}(\mathbf{x},\omega') = \mathcal{E}_i(\mathbf{x},\omega) 2\pi\delta(\omega'-\omega) \quad \mathcal{E}_i(\mathbf{x},\omega) = \text{line strength} \quad (1.6.22)$$

(f) Overloaded Notation and Maxwell's Equations in ω space

A rigorous textbook probably should be careful about which of the above many field versions are the subject of any particular discussion. To the reader's possible dismay, we shall generally (but not always) refer to all these electric fields as $E_{\mathbf{i}}$ and shall depend on the reader to decipher which kind of field is implied in a given situation. The reason for this decision is that having a large number of notations for electric fields (and for magnetic fields, and various other derived quantities such as potential V and current i and current density $J_{\mathbf{i}}$) adds a level of visual font complexity to equations which are already complex enough to begin with. It is a tradeoff between precision and font/decoration clutter.

In particular, earlier in this section we have carefully denoted the Fourier Transform of $f(t)$ as $f^{\wedge}(\omega)$ which is a notation used by Stakgold and others (though Stakgold has our (1.6.8) phases negated as in his equation (5.32)). In the rest of this document, however, we represent the Fourier Transform of $f(t)$ as $f(\omega)$ to avoid a proliferation of hat \wedge symbols. Since the functions $f(t)$ and $f(\omega)$ are completely different functions, the symbol f is "overloaded" (in the sense of overloaded variable names in computer languages) and we trust the reader to understand that $f(\omega)$ always means $f^{\wedge}(\omega)$. It is the presence of the argument ω that cues the reader to this fact. This overloaded notation has already been used in Section 1.5 and we continue it below. Similarly, a generic field $E_{\mathbf{i}}(\omega)$ may refer to the full Fourier transform $E^{\wedge}_{\mathbf{i}}$, or it may refer to the line strength $\mathcal{E}_{\mathbf{i}}$ if monochromatic fields are being used. A field magnitude will always be properly indicated as a magnitude. The physical fields make only rare appearances.

In the Maxwell and related equations which include the $\partial_{\mathbf{t}}$ operator, if the fields are expanded onto their Fourier transformed components using (1.6.8b), then using the rule (1.6.9) one may instantly write the frequency-domain version of these equations, just as in the example at the start of Section 1.5. For example,

$$\text{curl } \mathbf{H}(\mathbf{x},\omega) = j\omega\mathbf{D}(\mathbf{x},\omega) + \mathbf{J}(\mathbf{x},\omega) \quad (1.6.23)$$

$$\text{curl } \mathbf{E}(\mathbf{x},\omega) = -j\omega\mathbf{B}(\mathbf{x},\omega) \quad (1.6.24)$$

$$\text{div } \mathbf{J}(\mathbf{x},\omega) = -j\omega\rho(\mathbf{x},\omega) \quad (1.6.25)$$

Other equations in the Section 1.1 list have the same form but in terms of the frequency-domain functions. For example,

$$\mathbf{J}(\mathbf{x},\omega) = \sigma(\mathbf{x}) \mathbf{E}(\mathbf{x},\omega) \quad (1.6.26)$$

where we momentarily allow $\sigma(\mathbf{x})$ to have spatial dependence but not time dependence. All these ω dependent fields can be regarded either as full Fourier transforms, or as the line strengths corresponding to those transforms, where the $2\pi\delta$ functions cancel on the two sides of the equation.

Chapter 2: The Round Wire and the Skin Effect

Chapter 1 dealt with the generalities of electromagnetic theory. Maxwell's equations were stated *ex machina*, as it were, and wave equations for the fields and potentials were then derived. Formal integral solutions of the potential wave equations were also derived using the Green's Function method. It was noted that the potentials ϕ and \mathbf{A} are parts of the same Lorentz 4-vector.

Whereas the approach of Chapter 1 was very general and abstract, the discussion of this chapter is highly specific. The goal here is to learn about the properties of a very simple object -- an infinite straight round wire. Although transmission lines are not always made out of round wires, there is a wealth of useful practical information that arises from the study of this simple example which applies to more general geometries.

The major issue here is called the "skin effect". At high frequencies, current is forced away from the central regions of a conductor and concentrates at the surface in a thin layer that has a characteristic depth called δ , the skin depth. In this chapter it will be shown exactly why this occurs. The significance of the effect is that the resistance (impedance) of a wire increases drastically at high frequency since the current is forced to flow only in this thin shell below the wire surface. This effect is manifested in a property of a wire called its surface impedance which is studied below in Section 2.4 and qualitatively in Section 2.5.

Our development is an extension of the excellent discussion of Matick's Chapter 4. It is fastest to solve the round wire problem starting with the ω -domain damped wave equation (1.5.32) which, inside the wire where there is no free charge, says $(\nabla^2 + \beta^2)\mathbf{E} = 0$ with $\beta^2 = \omega^2\mu\xi$ where μ and ξ apply to the conductor. Instead, we have chosen to start from the basic Maxwell curl equations and use simple "math loops" to derive the basic (first order differential) equations relating \mathbf{E} and \mathbf{B} fields. The general technique of putting loops in opportune places is extremely useful in analyzing the more complicated situation which arises in a transmission line. This method is carried out in Section 2.2 and the wire's interior solutions are then studied in Section 2.3.

In the work done below, we shall assume axial symmetry for the fields in the round wire. The problem is treated more generally in Appendix D where the Helmholtz equation $(\nabla^2 + \beta^2)\mathbf{E} = 0$ is directly solved. The partial wave $m = 0$ solution of Appendix D corresponds to the analysis below.

2.1 The Implicit Wave Context, Helmholtz Equations and the Skin Effect

In the sections below we don't explicitly consider the notion that a wave is traveling down our round wire, but that is in fact what is happening and this fact deserves a few comments before we delve into the interior solution of the wire. Specifically, imagine that \mathbf{E} has the following traveling-wave form,

$$\mathbf{E}(x,y,z,t) = e^{j(\omega t - kz)} \mathbf{E}(x,y,\omega) \quad (2.1.1)$$

where $\mathbf{E}(x,y,\omega)$ might have dependence on ω and might be complex. Inside the wire this field must satisfy the damped wave equation (1.3.36),

$$(\nabla^2 - \mu\epsilon \partial_t^2 - \mu\sigma\partial_t) \mathbf{E}(x,y,z,t) = 0. \quad (2.1.2)$$

When the form (2.1.1) is inserted into (2.1.2), the result is, using $\nabla^2 = \nabla_{2D}^2 + \partial_z^2$,

$$\begin{aligned}
 & (\nabla_{2D}^2 + \partial_z^2 - \mu\epsilon \partial_t^2 - \mu\sigma\partial_t) \{ e^{j(\omega t - kz)} \mathbf{E}(x,y,\omega)\} = 0 \\
 \text{or} \\
 & (\nabla_{2D}^2 - k^2 + \mu\epsilon \omega^2 - j\mu\sigma\omega) \{ e^{j(\omega t - kz)} \mathbf{E}(x,y,\omega)\} = 0 \\
 \text{or} \\
 & (\nabla_{2D}^2 - k^2 + \beta^2) \{ e^{j(\omega t - kz)} \mathbf{E}(x,y,\omega)\} = 0 \\
 \text{or} \\
 & (\nabla_{2D}^2 + \beta^2 - k^2) \mathbf{E}(x,y,\omega) = 0 \quad // \text{ a 2D Helmholtz equation} \quad (2.1.3)
 \end{aligned}$$

where

$$\beta^2 = \mu\epsilon\omega^2 - j\omega\mu\sigma = \omega^2\mu(\epsilon - j\sigma/\omega) = \omega^2\mu\xi \quad \xi \equiv \epsilon - j\sigma/\omega \quad (1.5.1c)$$

Comment: $\mathbf{E}(x,y,\omega)$ is proportional to the Fourier Transformed ω -domain version of $\mathbf{E}(x,y,z,t)$:

$$\mathbf{E}^\wedge(x,y,z,\omega') \equiv \text{FT}\{ \mathbf{E}(x,y,z,t), \omega'\} = e^{-jkz} \mathbf{E}(x,y,\omega) 2\pi\delta(\omega-\omega') \quad // \text{ see (1.6.11)}$$

A similar equation applies just outside the round wire in the dielectric medium in which it is embedded, and this medium has its own β which we call β_d . Thus we have

$$(\nabla_{2D}^2 + \beta^2 - k^2) \mathbf{E}(x,y,\omega) = 0 \quad \text{inside wire} \quad \beta = (j-1)\sqrt{\omega\mu\sigma/2} = \text{complex} \quad (2.1.4a)$$

$$(\nabla_{2D}^2 + \beta_d^2 - k^2) \mathbf{E}(x,y,\omega) = 0 \quad \text{outside wire} \quad \beta_d = \omega\sqrt{\mu_d\epsilon_d} = \omega/v_d \approx \text{real} \quad (2.1.4b)$$

We have assumed that

- the dielectric is non-conducting or only slightly conducting so $\xi_d \approx \epsilon_d$.
- the conductor is a good one, so $\beta^2 \approx (-j)\omega\mu\sigma$ and then $\beta = \sqrt{-j}\sqrt{\omega\mu\sigma}$. As will be shown below, the choice for $\sqrt{-j}$ is $e^{j3\pi/4} = (j-1)/\sqrt{2}$ which then gives $\beta = (j-1)\sqrt{\omega\mu\sigma/2}$ as in (2.1.4a).

In (2.1.4b) we then make the ansatz assumption,

$$k = \beta_d \quad (2.1.5)$$

which basically says that the wave form $e^{j(\omega t - kz)} \mathbf{E}(x,y,\omega)$ really does describe a wave traveling down the wire with $k = \beta_d$. This $k = \beta_d = \omega/v_d$ is then related to the speed of light in the dielectric and is the expected value of k for, say, a radio or light wave traveling through the dielectric with no wire present. Once we have assumed $e^{j(\omega t - \beta_d z)}$ for the dielectric solution, the boundary conditions (1.1.51) on field components at the wire surface will force this same dependence on the solution inside the wire.

It will be shown later that (2.1.5) is valid for a transmission line operating at sufficiently high frequency (see (Q.3.5)), or equivalently, if the conductor has sufficiently large conductivity σ . In this case, the resistive loss inside the conductors can be neglected and conductors are "perfect conductors". Even if they are not completely perfect, (2.1.5) is close to true for a conventional "low-loss" transmission line.

In (2.1.4a), since the conductor has such a large σ , $|\beta|$ is a large number and $|\beta| \gg \beta_d$ (unless ω is extremely large or, as we shall later see, very small), so k^2 can be ignored in (2.1.4a). We then have

$$(\nabla_{2D}^2 + \beta^2) \mathbf{E}(x,y,\omega) \approx 0 \quad \text{inside wire} \quad \beta = (j - 1) \sqrt{\omega\mu\sigma/2} = \text{complex} \quad (2.1.6a)$$

$$\nabla_{2D}^2 \mathbf{E}(x,y,\omega) = 0 \quad \text{outside wire} \quad (2.1.6b)$$

The second equation says that the \mathbf{E} field outside the wire must solve the 2D vector Laplace equation. See Appendix D.7 for comments on the general exterior solution. Appendix D uses $\beta'^2 \equiv \beta^2 - \beta_d^2$ and does not make the approximation that $\beta' \approx \beta$, but we make that approximation here.

To put our "isolated" round wire into a physical context, it helps to think of it as the round central conductor of a coaxial cable whose shield cylinder radius is very large compared to the central wire radius (the Great Cylinder, analogous to the Great Sphere of electrostatics). Then this central round wire is really part of a transmission line and we expect such a transmission line to carry a wave with $e^{j(\omega t - \beta_d z)}$ time and z dependence. Moreover, we expect the field solution inside such a coaxial cable central wire to have the axial symmetry that appears in our assumption list below.

It is equation (2.1.6a) for the wire interior that we shall encounter below, and hopefully we have now put that equation into the context of a wave traveling down the wire.

If β_d has a small negative imaginary part due to conductivity of the dielectric (see (1.5.1a)), the factor $e^{-j\beta_d z}$ says that the wave slowly damps out as it travels down the wire due to dielectric ohmic loss, as it well should. (In a laser inverted medium β_d has a positive imaginary part so the wave grows instead.)

On the other hand, β is huge and has equal real and imaginary part magnitudes. Due to our axial symmetry, (2.1.6a) really says $(\nabla_{2D}^2 + \beta^2) \mathbf{E}(r,\omega) = 0$ which can be thought of as a "wave equation" in the radial direction. Of course it is a *damped* wave equation of a very extreme sort. As one moves in from the surface of the wire toward the center, we show later that over a distance in which the "wave" phase changes by about $\pi/2$, the amplitude is already down by a factor $1/e$, so one can roughly say that the wave basically damps out before it even goes $1/2$ wavelength. This is the skin effect described below.

To understand this effect, it is useful to consider a 1D version of the situation. Imagine zooming the camera in very close to the left surface of the round wire's cross section, so that we see a half space of conductor on the right and a half space of dielectric on the left. Let the radial direction be called x which increases into the conductor with $x = 0$ at the interface. Then the inside-wire wave equation above says

$$(\partial_x^2 + \beta^2) E(x,\omega) = 0 \quad (2.1.7)$$

The solution to this equation is (we select a particular sign for the phase, and see (2.1.6a) for β)

$$\begin{aligned} E(x,\omega) &= E(0,\omega) e^{+j\beta x} = E(0,\omega) \exp\{j[(j-1)\sqrt{\omega\mu\sigma/2}]x\} \\ &= E(0,\omega) \exp\{-\sqrt{\omega\mu\sigma/2}x\} \exp\{-j\sqrt{\omega\mu\sigma/2}x\} \\ &= E(0,\omega) \exp\{-x/\delta\} \exp\{-jx/\delta\} \quad \delta \equiv \sqrt{2/(\omega\mu\sigma)} \\ &= E(0,\omega) e^{-x/\delta} e^{-jx/\delta} \quad // = E(0,\omega) e^{-(j+1)x/\delta} \end{aligned} \quad (2.1.8)$$

As one moves from $x=0$ to the right into the conductor, in distance δ the E field amplitude drops to $1/e$ and the phase has changed by $\pi/2$. Quantity δ is called the skin depth, and this is probably the most basic way to understand the notion of the skin effect. It is a result dictated by the Helmholtz equation having a complex parameter β of the type shown. Based on this argument, the skin effect occurs at any conductor

surface regardless of its cross-sectional shape. Below we see in the round wire example how the Helmholtz equation (2.1.6a) is in turn a result of the two Maxwell curl equations each of which relates \mathbf{E} and \mathbf{B} . Of course this is how the Helmholtz equation was derived in the first place starting with (1.2.1).

2.2 Derivation of $\mathbf{E}(\mathbf{r})$, $\mathbf{B}(\mathbf{r})$ and $\mathbf{J}(\mathbf{r})$ for a round wire

We convert (1.1.38) and (1.1.36) to the ω domain using rule (1.5.2),

$$\text{curl } \mathbf{B} = \mu (j\omega\epsilon \mathbf{E} + \mathbf{J}) \quad \Leftrightarrow \quad \oint_{\mathcal{C}} \mathbf{B} \cdot d\mathbf{s} = \mu \int_{\mathcal{S}} [j\omega\epsilon \mathbf{E} + \mathbf{J}] \cdot d\mathbf{S} \quad (2.2.1)$$

$$\text{curl } \mathbf{E} = -j\omega\mathbf{B} \quad \Leftrightarrow \quad \oint_{\mathcal{C}} \mathbf{E} \cdot d\mathbf{s} = -j\omega \int_{\mathcal{S}} \mathbf{B} \cdot d\mathbf{S} \quad . \quad (2.2.2)$$

The two terms on the right side of (2.2.1) have names (we sometimes omit the word "density")

$$\begin{aligned} j\omega\epsilon\mathbf{E} &= \text{displacement current (density)} && // \text{ amps/m}^2 \\ \mathbf{J} = \sigma\mathbf{E} &= \text{conduction current (density)} && // \text{ amps/m}^2 \end{aligned} .$$

The sum of both currents may be written as

$$(j\omega\epsilon + \sigma) \mathbf{E}(\mathbf{x},\omega) \quad .$$

For any metal conductor such as copper, the displacement term is completely negligible as long as $\omega\epsilon \ll \sigma$. The value of ϵ for a metal is not very obvious (see Jackson pp 309-313) so we will follow Matick p 118 and blindly set $\epsilon = \epsilon_0$ for a crude comparison. The condition for negligible displacement current $\omega\epsilon \ll \sigma$ then becomes $f \ll \sigma/[2\pi\epsilon_0]$. Using $\sigma = 5.81 \times 10^7$ mho/m and $\epsilon_0 = 8.85 \times 10^{-12}$ F/m, one gets

$$f \ll (\sigma/2\pi\epsilon) = 1.04 \times 10^{18} \text{ Hz} \approx \text{one billion GHz} \quad .$$

Therefore, the displacement current is always ignored inside a conductor for any conventional transmission line application. Whatever ϵ really is, we shall ignore $j\omega\epsilon$ compared to σ . All the current inside a good conductor is conduction current. With respect to (1.5.1c), this same approximation means that inside a conductor,

$$\xi \approx -j\sigma/\omega \quad \beta^2 \approx -j\omega\mu\sigma \quad . \quad // f \ll 10^{18} \text{ H} \quad (2.2.3)$$

We now make a set of assumptions:

- (a) the round wire conductor medium is uniform (homogeneous) and isotropic (2.2.4)
- (b) the current pattern in the wire is axially symmetric (no dependence on azimuth θ ; it is invariant under any rotation of the wire about its center line)
- (c) the current is axial (longitudinal), so $\mathbf{J} = J\hat{\mathbf{z}}$, so $J = J_z$
- (d) the \mathbf{E} field is also axial so $\mathbf{E} = E\hat{\mathbf{z}}$ (this follows from (c) and $\mathbf{J} = \sigma\mathbf{E}$), so $E = E_z$
- (e) The \mathbf{B} field lines go around in circles centered at the wire axis. The relation between the direction of \mathbf{B} and the current flow \mathbf{J} is given by the right hand rule. If $J = J_z > 0$, then $\mathbf{B} = B_\theta \hat{\boldsymbol{\theta}} > 0$.

Thus, we represent $J_z(x,y,\omega) = J(r)$, $E_z(x,y,\omega) = E(r)$, and $B_\theta(x,y,\omega) = B(r)$ -- no dependence on θ or z . The fields like $E_z(x,y,\omega)$ are of the type shown on the right of (2.1.3) where the z dependence has already been extracted. Fields $\mathbf{E}(x,y,\omega)$, $\mathbf{B}(x,y,\omega)$ and $\mathbf{J}(x,y,\omega)$ are complex, so $E(r)$, $B(r)$ and $J(r)$ are all complex. They all depend on ω , but we suppress the ω arguments. As noted above, $\mathbf{E} = E(r) \hat{\mathbf{z}}$ and $\mathbf{B} = B(r) \hat{\boldsymbol{\theta}}$.

Here is another way to state assumption (b). We search for an axially symmetric solution of Maxwell's equations for the round wire, and if we find one, we accept it as a possible way fields and currents could exist in the wire. If the wire were in idealized perfect isolation with an axially symmetric source and load, the invariance of the physical situation with regard to rotation about the wire axis would require (b) to be valid. This symmetry is also implied by our "fat" coaxial cable context noted earlier.

Consider now the thin (width is dr) red loop shown in Fig 2.1:

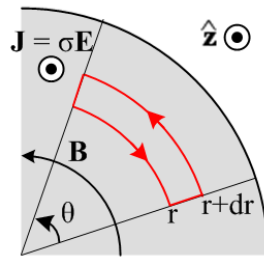


Fig 2.1

Cross section view of wire, current flowing in $\hat{\mathbf{z}}$ direction toward viewer

According to (2.2.1) with $\mathbf{J} = \sigma \mathbf{E}$ and no displacement current,

$$\oint_C \mathbf{B} \cdot d\mathbf{s} = (\mu\sigma) \int_S \mathbf{E} \cdot d\mathbf{S} \quad (2.2.5)$$

For the CCW loop shown, the "right hand rule" says area $d\mathbf{S}$ points out of the plane of paper. The two sides of this equation can be easily evaluated ($B = B_\theta$ and $E = E_z$)

$$[B(r+dr) (r+dr) - B(r) r] \theta = (\mu\sigma) E(r) [r\theta dr] \quad (2.2.6)$$

which simplifies to

$$\frac{\partial [r B(r)]}{\partial r} = (\mu\sigma) [r E(r)] \quad (2.2.7)$$

Comment: When one says in Fig 2.1 that " \mathbf{J} points in the $\hat{\mathbf{z}}$ direction", one interpretation might be that the vector \mathbf{J} has the form $\mathbf{J} = J_z \hat{\mathbf{z}}$ and that $J_z > 0$. That is not the correct interpretation for our pictures. The quoted phrase just means that $\mathbf{J} = J_z \hat{\mathbf{z}}$ and nothing is implied about the "sign" of J_z . In our case, $J_z = J(r)$ is a complex number which has no "sign". If we said " \mathbf{J} points in the $-\hat{\mathbf{z}}$ direction" we would just mean that $\mathbf{J} = J_z(-\hat{\mathbf{z}}) = -J_z \hat{\mathbf{z}}$. Our only interest in clarifying these "directions" is to get the signs right in our application of Stokes's law. The same comment applies to the direction of \mathbf{B} in the next figure. By saying that " \mathbf{B} points out of the plane of paper", we just mean that $\mathbf{B} = +B(r) \hat{\boldsymbol{\theta}}$ which is consistent with the

fact that $\mathbf{J} = +J_z \hat{\mathbf{z}}$ according to the right hand rule: thumb in the "direction" of \mathbf{J} at the wire axis, curled fingers are in the "direction" of \mathbf{B} .

Now consider the thin red loop shown in Fig. 2.2,

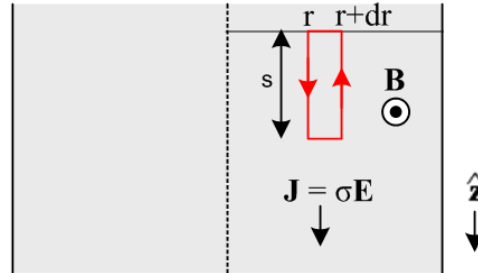


Fig 2.2

Top view of wire's central plane, current flowing in $\hat{\mathbf{z}}$ direction (down)

According to (2.2.2),

$$\oint_C \mathbf{E} \cdot d\mathbf{s} = -j\omega \int_S \mathbf{B} \cdot d\mathbf{S} \quad (2.2.2)$$

where, for the CCW loop shown, the right hand rule puts $d\mathbf{S}$ pointing to the viewer (aligned with \mathbf{B} which points to the viewer due to its right hand rule with \mathbf{J}). The two sides of this equation are easily evaluated (the first term on the left is negative because $\hat{\mathbf{z}}$ points down while the red arrow points up)

$$[-E(r+dr) + E(r)] s = -j\omega B(r) [s dr] \quad (2.2.8)$$

which simplifies to

$$\frac{\partial E(r)}{\partial r} = j\omega B(r) \quad (2.2.9)$$

This equation says that $E(r)$ changes with radius as long as $\omega \neq 0$ and $B(r) \neq 0$. Since everything is complex, we cannot really tell from (2.2.9) that $|E(r)|$ increases with radius, but we shall see below that it does, and this fact gives rise to the "skin effect" where current is maximum at the wire surface.

Reader Exercise: Why can't one take the absolute value of both sides of (2.2.9) and reach the conclusion that $\partial_{\mathbf{x}}|E(r)| = \omega|B(r)| > 0$ and conclude that $|E(r)|$ increases with r ? Hint: $\partial_{\mathbf{x}}|f| \neq |\partial_{\mathbf{x}}f|$

Now solve (2.2.9) for $B(r)$ and put this into (2.2.7) to get

$$\frac{1}{r} \frac{\partial}{\partial r} \left(r \frac{\partial E(r)}{\partial r} \right) = (j\omega\mu\sigma) E(r) = -\beta^2 E(r) \quad (2.2.10)$$

where $\beta^2 = -j\omega\mu\sigma$ from (2.2.3). The operator on the left is ∇^2 in cylindrical coordinates for a function that does not depend on θ or z . For such functions, $\nabla^2 = (\partial_z^2 + \nabla_{2D}^2)$ and ∇_{2D}^2 are equivalent. Thus, (2.2.10) is really a special case of the following

$$[\nabla_{2D}^2 + \beta^2] E(r) = 0 \quad (2.2.11)$$

This in turn is a special case of the \mathbf{E} field wave equation (2.1.6a),

$$(\nabla_{2D}^2 + \beta^2) \mathbf{E}(x,y,\omega) = 0 \quad (2.1.6a)$$

The Helmholtz parameter β^2 is given by (1.5.1c),

$$\beta^2 = \mu\epsilon\omega^2 - j\omega\mu\sigma = \omega^2\mu(\epsilon - j\sigma/\omega) \approx -j\omega\mu\sigma \quad (1.5.1c)$$

The ϵ term in β^2 has been neglected since σ is very large. Parameter $\beta = 2\pi/\lambda$ is a "wavenumber" and has dimensions of m^{-1} . If λ were real (it is not), then β would be the number of wave radians per meter just as ω is the number of wave radians per second.

The complex number $-j$ has two square roots which are $e^{j3\pi/4}$ and $e^{-j\pi/4}$,

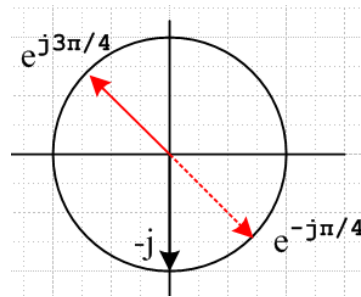


Fig 2.3

and we specify the upper red arrow as the square root in the definition of β ,

$$\beta \equiv e^{j3\pi/4} \sqrt{\omega\mu\sigma} \quad // \quad \beta = (j - 1) \sqrt{\omega\mu\sigma/2} = (j-1)\delta \quad (2.2.12)$$

We could have started out with (2.2.11) and skipped all the above analysis of loops, but this method of using loops emphasizes the direct action of Maxwell's equations and seems instructive.

Comment: One could of course take the other square root of $-j$ and develop things that way. Historically the root selected above has been used. Taking the other root means $\beta \rightarrow -\beta$. A review of the solutions obtained below shows that they are invariant under $\beta \rightarrow -\beta$. Such a review can use the facts that $J_0(-z) = J_0(z)$, and $J_1(-z) = -J_1(z)$. In general $J_\nu(z)$ is analytic at $z = 0$ for $\text{Re}\nu \geq 0$ and the rules just stated follow from the series representations of J_0 and J_1 as shown for example in Spiegel 24.5 and 25.6. In "exterior" problems involving the Hankel functions, there is significance as to whether $z = \beta r$ is in the upper or lower z -plane in terms of convergence for large r . For example, if β is in the upper half plane, then $H^{(1)}(\beta r)$ is the function that converges as $r \rightarrow \infty$ and $H^{(2)}(\beta r)$ blows up:

The asymptotic forms for the Hankel functions are:

$$H_{\alpha}^{(1)}(z) \sim \sqrt{\frac{2}{\pi z}} \exp\left(i\left(z - \frac{\alpha\pi}{2} - \frac{\pi}{4}\right)\right) \text{ for } -\pi < \arg z < 2\pi$$

$$H_{\alpha}^{(2)}(z) \sim \sqrt{\frac{2}{\pi z}} \exp\left(-i\left(z - \frac{\alpha\pi}{2} - \frac{\pi}{4}\right)\right) \text{ for } -2\pi < \arg z < \pi$$

http://en.wikipedia.org/wiki/Bessel_function

The next step is to expand (2.2.10) as follows:

$$\frac{\partial^2 E(r)}{\partial r^2} + \frac{1}{r} \frac{\partial E(r)}{\partial r} + \beta^2 E(r) = 0$$

or

$$r^2 \frac{\partial^2 E(r)}{\partial r^2} + r \frac{\partial E}{\partial r} + r^2 \beta^2 E(r) = 0 \quad (2.2.13)$$

Change variables to dimensionless $x = \beta r$. Then

$$r = x/\beta \quad x = \beta r \quad \partial x/\partial r = \partial_{\mathbf{r}} x = \beta$$

$$\partial_{\mathbf{r}} E = \frac{\partial E}{\partial r} = \frac{\partial E}{\partial x} \frac{\partial x}{\partial r} = \beta \frac{\partial E}{\partial x} \quad (2.2.14)$$

$$\frac{\partial^2 E}{\partial r^2} = \partial_{\mathbf{r}}^2 E = \partial_{\mathbf{r}}(\partial_{\mathbf{r}} E) = \partial_{\mathbf{r}}(\beta \partial_{\mathbf{x}} E) = \beta \partial_{\mathbf{x}}(\partial_{\mathbf{r}} E) = \beta \partial_{\mathbf{x}}(\beta \partial_{\mathbf{x}} E) = \beta^2 \partial_{\mathbf{x}}^2 E = \beta^2 \frac{\partial^2 E}{\partial x^2} \quad (2.2.15)$$

Inserting these quantities into (2.2.13) gives

$$r^2 \beta^2 \frac{\partial^2 E}{\partial x^2} + r \beta \frac{\partial E}{\partial x} + r^2 \beta^2 E = 0$$

or

$$x^2 \frac{\partial^2 f(x)}{\partial x^2} + x \frac{\partial f(x)}{\partial x} + x^2 f(x) = 0 \quad (2.2.16)$$

where $f(x) = E(x/\beta)$. Now (2.2.16) happens to be Bessel's Equation with $\nu = 0$ [NIST 10.2.1], and the solution must therefore be a linear combination of this form, where C and D are constants,

$$f(x) = C J_0(x) + D Y_0(x) \quad (2.2.17)$$

So far, we still don't know which way $\partial E/\partial r$ in (2.2.9) is changing, but we are about to find out. Since $f(x)$ represents the current and the electric field, we know $f(0)$ cannot be infinite. But $Y_0(x)$ blows up at $x=0$ [NIST 10.8.2], therefore constant $D = 0$. We now have an exact solution for the electric field in the wire:

$$E(r) = f(x) = C J_0(\beta r) \quad (2.2.18)$$

where

$$\beta = e^{j3\pi/4} \sqrt{\omega\mu\sigma} = (j-1) \sqrt{\omega\mu\sigma/2} \quad (2.2.19)$$

The following definition is usually made (factor of 2 explained later)

$$\delta \equiv \sqrt{2/\omega\mu\sigma} = \text{skin depth} \quad // \quad \omega\mu\sigma = 2/\delta^2 \quad (2.2.20)$$

so that

$$\beta = e^{j3\pi/4} (\sqrt{2}/\delta) = (j-1)/\delta \quad \text{and} \quad \beta^2 = -2j/\delta^2 \quad (2.2.21)$$

It is convenient to divide (2.2.18) by itself evaluated at $r=a$ which we shall assume is the **radius** of our round wire, so (plots coming soon),

$$E(r) = E(a) \frac{J_0(\beta r)}{J_0(\beta a)} \quad (2.2.22)$$

According to (2.2.9) which says $\partial_r E(r) = j\omega B(r)$ we can write

$$B(r) = (1/j\omega) \partial_r E(r) = (1/j\omega) E(a) \frac{\partial_r [J_0(\beta r)]}{J_0(\beta a)} = (1/j\omega) E(a) \frac{\beta J_0'(\beta r)}{J_0(\beta a)} = (\beta/j\omega) E(a) \frac{J_0'(\beta r)}{J_0(\beta a)} \quad (2.2.23)$$

Since $J_0'(x) = -J_1(x)$ [NIST 10.6.2] this gives,

$$B(r) = -(\beta/j\omega) E(a) \frac{J_1(\beta r)}{J_0(\beta a)} \quad (2.2.23)$$

which when evaluated at $r = a$ gives

$$B(a) = -(\beta/j\omega) E(a) \frac{J_1(\beta a)}{J_0(\beta a)} \quad \Rightarrow \quad E(a) = - (j\omega/\beta) \frac{J_0(\beta a)}{J_1(\beta a)} B(a) \quad (2.2.24)$$

which relates the two surface values $B(a)$ and $E(a)$. An alternative way to write $B(r)$ is

$$B(r) = B(a) \frac{J_1(\beta r)}{J_1(\beta a)} = \left\{ -(\beta/j\omega) E(a) \frac{J_1(\beta a)}{J_0(\beta a)} \right\} \frac{J_1(\beta r)}{J_1(\beta a)} = -(\beta/j\omega) E(a) \frac{J_1(\beta r)}{J_0(\beta a)} \quad (2.2.25)$$

Ampere's law with a circular loop just below the surface gives, where I is the total wire current,

$$2\pi a H_\theta = I \quad \Rightarrow \quad 2\pi a B_\theta / \mu = I \quad \Rightarrow \quad B(a) = \frac{\mu I}{2\pi a} \quad (2.2.26)$$

from which we find from (2.2.24) that

$$E(a) = - (j\omega/\beta) \frac{\mu I}{2\pi a} \frac{J_0(\beta a)}{J_1(\beta a)} \quad (2.2.27)$$

Using (2.2.26) for B(a) in (2.2.25) gives

$$B(r) = \frac{\mu I}{2\pi a} \frac{J_1(\beta r)}{J_1(\beta a)} \quad (2.2.28)$$

and using (2.2.24) for E(a) in (2.2.22) gives

$$E(r) = E(a) \frac{J_0(\beta r)}{J_0(\beta a)} = \left\{ - (j\omega/\beta) \frac{\mu I}{2\pi a} \frac{J_0(\beta a)}{J_1(\beta a)} \right\} \frac{J_0(\beta r)}{J_0(\beta a)} = - (j\omega/\beta) \frac{\mu I}{2\pi a} \frac{J_0(\beta r)}{J_1(\beta a)} \quad (2.2.29)$$

Let us gather up some of the main results obtained so far and put them in a box:

Interior Field Solution of a Round Wire		(2.2.30)
$\frac{\partial [rB(r)]}{\partial r} = (\mu\sigma) [rE(r)]$	(2.2.7)	$\frac{\partial E(r)}{\partial r} = j\omega B(r)$
$B(r) = \frac{\mu I}{2\pi a} \frac{J_1(\beta r)}{J_1(\beta a)}$	(2.2.28)	$B(a) = \frac{\mu I}{2\pi a}$
$E(r) = \frac{\mu I}{2\pi a} \frac{J_0(\beta r)}{J_1(\beta a)} (-j\omega/\beta)$	(2.2.29)	$E(a) = \frac{\mu I}{2\pi a} \frac{J_0(\beta a)}{J_1(\beta a)} (-j\omega/\beta)$
$J(r) = \frac{\mu I}{2\pi a} \frac{J_0(\beta r)}{J_1(\beta a)} (-j\omega\sigma/\beta) = \frac{I}{2\pi a} \frac{J_0(\beta r)}{J_1(\beta a)} \beta$		from $J(r) = \sigma E(r)$
$\beta = e^{j3\pi/4} (\sqrt{2}/\delta) = e^{j3\pi/4} \sqrt{\omega\mu\sigma} = (j-1)\sqrt{\omega\mu\sigma/2} = (j-1)\delta$		(2.2.19), (2.2.21)
$\delta \equiv \sqrt{2/\omega\mu\sigma} = \text{skin depth}$	$\beta^2 = -2j/\delta^2 = -j\omega\mu\sigma$	(2.2.20), (2.2.21)

The reader is reminded once again that E(r), B(r) and J(r) are complex functions of r and ω since they are components of the Fourier Integral Transform of the time-domain fields and current density. Since β is complex, the various $J_\nu(\beta r)$ are also complex. Thus, the nature of the solutions in the above box is not very obvious at this point.

Comment: Appendix D does an exact calculation of the **E** and **B** fields inside a round wire using a partial wave analysis with index m. The solution for the problem considered here in Chapter 2 corresponds to the partial wave $m = 0$ and is stated in summary box (D.6.3) and then in (D.6.6). It is shown that the E_z and

B_θ fields there match those obtained here, but in addition there is an extra field component E_r which is very small in the ratio $|\beta_{a0}/\beta|$. The reason our calculation here failed to discover this smaller field component was that we assumed $\mathbf{E} = E(r) \hat{z}$ and $\mathbf{B} = B(r) \hat{\theta}$. An implication of $E_r \neq 0$ is that $E_r(r=a) \neq 0$ which, as shown in (D.2.24), implies the existence of a surface charge on the round wire. This then fits with our context model of the round wire as the central conductor of a fat coaxial transmission line as discussed in Section 2.1.

2.3 A study of the solution of a round wire

(a) Kelvin Functions

The reader may be aware of the so-called first-kind *modified* Bessel function defined by

$$I_\nu(x) \equiv e^{-j\pi\nu/2} J_\nu(e^{j\pi/2}x),$$

where the J_ν function argument has phase $\pi/2$. Unfortunately, our $J_\nu(\beta r)$ functions have phase $3\pi/4$ so the I_ν functions are not particularly useful.

The real and imaginary parts of a Bessel function having an argument with phase $(3/4)\pi$ have the following historic names (bessel real and bessel imaginary) called Kelvin functions [NIST 10.61.1],

$$J_\nu(e^{j3\pi/4}z) = \text{ber}_\nu(z) + j \text{bei}_\nu(z) . \quad (2.3.1)$$

In our application $e^{j3\pi/4}z = \beta r = e^{j3\pi/4}(\sqrt{2}/\delta) r$ so that $z = \sqrt{2} (r/\delta)$. Thus, the solution $E(r)$ in (2.2.22) may be written as,

$$E(r) = E(a) \frac{\text{ber}_0[\sqrt{2}(r/\delta)] + j \text{bei}_0[\sqrt{2}(r/\delta)]}{\text{ber}_0[\sqrt{2}(a/\delta)] + j \text{bei}_0[\sqrt{2}(a/\delta)]} \quad z = \sqrt{2} (r/\delta) \quad (2.3.2)$$

The Kelvin functions are real when the arguments are real and positive. This is the case for almost all special functions (they are "real analytic"), though derived functions like $H_n^{(1)}(z)$ are an exception. Similar functions \ker_ν and \kei_ν are associated with $K_\nu(e^{j3\pi/4}z)$ where K_ν is the second-kind modified Bessel function. Since $J(r) = \sigma E(r)$, we could replace E with J on both sides of (2.3.2). This equation for J appears in Matick as p 101 (4-18).

Note: Lord Kelvin (William Thomson) introduced the ber and bei notation for these functions while considering the same problem we are dealing with here. The functions appear in the Appendix of his 34 page 1889 inaugural address used when he became president of the Institute of Electrical Engineers (see Refs) :

„ ber and bei denote two functions defined as follows:—

$$\text{ber } q = 1 - \frac{q^4}{2^2 4^2} + \frac{q^8}{2^2 4^2 6^2 8^2} - \&c. ;$$

$$\text{bei } q = \frac{q^2}{2^2} - \frac{q^6}{2^2 4^2 6^2} + \&c.$$

We can verify using Maple (which Kelvin would have enjoyed) that these are the ber_0 and bei_0 functions:

```

series(KelvinBer(0,q),q=0,10);
1 - 1/64 q^4 + 1/147456 q^8 + O(q^10)
series(KelvinBei(0,q),q=0,10);
1/4 q^2 - 1/2304 q^6 + O(q^10)
(2*4*6*8)^2;
147456
(2*4)^2;
64
(2*4*6)^2;
2304

```

Some authors, not liking Kelvin's notation, use Ber, Bei, Ker, Kei for ber, bei, ker, kei. Perhaps the idea is that Be is more obviously Bessel and perhaps Ke is then for Kelvin.

Since these Bessel forms occur frequently, there are standard functions for their magnitude and phase [NIST 10.68.1]

$$J_\nu(e^{j3\pi/4}z) = M_\nu(z) e^{j\theta_\nu(z)}. \quad (2.3.3)$$

Of particular interest is the magnitude of $E(r)$. Applying (2.3.3) to the $E(r)$ in (2.2.22) gives

$$|E(r)| = |E(a)| \frac{M_0[\sqrt{2}(r/\delta)]}{M_0[\sqrt{2}(a/\delta)]}. \quad (2.3.4)$$

(b) Plots of $|E(r)/E(a)|$ for various δ values

Finally we are in a position to make some plots to see how the electric field magnitude varies with radius in a round wire as a function of the skin depth parameter $\delta \equiv \sqrt{2/\omega\mu\sigma}$. As ω increases, δ decreases. Our aging Maple V knows about the Kelvin functions but not M , so here is the code

```

restart; with(plots):
z := sqrt(2)*r/d:
za := sqrt(2)*a/d:
M := (nu,z) -> abs(KelvinBer(nu,z) + I*KelvinBei(nu,z)):
a := 20:
p1 := plot([seq(M(0,z)/M(0,za), d = 1..10)], r = 1..a, color = red):
display(p1);

```

and here are plots of $|E(r)|/|E(a)|$ for $a = 20$ and $\delta = 1$ to 10, The steepest curve is for $\delta = 1$:

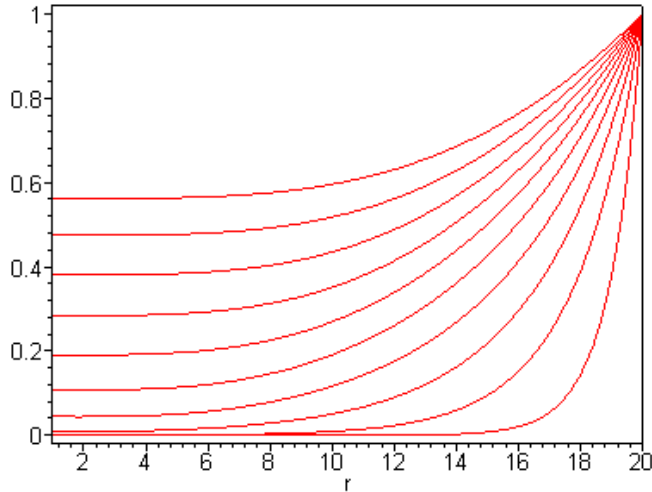


Fig 2.4

The same plots apply to $|J(r)| / |J(a)|$. One sees clearly how the current and electric field magnitude drop off quickly moving in from the edge of the round wire (right edge of graph) toward the wire axis when δ is small relative to radius a .

Asymptotic expansions for $M_n(z)$ and $\theta_n(z)$ for large z are given by NIST 10.68.16 and 10.68.18,

$$\begin{aligned} M_\nu(z) &\approx \frac{\exp(z/\sqrt{2})}{\sqrt{2\pi z}} \left[1 - \frac{4\nu^2-1}{8\sqrt{2} z} + O(1/z^2) \right] \\ \theta_\nu(z) &\approx (z/\sqrt{2}) + (\pi/2) [\nu - 1/4] + \frac{4\nu^2-1}{8\sqrt{2} z} + O(1/z^2) . \end{aligned} \quad (2.3.5)$$

For $\nu = 0$ we find

$$\begin{aligned} M_0(z) &\approx \frac{\exp(z/\sqrt{2})}{\sqrt{2\pi z}} \left[1 + \frac{1}{8\sqrt{2} z} \right] \\ \theta_0(z) &\approx (z/\sqrt{2}) - (\pi/8) - \frac{1}{8\sqrt{2} z} . \end{aligned} \quad (2.3.6)$$

For $z > 3$ the correction term $\frac{1}{8\sqrt{2} z}$ in $M_0(z)$ is less than .03 so we can ignore it for rough estimates. In this case one gets

$$\begin{aligned} |E(r)| &= |E(a)| \frac{M_0[\sqrt{2} (r/\delta)]}{M_0[\sqrt{2} (a/\delta)]} = |E(a)| \frac{M_0(z)}{M_0(z_a)} \quad z = \sqrt{2} (r/\delta) \quad z_a = \sqrt{2} (a/\delta) \\ &\approx |E(a)| \frac{\exp(z/\sqrt{2})}{\exp(z_a/\sqrt{2})} \frac{\sqrt{2\pi z_a}}{\sqrt{2\pi z}} = |E(a)| \exp([z-z_a]/\sqrt{2}) \sqrt{z_a/z} . \end{aligned}$$

But $[z-z_a]/\sqrt{2} = (r/\delta)-(a/\delta) = (r-a)/\delta$ and $\sqrt{z_a/z} = \sqrt{a/r}$. Thus we find that

$$\frac{|E(r)|}{|E(a)|} = \sqrt{\frac{a}{r}} e^{-(r-a)/\delta} \quad r/\delta > 3/\sqrt{2} = 2.1 \quad (2.3.7)$$

This is the famous skin depth result as it appears for a round wire. This ratio is 1 at the surface and then drops off exponentially with characteristic distance δ moving inside the wire. One sees now why the $\sqrt{2}$ was included in the definition of δ : there is then no $\sqrt{2}$ in equation (2.3.7). Comparing (2.3.7) to the one-dimensional skin depth formula (2.1.8) one sees an extra $\sqrt{a/r}$ factor arising from the cylindrical geometry.

Equation (2.3.7) is valid down to within about 2 skin depths of the center axis of the wire. In general, one can assume the field $E(r)$ is zero for all practical purposes perhaps 5 skin depths in from the surface (if $a > 5\delta$). Here are plots of $|E(r)|/|E(a)|$ using the approximate formula (2.3.7) for the same ten δ values as our previous plots,

```
f := sqrt(a/r)*exp((r-a)/d):
p2 := plot([seq(f, d = 1..10)], r = 1..a, color = black):
display(p2);
```

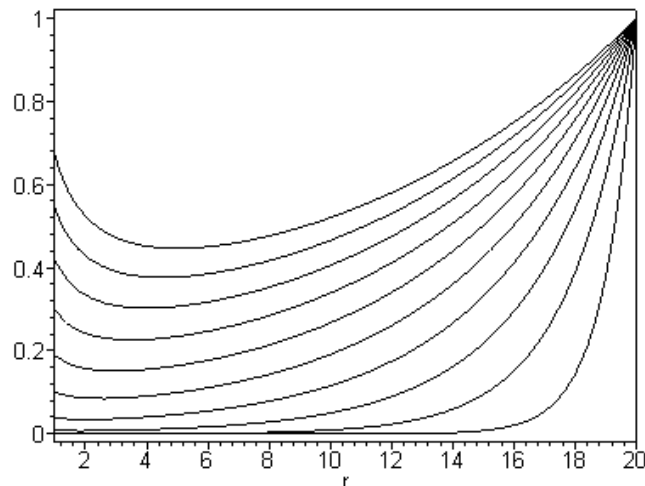


Fig 2.5

Previous plot using a certain approximation discussed above

and here are the two sets of plots superimposed with some notations added:

display(p1,p2);

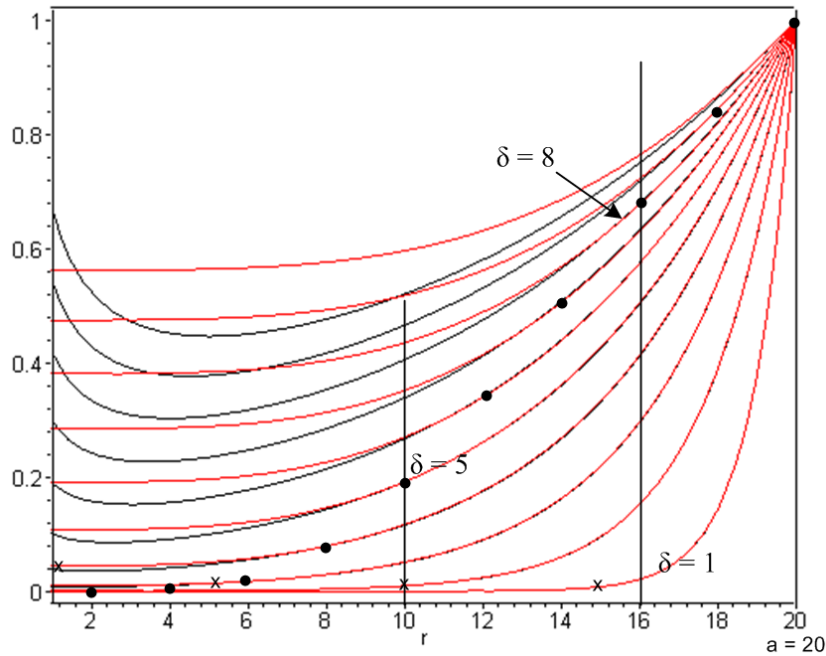


Fig 2.6

The wire radius is $a = 20$, and the curves are for $\delta = 1$ to 10 , with $\delta = 1$ being the rightmost and steepest curve. The red (exact) and black (approximate) curves for $\delta = 1$ agree down to $r = 2$ at least. The $\delta = 5$ red/black pair of curves start to pull apart around $r = 10$ which is 2 skin depths from the center. The $\delta = 8$ red/black pair of curves start to pull apart around $r = 16$. We thus verify the claim made above that each red/black pair of curves agree starting at $r = a$ and moving in to about 2 skin depths from the center line (the pull-apart points are marked by dots). One can also see that the electric field is roughly zero about 5 skin depths in from the surface (marked by x's).

Here are some skin depth values in copper based on (2.2.20) $\delta = \sqrt{2/(\omega\mu\sigma)}$ with $\sigma = 5.81 \times 10^7$ mho/m, and $\mu = \mu_0 = 4\pi \times 10^{-7}$ H/m. Selecting a reference point of 1 GHz, we have,

$$\delta = \sqrt{2/(2\pi f\mu_0\sigma)} = \sqrt{1/(\pi f\mu_0\sigma)} = \sqrt{1/f} \sqrt{1/(\pi 10^9\mu_0\sigma)} = 2.09 \times \sqrt{1/f(\text{GHz})} \mu . \quad (2.3.8)$$

Here then is a table of copper skin depths ($\mu = \text{microns}$),

f	δ	f	δ
100 GHz	0.21 μ	100 KHz	209 μ
10 GHz	0.66 μ	10 KHz	661 μ
1 GHz	2.09 μ	1 KHz	0.21 cm
100MHz	6.61 μ	100 Hz	0.66 cm
10 MHz	20.9 μ	10 Hz	2.09 cm
1 MHz	66.1 μ	1 Hz	6.61 cm

(2.3.9)

The radius of the center conductor of Belden 8281 coaxial cable is 15.5 mil = 394 μ , so the skin effect restriction occurs for $f \approx 1$ MHz and above. At 1 GHz δ is about 1/200th the radius.

As we get into the lower frequencies, the exponential decay no longer applies for Belden 8281. For very low frequencies, we can use the small z limit of $J_0(z)$ to see how the distortion begins at low frequency,

$$J_0(z) = 1 - z^2/4 \quad z \ll 1 \quad // \text{ Spiegel 24.5} \quad z = \sqrt{2} (r/\delta) .$$

Using the expression for $E(r)$ and β^2 in box (2.2.26) we find

$$\frac{E(r)}{E(a)} = \frac{1 + j (r/\delta)^2/2}{1 + j (a/\delta)^2/2} \quad \frac{|E(r)|}{|E(a)|} = \sqrt{\frac{1 + (r/\delta)^4/4}{1 + (a/\delta)^4/4}} \quad (2.3.10)$$

This shows the very early phase of the skin effect happening at low frequencies. Eq. (2.3.10) would apply for example in Belden 8281 at 1 KHz and below where $\delta/a \geq 5$. There is a *very slight* dip in the $E(r)$ and $J(r)$ distribution at $r=0$ compared to $r=a$. For example, with $a = 20$ and $\delta = 100$ one has $z \leq \sqrt{2} (a/\delta) = \sqrt{2} (1/5) = .28$ for all values of r , so z is "small" in the whole range. Below is a plot of $|E(r)/E(a)|$ in this case. Notice the offset zero so the drop is only 2 parts in 10,000.

```
num := (1+(1/4)*(r/d)^4):
den := (1+(1/4)*(a/d)^4):
f := sqrt(num/den):
d := 100: a := 20:
plot(f, r = 0..a);
```

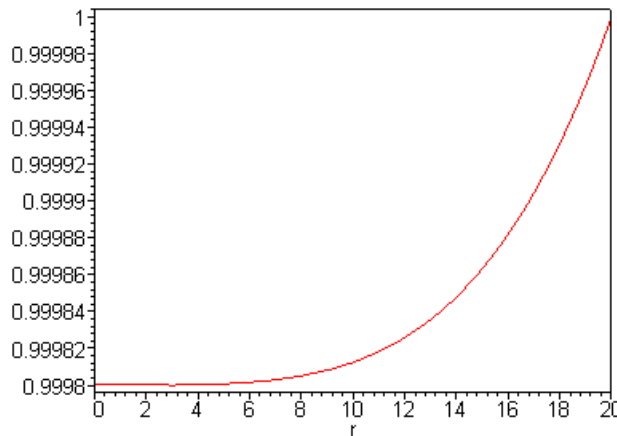


Fig 2.7

Slight dip in $E(r)$ or $J(r)$ moving from surface to center for a round wire in the low frequency limit. In this case radius $a = 20$ and skin depth $\delta = 200$.

(c) Review of the round wire solution

To conclude this section, we state in full notation the solution of the round wire as outlined above, using ω rather than δ as the argument of interest, where recall $\delta = \sqrt{2/\omega\mu\sigma}$ so $z = \sqrt{2} (r/\delta) = r \sqrt{\omega\mu\sigma}$. The following two expressions are (2.2.22) and (2.2.25) with $(\beta/j\omega) = e^{j\pi/4} \sqrt{\omega\mu\sigma} / \omega$ as in (2.2.12):

$$E(r,\omega) = E(a,\omega) \frac{\text{ber}_0[r\sqrt{\omega\mu\sigma}] + j \text{bei}_0[r\sqrt{\omega\mu\sigma}]}{\text{ber}_0[a\sqrt{\omega\mu\sigma}] + j \text{bei}_0[a\sqrt{\omega\mu\sigma}]} \quad (2.3.11)$$

$$B(r,\omega) = E(a,\omega) \frac{\text{ber}_1[r\sqrt{\omega\mu\sigma}] + j \text{bei}_1[r\sqrt{\omega\mu\sigma}]}{\text{ber}_0[a\sqrt{\omega\mu\sigma}] + j \text{bei}_0[a\sqrt{\omega\mu\sigma}]} \left(-e^{j\pi/4} \sqrt{\frac{\mu\sigma}{\omega}} \right) . \quad (2.3.12)$$

The ratio is then

$$\frac{B(r,\omega)}{E(r,\omega)} = \frac{\text{ber}_1[r\sqrt{\omega\mu\sigma}] + j \text{bei}_1[r\sqrt{\omega\mu\sigma}]}{\text{ber}_0[r\sqrt{\omega\mu\sigma}] + j \text{bei}_0[r\sqrt{\omega\mu\sigma}]} \left(-e^{j\pi/4} \sqrt{\frac{\mu\sigma}{\omega}} \right) . \quad (2.3.13)$$

The time-domain fields are, from (2.1.1) and our assumptions (2.2.4) (d) and (e),

$$\begin{aligned} \mathbf{E}(x,y,z,t) &= e^{j(\omega t - \beta_d z)} E(r,\omega) \hat{\mathbf{z}} \\ \mathbf{B}(x,y,z,t) &= e^{j(\omega t - \beta_d z)} B(r,\omega) \hat{\boldsymbol{\theta}} \end{aligned} \quad (2.3.14)$$

so that, in terms of the complex value $E(a,\omega)$,

$$\begin{aligned} \mathbf{E}(x,y,z,t) &= e^{j(\omega t - \beta_d z)} E(a,\omega) \frac{\text{ber}_0[r\sqrt{\omega\mu\sigma}] + j \text{bei}_0[r\sqrt{\omega\mu\sigma}]}{\text{ber}_0[a\sqrt{\omega\mu\sigma}] + j \text{bei}_0[a\sqrt{\omega\mu\sigma}]} \hat{\mathbf{z}} \\ \mathbf{B}(x,y,z,t) &= -e^{j(\omega t - \beta_d z)} E(a,\omega) e^{j\pi/4} \sqrt{\frac{\mu\sigma}{\omega}} \frac{\text{ber}_1[r\sqrt{\omega\mu\sigma}] + j \text{bei}_1[r\sqrt{\omega\mu\sigma}]}{\text{ber}_0[a\sqrt{\omega\mu\sigma}] + j \text{bei}_0[a\sqrt{\omega\mu\sigma}]} \hat{\boldsymbol{\theta}} . \end{aligned} \quad (2.3.15)$$

In the notation of Section 1.6 (d) these equations can be written,

$$\begin{aligned} \mathbf{E}(x,y,z,t) &= e^{j(\omega t - \beta_d z)} e^{j\varphi_{\mathbf{ez}}(r,\omega)} E(r,\omega) \hat{\mathbf{z}} & E(r,\omega) &= e^{j\varphi_{\mathbf{ez}}(r,\omega)} E(r,\omega) \\ \mathbf{B}(x,y,z,t) &= e^{j(\omega t - \beta_d z)} e^{j\varphi_{\mathbf{b\theta}}(r,\omega)} B(r,\omega) \hat{\boldsymbol{\theta}} & B(r,\omega) &= e^{j\varphi_{\mathbf{b\theta}}(r,\omega)} B(r,\omega) \end{aligned} \quad (2.3.16)$$

where $E(r,\omega) = |E(r,\omega)|$ and $B(r,\omega) = |B(r,\omega)|$ are real. From (1.6.8) we see that $E(r,\omega)$ and $B(r,\omega)$ are really "line strength" type fields. As shown in (1.6.6), the physical fields could be taken as either of the following pairs

$$\begin{aligned} \mathbf{E}_{\text{phys}}(x,y,z,t) &= \text{Re} \{ \mathbf{E}(x,y,z,t) \} = \cos[\omega t - \beta_d z + \varphi_{\mathbf{ez}}(r,\omega)] E(r,\omega) \hat{\mathbf{z}} \\ \mathbf{B}_{\text{phys}}(x,y,z,t) &= \text{Re} \{ \mathbf{B}(x,y,z,t) \} = \cos[\omega t - \beta_d z + \varphi_{\mathbf{b\theta}}(r,\omega)] B(r,\omega) \hat{\boldsymbol{\theta}} \end{aligned} \quad (2.3.17)$$

or

$$\begin{aligned} \mathbf{E}_{\text{phys}}(x,y,z,t) &= \text{Im} \{ \mathbf{E}(x,y,z,t) \} = \sin[\omega t - \beta_d z + \varphi_{\mathbf{ez}}(r,\omega)] E(r,\omega) \hat{\mathbf{z}} \\ \mathbf{B}_{\text{phys}}(x,y,z,t) &= \text{Im} \{ \mathbf{B}(x,y,z,t) \} = \sin[\omega t - \beta_d z + \varphi_{\mathbf{b\theta}}(r,\omega)] B(r,\omega) \hat{\boldsymbol{\theta}} \end{aligned} \quad (2.3.18)$$

(d) Plots of the round wire solution for Belden 8281 at 5 MHz.

Here is some Maple code to generate various plots, where we arbitrarily set $E_0 = E(a, \omega) = 1$ volt/m, $\mu = \mu_0 = 4\pi \times 10^{-7}$, $\sigma_{\text{copper}} = 5.81 \times 10^7$, $\omega = 2\pi [5 \text{ MHz}]$, and $a = 394 \mu$ -- all as appropriate for the center conductor of Belden 8281 coaxial cable. Notice that the factor

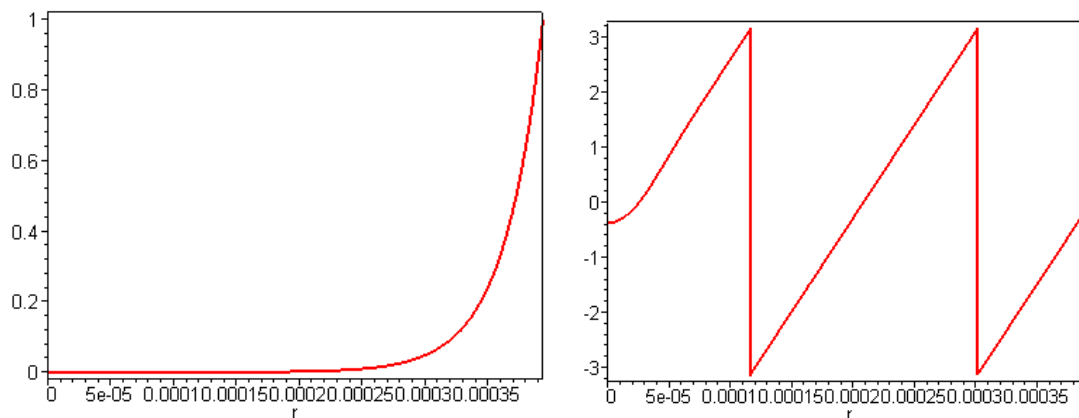
$$\sqrt{\frac{\mu\sigma}{\omega}} = \sqrt{4\pi \cdot 5.81 / 2\pi \cdot 10^6} = 10^{-3} \sqrt{2 \cdot 5.81} = 3.4 \times 10^{-3}$$

causes B to be small even at the surface $r = a$. We first set in the parameters just quoted,

```
restart; alias(I=I, j=sqrt(-1)):
E0 := 1: # volts/meter
u := 4*Pi*10^(-7): # mu-zero
s := 5.81*10^(+7): # sigma for copper
a := 394*10^(-6): # 394 microns
w := 2*Pi*5*10^(6): # 5 MHz
z := r*sqrt(w*u*s): # dimensionless arg
za := a*sqrt(w*u*s): # same at r = a
```

and then do the plots as follows, using (2.3.11) for E and (2.3.12) for B :

```
numE := KelvinBer(0,z)+ j*KelvinBei(0,z):
denE := KelvinBer(0,za)+ j*KelvinBei(0,za):
E := E0*numE/denE:
plot(abs(E), r = 0..a, thickness = 2, axes=boxed);
plot(argument(E), r = 0..a, thickness = 2, axes=boxed);
numB := KelvinBer(1,z)+ j*KelvinBei(1,z):
denB := KelvinBer(0,za)+ j*KelvinBei(0,za):
B := -E0*exp(j*Pi/4)*sqrt(u*s/w)*numB/denB:
plot(abs(B), r = 0..a, thickness = 2, axes=boxed);
plot(argument(B), r = 0..a, thickness = 2, axes=boxed);
plot(abs(B/E), r = 0..a, thickness = 2, axes=boxed);
plot(argument(B/E), r = 0..a, thickness = 2, numpoints = 100, axes=boxed);
```



E = Magnitude of E

φ_{ez} = Phase of E

Fig 2.8

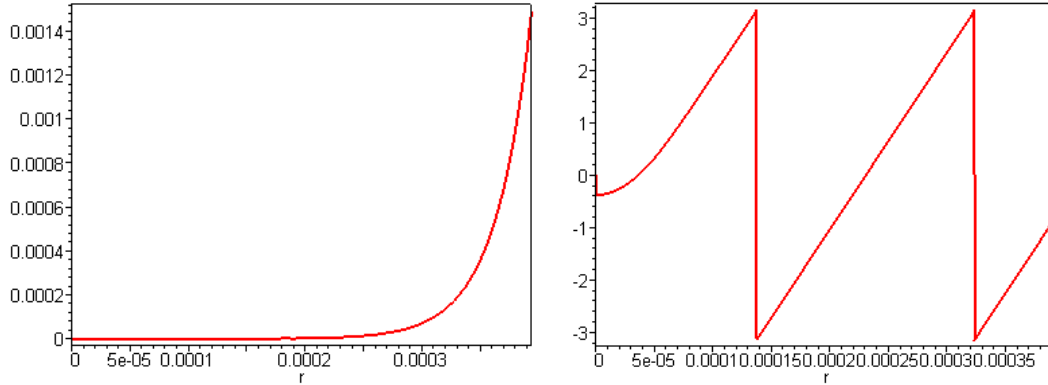


Fig 2.9

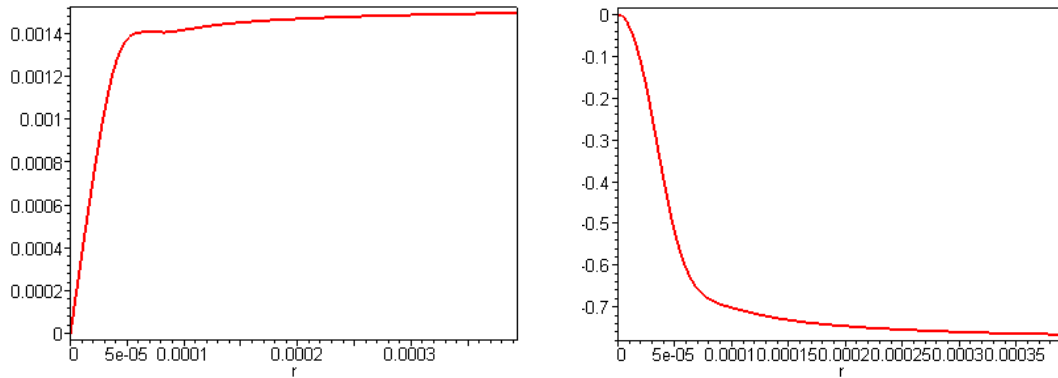
 $B = \text{Magnitude of } B$
 $\varphi_{B\theta} = \text{Phase of } B$


Fig 2.10

 $B/E = \text{Magnitude of } B/E$
 $\varphi_{B\theta} - \varphi_{Ez} = \text{Phase of } B/E$

Regarding the fast cycling of the phases of E and B, recall the discussion above (2.1.7) concerning the notion of the field being a highly damped radial wave, and below (2.1.7) where it was noted that in the 1D analog, the amplitude drops to $1/e$ when that radial wave has progressed a mere $\pi/2$ worth of phase. We see that happening here for both E and B.

The nature of these plots for moderate to large $z = r\sqrt{\omega\mu\sigma}$ can be obtained from the large z limit of the J_ν functions as noted earlier,

$$J_\nu(e^{j3\pi/4}z) = M_\nu(z) e^{j\theta_\nu(z)} \quad z = r\sqrt{\omega\mu\sigma} \quad (2.3.3)$$

$$M_\nu(z) \approx \frac{\exp(z/\sqrt{2})}{\sqrt{2\pi z}} \quad \theta_\nu(z) \approx (z/\sqrt{2}) + (\pi/2) [\nu - 1/4] \quad (2.3.5)$$

Example: For the electric field in (2.2.22) we have this large z limit,

$$\begin{aligned} E(r,\omega) &= E_0 \frac{J_0(\beta r)}{J_0(\beta a)} = E_0 \frac{J_0(e^{j3\pi/4} r \sqrt{\omega\mu\sigma})}{J_0(e^{j3\pi/4} a \sqrt{\omega\mu\sigma})} = E_0 \frac{M_0(r\sqrt{\omega\mu\sigma})}{M_0(a\sqrt{\omega\mu\sigma})} \frac{e^{jx\sqrt{\omega\mu\sigma/2}}}{e^{ja\sqrt{\omega\mu\sigma/2}}} \\ &\approx E_0 \frac{\exp(z/\sqrt{2})}{\exp(z_a/\sqrt{2})} \frac{\sqrt{2\pi z_a}}{\sqrt{2\pi z}} e^{j(x-a)\sqrt{\omega\mu\sigma/2}} \quad // E_0 = E(a,\omega) \end{aligned}$$

$$\begin{aligned}
 &\approx E_0 \exp[-(a-r) \sqrt{\omega\mu\sigma/2}] \sqrt{\frac{a}{r}} e^{-j(a-r) \sqrt{\omega\mu\sigma/2}} \\
 &\approx E(a,\omega) \sqrt{\frac{a}{r}} e^{-(a-r)/\delta} e^{-j(a-r)/\delta} \quad \delta \equiv \sqrt{2/(\omega\mu\sigma)} \quad (2.3.19)
 \end{aligned}$$

which shows both the exponential decay in magnitude and the phase linear in r ,

$$\varphi_{\mathbf{e}_z}(r,\omega) \approx -(a-r)/\delta .$$

Again, (2.3.19) is reminiscent of the 1D skin depth solution shown in (2.1.8),

$$E(x,\omega) = E(0,\omega) e^{-x/\delta} e^{-jx/\delta} . \quad (2.1.8)$$

2.4 The Surface Impedance $Z_s(\omega)$ of a Round Wire

A piece of round wire can be thought of as a resistor. Consider Fig. 2.11:

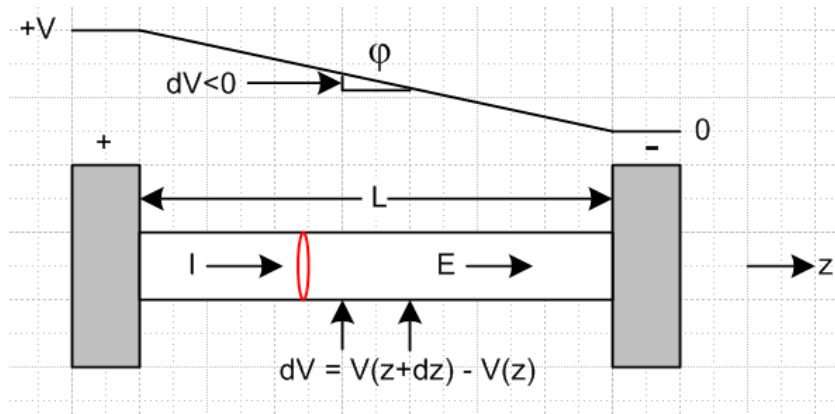


Fig 2.11

Here a piece of finite- σ wire is attached to a pair of $\sigma = \infty$ contacts. The total impedance of the wire is then determined by $Z = V/I$ ohms where V is the voltage applied to the contacts and I is the total current through the wire.

Alternatively, one could probe the wire along its surface as shown by the two arrows separated by dz . There is some voltage dV between the probes due to the field $E_z(a) \equiv E(a)$ at the surface of the wire. By definition, the surface impedance per unit length is

$$Z_s \equiv (-dV/dz) / I = E(a) / I \text{ ohms/m} . \quad (2.4.1)$$

Since the fields and currents derived under the assumptions (2.2.4) vary only with r , Z_s is independent of z and we get

$$V = V(0) - V(L) = - \int_0^L dV = - \int_0^L (dV/dz) dz = \int_0^L I Z_s dz = I Z_s L = I Z \quad (2.4.2)$$

so

$$Z = Z_s L . \quad (2.4.3)$$

Our analysis above treats the infinitely long wire, so one must imagine L here as very large compared to the wire radius a , so that end effects influencing Z_s can be ignored.

As one might expect, Z_s plays a role in transmission line attenuation.

(a) Expressions for Surface Impedance

To compute the surface impedance of the round wire, we have to make a connection to the total current I in the wire. This time, our "math loop" is a circular ring lying just below the wire surface as shown in red in Fig 2.11. Apply (2.2.1) to this loop (with $\varepsilon = 0$) to get:

$$2\pi a B(a) = \mu I \quad . \quad (2.4.4)$$

Thus, from the Z_s definition (2.4.1),

$$Z_s = E(a)/I = E(a) \mu / [2\pi a B(a)] = (\mu/2\pi a) E(a)/B(a) \quad . \quad (2.4.5)$$

Recalling from (2.2.24) that

$$E(a) = - (j\omega/\beta) \frac{J_0(\beta a)}{J_1(\beta a)} B(a) \quad . \quad (2.2.24)$$

we find that

$$Z_s = Z_s(\omega) = - (\mu/2\pi a) (j\omega/\beta) \frac{J_0(\beta a)}{J_1(\beta a)}$$

or

$$Z_s(\omega) = \frac{-j\omega\mu}{2\pi a\beta} \frac{J_0(\beta a)}{J_1(\beta a)} \quad (2.4.6)$$

where $\beta = (\sqrt{2}/\delta) e^{j3\pi/4}$ and $\delta \equiv \sqrt{2/\omega\mu\sigma}$ as in box (2.2.30). Using these last two facts and the fact that $e^{j3\pi/4}$ is a square root of $-j$, the leading factor may be written

$$\frac{-j\omega\mu}{2\pi a\beta} = \frac{-j2/(\sigma\delta^2)}{2\pi a e^{j3\pi/4} (\sqrt{2}/\delta)} = \frac{e^{j3\pi/4}}{\sqrt{2} \pi a \sigma \delta}$$

giving this alternate form for (2.4.6) in which ω does not explicitly appear,

$$Z_s(\omega) = \frac{e^{j3\pi/4}}{\sqrt{2} \pi a \sigma \delta} \frac{J_0(\beta a)}{J_1(\beta a)} \quad . \quad \beta = (\sqrt{2}/\delta) e^{j3\pi/4} = (j-1)/\delta \quad (2.4.7)$$

Below we shall use form (2.4.7) to plot $Z_s(\omega)$ as a function of skin depth δ .

Equation (2.4.7) is, as expected, rather complex. In terms of the Kelvin functions defined in (2.3.1) we may write (2.4.6) as

$$Z_s(\omega) = \frac{-j\omega\mu}{2\pi a (\sqrt{2}/\delta) e^{j3\pi/4}} \frac{\text{ber}_0[\sqrt{2}(a/\delta)] + j \text{bei}_0[\sqrt{2}(a/\delta)]}{\text{ber}_1[\sqrt{2}(a/\delta)] + j \text{bei}_1[\sqrt{2}(a/\delta)]} \quad (2.4.8)$$

According to (2.3.1) one finds, with $\alpha \equiv e^{j3\pi/4}$, that

$$\text{ber}_\nu'(z) + j \text{bei}_\nu'(z) = \frac{dJ_\nu(\alpha z)}{dz} = \frac{dJ_\nu(\alpha z)}{d(\alpha z)} \frac{d(\alpha z)}{dz} = \alpha J_\nu'(\alpha z) = e^{j3\pi/4} J_\nu'(e^{j3\pi/4} z) \quad (2.4.9)$$

Then since $J_0'(x) = -J_1(x)$ one gets

$$\begin{aligned} \text{ber}_0'(z) + j \text{bei}_0'(z) &= e^{j3\pi/4} J_0'(e^{j3\pi/4} z) = - e^{j3\pi/4} J_1(e^{j3\pi/4} z) \\ &= - e^{j3\pi/4} [\text{ber}_1(z) + j \text{bei}_1(z)] \quad (2.4.10) \end{aligned}$$

Then (2.4.8) may be rewritten as

$$Z_s(\omega) = \frac{+j\omega\mu}{2\pi a (\sqrt{2}/\delta)} \frac{\text{ber}_0[\sqrt{2}(a/\delta)] + j \text{bei}_0[\sqrt{2}(a/\delta)]}{\text{ber}_0'[\sqrt{2}(a/\delta)] + j \text{bei}_0'[\sqrt{2}(a/\delta)]} \quad (2.4.11)$$

and this form for $Z_s(\omega)$ appears in Matlick p 104 (4-28).

(b) Low frequency limit of $Z_s(\omega)$

Small $\omega \Rightarrow$ large $\delta \Rightarrow$ small β , so we expand both Bessel functions of (2.4.7) for small argument:
[Spiegel 24.5 and 24.6]

$$J_0(x) \approx 1 - x^2/4$$

$$J_1(x) \approx (x/2)(1 - x^2/8) \quad \Rightarrow \quad 1/J_1(x) \approx (2/x) (1 + x^2/8)$$

$$\Rightarrow J_0(x)/J_1(x) \approx (2/x) (1 + x^2/8) (1 - x^2/4) \approx (2/x)(1 - x^2/8) = 2/x - x/4$$

$$\Rightarrow J_0(\beta a)/J_1(\beta a) \approx 2/(\beta a) - (\beta a)/4 \quad .$$

Then from (2.4.6)

$$\begin{aligned} Z_s(\omega) &= \frac{-j\omega\mu}{2\pi a\beta} \frac{J_0(\beta a)}{J_1(\beta a)} \approx \frac{-j\omega\mu}{2\pi a\beta} [2/(\beta a) - (\beta a)/4] = \frac{-j\omega\mu}{\pi a^2 \beta^2} + \frac{j\omega\mu}{8\pi} \\ &= \frac{-j\omega\mu}{\pi a^2 [-j\omega\mu\sigma]} + \frac{j\omega\mu}{8\pi} \quad // \beta^2 \text{ from (2.2.3)} \end{aligned}$$

or

$$Z_s(\omega) = \frac{1}{\sigma\pi a^2} + j\omega \frac{\mu}{8\pi} = R_s + j\omega L_s \quad // \text{ low frequency limit} \quad (2.4.12)$$

The first term is the uniform DC resistance of the wire per unit length, normally written ρ/A as in (C.1.1) of Appendix C. The second term is $j\omega$ times the DC internal inductance $L_i = (\mu/8\pi)$ H/m, as derived in (C.3.10). Recall that this is exactly 50 nH/m if $\mu=\mu_0$, quite small, and independent of radius.

(c) High frequency limit of $Z_s(\omega)$

We first use (2.3.3) to write (2.4.6) as

$$Z_s(\omega) = (-j\omega\mu/2\pi a\beta) [M_0(\sqrt{2} a/\delta) / M_1(\sqrt{2} a/\delta)] \exp[j\{\theta_0(\sqrt{2} a/\delta) - \theta_1(\sqrt{2} a/\delta)\}] \quad (2.4.13)$$

Since large $\omega \Rightarrow$ small $\delta \Rightarrow$ large arguments for the functions in (2.4.13), we use these large z limits which can easily be obtained from (2.3.5) using $\nu = 0$ and 1,

$$\begin{aligned} M_0(z) / M_1(z) &= [1 + \frac{1}{2\sqrt{2} z} + O(1/z^2)] \\ \theta_0(z) - \theta_1(z) &= - [(\pi/2) + \frac{1}{2\sqrt{2} z} + O(1/z^2)] \end{aligned} \quad (2.4.14)$$

Insertion of these large-argument expressions into (2.4.13) with $z = \sqrt{2} \delta/a$ gives

$$\begin{aligned} Z_s(\omega) &= (-j\omega\mu/2\pi a\beta) \left(1 + \frac{1}{2\sqrt{2} \sqrt{2} a/\delta} \right) \exp(-j [\pi/2 + \frac{1}{2\sqrt{2} \sqrt{2} a/\delta}]) \\ &= (-j\omega\mu/2\pi a\beta) [1 + \delta/(4a)] \exp(-j [\pi/2 + \delta/(4a)]) \\ &= \frac{e^{-j\pi/2} \omega\mu}{2\pi a(\sqrt{2}/\delta) e^{j3\pi/4}} [1 + \delta/(4a)] e^{-j\pi/2} e^{-j\delta/(4a)} \quad // -j = e^{-j\pi/2} \end{aligned}$$

The phasor factors combine to give

$$e^{-j\pi/2} e^{-j3\pi/4} e^{-j\pi/2} = e^{-j\pi[1+3/4]} = e^{-j\pi[2-1/4]} = e^{-j\pi 2} e^{j\pi/4} = e^{j\pi/4} = (1+j)/\sqrt{2}$$

and then

$$Z_s(\omega) = \frac{\omega\mu}{4\pi(a/\delta)} (1+j) [1 + \delta/(4a)] e^{-j\delta/(4a)} \quad (2.4.15)$$

Then if $\delta \ll 4a$ the last two factors are unity and we have

$$\begin{aligned}
Z_s(\omega) &\approx \frac{\omega\mu}{4\pi(a/\delta)} (1+j) = \frac{\omega\mu\delta^2}{4\pi a\delta} (1+j) = \frac{\omega\mu[2/\omega\mu\sigma]}{4\pi a\delta} (1+j) \quad // \text{ using } \delta^2 = 2/\omega\mu\sigma \text{ from (2.2.20)} \\
&\approx \frac{1}{\sigma(2\pi a)\delta} (1+j) \quad \delta \ll 4a \quad . \quad (2.4.16)
\end{aligned}$$

Writing this as the sum of a resistive and inductive part,

$$Z_s(\omega) = R_s(\omega) + j\omega L_s(\omega) \quad (2.4.17)$$

we find

$$R_s(\omega) = \frac{1}{\sigma(2\pi a)\delta} = \omega L_s(\omega) = X_{L_s}(\omega) \quad . \quad (2.4.18)$$

The inductance can be written several ways,

$$L_s(\omega) = \frac{1}{\omega\sigma(2\pi a)\delta} = \frac{1}{\omega\sigma(2\pi a)\sqrt{2/\omega\mu\sigma}} = \frac{1}{2\pi a} \sqrt{\frac{\mu}{2\sigma\omega}} \quad . \quad (2.4.19)$$

The resistance has a simple interpretation. It is $R = 1/(\sigma A)$ where area $A = (2\pi a)\delta$. This is the area of a thin washer at the periphery of the wire of thickness δ .

The inductance is harder to understand. Its origin can be traced back to (2.4.5) above which shows that the phase of Z_s is equal to the phase of the ratio $E(a)/B(a)$. It is a result of Maxwell's curl equations that the phase of this ratio as seen in (2.4.16) is $\pi/4$ at the surface of a conductor in the skin effect limit. The inductive *reactance* is the same as the resistance, but the inductance itself increases as frequency decreases, behaving as $L \sim 1/\sqrt{\omega}$ as shown.

Quantity $R_s(\omega)$ in (2.4.18) is called R_{hf} by Matlick p 105 in his (4-35), and (2.4.16) appears as (4-36).

(d) Plots of $Z_s(\omega)$ versus skin depth δ

From (2.4.7) we found that

$$Z_s(\omega) = \frac{e^{j3\pi/4}}{\sqrt{2}} \frac{J_0(\beta a)}{\pi a \sigma \delta} \frac{J_0(\beta a)}{J_1(\beta a)} \quad \beta = (\sqrt{2}/\delta) e^{j3\pi/4} = (j-1)/\delta \quad \delta \equiv \sqrt{2/\omega\mu\sigma} \quad . \quad (2.4.7)$$

This is in SI units, but we will use $a = [a(\mu)10^{-6}]$ m and $\delta = [\delta(\mu) 10^{-6}]$ m and $\sigma = 5.81 \times 10^7$ mho/m for copper, where $a(\mu)$ and $\delta(\mu)$ means the wire radius and skin depth in microns. Then:

$$Z_s(\omega) = \frac{N e^{j3\pi/4}}{\sqrt{2}} \frac{J_0(\beta a)}{\pi a(\mu)\sigma\delta(\mu)} \frac{J_0(\beta a)}{J_1(\beta a)} \quad \text{ohms/m} \quad N = 10^{12} \quad .$$

The two limits obtained above were :

$$Z_s(\omega) \approx \frac{1}{\sigma\pi a^2} + j\omega \frac{\mu}{8\pi} = \frac{1}{\sigma\pi a^2} + j \frac{1}{4\pi\sigma\delta^2} \quad \text{small } \omega, \text{ large } \delta \quad (2.4.12)$$

Real part goes to a constant, imaginary part decays as $1/\delta^2$

$$Z_s(\omega) \approx \frac{1}{\sigma(2\pi a)\delta} (1+j) = \frac{1}{\sigma(2\pi a)\delta} + j \frac{1}{\sigma(2\pi a)\delta} \quad \text{large } \omega, \text{ small } \delta \quad (2.4.16)$$

Real and Imaginary part are the same and blow up as $1/\delta$

In our units above, the low frequency constant limit is $R_{LF} \equiv \frac{1}{\sigma\pi a^2} = \frac{N}{\sigma\pi a(\mu)^2}$.

Example: For $a = 1000\mu$, the DC resistance is $R_{LF} = 1/(\sigma\pi a^2) = .00548 \Omega/\text{m}$. Since $a = 1000/25.4 = 39.37$ mils, $2a = 78.74$ mils. From the following British units graphic, 12 gauge house wire has $2a = 80.808$ mils and has $R = .001588 \Omega/\text{ft}$ which is $.005210 \Omega/\text{m}$

TYPICAL USES	WIRE GAUGE #	DIAMETER in MILS.	AREA DIAMETER	OHMS PER 100 FT.	OHMS PER 10 FT.	OHMS PER FOOT
House Wiring	12	80.808	6,529.90	0.15880	0.015880	0.001588

Here is Maple code which plots the natural log of the real (red) and imaginary (black) part of $Z_s(\omega)$ as a function of δ , and also computes the constant limit (gray) just mentioned. The copper wire radius is set to $a=1000 \mu$.

```
restart; with(plots):
beta := (sqrt(2)/delta)*ph;
```

$$\beta = \frac{\sqrt{2} ph}{\delta}$$

```
Z := N*(ph/(sqrt(2)*Pi*a*sigma*delta))*BesselJ(0,beta*a)/BesselJ(1,beta*a);
```

$$Z = \frac{1}{2} \frac{N ph \sqrt{2} \text{BesselJ}\left(0, \frac{\sqrt{2} ph a}{\delta}\right)}{\pi a \sigma \delta \text{BesselJ}\left(1, \frac{\sqrt{2} ph a}{\delta}\right)}$$

```
ph := exp(I*3*Pi/4): N := 1e12: # phasor and scale number N
a := 1000: sigma := 5.81e7: # copper wire with radius 1000 microns
RLF := evalf(N/(sigma*Pi*a^2)): # low frequency limit
plot([log(Re(Z)), log(Im(Z)), log(RLF)], delta = 0..a, color = [red,black,gray]);
```

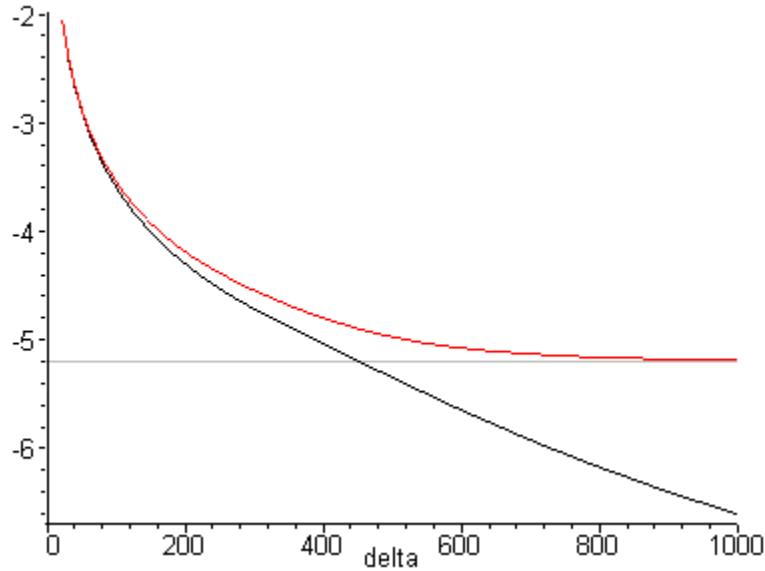


Fig 2.12

Plot of $\ln(\text{Re } Z_s)$ and $\ln(\text{Im } Z_s)$ as function of skin depth $\delta \approx 40$ to 1000μ for a copper wire of radius 1000μ . Red is real part, black is imaginary.

The general idea is that surface impedance goes up as δ goes down (left end of graph).

Here is the same plot for $\delta = 100$ to 1000 without the natural logs ($\ln = \text{"log"}$ in Maple) :

```
plot([Re(Z),Im(Z),RLF], delta = 1..10, color = [red,black,gray], labels = ["delta","Z(ohms/m)"]);
```

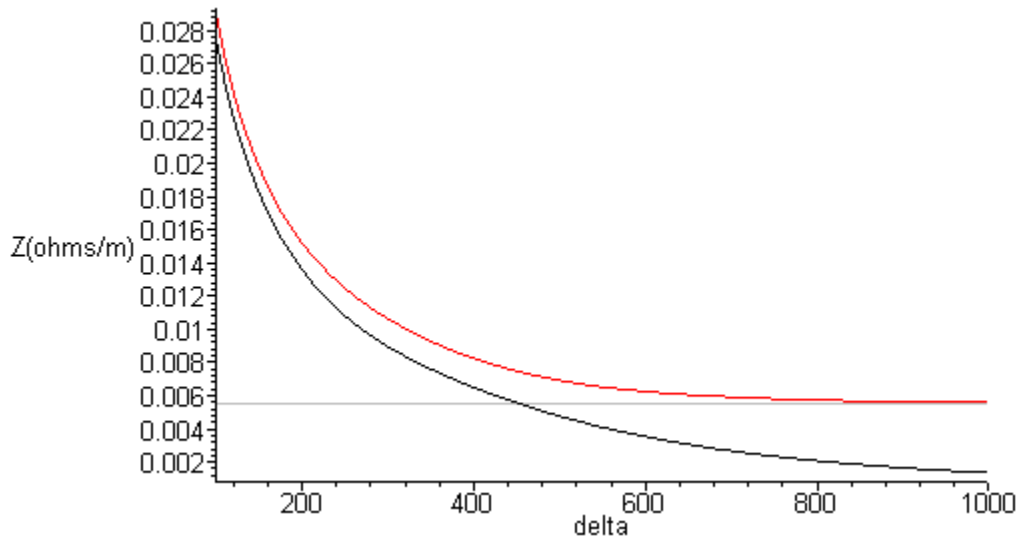


Fig 2.13

Plot of surface impedance Z_s as function of skin depth $\delta = 100$ to 1000μ for a copper wire of radius 1000μ . Red is real part, black is imaginary.

Either plot type realizes the two limits discussed above.

For the limited range $\delta = 1$ to 10μ the above plot has this appearance (the red and black curves are superposed and the gray constant line at $.00555\Omega/m$ is indistinguishable from the x axis) :

```
plot([Re(Z),Im(Z),RLF], delta = 1..10, color = [red,black,gray], labels = ["delta", "Z(ohms/m)"]);
```

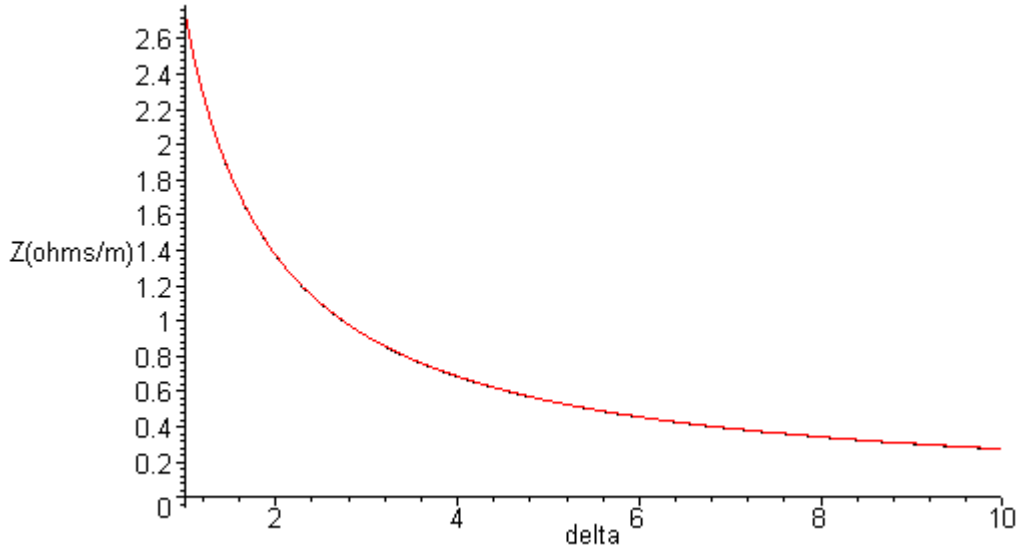


Fig 2.14

Plot of surface impedance Z_s as function of skin depth $\delta = 1$ to 10μ for a copper wire of radius 1000μ . Red is real part, black is imaginary.

The resistance of our near-12-gauge house wire at $\delta = 1$ micron (4.37 GHz) is about $2.7 \Omega/m$, which is some 500 times larger than the DC resistance.

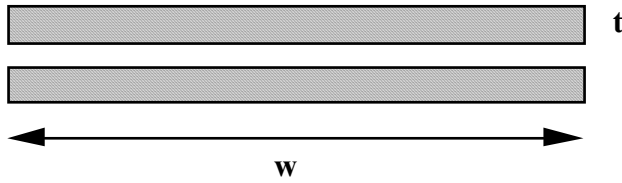
2.5 Surface Impedance for a Transmission Line

What is the surface impedance of an arbitrary conductor? As we have seen, a significant amount of work was needed to obtain the exact result even for the simple geometry of a round wire with a symmetric current distribution. One can repeat this calculation for other geometries such as a parallel plate transmission line. The general nature of the result is always the same when δ is much smaller than the depth of the conductor. That result is this (with comparison),

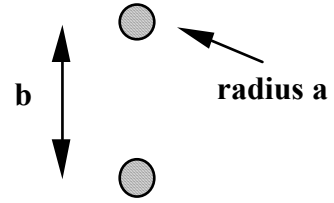
$$Z_s(\omega) \approx \frac{1}{\sigma p \delta} (1 + j) \quad // \text{ general case} \quad (2.5.1)$$

$$Z_s(\omega) \approx \frac{1}{\sigma(2\pi a)\delta} (1+j) \quad \delta \ll 4a \quad // \text{ round wire} \quad (2.4.16)$$

where p is the *effective* perimeter distance around the cross-sectional surface of a conductor where significant current flows. For the (coaxial) round wire this was $p = 2\pi a$, the circumference. For a parallel plate line of width w , $p = w$. Consider these two possible transmission line cross sections:



Cross section of a parallel plate line

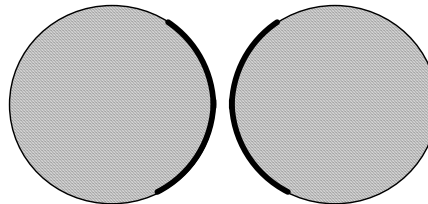


Cross section of a twin-lead line

Fig 2.15

In both cases we assume a frequency ω such that skin depth δ is small compared to the thickness of the conductors. Although the total cross sectional perimeter of one of the parallel plates is $2w + 2t$, it seems clear that the length of the "active surface" is only w , and one sets $p = w$ in the surface impedance formula. For the twin lead case with leads assumed far apart ($b \gg a$), both conductors are immersed in roughly uniform active fields, so the full $p = 2\pi a$ is applicable just as it is for a coaxial cable.

As the two round wires are brought very close together, certainly there will develop an asymmetry so that the currents are largest on the parts of the wires closest to the other wire. In this case, one must make an estimate of the "effective perimeter" p . Here is a picture,



Fat twinlead

Fig 2.16

where we have indicated a crude graphical estimate of the "active perimeter" of current flow.

King [TLT p 30 Eq (45)] quotes an approximate surface impedance result for the case of Figure 2.16. The effective distance is,

$$p = 2\pi a \sqrt{1 - (2a/b)^2} \quad . \quad a = \text{wire radius, } b = \text{center line separation} \quad (2.5.2)$$

If the gap between the conductors is $a/6$, a rough estimate for Fig 2.16, then the radical in this formula becomes .38, so the dark lines shown should cover 38% of the circumference. If the conductors almost touch, then p becomes extremely small.

King makes the interesting remark (p 30) that "accurate formulas for the internal (i.e., surface) impedance of one cylindrical conductor in the presence of another with *different radius* are not available." From the potential results of Chapter 6 below one can obtain the surface charge density $n(\theta)$ in terms of $\partial_n \phi$ on such cylindrical conductors and thus the charge partial wave moments η_m used in Appendix D. From these one could find E_z at the conductor surfaces using (D.4.13) and that would seem to determine Z_s .

In general, the high frequency skin current will be large where the E and B fields are large. These fields are large where the electric field would be large in a capacitor whose "plates" are the two conductors in cross section. Recall that such a 2D capacitor problem seeks potential ϕ as a solution of the

equation $\nabla^2_{2D}\phi(x,y) = 0$. In regions where ϕ is very large, $\mathbf{E} = -\nabla\phi$ will also be large. This subject is addressed in Chapter 5 below.

There is an interesting transmission line "paradigm shift" which occurs as one moves from the low frequency domain to that of high frequency. For small ω , one thinks of the currents in the two conductors of a transmission line as being there because they are "applied" by some external agency. The current then creates a B field around each wire which, since it is changing, creates an E field.

In the high frequency skin-effect limit, it is easier to think of the currents in the conductor surfaces as being generated by the field activity near the surfaces. The E and B fields just outside the conductors force themselves slightly into the surface. The resulting E field in the surface layer is then what creates the current.

Matick's Chapter 4 computes the surface impedance for the round wire and for strip line conductors (but not the official Stripline).

Chapter 3: Transmission Line Preliminaries

3.1 Why is there no free charge inside a conductor or a dielectric?

Imagine that at time $t = 0$ there were some free charge ρ inside a medium having conductivity σ . What would this free charge do? Intuition suggests that the individual charges in the little charge cloud would repel each other and the cloud would spread out until it encountered boundaries. In this Section we put that intuition on a more technical footing.

As discussed in Appendix E, for a non-neutral medium Ohm's Law takes the form

$$\mathbf{J} = \sigma \mathbf{E} - D \text{grad } \rho, \quad (3.1.1)$$

where \mathbf{J} is conduction current and the second term on the right, associated with Fick's Law, is non-zero when the free charge density ρ varies in space. This term is a diffusion term, D is the (electron) diffusion constant for the medium at hand, and the diffusion current flows from a region of higher charge density to one of lower density, hence the minus sign. Taking the divergence of the above equation, one finds

$$\text{div } \mathbf{J} = \sigma \text{div } \mathbf{E} - D \nabla^2 \rho$$

or

$$-\partial_t \rho = \sigma \rho / \epsilon - D \nabla^2 \rho \quad // \text{ using (1.1.25) for div } \mathbf{J}, \text{ and (1.1.3) with (1.1.6) for div } \mathbf{E}$$

or

$$\partial_t \rho - D \nabla^2 \rho + (\sigma/\epsilon)\rho = 0 \quad (3.1.2)$$

or

$$\partial_t \rho - a \nabla^2 \rho - b \rho = 0 \quad \text{where} \quad a \equiv D, \quad b \equiv -(\sigma/\epsilon). \quad (3.1.3)$$

Now let $\rho' = \rho e^{-bt}$ be an "adjusted" charge density. Then, since $\rho = \rho' e^{bt}$, (3.1.3) becomes

$$[(\partial_t \rho') e^{bt} + \rho' b e^{bt}] - a e^{bt} \nabla^2 \rho' - b e^{bt} \rho' = 0$$

or

$$\partial_t \rho' - a \nabla^2 \rho' = 0 \quad (3.1.4)$$

which is the standard heat/diffusion equation. If one starts at $t = 0$ with a point charge $\rho' = q \delta(\mathbf{r})$ at the origin, and if one assumes an infinite isotropic medium, one finds that at time t the charge density is given by

$$\rho'(r,t) = q \exp(-r^2/4at) / (4\pi at)^{3/2}. \quad t \geq 0 \quad (3.1.5)$$

This is the 3D causal free-space propagator (Green function) for the heat equation. It is the solution of

$$(\partial_t - a \nabla^2) \rho'(r,t) = \delta(\mathbf{r})\delta(t) \quad \rho'(r,t) = 0 \text{ for } t < 0. \quad (3.1.6)$$

See Stakgold (5.133) and (5.136). In n spatial dimensions, the propagator is as in (3.1.5) with $3/2 \rightarrow n/2$ and is derived in the text leading up to Stakgold (5.140).

Consider now (3.1.3) with a source term $\delta(\mathbf{r})\delta(t)$ added to the right side,

$$(\partial_t - a\nabla^2 - b)\rho(r,t) = \delta(r)\delta(t) \quad \rho(r,t) = 0 \text{ for } t < 0 \quad (3.1.7)$$

Replacing $\rho = \rho' e^{bt}$ gives

$$\partial_t \rho' - a\nabla^2 \rho' = \delta(r)\delta(t)e^{-bt} = \delta(r)\delta(t)$$

which is the same as (3.1.6). Therefore, the solution of (3.1.7) is

$$\begin{aligned} \rho(r,t) &= \rho' e^{bt} = q e^{bt} \exp(-r^2/4at) / (4\pi at)^{3/2} & \rho(r,0) &= q \delta(r) \\ \text{or} & & & \\ \rho(r,t) &= q e^{-(\sigma/\epsilon)t} \exp(-r^2/4Dt) / (4\pi Dt)^{3/2} & \rho(r,0) &= q \delta(r) \end{aligned} \quad (3.1.8)$$

The first factor $e^{-(\sigma/\epsilon)t}$ says that $\rho(r,t)$ decays exponentially in time in a uniform manner over space, while the second term says that the rough radius of the diffusing charge cloud is given by $r_t = \sqrt{4Dt}$.

The main point of all this math is the following: if there is any free charge in a medium, it goes away in a timely manner. In our idealized analysis above, it runs off to $r = \infty$, but in a finite medium it runs off to the boundary surface of the medium and becomes surface charge.

Let's now look at two extreme cases.

For a good conductor with a low diffusion rate, equation (3.1.2) becomes

$$\partial_t \rho + (\sigma/\epsilon)\rho = 0 \quad (3.1.9)$$

which has the obvious solution $\rho(r,t) = \rho(r,0) e^{-(\sigma/\epsilon)t}$ which replicates the first factor of (3.1.8). The charge just "flows away" due to the large σ .

For a dielectric with a very small conductivity, equation (3.1.2) instead becomes

$$D\nabla^2 \rho - \partial_t \rho = 0 \quad (3.1.10)$$

which is just the heat equation whose impulse response solution is (3.1.8) with $\sigma = 0$, as was shown in (3.1.5). In this case, the charge at least has time to diffuse out before it goes away!

There are then two time constants involved. The first is for the $e^{-(\sigma/\epsilon)t}$ factor where $\tau = \epsilon/\sigma$. We can estimate this time constant for a conductor and dielectric using $\epsilon \approx \epsilon_0$, and

$$\begin{aligned} \text{copper} \quad \sigma &= 5.81 \times 10^7 \text{ mho/m} \\ \epsilon_0 &= 8.8541877 \times 10^{-12} \text{ farad/m (from 1.1.28)} \\ \tau = \epsilon/\sigma &\approx 10^{-11} / 10^8 \approx 10^{-18} \text{ sec} \end{aligned} \quad (3.1.11)$$

so in copper, free charge runs off to the surface in one thousandth of a femtosecond, so we don't worry about the diffusion time constant.

For a dielectric with $\sigma = 10^{-15}$ mho/m we get τ larger by 10^{23} which is then 10^5 seconds or about a day. But in this case, the diffusion mechanism wins out. As an example, for pure silicon, $D \approx 40 \text{ cm}^2/\text{sec} = 4 \times 10^{-3} \text{ m}^2/\text{sec}$. The time to diffuse from a delta function out to say $r = 1 \text{ mm}$ is given by

$$r = \sqrt{4Dt} \Rightarrow t = r^2/(4D) = (10^{-3}\text{m})^2 / (4 \times 10^{-3} \text{ m}^2/\text{sec}) = (1/4) \times 10^{-3} \text{ sec} \quad (3.1.12)$$

so in this case the charge is pretty much gone in a quarter of a millisecond.

We arrive then at this fact:

Fact 1: In a transmission line, charge exists only on the surface of conductors. (3.1.13)

Comment: If one wants an initial charge distribution $\rho'(r,0)$ to be something *other* than a delta function, one may use this solution to the heat equation (3.1.4),

$$\rho'(r,t) = [2r\sqrt{\pi at}]^{-1} \int_0^\infty r' dr' \rho'(r',0) \{ \exp[-(r-r')^2/4at] - \exp[-(r+r')^2/4at] \} \quad (3.1.14)$$

which appears in Polyanin 1.2.3-10. Setting $\rho'(r',0) = q \delta(\mathbf{r}') = q \delta(r')/(4\pi r'^2)$ then replicates the earlier result (3.1.5), after using L'Hôpital's Rule on the integrand. The reason $\delta(\mathbf{r}) = \delta(r)/4\pi r^2$ is that it makes $\int dV \delta(\mathbf{r}) = 1$ when integrated over a sphere of any radius.

There is an exception to our rule that $\rho = 0$ inside a conductor. If magnetic fields are present in the right manner, it is possible to have an *extremely* small $\rho \neq 0$ inside a conductor -- so small that one can ignore it in any practical application. An example of this situation is presented in Section N.7 which concerns what we call the Radial Hall Effect in a round wire. The tiny charge density is required to produce a radial Hall field which offsets conduction electrons' radial Lorentz force. In the regular Hall effect, this Hall field is generated by surface charges on opposite faces of a sample, but in the round wire case only one surface is available, which is the surface of the round wire.

3.2 How thick is the surface charge layer on a conductor?

This is a fascinating subject and the interested reader will find an analysis in Appendix E from which we now quote. Since there is no free charge in the dielectric outside the conductor, and since electrons at normal temperatures cannot jump off the conductor due to its so-called work function, the surface charge is actually a layer just below the nominal surface of the conductor, but can essentially be regarded as being right at the surface. The situation is much different when a conductor is immersed in a solution of charge-carrying ions or molecules.

It turns out that the charge density decays exponentially away from the surface into the conductor and drops to $1/e$ of its surface value at a distance called the Debye length. For copper, this distance is roughly

0.6Å (Angstroms), which is 6×10^{-11} m. The crystal spacing for copper is 3.6Å, and the copper atom radius is about 1.3Å. Thus,

Fact 2: The thickness of the surface charge density on the surface of a conductor is incredibly small. For copper, it is less than the radius of one copper atom, and the general result applies to any metal. (3.2.1)

Table (2.3.9) shows that the skin depth δ for copper at 100 GHz is about 0.2 microns which is 2×10^{-7} m \approx 2000Å. Even at this large frequency, the skin depth is still about 4000 times larger than the thickness of the surface charge layer. At 1 GHz this ratio is 40,000.

Fact 3: Whereas current can exist "deep" under the surface of a conductor, even when the skin effect is dominant, the surface charge can always be thought of as being exactly at the surface. (3.2.2)

Motions of surface charges can create a 2D current density on the surface, which we might refer to as a Debye Surface Current (see Section D.9). In a transmission line, even in the extreme skin effect regime, any such Debye surface current is completely swamped by the skin effect current, and so can be ignored. In effect, one can regard such a Debye current as a very tiny fraction of the total skin effect current. We just saw above how the Debye current layer might be 0.6 Å thick, while the skin effect current at 100 GHz is 2000Å thick.

3.3 How does loss tangent affect dielectric conductivity?

The total current in a dielectric may be written, as noted in (2.2.1),

$$\mathbf{J}_{\text{tot}} = j\omega\epsilon_{\text{d}}\mathbf{E} + \sigma_{\text{d}}\mathbf{E} . \quad (3.3.1)$$

The first term is the displacement current and the second term is the conduction current. At high frequencies (say 1 GHz), the dielectric constant ϵ_{d} acquires a small imaginary part due to the presence of absorption resonances in the medium at infrared frequencies. One can write,

$$\epsilon_{\text{d}} = \epsilon'_{\text{d}} - j\epsilon''_{\text{d}} = \epsilon'_{\text{d}} [1 - j (\epsilon''_{\text{d}}/\epsilon'_{\text{d}})] = \epsilon'_{\text{d}} [1 - j \tan_{\text{L}}] , \quad \tan_{\text{L}} \equiv (\epsilon''_{\text{d}}/\epsilon'_{\text{d}}) . \quad (3.3.2)$$

If one plots ϵ_{d} in the complex plane, \tan_{L} (called the **loss tangent**, aka $\tan\delta$) is the tangent of the small angle θ_{L} of the triangle whose perpendicular sides have length ϵ'_{d} and ϵ''_{d} where ϵ''_{d} is normally very small. That is to say, the loss tangent is (minus) the ratio of the small imaginary part to the dominant real part of ϵ_{d} . \tan_{L} is commonly referred to as the **dissipation factor**. When this expression is inserted into (3.3.1) the result is,

$$\begin{aligned} \mathbf{J}_{\text{tot}} &= j\omega\epsilon_{\text{d}}\mathbf{E} + \sigma_{\text{d}}\mathbf{E} = j\omega\epsilon'_{\text{d}}[1 - j \tan_{\text{L}}]\mathbf{E} + \sigma_{\text{d}}\mathbf{E} \\ &= j\omega\epsilon'_{\text{d}}\mathbf{E} + (\sigma_{\text{d}} + \omega\epsilon'_{\text{d}}\tan_{\text{L}})\mathbf{E} \\ &= j\omega\epsilon'_{\text{d}}\mathbf{E} + \sigma_{\text{eff}}\mathbf{E} . \end{aligned} \quad (3.3.3)$$

In effect, the dielectric has now acquired an effective conductivity,

$$\sigma_{\text{eff}} = (\sigma_d + \omega \epsilon'_d \tan \delta) . \tag{3.3.4}$$

Because the DC conductivity of a good dielectric is so small, the loss tangent contribution to σ_{eff} dominates even at quite low frequencies. For polyethylene we can use these ballpark numbers,

$$\sigma_d \approx 10^{-15} \text{ mho/m} \quad \epsilon'_d \approx 2.3 \quad \tan \delta \approx 2 \times 10^{-4} \tag{3.3.5}$$

taken from the following 2008 studies of Low and High Density Polyethylene done by Eaton and Kmiec,

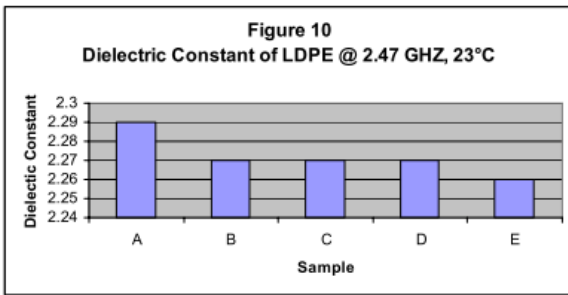


Figure 10: Dielectric Constant of LDPE @ 2.47 GHz, 23°C

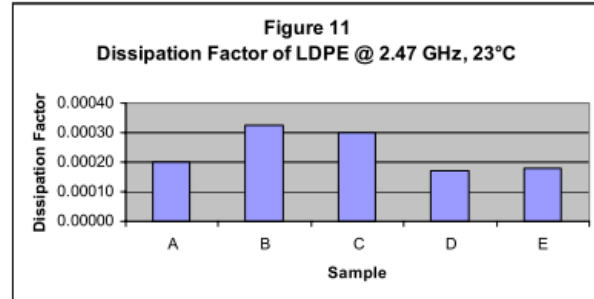


Figure 11: Dissipation Factor of LDPE @ 2.47 GHz, 23°C

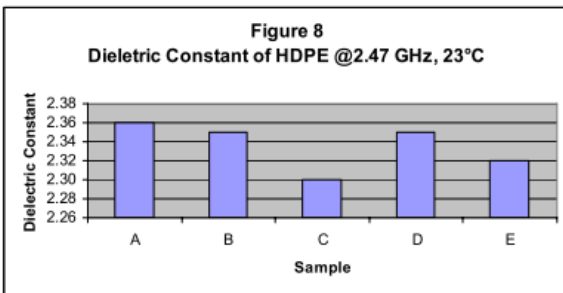


Figure 8: Dielectric Constant of HDPE @ 2.47 GHz, 23°C

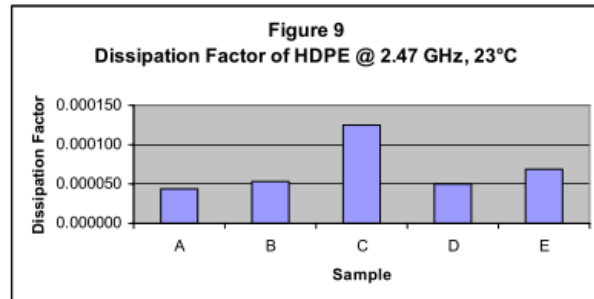


Figure 9: Dissipation Factor of HDPE @ 2.47 GHz, 23°C

and for conductivity,

Fig 3.1

Typical properties of polyethylene

ASTM test	Property	Low density	Medium density	High density	Ultrahigh molecular weight
D149	Dielectric strength (V/mil) short time, 1/8-in. thick	460-700	460-650	450-500	900 kV/cm
D150	Dielectric constant At 1kHz	2.25-2.35	2.25-2.35	2.30-2.35	2.30-2.35
D150	Dissipation factor At 1kHz	0.0002	0.0002	0.0003	0.0002
D257	Volume resistivity (ohm-cm) At 73°F, 50% RH	10~15	10~15	10~15	10~18
D495	Arc resistance(s)	135-160	200-235	-	-

<http://www.sdplastics.com/polyeth.html>

San Diego Plastics, Inc.

Note: This table claims $\rho_d = 10^{15} \text{ ohm-cm} = 10^{13} \text{ ohm-m}$, but most other sources give larger values. We assume $\rho_d \sim 10^{17} \text{ ohm-cm} = 10^{15} \text{ ohm-m}$ and therefore $\sigma_d \sim 10^{-15} \text{ mho/m}$. It does not matter much!

Even at 1 Hz, the loss tangent contribution dominates in (3.3.4). Using the above figure for $\tan \delta$, here are a few values of $\sigma_{\text{eff}} \approx (\epsilon'_d \tan \delta) \omega$ versus frequency: ($f = .0$ is really $10^0 = 1 \text{ Hz}$)

```

e0 := 8.85e-12:  tanL := .0002:  ep := 2.3*e0:
sig_eff := (f) -> evalf(1e-15 + 2*Pi*f*ep*tanL):
printf("      f(GHz)  sigma_eff(mho/m)\n");
for n in [0,8,9,10,11] do f := 10^n;
  printf("      %5.1f,      %4.1e\n",f/1e9,sig_eff(f));
od:

      f(GHz)  sigma_eff(mho/m)
      .0,      2.7e-14
      .1,      2.6e-06
      1.0,      2.6e-05
      10.0,      2.6e-04
      100.0,      2.6e-03

```

// = 2.6×10^{-3}

so

$$\sigma_{d,\text{eff}}(\omega) \approx (\epsilon_d \tan_L) \omega = 4.1 \times 10^{-15} \omega = 2.6 \times 10^{-5} f(\text{GHz}) \quad // \text{PE} \quad (3.3.6)$$

Thus, in a transmission line, although the nominal DC dielectric conductance might be 10^{-15} mho/m, at operating frequencies the effective σ_d is much larger, being for example 2.6×10^{-5} mho/m in polyethylene at 1 GHz. However, even if we replace σ_d by the much larger σ_{eff} in the complex dielectric constant ξ_d ,

$$\begin{aligned} \xi_d &= \epsilon'_d + \sigma_{\text{eff}}/j\omega = \epsilon'_d + [\sigma_d + \omega \epsilon'_d \tan_L]/j\omega \approx \epsilon'_d + [\omega \epsilon'_d \tan_L]/j\omega \\ &= \epsilon'_d [1 + \tan_L/j] \approx \epsilon'_d \approx \epsilon_d \end{aligned} \quad (3.3.7)$$

we still find for a material like polyethylene that

$$\xi_d \approx \epsilon_d \quad (3.3.8)$$

at least to 2.5 GHz. It is not hard to write an expression for \tan_L as a function of frequency since it involves the real and imaginary parts of the dielectric constant $\epsilon_d(\omega)$ which has infrared resonances dependent on the medium. Since RF frequencies up to perhaps 10 GHz are much less than infrared frequencies, although \tan_L does increase somewhat with ω in this range, one still has $\tan_L \ll 1$. Advanced dielectrics typically have \tan_L in the range .002 or less at 10 GHz.

3.4 Size of E fields in conductor and dielectric; conservation of total current at a boundary

We know from (1.1.48) that the following E field condition applies at a boundary between two media, where n refers to the normal component,

$$\xi_1 E_{n1} = \xi_2 E_{n2} \quad // \text{ frequency domain} \quad (1.1.48)$$

or

$$(\epsilon_1 + \sigma_1/j\omega) E_{n1} = (\epsilon_2 + \sigma_2/j\omega) E_{n2} \quad (3.4.1)$$

or

$$\frac{E_{n1}}{E_{n2}} = \frac{\xi_2}{\xi_1} = \frac{\epsilon_2 + \sigma_2/j\omega}{\epsilon_1 + \sigma_1/j\omega} = \frac{j\omega\epsilon_2 + \sigma_2}{j\omega\epsilon_1 + \sigma_1} \quad (3.4.2)$$

Since most dielectrics have a small imaginary part for ϵ_1 , we must interpret σ_1 as being the σ_{eff} shown in (3.3.4).

$$\sigma_1 \approx (\sigma_{1\text{DC}} + \omega\epsilon_1 \tan_L) \quad (3.4.3)$$

Let 1 = dielectric = polyethylene and 2 = conductor = copper with these assumed parameters

$$\begin{array}{lll} \epsilon_1 = 2.3 \epsilon_0 & \epsilon_2 = \epsilon_0 & \epsilon_0 = 8.85 \times 10^{-12} \\ \sigma_{1\text{DC}} = 10^{-15} & \sigma_2 = 5.81 \times 10^7 & \tan_L = .0002 \end{array} \quad (3.4.4)$$

Then

$$\text{rat} \equiv \frac{E_{n1}}{E_{n2}} = \frac{j\omega\epsilon_2 + \sigma_2}{j\omega\epsilon_1 + \sigma_1} = \frac{j2\pi f\epsilon_2 + \sigma_2}{j2\pi f\epsilon_1 + \sigma_1} \quad (3.4.5)$$

```

pi := evalf(Pi):
e1 := 2.3*e0: e2 := e0: e0 := 8.85e-12:
s1dc := 1e-15: s2 := 5.81e7: tanL := .0002:
s1 := s1dc + 2*pi*f*e1*tanL:
rat := (j*2*pi*f*e2+s2)/(j*2*pi*f*e1+s1): collect(%,f);

```

$$\frac{.5560618998 \cdot 10^{-10} j f + .581 \cdot 10^8}{(.2557884738 \cdot 10^{-13} + .1278942369 \cdot 10^{-9} j) f + .1 \cdot 10^{-14}}$$

Looking at this ratio, for f in the range (10 Hz, 10^{16} Hz) we can approximate the ratio as

$$\text{rat} = \frac{E_{n1}}{E_{n2}} = \frac{\sigma_2}{j2\pi f\epsilon_1} \quad \left| \frac{E_{n1}}{E_{n2}} \right| \approx \frac{\sigma_2}{2\pi f\epsilon_1} = .45 \times 10^{18} / f \quad (3.4.6)$$

Then for the "practical" range (10 Hz, 500 GHz) this ratio varies from $\sim 10^{17}$ to 10^6 . We conclude:

Fact 1: At a boundary between a good dielectric and a good conductor, the normal E field is at least 1 million times larger in the dielectric than it is in the conductor for frequencies under 500 GHz. (3.4.7)

Fact 2: This large jump in E_n at the boundary must be supported by a significant surface charge density n_s on the boundary since, according to (1.1.47), $n_s = \epsilon_1 E_{n1} - \epsilon_2 E_{n2} \approx \epsilon_1 E_{n1}$. (3.4.8)

Using $J_i = \sigma_i E_i$ we can restate the above facts in terms of current densities,

$$(j\omega\epsilon_1 + \sigma_1) E_{n1} = (j\omega\epsilon_2 + \sigma_2) E_{n2} . \tag{3.4.1}$$

$$(j\omega\epsilon_1 + \sigma_1) (J_{n1}/\sigma_1) = (j\omega\epsilon_2 + \sigma_2) (J_{n2}/\sigma_2) .$$

$$[1 + j\omega(\epsilon_1/\sigma_1)] J_{n1} = [1 + j\omega(\epsilon_2/\sigma_2)] J_{n2} \tag{3.4.9}$$

$$\left[1 + \frac{j\omega\epsilon_1}{\sigma_{1DC} + \omega\epsilon_1 \tan_L} \right] J_{n1} = [1 + j\omega(\epsilon_2/\sigma_2)] J_{n2} \quad // \text{ using (3.4.3)}$$

$$\left[1 + \frac{j2\pi f\epsilon_1}{\sigma_{1DC} + 2\pi f\epsilon_1 \tan_L} \right] J_{n1} = [1 + j2\pi f(\epsilon_2/\sigma_2)] J_{n2} \quad // \omega = 2\pi f \tag{3.4.10}$$

For $f \gg \sigma_{1DC}/(2\pi\epsilon_1 \tan_L) = .04 \text{ Hz}$, one can ignore σ_{1DC} on the left to get

$$\begin{array}{ccc} \text{dielectric} & & \text{conductor} \\ [1 + \underset{\text{cond}}{j/\tan_L}] \underset{\text{disp}}{J_{n1}} = [1 + j2\pi f(\epsilon_2/\sigma_2)] \underset{\text{cond}}{J_{n2}} & f \gg \sigma_{1DC}/(2\pi\epsilon_1 \tan_L) & \\ \text{cond} & \text{disp} & \text{cond} \quad \text{disp} \end{array} \tag{3.4.11}$$

where we have now labeled the conduction current and displacement current terms. Using the numbers above one finds,

$$\begin{array}{ccc} \text{dielectric} & & \text{conductor} \\ [1 + 5000 \underset{\text{cond}}{j}] \underset{\text{disp}}{J_{n1}} = [1 + 10^{-18} \underset{\text{cond}}{f}] \underset{\text{disp}}{J_{n2}} & & \\ \text{cond} & \text{disp} & \text{cond} \quad \text{disp} \end{array} \tag{3.4.12}$$

For f in the range (10 Hz, 10^{16} Hz) it is clear that in the dielectric, essentially all the current is displacement current, while in the conductor it is essentially all conduction current. We conclude:

Fact 3: For any practical frequency and good dielectric, the total current in the dielectric is almost all displacement current, while that in the conductor it is almost all conduction current. (3.4.13)

Imagine now a tiny patch of area (bordered in red) on the surface between a conductor and a dielectric,

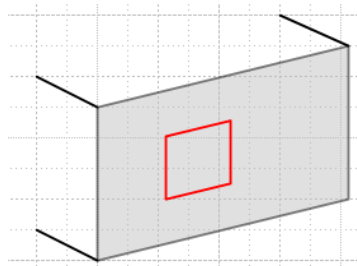


Fig 3.2

Defining a total current $J_{\text{tot},n} \equiv j\omega\epsilon E_n + \sigma E_n$, as in (2.2.1), we have shown that this total current flows right through the patch but changes its nature from nearly all conduction current in the conductor to nearly all displacement current in the dielectric. In the next section, we identify the normal direction with the local radial direction. Then the total current passing through a tiny square patch like that in Fig 3.2 can be regarded as being "fed" by the radial conduction current J_r just inside the conductor where $J_r = \sigma E_r$. This current feeds the surface charge on the boundary which creates a large E field and thus a large displacement current in the dielectric. We sometimes refer to this mechanism as "charge pumping".

Recall now some results from Section 1.5,

$$J_{n1} = n_s(\sigma_1/\epsilon_1) \quad (1.5.15)$$

$$J_{2n} = (\xi_1/\epsilon_1) (j\omega) n_s = [j\omega + (\sigma_1/\epsilon_1)] n_s \quad (1.5.16)$$

It follows that (remember that these J's are conduction currents)

$$J_{2n} = j\omega n_s + J_{n1} \quad (3.4.14)$$

We interpret this to say that during the charge pumping process, some of J_{2n} is used to feed the change in the surface charge n_s (think $\partial_t n_s$), and the rest flows through into the dielectric as J_{n1} . This last equation is just an application of continuity (1.1.35) at the boundary.

3.5 The TEM mode fields and currents for an *ideal* transmission line

In this and the next section, we take a crude qualitative look at the various E, B and J components first for an ideal transmission line, then for a practical one. An example is repeatedly used in which the conductor of interest is the round center conductor (radius $a = 1$ mm) of a properly terminated 75Ω coaxial cable driven by 7.5 volts, and thus having a current of 100 mA. The two tables obtained (one ideal, one practical) mainly serve as an exercise in applying the various concepts reviewed in previous sections.

By "ideal" we mean that the conductors have near infinite conductivity and the dielectric has zero conductivity. Consider a cross sectional view of one conductor of a transmission line having arbitrarily shaped conductors (the shape is uniform in the z direction). For a given point on the surface, define a cylindrical coordinate system (axis through red dot) so that

- r = radial direction = the normal outward from the surface (local x)
- θ = azimuthal direction = tangential to the surface in the cross section plane (local y)
- z = tangential to the surface along the transmission line (local and global z)

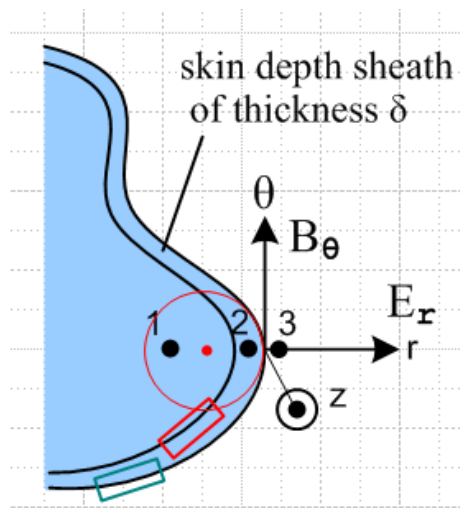


Fig 3.3

The following table shows the qualitative sizes of various components of E, B and J (conduction current) near the surface of a transmission line conductor. Several regions of space are of interest:

1. Deep in the conductor, under the surface charge layer and under any current layer.
2. In the conductor, just under the surface charge layer, and in the skin current layer.
3. In the dielectric, just outside the super-thin surface charge layer.

The reader is warned that the rest of this section and Section 3.6 make very tedious reading because an argument must be made for the general size of every single item in the two large Tables. We recommend that the reader just peruse the two Tables and ignore the Explanation sections unless there is an interest in some particular table value.

First is the Table for the ideal transmission line conductor :

Table 1: E,B,J for an ideal transmission line

Region 1. Deep in the conductor, under the surface charge layer and under any current layer.

$$\begin{array}{lll} E_{\mathbf{x}} = 0 & B_{\mathbf{x}} = 0 & J_{\mathbf{x}} = 0 \\ E_{\boldsymbol{\theta}} = 0 & B_{\boldsymbol{\theta}} = 0 & J_{\boldsymbol{\theta}} = 0 \\ E_{\mathbf{z}} = 0 & B_{\mathbf{z}} = 0 & J_{\mathbf{z}} = 0 \end{array}$$

Region 2. In the conductor, just under the surface charge layer, and in the current layer.

$$\begin{array}{lll} E_{\mathbf{x}} = \text{very small} & B_{\mathbf{x}} = 0 & J_{\mathbf{x}} = \text{small} \\ E_{\boldsymbol{\theta}} = 0 & B_{\boldsymbol{\theta}} = \text{large} & J_{\boldsymbol{\theta}} = 0 \\ E_{\mathbf{z}} = \text{small} & B_{\mathbf{z}} = \text{small} & J_{\mathbf{z}} = \text{very large} \end{array}$$

Region 3. In the dielectric, just outside the super-thin surface charge layer (explanations below):

$$\begin{array}{lll} E_{\mathbf{x}} = \text{large} & B_{\mathbf{x}} = 0 & J_{\mathbf{x}} = 0 \\ E_{\boldsymbol{\theta}} = 0 & B_{\boldsymbol{\theta}} = \text{large} & J_{\boldsymbol{\theta}} = 0 \\ E_{\mathbf{z}} = \text{small} & B_{\mathbf{z}} = \text{small} & J_{\mathbf{z}} = 0 \end{array} \quad (3.5.1)$$

Explanations of Table Entries

Region 1: (the interior) In the interior we know that \mathbf{E} must satisfy the Helmholtz equation (2.1.6a). Due to the powerful exponential effect of this equation (see (2.1.8) and (2.3.7) for the round wire), we know that \mathbf{E} fields cannot exist deep inside the conductor, and can exist only in the skin depth region. Maxwell (1.1.2) says $\text{curl } \mathbf{E} = -j\omega\mathbf{B}$ in the ω domain, so if $\mathbf{E} = 0$ in the interior, so also is \mathbf{B} . A "perfect conductor" has $\sigma = \text{extremely large}$, and $\delta = \text{extremely small}$ since $\delta = \sqrt{2/\mu\sigma\omega}$. Thus, conductor \mathbf{E} and \mathbf{B} fields can only exist very close to the surface. In region 1 of the above table, we show all fields as being 0 underneath the very thin current sheath. Since $\mathbf{E} = 0$ in the perfect conductor interior, it follows from $\mathbf{J} = \sigma\mathbf{E}$ that $\mathbf{J} = 0$ there as well (region 1). Thus, all current is confined to the thin current sheath of regions 2. Everything is quiet in Region 1.

Region 2: (the current sheath) As just noted, all currents flow in a very thin sheath at the surface of thickness δ . Since the thickness is tiny, the current density $J_{\mathbf{z}}$ there is "very large" as marked in the table. Imagine a total current I flowing down the conductor, but it is restricted to flow only in the thin sheath.

In this thin layer, there is some radial pumping of charge to the surface to "feed" the surface charge which is always changing in time, so we indicate a small $J_{\mathbf{x}}$ term. As noted in Section 3.4, this same $J_{\mathbf{x}}$ is "feeding" the total current flow through the surface, and the surface converts this total current from conduction current on the inside to displacement current on the outside. An argument will be given below for why $J_{\mathbf{x}}$ is small compared with $J_{\mathbf{z}}$ and we duly mark $J_{\mathbf{x}}$ as "small" in region 2.

Application of Ampere's Law (1.1.37) to the small red loop in Fig 3.3 ($B_{\boldsymbol{\theta}} = 0$ on the left long edge) shows that the large $J_{\mathbf{z}}$ sheath current creates a "large" $B_{\boldsymbol{\theta}}$ field in the sheath which grows from 0 on the sheath's inner boundary to some large value at the conductor surface. Ignoring dramatic μ differences, this

B_θ then exists just outside the surface as well according to (1.1.42). We thus mark B_θ as "large" in both regions 2 and 3. If $I = 100$ mA and $a = 1$ mm for a round conductor, then $B_\theta = \mu_0 I / (2\pi a) = 20$ μ T at the wire surface. (Earth field is 32 μ T). This is a large value for B_θ in our current context.

Since $\mathbf{E} = \mathbf{J}/\sigma$, even though J_z is very large, σ is extremely large, so we shall mark E_z as being "small". And since J_r is already marked "small", we mark $E_r = J_r/\sigma$ as "very small". The small radial current J_r might create some small B_z , so we throw in a small B_z entry as well (see Region 3 below).

The remaining three entries (B_r , E_θ , J_θ) in region 2 we leave at 0, though they might have some very tiny values.

Region 3: (the dielectric) Since we are now outside the surface charge layer, (1.1.47) says there is a large radial electric field E_r which is supported by this charge density (Gauss's Law), so we mark E_r as "large" in region 3. The tangential electric fields are continuous through the boundary according to (1.1.41). Therefore, we give E_θ and E_z the same values they had in region 2.

We already observed that B_θ continues being "large" just above the surface.

It was noted above that there is a radial pumping current J_r inside the conductor. This pumps charge onto the conductor surface, and is converted to displacement current in the dielectric, as discussed above in Section 3.4 (think of a simple parallel plate capacitor where this also happens). This displacement current and J_r are relatively small currents and they create a small B_z field as we now crudely demonstrate. Consider a very tall and thin (small w) red math loop whose one edge lies parallel to the z direction between the conductors and whose top edge is very distant.

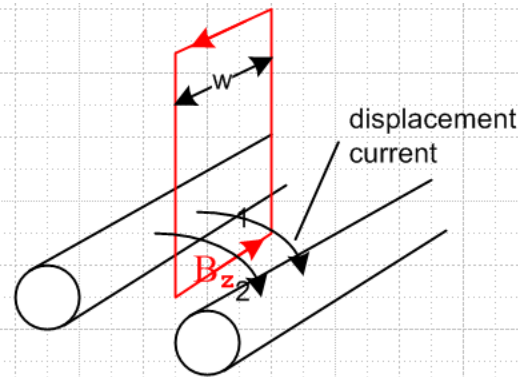


Fig 3.4

Consider Ampere's law (1.1.37) relative to this loop and with respect to the displacement current flowing through the loop between the conductors,

$$\oint \mathbf{H} \cdot d\mathbf{s} = \int_S \partial_t \mathbf{D} \cdot d\mathbf{S} \quad . \quad (1.1.37)$$

Integration of the small displacement current $\partial_t \mathbf{D}$ passing through the loop gives some small non-zero value for the area integral on the right. Meanwhile, the line integral on the left has cancelling contributions from the vertical loop sides (w is very small), while the loop top is far away so contributes nothing. The result is some small H_z and hence small B_z in the region between the conductors. Since B_z is a tangential field, it will exist also just inside the conductor surface, as indicated by (1.1.42). Both these B_z fields are marked "small" in the table for regions 2 and 3. As a crude estimate, a loop of width $w = \lambda/2$

would capture a full I worth of displacement current, so our thin loop captures $\sim I w/(\lambda/2)$. If $I \sim 100$ mA and $\lambda \approx 1$ m, then Ampere's law above says $(B_z/\mu_0)w = I w/(\lambda/2)$ so $B_z \approx \mu_0 I(\lambda/2) = 4\pi \times 10^{-7}(0.1)(1/2) \approx 6.3 \times 10^{-8} = .06 \mu\text{T}$, which is small compared to our $20\mu\text{T}$ estimate for B_θ .

Since the ideal dielectric has zero conductivity, the conduction current components are all set to zero.

In the dielectric, if we ignore the small E_z and B_z field components relative to the large E_r and B_θ , we find that (see Fig 3.3) just outside the surface, the \mathbf{E} and \mathbf{B} fields are perpendicular and are both transverse to the z direction. Hence this is a TEM (Transverse Electric and Magnetic) mode of the transmission line. Their cross product is the Poynting vector $(1/\mu_d) \mathbf{E} \times \mathbf{B}$ which is in the $+z$ direction coming at the viewer in Fig 3.3. This is the direction of power flow along the transmission line. (Jackson p 259, Eq. 6.109: $\mathbf{S} = \mathbf{E} \times \mathbf{H}$ in SI units).

The remaining two entries (B_r , E_θ) in the region 3 we leave at 0, though they might have some very tiny values.

3.6 The TEM mode fields and currents for a *practical* transmission line

We now "turn on" the imperfections of the transmission line. As soon as σ in the conductor becomes large but finite, the infinitely thin current sheath spreads out over some moderate skin depth δ . At very low frequencies, the current J_z is spread across the entire conductor and there is no Region 1.

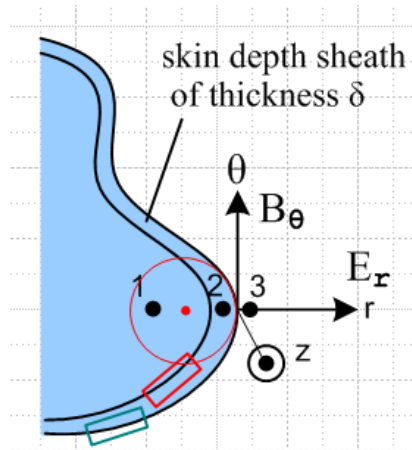


Fig 3.3

At higher ω there still is a Region 1, but we shall ignore it from now on. We are still interested in region 2 which is just below the surface charge layer. Recall from Section 3.2 that the surface charge layer remains nearly infinitely thin even for a non-perfect conductor.

So here is the new table. The superscripts refer to descriptive sections below. Other values are just carried from the previous table. In order to make ballpark magnitude estimates, we again assume that the transmission line is 75 ohms, is properly terminated, and is driven by a voltage of amplitude 7.5 volts, so the current is 100 mA.

Table 2: E,B,J for a practical transmission line

Region 2. In the conductor, just under the surface charge layer, and in the current layer.

$$\begin{array}{lll} E_x = \text{very small}^{[c]} & B_x = 0 & J_x = \text{small} \\ E_\theta = 0 & B_\theta = \text{large} & J_\theta = 0 \\ E_z = \text{small}^{[a]} & B_z = \text{small} & J_z = \text{large}^{[a]} \end{array}$$

Region 3. In the dielectric, just outside the super-thin surface charge layer.

$$\begin{array}{lll} E_x = \text{large}^{[a]} & B_x = 0 & J_x = \text{very small}^{[b]} \\ E_\theta = 0 & B_\theta = \text{large} & J_\theta = 0 \\ E_z = \text{small}^{[a]} & B_z = \text{small} & J_z = \text{very small}^{[b]} \end{array} \quad (3.6.1)$$

Explanations of Table Entries

[a] E_z and J_z in the conductor; E_z and E_x outside the conductor

Inside the conductor, a non-zero E_z exists due to the current flow in the z direction and the finite conductivity of the conductor. As an estimate for a round wire not too close to the other conductor, assume that the wire has diameter 1 mm, and is operating at 1 GHz with a skin depth $\delta = 2$ microns as in (2.3.9). The cross sectional area for current flow is then about $2\pi r\delta = 4\pi \times 10^{-9} \text{ m}^2$. If 100 mA flows through this wire, then $J_z = 0.1/(2\pi r\delta) = 8 \times 10^6 \text{ amps/m}^2$, and this J_z is marked "large" for region 2 in the above table. Then $E_z = J_z/\sigma = 8 \times 10^6 / 5.81 \times 10^7 = 0.14 \text{ volts/meter}$. This E_z is marked "small" in the region 2 part of the above table. At lower frequencies where skin depth is larger, E_z is less.

Since E_z is a tangential (parallel to conductor surface) E field, according to (1.1.41) it has the same value in region 3, so that is also marked "small" above.

In contrast, if the conductor separation is 0.5 cm, and if we crudely assume the E field is constant between the conductors, then E_x between the conductors is $7.5 \text{ volts} / 5 \times 10^{-3} \text{ m} = 1500 \text{ volts/m}$. This is marked "large" in region 3 above. So in region 3 just outside the conductor,

$$E_x \sim 1500 \text{ V/m} \quad E_z \sim 0.14 \text{ V/m} \quad \text{ratio } (E_z/E_x) \leq 10^{-4} \quad (3.6.2)$$

[b] J_x , E_x and J_z in the dielectric

As shown in (3.3.4), the effective conductivity in the dielectric is given by

$$\sigma_{\text{eff}} = (\sigma_d + \omega \epsilon'_d \tan \delta) \quad (3.3.4)$$

For polyethylene, $\sigma_d \sim 10^{-15}$ and can be ignored, while $\epsilon'_d \approx 2.3 \epsilon_0$ and $\tan \delta \approx 2 \times 10^{-4}$ as in (3.3.5). For a frequency of 1 GHz, we then find

$$\sigma_{\text{eff}} \approx \omega \epsilon'_d \tan \delta \approx 2\pi \cdot 10^9 * [2.3 * 8.85 \times 10^{-12}] * 2 \times 10^{-4} \approx 2.6 \times 10^{-5} \text{ mho/m} \quad (3.6.3)$$

This is 12 orders of magnitude smaller than the σ of copper $\sim 10^7$, but it is 10 orders of magnitude larger than the DC conductivity of the dielectric $\sim 10^{-15}$.

It was shown in (3.4.12) that the conduction current in any good dielectric is much smaller than the displacement current by a factor of $1/\tan\delta$. Thus, since the dielectric's *total* radial dielectric current equals J_r in region 2, and since that is marked small, we mark J_r in the dielectric as "very small".

Finally, we already noted a small E_z just outside the conductor, and since the dielectric has some very small conductivity (σ_{eff}), there will be some J_z in region 3 which is also "very small".

[c] E_r and J_r inside the conductor

We have already estimated that E_r inside the conductor surface is less than 10^{-6} what it is outside the surface, see (3.4.7) Fact 1. Thus, if E_r outside is 1500 volts/m as in our section (a) example, E_r inside is less than 1.5 mV/m at 500 GHz, and is proportionally less than this at lower frequencies, so E_r in region 2 is marked "very small", just as in the previous Table. In the example above we found $E_z \approx .14$ V/m inside the conductor. Thus we have $E_r \ll E_z$ inside the conductor which in turn means $J_r \ll J_z$. Below we shall provide more support for the idea that $J_r \ll J_z$.

3.7 The general shape of fields, charges, and currents on a transmission line

(a) E_θ at a conductor surface vanishes

We start by borrowing Fig B.6 from Appendix B (similar to Fig 3.3 above),

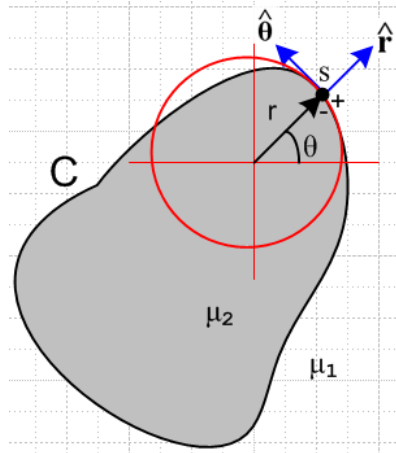


Fig B.6

The figure shows a transmission line conductor of some arbitrary (but reasonably smooth) cross sectional shape. At the point of interest s we construct a cylindrical coordinate system as shown, such that the coordinates (r, θ, z) are appropriate for point s and its immediate neighborhood. Basically we approximate the piece of conductor surface near s as if it were the surface of a round wire of some radius r . At this point s , then, we can talk about fields E_θ , E_z , B_θ , and B_z .

For a transmission line we shall use E_t to refer to the transverse components of an electric field, as opposed to the longitudinal component E_z . In Cartesian coordinates $E_t = (E_x, E_y)$ and in the local cylindrical coordinates just defined at a surface point s , $E_t = (E_r, E_\theta)$. The important point is that E_θ is our

notation for the component of \mathbf{E}_t which at some surface point is tangent to the surface, while E_x is normal to the surface (we will also call this E_n below).

A fundamental assumption of our transmission line theory is that the cross-section tangential electric field at a conductor surface vanishes, which is to say, E_θ as defined above vanishes at all points on the surface. This assumption is examined in Appendix D.8 and here we accept it as fact. The basic idea is that surface charge is free to move along the conductor surface in a $z=\text{constant}$ plane to neutralize any E_θ that might develop, and this mechanism of maintaining $E_\theta = 0$ on the surface works from DC up to perhaps 1000 GHz. So:

Fact 0: $E_\theta = 0$ at the surface of a transmission line conductor. (3.7.0)

This assumption, stated in partial waves, appears in (D.2.27) and is one of two boundary conditions used in Appendix D to determine the internal fields of a round wire, the other boundary condition being (D.2.26). One can consider Fact 0 to be part of the "electro-quasi-static" model of a transmission line.

(b) The transverse vector potential components are small

Fact 1: In the King gauge, for a transmission line operating in the transmission line limit, the transverse vector potential is very small: $|\mathbf{A}_t| < 10^{-4} |\mathbf{A}_z|$ for $f = 0$ to 500 GHz. (3.7.1)

This is demonstrated in Appendix M, see (M.16). The basic idea is that in a transmission line the major current is in the z direction, and $\mathbf{A} \sim \mathbf{J}$ according to the Helmholtz integral. Then since $|\mathbf{J}_t| \ll |\mathbf{J}_z|$, one finds that $|\mathbf{A}_t| \ll |\mathbf{A}_z|$.

(c) The scalar potential ϕ on a conductor surface

By "conductor surface" we mean the boundary of a cross-sectional slice at $z = \text{constant}$ through a transmission line conductor. In electrostatics one has $\mathbf{E} = -\nabla\phi$ and then $\mathbf{E}_t = \nabla_t\phi$ for the transverse electric field. In the neighborhood of a surface point \mathbf{s} we write this as $E_\theta = (1/r)\partial_\theta\phi$ and $E_x = \partial_x\phi$. Since Fact 0 says $E_\theta = 0$ at any \mathbf{s} on the surface, we conclude that $\phi = \text{constant}$ all the way around the conductor boundary. This is fine for $\omega = 0$, but for $\omega > 0$ we have from (1.3.1) that $\mathbf{E} = -\nabla\phi - j\omega\mathbf{A}$ and so

$$\mathbf{E}_t = -\nabla_t\phi - j\omega\mathbf{A}_t \quad (3.7.2)$$

and now it is no longer possible to immediately claim $E_\theta = 0 \Rightarrow \phi = \text{constant}$ on the boundary. We shall now show that, under suitable conditions, the last term $-j\omega\mathbf{A}_t$ is much smaller (in magnitude) than the first term $-\nabla_t\phi$, and therefore we have $\mathbf{E}_t \approx -\nabla_t\phi$ and then $\phi \approx \text{constant}$ by our argument above.

An arm-waving argument is to say that Fact 1 implies that the transverse potential \mathbf{A}_t can be neglected in a transmission line and therefore $\mathbf{E}_t \approx -\nabla_t\phi$. But $|\mathbf{A}_t| \ll |\mathbf{A}_z|$ does not prove $|\omega\mathbf{A}_t| \ll |\nabla_t\phi|$ so we shall try to do better with a more substantial argument.

First, we divide up the frequency domain (relative to some transmission line geometry) into a set of regimes. We state these for a round wire of radius a , but for a general conductor one can replace a with some typical transverse dimension of the conductor :

$$\begin{array}{lll}
 \delta > a/10 & \delta < a/10 & \delta < a/1000 \\
 \text{low frequency} & \text{strong skin effect} & \text{extreme skin effect}
 \end{array} \tag{3.7.3}$$

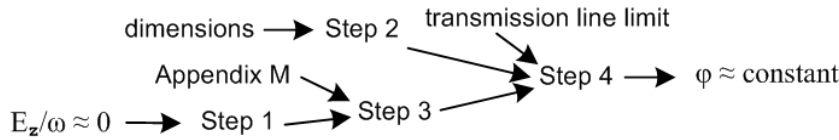
Here $\delta \equiv \sqrt{2/(\omega\mu\sigma)}$ is the skin depth of (2.1.8) or (2.2.20). Obviously the classification is arbitrary, we might have taken $\delta = a/5$ as the strong skin effect boundary. We shall find that some facts which are approximately valid for the strong skin effect regime are almost exactly valid in the extreme skin effect regime.

Here then is what we want to show:

Fact 2: $\varphi \approx \text{constant}$ on a conductor boundary ($z = \text{constant}$) in the strong or extreme skin effect regimes within the Transmission Line Limit. (3.7.4)

See Comments below the proof regarding the significance of Fact 2.

Our proof proceeds in a set of Steps (the Transmission Line Limit is defined in Step 4). As a guide, here is a little graphic showing how this proof works:



Step 1. In the strong or extreme skin depth regime, $A_z \approx (1/v_d) \varphi$. (3.7.5)

As usual, the subscript "d" refers to a value in the dielectric between conductors, and here $v_d = 1/\sqrt{\mu_d \epsilon_d}$ is the speed of light in the dielectric and also the phase velocity of a wave going down our low-loss transmission line. Similarly, $\beta_d = (\omega/v_d)$ is the wave's wavenumber in the dielectric. Using $\partial_z \rightarrow -j\beta_d$ as in (D.1.16) and our usual $\partial_t \rightarrow j\omega$ we find from (1.3.1) that

$$\begin{aligned}
 E_z &= -\partial_z \varphi - j\omega A_z = j\beta_d \varphi - j\omega A_z = j(\omega/v_d)\varphi - j\omega A_z = j\omega [\varphi/v_d - A_z] . & \beta_d &= (\omega/v_d) \\
 \Rightarrow \varphi/v_d - A_z &= E_z/(j\omega)
 \end{aligned} \tag{3.7.6}$$

Inside a good conductor E_z is small to begin with, and in the limit $\delta \rightarrow 0$ ($\omega \rightarrow \infty$) the right side of (3.7.6) is small due to this fact and due to the $1/\omega$ factor. Therefore,

$$A_z \approx \varphi/v_d \quad \text{small or extreme skin effect} \tag{3.7.7}$$

Sometimes a different argument is given to obtain (3.7.7). In the King gauge we know from (1.5.5) that in the dielectric,

$$\operatorname{div} \mathbf{A} = -j (\beta_d^2/\omega)\phi \quad (1.5.5)$$

or

$$(\partial_x A_x + \partial_y A_y) + \partial_z A_z = -j (\beta_d^2/\omega)\phi$$

or

$$(\partial_x A_x + \partial_y A_y) - j\beta_d A_z = -j (\beta_d^2/\omega)\phi . \quad (3.7.8)$$

Without a proof, we extend the usual arm-waving argument that \mathbf{A}_t components can be neglected to say that transverse *derivatives* of \mathbf{A}_t can also be neglected so $(\partial_x A_x + \partial_y A_y) \approx 0$, and then we have

$$-j\beta_d A_z \approx -j (\beta_d^2/\omega)\phi$$

or

$$A_z \approx (\beta_d/\omega)\phi = \phi/v_d$$

which replicates the conclusion (3.7.7) seemingly without the skin effect restriction. A more careful analysis must show that $(\partial_x A_x + \partial_y A_y)$ can only be so neglected in the strong or extreme skin effect limits. This issue reappears in (M.17) and Section 7.5.

Step 2. Claims that $|\nabla_t \phi| \approx (1/D)|\phi|$ where D is a characteristic transverse dimension of the transmission line.

We might argue this on dimensional grounds alone, but consider

$$|\partial_x \phi| \approx \frac{\Delta\phi}{\Delta x} \approx \frac{V}{D} \approx (1/D) |\phi| . \quad (3.7.9)$$

This is a very crude use of the \approx sign, there could be a factor of 10 or 1/10 on either side, but when combined with \ll in Step 4 below we still obtain a reasonable conclusion. Here V is the potential difference between the two transmission line conductors, and D is their "separation". Obviously $|\partial_x \phi|$ is not the exact constant V/D at every point in space between the conductors, this is meant only as a ballpark estimate of the size of $|\partial_x \phi|$ in some average sense.

Step 3. Claims that $|\omega A_x| \ll 2\pi |\phi| (1/\lambda)$ where $\lambda =$ traveling wave's wavelength.

From Fact 1 we have,

$$|A_x| \ll |A_z| . \quad (3.7.10)$$

With Step 1 (3.7.7) this says

$$|A_x| \ll |\phi| / v_d = |\phi| (\beta_d/\omega)$$

or

$$|\omega A_x| \ll (2\pi/\lambda) |\phi| \quad \beta_d = 2\pi/\lambda \quad (3.7.11)$$

where λ is the wavelength of our transmission line wave.

Step 4. Claims that $|\omega \mathbf{A}_x| \ll |\partial_x \phi|$

In Chapter 4 we shall introduce the notion of the Transmission Line Limit which is a requirement that on a transmission line, the wavelength λ must be much larger than any transverse dimension D of the line,

$$\lambda \gg D \quad (3.7.12)$$

or

$$(1/\lambda) \ll (1/D)$$

or

$$2\pi |\phi| (1/\lambda) \ll 2\pi |\phi| (1/D) . \quad (3.7.13)$$

Combining this with Step 3 (3.7.11) we find

$$|\omega \mathbf{A}_x| \ll (2\pi/\lambda) |\phi| \ll 2\pi |\phi| (1/D)$$

or

$$|\omega \mathbf{A}_x| \ll 2\pi |\phi| (1/D) .$$

Bringing in the ballpark estimate Step 2 (3.7.9) that $|\partial_x \phi| \approx (1/D) |\phi|$ we then have

$$|\omega \mathbf{A}_x| \ll |\partial_x \phi|$$

where we just ignore the 2π factor relative to our extreme \ll situation. Doing this also for y , we have

$$|\omega \mathbf{A}_t| \ll |\nabla_t \phi| . \quad (3.7.14)$$

Looking then at (3.7.2) one finds

$$\mathbf{E}_t = -\nabla_t \phi - j\omega \mathbf{A}_t \approx -\nabla_t \phi$$

and this concludes our longwinded explanation of why $\phi \approx$ constant on a transmission line conductor's cross section surface. We had to assume the Transmission Line Limit ($\lambda \gg D$) and we had to assume the strong or extreme skin effect regime to show $\phi \approx$ constant.

Comments:

1. Intuitive proof: We need high ω to get small δ . Currents in the thin δ surface sheath are in the z direction and there is "no room" for transverse currents in the sheath so $\mathbf{J}_t \approx 0$ and then $\mathbf{A}_t \approx 0$ so $\omega \mathbf{A}_t \approx 0$ so $\mathbf{E}_t \approx -\nabla_t \phi$ and then finally $E_\theta = 0 \Rightarrow \phi \approx$ constant.

2. The fact that $\phi \approx$ constant on each conductor surface embodies the **electro-quasi-static** transmission line theory. It will allow us to treat the transmission line as a "capacitor problem" in Chapter 5, as if we were doing electrostatics, even though we are at high ω and in the skin depth regime.

3. We know that $\varphi = \text{constant}$ at $\omega = 0$, but in order to prove that $\varphi = \text{constant}$ at $\omega > 0$ we had to make the extra assumptions stated above. We have not provided any proof that $\varphi = \text{constant}$ for the "low frequency" range of (3.7.3), except for $\omega = 0$. It seems likely that $\varphi = \text{constant}$ is correct for very low frequencies close to $\omega = 0$ and below some ω_1 , and probably $\varphi \approx \text{constant}$ is reasonable for the rest of the low frequency range (but we have not proved this). Here then is the situation:

very low ω	low ω	strong skin effect	extreme skin effect	
$0 \leq \omega < \omega_1$	$\delta_1 > \delta > a/10$	$\delta < a/10$	$\delta < a/1000$	
$\varphi = \text{constant}$	$\varphi \approx \text{constant} ?$	$\varphi \approx \text{constant}$	$\varphi = \text{constant}$	(3.7.15)

(d) \mathbf{B} and A_z on a conductor surface

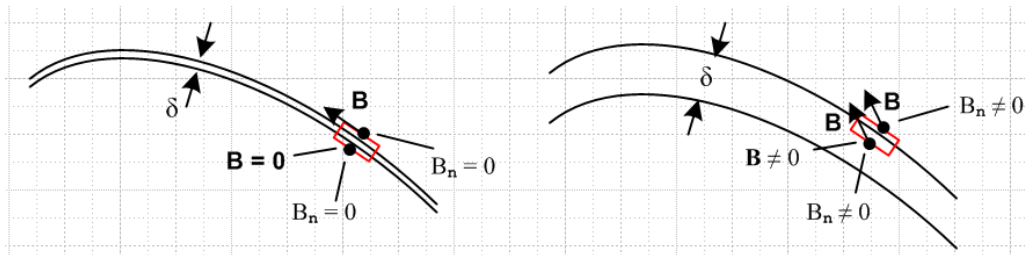
Fact 1 (3.7.1) says that $|A_{\mathbf{x}, \mathbf{y}}| \ll A_z$ for a transmission line, and so we just set $A_{\mathbf{x}} = A_{\mathbf{y}} \approx 0$. In this case we find that

$$\begin{aligned} \mathbf{B} &= \text{curl } \mathbf{A} = \hat{\mathbf{x}} (\partial_y A_z - \partial_z A_y) + \hat{\mathbf{y}} (\partial_z A_x - \partial_x A_z) + \hat{\mathbf{z}} (\partial_x A_y - \partial_y A_x) \\ &\approx \hat{\mathbf{x}} (\partial_y A_z) + \hat{\mathbf{y}} (-\partial_x A_z) = \mathbf{B}_t \end{aligned} \tag{3.7.16}$$

which says $\mathbf{B} \approx \mathbf{B}_t$ is mainly in the transverse direction. In the extreme skin effect regime, we know that inside the conductor \mathbf{B} decays to 0 quickly over distance δ (see Fig 2.9 for an isolated round wire). This is akin to the Meissner Effect where magnetic fields are excluded from the interior of a superconductor. In the extreme skin effect limit $\delta \rightarrow 0$, just below the thin surface current sheath we then have $B_n = 0$ (since $\mathbf{B} = 0$), where B_n is the component of \mathbf{B}_t normal to the surface. According to box (1.1.51) we know that B_n is continuous through the boundary, so we must have $B_n = 0$ just *outside* the surface as well. This is an application of

$$\text{div } \mathbf{B} = 0 \quad \Leftrightarrow \quad \int_S \mathbf{B} \cdot d\mathbf{S} = 0 \quad S \text{ is any closed surface} \tag{1.1.34}$$

for a thin red Gaussian box shown here end-on on the left:



On the left we imagine $\delta \rightarrow 0$ so the box can be made extremely thin so the left and right sides of the box then make no contribution to the flux. The front and back sides have no flux since $B_z \approx 0$ and because the sides are thin. Thus B_n vanishes on the top face of the box since it vanishes on the bottom face. For finite δ on the right, this same thin box does not deliver this result. A more detailed argument would show that $B_n = 0$ to the extent that skin depth $\delta \ll r$ where r is the local radius of curvature of the surface. For a "perfect conductor" we have $\delta = 0$ and $B_n = 0$ exactly. We summarize our conclusions:

Fact 3: (a) In general, the \mathbf{B} field at a transmission line conductor surface has a negligible z component and so $\mathbf{B} \approx \mathbf{B}_t$; (b) In the extreme skin effect regime, $\mathbf{B} \approx \mathbf{B}_t$ has no normal component B_n at the conductor surface. This is approximately true in the strong skin effect regime. (3.7.17)

Corollary: In the plane of a transmission line conductor cross section, and in the extreme skin effect regime, the magnetic field line pattern in the dielectric is such that just above the surface of each conductor there is a closed tangential \mathbf{B} field line enclosing the conductor which is almost exactly parallel to the surface at every point. This fact is approximately true for the strong skin depth regime. (3.7.18)

This is illustrated in the following figure where \mathbf{B} field lines are shown in red:

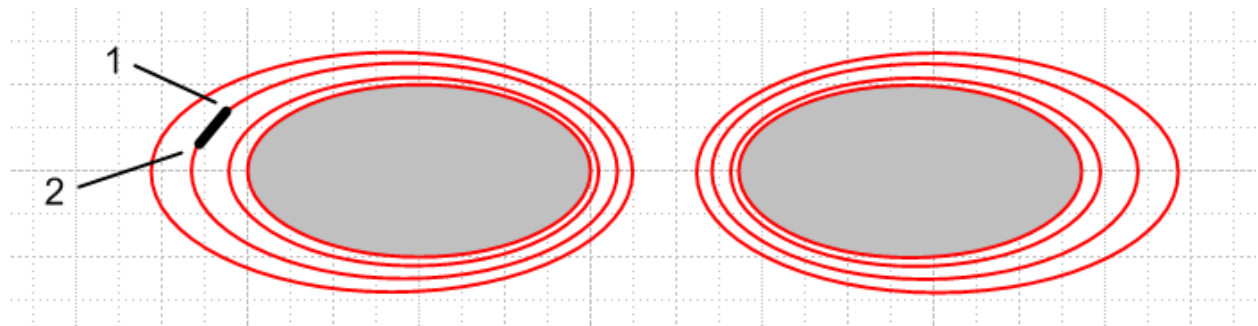


Fig 3.5

Fact 4: In a situation where $A_{x,y}$ can be neglected relative to A_z we have seen that the \mathbf{B} field lines are constrained to cross sectional planes. For any such planar set of \mathbf{B} field lines, each \mathbf{B} field line is an equipotential contour for A_z . (3.7.19)

Proof: Consider a small rectangular "math loop" into the plane of paper (depth dz) as shown in the above Figure. The black segment shows this loop edge on. Since this loop is parallel to a \mathbf{B} field line, the magnetic flux through the loop is zero. According to (1.1.39) we know that

$$\text{curl } \mathbf{A} = \mathbf{B} \quad \Leftrightarrow \quad \oint_C \mathbf{A} \cdot d\mathbf{s} = \int_S \mathbf{B} \cdot d\mathbf{S}. \quad (1.1.39)$$

The line integral of \mathbf{A} around our math loop must therefore vanish. But since \mathbf{A} has only the component A_z , the line integral has contributions only from the two sides of the loop (both of which are perpendicular to paper). Thus $\oint_C \mathbf{A} \cdot d\mathbf{s} = [A_z(1) - A_z(2)] dz = 0$ so $A_z(1) = A_z(2)$. By this argument, all points on the red \mathbf{B} field line shown have the same value of A_z and thus that red \mathbf{B} field line is an equipotential contour for A_z . But this applies to any of the red \mathbf{B} field lines, so in general, each such \mathbf{B} field line is an equipotential for A_z . This is reminiscent of the fact that \mathbf{E} field lines are equipotentials for ϕ in electrostatics.

Fact 5: On each conductor boundary, $A_z \approx \text{constant}$ in the extreme or strong skin effect regimes. (3.7.20)

From (3.7.18) we know that in the extreme skin depth regime, the innermost B field line almost exactly skirts the conductor perimeter. From (3.7.19) we know that any B field line is an equipotential contour. Thus, the cross section perimeter itself is very close to an equipotential contour of the function $A_z(x,y,z)$. In the strong skin effect regime this constancy of A_z on the boundary is only approximately true.

Comment: In Fact 2 we argued that $\phi \approx \text{constant}$ on a conductor perimeter in the extreme skin effect regime. We also argued in Step 1 that $A_z \approx (1/v_d)\phi$ everywhere inside the conductor and therefore also at the conductor surface. Thus, Fact 2 that $\phi \approx \text{constant}$ on the perimeter is consistent with Fact 5 that $A_z \approx \text{constant}$ on the perimeter, and these two constants are related by $A_z \approx (1/v_d) \phi$. That is,

$$A_z(\text{ any point on perimeter}) \approx (1/v_d) \phi(\text{any point on perimeter}) \quad //\text{extreme } \delta \quad (3.7.21)$$

and for the strong δ regime, this is approximately true.

A Counter Example and Comments on the Low Frequency Regime

We have argued above that in the strong/extreme skin effect regime, the perimeter of a transmission line conductor's cross section will align with a B field line and will have a constant value of A_z . This is in general *not* true for low frequencies. In particular, it is not true at $\omega = 0$. As an example of this fact, we consider a pair of parallel round wires carrying current I and $-I$. Since the current density in the wires is uniform, it is an easy matter to compute \mathbf{B} for each conductor and superpose to get the total \mathbf{B} field due to both conductors. Here is a plot of the resulting magnetic field lines (details in Appendix O),

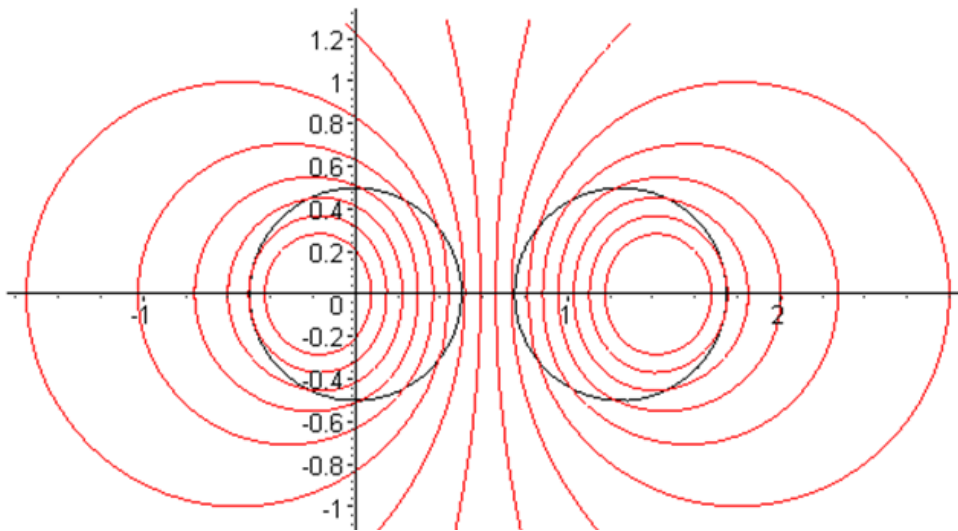


Fig 3.6a

Notice that the red magnetic field lines, being loci of constant A_z , do not align with the black conductor surfaces. One can conclude that the conductor surfaces are *not* surfaces of constant A_z in this very low frequency example ($\omega= 0$).

Now, having said this, we can make some very approximate low frequency remarks. In Chapter 5 we will arrive at following equations involving ϕ and A_z and their transverse partners ϕ_t and A_{zt} :

$$\varphi(x,y,z) = \frac{1}{4\pi\epsilon} q(z) \varphi_t(x,y) \tag{5.1.1}$$

$$A_z(x,y,z) = \frac{\mu}{4\pi} i(z) A_{zt}(x,y) \tag{5.2.1}$$

$$[\nabla_t^2 + (\beta_d^2 - k^2)] \varphi_t(x,y) = 0 \quad \varphi_t(C_1) = K_1 \quad \varphi_t(C_2) = K_2 \quad K_1 - K_2 = K \tag{5.3.10}$$

$$[\nabla_t^2 + (\beta_d^2 - k^2)] A_{zt}(x,y) = 0 \quad A_{zt}(C_1) = W_1 \quad A_{zt}(C_2) = W_2 \quad W_1 - W_2 = K \tag{5.3.11}$$

These two boundary value problems assume the extreme skin effect regime so that φ_t and A_{zt} are constants on both black circles. For the $\delta \rightarrow 0$ skin depth limit, we expect then to have $A_{zt}(x,y) = \varphi_t(x,y)$. Using $\mu\epsilon = 1/v_d^2$ and

$$i(z) = q(z) v_d, \tag{4.11.17}$$

if one has $A_{zt}(x,y) = \varphi_t(x,y)$, then from the ratio of the first two equations above one also has $A_z(x,y,z) = (1/v_d) \varphi(x,y,z)$ which is the Step 1 fact (3.7.5) above (stated there for finite δ).

The question then is this: to what extent is it true that $A_z \approx (1/v_d) \varphi$ in the *low*-frequency regime shown in (3.7.3), all the way down to $\omega = 0$? Looking at Fig 3.6a, we can certainly find two red loci which are somewhat similar to our black conductor boundaries, missing perhaps by 30%. These two red closed curves would then define a boundary value problem with a solution A_{zt} that is roughly on the same *scale* as the solution A_{zt} at high frequency. So our answer is this:

$$A_z \sim (1/v_d) \varphi \quad \text{in the low frequency regime} \tag{3.7.5}_{low \ \omega}$$

where \sim means both sides have the same general scale. Here is another version of Fig 3.6a in which the A_z values of some of the red curves are shown,

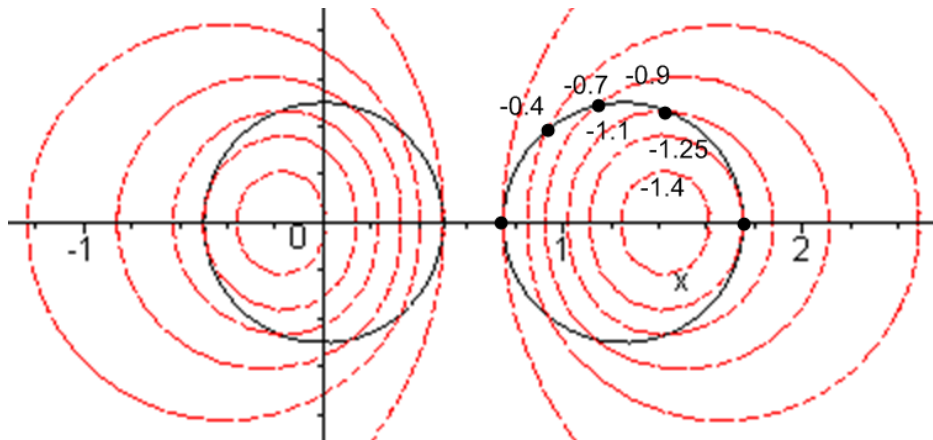


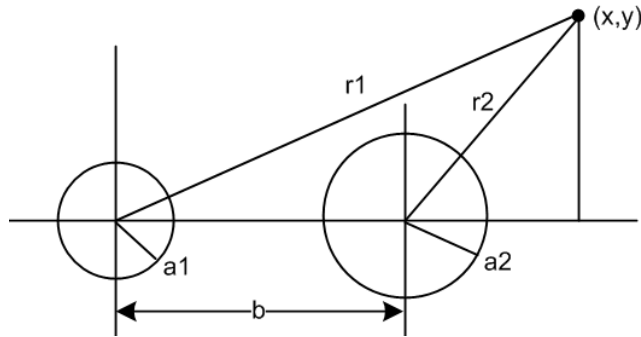
Fig 3.6b

As an alternate to the above language, we could say that A_z is *ballpark* constant on the right black circle, in that A_z only varies from -0.4 to -1.25 (and not, say, from -0.001 and -1000).

How Fig 3.6b was made. $A_z(x,y)$ for one cylinder at DC is computed in Appendix B with result (B.7.7). We can superpose that A_z with a similar A_z for the other cylinder giving this result,

$$A_z(x,y) = \frac{\mu I}{2\pi} * \{ -\ln r_1 \theta(r_1 > a_1) + [(1-r_1^2/a_1^2)/2 - \ln a_1] \theta(r_1 < a_1) \\ + \ln r_2 \theta(r_2 > a_2) - [(1-r_2^2/a_2^2)/2 - \ln a_2] \theta(r_2 < a_2) \} .$$

The drawing below shows the r_i and a_i with origin at the center of the left cylinder :



Setting $a_1 = a_2 = 0.5$ and $b = 1.25$, and ignoring the overall constant $\mu I/2\pi$, the plot was made using Maple's implicitplot call which is an x-y scanner producing a crude but acceptable plot:

```
kvals := [-1.4, -1.25, -1.1, -0.9, -0.7, -0.4, 0.4, 0.7, 0.9, 1.1, 1.25, 1.4]:
p := implicitplot({seq(Az(x,y) = k, k = kvals)}, x=-3..3, y=-2..2, scaling =
constrained, grid = [50,50], view = [-2..3, -2..2]):
c1 := circle([0,0], a1, color=black):
c2 := circle([b,0], a2, color=black):
display(p, c1, c2);
```

(e) Observations about the E and B field lines in a transmission line dielectric

Fact 6: In a *cross sectional* sketch of a transmission line, the E field lines land on the conductors at right angles to the conductor surface. This is exactly true for the TEM mode, and applies to all points on the conductor surfaces. (3.7.22)

Proof: This follows from Fact 1 (3.7.0) which says $E_\theta = 0$ at the conductor surface.

Fact 7: In a *longitudinal* sketch of a transmission line, the E field lines still land on the conductors at very close to right angles. (3.7.23)

Proof: Although $E_\theta = 0$ at the conductor surface, E_z is not zero, though it is very small. We know that E_z exists inside the conductor to support $J_z = \sigma E_z$, and we know by (1.1.41) that E_z is continuous through the boundary, so the longitudinal E field landing angle will not quite be $\pi/2$. The deviation from $\pi/2$ is less than 10^{-4} radians according to (3.6.2), and the deviation is in the direction of current flow at each conductor. This causes a very slightly warping of the otherwise planar cross-sectional field line grid.

Fact 8: Apart from an overall scale factor, the cross-sectional field shape of a TEM wave on a transmission line is independent of position z along the transmission line, and is independent of time t . The shape is also independent of ω . (3.7.24)

Proof: As we shall see below, the TEM form of any field or current is $\mathbf{F}(x,y,z,t) = e^{j[\omega t - kz + \phi_{\mathbf{F}}(\omega)]} \mathbf{F}(x,y)$ where $\mathbf{F}(x,y)$ is real and all t and z dependence is in the exponential. We can take the physical field to be the real part as discussed in Section 1.6 so $\mathbf{F}_{\text{physical}}(x,y,z,t) = \cos[\omega t - kz + \phi_{\mathbf{F}}(\omega)] \mathbf{F}(x,y)$. Thus, the cross sectional shape of the field is determined by $\mathbf{F}(x,y)$ and is the same at all values of z apart from an overall scale factor $\cos[\omega t - kz + \phi_{\mathbf{F}}(\omega)]$. This scale factor varies between +1 and -1 as one moves down the line in z at some fixed t , or as one observes at some fixed z as time varies. Later we will see that this shape $\mathbf{F}(x,y)$ can be found by solving a certain 2D Helmholtz equation, and we find that the shape is determined entirely by the shape of the boundaries of the conductors. Different vector fields (e.g., \mathbf{J} and \mathbf{E}) might have different ω -dependent phases in this wave motion which we indicate by $\phi_{\mathbf{F}}(\omega)$ for $\mathbf{F}(x,y,z,t)$.

Fact 9: In a cross sectional sketch of a transmission line operating in the extreme skin effect regime, the \mathbf{E} and \mathbf{B} field lines are very nearly perpendicular at every point in the dielectric. In the strong skin effect regime, the fields are approximately perpendicular. (3.7.25)

Proof: From Maxwell's curl \mathbf{E} equation (1.1.2) in the ω domain we have

$$\text{curl } \mathbf{E} = -j\omega \mathbf{B} \quad (1.1.2)$$

Then

$$\begin{aligned} \mathbf{B} \bullet \mathbf{E} &= (-j\omega)^{-1} \text{curl } \mathbf{E} \bullet \mathbf{E} \\ &= (-j\omega)^{-1} [(\partial_x E_y - \partial_y E_x) E_z + (\partial_y E_z - \partial_z E_y) E_x + (\partial_z E_x - \partial_x E_z) E_y] \end{aligned} \quad (3.7.26)$$

In the extreme skin effect regime, for a given ω we think of conductivity σ being very large, and so the conductor's E_z is very small. Since E_z is continuous at the conductor boundary, E_z is also very small in the dielectric. In contrast, due to the surface charge on the conductors, the transverse fields E_x and E_y are very large in the dielectric. If we neglect E_z and its derivatives in the above expression we find that

$$\begin{aligned} \mathbf{B} \bullet \mathbf{E} &\approx (-j\omega)^{-1} [(-\partial_z E_y) E_x + (\partial_z E_x) E_y] \\ &\approx (-j\omega)^{-1} [E_y^2 \partial_z (E_x/E_y)] \end{aligned} \quad (3.7.27)$$

However, we argued in Fact 8 that the shape of fields does not vary with z . Thus, the ratio of two components like E_x/E_y cannot vary with z , so $\partial_z (E_x/E_y) = 0$. Alternatively, we make the usual replacement $\partial_z \rightarrow -jk$ (see Fact 8 proof) to get

$$\begin{aligned} \mathbf{B} \bullet \mathbf{E} &\approx (-j\omega)^{-1} [(-\partial_z E_y) E_x + (\partial_z E_x) E_y] = (-j\omega)^{-1} [(jk E_y) E_x + (-jk E_x) E_y] \\ &= (-j\omega)^{-1} (jk) [(E_y) E_x + (-E_x) E_y] = 0 \end{aligned} \quad (3.7.28)$$

We have already shown that at the conductor surfaces, \mathbf{E} is normal to the surface and in the extreme skin effect regime \mathbf{B} is nearly tangent to the surface, so we certainly have $\mathbf{B} \cdot \mathbf{E} \approx 0$ at the conductor surfaces.

(f) Drawings of the fields

We are now in a position to draw some sketches of fields on a transmission line. Let's start with the transverse or cross section picture:

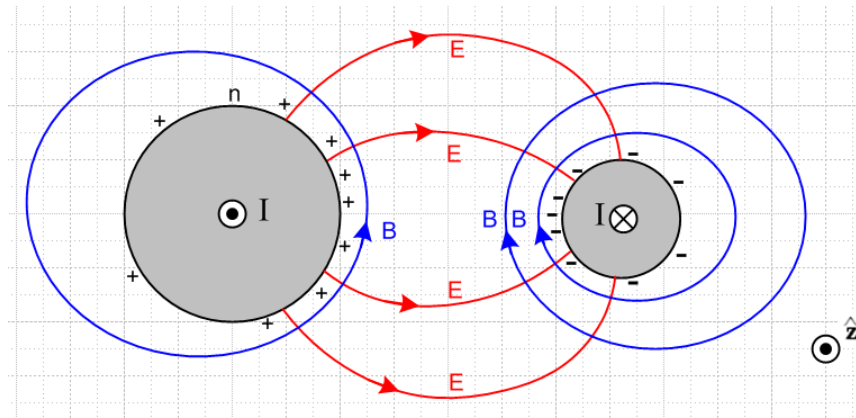


Fig 3.7: Cross section view

Fig 3.7

Although this figure is drawn for two round conductors, its general features apply to any conductors. The figure is a snapshot at one instant in time and at some value of z . The \bullet and \otimes indicate current flow direction in the conductors. Positive charge exists on the surface of the left conductor, and is strongest on the face of that conductor which is closest to the other conductor. Negative surface charge lies on the right conductor. The electric fields are as shown and are strongest in the region between the conductors. The magnetic field directions derive from the right hand rule relative to the current in each conductor. The lines of \mathbf{E} and \mathbf{B} always intersect at right angles as noted in (3.7.25).

The magnitude of the \mathbf{E} field is determined by the potential difference between the conductors and the geometry. It is independent of frequency. Similarly, the magnitude of the \mathbf{B} field is determined by the size of the current in either conductor and is also independent of frequency.

Consider a $75\ \Omega$ transmission line that is properly terminated and is driven by a 7.5 volt amplitude sine wave. Regardless of frequency ω (but ω large enough so $Z_0 = 75\ \Omega$, see (4.12.18)), the magnitude of the current in this transmission line is 100 mA, and the magnitude of the potential difference is 7.5 volts. Of course both these quantities have sinusoidal time dependence. At some instant in time, the fields and currents are as in Fig 3.7.

We are always talking a lossless or very low-loss transmission line here. If the conductor resistance and/or dielectric conductivity are significant, then yes, both I and V decrease as z increases down the line. This decrease is realized by the k in $e^{j(\omega t - kz)}$ having a small negative imaginary part (Appendix Q).

We have just argued then that not much happens in the transverse directions x and y as frequency sweeps up from strong skin effect to extreme skin effect. The rate at which the pattern oscillates back and forth increases, but the field pattern shape does not change. This may seem contradictory. In general, one is used to ω affecting things due to equations like

$$\text{curl } \mathbf{E} = -j\omega\mathbf{B} \qquad \text{Maxwell curl E equation} \qquad (1.1.2)$$

The resolution is that all the spatial variation happens in the *longitudinal* direction. Here then is a top view of the same transmission line:

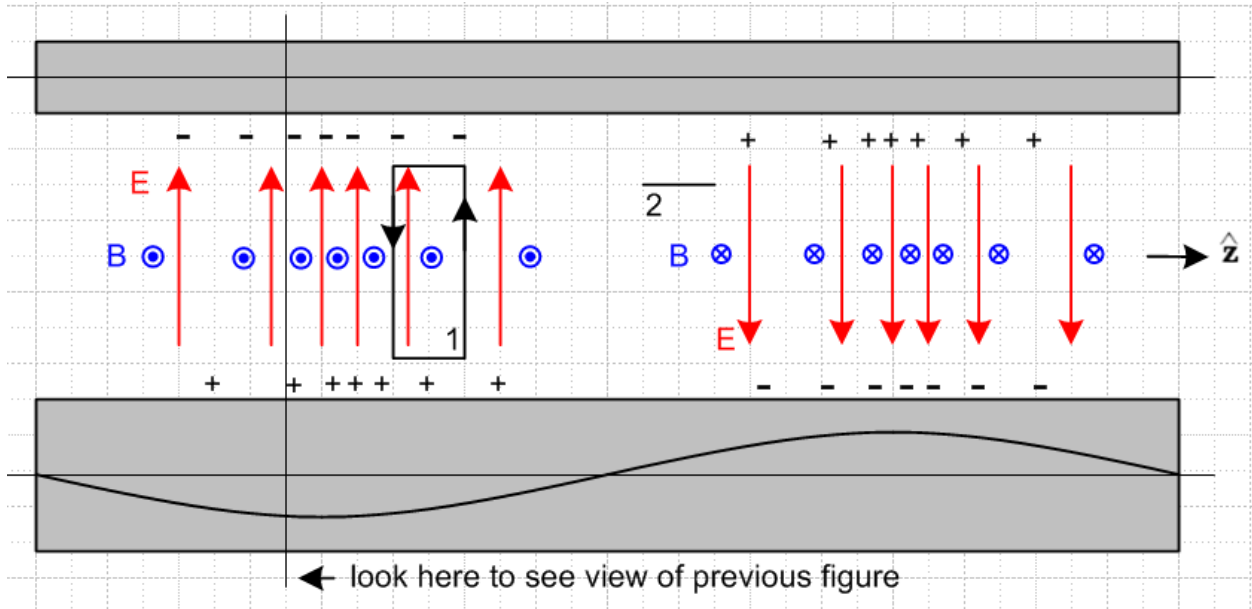


Fig 3.8: Top view of transmission line

Fig 3.8

The red E arrows are all of unit length and serve to mark the direction and density of electric field lines lying in the plane containing the center lines of the conductors. The blue B arrows are seen end-on and indicate the same for the magnetic field. On the left they come out of the plane of paper and on the right they go into it. Later we shall learn about the "transmission line limit" in which the wavelength λ of the wave propagating down a transmission line is assumed to be much larger than all transverse dimensions of the line. The reader should understand the above picture as being in that limit, but one would have to stretch the picture at least 10X horizontally to make it be reasonable. At all places $\mathbf{E} \times \mathbf{B}$ points to the right (+z).

Now apply the Maxwell curl equations using the two loops shown. Loop 1 is positioned to pick up magnetic flux, so we use (1.1.36) which in the frequency domain says

$$\text{curl } \mathbf{E} = -j\omega\mathbf{B} \qquad \Leftrightarrow \qquad \oint \mathbf{E} \cdot d\mathbf{s} = -j\omega \left[\int \mathbf{B} \cdot d\mathbf{S} \right] \qquad (3.7.29)$$

Notice the ω sitting on the right side. We argued in the last section that the amplitude of the B field does not change as ω changes. Thus, the right side of (3.7.29) is proportional to ω . As ω increases, the line integral of the E field around loop 1 must increase. Thus, the rate of change of E must increase in the z direction! In other words, as ω increases, the whole pattern of Fig 2 contracts in the z direction, which causes all z derivatives to increase, thus increasing $\oint \mathbf{E} \cdot d\mathbf{s}$ for the same fixed loop 1. Remember that the

strength of the E field is indicated in Fig 2 by the density of the red arrows, not by the length of the red arrows.

A similar argument applies to loop 2. This loop appears end-on in Fig 3.8. It is set up to sense the electric field flux. The appropriate curl equation is (1.1.38) which says

$$\begin{aligned} \text{curl } \mathbf{B} = \mu_d \epsilon_d j \omega \mathbf{E} + \mu \mathbf{J}_c & \Leftrightarrow \oint \mathbf{B} \cdot d\mathbf{s} = \mu_d \int_S [\epsilon_d j \omega \mathbf{E} + \mathbf{J}_c] \cdot d\mathbf{S} \\ & \approx j \omega \mu_d \epsilon_d \int \mathbf{E} \cdot d\mathbf{S}. \end{aligned} \quad (3.7.30)$$

Since we are now in the dielectric, we have ignored the small conduction current, and have kept the dominant displacement current, see (3.4.12). Again there is a factor of ω on the right side, arising from a time derivative. As ω increases, the line integral of the B field must increase. Thus, the B field must change faster in the z direction. As ω increases, the curl equation (3.7.30) is satisfied by having the entire pattern contract in the z dimension.

If the frequency ω doubles, the wavelength λ goes to half. This of course is no surprise, since ω and λ are related by the speed of light v_d in the dielectric,

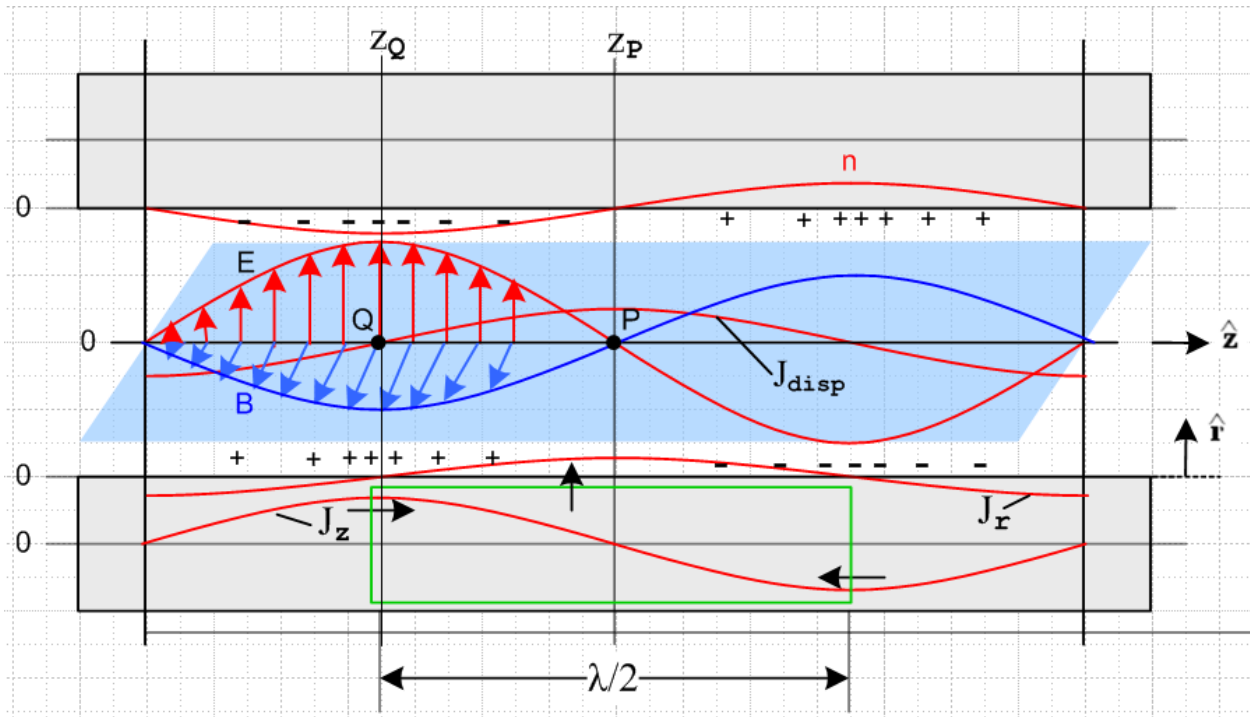
$$\lambda = v_d / f = 2\pi v_d / \omega. \quad (3.7.31)$$

The main point of the above discussion is to show how the Maxwell curl equations force the field pattern to contract in the z direction as ω increases. In the transverse direction, the field pattern *shape* stays constant.

(g) More on the field and current structure

Here we explore in more detail the general distribution of fields and currents in a transmission line. The goal is to establish the phase relationships among the electromagnetic fields and various currents. Once this is done, it is possible to make an estimate of the ratio J_x/J_z and that is done in the following section.

Consider the following more elaborate version of Figure 3.8 :



Tilted overhead view of a transmission line

Fig 3.9

The picture is quite complicated and deserves clarifying comments:

- (1) Unlike in Fig 3.8, the \mathbf{E} and \mathbf{B} arrows indicate the \mathbf{E} and \mathbf{B} vectors, and are not just field direction and field line density indicators.
- (2) The \mathbf{E} and \mathbf{B} field vectors are shown along some line which lies in the plane of the center lines of the two conductors and which points in the \hat{z} direction, as do those center lines.
- (3) The blue \mathbf{B} field arrows lie in the blue plane which is meant to be perpendicular to the plane of the conductor center lines, which is the plane of the paper. The red \mathbf{E} field arrows are in the plane of the paper.
- (4) Looking at $\mathbf{E} \times \mathbf{B}$, one sees that the wave is traveling to the right in the \hat{z} direction.
- (5) The \mathbf{E} field arrows point from positive charge to negative charge, so this is why the + and - signs are distributed as shown.
- (6) The conductors are fixed to the paper, everything else is moving to the right at velocity v_d . This includes the \mathbf{E} and \mathbf{B} arrows and their curves, the charge density and its curve n , and the two current curves drawn on the bottom conductor.
- (7) At point Q on plane $z = z_Q$, since \mathbf{B} is coming out of paper to the viewer, the longitudinal current J_z in the lower conductor must be pointing to the right. This is why J_z is shown positive at this point in the lower conductor, and this calibrates the position of the J_z curve. Maximum J_z occurs with maximum \mathbf{B} .

(8) There exists a displacement current $\mathbf{J}_{\text{disp}} = \partial_t \mathbf{D} = \epsilon_d \partial_t \mathbf{E}$ in the dielectric whose magnitude is shown as a red curve. For an observer sitting at fixed point P, since the wave is moving to the right, the value of $\partial_t \mathbf{E}$ is at its instantaneous maximum positive value. This is why the red \mathbf{J}_{disp} curve has a positive maximum at point P.

(9) As discussed in Section 3.4, the displacement current is "fed" by the radial current \mathbf{J}_r inside the lower conductor, so the \mathbf{J}_r curve also has its maximum positive value at point P. This \mathbf{J}_r current is busily radially pumping positive charge to the surface of the lower conductor at point P so that charge will be there when the wave has moved $\lambda/4$ to the right. Of course this radial \mathbf{J}_r is doing this charge pumping all around the lower conductor, but we only show it in the plane of paper. [See Section D.9 (c)]

(10) We have glossed over the fact that the E and B fields track each other in magnitude. The Maxwell equation $\text{curl } \mathbf{E} = -j\omega \mathbf{B}$ requires that E and B vanish at the same place ($z = z_p$). Since E and B have the same wavelength, they must also have their maxima at the same place ($z = z_Q$). This same correlation occurs in a normal plane wave. The maximum of E at $z = z_Q$ is associated with a maximum of the surface charge, while the maximum of B is associated with a maximum of \mathbf{J}_z .

(h) Estimate of the ratio $\mathbf{J}_r/\mathbf{J}_z$

Having drawn and described this elaborate Fig 3.9, we now consider the inscribed green Gaussian box which contains no surface charge. We first assume cylindrical conductors so this box is a cylinder. At the instant in time for which Fig 3.9 is drawn, the total current flowing into the endcaps of the box is $2I$, where I is the peak longitudinal current -- the magnitude of the longitudinal sine wave. Therefore, the total \mathbf{J}_r integrated over the sides of the green cylinder must also be $2I$.

To obtain a ballpark estimate of the situation, we assume that the two round conductors are far apart compared to their radii, in which case \mathbf{J}_r is roughly symmetric around the conductor surface. Then the total radial current emitted by the curved surface of the green Gaussian cylinder is:

$$\text{radial current total} = [(2/\pi)\mathbf{J}_r] * 2\pi a * (\lambda/2) = 2I$$

Since \mathbf{J}_r is a longitudinal sine wave, we have added a factor $2/\pi$ to get its value averaged over the length of the Gaussian box. In a more general case, we can replace $2\pi a$ with distance p which represents the active portion of the conductor perimeter, as illustrated in Fig 2.16. Then we have

$$[(2/\pi)\mathbf{J}_r] * p * (\lambda/2) = 2I \quad \Rightarrow$$

$$\mathbf{J}_r = 2\pi I / (\lambda p) \quad . \quad (3.7.32)$$

On the other hand, for a round conductor operating in the strong skin effect regime

$$\mathbf{J}_z \approx I/(p\delta) \quad (3.7.33)$$

where p is the same active perimeter just mentioned. So

$$\mathbf{J}_r/\mathbf{J}_z \approx 2\pi (\delta/\lambda) \quad . \quad (3.7.34)$$

For δ we had

$$\delta \equiv \sqrt{2/\omega\mu\sigma} \quad . \quad (2.2.20)$$

From (3.7.31) we have $\lambda = v_d/f = 2\pi v_d/\omega$ where v_d is the wave phase velocity. Then

$$(\delta/\lambda) = \sqrt{\frac{2}{\omega\mu\sigma}} \frac{\omega}{2\pi v_d} = \sqrt{\frac{2\omega}{\mu\sigma}} \frac{1}{2\pi v_d} = \sqrt{\frac{4\pi f}{\mu\sigma}} \frac{1}{2\pi v_d} \quad . \quad (3.7.35)$$

Setting $v_d \approx c$ and $\mu = \mu_0 = 4\pi \times 10^{-7}$ and $\sigma = 5.81 \times 10^7$ (copper) and $f = 10^9$ f(GHz) we get

$$\begin{aligned} (\delta/\lambda) &\approx \sqrt{\frac{4\pi f}{\mu\sigma}} \frac{1}{2\pi v_d} = \sqrt{\frac{4\pi \cdot 10^9 \text{ f(GHz)}}{4\pi \times 10^{-7} \times 5.81 \times 10^7}} \frac{1}{2\pi} \frac{1}{3 \times 10^8} \\ &= \sqrt{\frac{10^{10} \text{ f(GHz)}}{58.1}} \frac{1}{2\pi} \frac{1}{3 \times 10^8} = \sqrt{\frac{\text{f(GHz)}}{58.1}} \frac{1}{6\pi} 10^{-3} = 7 \times 10^{-6} \sqrt{\text{f(GHz)}} \end{aligned}$$

and so

$$J_x/J_z \approx (2\pi) (\delta/\lambda) \approx 4.4 \times 10^{-5} \sqrt{\text{f(GHz)}} \quad . \quad (3.7.36)$$

For $f \leq 10$ GHz we then find

$$J_x/J_z \leq 1.4 \times 10^{-4} \quad . \quad f \leq 10 \text{ GHz} \quad \text{strong skin effect regime} \quad (3.7.37)$$

showing that the radial charge-pumping current density J_x is much smaller than the longitudinal current density J_z in the conductor sheath.

What about the low-frequency situation with no skin-effect sheath? For simplicity, we assume now two round conductors of radius a which are widely spaced. No skin effect means roughly $\delta > a$ which means

$$\sqrt{2/\omega\mu\sigma} > a \quad \Rightarrow \quad \omega < 2/(\mu\sigma a^2) \quad \text{or} \quad \omega a/2 < 1/(\mu\sigma a) \quad . \quad (3.7.38)$$

In this low frequency regime we must replace (3.7.33) by

$$J_z \approx I/(\pi a^2) \quad . \quad (3.7.39)$$

Since (3.7.32) is still valid, we find now that

$$\begin{aligned} J_z &\approx I/(\pi a^2) \\ J_x &\approx 2\pi I/(\rho\lambda) \approx 2\pi I/(2\pi a\lambda) \approx I/(a\lambda) \end{aligned}$$

so

$$J_x/J_z \approx \pi(a/\lambda) \approx (\pi a)(\omega/2\pi v_d) \approx \omega a/2v_d = (\omega a/2)(1/v_d) \quad . \quad (3.7.40)$$

Using (3.7.38) for $\omega a/2$ we get

$$J_x/J_z < 1/(\mu\sigma av_d) . \quad (3.7.41)$$

With $\mu = \mu_0 = 4\pi \times 10^{-7}$, $\sigma = 5.81 \times 10^7$ (copper) and $v_d = c = 3 \times 10^8$ we find for a wire of radius 1 mm,

$$J_x/J_z < \frac{1}{4\pi * 5.81 * 10^{-3} * 3 * 10^8} = \frac{10^{-5}}{4\pi * 5.81 * 3} = 4.6 \times 10^{-8} . \text{ low frequency} \quad (3.7.42)$$

The conclusion is that in general $J_x \ll J_z$ under 10 GHz and finally we justify entries made in the tables of Sections 3.5 and 3.6. The basic fact is that the green cylinder in Fig 3.9 is long, so the surface area through which J_x flows is much larger than the area through which J_z flows.

Comment: The explicit round wire field solution of Appendix D verifies that $|J_x/J_z| \ll 1$. See (D.2.33) and Observation (3) following. Roughly the conclusion is that $|J_x/J_z| \approx |\beta_d/\beta'| \ll 1$.

3.8 Review of Transmission Line Preliminaries

A transmission line normally has two conductors. The cross sectional shape of these conductors is assumed constant in the direction z along the transmission line. The transverse directions are x and y .

A wave propagates down a transmission line in what is called the TEM mode. TEM means that the electric and magnetic fields of a wave traveling down the line are transverse, as in Figures 3.7-9. What this really means is that an electromagnetic wave goes straight down the conductors as guides with no surface reflections, unlike what happens in a waveguide, see Appendix F. Apart from a small drag on the wave due to losses in the conductors, the wave proceeds with wavenumber β_d and velocity v_d as it would in an open medium. The conductors *shape* the \mathbf{E} and \mathbf{B} fields as in Fig 3.7, so the wave is not a "plane wave". Nevertheless, at each point in the dielectric, \mathbf{E} and \mathbf{B} are perpendicular (strong skin effect regime) and $\mathbf{E} \times \mathbf{B}$ points down the transmission line.

We now summarize a set of basic facts about this TEM mode, most of which were addressed in the previous Section.

Fact 1: The major current for the TEM mode is the *longitudinal* current J_z . We just showed in the last section that $J_x \ll J_z$. Moreover, $J_\theta = \sigma E_\theta$ vanishes at the surface from (3.7.0) and is presumably either tiny or non-existent inside the conductor. (3.8.1)

Fact 2: There is no cutoff frequency one has to operate above. The TEM mode works all the way down to DC (although at low frequencies, the attenuation per wavelength becomes large). See Appendix F for why operation down to DC is not possible in a waveguide. (3.8.2)

Comment: In the low frequency regime of (3.7.3) there is still a TEM wave going down the transmission line, but since we are not then in the strong or extreme skin depth limits, some of the facts of Section 3.7 do not apply. For example, looking at Fig 3.6, the conductors are no longer wrapped by tangent \mathbf{B} field lines, and A_z is no longer constant on the conductor perimeter, and $\mathbf{E} \cdot \mathbf{B}$ is no longer 0 at the surface.

Corollary 2: If one operates a transmission line below the cutoff of the lowest waveguide mode, the TEM mode is the only possible way of moving energy down the line. (3.8.3)

Fact 3: The simplest expression of the boundary conditions (at least for large ω) are in terms of *potentials*, not fields, so the potential wave equations are used to solve problems. (3.8.4)

Those boundary conditions are that ϕ and A_z are constant on conductor cross sections at a given z , as stated below in Facts 6 and 7.

Fact 4: The transverse components of the vector potential \mathbf{A} can be neglected, so A_z is the only component of \mathbf{A} we have to worry about. (3.8.5)

Proof: This is addressed in (3.7.1) and Appendix M, but we give a brief summery here. Consider equation (1.5.9) where both conductors have the same μ ,

$$\mathbf{A}(\mathbf{x},\omega) = \frac{\mu}{4\pi} \int \mathbf{J}(\mathbf{x}',\omega) \frac{e^{-j\beta_0 R}}{R} dV' \quad . \quad (3.8.6)$$

Here, \mathbf{J} represents the currents in the conductors and the volume integration is over both conductors in x,y and z , and $R = |\mathbf{x}-\mathbf{x}'|$. There is clearly going to be a strong A_z component since the predominant conductor currents are in the longitudinal direction. According to Fact 1 above, transverse currents are very small, so the corresponding transverse components of \mathbf{A} will also be very small and we shall completely neglect them.

When we compute \mathbf{A} in the above integral, we can still decompose \mathbf{A} into A_z , A_x and A_θ . These components are, however, with respect to some fixed coordinate system located perhaps on some approximate center line between the two conductors. Thus, each potential of the pair A_x and A_θ will feel the effect of both J_x and J_θ , but these are both very small. Moreover, there is considerable cancellation which takes place as pieces of J_x and J_θ are added up in the integration. We rely mainly on the fact that J_x and J_θ are very small to conclude that A_x and A_θ may be safely neglected.

This is very different from what happens with A_z . In the region of one conductor, the summation is additive for all nearby pieces of current J_z in that conductor, assuming that the wavelength λ of longitudinal propagation is much larger than any transverse dimension. The only place A_z is small is on a longitudinal line between the conductors where their contributions cancel.

We conclude then that A_x and A_θ can be neglected relative to A_z .

Fact 5: The potential $\phi(x)$ can be identified with the transverse "voltmeter voltage" . (3.8.7)

In the transverse direction ($z = \text{constant}$), and in the extreme/strong skin depth regime, we know from (3.7.14) that $\mathbf{E}_t = -\nabla_t \phi - j\omega \mathbf{A}_t \approx -\nabla_t \phi$. In the drawing below there is no difference then between the line integral of the electric field between the two black dots and the potential difference $\phi_1 - \phi_2$ between these same points. Since there is no B field perpendicular to the plane of paper, there is no time-varying magnetic flux through any loop containing the probe wires of our "planar" voltmeter, so there is no "EMF" induced in these leads to confuse the meter reading, and the meter directly reads $V = \phi_1 - \phi_2$. If in

the drawing we move the right black dot attachment point to a point on the left conductor in some other z plane, the meter leads then enclose B field flux *and* $-j\omega A_z$ comes into play in $E_z = -\partial_z\phi - j\omega A_z$ and it is then less clear what the voltmeter is reading :

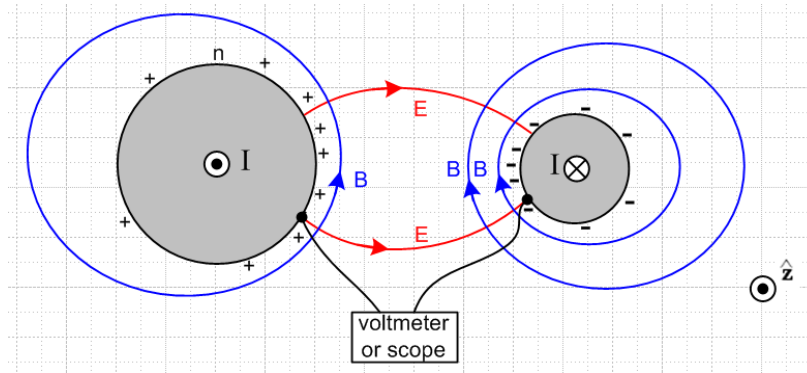


Fig 3.10

Fact 6: The potential ϕ is *constant* over the surface of either conductor at a fixed z . (3.8.8)

This was addressed in (3.7.4) where we had to add the assumptions that we are in the strong or extreme skin effect regimes and we are operating in the transmission line limit. Although $\phi = \text{constant}$ at $\omega = 0$, we concluded only that $\phi \approx \text{constant}$ in the low frequency regime of (3.7.3).

Fact 7: The potential A_z is *constant* over the surface of either conductor at a fixed z . (3.8.9)

This was addressed in (3.7.20) and is only valid in the strong or extreme skin effect regimes. At low frequencies Fact 7 is definitely not valid (see Fig 3.6a).

Chapter 4: Transmission Line Equations

In this Chapter we use the potential integral expressions derived in Chapter 1 to derive the classical transmission line equations. It is shown that most transmission line parameters are determined by a single geometric integral K . The approximations are clearly stated.

4.1 Computation of potential ϕ due to one conductor of a transmission line

Our starting point is the potential ϕ expression given in box (1.5.23) for the potential at some arbitrary point \mathbf{x} in the dielectric *due to conductor* C_1 of a transmission line,

$$\phi_1(\mathbf{x}, \omega) = \frac{1}{4\pi\xi_{\mathbf{d}}} \int_{C_1} \rho_1(x', y', z', \omega) \frac{e^{-j\beta_{\mathbf{d}}R}}{R} dx' dy' dz' . \quad R = |\mathbf{x} - \mathbf{x}'| \quad (4.1.1)$$

Here the integration point $\mathbf{x}' = (x', y', z')$ runs over the surface of C_1 and R is the distance between the observation point \mathbf{x} in the dielectric and the point \mathbf{x}' . Parameters $\beta_{\mathbf{d}}$ and $\xi_{\mathbf{d}}$ are for the dielectric.

Comments on ρ_1 :

1. ρ_1 is the volume charge density associated with "surface charge" n_1 according to $\rho_1 dV' = n_1 dS'$.
2. ρ_1 is a distribution. For example, for a round wire of radius a we expect ρ_1 to be proportional to $\delta(r'-a)$ where $r' = \sqrt{x'^2 + y'^2}$. Perhaps $\rho_1 = f(\theta')\delta(r'-a)$ where (r', θ', z') are cylindrical coordinates with axis at the round wire center.
3. Recall from Section 1.5 (c) and (1.5.17) the fact that there are two distinct areal charge distributions called $n_{\mathbf{e}}$ and $n_{\mathbf{s}}$ which are related by $n_{\mathbf{e}} = (\xi_{\mathbf{d}}/\epsilon_{\mathbf{d}})n_{\mathbf{s}}$. Here $n_{\mathbf{s}}$ is the *actual* surface charge distribution, whereas $n_{\mathbf{e}}$ is an *adjusted* charge density which is directly associated with the current I in the conductor and which accounts for possible leakage in the dielectric. Our n_1 and ρ_1 are associated with this $n_{\mathbf{e}}$ adjusted charge distribution, not with $n_{\mathbf{s}}$. That is why the external factor in (4.1.1) is $1/4\pi\xi_{\mathbf{d}}$ instead of $1/4\pi\epsilon_{\mathbf{d}}$.

Consider now this charge density $\rho_1(\mathbf{x})$. Following a standard methodology, we make the assumption that its functional form may be factored in the following manner,

$$\rho_1(x, y, z) = \alpha_1(x, y) q_1(z) \quad . \quad (4.1.2)$$

$\frac{C/m^3}{1/m^2} \quad \frac{C/m}{C/m}$

The dimensions of the functions in this factorization are as indicated, so the charge goes with q_1 . Moreover, without any loss of generality we select the relative scale of the two factors such that the integral of $\alpha_1(x, y)$ over a slice of conductor C_1 at any z is unity,

$$\int_{C_1} dx dy \alpha_1(x, y) = 1 . \quad (4.1.3)$$

Therefore, one can interpret $q_1(z)$ as the total charge per unit length on C_1 at location z :

$$\int_{C_1} dx dy \rho_1(x,y,z) = q_1(z) \int_{C_1} dx dy \alpha_1(x,y) = q_1(z) \cdot 1 = q_1(z) .$$

Assume that $q_2(z)$ is the charge on the other conductor C_2 of a two-conductor transmission line. If $q_1(z) + q_2(z) \neq 0$, then there is a net charge per unit length and the transmission line is acting as a radiating antenna as well as a transmission line. From now on, we ignore this superposed radiation problem and assume that at each value of z , the net charge on both conductors is 0 -- the line is "balanced". Thus,

$$q_2(z) = - q_1(z) \equiv -q(z) . \quad (4.1.4)$$

To simplify notation, we now dispense with the subscript and denote $q_1(z) = q(z)$. However, we maintain the subscript on $\alpha_1(x,y)$ to emphasize that the two conductors can have completely different cross sectional shapes. The shape of the transverse distribution of charge on C_1 is determined by $\alpha_1(x,y)$, but the total charge is $q(z)$ per unit length.

How can we justify assumption (4.1.2)? This is "separation of variables". The idea is that we assume it without any justification, and then we try to find a solution to our problem which is consistent with the assumption. All we really want is to find a solution to our basic differential equations with their boundary conditions, and any assumptions we make can be justified in the end once we have found a solution. On the other hand, if an assumption like (4.1.2) does not lead to a solution, then it must have been a bad assumption. We have seen earlier how the expected EM field pattern on a transmission line has a constant transverse "shape" and this certainly motivates the assumption (4.1.2).

Now insert (4.1.2) into (4.1.1) to get,

$$\phi_1(x,y,z) = \frac{1}{4\pi\epsilon_d} \int_{-\infty}^{\infty} dz' q(z') \int_{C_1} dx' dy' \alpha_1(x',y') \frac{e^{-j\beta_d R}}{R} \quad (4.1.5)$$

$$R^2 = (x-x')^2 + (y-y')^2 + (z-z')^2 .$$

Technical Note Concerning the condition (4.1.2) and (4.1.3)

For some general quantity Q we must in general assume the following

$$Q(x,y,z,t) = Q(x,y,z) e^{j\omega t} = |Q(x,y,z)| e^{j\phi_Q(x,y,z)} e^{j\omega t}$$

$$Q_{\text{physical}}(x,y,z,t) = \text{Re}(Q) = |Q(x,y,z)| \cos [\omega t + \phi_Q(x,y,z)] = \text{real} .$$

In general, $Q(x,y,z,t)$ can have a phase $\phi_Q(x,y,z)$ which is a function of position (x,y,z) . For example, in Chapter 2 we found for a round wire that $E(r) = E(a) \frac{J_0(\beta r)}{J_0(\beta a)}$ where $\beta = e^{j3\pi/4} (\sqrt{2} / \delta)$. In this case, $E(r)$ certainly has a phase which depends on location r in the wire.

In (4.1.2) we write the partition $\rho_1(x,y,z) = \alpha_1(x,y) q_1(z)$. In general, $\alpha_1(x,y)$ could have a phase which varies with x,y . Suppose that $\int_{C_1} dx dy \alpha_1(x,y) = \kappa$, where κ is some complex number. We can then define primed quantities $\alpha'_1(x,y) \equiv \alpha_1(x,y)/\kappa$ and $q'_1(z) \equiv q_1(z)\kappa$. In this new partition we then have $\rho_1(x,y,z) = \alpha'_1(x,y) q'_1(z)$ where $\int_{C_1} dx dy \alpha'_1(x,y) = 1$. The point is that, even though $\alpha_1(x,y)$ might be a complex function of variables x,y , we can always find a partition $\rho_1(x,y,z) = \alpha'_1(x,y) q'_1(z)$ where $\alpha'_1(x,y)$ is a complex function of x,y , but nevertheless $\int_{C_1} dx dy \alpha'_1(x,y) = 1$.

Having said all this, we now further claim that we can take $\alpha_1(x,y)$ to be purely real with zero phase in our development below. We will be assuming that $\varphi \approx \text{constant}$ on a conductor perimeter in any $z = \text{constant}$ plane. If it were possible for $\rho_1(x,y,z,t)$ to "peak" at different times at different points on the perimeter, then such a ρ_1 would differ from its quasi-static equilibrium form in which $\varphi = \text{constant}$, and then one would have $\varphi \neq \text{constant}$. Thus for all points on the perimeter $\rho_1(x,y,z,t)$ must reach a peak value at the same time, which then implies that $\alpha_1(x,y)$ does not have a phase which varies with x,y and can then be taken to be a real function.

4.2 Computation of potential φ due to both conductors of a transmission line

We now write the potential at an arbitrary point \mathbf{x} in the dielectric due to *both* conductors C_1 and C_2 :

$$\begin{aligned} \varphi_{12}(\mathbf{x}) &= \varphi_1(\mathbf{x}) + \varphi_2(\mathbf{x}) = \\ &= \frac{1}{4\pi\xi} \int_{-\infty}^{\infty} dz' q(z') \left\{ \int_{C_1} dx_1' dy_1' \alpha_1(x_1',y_1') \frac{e^{-j\beta_d R}}{R} - \int_{C_2} dx_2' dy_2' \alpha_2(x_2',y_2') \frac{e^{-j\beta_d R}}{R} \right\} \\ R_1^2 &= (x-x_1')^2 + (y-y_1')^2 + (z-z')^2 = s_1^2 + (z-z')^2 & s_1^2 &= (x-x_1')^2 + (y-y_1')^2 \\ R_2^2 &= (x-x_2')^2 + (y-y_2')^2 + (z-z')^2 = s_2^2 + (z-z')^2 & s_2^2 &= (x-x_2')^2 + (y-y_2')^2 \end{aligned} \quad (4.2.1)$$

The minus sign between the terms is due to (4.1.4). Each conductor has its own arbitrary transverse charge distribution α_i . The transverse integration variables on C_1 are $dx_1' dy_1'$, while those on C_2 are instead $dx_2' dy_2'$. In the last two lines we introduce certain transverse distances s_1 and s_2 as shown. The same dz' integration variable is used for both conductors. The following drawing shows an arbitrary dielectric point $\mathbf{x} = (x,y,z)$ located in the $z = z$ plane. The point $\mathbf{x}_1' = (x_1',y_1',z')$ lies on C_1 at some point of the C_1 integration and similarly for $\mathbf{x}_2' = (x_2',y_2',z')$. The full distances R_1 and R_2 and the transverse distances s_1 and s_2 are shown. We show \mathbf{x}_1' and \mathbf{x}_2' on the surfaces based on Comment 2 above.

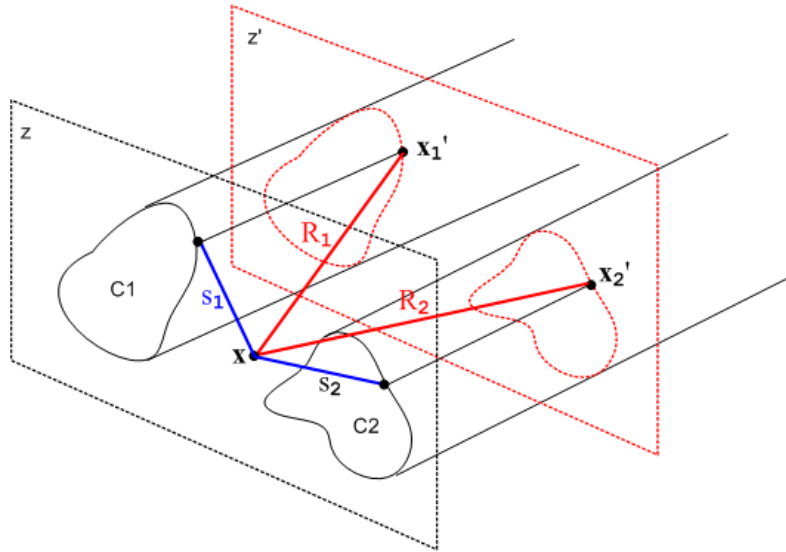


Fig 4.1

One can imagine an expression similar to (4.2.1) for a transmission line consisting of N conductors where $\sum_{i=1}^N q_i(z) = 0$, but we shall restrict our interest to $N = 2$.

4.3 The Transmission Line Limit

Consider again the potential at \mathbf{x} due to both conductors shown in (4.2.1),

$$\varphi_{12}(\mathbf{x}) = \frac{1}{4\pi\xi} \int_{-\infty}^{\infty} dz' q(z') \left\{ \int_{C_1} dx_1' dy_1' \alpha_1(x_1', y_1') \frac{e^{-j\beta_a R_1}}{R_1} - \int_{C_2} dx_2' dy_2' \alpha_2(x_2', y_2') \frac{e^{-j\beta_a R_2}}{R_2} \right\} \quad (4.3.1)$$

As the red-dashed $z = z'$ plane shown in Fig 4.1 is pushed back far from the $z = z$ plane, the vectors which are labeled by distances R_1 and R_2 become more aligned, and both R_1 and R_2 become larger. During the transverse integrations over \mathbf{x}_1' and \mathbf{x}_2' , these R_i vectors then don't vary much. One could then replace the transverse charge density $\alpha_1(x_1', y_1')$ with a point charge at the "center of the conductor" and not make much difference in the \mathbf{R}_1 vector and its length R_1 . In this situation, the $\{ \dots \}$ integrand of the above integral has this form

$$\left\{ \frac{e^{-j\beta_a R_1}}{R_1} - \frac{e^{-j\beta_a R_2}}{R_2} \right\} \quad // \text{ when } |z-z'| \text{ is large} \quad (4.3.2)$$

If we then expand the exponentials showing the first few terms, this becomes

$$\begin{aligned} \left\{ \frac{1 - j\beta_a R_1 + (j\beta_a)^2 R_1^2 / 2}{R_1} - \frac{1 - j\beta_a R_2 + (j\beta_a)^2 R_2^2 / 2}{R_2} \right\} &= \left\{ \left[\frac{1}{R_1} - \frac{1}{R_2} \right] + [-j\beta_a + j\beta_a] + (j\beta_a)^2 / 2 [R_1 - R_2] + \dots \right\} \\ &= \left\{ \left[\frac{1}{R_1} - \frac{1}{R_2} \right] - (\beta_a^2 / 2) [R_1 - R_2] + \text{order}(\beta_a^3) \right\} \end{aligned} \quad (4.3.3)$$

Since $R_1 \approx R_2$ for large $|z-z'|$ as just discussed, both the leading term and the β_d^2 term are small in an absolute sense as long as β_d^2 is not huge. When $|z-z'|$ is large, both R_1 and R_2 are large and thus both $1/R_1$ and $1/R_2$ are small, and $[1/R_1 - 1/R_2]$ is smaller still due to cancellation between the terms.

So our first point is that, in the dz' integration, the main contribution to $\phi_{12}(\mathbf{x})$ comes from regions of z' for which $|z-z'|$ is small.

Given then that the dz' integration in (4.3.1) is dominated by that part for which $|z-z'|$ is small, we can see that for this controlling integration region the size of distances R_1 and R_2 will be on the order of the transverse dimension of the transmission line, assuming that we select the point \mathbf{x} somewhere between the two conductors. If we vaguely define the transmission line's transverse extent as distance D , then suppose we make the following assumption concerning β_d :

$$\beta_d D \ll 1 \quad \text{"small } \beta_d \text{"} . \quad (4.3.4)$$

In this case, we can replace $e^{-j\beta_d R_1} = 1$ and $e^{-j\beta_d R_2} = 1$ in the integration without significantly changing the result. Then as shown in (4.3.3) there will be a correction term that is order β_d^2 which we shall neglect, as well as higher terms of order β_d^n with $n > 2$.

Notice that the linear β_d term vanished exactly in our large $|z-z'|$ analysis. This linear term also vanishes in the full analysis since the α_i transverse charge functions are normalized to unity:

$$\begin{aligned} & \left\{ \int_{C_1} dx_1' dy_1' \alpha_1(x_1', y_1') \frac{-j\beta_d R_1}{R_1} - \int_{C_2} dx_2' dy_2' \alpha_2(x_2', y_2') \frac{-j\beta_d R_2}{R_2} \right\} \\ & = (-j\beta_d) \left\{ \int_{C_1} dx_1' dy_1' \alpha_1(x_1', y_1') - \int_{C_1} dx_1' dy_1' \alpha_1(x_1', y_1') \right\} = (-j\beta_d) \{1 - 1\} = 0. \end{aligned} \quad (4.3.5)$$

Thus, by setting $\beta_d = 0$ in (4.3.1) we are ignoring corrections on the order of β_d^2 and higher, and if β_d is small, these corrections are very small.

The Helmholtz parameter β_d for the dielectric is $2\pi/\lambda$ where λ is the wavelength of a wave passing down the transmission line. Thus, our "small β_d " assumption stated above can also be written

$$\lambda \gg D \quad (4.3.6)$$

which says the wavelength is much longer than the size of the transmission line transverse dimensions. This assumption is called the **Transmission Line Limit**. If we operate within this limit, then (4.3.1) may be approximated as

$$\phi_{12}(\mathbf{x}) = \frac{1}{4\pi\epsilon_d} \int_{-\infty}^{\infty} dz' q(z') \left\{ \int_{C_1} dx_1' dy_1' \alpha_1(x_1', y_1') \frac{1}{R_1} - \int_{C_2} dx_2' dy_2' \alpha_2(x_2', y_2') \frac{1}{R_2} \right\} . \quad (4.3.7)$$

We shall now use the small β_d assumption one more time. We assume that the linear charge density $q(z')$ has the characteristics of a wave traveling down the transmission line (see also Chapter 5),

$$q(z) = q(0) e^{-j\beta_d z} \quad // \quad q(z, t) = q(0, 0) e^{j(\omega t - \beta_d z)} \quad (4.3.8)$$

which is appropriate for a lossless line (see below for a lossy line). Therefore,

$$q'(z) = -j\beta_d q(z)$$

$$q''(z) = (-j\beta_d)^2 q(z) \quad \text{and so on.}$$

We can then write a Taylor expansion for charge density $q(z')$ which appears in our integration,

$$\begin{aligned} q(z') &= q(z) + (z'-z) q'(z) + (1/2) (z'-z)^2 q''(z) + \dots \\ &= q(z) + (-j\beta_d) q(z) (z'-z) + (1/2) (-j\beta_d)^2 q(z) (z'-z)^2 + \dots \\ &= q(z) [1 + (-j\beta_d) (z'-z) + (1/2) (-j\beta_d)^2 (z'-z)^2 + \dots] . \end{aligned} \quad (4.3.9)$$

Since both R_1 and R_2 are even functions of the quantity $(z'-z)$, and since there is no other $(z'-z)$ dependence in the (4.3.7) integrand, the $(-j\beta_d)$ term in (4.3.9) contributes nothing (this is also true more generally for (4.3.1)). Thus, if we assume small β_d , we can approximate $q(z') \approx q(z)$ where we are then ignoring a β_d^2 size term. Once again, if β_d is small, β_d^2 is very small so our error in replacing $q(z')$ by $q(z)$ is very small. We are only interested in the contributing region where $|z-z'|$ is on the order of transverse dimension D , so one is using the same $\beta_d D \ll 1$ as assumed earlier.

We arrive then at our final result for the potential at a point \mathbf{x} between the conductors,

$$\phi_{12}(\mathbf{x}) = \frac{1}{4\pi\epsilon_d} q(z) \int_{-\infty}^{\infty} dz' \left\{ \int_{C_1} dx_1' dy_1' \alpha_1(x_1', y_1') \frac{1}{R_1} - \int_{C_2} dx_2' dy_2' \alpha_2(x_2', y_2') \frac{1}{R_2} \right\} \quad (4.3.10)$$

where we have thrown out terms of order β_d^2 and higher. In this transmission line limit approximation, our Helmholtz integral (4.3.1) has been reduced to essentially an electrostatics Coulomb integral where we just sum over the contribution of each piece of charge to the total potential. As noted earlier, $q(z)$ has the normalization of n_e and not n_s as discussed in Section 1.5 (c) which explains why the leading factor is $\frac{1}{4\pi\epsilon_d}$ and not $\frac{1}{4\pi\epsilon_s}$. This allows for the dielectric to have some conductance.

It should be noted that the integral of (4.3.10) converges due to the subtraction of the two terms which in turn results from the two conductors having opposite longitudinal charge densities $q(z)$ and $-q(z)$. The individual terms in (4.3.10) do not converge and are in fact each logarithmically divergent in the sense that

$$\int_0^{\infty} dz' (1/z') = \ln(\infty) = \infty .$$

This will become clearer in (4.4.5) below.

Transmission Line Limit for a Transmission Line with Losses

When a transmission line has losses, we will show later in (5.3.5) that the z dependence of $q(z)$ and other line quantities is not $e^{-j\beta_d z}$ but rather e^{-jkz} where $jk = \sqrt{(R+j\omega L)(G+j\omega C)}$ where R, L, G, C are certain transmission line parameters. The lossless case is recovered by setting $R = G = 0$ so $jk = \sqrt{-\omega^2 LC}$ and then $k = \omega\sqrt{LC}$. It will be shown in (4.12.19) that in this case $\sqrt{LC} = 1/v_d$ so then $k = \omega/v_d = \beta_d$. In the lossy case, to make the argument above concerning $q(z') \approx q(z)$, we must show that $|k| D \ll 1$ in addition

to $\beta_a D \ll 1$ of (4.3.4). Appendix (Q.2.1) shows that $|k| = [(R^2 + \omega^2 L^2)(G^2 + \omega^2 C^2)]^{1/4}$, so the "transmission line limit" then requires that these two conditions be met :

$$\begin{aligned} \omega \sqrt{LC} D &\ll 1 && // \beta_a D \ll 1 \\ [(R^2 + \omega^2 L^2)(G^2 + \omega^2 C^2)]^{1/4} D &\ll 1 . && // \text{for a lossy line, } |k| D \ll 1 \end{aligned} \quad (4.3.11)$$

Since $|k| \geq \beta_a$ (see Fig Q.5.8), the second inequality is more stringent in determining the maximum general ω for which the analysis presented above is valid. Using the quadratic formula, the last inequality can be written as

$$\omega^2 \ll [-b + \sqrt{b^2 - 4ac}] / (2a) \quad // \text{transmission line limit for lossy line} \quad (4.3.12)$$

$$\begin{aligned} a &= L^2 C^2 &> 0 \\ b &= L^2 G^2 + R^2 C^2 &> 0 \\ c &= R^2 G^2 - 1/D^4 &< 0 \text{ (for } D \text{ small enough to put things in the transmission line limit)} \end{aligned}$$

As an example, if we insert the parameters appropriate for Belden 8281 coaxial cable (see Appendix R), and use $D = a_2 =$ the cable radius, we obtain from (4.3.12) that $\omega^2 \ll 6 \times 10^{21}$ so $\omega \ll 8 \times 10^{10}$ and finally $f \ll 12$ GHz. At such a high frequency, Fig Q.5.8 shows that $\text{Im}(k) \approx 0.1$ so a signal would decay to $1/e$ in 10 meters of cable.

4.4 General Calculation of $V(z)$

We now introduce two new points \mathbf{x}_1 and \mathbf{x}_2 . The point \mathbf{x}_1 lies on C_1 in the $z = z$ plane, while \mathbf{x}_2 lies on C_2 in this same plane. We then evaluate $\phi_{12}(\mathbf{x})$ at $\mathbf{x} = \mathbf{x}_1$ and subtract from that $\phi_{12}(\mathbf{x})$ at $\mathbf{x} = \mathbf{x}_2$ and in this way we obtain the potential difference between the surfaces of the two conductors at $z = z$. Recall,

Fact 2: $\phi \approx$ constant on a conductor boundary ($z = \text{constant}$) in the strong or extreme skin effect regimes within the Transmission Line Limit. (3.7.4)

Thus, assuming the small δ regime and treating $\phi \approx$ constant as an equality, the potential difference will be independent of the locations of \mathbf{x}_2 and \mathbf{x}_1 as long as they are on their respective surfaces and both have $z = z$. For this reason, the potential difference is a function only of z . Thus we write, using two copies of (4.3.10),

$$\begin{aligned} V(z) &\equiv \phi_{12}(\mathbf{x}_1) - \phi_{12}(\mathbf{x}_2) \\ &= \frac{1}{4\pi\epsilon_d} q(z) \int_{-\infty}^{\infty} dz' \left\{ \int_{C_1} dx_1' dy_1' \alpha_1(x_1', y_1') \frac{1}{R_{11}} - \int_{C_2} dx_2' dy_2' \alpha_2(x_2', y_2') \frac{1}{R_{12}} \right\} \\ &\quad - \frac{1}{4\pi\epsilon_d} q(z) \int_{-\infty}^{\infty} dz' \left\{ \int_{C_1} dx_1' dy_1' \alpha_1(x_1', y_1') \frac{1}{R_{21}} - \int_{C_2} dx_2' dy_2' \alpha_2(x_2', y_2') \frac{1}{R_{22}} \right\} \end{aligned} \quad (4.4.1)$$

where

$$\begin{aligned}
 R_{11}^2 &= (x_1-x_1')^2 + (y_1-y_1')^2 + (z-z')^2 = s_{11}^2 + (z-z')^2 & s_{11}^2 &= (x_1-x_1')^2 + (y_1-y_1')^2 \\
 R_{12}^2 &= (x_1-x_2')^2 + (y_1-y_2')^2 + (z-z')^2 = s_{12}^2 + (z-z')^2 & s_{12}^2 &= (x_1-x_2')^2 + (y_1-y_2')^2 \\
 R_{22}^2 &= (x_2-x_2')^2 + (y_2-y_2')^2 + (z-z')^2 = s_{22}^2 + (z-z')^2 & s_{22}^2 &= (x_2-x_2')^2 + (y_2-y_2')^2 \\
 R_{21}^2 &= (x_2-x_1')^2 + (y_2-y_1')^2 + (z-z')^2 = s_{21}^2 + (z-z')^2 & s_{21}^2 &= (x_2-x_1')^2 + (y_2-y_1')^2 .
 \end{aligned} \tag{4.4.2}$$

The vector \mathbf{R}_{12} points from our new point \mathbf{x}_1 to an integration point \mathbf{x}_2' on C_2 . Here is a drawing of our new and more complicated situation:

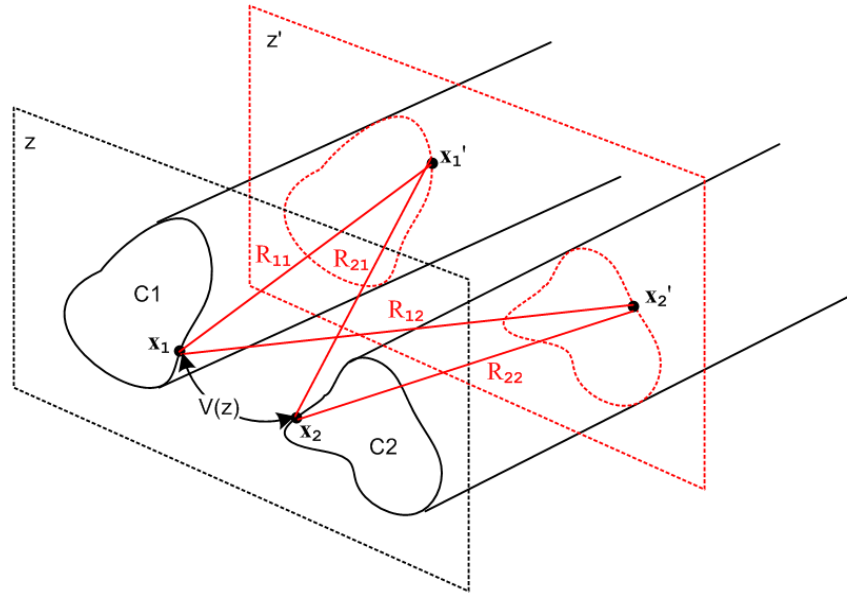


Fig 4.2

We next rearrange the four terms in (4.4.1) to get

$$\begin{aligned}
 V(z) & & (4.4.3) \\
 &= q(z) \frac{1}{4\pi\epsilon_0 a} \int_{-\infty}^{\infty} dz' \left\{ \int_{C_1} dx_1' dy_1' \alpha_1(x_1', y_1') \left(\frac{1}{R_{11}} - \frac{1}{R_{21}} \right) - \int_{C_2} dx_2' dy_2' \alpha_2(x_2', y_2') \left(\frac{1}{R_{12}} - \frac{1}{R_{22}} \right) \right\} .
 \end{aligned}$$

It is now possible to carry out the dz' integrations. The generic integral of interest is the following,

$$\int_{-\infty}^{\infty} dx \left\{ \frac{1}{\sqrt{a^2+x^2}} - \frac{1}{\sqrt{b^2+x^2}} \right\} = \ln(b^2/a^2) . \tag{4.4.4}$$

Since this is quite important, we confirm with Maple,

```
Int(1/sqrt(a^2+x^2) - 1/sqrt(b^2 +x^2), x=-infinity..infinity);
```

$$\int_{-\infty}^{\infty} \left(\frac{1}{\sqrt{a^2+x^2}} - \frac{1}{\sqrt{b^2+x^2}} \right) dx$$

```
value(%);
```

$$-\ln(a^2) + \ln(b^2)$$

The separate integrals here are logarithmically divergent, but the combination converges. Thus,

$$\int_{-\infty}^{\infty} dz' \left(\frac{1}{R_{11}} - \frac{1}{R_{21}} \right) = \int_{-\infty}^{\infty} dz' \left(\frac{1}{\sqrt{s_{11}^2 + (z-z')^2}} - \frac{1}{\sqrt{s_{21}^2 + (z-z')^2}} \right) = \ln(s_{21}^2/s_{11}^2)$$

$$\int_{-\infty}^{\infty} dz' \left(\frac{1}{R_{12}} - \frac{1}{R_{22}} \right) = \int_{-\infty}^{\infty} dz' \left(\frac{1}{\sqrt{s_{12}^2 + (z-z')^2}} - \frac{1}{\sqrt{s_{22}^2 + (z-z')^2}} \right) = \ln(s_{22}^2/s_{12}^2) \quad (4.4.5)$$

so that

$$V(z) = q(z) \frac{1}{4\pi\epsilon_0} \left\{ \int_{C_1} dx_1' dy_1' \alpha_1(x_1', y_1') \ln(s_{21}^2/s_{11}^2) - \int_{C_2} dx_2' dy_2' \alpha_2(x_2', y_2') \ln(s_{22}^2/s_{12}^2) \right\}$$

$$\begin{aligned} s_{21}^2 &= (x_2 - x_1')^2 + (y_2 - y_1')^2 & s_{22}^2 &= (x_2 - x_2')^2 + (y_2 - y_2')^2 \\ s_{11}^2 &= (x_1 - x_1')^2 + (y_1 - y_1')^2 & s_{12}^2 &= (x_1 - x_2')^2 + (y_1 - y_2')^2 \end{aligned} \quad (4.4.6)$$

The four transverse distances are shown in this figure,

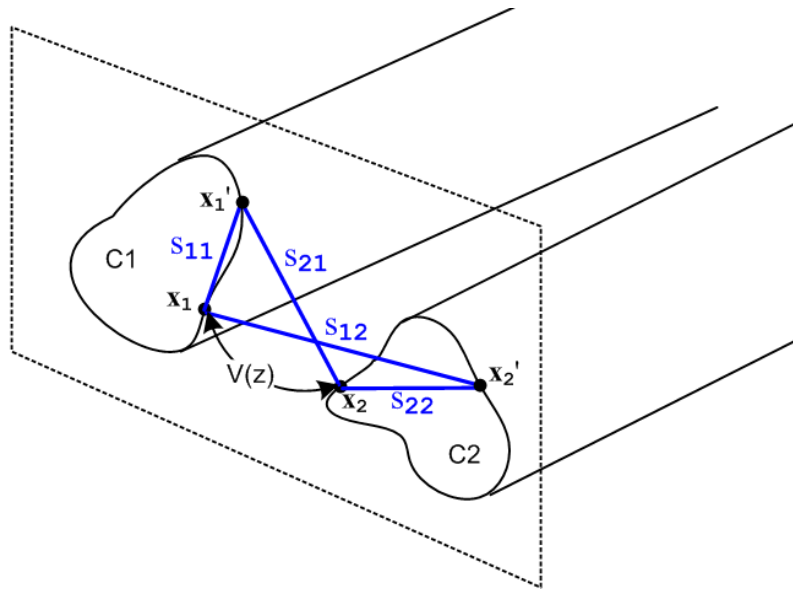


Fig 4.3

Equation (4.4.6) expresses the potential between the two transmission line conductors at some plane \$z\$ in terms of the charge distributions on the conductors \$\alpha_i\$. In general, these charge distributions are not known, so one cannot regard (4.4.6) as a general purpose silver bullet to solve transmission line problems. On the other hand, as we shall see, equation (4.4.6) is one of a group of equations which will allow us to express several different transmission line parameters in terms the same integral, and one then obtains a relation between these parameters.

For example, in analogy to what we did with a parallel plate capacitor in (1.5.19), we may define the complex capacitance \$C'\$ per unit length of our transmission line using (4.4.6) as follows:

$$\begin{aligned} \frac{1}{C'} &= \frac{V(z)}{q(z)} = \frac{1}{4\pi\xi_d} \left\{ \int_{C_1} dx_1' dy_1' \alpha_1(x_1', y_1') \ln(s_{21}^2/s_{11}^2) - \int_{C_2} dx_2' dy_2' \alpha_2(x_2', y_2') \ln(s_{22}^2/s_{12}^2) \right\} \\ &= \frac{1}{4\pi\xi_d} K \quad \text{and} \quad V(z) = q(z) \frac{1}{4\pi\xi_d} K \end{aligned} \quad (4.4.7)$$

where

$$K \equiv \int_{C_1} dx_1' dy_1' \alpha_1(x_1', y_1') \ln(s_{21}^2/s_{11}^2) - \int_{C_2} dx_2' dy_2' \alpha_2(x_2', y_2') \ln(s_{22}^2/s_{12}^2) . \quad (4.4.8)$$

Eq (4.1.2) shows that $\alpha_1(x,y)$ has dimensions $1/m^2$, so K is a dimensionless number. As observed at the end of Section 4.1, Fact 2 of (3.7.4) that $\varphi = \text{constant}$ on the cross section perimeter allows us to define $\alpha_1(x_1', y_1')$ to be a purely real function. Thus, K is a dimensionless real number obtained from a 2D geometric integral of the normalized transverse charge distributions α_i .

Recall from (1.5.20) that (C' , C and G are discussed further in Section 4.11 below)

$$C' = C + 1/(j\omega R) = C + G/(j\omega) \quad (4.4.9)$$

where conductance (per unit length) G is associated with the imaginary part of C' . We then have

$$4\pi\xi_d/K = C' = C + G/j\omega$$

or

$$4\pi(\varepsilon_d + \sigma_d/j\omega)/K = C + G/j\omega \quad // (1.5.1a) \text{ for } \xi_d$$

so that

$$C = 4\pi\varepsilon_d/K \quad \text{capacitance per unit length of the transmission line}$$

$$G = 4\pi\sigma_d/K \quad \text{conductance per unit length of the transmission line}$$

so

$$C/G = \varepsilon_d/\sigma_d . \quad (4.4.10)$$

Here $G = 1/R_G$ is the conductance across the dielectric *between* a unit length of the two conductors. This is unrelated to the longitudinal resistance R of the conductors themselves, though that parameter will arise later on in the form of surface impedance Z_s . We only have $G \neq 0$ if the dielectric has some conductance $\sigma_d \neq 0$ (or $\sigma_{eff} \neq 0$ as in (3.3.4)).

Note from above and (1.1.28) that $\dim(C) = \dim(\varepsilon) = \text{farad/m}$ and $\dim(G) = \dim(\sigma) = \text{mho/m}$.

We now quote several results that will be derived later in Section 4.11.

First, we show below in (4.10.8) with (4.12.20) that the external inductance per unit length of our transmission line is *also* related to this same constant K ,

$$L_e = (\mu_d/4\pi)K . \quad (4.4.11)$$

Second, we show in (4.12.18) that the **characteristic impedance** of the transmission line is given by

$$Z_0 \equiv \frac{V(z)}{i(z)} = \sqrt{\frac{R + j\omega L}{G + j\omega C}} \quad (4.4.12)$$

At sufficiently large ω we can neglect the R and G terms to get this real value,

$$Z_0 = \sqrt{\frac{L}{C}} \quad // \text{ large } \omega \quad (4.4.13)$$

Third, we show in (4.12.26) that, for large ω , $L \rightarrow L_e$ so

$$Z_0 = \sqrt{\frac{L_e}{C}} = \sqrt{\frac{(\mu_d/4\pi)K}{4\pi\epsilon_d/K}} = (1/4\pi) K \sqrt{\mu_d/\epsilon_d} = (1/4\pi) K Z_m \quad // \text{ large } \omega \quad (4.4.14)$$

where $Z_m \equiv \sqrt{\mu_d/\epsilon_d}$ is the "intrinsic impedance of the dielectric medium" having μ_d and ϵ_d . Recall that for free space we had in (1.1.29)

$$Z_{fs} = \sqrt{\mu_0/\epsilon_0} = 376.73032 \text{ ohms} \quad \Rightarrow \quad Z_{fs}/4\pi = 29.97948 \approx 30 \Omega \quad (4.4.15)$$

[Obscure fact: the color NTSC frame rate is $30 \cdot 1000/1001 = 29.97002997$ Hz. ≈ 30 Hz.]

Typically one has $\mu_d = \mu_0$ so then (note that ϵ_{re1} and K are dimensionless),

$$Z_m \equiv \sqrt{\mu_d/\epsilon_d} = \sqrt{\mu_0/\epsilon_d} = \sqrt{\mu_0/\epsilon_0} \sqrt{\epsilon_0/\epsilon_d} = Z_{fs} / \sqrt{\epsilon_{re1}} \quad // \epsilon_{re1} \equiv \epsilon_d/\epsilon_0 \quad (4.4.16)$$

so

$$Z_0 = (1/4\pi) K Z_m = (1/4\pi) K (Z_{fs}/\sqrt{\epsilon_{re1}}) = (K/\sqrt{\epsilon_{re1}}) (Z_{fs}/4\pi) = (K/\sqrt{\epsilon_{re1}}) 30\Omega.$$

We then summarize the parameters of a transmission line in terms of dimensionless real integral K :

$$C = 4\pi\epsilon_d/K \quad \text{capacitance per unit length} \quad (4.4.17)$$

$$G = 4\pi\sigma_d/K \quad \text{transverse conductance per unit length}$$

$$L_e = (\mu_d/4\pi) K \quad \text{external inductance per unit length}$$

$$Z_0 \approx (K/\sqrt{\epsilon_{re1}}) 30\Omega \quad \text{characteristic impedance } \mu_d = \mu_0, \epsilon_{re1} \equiv \epsilon_d/\epsilon_0$$

$$R = \text{Re}(Z_{s1} + Z_{s2}) \quad \text{resistance of conductors, see (4.12.24)}$$

$$L = L_e + (1/\omega) \text{Im}(Z_{s1} + Z_{s2}) \quad \text{total inductance, see (4.12.24)}$$

$$Z_{si} = \text{surface impedance of conductor } i, \text{ see (2.4.1) and (4.12.9)}$$

The last three items are *not* determined by integral K and we just mention them for completeness's sake. All these equations will be more fully developed in Section 4.11 below, but we have jumped ahead a bit in order to treat two important examples which hopefully will be refreshing after all the above "theory".

Intrinsic Impedance Comment: Notice that the intrinsic impedance of a dielectric medium $Z_m = \sqrt{\mu_d/\epsilon_d}$ is different from the characteristic impedance of a transmission line Z_0 , although the numbers are in the same ballpark. For large ω , we showed in (4.4.14) that they are related by the equation $Z_0 = (K/4\pi) Z_m$. Both have dimensions of ohms (not ohms/m).

One can define a different intrinsic impedance $Z_m = \sqrt{\mu_d/\xi_d}$ [recall (1.5.1a) that $\xi_d \equiv \epsilon_d - j\sigma_d/\omega$] and corresponding characteristic impedance Z_0 which have the relationship $Z_0 = \sqrt{L/C'} = (1/4\pi) K Z_m$ with C' as shown in (4.4.9) above. Belden sometimes refers to Z_m as η . We shall have no need for the quantities Z_0 and Z_m since we handle conducting dielectrics without involving these quantities.

4.5 Example: Transmission line with widely-spaced round wires of unequal diameters

Consider a transmission line made from two round wires of radii a_1 and a_2 and center line spacing b . In the case that $b \gg a_1$ and a_2 , the charge distribution on each round wire is symmetric about the wire and in this situation (a rare one admittedly) we *know* the two transverse charge distributions:

$$\begin{aligned}\alpha_1(x,y) &= \alpha_1(r,\theta) = \delta(r - a_1)/(2\pi a_1) \\ \alpha_2(x,y) &= \alpha_2(r,\theta) = \delta(r - a_2)/(2\pi a_2) \quad .\end{aligned}\tag{4.5.1}$$

The $1/(2\pi a_1)$ factor is required so that the integral of α_1 is unity as required by (4.1.3),

$$\begin{aligned}\int_{C_1} dx dy \alpha_1(x,y) &= \int_0^{2\pi} d\theta \int_0^\infty r dr \alpha_1(r,\theta) = \int_0^{2\pi} d\theta \int_0^\infty r dr \delta(r - a_1)/(2\pi a_1) \\ &= \int_0^{2\pi} d\theta a_1/(2\pi a_1) = 2\pi a_1/(2\pi a_1) = 1 \quad .\end{aligned}\tag{4.5.2}$$

Note: The reason the α_i are symmetric is that the two conductors are so far apart that each one is essentially "in isolation" and so the charge assumes an axially symmetric distribution. An analogy would be that for two point charges far apart, the E field close to either point charge is spherically symmetric because close to one charge the field of the other can be neglected.

Our task is then to compute the integral K shown in (4.4.8),

$$\begin{aligned}K &= \int_0^{2\pi} d\theta_1 \int_0^{a_1} r_1 dr_1 [\delta(r_1 - a_1)/(2\pi a_1)] \ln(s_{21}^2/s_{11}^2) \\ &\quad - \int_0^{2\pi} d\theta_2 \int_0^{a_2} r_2 dr_2 [\delta(r_2 - a_2)/(2\pi a_2)] \ln(s_{22}^2/s_{12}^2) \quad . \\ &= \int_0^{2\pi} d\theta_1 1/(2\pi) \ln(s_{21}^2/s_{11}^2) \\ &\quad - \int_0^{2\pi} d\theta_2 1/(2\pi) \ln(s_{22}^2/s_{12}^2) \\ &= 1/(2\pi) \left\{ \int_0^{2\pi} d\theta_1 [\ln(s_{21}^2) - \ln(s_{11}^2)] - \int_0^{2\pi} d\theta_2 [\ln(s_{22}^2) - \ln(s_{12}^2)] \right\}\end{aligned}\tag{4.5.3}$$

where we then have four integrals to evaluate.

We shall choose our $V(z)$ potential-determining reference points \mathbf{x}_1 and \mathbf{x}_2 as shown in this drawing,

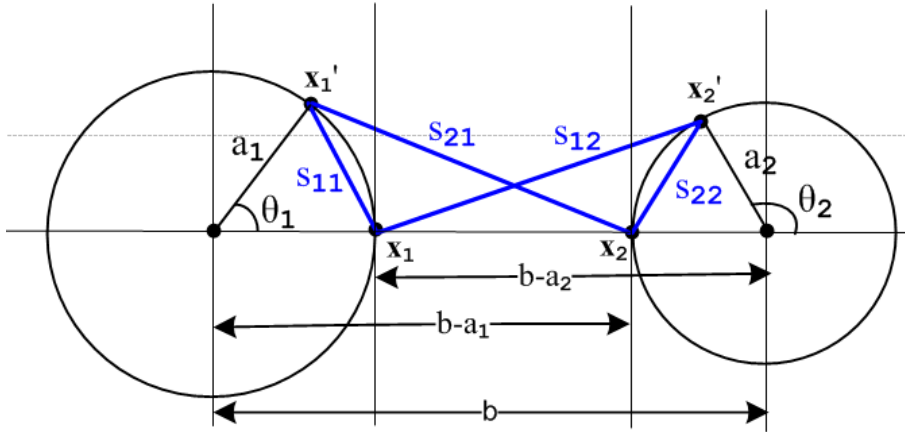


Fig 4.4

The four $s_{i,j}$ distances can be read off from the drawing using the law of cosines,

$$\begin{aligned}
 s_{21}^2 &= a_1^2 + (b-a_1)^2 - 2 a_1(b-a_1) \cos(\theta_1) \\
 s_{11}^2 &= a_1^2 + a_1^2 - 2 a_1 a_1 \cos(\theta_1) = 2a_1^2(1 - \cos(\theta_1)) \\
 s_{22}^2 &= a_2^2 + a_2^2 - 2 a_2 a_2 \cos(\pi-\theta_2) = 2a_2^2(1 + \cos(\theta_2)) \\
 s_{12}^2 &= a_2^2 + (b-a_2)^2 + 2 a_2(b-a_2) \cos(\theta_2) .
 \end{aligned} \tag{4.5.4}$$

We then invoke the following integral from p 531 of GR7,

$$9.^8 \quad \int_0^\pi \ln(a + b \cos x) dx = \pi \ln \frac{a + \sqrt{a^2 - b^2}}{2} \quad [a \geq |b| > 0] \quad \text{GW (322)(15)}$$

which we rewrite as

$$\int_0^{2\pi} d\theta \ln(A \pm B \cos \theta) = 2\pi \ln\left[\frac{1}{2}(A + \sqrt{A^2 - B^2})\right] . \tag{4.5.5}$$

The four integrals are then easily evaluated. First,

$$\int_0^{2\pi} d\theta_1 \ln(s_{21}^2) = \int_0^{2\pi} d\theta_1 \ln([a_1^2 + (b-a_1)^2 - 2 a_1(b-a_1) \cos(\theta_1)])$$

$$A = a_1^2 + (b-a_1)^2 \quad B = 2 a_1(b-a_1)$$

$$A^2 - B^2 = [a_1^2 + (b-a_1)^2]^2 - 4 a_1^2(b-a_1)^2 = [a_1^2 - (b-a_1)^2]^2 \Rightarrow \sqrt{A^2 - B^2} = (b-a_1)^2 - a_1^2 > 0 \quad b \gg a_1$$

$$\Rightarrow \int_0^{2\pi} d\theta_1 \ln(s_{21}^2) = 2\pi \ln\left[\frac{1}{2}(a_1^2 + (b-a_1)^2 + (b-a_1)^2 - a_1^2)\right] = 2\pi \ln[(b-a_1)^2] .$$

The fourth integral is the same with $1 \leftrightarrow 2$, and the different sign of the second term in s_{12}^2 makes no difference,

$$\int_0^{2\pi} d\theta_2 \ln(s_{12}^2) = 2\pi \ln[(b-a_2)^2] .$$

The second integral is

$$\begin{aligned} \int_0^{2\pi} d\theta_1 \ln(s_{11}^2) &= \int_0^{2\pi} d\theta_1 \ln([2a_1^2(1 - \cos(\theta_1))]) & A = B = 2a_1^2, A^2 - B^2 = 0 \\ &= 2\pi \ln[(1/2) 2a_1^2] = 2\pi \ln(a_1^2) . \end{aligned}$$

The third integral is similar giving

$$\int_0^{2\pi} d\theta_2 \ln(s_{22}^2) = 2\pi \ln(a_2^2) .$$

To summarize:

$$\begin{aligned} \int_0^{2\pi} d\theta_1 \ln(s_{21}^2) &= 2\pi \ln[(b-a_1)^2] \\ \int_0^{2\pi} d\theta_1 \ln(s_{11}^2) &= 2\pi \ln(a_1^2) \\ \int_0^{2\pi} d\theta_2 \ln(s_{22}^2) &= 2\pi \ln(a_2^2) \\ \int_0^{2\pi} d\theta_2 \ln(s_{12}^2) &= 2\pi \ln[(b-a_2)^2] . \end{aligned} \tag{4.5.6}$$

Then from (4.5.3) we find

$$\begin{aligned} K &= 1/(2\pi) \{ \int_0^{2\pi} d\theta_1 [\ln(s_{21}^2) - \ln(s_{11}^2)] - \int_0^{2\pi} d\theta_2 [\ln(s_{22}^2) - \ln(s_{12}^2)] \} \\ &= \ln[(b-a_1)^2] - \ln(a_1^2) - \ln(a_2^2) + \ln[(b-a_2)^2] = \ln \left[\frac{(b-a_1)^2(b-a_2)^2}{a_1^2 a_2^2} \right] \\ &= 2 \ln \left[\frac{(b-a_1)(b-a_2)}{a_1 a_2} \right] = 2 \ln \left[\frac{b^2}{a_1 a_2} \right] \quad // \text{ since we assumed at the start that } b \gg a_1, a_2 \\ &= 4 \ln(b/\sqrt{a_1 a_2}) . \end{aligned} \tag{4.5.7}$$

Therefore the transmission line parameters from (4.5.7) and (4.4.17) are,

$$\begin{aligned}
 K &= 4 \ln(b/\sqrt{a_1 a_2}) && // \text{widely-space round wires, } b \gg a_1, a_2 \\
 C &= 4\pi\epsilon_d/K && = \pi\epsilon_d / \ln(b/\sqrt{a_1 a_2}) \\
 G &= 4\pi\sigma_d/K && = \pi\sigma_d / \ln(b/\sqrt{a_1 a_2}) \\
 L_e &= (\mu_d/4\pi) K && = (\mu_d/\pi) \ln(b/\sqrt{a_1 a_2}) \\
 Z_0 &= (K / \sqrt{\epsilon_{re1}}) 30\Omega && = (1/\sqrt{\epsilon_{re1}}) \ln(b/\sqrt{a_1 a_2}) 120\Omega .
 \end{aligned}
 \tag{4.5.8}$$

Sometimes these formulas are written in terms of wire diameters $d_i = 2a_i$ in which case

$$K = 4 \ln[b/\sqrt{a_1 a_2}] = 4 \ln[2b/\sqrt{d_1 d_2}] = 2 \ln[4b^2/d_1 d_2] .
 \tag{4.5.9}$$

Since we are assuming $b \gg d_1, d_2$ we know that $x \equiv 2b^2/d_1 d_2 \gg 1$. Therefore

$$\text{ch}^{-1}x = \ln[x + \sqrt{x^2-1}] \approx \ln(2x) \quad // \text{an identity Siegel 8.56, then an approximation}
 \tag{4.5.10}$$

so

$$\text{ch}^{-1}(2b^2/d_1 d_2) \approx \ln(4b^2/d_1 d_2) .$$

Then we can write K as

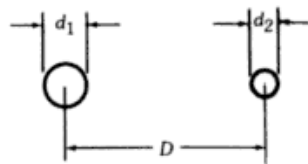
$$K = 2 \ln[4b^2/d_1 d_2] = 2 \text{ch}^{-1}(2b^2/d_1 d_2)
 \tag{4.5.11}$$

and so

$$Z_0 = (K / \sqrt{\epsilon_{re1}}) 30\Omega = (1/\sqrt{\epsilon_{re1}}) \text{ch}^{-1}(2b^2/d_1 d_2) 60\Omega .
 \tag{4.5.12}$$

It is not easy to find expressions for C,G and L_e for the unequal radii geometry, but Z_0 does appear for example in Reference RDE page 29-23 where we find:

N. Balanced 2-wire—unequal diameters



$$\begin{aligned}
 Z_0 &= (60/\epsilon^{1/2}) \cosh^{-1}N \\
 N &= \frac{1}{2}[(4D^2/d_1 d_2) - (d_1/d_2) - (d_2/d_1)]
 \end{aligned}$$

Fig 4.5

with $D =$ our b . For $D \gg d_1, d_2$ this shows $N = 2D^2/(d_1 d_2)$, and this then agrees with (4.5.12). This quoted result is in fact correct (with the two extra terms shown in N) even when D is not large. We shall derive this full result in Chapter 6, equation (6.3.12).

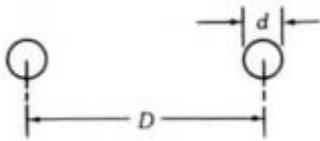
In the special case that $a_1 = a_2 \equiv a$ we get,

$$\begin{aligned}
 K &= 4 \ln(b/a) && // \text{ widely-space round wires, } b \gg a_1=a_2 \\
 C &= 4\pi\epsilon_d/K && = \pi\epsilon_d/ \ln(b/a) \\
 G &= 4\pi\sigma_d/K && = \pi\sigma_d/ \ln(b/a) \\
 L_e &= (\mu_d/4\pi) K && = (\mu_d/\pi) \ln(b/a) \\
 Z_0 &= (K/\sqrt{\epsilon_{rel}}) 30\Omega = (1/\sqrt{\epsilon_{rel}}) \ln(b/a) 120\Omega \\
 &= (1/\sqrt{\epsilon_{rel}}) \ln(2b/d) 120\Omega && d = 2a .
 \end{aligned} \tag{4.5.13}$$

The first three results agree with King TLT p17 (30b),

$$g \equiv \frac{\pi\sigma}{\ln(b/a)} \quad c \equiv \frac{\pi\epsilon}{\ln(b/a)} \quad l^e = \frac{y}{\pi} \ln \frac{b}{a} \tag{30b}$$

The expression for Z_0 agrees with the RDE source quoted above,



$$\begin{aligned}
 Z_0 &= 120 \cosh^{-1}(D/d) \\
 &\approx 276 \log_{10}(2D/d) \\
 &\approx 120 \log_e(2D/d)
 \end{aligned}$$

Fig 4.6

where again $D = b$ and $\epsilon_{rel} = 1$.

Power Transmission Lines (also Telephone and Telegraph)

Ignoring proximity effects of the ground and possible ground wires, one can consider a single phase power transmission line as fitting into this example. The first interesting number is skin depth. For aluminum at $f = 60$ Hz one finds,

$$\begin{aligned}
 \sigma_{\text{aluminum}} &= 3.7 \times 10^7 \text{ mho/m} && // \text{ recall } \sigma_{\text{copper}} \approx 5.8 \times 10^7 \text{ (annealed)} \\
 \mu_0 &= 4\pi \times 10^{-7} \text{ henry/m}
 \end{aligned}$$

$$\delta \equiv \sqrt{2/(\omega\mu\sigma)} \approx \sqrt{2/(2\pi f\mu_0\sigma)} = \sqrt{1/(\pi f\mu_0\sigma)}$$

```

delta := sqrt(1/(Pi*60*4*Pi*3.7)): evalf(%);
.01068178037
    
```

So $\delta \approx 1$ cm. Thus, skin effect could be significant for a very large diameter wire. Typically the individual strands of a 1500 amp cable are 1/6" in diameter or 0.2 cm in radius, so there is some slight non-uniformity in the current distribution. If the strands are not insulated one should think of this more in terms of the total cable diameter including all strand layers which might be 1".

Usually the requirement of low power loss requires that R be relatively small compared to ωL . The 1500A cable just noted has $R = .02\Omega$ per thousand feet. Similarly, the conductance G (mostly from

insulator leakage) is very small compared to ωC . Thus, (4.4.12) leads to (4.4.16) stating $Z_0 \approx K 30\Omega$. If the full cable is 1" in diameter and the two lines are spaced 1 m apart, we can compute K from (4.5.13),

$$K = 4 \ln(b/a) = 4 \ln(1\text{m}/0.5\text{")}) = 4 \ln(39.37 \times 2) = 17.5$$

so then from (4.4.16),

$$Z_0 \approx K 30\Omega = 17.5 * 30\Omega = 524\Omega .$$

Notice that halving radius a (or doubling b) increases K by $4\ln 2 = 2.77$ which is only 16% of 17.5, so Z_0 is fairly insensitive to the line geometry. Rajput (p 554) claims power lines typically range from 400 to 600 Ω . See southwire.com for data on transmission line cables.

A twin-line telegraph or telephone cable falls into this same impedance class, with 600 ohms being the traditional Z_0 number. A single telegraph wire over the ground plane has a similar Z_0 . For $a = 1/8" = 0.32\text{ cm}$ and height 4 m, $K = 2 \ln(2h/a)$ from (6.3.21) below, so $K = 2 \ln(8/[.32 \times 10^{-2}]) = 2 \ln(2500) = 15.64$ giving $Z_0 = 469\Omega$.

4.6 Example: A coaxial cable

A coaxial cable is the other transmission line where we know the surface charge distribution is that given by (4.5.1). The analysis of the previous section resulting in (4.5.3) is then unchanged, and we find that K is still given by (4.5.3),

$$K = 1/(2\pi) \left\{ \int_0^{2\pi} d\theta_1 [\ln(s_{21}^2) - \ln(s_{11}^2)] - \int_0^{2\pi} d\theta_2 [\ln(s_{22}^2) - \ln(s_{12}^2)] \right\} . \quad (4.5.3)$$

What is different is that we have a different picture describing the various s_{ij} distances. The new picture is this, where the cross section circles have radii $a_2 > a_1$:

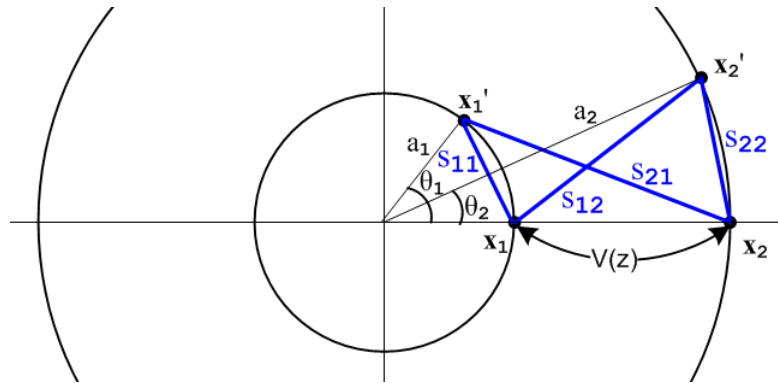


Fig 4.7

As done in the previous section, we "read off" the s_{ij} expressions using the law of cosines:

$$\begin{aligned} s_{21}^2 &= a_1^2 + a_2^2 - 2 a_1 a_2 \cos(\theta_1) \\ s_{11}^2 &= a_1^2 + a_1^2 - 2 a_1 a_1 \cos(\theta_1) = 2a_1^2(1 - \cos(\theta_1)) \\ s_{22}^2 &= a_2^2 + a_2^2 - 2 a_2 a_2 \cos(\theta_2) = 2a_2^2(1 - \cos(\theta_2)) \\ s_{12}^2 &= a_2^2 + a_1^2 - 2 a_1 a_2 \cos(\theta_2) . \end{aligned} \quad (4.6.1)$$

Recalling,

$$\int_0^{2\pi} d\theta \ln (A \pm B \cos\theta) = 2\pi \ln[(1/2)(A + \sqrt{A^2 - B^2})] . \quad (4.5.5)$$

one finds,

$$\int_0^{2\pi} d\theta_1 \ln(s_{21}^2) = \int_0^{2\pi} d\theta_1 \ln[a_1^2 + a_2^2 - 2a_1 a_2 \cos(\theta_1)] \quad A = a_1^2 + a_2^2 \quad B = 2a_1 a_2$$

$$A^2 - B^2 = (a_1^2 + a_2^2)^2 - 4a_1^2 a_2^2 = (a_1^2 - a_2^2)^2 \Rightarrow \sqrt{A^2 - B^2} = (a_2^2 - a_1^2) > 0 \quad \text{since } a_2 > a_1$$

so

$$\int_0^{2\pi} d\theta_1 \ln(s_{21}^2) = 2\pi \ln[(1/2)(a_1^2 + a_2^2 + (a_2^2 - a_1^2))] = 2\pi \ln(a_2^2) .$$

Similarly

$$\int_0^{2\pi} d\theta_2 \ln(s_{12}^2) = 2\pi \ln[(1/2)(a_1^2 + a_2^2 + (a_2^2 - a_1^2))] = 2\pi \ln(a_2^2) = \text{same as above} .$$

The other two integrals are,

$$\begin{aligned} \int_0^{2\pi} d\theta_1 \ln(s_{11}^2) &= \int_0^{2\pi} d\theta_1 \ln[2a_1^2(1 - \cos(\theta_1))] & A = B = 2a_1^2 \\ &= 2\pi \ln[(1/2)2a_1^2] = 2\pi \ln(a_1^2) \end{aligned}$$

$$\begin{aligned} \int_0^{2\pi} d\theta_2 \ln(s_{22}^2) &= \int_0^{2\pi} d\theta_2 \ln[2a_2^2(1 - \cos(\theta_2))] & A = B = 2a_2^2 \\ &= 2\pi \ln[(1/2)2a_2^2] = 2\pi \ln(a_2^2) . \end{aligned}$$

To summarize:

$$\begin{aligned} \int_0^{2\pi} d\theta_1 \ln(s_{21}^2) &= 2\pi \ln(a_2^2) \\ \int_0^{2\pi} d\theta_1 \ln(s_{11}^2) &= 2\pi \ln(a_1^2) \\ \int_0^{2\pi} d\theta_2 \ln(s_{22}^2) &= 2\pi \ln(a_2^2) \\ \int_0^{2\pi} d\theta_2 \ln(s_{12}^2) &= 2\pi \ln(a_2^2) . \end{aligned} \tag{4.6.2}$$

Then from (4.5.3) one gets,

$$\begin{aligned} K &= 1/(2\pi) \left\{ \int_0^{2\pi} d\theta_1 [\ln(s_{21}^2) - \ln(s_{11}^2)] - \int_0^{2\pi} d\theta_2 [\ln(s_{22}^2) - \ln(s_{12}^2)] \right\} \\ &= \ln(a_2^2) - \ln(a_1^2) - \ln(a_2^2) + \ln(a_2^2) = \ln(a_2^2/a_1^2) = 2 \ln(a_2/a_1) . \end{aligned} \tag{4.6.3}$$

The coaxial transmission line parameters are then given by,

$$\begin{aligned} K &= 2 \ln(a_2/a_1) && // \text{ centered coaxial} \\ C &= 4\pi\epsilon_d/K && = 2\pi\epsilon_d / \ln(a_2/a_1) \\ G &= 4\pi\sigma_d/K && = 2\pi\sigma_d / \ln(a_2/a_1) \\ L_e &= (\mu_d/4\pi)K && = (\mu_d/2\pi) \ln(a_2/a_1) \\ Z_0 &= (K / \sqrt{\epsilon_{re1}}) 30\Omega && = (1/\sqrt{\epsilon_{re1}}) \ln(a_2/a_1) 60\Omega \end{aligned} \tag{4.6.4}$$

We verify the C and L_e parameters from http://en.wikipedia.org/wiki/Coaxial_cable ,

Fundamental electrical parameters [\[edit\]](#)

- Shunt **capacitance** per unit length, in **farads** per metre. ^[6]

$$\left(\frac{C}{h}\right) = \frac{2\pi\epsilon}{\ln(D/d)} = \frac{2\pi\epsilon_0\epsilon_r}{\ln(D/d)}$$

- Series **inductance** per unit length, in **henrys** per metre.

$$\left(\frac{L}{h}\right) = \frac{\mu}{2\pi} \ln(D/d) = \frac{\mu_0\mu_r}{2\pi} \ln(D/d)$$

Fig 4.8

To verify the Z_0 value, first recall that (the positive square root is implied here)

$$\operatorname{ch}^{-1}x = \ln[x + \sqrt{x^2 - 1}] \quad // \text{ Spiegel identity 8.56, valid for } x \geq +1 \quad (4.6.5)$$

Setting $x \equiv \frac{1}{2} \left(\frac{a}{b} + \frac{b}{a} \right) = \frac{1}{2} \frac{a^2 + b^2}{ab}$ and assuming $a > 0$ and $b > 0$,

$$x^2 - 1 = \frac{1}{4} \frac{(a^2 + b^2)^2}{a^2 b^2} - 1 = \frac{1}{4} \left\{ \frac{(a^2 + b^2)^2 - 4a^2 b^2}{a^2 b^2} \right\} = \frac{1}{4} \frac{(a^2 - b^2)^2}{a^2 b^2}$$

$$\Rightarrow \sqrt{x^2 - 1} = \frac{1}{2} \frac{|b^2 - a^2|}{ab} = \operatorname{sign}(b-a) \frac{1}{2} \left(\frac{b}{a} - \frac{a}{b} \right)$$

$$\Rightarrow x + \sqrt{x^2 - 1} = \frac{1}{2} \left(\frac{a}{b} + \frac{b}{a} \right) + \operatorname{sign}(b-a) \frac{1}{2} \left(\frac{b}{a} - \frac{a}{b} \right) = \begin{cases} b/a & b \geq a \\ a/b & a \geq b \end{cases}$$

$$\Rightarrow \ln [x + \sqrt{x^2 - 1}] = \ln \left[\begin{cases} b/a & b \geq a \\ a/b & a \geq b \end{cases} \right] = \operatorname{sign}(b-a) \ln(b/a) \quad .$$

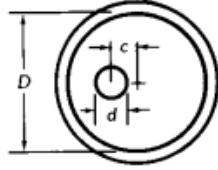
Thus we have shown that (note that both sides are invariant under $a \leftrightarrow b$)

$$\operatorname{ch}^{-1} \left[\frac{1}{2} \left(\frac{a}{b} + \frac{b}{a} \right) \right] = \operatorname{sign}(b-a) \ln \frac{b}{a} \quad . \quad a > 0 \text{ and } b > 0 \quad (4.6.6)$$

With this rather elaborate fact, and since $b > a$, rewrite Z_0 above as

$$Z_0 = (1/\sqrt{\epsilon_{re1}}) \operatorname{ch}^{-1} \left[\frac{1}{2} \left(\frac{a}{b} + \frac{b}{a} \right) \right] 60 \Omega \quad . \quad (4.6.7)$$

Again we quote from reference RDE page 29-24

U. Eccentric line

$$Z_0 = (60/\epsilon^{1/2}) \cosh^{-1} U$$

$$U = \frac{1}{2} [(D/d) + (d/D) - (4c^2/dD)]$$

Fig 4.9

In our centered case $c = 0$ so $U = (1/2)(D/d+d/D)$ and we have agreement. The full off-center result is derived later in Chapter 6, equation (6.3.15).

Comment: In the examples of Sections 4.5 and 4.6, the current distributions in the involved round wires are axially symmetric. Therefore all the results of Chapter 2 apply. In particular, Chapter 2 calculates the surface impedance Z_s for a round wire in complete detail, including its limits for large and small ω . For example, at low frequency for a wire of radius a ,

$$Z_s(\omega) = \frac{1}{\sigma\pi a^2} + j\omega \frac{\mu}{8\pi} = R_s + j\omega L_s \quad // \text{ low frequency limit} \quad (2.4.12)$$

and one sees that R_s is the expected DC resistance (C.1.1) and L_s is the internal impedance L_i as computed in (C.3.5).

Having presented our two Examples, we now resume development of the transmission line equations.

4.7 Computation of A_z due to one conductor of a transmission line

Summary box (1.5.23) states the following Helmholtz integral for the vector potential arising from currents in a set of conductors,

$$\mathbf{A}(\mathbf{x},\omega) = \frac{1}{4\pi} \sum_i \int \mu_i \mathbf{J}_i(\mathbf{x}',\omega) \frac{e^{-j\beta_d R}}{R} dV' \quad (1.5.23)$$

where the sum \sum_i is over the conductors and μ_i is the permeability of conductor i .

In our transmission line context, and as discussed in Chapter 3, the dominant current is in the z (longitudinal) direction, while transverse currents are very small. For example, in the estimate of Section 3.7 (h) we found that $J_x/J_z < 1.4 \times 10^{-4}$ below 10 GHz and $J_x/J_z < 4.6 \times 10^{-8}$ at low frequency. Looking at the above Helmholtz solution to the Helmholtz equation, if we neglect these transverse currents, we are then in effect neglecting the transverse components of \mathbf{A} , and this is what we shall do from now on. This approximation, discussed in Chapter 3 as Fact 1 (3.7.1), is restated below, and details are given in Appendix M.

Fact: The transverse components A_x and A_y can be neglected so that $\mathbf{A} = A_z \hat{\mathbf{z}}$. (Appendix M) (4.7.1)

Our starting point then is the following expression for the potential A_z at some arbitrary point \mathbf{x} in the dielectric due to conductor C_1 of a transmission line,

$$A_{z1}(\mathbf{x},\omega) = \frac{\mu_1}{4\pi} \int_{C_1} J_{z1}(x',y',z',\omega) \frac{e^{-j\beta_d R}}{R} dx'dy'dz' \quad R = |\mathbf{x} - \mathbf{x}'| \quad (4.7.2)$$

Here the integration point $\mathbf{x}' = (x',y',z')$ runs over the *volume* of C_1 and R is the distance between the observation point \mathbf{x} in the dielectric and the point \mathbf{x}' . Parameter β_d is for the dielectric while μ_1 is for the conductor.

In the analogous ϕ solution (4.1.1) everything has the same form as (4.7.2) but in (4.1.1) the charge density exists only on the conductor surface. Nevertheless, we represented that charge density as a volume density, and only later in examples set that volume density to a surface distribution. Thus, the parallel between the ϕ and the A_z analysis is very close, not surprising in light of (1.3.11). Another difference is that for ϕ the leading factor is $1/(4\pi\epsilon_d)$ where ϵ_d was the complex dielectric constant of the dielectric. In (4.7.2) this factor is replaced by $(\mu_1/4\pi)$ where μ_1 is the magnetic permeability of the conductor C_1 .

We next make the same assumption of separation of variables to write

$$J_{z1}(x,y,z) = b_1(x,y) i_1(z) \quad \begin{array}{l} \text{A/m}^2 \quad \quad \quad 1/\text{m}^2 \quad \text{A} \end{array} \quad (4.7.3)$$

where i_1 is scaled such that

$$\int_{C_1} dx dy b_1(x,y) = 1 . \quad (4.7.4)$$

As shown in the Technical Note below (4.1.5), even though $b_1(x,y)$ is in general a complex function with a phase which varies with x,y , we can always find a partition (4.7.3) such that (4.7.4) is true. As that same Technical Note points out, we expect $J_{z1}(x,y,z)$ inside a conductor to have a phase which varies as x and y vary over the conductor cross section, just the way $E(r)$ of Chapter 2 has a variable phase. For this reason, we cannot partition the current so that $b_1(x,y)$ is a purely real function as we could with $\alpha_1(x,y)$.

Function $b_1(x,y)$ describes the distribution of the current density across the conductor C_1 cross section. At DC this density is a uniform constant, but at higher ω the density becomes non-uniform in two ways. First, it becomes concentrated away from the central region due to the skin effect. Second it is non-uniform in that it tends to concentrate on the portion of conductor C_1 which is closest to conductor C_2 . In the corresponding equation $\rho_1(x,y,z) = \alpha_1(x,y) q_1(z)$ of (4.1.2), $\alpha_1(x,y)$ exists only on the conductor surface, and is generally non-uniform in the second sense noted above for $b_1(x,y)$.

As before, we can now interpret $i_1(z)$ as the *total current* in C_1 at z . Again assuming that there is no net superposed radiating antenna current, we have equal and opposite currents in the two conductors so the line is a balanced line, and then

$$i_2(z) = -i_1(z) = -i(z) . \quad (4.7.5)$$

This then leads to

$$A_{z1}(x,y,z) = \frac{\mu_1}{4\pi} \int_{-\infty}^{\infty} dz' i(z') \int_{C_1} dx' dy' b_1(x',y') \frac{e^{-j\beta_d R}}{R} . \quad (4.7.6)$$

Note: In the ω domain, $J_{z1}(x,y,z)$ is complex with a position-dependent phase, as for example in the plot of $E_z = J_z/\sigma$ shown in Fig 2.8. Thus, $b_1(x,y)$ is complex and has a position-dependent phase. This does not stop us from allocating the phase between the two terms in (4.7.3) so that the integral of $b_1(x,y)$ is unity as in (4.7.4). One ends up then with $i_1(z)$ having some phase that in general is non-zero.

Comments regarding μ

This is a subtle subject and is not discussed in King's transmission line theory book. In this section we regard conductor C_1 as having parameters ϵ_1, μ_1 while the dielectric outside the conductor has ϵ_d and μ_d .

Before dealing with A_z and μ , it is useful to start with ϕ and ϵ . Our Helmholtz integral solution for ϕ at a point \mathbf{x} in the dielectric, expressed for a single conductor C_1 , can be written as follows based on (1.5.13),

$$\phi(\mathbf{x},\omega) = \frac{1}{4\pi\epsilon_d} \int_{C_1} n_s(\mathbf{x}',\omega) \frac{e^{-j\beta_d R}}{R} dS' . \quad R = |\mathbf{x} - \mathbf{x}'| \quad (1.5.13)$$

The potential ϕ is continuous at the boundary, but $\partial_n\phi$ is not continuous, having a jump there, though this fact is not obvious since we only have ϕ stated for \mathbf{x} in the dielectric. We do know from (1.1.47) that,

$$[\epsilon_a E_{an} - \epsilon_b E_{bn}] = n_{free} . \quad (1.1.47)$$

Letting a = dielectric and b = conductor, and with $\hat{\mathbf{n}}$ pointing out from the conductor, we translate this equation to read,

$$\epsilon_d E_{n,d} - \epsilon_1 E_{n,c} = n_s \quad (4.7.7)$$

where n_s is the free surface charge appearing in (1.5.13). According to (4.7.1) we can set transverse A_i components to zero, so then (1.3.1) which says $\mathbf{E} = -\text{grad } \phi - j\omega\mathbf{A}$ tells us that $E_n = -\partial_n\phi$. We then have

$$\epsilon_d (-\partial_n\phi(\mathbf{x}+)) - \epsilon_1 (-\partial_n\phi(\mathbf{x}-)) = n_s(\mathbf{x}) \quad (4.7.8)$$

where $\mathbf{x}+$ is just outside the conductor surface and $\mathbf{x}-$ is just inside. From this result one can compute the discontinuity or jump in $\partial_n\phi$ at the conductor boundary. If $\epsilon_d = \epsilon_1 = \epsilon_0$, then $\partial_n\phi(\mathbf{x}+) - \partial_n\phi(\mathbf{x}-) = -n_s/\epsilon_0$, for example.

Normally, however, $E_{n,c} \approx 0$ so (4.7.7) reads $\epsilon_d E_{n,d} = n_s$ and then $E_{n,d} = n_s/\epsilon_d$ is the normal E field in the dielectric just outside the conductor. And since $E_{n,c} \approx 0$, we have $\phi(\mathbf{x},\omega) \approx \text{constant}$ inside the conductor, so we are generally not interested in finding a version of (1.5.13) that is valid inside the conductor. We just evaluate (1.5.13) at the surface for some $\mathbf{x}+$ and that gives ϕ inside the conductor. Thus, the Helmholtz integral (1.5.13) provides our full solution of interest, and we have no homogeneous adder terms to worry about of the type discussed below. Another interpretation is that $n_s(\mathbf{x})$ just assumes whatever value is needed to make (4.7.8) be valid.

With this as warm up, we now consider the case of A_z and μ . Our Helmholtz integral solution for A_z at a point \mathbf{x} in the dielectric, expressed for a single conductor C_1 , can be written as follows based on (4.7.2),

$$A_{z1}(\mathbf{x},\omega) = \frac{\mu_1}{4\pi} \int_{C_1} J_{z1}(x',y',z',\omega) \frac{e^{-j\beta_d R}}{R} dx'dy'dz' . \quad R = |\mathbf{x} - \mathbf{x}'| \quad (4.7.2)$$

where μ_1 is for the conductor C_1 . The potential A_{z1} is continuous at the boundary but $\partial_n A_{z1}$ is not continuous, having a jump.

Appendix D.9 shows that there is a miniscule free surface current K_z^D which flows on the surface of a transmission line conductor, which we call the Debye surface current. It is n_s being moved by E_z at the surface. Although n_s is significant from the point of view of the $E_{n,d}$ field it creates in the dielectric, its effective 3D density is tiny compared to the density of conduction electrons in the conductor. Equation (D.9.3) shows that the Debye current contribution to the above integral is totally negligible relative to bulk current contribution, so the left side of (4.7.2) is unchanged if we completely ignore this Debye current contribution to J_z . Thus, we are in effect setting $K_z^D = 0$ in this well-justified approximation. We may then apply (1.1.46) to find that

$$(1/\mu_d) (\partial_n A_{z1}(x+)) - (1/\mu_1) (\partial_n A_{z1}(x-)) = 0 . \quad (1.1.46)$$

Thus we arrive at these boundary conditions on A_{z1} produced by conductor C_1 :

$$\begin{aligned} A_{z1}(x+) &= A_{z1}(x-) \\ (1/\mu_d) \partial_n A_{z1}(x+) &= (1/\mu_1) \partial_n A_{z1}(x-) \end{aligned} \quad (4.7.9)$$

where again $x+$ is just outside the conductor surface and $x-$ is just inside.

If $\mu_1 = \mu_d$, there is no "magnetic boundary" at the surface, and (4.7.9) says $\partial_n A_{z1}(x+) = \partial_n A_{z1}(x-)$, so both the function A_{z1} and its normal derivative are continuous through the boundary -- nothing special is happening there. Thus, the Helmholtz integral solution (4.7.2) provides the whole solution for A_{z1} in both the dielectric and conductor since it meets both "boundary conditions" at this pseudo boundary.

If on the other hand we have $\mu_1 \neq \mu_d$, then there *is* a magnetic boundary between conductor and dielectric which we have to worry about. In this case, (4.7.2) applied in both dielectric and conductor cannot possibly satisfy the second boundary condition of (4.7.9) since, as already noted, the A_{z1} of (4.7.2) satisfies $\partial_n A_{z1}(x+) = \partial_n A_{z1}(x-)$. Thus, in this case (4.7.2) is not the full solution for A_{z1} . One must add a homogeneous Helmholtz equation solution to (4.7.2) in order to have a proper solution for A_{z1} that satisfies both equations in (4.7.9).

It *turns out* that the correct total A_{z1} solution can be generated by adding a certain fictitious surface current term to $\mu_1 J_{z1}$ in (4.7.2). Since such a surface current vanishes on both sides of the boundary between μ_d and μ_1 , the Helmholtz solution due just to this surface current term is in fact a homogeneous solution to the Helmholtz equation in both the conductor and dielectric regions, away from that boundary. It turns out moreover that the correct fictitious surface current to add is in fact the magnetization surface current J_m which is created at the boundary between $\mu_d \neq \mu_1$. Adding this surface current is just a "trick" in order to generate the correct homogeneous adder solution so that the resulting total A_{z1} satisfies both boundary conditions in (4.7.9). Formally speaking, the J_i appearing in (1.5.4) and then J_{z1} in (4.7.2) should *not* include such magnetization currents since this J is really the J in Maxwell's equation $\text{curl } \mathbf{H} = \partial_t \mathbf{D} + \mathbf{J}$, and this J does not include magnetization currents -- it includes only normal conduction currents.

In our current Chapter 4, we *want* (4.7.2) to represent the complete solution for A_{z1} and for that reason we must restrict our analysis to the situation where dielectric and all conductors have the same permeability which we shall just call μ_d . In practice, one normally has $\mu_d = \mu_1 = \mu_0$. In order to handle the more general case of $\mu_d \neq \mu_1$, we have to deal with the inhomogeneous adder solutions or equivalently with the abovementioned fictitious surface current, and this complicates our analysis which is already quite complicated. So, for the moment, we now make the same assumption made by King and other authors:

Fact: From now on, conductors and dielectric must have the same permeability μ_d . (4.7.10)

After fully developing this special case, we extend the theory in Section 4.13 to allow for $\mu_d \neq \mu_1$.

There are several Appendices which relate to this subject :

Appendix G shows for the round wire how the inhomogeneous adder solution is found and how it then causes the boundary conditions (4.7.9) to be met when $\mu_1 \neq \mu_d$. However, in Appendix G the notation is different: 1 = dielectric and 2 = conductor, so that $\mu_1 \neq \mu_d \rightarrow \mu_2 \neq \mu_1$.

Appendix B shows how the addition of a fictitious surface current term $\mu_0 J_m$ provides an alternate and simpler solution to the same problem of meeting boundary conditions (4.7.9) when $\mu_1 \neq \mu_d$. It then shows exactly how this works in the special case of a round wire (same notation as Appendix G).

4.8 Computation of potential A_z due to both conductors of a transmission line

We now write the potential at an arbitrary point \mathbf{x} in the dielectric due to *both* conductors C_1 and C_2 . We accept the requirement of (4.7.10) and require that all conductors have the same μ as the dielectric, so then $\mu_1 = \mu_2 = \mu_d$. Then,

$$A_{z12}(\mathbf{x}) = A_{z1}(\mathbf{x}) + A_{z2}(\mathbf{x}) =$$

$$\frac{\mu_d}{4\pi} \int_{-\infty}^{\infty} dz' i(z') \left\{ \int_{C_1} dx_1' dy_1' b_1(x_1', y_1') \frac{e^{-j\beta_d R_1}}{R_1} - \int_{C_2} dx_2' dy_2' b_2(x_2', y_2') \frac{e^{-j\beta_d R_2}}{R_2} \right\}$$

$$R_1^2 = (x-x_1')^2 + (y-y_1')^2 + (z-z')^2 = s_1^2 + (z-z')^2 \quad s_1^2 = (x-x_1')^2 + (y-y_1')^2 \quad (4.8.1)$$

$$R_2^2 = (x-x_2')^2 + (y-y_2')^2 + (z-z')^2 = s_2^2 + (z-z')^2 \quad s_2^2 = (x-x_2')^2 + (y-y_2')^2 .$$

The picture going with the above equation is identical to Fig 4.1 [below (4.2.1)] except the points \mathbf{x}_1' and \mathbf{x}_2' can be in the interior of the conductors, not just on the boundary of the conductors.

4.9 Transmission Line Limit Revisited

Section 4.3 discussed the so-called transmission line limit of small β_d in the context of the scalar potential ϕ . The flow of that section applies to A_z with the following substitutions:

$$q(z) \rightarrow i(z) \quad \alpha_i \rightarrow b_i \quad \phi_{12} \rightarrow A_{z12} \quad \frac{1}{4\pi\xi} \rightarrow \frac{\mu}{4\pi} .$$

The conclusion is that in the transmission line limit (small β_d , long wavelength $\lambda = 2\pi/\beta_d$) one may write

$$A_{z12}(\mathbf{x}) = \frac{\mu_d}{4\pi} i(z) \int_{-\infty}^{\infty} dz' \left\{ \int_{C_1} dx_1' dy_1' b_1(x_1', y_1') \frac{1}{R_1} - \int_{C_2} dx_2' dy_2' b_2(x_2', y_2') \frac{1}{R_2} \right\} \quad (4.9.1)$$

which is analogous to (4.3.10). Also, in analogy with (4.3.8) we write for a lossless line,

$$i(z) = i(0) e^{-j\beta_d z} \quad // \quad i(z,t) = i(0,0) e^{j(\omega t - \beta_d z)} \quad (4.9.2)$$

and for a lossy line

$$i(z) = i(0) e^{-jkz} \quad // \quad i(z,t) = i(0,0) e^{j(\omega t - kz)} \quad (4.9.3)$$

as explained in the discussion leading up to (4.3.11).

4.10 General Calculation of $W(z)$

As before, we now introduce the two new points \mathbf{x}_1 and \mathbf{x}_2 . The point \mathbf{x}_1 lies on C_1 in the $z = z$ plane, while \mathbf{x}_2 lies on C_2 in this same plane. We then evaluate $A_{z12}(\mathbf{x})$ at $\mathbf{x} = \mathbf{x}_1$ and subtract from that $A_{z12}(\mathbf{x})$ at $\mathbf{x} = \mathbf{x}_2$ and in this way we obtain the A_z potential difference between the surfaces of the two conductors at $z = z$ which we shall call $W(z)$. Recall,

Fact 5: On each conductor boundary, $A_z \approx$ constant in the extreme or strong skin effect regimes. (3.7.20)

Thus, assuming the small δ regime and treating $A_z \approx$ constant as an equality, the A_z potential difference will be independent of the locations of \mathbf{x}_2 and \mathbf{x}_1 as long as they are on their respective surfaces and both have $z = z$. For this reason, the A_z potential difference is a function only of z . Thus we write, using two copies of (4.9.1),

$$\begin{aligned} W(z) &\equiv A_{z12}(\mathbf{x}_1) - A_{z12}(\mathbf{x}_2) \\ &= \frac{\mu_d}{4\pi} i(z) \int_{-\infty}^{\infty} dz' \left\{ \int_{C_1} dx_1' dy_1' b_1(x_1', y_1') \frac{1}{R_{11}} - \int_{C_2} dx_2' dy_2' b_2(x_2', y_2') \frac{1}{R_{12}} \right\} \\ &\quad - \frac{\mu_d}{4\pi} i(z) \int_{-\infty}^{\infty} dz' \left\{ \int_{C_1} dx_1' dy_1' b_1(x_1', y_1') \frac{1}{R_{21}} - \int_{C_2} dx_2' dy_2' b_2(x_2', y_2') \frac{1}{R_{22}} \right\} \quad (4.10.1) \end{aligned}$$

where

$$\begin{aligned} R_{11}^2 &= (x_1 - x_1')^2 + (y_1 - y_1')^2 + (z - z')^2 = s_{11}^2 + (z - z')^2 & s_{11}^2 &= (x_1 - x_1')^2 + (y_1 - y_1')^2 \\ R_{12}^2 &= (x_1 - x_2')^2 + (y_1 - y_2')^2 + (z - z')^2 = s_{12}^2 + (z - z')^2 & s_{12}^2 &= (x_1 - x_2')^2 + (y_1 - y_2')^2 \\ R_{22}^2 &= (x_2 - x_2')^2 + (y_2 - y_2')^2 + (z - z')^2 = s_{22}^2 + (z - z')^2 & s_{22}^2 &= (x_2 - x_2')^2 + (y_2 - y_2')^2 \\ R_{21}^2 &= (x_2 - x_1')^2 + (y_2 - y_1')^2 + (z - z')^2 = s_{21}^2 + (z - z')^2 & s_{21}^2 &= (x_2 - x_1')^2 + (y_2 - y_1')^2 \end{aligned} \quad (4.10.2)$$

The picture going with the above equation is identical to Fig 4.2 [below (4.4.2)] except, once again, the points \mathbf{x}_1' and \mathbf{x}_2' can be in the interior of the conductors, not just on the surface of the conductors. Also, we replace the figure's double arrow label $V(z)$ with $W(z)$. We then reorder the four terms to get

$$\begin{aligned} W(z) & \quad (4.10.3) \\ &= \frac{\mu_d}{4\pi} i(z) \int_{-\infty}^{\infty} dz' \left\{ \int_{C_1} dx_1' dy_1' b_1(x_1', y_1') \left(\frac{1}{R_{11}} - \frac{1}{R_{21}} \right) - \int_{C_2} dx_2' dy_2' b_2(x_2', y_2') \left(\frac{1}{R_{12}} - \frac{1}{R_{22}} \right) \right\} \end{aligned}$$

The dz' integrals are the same as those done in Section 4.4 and we then arrive at

$$W(z) = i(z) \frac{\mu_0}{4\pi} \left\{ \int_{C_1} dx_1' dy_1' b_1(x_1', y_1') \ln(s_{21}^2/s_{11}^2) - \int_{C_2} dx_2' dy_2' b_2(x_2', y_2') \ln(s_{22}^2/s_{12}^2) \right\}$$

$$\begin{aligned} s_{21}^2 &= (x_2 - x_1')^2 + (y_2 - y_1')^2 & s_{22}^2 &= (x_2 - x_2')^2 + (y_2 - y_2')^2 \\ s_{11}^2 &= (x_1 - x_1')^2 + (y_1 - y_1')^2 & s_{12}^2 &= (x_1 - x_2')^2 + (y_1 - y_2')^2 \end{aligned} \quad (4.10.4)$$

which is analogous to (4.4.6) for $V(z)$. The corresponding drawing is analogous to Fig 4.3 where, once again, the integration points x_1' and x_2' are inside the conductor :

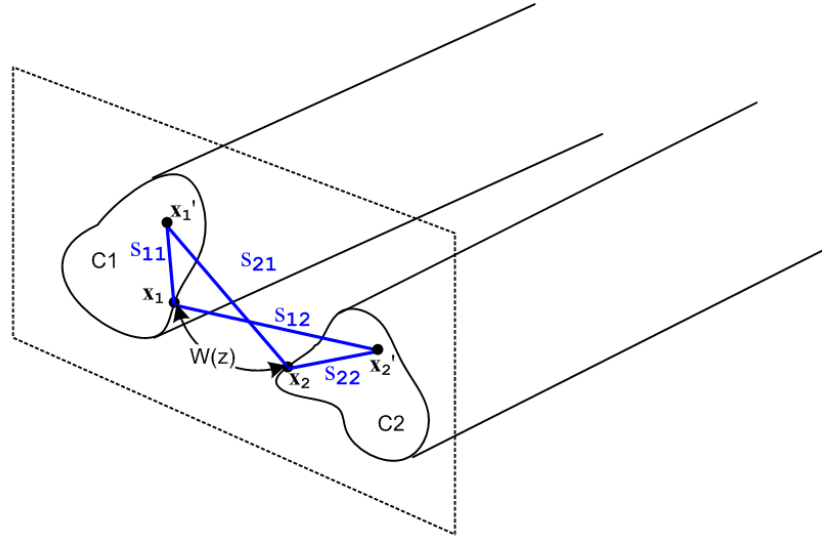


Fig 4.10

Equation (4.10.4) expresses the A_z potential between the two transmission line conductors at some plane z in terms of the current distributions b_1 within the conductors.

Now, the Stokes theorem applied to $\mathbf{B} = \text{curl } \mathbf{A}$ says

$$\text{curl } \mathbf{A} = \mathbf{B} \quad \Leftrightarrow \quad \oint \mathbf{A} \cdot d\mathbf{s} = \int_{\mathbf{s}} \mathbf{B} \cdot d\mathbf{S} \quad (1.1.39)$$

Consider the red loop shown in this top view of the two transmission line conductors. The loop is intended to have a tiny width dz , and the top view obscures the fact that each conductor has an arbitrary cross section. The loop makes contact with the points x_1 and x_2 shown in the previous figure,

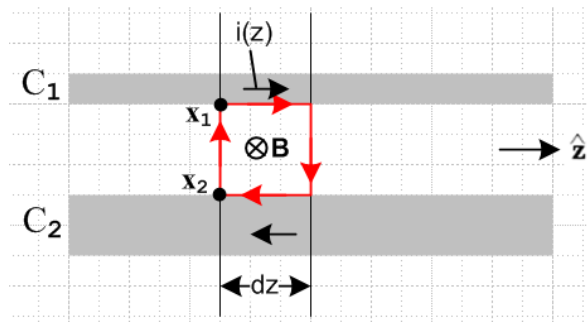


Fig 4.11

Since we neglect any transverse components of \mathbf{A} , the Stokes theorem says

$$[A_{z1}(\text{top}) - A_{z2}(\text{bottom})] dz = [\text{magnetic flux through red loop}] = \int_{\mathbf{s}} \mathbf{B} \cdot d\mathbf{S} . \quad (4.10.5)$$

If we regard the two short dz length conductor pieces as forming a tiny "inductor", closed on the ends by the vertical red lines, we can use this definition of inductance to compute the inductance of that inductor:

$$[\text{magnetic flux through red loop}] = (L_e dz) i(z) . \quad (4.10.6)$$

Here $(L_e dz)$ is the inductance of our tiny loop, so L_e is the transmission line inductance per unit length. We know (as in Appendix C) that there will be magnetic flux inside the conductors as well as between them, and for that reason L_e as defined here only accounts for the "external" inductance of the transmission line, again see Appendix C.

Since $[A_{z1}(\text{top}) - A_{z2}(\text{bottom})] = W(z)$ according to (4.10.1), we may combine (4.10.5) and (4.10.6) to obtain

$$W(z) = L_e i(z) . \quad (4.10.7)$$

Therefore from (4.10.4) we have found that

$$L_e = \frac{W(z)}{i(z)} = \frac{\mu_d}{4\pi} K_L \quad (4.10.8)$$

where K_L is the following dimensionless number,

$$K_L \equiv \int_{C_1} dx_1' dy_1' b_1(x_1', y_1') \ln(s_{21}^2/s_{11}^2) - \int_{C_2} dx_2' dy_2' b_2(x_2', y_2') \ln(s_{22}^2/s_{12}^2) . \quad (4.10.9)$$

This number is reminiscent of the dimensionless real number K obtained in Section 4.4,

$$K \equiv \int_{C_1} dx_1' dy_1' \alpha_1(x_1', y_1') \ln(s_{21}^2/s_{11}^2) - \int_{C_2} dx_2' dy_2' \alpha_2(x_2', y_2') \ln(s_{22}^2/s_{12}^2) . \quad (4.4.8)$$

As noted in the comments after (4.7.4), the transverse current density $b_1(x, y)$ is in general complex and not real, just based on the fact that we know that the skin effect warps current phase as a function of r from Chapter 2. For this reason, it would appear that the integral K_L might be complex as well. In an integral of a complex function, it is possible for the imaginary part to cancel out. That seems to be the case with K_L , since we will later show in (4.12.20) that $K_L = K$ and K is real. Thus, L_e is also real.

4.11 Relations involving C and G and the charges and currents in a transmission line

Before continuing our development of the transmission line equations, we need to establish the connections between parameters C and G and the charges and currents in a transmission line. Then we resume the development in Section 4.12.

Consider this picture showing a section of a transmission line of length dz :

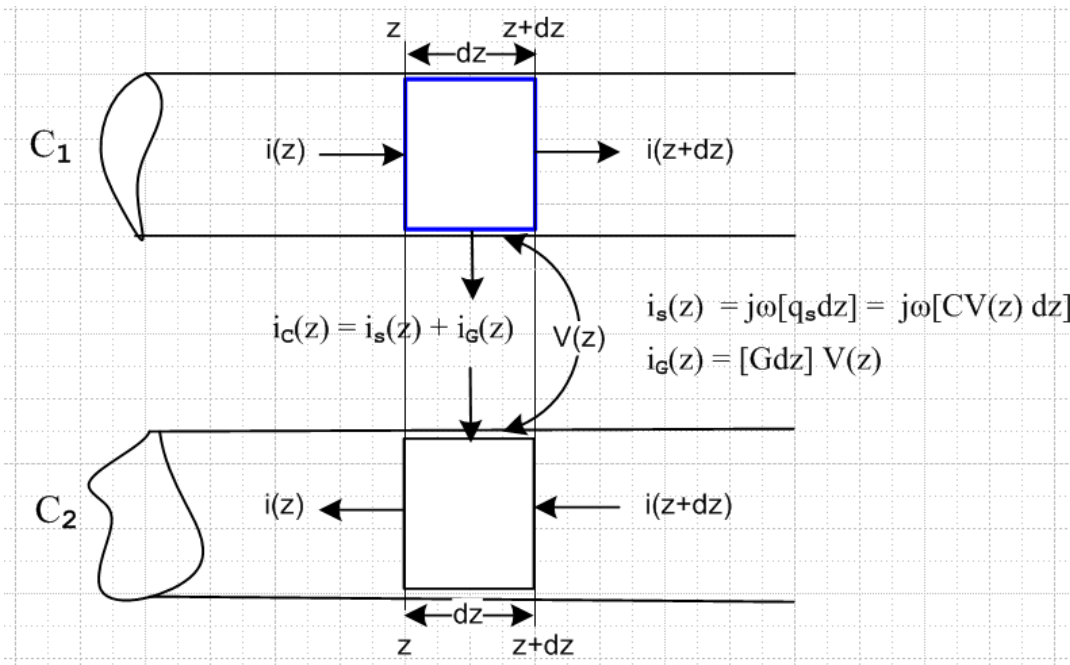


Fig 4.12

We focus on the upper conductor C_1 . Over the distance dz , the current $i(z)$ in this conductor is reduced by amount $-di(z) = i(z) - i(z+dz) > 0$ by the fact that current flows transversely to feed the surface charge q_s and to feed the conductance G between the conductors.

Since the blue Gaussian box embedded just inside the upper conductor contains no free charge, we know from (1.1.35) that $\text{div } \mathbf{J} = 0$ and $\int_S \mathbf{J} \cdot d\mathbf{S} = 0$. The latter means that the sum of all currents crossing the box boundary is 0. Thus,

$$-di(z) = i_g(z) + i_s(z) \quad \text{" current loss feeds capacitance and conductance" } \quad (4.11.1)$$

The two currents may be written

$$i_g(z) = [Gdz] V(z) \quad // \ i_g \text{ flows through the dielectric} \quad (4.11.2)$$

$$i_s(z) = j\omega[q_s(z)dz] \quad // \ i_s \text{ feeds the true surface charge per length } q_s \quad (4.11.3)$$

The section of dielectric has some transverse resistance $R_t = 1/[Gdz]$ and then $i_g(z) = V(z)/R_t$. Quantity G is the conductance of the dielectric per unit length of the transmission line. The true total surface charge

per length is q_s and i_s feeds this charge according to $i_s(z) = j\omega[q_s(z)dz]$ ($i_s = \partial_t[q_s dz]$ in the time domain). But we know for the dz -length capacitor that $q_s(z) = CV(z)$ where C is the capacitance per length. Then (4.11.1) can be written

$$-di(z) = i_G(z) + i_s(z) = [Gdz] V(z) + j\omega[CV(z)dz] = [G + j\omega C] V(z)dz \quad . \quad (4.11.4)$$

Dividing by dz and taking $dz \rightarrow 0$ then gives,

$$\partial_z i(z) = - [G + j\omega C] V(z) \quad . \quad (4.11.5)$$

This is in fact one of the two "transmission line equations" we shall be deriving below.

Quantity $q_s(z)$ is the true surface charge (per length) at location z . Corresponding to this charge is the so-called transport charge (per unit length) $q_c(z)$, where

$$q_c(z) = (\xi_d/\epsilon_d)q_s(z) \quad (4.11.6)$$

as shown in (1.5.17). Here q_s and q_c are the integrals of the corresponding surface charge densities n_s and q_s over the surface of the C_1 conductor section shown in Fig 4.12. The transport charge density q_c is larger than q_s because it accounts for both the surface charge and the charge lost due to leakage into the dielectric, as described in Section 1.5. The two charges are related to the real and complex capacitances in this manner

$$q_s(z) = C V(z) \quad C = \text{real capacitance (per length)} \quad (4.11.7)$$

$$q_c(z) = C' V(z) \quad C' = \text{complex capacitance including effect of } G \text{ (per length)} \quad (4.11.8)$$

where the second line really defines the complex capacitance C' . Therefore using (4.11.6) and (1.5.1c) for ξ_d ,

$$C'/C = q_c(z)/q_s(z) = (\xi_d/\epsilon_d) = [\epsilon_d - j\sigma_d/\omega]/\epsilon_d = 1 + (1/j\omega)(\sigma_d/\epsilon_d) \quad (4.11.9a)$$

or

$$C' = C + (C/j\omega)(\sigma_d/\epsilon_d) \quad (4.11.9b)$$

or

$$j\omega C' = C(\sigma_d/\epsilon_d) + j\omega C \quad . \quad (4.11.9c)$$

The current feeding the transport charge in the transmission line section of length dz is given by

$$i_c(z) = i_s(z) + i_G(z) \quad (4.11.10)$$

where

$$i_c(z) = j\omega [q_c(z)dz] \quad // \quad i_c = \partial_t[q_c dz] \text{ in the time domain} \quad (4.11.11)$$

Using (4.11.8) this says

$$i_c(z) = j\omega [C'V(z)dz] . \quad (4.11.12)$$

Then (4.11.10) and (4.11.4) imply

$$j\omega [C'V(z)dz] = [G + j\omega C] V(z)dz \quad (4.11.13)$$

so that

$$j\omega C' = G + j\omega C . \quad (4.11.14)$$

Comparing this with (4.11.9c) shows that

$$G = C(\sigma_d/\epsilon_d) \quad (4.11.15)$$

which is an interesting relationship between G and C for a transmission line with arbitrary conductor shapes. We saw this relationship just below (1.5.20) for the special case of a parallel plate capacitor.

Finally, were we to assume that transmission line quantities all have the simple z dependence e^{-jkz} (implying a traveling wave $e^{j(\omega t - kz)}$), then starting with (4.11.5),

$$\partial_z i(z) = - [G + j\omega C] V(z) \quad (4.11.5)$$

$$-jk i(z) = -j\omega C' V(z) \quad // e^{-jkz} \text{ dependence and (4.11.14)}$$

or

$$i(z) = (\omega/k) C' V(z)$$

or

$$i(z) = q_c(z) (\omega/k) \quad // \text{ using (4.11.8)}$$

or

$$i(z) = q_c(z) v . \quad // v \equiv (\omega/k) , e^{-jkz} \text{ assumed} \quad (4.11.16)$$

In the last line we use the fact that $v \equiv (\omega/k)$ is the complex phase velocity of the wave $e^{j(\omega t - kz)}$. This last equation can be interpreted as saying that the total current $i(z)$ *acts as if* the transport charge $q_c(z)$ were traveling at speed v down the transmission line. If $G = 0$, then $\xi_d = \epsilon_d$ and $q_c = q_s$. Furthermore, if ω is large, then $k = \beta_{d0} = \omega\sqrt{\mu_d\epsilon_d} = \omega/v_d$ [see (1.5.1b)] where v_d is the speed of light in the dielectric. In this case one finds that

$$i(z) = q_s(z) v_d . \quad G = 0 \text{ and large } \omega \quad (4.11.17)$$

Again, one has the illusion that the current $i(z)$ consists of the surface charge $q_s(z)$ moving at v_d . Since v_d is some large fraction of the the speed of light, we know that the surface charge electrons are not really flowing down the line at such a speed (they flow a few mm per second). This interesting issue is addressed in Appendix D.9 (c).

4.12 The Classical Transmission Line Equations

The results of the Sections 4.1 through 4.10 of this chapter may be succinctly summarized as:

$$\frac{1}{C'} = \frac{V(z)}{q(z)} = \frac{1}{4\pi\epsilon_d} K \quad (4.4.7) \quad (4.12.1)$$

$$L_e = \frac{W(z)}{i(z)} = \frac{\mu_d}{4\pi} K_L \quad (4.10.8)$$

$$K \equiv \int_{C_1} dx_1' dy_1' \alpha_1(x_1', y_1') \ln(s_{21}^2/s_{11}^2) - \int_{C_2} dx_2' dy_2' \alpha_2(x_2', y_2') \ln(s_{22}^2/s_{12}^2) \quad (4.4.8)$$

$$K_L \equiv \int_{C_1} dx_1' dy_1' b_1(x_1', y_1') \ln(s_{21}^2/s_{11}^2) - \int_{C_2} dx_2' dy_2' b_2(x_2', y_2') \ln(s_{22}^2/s_{12}^2) \quad (4.10.9)$$

Notice that we have made no assumptions whatsoever about the cross-sectional shape of the transmission line. We have only assumed that the transverse dimensions are small compared to the wavelength λ that corresponds to β_d -- this was the transmission line limit.

(a) Initial Processing

There are several equations from Chapter 1 we shall now press into service:

$$\mathbf{E} = - \text{grad } \varphi - \partial_t \mathbf{A} \quad (1.3.1)$$

$$\text{div } \mathbf{A} = - \mu_d \epsilon_d \partial_t \varphi - \mu_d \sigma_d \varphi \quad // \text{ the King gauge} \quad (1.3.18)$$

In the frequency domain these become,

$$\mathbf{E} = - \text{grad } \varphi - j\omega \mathbf{A}$$

$$\text{div } \mathbf{A} = - j (\beta_d^2/\omega) \varphi \quad // \text{ the King gauge, see (1.5.5)} \quad (4.12.2)$$

According to Fact (4.7.1), potential \mathbf{A} has only component A_z , so these equations become

$$E_z(\mathbf{x}) = - \partial_z \varphi(\mathbf{x}) - j\omega A_z(\mathbf{x})$$

$$\partial_z A_z(\mathbf{x}) = - j (\beta_d^2/\omega) \varphi(\mathbf{x}) \quad (4.12.3)$$

However, as was shown at the end of Step 1 below (3.7.8), the second line of (4.12.3) can only be justified in the strong or extreme skin effect regimes, and we continue then to assume our transmission line is operating at sufficiently high ω to be in the small δ regime.

The potentials in the above equations are those due to both conductors and were denoted as φ_{12} and A_{z12} in the previous sections. We then rewrite the above as

$$E_z(\mathbf{x}) = -\partial_z \varphi_{12}(\mathbf{x}) - j\omega A_{z12}(\mathbf{x}) \quad (4.12.4a)$$

$$\partial_z A_{z12}(\mathbf{x}) = -j(\beta_d^2/\omega)\varphi_{12}(\mathbf{x}) \quad (4.12.4b)$$

Recall now the conductor-surface-located points \mathbf{x}_1 and \mathbf{x}_2 as shown for example in Fig 4.10. If we evaluate each of the above equations at $\mathbf{x} = \mathbf{x}_1$ and then $\mathbf{x} = \mathbf{x}_2$ and then subtract, we get

$$E_z(\mathbf{x}_1) - E_z(\mathbf{x}_2) = -\partial_z[\varphi_{12}(\mathbf{x}_1) - \varphi_{12}(\mathbf{x}_2)] - j\omega[A_{z12}(\mathbf{x}_1) - A_{z12}(\mathbf{x}_2)] \quad (4.12.5a)$$

$$\partial_z[A_{z12}(\mathbf{x}_1) - A_{z12}(\mathbf{x}_2)] = -j(\beta_d^2/\omega)[\varphi_{12}(\mathbf{x}_1) - \varphi_{12}(\mathbf{x}_2)] \quad (4.12.5b)$$

Then using these definitions (again, we are assuming the strong or extreme skin depth regime),

$$V(z) \equiv \varphi_{12}(\mathbf{x}_1) - \varphi_{12}(\mathbf{x}_2) \quad (4.4.1)$$

$$W(z) \equiv A_{z12}(\mathbf{x}_1) - A_{z12}(\mathbf{x}_2) \quad (4.10.1)$$

we may rewrite (4.12.5) in this simple manner,

$$E_z(\mathbf{x}_1) - E_z(\mathbf{x}_2) = -\partial_z V - j\omega W \quad (4.12.6a)$$

$$\partial_z W = -j(\beta_d^2/\omega) V \quad (4.12.6b)$$

The quantity $E_z(\mathbf{x}_1)$ is the longitudinal electric field at point \mathbf{x}_1 on the surface of conductor C_1 . It is related to the conductor's at-the-surface current density by $J_z(\mathbf{x}_1) = \sigma E_z(\mathbf{x}_1)$. If the conductor were "perfect", we would have $\sigma = \infty$ and $E_z(\mathbf{x}_1) = 0$, but real conductors are not perfect. However, since we are assuming the strong or extreme skin effect all along here in our analysis, we do know that $E_z(\mathbf{x}_1)$ and $E_z(\mathbf{x}_2)$ are very small.

(b) Averaging Repair and the Transmission Line Equations

Our theory now has an inconsistency which needs to be fixed.

We know that for a general transmission line operating at $\omega > 0$, the current density J_z inside the conductors will not be uniformly distributed. It will be larger in the conductor region closest to the other conductor. This "proximity effect" is discussed in Appendix P from an eddy current point of view, see Fig P.13 for an example. The J_z current non-uniformity can be very dramatic as for example in a transmission line having this cross section, where J_z will be large near the gap and small far from the gap:



Fig 4.13

Since J_z is non-uniform in each conductor, so is E_z , and so we expect $E_z(\mathbf{x}_1)$ to be a strong function of the point \mathbf{x}_1 on the perimeter of C_1 , certainly for the above cross section example. This means that the left side of (4.12.6a) is a function of $\mathbf{x}_1 = (x_1, y_1, z)$ and $\mathbf{x}_2 = (x_2, y_2, z)$ whereas the right side in our theory is a function only of z . To remedy this inconsistency, we now have to think of V and W as having very slight dependence on \mathbf{x}_1 and \mathbf{x}_2 which we generally ignore, but which we must face up to in (4.12.6a). In reality we have $V(\mathbf{x}_1, \mathbf{x}_2)$ and $W(\mathbf{x}_1, \mathbf{x}_2)$. This is a manifestation of the fact that in reality $\varphi \approx \text{constant}$ and $A_z \approx$

constant on the boundaries (with \approx and not $=$). In the extreme skin effect regime (think a very good conductor), the left side of (4.12.6a) can be a violent function of \mathbf{x}_1 and \mathbf{x}_2 as in the case of the above figure, but the left side is always very small, even where it is largest, and its variation can be accommodated by the right side of (4.12.6a) which is the difference of large-valued functions which vary only slightly with \mathbf{x}_1 and \mathbf{x}_2 . So first rewrite (4.12.6a) as

$$E_{\mathbf{z}}(\mathbf{x}_1) - E_{\mathbf{z}}(\mathbf{x}_2) = -\partial_{\mathbf{z}} V(\mathbf{x}_1, \mathbf{x}_2) - j\omega W(\mathbf{x}_1, \mathbf{x}_2) . \quad (4.12.6a)'$$

Backing up another step, we write out of (4.12.4a) for the two perimeter points \mathbf{x}_1 and \mathbf{x}_2 ,

$$\begin{aligned} (1/\sigma)J_{\mathbf{z}}(\mathbf{x}_1) = E_{\mathbf{z}}(\mathbf{x}_1) &= -\partial_{\mathbf{z}}\phi_{12}(\mathbf{x}_1) - j\omega A_{\mathbf{z}12}(\mathbf{x}_1) && \mathbf{x}_1 \text{ on perimeter of } C_1 \\ (1/\sigma)J_{\mathbf{z}}(\mathbf{x}_2) = E_{\mathbf{z}}(\mathbf{x}_2) &= -\partial_{\mathbf{z}}\phi_{12}(\mathbf{x}_2) - j\omega A_{\mathbf{z}12}(\mathbf{x}_2) . && \mathbf{x}_2 \text{ on perimeter of } C_2 \end{aligned} \quad (4.12.4a)'$$

Calling the perimeter distances of the conductors P_1 and P_2 , we then average each of these equations around its appropriate perimeter. Apply $(1/P_1) \int_{C_1} ds_1$ to the first equation and $(1/P_2) \int_{C_2} ds_2$ to the second to get [ds_1 is a distance element along the perimeter of C_1],

$$\begin{aligned} (1/\sigma)\langle J_{\mathbf{z}}(\mathbf{x}_1) \rangle_{C_1} = \langle E_{\mathbf{z}}(\mathbf{x}_1) \rangle_{C_1} &= -\partial_{\mathbf{z}}\langle \phi_{12}(\mathbf{x}_1) \rangle_{C_1} - j\omega\langle A_{\mathbf{z}12}(\mathbf{x}_1) \rangle_{C_1} \\ (1/\sigma)\langle J_{\mathbf{z}}(\mathbf{x}_2) \rangle_{C_2} = \langle E_{\mathbf{z}}(\mathbf{x}_2) \rangle_{C_2} &= -\partial_{\mathbf{z}}\langle \phi_{12}(\mathbf{x}_2) \rangle_{C_2} - j\omega\langle A_{\mathbf{z}12}(\mathbf{x}_2) \rangle_{C_2} . \end{aligned}$$

Subtract the second line from the first to get,

$$\begin{aligned} [\langle E_{\mathbf{z}}(\mathbf{x}_1) \rangle_{C_1} - \langle E_{\mathbf{z}}(\mathbf{x}_2) \rangle_{C_2}] \\ = -\partial_{\mathbf{z}}[\langle \phi_{12}(\mathbf{x}_1) \rangle_{C_1} - \langle \phi_{12}(\mathbf{x}_2) \rangle_{C_2}] - j\omega [\langle A_{\mathbf{z}12}(\mathbf{x}_1) \rangle_{C_1} - \langle A_{\mathbf{z}12}(\mathbf{x}_2) \rangle_{C_2}] . \end{aligned}$$

We now *redefine* V and W to be the averages appearing in these equations, along with $E_{\mathbf{z}1}$ and $E_{\mathbf{z}2}$:

$$\begin{aligned} E_{\mathbf{z}1}(z) \equiv \langle E_{\mathbf{z}}(\mathbf{x}_1) \rangle_{C_1} &= (1/P_1) \int_{C_1} ds_1 E_{\mathbf{z}}(\mathbf{x}_1) \\ E_{\mathbf{z}2}(z) \equiv \langle E_{\mathbf{z}}(\mathbf{x}_2) \rangle_{C_2} &= (1/P_2) \int_{C_2} ds_2 E_{\mathbf{z}}(\mathbf{x}_2) \\ V(z) \equiv \langle \phi_{12}(\mathbf{x}_1) \rangle_{C_1} - \langle \phi_{12}(\mathbf{x}_2) \rangle_{C_2} &= \langle V(\mathbf{x}_1, \mathbf{x}_2) \rangle_{C_1, C_2} \\ W(z) \equiv \langle A_{\mathbf{z}12}(\mathbf{x}_1) \rangle_{C_1} - \langle A_{\mathbf{z}12}(\mathbf{x}_2) \rangle_{C_2} &= \langle W(\mathbf{x}_1, \mathbf{x}_2) \rangle_{C_1, C_2} \end{aligned} \quad (4.12.7)$$

with this result

$$[E_{\mathbf{z}1}(z) - E_{\mathbf{z}2}(z)] = -\partial_{\mathbf{z}} V(z) - j\omega W(z) . \quad (4.12.8)$$

Meanwhile, the surface impedances on C_1 and C_2 are defined by (see C.2.1) ,

$$\begin{aligned} E_{\mathbf{z}1}(\mathbf{x}_1) &= Z_{s1}(\mathbf{x}_1) i_1(z) \\ E_{\mathbf{z}2}(\mathbf{x}_2) &= Z_{s2}(\mathbf{x}_2) i_2(z) \end{aligned} \quad (C.2.1)$$

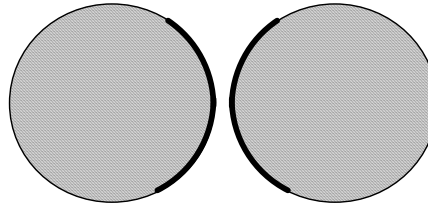
which we average in the same way to obtain

$$\begin{aligned} E_{z1}(z) &= Z_{s1} i_1(z) & Z_{s1} &\equiv (1/P_1) \int_{C_1} ds_1 Z_{s1}(x_1) \\ E_{z2}(z) &= Z_{s2} i_2(z) & Z_{s2} &\equiv (1/P_2) \int_{C_2} ds_2 Z_{s2}(x_2) \end{aligned} \quad (4.12.9)$$

There will be some location on C_1 where $E_{z1}(x_1)$ and thus $Z_{s1}(x_1)$ will be maximal (for example on the walls of the gap in Fig 4.13). Referring to this value as $Z_{s1,max}$ we can define

$$\begin{aligned} p_1 &\equiv (Z_{s1}/Z_{s1,max}) P_1 \\ p_2 &\equiv (Z_{s2}/Z_{s2,max}) P_2 \end{aligned} \quad (4.12.10)$$

where p_1 is the effective length of the "active perimeter" of C_1 . This then provides a crude model for the symbol p which appears in (2.5.1) and Fig 2.16 which we replicate here,



Fat twinlead

Fig 2.16

Now using $i(z) = i_1(z) = -i_2(z)$ and (4.12.9), rewrite (4.12.8) and (4.12.6b) as

$$\begin{aligned} [Z_{s1} + Z_{s2}] i(z) &= -\partial_z V(z) - j\omega W(z) \\ \partial_z W(z) &= -j(\beta_d^2/\omega) V(z) \end{aligned} \quad (4.12.11)$$

where the second equation above is the $\langle \rangle_{C_1, C_2}$ average of (4.12.6b).

Continuing this repair effort, we back up to box (4.12.1) and write

$$\begin{aligned} V(x_1, x_2) &= q(z) / C'(x_1, x_2) = q(z) \left[\frac{1}{4\pi\epsilon_d} K(x_1, x_2) \right] \\ W(x_1, x_2) &= i(z) L_e(x_1, x_2) = i(z) \left[\frac{\mu}{4\pi} K_L(x_1, x_2) \right] \end{aligned} \quad (4.12.12)$$

which we average in the same way to get

$$\begin{aligned} V(z) &= q(z) \frac{1}{C'} & W(z) &= i(z) L_e \\ \frac{1}{C'} &\equiv (1/P_1) \int_{C_1} ds_1 (1/P_2) \int_{C_2} ds_2 \frac{1}{C'(x_1, x_2)} = \langle \frac{1}{C'(x_1, x_2)} \rangle_{C_1, C_2} \\ L_e &\equiv (1/P_1) \int_{C_1} ds_1 (1/P_2) \int_{C_2} ds_2 L_e(x_1, x_2) = \langle L_e(x_1, x_2) \rangle_{C_1, C_2} \end{aligned} \quad (4.12.13)$$

The "constants" K and K_L in (4.12.1) are similarly replaced with their $\langle \cdot \rangle_{c1, c2}$ averages.

In the discussion below, we shall no longer mention the averaging process, but it should be understood that for closely spaced conductors the symbols Z_{s1} , Z_{s2} , L_e , C' , K , K_L , V , W are the perimeter-averaged values discussed above. For widely spaced conductors, J_z is roughly uniform over the conductor cross sections and perimeters and the averaging process is not needed. The whole subject of averaging is reviewed in more detail in Appendix S.

Inserting the equations on the first line of (4.12.13) into (4.12.11) we get

$$\begin{aligned}(Z_{s1} + Z_{s2}) i(z) &= -\partial_z V(z) - j\omega L_e i(z) \\ L_e \partial_z i(z) &= -j(\beta_d^2/\omega) V(z)\end{aligned}$$

which we then rearrange as

$$\begin{aligned}\partial_z V(z) &= -[Z_{s1} + Z_{s2} + j\omega L_e] i(z) \\ \partial_z i(z) &= -[j\beta_d^2/(\omega L_e)] V(z).\end{aligned}\tag{4.12.14}$$

These are the classical **transmission line equations**. They are usually written in this form: [$\partial/\partial z = d/dz$]

$$\frac{dV(z)}{dz} = -z i(z) \quad \frac{di(z)}{dz} = -y V(z)\tag{4.12.15}$$

where

$$\begin{aligned}z &= Z_{s1} + Z_{s2} + j\omega L_e &= R + j\omega L && // z \text{ and } R \text{ are ohms/m} \\ y &= j\beta_d^2/(\omega L_e) &= G + j\omega C = j\omega C' && // y \text{ and } G \text{ are mhos/m}\end{aligned}\tag{4.12.16}$$

Note: We have been using bold notation only for vectors, and we now break that guideline by bolding these complex quantities z and y . Our purpose for this bolding is to distinguish them from Cartesian coordinates z and y which typically appear in the same problem. In King's books, *all* complex parameters are put in bold font, but we do this only for z and y .

The quantities z and y are called the transmission line **impedance** and **admittance**. On the right we have partitioned the expressions for z and y into their real and imaginary parts in terms of four real parameters R, L, G and C .

Parameters R and L are defined to be the resistance and inductance of the transmission line (per unit length). When $\omega = 0$, $R = R_{dc}$ = the total DC resistance of both transmission line conductors, but when ω is large this is no longer true. One can associate this fact with the skin effect which displaces current away from the conductor's central region

Comparing the right equation in (4.12.15) to (4.11.5), we may immediately interpret the real parameters C and G as the capacitance and conductance of the transmission line (per unit length) as discussed in Section 4.11. The fact that $G + j\omega C = j\omega C'$ has been shown in (4.11.14), where C' is the complex capacitance (per unit length) of the transmission line.

If one applies ∂_z to either equation in (4.12.15) and then uses the other, one obtains these corresponding wave equations (but in the ω domain, so they are really Helmholtz equations),

$$\frac{d^2 V(z)}{dz^2} - zy V(z) = 0 \quad \frac{d^2 i(z)}{dz^2} - zy i(z) = 0 \quad (4.12.17)$$

We refer to (4.12.15) as the first order transmission line equations, and (4.12.17) as the second order transmission line equations.

Jumping the gun a bit, if we assume now a traveling-wave z dependence $e^{j(\omega t - kz)}$ for both $V(z)$ and $i(z)$, where k is the wave's (possibly complex) wavenumber, then $\partial_z \rightarrow -jk$ and the transmission line equations (4.12.15) become

$$\begin{aligned} -jk V(z) &= -z i(z) \quad \text{and} \quad -jk i(z) = -y V(z) \\ \text{or} \\ -jk &= -z i(z)/V(z) \quad \text{and} \quad -jk = -y V(z)/i(z) \end{aligned}$$

Equating these last two expressions gives

$$-z i(z)/V(z) = -y V(z)/i(z) \quad \Rightarrow \quad z/y = [V(z)/i(z)]^2$$

and we then have,

$$Z_0 \equiv V(z)/i(z) = \sqrt{\frac{z}{y}} = \sqrt{\frac{R + j\omega L}{G + j\omega C}} \quad (4.12.18)$$

where by definition Z_0 is the **characteristic impedance** of the transmission line. Obviously Z_0 is completely different from z even though both are referred to as an impedance.

Looking at (4.12.16) we see that

$$\begin{aligned} j\omega C' &= j\beta_d^2 / (\omega L_e) \\ \text{so} \\ L_e C' &= (\beta_d / \omega)^2 = \mu_d \xi_d \quad // \text{ using (1.5.1a)} \\ L_e C &= \mu_d \epsilon_d = 1/v_d^2 \quad // \text{ using (4.11.9a) that } C'/C = (\xi_d / \epsilon_d) \text{ and then (1.1.29)} \end{aligned} \quad (4.12.19)$$

Recall now from summary box (4.12.1) that

$$\frac{1}{C'} = \frac{V(z)}{q(z)} = \frac{1}{4\pi \xi_d} K \quad \Rightarrow \quad C' = 4\pi \xi_d / K \quad (4.4.7)$$

$$L_e = \frac{W(z)}{i(z)} = \frac{\mu_d}{4\pi} K_L \quad (4.10.8) \quad (4.12.1)$$

Inserting these expressions into (4.12.19) that $[L_e][C'] = \mu_d \xi_d$ gives

$$\left[\frac{\mu_0}{4\pi} K_L \right] [4\pi\zeta_d/K] = \mu_0\zeta_d$$

or

$$K_L = K \quad (4.12.20)$$

This is a remarkable connection between our two seemingly unrelated constants K and K_L ,

$$K \equiv \int_{C_1} dx_1' dy_1' \alpha_1(x_1', y_1') \ln(s_{21}^2/s_{11}^2) - \int_{C_2} dx_2' dy_2' \alpha_2(x_2', y_2') \ln(s_{22}^2/s_{12}^2) \quad (4.4.8)$$

$$K_L \equiv \int_{C_1} dx_1' dy_1' b_1(x_1', y_1') \ln(s_{21}^2/s_{11}^2) - \int_{C_2} dx_2' dy_2' b_2(x_2', y_2') \ln(s_{22}^2/s_{12}^2) \quad (4.10.9)$$

Since K involves a peripheral line integral of surface charge densities α_i whereas K_L involves a full cross sectional area integral of the current densities b_i , it seems unlikely these integrals would be equal, but they are equal.

(c) An example of $K = K_L$

The equality even seems unlikely in a case with symmetric densities on round wires, so let's do a check using our Section 4.5 example with widely-spaced round wires of unequal diameters. The first thing we need is a new picture to display the "kinematics" of the K_L integral (since densities are symmetric, one should regard this picture as having b much larger than shown relative to a_1 and a_2),

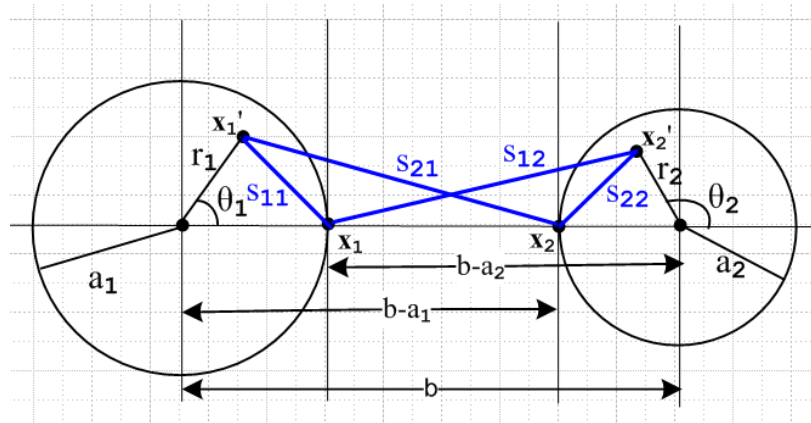


Fig 4.14

As before, we read off the four distances of interest using the law of cosines. The new distances are all different from before since x_1' and x_2' are now each integrated over their respective disks instead of the bounding circles.

$$\begin{aligned} s_{21}^2 &= r_1^2 + (b-a_1)^2 - 2 r_1(b-a_1) \cos(\theta_1) \\ s_{11}^2 &= r_1^2 + a_1^2 - 2 r_1 a_1 \cos(\theta_1) \\ s_{22}^2 &= r_2^2 + a_2^2 + 2 r_2 a_2 \cos(\theta_2) \\ s_{12}^2 &= r_2^2 + (b-a_2)^2 + 2 r_2(b-a_2) \cos(\theta_2) \end{aligned}$$

The integration rule is still

$$\int_0^{2\pi} d\theta \ln(A \pm B \cos\theta) = 2\pi \ln\left[\frac{1}{2}(A + \sqrt{A^2 - B^2})\right] . \quad (4.5.5)$$

The first integral is:

$$\int_0^{2\pi} d\theta_1 \ln(s_{21}^2) = \int_0^{2\pi} d\theta_1 \ln([r_1^2 + (b-a_1)^2 - 2 r_1(b-a_1) \cos(\theta_1)])$$

$$A = r_1^2 + (b-a_1)^2 \quad B = 2 r_1(b-a_1)$$

$$A^2 - B^2 = [r_1^2 + (b-a_1)^2]^2 - 4 r_1^2 (b-a_1)^2 = [r_1^2 - (b-a_1)^2]^2 \Rightarrow \sqrt{A^2 - B^2} = (b-a_1)^2 - r_1^2 > 0 \quad b \gg a_1$$

$$\Rightarrow \int_0^{2\pi} d\theta_1 \ln(s_{21}^2) = 2\pi \ln\left[\frac{1}{2}(r_1^2 + (b-a_1)^2 + (b-a_1)^2 - r_1^2)\right] = 2\pi \ln[(b-a_1)^2]$$

But this integral is the same as before! The s_{11}^2 integral is obtained from the above with $b-a_1 \rightarrow a_1$

$$\int_0^{2\pi} d\theta_1 \ln(s_{11}^2) = 2\pi \ln(a_1^2)$$

which is also the same as before. The other two integrals are found from $1 \rightarrow 2$. Our integral summary is then exactly the same as (4.5.6),

$$\begin{aligned} \int_0^{2\pi} d\theta_1 \ln(s_{21}^2) &= 2\pi \ln[(b-a_1)^2] \\ \int_0^{2\pi} d\theta_1 \ln(s_{11}^2) &= 2\pi \ln(a_1^2) \\ \int_0^{2\pi} d\theta_2 \ln(s_{22}^2) &= 2\pi \ln(a_2^2) \\ \int_0^{2\pi} d\theta_2 \ln(s_{12}^2) &= 2\pi \ln[(b-a_2)^2] . \end{aligned} \quad (4.5.6)$$

We now assume that the current densities b_i each have radial symmetry ("widely spaced wires"),

$$b_1(r_1, \theta_1) = b_1(r_1) \quad (4.12.21)$$

where $b_1(r_1)$ is a completely arbitrary function, with the following normalization of (4.7.4),

$$\int_0^{2\pi} d\theta_1 \int_0^{a_1} r_1 dr_1 b_1(r_1) = 1 \quad \Rightarrow \quad \int_0^{a_1} r_1 dr_1 b_1(r_1) = 1/2\pi . \quad (4.12.22)$$

We now proceed to calculate the constant K_L

$$\begin{aligned}
K_L &= \int_0^{2\pi} d\theta_1 \int_0^{a_1} r_1 dr_1 b_1(r_1) \ln(s_{21}^2/s_{11}^2) - \int_0^{2\pi} d\theta_2 \int_0^{a_2} r_2 dr_2 b_2(r_2) \ln(s_{22}^2/s_{12}^2) \\
&= \int_0^{a_1} r_1 dr_1 b_1(r_1) \int_0^{2\pi} d\theta_1 \ln(s_{21}^2/s_{11}^2) - \int_0^{a_2} r_2 dr_2 b_2(r_2) \int_0^{2\pi} d\theta_2 \ln(s_{22}^2/s_{12}^2) \\
&= 2\pi \int_0^{a_1} r_1 dr_1 b_1(r_1) [\ln[(b-a_1)^2] - \ln(a_1^2)] - \int_0^{a_2} r_2 dr_2 b_2(r_2) [\ln[(b-a_2)^2] - \ln(a_2^2)] \\
&= 2\pi [\ln[(b-a_1)^2/a_1^2] \int_0^{a_1} r_1 dr_1 b_1(r_1) - 2\pi [\ln[(b-a_2)^2/a_2^2] \int_0^{a_2} r_2 dr_2 b_2(r_2)] \\
&= [\ln[(b-a_1)^2/a_1^2] - \ln[(b-a_2)^2/a_2^2]] \\
&= \ln \left[\frac{(b-a_1)^2 (b-a_2)^2}{a_1^2 a_2^2} \right] \\
&= K \quad \text{as obtained in (4.5.7), third last line} \tag{4.12.23}
\end{aligned}$$

and we have then shown $K_L = K$ for this particular example. The key fact is that the $d\theta$ integrals *appear* to be functions of r_i , but the r_i^2 terms cancel and so the $d\theta$ integrals are independent of r_i .

The summary of results on the next page includes a few items not yet derived, as indicated by references. It seemed good to gather it all in one place.

(d) Summary of Results

Classical Transmission Line Equations and Parameters (ω domain) (4.12.24)

$$K \equiv \int_{C_1} dx_1' dy_1' \alpha_1(x_1', y_1') \ln(s_{21}^2/s_{11}^2) - \int_{C_2} dx_2' dy_2' \alpha_2(x_2', y_2') \ln(s_{22}^2/s_{12}^2) \quad (4.4.8)$$

$$K_L \equiv \int_{C_1} dx_1' dy_1' b_1(x_1', y_1') \ln(s_{21}^2/s_{11}^2) - \int_{C_2} dx_2' dy_2' b_2(x_2', y_2') \ln(s_{22}^2/s_{12}^2), \quad (4.10.9)$$

$$K = K_L \quad \text{real and dimensionless} \quad (4.12.20)$$

$$\frac{dV(z)}{dz} = -z i(z) \quad \left(\frac{d}{dz^2} - zy \right) V(z) = 0 \quad z = R + j\omega L \quad \text{transmission line equations}$$

$$\frac{di(z)}{dz} = -yV(z) \quad \left(\frac{d}{dz^2} - zy \right) i(z) = 0 \quad y = G + j\omega C \quad (4.12.15, 16 \text{ and } 17)$$

$$z = Z_{s1} + Z_{s2} + j\omega L_e \quad (4.12.16) \quad X_L \equiv \omega L_e, \quad X_C \equiv 1/(\omega C)$$

$$y = j\omega C' = j\omega C + G \quad (4.12.16) \quad G = (\sigma_d/\epsilon_d)C \quad (4.11.15)$$

$$R = \text{Re}(Z_{s1} + Z_{s2}) \quad L = L_e + (1/\omega) \text{Im}(Z_{s1} + Z_{s2}) = L_e + L_i \quad // \text{ from above}$$

$$L_e = \frac{\mu_d}{4\pi} K \quad (4.10.8) \text{ and } (4.12.20)$$

$$C' = 4\pi \xi_d / K \quad (4.4.7) \quad C' = (\xi_d/\epsilon_d)C \quad (4.11.9a)$$

$$C = 4\pi \epsilon_d / K \quad \text{above two equations}$$

$$G = 4\pi \sigma_d / K \quad \text{above and } (4.4.10) \quad G/C = \sigma_d/\epsilon_d \quad (4.4.10)$$

$$L_e C' = \mu_d \xi_d \quad (4.12.19)$$

$$L_e C = \mu_d \epsilon_d = 1/v_d^2 \quad (4.12.19)$$

$$Z_0 = \sqrt{\frac{z}{y}} = \sqrt{\frac{R + j\omega L}{G + j\omega C}} \quad (4.12.18) \quad jk = \sqrt{zy} = \sqrt{(R + j\omega L)(G + j\omega C)} \quad (5.3.6)$$

$$Z_0 \text{ (large } \omega) \approx \sqrt{\frac{L}{C}} \approx \sqrt{\frac{L_e}{C}} = (1/4\pi) K \sqrt{\mu_d/\epsilon_d} = (K/4\pi) Z_m \quad \text{facts above; } (4.4.14)$$

$$\lambda \gg D \quad (4.3.6) \quad \text{assumed transmission line limit where } \beta_d = 2\pi/\lambda$$

$$\beta_d^2 = \mu_d \epsilon_d \omega^2 - j\omega \mu_d \sigma_d = \omega^2 \mu_d (\epsilon_d - j\sigma_d/\omega) = \omega^2 \mu_d \xi_d \quad \xi_d \equiv \epsilon_d - j\sigma_d/\omega \quad (1.5.1a)$$

$$\beta_{d0}^2 = \omega^2 \mu_d \epsilon_d = (\omega^2/v_d^2) \quad \Rightarrow \quad \beta_{d0} = (\omega/v_d) \quad (1.5.1b)$$

$$F(z)/F(0) = e^{-jkz} = e^{-az} e^{-j bz} \quad a \equiv -\text{Im}(k) = \text{Re}(\sqrt{zy}) = \text{attenuation}$$

$$jk = a + jb = \sqrt{zy} \quad k = -ja + b = -j\sqrt{zy} \quad b \equiv \text{Re}(k) = \text{Im}(\sqrt{zy}) = \text{phase} \quad \text{see } (5.3.6)$$

Comments:

1. In Chapter 2 we computed the surface impedance Z_s for a round wire in the case of axially symmetric current and we found that, for large ω ,

$$Z_s(\omega) \approx \frac{1}{\sigma(2\pi a)\delta} (1+j) \quad (2.4.16)$$

$$\delta \equiv \sqrt{2/\omega\mu\sigma} = \text{skin depth} \quad (2.2.20)$$

so that

$$Z_s(\omega) \approx \frac{1}{2\pi a} \sqrt{\frac{\mu}{2\sigma}} (1+j) \sqrt{\omega} \quad (4.12.25)$$

Presumably the result will be $Z_s(\omega) \sim \sqrt{\omega}$ for any conductor cross section shape. Then

$$L = L_e + (1/\omega) \text{Im}(Z_{s1} + Z_{s2}) = L_e + (\text{stuff}) 1/\sqrt{\omega} \rightarrow L_e \quad \text{for large } \omega \quad (4.12.26)$$

For this reason, the high frequency characteristic impedance Z_0 can be written as shown in (4.12.24).

2. Conductors have internal inductance L_i as well as external inductance L_e . In Appendix C.3 (a) we compute the low frequency internal inductance of a round wire to be $L_i = \mu/8\pi = (\mu/\mu_0) * 50 \text{ nH/m}$. Our Chapter 4 transmission line development makes no mention of L_i . This can be traced to Figure 4.11 where only the external magnetic flux is involved. In fact, L_i is accounted for in the imaginary part of the surface impedance Z_s . For example, we found that for our round wire situation,

$$Z_s(\omega) = \frac{1}{\sigma\pi a^2} + j\omega \frac{\mu}{8\pi} = R_s + j\omega L_s \quad // \text{ low frequency limit} \quad (2.4.12)$$

and here one sees that $L_s = \frac{\mu}{8\pi} = L_i$.

3. We have assumed that ϵ_d and μ_d are real. If not, the usual adjustments can be made in (4.12.24) for the interpretations of R,L,G and C. See for example (3.3.4) concerning σ being replaced by σ_{eff} if ϵ has an imaginary part.

4. Apart from the symmetric cases like the examples of Section 4.5 and 4.6, we do not yet have a way to compute K and the transmission line parameters since the charge and current distributions α_i and b_i are not known. This matter will be remedied in Chapter 5.

5. A **strip** transmission line of width w and separation s with $s \ll w$ is the simplest example of the above summary:

$$E = V/s \quad n = \epsilon_d E = \epsilon_d V/s \quad q = nw \quad C = q/V = \epsilon_d w/s \Rightarrow K = 4\pi\epsilon_d/C = 4\pi(s/w)$$

so

$$\begin{aligned} C &= 4\pi\epsilon_d/K &= \epsilon_d (w/s) & \quad K = 4\pi (s/w) \\ G &= 4\pi\sigma_d/K &= \sigma_d (w/s) \\ L_e &= (\mu_d/4\pi) K &= \mu_d (s/w) \\ Z_0 &\approx (K/\sqrt{\epsilon_{re1}}) 30\Omega = 4\pi (s/w) (1/\sqrt{\epsilon_{re1}}) 30\Omega = (s/w) (1/\sqrt{\epsilon_{re1}}) 377\Omega \end{aligned} \quad (4.12.27)$$

(e) Time domain equations (telegraph equations)

The results above are all stated in the frequency domain, but it is a simple matter to convert them to the time domain using $j\omega \leftrightarrow \partial_t$. One then makes these replacements

$$\begin{aligned} \mathbf{z} &= R + j\omega L &\rightarrow & L\partial_t + R \\ \mathbf{y} &= G + j\omega C &\rightarrow & C\partial_t + G \\ \mathbf{zy} &= (R + j\omega L)(G + j\omega C) &\rightarrow & (R + L\partial_t)(G + C\partial_t) = LC\partial_t^2 + (LG + RC)\partial_t + RG. \end{aligned} \quad (4.12.28)$$

Here then are selected equations and their translations to the time domain:

Transmission Line Equations (4.12.14b) : [coupled first order PDE's]

$$\begin{aligned} \partial_z V &= -\mathbf{z} i &\Rightarrow & \partial_z V(z,t) = -L\partial_t i(z,t) - LR i(z,t) \\ \partial_z i &= -\mathbf{y} V &\Rightarrow & \partial_z i(z,t) = -C\partial_t V(z,t) - CGV(z,t) \end{aligned} \quad (4.12.29)$$

Transmission Line Wave Equations (4.12.15) [damped wave equations]

$$\begin{aligned} (\partial_z^2 - \mathbf{zy}) V(z) &= 0 &\Rightarrow & [\partial_z^2 - LC \partial_t^2 - (LG + RC)\partial_t - RG] V(z,t) = 0 \\ (\partial_z^2 - \mathbf{zy}) i(z) &= 0 &\Rightarrow & [\partial_z^2 - LC \partial_t^2 - (LG + RC)\partial_t - RG] i(z,t) = 0 \end{aligned} \quad (4.12.30)$$

If we set the loss parameters R and G both to 0 these equations become

$$\begin{aligned} \partial_z V(z,t) &= -L\partial_t i(z,t) & [\partial_z^2 - LC \partial_t^2] V(z,t) &= 0 & [\text{undamped wave equations}] \\ \partial_z i(z,t) &= -C\partial_t V(z,t) & [\partial_z^2 - LC \partial_t^2] i(z,t) &= 0 & // \text{lossless} \end{aligned} \quad (4.12.31)$$

At large ω one has $L \approx L_e$ (note 1 above) and since (4.12.19) says $L_e C = \mu_d \epsilon_d = 1/v_d^2$ we conclude that the factor LC appearing in the above wave equations is $1/v_d^2$ where v_d is the dielectric wave velocity.

The various transmission line equations shown above in the time domain are often referred to as **telegraph** (telegrapher, telegrapher's) **equations**. See wiki.

4.13 Modifications to account for $\mu_d \neq \mu_1 \neq \mu_2$

These modifications only affect the A_z and $W(z)$ part of this chapter, not the first six sections which are concerned with ϕ and $V(z)$. So changes start with Section 4.7.

If the equality $\mu_d = \mu_1 = \mu_2$ assumed in Section 4.7 is broken, the result is that surface magnetization currents appear on one or both of the conductor surfaces and these cause an alteration of the theory. Thanks to the "J_m Theorem" proven in Appendix B, this alteration can be carried through with a very minimal impact, as we now show.

In Appendix B conductor magnetization surface currents are studied in some detail. The reader interested in how the magnetic modification is carried out would do well to read Appendix B at this point. A reader less interested can accept the Appendix B results and continue here to learn that basically nothing changes except R and L and parameters like Z_0 and k which are functions of R and L.

So imagine starting with $\mu_d = \mu_1 = \mu_2$ and then changing μ_1 and μ_2 to new values. The question is: how do the various parameters and equations of the theory change? The first modification arises in Section 4.7. As described in Appendix B.6, the modified version of (4.7.2) is this,

$$A_{z1}(\mathbf{x}) = \frac{\mu_1}{4\pi} \int_{C_1} [J_{z1}(\mathbf{x}') + \frac{\mu_0}{\mu_1} J_{zm1}(\mathbf{x}')] \frac{e^{-j\beta_d R}}{R} dx'dy'dz' . \quad R = |\mathbf{x} - \mathbf{x}'| \quad (4.7.2)'$$

where J_{zm1} includes only the surface component of the magnetization current on conductor C_1 . Section B.6 shows how this J_{zm1} adder term in effect adds a certain homogeneous solution to the particular solution (first term above) of the A_z Helmholtz equation such that the A_z boundary conditions are duly satisfied at the magnetic conductor C_1 boundary. According to (B.1.10), the surface current J_{zm1} when expressed in surface rather than volume notation is given by $K_z = - \left(\frac{\mu_1}{\mu_0} - \frac{\mu_d}{\mu_0} \right) H_\theta$ and thus vanishes when $\mu_1 = \mu_d$, resulting in the unmodified version of (4.7.2).

We maintain the next two equations of Section 4.7 as is, involving separation of variables,

$$J_{z1}(x,y,z) = \underbrace{b_1(x,y)}_{A/m^2} \underbrace{i_1(z)}_{1/m^2 \quad A} \quad (4.7.3)$$

where i_1 is scaled such that

$$\int_{C_1} dx dy b_1(x,y) = 1 . \quad (4.7.4)$$

This $i_1(z)$ is still the total conduction current in C_1 . But we now add two new equations,

$$J_{z1m}(x,y,z) = \underbrace{b_{1m}(x,y)}_{A/m^2} \underbrace{i_{1m}(z)}_{1/m^2 \quad A} \quad (4.13.1)$$

where i_{1m} is scaled such that

$$\int_{C_1} dx dy b_{1m}(x,y) = 1 . \quad (4.13.2)$$

It is understood here that $b_{1m}(x,y)$ is a distribution which is restricted to the surface of C_1 , but we continue to write it as if it existed at all points in the cross section of C_1 . The integration in (4.13.2) is of course meant to include this surface distribution.

We know from (B.1.11) and (B.1.12) that, for an arbitrarily shaped conductor C_1 , the bound magnetic current is given by,

$$i_{1m}(z) \equiv - \left(\frac{\mu_1}{\mu_0} - \frac{\mu_d}{\mu_0} \right) i(z) , \quad [\mu_1 = \text{conductor } C_1, \mu_d = \text{dielectric}] \quad (4.13.3)$$

and the ratio of this to the total free current is therefore given by,

$$f_{1m} \equiv i_{1m}(z)/i(z) = - \left(\frac{\mu_1}{\mu_0} - \frac{\mu_d}{\mu_0} \right) . \quad (4.13.4)$$

With the above definitions, our modified (4.7.6) becomes

$$\begin{aligned} A_{z1}(x,y,z) &= \frac{\mu_1}{4\pi} \int_{-\infty}^{\infty} dz' i(z') \int_{C_1} dx' dy' [b_1(x',y') + \frac{\mu_0}{\mu_1} f_{1m} b_{1m}(x',y')] \frac{e^{-j\beta_d R}}{R} \\ &= \frac{\mu_d}{4\pi} \int_{-\infty}^{\infty} dz' i(z') \int_{C_1} dx' dy' [\frac{\mu_1}{\mu_d} b_1(x',y') + \frac{\mu_0}{\mu_d} f_{1m} b_{1m}(x',y')] \frac{e^{-j\beta_d R}}{R} \end{aligned} \quad (4.13.5)$$

where notice that μ_d is now out front in place of μ_1 . This leads us to define a new effective transverse current density,

$$\begin{aligned} b'_1(x,y) &\equiv \frac{\mu_1}{\mu_d} b_1(x',y') + \frac{\mu_0}{\mu_d} f_{1m} b_{1m}(x',y') \\ &= \frac{\mu_1}{\mu_d} b_1(x',y') + [1 - \frac{\mu_1}{\mu_d}] b_{1m}(x',y') . \end{aligned} \quad (4.13.6)$$

This new transverse density b'_1 is still normalized to unity, using (4.7.4) and (4.13.2) above :

$$\begin{aligned} \int_{C_1} dx dy b'_1(x,y) &= \frac{\mu_1}{\mu_d} \int_{C_1} dx dy b_1(x,y) + [1 - \frac{\mu_1}{\mu_d}] \int_{C_1} dx dy b_{1m}(x,y) \\ &= \frac{\mu_1}{\mu_d} * 1 + [1 - \frac{\mu_1}{\mu_d}] * 1 = 1 . \end{aligned} \quad (4.13.7)$$

How does b'_1 differ from b_1 ? The difference is that b_1 does not include a surface current and b'_1 does. We can represent equation (4.13.6) in this symbolic graphic manner:

$$\textcircled{b'_1} = \frac{\mu_1}{\mu_d} \textcircled{b_1} + \left[1 - \frac{\mu_1}{\mu_d}\right] \textcircled{b_{1m}} \quad (4.13.6)$$

Thus, from (4.13.5) and (4.13.6) we have this new version of (4.7.6),

$$A_{z1}(x,y,z) = \frac{\mu_d}{4\pi} \int_{-\infty}^{\infty} dz' i(z') \int_{C_1} dx' dy' b'_1(x,y) \frac{e^{-j\beta_d R}}{R} \quad (4.7.6')$$

The differences are that the leading factor is μ_d instead of μ_1 , and b_1 is replaced by b'_1 .

Moving into Section 4.8 we have this new version of (4.8.1),

$$A_{z12}(\mathbf{x}) = A_{z1}(\mathbf{x}) + A_{z2}(\mathbf{x}) = \frac{\mu_d}{4\pi} \int_{-\infty}^{\infty} dz' i(z') \left\{ \int_{C_1} dx_1' dy_1' b'_1(x_1',y_1') \frac{e^{-j\beta_d R}}{R} - \int_{C_2} dx_2' dy_2' b'_2(x_2',y_2') \frac{e^{-j\beta_d R}}{R} \right\} \quad (4.8.1')$$

which is identical to (4.8.1) except $b_i \rightarrow b'_i$. Then in the transmission line limit, we get this new version of (4.9.1),

$$A_{z12}(\mathbf{x}) = \frac{\mu_d}{4\pi} i(z) \int_{-\infty}^{\infty} dz' \left\{ \int_{C_1} dx_1' dy_1' b'_1(x_1',y_1') \frac{1}{R_{11}} - \int_{C_2} dx_2' dy_2' b'_2(x_2',y_2') \frac{1}{R_{12}} \right\} \quad (4.9.1')$$

From this point onward, all equations are the same apart from $b_i \rightarrow b'_i$. Here are some of those equations after modification:

$$W(z) \equiv A_{z12}(\mathbf{x}_1) - A_{z12}(\mathbf{x}_2) \quad (4.10.1')$$

$$\begin{aligned} &= \frac{\mu_d}{4\pi} i(z) \int_{-\infty}^{\infty} dz' \left\{ \int_{C_1} dx_1' dy_1' b'_1(x_1',y_1') \frac{1}{R_{11}} - \int_{C_2} dx_2' dy_2' b'_2(x_2',y_2') \frac{1}{R_{12}} \right\} \\ &- \frac{\mu_d}{4\pi} i(z) \int_{-\infty}^{\infty} dz' \left\{ \int_{C_1} dx_1' dy_1' b'_1(x_1',y_1') \frac{1}{R_{21}} - \int_{C_2} dx_2' dy_2' b'_2(x_2',y_2') \frac{1}{R_{22}} \right\} \end{aligned}$$

$$W(z) \quad (4.10.3')$$

$$= \frac{\mu_d}{4\pi} i(z) \int_{-\infty}^{\infty} dz' \left\{ \int_{C_1} dx_1' dy_1' b'_1(x_1',y_1') \left(\frac{1}{R_{11}} - \frac{1}{R_{21}} \right) - \int_{C_2} dx_2' dy_2' b'_2(x_2',y_2') \left(\frac{1}{R_{12}} - \frac{1}{R_{22}} \right) \right\} \cdot$$

$$W(z) = i(z) \frac{\mu_d}{4\pi} \left\{ \int_{C_1} dx_1' dy_1' b_1'(x_1', y_1') \ln(s_{21}^2/s_{11}^2) - \int_{C_2} dx_2' dy_2' b_2'(x_2', y_2') \ln(s_{22}^2/s_{12}^2) \right\} \quad (4.10.4)'$$

$$K_L \equiv \int_{C_1} dx_1' dy_1' b_1'(x_1', y_1') \ln(s_{21}^2/s_{11}^2) - \int_{C_2} dx_2' dy_2' b_2'(x_2', y_2') \ln(s_{22}^2/s_{12}^2) \quad (4.10.9)'$$

$$L_e = \frac{W(z)}{i(z)} = \frac{\mu_d}{4\pi} K_L \quad // \text{ no change} \quad (4.10.8)$$

Section 4.11 involving non-magnetic currents is unaltered. We then enter Section 4.12. The derivation of the transmission line equations (4.12.15) is *unaffected* by the above modifications; the only change is that the b_i appear in the integral K_L in place of the b_i . The derivation of the fact that $K = K_L$ ending in (4.12.20) is also unchanged! This at first seems strange since K has not changed, but we have apparently altered K_L by the replacements $b_i \rightarrow b_i'$. But K_L is not an evaluation -- it is an integral equation relating K_L to the b_i' . In the self-consistent solution, the new functions (distributions) b_i' adjust themselves so that K_L does not change. K_L cannot change because (4.12.20) says it must remain equal to K which is determined by the electrostatic side of the problem. It is perhaps helpful to look at (4.10.8) which says

$L_e = \frac{\mu_d}{4\pi} K_L$. We know that if the dielectric μ_d value does not change, the *external* inductance L_e of the transmission line cannot change so K_L stays fixed. Changing μ_1 and/or μ_2 away from the value μ_d will of course change the *internal* inductances of the conductors, and this is duly noted below in terms of surface impedances. As μ_1 is increased, the B field inside conductor C_1 increases (H stays the same) so the stored B field increases, and L_i increases.

Finally, if we look at the example associated with Fig 4.14, we still find explicitly that $K_L = K$ because the calculation leading to (4.12.23) is unchanged when b_i are replaced with b_i' , since the b_i' are still normalized to unity as shown in (4.13.7).

The happy bottom line is that all of summary box (4.12.24) is unchanged except $b_i \rightarrow b_i'$ in the K_L integral. The constant K can still be evaluated using the "capacitor problem" of Section 5.5 below and it is unaffected by conductors having $\mu_i \neq \mu_d$.

Having said this, let us now consider what happens to an operating transmission line which starts off with $\mu_1 = \mu_2 = \mu_d = \mu_0$ and we then gradually turn a magic "permeability knob" so that μ_1 gradually increases from μ_0 to some value $\mu_1 > \mu_0$. That is to say, we gradually cause conductor C_1 to become magnetic. The constant K (and therefore $K_L = K$) does not change at all. This K is determined by the potential ϕ part of the problem in Section 4.4 and does not even know about the magnetic modification. Thus, looking at (4.12.24), C' , C , G and L_e do not change. In particular, L_e does not change because we have not altered μ_d of the dielectric. The following two items shown in box (4.12.24) *do* change :

$$R = \text{Re}(Z_{s1} + Z_{s2}) \quad L = L_e + (1/\omega) \text{Im}(Z_{s1} + Z_{s2})$$

where Z_{s_i} is the surface impedance of conductor C_i . The non- L_e term in L can be interpreted as the internal inductance of the conductors. R and L change because Z_{s1} changes if we change μ_1 . This is so because Z_{s1} is always a function of the skin depth δ_1 , and $\delta_1 \equiv \sqrt{2/(\omega\mu_1\sigma_1)} = \delta(\mu_1)$ from (2.2.20). In the

special case that C_1 is a round wire of radius a_1 with an axially symmetric current distribution (such as the center wire of a coaxial cable), we showed in (2.4.11) that the surface impedance is given by

$$Z_{1s}(\omega) = \frac{+j\omega\mu_1}{2\pi a_1(\sqrt{2}/\delta_1)} \frac{\text{ber}_0[\sqrt{2}(a_1/\delta_1)] + j \text{bei}_0[\sqrt{2}(a_1/\delta_1)]}{\text{ber}_0'[\sqrt{2}(a_1/\delta_1)] + j \text{bei}_0'[\sqrt{2}(a_1/\delta_1)]} \quad (2.4.11)$$

so certainly this $Z_s(\omega)$ is a function of μ_1 both due to the leading constant and through the five occurrences of δ_1 . Both the real and imaginary parts of $Z_{1s}(\omega)$ will change as μ_1 changes, so the transmission line parameters R and L both change. In the high frequency limit ,

$$Z_{1s}(\omega) \approx \frac{1}{\sigma_1(2\pi a_1)\delta_1} (1+j) \quad \delta_1 \ll 16a \quad (2.4.16)$$

so now the variation with μ_1 is through the single δ_1 factor shown. Again, both real and imaginary parts of $Z_{1s}(\omega)$ vary with μ_1 .

Since R and L change as noted above, the transmission line characteristic impedance will also change,

$$Z_0 = \sqrt{\frac{R + j\omega L}{G + j\omega C}} = \sqrt{\frac{z}{y}} \quad (K.12) \text{ or } (4.12.18)$$

This means, for example, if we drive a semi-infinite transmission line with some fixed voltage $V(z)$, the driving current $i(z)$ will vary in amplitude and phase as we turn our "permeability knob" for conductor C_1 . This is simply because $i(z) = V(z)/Z_0$. In Chapter 5 we shall encounter the wave number k where

$$k = -j\sqrt{zy} = -j\sqrt{(R+j\omega L)(G+j\omega C)} \quad (K.7) \text{ or } (5.3.6)$$

and so this parameter will vary as well. Since losses are associated with the imaginary part of k , the transmission line loss will also be affected by turning this "permeability knob".

So **the good news** is that the theory of Chapter 4 is easily extended to allow for magnetic conductors and or dielectric. Once again, the summary box (4.12.24) is unchanged when $\mu_1 = \mu_2 = \mu_d$ is broken except for the appearance of b'_i in the K_L integral, and except for the fact that Z_{s1} and Z_{s2} change as noted above, causing changes in R, L and Z_0 . At very high frequency, one will have $Z_0 = \sqrt{(L_e/C)}$ and in this case Z_0 is not altered, see (4.12.26). As noted, k to be introduced below will also be altered, but not at high frequency where $k = -j\sqrt{(j\omega L)(j\omega C)} = \omega\sqrt{LC} = \omega\sqrt{L_e C} = \omega/v_d$.

Chapter 5: The Transverse Problem

In this Chapter we define a certain "transverse" potential theory problem and then give a prescription for obtaining K and thus the transmission line parameters C , G and L_e . Basically this amounts to computing the capacitance of a section of transmission line using standard (if obscure) electrostatic methods. Subsidiary topics involve a certain dipole scaling condition for infinite dielectrics, the equation of energy conservation for a transmission line, and an interpretation of the terms lossless, low-loss and lossy.

5.1 Separation of ϕ

Let $\phi \equiv \phi_{12}(\mathbf{x})$ of Section 4.2. Then in the transmission line limit we found in (4.3.10) that,

$$\phi(\mathbf{x}) = \frac{1}{4\pi\epsilon_d} q(z) \int_{-\infty}^{\infty} dz' \left\{ \int_{C_1} dx_1' dy_1' \alpha_1(x_1', y_1') \frac{1}{R_1} - \int_{C_2} dx_2' dy_2' \alpha_2(x_2', y_2') \frac{1}{R_2} \right\}. \quad (4.3.10)$$

Rewrite the above equation as,

$$\phi(x, y, z) = \frac{1}{4\pi\epsilon_d} q(z) \phi_t(x, y) \quad (5.1.1)$$

$$\phi_t(x, y) \equiv \int_{-\infty}^{\infty} dz' \left\{ \int_{C_1} dx_1' dy_1' \alpha_1(x_1', y_1') \frac{1}{R_1} - \int_{C_2} dx_2' dy_2' \alpha_2(x_2', y_2') \frac{1}{R_2} \right\} \quad (5.1.2)$$

where $R_1 = |\mathbf{x} - \mathbf{x}_1|$, $R_2 = |\mathbf{x} - \mathbf{x}_2|$, and \mathbf{x} is a point in the dielectric. We thus identify ϕ_t as a dimensionless "transverse potential" associated with the full potential ϕ .

Recall that \mathbf{x}_1 and \mathbf{x}_2 are points on the surfaces of conductors C_1 and C_2 at the same z . Evaluate (5.1.1) at \mathbf{x}_1 then at \mathbf{x}_2 and then subtract to get the right equation below,

$$V(z) = \phi(\mathbf{x}_1) - \phi(\mathbf{x}_2) = \frac{1}{4\pi\epsilon_d} q(z) [\phi_t(x_1, y_1) - \phi_t(x_2, y_2)].$$

The left side is just $V(z)$ according to (4.4.1). Recalling now from (4.4.7) that

$$V(z) = q(z) \frac{1}{4\pi\epsilon_d} K \quad (4.4.7)$$

one concludes that

$$\phi_t(x_1, y_1) - \phi_t(x_2, y_2) = K. \quad (5.1.3)$$

The Helmholtz equation for ϕ is given by (1.5.3) for a region including dielectric and conductors,

$$(\nabla^2 + \beta_d^2)\phi(x, y, z) = -(1/\epsilon_d) \rho(x, y, z) \quad (1.5.3) \quad (5.1.4)$$

where $\rho(x,y,z)$ exists on the boundary of the dielectric region (ie, on the conductor surfaces). Inside the dielectric there is no ρ so we then have

$$(\nabla^2 + \beta_d^2)\varphi(x,y,z) = 0 . \quad // \text{ dielectric region} \quad (5.1.5)$$

Inserting (5.1.1) into (5.1.5) yields,

$$(\nabla^2 + \beta_d^2) \frac{1}{4\pi\epsilon_d} q(z) \varphi_t(x,y) = 0$$

or

$$(\nabla_t^2 + \partial_z^2 + \beta_d^2) \frac{1}{4\pi\epsilon_d} q(z) \varphi_t(x,y) = 0 \quad // \nabla_t^2 = \nabla_{2D}^2 = \nabla^2 - \partial_z^2$$

or

$$q(z)\nabla_t^2\varphi_t(x,y) + \varphi_t(x,y)\partial_z^2q(z) + \beta_d^2\varphi_t(x,y)q(z) = 0 .$$

Divide through by $\varphi_t(x,y)q(z)$ to get

$$\frac{\nabla_t^2\varphi_t(x,y)}{\varphi_t(x,y)} + \frac{\partial_z^2q(z)}{q(z)} + \beta_d^2 = 0$$

or

$$\left[\frac{\nabla_t^2\varphi_t(x,y)}{\varphi_t(x,y)} \right] + \frac{\partial_z^2q(z)}{q(z)} = -\beta_d^2 \quad (5.1.6)$$

which has the general form,

$$[h(x,y)] + g(z) = -\beta_d^2 .$$

The only way this can be true for all x,y,z in a region is if $g(z) = \text{some constant}$, which call $-k_\phi^2$. Then,

$$\frac{\partial_z^2q(z)}{q(z)} = -k_\phi^2 \quad \frac{\nabla_t^2\varphi_t(x,y)}{\varphi_t(x,y)} = -\beta_d^2 + k_\phi^2 . \quad (5.1.7)$$

We can rewrite these equations as

$$[\nabla_t^2 + (\beta_d^2 - k_\phi^2)] \varphi_t(x,y) = 0 \quad (5.1.8)$$

$$[\partial_z^2 + k_\phi^2] q(z) = 0 . \quad (5.1.9)$$

According to Fact (3.8.8) and (5.1.1), for a particular z value, we expect $\varphi_t(x,y)$ to have some constant value K_1 on the entire perimeter of a cross section of conductor C_1 , and some other constant value K_2 on the entire perimeter of a cross section of conductor C_2 . These facts act as boundary conditions for (5.1.7),

$$\varphi_t(C_1) = K_1 \quad \varphi_t(C_2) = K_2 \quad K_1 - K_2 = K \quad (5.1.10)$$

so that (5.1.3) is realized.

Equation (5.1.9) has the following solution

$$q(z) = q(0) e^{-jk_\phi z} \quad \Rightarrow \quad q(z,t) = q(0) e^{j(\omega t - k_\phi z)} \quad (5.1.11)$$

and we find that $q(z)$ has the form of a wave traveling down the transmission line with wavenumber k_ϕ .

The reader of Chapter 2 or of Appendix D will recognize this as the form assumed for the electric field in (2.1.1) or (D.1.1) where it was assumed as an *ansatz* without much *a priori* justification. For example,

$$\mathbf{E}(r,\theta,z,t) = e^{j(\omega t - k_\phi z)} \mathbf{E}(r,\theta) . \quad (D.1.1)$$

When the dust settles below, for a low-loss transmission line we shall in fact end up with $k_\phi = k$ so that (D.1.1) has the same traveling wave form as (5.1.11).

5.2 Separation of A_z

Let $A_z \equiv A_{z12}(\mathbf{x})$ of Section 4.8. Then in the transmission line limit we found in (4.9.1) that

$$A_z(\mathbf{x}) = \frac{\mu_d}{4\pi} i(z) \int_{-\infty}^{\infty} dz' \left\{ \int_{C_1} dx_1' dy_1' b_1(x_1', y_1') \frac{1}{R_1} - \int_{C_2} dx_2' dy_2' b_2(x_2', y_2') \frac{1}{R_2} \right\} . \quad (4.9.1)$$

Rewrite the above equation as,

$$A_z(x,y,z) = \frac{\mu_d}{4\pi} i(z) A_{z\mathbf{t}}(x,y) \quad (5.2.1)$$

$$A_{z\mathbf{t}}(x,y) \equiv \int_{-\infty}^{\infty} dz' \left\{ \int_{C_1} dx_1' dy_1' b_1(x_1', y_1') \frac{1}{R_1} - \int_{C_2} dx_2' dy_2' b_2(x_2', y_2') \frac{1}{R_2} \right\} \quad (5.2.2)$$

where $R_1 = |\mathbf{x} - \mathbf{x}_1'|$, $R_2 = |\mathbf{x} - \mathbf{x}_2'|$, and \mathbf{x} is a point in the dielectric. We thus identify $A_{z\mathbf{t}}$ as a dimensionless "transverse vector potential" associated with the full vector potential A_z .

Recall that \mathbf{x}_1 and \mathbf{x}_2 are points on the surfaces of conductors C_1 and C_2 at the same z . Evaluate (5.2.1) at \mathbf{x}_1 then at \mathbf{x}_2 and then subtract to get the right equation below,

$$W(z) = A_z(\mathbf{x}_1) - A_z(\mathbf{x}_2) = \frac{\mu_d}{4\pi} i(z) [A_{z\mathbf{t}}(\mathbf{x}_1, y_1) - A_{z\mathbf{t}}(\mathbf{x}_2, y_2)] .$$

The left side is just $W(z)$ according to (4.10.1). Recalling now

$$L_e = \frac{W(z)}{i(z)} = \frac{\mu_d}{4\pi} K_L \quad \Rightarrow \quad W(z) = \frac{\mu_d}{4\pi} i(z) K_L \quad (4.10.8)$$

we conclude that

$$A_{\mathbf{z}\mathbf{t}}(x_1, y_1) - A_{\mathbf{z}\mathbf{t}}(x_2, y_2) = K_{\mathbf{L}}.$$

But (4.12.20) says $K_{\mathbf{L}} = K$, so write this last as

$$A_{\mathbf{z}\mathbf{t}}(\mathbf{x}_{1\mathbf{t}}) - A_{\mathbf{z}\mathbf{t}}(\mathbf{x}_{2\mathbf{t}}) = K. \quad (5.2.3)$$

The Helmholtz equation for $A_{\mathbf{z}}$ is given by (1.5.4) for a region including dielectric and conductors,

$$(\nabla^2 + \beta_{\mathbf{d}}^2)A_{\mathbf{z}}(x, y, z) = -\sum_{\mathbf{i}=2}^{\mathbf{N}} \mu_{\mathbf{i}} \mathbf{J}_{\mathbf{i}\mathbf{z}}. \quad (1.5.4) \quad (5.2.4)$$

The $\mathbf{J}_{\mathbf{i}}$ are currents inside the conductors. Although there is small conduction current in the dielectric, it has been absorbed into $\beta_{\mathbf{d}}^2$ as shown in (1.3.21) in the time domain with the use of the King gauge. If we take our region of interest to be the dielectric alone, we then have

$$(\nabla^2 + \beta_{\mathbf{d}}^2)A_{\mathbf{z}}(x, y, z) = 0. \quad // \text{ dielectric region} \quad (5.2.5)$$

Inserting (5.2.1) into (5.2.5) yields,

$$(\nabla^2 + \beta_{\mathbf{d}}^2) \frac{\mu_{\mathbf{d}}}{4\pi} i(z) A_{\mathbf{z}\mathbf{t}}(x, y) = 0$$

or

$$(\nabla_{\mathbf{t}}^2 + \partial_{\mathbf{z}}^2 + \beta_{\mathbf{d}}^2) \frac{\mu_{\mathbf{d}}}{4\pi} i(z) A_{\mathbf{z}\mathbf{t}}(x, y) = 0$$

or

$$i(z) \nabla_{\mathbf{t}}^2 A_{\mathbf{z}\mathbf{t}}(x, y) + A_{\mathbf{z}\mathbf{t}}(x, y) \partial_{\mathbf{z}}^2 i(z) + \beta_{\mathbf{d}}^2 A_{\mathbf{z}\mathbf{t}}(x, y) i(z) = 0.$$

Now divide through by $A_{\mathbf{z}\mathbf{t}}(x, y) i(z)$ to get

$$\left[\frac{\nabla_{\mathbf{t}}^2 A_{\mathbf{z}\mathbf{t}}(x, y)}{A_{\mathbf{z}\mathbf{t}}(x, y)} \right] + \frac{\partial_{\mathbf{z}}^2 i(z)}{i(z)} + \beta_{\mathbf{d}}^2 = 0 \quad (5.2.6)$$

which has the general form,

$$[h(x, y)] + g(z) = -\beta_{\mathbf{d}}^2.$$

The only way this can be true for all x, y, z in a region is if $g(z) = \text{some constant}$, which call $-k_{\mathbf{A}}^2$. Then,

$$\frac{\partial_{\mathbf{z}}^2 i(z)}{i(z)} = -k_{\mathbf{A}}^2 \quad \frac{\nabla_{\mathbf{t}}^2 A_{\mathbf{z}\mathbf{t}}(x, y)}{A_{\mathbf{z}\mathbf{t}}(x, y)} = -\beta_{\mathbf{d}}^2 + k_{\mathbf{A}}^2. \quad (5.2.7)$$

We can rewrite these equations as

$$[\nabla_{\mathbf{z}}^2 + (\beta_{\mathbf{d}}^2 - k_{\mathbf{A}}^2)] A_{\mathbf{z}\mathbf{t}}(x,y) = 0 \quad (5.2.8)$$

$$[\partial_{\mathbf{z}}^2 + k_{\mathbf{A}}^2] i(z) = 0 \quad (5.2.9)$$

According to Fact (3.8.9) and (5.2.1), for a particular z value, we expect $A_{\mathbf{z}\mathbf{t}}(x,y)$ to have some constant value W_1 on the entire perimeter of a cross section of conductor C_1 , and some other constant value W_2 on the entire perimeter of a cross section of conductor C_2 . These facts act as boundary conditions for (5.2.7). Since a potential has an arbitrary zero, we shall set

$$A_{\mathbf{z}\mathbf{t}}(C_1) = W_1 \quad A_{\mathbf{z}\mathbf{t}}(C_2) = W_2 \quad W_1 - W_2 = K \quad (5.2.10)$$

so that (5.2.3) is realized.

The second equation (5.2.9) has the following solution

$$i(z) = i(0) e^{-jk_{\mathbf{A}}z} \quad \Rightarrow \quad i(z,t) = i(0) e^{j(\omega t - k_{\mathbf{A}}z)} \quad (5.2.11)$$

and we find that $i(z)$ has the form of a wave traveling down the transmission line with wavenumber $k_{\mathbf{A}}$.

Comparing (5.2.11) with (5.1.11), it would certainly seem odd if $q(z)$ and $i(z)$ had the form of traveling waves with different wavenumbers $k_{\phi} \neq k_{\mathbf{A}}$. We will formally show in the next section that $k_{\phi} = k_{\mathbf{A}}$.

5.3 Development of the Transverse Problem

(a) $k_{\phi} = k_{\mathbf{A}}$ and the transverse equations

The longitudinal equations from the previous two sections are these:

$$[\partial_{\mathbf{z}}^2 + k_{\phi}^2] q(z) = 0 \quad (5.1.9)$$

$$[\partial_{\mathbf{z}}^2 + k_{\mathbf{A}}^2] i(z) = 0 \quad (5.2.9)$$

But,

$$\varphi(x,y,z) = \frac{1}{4\pi\epsilon_{\mathbf{d}}} q(z) \varphi_{\mathbf{t}}(x,y) \quad (5.1.1)$$

$$A_{\mathbf{z}}(x,y,z) = \frac{\mu_{\mathbf{d}}}{4\pi} i(z) A_{\mathbf{z}\mathbf{t}}(x,y) \quad (5.2.1)$$

Therefore,

$$\begin{aligned} [\partial_{\mathbf{z}}^2 + k_{\phi}^2] \varphi(x,y,z) &= 0 \\ [\partial_{\mathbf{z}}^2 + k_{\mathbf{A}}^2] A_{\mathbf{z}}(x,y,z) &= 0 \end{aligned} \quad (5.3.1)$$

Recall that \mathbf{x}_1 and \mathbf{x}_2 are points on the surfaces of conductors C_1 and C_2 . If we write equations (5.3.1) first at \mathbf{x}_1 and then at \mathbf{x}_2 and then subtract, we get longitudinal equations for $V(z)$ and $W(z)$,

$$\begin{aligned}
[\partial_z^2 + k_\phi^2] V(z) &= 0 & // V(z) &= \phi(\mathbf{x}_1) - \phi(\mathbf{x}_2) \\
[\partial_z^2 + k_A^2] W(z) &= 0 & // W(z) &= A_z(\mathbf{x}_1) - A_z(\mathbf{x}_2) \\
[\partial_z^2 + k_A^2] i(z) &= 0 & // \text{since } W(z) &= L_e i(z) \text{ from (4.10.8)}
\end{aligned} \tag{5.3.2}$$

where we have used the definitions $V(z)$ and $W(z)$ from (4.4.1) and (4.10.1). For low frequencies, we average (5.3.1) over the conductor perimeters and then $V(z)$ and $W(z)$ are as in (4.12.7).

Recall now the second order transmission line equations of (4.12.17),

$$\frac{d^2 V(z)}{dz^2} - zy V(z) = 0 \qquad \frac{d^2 i(z)}{dz^2} - zy i(z) = 0 \quad (4.12.17) \tag{5.3.3}$$

Comparison of (5.3.2) with (5.3.3) shows that

$$k_\phi^2 = k_A^2 \equiv k^2 = -zy = -(R+j\omega L)(G+j\omega C) \tag{5.3.4}$$

which fulfills the expectation earlier that we should have $k_\phi = k_A$. Recall the longitudinal behaviors,

$$q(z) = q(0) e^{-jk_\phi z} \qquad \Rightarrow \qquad q(z,t) = q(0) e^{j(\omega t - k_\phi z)} \tag{5.1.11}$$

$$i(z) = i(0) e^{-jk_A z} \qquad \Rightarrow \qquad i(z,t) = i(0) e^{j(\omega t - k_A z)} \tag{5.2.11}$$

We claim that the appropriate root for our $+\hat{z}$ directed wave is given by

$$\begin{aligned}
k &= k_\phi = k_A = -j\sqrt{zy} \qquad \Rightarrow \\
jk &= \sqrt{zy} \equiv \sqrt{(R+j\omega L)(G+j\omega C)} = a + jb \quad // a \text{ and } b \text{ are real and imag parts of } jk
\end{aligned} \tag{5.3.5}$$

For example, near $\omega = 0$ we get $jk \approx \sqrt{RG} > 0$ and then $e^{-jkz} \sim \exp(-\sqrt{RG} z)$ which shows that the wave *decays* as z increases to the right. The other root $k = +j\sqrt{zy}$ would be appropriate for a wave going in the $-\hat{z}$ direction.

All quantities like $q(z), i(z), V(z), W(z)$ have this longitudinal behavior for a wave traveling in the $+\hat{z}$ direction,

$$\begin{aligned}
F(z) &= F(0) e^{-jkz} = F(0) e^{-az} e^{-jbz} & jk &= a + jb = \sqrt{zy} = \sqrt{(R+j\omega L)(G+j\omega C)} \\
&= F(0) \exp[-\sqrt{zy} z] \\
&= F(0) \exp[-\sqrt{(R+j\omega L)(G+j\omega C)} z] \\
a &\equiv \text{Re}(\sqrt{zy}) = \text{Re}[\sqrt{(R+j\omega L)(G+j\omega C)}] = -\text{Im}(k) & // \text{attenuation per distance of } F(z) \\
b &= \text{Im}(\sqrt{zy}) = \text{Im}[\sqrt{(R+j\omega L)(G+j\omega C)}] = \text{Re}(k) & // \text{phase of } F(z)
\end{aligned} \tag{5.3.6}$$

Now recall from box (4.12.24) that

$$\begin{aligned} \mathbf{z} &= Z_s + j\omega L_e = Z_s + j\omega \frac{\mu_d}{4\pi} K & Z_s &\equiv Z_{s1} + Z_{s2} \\ \mathbf{y} &= j\omega C' = j\omega 4\pi\xi_d/K \end{aligned} \quad (5.3.7)$$

so

$$\begin{aligned} k^2 &= -\mathbf{z}\mathbf{y} = -[Z_s + j\omega \frac{\mu_d}{4\pi} K] j\omega 4\pi\xi_d/K \\ &= -Z_s j\omega 4\pi\xi_d/K + \omega^2 \mu_d \xi_d \\ &= -j\omega Z_s 4\pi\xi_d/K + \beta_d^2. \end{aligned} \quad // \text{ see (1.5.1a)} \quad (5.3.8)$$

Therefore,

$$\begin{aligned} (\beta_d^2 - k^2) &= j\omega Z_s 4\pi\xi_d / K = \frac{j\omega Z_s 4\pi\xi_d}{K} = j\omega Z_s C' \\ &= j\omega Z_s (\xi_d/\epsilon_d) C = j\omega (1/\epsilon_d) [\epsilon_d + \sigma_d/j\omega] Z_s C = [j\omega + \sigma_d/\epsilon_d] Z_s C. \end{aligned} \quad (5.3.9)$$

The transverse equations (5.1.8) and (5.2.8) and boundary conditions (5.1.10) and (5.2.10) may now be summarized:

$$[\nabla_t^2 + (\beta_d^2 - k^2)] \varphi_t(x, y) = 0 \quad \varphi_t(C_1) = K_1 \quad \varphi_t(C_2) = K_2 \quad K_1 - K_2 = K \quad (5.3.10)$$

$$[\nabla_t^2 + (\beta_d^2 - k^2)] A_{zt}(x, y) = 0 \quad A_{zt}(C_1) = W_1 \quad A_{zt}(C_2) = W_2 \quad W_1 - W_2 = K \quad (5.3.11)$$

$$\text{where } (\beta_d^2 - k^2) = \frac{j\omega Z_s 4\pi\xi_d}{K}.$$

For a lossless transmission line, $Z_s = 0$ and then $k = \beta_d = \omega/v_d$ where v_d is the dielectric light speed.

(b) The scaling boundary condition on $\varphi_t(\mathbf{x})$

There exists another boundary condition on φ_t in the case that the dielectric extends transversely to infinity. Recall (5.1.2) for $\varphi_t(x, y) = \varphi_t(\mathbf{x})$,

$$\varphi_t(\mathbf{x}) = \int_{-\infty}^{\infty} dz' \left\{ \int_{C_1} dx_1' dy_1' \alpha_1(x_1', y_1') \frac{1}{R_1} - \int_{C_2} dx_2' dy_2' \alpha_2(x_2', y_2') \frac{1}{R_2} \right\} \quad (5.1.2)$$

$$\begin{aligned} R_1^2 &= (x-x_1')^2 + (y-y_1')^2 + (z-z')^2 = s_1^2 + (z-z')^2 & s_1^2 &= (x-x_1')^2 + (y-y_1')^2 \\ R_2^2 &= (x-x_2')^2 + (y-y_2')^2 + (z-z')^2 = s_2^2 + (z-z')^2 & s_2^2 &= (x-x_2')^2 + (y-y_2')^2. \end{aligned} \quad (4.2.1)$$

If we take the point \mathbf{x} transversely far away from the conductors, the following drawing shows the distances R_1 and R_2 which appear in the above integration,

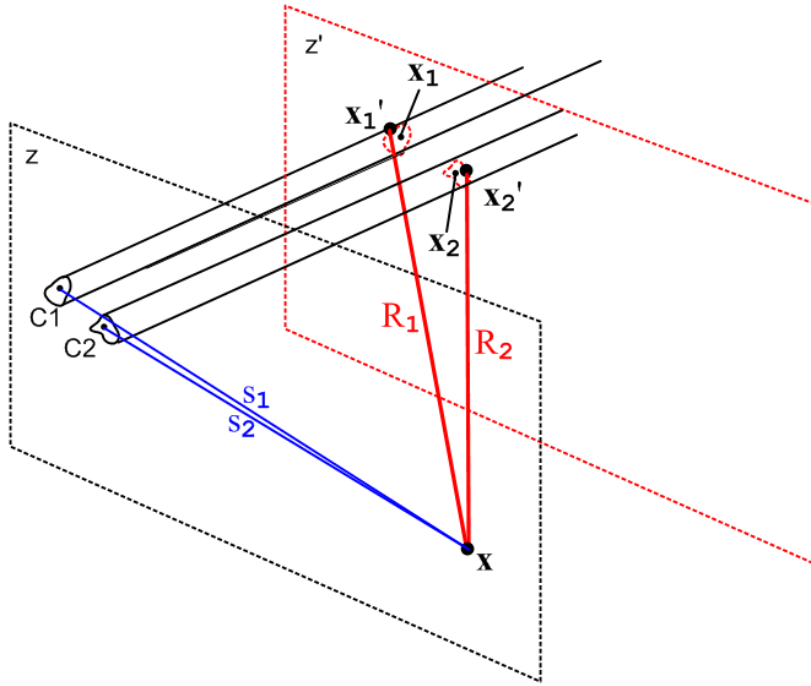


Fig 5.1

During the transverse integration $\int_{C_1} dx_1' dy_1'$, distance R_1 does not vary much and can be replaced with a distance from \mathbf{x} to the "center" of conductor C_1 without changing the integral significantly. The same can be said for R_2 . We shall refer to these "center points" as \mathbf{x}_1 and \mathbf{x}_2 (this is a new and different use for these variable names). In this case, we obtain

$$\begin{aligned} \varphi_{\mathbf{t}}(\mathbf{x}) &\approx \int_{-\infty}^{\infty} dz' \left\{ \frac{1}{R_1} \int_{C_1} dx_1' dy_1' \alpha_1(x_1', y_1') - \frac{1}{R_2} \int_{C_2} dx_2' dy_2' \alpha_2(x_2', y_2') \right\} \\ &= \int_{-\infty}^{\infty} dz' \left\{ \frac{1}{R_1} - \frac{1}{R_2} \right\} = \int_{-\infty}^{\infty} dz' \left(\frac{1}{\sqrt{s_1^2 + (z-z')^2}} - \frac{1}{\sqrt{s_2^2 + (z-z')^2}} \right) \end{aligned} \quad (5.3.12)$$

where we have used the fact (4.1.3) that the transverse charge densities are normalized to unity. The dz' integral was done in (4.4.5) and equals $\ln(s_2^2/s_1^2)$, so then

$$\varphi_{\mathbf{t}}(\mathbf{x}) \approx \ln(s_2^2/s_1^2) \quad // \text{ limiting form as point } \mathbf{x} = (x, y) \text{ moves far from the conductors} \quad (5.3.13)$$

$$\begin{aligned} s_1^2 &= (x-x_1)^2 + (y-y_1)^2 \\ s_2^2 &= (x-x_2)^2 + (y-y_2)^2. \end{aligned}$$

Whatever the exact solution $\varphi_{\mathbf{t}}(\mathbf{x})$ might be, in the limit discussed above one must obtain $\varphi_{\mathbf{t}}(\mathbf{x}) \approx \ln(s_2^2/s_1^2)$. Of course as one continues to move \mathbf{x} away to infinity, $s_1 \approx s_2$ and then $\varphi_{\mathbf{t}}(\mathbf{x}) \approx \ln(1) = 0$. Basically (5.3.13) is a boundary condition on the "scale" of the solution $\varphi_{\mathbf{t}}(\mathbf{x})$. If someone were to propose a possible solution $\varphi_{\mathbf{t}}(\mathbf{x}) = 2.6 \ln(s_2^2/s_1^2)$ for some conductor geometry, we could instantly rule

out that solution since it violates the boundary condition (5.3.13). The scale of $\phi_{\mathbf{t}}$ is restricted in this manner because the charge distributions α_i appearing in (5.3.12) are normalized to unity.

By the exact same argument presented above, we have

$$A_{\mathbf{z}\mathbf{t}}(\mathbf{x}) \approx \ln(s_2^2/s_1^2) \quad // \text{ limiting form as point } \mathbf{x} = (x,y) \text{ moves far from the conductors} \quad (5.3.14)$$

We shall give an interpretation of these limiting forms in Section 5.4 (b) below.

(c) Energy Conservation in a Transmission Line

In (5.3.6) we have seen how the voltage or current in a transmission line has z dependence $e^{-j\mathbf{kz}}$ where

$$k = -j\sqrt{\mathbf{zy}} \quad (5.3.6)$$

Now consider the following quantities:

$$u_{\mathbf{C}} = (1/2) C V(z)^2 dz = \text{capacitative energy stored in } dz$$

$$u_{\mathbf{L}} = (1/2) L i(z)^2 dz = \text{inductive energy stored in } dz \text{ (as in (C.3.5))}$$

$$p_{\mathbf{C}} = C dz V(z) \partial_{\mathbf{t}} V(z) = \text{rate of increase of the C stored energy}$$

$$p_{\mathbf{L}} = L dz i(z) \partial_{\mathbf{t}} i(z) = \text{rate of increase of the L stored energy}$$

$$p_{\mathbf{R}} = i(z)^2 R dz = \text{rate of energy burned in R}$$

$$p_{\mathbf{G}} = V(z)^2 G dz = \text{rate of energy burned in G} \quad // V(z) i_{\mathbf{G}}(z) = V(z) [V(z) G dz]$$

$$p(z) = \text{energy/sec entering a little transmission line segment of length } dz \text{ located at } z$$

$$p(z+dz) = \text{energy/sec leaving the segment at } z + dz \quad (5.3.15)$$

The power balance equation for the transmission line segment of length dz is then

$$p(z) - p(z+dz) = \text{power flow decrease over } dz = p_{\mathbf{C}} + p_{\mathbf{L}} + p_{\mathbf{R}} + p_{\mathbf{G}}$$

$$= C dz V(z) \partial_{\mathbf{t}} V(z) + L dz i(z) \partial_{\mathbf{t}} i(z) + i(z)^2 R dz + V(z)^2 G dz \quad (5.3.16)$$

so that

$$-\partial_{\mathbf{z}} p(z) = C V(z) \partial_{\mathbf{t}} V(z) + L i(z) \partial_{\mathbf{t}} i(z) + i(z)^2 R + V(z)^2 G$$

or

$$-\partial_{\mathbf{z}} p(z) = \partial_{\mathbf{t}} [(1/2) C V(z)^2 + (1/2) L i(z)^2] + i(z)^2 R + V(z)^2 G$$

Since $p(z) = V(z)i(z)$, one finds

$$-\partial_{\mathbf{z}} [V(z,t) i(z,t)] = \partial_{\mathbf{t}} [(1/2) C V(z,t)^2 + (1/2) L i(z,t)^2] + i(z,t)^2 R + V(z,t)^2 G \quad (5.3.17)$$

where we now show both space and time arguments. One can regard the above as a statement of energy conservation (per unit time) at location z on an infinite transmission line. For a lossless line, $R = G = 0$, and it is for such a line that the above equation appears in Haus and Melcher as Sec 14.2 Eq. (19).

Verification check "trust, but verify"

"doveryai, no proveryai"

Moving the time derivative back in one gets,

$$-\partial_z[V(z,t) i(z,t)] = [CV(z,t) \partial_t V(z,t) + L i(z,t) \partial_t i(z,t)] + i(z,t)^2 R + V(z,t)^2 G .$$

Since both V and i have the z dependence e^{-jkz} , $V i$ has dependence e^{-2jkz} so,

$$-2jk [V(z,t) i(z,t)] = [CV(z,t) \partial_t V(z,t) + L i(z,t) \partial_t i(z,t)] + i(z,t)^2 R + V(z,t)^2 G .$$

Taking $\partial_t \rightarrow j\omega$ and writing $V(z,\omega) = V$ and $i(z,\omega) = I$, the above becomes in the ω domain,

$$\begin{aligned} -2jk [VI] &= j\omega [CV^2 + LI^2] + I^2 R + V^2 G \\ &= I^2 (R + j\omega L) + V^2 (G + j\omega C) = I^2 \mathbf{z} + V^2 \mathbf{y} . \end{aligned}$$

Dividing both sides by VI gives

$$-2jk = (I/V) \mathbf{z} + (V/I) \mathbf{y} .$$

But (4.12.18) says that $V/I = Z_0 = \sqrt{\mathbf{z}/\mathbf{y}}$ so we find,

$$-2jk = (I/V) \mathbf{z} + (V/I) \mathbf{y} = \sqrt{\mathbf{y}/\mathbf{z}} \mathbf{z} + \sqrt{\mathbf{z}/\mathbf{y}} \mathbf{y} = \sqrt{\mathbf{zy}} + \sqrt{\mathbf{zy}} = 2\sqrt{\mathbf{zy}}$$

and we finally arrive at

$$-jk = \sqrt{\mathbf{zy}}$$

which matches the equation stated at the start of this subsection.

5.4 The Low-Loss Approximation

(a) Transverse Equations for a Low-Loss transmission line

For low loss, we take the conductor surface impedance $Z_s \approx 0$. Recall from (5.3.8) that

$$k^2 = \beta_d^2 - j\omega Z_s 4\pi\xi_d/K . \tag{5.3.8}$$

Our definition of a "low-loss" transmission line is one for which $k^2 \approx \beta_d^2$ and in this case the longitudinal wave number k as shown in (5.1.11) and (5.2.11) is $k \approx \beta_d$. So our low-loss condition is (using (1.5.1a) for β_d^2),

$$\begin{aligned}
& |j\omega Z_s 4\pi\xi_d/K| \ll |\beta_d^2| & \beta_d^2 = \omega^2 \mu_d \xi_d \\
\text{or} & \\
& |Z_s| \ll (1/4\pi) |\beta_d^2/(\omega\xi_d)| K = (1/4\pi) \omega |\beta_d^2/(\omega^2\xi_d)| K = (1/4\pi) \omega \mu_d K \\
\text{so} & \\
& |Z_s| \ll (1/4\pi) \omega \mu_d K . & (5.4.1)
\end{aligned}$$

For a symmetric-environment round wire of radius a we found in (2.4.16) that for **large** ω ,

$$Z_s \approx \frac{1}{\sigma(2\pi a)\delta} (1+j) \quad \text{for } \delta \ll 4a \quad \delta^2 = 2/\omega\mu\sigma . \quad (2.4.16)$$

For a transmission line of two round conductors either coaxial or widely spaced we can estimate

$$Z_s = Z_{s1} + Z_{s2} = \frac{1}{\sigma(2\pi)\delta} (1+j) \left(\frac{1}{a_1} + \frac{1}{a_2} \right) \equiv \frac{1}{\sigma(2\pi)\delta} (1+j) \frac{1}{a} \quad \frac{1}{a} \equiv \left(\frac{1}{a_1} + \frac{1}{a_2} \right)$$

so that (5.4.1) says [assuming $\mu = \mu_d$]

$$\begin{aligned}
\sigma |Z_s| &= \frac{1}{(2\pi a)\delta} \sqrt{2} \ll (1/4\pi) \sigma \omega \mu K = (1/4\pi) (2/\delta^2) K \\
\Rightarrow \frac{1}{(2\pi a)\delta} \sqrt{2} &\ll (1/4\pi) (2/\delta^2) K & \Rightarrow \frac{1}{\delta a} \sqrt{2} \ll (1/\delta^2) K \\
\Rightarrow (\delta/a) &\ll K/\sqrt{2} & (5.4.2)
\end{aligned}$$

We saw in the Example of Section 4.6 that $K = 2 \ln(a_2/a_1)$ for a coaxial cable, (4.6.4). Even for a very large radius ratio of 100 this would be $K = 2 \ln(100) = 9.2$. For a more typical ratio of perhaps 5, $K \approx 3.2$. Then our inequality above says roughly

$$(\delta/a) \ll 2 \quad \frac{1}{a} \equiv \left(\frac{1}{a_1} + \frac{1}{a_2} \right)$$

which is then our ball-park estimate for applicability of the "low-loss transmission line" condition at large ω . We showed in Section 2.5 (and Section 4.11) how Z_s can be modified for some other geometry. Basically this says we are in the low-loss limit if the skin depth is much smaller than the wire's transverse dimensions. That is to say, a transmission line has "low loss" when ω is *larger* than some value. The E and B fields in the dielectric wing along at v_d between the conductors, with little penetration into either conductor, and thus little ohmic loss in those conductors.

On the other hand, for **small** ω we found in (2.4.12) that

$$Z_s(\omega) = R_{dc} + j\omega \frac{\mu}{8\pi} = R_s + j\omega L_s \quad // \text{ low frequency limit} \quad (2.4.12)$$

where $R_{dc} = 1/(\sigma\pi a^2)$ for a round wire. If we use this as an estimate for Z_s of each conductor in the case of general conductors, then

$$Z_s = Z_{s1} + Z_{s2} = R_{dc1} + R_{dc2} + 2j\omega \frac{\mu}{8\pi} \equiv R_{DC} + 2j\omega \frac{\mu}{8\pi}$$

and then (5.4.1) says

$$|Z_s| = |R_{DC} + 2j\omega \frac{\mu}{8\pi}| \ll (1/4\pi) \omega \mu K$$

or

$$(R_{DC})^2 + (\mu/4\pi)^2 \omega^2 \ll (\mu/4\pi)^2 \omega^2 K^2$$

$$R_{DC} \ll (\mu/4\pi) \omega \sqrt{K^2 - 1} .$$

For a given low frequency ω , R_{DC} must be smaller than the above for the transmission line to be low-loss.

Low ω Example 1: Belden 8281 coaxial cable is treated as a case study in Appendix R. There it is shown that $R_{DC} = .036$ ohm/m and $K = 3.7$. The inequality above then requires that

$$\omega \gg (4\pi/\mu) R_{DC} 1/\sqrt{K^2 - 1} = 10^7 * .036 / 3.56 \approx 10^5 \quad \Rightarrow \quad f \gg 16 \text{ KHz}$$

So in the low frequency range, as long as f is not *too* low, one can treat 8281 cable as low-loss.

Low ω Example 2: At the end of Section 4.5 we considered a power transmission line with two 1" diameter conductors separated by 1 meter. It was found that $K = 17.5$ and that $R_{dc} = .02\Omega$ per thousand feet for each conductor which is 0.66×10^{-4} ohms/m for each conductor. Thus we need

$$\omega \gg (4\pi/\mu) R_{DC} 1/\sqrt{K^2 - 1} = 10^7 * [2 * 0.66 \times 10^{-4}] / 17.47 \approx 76 \quad \Rightarrow \quad f \gg 12 \text{ Hz}$$

Such power lines are normally operated at 50 or 60Hz so are in the low loss regime.

If we assume this low-loss limit is in effect, then

$$\beta_d^2 - k^2 = j\omega Z_s 4\pi\xi_d/K \approx 0$$

and our transverse equations (5.3.10) and (5.3.11) become 2D *Laplace* equations,

$$\nabla_t^2 \varphi_t(x,y) = 0 \quad \varphi_t(C_1) = K_1 \quad \varphi_t(C_2) = K_2 \quad K_1 - K_2 = K \quad (5.4.3)$$

$$\nabla_t^2 A_{zt}(x,y) = 0 \quad A_{zt}(C_1) = W_1 \quad A_{zt}(C_2) = W_2 \quad W_1 - W_2 = K \quad (5.4.4)$$

As commented earlier, the parallelism between φ_t and A_{zt} should not be surprising in light of Section 1.3 (b) where it was noted that \mathbf{A} and $\boldsymbol{\varphi}$ are components of the same relativistic 4-vector.

(b) The scaling boundary condition (5.3.13) revisited

First, a quick review.

In 3D the potential (SI units) of a point charge q located at \mathbf{x}_1 is $\varphi(\mathbf{x}) = (q/4\pi\epsilon|\mathbf{x}-\mathbf{x}_1|) = q/(4\pi\epsilon R_1)$.

In 2D the potential of a point charge q located at \mathbf{x}_1 is $\varphi(\mathbf{x}) = -(q/2\pi\epsilon) \ln|\mathbf{x}-\mathbf{x}_1| = -(q/2\pi\epsilon) \ln s_1$.

The 3D $\varphi(\mathbf{x})$ is the solution of $-\nabla^2(\varphi) = (q/\epsilon) \delta^{(3)}(\mathbf{x}-\mathbf{x}_1)$ as shown in (H.1.4) and as proven in Appendix H. The quantity $1/4\pi R_1$ is the 3D free-space propagator of the 3D Laplace equation. It is the Green's function of the equation $-\nabla^2 g(\mathbf{x}|\mathbf{x}_1) = \delta^{(3)}(\mathbf{x}-\mathbf{x}_1)$.

The 2D $\varphi(\mathbf{x})$ is the solution of $-\nabla_{2D}^2(\varphi) = (q/\epsilon) \delta^{(2)}(\mathbf{x}-\mathbf{x}_1)$ as shown in (I.1.4) and as proven in Appendix I. The quantity $-2\pi \ln s_1$ is the 2D free-space propagator of the 2D Laplace equation. It is the Green's function of the equation $-\nabla_{2D}^2 g(\mathbf{x}|\mathbf{x}_1) = \delta^{(2)}(\mathbf{x}-\mathbf{x}_1)$.

With this brief review, we now examine a 2D cross section view of the transmission line of Fig 5.1 at a scale that makes the two conductors appear very small and very close together, and at the same time we imagine more elaborate cross section shapes. The dielectric is assumed non-conducting, so $\xi_d = \epsilon_d$. The three points indicated by the three dots on the right all lie in the plane of paper; this is just a 2D drawing and $\mathbf{x} = (x,y)$.

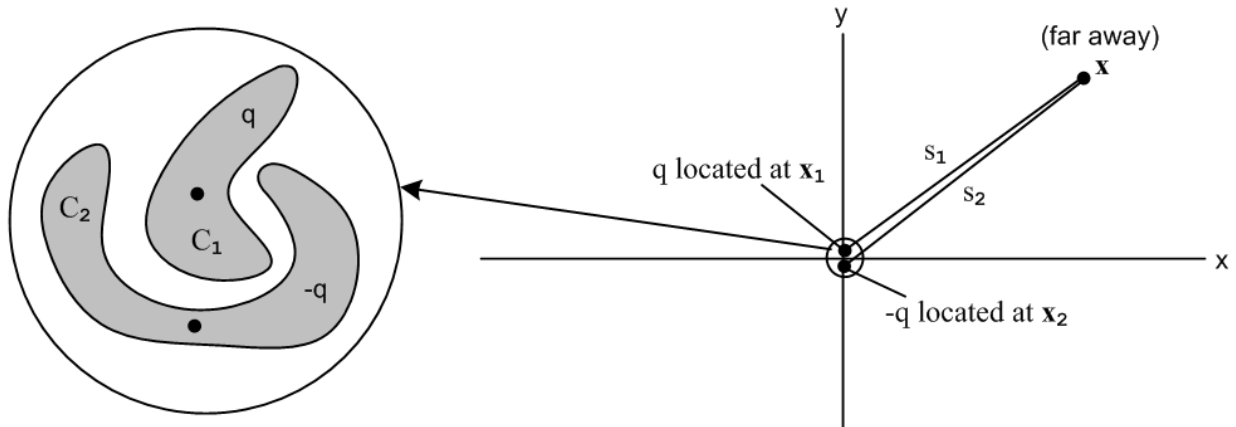


Fig 5.2

The dots on the left indicate the "center of charge" for each conductor and these dots appear also on the right. The claim is that when \mathbf{x} is very far away, the variation in s_1 as it moves over the perimeter of the conductor C_1 cross section is so small that we can replace s_1 with a distance to the center of charge of C_1 and similarly for R_2 . Thus, on the right we end up with the 2D potential of two point charges which form a 2D electric dipole. Using the results just quoted in the above review, we find that

$$\begin{aligned} \varphi(\mathbf{x}) &= \varphi_1(\mathbf{x}) + \varphi_2(\mathbf{x}) = -(q/2\pi\epsilon_d)\ln|\mathbf{x}-\mathbf{x}_1| - (-q/2\pi\epsilon_d)\ln|\mathbf{x}-\mathbf{x}_2| = -(q/2\pi\epsilon_d) \ln s_1 + (q/2\pi\epsilon_d) \ln s_2 \\ &= (q/2\pi\epsilon_d) \ln(s_2/s_1) = (q/4\pi\epsilon_d)\ln(s_2^2/s_1^2) . \end{aligned}$$

Recalling for $\xi_d = \epsilon_d$ that

$$\varphi(x,y,z) = \frac{1}{4\pi\epsilon_d} q(z) \varphi_t(x,y) \quad (5.1.1)$$

we find that

$$\varphi_t(x,y) = \ln(s_2^2/s_1^2) \quad // \text{ for } \mathbf{r} \text{ far away}$$

Thus we have an alternate derivation and 2D dipole interpretation of our earlier "scaling boundary condition" (5.3.13).

5.5 The Capacitor Problem: How to Find K

We have now boiled down the computation of transmission line parameters (in the transmission line limit and in the low-loss limit) to the problem of computing the capacitance of a section of transmission line. Here we assume the dielectric is non-conducting so $\xi = \epsilon$ and we don't have to worry about the distinction between charge densities q_c and q_s as discussed in (4.11.6).

Solving the capacitor problem using φ

A standard approach to a general 2D electrostatics capacitor problem is as follows. Start with

$$\nabla_{2D}^2 \varphi(x,y) = 0 \quad \varphi(C_1) - \varphi(C_2) = V = \text{voltage between conductors} \quad (5.5.1)$$

where we now (arbitrarily) use notation ∇_{2D}^2 in place of ∇_t^2 .

Since the dielectric presumably fills the region between the conductors, the dielectric is the official "region" of a Green's function problem. For a unit positive point charge placed at some location (x',y') in the dielectric region we can then formally (!) solve this 2D Green's function problem,

$$\begin{aligned} -\nabla_{2D}^2 g(x,y|x',y') &= \delta(x-x')\delta(y-y') & g(x,y|x',y') &= 0 \text{ for } (x,y) \text{ on both } C_1 \text{ and } C_2 \\ & & g(x,y|x',y') &= 0 \text{ for } (x,y) = \infty \text{ (if appropriate)} \end{aligned} \quad (5.5.2)$$

Here $g(x,y|x',y')$ is specific to our geometry; it is not the 2D free-space Green's function - $\ln(1/R)/2\pi$ shown in (I.1.4). The free-space solution has only the lower boundary condition stated above. We assume now that this Green's function problem has been solved, either analytically, approximately, or numerically, so that $g(x,y|x',y')$ is known (example coming in Chapter 6).

In very general notation, if a region contains some sources $q(\mathbf{x})$ and if the potential φ is *prescribed* on the entire closed boundary surrounding the region by a function f , then the solution to (5.5.1) is given in Stakgold notation as (1.5.11) (which we derive in the lines following (1.5.11) for both Laplace and Helmholtz equations),

$$\varphi(x) = \int_{\mathbf{R}} dx' g(x|x') \mathbf{q}(x') - \int_{\sigma} dS_{\xi} f(\xi) \partial_{\xi n} g(x|\xi) \quad // \text{Stakgold (6.81)} \quad (1.5.11)$$

where σ represents the closed boundary of the region of interest, dS_{ξ} is an integration over this boundary, and $\partial_{\xi n} g(x|\xi)$ is the derivative of the Green's function in a direction locally normal to the boundary surface. In potential theory, this type of problem is known as "the Dirichlet Problem". In our case the boundary consists of C_1 , C_2 and the Great Circle at ∞ . Stakgold deals in an arbitrary number of spatial dimensions, but we have only 2 dimensions here, so dS_{ξ} is a line integral around the boundary. A picture is in order, showing a cross section of the transmission line,

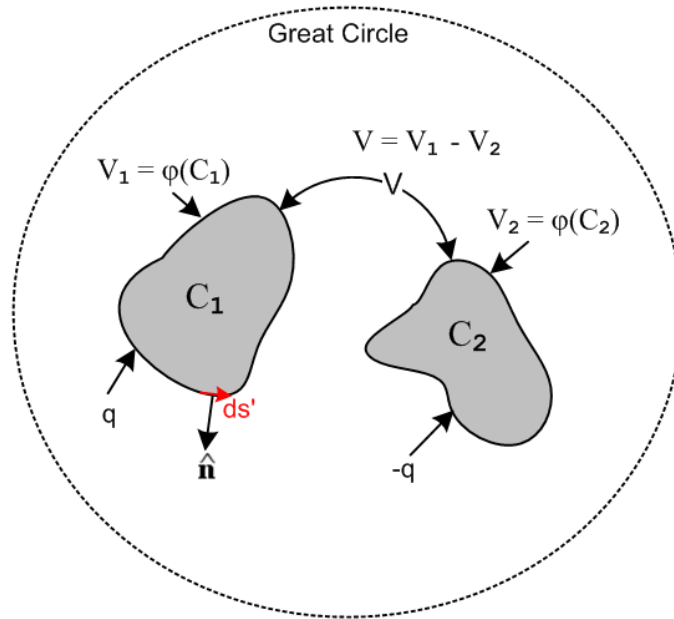


Fig 5.3

We know that on the great circle $\varphi = 0$, so there will be no contribution from that part of the Dirichlet boundary. What we do *not* know are V_1 and V_2 which are the constant potentials on C_1 and C_2 . If it happened that the picture had mirror symmetry in a plane separating the two conductors, we would know that $V_1 = V/2$ and $V_2 = -V/2$, but in the general case we don't know V_1 and V_2 *a priori*. For the moment, we leave them as to-be-determined quantities.

In our application of (1.5.11) there are no charges $\mathbf{q}(x)$ in the dielectric region. We put one there temporarily to obtain the Green's function, but it is now gone. Thus (1.5.11) reads,

$$\begin{aligned} \varphi(x,y) &= - \oint_{C_1} ds' f(C_1) \partial_{ng}(x,y|x',y') - \oint_{C_2} ds' f(C_2) \partial_{ng}(x,y|x',y') - \oint_{GC} ds' f(\infty) \partial_{ng}(x,y|x',y') \\ &= - \oint_{C_1} ds' V_1 \partial_{ng}(x,y|x',y') - \oint_{C_2} ds' V_2 \partial_{ng}(x,y|x',y') - \oint_{GC} ds' (0) \partial_{ng}(x,y|x',y') \\ &= -V_1 \oint_{C_1} ds' \partial_{ng}(x,y|x',y') - V_2 \oint_{C_2} ds' \partial_{ng}(x,y|x',y') \} \\ &= V_1 F_1(x,y) + V_2 F_2(x,y) \end{aligned} \quad (5.5.3)$$

where the $F_i(x,y)$ are determined by doing the line integrals for a given geometry. If $y = y_1(x)$ describes a piece of the C_1 perimeter, then

$$ds' = \sqrt{dx'^2 + dy'^2} = \sqrt{1 + \partial_{\mathbf{x}'} y_1(x')} dx' \quad (5.5.4)$$

which gives a candidate ds' for doing the line integral over that piece of the perimeter.

Once $\phi(x,y)$ is known, one can compute the normal electric field E_n at the conductor surfaces,

$$\begin{aligned} E_n(\mathbf{x}) &= -\partial_{n1}\phi(\mathbf{x}) = -V_1 [\partial_{n1}F_1(\mathbf{x})] - V_2 [\partial_{n1}F_2(\mathbf{x})] \equiv V_1 G_{11}(\mathbf{x}) + V_2 G_{12}(\mathbf{x}) & \mathbf{x} \text{ on } C_1 \\ E_n(\mathbf{x}) &= -\partial_{n2}\phi(\mathbf{x}) = -V_1 [\partial_{n2}F_1(\mathbf{x})] - V_2 [\partial_{n2}F_2(\mathbf{x})] \equiv V_1 G_{21}(\mathbf{x}) + V_2 G_{22}(\mathbf{x}) . & \mathbf{x} \text{ on } C_2 \end{aligned} \quad (5.5.5)$$

Since the conductors are different, the resulting four functions $G_{i,j}$ will in general be different. For example, we are taking normal derivatives of the F_i at different points in space on different (1D) surfaces.

Fig 5.3 is meant to represent the 2D cross section of a 3D transmission line, and in the following the symbol n refers to the true surface charge density in Coul/m^2 . We compute n using (1.1.47) assuming $E_n = 0$ inside the conductor,

$$\begin{aligned} n_1(x,y) &= \epsilon_d E_n(x,y) = \epsilon_d V_1 G_{11}(\mathbf{x}) + \epsilon_d V_2 G_{12}(\mathbf{x}) & \mathbf{x} \text{ on } C_1 \\ n_2(x,y) &= \epsilon_d E_n(x,y) = \epsilon_d V_1 G_{21}(\mathbf{x}) + \epsilon_d V_2 G_{22}(\mathbf{x}) & \mathbf{x} \text{ on } C_2 \end{aligned} \quad (5.5.6)$$

where ϵ_d is for the dielectric. One can then integrate over the boundaries of the conductors to get the total charges q_1 and q_2 residing on the conductors (per unit length),

$$\begin{aligned} q_1 &= \oint_{C_1} ds' n_1(x',y') = \epsilon_d V_1 H_{11} + \epsilon_d V_2 H_{21} \\ q_2 &= \oint_{C_2} ds' n_2(x',y') = \epsilon_d V_1 H_{21} + \epsilon_d V_2 H_{22} \end{aligned} \quad (5.5.7)$$

where the $H_{i,j}$ are now four constants which were computed in the above process. Since it turns out that $H_{12} = H_{21}$ as shown below, one can ignore H_{21} , $G_{21}(\mathbf{x})$, and $\partial_{n2}F_1(\mathbf{x})$ in the above set of calculations.

We now define some new constants $c_{i,j} = \epsilon_d H_{i,j}$ and write the above as

$$\begin{aligned} q_1 &= c_{11}V_1 + c_{12}V_2 \\ q_2 &= c_{21}V_1 + c_{22}V_2 . \end{aligned} \quad (5.5.8)$$

Comment: The coefficients $c_{i,j}$ are dimensionally capacitance, but they are a little strange. If we start off with the conductors holding charges q_1 and q_2 and then ground C_2 to the great circle (thin wire, $V_2=0$), and then measure V_1 relative to the great circle, we find that $V_1 = q_1/c_{11}$ and $q_2 = c_{21}V_1$. So c_{11} is the capacitance of C_1 *in the presence of* a grounded C_2 (which is not the same as the capacitance of C_1 in isolation). And c_{21} determines how much charge q_2 is "induced" onto C_2 by the presence of charged C_1 . Smythe (p 37) and Oughstun (p 23) refer to the $c_{i,j}$ both as "coefficients of capacitance" and "coefficients of induction". This should be distinguished from the notion of conductors C_1 and C_2 each having a "self-capacitance" (each in isolation) and having a "mutual capacitance" (to be called C below).

Writing the above pair of equations in matrix notation,

$$\begin{pmatrix} q_1 \\ q_2 \end{pmatrix} = \begin{pmatrix} c_{11} & c_{12} \\ c_{21} & c_{22} \end{pmatrix} \begin{pmatrix} V_1 \\ V_2 \end{pmatrix} \quad \text{or} \quad \mathbf{q} = \mathbf{c} \mathbf{V} \quad (5.5.9)$$

The c_{ij} are all known because they were computed above. Then invert to get

$$\begin{pmatrix} V_1 \\ V_2 \end{pmatrix} = \begin{pmatrix} s_{11} & s_{12} \\ s_{21} & s_{22} \end{pmatrix} \begin{pmatrix} q_1 \\ q_2 \end{pmatrix} \quad \text{or} \quad \mathbf{V} = \mathbf{s} \mathbf{q} \quad (5.5.10)$$

where matrix $s = c^{-1}$ is called the "mutual elastance" matrix by Smythe (p 36), and the "coefficients of potential" by Oughstun (p 21). Both authors deal with an arbitrary number of conductors.

The reader will not be surprised to learn that in general $c_{ij} = c_{ji}$ and $s_{ij} = s_{ji}$ so the matrices c and s are in fact symmetric matrices. Smythe shows this on pages 36-37 based on what he calls "Green's Reciprocation Theorem" on page 34 (George Green once again!). This theorem can be a lifesaver in certain electrostatic problems.

Now our problem as shown in Fig 5.3 is to compute the potential ϕ when C_1 has charge q and C_2 has charge $-q$. We then finally arrive at the appropriate values of V_1 and V_2 for our problem, which we said above were "to be determined". Here they are:

$$\begin{pmatrix} V_1 \\ V_2 \end{pmatrix} = \begin{pmatrix} s_{11} & s_{12} \\ s_{21} & s_{22} \end{pmatrix} \begin{pmatrix} q \\ -q \end{pmatrix} = q \begin{pmatrix} s_{11} & s_{12} \\ s_{21} & s_{22} \end{pmatrix} \begin{pmatrix} 1 \\ -1 \end{pmatrix} \quad (5.5.11)$$

so that

$$\begin{aligned} V_1 &= q (s_{11} - s_{12}) \\ V_2 &= q (s_{21} - s_{22}) \\ V &= V_1 - V_2 = q [s_{11} + s_{22} - 2s_{12}] \quad // s_{12} = s_{21} \text{ as noted above} \end{aligned} \quad (5.5.12)$$

Finally, here is the computed (inverse) capacitance of our transmission line section,

$$1/C = V/q = s_{11} + s_{22} - 2s_{12} .$$

But we know how to invert a simple 2x2 matrix ($T = \text{transpose}$, $\text{cof} = \text{cofactor}$, $\det(c) = |c|$)

$$s = c^{-1} = \text{cof}(c^T) / \det(c)$$

so that

$$s = \begin{pmatrix} s_{11} & s_{12} \\ s_{21} & s_{22} \end{pmatrix} = \begin{pmatrix} c_{22} & -c_{12} \\ -c_{21} & c_{11} \end{pmatrix} / \det(c) \quad (5.5.13)$$

Then

$$1/C = s_{11} + s_{22} - 2s_{12} = (c_{22} + c_{11} + 2c_{12})/\det(c) = \frac{c_{11} + c_{22} + 2c_{12}}{c_{11}c_{22} - c_{12}^2}$$

so

$$C = \frac{c_{11}c_{22} - c_{12}^2}{c_{11} + c_{22} + 2c_{12}} \quad (5.5.14)$$

Oughstun page 27 equation (27) verifies this result,

$$\boxed{C = \frac{c_{11}c_{22} - c_{12}^2}{c_{11} + c_{22} + 2c_{12}}} \quad (27)$$

for the mutual capacitance of a two conductor system.

Once C is known, K can be found from (4.12.24),

$$K = 4\pi\epsilon_d/C = 4\pi\epsilon_d \frac{c_{11} + c_{22} + 2c_{12}}{c_{11}c_{22} - c_{12}^2} \quad (5.5.15)$$

Thus, we have solved "The Capacitor Problem" to obtain K for the transmission line. The other line parameters are then given as in (4.12.24),

$$G = 4\pi\sigma_d/K \quad L_e = \frac{\mu_d}{4\pi} K$$

Statement of the capacitor problem in terms of φ_t

To show that our capacitor problem is the same as (5.4.3), we first quote the capacitor problem (5.5.1),

$$\nabla_{2D}^2 \varphi(x,y) = 0 \quad \varphi(C_1) - \varphi(C_2) = V \quad (5.5.1)$$

Then use (5.1.1) that $\varphi(x,y,z) = \frac{q(z)}{4\pi\epsilon} \varphi_t(x,y)$ to get

$$\nabla_{2D}^2 \varphi_t(x,y) = 0 \quad \frac{q(z)}{4\pi\epsilon} \varphi_t(C_1) - \frac{q(z)}{4\pi\epsilon} \varphi_t(C_2) = V$$

or

$$\nabla_{2D}^2 \varphi_t(x,y) = 0 \quad \varphi_t(C_1) - \varphi_t(C_2) = V \frac{4\pi\epsilon}{q(z)}$$

or

$$\nabla_{2D}^2 \varphi_t(x,y) = 0 \quad \varphi_t(C_1) - \varphi_t(C_2) = K$$

which is (5.4.3). In the last step we used (4.4.7) that $V(z) = \frac{q(z)}{4\pi\epsilon} K$. The potentials V_1 and V_2 are related to constants K_1 and K_2 by

$$V_1 = \frac{q(z)}{4\pi\epsilon} K_1 \quad V_2 = \frac{q(z)}{4\pi\epsilon} K_2 \quad (5.5.16)$$

Solution of the capacitor problem using φ_t

Here we just repeat the above analysis, showing how things differ. We leave out the words. The main differences are that the V_i are replaced by K_i and the factor $\frac{q(z)}{4\pi\epsilon}$ appears on the lines where n_i are computed. As before, K_1 and K_2 are initially unknown, but we find them in the end:

$$\begin{aligned}\varphi_t(x,y) &= - \oint_{C_1} ds' K_1 \partial_n g(x,y|x',y') - \oint_{C_2} ds' K_2 \partial_n g(x,y|x',y') \\ &= K_1 F_1(x,y) + K_2 F_2(x,y)\end{aligned}$$

$$E_n(x,y) = - \partial_{n1} \varphi = - \frac{q(z)}{4\pi\epsilon} \partial_{n1} \varphi_t(x,y) = \frac{q(z)}{4\pi\epsilon} \{ K_1 G_{11}(x) + K_2 G_{12}(x) \} \quad \mathbf{x} \text{ on } C_1$$

$$E_n(x,y) = - \partial_{n1} \varphi = - \frac{q(z)}{4\pi\epsilon} \partial_{n2} \varphi_t(x,y) = \frac{q(z)}{4\pi\epsilon} \{ K_1 G_{21}(x) + K_2 G_{22}(x) \} \quad \mathbf{x} \text{ on } C_2$$

$$n_1(x,y) = \epsilon E_n(x,y) = \frac{q(z)}{4\pi\epsilon} \epsilon K_1 G_{11}(x) + \frac{q(z)}{4\pi\epsilon} \epsilon K_2 G_{12}(x) \quad \mathbf{x} \text{ on } C_1$$

$$n_2(x,y) = \epsilon E_n(x,y) = \frac{q(z)}{4\pi\epsilon} \epsilon K_1 G_{21}(x) + \frac{q(z)}{4\pi\epsilon} \epsilon K_2 G_{22}(x) \quad \mathbf{x} \text{ on } C_2$$

$$q_1 = \oint_{C_1} ds' n_1(x',y') = \frac{q(z)}{4\pi\epsilon_d} [\epsilon_d K_1 H_{11} + \epsilon_d K_2 H_{21}] = \frac{q(z)}{4\pi\epsilon} [c_{11} V_1 + c_{12} V_2]$$

$$q_2 = \oint_{C_2} ds' n_2(x',y') = \frac{q(z)}{4\pi\epsilon_d} [\epsilon_d K_1 H_{21} + \epsilon_d K_2 H_{22}] = \frac{q(z)}{4\pi\epsilon} [c_{21} V_1 + c_{22} V_2]$$

$$\begin{pmatrix} q_1 \\ q_2 \end{pmatrix} = \frac{q(z)}{4\pi\epsilon_d} \begin{pmatrix} c_{11} & c_{12} \\ c_{21} & c_{22} \end{pmatrix} \begin{pmatrix} K_1 \\ K_2 \end{pmatrix} \quad \text{or} \quad \mathbf{q} = \frac{q(z)}{4\pi\epsilon_d} \mathbf{c} \mathbf{K}$$

$$\begin{pmatrix} K_1 \\ K_2 \end{pmatrix} = \frac{4\pi\epsilon_d}{q(z)} \begin{pmatrix} s_{11} & s_{12} \\ s_{21} & s_{22} \end{pmatrix} \begin{pmatrix} q_1 \\ q_2 \end{pmatrix} \quad \text{or} \quad \mathbf{K} = \frac{4\pi\epsilon_d}{q(z)} \mathbf{s} \mathbf{q}$$

$$\begin{pmatrix} K_1 \\ K_2 \end{pmatrix} = \frac{4\pi\epsilon_d}{q(z)} \begin{pmatrix} s_{11} & s_{12} \\ s_{21} & s_{22} \end{pmatrix} \begin{pmatrix} q(z) \\ -q(z) \end{pmatrix} = 4\pi\epsilon_d \begin{pmatrix} s_{11} & s_{12} \\ s_{21} & s_{22} \end{pmatrix} \begin{pmatrix} 1 \\ -1 \end{pmatrix}$$

$$K_1 = 4\pi\epsilon_d (s_{11} - s_{12})$$

$$K_2 = 4\pi\epsilon_d (s_{21} - s_{22})$$

$$K = K_1 - K_2 = 4\pi\epsilon_d [s_{11} + s_{22} - 2s_{12}]$$

so

$$K = 4\pi\epsilon_d \frac{c_{11} + c_{22} + 2c_{12}}{c_{11}c_{22} - c_{12}^2} \quad (5.5.17)$$

which is the same as (5.5.15).

For arbitrary conductor shapes, carrying out the Green's function program just outlined is quite difficult and usually requires expanding the Green's function in some complete set of eigenfunctions and then making various approximations. Perhaps conformal mapping is helpful in certain cases. Our main point is that the capacitor problem is a well-posed problem and has a solution value K . Numerical evaluations are always possible as noted earlier.

If the conductors are round, the problem can be solved *exactly* as we shall show in Chapter 6.

5.6 What happens if low-loss is not assumed?

We have seen how one can analyze a transmission line in the low-loss regime by studying the associated capacitor problem. The reader is reminded that the term low-loss does not mean no-loss! A low-loss transmission line does have losses, meaning it has attenuation. This attenuation is associated with the imaginary part of k as shown in (5.3.6) and as examined in Appendix Q. A specific attenuation example is presented in Appendix R for Belden 8281 cable, see Fig R.7. However, if losses are so great that the low-loss regime does not apply (the transmission line is "lossy"), the situation becomes much more complicated, and we address that case in a cursory manner below. Basically one cannot consider the transverse Helmholtz equation as a Laplace equation, so one cannot solve things in the capacitor electrostatics sense, and our rote formulas for K such as those derived in Chapter 6 (like $K = 2 \ln (a_2/a_1)$ for a coaxial cable) are no longer correct. It turns out that in the high-loss regime K must be determined by solving an unpleasant eigenvalue problem. One might argue that the high-loss regime is of little practical interest since practical transmission lines are always designed to be low-loss transmission lines.

Let's go back to our equation before the low-loss assumption that $Z_s \approx 0$,

$$\left[\nabla_{\mathbf{t}}^2 + \frac{j\omega Z_s 4\pi\epsilon_d}{K} \right] \varphi_{\mathbf{t}}(x,y) = 0 \quad \varphi_{\mathbf{t}}(C_1) = K/2 \quad \varphi_{\mathbf{t}}(C_2) = -K/2 \quad . \quad (5.3.10)$$

This is now a Helmholtz equation with Helmholtz parameter $\frac{j\omega Z_s 4\pi\epsilon_d}{K}$, whereas with $Z_s = 0$ we had the simpler Laplace Equation. Treating Z_s as some given value $\neq 0$, one could go ahead and find the Green's function for the above equation and it would be a function of K since K appears in the Helmholtz parameter. Call this Helmholtz Green's function $g_{\mathbf{K}}(x,y|x',y')$. We still have $\varphi = \frac{1}{4\pi\epsilon_d} q(z)$ $\varphi_{\mathbf{t}}$ being the full potential from which the electric field is obtained as $\mathbf{E}_{\mathbf{n}} = -\partial_{\mathbf{n}}\varphi$ [recall that transverse \mathbf{A} components are zero so this is consistent with $\mathbf{E} = -\text{grad } \varphi - \partial_{\mathbf{t}}\mathbf{A}$]. The solution of the above PDE system then starts off

$$\begin{aligned} \varphi_{\mathbf{t}}(x,y) &= - \oint_{C_1} ds' K_1 \partial_{\mathbf{n}} g_{\mathbf{K}}(x,y|x',y') - \oint_{C_2} ds' K_2 \partial_{\mathbf{n}} g_{\mathbf{K}}(x,y|x',y') \\ &= K_1 F_1(x,y,K) + K_2 F_2(x,y,K) \quad . \end{aligned} \quad (5.6.1)$$

From this point on, every function and constant acquires and argument K : $G_{i,j}(x,K)$, $H_{i,j}(K)$ and then $c_{i,j}(K)$. We end up then with

$$K = 4\pi\epsilon \frac{c_{11}(K) + c_{22}(K) + 2c_{12}(K)}{c_{11}(K)c_{22}(K) - [c_{12}(K)]^2} . \quad (5.6.2)$$

The new feature is that K appears on both sides of the last equation. This probably-complicated equation then has to be solved for K , and sometimes this is referred to as "an eigenvalue problem" for K . For example, if Z_s is very small but non-zero, one would expect the solution for K to be slightly different from the value obtained with $Z_s = 0$ and one could perhaps approach the problem using perturbation theory where the Helmholtz parameter is a "smallness parameter".

Recall that

$$k^2 = \beta_d^2 - j\omega Z_s 4\pi\xi_d / K \quad (5.3.8)$$

where now K is the "eigenvalue" of our solution above. If Z_s is very small but not zero, we end up then with

$$k = \beta_d - \Delta$$

where Δ is a small complex number. The longitudinal transmission line behavior of all z -dependent functions like ϕ , $A_{z,t}$, q , V , W , \mathbf{E} , \mathbf{B} is then given by (5.1.11),

$$\begin{aligned} q(z,t) &= q(z,t) = q(0) e^{j(\omega t - kz)} = q(0) e^{j(\omega t - [\beta_d - \Delta] z)} \\ &= q(0) e^{j(\omega t - [\beta_d - \text{Re}(\Delta)] z)} e^{-\text{Im}(\Delta) z} \end{aligned}$$

The real part of Δ causes a shift in the wavenumber k so the wave no longer propagates with the normal dielectric wavenumber β_d . Since $v = \omega/k$, one finds that the wave is "slowed down" due to the drag effect of the non-zero surface impedance of the conductors. The imaginary part of Δ then causes an exponential decay of the wave magnitude due to ohmic losses at the conductor surface. In our Chapter 2 analysis of the round wire we found that in general Z_s is itself complex, so computation of Δ is a somewhat complicated problem which we shall not attempt here (but see Appendix Q).

The problem of lossy transmission lines is usually approached using \mathbf{E} and \mathbf{B} fields, rather than potentials ϕ and A_z , and the analysis is then similar to the way waveguides in general are treated. Due to the skin effect, the \mathbf{E} and \mathbf{B} fields penetrate a distance $\sim\delta$ into the conductor surfaces and this results in ohmic losses and a "drag" on the propagating wave. In this approach, one ends up again with an eigenvalue problem to solve, not directly for K but for some other related parameter like k .

In the 12-page Section 4.5 of his book (p 106), Matick studies a lossy-transmission line in the simplest possible case which is a strip geometry whose gap S is small compared to the width, and whose metal strips are much thicker than the skin depth δ . His parameter γ is related to our parameter k by $\gamma = jk$, and his longitudinal direction is x instead of our z . He ends up with a transcendental "eigenvalue equation" (4-66) for γ , but if loss is very small, he can approximately solve for γ with these results [$\beta_d = \omega \sqrt{\mu_d \epsilon_d}$]

$$\text{Im}(\gamma) = \beta_a(1+\delta/2S) \qquad \text{Re}(\gamma) = \beta_a (\delta/2S) \qquad // \text{ Matick (4-75,76,77) p 115}$$

which with $\gamma = jk$ we translate to

$$\text{Im}(k) = -\text{Re}(\gamma) = -\beta_a (\delta/2S)$$

$$\text{Re}(k) = \text{Im}(\gamma) = \beta_a(1+\delta/2S)$$

$$k = \beta_a(1+\delta/2S) - j \beta_a (\delta/2S) = \beta_a [1 + (\delta/2S) + j(\delta/2S)]$$

so

$$\Delta = \beta_a[(\delta/2S) + j(\delta/2S)] .$$

Thus, for such a thick strip transmission line, the longitudinal dependence of all functions has this form,

$$\begin{aligned} q(z,t) &= e^{j(\omega t - [\beta_a - \text{Re}(\Delta)]z)} e^{-\text{Im}(\Delta)z} \\ &= e^{j(\omega t - [\beta_a + \delta/2S]z)} e^{-(\delta/2S)z} \end{aligned}$$

which shows the exponential loss factor and an increased wavenumber $\beta + \delta/2S$ which corresponds to a decreased wavelength λ and a decreased wave velocity $v = \omega/k = \omega\lambda/2\pi = f\lambda$, the "drag effect".

Matick has an erratum in this section which is a bit confusing, so we repair it right here. His equation (4-50) p 110 should read (in his notation)

$$\nabla^2 \mathbf{E} = \left(\frac{\partial^2 E_x}{\partial x^2} + \frac{\partial^2 E_x}{\partial z^2} \right) \hat{\mathbf{x}} + \left(\frac{\partial^2 E_z}{\partial x^2} + \frac{\partial^2 E_z}{\partial z^2} \right) \hat{\mathbf{z}} = (j\omega\mu\sigma - \omega^2\mu\epsilon)(E_x \hat{\mathbf{x}} + E_z \hat{\mathbf{z}}) \qquad \text{Matick (4-50)}$$

Chapter 6: Two Cylindrical Conductors

6.1 A candidate transverse potential ϕ_{t}

In Sections 5.3 (b) and 5.4 (b) we showed that the transverse potential of a 2-conductor balanced transmission line must have this form when viewed from far away,

$$\phi_{\text{t}}(\mathbf{x}) \approx \ln(s_2^2/s_1^2) \quad // \text{ limiting form as point } \mathbf{x} = (x,y) \text{ moves far from the conductors} \quad (5.3.13)$$

$$\begin{aligned} s_1^2 &= (x-x_1)^2 + (y-y_1)^2 = |\mathbf{x} - \mathbf{x}_1|^2 \\ s_2^2 &= (x-x_2)^2 + (y-y_2)^2 = |\mathbf{x} - \mathbf{x}_2|^2 \end{aligned} \quad (6.1.1)$$

where the points \mathbf{x}_1 and \mathbf{x}_2 are the "center of charge" points for the C_1 and C_2 conductor cross sections.

Suppose now we take, as a candidate dimensionless transverse potential ϕ_{t} , *exactly* the above limiting expression. Our candidate ϕ_{t} is

$$\phi_{\text{t}}(\mathbf{x}) = \ln(s_2^2/s_1^2) . \quad \text{for all values of } \mathbf{r}, \text{ close and far} \quad (6.1.2)$$

where we specify the center of charge points to be $\mathbf{x}_1 = (d,0)$ and $\mathbf{x}_2 = (-d,0)$.

Certainly this meets the limiting form boundary condition (5.3.13)! We know also that this potential is a valid solution of the 2D Laplace equation, since $\ln(s_1)$ and $\ln(s_2)$ are each valid solutions. This fact was shown at the start of Section 5.4 (b). Since $-2\pi\ln s_1$ is the 2D free-space propagator, it follows that $-2\pi\ln s_1$ is a solution of $\nabla_{2D}^2(\phi) = 0$ away from the point where $s_1 = 0$, and then so is $\ln s_1$. Then by superposition, $2\ln s_2 - 2\ln s_1$ is also a valid solution, and thus so is $\ln(s_2^2/s_1^2)$. Thus, ϕ_{t} is a valid candidate for a lossless transmission line since ϕ_{t} satisfies the 2D Laplace equation according to (5.4.3),

$$\nabla_{\text{t}}^2 \phi_{\text{t}}(x,y) = 0 \quad \phi_{\text{t}}(C_1) = K_1 \quad \phi_{\text{t}}(C_2) = K_2 \quad K_1 - K_2 = K . \quad (5.4.3)$$

The question then becomes: what are the surfaces C_i in 2D space on which this candidate ϕ_{t} is a constant? Such surfaces can then serve as possible conductor cross sections for a transmission line.

6.2 Ancient Greece circa 230 BC

Apollonius of Perga (262BC-190BC) [like Joe of Chicago] was a pretty smart guy as wiki explains. He did astronomy and therefore he did geometry. Besides giving conic sections their current names and writing eight books about them, he learned about what are now called the Apollonian Circles. These circles form the "level surfaces" for 2D bipolar (orthogonal) coordinates as shown in this picture,

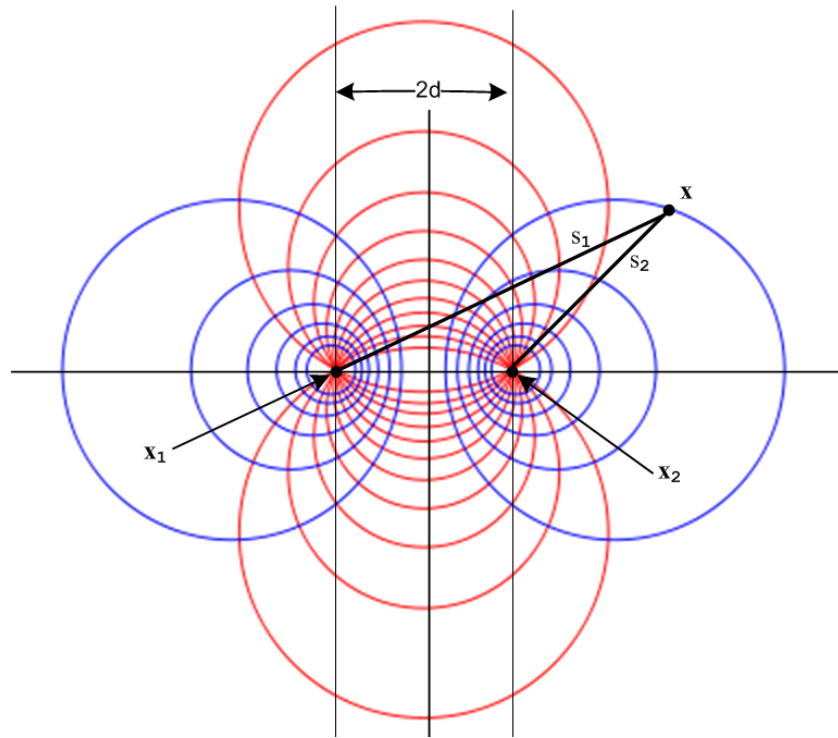


Fig 6.1

http://en.wikipedia.org/wiki/Apollonian_circles

When this picture is rotated around its vertical axis, the blue level circles become toroids and one then arrives at 3D toroidal coordinates, but that is another story. Our interest is in the 2D blue circles.

It turns out, as the reader may suspect, that the blue circles have the following simple property,

$$s_2/s_1 = \text{constant} ,$$

which we shall prove in a moment. Calling this constant e^{-B} we get

$$s_2/s_1 = e^{-B} \quad \Rightarrow \quad \ln(s_2/s_1) = -B . \quad (6.2.1)$$

Thus, since $\varphi_t(\mathbf{x}) = \ln(s_2^2/s_1^2) = 2 \ln(s_2/s_1)$, the blue circles are candidate equipotential surfaces for our potential $\varphi_t(\mathbf{x})$.

To show that $s_2/s_1 = e^{-B}$ describes a circle, consider:

$$|\mathbf{x}-\mathbf{x}_2| / |\mathbf{x}-\mathbf{x}_1| = e^{-B}$$

$$|\mathbf{x}-\mathbf{x}_2|^2 = e^{-2B} |\mathbf{x}-\mathbf{x}_1|^2$$

$$(x-x_2)^2 + (y-y_2)^2 = e^{-2B} [(x-x_1)^2 + (y-y_1)^2] .$$

This equation has the following form

$$A(x^2 + y^2) + Bx + Cy + D = 0 \quad A = (1 - e^{-2B})$$

or

$$x^2 + y^2 + \alpha x + \beta y + \gamma = 0 .$$

One can then "complete the squares" to obtain the equation of a circle of radius r centered at (x_c, y_c) ,

$$(x - x_c)^2 + (y - y_c)^2 = r^2$$

$$\text{where} \quad -2x_c = \alpha \quad -2y_c = \beta \quad x_c^2 + y_c^2 - r^2 = \gamma . \quad (6.2.2)$$

For the particular locations of x_1 and x_2 shown in Fig 6.1 one has

$$\begin{aligned} x_1 = -d \quad x_2 = d \quad y_1 = y_2 = 0 \\ s_1^2 = (x+d)^2 + y^2 \quad s_2^2 = (x-d)^2 + y^2 \end{aligned} \quad (6.2.3)$$

so

$$s_2/s_1 = e^{-B} \Rightarrow s_1/s_2 = e^B \Rightarrow e^{2B} s_2^2 = s_1^2 \Rightarrow (e^B/2) s_2^2 = (e^{-B}/2) s_1^2 \Rightarrow$$

$$(e^B/2) [x^2 - 2dx + d^2 + y^2] = (e^{-B}/2) [x^2 + 2dx + d^2 + y^2]$$

$$\text{sh}B (x^2 + d^2 + y^2) + \text{ch}B(-2dx) = 0 \quad // \quad \text{sh}B = (e^B - e^{-B})/2, \text{ch}B = (e^B + e^{-B})/2$$

$$(x^2 + d^2 + y^2) + \text{coth}B (-2dx) = 0$$

$$x^2 - 2d x \text{coth}B + y^2 = -d^2$$

$$x^2 - 2d x \text{coth}B + d^2 \text{coth}^2 B + y^2 = -d^2 + d^2 \text{coth}^2 B \quad // \text{complete the square}$$

$$(x - d \text{coth}B)^2 + y^2 = d^2 \text{csch}^2 B . \quad (6.2.4)$$

We conclude that our blue equipotential circles have this simple form

$$(x - x_c)^2 + y^2 = r^2 \quad x_c = d \text{coth}B \quad r = |d \text{csch}B| . \quad (6.2.5)$$

Using $d = 5$, here is a plot of these circles for 10 different B values:

```

restart; with(plots):with(plottools):
xc := d*coth(B):
r := d*csch(B):
d := 5:
Bvals := [-3,-2,-1.5,-1,-.75,.75,1,1.5,2,3]:N := nops(Bvals):
for n from 1 to N do
  B := Bvals[n];
  c[n] := circle([xc,0],r);
od:
display(seq(c[n],n=1..N),color=blue,scaling = constrained,thickness=2);

```

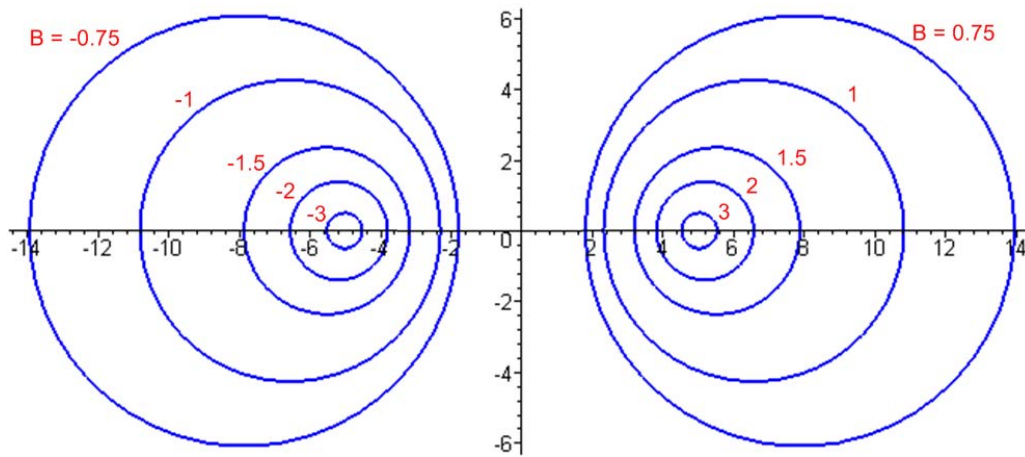


Fig 6.2

Since $x_c = d \coth B$, the right side circles have $B > 0$ while the left side have $B < 0$. The value $B = 0$ corresponds to the vertical y axis, while $B = \pm\infty$ correspond to the two focal points at $d = \pm 5$.

6.3 Back to the Future: Calculation of K

Let C_2 to be a circle on the right side, so that $B_2 > 0$.

For C_1 select a second circle from either the left or the right, so B_1 can have either sign.

If one selects C_1 from the left side, one has a two-wire transmission line (dielectric = gray),

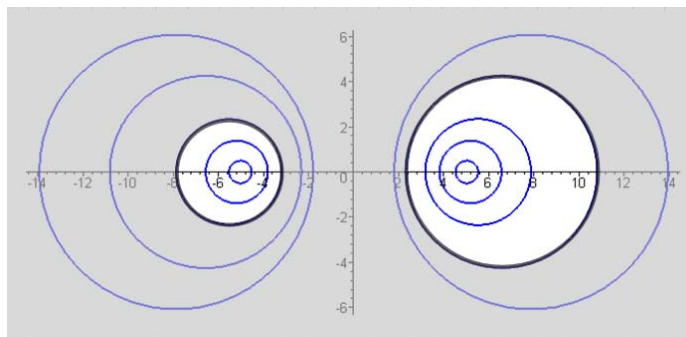


Fig 6.3

If one selects C_2 from the right, one has an off-center coaxial transmission line,

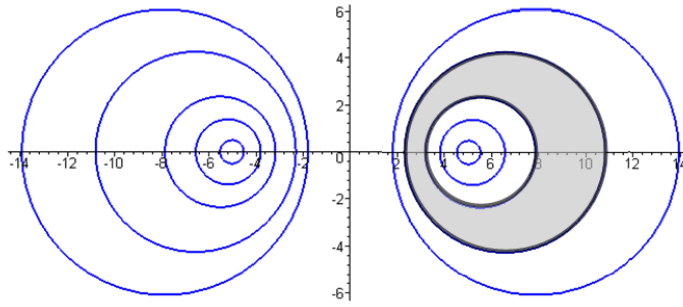


Fig 6.4

Fig 6.3 shows a transmission line cross section where the two conductors are round wires with unequal radii a_1 and a_2 . Treated as a 2D capacitor, one's intuition at least suggests that the two focal points might be the conductor "centers of charge". The gray dielectric is of course outside the two conductors and it is possible to select a point in the dielectric that is "far away" from both conductors, so our limiting form discussion applies and the points \mathbf{x}_1 and \mathbf{x}_2 should be the centers of charge.

Figure 6.4 shows an off-center coaxial transmission line for which the dielectric is the region between the two black circles. In this case, one cannot take a point in the dielectric that is "far away" from both conductors, so the limiting form discussion does not apply. Here it appears that both conductors have the same center of charge located at \mathbf{x}_2 .

We shall now determine K and therefore the 2D capacitance $C = 4\pi\epsilon/K$ for the above cases.

Let $\sigma_1 = \text{sign}(B_1)$. Then from (6.1.2) and (6.2.1),

$$\begin{aligned}\varphi_{\mathbf{t}}(\mathbf{x}) &= \ln(s_2^2/s_1^2) = 2 \ln(s_2/s_1) \\ \varphi_{\mathbf{t}}(C_1) &= 2 \ln(s_2/s_1)|^{C_1} = -2B_1 \\ \varphi_{\mathbf{t}}(C_2) &= 2 \ln(s_2/s_1)|^{C_2} = -2B_2.\end{aligned}\tag{6.3.1}$$

Recall from (5.1.3) that $\varphi_{\mathbf{t}}(C_1) - \varphi_{\mathbf{t}}(C_2) = K$. Therefore,

$$K = 2(B_2 - B_1) = 2(|B_2| - \sigma_1|B_1|).\tag{6.3.2}$$

Knowing K , one knows C , G and L_e for the transmission line from box (4.12.24).

We must now do some slightly painful algebra. First, we know from (6.2.5) that

$$\begin{aligned}a_1 &= d |\text{csch}B_1| \quad \Rightarrow \quad (d/a_1) = \text{sh}(|B_1|) \quad \Rightarrow \quad |B_1| = \text{sh}^{-1}(d/a_1) \\ a_2 &= d |\text{csch}B_2| \quad \Rightarrow \quad (d/a_2) = \text{sh}(|B_2|) \quad \Rightarrow \quad |B_2| = \text{sh}^{-1}(d/a_2).\end{aligned}\tag{6.3.3}$$

The separation of the centers of the two round wires is b , where, again using (6.2.5),

$$b = |x_{c2} - x_{c1}| = |d \coth B_2 - d \coth B_1| = d |\coth B_2 - \coth B_1|.\tag{6.3.4}$$

From (6.3.2) one has

$$\begin{aligned}
 \text{ch}(K/2) &= \text{ch} [|B_2| - \sigma_1 |B_1|] \\
 &= \text{ch}|B_2| \text{ch}|B_1| - \sigma_1 \text{sh}|B_2| \text{sh}|B_1| \\
 &= \sqrt{1+\text{sh}^2 B_2} \sqrt{1+\text{sh}^2 B_1} - \sigma_1 \text{sh}|B_2| \text{sh}|B_1| \\
 &= \sqrt{1+(d/a_2)^2} \sqrt{1+(d/a_1)^2} - \sigma_1 (d/a_2) (d/a_1) .
 \end{aligned} \tag{6.3.5}$$

Meanwhile,

$$\begin{aligned}
 b &= d |\coth B_2 - \coth B_1| = |d [\text{ch} B_2 / \text{sh} B_2 - \text{ch} B_1 / \text{sh} B_1]| = |d [\text{ch}|B_2| / \text{sh}|B_2| - \sigma_1 \text{ch}|B_1| / \text{sh}|B_1|]| \\
 &= |d [\text{ch}|B_2| \text{sh}|B_1| - \sigma_1 \text{ch}|B_1| \text{sh}|B_2|] / \text{sh}|B_1| \text{sh}|B_2|| \\
 &= |d [\sqrt{1+(d/a_2)^2} (d/a_1) - \sigma_1 \sqrt{1+(d/a_1)^2} (d/a_2)] / (d/a_2) (d/a_1)| \\
 &= |[\sqrt{1+(d/a_2)^2} (1/a_1) - \sigma_1 \sqrt{1+(d/a_1)^2} (1/a_2)] / (1/a_2) (1/a_1)| \\
 &= |[a_2 \sqrt{1+(d/a_2)^2} - \sigma_1 a_1 \sqrt{1+(d/a_1)^2}]| .
 \end{aligned} \tag{6.3.6}$$

Square this to get

$$\begin{aligned}
 b^2 &= a_2^2 [1+(d/a_2)^2] + a_1^2 [1+(d/a_1)^2] - 2\sigma_1 a_1 a_2 \sqrt{1+(d/a_2)^2} \sqrt{1+(d/a_1)^2} \\
 \text{so} \\
 2\sigma_1 a_1 a_2 \sqrt{1+(d/a_2)^2} \sqrt{1+(d/a_1)^2} &= a_2^2 [1+(d/a_2)^2] + a_1^2 [1+(d/a_1)^2] - b^2 \\
 &= a_2^2 + d^2 + a_1^2 + d^2 - b^2 = a_1^2 + a_2^2 + 2d^2 - b^2 .
 \end{aligned}$$

The purpose of doing all this work is to obtain the following expression for the radical product,

$$\sqrt{1+(d/a_2)^2} \sqrt{1+(d/a_1)^2} = (a_1^2 + a_2^2 + 2d^2 - b^2) / (2\sigma_1 a_1 a_2) . \tag{6.3.7}$$

Install this into expression (6.3.5) above for $\text{ch}(K/2)$ to get

$$\begin{aligned}
 \text{ch}(K/2) &= \sqrt{1+(d/a_2)^2} \sqrt{1+(d/a_1)^2} - \sigma_1 (d/a_2) (d/a_1) \\
 &= (a_1^2 + a_2^2 + 2d^2 - b^2) / (2\sigma_1 a_1 a_2) - 2d^2 / (2\sigma_1 a_2 a_1) \\
 &= (a_1^2 + a_2^2 - b^2) / (2\sigma_1 a_2 a_1) = \sigma_1 (1/2) (a_1^2 + a_2^2 - b^2) / (a_1 a_2)
 \end{aligned}$$

$$= \sigma_1 (1/2) [(a_1/a_2) + (a_2/a_1) - (b^2/a_1 a_2)] \quad (6.3.8)$$

and the focal distance d has vanished from the $\text{ch}(K/2)$ expression. Therefore

$$K = 2 \text{ch}^{-1} \{ \sigma_1 (1/2) [(a_1/a_2) + (a_2/a_1) - (b^2/a_1 a_2)] \} . \quad (6.3.9)$$

Notice that the result is symmetric under $a_1 \leftrightarrow a_2$.

We now distinguish our two cases of interest. For the unequal twin-lead type transmission line of Fig 6.3 we know that $B_1 < 0$ since the C_1 circle is on the left, so $\sigma_1 = \text{sign}(B_1) = -1$ and then

$$K = 2 \text{ch}^{-1} \{ (1/2) [(b^2/a_1 a_2) - (a_1/a_2) - (a_2/a_1)] \} \quad // \text{ Fig 6.3} \quad (6.3.10)$$

which is an amazingly simple result. Recall from (4.4.16) that

$$Z_0 = (K / \sqrt{\epsilon_{re1}}) 30 \Omega \quad (4.4.16)$$

so then

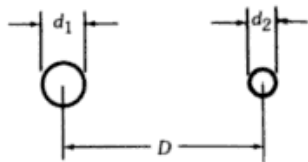
$$Z_0 = \text{ch}^{-1} \{ (1/2) [(b^2/a_1 a_2) - (a_1/a_2) - (a_2/a_1)] \} (1/\sqrt{\epsilon_{re1}}) 60 \Omega . \quad (6.3.11)$$

If the wires have diameters $d_1 = 2a_1$ and $d_2 = 2a_2$ this becomes

$$Z_0 = \text{ch}^{-1} \{ (1/2) [(4b^2/d_1 d_2) - (d_1/d_2) - (d_2/d_1)] \} (1/\sqrt{\epsilon_{re1}}) 60 \Omega . \quad (6.3.12)$$

For verification, we quote again from Reference RDE page 29-23,

N. Balanced 2-wire—unequal diameters



$$Z_0 = (60/\epsilon^{1/2}) \cosh^{-1} N$$

$$N = \frac{1}{2} [(4D^2/d_1 d_2) - (d_1/d_2) - (d_2/d_1)]$$

where our b is their D .

On the other hand, if we are interested in an off-center coaxial transmission line as in Fig 6.4, we select C_1 from the right side of Fig 6.2 and then $\sigma_1 = \text{sign}(B_1) = +1$ and we find

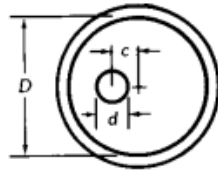
$$K = 2 \operatorname{ch}^{-1} \left\{ (1/2) \left[(a_1/a_2) + (a_2/a_1) - (b^2/a_1a_2) \right] \right\} \quad // \text{ Fig 6.4} \quad (6.3.13)$$

$$Z_0 = \operatorname{ch}^{-1} \left\{ (1/2) \left[(a_1/a_2) + (a_2/a_1) - (b^2/a_1a_2) \right] \right\} (1/\sqrt{\epsilon_{re1}}) 60 \Omega \quad (6.3.14)$$

$$Z_0 = \operatorname{ch}^{-1} \left\{ (1/2) \left[(d_1/d_2) + (d_2/d_1) - (4b^2/d_1d_2) \right] \right\} (1/\sqrt{\epsilon_{re1}}) 60 \Omega \quad (6.3.15)$$

For verification, we quote again from Reference RDE page 29-24,

U. Eccentric line



$$Z_0 = (60/\epsilon^{1/2}) \cosh^{-1} U$$

$$U = \frac{1}{2} [(D/d) + (d/D) - (4c^2/dD)]$$

where we may take $d =$ our d_1 and $D =$ our d_2 and $c =$ our $b =$ the center-line separation.

One more case of interest falls out from this analysis. Taking $B_1 = 0$ we have

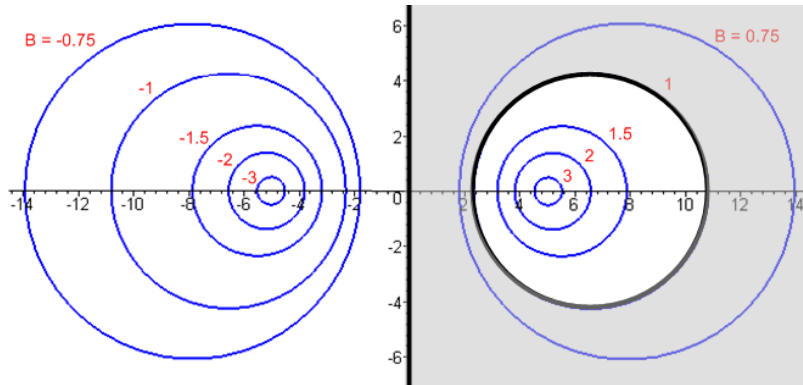


Fig 6.5

which is a transmission line consisting of a round wire above an infinite flat plane. This is a tricky limit of (6.3.10) where both $a_1 \rightarrow \infty$ and $b \rightarrow \infty$, so we ignore (6.3.10) and work from scratch. Since $B_1 = 0$ one finds from (6.3.2) that

$$K = 2B_2 \quad (6.3.16)$$

But from (6.2.5),

$$\begin{aligned} x_{2c} &= d \coth B_2 = d \operatorname{ch} B_2 / \operatorname{sh} B_2 \\ a_2 &= d / \operatorname{sh}(B_2) . \end{aligned} \quad (6.3.17)$$

Therefore

$$x_{2c}/a_2 = \operatorname{ch} B_2 \quad \Rightarrow \quad B_2 = \operatorname{ch}^{-1}(x_{2c}/a_2) \quad \Rightarrow \quad K = 2 \operatorname{ch}^{-1}(x_{2c}/a_2) . \quad (6.3.18)$$

Here x_{2c} is the distance from the wire *center line* to the ground plane. Calling this h and the wire radius a , we get the following extremely simple and exact result,

$$\begin{aligned} K &= 2 \operatorname{ch}^{-1}(h/a) && // \text{ wire radius } a \text{ with center } h \text{ over ground plane, exact} \\ Z_0 &= (K / \sqrt{\epsilon_{re1}}) 30 \Omega = \operatorname{ch}^{-1}(h/a) (1/\sqrt{\epsilon_{re1}}) 60 \Omega \end{aligned} \quad (6.3.19)$$

where one must have $h > a$ to keep the wire from touching the ground plane. Using the identity $\operatorname{ch}^{-1}x = \ln(x + \sqrt{x^2 - 1})$ for $x \geq 1$, one can write the above as

$$\begin{aligned} K &= 2 \ln [(h/a) + \sqrt{(h/a)^2 - 1}] && // \text{ wire radius } a \text{ with center } h \text{ over ground plane, exact} \\ Z_0 &= \ln [(h/a) + \sqrt{(h/a)^2 - 1}] (1/\sqrt{\epsilon_{re1}}) 60 \Omega . \end{aligned} \quad (6.3.20)$$

For $h \gg a$ this becomes ("thin wire")

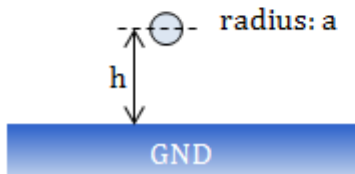
$$\begin{aligned} K &= 2 \ln(2h/a) && // \text{ wire radius } a \text{ center } h \text{ over ground plane, } h \gg a \\ Z_0 &= \ln(2h/a) (1/\sqrt{\epsilon_{re1}}) 60 \Omega . \end{aligned} \quad (6.3.21)$$

For verification, we found the following web offering (where log means ln),

The characteristic impedance of a wire over a ground plane:

$$Z_0 = \frac{1}{2\pi} \sqrt{\frac{\mu}{\epsilon}} \log \left(\frac{h}{a} + \sqrt{\left(\frac{h}{a}\right)^2 - 1} \right) \cong \frac{1}{2\pi} \sqrt{\frac{\mu}{\epsilon}} \log \left(\frac{2h}{a} \right) \quad (a \ll h)$$

$$\frac{1}{2\pi} \sqrt{\frac{\mu}{\epsilon}} \cong \frac{60[\Omega]}{\sqrt{\epsilon_r}}$$



http://members3.jcom.home.ne.jp/zakii/tline_e/14_microstripline_z0.htm

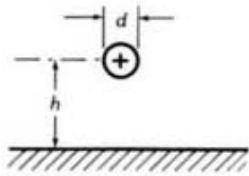
which results are derived using an image method to handle the ground plane.

For some odd reason, our usual RDE source on this subject only gives the result for $h \gg a$. Taking d to be the wire diameter,

$$\begin{aligned} Z_0 &= \ln(4h/d) (1/\sqrt{\epsilon_{re1}}) 60 \Omega \\ &= \ln(10) \log(4h/d) (1/\sqrt{\epsilon_{re1}}) 60 \Omega \\ &\approx \log(4h/d) (1/\sqrt{\epsilon_{re1}}) 138.2 \Omega \end{aligned} \quad (6.3.22)$$

which then compare to RDE p 29-22 ,

G. Single wire, near ground



For $d \ll h$

$$Z_0 = (138/\epsilon^{1/2}) \log_{10}(4h/d)$$

Reader Exercise: Given $\varphi(\mathbf{x}) = \ln(s_2^2/s_1^2)$, compute $\mathbf{E} = -\nabla\varphi$, compute $E_n = \mathbf{E} \cdot \hat{\mathbf{n}}$ as the normal electric field at the surface of C_2 , compute $n = \epsilon_d E_n$ as the charge density on C_2 , then using that n , find the "center of charge" $\langle x \rangle = [\int_{C_2} ds \, x \, n(\mathbf{x}) / \int_{C_2} ds \, n(\mathbf{x})]$ and see if $\langle x \rangle = d$. Decide whether or not it is worth while learning how to work in bipolar coordinates to carry out this exercise. [The solution to this exercise appears in the author's *Bipolar Coordinates* document, see References. See also Section 6.5 below.]

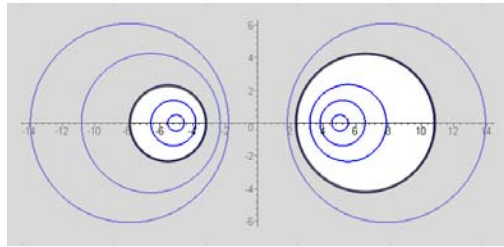
6.4 Summary of Line Parameter Results

Summary for Transmission Line with Two Round Conductors (6.4.1)

Identities: $\text{ch}^{-1}x = \ln(x + \sqrt{x^2 - 1})$, $x \geq 1$ $\text{ch}^{-1}x \approx \ln(2x)$, $x \gg 1$
 $\text{ch}^{-1}\left[\frac{1}{2}\left(\frac{b}{a} + \frac{a}{b}\right)\right] = \ln \frac{b}{a}$ $b > a > 0$ (4.6.6)

Line Properties: $C = 4\pi\epsilon_d/K$, $G = 4\pi\sigma_d/K$, $L_e = \frac{\mu_d}{4\pi} K$ $\epsilon_d, \sigma_d, \mu_d$ for dielectric (4.12.24)

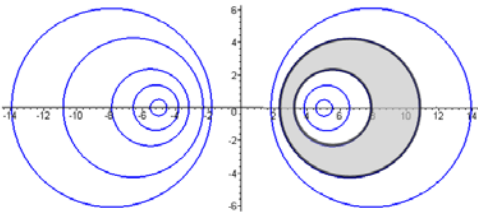
dielectric is gray



Special case $a_1 = a_2 = a$:
 Special case $b \gg a_1, a_2$:
 Special case $b \gg a_1 = a_2 = a$:

$$K = 2 \text{ch}^{-1} \left\{ \frac{1}{2} \left[\frac{b^2}{a_1 a_2} - \left(\frac{a_1}{a_2} \right) - \left(\frac{a_2}{a_1} \right) \right] \right\}$$

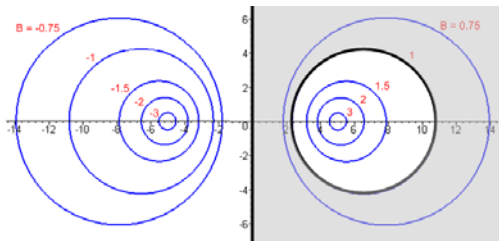
$a_i = \text{radii}$ $b = \text{center separation}$
 $K = 2 \text{ch}^{-1} \left[\frac{b^2}{2a^2} - 1 \right]$ (twin-lead)
 $K = 4 \ln(b/\sqrt{a_1 a_2})$
 $K = 4 \ln(b/a)$



Special case $b = 0$ and $a_2 > a_1$:

$$K = 2 \text{ch}^{-1} \left\{ \frac{1}{2} \left[\left(\frac{a_1}{a_2} \right) + \left(\frac{a_2}{a_1} \right) - \frac{b^2}{a_1 a_2} \right] \right\}$$

$a_i = \text{radii}$ $b = \text{center separation}$
 $K = 2 \ln(a_2/a_1)$ (centered coaxial)



Special case $h \gg a$:

$$K = 2 \text{ch}^{-1}(h/a) = 2 \ln \left[\frac{h}{a} + \sqrt{\left(\frac{h}{a} \right)^2 - 1} \right]$$

$a = \text{radius}$ $h = \text{height of center over plane}$
 $K = 2 \ln(2h/a)$ (thin wire)

6.5. The Proximity Effect for a Transmission Line made of Two Round Wires

This effect is discussed qualitatively in Appendix P in terms of eddy currents, and we quote the following Figure P.13,

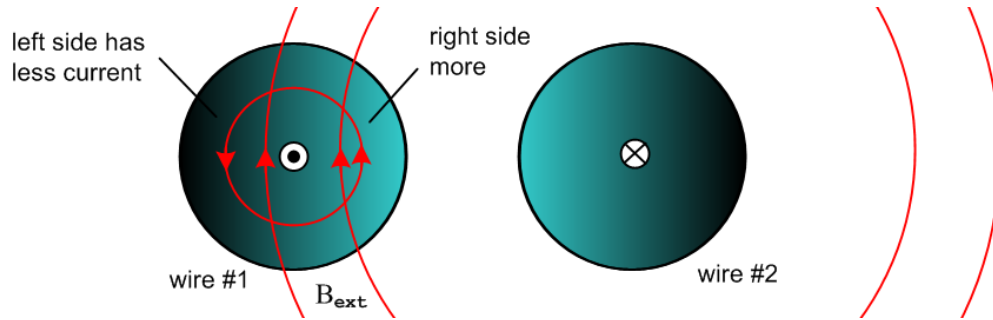


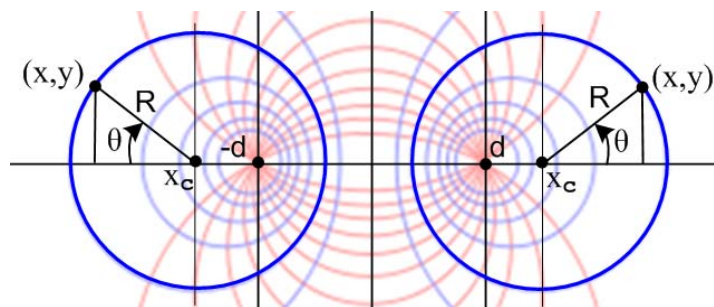
Fig 6.6

The effect is that for $\omega > 0$ the current density J_z is not uniform in the conductor cross sections but is larger on the side of each conductor which faces the other conductor.

In this section we shall compute J_z over the wire cross section and perimeter to get a quantitative result.

(a) The surface charge density and its moments

On either of the conductors shown above there is some surface charge density $n(\theta)$ which has moments called N_m and η_m in Appendix D. Using the electro-quasi-static model for a transmission line, one can analyze the transmission line as if it were an electrostatics capacitor problem: the two cylinders form a capacitor (per unit length). If one assumes a potential V between the conductors, one can solve the Laplace equation to get the potential ϕ in the dielectric between the conductors, which ϕ will be constant on the surface of either conductor. From this one may compute the electric field in the dielectric, and from the electric field just above the conductor surfaces one can compute $n(\theta)$. This calculation is carried out in our (downloadable) document *Bipolar Coordinates and the Two-Cylinder Capacitor* from which we quote results below. Each cylinder of the transmission line is characterized by a certain value of B as shown in Fig 6.2. In *Bipolar* B is called ξ which is one of the bipolar coordinates (ξ, u) . The angle θ is measured as indicated in this figure taken from *Bipolar*, which happens to show the two cylinders having the same radius:

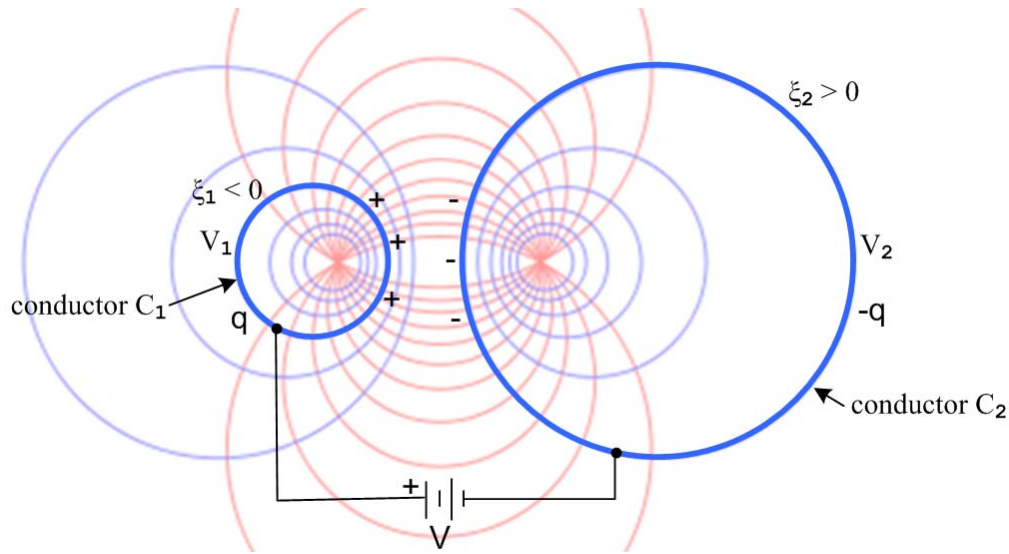


Bipolar (7.1) Fig 6.7

Notice that the two bipolar "focal points" are at $x = \pm d$, while the radii of the left and right cylinders we shall call a_1 and a_2 . In *Bipolar* these parameters d , a_1 , a_2 are called a , R_1 , R_2 .

Comment: It is shown in *Bipolar* Section 10 (d) that the "center of charge" for the surface charge distribution $n(\theta)$ is in fact the focal point for each conductor.

Here is the more general picture where the cylinders have different radii. The right cylinder has bipolar coordinate $\xi_2 > 0$ and the left has $\xi_1 < 0$



Bipolar (10.2)

Fig 6.8

The angular surface charge densities on the conductors are found to be (Cou/m),

$$\begin{aligned} n_1(\xi_1, \theta) &= \frac{q}{2\pi} \frac{|\operatorname{sh}\xi_1|}{\operatorname{ch}\xi_1 + \cos\theta} \\ n_2(\xi_2, \theta) &= -\frac{q}{2\pi} \frac{|\operatorname{sh}\xi_2|}{\operatorname{ch}\xi_2 + \cos\theta} \end{aligned} \quad \text{Bipolar (10.28)} \quad (6.5.1)$$

where q is

$$q = 2\pi\epsilon_a \frac{V}{\xi_2 - \xi_1} \quad \text{Bipolar (10.15)} \quad (6.5.2)$$

and ϵ_a is for the dielectric between the conductors. Here q is the charge per unit length in z on the left conductor so has dimensions Cou/m. The surface charge density n_1 is normalized so $\int n_1(\theta)d\theta = q$ so the dimensions of n_1 are Cou/m. The true charge density is $n_1(\theta) = n_1(\theta)/a_1$ Cou/m².

The capacitance per unit length is then

$$C = q/V = 2\pi\epsilon_d \frac{1}{\xi_2 - \xi_1} . \quad \dim(\epsilon_d) = \text{farad/m} \quad \text{Bipolar (10.16)} \quad (6.5.3)$$

This is in agreement with (6.3.2) which says $K = 2(B_2 - B_1) = 2(\xi_2 - \xi_1)$ and (4.12.24) that $C = 4\pi\epsilon_d/K$.

Notice that for fixed q the charge distribution on each conductor is independent of the ξ value of the other conductor. Thus, if the battery in Fig 6.8 is disconnected (to maintain a constant q), $n_1(\xi_1, \theta)$ does not change if ξ_2 is varied.

Using (D.1.5b) the moments of the surface charge distribution $n_1(\xi_1, \theta)$ are computed in *Bipolar* Appendix A and are found to be,

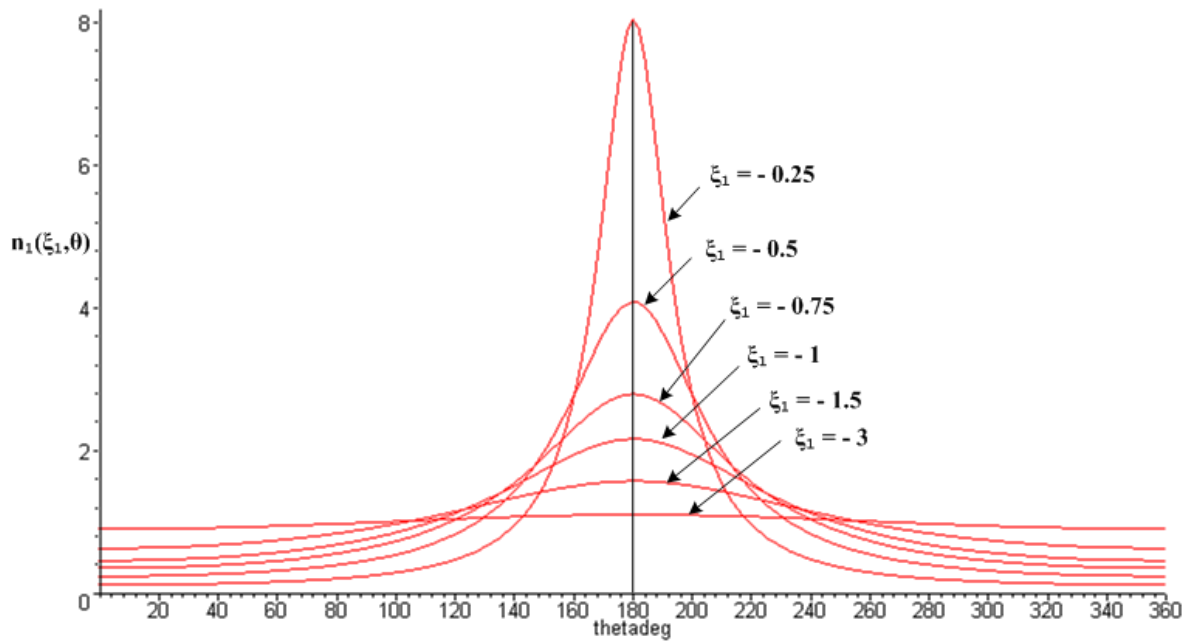
$$\eta_m \equiv N_m/N_0 = (-1)^m e^{-|m\xi_1|} . \quad \text{Bipolar (A.12)} \quad (6.5.4)$$

Using (D.1.5a) one then finds,

$$n_1(\xi_1, \theta) = (q/2\pi) \left[1 + 2 \sum_{m=1}^{\infty} (-1)^m e^{-m|\xi_1|} \cos(m\theta) \right] . \quad \text{Bipolar (A.13)} \quad (6.5.5)$$

and in *Bipolar* Appendix A it is verified that this series sums to the expression in (6.5.1).

For small ξ_1 (closely spaced) there are many significant partial waves in the sum. At $\theta = 0$ the partial waves tend to cancel due to the alternating signs of the terms due to $(-1)^m$, whereas at $\theta = \pi$ the terms reinforce. As expected, the charge density peaks on the side of the conductor facing the other conductor. Here are plots of the charge distribution $n_1(\xi_1, \theta)$ (6.5.1) for various values of ξ_1 and for fixed q ($q/2\pi=1$):



Bipolar (10.40)

Fig 6.9

And here are some equations of interest (also stated in *Bipolar* (11.3)),

$$a_1 = -d/\text{sh}\xi_1 \quad // \text{ radius of left circle} \quad (6.3.3)$$

$$a_2 = d/\text{sh}\xi_2 \quad // \text{ radius of right circle} \quad (6.3.3)$$

$$b = d (\text{coth}\xi_2 - \text{coth}\xi_1) \quad // \text{ distance between center lines} \quad (6.3.4) \quad (6.5.6)$$

and the inverse equations,

$$\begin{aligned} d &= (1/2b) \sqrt{b^2 - (a_2 + a_1)^2} \sqrt{b^2 - (a_2 - a_1)^2} \\ \xi_1 &= -\text{sh}^{-1}(d/a_1) \\ \xi_2 &= \text{sh}^{-1}(d/a_2) \quad . \end{aligned} \quad \text{Bipolar (11.10)} \quad (6.5.7)$$

The first equation of the second set determines the bipolar focal distance d from the two cylinder radii a_1 and a_2 and the distance b between their center lines. For $a_1 = a_2 = a$ this says $d = (1/2)\sqrt{b^2 - 4a^2}$.

(b) The Proximity Effect

Appendix D computes the E fields inside a round wire of radius a in terms of the surface charge moments η_m under the assumption that a wave $e^{j(\omega t - kz)}$ is traveling down the wire. We first remind the reader of the parameters involved. From (D.2.2),

$$\beta'^2 \equiv \beta^2 - k^2 \quad (D.2.2)$$

where

$$\beta = e^{j3\pi/4} (\sqrt{2}/\delta) = (j-1)/\delta = e^{j3\pi/4} \sqrt{\omega\mu\sigma} \quad (2.2.30)$$

$$k = -j\sqrt{zy} = -j\sqrt{(R+j\omega L)(G+j\omega C)} \quad (5.3.5)$$

$$(6.5.8)$$

Here β is the wavenumber in the conductor medium shown in (1.5.1c), while k is a low-loss effective wavenumber for the transmission line wave having the form $e^{j(\omega t - kz)}$. Although k is a free parameter in Appendix D, it is forced equal to $-j\sqrt{zy}$ in Chapter 5 where the Helmholtz equation is separated into longitudinal and transverse parts. This identification $k = -j\sqrt{zy}$ is established only for high frequencies (= low-loss), but can be assumed approximately true at lower frequencies. This subject is discussed in detail in Section D.11 (a), and the high and low ω limits of k are obtained in Appendix Q.

Now, since $n(\theta)$ is real and an even function of θ for our two-cylinder transmission line, $\eta_{-m} = \eta_m$ and from (D.10.4a) the longitudinal electric field $E_z(r, \theta)$ is shown to be (f_m a few lines below),

$$E_z(r, \theta) = (1/4) \mathcal{B}(\omega a) (\beta'/k) [f_0(r) + 2 \sum_{m=1}^{\infty} f_m(r) \eta_m \cos(m\theta)] \quad (D.10.4a)$$

$$\text{where } \mathcal{B} \equiv (\xi_d/\epsilon_d) \text{ CV } R_{dc} = [1 + (\sigma_d/\epsilon_d)/j\omega] \text{ CV } (1/\sigma\pi a^2) \quad (6.5.9)$$

Using (6.5.4) for the η_m and multiplying overall by σ to get $J_z = \sigma E_z$, one finds

$$J_z(r, \theta) = (1/4) \sigma \mathcal{B}(\omega a) (\beta'/k) [f_0(r) + 2 \sum_{m=1}^{\infty} (-1)^m e^{-m|\xi_1|} f_m(r) \cos(m\theta)] \quad (6.5.10)$$

The leading factors we combine into a function $F(\omega)$ so that,

$$J_z(r,\theta) = F(\omega) [f_0(r) + 2 \sum_{m=1}^{\infty} (-1)^m e^{-m|\xi_1|} f_m(r) \cos(m\theta)] \tag{6.5.11}$$

where

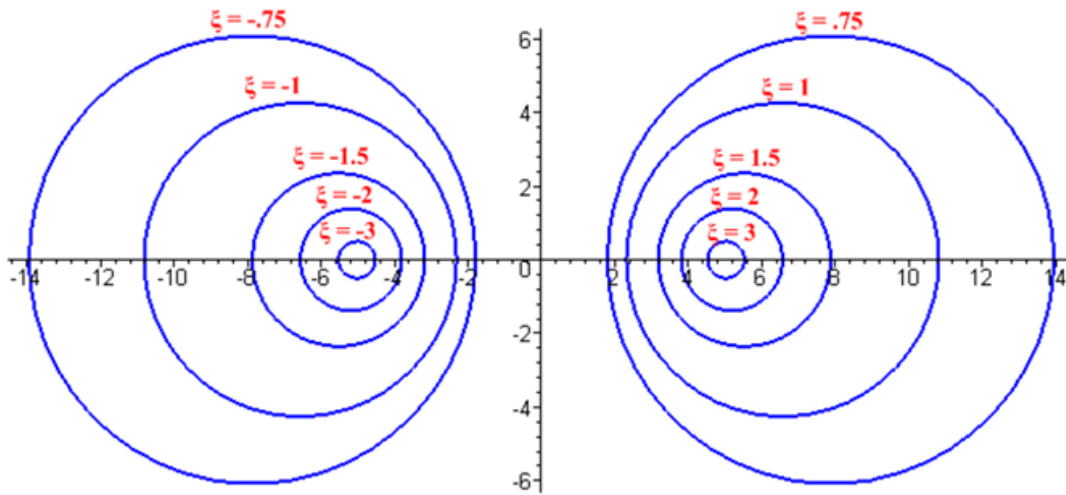
$$\begin{aligned} F(\omega) &\equiv (1/4) \sigma \mathcal{B}(\omega a) (\beta'/k) & \beta'^2 &= \beta^2 - k^2 & \beta &= e^{j3\pi/4} (\sqrt{2}/\delta) \\ f_m(r) &\equiv \left[\frac{J_m(x)}{J_{m+1}(x_a)} - \frac{J_m(x)}{J_{m-1}(x_a)} \right] & x &= \beta'r & x_a &= \beta'a \end{aligned} \tag{6.5.12}$$

$J_z(r,\theta)$ is the longitudinal current density in the left round conductor (the one with $\xi_1 < 0$) and just the fact that it is not constant in θ and r shows that we have a **proximity effect** as illustrated in Fig 6.6 above. We refer to this current density J_z as being "asymmetric" as opposed to "uniform".

For large ω we know (see below (D.2.2)) that $k \approx \beta_{a0}$ and $|k/\beta| \ll 1$ so $\beta' \approx \beta = e^{j3\pi/4} (\sqrt{2}/\delta)$. In the following plots, we shall assume this large ω regime, and shall set $F(\omega) = 1$ to produce normalized plots.

(c) Plots of the Proximity and Skin Effects

First, it is helpful to have a plot showing the conductors for various values of ξ so one can get a feel for how "fat" the cylinders are relative to their separation distance (same as Fig 6.2),



Bipolar (2.5) Fig 6.10

In Maple code we first enter all the expressions of interest:

$$J_z = (6.5.11) \quad \beta = (6.5.8) \quad f_m = (6.5.12) \quad \eta_m = (6.5.4) \quad x = \beta'r \quad x_a = \beta'a$$

```

restart; alias(J=BesselJ,I=I,j=sqrt(-1));

$$J_z := F * ( f(0) + 2 * \sum_{m=1}^N \eta(m) * f(m) * \cos(m * \theta) );$$


$$J_z := F \left( f(0) + 2 \left( \sum_{m=1}^N \eta(m) f(m) \cos(m \theta) \right) \right)$$

beta := exp(j*3*Pi/4) * sqrt(2) / delta;

$$\beta = \frac{\left( -\frac{1}{2}\sqrt{2} + \frac{1}{2}j\sqrt{2} \right) \sqrt{2}}{\delta}$$

f := m -> J(m,x)/J(m+1,xa) - J(m,x)/J(m-1,xa);

$$f = m \rightarrow \frac{J(m,x)}{J(m+1,xa)} - \frac{J(m,x)}{J(m-1,xa)}$$

eta := m -> (-1)^m * exp(-m*abs(xil));

$$\eta = m \rightarrow (-1)^m e^{(-m|\xi_1|)}$$

x := beta*r: xa := beta*a:

```

Next, specific parameters are entered ($\xi_1 = \xi_1 = -1$ and $\delta/a = 1/10$),

```

N := 10:      # number of terms in sum
F := 1:      # normalize plot
xil := -1.00: # label for left cylinder
a := 10:    # wire radius
delta := 1:  # skin depth

```

The first plot is of $|J_z(r,\theta)|$ where the axes are r and θ :

```

plot3d(abs(evalf((Jz))), r = 0..a, theta = 0..2*Pi, axes = boxed);

```

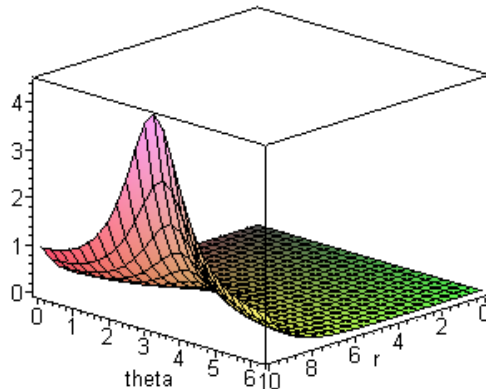


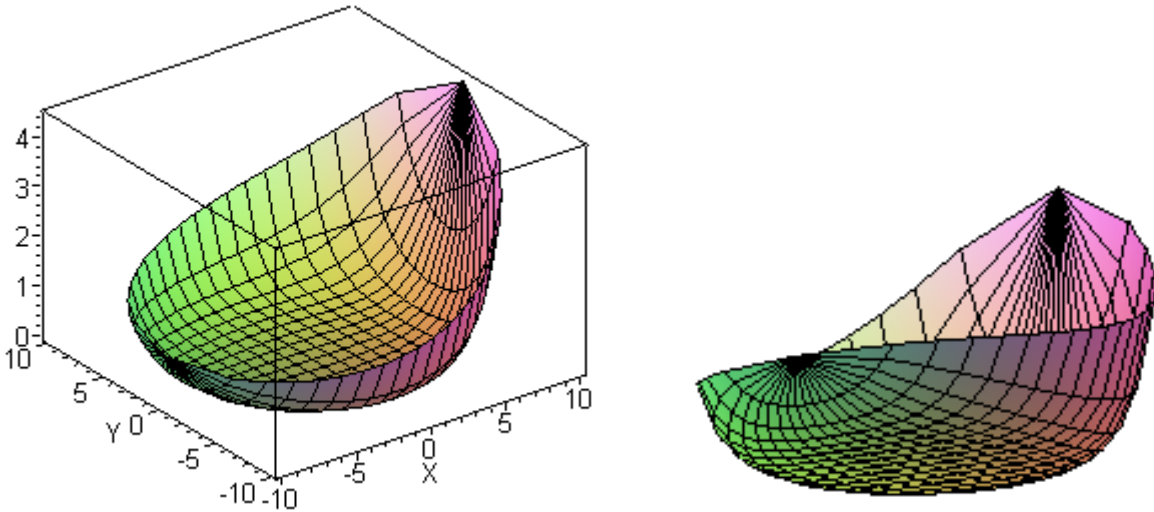
Fig 6.11

This shows the general peaking of $|J_z(r,\theta)|$ at $\theta = \pi$ (see Fig 6.7) , but the plot we really want to see is $|J_z(r,\theta)|$ displayed over the cross section of the round wire:

```

r := sqrt(X^2+Y^2):
theta := arctan(Y,-X): # note that X = -r*cos(theta) for left wire
plot3d(abs(evalf(Jz)),X = -a..a,Y = -sqrt(a^2-X^2)..sqrt(a^2-X^2), axes = boxed,
grid = [20,20]);

```



$|J_z|$ Distribution in left round wire for $a = 10$, $\delta = 1$ and $\xi_1 = -1.00$

Fig 6.12

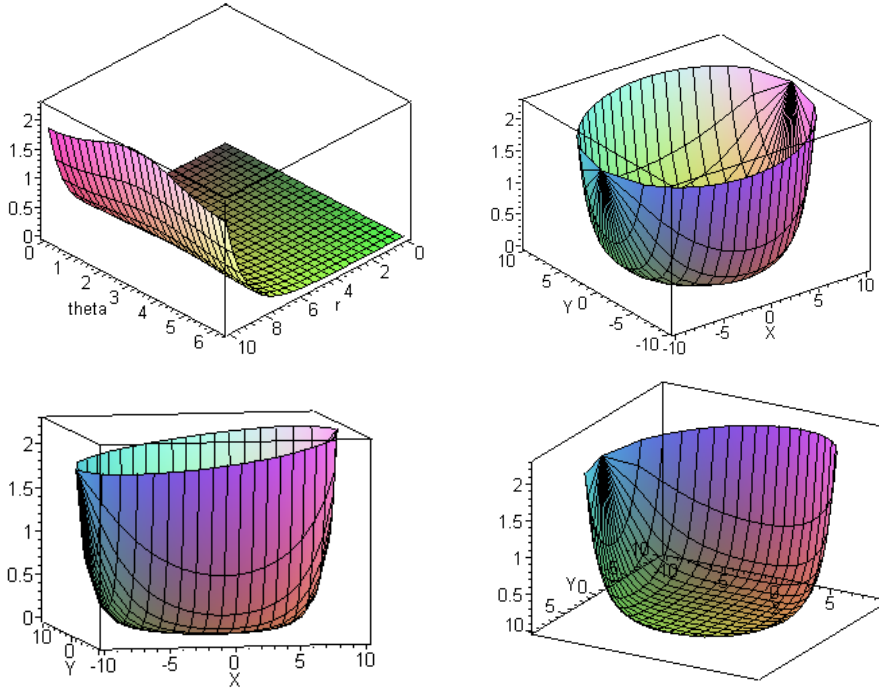
Observations:

- The skin effect for $|J_z|$ appropriate to $\delta/a = 1/10$ is seen in the cross section. The "bottom" of the plot is flat at value 0 and indicates no current in the central conductor region -- all current is in the sheath of thickness ≈ 1 just inside the wire radius $a = 10$.
- The distribution is strongly peaked on the side of the conductor facing the other conductor; this is the proximity effect (currents in opposite directions), though some authors include the skin effect as part of the proximity effect.
- Using the formula given in (P.10.7),

$$\mathcal{R} = \mathcal{R}_{dc} \frac{E(J_z^2)}{[E(J_z)]^2}, \quad (P.10.7)$$

one can compute the effective wire resistance $\mathcal{R} > \mathcal{R}_{dc}$ using (6.5.11) for J_z . The high and low ω limits of f_m and $J_z = \sigma E_z$ appearing in Appendix D.10 and D.11 simplify this task.

We now present a few such plots for different values of δ and ξ_1 . First, for $\delta/a = 1/10$ and $\xi_1 = -3$:

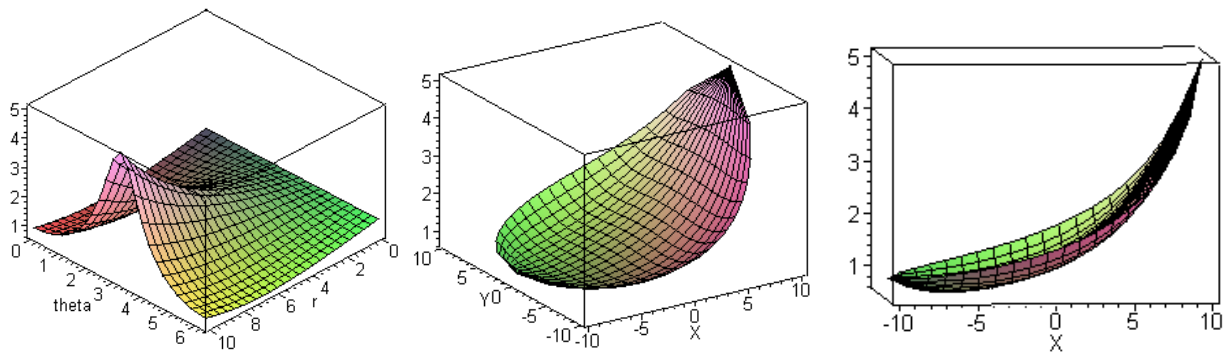


$|J_z|$ Distribution in left round wire for $a = 10$, $\delta = 1$ and $\xi_1 = -3.00$

Fig 6.13

Here, for two equal-radius round wires of $\xi_1 = -3$ and $\xi_2 = 3$, the wires are "far apart" (see Fig 6.10 above). The proximity effect is still present as shown in the lower left picture (larger at $x = 10$ than at $x = -10$), but the effect is small. On the other hand, the skin effect is still strongly in evidence, and again the entire current is in a sheath just inside $r = a = 10$ of thickness about $\delta = 1$ unit.

Next is an example with $\delta/a = 1/2$ and $\xi_1 = -1$:



$|J_z|$ Distribution in left round wire for $a = 10$, $\delta = 5$ and $\xi_1 = -1.00$

Fig 6.14

In the central drawing we are looking into the bowl of the distribution from above. Since $\delta/a = 1/2$ now, the skin effect is much less pronounced: J_z is no longer 0 in the central region as shown on the right. There is only a shallow "lip" around the bowl edge suggesting some skin effect. On the other hand, the

proximity effect is still strong since for $\xi_1 = -1$ and $\xi_2 = 1$ the wires are fairly close together as shown in Fig 6.10. For such wires, using (6.5.6),

$$a/b = a_1/b = \frac{|\operatorname{csch}\xi_1|}{\operatorname{coth}\xi_2 - \operatorname{coth}\xi_1} = \frac{|\operatorname{csch}(-1)|}{\operatorname{coth}(1) - \operatorname{coth}(-1)} = \frac{\operatorname{csch}(1)}{2 \operatorname{coth}(1)} = \frac{1}{2 \cosh(1)} = 0.324$$

$$\implies b/a = 3.08 \quad \text{and} \quad b/(2a) = 1.54$$

so the ratio of wire center separation to wire diameter is about 1.5 (which agrees with ruler measurements made on Fig 6.10 above). The two conductors touch when this ratio drops to 1.0.

In the next plot, we have $a = 10$ and $\delta = 1$, but now we plot the value of $|J_z|$ at $r = a$ going around the perimeter of the conductor for a set of different ξ_1 values:

```
r := a: N := 30: unassign('theta', 'xi1');
plot([seq(abs(evalf(Jz)), xi1 = [-0.25, -0.5, -0.75, -1, -1.5, -3])], theta =
0..2*Pi, color=red);
```

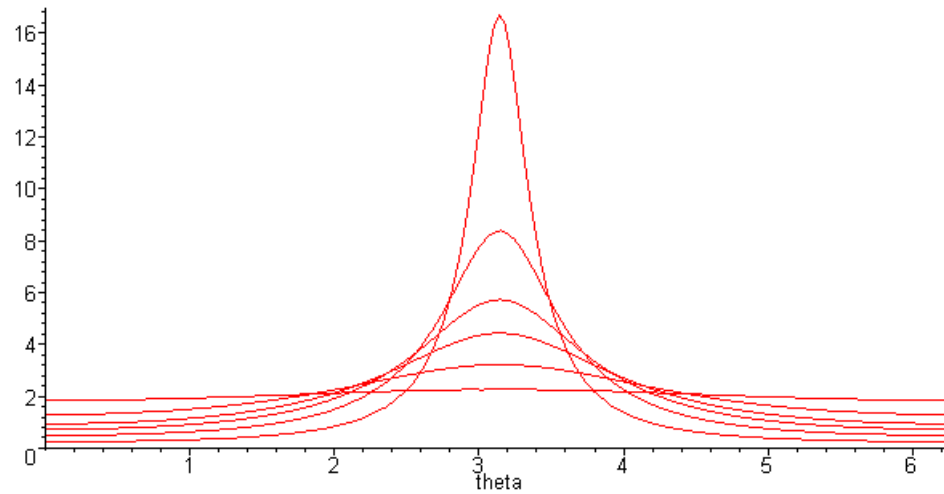


Fig 6.15

These plots of $|J_z|$ bear a strong resemblance to the surface charge density plots shown above in Fig 6.9 for the same set of ξ_1 values. It is shown in (D.10.15) that in the extreme skin effect regime one has

$$J_z(r, \theta) = - (j\omega) (\beta/\beta_{a0}) \sqrt{\frac{a}{r}} e^{(1+j)(r-a)/\delta} n(\theta) \quad \text{large } \omega \text{ (D.10.15)} \quad (6.5.13)$$

so we are not surprised to see that $J_z(r, \theta)$ tracks $n(\theta)$ in this manner. In the following section, we derive the above tracking relationship directly from $\operatorname{div} \mathbf{E} = 0$.

(d) The relationship between $J_z(a, \theta)$ and $n(\theta)$ obtained from $\text{div } \mathbf{E} = 0$

Here, assuming the skin effect regime and making a few assumptions, we obtain (6.5.13) directly from the $\text{div } \mathbf{E} = 0$ equation and the two Appendix D boundary conditions, just to provide some intuition about the linkage between J_z and $n(\theta)$.

The charge pumping boundary condition of Appendix D says ($r = a$ means $r = a - \epsilon$, and $\sigma_d = G = 0$),

$$E_r(r=a, \theta) = (j\omega/\sigma) n(\theta) \quad (D.2.24) \quad (6.5.14)$$

so the pattern of $n(\theta)$ is directly mapped to $E_r(r=a, \theta)$ at the surface by charge conservation there. But we are interested in E_z since our current density of interest is $J_z = \sigma E_z$. The condition $\text{div } \mathbf{E} = 0$ in cylindrical coordinates reads,

$$\partial_r (r E_r(r, \theta, z)) + \partial_\theta E_\theta(r, \theta, z) + r \partial_z E_z(r, \theta, z) = 0 .$$

The second Appendix D boundary condition is (D.2.27) which follows from (3.7.0) that $E_\theta(a, \theta) = 0$ at the surface, so $\partial_\theta E_\theta(r, \theta) = 0$ as well.. Then for r just below the surface one expects,

$$\begin{aligned} \partial_r (r E_r(r, \theta, z)) + r \partial_z E_z(r, \theta, z) &\approx 0 && // \text{ near } r = a \\ \partial_r (r E_r(r, \theta)) - jk r E_z(r, \theta) &\approx 0 && // \text{ using } \partial_z \rightarrow -jk, \text{ see (D.1.16), then cancel } e^{jkz} \text{ factors} \\ E_z(r, \theta) &\approx (1/jk) (1/r) \partial_r (r E_r(r, \theta)) . && // \text{ near } r = a \end{aligned} \quad (6.5.15)$$

which then relates E_z to E_r near the surface. For the symmetric-environment round wire (2.2.29) showed that

$$E_z(r) = E_z(a) \frac{J_0(\beta r)}{J_0(\beta a)} . \quad (2.2.29)$$

Taking the large argument limits of the two Bessel functions using (2.3.3) and (2.3.6), one finds that in the skin effect regime,

$$E_z(r, \theta) \approx E_z(a, \theta) \sqrt{\frac{a}{r}} e^{(r-a)/\delta} e^{j(r-a)/\delta} \quad (6.5.16)$$

which has the same general form as the simple result (2.1.8) with $x = a - r$ which is $e^{-x/\delta} e^{-jx/\delta}$ and is also consistent with (2.3.7) for magnitude. If one blindly assumes this same equation applies for $E_r(r, \theta)$ and $E_r(a, \theta)$, then

$$E_r(r, \theta) \approx E_r(a, \theta) \sqrt{\frac{a}{r}} e^{(r-a)/\delta} e^{j(r-a)/\delta} . \quad (6.5.17)$$

Then (6.5.15) says [since now at large ω (skin effect regime), $k \approx \beta_{a0}$],

$$\begin{aligned}
 E_z(a,\theta) &= (1/jk) E_x(a,\theta) \left[(1/r) \partial_x \left(r \sqrt{\frac{a}{r}} e^{(x-a)/\delta} e^{j(x-a)/\delta} \right) \right]_{r=a} \\
 &= (1/jak) E_x(a,\theta) [1/2 + (1+j)a/\delta] \tag{6.5.18}
 \end{aligned}$$

where the derivative is done by Maple,

```

f := r*sqrt(a/r)*exp((r-a)/delta)*exp(j*(r-a)/delta);
g := (1/r)*diff(f,r):
r := a;
g;

```

$$f = r \sqrt{\frac{a}{r}} e^{\left(\frac{r-a}{\delta}\right)} e^{\left(\frac{j(r-a)}{\delta}\right)}$$

$$\frac{\frac{1}{2} + \frac{a}{\delta} + \frac{aj}{\delta}}{a}$$

Using in (6.5.18) the charge pumping boundary condition (6.5.14) that $E_x(a,\theta) = (j\omega/\sigma) n(\theta)$, one obtains

$$\begin{aligned}
 E_z(a,\theta) &= (1/ja k) \{ (j\omega/\sigma) n(\theta) \} [1/2 + (1+j)a/\delta] \\
 &= (1/ja k) \{ (j\omega/\sigma) n(\theta) \} (1+j)a/\delta \quad // \text{ ignore } 1/2 \text{ relative to } a/\delta \\
 &= (1/jk) \{ (\omega/\sigma) n(\theta) \} (j-1)/\delta] \\
 &= (1/jk) \{ (\omega/\sigma) n(\theta) \} \beta] \quad // (6.5.8) \\
 &= (-j\omega/\sigma) (\beta/k) n(\theta) . \tag{6.5.19}
 \end{aligned}$$

Putting this into (6.5.16) then gives

$$E_z(r,\theta) \approx (-j\omega/\sigma) (\beta/k) n(\theta) \sqrt{\frac{a}{r}} e^{(x-a)/\delta} e^{j(x-a)/\delta} \quad // k \approx \beta_{a0} \tag{6.5.20}$$

which agrees with our earlier result (6.5.13) quoted from Appendix D. Although we just guessed at the form (6.5.17), that form is verified in box (D.10.13). The bottom line here is that E_z (and thus J_z) "tracks" $n(\theta)$ for its θ dependence and this fact is forced by $\text{div } \mathbf{E} = 0$ and the two boundary conditions at $r = a$. Notice that large ω (skin effect regime) was assumed in this derivation.

(e) The Proximity Effect At Low Frequencies

As discussed in Section D.11(a) (and Chapter 7) the Appendix D ansatz that the transmission line fields has the simple z dependence e^{-jkz} is incorrect at low frequencies. This is so because the physics-derived transmission line equations (4.12.17) which imply this z dependence are themselves inaccurate at low frequencies. Thus, although we might expect our transmission line theory to be *approximately* accurate at low frequencies, we should be prepared for incorrect predictions. One such anomaly is noted in (D.11.15) where the theory blindly extended down to very low frequencies (near and at DC) says,

$$J_z(r,\theta) = \frac{I}{\pi a^2} \left[1 + \sum_{m=1}^{\infty} \eta_m (r/a)^m (m+1) \cos(m\theta) \right] \quad (D.11.15)$$

and for the two-cylinder transmission line (6.5.4) gives

$$J_z(r,\theta) = \frac{I}{\pi a^2} \left[1 + \sum_{m=1}^{\infty} (-1)^m e^{-m|\xi_1|} (r/a)^m (m+1) \cos(m\theta) \right]. \quad (6.5.21)$$

In the DC limit, and very close to it, we expect the longitudinal current $J_z = \sigma E_z$ to be completely uniform across the conductor cross section (non-conducting dielectric), and we should then have only the "1" term shown above. Yet the above expression says J_z is non-uniform since it is a function of r and θ . For closely spaced conductors (small ξ_1), the predicted non-uniformity is quite dramatic and gives plots similar to those shown earlier.

We know that for the problem of two parallel cylindrical conductors (or any uniform parallel conductors) which carry I and $-I$ (perhaps they are shorted together at one end), J_z is uniform at DC. We know this because at $\omega = 0$ there are no eddy currents induced by one wire into the other (or by one wire into itself). The DC B field of wire #2 has no influence on the current density distribution $J_z(r,\theta)$ in wire #1. It does induce a tiny Hall charge onto the surface of wire #1 and a corresponding transverse Hall E field, since the B field of wire #2 temporarily deflects electrons in wire #1 (see Appendix N for various Hall examples). This tiny deflection effect is mentioned in the text below Fig P.12 in Appendix P, but there is no effect on the J_z distribution. From a current density standpoint, J_z in wire #1 doesn't even know that wire #2 is present, so wire #2 could just as well be removed. The isolated wire #1 then if round (Chapter 2) would certainly have a current distribution at DC that was independent of θ .

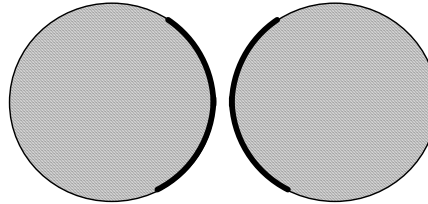
So we accept that our theory makes this incorrect prediction as $\omega \rightarrow 0$ and we chalk it up to the expected inaccuracy of the theory at low ω . This anomaly is somewhat softened when we remember that our theory only applies to infinite transmission lines, or finite transmission lines terminated in the correct Z_0 . As $\omega \rightarrow 0$, that correct $Z_0 \rightarrow \infty$ (non-conducting dielectric) and the current in the wire $I \rightarrow 0$. In the case of a conducting dielectric, we might expect a non-uniformity in J_z . The theory prediction is (D.11.9) in this case and the accuracy of this prediction is left as an unresolved Reader Exercise at the end of Appendix D. The low ω behavior of our theory is investigated more in Chapter 7.

In a proper treatment of the *fixed-load* finite-length two-cylinder transmission line problem, as $\omega \rightarrow 0$ one would see the eddy currents gradually decrease, one would arrive at a DC current $I \neq 0$, and one would have $J_z \rightarrow$ uniform. A solution to this problem could be based on the eddy current methods

outlined qualitatively in Appendix P and is no doubt available somewhere in the literature. This solution would then show the proximity and skin effects gradually vanishing as $\omega \rightarrow 0$, leaving a uniform J_z .

(f) Active perimeter p and Z_s for a two-cylinder transmission line

This active perimeter p was roughly illustrated for same-radius cylinders in Fig 2.16,



Fat twinlead

Fig 2.16

First, recall these high-frequency results for such a transmission line,

$$E_z(a, \theta) = (-j\omega/\sigma) (\beta/\beta_{d0}) n(\theta) \quad // E_z \text{ just below the surface} \quad (6.5.19)$$

$$n(\theta) = (-q/2\pi)(1/a) \frac{\text{sh}\xi_2}{\text{ch}\xi_2 + \cos\theta} \quad // n = n_2 \quad (6.5.1)$$

$$= (-q/2\pi)(1/a) \left[1 + 2 \sum_{m=1}^{\infty} (-1)^m e^{-m\xi_2} \cos(m\theta) \right] \quad (6.5.5)$$

where $\xi_2 > 0$ is for the right conductor in Fig. 6.7 and the fact that $n = n/a_2$. For this right conductor, (charge $-q$) these expressions take their maximum values when $\theta = \pi$:

$$E_z(a, \theta)_{\max} = E_z(a, \pi) = (-j\omega/\sigma) (\beta/\beta_{d0}) n(\pi) \quad n(\pi) = (-q/2\pi)(1/a) \frac{\text{sh}\xi_2}{\text{ch}\xi_2 - 1} \quad (6.5.22)$$

Meanwhile, the average values are

$$\langle E_z(a, \theta) \rangle = (-j\omega/\sigma) (\beta/\beta_{d0}) \langle n(\theta) \rangle \quad \text{with}$$

$$\langle n(\theta) \rangle = (-q/2\pi)(1/a) \quad // \text{(D.1.8) with } q \rightarrow -q \quad (6.5.23)$$

Thus,

$$\frac{\langle E_z(a, \theta) \rangle}{E_z(a, \theta)_{\max}} = \frac{\langle n(\theta) \rangle}{n(\pi)} = \frac{\text{ch}\xi_2 - 1}{\text{sh}\xi_2} \quad (6.5.24)$$

Our active perimeter distance p is defined in (4.12.10) as [using $Z_s(\theta) = E_z(a, \theta)/I$]

$$p \equiv \frac{Z_s}{Z_{s\max}} P = \frac{\langle Z_s(\theta) \rangle}{Z_{s\max}} P = \frac{\langle E_z(a, \theta) \rangle}{E_{z\max}} P = \frac{\text{ch}\xi_2 - 1}{\text{sh}\xi_2} 2\pi a \quad // P = 2\pi a \quad (6.5.25)$$

Using

$$\text{sh}\xi_2 = (d/a) \quad (6.5.6)$$

$$b = 2d \coth\xi_2 = 2d \text{ch}\xi_2/\text{sh}\xi_2 \quad // \ a_1 = a_2 \ \text{so} \ |\xi_1| = |\xi_2| \quad (6.5.6)$$

$$d = (1/2)\sqrt{b^2 - 4a^2} \quad (6.5.7)$$

one finds that

$$\text{ch}\xi_2 = (b/2d) \text{sh}\xi_2 = (b/2d)(d/a) = b/2a \quad (6.5.26)$$

Therefore

$$\begin{aligned} p &= \frac{\text{ch}\xi_2 - 1}{\text{sh}\xi_2} 2\pi a = \frac{(b/2a) - 1}{(d/a)} 2\pi a = \frac{b-2a}{2d} = \frac{b-2a}{\sqrt{b^2 - 4a^2}} 2\pi a = \frac{\sqrt{b-2a}}{\sqrt{b+2a}} 2\pi a = \frac{\sqrt{1-2a/b}}{\sqrt{1+2a/b}} 2\pi a \\ &= 2\pi a_e \ \text{where} \ a_e = a \frac{\sqrt{1-2a/b}}{\sqrt{1+2a/b}} \quad (6.5.27) \end{aligned}$$

Using E_z from (6.5.23) we next compute the average Z_s quantity defined in (4.12.9) :

$$Z_s \equiv \langle Z_s(\theta) \rangle = \langle E_z(a, \theta) \rangle / I = (-j\omega/\sigma) (\beta/\beta_{a0}) (-q/2\pi)(1/a)/I \quad (6.5.28)$$

But using (4.11.17) that $I = (-q) v_d$ along with $\beta_{a0} = \omega/v_d$ and $\beta = (j-1)/\delta$, this becomes,

$$\begin{aligned} Z_s &\equiv \langle Z_s(\theta) \rangle = -(j\omega/\sigma) (j-1)/\delta * (v_d/\omega) (1/a) (-q/2\pi) (-1/qv_d) \\ &= -(j/\sigma) (j-1)/\delta * (1/a) (1/2\pi) = (-j) (j-1) (1/2\pi a \sigma \delta) = \frac{1}{2\pi a \sigma \delta} (1+j) \quad (6.5.29) \end{aligned}$$

This is the same high- ω result found in (2.4.16) for the axially symmetric round wire situation. In the closely-spaced transmission line, $Z_s(\theta)$ is very large near $\theta = \pi$, but is very small near $\theta = 0$, but the average is the same as for a wide-spaced transmission line where each round wire is effectively in isolation. This average Z_s is what we use in (4.12.16) to evaluate the transmission line parameters. This calculation already accounts for the "proximity effect" since that effect is built into the theory as shown in the various plots of section (c) above. One *can* say that

$$Z_{s\max} = Z_s \frac{P}{p} = Z_s \frac{a}{a_e} = \frac{1}{2\pi a \sigma \delta} (1+j) \frac{a}{a_e} \quad (6.5.30)$$

which perhaps is the meaning of King's equation (46) quoted below.

On page 30 of TLT King discusses the notion of an effective radius a_e but his expression for a_e is

$$a_e = a \sqrt{1 - (2a/b)^2} \quad \text{King (45)}$$

and it is not clear how his perimeter $2\pi a_e$ is defined. King's expression for a_e at least agrees with ours in the two important cases $b \rightarrow \infty$ ($a_e = a$) and $b \rightarrow 2a$ ($a_e = 0$). He is quoting work from other people in this section, and we leave the reader to ponder King's comments directly. His "internal impedance" z_1^i is the same as our "surface impedance" Z_s . [We were unable to access King's two references shown below.]

The internal impedance per unit length is modified when two parallel conductors are close together by the so-called proximity effect. The density of axial current is increased in adjacent parts of parallel conductors with oppositely directed currents and is decreased at more remote parts. This increases the effective internal impedance, since more current is confined to a smaller volume. Accurate formulas for z_1^i for one cylindrical conductor in the presence of another with different radius are not available. If the two conductors are identical, an approximate high-frequency formula involves an effective radius

$$a_e = a \sqrt{1 - (2a/b)^2} \quad (45)$$

in place of a in the formula for z_1^i for a cylindrical rotationally symmetrical conductor.† Thus for each conductor⁴⁰

$$z_1^i \doteq \frac{1 + j}{2\pi a} \sqrt{\frac{\mu_c \omega}{2\sigma_c [1 - (2a/b)^2]}} \quad (46)$$

The internal impedance per unit length of a two-wire line is $z^i = 2z_1^i$. For the single wire over the conducting plane, $z^i = z_1^i$ if losses in the plane are neglected.

†

57. Sim, A. C.: New High-frequency Proximity Effect Formula, *Wireless Engr.*, **30**: 203 (1953).
 40. Carson, J. R.: Wave Propagation over Parallel Wires. The Proximity Effect, *Phil. Mag.*, ser. 6, **41**: 607 (1921).

(g) The Proximity Effect For Currents in the Same Direction

Our theory does not model this situation. If the currents in the two conductors are in the same direction, we don't even have a transmission line. However, one could regard two such conductors as the central conductors of a coaxial cable with a distant return sheath :

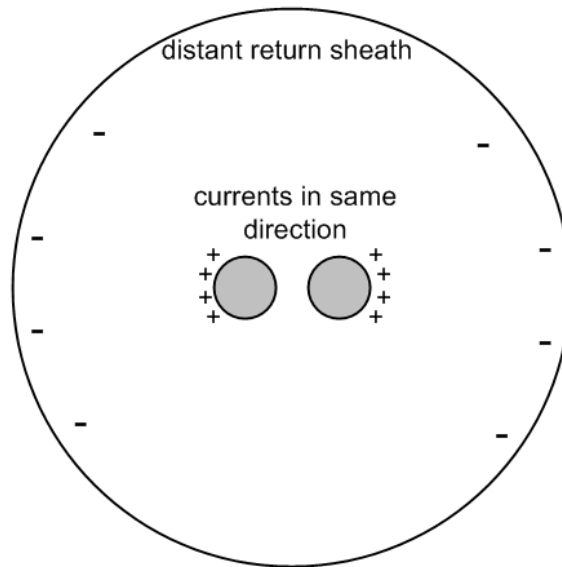


Fig 6.16

We then have a transmission line, and it has an associated "capacitor problem" which one could solve to determine the potential, the E field, and finally the surface charge $n(\theta)$ on each central conductor. From that one could compute the moments η_m and from that the current distributions $J_z(r,\theta)$ in the two wires using the methods given above. Even if the two central conductors touch, the problem is well defined and non-singular (unlike our regular twin-lead transmission line problem). We know from Fig P.12 that the currents will be largest near the surfaces most distant from the other conductor. Conceptually this can be regarded as just the skin effect applied to the composite central conductor. Multiple central conductor strands could be treated in principle in the same manner. This is the subject of the paper by Smith mentioned in Appendix P.9.

Chapter 7: The Low Frequency Limit of the Theory

By "the theory" we mean a combination of the developments of Chapters 1 through 6 on transmission lines, and the development of Appendix D which describes the E fields inside a round wire. It would seem to be a simple process to take the various results of this theory and evaluate expressions in the limit $\omega \rightarrow 0$ (the DC limit). However, carrying out and interpreting this task is like trying to run lengthwise through a Pyracantha hedge in one's birthday suit. The theory has many moving parts, and each attempted step forward seems to result in a newfound pain. In this chapter we shall explore this low-frequency issue in as systematic a fashion as possible. We shall show that our entire theory is invalid as $\omega \rightarrow 0$, and shall conjecture why that is the case.

7.1 A Review of Appendix D

Since the reader has likely not read the very long Appendix D, we summarize it here.

The appendix considers a round wire of radius a which is one conductor of an infinite transmission line. The other conductor(s) may or may not be round in cross section.

A cylindrical coordinate system is set up in the round conductor with the conductor center line as the z axis. The azimuthal angle θ is replaced by an integer m in a complex Fourier Series transform, for example $f(\theta) = \sum_{m=-\infty}^{\infty} e^{jm\theta} F(m)$. This has the benefit of allowing the replacement of ∂_{θ} in " θ space" by jm in " m space": $\partial_{\theta} f(\theta) = \sum_{m=-\infty}^{\infty} e^{jm\theta} [jmF(m)]$.

Time dependence of everything is taken to be $e^{j\omega t}$.

We then consider a set of four equations, two boundary conditions, and a special ansatz.

(a) The Four Equations

One of the four equations is $\text{div } \mathbf{E} = 0$, which we presume is true inside our conducting round wire. We ignore the miniscule deviation due to the radial Hall effect described in Appendix N.7 which causes a tiny charge density ρ to exist inside the conductor. The other three equations are $(\nabla^2 + \beta^2) \mathbf{E} = 0$ which is a vector Helmholtz equation treated in cylindrical coordinates. This vector equation is of course three separate equations, two of which cross-couple field components. Parameter β is the wavenumber inside the conductor and for all practical purposes we know from (1.5.1d) that that $\beta^2 = -j\omega\mu\sigma$ where μ and σ are the magnetic permeability and electrical conductivity of the conductor, which we often imagine to be made of copper which has $\mu = \mu_0$.

(b) The Two Boundary Conditions

The first boundary condition is charge conservation at the wire surface $r = a$. If the dielectric is a vacuum, this boundary condition takes the form $E_r(r=a, \theta) = (j\omega/\sigma) n(\theta)$ in θ -space, and $E_r(r=a, m) = (j\omega/\sigma) N_m$ in m -space, where N_m are the Fourier Series projections of the surface charge $n(\theta)$. Location a really means $a-\epsilon$, a point just below the surface. The idea is that the charge on the surface is fed by the radial current just below the surface, so $J_r(r=a-\epsilon, \theta) = j\omega n(\theta)$, which would say $J_r = \partial_t n(\theta)$ in the time domain. One might fairly wonder about the validity of this condition, imagining that $n(\theta)$ could also be fed by surface currents flowing in either the θ or z direction. By surface currents, we do not mean the skin effect current sheath which exists at large ω ; we refer instead to the current of the actual free surface charge on the

conductor surface moving around, and we refer to such currents as Debye surface currents, since the surface charge has a tiny thickness on the order of the Debye length (Appendix E). We have convinced ourselves that such surface currents are not large enough compared to the bulk conductor currents to alter the boundary condition, but it is not a slam dunk argument, and the reader is referred to our fretting in Section D.9. In Section D.9 (d) this boundary condition is generalized for a conducting dielectric.

The second boundary condition is that the azimuthal tangential electric field E_θ must vanish at the round wire surface. This is written $E_\theta(r=a, \theta) = 0$ in θ -space and $E_\theta(r=a, m) = 0$ in m -space. The main argument here is that up to quite a large frequency one has a quasi-electrostatic situation in this θ dimension of the problem, and any surface E_θ field that might appear would be instantly neutralized by an adjustment of the free surface charges on the conductor surface. Again, the argument is not a slam dunk, and the reader is referred to our further fretting in Section D.8.

(c) The e^{-jkz} Ansatz

In addition to our four equations and two boundary conditions, we make a rather brutal assumption at the start of Appendix D which is this: the z dependence of all three E field components is the same and is given by e^{-jkz} where k is some complex number. This is our "traveling wave ansatz" since it then implies that the E field components in θ -space have the form $E_i(r, \theta, z, t) = e^{j(\omega t - kz)} E_i(r, \theta)$, and we just replace θ by m for m -space. Here (as usual) we use the overloaded notation of Section 1.6 (f).

We select e^{-jkz} instead of e^{+jkz} to have a wave that travels in the $+z$ direction for $\text{Re}(k) > 0$.

This then injects an unspecified constant k into the machinery of Appendix D. We imagine that in the dielectric there exists a moving field pattern of strong E and B fields which slides down the transmission line. In order to match fields at the conductor boundary, these external fields must also have the traveling wave form $e^{j(\omega t - kz)}$ with the same constant k , a point we return to momentarily.

Within the context of the round wire and ignoring what is going on outside, any value of k is viable in solving our set of 4 equations, 2 boundary conditions, and the e^{-jkz} ansatz. Since the four equations are linear, new solutions can be formed by superposing solutions with different values of k .

In fact, the E_z equation is just a scalar Helmholtz equation $(\nabla^2 + \beta^2)E_z = 0$ (since E_z is a Cartesian coordinate). This equation is "separable" and any solution must be writable as a linear combination of the equation's atomic forms (harmonics). In this case those atoms are $[e^{jm\theta}] [J_m(\sqrt{\beta^2 - k^2} r)] [e^{-jkz}]$. We then recognize m and k as the two "separation constants". Since the geometry requires all θ dependence to be periodic in θ with period 2π , constant m must be an integer, and we identify this with our m -space "m" already discussed. Similarly, we identify separation constant k with the k in our ansatz e^{-jkz} . To really be complete, we let m take all integral values and k take all real values. $Y_m(\sqrt{\beta^2 - k^2} r)$ is rejected since it blows up at $r = 0$ which is the center of the physical wire.

So in general, whatever $E_z(r, \theta, z)$ is inside the round wire, one must be able to write it this way

$$E_z(r, \theta, z) = \sum_{m=-\infty}^{\infty} \int_{-\infty}^{\infty} dk A_{mk} e^{jm\theta} J_m(\sqrt{\beta^2 - k^2} r) e^{-jkz}$$

where A_{mk} are appropriate coefficients. In Appendix D, we take a particular value of k so we don't have this general $\int dk$ integration appearing, but we must allow in a general sense that it could be required to produce a viable solution for the transmission line.

Given then this discussion of the atomic forms of the scalar E_z Helmholtz equation, our ansatz that the z dependence is e^{-jkz} seems slightly less "brutal", and slightly more justifiable. The idea that a single value of k might suffice for the problem solution (finding the E fields inside the conductor) is then based on the idea that this internal k must be the same as the external k which arises in the transmission line dielectric region. Either from the physics model of Chapters 4 and 5, or from the electrical engineering network model of Appendix K, we have this familiar form for k

$$k = -j\sqrt{zy} = -j\sqrt{(R+j\omega L)(G+j\omega C)}$$

and to get the internal/external boundary condition to match, *this* is the k we use for the k of the interior solution. Note that the network model with its lumped components says nothing about E fields inside conductors. It is a model for the action in the dielectric.

"Where does the above expression for k come from?", the reader might ask. In both the physics model and the network model, one obtains certain "transmission line equations" of first and second order,

$\frac{dV(z)}{dz} = -z i(z)$	$(\frac{d}{dz^2} - zy) V(z) = 0$	$z = R + j\omega L$	transmission line equations
$\frac{di(z)}{dz} = -yV(z)$	$(\frac{d}{dz^2} - zy) i(z) = 0$	$y = G + j\omega C$	(4.12.15), (4.12.17), (4.12.16)

In Appendix K these appear as (K.5) and (K.6). Looking at the second order equations, one sees that both $V(z)$ and $i(z)$ must have the form e^{-jkz} where $k^2 = -zy$, and this basically forces all E and B fields to have this same form. This then dovetails perfectly with our e^{-jkz} ansatz and furthermore provides a specific formula for k . It all seems so nice!

(d) The Appendix D E-field Solutions

Grinding through Appendix D, one obtains the following exact E and B field component expressions which solve the above stated problem :

Summary of E and B fields inside a round wire			(D.9.39)
$E_z(r,m) = (1/4) \eta_m \mathcal{B}(\omega/k) (a\beta') f_m$	$x = \beta'r$	$x_a = \beta'a$	$\beta'^2 = \beta^2 - k^2$
$E_r(r,m) = (j/4) \eta_m \mathcal{B}(\omega a) g_m$			
$E_\theta(r,m) = (1/4) \eta_m \mathcal{B}(\omega a) h_m$			$\mathcal{B} \equiv (\xi_d/\epsilon_d) CV R_{dc}$
$B_z(r,m) = (j/4) (a) \eta_m \mathcal{B}(\beta' e_m)$			$(\xi_d/\epsilon_d) = 1 + (G/j\omega C)$
$B_r(r,m) = - (1/4) (a) \eta_m \mathcal{B}(1/k) (r^{-1} m \beta' f_m + k^2 h_m)$			
$B_\theta(r,m) = (j/4) (a) \eta_m \mathcal{B}(1/k) (k^2 g_m - \beta'^2 f_m [(m/x) - J_{m+1}(x)/J_m(x)])$			$\eta_m = N_m/N_0$
$e_m = [\frac{J_m(x)}{J_{m+1}(x_a)} + \frac{J_m(x)}{J_{m-1}(x_a)}]$	$g_m = [\frac{J_{m+1}(x)}{J_{m+1}(x_a)} + \frac{J_{m-1}(x)}{J_{m-1}(x_a)}]$		$R_{dc} = \frac{1}{\sigma\pi a^2}$
$f_m = [\frac{J_m(x)}{J_{m+1}(x_a)} - \frac{J_m(x)}{J_{m-1}(x_a)}]$	$h_m = [\frac{J_{m+1}(x)}{J_{m+1}(x_a)} - \frac{J_{m-1}(x)}{J_{m-1}(x_a)}]$		$G \geq 0$

7.2 First Sign of Trouble: J_z Asymmetry at DC

As a simple "check" on our theory, it seems reasonable to casually take $\omega \rightarrow 0$ and make sure the obvious DC results are replicated. As we now show, something is wrong with this limit.

Using E_z from the above box, consider this ratio, where we have canceled all common factors,

$$\frac{E_z(r,m)}{E_z(r,0)} = \eta_m \frac{f_m(x,x_a)}{f_0(x,x_a)}, \quad f_m(x,x_a) = \left[\frac{J_m(x)}{J_{m+1}(x_a)} - \frac{J_m(x)}{J_{m-1}(x_a)} \right], \quad x = \beta'r, \quad x_a = \beta'a. \quad (7.2.1)$$

Let us assume that as $\omega \rightarrow 0$, $\beta' \rightarrow \beta'_0$, some finite value. One then finds that

$$\lim_{\omega \rightarrow 0} \frac{E_z(r,m)}{E_z(r,0)} = \eta_m \frac{f_m(\beta'_0 r, \beta'_0 a)}{f_0(\beta'_0 r, \beta'_0 a)} \quad f_m(x,x_a) = \left[\frac{J_m(x)}{J_{m+1}(x_a)} - \frac{J_m(x)}{J_{m-1}(x_a)} \right]. \quad (7.2.2)$$

This ratio does not vanish as $\omega \rightarrow 0$! It is some complicated function of β'_0 , m , r and a . The moments η_m do not vanish for $m \neq 0$, see for example (6.5.4) for two round wires.

Suppose β'_0 is very small such that $|\beta'_0 a| \ll 1$. Then we can use these Section D.11 limits of the f_m functions for small argument,

$$f_m \rightarrow (r/a)^{|m|} (|m|+1) (2/\beta'a) \quad f_0 \rightarrow 4/(a\beta') \quad (D.11.6)$$

to find that

$$\lim_{\omega \rightarrow 0} \frac{E_z(r,m)}{E_z(r,0)} \approx \eta_m \frac{(r/a)^{|m|} (|m|+1)}{2} \quad |\beta'_0 a| \ll 1 \quad (7.2.3)$$

where the fact that the ratio is non-zero is quite explicit and dramatic.

This ratio is the same even if $\beta'_0 = 0$.

If at DC we have $E_z(r,m) \neq 0$, there must be some $\cos(m\theta)$ component in $J_z = \sigma E_z$ and therefore the current density J_z is not uniform over the round wire cross section. It happens that the current $I \rightarrow 0$ for a transmission line having conductance $G = 0$ (since $Z_0 \rightarrow \infty$), but we would expect that *very close to* $\omega = 0$ we should see J_z at least *approaching* uniformity on the cross section, but that is not happening.

Our conclusion is that, according to our theory, regardless of the value of $\beta' = \sqrt{\beta^2 - k^2}$ as $\omega \rightarrow 0$, the above ratio is non-zero. The implication is that E_z and therefore the current distribution $J_z = \sigma E_z$ is not uniform over the round wire cross section at DC!

We know that this conclusion is incorrect and that in fact J_z is uniform across a wire cross section at DC. We know this from eddy current arguments as in Appendix P, and from the proof which follows in the next section. Therefore, something is wrong with our theory as $\omega \rightarrow 0$, the first sign of trouble.

Superposition does not help.

The above conclusion is unchanged even if we allow a superposition of k values for E_z (and thereby don't invoke any connection between k and $k(\omega) = -j\sqrt{(R+j\omega L)(G+j\omega C)}$). Such a superposition really makes no sense since we really want to match interior and exterior boundary conditions and have $k = k(\omega)$, but we discuss it anyway just to show that, even if it could somehow make sense, it still results in an asymmetric J_z at $\omega = 0$.

In order to find the nature of a possible k -superposed solution, we require it to satisfy these two boundary conditions,

$$\begin{aligned} E_z(r=a-\varepsilon, \theta, z) &= (j\omega/\sigma) n(\theta, z, \omega) = (j\omega/\sigma) n(\theta) c(z, \omega) \\ E^r(r=a-\varepsilon, \theta, z) &= 0 \end{aligned} \quad (7.2.4)$$

where the new feature is that $c(z, \omega)$ describes how the surface charge density varies with z . For the single- k solution we of course have $c(z, \omega) = e^{-jkz}$. It is useful to define $C(k, \omega)$ as the Fourier Transform of $c(z, \omega)$ with the convention of (1.6.8),

$$C(k, \omega) = (1/2\pi) \int dz e^{jkz} c(z, \omega). \quad (7.2.5)$$

We shall now skip a few details and just outline the development. We first assume that

$$E_z(r, m, z) = \int dk d_m(k, \omega) e^{-jkz} J_m(\beta'r) \quad (7.2.6)$$

which is the most general form noted above, and we then determine $d_m(k, \omega)$ using the Helmholtz equations and $\text{div } E = 0$ and the two boundary conditions noted above. We find that $d_m(k, \omega) = C_{zm}$, a constant appearing in (D.2.4) which we also identify with $C_{zm} = (1/2j)(\beta'/k)K_m$ as in (D.2.9). We end up with unknown constants a_m and K_m just as we do in (D.2.21). It turns out, however, that these a_m and K_m have an extra factor of $C(k, \omega)$ [the Fourier Transform of $c(z, \omega)$ above] relative to the coefficients stated in (D.2.28). The continuous superposition solution which solves this problem is then the following

$$E_z(r, m, z) = \int dk C(k, \omega) e^{-jkz} E_z(r, m; \text{single-}k) \quad (7.2.7)$$

where $E_z(r, m; \text{single-}k)$ is what appears in (D.9.39) quoted above,

$$E_z(r, m; \text{single-}k) = (1/4) \eta_m \mathcal{B}(\omega/k) (a\beta') f_m \quad (D.2.33) \quad (7.2.8)$$

where

$$f_m = \left[\frac{J_m(x)}{J_{m+1}(x_a)} - \frac{J_m(x)}{J_{m-1}(x_a)} \right], \quad x = \beta'r, \quad x_a = \beta'a, \quad \beta' = \sqrt{\beta^2 - k^2}.$$

We then find from the last two equations that

$$\frac{E_z(r,m,z)}{E_z(r,0,z)} = \eta_m \frac{\int dk C(k,\omega) e^{-jkz} E_z(r,m; \text{single-}k)}{\int dk C(k,\omega) e^{-jkz} E_z(r,0; \text{single-}k)} = \eta_m \frac{\int dk C(k,\omega) e^{-jkz} (\beta'/k) f_m}{\int dk C(k,\omega) e^{-jkz} (\beta'/k) f_0} \quad (7.2.9)$$

where $\beta' = \sqrt{\beta^2 - k^2}$. Taking $\omega \rightarrow 0$ causes $\beta \rightarrow 0$ since $\beta^2 = j\mu\sigma\omega$, so $\beta' \rightarrow jk$. In this limit,

$$\lim_{\omega \rightarrow 0} \frac{E_z(r,m,z)}{E_z(r,0,z)} = \eta_m \frac{\int dk' C(k',0) e^{-jk'z} f_m}{\int dk' C(k',0) e^{-jk'z} f_0} \quad // \beta' = jk' \text{ inside } f_m \text{ and } f_0 \quad (7.2.10)$$

where f_m and f_0 are complicated functions of $\beta' = jk'$, r and a . Just looking at the z dependence and ignoring all the rest, one sees that the numerator only vanishes if $C(k',0) \equiv 0$, giving a limit of $0/0$ which is meaningless. Also, if $C(k',0) = 0$, it must be that $c(z,0) = 0$ and then $n(\theta,z) = 0$ and the transmission line has no surface charge. This is impossible since at DC it is a capacitor driven by voltage V .

The point is that the superposition idea does not cause the ratio $J_z(r,m,z) / J_z(r,0,z)$ to vanish as $\omega \rightarrow 0$, and therefore even with a superposition solution (were it even sensible) one cannot eliminate the paradoxical result that J_z is non-uniform across the round wire cross section at DC.

Taking $C(k',0) = \delta(k'-k)$ reproduces the single- k ratio appearing earlier in (7.2.2).

An interesting superposition is to try $C(k',0) = A(k')\delta(k'-k) + B(k')\delta(k'+k)$ which is then a sum of oppositely directed waves on the transmission line. One can construct a reflection scenario where the transmission line voltage vanishes at some $z = L$ where we assume the presence of a shorting bar. In this reflection scenario, it is possible to have a finite current I in the transmission line, but the J_z asymmetry still persists as $\omega \rightarrow 0$, as it does for any superposed solution. But we know that for two parallel round wires carrying a finite current I and $-I$ at DC, the current density J_z should be uniform over the cross section.

7.3 A proof that J_z must be uniform at DC

Most readers would agree that the current in any uniform wire is evenly spread out over the cross section of the wire at DC. This seems a natural result, but still it is not totally obvious. For example, the electrons in our transmission line's round wire experience the magnetic field of both the round wire and the other conductor. This magnetic field causes an initial transverse deflection of the flowing conduction electrons due to the Lorentz force acting on them. But this deflection ceases when tiny charges accumulate on the wire surfaces which create a transverse electric field which then neutralizes the deflection. There is then "no reason" for the current to be non-uniform. This DC Hall effect is described in much detail in Appendix N.

Perhaps a better explanation is in terms of the eddy current analysis of Appendix P. In that Appendix, all J_z asymmetry in a round wire (skin effect and proximity effect) is associated with eddy currents, and eddy currents vanish at DC.

Since we have found anomalous J_z behavior of our Appendix D theory as $\omega \rightarrow 0$, we want to examine the Appendix D method where we *start off* at $\omega = 0$ instead of obtaining a result for $\omega > 0$ and then taking the limit $\omega \rightarrow 0$. It should be useful to see exactly what happens in this approach.

Since $\beta^2 = -j\omega\mu\sigma$ from (1.5.1d), the vector Helmholtz equation $(\nabla^2 + \beta^2)\mathbf{E} = 0$ becomes a vector Laplace equation $\nabla^2\mathbf{E} = 0$. At $\omega = 0$ we have

$$k(\omega) = -j\sqrt{(R+j\omega L)(G+j\omega C)} \rightarrow -j\sqrt{RG} \quad \Rightarrow \quad k = -j\sqrt{RG} \quad (7.3.1)$$

$$Z_0(\omega) = \sqrt{\frac{R+j\omega L}{G+j\omega C}} \rightarrow \sqrt{R/G} \quad \Rightarrow \quad Z_0 = \sqrt{R/G} \quad (7.3.2)$$

The current I is then finite,

$$I = V/Z_0 = V\sqrt{G/R} \quad (7.3.3)$$

At this point, we imagine that G is extremely small but non-zero (perhaps $G = 10^{-18}$ mho/m), so the current I is then very small but non-zero. Since $k = -j\sqrt{RG} \approx 0$ (R is likely also small), we take $\partial_z \rightarrow -jk \approx 0$ wherever it appears. Since $k = k(\omega) \approx 0$, the ansatz factor $e^{-jkz} \approx 1$, and there is no z-dependence in the problem. Yes, moving a great distance down the line there is a very slight exponential decay in all fields due to $\text{Im}(k) = -\sqrt{RG}$, but we shall just ignore this slight decay. Since $\partial_z \rightarrow 0$ wherever it appears, we will replace ∇^2 by its 2D version ∇_{2D}^2 in the vector Laplace equation examined below.

The two Appendix D boundary conditions (D.2.24) and (D.2.27) in θ space become, since $\omega = 0$,

$$\begin{aligned} E_r(r=a,\theta) &= 0 && \text{no charge pumping at DC since } n(\theta) \text{ is constant} \\ E_\theta(r=a,\theta) &= 0 && \text{surface charge adjusts to make this be so} \end{aligned} \quad (7.3.4)$$

and in m space,

$$\begin{aligned} E_r(r=a,m) &= 0 \\ E_\theta(r=a,m) &= 0 \end{aligned} \quad (7.3.5)$$

The entire Appendix D problem (at $\omega=0$) can then be represented by this system of equations:

$$\nabla_{2D}^2 \mathbf{E}(r,\theta) = 0 \quad \text{div}_{2D} \mathbf{E}(r,\theta) = 0 \quad E_r(r=a,\theta) = 0 \quad E_\theta(r=a,\theta) = 0 \quad (7.3.6)$$

which we restate in m space using $\partial_\theta \rightarrow jm$,

$$\nabla_{2D}^2 \mathbf{E}(r,m) = 0 \quad \text{div}_{2D} \mathbf{E}(r,m) = 0 \quad E_r(r=a,m) = 0 \quad E_\theta(r=a,m) = 0 \quad (7.3.7)$$

As our first step in solving this system, we confiscate the equation set (D.1.20) setting $\beta = 0$ and $k = 0$ to obtain these simplified results:

The Three Laplace Equations and the $\text{div } \mathbf{E} = 0$ equation (in partial waves) (D.1.20)

$$[\nabla^2 \mathbf{E}]_z = 0 : \\ [r^2 \partial_r^2 + r \partial_r - m^2] E_z(r, m) = 0 \quad (D.1.15)$$

$$[\nabla^2 \mathbf{E}]_r = 0 : \\ [r^2 \partial_r^2 + r \partial_r - (m^2 + 1)] E_r(r, m) - 2jm E_\theta(r, m) = 0 \quad (D.1.17)$$

$$[\nabla^2 \mathbf{E}]_\theta = 0 : \\ [r^2 \partial_r^2 + r \partial_r - (m^2 + 1)] E_\theta(r, m) + 2jm E_r(r, m) = 0 \quad (D.1.18)$$

$$\text{div } \mathbf{E} = 0 : \\ \partial_r [r E_r(r, m)] + jm E_\theta(r, m) = 0 \quad (D.1.19)$$

The E_z equation

Since $E_z(r, m) = E_z(r, -m)$ according to the first equation in the box, we assume $m \geq 0$ for simplicity. Since the first equation is the radial equation of the 2D Laplace equation, we know the solutions are $A_m r^m + B_m r^{-m}$ for $m > 0$, and $C + D \ln r$ for $m = 0$. Since E_z is finite at $r = 0$, we reject $\ln r$ and r^{-m} for $m > 0$. Thus, for $m \geq 0$ one has $E_z(r, m) = A_{zm} r^m$ where A_{zm} are constants to be determined :

$$\begin{aligned} E_z(r, m) &= A_{zm} r^m & m > 0 \\ E_z(r, 0) &= A_{z0} & m = 0 \end{aligned} \quad (7.3.8)$$

Maple is happy to verify the claimed general solutions:

```
f := r^2*Diff(Ez,r,r) + r*Diff(Ez,r) - m^2*Ez;
```

$$f := r^2 \left(\frac{\partial^2}{\partial r^2} E_z \right) + r \left(\frac{\partial}{\partial r} E_z \right) - m^2 E_z$$

```
Ez := A*r^m + B*r^(-m);
```

$$E_z := A r^m + B r^{(-m)}$$

```
value(f): simplify(%);
```

0

```
m := 0;
```

$m = 0$

```
Ez := C + D*ln(r);
```

$$E_z := C + D \ln(r)$$

```
value(f): simplify(%);
```

0

The E_r equation

For $m = 0$ this equation reads

$$[r^2 \partial_r^2 + r \partial_r - 1] E_r(r, 0) = 0 .$$

This is the same as the E_z equation for $m = 1$, so $E_r(r, 0) = A_{r0} r$.

For $m > 0$ we solve the $\text{div } \mathbf{E} = 0$ equation to get $j m E_\theta(r, m) = -\partial_r [r E_r(r, m)]$. Just as in Appendix D, we insert this into the E_r equation to eliminate E_θ with this result

$$[r^2 \partial_r^2 + r \partial_r - (m^2 + 1)] E_r(r, m) - 2 j m E_\theta(r, m) = 0$$

$$[r^2 \partial_r^2 + r \partial_r - (m^2 + 1)] E_r(r, m) - 2 \{-\partial_r [r E_r(r, m)]\} = 0$$

$$[r^2 \partial_r^2 + r \partial_r - (m^2 + 1)] E_r(r, m) + 2 \{ [r \partial_r + 1] E_r(r, m) \} = 0$$

$$[r^2 \partial_r^2 + 3 r \partial_r - (m^2 - 1)] E_r(r, m) = 0 .$$

Since this equation contains only m^2 , we know that $E_r(r, -m) = E_r(r, m)$ so again assume $m \geq 0$. Maple gives the solution as

```
eq := r^2*Diff(Ez(r), r, r) + 3*r*Diff(Ez(r), r) - (m^2-1)*Ez(r);
```

$$eq = r^2 \left(\frac{\partial^2}{\partial r^2} E_z(r) \right) + 3 r \left(\frac{\partial}{\partial r} E_z(r) \right) - (m^2 - 1) E_z(r)$$

```
dsolve(eq);
```

$$E_z(r) = _C1 r^{(-1+m)} + _C2 r^{(-1-m)}$$

Since $m > 0$, we reject r^{-1-m} and conclude that

$$\begin{aligned} E_r(r, m) &= A_{rm} r^{m-1} & m > 0 \\ E_r(r, 0) &= A_{r0} r & m = 0 \end{aligned} \quad (7.3.9)$$

The E_θ equation

For $m = 0$ the equation reads,

$$[r^2 \partial_r^2 + r \partial_r - (1)] E_\theta(r, 0) = 0,$$

which is again the same as the E_z equation for $m = 1$ and so has solution $E_\theta(r, 0) = A_{\theta 0} r$.

For $m > 0$ we use the $\text{div } \mathbf{E} = 0$ equation to find that

$$jmE_{\theta}(r,m) = -\partial_r [r E_r(r,m)] = -\partial_r [r A_{rm} r^{m-1}] = -A_{rm} \partial_r [r^m] = -A_{rm} m r^{m-1}$$

or

$$jE_{\theta}(r,m) = -A_{rm} r^{m-1} .$$

Thus

$$\begin{aligned} E_{\theta}(r,m) &= j A_{rm} r^{m-1} & m > 0 \\ E_{\theta}(r,0) &= A_{\theta 0} r & m = 0 \end{aligned} \tag{7.3.10}$$

Alternatively, we could write the E_{θ} equation as

$$[r^2 \partial_r^2 + r \partial_r - (m^2+1)] E_{\theta}(r,m) + 2jmE_r(r,m) = 0$$

or

$$\begin{aligned} [r^2 \partial_r^2 + r \partial_r - (m^2+1)] E_{\theta}(r,m) + 2jm A_r r^{m-1} &= 0 & m > 0 \\ [r^2 \partial_r^2 + r \partial_r - (1)] E_{\theta}(r,0) &= 0 & m = 0 \end{aligned}$$

The $m = 0$ equation is as above. Maple then verifies that $E_{\theta}(r,m) = j A_{rm} r^{m-1}$ satisfies the $m > 0$ equation,

```
f := r^2*Diff(Eth(r),r,r) + r*Diff(Eth(r),r) - (m^2+1)*Eth(r) + 2*j*m*Arm*r^(m-1);
f:=r^2*(d^2/d^2r Eth(r)) + r*(d/d r Eth(r)) - (m^2+1) Eth(r) + 2j m Arm r^(m-1)
Eth := r -> j*Arm*r^(m-1);
value(f): simplify(%);
0
```

and we end up with the same results as above,

$$\begin{aligned} E_{\theta}(r,m) &= j A_{rm} r^{m-1} & m > 0 \\ E_{\theta}(r,0) &= A_{\theta 0} r & m = 0 . \end{aligned}$$

We now summarize our partial wave E field solutions at this point:

$$\begin{aligned} E_z(r,m) &= A_{zm} r^m & m > 0 \\ E_z(r,0) &= A_{z0} & m = 0 \\ E_r(r,m) &= A_{rm} r^{m-1} & m > 0 \\ E_r(r,0) &= A_{r0} r & m = 0 \\ E_{\theta}(r,m) &= j A_{rm} r^{m-1} & m > 0 \\ E_{\theta}(r,0) &= A_{\theta 0} r & m = 0 . \end{aligned} \tag{7.3.11}$$

Finally we apply the two boundary conditions $E_r(r=a,m) = 0$ and $E_{\theta}(r=a,m) = 0$. They require that $A_{rm} = 0$ for $m > 0$, and that $A_{r0} = A_{\theta 0} = 0$ for $m = 0$, giving these final field results:

$$\begin{aligned}
 E_z(r,m) &= A_{zm}r^m & m > 0 \\
 E_z(r,0) &= A_{z0} & m = 0 \\
 E_r(r,m) &= 0 & m \geq 0 \\
 E_\theta(r,m) &= 0 & m \geq 0 \quad .
 \end{aligned} \tag{7.3.12}$$

The current I must be the cross-section integral of $J_z(r,0) = \sigma E_z(r,0) = \sigma A_{z0}$, so

$$I = \sigma A_{z0} * \pi a^2 \quad \Rightarrow \quad A_{z0} = I/(\pi a^2 \sigma) = IR . \tag{7.3.13}$$

The fields are then,

$$\begin{aligned}
 E_z(r,m) &= A_{zm}r^m & m > 0 \\
 E_z(r,0) &= IR & m = 0 \\
 E_r(r,m) &= 0 & m \geq 0 \\
 E_\theta(r,m) &= 0 & m \geq 0 \quad .
 \end{aligned} \tag{7.3.14}$$

We now arrive at an interesting fact: the vector Helmholtz equation (which became a vector Laplace equation), the $\text{div}\mathbf{E} = 0$ condition and the two boundary conditions are insufficient to determine the coefficients A_{zm} for $m > 0$. The system is underspecified! This situation did not arise in Appendix D as presented for general ω .

To nail down these coefficients -- which of course are critical to our proof that J_z is uniform in this DC problem -- we must call upon the Maxwell curl \mathbf{E} equation (1.1.2) with $\partial_t \rightarrow j\omega$,

$$\text{curl } \mathbf{E} = -j\omega\mathbf{B} = 0 \quad \text{at } \omega = 0 . \tag{7.3.15}$$

We write this as

$$\text{curl } \mathbf{E}(r,\theta,z) = \hat{\mathbf{r}} [r^{-1}\partial_\theta E_z - \partial_z E_\theta] + \hat{\boldsymbol{\theta}} [\partial_z E_r - \partial_r E_z] + \hat{\mathbf{z}} [r^{-1}\partial_r(rE_\theta) - r^{-1}\partial_\theta E_r] \tag{7.3.16}$$

or

$$\text{curl } \mathbf{E}(r,m,z) = \hat{\mathbf{r}} [r^{-1}jmE_z + jkE_\theta] + \hat{\boldsymbol{\theta}} [-jkE_r - \partial_r E_z] + \hat{\mathbf{z}} [r^{-1}\partial_r(rE_\theta) - r^{-1}jmE_r] . \tag{7.3.17}$$

Setting $k \approx 0$ as above this becomes

$$\text{curl } \mathbf{E}(r,m,z) = \hat{\mathbf{r}} [r^{-1}jmE_z(r,m)] + \hat{\boldsymbol{\theta}} [-\partial_r E_z(r,m)] + \hat{\mathbf{z}} [r^{-1}\partial_r(rE_\theta(r,m)) - r^{-1}jmE_r(r,m)] .$$

But from (7.3.14) only E_z is non-vanishing, so this simplifies to

$$\text{curl } \mathbf{E}(r,m,z) = \hat{\mathbf{r}} [r^{-1}jmE_z(r,m)] + \hat{\boldsymbol{\theta}} [-\partial_r E_z(r,m)] \tag{7.3.18}$$

so $\text{curl } \mathbf{E} = 0$ requires

$$\begin{aligned} r^{-1}jmE_z(r,m) &= 0 \\ -\partial_r E_z(r,m) &= 0 \end{aligned} \quad (7.3.19)$$

We evaluate these first for $m = 0$,

$$\begin{aligned} 0 &= 0 E_z(r,0) && \text{condition met} \\ \partial_r E_z(r,0) &= 0 && \text{condition met since } E_z(r,0) = IR = \text{constant} \end{aligned} \quad (7.3.20)$$

For $m > 0$ the conditions say that

$$\begin{aligned} r^{-1}jm A_{zm}r^m &= 0 \\ \partial_r A_{zm}r^m &= 0 \quad \text{or} \quad A_{zm} m r^{m-1} = 0 \end{aligned} \quad (7.3.21)$$

Both conditions are satisfied only if $A_{zm} = 0$ for $m > 0$. We then arrive at a final field set:

$$\begin{aligned} E_z(r,m) &= 0 && m > 0 \\ E_z(r,0) &= IR && m = 0 \\ E_r(r,m) &= 0 && m \geq 0 \\ E_\theta(r,m) &= 0 && m \geq 0 \end{aligned} \quad (7.3.22)$$

which then tells us that $J_z = \sigma E_z$ is in fact uniform over the round wire cross section at DC.

7.4 Second Sign of Trouble: Infinite B fields as $\omega \rightarrow 0$

Recall from (D.11.7) the E fields for small ω ,

$E_z(r,m) = (1/2) \eta_m \mathcal{B}(\omega/k) (r/a)^m (m+1)$	<i>(D.11.7)</i>	<i>(7.4.1)</i>
$E_r(r,m) = (j/4) \eta_m \mathcal{B}(\omega a) [(r/a)^{m+1} + (r/a)^{m-1}]$		
$E_\theta(r,m) = (1/4) \eta_m \mathcal{B}(\omega a) [(r/a)^{m+1} - (r/a)^{m-1}]$	$m > 0$	
$E_z(r,0) = \mathcal{B}(\omega/k)$	$\mathcal{B} \equiv (\xi_d/\epsilon_d) CV R_{dc}$	
$E_r(r,0) = (j/2) \mathcal{B}(\omega r)$		
$E_\theta(r,0) = 0$	$m = 0$	$G \geq 0$

Next, recall (D.4.7), which expresses the Maxwell equation $\mathbf{B} = (j/\omega) \text{curl } \mathbf{E}$ in cylindrical coordinates,

$$\begin{aligned} B_r(r,m) &= (j/\omega) [\text{curl } \mathbf{E}]_r = (j/\omega) [r^{-1}jmE_z + jkE_\theta] \\ B_\theta(r,m) &= (j/\omega) [\text{curl } \mathbf{E}]_\theta = (j/\omega) [-jkE_r - \partial_r E_z] \\ B_z(r,m) &= (j/\omega) [\text{curl } \mathbf{E}]_z = (j/\omega) [r^{-1}\partial_r(rE_\theta) - r^{-1}jmE_r] \end{aligned} \quad (D.4.7)$$

These are duly entered into Maple :

Enter the Bi expressions

`Br := (j/omega)*((j*m/r)*Ez + j*k*Eth);`

$$B_r = \frac{j \left(\frac{j m E_z}{r} + j k E_{th} \right)}{\omega}$$

`Bth := (j/omega)*(-j*k*Er - Diff(Ez,r));`

$$B_{th} = \frac{j \left(-j k E_r - \left(\frac{\partial}{\partial r} E_z \right) \right)}{\omega}$$

`Bz := (j/omega)*(1/r)*(Diff(r*Eth,r) - j*m*Er);`

$$B_z = \frac{j \left(\left(\frac{\partial}{\partial r} r E_{th} \right) - j m E_r \right)}{\omega r}$$

Before continuing, look at the first term above for B_r which has the form $\frac{j}{\omega} \frac{j m E_z}{r}$. If we install E_z from (7.4.1), the (ω/k) factor in E_z results in a $1/k$ factor in B_r . This is a preview of our upcoming problem.

Momentarily omitting the common factor $\eta_m \mathcal{B}$, enter the E fields for $m > 0$ from (7.4.1) above,

Enter the Ei expressions for $m > 0$

`Ez := (1/2)*(omega/k)*(r/a)^m*(m+1);`

$$E_z = \frac{1}{2} \omega \left(\frac{r}{a} \right)^m (m+1)$$

`Er := (j/4)*(omega*a)*((r/a)^(m+1) + (r/a)^(m-1));`

$$E_r = \frac{1}{4} j \omega a \left(\left(\frac{r}{a} \right)^{m+1} + \left(\frac{r}{a} \right)^{m-1} \right)$$

`Eth := (1/4)*(omega*a)*((r/a)^(m+1) - (r/a)^(m-1));`

$$E_{th} = \frac{1}{4} \omega a \left(\left(\frac{r}{a} \right)^{m+1} - \left(\frac{r}{a} \right)^{m-1} \right)$$

Maple then computes the resulting B fields:

`Br: simplify(%);`

$$\frac{1}{4} \frac{\left(\frac{r}{a} \right)^m (-2 m^2 - 2 m - k^2 r^2 + k^2 a^2)}{r k}$$

`value(Bth): simplify(%);`

$$\frac{1}{4} \frac{j \left(\frac{r}{a} \right)^m (k^2 r^2 + k^2 a^2 - 2 m^2 - 2 m)}{r k}$$

`value(Bz): simplify(%);`

$$\frac{1}{2} j \left(\frac{r}{a} \right)^m (m+1)$$

Using $(r/a)^m/r = (r/a)^m (a/r)(1/a) = (r/a)^{m-1}(1/a)$, the Maple results for $m > 0$ are,

$$\begin{aligned} B_r &= (1/4) (r/a)^{m-1} (1/ak) [-2m(m+1) + k^2(a^2-r^2)] \\ B_\theta &= (j/4) (r/a)^{m-1} (1/ak) [-2m(m+1) + k^2(r^2+a^2)] \\ B_z &= (j/2) (r/a)^m (m+1) \end{aligned}$$

We repeat the effort for $m = 0$:

Enter the Ei expressions for $m = 0$

`Ez := (omega/k);`

$$Ez = \frac{\omega}{k}$$

`Er := (j/2)*omega*r;`

$$Er = \frac{1}{2} j \omega r$$

`Eth := 0;`

$$Eth = 0$$

to get

`m := 0;`

$$m = 0$$

`Br: simplify(%);`

$$0$$

`value(Bth): simplify(%);`

$$\frac{1}{2} j k r$$

`value(Bz): simplify(%);`

$$0$$

Thus, restoring the $\eta_m \mathcal{B}$ factor, for small ω the B fields inside the round wire are given by

B fields in round wire for small ω

(7.4.2)

$$B_z(r,m) = (j/2) \eta_m \mathcal{B} (r/a)^m (m+1) \quad m > 0$$

$$B_r(r,m) = (1/4) \eta_m \mathcal{B} (r/a)^{m-1} (1/ak) [-2m(m+1) + k^2(a^2-r^2)]$$

$$B_\theta(r,m) = (j/4) \eta_m \mathcal{B} (r/a)^{m-1} (1/ak) [-2m(m+1) + k^2(r^2+a^2)]$$

$$B_z(r,0) = 0 \quad m = 0$$

$$B_r(r,0) = 0$$

$$B_\theta(r,0) = (j/2) \mathcal{B} kr$$

$$\mathcal{B} \equiv (\xi_d/\epsilon_d) CV R_{dc}$$

$$G \geq 0$$

These same B fields can be obtained by taking the small-x limit of the full B fields shown in (D.9.39) and making use of (D.11.6).

So far we have no infinite B problem. Recall that in Appendix D, the parameter k is an arbitrary complex number. But in order to take the "small ω limit" as we did in Section D.11, we have to assume at least that k is "small" for small ω , so that then $\beta'^2 = \beta^2 - k^2 = -j\omega\mu\sigma - k^2$ will be small, allowing a power series expansion for the various Bessel functions (recall $x = \beta'r$). So as long as k is some small number (in magnitude), we know that the E and B fields given in (7.4.1) and (7.4.2) represent a solution to the Helmholtz equation for E, the $\text{div } E = 0$ equation, all four Maxwell equations, and in fact also the Helmholtz equation for B, though we did not demonstrate this fact. The fields also satisfy the two boundary conditions (D.2.26) and (D.2.27). By assuming small ω and small k and hence small β' , we were able to replace the Bessel functions with their leading expansion terms resulting in the various simple polynomial terms in (7.4.1) and (7.4.2).

The trouble now arises if we *further* assume that our small k value of the last paragraph is identified with the $\omega \rightarrow 0$ value of $k = -j\sqrt{zy} = -j\sqrt{(R+j\omega L)(G+j\omega C)}$. This is the k value for the wave proceeding down the dielectric of the transmission line, *based on* the transmission line equations (4.12.17).

G = 0 Case

We first assume that $G = 0$ which in turn implies $(\xi_{\mathbf{d}}/\epsilon_{\mathbf{d}}) = 1$ since $\sigma_{\mathbf{d}} = 0$. According to (Q.4.9), and assuming that $k = -j\sqrt{(R+j\omega L)(G+j\omega C)}$, we see that as $\omega \rightarrow 0$,

$$k \rightarrow \sqrt{R_{\mathbf{dc}2}C/2} \sqrt{\omega} (1-j) = \sqrt{R_{\mathbf{dc}2}C} \sqrt{\omega} e^{-j\pi/4} \quad \text{as } \omega \rightarrow 0 \quad . \quad (7.4.3)$$

We are now using $R_{\mathbf{dc}}$ as the resistance per length of our round wire conductor, while $R_{\mathbf{dc}2}$ is the resistance of both transmission line conductors per length. Note that $k \rightarrow 0$ as $\sqrt{\omega}$. The above B fields (7.4.2) then become

$B_{\mathbf{z}}(r,m) = (j/2) \eta_{\mathbf{m}} CV R_{\mathbf{dc}} (r/a)^m (m+1)$	$m > 0$	(7.4.4)
$B_{\mathbf{r}}(r,m) = (1/4) \eta_{\mathbf{m}} CV R_{\mathbf{dc}} (r/a)^{m-1} (1/a) [-2m(m+1)] / [\sqrt{R_{\mathbf{dc}2}C} \sqrt{\omega} e^{-j\pi/4}]$		
$B_{\theta}(r,m) = (j/4) \eta_{\mathbf{m}} CV R_{\mathbf{dc}} (r/a)^{m-1} (1/a) [-2m(m+1)] / [\sqrt{R_{\mathbf{dc}2}C} \sqrt{\omega} e^{-j\pi/4}]$		
$B_{\mathbf{z}}(r,0) = 0$	$m = 0$	
$B_{\mathbf{r}}(r,0) = 0$		
$B_{\theta}(r,0) = (j/2) CV R_{\mathbf{dc}} r [\sqrt{R_{\mathbf{dc}2}C} \sqrt{\omega} e^{-j\pi/4}]$		$G = 0$

As $\omega \rightarrow 0$, the three $m = 0$ B fields go to zero. This is as expected since the current vanishes:

$$I = CV (\omega/k) = CV \omega / [\sqrt{R_{\mathbf{dc}2}C} \sqrt{\omega} e^{-j\pi/4}] = CV \sqrt{\omega} / [\sqrt{R_{\mathbf{dc}2}C} e^{-j\pi/4}] \rightarrow 0 \quad . \quad (7.4.5)$$

However, as $\omega \rightarrow 0$, the $m > 0$ B fields all diverge as $1/\sqrt{\omega}$!! In the DC limit, there will still be some asymmetric $n(\theta)$ on the round wire surface just because this round wire is part of a long capacitor connected to a battery of voltage V , so the $\eta_{\mathbf{m}}$ coefficients do not vanish for $m > 0$. Looking at (7.4.1) we

see that as $\omega \rightarrow 0$, all the E field components vanish in all partial waves m, as we would expect since the transmission line impedance goes to ∞ . It seems a bit unphysical for our round wire at DC to have no E fields, no current, but some infinite internal B fields. One can show that curl B is finite in the $\omega \rightarrow 0$ limit (and $\text{div B} = 0$), but this is not much respite.

G > 0 Case

We start again with (7.4.2), but now

$$(\xi_d/\epsilon_d) = 1 + (G/j\omega C) \rightarrow (G/j\omega C) \quad \text{as } \omega \rightarrow 0$$

$$\mathcal{B} \rightarrow (G/j\omega C) CV R_{dc} = (G/j\omega) V R_{dc} \quad (7.4.6)$$

Moreover, according to (Q.4.6), and assuming that $k = -j\sqrt{(R+j\omega L)(G+j\omega C)}$, we see that

$$k \rightarrow -j\sqrt{R_{dc}G} \equiv k_1 \quad \text{as } \omega \rightarrow 0 \quad // \text{ a very small constant value} \quad (7.4.7)$$

Then (7.4.2) reads,

$B_z(r,m) = (j/2) \eta_m (G/j\omega) V R_{dc} (r/a)^m (m+1) \quad m > 0 \quad (7.4.8)$
$B_r(r,m) = (1/4) \eta_m (G/j\omega) V R_{dc} (r/a)^{m-1} (1/ak_1) [-2m(m+1) + k_1^2(a^2-r^2)]$
$B_\theta(r,m) = (j/4) \eta_m (G/j\omega) V R_{dc} (r/a)^{m-1} (1/ak_1) [-2m(m+1) + k_1^2(r^2+a^2)]$
$B_z(r,0) = 0 \quad m = 0$
$B_r(r,0) = 0$
$B_\theta(r,0) = (j/2) (G/j\omega C) CV R_{dc} k_1 r \quad G > 0$

We find that for $G > 0$, all the non-zero B field components diverge as $1/\omega$ as $\omega \rightarrow 0$!! This is even worse than that $G = 0$ case where divergence was $1/\sqrt{\omega}$.

This then is our second sign of trouble: B fields are going infinite as $\omega \rightarrow 0$. It seems clear that the physical B field of a transmission line operating at DC should be finite since there are no infinite currents anywhere. Thus, the theory of Appendix D combined with the idea that $k = -j\sqrt{(R+j\omega L)(G+j\omega C)}$ is *invalid* as $\omega \rightarrow 0$.

7.5 What is the cause of the Trouble as $\omega \rightarrow 0$?

There are likely several causes of " $\omega \rightarrow 0$ trouble", but here we discuss just one problem source.

In Appendix M it is argued that $|\mathbf{A}_t| < 10^{-4} |\mathbf{A}_z|$ from 0 to 500 GHz, where $\mathbf{A}_t = A_x \hat{x} + A_y \hat{y}$ is the transverse vector potential. This relative smallness of the transverse vector potential for a transmission line does not seem to translate into the relative smallness of transverse *derivatives* of the potential at low frequencies.

In Step 1 (3.7.5) it was shown indirectly that one can approximate div A as $\partial_z A_z$ only when ω is large. In other words, $(\partial_x A_x + \partial_y A_y)$ cannot be neglected relative to $\partial_z A_z$ when ω is small. Since we have

never studied the small transverse potentials, it is not clear just how small ω has to be for this neglect to be unjustified, but one might vaguely assume for a round conductor of radius a that $a = \delta = \sqrt{2/(\omega\mu\sigma)}$ might provide a ballpark value below which $(\partial_{\mathbf{x}}A_{\mathbf{x}} + \partial_{\mathbf{y}}A_{\mathbf{y}})$ should not be neglected. Certainly then in the limit $\omega \rightarrow 0$, one should not be neglecting $(\partial_{\mathbf{x}}A_{\mathbf{x}} + \partial_{\mathbf{y}}A_{\mathbf{y}})$.

A more generic argument comparing $(\partial_{\mathbf{x}}A_{\mathbf{x}} + \partial_{\mathbf{y}}A_{\mathbf{y}})$ to $(\partial_{\mathbf{z}}A_{\mathbf{z}})$ is this. If we were to assume that $A_{\mathbf{z}}$ behaves as $e^{-j\mathbf{kz}}$, we would then be comparing $|\partial_{\mathbf{x}}A_{\mathbf{x}} + \partial_{\mathbf{y}}A_{\mathbf{y}}|$ with $|k A_{\mathbf{z}}|$. In a scale sense, we might expect the scale of these transverse derivatives to be such that $\partial_{\mathbf{x}}A_{\mathbf{x}} \sim (1/D_{\mathbf{x}})A_{\mathbf{x}}$ and $\partial_{\mathbf{y}}A_{\mathbf{y}} \sim (1/D_{\mathbf{y}})A_{\mathbf{y}}$ where $D_{\mathbf{x}}$ and $D_{\mathbf{y}}$ are some ballpark transverse dimensions of the transmission line. Then our comparison is between $|(1/D_{\mathbf{x}})A_{\mathbf{x}} + (1/D_{\mathbf{y}})A_{\mathbf{y}}|$ and $|k A_{\mathbf{z}}|$. In this same scale sense, we expect to have $k \sim 1/\lambda$ where λ is the wavelength of a wave going down the transmission line. The assumption made in neglecting the transverse derivatives is then roughly this

$$|(1/D_{\mathbf{x}})A_{\mathbf{x}} + (1/D_{\mathbf{y}})A_{\mathbf{y}}| \ll |(1/\lambda)A_{\mathbf{z}}|.$$

Even though we have $|A_{\mathbf{x}}, A_{\mathbf{y}}| \ll |A_{\mathbf{z}}|$ from Appendix M, as ω becomes smaller, we expect λ to become larger, so the right side of this inequality gets arbitrarily small as $\omega \rightarrow 0$ and $\lambda \rightarrow \infty$, and at some value of ω the neglect of the left side is no longer justified.

In Chapter 4 it was assumed that $|\partial_{\mathbf{x}}A_{\mathbf{x}} + \partial_{\mathbf{y}}A_{\mathbf{y}}| \ll |k A_{\mathbf{z}}|$. This assumption, which we quietly justified there based on $|A_{\mathbf{t}}| < 10^{-4} |A_{\mathbf{z}}|$, was made in going from (4.12.2) to (4.12.3). We then ended up with the second-order transmission line equations of (4.12.17),

$$\frac{d^2V(z)}{dz^2} - \mathbf{zy} V(z) = 0 \quad \frac{d^2i(z)}{dz^2} - \mathbf{zy} i(z) = 0. \quad (4.12.17)$$

The solutions to these equations indicate that $V(z)$ and $i(z)$ have $e^{-j\mathbf{kz}}$ dependence on z , with $k = -j\sqrt{\mathbf{zy}}$. This suggests at least indirectly that the E and B fields at the surface of and inside the conductors have this same z dependence, which is the ansatz of (D.1.1) at the very start of Appendix D.

We see now that the above situation only applies if ω is not too small. If we *maintain* the transverse derivatives $(\partial_{\mathbf{x}}A_{\mathbf{x}} + \partial_{\mathbf{y}}A_{\mathbf{y}})$ and carry through the analysis of Chapter 4, we arrive at these modified second-order transmission line equations (see Appendix S, equation (S.29)),

$$\frac{d^2V(z)}{dz^2} - \mathbf{zy} V(z) = (-\mathbf{z}/L_{\mathbf{e}})T(z) \quad \frac{d^2i(z)}{dz^2} - \mathbf{zy} i(z) = (1/L_{\mathbf{e}}) \partial_{\mathbf{z}}T(z). \quad (4.12.17) \quad (S.29)$$

In Appendix S we implement an averaging procedure where $V(z)$, $T(z)$ and $L_{\mathbf{e}}$ are certain double averages over the perimeters of the two conductors, though the averaging can be ignored for widely spaced conductors. The quantity $T(z)$ is given by such a double average,

$$T(z) \equiv \langle T(\mathbf{x}_1, \mathbf{x}_2) \rangle_{\mathbf{c}_1, \mathbf{c}_2} \quad (S.19)$$

where

$$T(\mathbf{x}_1, \mathbf{x}_2) \equiv (\partial_{\mathbf{x}}A_{\mathbf{x}12}(\mathbf{x}_1) - \partial_{\mathbf{x}}A_{\mathbf{x}12}(\mathbf{x}_2)) + (\partial_{\mathbf{y}}A_{\mathbf{y}12}(\mathbf{x}_1) - \partial_{\mathbf{y}}A_{\mathbf{y}12}(\mathbf{x}_2)), \quad // \dim(T) = \text{tesla} \quad (S.17)$$

which involves those transverse vector potential derivatives evaluated at points on the boundaries. We don't know how to compute the function T because we don't know the transverse potential functions, but the argument above suggests that at low ω we cannot just set $T(z) = 0$ as was done in Chapter 4.

With $T(z) \neq 0$, the two second order transmission line equations are inhomogeneous, meaning they have driving terms on the right side. It is true that $e^{\pm jkz}$ are still homogeneous "adder solutions" to the two equations in (S.29), but each equation also has a "particular" solution that cannot be ignored. For example, we might have

$$V(z) = V_{\text{particular}}(z) + A e^{-ikz} + B e^{+ikz}$$

where A and B can be adjusted. Therefore, for small ω , we do *not* simply have e^{-jkz} as the z dependence of $V(z)$, and we can deduce that this fact applies as well to the E and B fields in the dielectric and inside the conductors. For example, $V(z)$ is the line integral of E along a path in the $z = \text{constant}$ plane between the conductors (albeit averaged over the conductor boundaries). And $i(z)$ will be related to the B field inside the conductor as well as the E field.

Thus, at low ω , the e^{-jkz} ansatz for E_z inside the round conductor of Appendix D is unjustified. This is the main point. Since the ansatz of Appendix D is unjustified at low ω , it follows that the predictions of Appendix D for small ω are simply not valid. It is in this manner that we "explain away" our two low- ω anomalies: J_z being non-uniform inside the round conductor at $\omega = 0$, and B fields being infinite.

We must then also give up our simple traveling wave behavior for small ω , as given in (D.1.1)

$$\mathbf{E}(r,\theta,z,t) = e^{j(\omega t - kz)} \mathbf{E}(r,\theta) . \quad (D.1.1)$$

Once again, this led to all quantities in Appendix D having this same $e^{j(\omega t - kz)}$ dependence on z , and matching at the conductor boundary then required that fields in the dielectric have this same $e^{j(\omega t - kz)}$ form. This in turn resulted in the potential $V(z)$ having this same e^{-jkz} dependence. But we have just argued above that for small ω , this z dependence of $V(z)$ is unjustified since $T(z)$ cannot be neglected.

There are various other hints of trouble at low ω floating around in Chapters 3 and 4, where we often had to assume the strong or extreme skin effect limits, meaning large ω . A dramatic inconsistency at very low ω was shown in Figure 3.6a which is a plot of magnetic fields lines at DC for two round wires. Since the B fields are clearly not tangent to the conductor surfaces, we know that A_z is not constant on these surfaces, yet that was assumed true, as shown for example in (5.3.11).

Another possible source of our low- ω anomalies goes way back to Chapter 1 where, in our derivation of the King gauge potential wave equation (1.3.20) inside the conductors (like "region 2"), we dropped a certain term based on σ_2 being large in a conductor. Dropping this term is the same as assuming that the operating frequency f is larger than the amount shown in (1.3.38), which for the Belden 8281 cable requires that f be larger than 15KHz. Although this is a small frequency compared to the usual RF usage range of such a cable, it is considerably larger than "DC". We had to drop this σ_2 term in order to obtain (1.3.20) which in the ω domain becomes (1.5.4) $(\nabla^2 + \beta_d^2)\mathbf{A} = -\sum_i \mu_i \mathbf{J}_i$ where the sum is over currents in

all conductors. This PDE then has King's Helmholtz integral solution (1.5.9) which forms the *basis* of the $W(z)$ portion of Chapter 4 starting in Section 4.7 which eventually led to the transmission line equations (4.12.17). Thus, we really should be adding the condition (1.3.38) to our analysis if we wish to avoid still more "correction terms" in the transmission line equations like the $T(z)$ discussed above.

We reach the conclusion that the basic theory presented in Chapters 4 and 5 (and Appendix D for round wires) is adequate at "high frequency" which means in the skin effect regime, though results might be valid at significantly lower ω . On the other hand, the approximations of eddy current theory are valid at "low frequency", as presented qualitatively in Appendix P. More analytic eddy current analyses do exist, such as that of Rodrigues and Valli.

To find a complete analytic solution valid for all ω for the infinite transmission line one must face up to a full-bore boundary value problem for the two (or more) conductors, where all the conductor interior problems and the overall dielectric exterior problem are treated simultaneously with Maxwell's Equations, with fulfillment of boundary conditions on all \mathbf{E} and \mathbf{B} field components on all conductor surfaces. We have not attempted such a solution in this document. Since the vector potential is not constant on conductor surfaces at all ω , it seems unlikely that the King potential approach of Chapter 4 would be useful. Moreover, the simplification of being able to ignore the transverse vector potentials $A_{\mathbf{x}}$ and $A_{\mathbf{y}}$ leading to only two working variables ϕ and $A_{\mathbf{z}}$ is no longer viable at low ω .

We close with some comments on the network model of Appendix K which uses differentially small lumped electronics components to model a transmission line. The model treats the conductors as if each were an alternating series of inductances and resistances with no mention of what might actually be going on inside the conductor volumes. If one is interested in what goes on inside, this model is lacking. On the other hand, the conductance and capacitance aspects of the model seem very reasonable.

It is shown in Section k (c) that this network model implies the transmission line equations with no $T(z)$ term on the right side, see (K.6). Since these transmission line equations are invalid for small ω , as just shown above, we must conclude that the entire network model itself is invalid at small ω . An implication is that the values of k and Z_0 for very small ω based on this model are not to be trusted. It does seem, however, that the expression for Z_0 is still reasonable even at small ω , and approaches the correct DC limit. But the whole *notion* of k , including its small ω limits, is based on the traveling wave idea which we have seen is invalid at small ω .

Appendix A: Gauge Invariance

Here we show why it is that, in choosing potentials ϕ and \mathbf{A} , one is allowed to set the divergence of the vector potential \mathbf{A} equal to an arbitrary function. This freedom of setting $\text{div } \mathbf{A}$ is associated with "gauge invariance" as explained below. Our step-by-step approach here is somewhat unconventional and brings in the notion of a Green's function and the particular solution of the Poisson Equation. Some extracurricular topics are brought up which may or may not interest the reader. Each section builds on the previous section. Before getting launched, here is some terminology:

$\nabla^2\phi = 0$ The Laplace Equation ($\nabla^2 =$ The Laplacian, has a Laplace propagator)
 $\nabla^2\phi = f$ the inhomogeneous Laplace Equation = The Poisson Equation (Poisson's Equation)

$(\nabla^2 + \beta^2)\phi = 0$ The Helmholtz Equation ($\nabla^2 + \beta^2 =$ the Helmholtz operator, has a Helmholtz propagator)
 $(\nabla^2 + \beta^2)\phi = f$ the inhomogeneous Helmholtz Equation = has no special name

A.0 The Poisson Equation and its Solution

Fact 0: The Poisson Equation $-\nabla^2\phi = \rho/\epsilon_0$ with $\phi(\infty) = 0$ has a unique solution as stated below. (A.0.0)

For *electrostatics* in an isotropic medium equations (1.1.3) and (1.1.6) indicate that $\text{div } \mathbf{E} = \rho/\epsilon$ while (1.1.2) says that $\text{curl } \mathbf{E} = 0$. Since $\text{curl grad } f = 0$ for any function f , if one lets $\mathbf{E} = -\text{grad } \phi$, then

$$\text{curl } \mathbf{E} = -\text{curl grad } \phi = 0$$

$$\rho/\epsilon = \text{div } \mathbf{E} = -\text{div grad } \phi = -\nabla^2\phi \quad \Rightarrow \quad -\nabla^2\phi = \rho/\epsilon,$$

an equation known as the **Poisson Equation**. The problem of electrostatics ("potential theory") is then to solve $-\nabla^2\phi = \rho/\epsilon$ for the potential ϕ , and then $\mathbf{E} = -\text{grad } \phi$ produces the resulting electric field. For a static physical situation (nothing varies with time t), the electrostatic potential ϕ matches the scalar potential ϕ appearing in (1.3.1). Here $\rho(\mathbf{x})$ refers to the electric charge density.

(a) Imagine some static charge distribution $\rho(\mathbf{x})$ that is constrained to a localized region near the origin within infinite space. The distribution $\rho(\mathbf{x})$ includes *all* charges in this region. Here are some types of charges which would be included in $\rho(\mathbf{x})$:

- point charges which are "glued down" to certain points in space.
- linear continuous charge densities that are glued down along curved filaments in space or which are stable on conducting filaments.
- surface charge densities that are either glued to certain surfaces, or which are stable because they lie on the surfaces of pieces of conductor (like metal).
- 3D continuous charge densities that are glued down in 3D space so they cannot move, or which manage to achieve a stable configuration as free charge (if that is possible!)
- surface polarization charge densities not already accounted for by the ϵ in $-\nabla^2\phi = \rho/\epsilon$.

By including all these types of charge in ρ , we are able to avoid the complicating issue of "boundary surfaces" in our discussion below, and our only boundary of interest is The Great Sphere which is a sphere of infinite radius surrounding our localized region of interest.

From **Coulomb's Law** (in SI units, and in an isotropic medium of dielectric constant ϵ) we know that the electric potential ϕ of a point charge q located at point \mathbf{x}' is $\phi(\mathbf{x}) = q/[4\pi\epsilon R]$ where $R = |\mathbf{x}-\mathbf{x}'|$ is the distance between charge q at \mathbf{x}' and an observation point \mathbf{x} . Such a point charge is described by $\rho(\mathbf{x}) = q\delta(\mathbf{x}-\mathbf{x}')$. The general equation which relates $\phi(\mathbf{x})$ to $\rho(\mathbf{x})$ is the Poisson Equation,

$$-\nabla^2\phi(\mathbf{x}) = \rho(\mathbf{x})/\epsilon \quad \phi(\infty) = 0 \quad . \quad (\text{A.0.1})$$

By including the condition $\phi(\infty) = 0$, we are really describing a Poisson "boundary value problem". We add $\phi(\infty) = 0$ because we are assuming that $\rho(\mathbf{x})$ is localized as just noted.

Both the PDE and the boundary condition are linear. Letting $\phi = \alpha\phi_1 + \beta\phi_2$, and $\rho = \alpha\rho_1 + \beta\rho_2$,

$$\nabla^2\phi = \nabla^2(\alpha\phi_1 + \beta\phi_2) = \alpha\nabla^2\phi_1 + \beta\nabla^2\phi_2 = \alpha\rho_1(\mathbf{x})/\epsilon + \beta\rho_2(\mathbf{x})/\epsilon = [\alpha\rho_1(\mathbf{x}) + \beta\rho_2(\mathbf{x})]/\epsilon = \rho/\epsilon$$

$$\phi(\infty) = \alpha\phi_1(\infty) + \beta\phi_2(\infty) = 0 + 0 = 0. \quad // \text{ boundary condition is linear}$$

Therefore, we may superpose the potentials of multiple charges to get the potential resulting from a distribution of charges. Thus, we at once obtain this superposed version of Coulomb's Law,

$$\phi(\mathbf{x}) = \frac{1}{4\pi\epsilon} \int d^3\mathbf{x}' \frac{\rho(\mathbf{x}')}{|\mathbf{x}-\mathbf{x}'|} \quad . \quad (\text{A.0.2})$$

Here $d^3\mathbf{x}' \rho(\mathbf{x}') = dq(\mathbf{x}')$ is a differential chunk of charge located at \mathbf{x}' contained in tiny volume $d^3\mathbf{x}'$. Thus, (A.0.2) must be a solution of (A.0.1). If we allow the observation point \mathbf{x} to move right on top of some point charge in the distribution ρ , we will get $\phi = \infty$, so we generally avoid such observation points.

(b) We would like to explicitly show that (A.0.2) is a solution of (A.0.1) for a general distribution ρ . To this end, we digress to consider the following equation and its solution,

$$-\nabla^2 g(\mathbf{x},\mathbf{x}') = \delta(\mathbf{x}-\mathbf{x}') \quad \text{with} \quad g(\infty,\mathbf{x}') = 0 \quad \Rightarrow \quad g(\mathbf{x},\mathbf{x}') = \frac{1}{4\pi} \frac{1}{|\mathbf{x}-\mathbf{x}'|} \quad . \quad (\text{A.0.3})$$

The equation on the left is Poisson's Equation where ρ consists of a positive point charge of $q = \epsilon$ units sitting at position \mathbf{x}' . Recall from above that $\rho(\mathbf{x}) = q\delta(\mathbf{x}-\mathbf{x}')$ for a point charge. Coulomb's Law gives the solution shown on the right. Therefore it must be true that

$$-\nabla^2 \left\{ \frac{1}{4\pi} \frac{1}{|\mathbf{x}-\mathbf{x}'|} \right\} = \delta(\mathbf{x}-\mathbf{x}') \quad \text{or} \quad -\nabla^2 \left\{ \frac{1}{|\mathbf{x}-\mathbf{x}'|} \right\} = 4\pi \delta(\mathbf{x}-\mathbf{x}') \quad . \quad (\text{A.0.4})$$

This last equation is derived in Appendix H (see H.1.4), but we have already shown it is true, given Coulomb's Law. We can now show that (A.0.2) is a solution of (A.0.1) for an arbitrary distribution ρ as follows:

$$-\nabla^2\phi(\mathbf{x}) = \frac{1}{4\pi\epsilon} \int d^3\mathbf{x}' \rho(\mathbf{x}') \left\{ -\nabla^2 \frac{1}{|\mathbf{x}-\mathbf{x}'|} \right\} = \frac{1}{4\pi\epsilon} \int d^3\mathbf{x}' \rho(\mathbf{x}') 4\pi \delta(\mathbf{x}-\mathbf{x}') = \rho(\mathbf{x})/\epsilon \quad . \quad \text{QED.}$$

The assisting function $g(\mathbf{x}, \mathbf{x}')$ has various names with respect to (A.0.3): the **Green's Function** or Green function, the fundamental solution, the free-space **propagator**, or the kernel. It is nothing more than the potential created by a point charge of ϵ units located at \mathbf{x}' and viewed from \mathbf{x} . Some authors put a 4π in front of the δ in the left equation of (A.0.3) which causes the $1/(4\pi)$ to be absent in the right equation of (A.0.3).

(c) We have found the particular solution of (A.0.1) given by (A.0.2). There are many *other* PDE solutions which can be obtained by adding to the solution (A.0.2) a solution of $-\nabla^2 u = 0$. This last equation, usually written $\nabla^2 u = 0$, is called the Laplace Equation, and it is the "homogeneous" form of the Poisson Equation, that is, the right side of the Poisson Equation is set to 0. Solutions u are called **homogeneous solutions**. One obvious solution is $u = 2$, so we could then add 2 to (A.0.2) and get a new solution to (A.0.1). Since we have specified that our charge distribution $\rho(\mathbf{x})$ is localized to some region of space, we expect that as $x \rightarrow \infty$, we must have $\phi \rightarrow 0$, as (A.0.1) states. The solution (A.0.2) meets this requirement, but if we add 2, then our boundary condition $\phi(\infty) = 0$ is not met, so we must rule out adding a 2. We would also rule out $2x + 3$, for example, or $7xy$. Recall that $\nabla^2 = \partial_x^2 + \partial_y^2 + \partial_z^2$.

It turns out that the only solution of $\nabla^2 u = 0$ which meets the requirement $u \rightarrow 0$ as $\mathbf{x} \rightarrow \infty$ in all directions is the trivial function $u(\mathbf{x}) = 0$. In 2D one intuitively sees this because a massless taut thin rubber sheet (drum head) tied down to height $u = 0$ around a circular perimeter is going to be a *flat* rubber sheet with $u = 0$ everywhere. The solutions to the 3D equation $\nabla^2 u = 0$ are called harmonic functions, and it is not hard to show that any harmonic function must take both its max and min values on the boundary, which here is a 3D great sphere. Thus $u_{\max} = 0$ and $u_{\min} = 0$, so the only possibility is that $u(\mathbf{x}) \equiv 0$ everywhere.

The implication of the previous paragraph is that (A.0.2) is the only possible solution of (A.0.1) because the only homogeneous solution one is allowed to add to (A.0.2) is $u = 0$. One can suppose there are two different solutions of $-\nabla^2 \phi = \rho/\epsilon$ called ϕ and ϕ' both of which go to 0 on the great sphere. Then $-\nabla^2(\phi - \phi') = 0$ with $(\phi - \phi') \rightarrow 0$ on the great sphere. But then $(\phi - \phi') = 0$ so $\phi' = \phi$ and there cannot then exist two different physical solutions of (A.0.1).

(d) In the following discussions, we shall be less explicit about boundary conditions like $\phi(\infty) = 0$, but they are always implied because we shall always be considering only a local distribution of sources. One convenient implication of such boundary conditions is that the "parts" of **parts integrations** often vanish, since they involve functions evaluated on the Great Sphere (or Great Circle in 2D). To clarify this perhaps obscure comment, here is a statement of two integral theorems where V is an n dimensional volume and S is an $n-1$ dimensional surface enclosing that volume:

$$\int_V dV \nabla \phi = \int_S dS \phi \quad // \text{"integral of a gradient theorem"} \quad (\text{A.0.5})$$

$$\int_V dV \psi(\nabla \phi) = - \int_V dV (\nabla \psi) \phi + \int_S dS (\psi \phi) \quad // \text{"parts integration"} \quad (\text{A.0.6})$$

"the minus sign" "the parts"

The first theorem is just the divergence theorem (1.1.30) applied to $\mathbf{F}(\mathbf{x}) = \phi(\mathbf{x}) \mathbf{a}$ where \mathbf{a} is a constant vector. It happens that $\nabla \cdot \mathbf{F} = \partial_i F_i = \partial_i [\phi a_i] = (\partial_i \phi) a_i = \nabla \phi \cdot \mathbf{a}$, so

$$\int_{\mathbf{v}} dV \nabla \cdot \mathbf{F} = \int_{\mathbf{s}} d\mathbf{S} \cdot \mathbf{F} \quad \Rightarrow \quad \left(\int_{\mathbf{v}} dV \nabla \varphi \right) \cdot \mathbf{a} = \int_{\mathbf{s}} d\mathbf{S} \cdot [\varphi \mathbf{a}] = \left(\int_{\mathbf{s}} d\mathbf{S} \varphi \right) \cdot \mathbf{a}$$

By setting $\mathbf{a} = \hat{\mathbf{x}}, \hat{\mathbf{y}}$ and $\hat{\mathbf{z}}$ one concludes that $\int_{\mathbf{v}} dV \nabla \varphi = \int_{\mathbf{s}} d\mathbf{S} \varphi$.

The second theorem is the first applied to the function $\varphi \rightarrow \psi \varphi$ and is the generalization of 1D parts integration to n dimensional space. The "parts" is $\int_{\mathbf{s}} d\mathbf{S} (\psi \varphi)$ and if S is the Great Sphere, then this integral involves ψ and φ evaluated on the Great Sphere, and usually one of these functions is 0 there. In what follows, we shall often be swinging a derivative from one function to the other inside an integral, and we ignore the parts for the reason just stated.

A.1 Existence of \mathbf{A} such that $\mathbf{B} = \text{curl } \mathbf{A}$ and $\text{div } \mathbf{A} = 0$

Fact 1: If $\text{div } \mathbf{B} = 0$, there exists an \mathbf{A} such that $\mathbf{B} = \text{curl } \mathbf{A}$ and $\text{div } \mathbf{A} = 0$. (A.1.0)

The "gauge choice" $\text{div } \mathbf{A} = 0$ is known as the Coulomb or Transverse Gauge. More on gauges later.

Proof: There are several parts to the proof:

(a) If \mathbf{A} exists such that $\mathbf{B} = \text{curl } \mathbf{A}$, then it will certainly be true that $\text{div } \mathbf{B} = 0$, since $\text{div curl } \mathbf{A} = 0$ for any vector field \mathbf{A} . The problem is showing that \mathbf{A} exists, and moreover, that an \mathbf{A} exists with $\text{div } \mathbf{A} = 0$.

(b) Consider the following differential equation (at this point \mathbf{A} is some undefined vector field):

$$-\nabla^2 \mathbf{A} = \text{curl } \mathbf{B} \tag{A.1.1a}$$

or, in Cartesian coordinates,

$$-\nabla^2 (A_{\mathbf{i}}) = [\text{curl } \mathbf{B}]_{\mathbf{i}} . \tag{A.1.1b}$$

We may regard this as the Poisson equation (A.0.1) where $\varphi \rightarrow A_{\mathbf{i}}$ and $\rho \rightarrow \epsilon [\text{curl } \mathbf{B}]_{\mathbf{i}}$. We know that a Poisson equation of the form (A.0.1) has a unique physical solution of the form (A.0.2), so the solution of (A.1.1) is given by

$$\mathbf{A}(\mathbf{x}) = \frac{1}{4\pi} \int d^3 \mathbf{x}' \frac{\text{curl}' \mathbf{B}(\mathbf{x}')}{|\mathbf{x} - \mathbf{x}'|} . \tag{A.1.2}$$

As with ρ in the previous section, we think of $\text{curl } \mathbf{B}$ as being localized in some region near the origin and dropping off at large distances. Perhaps \mathbf{B} is generated by some currents in this localized region.

We take (A.1.2) to be a *candidate* expression for the vector field \mathbf{A} . If we can show that $\text{div } \mathbf{A} = 0$ and that $\mathbf{B} = \text{curl } \mathbf{A}$, then (A.1.2) is a viable expression for \mathbf{A} ("proof by construction").

(c) Take the divergence of both sides of (A.1.2) [implied sum on i]

$$\operatorname{div} \mathbf{A}(\mathbf{x}) = \partial_i A_i(\mathbf{x}) = \frac{1}{4\pi} \int d^3 \mathbf{x}' [\operatorname{curl}' \mathbf{B}(\mathbf{x}')]_i \partial_i \frac{1}{|\mathbf{x} - \mathbf{x}'|} . \quad (\text{A.1.3})$$

We can replace ∂_i by $-\partial'_i$ acting on $1/|\mathbf{x} - \mathbf{x}'|$. Then we can do parts integration and move ∂'_i onto $[\operatorname{curl}' \mathbf{B}(\mathbf{x}')]_i$ with a parts sign change. In doing so, we assume that at infinity we pick up no "parts" since $\operatorname{curl} \mathbf{B}$ is assumed to drop off sufficiently fast. We end up then with:

$$\operatorname{div} \mathbf{A}(\mathbf{x}) = \frac{1}{4\pi} \int d^3 \mathbf{x}' \frac{\operatorname{div}' \operatorname{curl}' \mathbf{B}(\mathbf{x}')}{|\mathbf{x} - \mathbf{x}'|} . \quad (\text{A.1.4})$$

But $\operatorname{div} \operatorname{curl} \mathbf{F} = 0$ for any vector field \mathbf{F} , so the integrand and integral vanish. Thus, we conclude that

$$\operatorname{div} \mathbf{A} = 0 . \quad (\text{A.1.5})$$

(d) Next, take the curl of both sides of (A.1.2). Here is the i^{th} component [implied sums on j and k, and ε_{ijk} is the totally antisymmetric permutation tensor used to express curl components]

$$[\operatorname{curl} \mathbf{A}(\mathbf{x})]_i = \varepsilon_{ijk} \partial_j A_k(\mathbf{x}) = + \varepsilon_{ijk} \frac{1}{4\pi} \int d^3 \mathbf{x}' [\operatorname{curl}' \mathbf{B}(\mathbf{x}')]_k \partial_j \frac{1}{|\mathbf{x} - \mathbf{x}'|} . \quad (\text{A.1.6})$$

As before, replace ∂_j by $-\partial'_j$ acting on $(1/|\mathbf{x} - \mathbf{x}'|)$. Then do parts to move ∂'_j onto $[\operatorname{curl}' \mathbf{B}(\mathbf{x}')]_k$. As before, there is no "parts contribution". The result can then be put back into full vector notation to give:

$$\operatorname{curl} \mathbf{A}(\mathbf{x}) = + \frac{1}{4\pi} \int d^3 \mathbf{x}' \frac{\operatorname{curl}' \operatorname{curl}' \mathbf{B}(\mathbf{x}')}{|\mathbf{x} - \mathbf{x}'|} . \quad (\text{A.1.7})$$

Now use the vector identity $\operatorname{curl} \operatorname{curl} \mathbf{B} = \operatorname{grad} \operatorname{div} \mathbf{B} - \nabla^2 \mathbf{B} = -\nabla^2 \mathbf{B}$, since $\operatorname{div} \mathbf{B} = 0$. This gives

$$\operatorname{curl} \mathbf{A}(\mathbf{x}) = - \frac{1}{4\pi} \int d^3 \mathbf{x}' \frac{\nabla'^2 \mathbf{B}(\mathbf{x}')}{|\mathbf{x} - \mathbf{x}'|} . \quad (\text{A.1.8})$$

The next step is to move the operator ∇'^2 onto the other integrand factor $1/|\mathbf{x} - \mathbf{x}'|$ by doing a *double* parts, and again for each parts operation there is no parts contribution from the Great Sphere at infinity. We then use the fact (A.0.4) that $\nabla^2(1/|\mathbf{x} - \mathbf{x}'|) = -4\pi \delta(\mathbf{x} - \mathbf{x}')$ to get

$$\operatorname{curl} \mathbf{A}(\mathbf{x}) = - \frac{1}{4\pi} [-4\pi \mathbf{B}(\mathbf{x})] = \mathbf{B}(\mathbf{x}) . \quad (\text{A.1.9})$$

Thus, assuming $\operatorname{div} \mathbf{B} = 0$, we have formally constructed in (A.1.2) a vector field \mathbf{A} such that $\mathbf{B} = \operatorname{curl} \mathbf{A}$ and $\operatorname{div} \mathbf{A} = 0$, and this was the claim of Fact 1 stated above.

A.2 Existence of \mathbf{A}' such that $\mathbf{B} = \text{curl } \mathbf{A}'$ and $\text{div } \mathbf{A}' = \mathbf{f}$.

Fact 2: If $\text{div } \mathbf{B} = 0$, there exists \mathbf{A}' such that $\mathbf{B} = \text{curl } \mathbf{A}'$ and $\text{div } \mathbf{A}' = \mathbf{f}(\mathbf{x})$, where $\mathbf{f}(\mathbf{x})$ is an arbitrary scalar field which "drops off" in some reasonable (sufficient) manner as $|\mathbf{x}| \rightarrow \infty$. (A.2.0)

Proof: From Fact 1, we first find \mathbf{A} such that $\mathbf{B} = \text{curl } \mathbf{A}$ and $\text{div } \mathbf{A} = 0$. We then define

$$\mathbf{A}' \equiv \mathbf{A} + \text{grad } \Lambda \quad \text{dim}(\Lambda) = \text{volt-sec} \quad (\text{A.2.1})$$

where Λ is some so-far arbitrary function (scalar field). As shown below (1.3.1), $\text{dim}(\mathbf{A}) = \text{volt-sec/m}$, and therefore $\text{dim}(\Lambda) = \text{volt-sec}$. It follows from (A.2.1) that

$$\text{div } \mathbf{A}' = \text{div } \mathbf{A} + \nabla^2 \Lambda = \nabla^2 \Lambda. \quad (\text{A.2.2})$$

We would like to have $\text{div } \mathbf{A}' = \mathbf{f}$, so we must find Λ such that

$$\nabla^2 \Lambda = \mathbf{f}. \quad \text{dim}(\mathbf{f}) = \text{volt-sec/m}^2 \quad (\text{A.2.3})$$

But this is once again Poisson's Equation (A.0.1) with $\phi \rightarrow \Lambda$ and $\rho \rightarrow -\epsilon \mathbf{f}$. Translating (A.0.2) we then find that

$$\Lambda(\mathbf{x}) = -\frac{1}{4\pi} \int d^3 \mathbf{x}' \frac{\mathbf{f}(\mathbf{x}')}{|\mathbf{x} - \mathbf{x}'|}. \quad (\text{A.2.4})$$

Meanwhile, from (A.2.1) we also conclude that, since $\text{curl grad } g = 0$ for any function g ,

$$\text{curl } \mathbf{A}' = \text{curl } \mathbf{A} + \text{curl grad } \Lambda = \text{curl } \mathbf{A} = \mathbf{B}. \quad (\text{A.2.5})$$

Thus, assuming $\text{div } \mathbf{B} = 0$, we have formally constructed a vector field \mathbf{A}' such that $\mathbf{B} = \text{curl } \mathbf{A}'$ and $\text{div } \mathbf{A}' = \mathbf{f}(\mathbf{x})$ where $\mathbf{f}(\mathbf{x})$ is any function we like that drops off sufficiently fast as $|\mathbf{x}| \rightarrow \infty$, and this is the claim of Fact 2. If $\mathbf{f}(\mathbf{x})$ drops off away from the origin, this is like the $\rho(\mathbf{x})$ of Fact 0, and we find that $\Lambda \rightarrow 0$ as $\mathbf{x} \rightarrow \infty$ in any direction. Then since $\Lambda = 0$ on the Great Sphere, we know that there are no homogenous solutions to $\nabla^2 \Lambda = 0$ which could be added to (A.2.4) and so $\Lambda(\mathbf{x})$ is uniquely determined by our selected function $\mathbf{f}(\mathbf{x})$. The function $\Lambda(\mathbf{x})$ is called a gauge function for reasons given below.

A.3 Existence of ϕ such that $\mathbf{E} = -\text{grad } \phi$

Fact 3: If $\text{curl } \mathbf{E} = 0$, then there exists a ϕ such that $\mathbf{E} = -\text{grad } \phi$. (A.3.0)

Proof: This proof is almost identical to that of Fact 1, but a little simpler.

(a) If ϕ exists such that $\mathbf{E} = -\text{grad } \phi$, then it will certainly be true that $\text{curl } \mathbf{E} = 0$, since $\text{curl grad } \phi = 0$ for any function ϕ . The problem is showing that ϕ exists.

(b) Consider the following differential equation (at this point ϕ is some undefined scalar field):

$$\nabla^2 \varphi = - \operatorname{div} \mathbf{E} . \quad (\text{A.3.1})$$

This is yet again Poisson's equation (A.0.1) for φ , this time with $\rho \rightarrow \varepsilon \operatorname{div} \mathbf{E}$, we solve it as in (A.0.2) to get,

$$\varphi(\mathbf{x}) = \frac{1}{4\pi} \int d^3 \mathbf{x}' \frac{\operatorname{div}' \mathbf{E}(\mathbf{x}')}{|\mathbf{x} - \mathbf{x}'|} . \quad (\text{A.3.2})$$

As usual, we assume that $\operatorname{div} \mathbf{E}$ drops off in some sufficient manner away from the origin going to infinity. Perhaps \mathbf{E} is generated by a charge distribution in some region near the origin.

(c) Next, take the grad of both sides of (A.3.2). Here is the i^{th} component:

$$\partial_i \varphi(\mathbf{x}) = \frac{1}{4\pi} \int d^3 \mathbf{x}' \operatorname{div}' \mathbf{E}(\mathbf{x}') \partial_j \frac{1}{|\mathbf{x} - \mathbf{x}'|} . \quad (\text{A.3.3})$$

As usual, replace ∂_j by $-\partial'_j$ acting on $(1/|\mathbf{x} - \mathbf{x}'|)$. Then do parts to move ∂'_j onto $\operatorname{div}' \mathbf{E}(\mathbf{x}')$ with a second sign change, and also as usual there is no "parts contribution" from the Great Sphere. The result can then be put back into full vector notation to give:

$$\operatorname{grad} \varphi(\mathbf{x}) = + \frac{1}{4\pi} \int d^3 \mathbf{x}' \frac{\operatorname{grad}' \operatorname{div}' \mathbf{E}(\mathbf{x}')}{|\mathbf{x} - \mathbf{x}'|} . \quad (\text{A.3.4})$$

Now use the vector identity $\operatorname{grad} \operatorname{div} \mathbf{E} = \operatorname{curl} \operatorname{curl} \mathbf{E} + \nabla^2 \mathbf{E} = \nabla^2 \mathbf{E}$, since $\operatorname{curl} \mathbf{E} = 0$. This gives

$$\operatorname{grad} \varphi(\mathbf{x}) = \frac{1}{4\pi} \int d^3 \mathbf{x}' \frac{\nabla'^2 \mathbf{E}(\mathbf{x}')}{|\mathbf{x} - \mathbf{x}'|} . \quad (\text{A.3.5})$$

As before, move the operator ∇'^2 onto the other term $1/|\mathbf{x} - \mathbf{x}'|$ by doing a double parts. We then use the fact (A.0.4) that $\nabla'^2(1/|\mathbf{x} - \mathbf{x}'|) = -4\pi \delta(\mathbf{x} - \mathbf{x}')$ to get

$$\operatorname{grad} \varphi(\mathbf{x}) = \frac{1}{4\pi} [-4\pi \mathbf{E}(\mathbf{x})] = -\mathbf{E}(\mathbf{x}) \quad (\text{A.3.6})$$

Thus, assuming $\operatorname{curl} \mathbf{E} = 0$, we have constructed a function φ in (A.3.2) such that $\mathbf{E} = -\operatorname{grad} \varphi$, so φ must exist, and this is the claim of Fact 3.

A.4 Existence of \mathbf{A}' and φ' such that $\mathbf{B} = \operatorname{curl} \mathbf{A}'$, $\mathbf{E} = -\operatorname{grad} \varphi' - \partial_t \mathbf{A}'$, and $\operatorname{div} \mathbf{A}' = \mathbf{f}$.

Fact 4: If $\operatorname{div} \mathbf{B} = 0$ and $\operatorname{curl} \mathbf{E} = -\partial \mathbf{B} / \partial t$, then there exist both \mathbf{A}' and φ' such that $\mathbf{B} = \operatorname{curl} \mathbf{A}'$ and $\mathbf{E} = -\operatorname{grad} \varphi' - \partial \mathbf{A}' / \partial t$, and the quantity $\operatorname{div} \mathbf{A}'$ may be set to any function \mathbf{f} . (A.4.0)

Proof: We know from Fact 2 that \mathbf{A}' exists such that $\mathbf{B} = \text{curl } \mathbf{A}'$ and such that $\text{div } \mathbf{A}'$ equals any arbitrary function f . If we start with some arbitrary \mathbf{A} and ϕ , the successful \mathbf{A}' from (A.2.1) is $\mathbf{A}' = \mathbf{A} + \text{grad } \Lambda$ where Λ is given by (A.2.4) as an integral over f . What is the corresponding ϕ' ? Since the \mathbf{E} field corresponding to (\mathbf{A}, ϕ) and (\mathbf{A}', ϕ') must be the same, we must have $-\mathbf{E} = -\mathbf{E}'$ or

$$\text{grad } \phi + \partial_t \mathbf{A} = \text{grad } \phi' + \partial_t \mathbf{A}' .$$

Since $\mathbf{A}' = \mathbf{A} + \text{grad } \Lambda$, then $\partial_t \mathbf{A}' = \partial_t \mathbf{A} + \text{grad } \partial_t \Lambda$, so the above reads

$$\text{grad } \phi = \text{grad } \phi' + \text{grad } \partial_t \Lambda$$

which is satisfied by $\phi' = \phi - \partial_t \Lambda$. Thus, the successful potential pair giving $\text{div } \mathbf{A}' = f$ is this:

$$\begin{aligned} \mathbf{A}' &= \mathbf{A} + \text{grad } \Lambda \\ \phi' &= \phi - \partial_t \Lambda \end{aligned} \quad // \text{dim}(\Lambda) = \text{volt-sec} \quad (\text{A.4.1})$$

where from (A.2.4),

$$\Lambda(\mathbf{x}) = -\frac{1}{4\pi} \int d^3 \mathbf{x}' \frac{f(\mathbf{x}')}{|\mathbf{x} - \mathbf{x}'|} \quad (\text{A.2.3})$$

The pair of equations (A.4.1) is called a **gauge transformation** and we have just seen in Facts 2 and 4 that a gauge transformation preserves both \mathbf{E} and \mathbf{B} . That $\mathbf{E}' = \mathbf{E}$ was built into (A.4.1), and $\mathbf{B}' = \mathbf{B}$ since $\mathbf{B}' = \text{curl } \mathbf{A}' = \text{curl } \mathbf{A} + \text{curl } \text{grad } \Lambda = \mathbf{B} + 0 = \mathbf{B}$. Each possible choice for f implies a **gauge function** Λ from (A.2.3) which then creates the gauge transformation (A.4.1). There are an infinite set of f and corresponding Λ functions, so there are an infinite number of gauge transformations which leave the \mathbf{E} and \mathbf{B} fields invariant. We are free to **choose a gauge** such that $\text{div } \mathbf{A}' = f$ for any f we like.

A.5 Gauge Invariance

In electromagnetism, the situation of Fact 4 arises for

$$\begin{aligned} \mathbf{B} &= \text{magnetic field} \\ \mathbf{A} &= \text{vector potential} \\ \mathbf{E} &= \text{electric field} \\ \phi &= \text{scalar potential} \end{aligned}$$

Using the gauge transformation (A.4.1), one transforms from \mathbf{A}, ϕ to \mathbf{A}', ϕ' without altering the physical electromagnetic fields \mathbf{E} and \mathbf{B} . The electromagnetic fields are thus **invariant** under such a gauge transformation, and one says that the classical theory of electromagnetism is **gauge invariant**.

The word "gauge" was first used by Hermann Weyl in the context of general relativity. Gauge invariant there means that a certain "covariant derivative" transforms as a proper tensor object so that things have the same form in different coordinate systems used to measure things. These different coordinate systems were referred to as different "gauges" in the sense that a gauge is a marked-off measuring instrument used

to measure something (like the marked-off x-axis of a coordinate system). In general relativity the metric tensor $g_{\mu\nu}$, which defines the meaning of distance in the 4 dimensions of spacetime, is a function $g_{\mu\nu}(x)$ of the local location in spacetime x . Weyl considered the effect of rescaling the metric tensor according to $g_{\mu\nu}(x) \rightarrow \lambda(x)g_{\mu\nu}(x)$ where $\lambda(x)$ was an arbitrary "gauge function" (like our $\Lambda(x)$). Nowadays, gauge invariance is associated with any continuous degree(s) of freedom of a theory which don't affect physical measurements derived from the theory, such as our gauge transformation (A.4.1). See Quigley.

A.6 The Lorenz Gauge and QED

This section is certainly off the transmission-lines beaten path, but the author thought the reader might find it interesting. It is true that the nature of a transmission line results from photons "jumping back and forth" between the conductors. Unlike elsewhere in this document, everything is not fully explained in the following quick outline. A more detailed description of the tensor notation used below may be found in the author's *Tensor Analysis* document and elsewhere.

In relativistic notation one uses 4-vectors which have one time component and three spatial components such as $x^\mu = (ct, x, y, z)$ which denotes a point in "spacetime". The time component t is multiplied by the speed of light c so that all four components have the same units -- distance L . Often people measure distance in light-seconds instead of meters so in such units $c = 1$, but we shall display the c to keep track of units. This x^μ is a "contravariant" (index up) 4-vector and the corresponding "covariant" (index down) 4-vector is $x_\mu = (ct, -x, -y, -z)$. Thus, one has $x^0 = x_0 (= ct)$ but $x^i = -x_i$. We are assuming here the "Bjorken-Drell metric" $g_{\mu\nu} = \text{diag}(1, -1, -1, -1)$. The gradient operator ∂_i "transforms as" the spatial part of the covariant 4-vector ∂_μ , and one can write $\partial^i = -\partial_i$ just as $x^i = -x_i$ for $i = 1, 2, 3$. This four-vector gradient operator can be written $\partial_\mu = (\partial_0, \partial_i)$ and $\partial^\mu = (\partial^0, \partial^i) = (\partial_0, -\partial_i)$ where $\partial^0 = \partial_0 = \frac{1}{c} \partial_t = \frac{1}{c} \frac{\partial}{\partial t}$. The four components of ∂^μ all have dimension L^{-1} . The Laplacian is $\nabla^2 = \partial_i \partial_i = \frac{\partial}{\partial x^i} \frac{\partial}{\partial x^i}$

(implied sum on i) while the corresponding object $\square \equiv \partial_\mu \partial^\mu = \frac{1}{c^2} \partial_t^2 - \nabla^2$ is the D'Alembertian which appears in wave equations.

Consider then the gauge transformation (A.4.1) which in relativistic tensor notation is

$$\begin{aligned} A^{i'} &= A^i + \partial_i \Lambda = A^i - \partial^i \Lambda & i &= 1, 2, 3 \\ \varphi' &= \varphi - \partial_t \Lambda = \varphi - c \partial^0 \Lambda \end{aligned} \quad (\text{A.6.1})$$

The components of a classical vector like \mathbf{A} , normally written as A_i , are in fact the contravariant components A^i in tensor notation. If we now define $A^0 \equiv \frac{1}{c} \varphi$ we can combine the two gauge transformation equations into a single equation involving three 4-vectors (one of which is $\partial^\mu \Lambda$),

$$A^{\mu'} = A^\mu - \partial^\mu \Lambda \quad \mu = 0, 1, 2, 3 \quad (\text{A.6.2})$$

Suppose we want $\partial_\mu A^{\mu'} = 0$ (implicit sum on $\mu = 0, 1, 2, 3$). This would be a relativistic version of the Coulomb gauge choice that $\partial_i A^i = \text{div } \mathbf{A} = 0$. If we could find a potential $A^{\mu'}$ with this property, that would be very convenient for the following reason: In general $a_\mu b^\mu (= a^\mu b_\mu = \mathbf{a} \cdot \mathbf{b})$ is the same in all

frames of reference related by Lorentz Transformations. If $\partial_{\mu}A^{\mu} = 0$ in one frame, it is 0 in all frames, and that makes computational life simple. For example, let S and S'' be two frames of reference related by a Lorentz transformation. Then the implication is that

$$\underset{\text{frame S observer}}{\partial_{\mu}A^{\mu}(x^{\nu}) = 0} \quad \Rightarrow \quad \underset{\text{frame S'' observer}}{\partial''_{\mu}A^{\mu}(x''^{\nu}) = 0} \quad \text{where} \quad \partial_{\mu} \equiv \partial/\partial x^{\mu} \quad \text{and} \quad \partial''_{\mu} \equiv \partial/\partial x''^{\mu}$$

So, is it possible to have $\partial_{\mu}A^{\mu} = 0$? Writing this out we get

$$\partial_0 A'^0 + \partial_i A'^i = 0 \quad \Rightarrow \quad \frac{1}{c} \partial_t \left[\frac{1}{c} \phi' \right] + \text{div } \mathbf{A}' = 0 \quad \Rightarrow \quad \frac{1}{c^2} \partial_t \phi' + \text{div } \mathbf{A}' = 0$$

so

$$\text{div } \mathbf{A}' = -\frac{1}{c^2} \partial_t \phi'. \tag{A.6.3}$$

But we showed in Fact 2 that given any \mathbf{A} , we can find an E-B-fields-equivalent \mathbf{A}' which has $\text{div } \mathbf{A}' =$ any $f(\mathbf{x})$ we want, so we just select $f(\mathbf{x}) = -(1/c^2) \partial\phi'/\partial t$. By selecting this $f(\mathbf{x})$, we are **selecting the Lorenz Gauge**. In this gauge (now dropping the prime on A), one has $\partial_{\mu}A^{\mu} = 0$. Thus, the condition defining the Lorenz Gauge is Lorentz covariant under all Lorentz transformations. The reason is that both sides of $\partial_{\mu}A^{\mu} = 0$ "transform" as the same kind of tensor object, in this case a scalar object. One can interpret $\partial_{\mu}A^{\mu} = 0$ as $\partial \bullet \mathbf{A} = 0$ where ∂ is a 4-divergence operator. Thus, in the Lorenz gauge, the 4-divergence of A^{μ} is always exactly 0 at every point in spacetime. [Lorenz and Lorentz are two different people, see the Comment below equation (1.3.6).]

In 3D if we said that $\text{div } \mathbf{F} = \partial_i F^i = 0$ defined something called a gauge condition, it would be clear that \mathbf{F} was not uniquely determined by that condition since many vector fields have zero divergence. Just so, the Lorenz gauge condition $\partial_{\mu}A^{\mu} = 0$ does not uniquely determine A^{μ} , it is just a condition on A^{μ} . So in fact there are many pairs (\mathbf{A}, ϕ) which satisfy the Lorenz gauge condition, so the term "the Lorenz gauge" is a little misleading, though we shall use it anyway. It is a class of gauges.

In relativistic quantum field theory (aka quantum electrodynamics, or QED), the potential A^{μ} is interpreted as the quantum field of a massless vector particle called the photon. The potentials ϕ and \mathbf{A} are thus promoted from being mere "helper functions" to having their own particle interpretation. In the Lagrangian density for the photon-electron system an interaction term - $J_{\mu}A^{\mu}$ appears,

$$\mathcal{L} = \dots - J_{\mu}A^{\mu} \quad J_{\mu} = e_0 \bar{\psi} \gamma_{\mu} \psi \tag{A.6.4}$$

where J_{μ} is the electric current, an operator built from the quantum field ψ of the electron. The number e_0 is the so-called bare (unrenormalized) charge of the electron. According to (A.6.2), a gauge transformation on A^{μ} creates a new term - $J_{\mu} \partial^{\mu} \Lambda$ in the Lagrangian density. In Lagrangian dynamics, the physics of QED is determined by $S = \int d^4x \mathcal{L} = \int d^3x \int dt \mathcal{L}$ which is called the action. If we insert the gauge term - $J_{\mu} \partial^{\mu} \Lambda$ into the action and do parts integration to move ∂^{μ} from Λ to J_{μ} , we end up with an action change $\Delta S = \int d^4x (\partial^{\mu} J_{\mu}) \Lambda$. But at every point in spacetime, we know that $\partial^{\mu} J_{\mu} = 0$ (shown in a

moment) so we find that $\Delta S = 0$ which means the action S is invariant under any gauge transformation. The reason $\partial^\mu J_\mu = \partial_\mu J^\mu = 0$ is because $J^\mu = (c\rho, \mathbf{J}^\dagger)$ where ρ is charge density and \mathbf{J}^\dagger is electric current, and then the statement $\partial_\mu J^\mu = 0$ says that $\frac{1}{c} \partial_t(c\rho) + \partial_i J^i = 0$ or $\text{div } \mathbf{J} = -\partial\rho/\text{dt}$. This is the equation of continuity (1.1.8) which says that if there is a current flowing out of a tiny volume of space, the charge density in that volume must be correspondingly decreasing. In other words, charge is "conserved". We can reverse our logic to conclude that the reason electric charge is conserved and cannot "leak away into the vacuum" is due to the invariance of the QED action under gauge transformations (A.6.2). More generally, symmetries (invariances) of the action always result in conserved quantities. Since 1949, unusual names have been given to similar conserved quantities: isospin, strangeness, color, charm, etc. The association of a conserved quantity with a differential symmetry of the action is known as Noether's Theorem, in honor of Ms. Emmy Noether who first showed this connection in 1915.

A.7 Finding the gauge function Λ for the Lorentz Gauge: time-domain propagators

In Fact 4 (A.4.0) it was noted that if one already has a potential set (\mathbf{A}, φ) , it is possible to find a new potential set (\mathbf{A}', φ') such that $\text{div } \mathbf{A}' = f$ for any reasonable f . The method of finding the new set (\mathbf{A}', φ') was to find the function Λ from f as shown in (A.2.4) and then use the gauge transformation implied by Λ as shown in (A.4.1) to find the new potentials (\mathbf{A}', φ') .

In the discussion of the Lorenz Gauge, we thus imagine we have some (\mathbf{A}, φ) and we want then to find a potential set (\mathbf{A}', φ') such that $\text{div } \mathbf{A}' = -\frac{1}{c^2} \partial_t \varphi'$, which is the Lorenz Gauge (A.6.3). We are thus using $f = -\frac{1}{c^2} \partial_t \varphi'$ where φ' is the partner to \mathbf{A}' . One might fairly inquire what this function f actually is in terms of the starting potentials (\mathbf{A}, φ) , since one does not *a priori* know what φ' is. In other words, since we don't *a priori* know what $f(x)$ is, we cannot use (A.2.3) to find the right gauge function Λ to give the right new potentials (\mathbf{A}', φ') , so we seem to be in a circular conundrum when we try to fit this Lorenz gauge situation into the framework of our accumulated Facts above.

Here is one way to find the right function Λ in terms of (\mathbf{A}, φ) . We know from (A.2.3) and (A.4.1) that

$$\nabla^2 \Lambda = f = -\frac{1}{c^2} \partial_t \varphi' = -\frac{1}{c^2} \partial_t [\varphi - \partial_t \Lambda] .$$

This can be written as follows, where the left side is the 3D wave equation operator acting on Λ ,

$$(\partial_t^2 - c^2 \nabla^2) \Lambda = \partial_t \varphi . \tag{A.7.1}$$

Since we know φ from (\mathbf{A}, φ) , we can obtain Λ by *solving* this differential equation. The equation is similar to the Poisson equation (A.0.1) when written this way in terms of the \square symbol introduced above,

$$c^2 \square \Lambda = \partial_t \varphi . \quad // \text{ Stakgold (5.141) with } u \rightarrow \Lambda \text{ and } q \rightarrow \partial_t \varphi \tag{A.7.2}$$

Here and below we include some supporting equation numbers from Stakgold Vol II. The formal solution of (A.7.2) can be found by first defining a Green's Function as we did above in (A.0.3),

$$c^2 \square g(\mathbf{x}, t; \mathbf{x}', t') = \delta(\mathbf{x} - \mathbf{x}') \delta(t - t') \quad // \text{Stakgold (5.142)} \quad (\text{A.7.3})$$

The solution Green's function (propagator) is given by

$$\overset{\leftarrow}{c^2 g(\mathbf{x}, t; \mathbf{x}', t')} = (1/4\pi R) \delta(t - t' - R/c) \quad \text{with } R = |\mathbf{x} - \mathbf{x}'| \quad // \text{Stakgold (5.155) } n=3 \quad (\text{A.7.4})$$

We have added an arrow that shows the direction of the propagator: it runs from time t' in the past to time t in the future, in which case $t > t'$. The propagator vanishes for all $t < t'$ since in that case $t - t' - R/c < 0$ and the δ function can never get a hit. This g is an example of a "causal" Green's function and it describes an expanding spherical wavefront seen at observation point \mathbf{x} at time t propagating at velocity c from a point source at location \mathbf{x}' and time t' in the past. Formally one can then express a solution to (A.7.2) in a form similar to (A.0.2),

$$\Lambda(\mathbf{x}, t) = \int d^3x' \int dt' g(\mathbf{x}, t; \mathbf{x}', t') \partial_{t'} \phi(\mathbf{x}', t') \quad . \quad (\text{A.7.5})$$

Application of $c^2 \square$ to both sides of (A.7.5) with use of (A.7.3) reproduces (A.7.2) showing that (A.7.5) is indeed the particular solution of (A.7.2). Inserting the propagator (A.7.4) we find that

$$\Lambda(\mathbf{x}, t) = \frac{1}{4\pi c^2} \int d^3x' \frac{\partial_{t'} \phi(\mathbf{x}', t - R/c)}{R} \quad R = |\mathbf{x} - \mathbf{x}'| \quad . \quad (\text{A.7.6})$$

Thus we have solved our conundrum in that we have Λ expressed in terms of ϕ from the set (\mathbf{A}, ϕ) . The solution (A.7.6) has the same form as the retarded solutions of Section 1.4. Once we have this Λ , we may use (A.4.1) to find the set (\mathbf{A}', ϕ') given the set (\mathbf{A}, ϕ) .

Comments:

1. Whereas the Laplace equation with ∇^2 is "elliptic" in nature, the wave equation is "hyperbolic" since the various second derivatives in \square don't all have the same sign, resulting in a change in the nature of the Green's function solution, the principle fact being that it is a causal function in terms of the time coordinates. For details on the above discussion, see Stakgold Vol II p 61-63 (fundamental solutions) and p 246-256 (Green's functions for the wave equation). Stakgold treats this subject with an arbitrary number of spatial dimensions n . One finds, for example, that for $n = 3$ the propagator (A.7.4) is an expanding infinitely thin spherical shell with no wake, whereas for $n = 2$ there is a wake behind the front as in his (5.151) which says

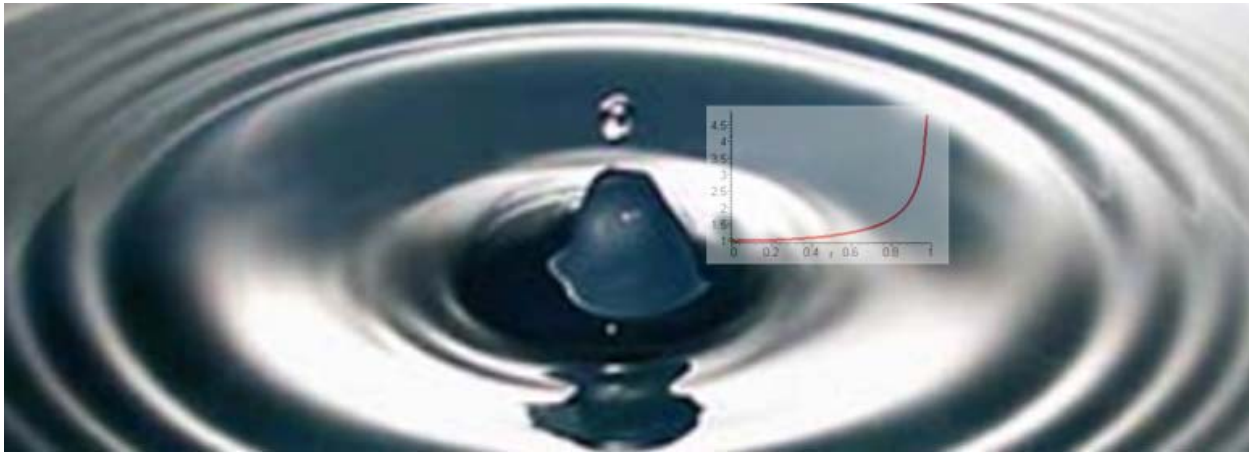
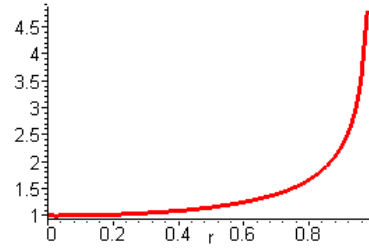
$$g(r, t) = \theta(t - r/v) 1/\sqrt{(vt)^2 - r^2} \quad (\text{A.7.7})$$

where v is wave velocity. It is difficult to create a clean unit impulse in water, but here is the rough idea:

```

g := 1/sqrt(v^2*t^2-r^2);
g = 1 / sqrt(v^2*t^2 - r^2)
v := 1; t := 1;
v = 1
plot(g, r=0..t, thickness = 3);

```



<http://physicsilluminati.blogspot.com/2012/10/wave-optics.html>

2. The time-domain Green's functions quoted in (A.7.4) for $n = 3$ and (A.7.7) for $n = 2$ are propagators for the wave equation (A.7.3) in 3D and 2D. When these Green's functions are Fourier transformed to the frequency ω domain, they become the 3D and 2D Helmholtz propagators discussed in Appendix H and I, namely

$$g_{\mathbf{F}}(\mathbf{r}, \mathbf{r}'; \omega) = e^{-jkR}/4\pi R = \text{the Helmholtz 3D free-space propagator} \quad R = |\mathbf{r} - \mathbf{r}'| \quad (H.1.7)$$

$$g_{\mathbf{F}}(\mathbf{r}, \mathbf{r}'; \omega) = (j/4) H_0^{(1)}(kR) = \text{the Helmholtz 2D free-space propagator} \quad k^2 = \omega^2 \mu \epsilon \quad (I.1.7)$$

Appendix B: Magnetization Surface Currents on a Conductor

Overview

When a conductor of magnetic permeability μ_2 is embedded in a medium of μ_1 with $\mu_1 \neq \mu_2$, a "bound current" (magnetization current) appears on the conductor surface.

Section B.1 shows how this surface current K is related to the H field at the surface.

Section B.2 shows how to compute H from the volume conduction current density J .

Section B.3 then outlines a general plan for computing surface current K for an arbitrary conductor.

Section B.4 computes H and the surface current for a round wire using symmetry.

Section B.5 repeats the calculation using the general method outlined in Section B.3.

Section B.6 presents what we call "the J_m Theorem" which shows that adding the magnetization surface current of Section B.3 to the conduction current of a transmission line conductor adjusts the Helmholtz integral for A_z so it gives the correct A_z when the conductor and dielectric have different permeabilities, $\mu_1 \neq \mu_2$.

Section B.7 shows how this " J_m Theorem" works for a round conductor. Plots are displayed for the three quantities A_z , B_θ and H_θ .

The conductors considered here are those of a transmission line in the "transmission line limit" in which it is assumed that the wavelength along the line is much longer than the transverse dimensions of the line. In this case, it is reasonable to use 2D wave equations whose solutions then involve use of the 2D Laplace free-space propagator $\ln(R/2\pi)$ as discussed in Appendix I.

B.1 Relationship between surface current K and the field H at a conductor boundary

First, consider this blowup of a piece of the boundary between a conductor (medium 2) and a dielectric (medium 1). Both media extend uniformly in the z direction, so we are looking at a piece of the cross section of a transmission line at a particular point on the surface of one of the conductors.

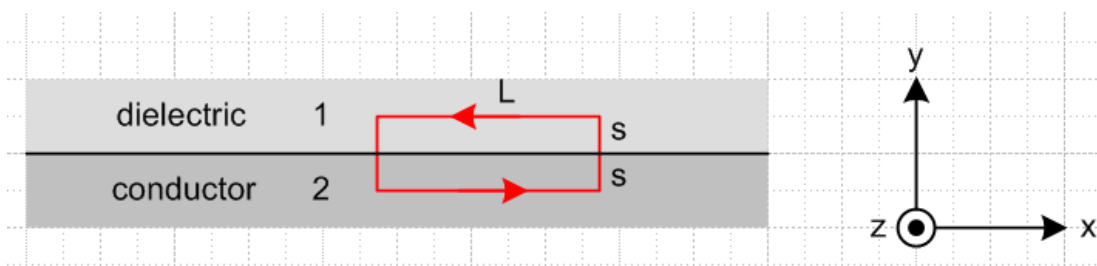


Fig B.1

We shall assume that the conduction current is positive in the z direction, so $\mathbf{J} = J_z \hat{\mathbf{z}}$ with $J_z > 0$. Since the lower medium is the conductor in the drawing, the \mathbf{B} and \mathbf{H} field at the boundary are in the $-\hat{\mathbf{x}}$ direction, that is to say, they point to the left due to the right hand rule relating \mathbf{J} and \mathbf{B} or \mathbf{H} .

According to (1.1.44), the tangential component of the \mathbf{H} field is continuous at a boundary provided the boundary does not carry a *free* surface current, which is our situation here (we ignore any Debye surface currents, see text above (4.7.9)). Therefore,

$$H_{\mathbf{x}2} = H_{\mathbf{x}1} \quad (1/\mu_1)\mathbf{B}_{\mathbf{x}1} = (1/\mu_2)\mathbf{B}_{\mathbf{x}2} \quad . \quad (\text{B.1.1})$$

Assuming $\mu_2 \geq \mu_1$ (which would be the case if $\mu_1 = \mu_0$), the right equation implies $|\mathbf{B}_{\mathbf{x}2}| \geq |\mathbf{B}_{\mathbf{x}1}|$ so the \mathbf{B} field is larger inside the conductor. But in our picture, both $\mathbf{B}_{\mathbf{x}2}$ and $\mathbf{B}_{\mathbf{x}1}$ are negative, so $-\mathbf{B}_{\mathbf{x}2} \geq -\mathbf{B}_{\mathbf{x}1}$ which then says $\mathbf{B}_{\mathbf{x}2} \leq \mathbf{B}_{\mathbf{x}1}$ and finally $(\mathbf{B}_{\mathbf{x}2} - \mathbf{B}_{\mathbf{x}1}) \leq 0$. Also, $H_{\mathbf{x}2} = H_{\mathbf{x}1} \leq 0$. For the red loop shown in the figure one then has, as $s \rightarrow 0$,

$$\oint \mathbf{B} \cdot d\mathbf{s} = B_{\mathbf{x}2}L - B_{\mathbf{x}1}L = (\mathbf{B}_{\mathbf{x}2} - \mathbf{B}_{\mathbf{x}1})L \leq 0 \quad . \quad (\text{B.1.2})$$

Now consider Stokes's theorem (1.1.31) and (1.1.24) which say (in the ω domain),

$$\oint \mathbf{B} \cdot d\mathbf{s} = \int_{\mathbf{s}} \text{curl } \mathbf{B} \cdot d\mathbf{S} = \mu_0 \int_{\mathbf{s}} [j\omega\epsilon\mathbf{E} + \mathbf{J}_c + \mathbf{J}_m] \cdot d\mathbf{S} \quad (\text{B.1.3})$$

where $d\mathbf{S} = dS \hat{\mathbf{z}}$. Since $\mathbf{E} \cdot d\mathbf{S}$ involves only E_z (parallel to surface), and since by (1.1.41) such E_z is continuous at the boundary, and since $E_z \approx 0$ inside the conductor, the $\epsilon j\omega\mathbf{E}$ term makes no contribution, giving then

$$\oint \mathbf{B} \cdot d\mathbf{s} = \mu_0 \int_{\mathbf{s}} [\mathbf{J}_c + \mathbf{J}_m] \cdot d\mathbf{S} \quad . \quad (\text{B.1.4})$$

As the distance s is taken to 0 in the red math loop above, $\int_{\mathbf{s}} \mathbf{J}_c \cdot d\mathbf{S} \rightarrow 0$ because the conduction current is non-singular at the boundary. That is to say, $\int_{\mathbf{s}} \mathbf{J}_c \cdot d\mathbf{S} \rightarrow \mathbf{J}_c \cdot \int_{\mathbf{s}} d\mathbf{S} \rightarrow 0$. Since we shall take this limit in the end, we can then ignore the \mathbf{J}_c term in (B.1.4) and write

$$\oint \mathbf{B} \cdot d\mathbf{s} = \mu_0 \int_{\mathbf{s}} \mathbf{J}_m \cdot d\mathbf{S} \quad \text{intending to take } s \rightarrow 0 \quad . \quad (\text{B.1.5})$$

Since \mathbf{J}_c flows in the $+\hat{\mathbf{z}}$ direction, the surface current \mathbf{J}_m flows in the $-\hat{\mathbf{z}}$ direction (as shown below), so write

$$\mathbf{J}_m = K_z \delta(y) \hat{\mathbf{z}} \quad (\text{B.1.6})$$

where $K_z \leq 0$ is the magnitude of the magnetization surface current. Then

$$\int_S \mathbf{J}_m \cdot d\mathbf{S} = K_z \int_0^L dx \int_{-s}^s dy \delta(y) \hat{\mathbf{z}} \cdot \hat{\mathbf{z}} = K_z \int_0^L dx = K_z L . \quad (\text{B.1.7})$$

Thus from (B.1.2), (B.1.5) and (B.1.7) we find that

$$\mu_0 K_z = B_{x2} - B_{x1} . \quad (\text{B.1.8})$$

Compare this with (1.1.44) which says (as noted earlier, $K_z^{\text{free}} = 0$ on the boundary)

$$0 = H_{x2} - H_{x1} . \quad (1.1.44)$$

The H field does not "see" the magnetization surface current K_z , but the B field does see it.

The signs are consistent with $K_z \leq 0$ and $(B_{x2} - B_{x1}) \leq 0$ as noted above. Then from (B.1.1) we find

$$\mu_0 K_z = B_{x2} - B_{x1} = (\mu_2 H_{x2} - \mu_1 H_{x1}) = (\mu_2 - \mu_1) H_{x2}$$

and finally

$$K_z = \left(\frac{\mu_2}{\mu_0} - \frac{\mu_1}{\mu_0} \right) H_{x2} . \quad (\text{B.1.9})$$

As noted earlier, $H_{x2} < 0$ so $K_z \leq 0$ is consistent with $\mu_2 \geq \mu_1$.

We now rewrite this result in terms of a different picture: $\hat{\mathbf{z}}$

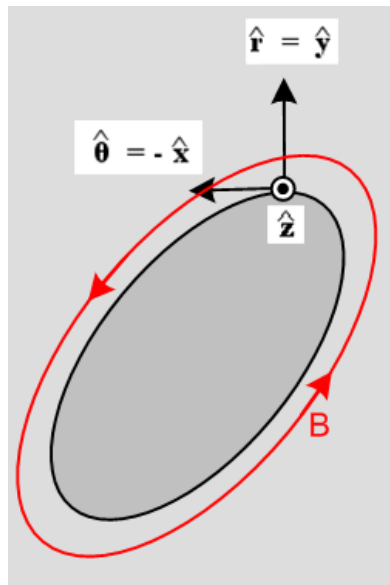


Fig B.2

This shows the cross section of the entire conductor in gray, and \mathbf{J}_c is still directed toward the viewer. In this picture a point on the surface is associated with a local coordinate system for which $\hat{\mathbf{r}} = \hat{\mathbf{y}}$ is normal

to the surface and $\hat{\boldsymbol{\theta}} = -\hat{\boldsymbol{x}}$ is tangent to the surface (so $H_{\boldsymbol{\theta}} = -H_{\boldsymbol{x}}$). We are thinking of (r,θ,z) as local cylindrical coordinates at the point shown on the conductor surface, where $\hat{\boldsymbol{r}} \times \hat{\boldsymbol{\theta}} = \hat{\boldsymbol{z}}$, and the x,y,z directions of the figure match those of the previous figure where as usual $\hat{\boldsymbol{x}} \times \hat{\boldsymbol{y}} = \hat{\boldsymbol{z}}$. Then (B.1.9) says

$$\mathbf{K}_{\mathbf{z}} = - \left(\frac{\mu_2}{\mu_0} - \frac{\mu_1}{\mu_0} \right) H_{\boldsymbol{\theta}} \quad \text{amps/m} \quad (\text{B.1.10})$$

where $H_{\boldsymbol{\theta}} > 0$ and $\mathbf{K}_{\mathbf{z}} \leq 0$.

In general, $\mathbf{K}_{\mathbf{z}}$ is a function of position on the perimeter of the conductor cross section.

We can compute the total magnetization current $I_{\mathbf{m}}$ (amps) by integrating $\mathbf{K}_{\mathbf{z}}$ around the perimeter of the conductor:

$$\int_{\mathbf{C}} \mathbf{K}_{\mathbf{z}} \, ds = - \left(\frac{\mu_2}{\mu_0} - \frac{\mu_1}{\mu_0} \right) \int_{\mathbf{C}} H_{\boldsymbol{\theta}} \, ds = - \left(\frac{\mu_2}{\mu_0} - \frac{\mu_1}{\mu_0} \right) \oint_{\mathbf{C}} \mathbf{H} \cdot d\mathbf{s}$$

But by (1.1.37),

$$\oint_{\mathbf{C}} \mathbf{H} \cdot d\mathbf{s} = \int_{\mathbf{S}} [j\omega\epsilon\mathbf{E} + \mathbf{J}] \cdot d\mathbf{S} = \int_{\mathbf{S}} [j\omega\epsilon E_z + J_z] \, dS \approx \int_{\mathbf{S}} J_z \, dS = I$$

and therefore

$$I_{\mathbf{m}} \equiv \int_{\mathbf{C}} \mathbf{K}_{\mathbf{z}} \, ds = - \left(\frac{\mu_2}{\mu_0} - \frac{\mu_1}{\mu_0} \right) I \quad (\text{B.1.11})$$

The ratio of the magnetization current to the conduction current is given by constant $f_{\mathbf{m}}$,

$$f_{\mathbf{m}} \equiv I_{\mathbf{m}}/I = - \left(\frac{\mu_2}{\mu_0} - \frac{\mu_1}{\mu_0} \right). \quad (\text{B.1.12})$$

and this result is independent of the shape of the conductor. Of course if $\mu_1 = \mu_2$, there is no magnetization current and $\mathbf{K}_{\mathbf{z}}$ and $I_{\mathbf{m}}$ are both zero.

Example: For a round wire of radius a carrying an axially symmetric current distribution, we know that $2\pi a H_{\boldsymbol{\theta}} = I$ so $H_{\boldsymbol{\theta}} = I/(2\pi a)$ at the surface. Then

$$\mathbf{K}_{\mathbf{z}} = - \left(\frac{\mu_2}{\mu_0} - \frac{\mu_1}{\mu_0} \right) [I/(2\pi a)] \quad // \text{ round wire of radius } a \text{ and } \mu_2, \text{ dielectric } \mu_1 \quad (\text{B.1.13})$$

The total surface magnetization current integrated around the round wire surface is then

$$I_{\mathbf{m}} = 2\pi a \mathbf{K}_{\mathbf{z}} = - \left(\frac{\mu_2}{\mu_0} - \frac{\mu_1}{\mu_0} \right) I \quad (\text{B.1.14})$$

in agreement with (B.1.11).

For example, if the dielectric has $\mu_1 = \mu_0$ and the conductor has $\mu_2 = 2\mu_0$, then $I_{\text{mag}} = -I$.

We return to this example in Section B.4 below.

Physical mechanism of the magnetization surface current. As a reminder, a surface magnetization current arises at a boundary between media with different μ values just the way surface polarization charge arises at a boundary between media with different ϵ . In the μ case, here is a suggestive picture :

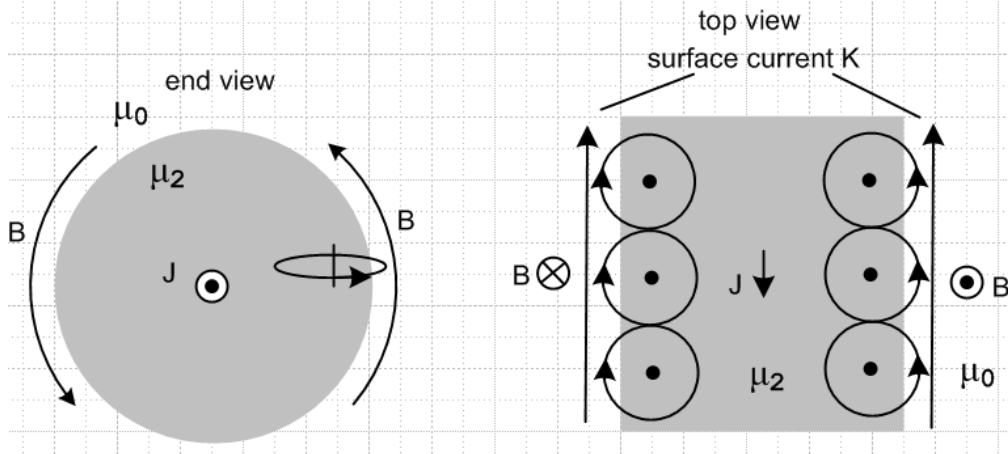


Fig B.3

On the left we look at a round wire end on, while the right shows a top view where the front end of the wire on the left has been tilted down. Here $\mu_1 = \mu_0$ so there is only vacuum outside the wire. The \mathbf{B} field lines up the little magnetic dipoles (or creates them) according to the right hand rule which we represent schematically as little atoms with orbiting electrons. On the right, \mathbf{B} comes out of paper and lines up the magnetic moments CCW as shown there. On the left, \mathbf{B} goes into paper so the moments are lined up clockwise instead. In both cases, the resulting magnetization surface current is in the same direction, as indicated by the arrows of the loops hanging outside the wire. The picture shows why it is that the surface current is directed opposite to the current \mathbf{J} which creates it, a sort of magnetization Lenz's Law. Note that this surface current is "not seen" by \mathbf{H} , but it is seen by \mathbf{B} , as mentioned in (1.1.24). [Atom arrows represent current, electrons go in the opposite direction.]

In the case that the outer medium has some $\mu_1 > \mu_0$, both media have surface currents at the boundary, and then when $\mu_1 \neq \mu_2$ there is a surface current imbalance resulting in a net surface current. If it happens that $\mu_1 < \mu_2$, then the directions shown above are correct, but if $\mu_1 > \mu_2$, the surface current runs in the opposite direction to that shown.

There is also a bulk volume magnetization current away from the surface, not shown above. Details of the magnetization current \mathbf{J}_m for a round wire are computed (DC) in Appendix G (G.3.4) where the current density \mathbf{J}_{mz} includes a surface delta function.

B.2 Calculation of \mathbf{H} from the current \mathbf{J} in a conductor

(a) An expression for \mathbf{H} in terms of \mathbf{J}

First, we want to clarify the connection between \mathbf{H} and \mathbf{J} in terms of Maxwell's equations. Since $\mathbf{J} = \sigma\mathbf{E}$, we can write the curl \mathbf{H} equation (1.1.1) in these three equivalent ways:

$$\text{a} \quad \text{curl } \mathbf{H} = j\omega\epsilon\mathbf{E} + \mathbf{J} = \text{displacement current} + \text{conduction current} \quad (1.1.1) \quad (\text{B.2.1a})$$

$$\text{b} \quad \text{curl } \mathbf{H} = j\omega(\xi/\sigma)\mathbf{J} \quad \xi \equiv \epsilon - j\sigma/\omega = \epsilon + \sigma/j\omega \quad (\text{B.2.1b})$$

$$\text{c} \quad \text{curl } \mathbf{H} = j\omega\xi\mathbf{E} . \quad (\text{B.2.1c})$$

Using the identity $\text{curl curl} = \text{grad div} - \nabla^2$ and noting that $\text{div } \mathbf{H} = \mu \text{div } \mathbf{B} = 0$ from (1.1.4) we find

$$\text{curl curl } \mathbf{H} = -\nabla^2\mathbf{H} . \quad (\text{B.2.2})$$

Applying curl to the three forms above, then using (B.2.2) and doing some small algebra as shown below, one obtains these three exactly equivalent equations for \mathbf{H} :

$$\text{a} \quad (\nabla^2 + \kappa^2)\mathbf{H} = -\text{curl } \mathbf{J} \quad \kappa^2 = \omega^2\epsilon\mu \quad // \text{ agrees with (1.5.26)} \quad (\text{B.2.3a})$$

$$\text{b} \quad \nabla^2\mathbf{H} = -j\omega(\xi/\sigma)\text{curl } \mathbf{J} = -[1 + j\omega(\epsilon/\sigma)]\text{curl } \mathbf{J} \quad \xi \equiv \epsilon + \sigma/j\omega \quad (\text{B.2.3b})$$

$$\text{c} \quad (\nabla^2 + \beta^2)\mathbf{H} = 0 \quad \beta^2 = \omega^2\xi\mu \quad // \text{ agrees with (1.5.27)} \quad (\text{B.2.3c})$$

Forms a and c make use of (1.1.2) which says $\text{curl } \mathbf{E} = -j\omega\mathbf{B} = -j\omega\mu\mathbf{H}$.

Algebra:

$$\text{a} \quad -\nabla^2\mathbf{H} = \text{curl}(j\omega\epsilon\mathbf{E} + \mathbf{J}) = j\omega\epsilon(-j\omega\mu\mathbf{H}) + \text{curl } \mathbf{J} = \omega^2\epsilon\mu\mathbf{H} + \text{curl } \mathbf{J} = \kappa^2\mathbf{H} + \text{curl } \mathbf{J}$$

$$\text{b} \quad -\nabla^2\mathbf{H} = \text{curl}(j\omega(\xi/\sigma)\mathbf{J}) = j\omega(\xi/\sigma)\text{curl } \mathbf{J}$$

$$\text{c} \quad -\nabla^2\mathbf{H} = \text{curl}(j\omega\xi\mathbf{E}) = (j\omega\xi)(-j\omega\mu\mathbf{H}) = \omega^2\xi\mu\mathbf{H} = \beta^2\mathbf{H}$$

We showed below (2.2.2) that for $f \ll 10^{18}$ Hz, we have $\omega\epsilon/\sigma \ll 1$ (copper). Assuming this inequality for any practical ω , we know that $\epsilon \ll \sigma/\omega$ so $\xi = \sigma/j\omega$ and $\beta^2 = \omega^2(\sigma/j\omega)\mu = -j\omega\mu\sigma$ which agrees with (1.5.1d). In this situation, since $-j\omega(\xi/\sigma) = -1$, we can write (B.2.3b) above as

$$\nabla^2\mathbf{H} = -\text{curl } \mathbf{J} . \quad // \text{ copper for } f \ll 10^{18} \text{ Hz} \quad (\text{B.2.4})$$

One might wonder how this last equation and (B.2.3a) can both be valid. The reason is that

$$|\kappa^2/\beta^2| = \omega^2\epsilon\mu/(-j\omega\mu\sigma) = |-\omega\epsilon/\sigma| = \omega\epsilon/\sigma \ll 1 . \quad (\text{B.2.5})$$

Then using this fact and (B.2.3c) we find

$$|\kappa^2 \mathbf{H}| \ll |\beta^2 \mathbf{H}| = |\nabla^2 \mathbf{H}| \quad \text{so} \quad |\kappa^2 \mathbf{H}| \ll |\nabla^2 \mathbf{H}| \quad (\text{B.2.6})$$

so the κ^2 term in (B.2.3a) makes no significant contribution.

Recalling (H.1.8),

$$\begin{aligned} -\nabla^2 f(\mathbf{x}) = s(\mathbf{x}) & \Rightarrow f(\mathbf{x}) = \int d^3x' [1/4\pi R] s(\mathbf{x}') + \text{homogeneous solutions} \\ \text{The Poisson Equation} & \end{aligned} \quad (\text{H.1.8})$$

one can write the Helmholtz particular integral solution of (B.2.4) as

$$\mathbf{H}(\mathbf{x}) = \int d^3x' [1/4\pi R] \text{curl}' \mathbf{J}(\mathbf{x}') \quad (\text{B.2.7})$$

where $[1/4\pi R]$ is the Laplace free-space propagator.

(b) An alternative derivation using the vector potential \mathbf{A}

Consider a conductor with $\mu, \epsilon, \sigma, \xi$ surrounded by a dielectric with $\mu_d, \epsilon_d, \sigma_d, \xi_d$. Here are two equations for the vector potential associated with the conductor current \mathbf{J} . The first equation is for the King gauge, while the second is for the Lorenz gauge:

$$(\nabla^2 + \beta_d^2) \mathbf{A}(\mathbf{x}) = -\mu \mathbf{J}(\mathbf{x}) \quad (1.5.4) \quad \beta_d^2 = \omega^2 \mu_d \xi_d \quad // \text{King gauge} \quad (\text{B.2.8a})$$

$$(\nabla^2 + \beta_0^2) \mathbf{A}(\mathbf{x}) = -\mu \mathbf{J}(\mathbf{x}) \quad (1.5.28) \quad \beta_0^2 = \omega^2 \mu \epsilon \quad // \text{Lorenz gauge} \quad (\text{B.2.8b})$$

Recalling (H.1.9),

$$\begin{aligned} -(\nabla^2 + k^2) f(\mathbf{x}) = s(\mathbf{x}) & \Rightarrow f(\mathbf{x}) = \int d^3x' [e^{-j\beta R}/4\pi R] s(\mathbf{x}') + \text{homogeneous solutions} \\ \text{The Helmholtz Equation} & \end{aligned} \quad (\text{H.1.9})$$

we may write down the Helmholtz particular integral solutions to (B.2.8),

$$\mathbf{A}(\mathbf{x}) = \mu \int d^3x' [e^{-j\beta_d R}/4\pi R] \mathbf{J}(\mathbf{x}') \quad \text{King gauge} \quad R = |\mathbf{x} - \mathbf{x}'| \quad (\text{B.2.9a})$$

$$\mathbf{A}(\mathbf{x}) = \mu \int d^3x' [e^{-j\beta_0 R}/4\pi R] \mathbf{J}(\mathbf{x}') \quad \text{Lorenz gauge} \quad R = |\mathbf{x} - \mathbf{x}'| \quad (\text{B.2.9b})$$

where $[e^{-j\beta_0 R}/4\pi R]$ is the usual 3D Helmholtz propagator.

We know that $\mathbf{B} = \text{curl } \mathbf{A}$ and therefore, using $\beta_{\mathbf{x}}$ to stand for either β_d or β_0 ,

$$\mathbf{H}(\mathbf{x}) = (1/\mu) \text{curl } \mathbf{A}(\mathbf{x}) = \int d^3x' \text{curl} ([e^{-j\beta_{\mathbf{x}} R}/4\pi R] \mathbf{J}(\mathbf{x}')) \quad (\text{B.2.10})$$

Notice that $\mathbf{J}(\mathbf{x}')$ is a constant in terms of the unprimed curl operator. A useful vector identity then is

$$\nabla \times (\varphi \mathbf{Q}) = \nabla \varphi \times \mathbf{Q} + \varphi (\nabla \times \mathbf{Q}) = (\nabla \varphi) \times \mathbf{Q} \quad \mathbf{Q} = \text{constant vector} .$$

Thus one may write

$$\mathbf{H}(\mathbf{x}) = \int d^3x' \nabla [e^{-j\beta \mathbf{x} \cdot \mathbf{R}} / 4\pi R] \times \mathbf{J}(\mathbf{x}') .$$

Since $R = |\mathbf{x} - \mathbf{x}'|$ we know ∇ acting on any function of R is the same as $-\nabla'$ on that function, so

$$\mathbf{H}(\mathbf{x}) = - \int d^3x' \nabla' [e^{-j\beta \mathbf{x} \cdot \mathbf{R}} / 4\pi R] \times \mathbf{J}(\mathbf{x}')$$

or in components (implied sum on r and s),

$$H_i = - \int d^3x' \varepsilon_{irs} \partial'_r [e^{-j\beta \mathbf{x} \cdot \mathbf{R}} / 4\pi R] J_s(\mathbf{x}') .$$

Doing parts integration and dropping the parts (see Section A.0 (d)), we get

$$H_i = + \int d^3x' [e^{-j\beta \mathbf{x} \cdot \mathbf{R}} / 4\pi R] \varepsilon_{irs} [\partial'_r J_s(\mathbf{x}')] .$$

or

$$\mathbf{H}(\mathbf{x}) = \int d^3x' [e^{-j\beta \mathbf{x} \cdot \mathbf{R}} / 4\pi R] \text{curl}' \mathbf{J}(\mathbf{x}') . \quad (\text{B.2.11})$$

We can compare this result to (B.2.7) obtained assuming $f \ll 10^{18}$ Hz,

$$\mathbf{H}(\mathbf{x}) = \int d^3x' [1/4\pi R] \text{curl}' \mathbf{J}(\mathbf{x}') . \quad \text{3D} \quad R = |\mathbf{x} - \mathbf{x}'| \quad (\text{B.2.7})$$

We conclude that in either gauge, and for this frequency range with copper, the exponential factor $e^{-j\beta \mathbf{x} \cdot \mathbf{R}}$ in (B.2.11) may be ignored. This basically says that the main contribution to the integral comes from the region near $R = 0$.

At low ω and in particular at DC with $\omega = 0$, we may assume that $\mathbf{J} = \mathbf{J}(x,y)$ with no z dependence. In this case we can do the dz' integration in (B.2.7) as shown in (J.10) which converts $[1/4\pi R]$ to $[-\ln(s)/2\pi]$. Renaming s to be R in 2D, we obtain

$$\mathbf{H}(x,y) = \int d^2x' [-\ln(R)/2\pi] \text{curl}' \mathbf{J}(x',y') \quad \text{2D} \quad R = |\mathbf{x} - \mathbf{x}'| \quad (\text{B.2.12})$$

where now $[-\ln(R)/2\pi]$ is the 2D Laplace free-space propagator of (I.1.8). In fact, this 2D result follows directly from (I.1.8) if we assume that $\mathbf{H} = \mathbf{H}(x,y)$ so that $\nabla^2 \mathbf{H} = \nabla_{2D}^2 \mathbf{H}$.

(c) Boundary conditions

Recall from (B.1.1) that the tangential component of \mathbf{H} is continuous through the boundary between conductor and dielectric, even if $\mu_1 \neq \mu_2$. Consider then the transverse component of (B.2.7) at some point on the conductor surface such as the point shown in Fig 3.3. We have ($t = \text{transverse}$)

$$\mathbf{H}_t(\mathbf{x}) = \int d^2x' [1/4\pi R] [\text{curl}' \mathbf{J}(\mathbf{x}')]_t \quad R = |\mathbf{x} - \mathbf{x}'| \quad .$$

This particular integral is naturally continuous at the boundary between the media, and this agrees with the fact that $\mathbf{H}_t(\mathbf{x})$ must have this property. Therefore, no homogeneous solutions of (B.2.4) $\nabla^2 \mathbf{H}_t = 0$ need be added in, so (B.2.12) is the complete solution for $\mathbf{H}_t(\mathbf{x})$. This solution can then be used in (B.1.10) to find the magnetization surface current.

(d) The Biot-Savart Law in 3D and 2D

Recall from above the 3D vector Helmholtz equation valid for $f \ll 10^{18}$ Hz, and its solution

$$\nabla^2 \mathbf{H} = - \text{curl}' \mathbf{J} \quad (B.2.4)$$

$$\mathbf{H}(\mathbf{x}) = \int d^3x' [1/4\pi R] \text{curl}' \mathbf{J}(\mathbf{x}') \quad R = |\mathbf{x} - \mathbf{x}'| \quad (B.2.7) \quad (B.2.13)$$

We shall now reverse the steps done in the previous section, but this time with $e^{-j\beta \cdot \mathbf{x}R} = 1$ based on the conclusion just drawn above. In components (B.2.7) reads,

$$H_i(\mathbf{x}) = \int d^3x' \left[\frac{1}{4\pi R} \right] \varepsilon_{ijk} \partial'_j J_k(\mathbf{x}') \quad \mathbf{R} \equiv \mathbf{x} - \mathbf{x}' = \text{points to observation point } \mathbf{x} \quad (B.2.14)$$

Then move ∂'_j from J_k to $(1/R)$ by parts integration (pick up minus sign) and throw out the parts for the usual reasons (see Section A.0 (d)),

$$H_i(\mathbf{x}) = - \int d^3x' \frac{1}{4\pi} \partial'_j \left(\frac{1}{R} \right) \varepsilon_{ijk} J_k(\mathbf{x}') \quad (B.2.15)$$

Then note that $\partial'_j R^{-1} = -R^{-2} \partial'_j R$ and

$$\partial'_j R = \partial'_j \sqrt{\Sigma_{\mathbf{k}}(x'_k - x_k)^2} = (1/2)(1/R) 2(x'_j - x_j) = R^{-1} (x'_j - x_j) = - R^{-1} R_j \quad (B.2.16)$$

so that $\partial'_j R^{-1} = +R^{-3} R_j$. Only the parts minus sign remains, so

$$H_i(\mathbf{x}) = - \int d^3x' \left[\frac{1}{4\pi R^3} \right] \varepsilon_{ijk} R_j J_k(\mathbf{x}') \quad (B.2.17)$$

or reversing the cross product order,

$$\mathbf{H}(\mathbf{x}) = \int d^3x' \frac{1}{4\pi R^3} \mathbf{J}(\mathbf{x}') \times \mathbf{R} \quad \mathbf{R} \equiv \mathbf{x} - \mathbf{x}' \quad (\text{B.2.18})$$

This equation is basically the **3D Biot-Savart Law**, see for example Panofsky and Philips p 125 (7.31). For a short piece ds' of thin wire carrying current I , one writes $\mathbf{J}(\mathbf{x}') d^3x' = I ds'$ so the above becomes,

$$\mathbf{H}(\mathbf{x}) = \oint \frac{1}{4\pi R^3} I ds' \times \mathbf{R} \quad \text{or} \quad d\mathbf{H}(\mathbf{x}) = \frac{1}{4\pi R^3} I ds' \times \mathbf{R} \quad (\text{B.2.19})$$

We can apply the same process to obtain a 2D Biot-Savart Law as follows. Start with

$$\nabla_{2D}^2 \mathbf{H}(x,y) = - \text{curl } \mathbf{J} \quad \mathbf{J} = J_z(x,y) \hat{\mathbf{z}} \quad (\text{B.2.4})$$

and its solution (B.2.5) obtained from (I.1.8)

$$\mathbf{H}(x,y) = \int d^2x' \left[\frac{1}{2\pi} \ln(1/R) \right] \text{curl}' \mathbf{J}(\mathbf{x}') \quad R = |\mathbf{x} - \mathbf{x}'| \quad (\text{B.2.5})$$

where $\frac{1}{2\pi} \ln(1/R)$ is the Laplace 2D free-space propagator. Then, inverting $1/R$,

$$H_{\mathbf{i}}(x,y) = - \int d^2x' \left[\frac{1}{2\pi} \ln(R) \right] \varepsilon_{\mathbf{i}j\mathbf{k}} \partial'_j J_{\mathbf{k}}(\mathbf{x}') \quad (\text{B.2.20})$$

Doing the same parts integration gives

$$H_{\mathbf{i}}(x,y) = + \int d^2x' \left[\frac{1}{2\pi} \partial'_j \ln(R) \right] \varepsilon_{\mathbf{i}j\mathbf{k}} J_{\mathbf{k}}(\mathbf{x}') \quad (\text{B.2.21})$$

and now using result (B.2.16) from above,

$$\partial'_j \ln(R) = R^{-1} \partial'_j R = R^{-1} [-R^{-1} R_j] = -R^{-2} R_j \quad (\text{B.2.22})$$

we get

$$H_{\mathbf{i}}(x,y) = - \int d^2x' \left[\frac{1}{2\pi} R^{-2} R_j \right] \varepsilon_{\mathbf{i}j\mathbf{k}} J_{\mathbf{k}}(\mathbf{x}') = - \int d^2x' \frac{1}{2\pi R^2} \varepsilon_{\mathbf{i}j\mathbf{k}} R_j J_{\mathbf{k}}(\mathbf{x}') \quad (\text{B.2.23})$$

or

$$\mathbf{H}(x,y) = \int d^2x' \frac{1}{2\pi R^2} \mathbf{J}(\mathbf{x}') \times \mathbf{R} \quad \mathbf{R} \equiv \mathbf{x} - \mathbf{x}' \quad (\text{B.2.24})$$

which is the **2D Biot-Savart Law**. It provides a way to obtain \mathbf{H} from \mathbf{J} in a 2D problem. In such a problem, we assume that $\mathbf{J} = \mathbf{J}(x,y)$ with no z dependence.

B.3 General Method for computing the surface current \mathbf{J}_m on a wire

Here are the steps for a wire of arbitrary cross sectional shape:

1. Compute \mathbf{H} from \mathbf{J} . Consider these sets of equations obtained above:

3D

$$\mathbf{H}(\mathbf{x}) = \int d^3x' \frac{1}{4\pi R} \text{curl}' \mathbf{J}(\mathbf{x}') \quad \mathbf{R} = |\mathbf{x} - \mathbf{x}'| \quad (\text{B.2.7})$$

$$\mathbf{H}(\mathbf{x}) = \int d^3x' \frac{1}{4\pi R^3} \mathbf{J}(\mathbf{x}') \times \mathbf{R} \quad \mathbf{R} \equiv \mathbf{x} - \mathbf{x}' \quad \text{Biot-Savart} \quad (\text{B.2.18})$$

$$\mathbf{A}(\mathbf{x}) = \mu \int d^3x' \frac{1}{4\pi R} \mathbf{J}(\mathbf{x}') \quad \mathbf{R} = |\mathbf{x} - \mathbf{x}'| \quad \mathbf{H} = (1/\mu) \text{curl } \mathbf{A} \quad (\text{B.2.9})$$

2D

$$\mathbf{H}(x,y) = \int d^2x' \frac{\ln(1/R)}{2\pi} \text{curl}' \mathbf{J}(x',y') \quad \mathbf{R} = |\mathbf{x} - \mathbf{x}'| \quad (\text{B.2.12})$$

$$\mathbf{H}(x,y) = \int d^2x' \frac{1}{2\pi R^2} \mathbf{J}(x',y') \times \mathbf{R} \quad \mathbf{R} \equiv \mathbf{x} - \mathbf{x}' \quad \text{Biot-Savart} \quad (\text{B.2.24})$$

$$\mathbf{A}(x,y) = \mu \int d^2x' \frac{\ln(1/R)}{2\pi} \mathbf{J}(x',y') \quad \mathbf{R} = |\mathbf{x} - \mathbf{x}'| \quad \mathbf{H} = (1/\mu) \text{curl } \mathbf{A} \quad (\text{B.3.1})$$

where the last line for \mathbf{A} is the same 3D \rightarrow 2D reduction used for \mathbf{H} . For either 3D or 2D, we thus provide three different methods for computing \mathbf{H} from \mathbf{J} .

2. Evaluate this \mathbf{H} field at $\mathbf{x}_b = (x_b, y_b)$ for all points \mathbf{x}_b on the cross section boundary.

3. Compute the component of \mathbf{H} which is tangential to the boundary in the cross sectional plane. Call this component H_θ .

4. The surface current density is then given by (B.1.10),

$$\mathbf{K}_z = - \left(\frac{\mu_2}{\mu_0} - \frac{\mu_1}{\mu_0} \right) H_\theta \quad \text{amps/m} \quad (\text{B.1.10})$$

B.4 Surface current on a round wire with uniform \mathbf{J}

For a round wire of radius a with uniform \mathbf{J}_z (as would be the DC case $\omega = 0$), geometric symmetry makes the calculation of \mathbf{H} very easy. One need only apply Ampere's Law separately for a point r outside the wire, and for another point r inside the wire. For the outside case one finds

$$2\pi r H_\theta(r) = I \quad \Rightarrow \quad H_\theta(r) = I/(2\pi r) \quad r \geq a \quad (\text{B.4.1})$$

And then for the inside case the "current enclosed" is determined by a simple area fraction.

$$2\pi r H_{\theta}(r) = I (\pi r^2 / \pi a^2) \quad \Rightarrow \quad H_{\theta}(r) = I r / (2\pi a^2) \quad r \leq a \quad . \quad (B.4.2)$$

At the boundary the two expressions agree and we have

$$H_{\theta} = I / (2\pi a) \quad . \quad (B.4.3)$$

If this wire has magnetic permeability μ_2 and is embedded in an infinite medium of μ_1 , then the surface magnetization current induced on the wire is

$$\mathbf{K}_z = - \left(\frac{\mu_2}{\mu_0} - \frac{\mu_1}{\mu_0} \right) H_{\theta} = - \left(\frac{\mu_2}{\mu_0} - \frac{\mu_1}{\mu_0} \right) I / (2\pi a) \quad \text{amp/m} \quad (B.4.4)$$

$$\mathbf{K}_z = K_z \hat{\mathbf{z}} \quad (B.4.5)$$

and this surface current is in the direction opposite \mathbf{J} if $\mu_2 > \mu_1$. If $\mu_1 = \mu_2$, the surface current vanishes. This surface current could be expressed in volume density form as

$$\mathbf{J}_m = K_z \delta(r-a) \hat{\mathbf{z}} \quad \text{amp/m}^2 \quad . \quad (B.4.6)$$

B.5 Computing H_{θ} for a round wire using the General Method of B.3

For a wire of some general cross section, symmetry is not available to allow the simple solution for H_{θ} outlined in the previous section. We then have to use the more general method outlined in Section B.3 above. As a check on the viability of this general method, we shall carry out "step 1" of the method and show how H_{θ} may be computed from \mathbf{J} using the 2D formula (B.2.12).

The conduction current density in a round wire with uniform J_z is given by

$$\mathbf{J}_z(r) = J_0 \theta(a-r) \quad (B.5.1)$$

where θ is the Heaviside step function. Our first step is to compute curl \mathbf{J} , and we do this in cylindrical coordinates by just staring at the cylindrical-coordinates curl formula,

$$\text{curl } \mathbf{J} = \hat{\mathbf{r}} [r^{-1} \partial_{\theta} J_z - \partial_z J_{\theta}] + \hat{\boldsymbol{\theta}} [\partial_z J_r - \partial_r J_z] + \hat{\mathbf{z}} [r^{-1} \partial_r (r J_{\theta}) - r^{-1} \partial_{\theta} J_r] \quad (B.5.2)$$

and finding the only non-zero piece which is this (uniform J_z),

$$\text{curl } \mathbf{J} = [-\partial_r J_z(r)] \hat{\boldsymbol{\theta}} \quad (B.5.3)$$

Inserting $J_z(r)$ from above we find

$$\partial_r J_z(r) = J_0 \partial_r \theta(a-r) = -J_0 \delta(r-a) \quad (B.5.4)$$

$$\Rightarrow \text{curl } \mathbf{J}(\mathbf{r}) = \hat{\boldsymbol{\theta}} J_0 \delta(r-a) . \quad (\text{B.5.5})$$

so we have a "ring source of curl \mathbf{J} ". For use in our integral for \mathbf{H} we then have

$$\text{curl}' \mathbf{J}(\mathbf{r}') = \hat{\boldsymbol{\theta}}' J_0 \delta(r'-a) . \quad (\text{B.5.6})$$

For a current distribution which tapers off smoothly to 0 at the wire edge one would not have this singular contribution, but for a wire with prescribed uniform current, it is present, and curl \mathbf{J} vanishes everywhere but on the boundary. The relevant picture is this:

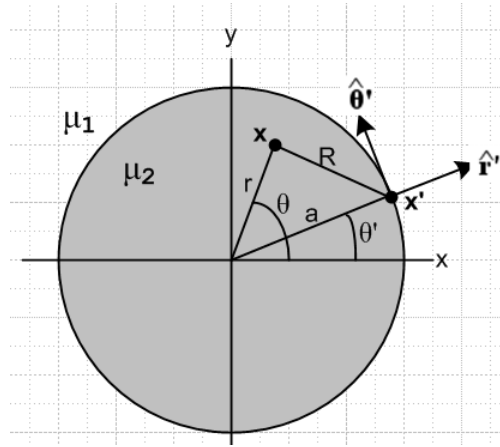


Fig B.4

From (B.2.12) the \mathbf{H} field at any point $\mathbf{x} = (x,y)$ is then given by

$$\begin{aligned} \mathbf{H}(x,y) &= -\frac{1}{4\pi} \int d^2\mathbf{x}' \ln(R^2) \text{curl}' \mathbf{J}(\mathbf{x}') = -\frac{1}{4\pi} \int d^2\mathbf{x}' \ln(R^2) \hat{\boldsymbol{\theta}}' J_0 \delta(r'-a) \\ &= -\frac{J_0 a}{4\pi} \int_{-\pi}^{\pi} d\theta' \ln(R^2)|_{r'=a} \hat{\boldsymbol{\theta}}' \end{aligned}$$

or

$$\mathbf{H}(r,\theta) = -\frac{J_0 a}{4\pi} \int_{-\pi}^{\pi} d\theta' \ln [r^2 + a^2 - 2ar \cos(\theta'-\theta)] \hat{\boldsymbol{\theta}}' . \quad (\text{B.5.7})$$

The figure shows that

$$\hat{\boldsymbol{\theta}}' = \cos\theta' \hat{\mathbf{y}} - \sin\theta' \hat{\mathbf{x}} \quad (\text{B.5.8})$$

so then

$$\mathbf{H}(r,\theta) = -\frac{J_0 a}{4\pi} \int_{-\pi}^{\pi} d\theta' \ln [r^2 + a^2 - 2ar \cos(\theta'-\theta)] [\cos\theta' \hat{\mathbf{y}} - \sin\theta' \hat{\mathbf{x}}] . \quad (\text{B.5.9})$$

Next, let $x \equiv \theta'-\theta$. Since the $\int d\theta'$ has full range 2π , one can replace $\int_{-\pi}^{\pi} d\theta' = \int_{-\pi}^{\pi} dx$. Then

$$\mathbf{H}(r,\theta) = - \frac{J_0 a}{4\pi} \int_{-\pi}^{\pi} dx \ln [r^2 + a^2 - 2ar \cos(x)] [\cos(x+\theta) \hat{\mathbf{y}} - \sin(x+\theta) \hat{\mathbf{x}}] . \quad (\text{B.5.10})$$

Now writing $\mathbf{H} = H_x \hat{\mathbf{x}} + H_y \hat{\mathbf{y}}$, decompose the above into two equations

$$\begin{aligned} H_x(r,\theta) &= + \frac{J_0 a}{4\pi} \int_{-\pi}^{\pi} dx \ln [r^2 + a^2 - 2ar \cos(x)] \sin(x+\theta) \\ H_y(r,\theta) &= - \frac{J_0 a}{4\pi} \int_{-\pi}^{\pi} dx \ln [r^2 + a^2 - 2ar \cos(x)] \cos(x+\theta) \end{aligned} \quad (\text{B.5.11})$$

or

$$\begin{aligned} H_x(r,\theta) &= + \frac{J_0 a}{4\pi} \int_{-\pi}^{\pi} dx \ln [r^2 + a^2 - 2ar \cos(x)] [\sin x \cos \theta + \cos x \sin \theta] \\ H_y(r,\theta) &= - \frac{J_0 a}{4\pi} \int_{-\pi}^{\pi} dx \ln [r^2 + a^2 - 2ar \cos(x)] [\cos x \cos \theta - \sin x \sin \theta] . \end{aligned} \quad (\text{B.5.12})$$

Since $\int_{-\pi}^{\pi} dx$ is over an even range, throw out odd integrand terms, and *then* fold the negative range into the positive adding a factor of 2 to get

$$\begin{aligned} H_x(r,\theta) &= + \sin \theta \frac{J_0 a}{2\pi} \int_0^{\pi} dx \ln [r^2 + a^2 - 2ar \cos(x)] \cos x \quad \equiv \quad \sin \theta \frac{J_0 a}{2\pi} Q \\ H_y(r,\theta) &= - \cos \theta \frac{J_0 a}{2\pi} \int_0^{\pi} dx \ln [r^2 + a^2 - 2ar \cos(x)] \cos x \quad = -\cos \theta \frac{J_0 a}{2\pi} Q \end{aligned} \quad (\text{B.5.13})$$

where

$$Q \equiv \int_0^{\pi} dx \ln [r^2 + a^2 - 2ar \cos(x)] \cos x . \quad (\text{B.5.14})$$

Before evaluating this integral, we see that

$$\mathbf{H} = H_x \hat{\mathbf{x}} + H_y \hat{\mathbf{y}} = - \frac{J_0 a}{2\pi} Q [\cos \theta \hat{\mathbf{y}} - \sin \theta \hat{\mathbf{x}}] = - \frac{J_0 a}{2\pi} Q \hat{\boldsymbol{\theta}} = H_{\boldsymbol{\theta}} \hat{\boldsymbol{\theta}} . \quad (\text{B.5.15})$$

Thus we find that the resulting \mathbf{H} is entirely in the $\hat{\boldsymbol{\theta}}$ direction and

$$H_{\boldsymbol{\theta}} = - \frac{J_0 a}{2\pi} Q . \quad (\text{B.5.16})$$

We seek now to evaluate this integral Q ,

$$Q \equiv \int_0^{\pi} dx \ln [r^2 + a^2 - 2ar \cos(x)] \cos x$$

$$\begin{aligned}
 &= \int_0^\pi dx \ln [\{a^2\} \{ (r/a)^2 + 1 - 2(r/a) \cos(x) \}] \cos x \\
 &= \int_0^\pi dx \{ \ln (a^2) + \ln[(r/a)^2 + 1 - 2(r/a) \cos(x)] \} \cos x \\
 &= \ln (a^2) [\int_0^\pi dx \cos x] + \int_0^\pi dx \ln[(r/a)^2 + 1 - 2(r/a) \cos(x)] \cos x \\
 &= \ln (a^2)[0] + \int_0^\pi dx \ln[\alpha^2 + 1 - 2\alpha \cos(x)] \cos x \quad \text{where } \alpha \equiv r/a \\
 &= \int_0^\pi dx \ln[\alpha^2 + 1 - 2\alpha \cos(x)] \cos x \quad // = Q \tag{B.5.17}
 \end{aligned}$$

This integral is the $n=1$ special case of the following integral from GR7 page 589 4.379.6,

$$\begin{aligned}
 6. \quad &\int_0^\pi \ln (1 - 2a \cos x + a^2) \cos nx \, dx \\
 &= \frac{1}{2} \int_0^{2\pi} \ln (1 - 2a \cos x + a^2) \cos nx \, dx \\
 &= -\frac{\pi}{n} a^n \quad [a^2 < 1] \quad \text{BI (330)(11), BI (332)(5)} \\
 &= -\frac{\pi}{na^n} \quad [a^2 > 1] \quad \text{GW (338)(13a)}
 \end{aligned}$$

Therefore we find

$$Q = \begin{cases} -\pi(r/a) & r < a \\ -\pi(a/r) & r > a \end{cases} \tag{B.5.18}$$

so

$$H_\theta = -\frac{J_0 a}{2\pi} Q = \begin{cases} (aJ_0/2) (r/a) & r < a \\ (aJ_0/2) (a/r) & r > a \end{cases} \tag{B.5.19}$$

Now the total current in the wire is $I = J_0 \pi a^2$ so $(aJ_0/2) = (I/2\pi a)$ and then

$$H_\theta = \begin{cases} (I/2\pi a) (r/a) & r < a \\ (I/2\pi a) (a/r) & r > a \end{cases} = \begin{cases} I (r/2\pi a^2) & r < a \\ I (1/2\pi r) & r > a \end{cases} \tag{B.5.20}$$

Thus, we finally arrive at the same results for H_θ as obtained in (B.4.2) and (B.4.1).

B.6 Modification of King's Helmholtz integral solution when $\mu_1 \neq \mu_2$

(a) General Discussion

In Section 4.7 we wrote the King gauge vector potential for transmission line conductor C in this manner,

$$A_{\mathbf{z}}(\mathbf{x}, \omega) = \frac{1}{4\pi} \int_C \mu_2 J_{\mathbf{zc}}(x', y', z', \omega) \frac{e^{-j\beta_d R}}{R} dx' dy' dz' \quad R = |\mathbf{x} - \mathbf{x}'| \quad (4.7.2)$$

where we have made a notational change to be consistent with previous sections of Appendix B. Here we use μ_2 to refer to the permeability of the conductor, and μ_1 to be that of the dielectric (these are called μ and μ_d in Section 4). The above "Helmholtz integral" is only the "particular solution" of the Helmholtz equation $(\nabla^2 + \beta_1^2)A_{\mathbf{z}} = -\mu_2 J_{\mathbf{zc}}$. When $\mu_1 \neq \mu_2$, it turns out that one must add a homogeneous solution $A_{\mathbf{z}}^{(\text{homo})}$ [that is, $(\nabla^2 + \beta_1^2)A_{\mathbf{z}}^{(\text{homo})} = 0$] to the Helmholtz solution shown above in order to meet boundary conditions. Appendix G.4 provides a very detailed study of just how this works for a round conductor with a uniform current distribution.

To avoid this major complication, we limited the analysis of Chapter 4 to the case that $\mu_1 = \mu_2$. This means, for example, that Chapters 4,5,6 are applicable for non-magnetic conductors in a non-magnetic dielectric, in which case $\mu_1 = \mu_2 = \mu_0$. The work presented below generalizing to $\mu_1 \neq \mu_2$ is then summarized in Section 4.13.

With the reader's permission, we replicate an abbreviated version of the comments below (4.7.6), making a few small notational changes:

Comments regarding μ

This is a subtle subject and is not discussed in King's transmission line theory book.

The solution $A_{\mathbf{z}}$ of (4.7.2) is continuous at the conductor boundary whether or not $\mu_1 = \mu_2$. The condition on the normal *slope* of $A_{\mathbf{z}}$ at the boundary is given by (1.1.46) since there is no *free* surface current on the boundary (ignoring the tiny Debye surface charge current). Thus we have these boundary conditions :

$$\begin{aligned} A_{\mathbf{z}}(\mathbf{x}+) &= A_{\mathbf{z}}(\mathbf{x}-) \\ (1/\mu_1) \partial_n A_{\mathbf{z}}(\mathbf{x}+) &= (1/\mu_2) \partial_n A_{\mathbf{z}}(\mathbf{x}-) \end{aligned} \quad (4.7.9) \quad (B.6.0)$$

where $\mathbf{x}+$ is just outside the conductor surface and $\mathbf{x}-$ is just inside.

If $\mu_1 = \mu_2$, there is no "magnetic boundary" at the surface, and (B.6.0) says $\partial_n A_{\mathbf{z}1}(\mathbf{x}+) = \partial_n A_{\mathbf{z}1}(\mathbf{x}-)$, so both the function $A_{\mathbf{z}}$ and its normal derivative are continuous through the boundary -- nothing special is happening there. Thus, the Helmholtz integral solution (4.7.2) provides the whole solution for $A_{\mathbf{z}}$ in both the dielectric and conductor since it meets both "boundary conditions" at this pseudo boundary.

If $\mu_1 \neq \mu_2$, then there *is* a magnetic boundary between conductor and dielectric which we have to worry about. In this case, (4.7.2) applied in both dielectric and conductor cannot possibly satisfy the second boundary condition of (B.6.0) since, as already noted, the $A_{\mathbf{z}}$ of (4.7.2) satisfies $\partial_n A_{\mathbf{z}1}(\mathbf{x}+) = \partial_n A_{\mathbf{z}1}(\mathbf{x}-)$. Thus, in this case (4.7.2) is not the full solution for $A_{\mathbf{z}1}$. One must add a homogeneous

Helmholtz equation solution to (4.7.2) in order to have a proper solution for A_z that satisfies both equations in (4.7.9).

It *turns out* that the correct total A_z solution can be generated by adding a certain fictitious surface current to $\mu_2 J_z$ in (4.7.2). Since such a surface current vanishes on both sides of the boundary between μ_1 and μ_2 , the Helmholtz solution due just to this surface current is in fact *a homogeneous solution* to the Helmholtz equation in both the conductor and dielectric regions, away from that boundary. It turns out moreover that the correct fictitious surface current to add is in fact the magnetization surface current J_m which is created at the boundary between $\mu_1 \neq \mu_2$. Adding this surface current is just a "trick" in order to generate the correct homogeneous adder solution so that the resulting total A_z satisfies both boundary conditions in (B.6.0). Formally speaking, the \mathbf{J} appearing in (1.5.3) and then J_z in (4.7.2) should *not* include such magnetization currents since this \mathbf{J} is really the \mathbf{J} in Maxwell's equation $\text{curl } \mathbf{H} = \partial_t \mathbf{D} + \mathbf{J}$, and this \mathbf{J} does not include magnetization currents -- it includes only normal conduction currents.

Here we wish to prove the claim that adding the *surface* magnetization current to the conduction current does in fact make the boundary conditions work. After doing this proof, we will show in Section B.7 just how this works out in the case of a round conductor.

We stress that only the surface part of J_m gets added in. In general J_m will also have a "bulk" component in the dielectric and conductor. If we were to include this bulk component, we would not be adding a homogeneous solution to the particular solution, and we would in fact be creating a non-solution! In (G.3.4) we show the complete J_m for a round wire carrying a uniform current, and it does have both bulk and surface components.

(b) Statement and Proof of the J_m Lemma

The J_m Lemma. If J_{mz} represents the surface component of magnetization current density for a transmission line conductor C of μ_2 with conduction current density J_{cz} , embedded in a dielectric medium of μ_1 , then if we write

$$A_z(\mathbf{x}) = \frac{1}{4\pi} \int_C [\mu_2 J_{cz}(\mathbf{x}') + \mu_0 J_{mz}(\mathbf{x}')] \frac{e^{-j\beta_d R}}{R} dV' \quad R = |\mathbf{x} - \mathbf{x}'| \quad (\text{B.6.1})$$

this $A_z(x)$ will satisfy the boundary conditions (B.6.0) shown above. Parameter β_d is for the dielectric, and should be called β_1 , but we leave it as β_d as used in Chapter 4.

Comments.

1. In this Lemma, we are showing that the contribution to $A_z(\mathbf{x})$ *just from conductor C* satisfies the boundary condition (B.6.0) at the surface of conductor C if we add in the surface current term $\mu_0 J_{mz}(\mathbf{x}')$ as shown. What we really want to show is that the *total* $A_z(\mathbf{x})$ due to *all* the transmission line conductors satisfies (B.6.0) at the surface of conductor C . This will be the content of the J_m Theorem presented in Section (c) below. Once this Theorem is proved, we know that "the other conductors" don't interfere with

the J_m Lemma and we can regard the boundary conditions on $A_z(\mathbf{x})$ given in (B.6.1) as applying also to the full $A_z(\mathbf{x})$ which includes the contributions of all conductors.

2. Our proof below applies in the "transmission line limit" of Sections 4.3 and 4.9 which is essentially a long wavelength and small β_a limit. In this limit, we can replace our various Helmholtz propagators below with Laplace propagators. Nevertheless, we maintain the Helmholtz forms in the hope that the above theorem is valid for reasonably moderate β_a values. At large β_a values (relative to transverse dimension D so that $\beta_a D$ no longer $\ll 1$ as in (4.3.4)) our whole TEM transmission line framework collapses, the transmission line limit is violated and the entire theory of Chapters 4 and 5 no longer applies.

(1) Preliminaries

We first quote a key result from Stakgold concerning a boundary layer function $a(\xi)$:

$$\begin{aligned} u(\mathbf{x}) &= \int_{\sigma} dS_{\xi} a(\xi) E(\mathbf{x}|\xi) \\ u(s) &= \int_{\sigma} dS_{\xi} a(\xi) E(s|\xi) \end{aligned} \quad (\text{B.6.2})$$

$$\begin{aligned} \partial_{\mathbf{v}} u(\mathbf{x}) &= \int_{\sigma} dS_{\xi} a(\xi) \partial_{\mathbf{v}} E(\mathbf{x}|\xi) \\ \partial_{\mathbf{v}} u(s) &= [\partial_{\mathbf{n}} u(\mathbf{x})]^{\mathbf{x} \rightarrow s^{\pm}} = \int_{\sigma} dS_{\xi} a(\xi) \partial_{\mathbf{v}} E(s|\xi) \mp a(s)/2 \quad // \text{ extra term !} \end{aligned} \quad (\text{B.6.3})$$

This is a tricky subject and some words are certainly in order. In the Stakgold world, σ is a surface of $n-1$ dimensions existing in an n dimensional space. $E(\mathbf{x}|\xi)$ is the free-space propagator in that n dimensional space (the "fundamental solution"). The integrals shown above are over the surface σ , and ξ represents the $n-1$ dimensional coordinate of a point on the surface σ , while dS_{ξ} is a piece of "area" on the surface. (Stakgold does not write vectors in bold font as we do in this document.) Function $a(\xi)$ is defined on the surface and is called a simple (monopole) boundary layer. Stakgold also deals with dipole layers (as in a cell membrane), but we don't care about them right now.

The question at hand is this: What happens as a point \mathbf{x} away from the surface approaches the surface where it becomes point s ? We are interested in the limit $\mathbf{x} \rightarrow s$. As shown in the first pair of equations (B.6.2), nothing unusual happens for the function $u(\mathbf{x})$ defined as shown by the integral. One then says that $u(\mathbf{x})$ is "continuous" at $\mathbf{x} = s$. But something very unusual happens for the function $\partial_{\mathbf{v}} u(\mathbf{x})$ where $\partial_{\mathbf{v}}$ denotes a derivative locally normal to the surface at s . As $\mathbf{x} \rightarrow s$ an "extra term" appears as shown above having value $\mp a(s)/2$. If normal \mathbf{v} points "out" from the surface then as one approaches from the outside (call it the $+$ side), the extra term is $-a(s)/2$, but if the approach is from the inside ($-$ side), the extra term changes sign. Here is a picture illustrating the geometry of the above equations: (\mathbf{n} is normal at ξ , \mathbf{v} is normal at s)

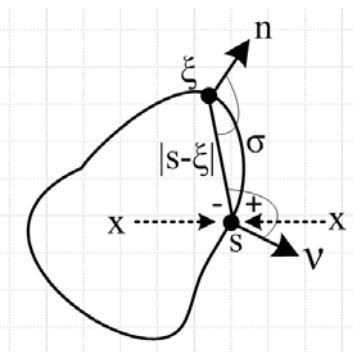


Fig B.5

The reason the extra term appears has to do with the nature of the $d\xi$ integration when ξ is very close to s which is somewhat of a singular situation since $R \equiv |s-\xi| \rightarrow 0$. Stakgold treats surface layers in Section 6.4 of his Volume II, pages 110-120, and his treatment involves a *lot* of detail. The claims shown above appear on pages 118 and 119, though the conclusions are a bit obscured in the detail. Stakgold works in 3D with $E(x|\xi) = (1/4\pi|x-\xi|) = 1/4\pi R$ and often uses these quantities,

$$k(s,\xi) = \cos(s \hat{\cdot} \xi, \hat{n}) / [4\pi|s-\xi|^2] \quad // \text{cos(upper marked angle)}$$

$$k(\xi,s) = \cos(\xi \hat{\cdot} s, \hat{v}) / [4\pi|s-\xi|^2] = \partial_v E(s|\xi) \quad // \text{cos(lower marked angle)}$$

Later in his Problem 6.18 through 6.20 Stakgold has the reader verify that the results are also valid in 2D where surface σ is then just a curve. These are the results we shall use. Although he does not state it outright, we think his results are probably valid for σ being a surface of any number of dimensions, but our only interest will be the 2D case.

(2) Outline of Proof of the J_m Lemma

We break up (B.6.1) into these two terms, a "conduction term" and a "magnetization" term,

$$A_z^{(c)}(\mathbf{x}) = \frac{1}{4\pi} \int_C [\mu_2 J_{cz}(x')] \frac{e^{-j\beta_d R}}{R} dV' \quad R = |\mathbf{x} - \mathbf{x}'| \quad (B.6.4)$$

$$A_z^{(m)}(\mathbf{x}) = \frac{1}{4\pi} \int_C [\mu_0 J_{mz}(x')] \frac{e^{-j\beta_d R}}{R} dV' \quad R = |\mathbf{x} - \mathbf{x}'| \quad (B.6.5)$$

$$A_z(\mathbf{x}) = A_z^{(c)}(\mathbf{x}) + A_z^{(m)}(\mathbf{x}) \quad \text{two terms} \quad (B.6.6)$$

As noted earlier, the first term is smooth at a point s on a conductor surface and satisfies the two boundary conditions,

$$\begin{aligned} A_z^{(c)}(s+) &= A_z^{(c)}(s-) \\ \partial_n A_z^{(c)}(s+) &= \partial_n A_z^{(c)}(s-) \end{aligned} \quad (B.6.7)$$

so one can write $A_z^{(c)}(s)$ or $\partial_n A_z^{(c)}(s)$ without concern for whether s is $s+$ or $s-$. For this term, which is the Helmholtz "particular" integral, we may then trivially write,

$$\frac{1}{\mu_1} \partial_n A_z^{(c)}(s^+) - \frac{1}{\mu_2} \partial_n A_z^{(c)}(s^-) = + \left[\frac{1}{\mu_1} - \frac{1}{\mu_2} \right] \partial_n A_z^{(c)}(s). \quad (\text{B.6.8})$$

Since this is non-zero, the term $A_z^{(c)}$ on its own does not meet the required slope boundary condition (B.6.0) at an interface between μ_1 and μ_2 , and that is precisely why we need the $A_z^{(m)}$ term. Our goal is to show that

$$\frac{1}{\mu_1} \partial_n A_z^{(m)}(s^+) - \frac{1}{\mu_2} \partial_n A_z^{(m)}(s^-) = - \left[\frac{1}{\mu_1} - \frac{1}{\mu_2} \right] \partial_n A_z^{(c)}(s) \quad (\text{B.6.9})$$

so that when we add the two terms we will get

$$\frac{1}{\mu_1} \partial_n A_z(s^+) - \frac{1}{\mu_2} \partial_n A_z(s^-) = 0 \quad (\text{B.6.10})$$

as required by (1.1.46). This concludes our proof outline, and it remains then to demonstrate (B.6.9).

(3) Verification of (B.6.9)

We start with (B.6.5) where $\int dV'$ is over the entire transmission line conductor C ,

$$\begin{aligned} A_z^{(m)}(\mathbf{x}) &= \frac{1}{4\pi} \int_C dV' [\mu_0 J_{mz}(\mathbf{x}')] \frac{e^{-j\beta_d R}}{R} \\ &= \int_C dV' [\mu_0 J_{mz}(\mathbf{x}') E_3(\mathbf{x}|\mathbf{x}')] \end{aligned} \quad (\text{B.6.11})$$

where

$$E_3(\mathbf{x}|\mathbf{x}') = \frac{e^{-j\beta_d R}}{R} \rightarrow \frac{1}{4\pi R} \text{ as } \beta_d \rightarrow 0. \quad (\text{B.6.12})$$

We know from Chapter 4 that in the transmission line limit we can do the dz' integration in dV' and arrive at a 2D-propagator expression for the above potential, where the integral is now over the cross section area of the conductor C ,

$$A_z^{(m)}(\mathbf{x}) = \int_C dS' [\mu_0 J_{mz}(\mathbf{x}')] E_2(\mathbf{x}|\mathbf{x}') \quad (\text{B.6.13})$$

where

$$E_2(\mathbf{x}|\mathbf{x}') = (j/4) H_0^{(1)}(\beta_d R) \rightarrow -\frac{1}{2\pi} \ln(R^2) \text{ as } \beta_d \rightarrow 0. \quad (\text{B.6.14})$$

This whole subject of transitioning from the 3D to 2D analysis is reviewed in Appendix J, and it occurs in many places in this document.

We are only using that portion of $\mathbf{J}_{\mathbf{mz}}$ which is a surface current on the perimeter of C , so we rewrite the above as

$$\mathbf{A}_{\mathbf{z}}^{(m)}(\mathbf{x}) = \oint_C ds' [\mu_0 \mathbf{K}_{\mathbf{z}}(\mathbf{x}')] E_2(\mathbf{x}|\mathbf{x}') \quad (\text{B.6.15})$$

where $\mathbf{K}_{\mathbf{z}}(\mathbf{x}')$ is the magnetization surface current (amps/m) discussed in Section B.1. Stakgold's surface integral over σ is now just a line integral around the perimeter of the conductor C cross section. Recall from (B.1.10) that the magnetization surface current is given by,

$$\mathbf{K}_{\mathbf{z}} = - \left(\frac{\mu_2}{\mu_0} - \frac{\mu_1}{\mu_0} \right) \mathbf{H}_{\theta} \quad (\text{B.1.10})$$

where \mathbf{H}_{θ} is the \mathbf{H} field tangent to the cross section surface. Inserting this $\mathbf{K}_{\mathbf{z}}$ into (B.6.15) gives

$$\mathbf{A}_{\mathbf{z}}^{(m)}(\mathbf{x}) = \oint_C ds' [(\mu_1 - \mu_2) \mathbf{H}_{\theta}(\mathbf{x}')] E_2(\mathbf{x}|\mathbf{x}') \quad (\text{B.6.16})$$

We now identify this with the first of Stakgold's equations (B.6.2) where $[(\mu_1 - \mu_2) \mathbf{H}_{\theta}(\mathbf{x}')]$ plays the role of the boundary monolayer function $a(\xi)$. We know we can take $\mathbf{x} \rightarrow \mathbf{s}$ with no surprises. If we now replace Stakgold's normal direction \mathbf{v} with our usual normal symbol \mathbf{n} , we can write (B.6.3) as

$$\partial_{\mathbf{n}} \mathbf{A}_{\mathbf{z}}^{(m)}(\mathbf{x}) = \oint_C ds' [(\mu_1 - \mu_2) \mathbf{H}_{\theta}(\mathbf{x}')] \partial_{\mathbf{n}} E_2(\mathbf{x}|\mathbf{x}') \quad (\text{B.6.17})$$

$$\partial_{\mathbf{n}} \mathbf{A}_{\mathbf{z}}^{(m)}(\mathbf{s}\pm) = \oint_C ds' [(\mu_1 - \mu_2) \mathbf{H}_{\theta}(\mathbf{x}')] \partial_{\mathbf{n}} E_2(\mathbf{s}|\mathbf{x}') \mp [(\mu_1 - \mu_2) \mathbf{H}_{\theta}(\mathbf{s})]/2 \quad (\text{B.6.18})$$

Now since we want to prove (B.6.9), we first evaluate its left hand side using (B.6.18) twice,

$$\begin{aligned} & \frac{1}{\mu_1} \partial_{\mathbf{n}} \mathbf{A}_{\mathbf{z}}^{(m)}(\mathbf{s}+) - \frac{1}{\mu_2} \partial_{\mathbf{n}} \mathbf{A}_{\mathbf{z}}^{(m)}(\mathbf{s}-) \\ &= \frac{1}{\mu_1} \left\{ \oint_C ds' [(\mu_1 - \mu_2) \mathbf{H}_{\theta}(\mathbf{x}')] \partial_{\mathbf{n}} E_2(\mathbf{s}|\mathbf{x}') - [(\mu_1 - \mu_2) \mathbf{H}_{\theta}(\mathbf{s})]/2 \right\} \\ & - \frac{1}{\mu_2} \left\{ \oint_C ds' [(\mu_1 - \mu_2) \mathbf{H}_{\theta}(\mathbf{x}')] \partial_{\mathbf{n}} E_2(\mathbf{s}|\mathbf{x}') + [(\mu_1 - \mu_2) \mathbf{H}_{\theta}(\mathbf{s})]/2 \right\} \quad (\text{B.6.19}) \\ &= (\mu_1 - \mu_2) \left[\frac{1}{\mu_1} - \frac{1}{\mu_2} \right] \oint_C ds' \mathbf{H}_{\theta}(\mathbf{x}') \partial_{\mathbf{n}} E_2(\mathbf{s}|\mathbf{x}') - \left[\frac{1}{\mu_1} + \frac{1}{\mu_2} \right] (\mu_1 - \mu_2) \mathbf{H}_{\theta}(\mathbf{s})/2 \end{aligned}$$

Our task of showing that (B.6.9) is true then boils down to showing that the last expression above is equal to $-\left[\frac{1}{\mu_1} - \frac{1}{\mu_2}\right] \partial_{\mathbf{n}} \mathbf{A}_{\mathbf{z}}^{(c)}(\mathbf{s})$. That is to say, we have to show

$$(\mu_1 - \mu_2) \left[\frac{1}{\mu_1} - \frac{1}{\mu_2} \right] \oint_C ds' H_{\theta}(\mathbf{x}') \partial_n E_2(\mathbf{s}|\mathbf{x}') - \left[\frac{1}{\mu_1} + \frac{1}{\mu_2} \right] (\mu_1 - \mu_2) H_{\theta}(\mathbf{s})/2 = - \left[\frac{1}{\mu_1} - \frac{1}{\mu_2} \right] \partial_n A_z^{(c)}(\mathbf{s}) \quad ? \quad (\text{B.6.20})$$

A question mark indicates an equation that we want to show is true, but have not yet done so.

Canceling $(\mu_1 - \mu_2)$ factors, (B.6.20) becomes

$$\left[\frac{1}{\mu_1} - \frac{1}{\mu_2} \right] \oint_C ds' H_{\theta}(\mathbf{x}') \partial_n E_2(\mathbf{s}|\mathbf{x}') - \left[\frac{1}{\mu_1} + \frac{1}{\mu_2} \right] H_{\theta}(\mathbf{s})/2 = + \frac{1}{\mu_1 \mu_2} \partial_n A_z^{(c)}(\mathbf{s}) \quad ? \quad (\text{B.6.21})$$

or

$$(\mu_2 - \mu_1) \oint_C ds' H_{\theta}(\mathbf{x}') \partial_n E_2(\mathbf{s}|\mathbf{x}') - (1/2)(\mu_2 + \mu_1) H_{\theta}(\mathbf{s}) = \partial_n A_z^{(c)}(\mathbf{s}) \quad ? \quad (\text{B.6.22})$$

The integral in (B.6.22) can be replaced using (B.6.18) with the $\mathbf{s}+$ choice,

$$\partial_n A_z^{(m)}(\mathbf{s}+) = \oint_C ds' [(\mu_1 - \mu_2) H_{\theta}(\mathbf{x}')] \partial_n E_2(\mathbf{s}|\mathbf{x}') - (1/2)[(\mu_1 - \mu_2) H_{\theta}(\mathbf{s})] \quad (\text{B.6.18})+$$

so

$$(\mu_2 - \mu_1) \oint_C ds' H_{\theta}(\mathbf{x}') \partial_n E_2(\mathbf{s}|\mathbf{x}') = - \partial_n A_z^{(m)}(\mathbf{s}+) - (1/2)(\mu_1 - \mu_2) H_{\theta}(\mathbf{s}) \quad (\text{B.6.23})$$

Equation (B.6.22) then becomes,

$$- \partial_n A_z^{(m)}(\mathbf{s}+) - (1/2)(\mu_1 - \mu_2) H_{\theta}(\mathbf{s}) - (1/2)(\mu_2 + \mu_1) H_{\theta}(\mathbf{s}) = \partial_n A_z^{(c)}(\mathbf{s}) \quad ?$$

or

$$- \partial_n A_z^{(m)}(\mathbf{s}+) - \mu_1 H_{\theta}(\mathbf{s}) = \partial_n A_z^{(c)}(\mathbf{s}) \quad ?$$

or

$$- \mu_1 H_{\theta}(\mathbf{s}) = \partial_n [A_z^{(c)}(\mathbf{s}) + A_z^{(m)}(\mathbf{s}+)] \quad ?$$

or

$$- \mu_1 H_{\theta}(\mathbf{s}) = \partial_n A_z(\mathbf{s}+) \quad ? \quad // \text{ using (B.6.6)} \quad (\text{B.6.24})$$

We now introduce a local cylindrical coordinate system in this manner relative to point \mathbf{s} :

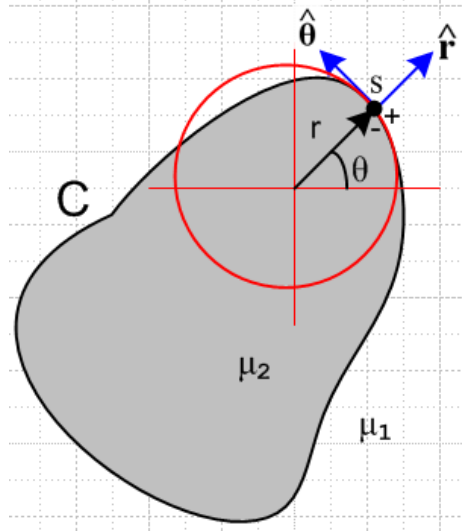


Fig B.6

Notice that $\hat{\mathbf{r}}$ is the normal vector at point s , so $\partial_{\mathbf{r}} = \partial_{\mathbf{n}}$. Then first we determine $\mathbf{B}_{\boldsymbol{\theta}}$,

$$\begin{aligned} \mathbf{B} &= \text{curl } \mathbf{A} = \hat{\mathbf{r}} [r^{-1} \partial_{\boldsymbol{\theta}} A_{\mathbf{z}} - \partial_{\mathbf{z}} A_{\boldsymbol{\theta}}] + \hat{\boldsymbol{\theta}} [\partial_{\mathbf{z}} A_{\mathbf{r}} - \partial_{\mathbf{r}} A_{\mathbf{z}}] + \hat{\mathbf{z}} [r^{-1} \partial_{\mathbf{r}} (r A_{\boldsymbol{\theta}}) - r^{-1} \partial_{\boldsymbol{\theta}} A_{\mathbf{r}}] \\ &= \hat{\mathbf{r}} [r^{-1} \partial_{\boldsymbol{\theta}} A_{\mathbf{z}}] + \hat{\boldsymbol{\theta}} [-\partial_{\mathbf{r}} A_{\mathbf{z}}] \\ &= \hat{\boldsymbol{\theta}} [-\partial_{\mathbf{r}} A_{\mathbf{z}}] . \end{aligned}$$

Here we have set $\partial_{\boldsymbol{\theta}} A_{\mathbf{z}} = 0$ according to Fact 7 of (3.8.9) which says $A_{\mathbf{z}}$ is constant on the cross section surface (which implies the strong or extreme skin effect regime). The result is then,

$$\mathbf{B}_{\boldsymbol{\theta}}(s^+) = -\partial_{\mathbf{n}} A_{\mathbf{z}}(s^+) . \quad (\text{B.6.25})$$

Since s^+ is in the dielectric with μ_1 we then have

$$\mathbf{H}_{\boldsymbol{\theta}}(s^+) = (1/\mu_1) \mathbf{B}_{\boldsymbol{\theta}}(s^+) = -(1/\mu_1) \partial_{\mathbf{r}} A_{\mathbf{z}}(s^+) \quad // \mathbf{H}_{\boldsymbol{\theta}}(s^+) = \mathbf{H}_{\boldsymbol{\theta}}(s^-) = \mathbf{H}_{\boldsymbol{\theta}}(s) \text{ says (1.1.42)}$$

so

$$-\mu_1 \mathbf{H}_{\boldsymbol{\theta}}(s) = \partial_{\mathbf{r}} A_{\mathbf{z}}(s^+) = \partial_{\mathbf{n}} A_{\mathbf{z}}(s^+) . \quad (\text{B.6.26})$$

But this last equation matches our equation in question (B.6.24), so we can then go back and erase all the question marks and we have then verified equation (B.6.9) and our proof is complete.

Comment: We noted that Stakgold's analysis is quite complicated. He uses the Laplace free-space propagators such as $E_{\mathbf{z}}(x|x') = -(1/2\pi) \ln(R^2)$, but we think his analysis also applies for the Helmholtz propagators. The reason is that the Helmholtz complication does not really change the singular nature of things near $R = 0$. This is most obvious when comparing $e^{-j\beta_a R} / 4\pi R$ to $1/4\pi R$. If we are wrong about this conjecture, we can regard the above theorem as proven only for small β_a which in fact defines the transmission line limit.

(c) Statement and Proof of the J_m Theorem

The J_m Theorem. A transmission line consists of two conductors called C_2 and C_3 , since index 1 is reserved for the dielectric. For example, the dielectric has permeability μ_1 (but we write β_d in place of β_1). The total "particular" vector potential $A_z(\mathbf{x})$ due to the conduction currents in these two conductors is, according to (1.5.9),

$$A(\mathbf{x})^{\text{part}} = \frac{1}{4\pi} \sum_{i=2}^3 \int_{C_i} \mu_i \mathbf{J}_{ci}(\mathbf{x}') \frac{e^{-j\beta_d R}}{R} dV' \quad R = |\mathbf{x} - \mathbf{x}'| \quad (1.5.9)$$

The theorem claims that (1) the correct adjusted total potential is given by

$$A(\mathbf{x}) = \frac{1}{4\pi} \sum_{i=2}^3 \int_{C_i} [\mu_i \mathbf{J}_{ci}(\mathbf{x}') + \mu_0 \mathbf{J}_{mi}(\mathbf{x}')] \frac{e^{-j\beta_d R}}{R} dV' \quad (B.6.27)$$

where $\mathbf{J}_{mi}(\mathbf{x}')$ represents the surface current at the surface of conductor C_i , and (2) this correct total potential satisfies the boundary conditions (B.6.0) at the surface of both conductors.

We claim the theorem is also true for a transmission line consisting of any number of conductors, but we restrict our interest to two conductors. We shall show for (B.6.27) that (B.6.0) is valid at the surface of conductor C_2 and a similar argument then shows it is also valid at the surface of C_3 .

In the theory of Chapters 4 and 5, the transverse components of \mathbf{A} are ignored, and our real interest is the z component of (B.6.27),

$$A_z(\mathbf{x}) = \frac{1}{4\pi} \sum_{i=2}^3 \int_{C_i} [\mu_i J_{czi}(\mathbf{x}') + \mu_0 J_{mzi}(\mathbf{x}')] \frac{e^{-j\beta_d R}}{R} dV' \quad (B.6.28)$$

To enhance clarity, we shall give each conductor its own custom integration variable. By adding primes, we shadow the equation numbers from section (b) (2) above which proves the J_m Lemma.

The expression above contains four terms which we now write out:

$$\begin{aligned}
 A_{\mathbf{z}}^{(c2)}(\mathbf{x}) &= \frac{1}{4\pi} \int_{C_2} [\mu_2 J_{c\mathbf{z}2}(\mathbf{x}_2')] \frac{e^{-j\beta d R_2}}{R_2} dV_2' & R_2 &= |\mathbf{x} - \mathbf{x}_2'| \\
 A_{\mathbf{z}}^{(c3)}(\mathbf{x}) &= \frac{1}{4\pi} \int_{C_3} [\mu_3 J_{c\mathbf{z}3}(\mathbf{x}_3')] \frac{e^{-j\beta d R_3}}{R_3} dV_3' & R_3 &= |\mathbf{x} - \mathbf{x}_3'|
 \end{aligned} \tag{B.6.4}'$$

$$\begin{aligned}
 A_{\mathbf{z}}^{(m2)}(\mathbf{x}) &= \frac{1}{4\pi} \int_{C_2} [\mu_0 J_{m\mathbf{z}2}(\mathbf{x}_2')] \frac{e^{-j\beta d R_2}}{R_2} dV_2' & R_2 &= |\mathbf{x} - \mathbf{x}_2'| \\
 A_{\mathbf{z}}^{(m3)}(\mathbf{x}) &= \frac{1}{4\pi} \int_{C_3} [\mu_0 J_{m\mathbf{z}3}(\mathbf{x}_3')] \frac{e^{-j\beta d R_3}}{R_3} dV_3' & R_3 &= |\mathbf{x} - \mathbf{x}_3'|
 \end{aligned} \tag{B.6.5}'$$

$$A_{\mathbf{z}}(\mathbf{x}) = A_{\mathbf{z}}^{(c2)}(\mathbf{x}) + A_{\mathbf{z}}^{(c3)}(\mathbf{x}) + A_{\mathbf{z}}^{(m2)}(\mathbf{x}) + A_{\mathbf{z}}^{(m3)}(\mathbf{x}) . \tag{B.6.6}'$$

Without loss of generality, we shall consider $\mathbf{x} \rightarrow \mathbf{s}$ where \mathbf{s} is a point on the surface of conductor C_2 .

The "conduction solutions" $A_{\mathbf{z}}^{(ci)}$ (that is to say, the particular solutions) are naturally smooth at point \mathbf{s} , as described in the text surrounding (B.6.0). Thus, we know that

$$\begin{aligned}
 A_{\mathbf{z}}^{(ci)}(\mathbf{s}+) &= A_{\mathbf{z}}^{(ci)}(\mathbf{s}-) \\
 \partial_{\mathbf{n}} A_{\mathbf{z}}^{(ci)}(\mathbf{s}+) &= \partial_{\mathbf{n}} A_{\mathbf{z}}^{(ci)}(\mathbf{s}-) . & i &= 2, 3
 \end{aligned} \tag{B.6.7}'$$

Since $\mathbf{s} = \mathbf{s}+ = \mathbf{s}-$ for these functions, we may trivially write

$$\begin{aligned}
 &\frac{1}{\mu_1} \partial_{\mathbf{n}} [A_{\mathbf{z}}^{(c2)}(\mathbf{s}+) + A_{\mathbf{z}}^{(c3)}(\mathbf{s}+)] - \frac{1}{\mu_2} \partial_{\mathbf{n}} [A_{\mathbf{z}}^{(c2)}(\mathbf{s}-) + A_{\mathbf{z}}^{(c3)}(\mathbf{s}-)] \\
 &= + \left[\frac{1}{\mu_1} - \frac{1}{\mu_2} \right] \partial_{\mathbf{n}} [A_{\mathbf{z}}^{(c2)}(\mathbf{s}) + A_{\mathbf{z}}^{(c3)}(\mathbf{s})].
 \end{aligned} \tag{B.6.8}'$$

Since this is non-zero, the term $[A_{\mathbf{z}}^{(c2)}(\mathbf{s}+) + A_{\mathbf{z}}^{(c3)}(\mathbf{s}+)]$ on its own does not meet the required slope boundary condition (B.6.0) at an interface between μ_1 and μ_2 , and that is precisely why we need the $A_{\mathbf{z}}^{(m)}$ terms. Our goal is to show that

$$\begin{aligned}
 &\frac{1}{\mu_1} \partial_{\mathbf{n}} [A_{\mathbf{z}}^{(m2)}(\mathbf{s}+) + A_{\mathbf{z}}^{(m3)}(\mathbf{s}+)] - \frac{1}{\mu_2} \partial_{\mathbf{n}} [A_{\mathbf{z}}^{(m2)}(\mathbf{s}-) + A_{\mathbf{z}}^{(m3)}(\mathbf{s}-)] \\
 &= - \left[\frac{1}{\mu_1} - \frac{1}{\mu_2} \right] \partial_{\mathbf{n}} [A_{\mathbf{z}}^{(c2)}(\mathbf{s}) + A_{\mathbf{z}}^{(c3)}(\mathbf{s})] .
 \end{aligned} \tag{B.6.9}'$$

so that when we add the four terms of (B.6.6)' we will get

$$\frac{1}{\mu_1} \partial_n A_z(\mathbf{s}+) - \frac{1}{\mu_2} \partial_n A_z(\mathbf{s}-) = 0 \quad (B.6.10)$$

as required by (1.1.46). This concludes our proof outline, and it remains then to demonstrate (B.6.9)'.

At this point, we skip over several equations of the Lemma proof since they are all generalized simply by adding 2 or 3 subscripts in the right places. For example, the surface currents are given by,

$$\begin{aligned} K_{z2} &= - \left(\frac{\mu_2}{\mu_0} - \frac{\mu_1}{\mu_0} \right) H_{\theta 2} && \text{on } C_2 \\ K_{z3} &= - \left(\frac{\mu_3}{\mu_0} - \frac{\mu_1}{\mu_0} \right) H_{\theta 3} && \text{on } C_3 \end{aligned} \quad (B.1.10)$$

We arrive then at (B.6.16)' as follows (recall that E_2 is the 2D Helmholtz propagator),

$$\begin{aligned} A_z^{(m2)}(\mathbf{x}) &= \oint_{C_2} ds_2' [(\mu_1 - \mu_2) H_{\theta 2}(\mathbf{x}_2')] E_2(\mathbf{x}|\mathbf{x}_2') \\ A_z^{(m3)}(\mathbf{x}) &= \oint_{C_3} ds_3' [(\mu_1 - \mu_3) H_{\theta 3}(\mathbf{x}_3')] E_2(\mathbf{x}|\mathbf{x}_3') \end{aligned} \quad (B.6.16)'$$

We regard these as two representations of Stakgold's first equation (B.6.2). Nothing special happens in these equations as $\mathbf{x} \rightarrow \mathbf{s}$. Thus, we can say that in either case, $A_z^{(mi)}(\mathbf{s}+) = A_z^{(mi)}(\mathbf{s}-)$. When this is combined with the first line of (B.6.7)', we find by adding all four terms in (B.6.6)' that $A_z(\mathbf{s}+) = A_z(\mathbf{s}-)$ and we have thus shown that the first boundary condition of the pair (B.6.0) is satisfied.

A major difference appears at the next step (B.6.18)',

$$\begin{aligned} \partial_n A_z^{(m2)}(\mathbf{s}\pm) &= \oint_{C_2} ds_2' [(\mu_1 - \mu_2) H_{\theta 2}(\mathbf{x}')] \partial_n E_2(\mathbf{s}|\mathbf{x}_2') \mp [(\mu_1 - \mu_2) H_{\theta 2}(\mathbf{s})]/2 \quad . \\ \partial_n A_z^{(m3)}(\mathbf{s}\pm) &= \oint_{C_3} ds_3' [(\mu_1 - \mu_3) H_{\theta 3}(\mathbf{x}')] \partial_n E_2(\mathbf{s}|\mathbf{x}_3') \end{aligned} \quad (B.6.18)'$$

The "extra Stakgold term" only appears when a point \mathbf{s} lies on the surface being integrated over since it is this integration which gives rise to the singular situation. Since our \mathbf{s} lies on C_2 and not on C_3 , there is no "extra term" in the last equation above.

Now since we want to prove (B.6.9)', we first evaluate its left hand side using each equation of (B.6.18)' twice,

$$\begin{aligned}\partial_n A_z^{(m2)}(s+) &= \oint_{C_2} ds_2' [(\mu_1 - \mu_2) H_{\theta 2}(x_2')] \partial_n E_2(s|x_2') - (1/2)[(\mu_1 - \mu_2) H_{\theta 2}(s)] \\ \partial_n A_z^{(m3)}(s) &= \oint_{C_3} ds_3' [(\mu_1 - \mu_3) H_{\theta 3}(x_3')] \partial_n E_2(s|x_3')\end{aligned}\quad (B.6.18) +$$

so

$$\begin{aligned}(\mu_2 - \mu_1) \oint_{C_2} ds_2' H_{\theta 2}(x_2') \partial_n E_2(s|x_2') &= -\partial_n A_z^{(m2)}(s+) - (1/2)[(\mu_1 - \mu_2) H_{\theta 2}(s)] \\ (\mu_3 - \mu_1) \oint_{C_3} ds_3' H_{\theta 3}(x_3') \partial_n E_2(s|x_3') &= -\partial_n A_z^{(m3)}(s) \quad .\end{aligned}\quad (B.6.23)'$$

Equation (B.6.22)' then becomes

$$\begin{aligned}-\partial_n A_z^{(m2)}(s+) - (1/2)[(\mu_1 - \mu_2) H_{\theta 2}(s) - (\mu_2 + \mu_1) H_{\theta 2}(s)]/2 \\ -\partial_n A_z^{(m3)}(s) = \partial_n [A_z^{(c2)}(s) + A_z^{(c3)}(s)]\end{aligned}\quad ?$$

or

$$\begin{aligned}-\partial_n A_z^{(m2)}(s+) - \mu_1 H_{\theta 2}(s) \\ -\partial_n A_z^{(m3)}(s) = \partial_n [A_z^{(c2)}(s) + A_z^{(c3)}(s)]\end{aligned}\quad ?$$

or

$$-\mu_1 H_{\theta 2}(s) = \partial_n [A_z^{(c2)}(s) + A_z^{(c3)}(s) + A_z^{(m2)}(s+) + \partial_n A_z^{(m3)}(s)] \quad ?$$

or

$$-\mu_1 H_{\theta 2}(s) = \partial_n A_z(s+) \quad ? \quad // \text{ using (B.6.6)'.} \quad (B.6.24)'$$

But this last equation is true as shown in Fig B.6 (with $C = C_2$) and (B.6.26), so we can then go back and erase all the question marks and we have then verified equation (B.6.9)' and our proof is complete.

By then taking s to be a point on the surface of C_3 , we would find $-\mu_1 H_{\theta 3}(s) = \partial_n A_z(s+)$ for (B.6.24)' and then Fig B.6 with $C = C_3$ would verify this result as well.

B.7 Application of the J_m Lemma to a round wire with uniform J_z

We shall here verify the J_m Lemma for a round wire which we can regard as the central conductor of a coaxial transmission line with distant shield return. We know from Comment 1 below (B.6.1) that the potential of the shield is not going to interfere with the J_m Lemma and that a verification of the boundary conditions (B.6.0) for the potential of this Lemma applies as well to the combined potential of both conductors.

Assuming the transmission line limit of small β_d , so $e^{-j\beta_d R} \approx 1$, we start then with (B.6.1),

$$A_z(\mathbf{x}) = \int_C dV' [\mu_2 J_{cz}(\mathbf{x}') + \mu_0 J_{mz}(\mathbf{x}')] \frac{1}{4\pi R} \quad . \quad R = |\mathbf{x} - \mathbf{x}'| \quad (B.6.1)$$

but we go at once to the 2D solution $[\nabla_{2D}^2 \mathbf{A}(\mathbf{x}) = -\mu_2 \mathbf{J}_c(\mathbf{x})]$ limit to get

$$-A_{\mathbf{z}}(\mathbf{x}) = \int_C dS' [\mu_2 J_{\mathbf{cz}}(\mathbf{x}') + \mu_0 J_{\mathbf{mz}}(\mathbf{x}')] \frac{\ln(R^2)}{4\pi} \quad // \frac{1}{2\pi} \ln(1/R) = -\frac{\ln(R^2)}{4\pi} \quad (\text{B.7.1})$$

The two currents are given by

$$\begin{aligned} J_{\mathbf{cz}}(\mathbf{x}') &= J_{\mathbf{cz}} = I/(\pi a^2) \quad // \text{uniform} \\ J_{\mathbf{mz}}(\mathbf{x}') &= K_{\mathbf{z}} \delta(r'-a) \quad \text{with} \quad K_{\mathbf{z}} = - \left(\frac{\mu_2}{\mu_0} - \frac{\mu_1}{\mu_0} \right) H_{\theta} \quad . \quad (\text{B.1.10}) \quad (\text{B.7.2}) \end{aligned}$$

(a) The $A_{\mathbf{z}}^{(c)}$ term

The first term in (B.7.1) is then

$$\begin{aligned} -A_{\mathbf{z}}^{(c)}(r,\theta) &= \frac{\mu_2 I}{\pi a^2} \int_C dS' \frac{\ln(R^2)}{4\pi} = \frac{\mu_2 I}{\pi a^2} \int_0^a r' dr' \int_{-\pi}^{\pi} d\theta' \frac{\ln(R^2)}{4\pi} \\ &= \frac{\mu_2 I}{4\pi^2 a^2} \int_0^a r' dr' \int_{-\pi}^{\pi} d\theta' \ln(r'^2 + r^2 - 2r r' \cos(\theta - \theta')) \\ &= \frac{\mu_2 I}{2\pi^2 a^2} \int_0^a r' dr' \int_0^{\pi} dx \ln(r'^2 + r^2 - 2r r' \cos x) \\ &= \frac{\mu_2 I}{2\pi^2 a^2} \int_0^a r' dr' Q(r',r) \quad (\text{B.7.3}) \end{aligned}$$

where we have defined the integral

$$Q(r',r) \equiv \int_0^{\pi} dx \ln [r'^2 + r^2 - 2r r' \cos x] \quad . \quad (\text{B.7.4})$$

The round wire geometry is shown in this drawing, where R^2 shown above comes from the law of cosines,

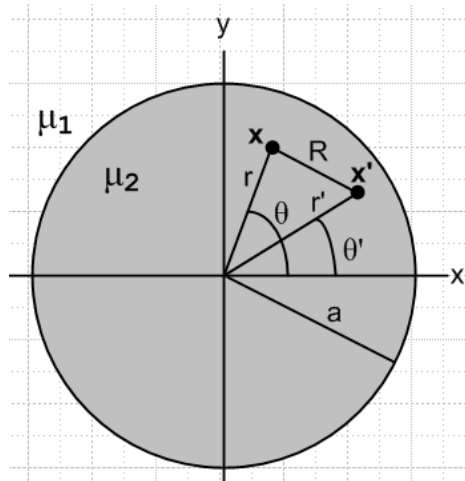


Fig B.7

The integral $Q(r',r)$ may be evaluated using GR7 p 531 4.224,

$$9.8 \quad \int_0^\pi \ln(a + b \cos x) dx = \pi \ln \frac{a + \sqrt{a^2 - b^2}}{2} \quad [a \geq |b| > 0] \quad \text{GW (322)(15)}$$

with $a = r'^2 + r^2$ and $b = -2rr'$ and $a^2 - b^2 = (r'^2 - r^2)^2$ so that $\sqrt{a^2 - b^2} = |r'^2 - r^2|$. The condition $a > |b| > 0$ is met since $(r \pm r')^2 > 0 \Rightarrow r^2 + r'^2 > \pm 2rr'$ which says $a > \pm b$ so $a > |b|$. Thus,

$$\begin{aligned} Q(r',r) &= \int_0^\pi dx \ln [r'^2 + r^2 - 2rr' \cos x] = \pi \ln \left[\frac{(r'^2 + r^2) + |r'^2 - r^2|}{2} \right] = \begin{cases} \pi \ln [r'^2] & r' > r \\ \pi \ln [r^2] & r' < r \end{cases} \\ &= 2\pi \begin{cases} \ln(r') & r' > r \\ \ln(r) & r' < r \end{cases} \end{aligned} \quad (\text{B.7.5})$$

We then have

$$\begin{aligned} -A_z^{(c)}(r,\theta) &= \frac{\mu_2 I}{2\pi^2 a^2} \int_0^a dr' r' Q(r',r) = \frac{\mu_2 I}{\pi a^2} \int_0^a dr' r' \begin{cases} \ln(r') & r' > r \\ \ln(r) & r' < r \end{cases} \\ &= \frac{\mu_2 I}{\pi a^2} \int_0^a dr' r' \{ \ln r' \theta(r' > r) + \ln r \theta(r' < r) \} \\ &= \frac{\mu_2 I}{\pi a^2} [\theta(r < a) \int_r^a dr' r' \ln r' + \ln r \int_0^{\min(a,r)} dr' r'] \\ &= \frac{\mu_2 I}{\pi a^2} \{ \theta(r < a) (1/2) \{ a^2 \ln a - r^2 \ln r - (a^2 - r^2)/2 \} + (1/2) \ln r [\min(a,r)]^2 \} \end{aligned} \quad (\text{B.7.6})$$

where Maple says

$$\begin{aligned} &\text{int}(x*\ln(x), x=r..a); \\ &\frac{1}{2}a^2 \ln(a) - \frac{1}{4}a^2 - \frac{1}{2}r^2 \ln(r) + \frac{1}{4}r^2 \end{aligned}$$

We then write out $A_z^{(c)}(r)$ in its two regions

$$A_z^{(c)}(r > a) = -\frac{\mu_2 I}{\pi a^2} \{ (1/2) a^2 \ln r \} = -\frac{\mu_2 I}{2\pi} \ln r \quad (\text{B.7.7})$$

$$A_z^{(c)}(r < a) = -\frac{\mu_2 I}{\pi a^2} \{ (1/2) \{ a^2 \ln a - r^2 \ln r - (a^2 - r^2)/2 \} + (1/2) r^2 \ln r \} = \frac{\mu_2 I}{2\pi a^2} \{ (a^2 - r^2)/2 - a^2 \ln a \}$$

(b) The $A_z^{(m)}$ term

From (B.7.1) and (B.7.2),

$$\begin{aligned}
 -A_z^{(m)}(\mathbf{x}) &= \mu_0 \int_C dS' J_{mz}(x') \frac{\ln(R^2)}{4\pi} \\
 &= \frac{\mu_0}{4\pi} \int_0^a r' dr' \int_{-\pi}^{\pi} d\theta' \left[-\left(\frac{\mu_2}{\mu_0} - \frac{\mu_1}{\mu_0}\right) H_{\theta}(r') \right] \delta(r'-a) \ln(R^2) \\
 &= -\frac{a}{4\pi} H_{\theta}(a) (\mu_2 - \mu_1) \int_{-\pi}^{\pi} d\theta' \ln(a^2 + r'^2 - 2ra \cos(\theta - \theta')) \\
 &= -\frac{a}{2\pi} H_{\theta}(a) (\mu_2 - \mu_1) \int_0^{\pi} dx \ln(a^2 + r'^2 - 2ra \cos(x)) \\
 &= -\frac{a}{2\pi} H_{\theta}(a) (\mu_2 - \mu_1) Q(a, r) \\
 &= -\frac{a}{2\pi} H_{\theta}(a) (\mu_2 - \mu_1) 2\pi \begin{cases} \ln(a) & a > r \\ \ln(r) & a < r \end{cases} \quad // \text{ using (B.7.5)} \\
 &= a H_{\theta}(a) (\mu_1 - \mu_2) \begin{cases} \ln(a) & a > r \\ \ln(r) & a < r \end{cases} \quad . \quad (B.7.8)
 \end{aligned}$$

From Ampere's law (1.1.37) we have (ignoring displacement current inside the conductor)

$$\oint \mathbf{H} \cdot d\mathbf{s} = 2\pi a H_{\theta}(a) = \int_S \mathbf{J} \cdot d\mathbf{S} = I \quad \Rightarrow \quad H_{\theta}(a) = \frac{I}{2\pi a}$$

and so

$$-A_z^{(m)}(\mathbf{x}) = \frac{I}{2\pi} (\mu_1 - \mu_2) \begin{cases} \ln(a) & a > r \\ \ln(r) & a < r \end{cases} \quad . \quad (B.7.9)$$

Then

$$\begin{aligned}
 A_z^{(m)}(r > a) &= \frac{I}{2\pi} (\mu_2 - \mu_1) \ln r \\
 A_z^{(m)}(r < a) &= \frac{I}{2\pi} (\mu_2 - \mu_1) \ln a \quad . \quad (B.7.10)
 \end{aligned}$$

(c) Adding the two terms and checking boundary conditions

Adding the results of (B.7.7) and (B.7.10) we obtain the total A_z vector potential,

$$\begin{aligned}
 A_z(r > a) &= -\frac{\mu_2 I}{2\pi} \ln r + \frac{I}{2\pi} (\mu_2 - \mu_1) \ln r = -\frac{\mu_1 I}{2\pi} \ln r \\
 A_z(r < a) &= \frac{\mu_2 I}{2\pi a^2} \left\{ (a^2 - r^2)/2 - a^2 \ln a \right\} + \frac{I}{2\pi} (\mu_2 - \mu_1) \ln a
 \end{aligned}$$

$$\begin{aligned}
 &= \frac{\mu_2 I}{2\pi} \{ (a^2 - r^2)/(2a^2) - \ln a \} + \frac{I}{2\pi} (\mu_2 - \mu_1) \ln a \\
 &= -\frac{I}{2\pi} \{ \mu_2 (r^2 - a^2)/(2a^2) + \mu_1 \ln a \}
 \end{aligned}$$

Here then are the final results for the potential $A_z = A_z^{(c)} + A_z^{(m)}$,

$$\begin{aligned}
 A_z(r > a) &= -\frac{I}{2\pi} \mu_1 \ln r \\
 A_z(r < a) &= -\frac{I}{2\pi} \left\{ \mu_1 \ln a + \mu_2 \frac{r^2 - a^2}{2a^2} \right\} .
 \end{aligned} \tag{B.7.11}$$

As a check, we calculate the **B and H fields** implied by these potentials

$$\begin{aligned}
 \mathbf{B} = \text{curl } \mathbf{A} &= \hat{\mathbf{r}} [r^{-1} \partial_\theta A_z - \partial_z A_\theta] + \hat{\boldsymbol{\theta}} [\partial_z A_r - \partial_r A_z] + \hat{\mathbf{z}} [r^{-1} \partial_r (r A_\theta) - r^{-1} \partial_\theta A_r] \\
 &= \hat{\boldsymbol{\theta}} [-\partial_r A_z] \quad \Rightarrow \quad B_\theta = -\partial_r A_z(r)
 \end{aligned}$$

Then

$$\begin{aligned}
 B_\theta(r > a) &= \frac{I}{2\pi} \mu_1 (1/r) \\
 B_\theta(r < a) &= \frac{I}{2\pi} \mu_2 \frac{2r}{2a^2} = \frac{I}{2\pi} \mu_2 (r/a^2)
 \end{aligned} \tag{B.7.12}$$

so the H fields are then

$$\begin{aligned}
 H_\theta(r > a) &= \frac{I}{2\pi} (1/r) \\
 H_\theta(r < a) &= \frac{I}{2\pi} (r/a^2) .
 \end{aligned} \tag{B.7.13}$$

This agrees with Ampere's Law applied in these two regions:

$$\begin{aligned}
 2\pi r H_\theta(r > a) &= I \quad \Rightarrow \quad H_\theta(r > a) = \frac{I}{2\pi} (1/r) \\
 2\pi r H_\theta(r < a) &= I(\pi r^2 / \pi a^2) \quad \Rightarrow \quad H_\theta(r < a) = \frac{I}{2\pi} (r/a^2) .
 \end{aligned} \tag{B.7.14}$$

Next, we check the two **boundary conditions** required by (B.6.0) :

value at $r = a$:

$$A_z(r > a)|_{r=a} - A_z(r < a)|_{r=a} = -\frac{I}{2\pi} \mu_1 \ln a - \left(\frac{I}{2\pi} \left[\mu_2 \frac{a^2 - a^2}{2a^2} - \mu_1 \ln a \right] \right) = 0 \quad \text{OK}$$

slope at $r = a$: $[\partial_r A_z = -B_\theta \text{ so use (B.7.12) }]$

$$\partial_r A_z(r > a) \Big|_{r=a} = -\frac{I}{2\pi} \mu_1 (1/a)$$

$$\partial_r A_z(r < a) \Big|_{r=a} = -\frac{I}{2\pi} \mu_2 (a/a^2) = -\frac{I}{2\pi} \mu_2 (1/a)$$

$$\frac{1}{\mu_1} \partial_r A_z(r > a) \Big|_{r=a} - \frac{1}{\mu_2} \partial_r A_z(r < a) \Big|_{r=a} = -\frac{I}{2\pi} (1/a) - \left[-\frac{I}{2\pi} (1/a) \right] = 0 \quad \text{OK}$$

Thus we have shown for the round conductor with uniform J_z that "the J_m Lemma" works. By adding the bogus surface current term, we generate the correct homogeneous solution which when added to the Helmholtz integral provides the correct total solution which meets both boundary conditions.

(d) Plots of A_z and B_θ and H_θ

Maple provides plots of A_z from (B.7.11), B_θ from (B.7.12) and H_θ from (B.7.13) for this round wire situation. Parameters are set to $I = 1$, $a = 2$, $\mu_1 = 2$ (dielectric), $\mu_2 = 3$ (wire).

```
restart; alias(I=I);
Az := -(I/2*Pi)*piecewise(r>a,mu1*log(r),r<=a,mu1*log(a) + mu2*(r^2-a^2)/(2*a^2));
```

$$A_z = -\frac{1}{2} I \pi \begin{cases} \mu_1 \ln(r) & a < r \\ \mu_1 \ln(a) + \frac{1}{2} \frac{\mu_2 (r^2 - a^2)}{a^2} & r \leq a \end{cases}$$

```
B := (I/2*Pi)*piecewise(r>a,mu1/r,r<=a,mu2*r/(a^2));
```

$$B = \frac{1}{2} I \pi \begin{cases} \frac{\mu_1}{r} & a < r \\ \frac{\mu_2 r}{a^2} & r \leq a \end{cases}$$

```
H := (I/2*Pi)*piecewise(r>a,1/r,r<=a,r/(a^2));
```

$$H = \frac{1}{2} I \pi \begin{cases} \frac{1}{r} & a < r \\ \frac{r}{a^2} & r \leq a \end{cases}$$

```
I := 1: a := 2: mu1 := 2: mu2 := 3:
plot([Az,B,H],r=0..8, color=[black,red,blue]);
```

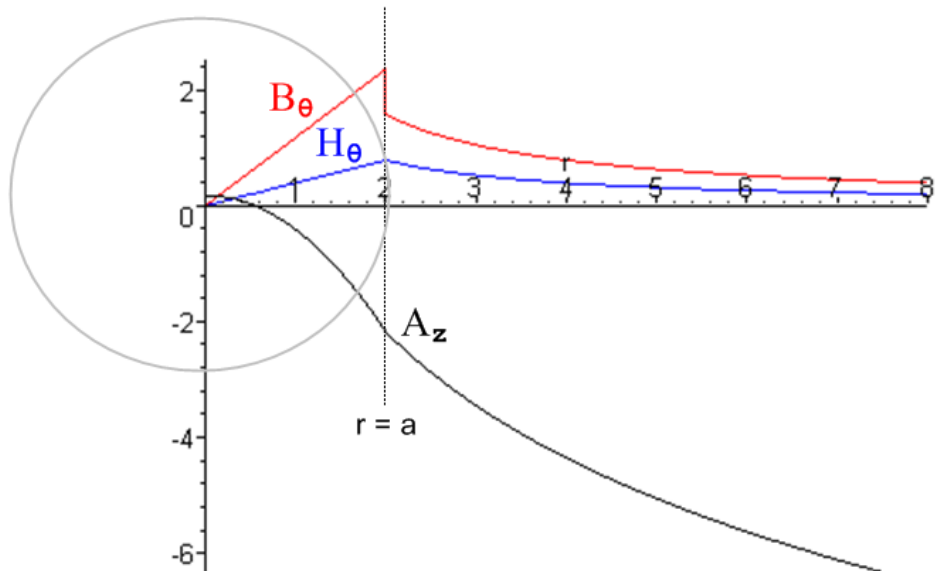


Fig B.8

A_z wanders down as $\sim -\ln(r)$ for large r ; B_θ jumps down at $r = a$ while H_θ is continuous there.

Appendix C: DC Properties of a Wire

C.1 The DC resistance of a wire

The resistance per unit length R of a differential piece of wire of length dz and area dA is derived as follows (σ = conductivity),

$$dV = E dz, \quad J = \sigma E, \quad I = J dA \quad \Rightarrow$$

$$R dz = dV/I = Edz/JdA = (1/\sigma) dz/dA \quad \Rightarrow \quad R = (1/\sigma) /dA .$$

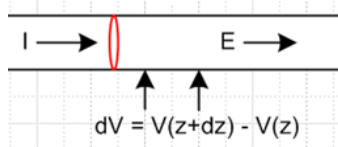
If current density J is constant across the wire cross section (which is the case at DC), we repeat the above with $dA \rightarrow A$ where A is the total wire cross sectional area to find this resistance per unit length for the wire,

$$R = 1/(\sigma A) = \rho/A . \quad // \quad \rho = 1/\sigma = \text{resistivity} \quad (\text{C.1.1})$$

For a round wire of radius a , $A = \pi a^2$, so $R = 1/(\sigma \pi a^2) \equiv R_{dc}$. Current density J is uniform at DC because there are no eddy currents to make it non-uniform as described in Appendix P. We of course assume that the wire is made of an isotropic and homogeneous substance where σ is the same in all directions at all points inside the wire.

C.2 The DC surface impedance of a wire

Imagine a fat wire carrying current I ,



If, at the surface of the wire, one puts voltmeter probes at longitudinal spacing dz , one measures some potential difference which is $dV = E_z dz$. When probed at the surface, the wire appears to have this impedance,

$$(Z_s dz) = dV/I .$$

The quantity Z_s is the surface impedance per unit length and is thus given by

$$Z_s = E_z / I \quad (\text{C.2.1})$$

where E_z is the component of electric field *at the surface* in the direction of the wire. For a wire operating at DC, the current density is uniform across the wire so $J_z = I/A$ and $E_z = J_z/\sigma = I/(A\sigma)$. Thus,

$$Z_s = 1/(A\sigma) = \rho/A \quad // = R \text{ of (C.1.1)} \quad (\text{C.2.2})$$

where A is the cross sectional area. For a round wire of radius a , $A = \pi a^2$, so

$$Z_s = \rho / (\pi a^2) . \quad (C.2.3)$$

If the wire is a perfect conductor, $\rho = 0$ and $Z_s = 0$. For DC, we have $Z_s = R$, but for AC this is no longer true due to the skin and proximity effects which make J_z non-uniform over the conductor cross section. Again, see Appendix P for a general discussion of both these effects, and Chapter 2 for skin effect.

C.3 The DC internal and external inductance of a round wire

We assume here that μ_i is the internal permeability of the wire, and μ_e of the region external to the wire.

The energy density (joules/m³) stored in an electromagnetic field within a medium of negligible loss is given by $u_{em} = (\mathbf{E} \cdot \mathbf{D} + \mathbf{B} \cdot \mathbf{H})/2$ [Jackson p 259 Eq. (6.106)]. We are interested only in the portion of this energy density stored in the magnetic field, so $u = (1/2) \mathbf{B} \cdot \mathbf{H}$. Since μ and ϵ are assumed to be scalars,

$$u = (1/2) \mu H^2 . \quad // (1.1.5) \mathbf{B} = \mu \mathbf{H} \quad (C.3.1)$$

For any inductor of inductance L carrying current I and having potential difference V , we know that

$$V = L \, dI/dt \quad (C.3.2)$$

$$P = IV = I (L \, dI/dt) = d/dt [(1/2)L I^2] . \quad (C.3.3)$$

Since the power fed into an ideal inductor goes into the magnetic field energy, $P = dU/dt$ and so

$$U = (1/2)L I^2 . \quad (C.3.4)$$

For a straight wire, we now redefine symbol L to mean inductance per unit length, so then

$$U = (1/2)[Ldz] I^2 . \quad (C.3.5)$$

For either the internal or external region we have $U = \int d\mathcal{V} u = dz \int dS u$ where $d\mathcal{V}$ is a volume element and dS is a cross sectional area element. Thus from (C.3.1) and (C.3.5),

$$U = dz \int dS (1/2) \mu H^2 = (1/2)[Ldz] I^2 \quad \Rightarrow \quad L = \mu \int dS (H/I)^2 . \quad (C.3.6)$$

In particular [elsewhere we have used $\mu_i = \mu$ and $\mu_e = \mu_d$]

$$L_i = \mu_i \int_{in} dS (H_i/I)^2 \quad (C.3.7)$$

$$L_e = \mu_e \int_{out} dS (H_e/I)^2 . \quad (C.3.8)$$

For the round wire at DC it is a simple matter to compute H_i and H_e using Ampere's Law (1.1.37),

$$\oint \mathbf{H} \cdot d\mathbf{s} = \int \mathbf{J} \cdot d\mathbf{S}$$

$$\begin{aligned} 2\pi r H_i &= I(\pi r^2/\pi a^2) \Rightarrow H_i/I = \frac{1}{2\pi} (r/a^2) \\ 2\pi r H_e &= I \Rightarrow H_e/I = \frac{1}{2\pi} (1/r) . \end{aligned} \quad (\text{C.3.9})$$

We then compute the two inductances as follows:

$$\begin{aligned} L_i &= \mu_i \int dS (H_i/I)^2 = \mu_i \int_0^a r dr \int_{-\pi}^{\pi} d\theta \left[\frac{1}{2\pi} (r/a^2) \right]^2 = \frac{\mu_i}{2\pi a^4} \int_0^a r^3 dr = \frac{\mu_i}{8\pi} \\ L_e &= \mu_e \int dS (H_e/I)^2 = \mu_e \int_a^\infty r dr \int_{-\pi}^{\pi} d\theta \left[\frac{1}{2\pi} (1/r) \right]^2 = \frac{\mu_e}{2\pi} \int_a^\infty (1/r) dr = \infty . \end{aligned}$$

Both results are interesting. L_i is interesting because it is independent of the wire radius a . For the same current, a smaller a results in a larger H and B field, which is then offset by the smaller volume (area).

L_e is interesting because it is infinite! Even a tiny 1 cm piece of our infinitely long round wire stores an infinite amount of energy in its magnetic field. We therefore limit the external region by some large radius R and then we have

$$L_i = \frac{\mu_i}{8\pi} = \frac{\mu_i}{\mu_0} \frac{\mu_0}{8\pi} = \frac{\mu_i}{\mu_0} \frac{4\pi \times 10^{-7}}{8\pi} = \frac{\mu_i}{\mu_0} * 50 \text{ nH/m} \quad (\text{C.3.10})$$

$$L_e = \frac{\mu_e}{2\pi} \ln(R/a) . \quad (\text{C.3.11})$$

Thus for a non-magnetic round wire in air the internal inductance is exactly 50 nH/m.

A "practical wire" is more like a loop of wire than an infinitely long wire. It is difficult to conjure up an experiment to test (C.3.11) even for a very long straight piece of wire without having some return path for the current to return to the driving "battery". For wire and dielectric both having μ_0 , Jackson shows (p 216-218) that the inductance per unit length of a loop of projected area A of radius- a wire is given by $L_e + L_i = (\mu_0/4\pi) [\ln(\xi A/a^2) + 1/2]$, where ξ is a near-unity factor which accounts for messy details of the calculation. The 1/2 term accounts for the internal inductance $L_i = \mu_0/8\pi$ as in (C.3.10).

For a *circular* loop of radius R , one has $A = \pi R^2$ and, if $R \gg a$, $\xi = 64/(\pi e^4) \approx .373$. So,

$$\ln(\xi A/a^2) = \ln(64 \pi R^2/\pi e^4 a^2) = 2 \ln(8R/ae^2) = 2 \ln(8R/a) + 2 \ln(e^{-2}) = 2 \ln(8R/a) - 4$$

and then the total inductance per unit length is

$$L_e + L_i = (\mu_0/4\pi) [2 \ln(8R/a) - 4 + 1/2] = (\mu_0/2\pi) [\ln(8R/a) - 2 + 1/4] = (\mu_0/2\pi) [\ln(8R/a) - 7/4] .$$

The *total* inductance of such a loop is then

$$L = 2\pi R(\mu_0/2\pi) [\ln(8R/a) - 7/4] = \mu_0 R [\ln(8R/a) - 7/4] \quad (\text{C.3.12})$$

in agreement with Jackson Problem 5.32 p 234. If one omits the internal inductance, the last factor is -2 instead of -7/4, and this result is seen in some sources. The point is that this is a finite result, even though the (dipole) magnetic field of such a loop extends to infinity. A loop of N turns gets an extra factor N^2 because in effect current $I \rightarrow NI$ in (C.3.5), so the total field energy increases by factor N^2 .

Suppose there were two parallel wires with currents flowing in opposite directions. In this case, we could compute the magnetic field H at any point in space as the vector sum of the fields of the two wires, then we could integrate H^2 over all space to get the total energy U and from that the external inductance L_e . In this case, the $\ln(R)$ divergence does not appear. In effect, the divergence cancels between the two wires, similar to the way opposite short segments of the circular wire cancel to give the finite result quoted above.

We really only care about the internal inductance L_i of a wire in our transmission line analysis because the external inductance L_e is already accounted for by the techniques of Chapter 4. That is, L_e is computed by considering the magnetic potential A_z (or W) between the wires, see (4.10.8).

C.4 The DC internal inductance of a wire of rectangular cross section

The inductance expressions above apply to *any* cross sectional shape,

$$L_i = \mu_i \int_{in} dS (H_i/I)^2 \quad (C.3.7)$$

$$L_e = \mu_e \int_{out} dS (H_e/I)^2 \quad (C.3.8)$$

so the only problem is how to compute H for a non-round wire. That problem is solved in Appendix B where it is shown that

$$\mathbf{H}(x,y) = -\frac{1}{4\pi} \int d^2x' \ln(R^2) \text{curl}' \mathbf{J}(x',y') \quad R = |\mathbf{x}-\mathbf{x}'| \quad (B.2.12) \quad (C.4.1)$$

Consider a wire of rectangular cross section $2a \times 2b$ (uniform \mathbf{J}_z) as an example.

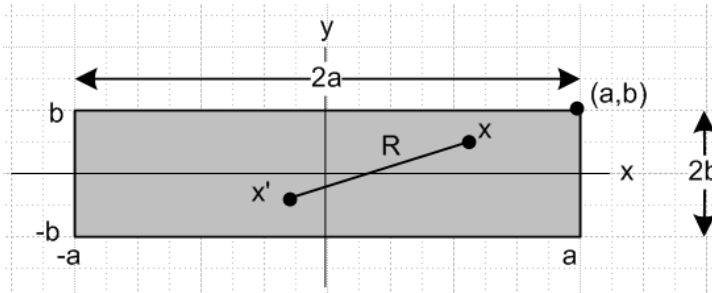


Fig C.1

The uniform current density is given by

$$\begin{aligned} J_z(x) &= (I/4ab)\theta(-a \leq x \leq a) \theta(-b \leq y \leq b) \\ &= (I/4ab) \theta(x \leq a)\theta(x \geq -a) \theta(y \leq b)\theta(y \geq -b) \quad // \theta(s \geq r) \text{ means } \theta(s-r) \text{ Heaviside} \\ &= (I/4ab) \theta(a-x)\theta(x+a) \theta(b-y)\theta(y+b) \quad (C.4.2) \end{aligned}$$

Calculate $\text{curl } \mathbf{J}$ to be used in (C.4.1) :

$$\begin{aligned} \text{curl } \mathbf{J} &= \hat{\mathbf{x}} (\partial_y J_z - \partial_z J_y) + \hat{\mathbf{y}} (\partial_z J_x - \partial_x J_z) + \hat{\mathbf{z}} (\partial_x J_y - \partial_y J_x) \\ &= \hat{\mathbf{x}} (\partial_y J_z) + \hat{\mathbf{y}} (-\partial_x J_z) \quad (C.4.3) \end{aligned}$$

$$\begin{aligned} \partial_x J_z &= (I/4ab) \partial_x [\theta(a-x)\theta(x+a)] \theta(b-y)\theta(y+b) \\ &= (I/4ab) [\theta(a-x)\delta(x+a) - \delta(x-a)\theta(x+a)] \theta(b-y)\theta(y+b) \quad // \partial_x \theta(a-x) = -\delta(x-a) \end{aligned}$$

$$\begin{aligned} \partial_y J_z &= (I/4ab) \theta(a-x)\theta(x+a) \partial_y [\theta(b-y)\theta(y+b)] \\ &= (I/4ab) \theta(a-x)\theta(x+a) [\theta(b-y)\delta(y+b) - \delta(y-b)\theta(y+b)] \end{aligned}$$

so then

$$\begin{aligned} [\text{curl } \mathbf{J}]_{\mathbf{x}} &= (I/4ab) \theta(a-x)\theta(x+a) [\theta(b-y)\delta(y+b) - \delta(y-b)\theta(y+b)] \\ [\text{curl } \mathbf{J}]_{\mathbf{y}} &= - (I/4ab) [\theta(a-x)\delta(x+a) - \delta(x-a)\theta(x+a)] \theta(b-y)\theta(y+b) . \end{aligned} \quad (\text{C.4.4})$$

Notice that we can obtain $[\text{curl } \mathbf{J}]_{\mathbf{y}}$ from $[\text{curl } \mathbf{J}]_{\mathbf{x}}$ by doing $a \leftrightarrow b$, $x \leftrightarrow y$ and adding a minus sign.

Finally calculate $H_{\mathbf{x}}$ from (C.4.1).

$$\begin{aligned} H_{\mathbf{x}}(x,y) &= -\frac{1}{4\pi} \int d^2 \mathbf{x}' \ln(R^2) [\text{curl}' \mathbf{J}(\mathbf{x}')]_{\mathbf{x}} \quad R = |\mathbf{x}-\mathbf{x}'| \\ &= -\frac{I}{16\pi ab} \int_{-a}^a dx' \int_{-\infty}^{\infty} dy' \ln [(x-x')^2 + (y-y')^2] [\theta(b-y')\delta(y'+b) - \theta(y'+b)\delta(y'-b)] \} \\ &= -\frac{I}{16\pi ab} \int_{-a}^a dx' \int_{-\infty}^b dy' \ln [(x-x')^2 + (y-y')^2] \delta(y'+b) \\ &\quad + \frac{I}{16\pi ab} \int_{-a}^a dx' \int_{-b}^{\infty} dy' \ln [(x-x')^2 + (y-y')^2] \delta(y'-b) \\ &= -\frac{I}{16\pi ab} \int_{-a}^a dx' \ln [(x'-x)^2 + (y+b)^2] + \frac{1}{16\pi ab} \int_{-a}^a dx' \ln [(x'-x)^2 + (y-b)^2] \} \\ &\equiv \frac{I}{16\pi ab} (-I_1 + I_2) \quad I_1(b) = \int_{-a}^a dx' \ln [(x'-x)^2 + (y+b)^2] \\ &\quad I_2(b) \equiv \int_{-a}^a dx' \ln [(x'-x)^2 + (y-b)^2] = I_1(-b) . \quad (\text{C.4.5}) \\ &\equiv \frac{I}{16\pi ab} F(x,y,a,b) \quad F = -I_1 + I_2 . \end{aligned}$$

As an aid to Maple's grouping of elements, let $x'' = x'-x$, then take $x'' \rightarrow x'$ to get

$$I_1(b) = \int_{-a-x}^{a-x} dx' \ln [x'^2 + c^2] \quad \text{where } c = y+b .$$

Maple then evaluates I_1 and I_2 as follows (hoop jumping to get results in desired order),

```

[> I1a := int(ln(xp^2 + c^2), xp=-a-x..a-x):
[> I1b := collect(I1a, ln): c := y+b: # get logs together
[> e1 := 2*a*x = (a+x)^2 - a^2 - x^2:
[> e2 := -2*a*x = (a-x)^2 - a^2 - x^2: # for substitution
[> I1c := subs(e1, e2, I1b):
[> I1d := unapply(I1c, b): # make function of b
[> I1 := I1d(b):

I1 := (a-x) ln((a-x)^2 + (y+b)^2) + (a+x) ln((a+x)^2 + (y+b)^2)
      + 2(y+b) arctan((a+x)/(y+b)) - 2(y+b) arctan((-a+x)/(y+b)) - 4a

[> I2 := I1d(-b):

I2 := (a+x) ln((a+x)^2 + (y-b)^2) + (a-x) ln((a-x)^2 + (y-b)^2)
      + 2(y-b) arctan((a+x)/(y-b)) - 2(y-b) arctan((-a+x)/(y-b)) - 4a

```

In Maple, unapply(f,x) causes expression f to be a function of x which can then be called as f(x). Collect just orders terms in a certain way, while subs forces Maple to be a little smarter about expressions. The next step is to create function F(x,y,a,b) which is just $-I_1 + I_2$ as shown above

```

[> Fa := collect(I2-I1, arctan): # gather arctans
[> F := unapply(Fa, x, y, a, b): # make F(x, y, a, b)
[> F(x, y, a, b): # call the newly made function

(2y+2b) arctan((-a+x)/(y+b)) + (-2y-2b) arctan((a+x)/(y+b))
+ (2y-2b) arctan((a+x)/(y-b)) + (-2y+2b) arctan((-a+x)/(y-b))
+ (a+x) ln((a+x)^2 + (y-b)^2) + (a-x) ln((a-x)^2 + (y-b)^2)
- (a+x) ln((a+x)^2 + (y+b)^2) - (a-x) ln((a-x)^2 + (y+b)^2)

```

Reading from the above and putting x,y last in each parentheses, the four arctangents can be written

$$\begin{aligned}
 (1/2) F(x,y,a,b)^{\text{atan}} &= -(b-y) \left[-\tan^{-1} \frac{a+x}{b-y} \right] + (b-y) \tan^{-1} \frac{a-x}{b-y} - (b+y) \tan^{-1} \left(\frac{a+x}{b+y} \right) + (b+y) \left[-\tan^{-1} \left(\frac{a-x}{b+y} \right) \right] \\
 &= (b-y) \left[\tan^{-1} \frac{a+x}{b-y} + \tan^{-1} \frac{a-x}{b-y} \right] - (b+y) \left[\tan^{-1} \left(\frac{a+x}{b+y} \right) + \tan^{-1} \left(\frac{a-x}{b+y} \right) \right] .
 \end{aligned}$$

Next, the four log terms can be combined to give

$$(1/2) F(x,y,a,b)^{\text{ln}} = (1/2) (a-x) \ln \left[\frac{(a-x)^2 + (b-y)^2}{(a-x)^2 + (b+y)^2} \right] + (1/2) (a+x) \ln \left[\frac{(a+x)^2 + (b-y)^2}{(a+x)^2 + (b+y)^2} \right] .$$

Combining and reordering these terms, we get

$$\begin{aligned}
(1/2) F(x,y,a,b) = & (1/2) (a+x) \ln \left[\frac{(a+x)^2 + (b-y)^2}{(a+x)^2 + (b+y)^2} \right] + (1/2) (a-x) \ln \left[\frac{(a-x)^2 + (b-y)^2}{(a-x)^2 + (b+y)^2} \right] \\
& + (b-y) \left[\tan^{-1} \frac{a-x}{b-y} + \tan^{-1} \frac{a+x}{b-y} \right] - (b+y) \left[\tan^{-1} \left(\frac{a-x}{b+y} \right) + \tan^{-1} \left(\frac{a+x}{b+y} \right) \right] .
\end{aligned} \tag{C.4.6}$$

This expression agrees with Holloway and Kuester's W_1 if one replaces $a = w/2$ and $b = t/2$. With such replacements, we would have

$$H_{\mathbf{x}}(x,y) = \frac{I}{16\pi ab} F(x,y,a,b) = \frac{I}{4\pi wt} F(x,y, w/2, t/2) = \frac{I}{2\pi wt} \left[(1/2) F(x,y, w/2, t/2) \right] \equiv \frac{I}{2\pi wt} W_1 \tag{C.4.7a}$$

so our $H_{\mathbf{x}}$ then agrees with their equations (9) and (11).

Now based on the comment below (C.4.4) above, we may conclude for $H_{\mathbf{y}}$ that

$$\begin{aligned}
H_{\mathbf{y}}(x,y) = & -\frac{1}{4\pi} \int d^2 \mathbf{x}' \ln(R^2) [\text{curl}' \mathbf{J}(\mathbf{x}')]_{\mathbf{y}} = H_{\mathbf{x}}(x,y) \text{ if we swap } a \leftrightarrow b, x \leftrightarrow y \text{ and add a minus} \\
= & -\frac{1}{16\pi ab} F(y,x,b,a) .
\end{aligned} \tag{C.4.7b}$$

Just for the record,

> **F(y, x, b, a) ;**

$$\begin{aligned}
& (2x - 2a) \arctan\left(\frac{y+b}{-a+x}\right) + (2x - 2a) \arctan\left(\frac{b-y}{-a+x}\right) \\
& + (-2x - 2a) \arctan\left(\frac{y+b}{a+x}\right) + (-2x - 2a) \arctan\left(\frac{b-y}{a+x}\right) \\
& + (b-y) \ln((b-y)^2 + (-a+x)^2) + (y+b) \ln((y+b)^2 + (-a+x)^2) \\
& - (b-y) \ln((b-y)^2 + (a+x)^2) - (y+b) \ln((a+x)^2 + (y+b)^2)
\end{aligned}$$

We can now make a "field plot" showing the H field (direction and magnitude) in the cross section plane of our rectangular conductor, where we stick with the 4:1 ratio of edges as in Fig C.1 above,


```

a := 4: b := 1: I := 1:
Hx := F(x,y,a,b)/(16*Pi*a*b):
Hy := -F(y,x,b,a)/(16*Pi*a*b):
p1 := fieldplot([Hx,Hy],x= -2*a..2*a,y= -6*b..6*b,arrows=THICK,grid =
[30,30],scaling=constrained):
p2 := PLOT(CURVES([[a,b],[a,-b],[-a,-b],[-a,b],[a,b]],COLOR(1,0,0))):
display(p1,p2);

```

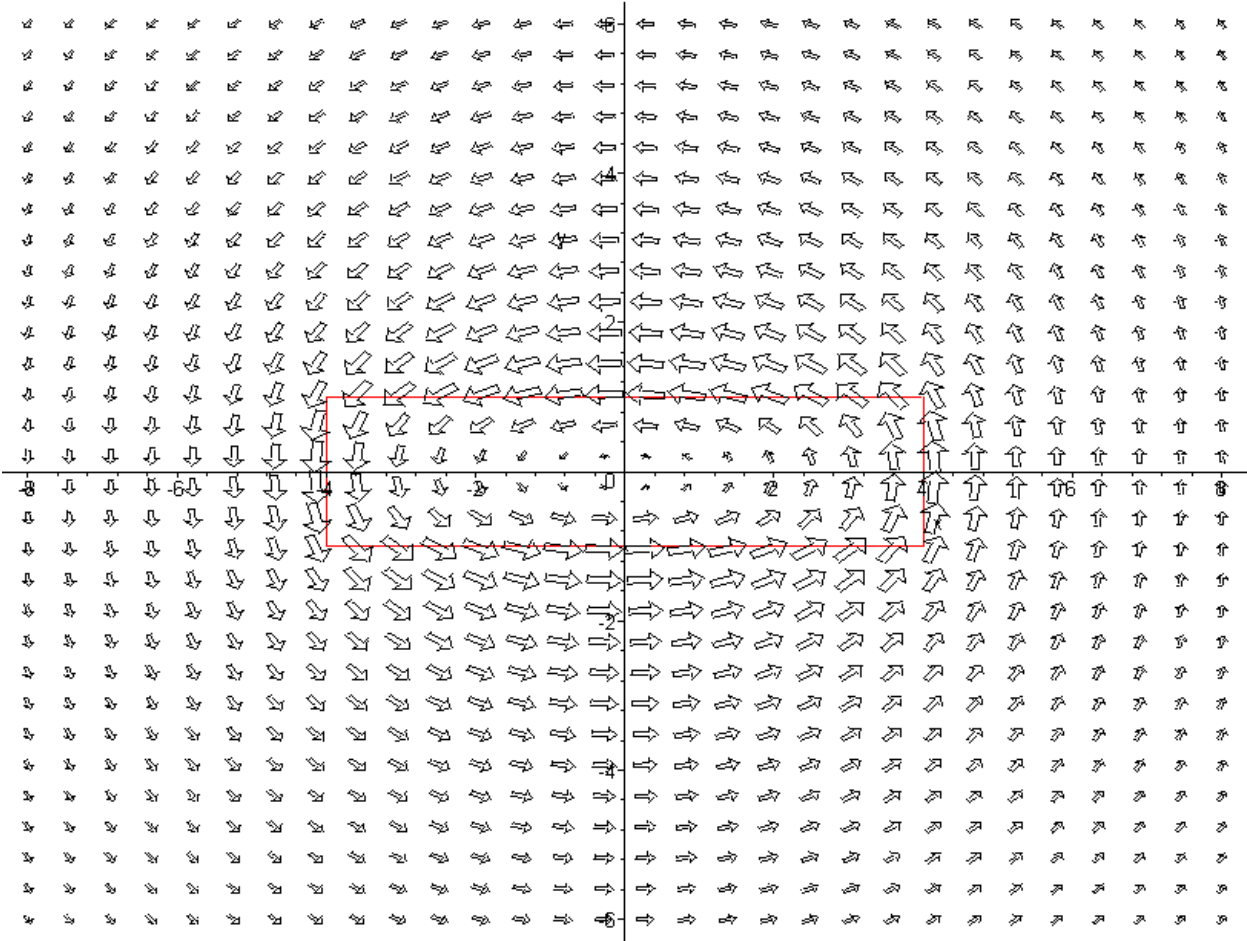


Fig C.2

In this plot the H field appears to be maximal at the conductor boundary (shown in red) and as one moves away it becomes the field of a thin round wire. Current J_z is flowing in the z direction toward the viewer.

The second plot is of $|\mathbf{H}|^2$ as a surface over the x,y plane. Recall that $|\mathbf{H}|^2$ is proportional to the energy density in the magnetic field which in turn contributes to inductance.

```
plot3d(3000*(Hx^2+Hy^2),x= -2*a..2*a,y= -6*b..6*b, grid = [40,40],projection = normal,axes=boxed,scaling=constrained);
```

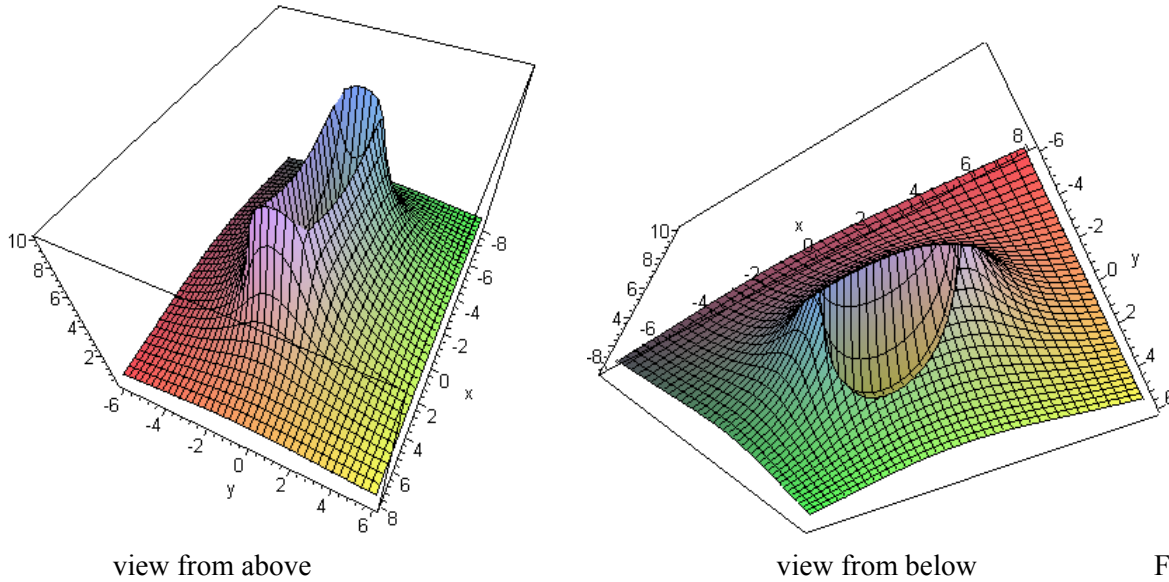


Fig C.3

The $|\mathbf{H}|^2$ surface is very steep at the conductor boundaries, somewhat resembling a rectangular volcano which dips all the way down to 0 in the center, as shown from below on the right. The L_i integration discussed below is over this central "cone" of the volcano.

The red plot below is a slice through the volcano at $x = 0$:

```
x := 0: plot([Hx^2+Hy^2, (0.03)*sqrt(Hx^2+Hy^2)],y=-6..6, color = [red,black],thickness=2,numpoints = 500);
```

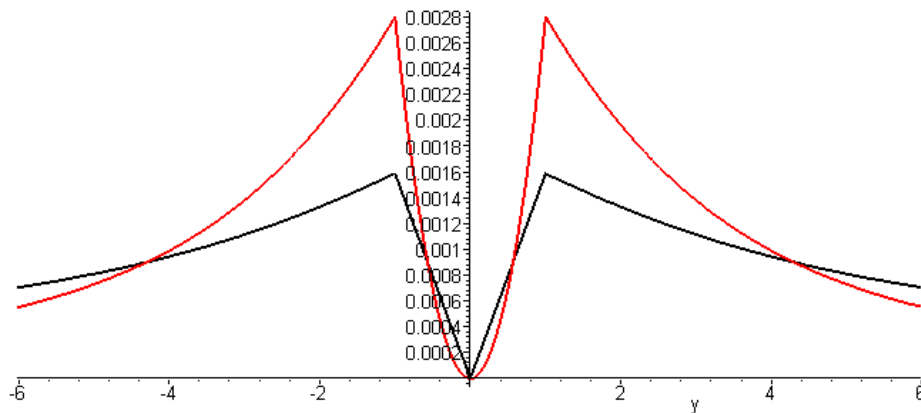


Fig C.4

The black plot is of $|\mathbf{H}|$ (but scaled down) and resembles the H_θ plot for the round wire shown in Fig B.8.

We return now to a computation of the **internal inductance** L_i of the rectangular wire. From (C.3.7),

$$L_i = \mu_i \int_i dS (H/I)^2 = \mu_i \left(\frac{1}{16\pi ab} \right)^2 \int_{-a}^a dx \int_{-b}^b dy [F(x,y,a,b)^2 + F(y,x,b,a)^2] . \quad (C.4.8)$$

Since $F(x,y,aa,ab) = aF(x/a,y/a,a,b)$ one can show that L_i must have this functional form

$$L_i = (\mu_i/8\pi) \ell(b/a) \quad (C.4.9)$$

though this conclusion is obvious based on dimensions alone. The factor $(\mu_i/8\pi)$ is L_i for a round wire of any radius, as shown in (C.3.10). The problem is to find function ℓ . We set $a = 1$ with no loss of generality and use the obvious four-fold symmetry of the energy density so that

$$\begin{aligned} L_i &= 4 \mu_i \left(\frac{1}{16\pi b} \right)^2 \int_0^1 dx \int_0^b dy [F(x,y,1,b)^2 + F(y,x,b,1)^2] \\ &= \left(\frac{\mu_i}{8\pi} \right) \left\{ \frac{1}{8\pi^2 b^2} \int_0^1 dx \int_0^b dy [F(x,y,1,b)^2 + F(y,x,b,1)^2] \right\} . \end{aligned} \quad (C.4.10)$$

Thus our function of interest is

$$\ell(b) = \frac{1}{8\pi^2 b^2} \int_0^1 dx \int_0^b dy [F(x,y,1,b)^2 + F(y,x,b,1)^2] \quad (C.4.11)$$

where the integrand is (look carefully to see top level brackets),

```
> F1 := F(x,y,1,b)^2 + F(y,x,b,1)^2;
```

$$\begin{aligned} F1 &= \left((1+x) \ln(1+2x+x^2+(y-b)^2) + (1-x) \ln(1-2x+x^2+(y-b)^2) + 2(y-b) \arctan\left(\frac{1+x}{y-b}\right) - 2(y-b) \arctan\left(\frac{-1+x}{y-b}\right) \right. \\ &\quad \left. - (1+x) \ln(1+2x+x^2+(y+b)^2) - (1-x) \ln(1-2x+x^2+(y+b)^2) - 2(y+b) \arctan\left(\frac{1+x}{y+b}\right) + 2(y+b) \arctan\left(\frac{-1+x}{y+b}\right) \right)^2 + \\ &\quad \left((y+b) \ln(b^2+2by+y^2+(-4+x)^2) + (b-y) \ln(b^2-2by+y^2+(-4+x)^2) + 2(-4+x) \arctan\left(\frac{y+b}{-4+x}\right) \right. \\ &\quad \left. - 2(-4+x) \arctan\left(\frac{y-b}{-4+x}\right) - (y+b) \ln(b^2+2by+y^2+(4+x)^2) - (b-y) \ln(b^2-2by+y^2+(4+x)^2) \right. \\ &\quad \left. - 2(4+x) \arctan\left(\frac{y+b}{4+x}\right) + 2(4+x) \arctan\left(\frac{y-b}{4+x}\right) \right)^2 \end{aligned}$$

If one were to expand this expression, there would be $16^2 + 16^2 = 256 + 256 = 512$ terms if no terms combined. In fact there are 232 distinct terms:

```
F2 := expand(F1): nops(F2);
```

Here are four sample terms in the integrand of (C.4.11),

```
for n from 13 to 16 do
  print(op(n,F2));
od;
```

$$\begin{aligned} & \ln(1-2x+x^2+(y-b)^2) x^2 \\ & -16 \ln(b^2-2by+y^2+(4+x)^2) b \arctan\left(\frac{y-b}{4+x}\right) \\ & -2 \ln(b^2+2by+y^2+(-4+x)^2) y^2 \ln(b^2-2by+y^2+(-4+x)^2) \\ & -8 \arctan\left(\frac{1+x}{y-b}\right) y^2 \arctan\left(\frac{-1+x}{y-b}\right) \end{aligned}$$

It seems rather unlikely that all 232 terms can be double-integrated analytically! For example, if we ask Maple to analytically integrate the last term shown above just over the x range, it gives up,

```
int(op(16,F2), x=0..1);
```

$$\int_0^1 -8 \arctan\left(\frac{1+x}{y-b}\right) y^2 \arctan\left(\frac{-1+x}{y-b}\right) dx$$

Thus, in order to compute $\mathcal{L}(b)$ we must turn to numerical integration which, for each value of b , requires doing 232 numerical double integrals and adding up the results. As is visible in Fig C.3 and Fig C.4, the overall integrand is singular at the conductor edge, so we might expect some difficulties with the numeric integrations near the upper endpoints.

We were not successful trying for a hour to get Maple to compute the integral (C.4.11) analytically or numerically, but certainly the numerical integration can be done. Holloway and Kuester quote the following numerical approximate formulas for two special cases,

$$\begin{aligned} L_{\mathbf{i}} &= (\mu_{\mathbf{i}}/8\pi) [0.96639] \quad a = b \text{ (square wire)} \quad // \text{ very close to the round conductor} \\ L_{\mathbf{i}} &= (\mu_{\mathbf{i}}/8\pi) [(4\pi/3) b/a] \quad b/a \ll 1 \text{ (flat wire)} \quad // L_{\mathbf{i}} = (1/6) \mu_{\mathbf{i}} (b/a) \end{aligned} \quad (\text{C.4.12})$$

We discuss the second case in Section C.5

Reader Exercise: Do the numerical integration outlined above to determine function $\mathcal{L}(b)$ for several b values and plot for $b = 1$ to 10. Is $\mathcal{L}(1) = 0.96639$? Holloway and Kuester have a plot in their Fig 2 which looks like this for $L_{\mathbf{i}}$ [$L_{\mathbf{i}}$ for a circular wire is 50 nH as shown in (C.3.10)],

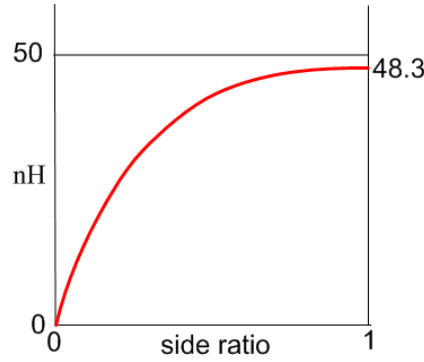


Fig C.5

Comment: Appendix B.3 provides three 2D methods of computing \mathbf{H} from \mathbf{J} . We chose to use the formula (B.2.12). Holloway and Kuester use the method of first computing \mathbf{A} then $\mathbf{B} = \text{curl } \mathbf{A}$. A third method is to use the 2D Biot-Savart Law (B.2.24). That third method begins this way :

$$\mathbf{H}(x,y) = \int d^2\mathbf{x}' \frac{1}{2\pi R^2} \mathbf{J}(\mathbf{x}') \times \mathbf{R} \quad \mathbf{R} \equiv \mathbf{x} - \mathbf{x}' \quad (\text{B.2.24})$$

and

$$\mathbf{J}_z(x) = (I/4ab)\theta(-a \leq x \leq a) \theta(-b \leq y \leq b)$$

so

$$\mathbf{H}(x,y) = \int_{-a}^a dx' \int_{-b}^b dy' \frac{1}{2\pi R^2} (I/4ab) \hat{\mathbf{z}} \times \mathbf{R} \quad .$$

But

$$\mathbf{R} = (x-x')\hat{\mathbf{x}} + (y-y')\hat{\mathbf{y}} \quad \Rightarrow \quad \hat{\mathbf{z}} \times \mathbf{R} = (x-x')\hat{\mathbf{y}} - (y-y')\hat{\mathbf{x}} \quad .$$

Thus,

$$H_x(x,y) = \int_{-a}^a dx' \int_{-b}^b dy' \frac{1}{2\pi R^2} (I/4ab) [-(y-y')]$$

$$H_y(x,y) = \int_{-a}^a dx' \int_{-b}^b dy' \frac{1}{2\pi R^2} (I/4ab) [(x-x')]$$

or

$$H_x(x,y) = (I/8\pi ab) \int_{-a}^a dx' \int_{-b}^b dy' (y'-y)/R^2$$

$$H_y(x,y) = -(I/8\pi ab) \int_{-a}^a dx' \int_{-b}^b dy' (x'-x)/R^2 \quad (\text{C.4.13})$$

These last integrals are the same as (7) and (8) of Holloway and Kuester with $2a = w$ and $2b = t$.

C.5 The DC internal inductance of a thin flat wire

This is a fascinating problem with a result that is non-obvious.

Consider an infinitely long conductor whose cross section has the shape of a *thin* strip of width w and height t with $t \ll w$,

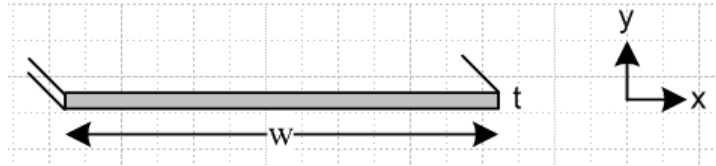


Fig C.6

The correct result for L_i was given earlier in (C.4.12) and we repeat it here, setting $w = 2a$ and $t = 2b$,

$$L_i = (\mu_i/8\pi) [(4\pi/3) t/w] = (1/6) \mu_i (t/w) \quad t \ll w \quad . \quad (C.4.12)$$

We shall now attempt to obtain this result in a simple manner, intentionally misleading the reader a bit.

The uniform current density is $J_z = I/(wt)$, flowing toward the viewer. Here is a blowup of a piece of the strip near its center,

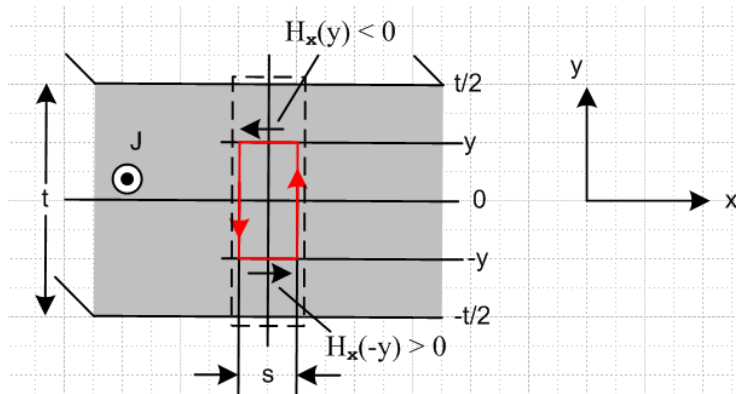


Fig C.7

The red math loop is positioned as shown for an application of Ampere's Law,

$$\int_s \mathbf{J} \cdot d\mathbf{S} = \oint_c \mathbf{H} \cdot d\mathbf{s} \quad . \quad (1.1.37)$$

Starting at the lower left corner of the red loop for \oint_c , this says

$$J_z 2y s = s H_x(-y) + 0 2y - H_x(y)s - 0 2y \quad . \quad (C.5.1)$$

We assume that "near the center of the strip" there is no significant transverse field component H_y , though we accept that such transverse fields do exist far away "near the edges" of the strip as in Fig C.2,

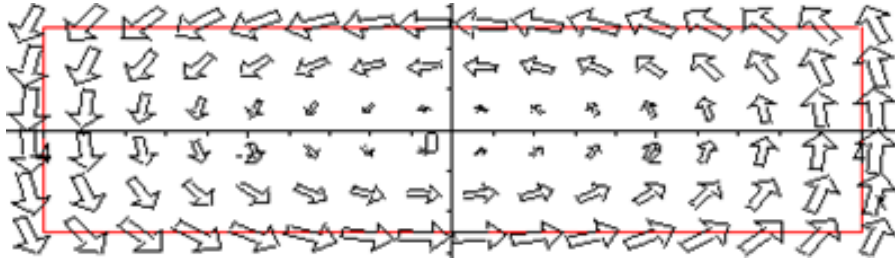


Fig C.8

Thus, the two vertical sections of the red loop make negligible contribution to the line integral in the main central region. Symmetry indicates that H_x on the upper red loop segment is equal and opposite to that on the lower segment, so the line integral is then $-2H_x(y)s$ and we continue :

$$J_z 2y s = -2 H_x(y)s$$

$$J_z y = - H_x(y)s$$

$$I/(wt)*y = - H_x(y)s$$

$$H_x(y)/I = - y/(wt) \quad . \quad (C.5.2)$$

The result is that $H_x(y) = -(I/wt)y$ which is a very reasonable linear function of y , with $H_x(y=0) = 0$. The fact that $H_x(y)$ does not depend on x is also reasonable since, when $w \gg t$, the central region of the strip is basically all of the strip excluding the tiny end regions which we ignore. A similar argument is made for the analysis of a parallel plate capacitor, where the end effects are ignored if $w \gg t$.

To get the internal inductance due to this H_x energy storage, we compute its contribution from the dotted rectangle in Fig C.6, then multiply by (w/s) to get L_i for the entire strip. So, using (C.3.7),

$$\begin{aligned} L_i &= (w/s) \mu \int_{\text{dotted}} dS (H/I)^2 = (w/s) \mu \int_{\text{dotted}} (sdy) [-y/(wt)]^2 \\ &= (w/s) \mu s (wt)^{-2} \int_{-t/2}^{t/2} dy y^2 = (w/s) \mu s (wt)^{-2} 2 \int_0^{t/2} dy y^2 \\ &= (w/s) \mu s (wd)^{-2} 2 (1/3) (t/2)^3 = w^{-1} \mu t^{-2} (2/3) t^3/8 \\ &= (1/12) \mu (t/w) = (\mu_i/8\pi) [2\pi/3 (t/w)] \quad // \text{ strip } w \gg t, \text{ due to } H_x \end{aligned} \quad (C.5.3)$$

But this is only half the correct result for L_i which was just quoted above. By luck, (C.5.3) happens to be the correct result for the H_x contribution to L_i ; by luck because it is derived from Fig C.7 with the assumption that $H_y \equiv 0$ which is not true. The other half of L_i in fact comes from the H_y field in the strip.

One can write

$$L_i = \mu \int_{-t/2}^{t/2} dy \int_{-w/2}^{w/2} dx [(H_x/I)^2 + (H_y/I)^2] = L_{ix} + L_{iy} \tag{C.5.4}$$

so the H_x and H_y contributions are simply additive with no interference.

So where did the argument above go wrong? It all seemed so reasonable. One is of course biased by the appearance of the fields in Fig C.8 shown just above. One's impression is that as the aspect ratio is increased from 4:1 to perhaps 100:1, the nature of the above plot should become even more convincing: large horizontal arrows to the left along the top of the strip, large horizontal arrows to the right along the bottom of the strip, and some minor edge effects at the distant ends.

But this is in fact not a correct impression! For a 10:1 aspect ratio strip, here is the field map (H_x, H_y) for the upper right quadrant of the strip

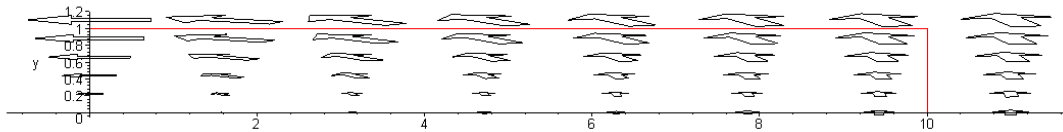


Fig C.9

If we plot only the H_x component by setting $H_y = 0$ in our field plot, we get

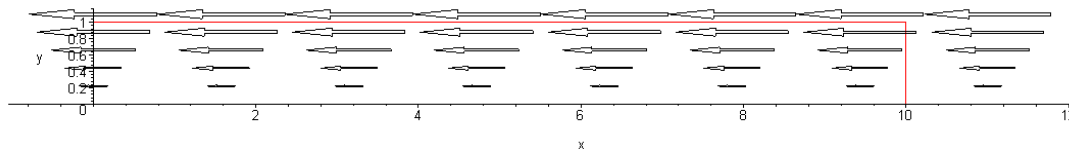


Fig C.10

and this displays our conjectured functional shape $H_x(y) = -(I/wt)y$ applying not just at the center of the strip, but all along the strip. This then explains graphically why our calculation above came up with the correct result for the H_x contribution to L_i . The other half of L_i comes from the transverse field component H_y which has this appearance (we now set $H_x = 0$ in the field plot)

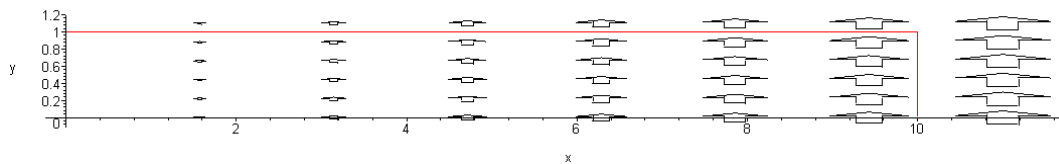


Fig C.11

The fact that the H_y contribution to L_i is exactly equal to the H_x contribution is just not obvious. One would think some simple argument could be concocted to explain this fact (perhaps an "equipartition theorem"). For example, one might conjecture looking at the above plot that $H_y \approx H_y(x)$ so that Ampere's law for the Fig C.7 red loop says, using $s = dx$,

$$J_z 2y \, dx = dx H_x(-y) + H_y(x+dx) 2y - H_x(y)dx - H_y(x)2y .$$

$$J_z 2y = -2 H_x(y) + [H_y(x+dx) - H_y(x)]/dx * 2y .$$

$$J_z y = - H_x(y) + y \partial_x H_y(x) . \tag{C.5.5}$$

We might then try $H_x(y) = -A(I/wt)y$ based on Fig C.10 with A some constant. Then (C.5.5) says

$$(I/wt) (1-A) = \partial_x H_y(x) \quad \Rightarrow \quad H_y(x) = [(I/wt) (1-A)] x \equiv Bx \tag{C.5.6}$$

which seems reasonable in terms Figure C.11. But $H_y(x) = Bx$ is problematical in two respects: (1) there is no obvious way to determine B without taking a limit of the complicated full H_y formula ; (2) Even when that is done, $H_y(x)$ is in fact not linear in x as a simple plot shows, so the model is inaccurate and does not give the result that L_i due to H_y is $(1/12) \mu (t/w)$.

The field plots shown above and the $|\mathbf{H}|^2$ energy plots of Fig C.3 are easy to produce from Maple. These latter plots are like topographical maps and they can be displayed in that manner as shown on the right below,

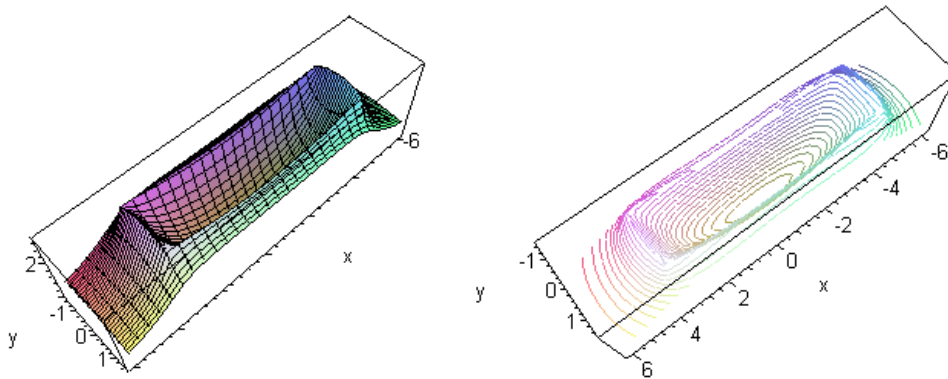


Fig C.12

where we have reverted to the 4:1 aspect ratio strip.

One should not confuse the $|\mathbf{H}|^2$ topo contour lines shown here with a plot of the H *field lines*. Making a field line plot is not a built-in function for our vintage Maple V and requires some minor coding to implement. Here is such a field line plot for a 20:1 aspect ratio thin strip (method given in Appendix O),

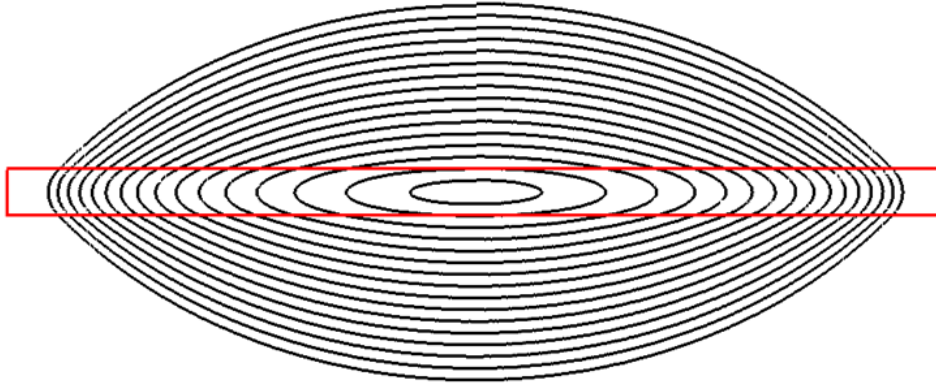


Fig C.13

Each contour starts at $x = 0$ and $y = \text{some value}$ and is iterated CCW (chasing the direction of the \mathbf{H} vector) until it arrives back where it started. The little jogs at the top represent the small error of this numerical process. Looking at this field line plot, it is totally obvious that there does not exist some "broad central region" in the strip where the field lines are mostly horizontal. The transverse field components (vertical) appear as soon as one leaves the exact center of the strip and it is totally wrong to ignore such transverse H_y components in the computation of L_i .

The correct calculation of L_i is done in the 2009 paper of Holloway and Kuester. They point out errors made by earlier authors and make the point that half the internal inductance comes from each field component. They do not claim that the transverse contribution is *exactly* half the result, but that it is half to a high degree of precision. In an email communication, Prof. Kuester made the appropriate point that, since $\text{div } \mathbf{H} = 0$ (there is no magnetic charge), the \mathbf{H} field lines must close on themselves and that is what forces the above figure to have the shape it has, where there is no "broad central region" having essentially horizontal field lines. In the corresponding parallel plate capacitor picture for electrostatics, since electric charge *does* exist, the \mathbf{E} fields lines do not need to close on themselves, and have sources and sinks all along the capacitor cross section, allowing for a uniform broad central region.

Here is one more field line plot showing a larger range of field lines,

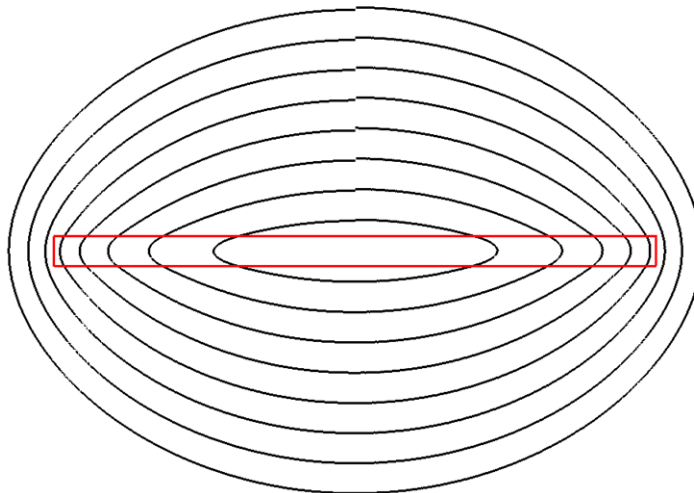


Fig C.14

As the field lines are continued outward, they eventually become circles as the strip eventually becomes a line source (a point source in cross section) when viewed from far away.

Reader Exercise: Come up with a simple explanation for why the H_x and H_y fields each contribute half the total L_i value for the thin strip. Is this perhaps true for any edge ratio of the rectangular cross section? That certainly seems unlikely.

C.6 The DC internal inductance of a hollow round wire

The pipe geometry is as follows, where we assume J_z is uniform and total current is I :

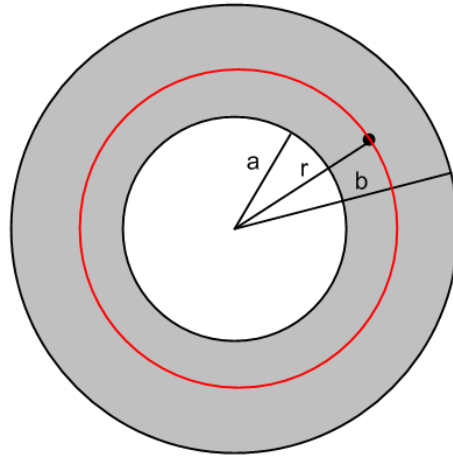


Fig C.15

As with the round wire case, we can avoid using (C.4.1) (or alternates) to compute H due to symmetry. The total current enclosed within the red circle is this,

$$I_{\text{enc}}(r) = \frac{\text{area inner annulus } a \text{ to } r}{\text{area full annulus } a \text{ to } b} = \frac{r^2 - a^2}{b^2 - a^2} I \quad \text{valid for } a \leq r \leq b \quad . \quad (\text{C.6.1})$$

For $r < a$, $I_{\text{enc}}(r) = 0$, and for $r > b$, $I_{\text{enc}}(r) = I$. Ampere's Law says

$$2\pi r H_{\theta}(r) = I_{\text{enc}}(r) \quad . \quad (\text{C.6.2})$$

Note that $H_{\theta}(r) = 0$ inside the tube, so this region makes no contribution to L_e or L_i . Inside the annulus,

$$H_{\theta}(r) = I_{\text{enc}}(r) / (2\pi r) = \frac{1}{2\pi} \frac{1}{r} \frac{r^2 - a^2}{b^2 - a^2} I \quad . \quad a \leq r \leq b \quad (\text{C.6.3})$$

Recalling that

$$L_i = \mu_i \int_{\text{in}} dS (H/I)^2 \quad (\text{C.3.7})$$

we conclude that

$$L_i = \mu_i \frac{1}{(2\pi)^2} \frac{1}{(b^2 - a^2)^2} \int_{in} dS \frac{1}{r^2} (r^2 - a^2)^2$$

and then using $dS = 2\pi r dr$ we find

$$\begin{aligned} L_i &= \mu_i \frac{1}{2\pi} \frac{1}{(b^2 - a^2)^2} \int_a^b dr \frac{1}{r} (r^2 - a^2)^2 \\ &= \mu_i \frac{1}{2\pi} \frac{1}{(b^2 - a^2)^2} J . \end{aligned} \tag{C.6.4}$$

Maple computes the integral J as follows

J := Int((r^2 - a^2)^2 / r, r = a..b);

$$J := \int_a^b \frac{(r^2 - a^2)^2}{r} dr$$

J := int((r^2 - a^2)^2 / r, r = a..b);

$$J := \frac{1}{4} b^4 - b^2 a^2 + a^4 \ln(b) + \frac{3}{4} a^4 - a^4 \ln(a)$$

which we restate as

$$J = (1/4)b^4 + (3/4)a^4 - a^2b^2 + a^4 \ln(b/a) \tag{C.6.5}$$

and then the final result for the internal inductance of a hollow pipe with $b > a$ is

$$L_i = \mu_i \frac{1}{2\pi} \frac{1}{(b^2 - a^2)^2} [(1/4)b^4 + (3/4)a^4 - a^2b^2 + a^4 \ln(b/a)] . \tag{C.6.6}$$

(a) limit as $a \rightarrow 0$: should be round wire of radius b

Reading off this limit from (C.6.6),

$$\begin{aligned} L_i &= \mu_i \frac{1}{2\pi} \frac{1}{(b^2 - a^2)^2} [(1/4)b^4 + (3/4)a^4 - a^2b^2 + a^4 \ln(b/a)] \\ &= \mu_i \frac{1}{2\pi} \frac{1}{b^4} [(1/4)b^4 + 0 - 0 + 0 \ln(b/a)] \\ &= \mu_i \frac{1}{8\pi} \end{aligned} \tag{C.6.7}$$

and we recover the L_i of a round wire as found in (C.3.10).

(b) External Verification of (C.6.6)

The result appears in a very fat (2,263 pages) 1922 handbook edited by Pender and Del Mar, from which we quote via Google books, page 827 (thank you anonymous scanner person),

External and Internal Self Inductance of a Round Wire. — The inductance of a round wire may be considered as made up of two parts, the inductance due to the flux *external* to the wire and that due to the flux *within* the wire. The first or “external” inductance is

$$L_e = 2l \left[\log_e \frac{2l}{r} - 1 \right], \quad (13)$$

the “internal” self inductance is

$$L_i = l \frac{\mu}{2}. \quad (13a)$$

Inductance of a Hollow Tube of Circular Section, Return Neglected. — The *external* inductance is the same as for a solid wire, i.e., equation (13), taking for r the external radius of the tube. The *internal* inductance of the tube, putting r_2 = external radius and r_1 = internal radius, is

$$L_i = 2 \mu l \left[\frac{r_1^4}{(r_2^2 - r_1^2)^2} \log_e \frac{r_2}{r_1} - \frac{1}{4} \frac{3 r_1^2 - r_2^2}{r_2^2 - r_1^2} \right]. \quad (14)$$

In their version which uses cgs units, the round wire has $L_i = (\mu/2)$ per unit length according to their (13a), so one must add $(1/4\pi)$ to their (14) result to compare with (C.6.6). Using $r_2 = b$ and $r_1 = a$ the results then agree after some algebra.

(c) limit as $b-a \rightarrow 0$: thin shell radius a and thickness d

In this limit, the hollow pipe is a thin cylindrical shell of inner radius a and thickness d . Continuing the Maple code, we first replace parameter b by $a+d$,

```
x := mu*(1/(2*Pi*(b^2-a^2)^2));
```

$$x := \frac{1}{2} \frac{\mu}{\pi (b^2 - a^2)^2}$$

```
LI := x*J;
```

$$LI := \frac{1}{2} \frac{\mu \left(\frac{1}{4} b^4 - b^2 a^2 + a^4 \ln(b) + \frac{3}{4} a^4 - a^4 \ln(a) \right)}{\pi (b^2 - a^2)^2}$$

```
b := a+d;
```

$$b := a + d$$

```
LI;
```

$$\frac{1}{2} \frac{\mu \left(\frac{1}{4} (a+d)^4 - (a+d)^2 a^2 + a^4 \ln(a+d) + \frac{3}{4} a^4 - a^4 \ln(a) \right)}{\pi ((a+d)^2 - a^2)^2}$$

Maple then expands this L_i function about $d = 0$,

```
series(LI, d=0, 4);
```

$$\frac{1}{6} \frac{\mu}{\pi a} d - \frac{1}{6} \frac{\mu}{\pi a^2} d^2 + \frac{3}{20} \frac{\mu}{\pi a^3} d^3 + O(d^4)$$

Of course our only interest is in the first term, so in this limit we have found that

$$L_i = \mu_i \frac{1}{6\pi} (d/a) = \frac{\mu_i}{8\pi} [(4/3)(d/a)] \quad \text{thin shell, valid for } d \ll a \quad (\text{C.6.8})$$

where again $(\mu_i/8\pi)$ is L_i for a round conductor of any radius.

(d) Maple Plot

Write (C.6.6) as

$$\begin{aligned}
 L_i &= \frac{\mu_i}{8\pi} \left\{ \frac{1}{(b^2-a^2)^2} [b^4 + 3a^4 - 4a^2b^2 + 4a^4 \ln(b/a)] \right\} & (C.6.6) \\
 &= \frac{\mu_i}{8\pi} \left\{ \frac{1}{(1-x^2)^2} [1 + 3x^4 - 4x^2 - 4x^4 \ln(x)] \right\} & x \equiv a/b \\
 &= \frac{\mu_i}{8\pi} f(x) .
 \end{aligned}$$

Maple then plots $f(x)$:

```

f := (1-x^2)^(-2)*(1 + 3*x^4-4*x^2 - 4*x^4*ln(x));
f := 
$$\frac{1 + 3x^4 - 4x^2 - 4x^4 \ln(x)}{(1-x^2)^2}$$

plot(f, x = 0..1, thickness=2);

```

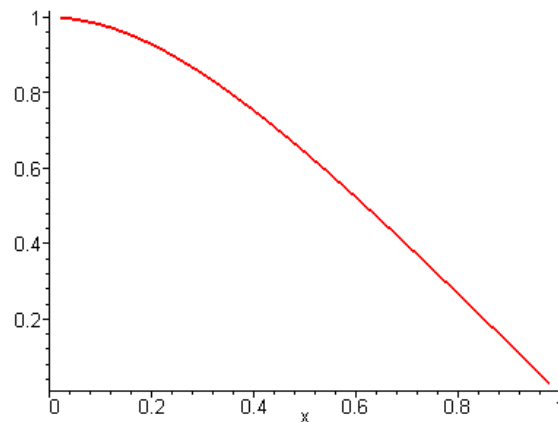


Fig C.16

As the pipe is hollowed out from a round wire to a foil shell, $f(x)$ drops from 1 to 0 as shown.

Appendix D: The General E and B Fields Inside an Infinite Straight Round Wire

This Appendix presents a rather lengthy calculation of the fields and currents inside a round wire *without* the Chapter 2 assumption that such fields and currents are symmetrical about the axis. This wire is regarded as one conductor of an infinite transmission line down which a wave is propagating.

Since this Appendix is quite long, a brief summary is in order (see also Table of Contents) :

Section D.1

(a) A longitudinal traveling wave form $\mathbf{E}(r,\theta,z,t) = e^{j(\omega t - kz)} \mathbf{E}(r,\theta)$ is assumed inside the round wire and $\mathbf{E}(r,\theta,z,t)$ is then shown to satisfy a certain vector Helmholtz equation.

(b) The field $\mathbf{E}(r,\theta)$ and the surface charge $n(\theta)$ are both expanded onto "azimuthal partial waves" $e^{jm\theta}$ with coefficients $\mathbf{E}(r,m)$ and N_m .

(c) The Helmholtz equation's vector Laplacian $\star \equiv \nabla^2$ is stated in cylindrical coordinates.

(d) The three Helmholtz component equations and $\text{div } \mathbf{E} = 0$ are written out in these coordinates.

Section D.2

(a),(b),(c): The z and r Helmholtz equations and the $\text{div } \mathbf{E} = 0$ equation are solved for E_z , then E_r , and then E_θ . These solutions are expressed in terms of Bessel J functions of a complex argument and two unknown constants a_m and K_m for each partial wave.

(d) a boundary condition relating E_r to surface charge density $n(\theta)$ is derived (see D.9 below)

(e) this and another boundary condition $E_\theta(a,m) = 0$ (see D.8 below) are used to evaluate a_m and K_m and then the solution \mathbf{E} field components are stated in box (D.2.33).

Section D.3

It is noted that the boxed \mathbf{E} field solutions also satisfy the ignored third θ Helmholtz equation.

Section D.4

The \mathbf{B} fields are computed from the \mathbf{E} fields using Maxwell $-j\omega\mathbf{B} = \text{curl } \mathbf{E}$, and then box (D.4.13) summarizes both the \mathbf{E} and \mathbf{B} partial wave fields inside a round wire.

Section D.5 These \mathbf{E} and \mathbf{B} fields are shown to exactly solve the other three Maxwell equations.

Section D.6 The $m = 0$ partial wave results are stated and compared to the results of Chapter 2.

Section D.7 The problem of finding an exterior field solution for the round wire is discussed.

Section D.8 Arguments supporting the second boundary condition $E_\theta(a,m) = 0$ are presented.

Section D.9 The "charge pumping boundary condition" is discussed in relation to surface currents.

Section D.10 High frequency limits of the round wire E fields are presented.

Section D.11 Low frequency limits of the round wire E fields are presented, along with comments on accuracy, the meaning of symbol k , and the e^{-jkz} ansatz made in Section D.1.

D.1 Partial Wave Expansion

Warning: In this appendix, we use the same function name \mathbf{E} to represent three *different* functions,

$$\mathbf{E}(r,\theta,z,t) \quad \mathbf{E}(r,\theta) \quad \mathbf{E}(r,m)$$

The functions are distinguished by the arguments shown, and if they are not shown, the general context of the discussion will indicate which function is implied. The symbol \mathbf{E} is thus "overloaded".

(a) The General Method

The starting point for the calculation is the damped wave equation (1.3.36, region 2) for the \mathbf{E} field inside the wire. Unsubscripted parameters refer to properties of the wire.

$$(\nabla^2 - \mu\epsilon \partial_t^2 - \mu\sigma\partial_t)\mathbf{E}(r,\theta,z,t) = 0. \quad (1.3.36)$$

Cylindrical coordinates (r,θ,z) are used, as appropriate for an infinite straight round wire. Recall that the damping term arises when the driving current \mathbf{J} on the right of (1.2.1) is replaced by Ohm's Law $\mathbf{J} = \sigma\mathbf{E}$.

We now make the ansatz that a solution to the above wave equation may be expressed in the following form where the t and z dependence is exposed and where $\mathbf{E}(r,\theta)$ is a complex function to be determined:

$$\mathbf{E}(r,\theta,z,t) = e^{j(\omega t - kz)} \mathbf{E}(r,\theta). \quad (D.1.1)$$

The idea here is that we take our round wire to be one of two conductors of a transmission line (the other wire may or may not have a round cross section). The form shown in (D.1.1) says that the \mathbf{E} field inside our round wire is assumed (an Ansatz!) to be a simple "traveling wave" moving down this transmission line in the $+z$ direction. As this interior wave moves down the line, we expect to have an exterior wave whose \mathbf{E} field takes the same general form shown in (D.1.1). If we match the \mathbf{E} and \mathbf{B} field boundary conditions of the interior and exterior waves, we expect k to have the same value on both sides of the round wire boundary.

About k

For a lossless wave, we expect the conductors to simply deform the exterior fields (for example, causing the \mathbf{E} field to be perpendicular to the conductor surfaces), but we expect the exterior wave to travel at the speed of light v_d in the dielectric, with no "drag" from the conductors. In this lossless case, we then expect to have $k = \omega \sqrt{\mu_d \epsilon_d} = \omega/v_d \equiv \beta_{d0}$ in (1.5.1b). If the dielectric conducts but the conductors are perfect, we have instead $k = \omega \sqrt{\mu_d \tilde{\epsilon}_d} \equiv \beta_d$ in (1.5.1a), and then k has a negative imaginary part which causes decay along the line, but k is still a characteristic of the dielectric medium.

However, if the conductors are not perfect, then they too contribute to the decay, and in this case we expect that our parameter k will no longer be a characteristic just of the dielectric. For example, we expect it will depend on R , the resistance per unit length of the conductors.

We shall continue to use the generic parameter k throughout this appendix, to make sure our theory can handle situations with loss. One should think of k as a general complex parameter which (hopefully) has a negative imaginary part and whose real part is the wave phase velocity. Only in the special case of a completely lossless line do we have $k = \omega/v_a = \beta_{a0}$.

In the strong and extreme skin effect regimes, Chapter 4 develops a *formula* for the parameter k based on Maxwell's equations. This formula states that $k = -j \sqrt{(R+j\omega L)(G+j\omega C)}$. This same formula arises in the network model of Appendix K, but in *that* model the formula applies all the way down to $\omega = 0$. Probably this extrapolation of the Maxwell-derived k expression down to low frequencies is reasonable though not exact. Having remarked on these two models for k , we shall ignore them until we reach Appendix D.11, so we continue to work with our generic parameter k .

When (D.1.1) is put into the above wave equation (1.3.36), time derivatives can be replaced $\partial_t \rightarrow j\omega$ with the result

$$(\nabla^2 + \beta^2) \mathbf{E}(r, \theta, z, t) = 0 \quad (D.1.2a)$$

or

$$[\nabla_{2D}^2 + (\beta^2 - k^2)] \mathbf{E}(r, \theta) = 0 \quad \nabla^2 = \nabla_{2D}^2 + \partial_z^2 \quad (D.1.2b)$$

where

$$\beta^2 = \mu \epsilon \omega^2 - j\omega \mu \sigma = \omega^2 \mu (\epsilon - j\sigma/\omega) = \omega^2 \mu \xi \quad \xi \equiv \epsilon - j\sigma/\omega \quad (1.5.1c)$$

We could have defined the temporal Fourier Transform of $\mathbf{E}(r, \theta, z, t)$,

$$\mathbf{E}^\wedge(r, \theta, z, \omega') \equiv \text{FT} \{ \mathbf{E}(r, \theta, z, t), \omega' \} = e^{-j\mathbf{kz}} \mathbf{E}(r, \theta) 2\pi \delta(\omega - \omega') = e^{-j\omega t} \mathbf{E}(r, \theta, z, t) 2\pi \delta(\omega - \omega')$$

as in (1.6.11) and then (D.1.2a) would be valid as well for $\mathbf{E}^\wedge(r, \theta, z, \omega)$ which would be a more conventional Helmholtz equation, but since $\mathbf{E}(r, \theta, z, t)$ is monochromatic, we leave (D.1.2a) as is.

One can regard (D.1.1) as an assumed variable-separated form for a solution, an "ansatz". If a consistent solution to the Maxwell equations can be found with this assumption, it is justified *de facto*.

Sign Convention Comment: Section 1.6 discusses the Fourier Transform (1.6.8) where $e^{+j\omega t}$ appears in the expansion formula. For $\mathbf{E}^\wedge(\mathbf{x}, \omega) = 2\pi \delta(\omega - \omega_1)$ one gets $\mathbf{E}(\mathbf{x}, t) = e^{+j\omega_1 t}$ and then the form of a wave solution is $e^{+j(\omega t - \mathbf{kz})}$ with the + sign associated with ωt . In general, EE people like to assume time dependence of the form $e^{+j\omega t}$ (and they prefer j in place of i for $\sqrt{-1}$). The Fourier Transform is of course valid with the other sign choice for the two exponentials, and for that other sign choice one would have $\mathbf{E}^\wedge(\mathbf{x}, \omega) = 2\pi \delta(\omega - \omega_1) \Rightarrow \mathbf{E}(\mathbf{x}, t) = e^{-j\omega_1 t}$ and one would think of a wave as $e^{-j(\omega t - \mathbf{kz})} = e^{+j(\mathbf{kz} - \omega t)$.

This sign convention is common in many physics texts [e.g. Jackson (7.8)], but in this document we use the $e^{+j(\omega t - \mathbf{kz})}$ convention usually used in EE texts [e.g. Haus-Melcher 13.1 (7)]. Jackson suggests a physics/EE conversion algorithm of $i \leftrightarrow -j$. It is all just a convention choice and, as in (1.6.6), only the sign of the imaginary physical field under consideration is affected. If one thinks of the physical field under consideration as $\text{Re}\{\mathbf{E}(\mathbf{x}, t)\}$, the sign convention choice makes no difference at all.

(b) Partial Wave Expansions

The next step is to do a "partial wave expansion" (that is, a complex Fourier series expansion) of $\mathbf{E}(r,\theta)$ in terms of "azimuthal harmonics" $e^{jm\theta}$, so that the variable θ is replaced with the partial wave index m :

$$\mathbf{E}(r,\theta) = \sum_{m=-\infty}^{\infty} \mathbf{E}(r,m) e^{jm\theta} \quad // \text{ expansion} \quad (\text{D.1.3a})$$

$$\mathbf{E}(r,m) = (1/2\pi) \int_{-\pi}^{\pi} d\theta \mathbf{E}(r,\theta) e^{-jm\theta} \quad // \text{ projection} \quad (\text{D.1.3b})$$

Note that $\dim[\mathbf{E}(r,m)] = \dim[\mathbf{E}(r,\theta)] = \text{volts/m}$. In analogy with (D.1.1) we define a surface charge density $n(\theta,z,t)$ which has the following ansatz variable-separated form,

$$n(\theta,z,t) = e^{j(\omega t - kz)} n(\theta) \quad (\text{D.1.4})$$

We then expand $n(\theta)$ as in (D.1.3),

$$n(\theta) = \sum_{m=-\infty}^{\infty} N_m e^{jm\theta} \quad // \dim[n(\theta)] = \text{Coul/m}^2 \quad (\text{D.1.5a})$$

$$N_m = (1/2\pi) \int_{-\pi}^{\pi} d\theta n(\theta) e^{-jm\theta} \quad // \dim[N_m] = \text{Coul/m}^2 \quad (\text{D.1.5b})$$

N_m is the "moment" of the surface charge distribution in the m^{th} partial wave. As with $\mathbf{E}(r,\theta)$, the function $n(\theta)$ is also a function of implicit arguments ω and k .

In principle, $n(\theta)$ could have a phase which varies with θ . If we momentarily assume this is not the case and assume that $n(\theta)$ is real, then (D.1.5b) says $N_{-m} = N_m^*$ and then

$$\begin{aligned} n(\theta) &= \sum_{m=-\infty}^{\infty} N_m e^{jm\theta} = N_0 + \sum_{m=1}^{\infty} [N_m e^{jm\theta} + N_m^* e^{-jm\theta}] = N_0 + 2 \sum_{m=1}^{\infty} \text{Re}\{N_m e^{jm\theta}\} \\ &= N_0 + 2 \sum_{m=1}^{\infty} \{ \text{Re}(N_m) \cos(m\theta) - \text{Im}(N_m) \sin(m\theta) \} \end{aligned} \quad (\text{D.1.6})$$

If we furthermore assume that $n(\theta)$ is an even function of θ , as symmetry implies for our particular figure below, then (D.1.5b) says the N_m are real and then we have

$$n(\theta) = N_0 + 2 \sum_{m=1}^{\infty} N_m \cos(m\theta) \quad // n(\theta) \text{ real and even in } \theta \quad (\text{D.1.7})$$

For a moderately closely spaced twin lead transmission line (we allow for different radii), one might expect the $m=0$ and $m=1$ partial waves to be dominant : [the moments appears in (6.5.4)]

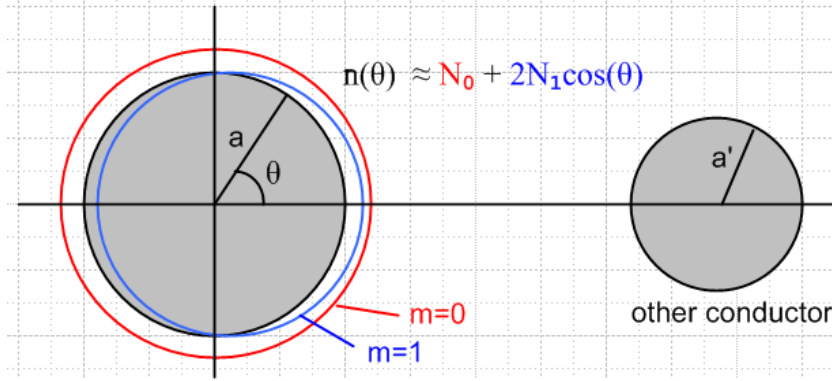


Fig D.1

Notice that

$$N_0 = (1/2\pi) \int_{-\pi}^{\pi} d\theta n(\theta) = (1/2\pi) (1/a)(1/dz) \int_{-\pi}^{\pi} [ad\theta dz] n(\theta) = (1/2\pi) (1/a)(1/dz) Q$$

where Q is the total charge on a thin ribbon of width dz wrapping the round wire. In (4.3.8) we refer to the quantity Q/dz as $q(0)$, where $q(z) = q(0) e^{jkz}$ is the total charge on the wire per unit length. Thus,

$$N_0 = (1/2\pi a) q(0) = \langle n(\theta) \rangle \quad // \quad q(0) = CV \quad (D.1.8)$$

(c) The Vector Laplacian in Cylindrical Coordinates

Given the following cylindrical-coordinates field components,

$$\mathbf{E}(r, \theta, z, t) = E_r(r, \theta, z, t) \hat{\mathbf{r}} + E_\theta(r, \theta, z, t) \hat{\boldsymbol{\theta}} + E_z(r, \theta, z, t) \hat{\mathbf{z}}$$

we may write out our ansatz wave form (D.1.1) and the Helmholtz equation (D.1.2a) in more detail,

$$\begin{aligned}
 E_r(r, \theta, z, t) &= e^{j(\omega t - kz)} E_r(r, \theta) & [\nabla^2 \mathbf{E}(r, \theta, z, t)]_r + \beta^2 E_r(r, \theta, z, t) &= 0 \\
 E_\theta(r, \theta, z, t) &= e^{j(\omega t - kz)} E_\theta(r, \theta) & [\nabla^2 \mathbf{E}(r, \theta, z, t)]_\theta + \beta^2 E_\theta(r, \theta, z, t) &= 0 \\
 E_z(r, \theta, z, t) &= e^{j(\omega t - kz)} E_z(r, \theta) & [\nabla^2 \mathbf{E}(r, \theta, z, t)]_z + \beta^2 E_z(r, \theta, z, t) &= 0
 \end{aligned} \quad (D.1.9)$$

where β^2 is the Helmholtz parameter of the conductor medium, not to be confused with k .

In Cartesian coordinates, it happens that $[\nabla^2 \mathbf{E}]_i = \nabla^2 (E_i)$, but this is not generally true for curvilinear coordinates. In cylindrical coordinates, it is true for the z coordinate only. The operator ∇^2 when applied to a vector field is called "the vector Laplacian" and it is very different from the scalar Laplacian, so much so that some authors (Moon and Spencer) replace $[\nabla^2 \mathbf{E}]$ by $[\star \mathbf{E}]$ which is defined in this manner

$$[\star \mathbf{E}] \equiv [\nabla^2 \mathbf{E}] \equiv \text{grad}(\text{div } \mathbf{E}) - \text{curl}(\text{curl } \mathbf{E}) = \nabla(\nabla \bullet \mathbf{E}) - \nabla \times (\nabla \times \mathbf{E}) \quad (D.1.10)$$

whereas

$$\nabla^2 \phi \equiv \text{div}(\text{grad } \phi) = \nabla \bullet (\nabla \phi) \quad (D.1.11)$$

It is the *vector* Laplacian that appears in our Helmholtz equation (D.1.2). For cylindrical coordinates it turns out that,

$$\begin{aligned}(\nabla^2 \mathbf{E})_{\mathbf{r}} &= \nabla^2 E_{\mathbf{r}} - (2/r^2) \partial_{\theta} E_{\theta} - (1/r^2) E_{\mathbf{r}} \\(\nabla^2 \mathbf{E})_{\theta} &= \nabla^2 E_{\theta} + (2/r^2) \partial_{\theta} E_{\mathbf{r}} - (1/r^2) E_{\theta} \\(\nabla^2 \mathbf{E})_{\mathbf{z}} &= \nabla^2 E_{\mathbf{z}}\end{aligned}\tag{D.1.12}$$

where ∇^2 is the scalar Laplacian, given in cylindrical coordinates by

$$\nabla^2 = (1/r)\partial_{\mathbf{r}}(r\partial_{\mathbf{r}}) + (1/r^2)\partial_{\theta}^2 + \partial_{\mathbf{z}}^2 = \partial_{\mathbf{r}}^2 + (1/r)\partial_{\mathbf{r}} + (1/r^2)\partial_{\theta}^2 + \partial_{\mathbf{z}}^2.\tag{D.1.13}$$

Notice in (D.1.12) that E_{θ} is mixed into the "r equation" and $E_{\mathbf{r}}$ is mixed into the " θ equation".

See for example Morse and Feshbach Vol I p 116, Moon and Spencer p 139, or do a web search on "vector Laplacian". The author's *Tensor Analysis* document, Sections 13, 14 and 15, derives these results for arbitrary coordinate systems. Here is a summary of vector differential operators in cylindrical coordinates taken from Morse and Feshbach, where the last line corresponds to the above discussion:

$$\begin{aligned}\text{grad } \psi &= \mathbf{a}_r \frac{\partial \psi}{\partial r} + \mathbf{a}_{\phi} \frac{1}{r} \frac{\partial \psi}{\partial \phi} + \mathbf{a}_z \frac{\partial \psi}{\partial z} \\ \text{div } \mathbf{A} &= \frac{1}{r} \frac{\partial}{\partial r} (rA_r) + \frac{1}{r} \frac{\partial A_{\phi}}{\partial \phi} + \frac{\partial A_z}{\partial z} \\ \text{curl } \mathbf{A} &= \mathbf{a}_r \left(\frac{1}{r} \frac{\partial A_z}{\partial \phi} - \frac{\partial A_{\phi}}{\partial z} \right) + \mathbf{a}_{\phi} \left(\frac{\partial A_r}{\partial z} - \frac{\partial A_z}{\partial r} \right) + \mathbf{a}_z \left(\frac{1}{r} \frac{\partial}{\partial r} rA_{\phi} - \frac{1}{r} \frac{\partial A_r}{\partial \phi} \right) \\ \nabla^2 \psi &= \frac{1}{r} \frac{\partial}{\partial r} \left(r \frac{\partial \psi}{\partial r} \right) + \frac{1}{r^2} \frac{\partial^2 \psi}{\partial \phi^2} + \frac{\partial^2 \psi}{\partial z^2} \\ \nabla^2 \mathbf{A} &= \mathbf{a}_r \left[\nabla^2 A_r - \frac{A_r}{r^2} - \frac{2}{r^2} \frac{\partial A_{\phi}}{\partial \phi} \right] + \mathbf{a}_{\phi} \left[\nabla^2 A_{\phi} - \frac{A_{\phi}}{r^2} + \frac{2}{r^2} \frac{\partial A_r}{\partial \phi} \right] + \mathbf{a}_z \nabla^2 A_z\end{aligned}\tag{D.1.14}$$

We use θ for azimuth instead of their ϕ since ϕ is our scalar potential.

Using the ansatz form (D.1.1) and partial wave expansions of the form (D.1.3) or (D.1.5), it is a simple matter to convert an equation containing the above differential operators and involving components like $E_{\mathbf{i}}(r,\theta,z,t)$ or $n(\theta,z,t)$ to a simpler equation involving components like $E_{\mathbf{i}}(r,m)$ and N_m and this will be done below.

(d) The three Helmholtz equations and $\text{div } \mathbf{E} = 0$ (in partial waves)

1. The z equation: The E_z Helmholtz Equation from (D.1.9) is $[\nabla^2 \mathbf{E}]_{\mathbf{z}} + \beta^2 E_z = 0$.

Using (D.1.12) and (D.1.13), the E_z equation may be written,

$$[\partial_{\mathbf{r}}^2 + (1/r) \partial_{\mathbf{r}} + (1/r^2) \partial_{\theta}^2 + \partial_{\mathbf{z}}^2 + \beta^2] e^{j(\omega t - \mathbf{kz})} E_z(r,\theta) = 0.\tag{1}$$

Inserting the expansion (D.1.3) for $E_z(r,\theta)$ and moving the m sum to the left gives

$$\sum_{m=-\infty}^{\infty} [\partial_r^2 + (1/r) \partial_r + (1/r^2) \partial_\theta^2 + \partial_z^2 + \beta^2] e^{j(\omega t - kz)} E_z(r,m) e^{jm\theta} = 0. \quad (2)$$

We can then make the obvious replacements $\partial_z = -jk$ and $\partial_\theta = +jm$ to get,

$$\sum_{m=-\infty}^{\infty} \{ [\partial_r^2 + (1/r) \partial_r - m^2 (1/r^2) - k^2 + \beta^2] e^{j(\omega t - kz)} E_z(r,m) \} e^{jm\theta} = 0. \quad (3)$$

Due to the completeness of functions $e^{jm\theta}$ on the interval $(-\pi, \pi)$, we conclude that $\{ \} = 0$, or

$$[\partial_r^2 + (1/r) \partial_r - m^2 (1/r^2) - k^2 + \beta^2] e^{j(\omega t - kz)} E_z(r,m) = 0. \quad (4)$$

Alternatively one can apply $\int_{-\pi}^{\pi} d\theta e^{-jm'\theta}$ to both sides of (3), use the orthogonality property

$$\int_{-\pi}^{\pi} d\theta e^{j(m-m')\theta} = 2\pi \delta_{m,m'}, \quad (5)$$

and then change m' to m to get (4).

Next, multiply both sides of (4) by $r^2 e^{-j(\omega t - kz)}$ to get,

$$[r^2 \partial_r^2 + r \partial_r - m^2 + r^2(\beta^2 - k^2)] E_z(r,m) = 0. \quad (D.1.15)$$

We may then write these rules for converting equation (1) to equation (D.1.15)

$$\begin{array}{ll} \text{Conversion Rules:} & \partial_z \rightarrow -jk & \partial_t \rightarrow +j\omega \\ & \partial_\theta \rightarrow +jm & f(r,\theta,z,t) \rightarrow f(r,m) \end{array} \quad (D.1.16)$$

We can now practice with these rules to convert various other equations of interest. A field with unstated arguments has the full arguments (r,θ,z,t) .

2. The r equation: The E_r Helmholtz Equation from (D.1.9) is $[\nabla^2 \mathbf{E}]_r + \beta^2 E_r = 0$.

Using (D.1.12) we find,

$$\nabla^2(E_r) - (2/r^2) \partial_\theta E_\theta - (1/r^2) E_r + \beta^2 E_r = 0$$

$$[\partial_r^2 + (1/r) \partial_r + (1/r^2) \partial_\theta^2 + \partial_z^2] E_r - (2/r^2) \partial_\theta E_\theta - (1/r^2) E_r + \beta^2 E_r = 0$$

$$[\partial_r^2 + (1/r) \partial_r + (1/r^2) \partial_\theta^2 + \partial_z^2 - (1/r^2) + \beta^2] E_r - (2/r^2) \partial_\theta E_\theta = 0.$$

Now apply the conversion rules to get

$$[\partial_{\mathbf{r}}^2 + (1/r)\partial_{\mathbf{r}} + (1/r^2)(-m^2) - k^2 - (1/r^2) + \beta^2] E_{\mathbf{r}}(r,m) - (2/r^2) jm E_{\theta}(r,m) = 0 .$$

Group like terms and multiply by r^2 to get

$$[r^2\partial_{\mathbf{r}}^2 + r\partial_{\mathbf{r}} - (m^2+1) + r^2(\beta^2-k^2)] E_{\mathbf{r}}(r,m) - 2jm E_{\theta}(r,m) = 0 . \quad (\text{D.1.17})$$

3. The θ equation: The E_{θ} Helmholtz Equation from (D.1.9) is $[\nabla^2 \mathbf{E}]_{\theta} + \beta^2 E_{\theta} = 0$.

Using (D.1.12) we find,

$$\nabla^2(E_{\theta}) + (2/r^2) \partial_{\theta} E_{\mathbf{r}} - (1/r^2) E_{\theta} + \beta^2 E_{\theta} = 0$$

$$[\partial_{\mathbf{r}}^2 + (1/r)\partial_{\mathbf{r}} + (1/r^2)\partial_{\theta}^2 + \partial_{\mathbf{z}}^2] E_{\theta} + (2/r^2) \partial_{\theta} E_{\mathbf{r}} - (1/r^2) E_{\theta} + \beta^2 E_{\theta} = 0$$

$$[\partial_{\mathbf{r}}^2 + (1/r)\partial_{\mathbf{r}} + (1/r^2)\partial_{\theta}^2 + \partial_{\mathbf{z}}^2 - (1/r^2) + \beta^2] E_{\theta} + (2/r^2) \partial_{\theta} E_{\mathbf{r}} = 0 .$$

Now apply the conversion rules to get

$$[\partial_{\mathbf{r}}^2 + (1/r)\partial_{\mathbf{r}} + (1/r^2)(-m^2) + (-k^2) - (1/r^2) + \beta^2] E_{\theta}(r,m) + (2/r^2) jm E_{\mathbf{r}}(r,m) = 0 .$$

Group like terms and multiply by r^2 to get

$$[r^2\partial_{\mathbf{r}}^2 + r\partial_{\mathbf{r}} - (m^2+1) + r^2(\beta^2-k^2)] E_{\theta}(r,m) + 2jm E_{\mathbf{r}}(r,m) = 0 . \quad (\text{D.1.18})$$

4. The $\text{div} \mathbf{E} = 0$ equation: Using (D.1.14) for $\text{div} \mathbf{E}$ (times r) we write $\text{div} \mathbf{E} = 0$ as

$$\partial_{\mathbf{r}} (r E_{\mathbf{r}}) + \partial_{\theta} E_{\theta} + r \partial_{\mathbf{z}} E_{\mathbf{z}} = 0 .$$

Applying the conversion rules gives

$$\partial_{\mathbf{r}} [r E_{\mathbf{r}}(r,m)] + jm E_{\theta}(r,m) + r (-jk) E_{\mathbf{z}}(r,m) = 0$$

or

$$[1 + r\partial_{\mathbf{r}}] E_{\mathbf{r}}(r,m) + jm E_{\theta}(r,m) + r (-jk) E_{\mathbf{z}}(r,m) = 0 . \quad (\text{D.1.19})$$

Here then is a summary of the above four results:

The Three Helmholtz Equations and the $\text{div } \mathbf{E} = 0$ equation (in partial waves) (D.1.20)

$$[\nabla^2 \mathbf{E}]_z + \beta^2 E_z = 0 : \\ [r^2 \partial_r^2 + r \partial_r - m^2 + r^2 (\beta^2 - k^2)] E_z(r,m) = 0 \quad (D.1.15)$$

$$[\nabla^2 \mathbf{E}]_r + \beta^2 E_r = 0 : \\ [r^2 \partial_r^2 + r \partial_r - (m^2 + 1) + r^2 (\beta^2 - k^2)] E_r(r,m) - 2jm E_\theta(r,m) = 0 \quad (D.1.17)$$

$$[\nabla^2 \mathbf{E}]_\theta + \beta^2 E_\theta = 0 : \\ [r^2 \partial_r^2 + r \partial_r - (m^2 + 1) + r^2 (\beta^2 - k^2)] E_\theta(r,m) + 2jm E_r(r,m) = 0 \quad (D.1.18)$$

$$\text{div } \mathbf{E} = 0 : \\ \partial_r [r E_r(r,m)] + jm E_\theta(r,m) - jk r E_z(r,m) = 0 \quad (D.1.19)$$

Helmholtz Comments: The *scalar* Helmholtz equation $(\nabla^2 + \beta^2)u(r,\theta,z) = 0$ is fully separable in cylindrical coordinates and the "harmonics" (we call them atomic forms) are as follows

$$[J_m(\beta'r), Y_m(\beta'r)] * [e^{jm\theta}, e^{-jm\theta}] * [e^{jkz}, e^{-jkz}] \quad (D.1.21)$$

where k is a free real parameter and where $\beta'^2 = \beta^2 - k^2$. Here we use parameter names relevant for our particular problem where $u = E_z$. These atomic forms appear for example in Moon and Spencer p15 with $\beta = \kappa$, $m = p$, $\beta' = iq$, $\alpha_2 = m^2$, and $-\alpha_3 = \beta'^2$. Whether a parameter like m or β' is real, imaginary or complex depends on the nature of the problem, and the above is a standard atoms choice for problems of our type. The θ "quantum number" m is quantized to be an integer by the fact that the problem region is the entire range $(-\pi, \pi)$ for θ and the solution must be single valued in θ . Our k is a parameter determined for a lossless line by $k = \omega \sqrt{\mu_d \epsilon_d}$ and is thus correlated with the selected frequency ω , whereas our parameter β is always complex as in (1.5.1c or d). In general, in any list of atomic forms like that shown above, two of the three atoms will be oscillatory and the third will be exponential, and in our case $J_m(\beta'r)$ is the exponential one, hence the skin effect with its exponential damping as shown in (2.3.7). Away from a singular point, any solution to $(\nabla^2 + \beta^2) u(r,\theta,z) = 0$ must be writable as a linear combination of the atoms, so

$$u = \int dk \sum_m [A_{k,m} J_m(\beta'r) + B_{k,m} Y_m(\beta'r)] [C_{k,m} e^{jm\theta} + D_{k,m} e^{-jm\theta}] [E_{k,m} e^{jkz} + F_{k,m} e^{-jkz}].$$

A general solution method is to find a subset of the above most-general form that is appropriate in each "region" of the problem, and then to match boundary conditions between regions. If the problem is well-posed, this will determine all the constants A,B,C,D,E,F. We refer to this solution method as "the method of Smythian forms" (Smythe used this method a lot). Often many of these constants are 0.

In contrast, the *vector* Helmholtz equation is *not* separable in cylindrical coordinates (see Moon and Spencer p 139), it is not even "R-separable", so there are no associated "harmonics" as there are with the

scalar Helmholtz equation. Nevertheless, the functions $e^{jm\theta}$ form a complete set for θ in $(-\pi, \pi)$ and our expansion of each E_i onto these $e^{jm\theta}$ is certainly allowed, even though these $e^{jm\theta}$ are not part of any associated harmonics for the vector Helmholtz equation.

However, in Cartesian coordinates each Helmholtz component equation *is* a scalar Helmholtz equation. In cylindrical coordinates z is a Cartesian coordinate, so we should not be surprised when we find below that $E_z \sim J_m(\beta'r) e^{im\theta} e^{-jkz}$ and this fits into the general form noted above. Neither E_r nor E_θ will have such a form.

D.2 Solutions for E_z , E_r and E_θ

(a) The E_z Solution

As shown in (D.1.15), the Helmholtz equation for $E_z(r, m)$ is

$$[r^2 \partial_r^2 + r \partial_r + (r^2 \beta'^2 - m^2)] E_z(r, m) = 0 \quad (D.2.1)$$

where

$$\beta'^2 = \beta^2 - k^2 \quad (D.2.2)$$

For a perfect conductor, $|\beta|$ is very large compared to the low-loss value $k = \beta_{d0} \approx \beta_{d0}$ (slight dielectric conductivity), so we *could* ignore the distinction between β and β' in that low-loss case. To show this, recall from (1.5.1b and d) that

$$\beta_{d0}^2 = \omega^2 \mu_d \epsilon_d \quad \beta^2 \approx -j\omega\mu\sigma \quad \Rightarrow \quad \left| \frac{\beta^2}{\beta_{d0}^2} \right| \approx \frac{\mu}{\mu_d} \frac{\sigma}{\omega\epsilon_d}$$

In scale, μ and μ_d are about the same, so using numbers from (1.1.28) and (1.1.29),

$$\left| \frac{\beta^2}{\beta_{d0}^2} \right| \approx \frac{\sigma}{\omega\epsilon_d} = \frac{5.81 \times 10^7}{2\pi f \cdot 8.85 \times 10^{-12}} \approx \frac{10^{18}}{f(\text{Hz})} = \frac{10^9}{f(\text{GHz})}$$

$$\left| \frac{\beta}{\beta_{d0}} \right| \approx \frac{3.2 \times 10^4}{\sqrt{f(\text{GHz})}}$$

For $f = 100$ GHz we then find that $|\beta/\beta_{d0}| \approx 3200$, so for $f < 100$ GHz, $|\beta/\beta_{d0}| > 3200$.

As noted earlier, we maintain k as a general complex parameter to be able to handle situations with loss, and thus we maintain the distinction between β and β' in all that follows.

Setting $x = \beta'r$ one finds $\partial_r = \beta' \partial_x$ and then $r \partial_r = x \partial_x$ and so on so that (D.2.1) reads

$$[x^2 \partial_x^2 + x \partial_x + (x^2 - m^2)] E_z(x/\beta', m) = 0 \quad x = \beta'r \quad (D.2.3)$$

This is Bessel's equation [Spiegel 24.1] and the solution subject to the condition that E_z be finite at $r = 0$ is $E_z(x/\beta', m) = C_{zm} J_m(x)$ or

$$E_z(r, m) = C_{zm} J_m(\beta' r) \quad (D.2.4)$$

where C_{zm} is an arbitrary constant for each partial wave m .

For $m = 0$, equation (D.2.4) is consistent with (2.2.22) found by other means. In Section 2.1 we dealt only with the $m=0$ partial wave, which embodies the symmetrical part of the problem.

(b) The E_r Solution

As shown in (D.1.17), the Helmholtz equation for $E_r(r, m)$ is, using (D.2.2),

$$[r^2 \partial_r^2 + r \partial_r - (m^2 + 1) + r^2 \beta'^2] E_r(r, m) - 2jm E_\theta(r, m) = 0 \quad (D.2.5)$$

while the $\text{div } \mathbf{E} = 0$ condition was stated in (D.1.19) as

$$\begin{aligned} [1 + r \partial_r] E_r(r, m) + jm E_\theta(r, m) + r (-jk) E_z(r, m) &= 0 \\ \text{or} \\ -jm E_\theta(r, m) &= [1 + r \partial_r] E_r(r, m) - r (jk) E_z(r, m) . \end{aligned} \quad (D.2.6)$$

Inserting this into (D.2.5) gives [$m = 0$ is a special case, but it falls out below correctly]

$$\begin{aligned} [r^2 \partial_r^2 + r \partial_r - (m^2 + 1) + r^2 \beta'^2] E_r(r, m) + [2 + 2r \partial_r] E_r(r, m) - 2r (jk) E_z(r, m) &= 0 \\ \text{or} \\ [r^2 \partial_r^2 + 3r \partial_r + (1 - m^2) + r^2 \beta'^2] E_r(r, m) &= 2r (jk) E_z(r, m) . \end{aligned} \quad (D.2.7)$$

Inserting solution (D.2.4) for $E_z(r, m)$ this becomes

$$\begin{aligned} [r^2 \partial_r^2 + 3r \partial_r + (1 - m^2) + r^2 \beta'^2] E_r(r, m) &= 2r (jk) C_{zm} J_m(\beta' r) \\ \text{or} \\ [r^2 \partial_r^2 + 3r \partial_r + (1 - m^2) + r^2 \beta'^2] E_r(r, m) &= 2j (k/\beta') C_{zm} \beta' r J_m(\beta' r) \\ \text{or} \\ [r^2 \partial_r^2 + 3r \partial_r + (1 - m^2) + r^2 \beta'^2] E_r(r, m) &= K_m \beta' r J_m(\beta' r) \end{aligned} \quad (D.2.8)$$

where

$$K_m \equiv 2j (k/\beta') C_{zm} . \quad (D.2.9)$$

In order to get the left side of (D.2.8) into something recognizable, we define

$$E_r(r, m) = x^{-1} F_m(x) \quad (D.2.10)$$

where x is a dimensionless radial variable which will play a major role in the following,

$$x \equiv \beta'r \quad \text{and} \quad x_a \equiv \beta'a \quad . \quad (D.2.11)$$

Then (D.2.8) becomes

$$[x^2 \partial_x^2 + 3x \partial_x + (1-m^2) + x^2] \{ x^{-1} F_m(x) \} = 2j (k/\beta') C_{zm} x J_m(x)$$

or

$$x [x^2 \partial_x^2 + 3x \partial_x + (1-m^2) + x^2] \{ x^{-1} F_m(x) \} = K_m x^2 J_m(x) . \quad (D.2.12)$$

Ever eager, Maple expands the left side of (D.2.12),

```

g := fm(x)/x;
L := x*(x^2*diff(g,x,x)+3*x*diff(g,x) + ((1-m^2) + x^2)*g):
simplify(%): expand(%): collect(%,fm(x));

```

$$(-m^2 + x^2) fm(x) + \left(\frac{\partial^2}{\partial x^2} fm(x) \right) x^2 + \left(\frac{\partial}{\partial x} fm(x) \right) x$$

so that (D.2.12) becomes

$$[x^2 \partial_x^2 + x \partial_x + (x^2 - m^2)] F_m(x) = K_m x^2 J_m(x) . \quad (D.2.13)$$

The left side of (D.2.13) is the normal Bessel operator [Spiegel 24.1], but the equation is also *driven* by a power times a Bessel function. The solution to the equation is the homogeneous solution of the Bessel equation plus the particular solution which is the response to the driving function on the right hand side.

The homogeneous solution is the usual linear combination of $J_m(x)$ and $Y_m(x)$, but we must reject $Y_m(x)$ since it blows up at $x=0$ and thereby causes the field E_r to be singular, which it cannot be, smack in the middle of a wire.

The particular solution is not very obvious and required some hunting to find. It is this

$$F_m(x)^{\text{particular}} = (1/2) K_m [x J_{m+1}(x)] . \quad (D.2.14)$$

as Maple confirms, continuing the above code,

```

fm := (x) -> (1/2)*Km*x*BesselJ(m+1,x);

```

$$fm := x \rightarrow \frac{1}{2} Km x BesselJ(m+1, x)$$

```

L: simplify(%);

```

$$x^2 Km BesselJ(m, x)$$

Therefore, we now have this full solution for $F_m(x)$

$$F_m(x) = F_m(x)^{\text{particular}} + F_m(x)^{\text{homogeneous}} = (1/2) K_m [x J_{m+1}(x)] + a_m J_m(x)$$

and then from (D.2.10) the full solution for E_r ,

$$E_{\mathbf{r}}(r,m) = a_m x^{-1} J_m(x) + \frac{K_m}{2} J_{m+1}(x) . \quad (D.2.15)$$

For each value of m , there are two as-yet undetermined constants, a_m and $(K_m/2)$. However, looking at (D.2.15), we see that, since $J_0(x) \approx 1$ for small x , we must have

$$a_0 = 0 \quad (D.2.16)$$

to keep $E_{\mathbf{r}}$ finite at $r = 0$. Later we shall obtain expressions for a_m and $(K_m/2)$.

(c) The E_{θ} Solution

Recall (D.2.6) in slightly altered form,

$$jmE_{\theta}(r,m) = -\partial_{\mathbf{r}}[rE_{\mathbf{r}}(r,m)] + r(jk)E_{\mathbf{z}}(r,m) . \quad (D.2.6)$$

We can then insert our known $E_{\mathbf{z}}$ and $E_{\mathbf{r}}$ to get E_{θ} :

$$E_{\mathbf{z}}(r,m) = C_{zm} J_m(x) \quad (D.2.4)$$

$$E_{\mathbf{r}}(r,m) = a_m x^{-1} J_m(x) + \frac{K_m}{2} J_{m+1}(x) . \quad (D.2.15)$$

so (D.2.6) just above becomes the following :

$$\begin{aligned} jmE_{\theta}(r,m) &= -\partial_{\mathbf{r}}[r\{a_m x^{-1} J_m(x) + \frac{K_m}{2} J_{m+1}(x)\}] + r(jk) C_{zm} J_m(x) \\ jmE_{\theta}(r,m) &= -\partial_{\mathbf{x}}[x\{a_m x^{-1} J_m(x) + \frac{K_m}{2} J_{m+1}(x)\}] + \frac{K_m}{2} x J_m(x) \quad // K_m \equiv 2j(k/\beta') C_{zm} \\ jmE_{\theta}(r,m) &= -\partial_{\mathbf{x}}[a_m J_m(x) + \frac{K_m}{2} x J_{m+1}(x)] + \frac{K_m}{2} x J_m(x) \\ jmE_{\theta}(r,m) &= -a_m J_m'(x) - \frac{K_m}{2} J_{m+1}(x) - \frac{K_m}{2} x J_{m+1}'(x) + \frac{K_m}{2} x J_m(x) \\ jmE_{\theta}(r,m) &= -a_m J_m'(x) + \frac{K_m}{2} [-J_{m+1}(x) - x J_{m+1}'(x) + x J_m(x)] . \end{aligned} \quad (D.2.17)$$

At this point we invoke the recurrence relations [NIST 10.6.2], where \mathcal{C}_{ν} is any Bessel function,

$$\begin{aligned} 10.6.2 \quad \mathcal{C}'_{\nu}(z) &= \mathcal{C}_{\nu-1}(z) - (\nu/z) \mathcal{C}_{\nu}(z), \\ \mathcal{C}'_{\nu}(z) &= -\mathcal{C}_{\nu+1}(z) + (\nu/z) \mathcal{C}_{\nu}(z). \end{aligned}$$

to write

$$\begin{aligned} J_{m+1}' &= J_m - (m+1)x^{-1}J_{m+1} && \text{first relation with } \nu = m+1 \\ J_m' &= -J_{m+1} + (m/x)J_m && \text{second relation with } \nu = m \end{aligned} \quad (D.2.18)$$

Insert these into (D.2.17) to get

$$\begin{aligned}
 jmE_{\theta}(r,m) &= -a_m J_m' + \frac{K_m}{2} [-x J_{m+1}' - J_{m+1} + xJ_m] \\
 &= -a_m \{-J_{m+1} + (m/x)J_m\} + \frac{K_m}{2} [-x \{J_m - (m+1)x^{-1}J_{m+1}\} - J_{m+1} + xJ_m] \\
 &= a_m J_{m+1} - a_m (m/x)J_m + \frac{K_m}{2} [-x J_m + (m+1) J_{m+1} - J_{m+1} + xJ_m] \\
 &= a_m J_{m+1} - a_m (m/x)J_m + \frac{K_m}{2} [m J_{m+1}] \\
 &= -a_m (m/x)J_m + \left(\frac{K_m}{2} m + a_m\right) J_{m+1} .
 \end{aligned}$$

Dividing by m then gives the final solution [again, $m = 0$ is a special case]

$$jE_{\theta}(r,m) = -a_m x^{-1} J_m(x) + \left(\frac{K_m}{2} + \frac{a_m}{m}\right) J_{m+1}(x) \quad x = \beta'r \quad (D.2.19)$$

We now gather up the solutions developed above, but first, recall that

$$K_m \equiv 2j (k/\beta') C_{zm} \quad (D.2.5)$$

which we can solve to get

$$C_{zm} = (1/2j)(\beta'/k) K_m . \quad (D.2.20)$$

Installing this into (D.2.4), our three E field components are then

$$\mathbf{First\ summary\ of\ the\ E\ field\ solutions} \quad (D.2.21)$$

$$E_z(r,m) = -j (\beta'/k) \frac{K_m}{2} J_m(x) \quad x = \beta'r \quad (D.1.27)$$

$$E_r(r,m) = a_m x^{-1} J_m(x) + \frac{K_m}{2} J_{m+1}(x) \quad \beta'^2 = \beta^2 - k^2 \quad (D.2.11)$$

$$jE_{\theta}(r,m) = -a_m x^{-1} J_m(x) + \left(\frac{K_m}{2} + \frac{a_m}{m}\right) J_{m+1}(x) \quad (D.2.15)$$

These solutions were obtained from the z and r Helmholtz equations and from the $\text{div } \mathbf{E} = 0$ equation. As will be shown below, for $m = 0$ it turns out that $a_0 = 0$ and also $\left(\frac{K_0}{2} + \frac{a_0}{0}\right) = 0$, so $E_{\theta}(r,0) \equiv 0$. This last result may be directly obtained by solving the $m = 0$ E_{θ} equation (D.1.18) to get $E_{\theta}(r,0) = C_{\theta 0} J_1(\beta'r)$ and then the boundary condition $E_{\theta}(a,0) = 0$ forces $C_{\theta 0} = 0$.

It is an easy matter to have Maple *verify* that this solution set solves the div E equation and *all three* of the Helmholtz equations z, r and θ :

`alias(I=I, j= sqrt(-1), J=BesselJ):`

Enter the left sides of the four equations in box (D.1.20):

`e1 := r^2*Diff(Ez,r,r) + r*Diff(Ez,r) -m^2*Ez + r^2*bp^2*Ez;`

$$e1 = r^2 \left(\frac{\partial^2}{\partial r^2} Ez \right) + r \left(\frac{\partial}{\partial r} Ez \right) - m^2 Ez + r^2 bp^2 Ez$$

`e2 := r^2*Diff(Er,r,r) + r*Diff(Er,r) -(m^2+1)*Er + r^2*bp^2*Er -2*j*m*Ephi;`

$$e2 = r^2 \left(\frac{\partial^2}{\partial r^2} Er \right) + r \left(\frac{\partial}{\partial r} Er \right) - (m^2 + 1) Er + r^2 bp^2 Er - 2j m Ephi$$

`e3 := r^2*Diff(Ephi,r,r) + r*Diff(Ephi,r) -(m^2+1)*Ephi + r^2*bp^2*Ephi +2*j*m*Er;`

$$e3 = r^2 \left(\frac{\partial^2}{\partial r^2} Ephi \right) + r \left(\frac{\partial}{\partial r} Ephi \right) - (m^2 + 1) Ephi + r^2 bp^2 Ephi + 2j m Er$$

`e4 := Diff(r*Er,r) + j*m*Ephi - j*k*r*Ez;`

$$e4 = \left(\frac{\partial}{\partial r} r Er \right) + j m Ephi - j k r Ez$$

Next, enter the claimed E field solutions from box (D.2.21):

`Ez := -j*(bp/k)*(Km/2)*J(m,x);`

$$Ez = -\frac{1}{2} \frac{j bp Km J(m, x)}{k}$$

`Er := am*(1/x)*J(m,x) + (Km/2)*J(m+1,x);`

$$Er = \frac{am J(m, x)}{x} + \frac{1}{2} Km J(m + 1, x)$$

`Ephi := (-j)*(-am*(1/x)*J(m,x) + (Km/2+am/m)*J(m+1,x));`

$$Ephi = -j \left(-\frac{am J(m, x)}{x} + \left(\frac{1}{2} Km + \frac{am}{m} \right) J(m + 1, x) \right)$$

`x := bp*r; set x`

$$x := bp r$$

Show that each left side evaluates to zero as box (D.1.20) requires

`value(e1): simplify(%)`

0

`value(e2): simplify(%)`

0

`value(e3): simplify(%)`

0

`value(e4): simplify(%)`

0

Maple Comment: In Maple one must be careful with this kind of verification to make sure Maple has not misunderstood something. For example, perhaps it thinks $\partial_x E_z = 0$ because it thinks E_z is a constant. This is the purpose of using the "inert" Diff operators (versus diff) when the function to be differentiated has not yet been defined, and then forcing them to evaluate later with the value() operator. One should

always view expressions before simplification to make sure things are kosher. For example, changing the colon to semicolon after value(e1) to force display, one gets

```
> value(e1); simplify(%);
```

$$\frac{\frac{1}{2} j r^2 b p^2 K m \left(- \left(J(m, b p r) - \frac{(m+1) J(m+1, b p r)}{b p r} \right) b p - \frac{m J(m, b p r)}{b p r^2} + \frac{m \left(-J(m+1, b p r) + \frac{m J(m, b p r)}{b p r} \right)}{r} \right)}{k} - \frac{1}{2} \frac{j r b p^2 K m \left(-J(m+1, b p r) + \frac{m J(m, b p r)}{b p r} \right)}{k} + \frac{1}{2} \frac{j m^2 b p K m J(m, b p r)}{k} - \frac{1}{2} \frac{j r^2 b p^3 K m J(m, b p r)}{k}$$

Here Maple has duly computed the Bessel function derivatives in expression e1 but does not yet realize that the expression is 0. This is brought out by the simplify(%) command (simplify the last computed expression) and the output of the simplify command is the 0 on the last line.

Here is an alternative verification of $\text{div}\mathbf{E} = 0$ and $(\nabla^2 + \beta^2)\mathbf{E} = 0$ using Maple's fancy differential operators and the fact that $\nabla^2\mathbf{E} = \text{grad}(\text{div}\mathbf{E}) - \text{curl}(\text{curl}\mathbf{E})$. We use the same field components as above, but tack on the θ and z dependence of the partial waves:

```
E := [Er, Etheta, Ez]:
c := [r, theta, z]:
Ez := -j*(bp/k)*(Km/2)*J(m,x)*exp(j*m*theta)*exp(-j*k*z):
Er := (am*(1/x)*J(m,x) + (Km/2)*J(m+1,x))*exp(j*m*theta)*exp(-j*k*z):
Etheta := (-j)*(-am*(1/x)*J(m,x) + (Km/2+am/m)*J(m+1,x))*exp(j*m*theta)*exp(-j*k*z):
x := bp*r: bp := sqrt(b^2-k^2):
diverge(E,c,coords=cylindrical):
0
gd := simplify(grad(diverge(E,c,coords=cylindrical),c,coords=cylindrical)):
cc := simplify(curl(curl(E,c,coords=cylindrical),c,coords=cylindrical)):
vlap := gd - cc:
evalm(vlap + b^2*E): simplify(%):
[0,0,0]
```

(d) The Charge Pumping Boundary Condition

The reason we are interested in the surface charge $n(\theta)$ of (D.1.5) is that it acts as a driving source of the radial electric field inside the wire. Recall the equation of continuity (1.1.35) converted to the ω domain

$$\text{div } \mathbf{J} = -j\omega\rho \quad \Leftrightarrow \quad -j\omega\left[\int_{\mathbf{v}} \rho \, dV\right] = \int_{\mathbf{s}} \mathbf{J} \cdot d\mathbf{S} . \quad (\text{D.2.22})$$

This is meant to be (1.1.25) where \mathbf{J} is conduction current and ρ is free charge. When applied to a thin box of radial area dS straddling the wire surface,

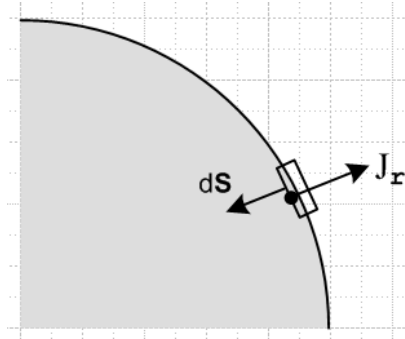


Fig D.2

one finds that $\int_{\mathbf{s}} \mathbf{J} \cdot d\mathbf{S} = -J_r(r=a-\epsilon, \theta)dS$ and $\int_{\mathbf{v}} \rho \, dV = n(\theta) \, dS$ so that (ϵ implies just below surface)

$$J_r(r=a-\epsilon, \theta) = j\omega \, n(\theta) . \quad (\text{D.2.23})$$

We assume there is no conduction current outside the wire to get this result (non-conducting dielectric). Since $\mathbf{J} = \sigma\mathbf{E}$, this is really a boundary condition on the radial electric field just below the surface,

$$E_r(r=a-\epsilon, \theta) = (j\omega/\sigma) \, n(\theta) . \quad (\text{D.2.24})$$

We convert this to m-space using the conversion rules (D.1.16) to obtain (dropping the ϵ)

$$E_r(r=a, m) = (j\omega/\sigma) \, N_m . \quad (\text{D.2.25})$$

Thus, the interior radial electric field must have a certain value at the $r=a$ boundary in each partial wave, and this value is determined by the moment of the surface charge distribution.

By way of interpretation, the surface charge of a transmission line is "pumped" by the radial current in the wire (in quadrature), see Fig D.7 far below. This radial current is accompanied by the usual longitudinal current one expects to find inside the conductors of a transmission line.

If the dielectric conducts with some $\sigma_d > 0$ but $\sigma_d \ll \sigma$, one must make these replacements in (D.2.24) and (D.2.25),

$$n(\theta) \rightarrow (\xi_d/\epsilon_d) n(\theta) \quad N_m \rightarrow (\xi_d/\epsilon_d) N_m .$$

See (D.9.23) and surrounding discussion. Generally we shall assume $\sigma_d = 0$ in the following work just to avoid having the extra (ξ_d/ϵ_d) factors floating around.

(e) Application of the Boundary Conditions

Our task here is to derive expressions for the constants a_m and K_m appearing in the above E field component equations.

We have two boundary conditions to impose:

$$E_r(r=a,m) = (j\omega/\sigma) N_m \quad (D.2.26)$$

$$E_\theta(r=a,m) = 0 . \quad (D.2.27)$$

The first is the radial charge pumping condition shown in (D.2.25) above. The second boundary condition is an assumption that requires its own discussion in Section D.8 below. It implies that the cross sectional wire surface is an equipotential surface and that therefore $E_\theta(r=a,\theta) = 0$. This in turn requires that in each partial wave $E_\theta(r,m) = 0$ since

$$E_\theta(r,m) = (1/2\pi) \int_{-\pi}^{\pi} d\theta E_\theta(r,\theta) e^{-jm\theta} \quad (D.1.3b)$$

$$E_\theta(a,m) = (1/2\pi) \int_{-\pi}^{\pi} d\theta E_\theta(a,\theta) e^{-jm\theta} = (1/2\pi) \int_{-\pi}^{\pi} d\theta 0 e^{-jm\theta} = 0 .$$

These two boundary conditions serve to determine the two constants a_m and K_m , though a bit of algebra is required. The first step is to use the E_r and E_θ expressions shown in summary box (D.2.21) to write out the two boundary conditions as

$$a_m x_a^{-1} J_m(x_a) + \frac{K_m}{2} J_{m+1}(x_a) = (j\omega/\sigma) N_m \quad (1)$$

$$- a_m x_a^{-1} J_m(x_a) + \left(\frac{K_m}{2} + \frac{a_m}{m} \right) J_{m+1}(x_a) = 0 . \quad (2)$$

Addition and subtraction of these equations gives two new equations,

$$\frac{K_m}{2} J_{m+1}(x_a) + \left(\frac{K_m}{2} + \frac{a_m}{m} \right) J_{m+1}(x_a) = (j\omega/\sigma) N_m \quad (3)$$

$$2 a_m x_a^{-1} J_m(x_a) - \frac{a_m}{m} J_{m+1}(x_a) = (j\omega/\sigma) N_m . \quad (4)$$

Using the recursion relation $2m x^{-1} J_m = [J_{m+1} + J_{m-1}]$, the second may be immediately solved for a_m ,

$$\frac{a_m}{m} = (j\omega/2\sigma) 2 N_m \frac{1}{J_{m-1}(x_a)} . \quad (5)$$

Using this same recursion relation and (5) for a_m , equation (2) may be solved to get

$$\left(\frac{K_m}{2} + \frac{a_m}{m}\right) = (j\omega/2\sigma) N_m \left[\frac{1}{J_{m+1}(x_a)} + \frac{1}{J_{m-1}(x_a)}\right] \quad (6)$$

Finally, subtracting (5) from (6) we find

$$\frac{K_m}{2} = (j\omega/2\sigma) N_m \left[\frac{1}{J_{m+1}(x_a)} - \frac{1}{J_{m-1}(x_a)}\right] \quad (7)$$

Notice the following situations for $m = 0$,

$$a_0 = 0 \quad (8) \quad // \text{ from (5)}$$

$$\frac{a_0}{0} = (j\omega/2\sigma) 2 N_0 \frac{1}{J_{-1}(x_a)} = - (j\omega/2\sigma) 2 N_0 \frac{1}{J_1(x_a)} \quad (9) \quad // \text{ from (5)}$$

$$\frac{K_0}{2} = (j\omega/2\sigma) N_0 \left[\frac{1}{J_1(x_a)} - \frac{1}{J_{-1}(x_a)}\right] = (j\omega/\sigma) N_0 \frac{1}{J_1(x_a)} \quad (10) \quad // \text{ from (7)}$$

$$\left(\frac{K_0}{2} + \frac{a_0}{0}\right) = 0 \quad (11) \quad // \text{ adding (9) and (10)}$$

We summarize the coefficients as follows:

$a_m = (j\omega/2\sigma) 2m N_m \frac{1}{J_{m-1}(x_a)} \cdot$	$a_0 = 0$	(D.2.28)
$\frac{K_m}{2} = (j\omega/2\sigma) N_m \left[\frac{1}{J_{m+1}(x_a)} - \frac{1}{J_{m-1}(x_a)}\right]$	$\frac{K_0}{2} = (j\omega/\sigma) N_0 \frac{1}{J_1(x_a)}$	
$\left(\frac{K_m}{2} + \frac{a_m}{m}\right) = (j\omega/2\sigma) N_m \left[\frac{1}{J_{m+1}(x_a)} + \frac{1}{J_{m-1}(x_a)}\right]$	$\left(\frac{K_0}{2} + \frac{a_0}{0}\right) = 0$	

The third equation is obvious from adding the first two, and Maple verifies that the first two satisfy (1) and (2). At this point it is convenient to introduce the DC resistance per unit length of the wire (C.1.1),

$$R_{dc} = \frac{1}{\sigma\pi a^2} \quad (D.2.29)$$

along with a new symbol to indicate the *relative* surface charge moment,

$$\eta_m \equiv \frac{N_m}{N_0} \quad (D.2.30)$$

The DC moment N_0 can be related to the total current I in the wire as follows:

$$\begin{aligned}
 I &= \int_0^{2\pi} d\theta \int_0^a r dr J_z(r,\theta) = \int_0^{2\pi} d\theta \int_0^a r dr \left\{ \sigma \sum_{m=-\infty}^{\infty} E_z(r,m) e^{jm\theta} \right\} \quad // (D.1.3a) \\
 &= \sigma \sum_{m=-\infty}^{\infty} \int_0^a r dr E_z(r,m) \int_0^{2\pi} d\theta e^{jm\theta} = 2\pi \sigma \int_0^a r dr E_z(r,0) \\
 &= 2\pi \sigma \int_0^a r dr \left\{ -j(\beta'/k) \frac{K_0}{2} J_0(x) \right\} \quad // (D.2.21) \text{ for } E_z(r,0) \\
 &= -j(\beta'/k) 2\pi \sigma \frac{K_0}{2} \int_0^a r dr J_0(x) \quad // x = \beta'r \text{ so } xdx = \beta'^2 r dr \\
 &= -j(\beta'k)^{-1} 2\pi\sigma \frac{K_0}{2} \left[\int_0^{x_a} dx x J_0(x) \right] = -j(\beta'k)^{-1} 2\pi\sigma \frac{K_0}{2} [x_a J_1(x_a)] \quad // \text{GR7 5.52.1} \\
 &= -j(\beta'k)^{-1} 2\pi\sigma \left\{ (j\omega/\sigma) N_0 / J_1(x_a) \right\} [x_a J_1(x_a)] \quad // (D.2.28) \text{ for } \frac{K_0}{2} \\
 &= (\beta'k)^{-1} 2\pi\omega N_0 x_a = (\beta'k)^{-1} 2\pi\omega N_0 \beta'a \\
 &= 2\pi\omega (a/k) N_0
 \end{aligned}$$

so that

$$I = 2\pi\omega (a/k) N_0 \quad (D.2.31a)$$

$$N_0 = (k/2\pi\omega a) I \quad // I \text{ is called } i(z=0) \text{ in (4.9.2) so } I = i(0) \quad (D.2.31b)$$

From (D.1.8) we know that $N_0 = \langle n(\theta) \rangle = (1/2\pi a) q$ and since $q = CV$ we get the alternate form,

$$I = 2\pi a (\omega/k) N_0 = 2\pi a (\omega/k) (1/2\pi a) q = (\omega/k) CV \quad (D.2.31c)$$

It follows from (D.2.31b) that the normalization factor appearing in (D.2.28) may be written as

$$\begin{aligned}
 (j\omega/2\sigma) N_m &= (j\omega/2\sigma) \frac{N_m}{N_0} N_0 = (j\omega/2\sigma) \eta_m [(k/2\pi\omega a) I] = (j/4) \eta_m (ak/\sigma\pi a^2) I \\
 &= (j/4) (ak) \eta_m I R_{dc} \quad (D.2.32)
 \end{aligned}$$

We may now construct the final form for our E field solutions in (D.2.21) using the coefficients in (D.2.28) and the replacement (D.2.32) :

$$\begin{aligned}
 E_z(r,m) &= -j(\beta'/k) \frac{K_m}{2} J_m(x) = -j(\beta'/k) (j\omega/2\sigma) N_m \left[\frac{1}{J_{m+1}(x_a)} - \frac{1}{J_{m-1}(x_a)} \right] J_m(x) \\
 &= -j(\beta'/k) [(j/4) (ak) \eta_m I R_{dc}] \left[\frac{1}{J_{m+1}(x_a)} - \frac{1}{J_{m-1}(x_a)} \right] J_m(x)
 \end{aligned}$$

$$\begin{aligned}
 &= (1/4) \eta_m I R_{dc} (a\beta') \left[\frac{J_m(x)}{J_{m+1}(x_a)} - \frac{J_m(x)}{J_{m-1}(x_a)} \right] \\
 E_r(r,m) &= a_m x^{-1} J_m(x) + \frac{K_m}{2} J_{m+1}(x) \\
 &= [(j\omega/2\sigma) N_m] \left\{ 2m \frac{1}{J_{m-1}(x_a)} x^{-1} J_m(x) + \left[\frac{1}{J_{m+1}(x_a)} - \frac{1}{J_{m-1}(x_a)} \right] J_{m+1}(x) \right\} \\
 &= (j/4) (ak) \eta_m I R_{dc} \left\{ \frac{2mx^{-1}J_m(x)}{J_{m-1}(x_a)} + \frac{J_{m+1}(x)}{J_{m+1}(x_a)} - \frac{J_{m+1}(x)}{J_{m-1}(x_a)} \right\} \\
 &= (j/4) (ak) \eta_m I R_{dc} \left\{ \frac{J_{m+1}(x)}{J_{m+1}(x_a)} + \frac{J_{m-1}(x)}{J_{m-1}(x_a)} \right\}
 \end{aligned}$$

where in the last line we used the NIST (10.6.1) Bessel identity $(2m/x)J_m(x) = J_{m-1}(x) + J_{m+1}(x)$. Finally,

$$\begin{aligned}
 jE_\theta(r,m) &= -a_m x^{-1} J_m(x) + \left(\frac{K_m}{2} + \frac{a_m}{m} \right) J_{m+1}(x) \\
 &= [(j\omega/2\sigma) N_m] \left\{ -2m x^{-1} \frac{1}{J_{m-1}(x_a)} + \left[\frac{1}{J_{m+1}(x_a)} + \frac{1}{J_{m-1}(x_a)} \right] J_{m+1}(x) \right\} \\
 &= (j/4) (ak) \eta_m I R_{dc} \left\{ -\frac{2mx^{-1}J_m(x)}{J_{m-1}(x_a)} + \left[\frac{J_{m+1}(x)}{J_{m+1}(x_a)} + \frac{J_{m+1}(x)}{J_{m-1}(x_a)} \right] \right\} \\
 &= (j/4) (ak) \eta_m I R_{dc} \left\{ \frac{J_{m+1}(x)}{J_{m+1}(x_a)} - \frac{J_{m-1}(x)}{J_{m-1}(x_a)} \right\}
 \end{aligned}$$

Gathering up one more time:

Second summary of the E field solutions :	$R_{dc} = \frac{1}{\sigma\pi a^2} \quad \beta'^2 = \beta^2 - k^2$	(D.2.33)
$E_z(r,m) = (1/4) \eta_m I R_{dc} (a\beta') f_m$	$f_m = \left[\frac{J_m(x)}{J_{m+1}(x_a)} - \frac{J_m(x)}{J_{m-1}(x_a)} \right]$	$x = \beta'r$
$E_r(r,m) = (j/4) \eta_m I R_{dc} (ak) g_m$	$g_m = \left[\frac{J_{m+1}(x)}{J_{m+1}(x_a)} + \frac{J_{m-1}(x)}{J_{m-1}(x_a)} \right]$	$x_a = \beta'a$
$E_\theta(r,m) = (1/4) \eta_m I R_{dc} (ak) h_m$	$h_m = \left[\frac{J_{m+1}(x)}{J_{m+1}(x_a)} - \frac{J_{m-1}(x)}{J_{m-1}(x_a)} \right]$	

Maple verification of these solutions is shown below.

Observations about the solution:

(1) We looked for a traveling wave solution inside a round wire in which phase fronts propagate down the wire (z direction) with angular frequency ω and wavelength $\lambda = 2\pi/\text{Re}(k)$. We found the solution shown in the above box. This solution satisfies all three components of the vector Helmholtz equation (D.1.2) as well as the $\text{div } \mathbf{E} = 0$ equation.

(2) For a low-loss line one has $\xi \approx \sigma/(j\omega)$ and $\xi_{\mathbf{d}} \approx \epsilon_{\mathbf{d}}$. These are the complex dielectric "constants". The corresponding wavenumbers are then

$$\beta' \approx \beta = \omega \sqrt{\mu \xi} \approx \omega \sqrt{\mu \sigma/(j\omega)} = e^{j3\pi/4} \sqrt{\omega \mu \sigma} = e^{j3\pi/4} (\sqrt{2}/\delta) \quad (1.5.1c), (2.2.19), (2.2.21)$$

$$k = \beta_{\mathbf{d}} = \omega \sqrt{\mu_{\mathbf{d}} \xi_{\mathbf{d}}} \approx \omega \sqrt{\mu_{\mathbf{d}} \epsilon_{\mathbf{d}}} = \omega / v_{\mathbf{d}} = \beta_{\mathbf{d}0} \quad v_{\mathbf{d}} = \text{speed of light in the dielectric} \quad (D.2.34)$$

Thus, in our wave solution (D.1.1), the phase fronts propagate down the *inside* of the wire at $v_{\mathbf{d}}$, the speed of light in the dielectric *outside* the wire. Although we have been quiet about the fields outside the wire, it seems reasonable to presume there is a wave outside also moving down the wire at $v_{\mathbf{d}}$. See Section D.7.

(3) For r near a , where most of the action occurs due to the skin effect, the Bessel function ratios appearing in (D.2.33) are on the general order of unity so we expect the three brackets [...] to be of the same general size. It then follows that the E_r and E_{θ} fields are smaller than E_z by the ratio $|k/\beta'|$ which we have shown in the discussion below (D.2.2) is very small at frequencies below 100 GHz (lossless). Since E_z is an electric field inside copper, it is already itself quite small, so the E_r and E_{θ} fields are extremely small. This then justifies their omission from the development of Chapter 2.

(4) If there exist moments N_m of the surface charge distribution on the wire with $m > 1$, then the corresponding $\eta_m \neq 0$ and it is clear that $E_z(r, \theta)$ and hence $J_z(r, \theta)$ are non-uniform inside the wire. That is, these fields vary with θ as $\cos(m\theta)$ as well as with r . The non-uniformity is not "small" but has the full strength of η_m . Of course we only expect to get significant moments of charge density $n(\theta)$ when conductors are "fat and close". See (6.5.4) for the special case of both conductors being round wires, and then Section 6 (b) for more on this "proximity effect".

(5) The surface impedance from (C.2.1) is just $Z_s(\theta) = E_z(r=a, \theta)/I$. Thus, from (D.1.3a),

$$Z_s(\theta) = (1/I) \sum_{m=-\infty}^{\infty} E_z(a, m) e^{jm\theta} \quad // (D.1.3a)$$

$$= (1/4) R_{\mathbf{dc}} \sum_{m=-\infty}^{\infty} \eta_m \left[\frac{x_a J_m(x_a)}{J_{m+1}(x_a)} - \frac{x_a J_m(x_a)}{J_{m-1}(x_a)} \right] e^{jm\theta} \quad // (D.2.33) \quad x_a = \beta' a$$

where,

$$\eta_m = N_m/N_0 = \frac{\omega a}{kI} \int_{-\pi}^{\pi} d\theta n(\theta) e^{-jm\theta} \quad // (D.1.5b) \text{ and } (D.2.31b) \quad (D.2.35)$$

Thus we see the expected non-uniformity of $Z_z(\theta)$ around the perimeter of the wire cross section due to the $m \neq 0$ surface charge components. $Z_z(\theta)$ is larger where $J_z(a, \theta)$ is larger.

Maple verification of box (D.2.33)

We use the same method illustrated below box (D.2.21). The same expressions e1,e2,e3,e4 are entered as the left sides of the four equations whose right sides we expect to be 0. Then:

Enter the claimed E field solutions from box (D.2.33)

```
Ez := C*xa*(J(m,x)/J(m+1,xa) - J(m,x)/J(m-1,xa));
```

$$E_z = C \, x a \left(\frac{J(m, x)}{J(m+1, x a)} - \frac{J(m, x)}{J(m-1, x a)} \right)$$

```
Er := C*j*(a*k)*(J(m+1,x)/J(m+1,xa) + J(m-1,x)/J(m-1,xa));
```

$$E_r = j \, C \, a \, k \left(\frac{J(m+1, x)}{J(m+1, x a)} + \frac{J(m-1, x)}{J(m-1, x a)} \right)$$

```
Ephi := C*(a*k)*(J(m+1,x)/J(m+1,xa) - J(m-1,x)/J(m-1,xa));
```

$$E_{\phi} = C \, a \, k \left(\frac{J(m+1, x)}{J(m+1, x a)} - \frac{J(m-1, x)}{J(m-1, x a)} \right)$$

```
x := bp*r: xa := bp*a: set x and xa
```

```
C := (1/4)*(Nm/NO)*I*Rdc;
```

$$C = \frac{1}{4} \frac{Nm \, I \, Rdc}{NO}$$

Show that each left side evaluates to zero as box (D.1.20) requires

```
> value(e1): simplify(%);
0
> value(e2): simplify(%);
0
> value(e3): simplify(%);
0
> value(e4): simplify(%);
0
```

Now check the boundary conditions

```
I := (2*Pi*omega*a/k)*NO: # (D.2.31)
```

```
Rdc := 1/(sigma*Pi*a^2):
```

```
eval(Er,r=a): # compare (D.2.26)
```

$$\frac{j \, Nm \, \omega}{\sigma}$$

```
eval(Ephi,r=a): # compare (D.2.27)
```

0

D.3 What about the E_θ Helmholtz Equation ?

A review of the above derivation of the three fields E_z , E_x and E_θ shows that the E_θ Helmholtz equation has been completely ignored. The E_θ expression was obtained from the $\text{div } \mathbf{E} = 0$ equation after the E_z and E_x fields were computed.

It is reasonable to wonder whether the solution fields found above in fact solve this θ Helmholtz equation which mixes the E_x and E_θ fields together in a manner similar to the r Helmholtz equation.

A related question is whether the three Helmholtz equations and $\text{div } \mathbf{E} = 0$ are four independent equations, or is one of the three Helmholtz equations dependent? In Cartesian coordinates suppose we know that (implied sums on repeated indices)

$$\begin{aligned} (\partial_j \partial_j + \beta^2) E_1 &= 0 \\ (\partial_j \partial_j + \beta^2) E_2 &= 0 \\ \partial_i E_i &= 0 \quad // \text{div } \mathbf{E} = 0 \end{aligned} \tag{D.3.1}$$

Can we show that $(\partial_j \partial_j + \beta^2) E_3 = 0$ so this third Helmholtz equation is dependent? Applying the operator $(\partial_j \partial_j + \beta^2)$ to the last equation above one gets

$$\begin{aligned} (\partial_j \partial_j + \beta^2) \partial_i E_i &= 0 \\ \text{or} \\ \partial_i (\partial_j \partial_j + \beta^2) E_i &= 0 \\ \text{or} \\ \partial_1 (\partial_j \partial_j + \beta^2) E_1 + \partial_2 (\partial_j \partial_j + \beta^2) E_2 + \partial_3 (\partial_j \partial_j + \beta^2) E_3 &= 0 \\ \text{or} \\ \partial_3 [(\partial_j \partial_j + \beta^2) E_3] &= 0 \end{aligned} \tag{D.3.2}$$

This does not prove that $(\partial_j \partial_j + \beta^2) E_3 = 0$ since $(\partial_j \partial_j + \beta^2) E_3 = f(x_1, x_2) \neq 0$ also satisfies (D.3.2).

Rather than pursue this question further, we simply note that the Maple code below box (D.2.21) verifies that the E field solutions given in that box do indeed satisfy the θ Helmholtz equation (as well as the other two Helmholtz equations and the $\text{div } \mathbf{E} = 0$ equation).

Reader Exercise: Come up with some reason that this had to be the case.

D.4 Computation of the \mathbf{B} fields in the round wire

The \mathbf{B} field components may be computed from the Maxwell curl \mathbf{E} equation (1.1.2),

$$-\partial_t \mathbf{B} = \text{curl } \mathbf{E} \quad \text{Maxwell curl E equation} \quad (1.1.2) \quad (\text{D.4.1})$$

In cylindrical coordinates one has from (D.1.14),

$$\text{curl } \mathbf{E} = \hat{\mathbf{r}} [r^{-1} \partial_\theta E_z - \partial_z E_\theta] + \hat{\boldsymbol{\theta}} [\partial_z E_r - \partial_r E_z] + \hat{\mathbf{z}} [r^{-1} \partial_r (r E_\theta) - r^{-1} \partial_\theta E_r] \quad (\text{D.4.2})$$

where the fields are of the traveling wave form shown in (D.1.1) which we assume also for the \mathbf{B} field. Thus, combining (D.1.1) with (D.1.3a), one has

$$\mathbf{E}(r, \theta, z, t) = e^{j(\omega t - \mathbf{kz})} \mathbf{E}(r, \theta) = e^{j(\omega t - \mathbf{kz})} \sum_{m=-\infty}^{\infty} \mathbf{E}(r, m) e^{jm\theta} \quad (\text{D.4.3})$$

$$\mathbf{B}(r, \theta, z, t) = e^{j(\omega t - \mathbf{kz})} \mathbf{B}(r, \theta) = e^{j(\omega t - \mathbf{kz})} \sum_{m=-\infty}^{\infty} \mathbf{B}(r, m) e^{jm\theta} \quad (\text{D.4.4})$$

Inserting the three cylindrical components of the \mathbf{E} expansion (D.4.3) into (D.4.2), one finds that these replacements may be made,

$$\partial_t \rightarrow +j\omega \quad \partial_z \rightarrow -jk \quad \partial_\theta \rightarrow +jm \quad (\text{D.4.5})$$

Similarly, inserting the \mathbf{B} expansion (D.4.4) into $-\partial_t \mathbf{B}$ one may replace $\partial_t \rightarrow +j\omega$. After doing this, both sides of (D.4.1) are expansions having the general form of (D.4.3) and one may then equate terms in the m sum [completeness of the $e^{jm\theta}$ on $(-\pi, \pi)$] to find that

$$-j\omega \mathbf{B}(r, m) = \hat{\mathbf{r}} [r^{-1} jm E_z + jk E_\theta] + \hat{\boldsymbol{\theta}} [-jk E_r - \partial_r E_z] + \hat{\mathbf{z}} [r^{-1} \partial_r (r E_\theta) - r^{-1} jm E_r] \quad (\text{D.4.6})$$

and this then gives the three partial wave components of the \mathbf{B} field

$$B_r(r, m) = (j/\omega) [\text{curl } \mathbf{E}]_r = (j/\omega) [r^{-1} jm E_z + jk E_\theta]$$

$$B_\theta(r, m) = (j/\omega) [\text{curl } \mathbf{E}]_\theta = (j/\omega) [-jk E_r - \partial_r E_z]$$

$$B_z(r, m) = (j/\omega) [\text{curl } \mathbf{E}]_z = (j/\omega) [r^{-1} \partial_r (r E_\theta) - r^{-1} jm E_r] \quad (\text{D.4.7})$$

It is now a simple task to insert into these B_i expressions the E_i field components from box (D.2.33),

Second summary of the E field solutions :	$R_{dc} = \frac{1}{\sigma\pi a^2} \quad \beta'^2 = \beta^2 - k^2$	(D.2.33)
$E_z(r,m) = (1/4) \eta_m I R_{dc} (a\beta') f_m$	$f_m = \left[\frac{J_m(x)}{J_{m+1}(x_a)} - \frac{J_m(x)}{J_{m-1}(x_a)} \right]$	$x = \beta'r$
$E_r(r,m) = (j/4) \eta_m I R_{dc} (ak) g_m$	$g_m = \left[\frac{J_{m+1}(x)}{J_{m+1}(x_a)} + \frac{J_{m-1}(x)}{J_{m-1}(x_a)} \right]$	$x_a = \beta'a$
$E_\theta(r,m) = (1/4) \eta_m I R_{dc} (ak) h_m$	$h_m = \left[\frac{J_{m+1}(x)}{J_{m+1}(x_a)} - \frac{J_{m-1}(x)}{J_{m-1}(x_a)} \right]$	

We have carried out this task manually to obtain the following results (which will be verified below),

$$\begin{aligned}
 B_r(r,m) &= -(1/4) (a/\omega) \eta_m I R_{dc} (r^{-1}m (\beta') f_m + k^2 h_m) \\
 B_\theta(r,m) &= (j/4)(a/\omega) \eta_m I R_{dc} (k^2 g_m - \beta'^2 f_m [(m/x) - J_{m+1}(x)/J_m(x)]) \\
 B_z(r,m) &= (j/4)(a/\omega) \eta_m I R_{dc} (k \beta' e_m) .
 \end{aligned} \tag{D.4.8}$$

Here the f_m , g_m and h_m are the same functions appearing in the box above, and the new function e_m is

$$e_m \equiv \left[\frac{J_m(x)}{J_{m+1}(x_a)} + \frac{J_m(x)}{J_{m-1}(x_a)} \right] . \tag{D.4.9}$$

Notice that the E_i and B_i fields all have the common factor $[(1/4) \eta_m I R_{dc} a]$. For purposes of *verifying* the B_i expressions above, we shall set this factor to 1 everywhere to obtain these scaled fields,

$$\begin{aligned}
 E_z(r,m) &= \beta' f_m \\
 E_r(r,m) &= j k g_m \\
 E_\theta(r,m) &= k h_m \\
 B_r(r,m) &= -(1/\omega) (r^{-1}m (\beta') f_m + k^2 h_m) \\
 B_\theta(r,m) &= j (1/\omega) (k^2 g_m - \beta'^2 f_m [(m/x) - J_{m+1}(x)/J_m(x)]) \\
 B_z(r,m) &= j (1/\omega) (k \beta' e_m) .
 \end{aligned} \tag{D.4.10}$$

To verify that $-j\omega\mathbf{B} = \text{curl } \mathbf{E}$ for the above set of fields, we shall check these three equations

$$-j\omega B_i = [\text{curl } \mathbf{E}]_i \quad ? \quad i = r, \theta, z \tag{D.4.11}$$

where from above

$$\begin{aligned}
 [\text{curl } \mathbf{E}]_r &= [r^{-1}j m E_z + j k E_\theta] \\
 [\text{curl } \mathbf{E}]_\theta &= [-j k E_r - \partial_r E_z] \\
 [\text{curl } \mathbf{E}]_z &= [r^{-1} \partial_r (r E_\theta) - r^{-1} j m E_r] .
 \end{aligned} \tag{D.4.12}$$

We start by entering these three curl expressions into Maple,

```
restart; alias(I=I, j=sqrt(-1), J=BesselJ):
```

Enter the curlE expressions

```
curlEr := (j*m/r)*Ez + j*k*Eth;
```

$$\text{curlEr} := \frac{j m E_z}{r} + j k E_{th}$$

```
curlEth := -j*k*Er - Diff(Ez,r);
```

$$\text{curlEth} := -j k E_r - \left(\frac{\partial}{\partial r} E_z \right)$$

```
curlEz := (1/r)*( Diff(r*Eth,r) - j*m*Er);
```

$$\text{curlEz} := \frac{\left(\frac{\partial}{\partial r} r E_{th} \right) - j m E_r}{r}$$

followed by the scaled B and E field expressions from (D.4.10) above,

Enter the B expressions

```
Br := -(1/omega)*( (m*bp*f/r) + k^2*h );
```

$$B_r := - \frac{\frac{m b p f}{r} + k^2 h}{\omega}$$

```
Bth := (j/omega)*(k^2*g - bp^2*f*(m/x - J(m+1,x)/J(m,x)));
```

$$B_{th} := \frac{j \left(k^2 g - b p^2 f \left(\frac{m}{x} - \frac{J(m+1, x)}{J(m, x)} \right) \right)}{\omega}$$

```
Bz := (j/omega)*k*bp*e;
```

$$B_z := \frac{j k b p e}{\omega}$$

Enter the E field expressions

```
Ez := bp*f;
```

$$E_z := b p f$$

```
Er := j*k*g;
```

$$E_r := j k g$$

```
Eth := k*h;
```

$$E_{th} := k h$$

Next come the various supporting functions,

Enter the supporting functions

$$e := J(m, x) / J(m+1, xa) + J(m, x) / J(m-1, xa);$$

$$e = \frac{J(m, x)}{J(m+1, xa)} + \frac{J(m, x)}{J(m-1, xa)}$$

$$f := J(m, x) / J(m+1, xa) - J(m, x) / J(m-1, xa);$$

$$f = \frac{J(m, x)}{J(m+1, xa)} - \frac{J(m, x)}{J(m-1, xa)}$$

$$g := J(m+1, x) / J(m+1, xa) + J(m-1, x) / J(m-1, xa);$$

$$g = \frac{J(m+1, x)}{J(m+1, xa)} + \frac{J(m-1, x)}{J(m-1, xa)}$$

$$h := J(m+1, x) / J(m+1, xa) - J(m-1, x) / J(m-1, xa);$$

$$h = \frac{J(m+1, x)}{J(m+1, xa)} - \frac{J(m-1, x)}{J(m-1, xa)}$$

$$x := bp * r;$$

$$x = bp r$$

$$xa := bp * a;$$

$$xa = bp a$$

Taking the precautions noted in the "Maple Comment" below (D.2.21), we now verify (D.4.11) that $-j\omega B_i = [\text{curl } E]_i$:

$$-j * \omega * B_r - \text{curl } E_r: \text{ simplify}(\%);$$

0

$$-j * \omega * B_{\theta} - \text{value}(\text{curl } E_{\theta}): \text{ simplify}(\%);$$

0

$$-j * \omega * B_z - \text{value}(\text{curl } E_z): \text{ simplify}(\%);$$

0

Here then is a summary of all the E and B field results in a single box

Summary of E and B fields inside a round wire		(D.4.13)
$E_z(r, m) = (1/4) \eta_m I R_{dc} (a\beta') f_m$ $E_r(r, m) = (j/4) \eta_m I R_{dc} (ak) g_m$ $E_{\theta}(r, m) = (1/4) \eta_m I R_{dc} (ak) h_m$	$x = \beta'r$	$x_a = \beta'a$
$\beta'^2 = \beta^2 - k^2$		
$B_z(r, m) = (j/4) (a/\omega) \eta_m I R_{dc} (k \beta' e_m)$ $B_r(r, m) = - (1/4) (a/\omega) \eta_m I R_{dc} (r^{-1} m \beta' f_m + k^2 h_m)$ $B_{\theta}(r, m) = (j/4) (a/\omega) \eta_m I R_{dc} (k^2 g_m - \beta'^2 f_m [(m/x) - J_{m+1}(x)/J_m(x)])$		
$e_m = \left[\frac{J_m(x)}{J_{m+1}(x_a)} + \frac{J_m(x)}{J_{m-1}(x_a)} \right]$	$g_m = \left[\frac{J_{m+1}(x)}{J_{m+1}(x_a)} + \frac{J_{m-1}(x)}{J_{m-1}(x_a)} \right]$	$R_{dc} = \frac{1}{\sigma \pi a^2}$
$f_m = \left[\frac{J_m(x)}{J_{m+1}(x_a)} - \frac{J_m(x)}{J_{m-1}(x_a)} \right]$	$h_m = \left[\frac{J_{m+1}(x)}{J_{m+1}(x_a)} - \frac{J_{m-1}(x)}{J_{m-1}(x_a)} \right]$	

D.5 Verification that the E and B fields satisfy the Maxwell equations

We already know that the Maxwell curl E equation is satisfied, since it was used in the previous section to derive the B fields. As for the other three Maxwell equations, we expect to find that

$$\begin{aligned}
 \operatorname{div} \mathbf{B} &= 0 && // \text{ since } \mathbf{B} = (1/j\omega) \operatorname{curl} \mathbf{E} \text{ so } \operatorname{div} \mathbf{B} = (1/j\omega) \operatorname{div} \operatorname{curl} \mathbf{E} = 0 \\
 \operatorname{div} \mathbf{E} &= 0 && // \text{ no free charge inside conductor} \\
 \operatorname{curl} \mathbf{B} &= \mu \mathbf{J} + \mu j\omega \epsilon \mathbf{E} = \mu(\sigma + j\omega \epsilon) \mathbf{E} = \mu(j\omega)(\epsilon - j\sigma/\omega) \mathbf{E} = j\omega \mu \xi \mathbf{E} && \text{(D.5.1)} \\
 &= j(\beta^2/\omega) \mathbf{E} \quad . && // \text{ see (1.5.1c)}
 \end{aligned}$$

In cylindrical coordinates the curl and div operators are, from (D.1.14),

$$\begin{aligned}
 \operatorname{curl} \mathbf{B} &= \hat{\mathbf{r}} [r^{-1} \partial_{\theta} B_z - \partial_z B_{\theta}] + \hat{\boldsymbol{\theta}} [\partial_z B_r - \partial_r B_z] + \hat{\mathbf{z}} [r^{-1} \partial_r (r B_{\theta}) - r^{-1} \partial_{\theta} B_r] \\
 \operatorname{div} \mathbf{B} &= r^{-1} \partial_r (r B_r) + r^{-1} \partial_{\theta} B_{\theta} + \partial_z B_z && \text{(D.5.2)}
 \end{aligned}$$

Using $\partial_z \rightarrow -jk$ and $\partial_{\theta} \rightarrow jm$ we can write these in m space as

$$\begin{aligned}
 \operatorname{curl} \mathbf{B}(r,m) &= \hat{\mathbf{r}} [r^{-1} jm B_z + jk B_{\theta}] + \hat{\boldsymbol{\theta}} [-jk B_r - \partial_r B_z] + \hat{\mathbf{z}} [r^{-1} \partial_r (r B_{\theta}) - r^{-1} jm B_r] \\
 \operatorname{div} \mathbf{B}(r,m) &= r^{-1} \partial_r (r B_r) + r^{-1} jm B_{\theta} - jk B_z \quad . && \text{(D.5.3)}
 \end{aligned}$$

We continue the Maple code of the previous section to verify that the other three Maxwell equations are satisfied:

Show that $\operatorname{div} \mathbf{B} = 0$

```
divB := (1/r)*diff(r*Br,r)+(1/r)*j*m*Bth-j*k*Bz: simplify(%);
0
```

Show that $\operatorname{div} \mathbf{E} = 0$

```
divE := (1/r)*diff(r*Er,r)+(1/r)*j*m*Eth-j*k*Ez: simplify(%);
0
```

Compute components of curl B

```
curlBr := (1/r)*j*m*Bz + j*k*Bth:
curlBth := -j*k*Br - diff(Bz,r):
curlBz := (1/r)*diff(r*Bth,r) - (1/r)*j*m*Br:
b := sqrt(bp^2+k^2): set in beta here called b
```

One component at a time, show that the curl B Maxwell equation is satisfied

```
curlBz - (j/omega)*b^2*Ez: simplify(%);
0
curlBr - (j/omega)*b^2*Er: simplify(%);
0
curlBth - (j/omega)*b^2*Eth: simplify(%);
0
```

The reader is again referred to the "Maple Comment" below (D.2.21). The expressions on the three last lines prior to simplification are quite complicated, for example

$$\begin{aligned}
 & > \text{curlBz} - (j/\omega) * b^2 * Ez; \text{simplify}(\%); \\
 & \left(\frac{j \left(k^2 \left(\frac{J(m+1, bpr)}{J(m+1, bpa)} + \frac{J(m-1, bpr)}{J(m-1, bpa)} \right) - bp^2 \left(\frac{J(m, bpr)}{J(m+1, bpa)} - \frac{J(m, bpr)}{J(m-1, bpa)} \right) \left(\frac{m}{bpr} - \frac{J(m+1, bpr)}{J(m, bpr)} \right) \right)}{\omega} + jr \left(\frac{J(m, bpr) - \frac{(m+1)J(m+1, bpr)}{bpr}}{J(m+1, bpa)} + \frac{\left(-J(m, bpr) + \frac{(m-1)J(m-1, bpr)}{bpr} \right) bp}{J(m-1, bpa)} \right) \right. \\
 & - bp^2 \left(\frac{\left(-J(m+1, bpr) + \frac{mJ(m, bpr)}{bpr} \right) bp}{J(m+1, bpa)} - \frac{\left(-J(m+1, bpr) + \frac{mJ(m, bpr)}{bpr} \right) bp}{J(m-1, bpa)} \right) \left(\frac{m}{bpr} - \frac{J(m+1, bpr)}{J(m, bpr)} \right) \\
 & \left. - bp^2 \left(\frac{J(m, bpr)}{J(m+1, bpa)} - \frac{J(m, bpr)}{J(m-1, bpa)} \right) \left(-\frac{m}{bpr^2} - \frac{\left(J(m, bpr) - \frac{(m+1)J(m+1, bpr)}{bpr} \right) bp}{J(m, bpr)} + \frac{J(m+1, bpr) \left(-J(m+1, bpr) + \frac{mJ(m, bpr)}{bpr} \right) bp}{J(m, bpr)^2} \right) \right) / \omega \\
 & \left. \right) / r + \frac{j m \left(\frac{J(m, bpr)}{J(m+1, bpa)} - \frac{J(m, bpr)}{J(m-1, bpa)} \right)}{r \omega} + k^2 \left(\frac{J(m+1, bpr)}{J(m+1, bpa)} - \frac{J(m-1, bpr)}{J(m-1, bpa)} \right) - \frac{j (bp^2 + k^2) bp \left(\frac{J(m, bpr)}{J(m+1, bpa)} - \frac{J(m, bpr)}{J(m-1, bpa)} \right)}{\omega}
 \end{aligned}$$

No approximations were made in the E fields, the B fields, or in these Maxwell verifications.

D.6 The exact E and B fields for the m=0 partial wave

The m=0 partial wave is all there is for an axially symmetric problem like that considered in Chapter 2, where the round wire is imagined in isolation, but is operationally the central conductor of a coaxial cable with a very distant return cylinder (outer shield). Here is the reduction of box (D.4.13) for m = 0:

$$\begin{aligned}
 e_0 &= \left[\frac{J_0(x)}{J_1(x_a)} + \frac{J_0(x)}{J_{-1}(x_a)} \right] = \left[\frac{J_0(x)}{J_1(x_a)} - \frac{J_0(x)}{J_1(x_a)} \right] = 0 \\
 f_0 &= \left[\frac{J_0(x)}{J_1(x_a)} - \frac{J_0(x)}{J_{-1}(x_a)} \right] = \left[\frac{J_0(x)}{J_1(x_a)} + \frac{J_0(x)}{J_1(x_a)} \right] = 2 \frac{J_0(x)}{J_1(x_a)} \\
 g_0 &= \left[\frac{J_1(x)}{J_1(x_a)} + \frac{J_{-1}(x)}{J_{-1}(x_a)} \right] = \left[\frac{J_1(x)}{J_1(x_a)} + \frac{J_1(x)}{J_1(x_a)} \right] = 2 \frac{J_1(x)}{J_1(x_a)} \\
 h_0 &= \left[\frac{J_1(x)}{J_1(x_a)} - \frac{J_{-1}(x)}{J_{-1}(x_a)} \right] = \left[\frac{J_1(x)}{J_1(x_a)} - \frac{J_1(x)}{J_1(x_a)} \right] = 0
 \end{aligned} \tag{D.6.1}$$

$$E_z(r,0) = (1/4) I R_{dc} (a\beta') f_0 = (1/4) I R_{dc} (a\beta') 2 \frac{J_0(x)}{J_1(x_a)}$$

$$E_r(r,0) = (j/4) I R_{dc} (ak) g_0 = (j/4) I R_{dc} (ak) 2 \frac{J_1(x)}{J_1(x_a)}$$

$$E_\theta(r,0) = (1/4) I R_{dc} (ak) h_0 = 0$$

$$B_z(r,0) = (j/4) (a/\omega) I R_{dc} (k\beta' e_0) = 0$$

$$B_r(r,0) = -(1/4) (a/\omega) I R_{dc} (k^2 h_0) = 0$$

$$\begin{aligned}
 B_{\theta}(r,0) &= (j/4) (a/\omega) I R_{dc} (k^2 g_0 + \beta'^2 f_0 [J_1(x)/J_0(x)]) \\
 &= (j/4) (a/\omega) I R_{dc} (k^2 2 \frac{J_1(x)}{J_1(x_a)} + \beta'^2 2 \frac{J_0(x)}{J_1(x_a)} [J_1(x)/J_0(x)]) \\
 &= (j/4) (a/\omega) I R_{dc} (k^2 2 \frac{J_1(x)}{J_1(x_a)} + \beta'^2 2 \frac{J_1(x)}{J_1(x_a)}) \\
 &= (j/4) (a/\omega) I R_{dc} (k^2 + \beta'^2) 2 \frac{J_1(x)}{J_1(x_a)} \\
 &= (j/4) (a/\omega) I R_{dc} \beta'^2 2 \frac{J_1(x)}{J_1(x_a)} \quad // \beta'^2 = \beta^2 - k^2 \tag{D.6.2}
 \end{aligned}$$

The results then are

Summary of E and B fields inside a round wire (m = 0 only)		(D.6.3)
$E_z(r,0) = (1/2) I R_{dc} (a\beta') \frac{J_0(x)}{J_1(x_a)}$	$B_z(r,0) = 0$	$x = \beta'r \quad x_a = \beta'a$
$E_r(r,0) = (j/2) I R_{dc} (ak) \frac{J_1(x)}{J_1(x_a)}$	$B_r(r,0) = 0$	$R_{dc} = \frac{1}{\sigma\pi a^2}$
$E_{\theta}(r,0) = 0$	$B_{\theta}(r,0) = (j/2) (a/\omega) I R_{dc} \beta'^2 \frac{J_1(x)}{J_1(x_a)}$	

For a low-loss transmission line $k \approx \beta_{d0} = \omega/v_d$. As implied by the comments below (D.2.2), in this situation one has $k \ll |\beta|$ and thus also $k \ll |\beta'|$. Ignoring the difference between J_0 and J_1 in scale, (D.6.3) shows that $|E_r / E_z| \sim |k/\beta'| \ll 1$ so the E_r field is very small and E_z is the main electric field. For such a transmission line one has,

$$\begin{aligned}
 E_z(r,0) &= (1/2) I R_{dc} (a\beta) \frac{J_0(x)}{J_1(x_a)} = (\omega/\beta) [(1/2) (a\beta^2/\omega) I R_{dc}] \frac{J_0(x)}{J_1(x_a)} \\
 B_{\theta}(r,0) &\approx (j/2) (a/\omega) I R_{dc} \beta'^2 \frac{J_1(x)}{J_1(x_a)} = j [(1/2) (a\beta^2/\omega) I R_{dc}] \frac{J_1(x)}{J_1(x_a)} \tag{D.6.4}
 \end{aligned}$$

where on the right we have rewritten the expressions in a seemingly obscure manner. As shown in (2.2.3), $\beta^2/\omega \approx -j\mu\sigma$ so that

$$[(1/2) (a\beta^2/\omega) I R_{dc}] = (1/2) a (-j\mu\sigma) I \frac{1}{\sigma\pi a^2} = -j \frac{\mu I}{2\pi a} \tag{D.6.5}$$

Since this is the bracket appearing in both field expressions in (D.6.4), we find that

$$\begin{aligned}
 E_z(r,0) &= (\omega/\beta) [-j \frac{\mu I}{2\pi a}] \frac{J_0(x)}{J_1(x_a)} = -j (\omega/\beta) \frac{\mu I}{2\pi a} \frac{J_0(x)}{J_1(x_a)} \\
 B_{\theta}(r,0) &= j [-j \frac{\mu I}{2\pi a}] \frac{J_1(x)}{J_1(x_a)} = \frac{\mu I}{2\pi a} \frac{J_1(x)}{J_1(x_a)} \tag{D.6.6}
 \end{aligned}$$

These results are in agreement with $E(r)$ and $B(r)$ shown in summary box (2.2.30) from the Chapter 2 calculation where we assumed $\mathbf{E} = E(r) \hat{z}$ and $\mathbf{B} = B(r) \hat{\theta}$.

D.7 What about the E fields *outside* the round wire?

The E field Helmholtz equation (D.1.2) outside the wire contains β_a instead of β . If we assume perfect conductors, then $k = \beta_a$ as well in (D.1.1). This means that

$$\beta'^2 = \beta_a'^2 - \beta_a^2 = 0.$$

We can then translate box (D.1.20) by replacing $\beta'^2 - k^2 \rightarrow 0$ and $\beta^2 \rightarrow k^2 = \beta_a^2$ to get the following "exterior" versions: (Note that $\nabla^2 = \nabla_{2D}^2 + \partial_z^2$)

$$\begin{aligned} [\nabla^2 \mathbf{E}]_z + k^2 E_z = 0 : & \quad // [\nabla_{2D}^2 \mathbf{E}]_z = 0 \\ [r^2 \partial_r^2 + r \partial_r - m^2] E_z(r,m) = 0 & \quad (D.1.15)_{\text{ext}} \end{aligned}$$

$$\begin{aligned} [\nabla^2 \mathbf{E}]_r + k^2 E_r = 0 : & \quad // [\nabla_{2D}^2 \mathbf{E}]_r = 0 \\ [r^2 \partial_r^2 + r \partial_r - (m^2+1)] E_r(r,m) - 2jm E_\theta(r,m) = 0 & \quad (D.1.17)_{\text{ext}} \end{aligned}$$

$$\begin{aligned} [\nabla^2 \mathbf{E}]_\theta + k^2 E_\theta = 0 : & \quad // [\nabla_{2D}^2 \mathbf{E}]_\theta = 0 \\ [r^2 \partial_r^2 + r \partial_r - (m^2+1)] E_\theta(r,m) + 2jm E_r(r,m) = 0 & \quad (D.1.18)_{\text{ext}} \end{aligned}$$

$$\begin{aligned} \text{div } \mathbf{E} = 0 : & \\ \partial_r [r E_r(r,m)] + jm E_\theta(r,m) - j k r E_z(r,m) = 0 & \quad (D.1.19)_{\text{ext}} \end{aligned}$$

The differential operators appearing in the above equations are no longer Bessel-style operators, they are Euler-style operators. Euler ODEs have the general form $[r^2 \partial_r^2 + a r \partial_r + b] f(r) = 0$, and the solutions have this form (from p 45 of Polyanin's excellent ODE compendium, or just use Maple),

$$118. \quad x^2 y''_{xx} + ax y'_x + by = 0.$$

The Euler equation.

Solution:

$$y = \begin{cases} |x|^{\frac{1-a}{2}} (C_1 |x|^\mu + C_2 |x|^{-\mu}) & \text{if } (1-a)^2 > 4b, \\ |x|^{\frac{1-a}{2}} (C_1 + C_2 \ln |x|) & \text{if } (1-a)^2 = 4b, \\ |x|^{\frac{1-a}{2}} [C_1 \sin(\mu \ln |x|) + C_2 \cos(\mu \ln |x|)] & \text{if } (1-a)^2 < 4b, \end{cases}$$

$$\text{where } \mu = \frac{1}{2} |(1-a)^2 - 4b|^{1/2}.$$

For $E_z(r,m)$ the equation (D.1.15)_{ext} shown just above is in fact an Euler equation which has $a = 1$ and $b = -m^2$ so $\mu = m$ and the solution forms are these ($r \geq a$ outside the wire),

$$\begin{aligned} E_z(r,m) &= A_m r^m + B_m r^{-m} & m > 0 \\ E_z(r,0) &= C_z \ln(r) + D_z & m = 0 \end{aligned} \quad (D.7.1)$$

Since z is a Cartesian coordinate, $[\nabla_{2D}^2 \mathbf{E}]_z = 0$ is the same as $\nabla_{2D}^2 E_z = 0$ which is just the 2D Laplace equation. When this equation is solved in polar coordinates (r, θ) , one finds $E_z = E_z(r, m) e^{jm\theta}$ and the expressions shown above are the standard atomic forms for the radial function. See for example Stakgold Vol II p 92 (6.7) and following discussion.

We can mimic our interior solution method presented in Section D.2 above, using the $\text{div } \mathbf{E} = 0$ equation to eliminate E_θ , and eventually end up with expressions for the three field components outside the wire. For $m > 1$ the general form for the exterior solution is found to be,

$$\begin{aligned} E_z(r, m) &= A_m r^m + B_m r^{-m} \\ E_r(r, m) &= -(jk/2) \frac{1}{m-1} B_m r^{1-m} - 2jk \frac{1}{m^2-1} A_m r^{1+m} + C_m r^{m-1} + D_m r^{-m-1} \\ jE_\theta(r, m) &= (jk/2) \frac{1}{m-1} B_m r^{1-m} + jk \frac{m^2+2m+3}{m(m^2-1)} A_m r^{1+m} - C_m r^{m-1} + D_m r^{-m-1} \end{aligned} \quad (\text{D.7.2})$$

where there are now four constants A_m , B_m , C_m and D_m to be determined in each partial wave. One could match the three E-field boundary conditions at $r = a$ as per (1.1.51) (subscript d means dielectric)

$$\begin{aligned} E_z(a, m) &= E_{zd}(a, m) \\ \xi E_r(a, m) &= \xi_d E_{rd}(a, m) \\ jE_\theta(a, m) &= jE_{\theta d}(a, m) \end{aligned} \quad (\text{D.7.3})$$

using the interior solutions shown in (D.2.33) where $E_\theta(a, m) = 0$. This gives 3 conditions on the 4 unknown constants so these boundary conditions can be met.

The *problem* with this exterior solution method is that more information is needed to solve the problem. The "Smythian Form" solution (D.7.2) is fine, but it only applies inside a thick cylindrical shell (blue) whose inner diameter is $r = a$ and whose outer diameter is $r = b$, where b causes this shell to touch the nearest other conductor, as illustrated here,

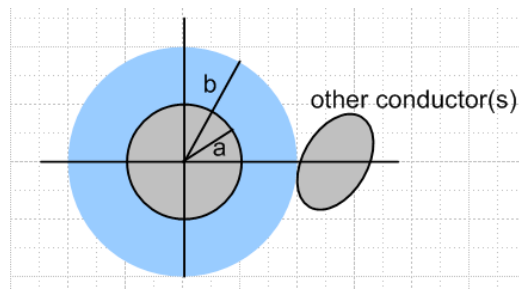


Fig D.3

The reason is that the dielectric E-field wave (Helmholtz) equation is not valid inside the "other conductor", so the form (D.7.2) cannot apply in a region which includes any of this other conductor. Since the blue shell region does not include $r = \infty$, one cannot rule out coefficients like A_m and C_m . One is now stuck worrying about boundary conditions at $r = b$ and the whole problem becomes intractable. But if one could find the complete exact exterior solution, one would find that inside the blue cylindrical shell the solution's partial wave fields would have the form shown in (D.7.2).

Reader Exercise:

(a) Verify (D.7.2).

(b) In Chapter 6 a transmission line with two round conductors is solved "exactly". Convert the solution to a coordinate system like that shown above, compute the $E_i(r,m)$ using (D.1.3b), and verify that these E_i field components fit into the form shown in (D.7.2).

D.8 About the boundary condition $E_\theta(a,m) = 0$

We start with a quick review.

In earlier sections of this Appendix we examined the electric field inside a round wire (radius a) which was regarded as a conductor in an infinite straight transmission line. The electric field was assumed to have the form of a longitudinal wave traveling down the conductor,

$$\mathbf{E}(r,\theta,z,t) = e^{j(\omega t - kz)} \mathbf{E}(r,\theta), \quad (D.1.1)$$

where k is the wavenumber parameter of the surrounding dielectric medium. We expanded the function $\mathbf{E}(r,\theta)$ onto azimuthal partial waves $e^{jm\theta}$ and solved the Helmholtz wave equation inside the wire with solutions as shown in box (D.2.21),

$$E_z(r,m) = -j(\beta'/k) \frac{K_m}{2} J_m(x) \quad x = \beta'r \quad (D.1.27)$$

$$E_r(r,m) = a_m x^{-1} J_m(x) + \frac{K_m}{2} J_{m+1}(x) \quad (D.2.11)$$

$$jE_\theta(r,m) = -a_m x^{-1} J_m(x) + \left(\frac{K_m}{2} + \frac{a_m}{m} \right) J_{m+1}(x) \quad (D.2.15)$$

where $\beta'^2 = \beta^2 - k^2$ with β being the (complex) wavenumber parameter of the conductor, and where a_m and K_m are undetermined constants.

At this point we applied the two boundary conditions, assuming a non-conducting dielectric,

$$E_r(r=a,m) = (j\omega/\sigma) N_m \quad (D.2.26)$$

$$E_\theta(r=a,m) = 0 \quad (D.2.27)$$

where N_m is the m^{th} partial wave moment of the surface charge $n(\theta)$ distribution, where

$$n(\theta,z,t) = e^{j(\omega t - kz)} n(\theta) \quad (D.1.4)$$

These conditions determined the constants a_m and K_m giving the resulting \mathbf{E} field inside the wire,

$$\begin{aligned}
 E_z(r,m) &= (1/4) \eta_m I R_{dc} (a\beta') \left[\frac{J_m(x)}{J_{m+1}(x_a)} - \frac{J_m(x)}{J_{m-1}(x_a)} \right] & a = \text{radius} \quad \eta_m &\equiv \frac{N_m}{N_0} & (D.2.33) \\
 E_r(r,m) &= (j/4) \eta_m I R_{dc} (ak) \left[\frac{J_{m+1}(x)}{J_{m+1}(x_a)} + \frac{J_{m-1}(x)}{J_{m-1}(x_a)} \right] & x &= \beta'r \\
 E_\theta(r,m) &= (1/4) \eta_m I R_{dc} (ak) \left[\frac{J_{m+1}(x)}{J_{m+1}(x_a)} - \frac{J_{m-1}(x)}{J_{m-1}(x_a)} \right] & x_a &= \beta'a
 \end{aligned}$$

where $R_{dc} = 1/(\pi a^2 \sigma)$ is the DC resistance of the wire per unit length, and I is the amplitude of the current in the wire. Everything is an implicit function of frequency ω . It was noted that, for $|k/\beta'| \ll 1$, the fields E_r and E_θ are much smaller than E_z , and this is the case for $f \sim 100$ GHz or below (but not too small).

An implication of the solution is that the E fields inside the wire for each partial wave are described by a single parameter N_m which is the surface charge moment noted above. If the other transmission line conductor(s) were to change their position relative to the round wire and/or to vary their cross sectional shape, the only effect this would have would be to adjust the set of parameters N_m , and the solutions would still be given by (D.2.33) quoted above. Although the set $\{N_m\}$ is infinite, it seems likely that for reasonable shapes of the other conductor(s), the lowest few N_m partial waves would provide a good approximation to the E fields inside the wire. Since Ohm's Law is assumed to apply inside the wire, one then knows in detail the current densities J_z , J_r and J_θ . The magnetic field \mathbf{B} inside the wire is then also known and was calculated above. The lowest moment is always $N_0 = (k/2\pi\omega a) I$ from (D.2.31b).

As an example, the following five-conductor transmission line might be expected to have a strong $m = 2$ quadrupole surface charge moment N_2 ,

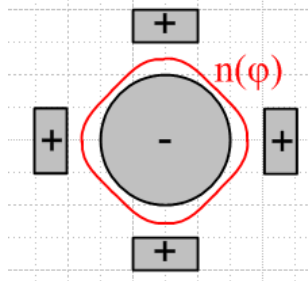


Fig D.4

A critical ingredient of our solution is the assumption that $E_\theta(r=a,m) = 0$ and that is the subject now addressed. We present two somewhat different arguments as to why $E_\theta(r=a,m) = 0$. It should be noted that King in his *Transmission-Line Theory* book always assumes that any straight transmission line conductor cross section has an equipotential surface (a ring, see for example middle p 14, top 15, 25 bottom). Due to the presence of small transverse vector potential components, $E_\theta = 0$ and "equipotential" for the scalar potential ϕ are not the same thing.

(a) The Quasi-Static Argument

In electrostatics, we are used to metal surfaces being equipotentials. For example, if we put a point charge q near a metal sphere, it induces a surface charge on that sphere. The electric field lines land on the sphere exactly perpendicular to the surface. One argues that if there were even some tiny E field component tangential to the surface, the surface charges would adjust their position to cancel out that tangential field.

Since the situation is static, any adjustment has already been made. Since $E_{tan} = 0$, the sphere's surface is an equipotential surface.

If we were to then slowly move the charge q around (perhaps it rotates in a circle around the sphere), the surface charge instantly adjusts at each new position of q , and those E field lines remain perpendicular to the surface, and $E_{tan} = 0$. While the charges are adjusting position, there is admittedly some very tiny surface current driven by some tiny E_{tan} , but if we move the charge slowly, we are "quasi-static" and the approximation $E_{tan} \approx 0$ is very good. One might compare the time constant of the moving sphere (T , the period of q 's revolution around the sphere) to the time constant of the surface charge adjustment. For copper the time constant is roughly the mean electron collision time which is on the order of 10^{-14} sec. The conclusion here is that for frequencies $\ll 10^{14}$ Hz (100,000 GHz), the quasi-static situation prevails and then $E_{tan} \approx 0$ is a very good approximation.

This then is our first argument for why we claim the boundary condition $E_{\theta} = 0$ on the surface of the round wire in a transmission line operating at a typical frequency.

We note from our solution $E_{\theta}(r,m)$ that if we assume $E_{\theta}(a,m) = 0$ on the round wire surface, we will still have $E_{\theta}(r,m) \neq 0$ inside the wire. This fact is consistent with our argument above since there are no free charges available to adjust themselves inside the wire.

However: if $E_{\theta} = 0$ by this quasi-static argument, then we should expect that $E_z = 0$ by the same argument, since E_z is also a tangential field at the round wire surface, and since E_z operates at the same frequency ω as E_{θ} . But we know that $E_z \neq 0$ because $J_z \neq 0$ just below the wire surface -- there is current flowing there -- and E_z is continuous through the surface by (1.1.51). So the E field lines are not quite perpendicular to the round wire surface in the z direction. This is not too surprising since we expect everything to vary in the z direction as $e^{j(\omega t - kz)}$ so we would expect the surface not to be an equipotential in this direction.

But what happened to that quasi-static argument we just applied to E_{θ} ? What happened is that there is external field activity associated with the wave going down the line which forces $E_z \neq 0$. One might say the EM wave traveling down the line induces a J_z in the round wire, with its associated $E_z \neq 0$. But then perhaps this same thing could somehow happen with E_{θ} and then our quasi-static argument that $E_{\theta} = 0$ collapses. We think this could happen in fact, but only if the transmission line is driven by an apparatus which creates a "torsion wave" in the line. For example, the apparatus could drive counter-rotating azimuthal currents onto the round wire surfaces of a twin-lead transmission line as suggested by this picture (which is not meant to imply that other field components vanish),

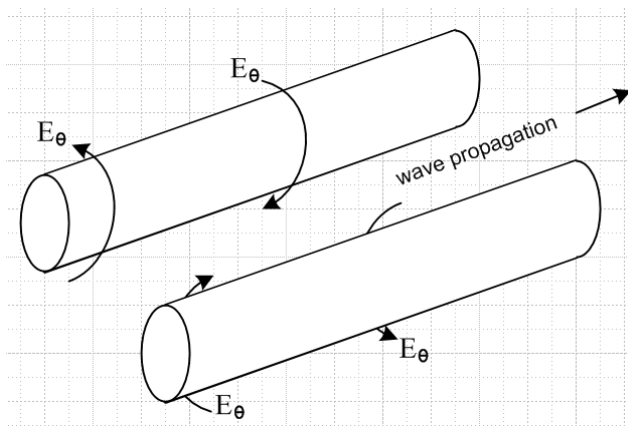


Fig D.5

It seems from our work above that such a wave would satisfy Maxwell's equations and be a viable mode of the transmission line. In this case, $E_\theta \neq 0$ because the EM wave going down the line forces $E_\theta \neq 0$, just as the normal wave forces $E_z \neq 0$.

We have not investigated whether this type of torsion wave is really viable. Whether or not it is, we assume in our transmission line discussion that this mode is not activated and that therefore the quasi-static argument for $E_\theta = 0$ is valid at the round wire surface.

(b) An Ansatz Argument

We make an ansatz that $E_x, E_\theta \ll E_z$ in our round wire \mathbf{E} field solution, perhaps based on an expectation that most current in the wire will be longitudinal. We assume this is true, and see if this assumption is born out in a final solution of Maxwell's equations. Given that E_θ is then very small, we can make an approximation (another ansatz) that this field E_θ is exactly zero on the surface of the round wire. This may not be exactly true, but again we assume it for our purposes and see where it leads. This is the nature of an "ansatz".

When we make this assumption, the cross section of the transmission line may be regarded (Chapter 5) as a two dimensional potential theory problem -- basically a capacitor problem where one conductor has potential $V/2$ and the other $-V/2$, say (for a symmetric line, at some fixed value of z). In such a potential problem, one always assumes that the electrostatic potential ϕ is a constant on the surface of each conductor, and that is precisely what our ansatz says: $E_\theta = -(\nabla\phi)_\theta = 0$, $\phi = \text{constant}$ in the θ direction. Now when we solve the capacitor problem for potential ϕ , that gives $\mathbf{E} = -\nabla\phi$ in the dielectric between the conductors, and from that we may deduce $\mathbf{E} \cdot \hat{\mathbf{n}}$ at the surface of one of the conductors. For the round wire with a cylindrical coordinate system whose axis is aligned with the wire center, that field is E_x . Next, from this surface value of E_x (which will be proportional to V) we may compute the surface charge density $n(\theta)$ on the round wire using (D.2.24) which says $E_x(r=a, \theta) = (j\omega/\sigma) n(\theta)$. For a "fat" twin lead transmission line for example we expect this to have a bulge in $n(\theta)$ on the side of the wire facing the other wire ($m = 1$, dipole), since that is what happens in such a capacitor. In any event, given $n(\theta)$ we may compute the moments N_m of the surface charge using (D.1.5b) and this then provides one "boundary condition" on our coefficients a_m and K_m which appear in all the field expressions we found above,

$$E_x(r=a, m) = (j\omega/\sigma) N_m . \quad (D.2.26)$$

But recall that, in order to carry out this entire process just described, we had to start with the assumption that $E_\theta = 0$ on the conductor cross section surface, so that we could have a capacitor problem in the first place. According to (D.1.3b), if $E_\theta(r=a, \theta) = 0$, then $E_\theta(r=a, m) = 0$, so that in fact we must have $E_x(a, m)$ being zero in all partial waves m . Thus our assumed ansatz condition is

$$E_\theta(r=a, m) = 0 \quad (D.2.27)$$

which is then a second boundary condition on a_m and K_m . Although (D.2.27) might not be exactly true, we know it is very close to being true. More importantly, we know that the above two conditions on a_m and K_m are consistent with each other, even though both boundary conditions might be slightly wrong. We then expect them to give good values for constants a_m and K_m .

Using these "perhaps slightly wrong" boundary conditions, we obtain the solutions shown in (D.2.33). It has already been noted above that for copper conductors and normal dielectrics, $|k/\beta'| \ll 1$ up to at least 100 GHz. The condition $|k/\beta'| \ll 1$ when applied to the (D.2.33) results shows that in fact our ansatz that $E_r, E_\theta \ll E_z$ is born out.

There are three footnotes to the above discussion.

First, we note that the second boundary condition does not force $E_\theta(r, m) = 0$ for $r < a$ inside the wire. In fact, there will be some small azimuthal "swirling" current inside the wire even if $E_\theta(r=a, m) = 0$, and this is just a result of Maxwell's equations and their solutions above.

Second, one might make the argument that the round wire surface is an equipotential since that is the way a line is driven at the source. For example, the center conductor of a coaxial cable plugs into a tiny driving cylinder (jack) in a BNC connector and this drives only the wire surface, and it does so in an azimuthally symmetric way so that one expects to have the wire surface be an equipotential at the driving point; this equipotential surface then moves down the line as the wave progresses.

Third, we have the complication that we don't really have a purely electrostatic situation, and the potential is in fact related to \mathbf{E} by equation (1.3.1) which says $\mathbf{E} = -\nabla\phi - \partial_t \mathbf{A}$. The rescue here comes by claiming that roughly $\mathbf{A} \approx A\hat{z}$ so that the transverse components A_r and A_θ are very small. In this case, we then do get $\mathbf{E} \approx -\nabla\phi$ so that $E_\theta = 0$ is associated with constant ϕ on the wire surface. The argument for $\mathbf{A} \approx A\hat{z}$ is that \mathbf{A} is driven by \mathbf{J} , and \mathbf{J} is mostly in the \hat{z} direction, which in turn is related to our starting ansatz (see Appendix M).

D.9 About the boundary condition $E_r(a, \theta) = (j\omega/\sigma) n(\theta)$.

The "charge pumping boundary condition" appears in (D.2.23) and here we want to examine it more closely. Our concern is that the derivation of (D.2.23) ignores surface currents that we know exist on the surface of a transmission line conductor as the surface charge moves around in response to tangential E fields. The first issue then is to define and quantify the nature of these surface currents.

(a) The notion of Debye Surface Currents

We continue in the context of our classical treatment of the conductor surface. In Appendix E it is pointed out that the surface charge on a transmission line conductor exists in an incredibly thin surface layer we shall call the Debye layer for want of a better name. For copper the thickness λ_D of this layer is on the order of one atomic radius. In addition to the normal conduction electrons, this thin layer contains extra free electrons that are piled up just below the surface (negative surface charge) or are depleted from this thin region (positive surface charge), as shown by the red curve in Fig E.1. We want first so show :

Fact 1: In a good conductor, the volume density of free electron carriers piled up at a surface (to make up the surface charge) is negligible compared to the volume density of conduction electrons. (D.9.1)

Proof: From (E.7) the free charge density in the Debye layer (assume x is the inward surface normal direction) is given by $\rho(x) = \rho(0) e^{-x/\lambda_D}$. The effective free surface charge n is then given by

$$n = \int_0^\infty dx \rho(x) = \rho(0) \int_0^\infty dx e^{-x/\lambda_D} = \rho(0)\lambda_D.$$

The free electron density n_e is then (n is the surface charge density)

$$n_e = \rho(0)/e = n / (e\lambda_D) .$$

As a typical example, consider a parallel plate capacitor with close plate spacing s . The E field in the gap is $E = V/s$ and the surface charge density from (1.1.47) is $n = \epsilon E = \epsilon V/s$. For $V = 10$ volts and $s = 1$ mm we find

$$n = \epsilon_0 V/s = 8.85 \times 10^{-12} * 10 / 10^{-3} \approx 10^{1-12+1+3} = 10^{-7} \text{ Coul/m}^2 .$$

Then the free electron density is

$$n_e = n / (e\lambda_D) \approx 10^{-7} \text{ Cou/m}^2 / [1.6 \times 10^{-19} \text{ Coul} * 10^{-10} \text{ m}]$$

$$\approx 0.6 * 10^{-7+19+10} \approx 10^{22} \text{ electrons/m}^3$$

As noted in (N.1.2), in copper the conduction electron density (one electron per atom) is $10^{29} / \text{m}^3$, QED.

Corollary: The conductivity σ_D inside the Debye layer is basically the same as σ outside that layer.

(D.9.2)

Proof: From (N.1.9) conductivity is $\sigma = (nq^2\tau/m)$ where n is the electron density. The Fact above shows that this density is the same in the Debye layer as in the bulk conductor, so $\sigma_D = \sigma$. (We ignore the possibility that the collision time τ could differ in the Debye layer vs. in the bulk volume.) QED

Consider now this crude drawing which shows a tiny slice of width dx of a piece of a transmission line conductor cross section at its surface. The yellow Debye surface charge layer is greatly exaggerated in thickness and is modeled as if it had a clean lower boundary. Recall from the comment below Fig E.2 that at 100 GHz one has $\delta \approx 4000 \lambda_D$ so $\delta \gg \lambda_D$ at all frequencies of transmission line interest.

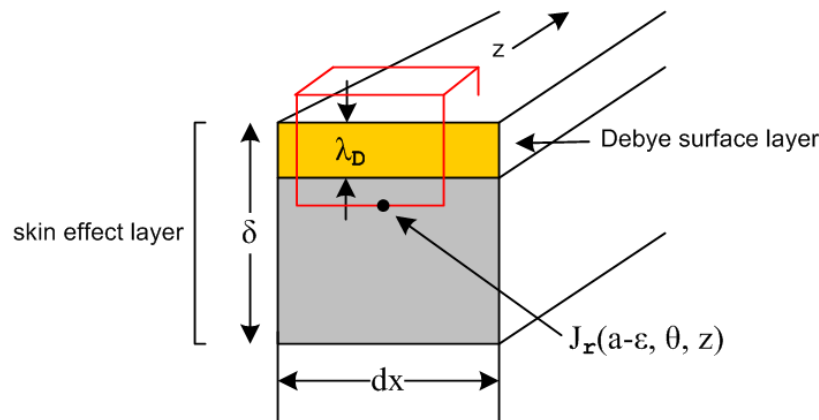


Fig D.6

The Debye layer holds the surface charge, and when this surface charge moves, one has a Debye surface current. We now show :

Fact 2: The total current in the Debye layer is negligible compared to that in the skin effect layer. (D.9.3)

Proof: The field E_z is parallel to the conductor surface, so we know from (1.1.41) that it is continuous through the boundary at the bottom of the Debye layer. Then the ratio of the currents in the two layers is,

$$\frac{I^D}{I^\delta} = \frac{J_z^D \lambda_d dx}{J_z^\delta \delta dx} = \frac{\sigma_D E_z^D \lambda_d}{\sigma E_z^\delta \delta} = \frac{\sigma_D}{\sigma} \frac{E_z}{E_z} \frac{\lambda_D}{\delta} \approx 1 * 1 * \frac{\lambda_D}{\delta} = \frac{\lambda_D}{\delta} \ll 1. \quad \text{QED}$$

(b) The role of Debye Surface Currents in the boundary condition

Now referring to the Debye surface currents as K_z^D and K_θ^D we reconsider the derivation of the charge pumping boundary condition of (D.2.24) where we had this figure,

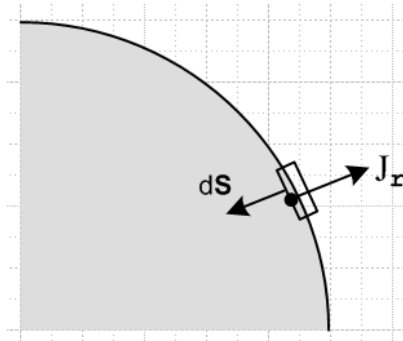


Fig D.2

If we include the Debye surface currents in the θ and z direction in our application of continuity,

$$\text{div } \mathbf{J} = -j\omega\rho \quad \Leftrightarrow \quad -j\omega[\int_V \rho dV] = \int_S \mathbf{J} \cdot d\mathbf{S}, \quad (D.2.22)$$

the result is

$$-j\omega n(\theta, z) = -J_r(r=a-\epsilon, \theta, z) + \partial_z K_z(\theta, z) + (1/a) \partial_\theta K_\theta(\theta, z) \quad (D.9.4)$$

where we assume that the dielectric outside the round wire is vacuum with $\sigma_a = 0$. The gaussian box selected here is that shown in red in Fig D.6. The bottom face lies below the Debye layer so $J_r(a-\epsilon, \theta, z)$ is the value of J_r in the normal skin effect region close to the surface. The Debye surface currents may be written approximately as

$$\begin{aligned} K_z^D &= J_z^D \lambda_D = \sigma_D E_z^D \lambda_D = \sigma E_z(r=a, \theta) \lambda_D && // \text{dim}(K) = \text{amp/m} \\ K_\theta^D &= J_\theta^D \lambda_D = \sigma_D E_\theta^D \lambda_D = \sigma E_\theta(r=a, \theta) \lambda_D = 0 && // (D.9.2) \text{ and } (3.7.0) \end{aligned} \quad (D.9.5)$$

where we use the Corollary above that $\sigma_D = \sigma$. From (3.7.0) we have $E_\theta = 0$ at the surface so $K_\theta^D = 0$ and we have only the Debye current K_z^D to worry about. Recall that $E_\theta(a, \theta) = 0$ is the second boundary

condition (D.2.27) used in Section D.2 to evaluate the a_m and K_m coefficients, and that this condition is itself a topic of interest in Section D.8, and we assume it is valid. We then have,

$$\begin{aligned} -j\omega n(\theta, z) &= -J_r(a, \theta, z) + \partial_z K_z^D(\theta, z) \\ &= -J_r(a, \theta, z) + \partial_z [\sigma E_z(a, \theta, z) \lambda_D] \end{aligned} \quad (D.9.6)$$

Assuming everything has z dependence $e^{j(\omega t - kz)}$ as in (D.1.4), we replace $\partial_z \rightarrow -jk$ and then suppress the z arguments to get

$$\begin{aligned} -j\omega n(\theta) &= -J_r(a, \theta) -jk [\sigma E_z(a, \theta) \lambda_D] \\ &= -\sigma E_r(a, \theta) -jk [\sigma E_z(a, \theta) \lambda_D] \\ &= -\sigma E_r(a, \theta) \left[1 - jk \lambda_D \frac{E_z(a, \theta)}{E_r(a, \theta)} \right] \end{aligned} \quad (D.9.7)$$

If we *assume* that the second term in (D.9.7) can be ignored, we get the charge pumping boundary condition

$$E_r(r=a-\epsilon, \theta) = (j\omega/\sigma) n(\theta) \quad (D.2.24) \quad (D.9.8)$$

which in return yields the E fields as stated in (D.2.33) where we see that roughly

$$\frac{E_z(a, \theta)}{E_r(a, \theta)} \sim \left| \frac{\beta}{k} \right| \quad (D.9.9)$$

Thus, our self-consistent condition for ignoring the second term in (D.9.7) is

$$\begin{aligned} k \lambda_D * \frac{E_z(a, \theta)}{E_r(a, \theta)} \ll 1 &\Leftrightarrow k \lambda_D * \left| \frac{\beta}{k} \right| \ll 1 \\ \Leftrightarrow \lambda_D |\beta| \ll 1 &\Leftrightarrow \lambda_D |e^{j3\pi/4} (\sqrt{2}/\delta)| \ll 1 \\ \Leftrightarrow (\lambda_D/\delta) \ll 1 &\Leftrightarrow (\delta/\lambda_D) \gg 1 \quad // \text{ ignore } \sqrt{2} \end{aligned}$$

But we know from above that $(\delta/\lambda_D) \gg 1$ for any $f < 100\text{GHz}$, so for such f the second term in (D.9.7) can in fact be ignored. We have just proven:

Fact 3: For $f < 100\text{ GHz}$, the Debye surface currents can be ignored in the derivation of the boundary condition $E_r(a-\epsilon, \theta) = (j\omega/\sigma) n(\theta)$. (D.9.10)

(c) Where does surface charge $n(\theta)$ come from?

According to our traveling-wave ansatz (D.1.1), all E field related quantities move down a transmission line at v_d as $e^{j(\omega t - kz)}$. For a low-loss line and a vacuum dielectric, $v_d \approx c$, the speed of light. Therefore,

$$n(\theta, z, t) = n(\theta, 0, 0) e^{j(\omega t - kz)} \quad k = (\omega/v_d) . \quad (D.9.11)$$

One can ponder and then discard a list of hypotheses concerning where $n(\theta)$ "comes from" as it increases and decreases over time at some location z on one of the conductors.

The first hypothesis might be that the individual electrons which make up $n(\theta)$ simply travel at v_d in the z direction down the conductor surface, and $n(\theta)$ is not fed by any radial currents inside the conductor. In this case one would have $K_z^D(\theta) = v_d n(\theta)$. But we know this is not what happens. Apart from the massive energy required to achieve relativistic electron velocities, we know from Appendix N.1 that the electrons in the Debye layer in fact drift along at something like ~ 1 mm/sec, just as do the regular conduction electrons in the conductor bulk.

The second hypothesis is a variation of the first, where we now allow that the Debye surface current works like any other conduction current, and when one electron moves "to the right" at some point z , a distant electron at $z+L$ moves to the right at nearly the same time, all electrons in a long string moving to the right one position, giving the illusion that a particular electron moved very fast. This does in fact happen, and if it were *all* that happened, again we would have $K_z^D(\theta) = v_d n(\theta)$.

Comment : Assume some skin depth $\delta \leq a/10$ so the bulk current is flowing in a sheath of thickness δ just under the conductor surface. The total sheath current is then roughly $2\pi a \delta J_z(a, \theta)$. We can regard this current flow as due to an effective "full surface current" $K_z = J_z \delta$. Notice that this "surface current" is different from the "Debye surface current". Based on Fact 2 above, we certainly expect $K_z \gg K_z^D$.

A third hypothesis is that somehow $n(\theta, z, t)$ is fed by azimuthal Debye surface currents, or some combination of these along with the z -directed $K_z^D(\theta)$. Our condition (3.7.0) that $E_\theta = 0$ puts a stop to the possibility of feeding by azimuthal Debye surface currents.

What we have learned from Fact 3 is that none of the above hypotheses explains where $n(\theta)$ comes from. The analysis above shows that, although the surface motions of the Debye surface charges do create Debye surface currents, these currents are so small that they play no role in $\text{div } \mathbf{J} = -\partial_t \rho$ for the Gaussian box shown in red in Fig D.6. The charge $n(\theta)$ "comes from" inside the wire and is fed by the radial current density J_r just below the surface according to (D.2.24),

$$J_r(r=a-\epsilon, \theta) = j\omega n(\theta) \quad n(\theta) = (1/j\omega) J_r(a-\epsilon, \theta) \quad (D.9.12)$$

Here is a suggestive picture,

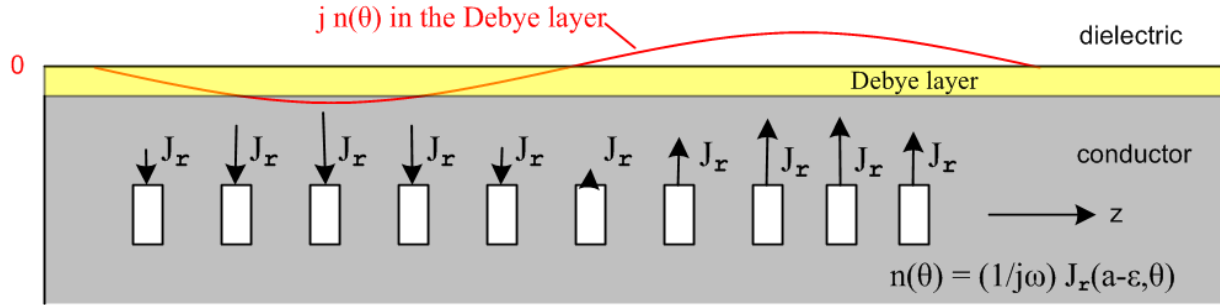


Fig D.7

where the white boxes are little "radial charge pumps" delivering the required J_r needed to feed the changing surface charge $n(\theta)$. Apart from the miniscule K_z^D , charges in $n(\theta)$ don't move in the z direction in this picture, they just appear to be doing that due to the choreographed radial pumping in and out at the wire surface. A wave front of the $n(\theta)$ wave travels at v_d , and this is just a phase velocity. In an analogous situation, in a deep ocean wave the individual particles of water travel in small ellipses and do not travel along with the wave, though there are small scale longitudinal motions due to those ellipses.

Comment: In our transmission line theory, the exterior problem in the dielectric is solved using the capacitor method, from which one learns $n(\theta)$. The boundary condition $J_r(r=a-\epsilon, \theta) = j\omega n(\theta)$ couples this exterior information into the wire interior, allowing one to solve for the fields and currents inside.

In Section 6.5 (d) we show how $\text{div } \mathbf{E} = 0$ inside the conductor (or $\text{div } \mathbf{J} = 0$) forces a relationship between J_r and J_z just below the conductor surface. When that relationship (6.5.18) is combined with the charge pumping boundary condition (D.9.8), one finds that

$$E_z(a, \theta) = (-j\omega/\sigma) (\beta/k) n(\theta) \quad (6.5.19)$$

or

$$J_z(a, \theta) = (-j\omega) (\beta/k) n(\theta) \quad (D.9.13)$$

This same result is obtained in a different manner as (6.5.13).

The "full surface current" K_z was defined in a Comment above as $K_z(\theta) = \delta J_z(a, \theta)$. Thus,

$$K_z(\theta) = \delta J_z(a, \theta) = [\delta (-j\omega) (\beta/k)] n(\theta) \quad (D.9.14)$$

But

$$\frac{\beta}{k} = \frac{e^{j3\pi/4} (\sqrt{2}/\delta)}{\omega/v_d}$$

so

$$\begin{aligned} [\delta (-j\omega) (\beta/k)] &= \delta (-j\omega) \frac{e^{j3\pi/4} (\sqrt{2}/\delta)}{\omega/v_d} = -j e^{j3\pi/4} \sqrt{2} v_d \\ &= -j (j-1)/\sqrt{2} * \sqrt{2} v_d = (1+j) v_d \end{aligned}$$

and we end up with

$$\begin{aligned} \mathbf{K}_z(\theta) &= (1+j) v_d n(\theta) \\ \operatorname{Re}(\mathbf{K}_z(\theta)) &= \operatorname{Im}(\mathbf{K}_z(\theta)) = v_d n(\theta) \end{aligned} \tag{D.9.15}$$

Once again, this last equation gives the illusion that the surface charge density $n(\theta)$ moves "to the right" at speed v_d to create the real or imaginary part of the full δ -thick surface current \mathbf{K}_z . This is the equation that replaces the incorrect equation $\mathbf{K}_z^D(\theta) = v_d n(\theta)$ which assumes there is no radial charge pumping.

Reader Exercise: Show using $\mathbf{F} = m\mathbf{a}$ and $\mathbf{F} = q\mathbf{E}$ (ignore magnetic fields) that, with a time-harmonic \mathbf{E} field, a classical electron inside a transmission line conductor traverses a tiny elliptical path and thus never really goes anywhere. That path is traversed once per period $T = 2\pi/\omega$. Mathematically, show that this amounts to proving that the three equations

$$\begin{aligned} x &= A\cos(\omega t - a) \\ y &= B\cos(\omega t - b) \\ z &= C\cos(\omega t - c) \end{aligned}$$

are parametric equations for an ellipse with some orientation in 3D space. As just noted above, this goes-nowhere aspect of the electron is similar to what happens with a droplet of water in an ocean wave. (Hint: first show that the first two equations describe an ellipse in the xy plane and that the semi-major axes in general are *not* A and B .)

(d) Modifications for a Conducting Dielectric

Ignoring the Debye surface currents as per section (b) above, if the dielectric has some conductivity σ_d , the charge pumping boundary condition (D.2.23) becomes

$$J_x(a-\alpha, \theta) - J_x(a+\alpha, \theta) = j\omega n(\theta)$$

or

$$\sigma E_x(a-\alpha, \theta) - \sigma_d E_x(a+\alpha, \theta) = j\omega n(\theta) \quad // \text{ this is } \text{div } \mathbf{J} = -j\omega\rho$$

where $\alpha > 0$ is a tiny distance (ϵ is already used for dielectric constant). Another boundary condition at the surface is provided by (1.1.47) which says ($\hat{\mathbf{n}}$ points into medium 1 which is the dielectric)

$$[\epsilon_1 E_{n1} - \epsilon_2 E_{n2}] = n_{\text{free}} \quad // \text{ this is continuity of } D_n \text{ at the surface}$$

or

$$[\epsilon_d E_{r1} - \epsilon_0 E_{r2}] = n(\theta) \quad // \text{ assuming } \epsilon_0 \text{ for the conductor}$$

or

$$[\epsilon_d E_x(a+\alpha, \theta) - \epsilon_0 E_x(a-\alpha, \theta)] = n(\theta) .$$

A seeming third boundary condition is (1.1.48),

$$\xi_1 E_{n1} = \xi_2 E_{n2}$$

or

$$(\epsilon_d + \sigma_d/j\omega) E_{rd} = (\epsilon_0 + \sigma/j\omega) E_r \approx (\sigma/j\omega) E_r$$

or

$$(\epsilon_d + \sigma_d/j\omega) E_x(a+\alpha, \theta) \approx (\sigma/j\omega) E_x(a-\alpha, \theta) .$$

There seem then to be three boundary conditions at the round wire surface,

$$\sigma E_x(a-\alpha, \theta) - \sigma_d E_x(a+\alpha, \theta) = j\omega n(\theta) \quad // \text{ modified cpbc from } \text{div } \mathbf{J} = -j\omega\rho \quad (\text{D.9.16})$$

$$\epsilon_d E_x(a+\alpha, \theta) - \epsilon_0 E_x(a-\alpha, \theta) = n(\theta) \quad // \text{ div } \mathbf{D} = \rho \text{ (straddle)} \quad (\text{D.9.17})$$

$$(\epsilon_d + \sigma_d/j\omega) E_x(a+\alpha, \theta) \approx (\sigma/j\omega) E_x(a-\alpha, \theta) \quad // \xi_1 E_{n1} = \xi_2 E_{n2} \quad (\text{D.9.18})$$

but only two of these conditions are independent. For example, multiply (D.9.16) by $(-1/j\omega)$ to get

$$(\sigma_d/j\omega) E_x(a+\alpha, \theta) - (\sigma/j\omega) E_x(a-\alpha, \theta) = -n(\theta) .$$

Adding this to (D.9.17) then gives

$$(\epsilon_d + \sigma_d/j\omega) E_x(a+\alpha, \theta) - (\sigma/j\omega) E_x(a-\alpha, \theta) = 0$$

which is in fact the same as (D.9.18).

When we solve the "capacitor problem" as in Section 6.5 (a) to obtain $n(\theta)$ on the round conductor surface, we are using (D.9.17) with the assumption that $E_{\mathbf{r}}(a+\alpha, \theta) \gg E_{\mathbf{r}}(a-\alpha, \theta)$. Typically one just says that in a good conductor $E_{\mathbf{r}}(a-\alpha, \theta) = 0$ and then $n(\theta) = \epsilon_{\mathbf{d}} E_{\mathbf{r}}(a+\alpha, \theta)$. That is fine, but it is not clear what happens to (D.9.16) above. The first term is the product of a large quantity σ times a small quantity $E_{\mathbf{r}}(a-\alpha, \theta)$ so can be the same size as the other terms in the equation.

The resolution is provided by the discussion in Section 1.5 (c) where we encountered the equation (1.5.17)

$$n_{\mathbf{c}}(\mathbf{x}, \omega) = (\xi_{\mathbf{1}}/\epsilon_{\mathbf{1}}) n_{\mathbf{s}}(\mathbf{x}, \omega) \quad (1.5.17)$$

which in our current context ($1 = \text{dielectric}$) becomes

$$n_{\mathbf{c}}(\theta) = (\xi_{\mathbf{d}}/\epsilon_{\mathbf{d}}) n(\theta) . \quad (D.9.19)$$

In that discussion it is noted that $n(\theta)$ is the actual free surface charge density, whereas $n_{\mathbf{c}}(\theta)$ is a related "transport charge density" having the same dimensions as $n(\theta)$. If we multiply (D.9.16) and (D.9.17) by $(\xi_{\mathbf{d}}/\epsilon_{\mathbf{d}})$, our (redundant) triplet of boundary conditions becomes,

$$\begin{aligned} 1 \quad & \sigma (\xi_{\mathbf{d}}/\epsilon_{\mathbf{d}}) E_{\mathbf{r}}(a-\alpha, \theta) - \sigma_{\mathbf{d}} (\xi_{\mathbf{d}}/\epsilon_{\mathbf{d}}) E_{\mathbf{r}}(a+\alpha, \theta) = j\omega n_{\mathbf{c}}(\theta) \\ 2 \quad & \xi_{\mathbf{d}} E_{\mathbf{r}}(a+\alpha, \theta) - (\xi_{\mathbf{d}}/\epsilon_{\mathbf{d}}) \epsilon_0 E_{\mathbf{r}}(a-\alpha, \theta) = n_{\mathbf{c}}(\theta) \\ 3 \quad & \xi_{\mathbf{d}} E_{\mathbf{r}}(a+\alpha, \theta) \approx \xi E_{\mathbf{r}}(a-\alpha, \theta) . \end{aligned} \quad (D.9.20)$$

We now use the last of these three equations to eliminate $E_{\mathbf{r}}(a+\alpha, \theta)$ in the first, which then becomes

$$\begin{aligned} & \sigma (\xi_{\mathbf{d}}/\epsilon_{\mathbf{d}}) E_{\mathbf{r}}(a-\alpha, \theta) - \sigma_{\mathbf{d}} (\xi/\epsilon_{\mathbf{d}}) E_{\mathbf{r}}(a-\alpha, \theta) = j\omega n_{\mathbf{c}}(\theta) \\ \text{or} & \\ & [\sigma \xi_{\mathbf{d}} - \sigma_{\mathbf{d}} \xi] / \epsilon_{\mathbf{d}} * E_{\mathbf{r}}(a-\alpha, \theta) = j\omega n_{\mathbf{c}}(\theta) \\ \text{or} & \\ & [\sigma (\epsilon_{\mathbf{d}} + \sigma_{\mathbf{d}}/j\omega) - \sigma_{\mathbf{d}} (\epsilon_0 + \sigma/j\omega)] / \epsilon_{\mathbf{d}} * E_{\mathbf{r}}(a-\alpha, \theta) = j\omega n_{\mathbf{c}}(\theta) \\ \text{or} & \\ & [(\sigma \epsilon_{\mathbf{d}} - \sigma_{\mathbf{d}} \epsilon_0)] / \epsilon_{\mathbf{d}} * E_{\mathbf{r}}(a-\alpha, \theta) = j\omega n_{\mathbf{c}}(\theta) \quad // \text{ two large terms cancelled} \\ \text{or} & \\ & [\sigma - \sigma_{\mathbf{d}} (\epsilon_0/\epsilon_{\mathbf{d}})] E_{\mathbf{r}}(a-\alpha, \theta) = j\omega n_{\mathbf{c}}(\theta) . \end{aligned}$$

Assume now that ϵ_0 (conductor) and $\epsilon_{\mathbf{d}}$ (dielectric) are the same order of magnitude, and assume that, even though the dielectric conducts, one still has $\sigma \gg \sigma_{\mathbf{d}}$. The last equation then reads

$$E_{\mathbf{r}}(a-\alpha, \theta) = (j\omega/\sigma) n_{\mathbf{c}}(\theta) = (j\omega/\sigma) (\xi_{\mathbf{d}}/\epsilon_{\mathbf{d}}) n(\theta) \quad // \theta \text{ space} \quad (D.9.21)$$

$$E_{\mathbf{r}}(a-\alpha, m) = (j\omega/\sigma) (\xi_{\mathbf{d}}/\epsilon_{\mathbf{d}}) N_{\mathbf{m}} . \quad // m \text{ space} \quad (D.9.22)$$

Above are the "**modified**" charge pumping boundary conditions which replace (D.2.24) and (D.2.25) for a mildly conducting dielectric,

$$E_{\mathbf{r}}(r=a, \theta) = (j\omega/\sigma) n(\theta) \quad (D.2.24)$$

$$E_{\mathbf{r}}(r=a, m) = (j\omega/\sigma) N_m . \quad (D.2.25)$$

How then does $\sigma_d \neq 0$ alter the E field results summarized in box (D.2.33)? The rule is this:

$$N_m \rightarrow N_m' \equiv (\xi_d/\epsilon_d) N_m \text{ everywhere .} \quad (D.9.23)$$

Here we use a prime to denote a parameter after the dielectric DC conductivity has been "turned on", and no prime for the case that $G_{dc} = 0 = \sigma_d$.

But there is another change which must not be overlooked. Although k is treated as a generic constant in Appendix D, we will eventually be setting k to a specific value $k(\omega)$ which is determined by activity in the dielectric, which in turn is affected by the dielectric conductance,

$$k = k(\omega) \equiv -j \sqrt{\mathbf{zy}} = -j \sqrt{[R(\omega)+j\omega L(\omega)][G(\omega)+j\omega C(\omega)]} , \quad (5.3.6)$$

where the four parameters are as given in the simple model of (Q.1.9). In particular, $C(\omega) = C$, a constant, whereas $G(\omega) = G_{dc} + C \tan_{\mathbf{L}}\omega$, so one may write (since $\tan_{\mathbf{L}} \ll 1$),

$$\begin{aligned} k(\omega) &= -j \sqrt{[R(\omega)+j\omega L(\omega)][G_{dc} + C \tan_{\mathbf{L}}\omega + j\omega C]} \\ &\approx -j \sqrt{[R(\omega)+j\omega L(\omega)][G_{dc}+j\omega C]} \end{aligned} \quad (D.9.24)$$

which shows the traditional dependence on G_{dc} and C . The combination $G_{dc} + j\omega C$ may be interpreted in terms of the complex capacitance C' where $G_{dc} + j\omega C = j\omega C'$ as in the line below (1.5.20). Then

$$k(\omega) = -j \sqrt{[R(\omega)+j\omega L(\omega)][j\omega C']} . \quad (D.9.25)$$

Thus one can write,

$$k' = -j \sqrt{[R(\omega)+j\omega L(\omega)][j\omega C']} \quad // G_{dc} > 0 \quad (D.9.26a)$$

$$k = -j \sqrt{[R(\omega)+j\omega L(\omega)][j\omega C]} . \quad // G_{dc} = 0 \quad (D.9.26b)$$

The point is that the value of k *changes* when G_{dc} is turned on. The k ratio is then

$$\frac{k'}{k} = \sqrt{\frac{C'}{C}} = \sqrt{\xi_d/\epsilon_d} \quad (D.9.27)$$

where the $\sqrt{\xi_d/\epsilon_d}$ factor follows from (1.5.19).

Here then is an improved statement of the Rule for how things change when the dielectric conductivity is turned on:

$$\begin{aligned}
 N_m &\rightarrow N_m' \equiv (\xi_d/\epsilon_d) N_m \\
 k &\rightarrow k' \equiv \sqrt{\xi_d/\epsilon_d} k \\
 C &\rightarrow C' = (\xi_d/\epsilon_d) C . \tag{D.9.28} \\
 \text{where } (\xi_d/\epsilon_d) &= \frac{C'}{C} = \frac{G_{dc} + j\omega C}{j\omega C} = 1 + \frac{(G_{dc}/C)}{j\omega} = 1 + \frac{(\sigma_d/\epsilon_d)}{j\omega} \quad // \text{ see (4.4.10)}
 \end{aligned}$$

For example, consider (D.1.8) in its form for $G_{dc} = 0$ [recall $I = 2\pi a (\omega/k) N_0$ from (D.2.31a)],

$$N_0 = \langle n(\theta) \rangle = q/(2\pi a) = CV/(2\pi a) \quad \Rightarrow \quad I = CV (\omega/k) . \tag{D.1.8}$$

Here $n = n_s$ and $q = q_s$ which are the surface charge and its cross section integral, so the above really says

$$N_0 = \langle n_s(\theta) \rangle = q_s/(2\pi a) = CV/(2\pi a) \quad \Rightarrow \quad I = CV (\omega/k) . \tag{D.1.8}$$

When $G_{dc} > 0$, the surface charges become their "transport charge" alter egos,

$$\begin{aligned}
 n_s &\rightarrow n' = n_c = (\xi_d/\epsilon_d)n_s && // (1.5.17) \\
 q_s &\rightarrow q' = q_c = (\xi_d/\epsilon_d)q_s && // \text{ integral of the above}
 \end{aligned} \tag{D.9.29}$$

and then (D.1.8) becomes

$$N_0' = \langle n_c(\theta) \rangle = q_c/(2\pi a) = C'V/(2\pi a) \quad \Rightarrow \quad I' = C'V (\omega/k') \tag{D.1.8}$$

or

$$\begin{aligned}
 (\xi_d/\epsilon_d)N_0 &= (\xi_d/\epsilon_d) \langle n_s(\theta) \rangle = (\xi_d/\epsilon_d) q_s/(2\pi a) = (\xi_d/\epsilon_d) C V/(2\pi a) \\
 \Rightarrow I' &= C'V (\omega/k') = (\xi_d/\epsilon_d) C V \frac{\omega}{\sqrt{\xi_d/\epsilon_d} k} = CV (\omega/k) \sqrt{\xi_d/\epsilon_d} = I \sqrt{\xi_d/\epsilon_d}
 \end{aligned} \tag{D.9.30}$$

and we find that the total current increases by this ratio when G_{dc} is turned on,

$$\frac{I'}{I} = \sqrt{\xi_d/\epsilon_d} . \tag{D.9.31}$$

A more direct path to this conclusion is the following, again using (D.2.31a) that $I = 2\pi a (\omega/k) N_0$:

$$\begin{aligned}
 I &= 2\pi a (\omega/k) N_0 \\
 \rightarrow I' &= 2\pi a (\omega/k') N_0' = 2\pi a \frac{\omega}{\sqrt{\xi_d/\epsilon_d} k} (\xi_d/\epsilon_d) N_0 = \sqrt{\xi_d/\epsilon_d} 2\pi a \frac{\omega}{k} N_0 = \sqrt{\xi_d/\epsilon_d} I .
 \end{aligned} \tag{D.9.32}$$

As a simple verification of this claim, consider the G_{dc} "turn on" viewed from this perspective,

$$I = V/Z_0 \quad \text{where} \quad 1/Z_0 = \sqrt{\frac{j\omega C}{R + j\omega L}} \quad (D.9.33a)$$

$$I' = V/Z_0' \quad \text{where} \quad 1/Z_0' = \sqrt{\frac{G_{dc} + j\omega C}{R + j\omega L}} = \sqrt{\frac{j\omega C'}{R + j\omega L}} \quad (D.9.33b)$$

where in general $Z_0 = \sqrt{\frac{z}{y}} = \sqrt{\frac{R + j\omega L}{G + j\omega C}}$ as in (4.12.18). From (D.9.33) we must have

$$\frac{I'}{I} = \sqrt{\frac{j\omega C'}{j\omega C}} = \sqrt{\frac{C'}{C}} = \sqrt{\xi_d/\epsilon_d}$$

which agrees with (D.9.31) above.

Now consider the Appendix D E fields from (D.2.33) as stated for $G_{dc} = 0$:

Second summary of the E field solutions :	$R_{dc} = \frac{1}{\sigma\pi a^2} \quad \beta'^2 = \beta^2 - k^2$	(D.2.33)
$E_z(r,m) = (1/4) \eta_m I R_{dc} (a\beta') f_m$	$f_m = \left[\frac{J_m(x)}{J_{m+1}(x_a)} - \frac{J_m(x)}{J_{m-1}(x_a)} \right]$	$x = \beta'r$
$E_r(r,m) = (j/4) \eta_m I R_{dc} (ak) g_m$	$g_m = \left[\frac{J_{m+1}(x)}{J_{m+1}(x_a)} + \frac{J_{m-1}(x)}{J_{m-1}(x_a)} \right]$	$x_a = \beta'a$
$E_\theta(r,m) = (1/4) \eta_m I R_{dc} (ak) h_m$	$h_m = \left[\frac{J_{m+1}(x)}{J_{m+1}(x_a)} - \frac{J_{m-1}(x)}{J_{m-1}(x_a)} \right]$	
$I = 2\pi a (\omega/k) N_0 = C V (\omega/k)$	(D.2.31a) and (D.1.8)	$G_{dc} = 0$

When G_{dc} is turned on, the fields are instead given by [taking $I \rightarrow I'$ and $k \rightarrow k'$ and $C \rightarrow C'$]

Second summary of the E field solutions :	$R_{dc} = \frac{1}{\sigma\pi a^2} \quad \beta'^2 = \beta^2 - k'^2$	(D.9.34)
$E_z(r,m) = (1/4) \eta_m I' R_{dc} (a\beta') f_m$	$f_m = \left[\frac{J_m(x)}{J_{m+1}(x_a)} - \frac{J_m(x)}{J_{m-1}(x_a)} \right]$	$x = \beta'r$
$E_r(r,m) = (j/4) \eta_m I' R_{dc} (ak') g_m$	$g_m = \left[\frac{J_{m+1}(x)}{J_{m+1}(x_a)} + \frac{J_{m-1}(x)}{J_{m-1}(x_a)} \right]$	$x_a = \beta'a$
$E_\theta(r,m) = (1/4) \eta_m I' R_{dc} (ak') h_m$	$h_m = \left[\frac{J_{m+1}(x)}{J_{m+1}(x_a)} - \frac{J_{m-1}(x)}{J_{m-1}(x_a)} \right]$	
$I' = 2\pi a (\omega/k') N_0' = C' V (\omega/k')$	(D.2.31a) and (D.1.8)	$G_{dc} > 0$

It is convenient to express everything in terms of k' , so we use

$$\Gamma = C' V (\omega/k') = (\xi_d/\epsilon_d) CV (\omega/k')$$

to rewrite the above box as

Second summary of the E field solutions :	$R_{dc} = \frac{1}{\sigma\pi a^2} \quad \beta'^2 = \beta^2 - k'^2$	(D.9.35)
$E_z(r,m) = (1/4) (\xi_d/\epsilon_d) \eta_m CV R_{dc} (\omega/k') (a\beta') f_m$	$f_m = \left[\frac{J_m(x)}{J_{m+1}(x_a)} - \frac{J_m(x)}{J_{m-1}(x_a)} \right]$	$x = \beta'r$
$E_r(r,m) = (j/4) (\xi_d/\epsilon_d) \eta_m CV R_{dc} (\omega a) g_m$	$g_m = \left[\frac{J_{m+1}(x)}{J_{m+1}(x_a)} + \frac{J_{m-1}(x)}{J_{m-1}(x_a)} \right]$	$x_a = \beta'a$
$E_\theta(r,m) = (1/4) (\xi_d/\epsilon_d) \eta_m CV R_{dc} (\omega a) h_m$	$h_m = \left[\frac{J_{m+1}(x)}{J_{m+1}(x_a)} - \frac{J_{m-1}(x)}{J_{m-1}(x_a)} \right]$	$G_{dc} > 0$

Then to get back to $G_{dc} = 0$, one replaces $(\xi_d/\epsilon_d) \rightarrow 1$ and $k' \rightarrow k$. Because k' appears as part of β' and β' appears in x and x_a and these are Bessel function arguments, one *cannot* simply say that the E_i fields are scaled up by the factor (ξ_d/ϵ_d) when the DC conductivity of the dielectric is turned on. This is the case, however, when $|k'| \ll |\beta|$ which is the situation for large ω (see (D.2.2) and following text).

Since the same factors appear repeatedly, we shall now define

$$\mathcal{B} \equiv (\xi_d/\epsilon_d) CV R_{dc} = C' V R_{dc} \quad . \quad // \dim(\mathcal{B}) = \text{tesla} \quad (D.9.36)$$

Now in our application of the above fields, we will always be using the symbol k *with the understanding* that $k = k(\omega) =$ with G_{dc} present or absent as appropriate, In this light we do a final rewrite, discarding the prime on k' , but keeping it in mind:

Second summary of the E field solutions :	$R_{dc} = \frac{1}{\sigma\pi a^2} \quad \beta'^2 = \beta^2 - k^2$	(D.9.37)
$E_z(r,m) = (1/4) \eta_m \mathcal{B} (\omega a) (\beta'/k) f_m$	$f_m = \left[\frac{J_m(x)}{J_{m+1}(x_a)} - \frac{J_m(x)}{J_{m-1}(x_a)} \right]$	$x = \beta'r \quad x_a = \beta'a$
$E_r(r,m) = (j/4) \eta_m \mathcal{B} (\omega a) g_m$	$g_m = \left[\frac{J_{m+1}(x)}{J_{m+1}(x_a)} + \frac{J_{m-1}(x)}{J_{m-1}(x_a)} \right]$	$\mathcal{B} \equiv (\xi_d/\epsilon_d) CV R_{dc}$
$E_\theta(r,m) = (1/4) \eta_m \mathcal{B} (\omega a) h_m$	$h_m = \left[\frac{J_{m+1}(x)}{J_{m+1}(x_a)} - \frac{J_{m-1}(x)}{J_{m-1}(x_a)} \right]$	$G \geq 0$

This form of the E fields is valid for $G_{dc} \geq 0$ if we interpret k properly and set $(\xi_d/\epsilon_d) = 1$ for $G_{dc} = 0$. In this form, one gets the misleading impression that all E fields are simply scaled up by the factor (ξ_d/ϵ_d) , when G_{dc} is turned on, but this is just an artifact of our notation due to the nature of k .

The B field expressions shown in (D.4.13) may be generalized in the same manner as the E fields: take $I \rightarrow I' = (\xi_d/\epsilon_d) CV (\omega/k')$ and then notationally replace k' by k . For example,

$$I R_{dc} \rightarrow I' R_{dc} = (\xi_d/\epsilon_d) CV R_{dc} (\omega/k') = \mathcal{B} (\omega/k') \rightarrow \mathcal{B} (\omega/k) . \quad (D.9.38)$$

One sees that this rule converts the E fields in (D.4.13) to those in (D.9.37). Applying this rule to both the E and B fields of (D.9.37) gives this final result

Summary of E and B fields inside a round wire			(D.9.39)
$E_z(r,m) = (1/4) \eta_m \mathcal{B} (\omega/k) (a\beta') f_m$	$x = \beta'r$	$x_a = \beta'a$	$\beta'^2 = \beta^2 - k^2$
$E_r(r,m) = (j/4) \eta_m \mathcal{B} (\omega a) g_m$			
$E_\theta(r,m) = (1/4) \eta_m \mathcal{B} (\omega a) h_m$			$\mathcal{B} \equiv (\xi_d/\epsilon_d) CV R_{dc}$
$B_z(r,m) = (j/4) (a) \eta_m \mathcal{B} (\beta' e_m)$			$(\xi_d/\epsilon_d) = 1 + (G/j\omega C)$
$B_r(r,m) = - (1/4) (a) \eta_m \mathcal{B} (1/k) (r^{-1} m \beta' f_m + k^2 h_m)$			
$B_\theta(r,m) = (j/4) (a) \eta_m \mathcal{B} (1/k) (k^2 g_m - \beta'^2 f_m [(m/x) - J_{m+1}(x)/J_m(x)])$			$\eta_m = N_m/N_0$
$e_m = [\frac{J_m(x)}{J_{m+1}(x_a)} + \frac{J_m(x)}{J_{m-1}(x_a)}]$	$g_m = [\frac{J_{m+1}(x)}{J_{m+1}(x_a)} + \frac{J_{m-1}(x)}{J_{m-1}(x_a)}]$		$R_{dc} = \frac{1}{\sigma \pi a^2}$
$f_m = [\frac{J_m(x)}{J_{m+1}(x_a)} - \frac{J_m(x)}{J_{m-1}(x_a)}]$	$h_m = [\frac{J_{m+1}(x)}{J_{m+1}(x_a)} - \frac{J_{m-1}(x)}{J_{m-1}(x_a)}]$		$G \geq 0$

D.10 High frequency limit of the round wire E fields

The box (D.9.39) above displays the round wire E_i and B_i field components in terms of functions e_m , f_m , g_m and h_m . Here we study first the symmetry under $m \leftrightarrow -m$ of these functions, and then we evaluate them at high frequency.

(a) Symmetry of e_m , f_m , g_m and h_m and expansions for $E_i(r, \theta)$

Although e_m does not appear in the E field expressions, it does in the B field ones so we include it here.

From NIST (10.4.1) we know that for integer m ,

$$J_{-m}(x) = (-1)^m J_m(x) \quad . \quad (D.10.1)$$

For f_m one then has,

$$f_m = \left[\frac{J_m(x)}{J_{m+1}(x_a)} - \frac{J_m(x)}{J_{m-1}(x_a)} \right]$$

$$f_{-m} = \left[\frac{J_{-m}(x)}{J_{-m+1}(x_a)} - \frac{J_{-m}(x)}{J_{-m-1}(x_a)} \right] = - \left[\frac{J_m(x)}{J_{m-1}(x_a)} - \frac{J_m(x)}{J_{m+1}(x_a)} \right] = f_m$$

With e_m the result is the same:

$$e_m = \left[\frac{J_m(x)}{J_{m+1}(x_a)} + \frac{J_m(x)}{J_{m-1}(x_a)} \right]$$

$$e_{-m} = \left[\frac{J_{-m}(x)}{J_{-m+1}(x_a)} + \frac{J_{-m}(x)}{J_{-m-1}(x_a)} \right] = - \left[\frac{J_m(x)}{J_{m-1}(x_a)} + \frac{J_m(x)}{J_{m+1}(x_a)} \right] = e_m$$

And coefficients g_m and h_m have the same symmetry,

$$g_m = \left[\frac{J_{m+1}(x)}{J_{m+1}(x_a)} + \frac{J_{m-1}(x)}{J_{m-1}(x_a)} \right]$$

$$g_{-m} = \left[\frac{J_{-m+1}(x)}{J_{-m+1}(x_a)} + \frac{J_{-m-1}(x)}{J_{-m-1}(x_a)} \right] = \left[\frac{J_{m-1}(x)}{J_{m-1}(x_a)} + \frac{J_{m+1}(x)}{J_{m+1}(x_a)} \right] = g_m$$

$$h_m = \left[\frac{J_{m+1}(x)}{J_{m+1}(x_a)} - \frac{J_{m-1}(x)}{J_{m-1}(x_a)} \right]$$

$$h_{-m} = \left[\frac{J_{-m+1}(x)}{J_{-m+1}(x_a)} - \frac{J_{-m-1}(x)}{J_{-m-1}(x_a)} \right] = \left[\frac{J_{m-1}(x)}{J_{m-1}(x_a)} - \frac{J_{m+1}(x)}{J_{m+1}(x_a)} \right] = - \left[\frac{J_{m+1}(x)}{J_{m+1}(x_a)} - \frac{J_{m-1}(x)}{J_{m-1}(x_a)} \right] = h_m$$

Thus we have shown that

$$\begin{aligned}
 e_{-m} &= e_m \\
 f_{-m} &= f_m \\
 g_{-m} &= g_m \\
 h_{-m} &= h_m .
 \end{aligned} \tag{D.10.2}$$

If the surface charge $n(\theta)$ happens to be even in θ , (D.1.7) shows that $\eta_m = N_m/N_0 = \eta_{-m}$. In this case, the E field components in (r, θ) can be written as in (D.1.7),

$$E_i(r, \theta) = E_i(r, m=0) + 2 \sum_{m=1}^{\infty} E_i(r, m) \cos(m\theta) \tag{D.10.3}$$

Then for even $n(\theta)$ the E fields are, using (D.9.39) with $\mathcal{B} \equiv (\xi_d/\epsilon_d) CV R_{dc}$,

$$\begin{aligned}
 E_z(r, \theta) &= (1/4) \mathcal{B} (\omega a) [f_0 + 2 \sum_{m=1}^{\infty} f_m \eta_m \cos(m\theta)] (\beta'/k) \\
 E_r(r, \theta) &= (j/4) \mathcal{B} (\omega a) [g_0 + 2 \sum_{m=1}^{\infty} g_m \eta_m \cos(m\theta)] \\
 E_\theta(r, \theta) &= (1/4) \mathcal{B} (\omega a) [h_0 + 2 \sum_{m=1}^{\infty} h_m \eta_m \cos(m\theta)] .
 \end{aligned} \tag{D.10.4a}$$

For general $n(\theta)$ where η_m and η_{-m} are no longer equal one has instead,

$$\begin{aligned}
 E_z(r, \theta) &= (1/4) \mathcal{B} (\omega a) [\sum_{m=-\infty}^{\infty} f_m \eta_m e^{jm\theta}] (\beta'/k) \\
 E_r(r, \theta) &= (j/4) \mathcal{B} (\omega a) [\sum_{m=-\infty}^{\infty} g_m \eta_m e^{jm\theta}] \\
 E_\theta(r, \theta) &= (1/4) \mathcal{B} (\omega a) [\sum_{m=-\infty}^{\infty} h_m \eta_m e^{jm\theta}] .
 \end{aligned} \tag{D.10.4b}$$

(b) High frequency evaluation of e_m , f_m , g_m and h_m and the E fields

For large ω we can use the following expressions for β' and k :

$$\beta^2 = -j\omega\mu\sigma \tag{1.5.1d} \text{ for good conductor}$$

$$k \approx \omega/v_d = \beta_{d0} = \omega\sqrt{L_e C} \approx \omega\sqrt{LC} \tag{Q.3.5}$$

$$\beta'^2 = \beta^2 - k^2 \approx -j\omega\mu\sigma - \omega^2 LC .$$

Although the second term appears to win out here for large ω , for frequencies of interest to us the first term is always much larger due to the large size of σ (see discussion below (D.2.2)) . Therefore

$$\beta' \approx \beta \approx \sqrt{-j\omega\mu\sigma} .$$

At high ω this β' parameter is very large, so $x_a = \beta'a$ will also be large and we need then to find the large x_a limits of the functions f_m , g_m and h_m . The $J_m(x)$ large- x limit is non-trivial, so we provide some detail.

From NIST 10.17.2, keeping a few leading terms in each inverse power expansion, we have this rather complicated large x behavior for $J_m(x)$,

$$J_m(x) = (2/\pi x)^{1/2} \{ \cos(w) [a_0(m) - a_2(m)/x^2 + O(1/x^4)] - \sin(w) [a_1(m)/x + O(1/x^3)] \}$$

$$w = x - m\pi/2 - \pi/4 \quad \Rightarrow \quad e^{-jw} = e^{-j(x - m\pi/2 - \pi/4)} = e^{-jx} e^{jm\pi/2} e^{j\pi/4}$$

$$a_0(m) = 1 \quad a_1(m) = \frac{4m^2 - 1}{8} \equiv c_m \quad a_2(m) = \frac{(4m^2 - 1)(4m^2 - 9)}{128} \equiv d_m \quad . \quad (D.10.5)$$

The expansion is in fact valid for all real and complex values of the parameter m , but we shall only use the expansion for integer m . Using the above abbreviations c_m and d_m one gets, for large x ,

$$J_m(x) = (2/\pi x)^{1/2} [\cos(w) (1 - d_m/x^2) - \sin(w) (c_m/x)] \quad . \quad (D.10.6)$$

Recall that inside the round wire,

$$\delta \equiv \sqrt{2/\omega\mu\sigma} = \text{skin depth} \quad // \quad \omega\mu\sigma = 2/\delta^2 \quad (2.2.20)$$

$$\beta = e^{j3\pi/4} (\sqrt{2}/\delta) = (j-1)/\delta \quad (2.2.21)$$

so

$$x = \beta r = e^{j3\pi/4} (\sqrt{2}/\delta) r = (j-1) (r/\delta)$$

$$x_a = \beta a = e^{j3\pi/4} (\sqrt{2}/\delta) a = (j-1) (a/\delta) \quad . \quad (D.10.7)$$

Since x has a large positive imaginary part for small δ , so does w . Then

$$\cos(w) = [e^{jw} + e^{-jw}] / 2 \approx (1/2) e^{-jw}$$

$$\sin(w) = [e^{jw} - e^{-jw}] / 2j \approx -(1/2j) e^{-jw} = (j/2) e^{-jw} \quad . \quad (D.10.8)$$

The large- x expansion above then becomes

$$J_m(x) = (2/\pi x)^{1/2} (1/2) [e^{-jw} (1 - d_m/x^2) - j e^{-jw} (c_m/x)]$$

$$= (1/2\pi x)^{1/2} e^{-jw} [1 - j c_m (1/x) - d_m (1/x^2) + \dots]$$

$$= (1/2\pi x)^{1/2} e^{-jx} e^{jm\pi/2} e^{j\pi/4} [1 - j c_m (1/x) - d_m (1/x^2) + \dots] \quad . \quad (D.10.9)$$

It is not hard to show that this agrees with (2.3.5) through order $1/x$. Notice from (D.10.7) that

$$e^{-jx} = e^{-j(j-1)(x/\delta)} = e^{(1+j)(x/\delta)}$$

giving a convenient hybrid large-x form for $J_m(x)$,

$$J_m(x) = (1/2\pi x)^{1/2} e^{(1+j)(x/\delta)} (j)^m e^{jn/4} [1 - j c_m(1/x) - d_m(1/x^2) + \dots] \quad (D.10.10)$$

From (D.10.10) we see by inspection that, through $O(1/x)$,

$$\begin{aligned} \frac{J_m(x)}{J_n(x_a)} &= (j)^{m-n} \sqrt{\frac{a}{r}} e^{(1+j)(x-a)/\delta} \frac{1 - j c_m(1/x) - d_m(1/x^2) + \dots}{1 - j c_n(1/x_a) - d_n(1/x_a^2) + \dots} \\ &\approx (j)^{m-n} \sqrt{\frac{a}{r}} e^{(1+j)(x-a)/\delta} [1 - j c_m/x + j c_n/x_a] \end{aligned} \quad (D.10.11)$$

and

$$\frac{J_m(x)}{J_m(x_a)} = \sqrt{\frac{a}{r}} e^{(1+j)(x-a)/\delta} \quad // \text{ independent of } m \quad (D.10.12)$$

Therefore, for large ω ,

$$\begin{aligned} g_m &= \left[\frac{J_{m+1}(x)}{J_{m+1}(x_a)} + \frac{J_{m-1}(x)}{J_{m-1}(x_a)} \right] = 2 \sqrt{\frac{a}{r}} e^{(1+j)(x-a)/\delta} \\ h_m &= \left[\frac{J_{m+1}(x)}{J_{m+1}(x_a)} - \frac{J_{m-1}(x)}{J_{m-1}(x_a)} \right] = 0 \\ f_m &= \left[\frac{J_m(x)}{J_{m+1}(x_a)} - \frac{J_m(x)}{J_{m-1}(x_a)} \right] = (j)^{-1} \sqrt{\frac{a}{r}} e^{(1+j)(x-a)/\delta} [1 - j c_m/x + j c_{m+1}/x_a] \\ &\quad - (j)^{+1} \sqrt{\frac{a}{r}} e^{(1+j)(x-a)/\delta} [1 - j c_m/x + j c_{m-1}/x_a] \\ &= -j \sqrt{\frac{a}{r}} e^{(1+j)(x-a)/\delta} [2 - 2j c_m(1/x) + j(c_{m+1} + c_{m-1})(1/x_a)] \\ &\approx -2j \sqrt{\frac{a}{r}} e^{(1+j)(x-a)/\delta} \end{aligned}$$

and we see that f_m , g_m and h_m are all independent of m . For e_m (which appears in the B field expressions),

$$\begin{aligned} e_m &= \left[\frac{J_m(x)}{J_{m+1}(x_a)} + \frac{J_m(x)}{J_{m-1}(x_a)} \right] = (j)^{-1} \sqrt{\frac{a}{r}} e^{(1+j)(x-a)/\delta} [1 - j c_m/x + j c_{m+1}/x_a] \\ &\quad + (j)^{+1} \sqrt{\frac{a}{r}} e^{(1+j)(x-a)/\delta} [1 - j c_m/x + j c_{m-1}/x_a] \end{aligned}$$

$$\begin{aligned}
 &= -j \sqrt{\frac{a}{r}} e^{(1+j)(x-a)/\delta} [(j/x_a)(c_{m+1} - c_{m-1})] = -j \sqrt{\frac{a}{r}} e^{(1+j)(x-a)/\delta} [(j/x_a) 2m] \\
 &\approx 0 \text{ due to } 1/x_a .
 \end{aligned}$$

The E field expressions from box (D.9.37) are then,

$$\begin{aligned}
 E_z(r,m) &= (1/4) \eta_m \mathcal{B}(\omega a) (\beta'/k) f_m & f_m &= -2j \sqrt{\frac{a}{r}} e^{(1+j)(x-a)/\delta} & x &= \beta'r \\
 E_r(r,m) &= (j/4) \eta_m \mathcal{B}(\omega a) g_m & g_m &= 2 \sqrt{\frac{a}{r}} e^{(1+j)(x-a)/\delta} & x_a &= \beta'a \\
 E_\theta(r,m) &= (1/4) \eta_m \mathcal{B}(\omega a) h_m & h_m &= 0 & k &= \beta_{d0}
 \end{aligned}$$

or

Large ω limits of the E field solutions : $R_{dc} = \frac{1}{\sigma \pi a^2}$ (D.10.13)

$$\begin{aligned}
 E_z(r,m) &= -(j/2) \eta_m \mathcal{B}(\omega a) (\beta/\beta_{d0}) \sqrt{\frac{a}{r}} e^{-(1+j)(a-r)/\delta} & x &= \beta r \\
 E_r(r,m) &= (j/2) \eta_m \mathcal{B}(\omega a) \sqrt{\frac{a}{r}} e^{-(1+j)(a-r)/\delta} & x_a &= \beta a \\
 E_\theta(r,m) &= 0 & \mathcal{B} &\equiv CV R_{dc}
 \end{aligned}$$

As observed earlier, the longitudinal current J_z is much larger than the radial current J_r by factor $|\beta/\beta_{d0}|$.

Notice the standard skin effect behavior both in amplitude and phase for both field components. We saw this earlier in several places:

$$E(x,\omega) = E(0,\omega) e^{-x/\delta} e^{-jx/\delta} = E(0,\omega) e^{-(1+j)x/\delta} \quad x \rightarrow (a-r) \quad \text{1D example} \quad (2.1.8)$$

$$\frac{|E_z(r)|}{|E_z(a)|} = \sqrt{\frac{a}{r}} e^{-(a-r)/\delta} \quad r/\delta > 3/\sqrt{2} = 2.1 \quad . \quad (2.3.7)$$

The θ -space fields from (D.10.4b) are then,

$$\begin{aligned}
 E_z(r,\theta) &= -(j/2) \mathcal{B}(\omega a) (\beta/k) \left\{ \sqrt{\frac{a}{r}} e^{-(1+j)(a-r)/\delta} \right\} \left[\sum_{m=-\infty}^{\infty} \eta_m e^{jm\theta} \right] \\
 E_r(r,\theta) &= (j/2) \mathcal{B}(\omega a) \left\{ \sqrt{\frac{a}{r}} e^{-(1+j)(a-r)/\delta} \right\} \left[\sum_{m=-\infty}^{\infty} \eta_m e^{jm\theta} \right] \\
 E_\theta(r,\theta) &= 0 & \eta_m &= N_m/N_0 . & & (D.10.14)
 \end{aligned}$$

But $[\sum_{m=-\infty}^{\infty} \eta_m e^{jm\theta}]$ is just $n(\theta)/N_0$ from (D.1.5a). Meanwhile,

$$\begin{aligned}
 (j/2) \mathcal{B}(\omega a)/N_0 &= (j/2) (\xi_d/\epsilon_d) CV R_{dc}(\omega a) / N_0 \\
 &= (j/2) (1) [2\pi a N_0] R_{dc}(\omega a) / N_0 && // (D.1.8) \text{ and } \xi_d/\epsilon_d = 1 \text{ for large } \omega \\
 &= (j/2) 2\pi a (1/\sigma\pi a^2) (\omega a) && // R_{dc} = 1/\sigma\pi a^2 \\
 &= (j\omega/\sigma)
 \end{aligned}$$

so then for large ω (D.10.14) becomes,

$$\begin{aligned}
 E_z(r,\theta) &= - (j\omega/\sigma) \sqrt{\frac{a}{r}} e^{-(1+j)(a-r)/\delta} n(\theta) (\beta/k) \\
 E_r(r,\theta) &= (j\omega/\sigma) \sqrt{\frac{a}{r}} e^{-(1+j)(a-r)/\delta} n(\theta) \\
 E_\theta(r,\theta) &= 0
 \end{aligned} \tag{D.10.15}$$

so both E_z and E_r track $n(\theta)$. From the first line of (D.10.15) the surface impedance is then

$$Z_s(\theta) \equiv E_z(a,\theta) / I = - (j\omega/\sigma) n(\theta) (\beta/k) / [2\pi a (\omega/k) N_0] = - (j/\sigma) (\beta/2\pi a) \frac{n(\theta)}{\langle n(\theta) \rangle}$$

where I comes from (D.2.31c) since $(\xi_d/\epsilon_d) = 1$ for large ω . But (2.2.21) says $\beta = (j-1)/\delta$, so

$$Z_s(\theta) \equiv - (j/\sigma) (j-1)(1/2\pi a\delta) \frac{n(\theta)}{\langle n(\theta) \rangle} = \frac{1}{\sigma(2\pi a)\delta} (1+j) \frac{n(\theta)}{\langle n(\theta) \rangle} \tag{D.10.16}$$

and $Z_s(\theta)$ is seen to track $n(\theta)$. Averaging over the round wire surface (as done in (4.12.9)) then gives

$$\langle Z_s(\theta) \rangle = \frac{1}{\sigma(2\pi a)\delta} (1+j) \tag{D.10.17}$$

which is the same as Z_s appearing in (2.4.16) for the symmetric round wire case.

Observations on the E fields for large ω

In the extreme skin effect (small δ , large ω) regime:

1. There is no azimuthal field E_θ inside or on the surface of the round wire.
2. Both E_z and E_r exhibit the standard skin effect form for amplitude and phase.
3. At least for low loss situations, the ratio $E_z(r,\theta)/E_r(r,\theta) = - (\beta'/k) = - (\beta'/\beta_{d0})$ is very large in magnitude and is constant in r and θ .

4. Both E_z and E_r track the surface charge density $n(\theta)$ for azimuthal dependence.

5. If $n(\theta) \neq \text{constant}$, then $J_z = \sigma E_z \neq \text{constant}$ in θ and the longitudinal current density is *asymmetric* across the round wire cross section, which is known as the proximity effect. This implies that the surface impedance Z_s is a function of θ , as shown in (D.10.16). In Section 2.4 the surface impedance was a constant since only the $m=0$ partial wave was involved.

Reader Exercise. Use $-j\omega\mathbf{B} = \text{curl } \mathbf{E}$ in the form (D.4.7), with (D.10.13) for \mathbf{E} , to obtain the following expressions for the partial wave magnetic fields inside a round wire at large ω :

$$B_z(r,m) = (j/2) \eta_m I R_{dc} (1/\omega) m\beta_{d0} \left(\frac{a}{r}\right)^{3/2} e^{-(1+j)(a-r)/\delta} \quad (\text{D.10.18})$$

$$B_r(r,m) = (j/2) \eta_m I R_{dc} (1/\omega) m\beta \left(\frac{a}{r}\right)^{3/2} e^{-(1+j)(a-r)/\delta}$$

$$B_\theta(r,m) = (j/2) \eta_m I R_{dc} (1/\omega) \beta \left(\frac{a}{r}\right)^{3/2} e^{-(1+j)(a-r)/\delta} [(\beta_{d0}r)(\beta_{d0}/\beta) - j/2 + (r/\delta)(j-1)].$$

In the transmission line limit $|(\beta_{d0}r)| \ll 1$ and from comments below (D.2.2) $|(\beta_{d0}/\beta)| \ll 1$, so the last bracket simplifies to $[-j/2 + (r/\delta)(j-1)]$. Since the exponential decays quickly in r , we could set $r \approx a$ in this bracket and make little difference to get $[-j/2 + (a/\delta)(j-1)]$. But $(a/\delta) \gg 1$ more or less in the large ω limit, so then the bracket is $\approx [(a/\delta)(j-1)]$ Observations:

- As expected, the B field components have the same skin effect exponential decay as the E field components.
- The B_z and B_r components vanish for $m = 0$ but the B_θ component does not. Why is this so?
[Hint: Look at (D.4.6)]
- B_θ is larger than B_r by roughly (a/δ) , and B_r is larger than B_z by the factor $|(\beta/\beta_{d0})| \gg 1$.

D.11 Low frequency limit of the round wire E fields

(a) A High Level Review of Appendix D and its Accuracy

As presented above, the general approach of Appendix D was to solve for the E and B fields inside a round wire assuming the ansatz traveling wave form

$$\mathbf{E}(r,\theta,z,t) = e^{j(\omega t - kz)} \mathbf{E}(r,\theta) \quad (D.1.1)$$

where k is an arbitrary complex parameter. For any k , we found the following E field solution, where k dependence is now shown more explicitly:

Second summary of the E field solutions :	$R_{dc} = \frac{1}{\sigma\pi a^2}$	$\beta'^2 = \beta^2 - k^2$	$(D.9.37)$
$E_z(r,m) = (1/4) \eta_m \mathcal{B}(\omega a) (\beta'/k) f_m$	$f_m = \left[\frac{J_m(x)}{J_{m+1}(x_a)} - \frac{J_m(x)}{J_{m-1}(x_a)} \right]$	$x = \beta'r$	$x_a = \beta'a$
$E_r(r,m) = (j/4) \eta_m \mathcal{B}(\omega a) g_m$	$g_m = \left[\frac{J_{m+1}(x)}{J_{m+1}(x_a)} + \frac{J_{m-1}(x)}{J_{m-1}(x_a)} \right]$	$\mathcal{B} \equiv (\xi_d/\epsilon_d) CV R_{dc}$	
$E_\theta(r,m) = (1/4) \eta_m \mathcal{B}(\omega a) h_m$	$h_m = \left[\frac{J_{m+1}(x)}{J_{m+1}(x_a)} - \frac{J_{m-1}(x)}{J_{m-1}(x_a)} \right]$	$G \geq 0$	

High Level Overview

These fields exactly solve Maxwell's equations and the two boundary conditions (D.2.26) and (D.2.27), and from these E fields we computed the corresponding B fields. The coefficients η_m are the moments of the surface charge distribution $n(\theta)$ on the round wire surface. In principle, any linear combination of these solutions for different k values (including a continuous superposition) is also a possible solution.

However, when this round wire is part of a transmission line, one must also take into consideration the field solution outside the round wire -- the solution within the transmission line dielectric region. This is the so-called exterior solution, whereas our round wire analysis provided an interior solution. The idea is that the exterior solution provides the correct value of parameter k to use for the interior solution. The solutions must have the same k value due to the boundary between interior and exterior.

Whereas Appendix D found the interior solution for the E field using the Helmholtz equation, Chapters 3 and 4 obtained the exterior solution in terms of the potentials ϕ and A_z using the King gauge condition. This analysis was not valid at low frequencies for a variety of reasons noted in those chapters, perhaps the most dramatic of which is shown in Fig 3.6.(b). This drawing illustrates how the round wires of a twin-lead transmission line are clearly not surfaces of constant A_z potential at very low frequency, whereas the theory assumes that they are. The main results of Chapter 4 were the first and second order "transmission line equations" (4.12.15) and (4.12.17) involving $i(z)$ and $V(z)$. The second order equations are (damped, ω domain) wave equations which directly imply an e^{-jkz} dependence on z . Through the boundary between the interior and exterior solutions, this implies a similar e^{-jkz} form for the interior solutions, which form is the ansatz of Appendix D. However, at low frequencies these wave equations are no longer valid, there are "correction terms" [see (S.29)], and thus the e^{-jkz} ansatz (D.1.1) of Appendix D is no longer valid. Therefore, we cannot expect low frequency predictions of Appendix D concerning interior fields to be accurate. See Chapter 7 for further discussion of low frequency issues.

Meanwhile, on a separate track altogether, Appendix K describes the so-called "network model" of the exterior solution [at least $i(z)$ and $V(z)$] for a transmission line, using lumped R,G,L,C components. In this model, the same transmission line equations obtained in Chapter 4 are found to be true, justifying the network model. However, in the network model, these transmission line equations are valid all the way down to DC ($\omega=0$) whereas we have just shown that the "physics model" does not support this conclusion. Nevertheless, we can use the network model's low frequency range as an approximation to the true exterior solution at low frequency. In other words, we can pretend that the transmission line equations are valid all the way down to DC. In so doing, we should not be surprised to find results which are inaccurate. Note that the network model says nothing about interior field solutions.

Above low frequencies both the physics and network models provide the same value of k to be used in the round wire interior solution. That value is $k = -j\sqrt{zy} = -j\sqrt{(R+j\omega L)(G+j\omega C)}$. Since k is a function of ω (explicitly and also through ω dependence of the parameters), the transmission line has "dispersion" and a group velocity $v_g = \partial\omega/\partial k$ different from the phase velocity $v_\phi = \omega/k$. Appendix Q obtains expressions for $k(\omega)$ appropriate for both high and low frequencies as limits of this rather complicated function. We then use these limits in our low frequency analysis below, aware that they can give inaccurate results. Appendix R makes use of the $k(\omega)$ function in a case study of a certain Belden cable.

(b) Low frequency values for β'

For low ω and $G > 0$: We seek an expression for β' at low ω . Since $\beta'^2 = \beta^2 - k^2$, we need to know about β and k . For any ω , we know first that

$$\beta^2 = -j\omega\mu\sigma \quad (1.5.1d) \text{ for good conductor}$$

so $\beta^2 \rightarrow 0$ as $\omega \rightarrow 0$. Meanwhile, the ultra-low frequency limit of k is known from (Q.4.6) to be,

$$\begin{aligned} \text{Re}(k) &\approx (\omega/2) (R_{dc2} + \omega_d L_{dc}) \sqrt{C/(\omega_d R_{dc2})} + O(\omega^2) & \omega < \omega_d = (\sigma_d/\epsilon_d) \\ \text{Im}(k) &\approx -\sqrt{R_{dc2}G} [1 + (\tan\tau/2) (\omega/\omega_d)] + O(\omega^2) \end{aligned} \quad (Q.4.6)$$

Here we use R_{dc2} to indicate the total DC resistance per unit length of the two transmission line conductors, to avoid confusion with R_{dc} appearing in (D.2.33) which is for the round conductor alone. Symbol G refers to the DC dielectric conductance of the transmission line, called G_{dc} in Appendix Q.

As $\omega \rightarrow 0$, one finds $\text{Re}(k) \rightarrow 0$ and $\text{Im}(k) \rightarrow -\sqrt{R_{dc2}G}$. Thus, at low ω ,

$$\begin{aligned} \beta^2 &\approx 0 \\ k &\approx -j\sqrt{R_{dc2}G} \quad \Rightarrow \quad k^2 = -R_{dc2}G \\ \beta'^2 = \beta^2 - k^2 &\approx -k^2 \approx R_{dc2}G \end{aligned} \quad (D.11.1)$$

For any reasonable transmission line $R_{dc2}G$ will very small so the Bessel argument $x_a = \beta'a \ll 1$.

Low Frequency Example: For Belden 8281 coaxial cable, Appendix R below Fig R.6 gives $R_{dc2} = .036$ and $G = 0.338 \times 10^{-14}$ so $\beta'^2 \approx R_{dc2}G \approx 1.22 \times 10^{-16}$ and then $\beta' \approx 1.1 \times 10^{-8} \text{ m}^{-1}$. The central conductor has $a = 3.94 \times 10^{-4} \text{ m}$ so $\beta'a \approx 5 \times 10^{-12} \ll 1$.

Since $\beta'a$ is very small, we shall need to evaluate f_m , g_m and h_m for small $x_a = \beta'a$.

For low ω and $G = 0$: When $G = 0$, the ultra-low ω behavior of k is given by (Q.4.9),

$$\begin{aligned} \text{Re}(k) &\approx +\sqrt{R_{dc2}C/2} \sqrt{\omega} (1 - \tan\epsilon/2) + O(\omega^{3/2}) \\ \text{Im}(k) &\approx -\sqrt{R_{dc2}C/2} \sqrt{\omega} (1 + \tan\epsilon/2) + O(\omega^{3/2}) \end{aligned} \quad (Q.4.9)$$

As $\omega \rightarrow 0$ one then has,

$$k \approx \sqrt{R_{dc2}C/2} \sqrt{\omega} (1 - j) = \sqrt{R_{dc2}C} \sqrt{\omega} e^{-j/4}$$

$$k^2 = -j\omega R_{dc2}C$$

$$\beta^2 = -j\omega\mu\sigma \quad (1.5.1d) \text{ for good conductor}$$

$$\beta'^2 = \beta^2 - k^2 \approx -j\omega\mu\sigma + j\omega R_{dc2}C = -j\omega(\mu\sigma - R_{dc2}C). \quad (D.11.2)$$

Again β' is very small at low frequency and in fact $\beta' \rightarrow 0$ as $\omega \rightarrow 0$. Thus again $\beta'a \ll 1$ so we need to evaluate f_m , g_m and h_m for small $x_a = \beta'a$.

(c) Low frequency evaluation of e_m , f_m , g_m and h_m

Although e_m does not appear in the E field expressions, it does in the B field ones so we include it here.

In the following we consider only $m \geq 0$, knowing from (D.10.2) that $*_{-m} = *_{m}$ for $* = e, f, g$ or h .

The small x limit for $J_m(x)$ is given by NIST 10.7.3,

$$J_n(x) = (x/2)^n / n! \quad \text{for } n = 0, 1, 2, \dots \quad (D.11.3)$$

Since J_{m-1} appears in our coefficient expressions and since $m = 0$ is encountered, we have to deal with $m = 0$ as a special case since the above limit is not valid for $n = -1$. To this end we use NIST 10.2.2 which is valid for integer n ,

$$J_{-n}(x) = (-1)^n J_n(x) \approx (-1)^n (x/2)^n / n! \quad (D.11.4)$$

so that $J_{-1}(x) = -J_1(x) \approx -(x/2)$. Our small- x forms of interest are then

$$\begin{aligned} J_n(x) &= (x/2)^n / n! && \text{for } n = 0, 1, 2, \dots \\ J_{-1}(x) &= -(x/2) && \text{for } n = -1 \end{aligned} \quad (D.11.5)$$

We now examine the small x limits of e_m , f_m , g_m , and h_m .

First f_m for $m > 0$, and then for $m = 0$:

$$\begin{aligned} f_m &= \left[\frac{J_m(x)}{J_{m+1}(x_a)} - \frac{J_m(x)}{J_{m-1}(x_a)} \right] = \left[\frac{(x/2)^m/m!}{(x_a/2)^{m+1}/(m+1)!} - \frac{(x/2)^m/m!}{(x_a/2)^{m-1}/(m-1)!} \right] \\ &= [(m+1) (x/x_a)^m (2/x_a) - (1/m) (x/x_a)^m (x_a/2)] = (x/x_a)^m [(m+1) (2/x_a) - (1/m) (x_a/2)] \\ &\approx (x/x_a)^m (m+1) (2/x_a) \quad // \text{ as } x_a \rightarrow 0 \end{aligned}$$

$$f_0 = \left[\frac{J_0(x)}{J_1(x_a)} - \frac{J_0(x)}{J_{-1}(x_a)} \right] = \left[\frac{J_0(x)}{J_1(x_a)} + \frac{J_0(x)}{J_1(x_a)} \right] = 2 \frac{J_0(x)}{J_1(x_a)} = 2 \frac{1}{(x_a/2)} = 4/x_a$$

Since only the first term in f_m survives the small x limit, the results for e_m are the same as for f_m :

$$e_m \approx \left[\frac{J_m(x)}{J_{m+1}(x_a)} + \frac{J_m(x)}{J_{m-1}(x_a)} \right] \approx (x/x_a)^m (m+1) (2/x_a).$$

But e_0 is different

$$e_0 = \left[\frac{J_0(x)}{J_1(x_a)} + \frac{J_0(x)}{J_{-1}(x_a)} \right] = \left[\frac{J_0(x)}{J_1(x_a)} - \frac{J_0(x)}{J_1(x_a)} \right] = 0.$$

First g_m for $m > 0$, and then for $m = 0$:

$$\begin{aligned} g_m &= \left[\frac{J_{m+1}(x)}{J_{m+1}(x_a)} + \frac{J_{m-1}(x)}{J_{m-1}(x_a)} \right] = \left[\frac{(x/2)^{m+1}/(m+1)!}{(x_a/2)^{m+1}/(m+1)!} + \frac{(x/2)^{m-1}/(m-1)!}{(x_a/2)^{m-1}/(m-1)!} \right] \\ &= (x/x_a)^{m+1} + (x/x_a)^{m-1} \\ g_0 &= \left[\frac{J_1(x)}{J_1(x_a)} + \frac{J_{-1}(x)}{J_{-1}(x_a)} \right] = \left[\frac{J_1(x)}{J_1(x_a)} + \frac{J_1(x)}{J_1(x_a)} \right] = 2 \frac{J_1(x)}{J_1(x_a)} = 2 (x/x_a) \end{aligned}$$

Results for h_m are then obvious since there is only a sign change between the terms in g_m .

$$h_m = (x/x_a)^{m+1} - (x/x_a)^{m-1} \quad h_0 = 0 \quad [\text{exactly, for any } x \text{ and } x_a]$$

The results are then,

$$\begin{array}{ll} e_m = (r/a)^m (m+1) (2/\beta'a) & e_0 = 0 \\ f_m = (r/a)^m (m+1) (2/\beta'a) & f_0 = 4/(a\beta') \\ g_m = (r/a)^{m+1} + (r/a)^{m-1} & g_0 = 2 (r/a) \\ h_m = (r/a)^{m+1} - (r/a)^{m-1} & h_0 = 0 \end{array}$$

for $m \geq 0$. Allowing for all integer values of m , using the symmetries (D.10.2) we can write,

$$\begin{aligned}
 e_m &= (r/a)^{|m|} (|m|+1) (2/\beta'a) & e_0 &= 0 \\
 f_m &= (r/a)^{|m|} (|m|+1) (2/\beta'a) & f_0 &= 4/(a\beta') \\
 g_m &= (r/a)^{|m|+1} + (r/a)^{|m|-1} & g_0 &= 2 (r/a) \\
 h_m &= (r/a)^{|m|+1} - (r/a)^{|m|-1} & h_0 &= 0 \quad .
 \end{aligned} \tag{D.11.6}$$

(d) Low frequency E fields

Recall that for the general case $G \geq 0$ we can write the E fields as

Second summary of the E field solutions :	$R_{dc} = \frac{1}{\sigma\pi a^2}$	$\beta'^2 = \beta^2 - k^2$	(D.9.37)
$E_z(r,m) = (1/4) \eta_m \mathcal{B}(\omega a) (\beta'/k) f_m$	$f_m = \left[\frac{J_m(x)}{J_{m+1}(x_a)} - \frac{J_m(x)}{J_{m-1}(x_a)} \right]$	$x = \beta'r$	$x_a = \beta'a$
$E_r(r,m) = (j/4) \eta_m \mathcal{B}(\omega a) g_m$	$g_m = \left[\frac{J_{m+1}(x)}{J_{m+1}(x_a)} + \frac{J_{m-1}(x)}{J_{m-1}(x_a)} \right]$	$\mathcal{B} \equiv (\xi_d/\epsilon_d) CV R_{dc}$	
$E_\theta(r,m) = (1/4) \eta_m \mathcal{B}(\omega a) h_m$	$h_m = \left[\frac{J_{m+1}(x)}{J_{m+1}(x_a)} - \frac{J_{m-1}(x)}{J_{m-1}(x_a)} \right]$	$G \geq 0$	

For small ω , use the small- x limits of (D.11.6) to get

$E_z(r,m) = (1/2) \eta_m \mathcal{B}(\omega/k) (r/a)^m (m+1)$	(D.11.7)
$E_r(r,m) = (j/4) \eta_m \mathcal{B}(\omega a) [(r/a)^{m+1} + (r/a)^{m-1}]$	
$E_\theta(r,m) = (1/4) \eta_m \mathcal{B}(\omega a) [(r/a)^{m+1} - (r/a)^{m-1}]$	$m > 0$
$E_z(r,0) = \mathcal{B}(\omega/k)$	$\mathcal{B} \equiv (\xi_d/\epsilon_d) CV R_{dc}$
$E_r(r,0) = (j/2) \mathcal{B}(\omega r)$	
$E_\theta(r,0) = 0$	$m = 0 \quad G \geq 0$

For $G = 0$ one has,

$$(\xi_d/\epsilon_d) = 1 \tag{D.9.28}$$

$$k = \sqrt{R_{dc} C} \sqrt{\omega} e^{-j/4} \Rightarrow C(\omega/k) = e^{j/4} \sqrt{\omega} \sqrt{C/R_{dc} C} \tag{D.11.2}$$

and then the E fields are

$$\begin{aligned}
 E_z(r,m) &= (1/2) \eta_m e^{j/4} V R_{dc} \sqrt{\omega} \sqrt{C/R_{dc2}} (r/a)^m (m+1) \\
 E_r(r,m) &= (j/4) \eta_m CV R_{dc} (\omega a) [(r/a)^{m+1} + (r/a)^{m-1}] \\
 E_\theta(r,m) &= (1/4) \eta_m CV R_{dc} (\omega a) [(r/a)^{m+1} - (r/a)^{m-1}] \quad m > 0 \\
 \\
 E_z(r,0) &= e^{j/4} V R_{dc} \sqrt{\omega} \sqrt{C/R_{dc2}} \\
 E_r(r,0) &= (j/2) CV R_{dc} (\omega r) \\
 E_\theta(r,0) &= 0 \quad m = 0 \quad G = 0 \quad \omega \rightarrow 0
 \end{aligned} \tag{D.11.8}$$

As $\omega \rightarrow 0$, all E fields go to zero as one might expect since $Z_0 \rightarrow \infty$. In the network model one has,

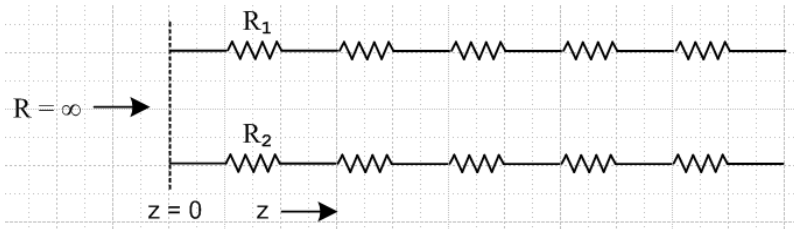


Fig D.8

The current is $I = CV(\omega/k) = V e^{j/4} \sqrt{\omega} \sqrt{C/R_{dc2}}$ and it too $\rightarrow 0$. With no current in the transmission line, it seems reasonable that all E fields should vanish.

For $G > 0$ one has instead, for small ω ,

$$(\xi_d/\epsilon_d) \approx (G/j\omega C) \tag{D.9.28}$$

$$k = -j\sqrt{R_{dc2}G} \tag{D.11.1}$$

and then the E fields of (D.11.7) are,

$$\begin{aligned}
 E_z(r,m) &= (1/2) \eta_m V R_{dc} \sqrt{G/R_{dc}} (r/a)^m (m+1) \\
 E_r(r,m) &= (1/4) \eta_m V R_{dc} (G a) [(r/a)^{m+1} + (r/a)^{m-1}] \\
 E_\theta(r,m) &= -j(1/4) \eta_m V R_{dc} (G a) [(r/a)^{m+1} - (r/a)^{m-1}] \quad m > 0 \\
 \\
 E_z(r,0) &= V R_{dc} \sqrt{G/R_{dc}} \\
 E_r(r,0) &= (1/2) V R_{dc} (G r) \\
 E_\theta(r,0) &= 0 \quad m = 0 \quad G > 0 \quad \omega \rightarrow 0
 \end{aligned} \tag{D.11.9}$$

As $\omega \rightarrow 0$, all E fields approach finite values except $E_\theta(r,0) = 0$. This seems reasonable since even at DC current flows between the conductors through the dielectric when $G > 0$.

Consider now the ratio $E_z(r,m)/E_z(r,0)$. For $G = 0$ or $G > 0$ the ratio is exactly the same, namely

$$\frac{J_z(r,m)}{J_z(r,0)} = \frac{E_z(r,m)}{E_z(r,0)} = (1/2) \eta_m (r/a)^m (m+1) \quad \text{as } \omega \rightarrow 0, m > 0 \quad (D.11.10)$$

where $J_z = \sigma E_z$ is used to obtain the leftmost ratio.

An anomaly. For the $G = 0$ case, the above result is rather disturbing. In the DC limit $\omega \rightarrow 0$, we expect the current density J_z inside our round wire to approach a uniform value. This is so because we expect there to be no eddy currents at $\omega = 0$ and these are the cause of J_z non-uniformity as discussed in Appendix P. In order for J_z to be uniform, the partial wave components $J(r,m)$ for $m \neq 0$ must all vanish. But the ratio above shows that they do not vanish in relation to $J(r,0)$. It is true that in the final limit $\omega \rightarrow 0$ all E fields vanish, as shown in (D.11.8), but we would have expected that, as we approach the limit, the current density would smoothly approach a uniform constant value.

Let us re-examine this situation in the θ domain rather than the m domain. Recall that for $n(\theta)$ even, one has $\eta_{-m} = \eta_m$ and then

$$E_z(r,\theta) = E_z(r,m=0) + 2 \sum_{m=1}^{\infty} E_z(r,m) \cos(m\theta) \quad (D.10.3)$$

Inserting the small- ω fields from (D.11.8) then gives

$$\begin{aligned} E_z(r,\theta) &= e^{j/4} V R_{dc} \sqrt{\omega} \sqrt{C/R_{dc2}} \\ &+ 2 \sum_{m=1}^{\infty} (1/2) \eta_m e^{j/4} V R_{dc} \sqrt{\omega} \sqrt{C/R_{dc2}} (r/a)^m (m+1) \cos(m\theta) \\ &= e^{j/4} V R_{dc} \sqrt{\omega} \sqrt{C/R_{dc2}} \left[1 + \sum_{m=1}^{\infty} \eta_m (r/a)^m (m+1) \cos(m\theta) \right] \end{aligned} \quad (D.11.11)$$

and therefore

$$J_z(r,\theta) = e^{j/4} \sigma V R_{dc} \sqrt{\omega} \sqrt{C/R_{dc2}} \left[1 + \sum_{m=1}^{\infty} \eta_m (r/a)^m (m+1) \cos(m\theta) \right] \quad (D.11.12)$$

The integral of J_z over the round wire cross section gives the total current I . In this integral, the partial waves with $m > 0$ make no contribution due to the $d\theta$ integral. Therefore

$$I = (e^{j/4} \sigma V R_{dc} \sqrt{\omega} \sqrt{C/R_{dc2}}) * \pi a^2 = e^{j/4} V \sqrt{\omega} \sqrt{C/R_{dc2}} \quad (D.11.13)$$

The expression for E_z and J_z can then be written in this simple form,

$$E_z(r,\theta) = I R_{dc} \left[1 + \sum_{m=1}^{\infty} \eta_m (r/a)^m (m+1) \cos(m\theta) \right] \quad \text{as } \omega \rightarrow 0 \quad (\text{D.11.14})$$

$$J_z(r,\theta) = \sigma I R_{dc} \left[1 + \sum_{m=1}^{\infty} \eta_m (r/a)^m (m+1) \cos(m\theta) \right] \quad \text{as } \omega \rightarrow 0 \quad (\text{D.11.15})$$

One sees explicitly now how $J_z(r,\theta)$ is not uniform but varies with both r and θ over the round wire cross section. As $\omega \rightarrow 0$, the shape of J_z over the round wire cross section approaches the bracketed function. The correct $\omega = 0$ result $I/(\pi a^2)$ is just the "1" term, as if all the η_m vanished for $m > 0$. But they don't vanish since a DC capacitor made from two infinite cylinders held at V in a vacuum holds charge which is asymmetric around the cross section perimeter.

There is a possible obscure argument that somehow, as $\omega \rightarrow 0$, the ratio of the eddy currents to the total current I is somehow constant and that is how the J_z asymmetry is maintained all the way to $\omega \rightarrow 0$. We don't think this argument is valid, so we really do have an anomaly of our theory as $\omega \rightarrow 0$.

The surface impedance for the round conductor is given by,

$$Z_s(\theta) \equiv E_z(a,\theta)/I = R_{dc} \left[1 + \sum_{m=1}^{\infty} \eta_m (r/a)^m (m+1) \cos(m\theta) \right] \quad \text{as } \omega \rightarrow 0 \quad (\text{D.11.16})$$

and so

$$\langle Z_s(\theta) \rangle = R_{dc} \quad \text{as } \omega \rightarrow 0 \quad (\text{D.11.17})$$

as one would expect.

Reader Exercise: Does (D.11.9) give the correct solution to the implied magnetostatics problem, or are there anomalies like the one noted above? Notice that Z_0 is certainly correct based on the reader exercise given in Appendix K (c). The "wave" decays in z according to $e^{-j\mathbf{k}z} = \exp(-\sqrt{RG} z)$ which also seems reasonable.

Appendix E: How Thick is Surface Charge on a Metal Conductor?

It is often said that surface charges exist only very close to the surface of a conductor. In this section, we will show how extremely true this statement is. Here is a crude sketch of what we expect surface charge distributions might look like at the plates of a capacitor.

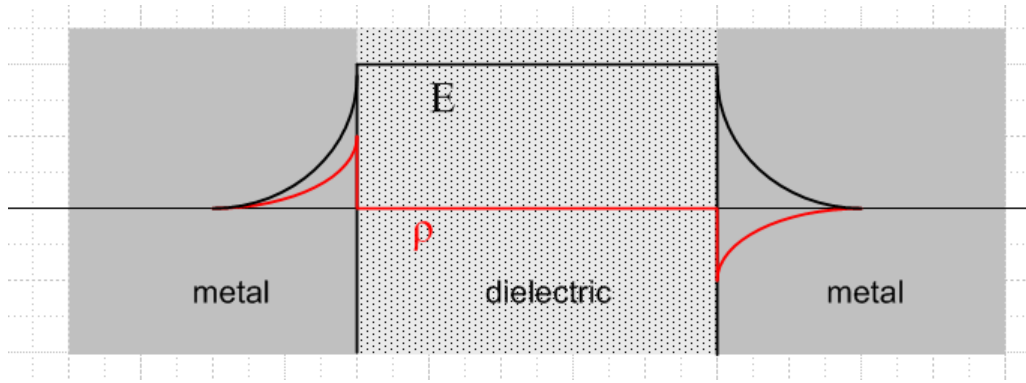


Fig E.1

The red plot is charge density ρ , and the black plot is the electric field magnitude. The charge density is exactly $\rho = 0$ in the dielectric region between the two plates simply because there are no available charge carriers as there are in a metal (the electron cloud), see Section 3.1. Barring a huge E field or very high temperatures, electrons cannot just "jump off" the metal surface into the dielectric region because of an energy cost to do so, called the work function.

The figure suggests that the charge distribution might have an exponential decay going into each metal surface, with some characteristic distance which we seek to find. The reader might wonder: is it the skin depth δ ? The answer to that question is: most definitely not!

We are accustomed to using Ohm's law $\mathbf{J} = \sigma \mathbf{E}$ in various forms. Application of this law in the regions of charge density in the above figure leads to a contradiction. In the DC static case, nothing moves, so there can be no \mathbf{J} , but there is clearly some \mathbf{E} , so how can $\mathbf{J} = \sigma \mathbf{E}$? The reason is that Ohm's law only applies in a neutral medium. When there is a net charge density, the corrected Ohm's law is this:

$$\mathbf{J} = \sigma \mathbf{E} - D \text{grad } \rho \quad \dim(D) = \text{m}^2/\text{sec} \quad (\text{E.1})$$

The grad term, associated with Fick's Law, represents a flux of charged particles (a current) created by a gradient of the charge density. The charge flows (diffuses) from a region of high density to one of lower density, hence the minus sign, just as heat flows from a region of higher temperature to one of lower temperature. In a static situation with no current, the second term balances the first term in a surface charge region,

$$\sigma \mathbf{E} = D \text{grad } \rho \quad (\text{E.2})$$

As electrons pile up on the boundary, they resist further pileup by their higher density. Basically this is a diffusion effect, and D is a diffusion coefficient.

There is another more familiar equation which relates \mathbf{E} and ρ , namely (1.1.3) + (1.1.6),

$$\text{div } \mathbf{E} = \rho/\epsilon \quad (\text{E.3})$$

Inside a metal conductor the dielectric constant ϵ requires some careful study, but here we shall just set it to ϵ_0 as if there were nothing in the electron cloud of the metal that could be polarized. Taking the divergence of (E.2) and using (E.3) we get this result

$$\nabla^2 \rho = (\sigma/D\epsilon_0) \rho \quad . \quad (E.4)$$

The inverse combination of symbols in (E.4) is the square of something called the Debye length,

$$\lambda_D^2 = (D\epsilon_0/\sigma) \quad (E.5)$$

which is associated with charge screening in plasmas (such as the electrons in a metal). Thus, (E.4) may be written,

$$\nabla^2 \rho = (1/\lambda_D^2) \rho \quad . \quad (E.6)$$

In our one-dimensional problem of the above figure, the solution of this equation is

$$\rho(x) = \rho(0) e^{-x/\lambda_D} \quad (E.7)$$

where x is a coordinate going into the surface. This says that the thickness of the charge surface layer inside the metal is basically λ_D .

If the electron cloud inside the metal is treated as a classical gas of particles of mass m , charge q , temperature T , and density n , one gets formulas for the various coefficients. Here are some expressions:

$$\begin{aligned} J &= nqv & v &= \text{average drift velocity} & // & \text{(N.1.1)} \\ \tau &= \text{mean lifetime between collisions} & // & \text{below (N.1.2)} \\ \mu &= (v/E) = (q/m)\tau = \text{mobility} & // & \text{(N.1.7)} \\ D &= kT(\mu/q) = kT(\tau/m) = \text{diffusion coefficient} & // & \text{" Einstein relation"} \\ \sigma &= (nq^2\tau/m) = \text{conductivity} & // & \text{(N.1.9)} \\ \lambda_D &= \sqrt{\epsilon_0 kT/nq^2} = \text{Debye length} & // & \text{(E.5) and last 2 equ. above} \end{aligned} \quad (E.8)$$

This set of equations represents a classical model for the free charge in a metal.

One major and one minor adjustment is needed (see Kittel p 278-280) when quantum theory is applied because electrons are fermions. This means that they cannot all park in the same state, so they "pile up" in higher and higher states in something known as the Fermi sphere. Only electrons at the surface of this sphere can do anything useful. Due to the pileup, the temperature of the active electrons is very much higher than one might think using classical physics. One finds this temperature by setting $kT = E_F$ where this latter is the Fermi energy,

$$E_F = (h^2/8\pi^2m)(3\pi^2n)^{2/3} = kT_F \quad . \quad (E.9)$$

The appearance of the Plank constant h is the clue that this is a quantum result. This was the major quantum adjustment. The minor one is that T in the Debye formula gets replaced by $(2/3)T$. Thus,

$$\lambda_D = \sqrt{\epsilon_0 k(2T_F/3)/nq^2} = \text{Debye length (quantum correct)} \quad . \quad (E.10)$$

We shall now run some numbers. Here are the basics,

$$n = 8.45 \times 10^{28} \text{ electrons/m}^3 \text{ for Copper}$$

$$k = 1.38 \times 10^{-23} = \text{Boltzmann constant}$$

$$m = 9.1 \times 10^{-31} \text{ kg} = \text{electron mass}$$

$$h = 6.63 \times 10^{-34} \text{ J sec} = \text{Planck constant}$$

Plugging these into (E.9) gives the following effective electron temperature

```
Tf := (1/k)*(h^2/(8*Pi*Pi*m))*(3*Pi*Pi*n)^(2/3):
n := 8.45e28:
k := 1.38e-23:
m := 9.1e-31:
h := 6.63e-34:
evalf(Tf);
81702.49481
```

so

$$T_F = 81,702 \text{ }^\circ\text{K} = \text{pretty hot} \quad . \quad (E.11)$$

We can now compute the Debye length, using (E.10) :

$$\epsilon_0 = 8.85 \times 10^{-12} \text{ F/m}$$

$$q = 1.60 \times 10^{-19} \text{ C}$$

```
Ld := sqrt(e0*k*(2/3)*Tf/(n*q*q)):
e0 := 8.85e-12:
q := 1.60e-19:
evalf(Ld);
.5545425447 10^-10
```

so

$$\lambda_D = 5.55 \times 10^{-11} \text{ m} = 0.55 \text{ \AA} \text{ (Angstroms)} \quad // = 55 \text{ pm} \quad (E.12)$$

and this result for λ_D appears on page 280 of Kittel. The atomic spacing in crystal copper is 3.6\AA , while the copper atomic radius is about 1.3\AA .

The basic discussion above through (E.7) appears in Portis pp 162-164 (Chap 5, Sec 11). Portis then gives a small table of metal parameters and λ_D for copper is quoted as 0.59Å, close to our result above.

Thus, we come to the dramatic conclusion of this section:

Fact: In our simple model, the thickness of the surface charge density below the surface of a conductor is incredibly small. For copper, it is less than the radius of one copper atom, and the general result applies to any metal. Thus, the surface charge decays away right in the very first atomic layer of a metal.

Fact: The thin layer of negative surface charge on the right plate in Fig E.1 above serves to neutralize the E field which would otherwise be present inside the right conductor due to the positive charge on the surface of the left plate. One says that the E field inside (and to the right of) the right plate is "screened" (killed off) by the negative surface charge layer on the right plate.

This is of course the principle behind the ever-popular Faraday Cage (note kids inside):



Fig E.2

http://www.wonderwhizkids.com/resources/content/imagesv4/apupdate/physics/Electricity/conductors/Faraday_cage.jpg

From Section 2.2, we found that the skin depth δ for copper at 100 GHz is about 0.2 microns which is $2 \times 10^{-7} \text{m} = 2000\text{Å}$. Even at this large frequency, the skin depth is still about 4000 times larger than the thickness of the surface charge layer. At 1 GHz this ratio is 40,000.

Fact: Whereas surface current can exist "deep" into the surface of a conductor, even when the skin effect is dominant, the surface charge can always be thought of as being exactly on the surface.

Appendix F: Waveguides

F.1 Discussion

A transmission line must have at least two distinct conductors to carry the TEM wave described in Section 3.7 and as illustrated in the figures there. For a two conductor transmission line the surfaces of the conductors have a potential difference of amplitude $V \neq 0$.

A single wire cannot carry a TEM wave except in the sense of Section 2.1 where it acts as the center conductor of a coaxial cable with a far-distant return sheath. A TEM wave cannot propagate down the inside of a hollow pipe regardless of cross section shape since the continuous conductor cross section "shorts out" any possible $V \neq 0$.

In this document we have associated the TEM wave with the phrase "transmission line". but certainly a waveguide is a form of transmission line. Normally one associates the word "waveguide" with the TE and TM modes such waveguides carry. The usual form of a waveguide is in fact a hollow pipe, often of rectangular or circular cross section. However, it is possible for a 2 conductor transmission line to have TE and TM modes. In this Appendix we shall not present a theory of waveguides since that is well done in Jackson and many other texts, but we would like to show that a transmission line made from two closely spaced parallel plates can carry waveguide modes in addition to the TEM mode. We want to use this simple example to illustrate the notion that waveguide modes have lower cutoff frequencies whereas the TEM mode can operate all the way down to $\omega = 0$ (albeit in a very lossy manner).

The terminology TEM (Transverse Electric and Magnetic) means that both the \mathbf{E} and \mathbf{B} fields are transverse, as shown in Figures 3.5 through 3.7. In reality, we know there is a very small longitudinal E_z field because E_z is continuous at a conductor surface and we know $\mathbf{J}_z = \sigma \mathbf{E}_z$ just inside the conductor. This E_z field exists and has a cosine-like shape between the conductors, having the opposite direction at the second conductor. This field might be smaller than the transverse \mathbf{E} field by a factor 10^{-4} as shown in (3.6.2).

A TEM wave is very much like a plane wave with its transverse \mathbf{E} and \mathbf{B} fields, but the fields are distorted by the presence of the conductors. As Fig 3.5 shows, this distortion is such that the Poynting vector $\mathbf{E} \times \mathbf{B}$ always points down the line (z direction), \mathbf{E} and \mathbf{B} are always perpendicular at any point [for sufficiently large ω , see (3.7.25)], and the \mathbf{E} field lands perpendicularly on the conductors. The TE and TM modes have much more complicated field patterns.

The waveguide modes are called TE (Transverse Electric) and TM (Transverse Magnetic). The nomenclature is a little confusing since both TE and TM waves generally have transverse \mathbf{E} and \mathbf{B} fields. The distinction is that the TE modes have no E_z field, while the TM modes have no B_z field. So TE means the \mathbf{E} field is "transverse only".

F.2 The TE waveguide modes for a parallel-plate transmission line

We shall assume (our usual "ansatz") that the entire \mathbf{E} field is given by

$$\mathbf{E}(x,y,z) = E_y(x) e^{j(\omega t - kz)} \hat{\mathbf{y}} \quad (\text{F.2.1})$$

where we have our usual overloading of the symbol E .

This field in the dielectric must satisfy the ω -domain wave equation (1.5.32) which says

$$(\nabla^2 + \beta_d^2) \mathbf{E} = 0 \quad . \quad (F.2.2)$$

Here β_d is the usual Helmholtz parameter of the dielectric as in (1.5.1a),

$$\beta_d^2 = \mu_d \epsilon_d \omega^2 - j\omega \mu_d \sigma_d = \omega^2 \mu_d (\epsilon_d - j\sigma_d/\omega) = \omega^2 \mu_d \xi_d \quad \xi_d \equiv \epsilon_d - j\sigma_d/\omega \quad . \quad (1.5.1a)$$

but in this Appendix we assume the dielectric is non-conducting so

$$\beta_d^2 = \omega^2 \mu_d \epsilon_d = \omega^2/v_d^2 \quad (\equiv \beta_{d0}^2 \text{ but we shall just call it } \beta_d^2). \quad (F.2.3)$$

Inserting the ansatz form (F.2.1) for \mathbf{E} into (F.2.2) one finds that,

$$(\partial_x^2 + \partial_y^2 + \partial_z^2 + \beta_d^2) E_y(x) e^{j(\omega t - kz)} = 0$$

or

$$(\partial_x^2 + 0 + (-k^2) + \beta_d^2) E_y(x) = 0 \quad . \quad (F.2.4)$$

Define

$$\gamma^2 \equiv \beta_d^2 - k^2 \quad (F.2.5)$$

so that

$$(\partial_x^2 + \gamma^2) E_y(x) = 0 \quad (F.2.6)$$

so

$$E_y(x) = A \sin(\gamma x) + B \cos(\gamma x) \quad . \quad (F.2.7)$$

We now introduce our parallel plate transmission line (the gap is exaggerated in width)

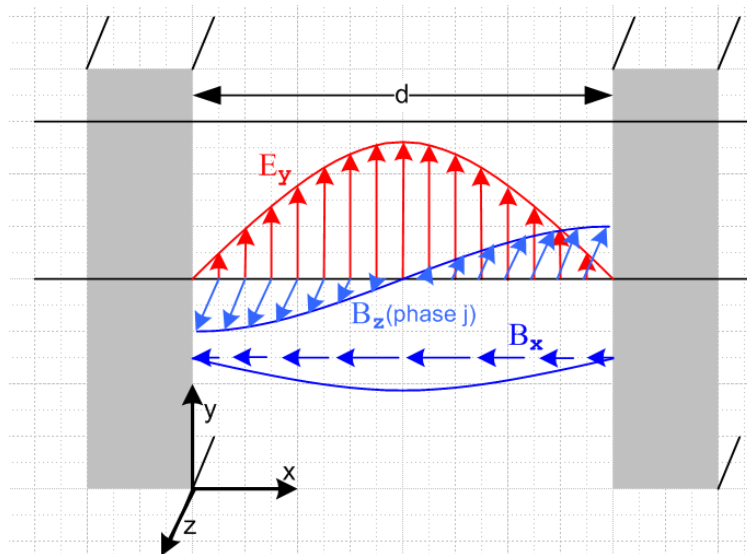


Fig F.1

Since we require $E_y = 0$ at the two inner plate surfaces, we find that

$$E_y(x) = A \sin(\gamma x) \quad \text{where } \sin(\gamma d) = 0 \quad \Rightarrow \quad \gamma d = m\pi . \quad (\text{F.2.8})$$

Thus, the parameter γ is quantized by the boundary conditions and we have

$$E_y^{(m)}(x) = A \sin(\gamma_m x) \quad \gamma_m = m(\pi/d) \quad m = 1, 2, 3, \dots \quad (\text{F.2.9})$$

Suddenly there are "modes" labeled by m . The lowest non-vanishing mode has $m = 1$, and this is the mode shown in the figure.

We find that the wave's wavenumber k is also quantized. From (F.2.5),

$$k_m = \sqrt{\beta_d^2 - \gamma_m^2} . \quad (\text{F.2.10})$$

In order to have a traveling wave $e^{j(\omega t - k z)}$, one needs k in (F.2.1) to be real, which requires that

$$\beta_d \geq \gamma_m . \quad (\text{F.2.11})$$

For a non-conducting dielectric one has $\beta_d = \omega \sqrt{\mu_d \epsilon_d} = \omega/v_d$ where v_d is the light speed in the dielectric. Recall from (1.1.29) that $\sqrt{\mu_0 \epsilon_0} = 1/c$. So the above condition is

$$\omega/v_d \geq m(\pi/d) \quad \Rightarrow \quad \omega \geq m(\pi/d)v_d$$

so

$$\omega \geq \omega_m \quad \omega_m \equiv m(\pi/d)v = \gamma_m v_d . \quad (\text{F.2.12})$$

Thus the m^{th} TE mode can only operate for ω above ω_m , and as m increases the low end mode cutoff increases. For $\omega < \omega_1$ there can be no TE action on this waveguide.

The B fields for our TE mode can be obtained from the Maxwell curl E (1.6.24),

$$\begin{aligned} \mathbf{B} &= (j/\omega) \text{curl } \mathbf{E} = (j/\omega) [\hat{\mathbf{x}} (\partial_y E_z - \partial_z E_y) + \hat{\mathbf{y}} (\partial_z E_x - \partial_x E_z) + \hat{\mathbf{z}} (\partial_x E_y - \partial_y E_x)] \\ &= (j/\omega) [\hat{\mathbf{x}} (-\partial_z E_y) + \hat{\mathbf{z}} (\partial_x E_y)] \end{aligned}$$

so then

$$B_x^{(m)}(x) = (j/\omega)(jk)E_y(x) = -(k_m/\omega) A \sin(\gamma_m x) \quad (\text{F.2.13})$$

$$B_z^{(m)}(x) = (j/\omega)\partial_x E_y(x) = (j/\omega) \gamma_m A \cos(\gamma_m x) . \quad (\text{F.2.14})$$

$$E_y^{(m)}(x) = A \sin(\gamma_m x) . \quad (\text{F.2.9})$$

If A is real, then E_y and B_x are real and in time phase, while B_z is 90° out of phase. An attempt has been made to display all three field components in Fig F.1.

To show that the waveguide mode outlined above is viable, we verify Maxwell's equations. Since the Maxwell curl \mathbf{E} equation was used to obtain \mathbf{B} , we need verify only the remaining three equations:

$$\text{div } \mathbf{E} = \partial_x E_x + \partial_y E_y + \partial_z E_z = \partial_y E_y(x) = 0 \quad (\text{F.2.15})$$

$$\begin{aligned} \text{div } \mathbf{B} &= \partial_x B_x + \partial_y B_y + \partial_z B_z = \partial_x B_x + \partial_z B_z \\ &= -(k_m/\omega) \gamma_m A \cos(\gamma_m x) - j k_m (j/\omega) \gamma_m A \cos(\gamma_m x) \\ &= -(k_m/\omega) \gamma_m A \cos(\gamma_m x) + k_m (1/\omega) \gamma_m A \cos(\gamma_m x) = 0 \end{aligned} \quad (\text{F.2.16})$$

Finally,

$$\begin{aligned} \text{curl } \mathbf{B} &= \hat{x} (\partial_y B_z - \partial_z B_y) + \hat{y} (\partial_z B_x - \partial_x B_z) + \hat{z} (\partial_x B_y - \partial_y B_x) \\ &= + \hat{y} (\partial_z B_x - \partial_x B_z) = \hat{y} [(-j k_m) - (k_m/\omega) A \sin(\gamma_m x) + (j/\omega) \gamma_m^2 A \sin(\gamma_m x)] \\ &= \hat{y} [(j k_m^2 / \omega) A \sin(\gamma_m x) + (j/\omega) \gamma_m^2 A \sin(\gamma_m x)] \\ &= \hat{y} [k_m^2 + \gamma_m^2] j (A/\omega) \sin(\gamma_m x) = \hat{y} \beta_d^2 j (A/\omega) \sin(\gamma_m x) . \end{aligned} \quad (\text{F.2.17})$$

According to (1.6.23)

$$\text{curl } \mathbf{H}(\mathbf{x}, \omega) = j\omega \mathbf{D}(\mathbf{x}, \omega) + \mathbf{J}(\mathbf{x}, \omega) \quad (1.6.18)$$

with $\mathbf{J} = 0$, $\mathbf{D} = \epsilon \mathbf{E}$ and $\mathbf{H} = \mathbf{B}/\mu$ one should have

$$\text{curl } \mathbf{B} = j\omega \epsilon \mu \mathbf{E} \quad (\text{F.2.18})$$

Installing curl \mathbf{B} from (F.2.17) and \mathbf{E} from (F.2.9), the Maxwell curl \mathbf{B} equation will be satisfied if

$$\begin{aligned} \beta_d^2 j (A/\omega) \sin(\gamma_m x) &= j\omega \epsilon \mu A \sin(\gamma_m x) \\ \text{or} \\ \beta_d^2 (1/\omega) &= \omega \epsilon_d \mu_d \\ \text{or} \\ \beta_d^2 &= \omega^2 \epsilon_d \mu_d \end{aligned}$$

which is (F.2.3) quoted above. Thus we have shown that our TE waveguide modes satisfy all four Maxwell equations.

Although the TE and TEM modes are both "transverse electric", there is a significant difference in the \mathbf{E} field pattern. In TEM the \mathbf{E} field lines run from one conductor to the other so that the line integral of \mathbf{E} generates the potential difference V , as shown in Fig 3.5. The \mathbf{E} field lines are "sourced by" (or "create")

the surface charge on the conductors. In the TE mode of Fig F.1, the E field is still transverse but is parallel to the conductors so the line integral of E between the conductors gives $V = 0$. These E lines are not sourced by charges on the conductors but are more like the E field lines in a free-space light wave.

Comments:

1. The parallel plate transmission line also has TM waveguide modes, and the cutoff frequencies are the same as for the TE mode.
2. A rectangular waveguide mode has two quantized integers and the cutoff frequency is then a function of both these integers. For TM the E_z field will have sine behavior in both x and y directions. See for example Jackson Section 8.4 page 361.
3. The obvious boundary condition is that $E_\tau = 0$ at the walls, while a less obvious condition is that $B_n = 0$ at the walls [see (3.7.17)]. Notice in our example that $B_x^{(m)}(x) = 0$ at the walls and this is a normal B field.
4. Waveguide problems are normally dealt with using the Helmholtz equation for the E and B fields, whereas the TEM transmission line problem is more easily dealt with using potentials ϕ and A_z .
5. We have dealt above with an ideal waveguide. In real waveguides the fields E and B penetrate distance δ (skin depth) into the walls and generate ohmic losses causing the wave to be damped. The same thing of course also happens for the transmission line TEM mode.

Reader Exercise: Make a 3D vector plot of the **E** and **B** fields for Fig F.1, and also plot the Poynting vector $\mathbf{S} = \mathbf{E} \times \mathbf{B}$ and compare with the TEM wave pattern. Except at the center, in addition to S_z there seems to be an S_x component suggesting a transverse power flow distribution in addition to the expected longitudinal power flow. (See below)

F.3 A waveguide interpretation

Adding the (F.2.1) ansatz z dependence $e^{-jk_z z}$ to (F.2.9) gives, with (F.2.10) for k_m ,

$$E_y(x,z) = A \sin(\gamma_m x) e^{-jk_m z} \quad k_m = \sqrt{\beta_d^2 - \gamma_m^2} \quad (\text{F.3.1})$$

The solution was approximate because it ignored skin depth effects.

It is convenient to think of (F.3.1) as the superposition of two "free space" plane waves of wavenumber β_d traveling at some skew angle $\pm\theta$ relative to the z direction, reflecting back and forth off the sides of the waveguide:

$$E_y(x,z) = (Aj/2) [e^{-j\beta_1 \bullet \mathbf{r}} - e^{-j\beta_2 \bullet \mathbf{r}}] = \text{sum of two plane waves} \quad (\text{F.3.2})$$

where

$$\begin{aligned}
 \boldsymbol{\beta}_1 &= \beta_x \hat{\mathbf{x}} + \beta_z \hat{\mathbf{z}} = \text{wavevector of the first wave} & \Rightarrow & \boldsymbol{\beta}_1 \cdot \mathbf{r} = \beta_x x + \beta_z z \\
 \boldsymbol{\beta}_2 &= -\beta_x \hat{\mathbf{x}} + \beta_z \hat{\mathbf{z}} = \text{wavevector of the second wave} & \Rightarrow & \boldsymbol{\beta}_2 \cdot \mathbf{r} = -\beta_x x + \beta_z z
 \end{aligned} \quad (\text{F.3.3})$$

$$(\beta_1)^2 = (\beta_2)^2 = \beta_x^2 + \beta_z^2 = \beta_d^2$$

$$\tan\theta = \beta_x/\beta_z . \quad (\text{F.3.4})$$

Adding the two terms in (F.3.2) gives

$$\begin{aligned}
 E_y(x,z) &= (Aj/2) [e^{-j\beta_1 \cdot \mathbf{r}} - e^{-j\beta_2 \cdot \mathbf{r}}] = (Aj/2) [e^{-j\beta_x x - j\beta_z z} - e^{+j\beta_x x - j\beta_z z}] \\
 &= (Aj/2) e^{-j\beta_z z} [e^{-j\beta_x x} - e^{+j\beta_x x}] = (Aj/2) e^{-j\beta_z z} [-2j \sin(\beta_x x)] \\
 &= A e^{-j\beta_z z} \sin(\beta_x x) .
 \end{aligned} \quad (\text{F.3.5})$$

Comparing with (F.3.1) one concludes that

$$\begin{aligned}
 \beta_x &= \gamma_m = m\pi/d & \beta_z &= k_m & // \omega_m &= \gamma_m v_d \\
 \tan\theta &= \beta_x/\beta_z = \gamma_m/k_m = \frac{\gamma_m}{\sqrt{\beta_d^2 - \gamma_m^2}} = \frac{(\omega_m/v_d)}{\sqrt{(\omega/v_d)^2 - (\omega_m/v_d)^2}} = \frac{\omega_m}{\sqrt{\omega^2 - \omega_m^2}} .
 \end{aligned} \quad (\text{F.3.6})$$

The two plane waves have wavenumber $\beta_d = \omega/v_d$ and not k . Their sum is the superposed wave going down the guide in the z direction with wavenumber k_m shown in Fig F.2. As ω approaches cutoff from above, $\tan\theta \rightarrow \infty$ and $\theta \rightarrow \pi/2$ and at cutoff the plane waves just bounce back and forth sideways and there is no propagation down the guide at all. Here is a picture:

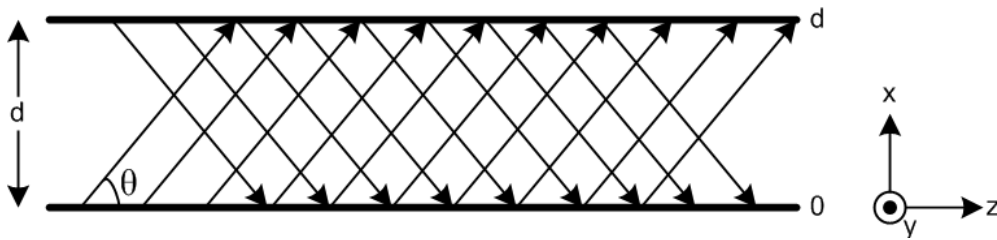


Fig F.2

Appendix G: The DC vector potential of a round wire carrying a uniform current

In this problem, an isolated, infinitely-long and z-aligned round wire ($\mu_2, \epsilon_2, \sigma_2$, radius a) carries a current I . The wire is immersed in an infinite dielectric medium ($\mu_1, \epsilon_1, \sigma_1$). We begin for general ω , but quickly go to the DC limit $\omega = 0$. We wish to calculate the vector potential \mathbf{A} of this wire *both inside and outside*.

Section G.1 sets up the problem, makes some ansatz assumptions, and then ends up with a 2D Poisson equation for the potential which is $\nabla^2_{2D} A_z(r) = - [I\mu_2/(\pi a^2)] \theta(r \leq a)$.

Section G.2 directly solves this Poisson equation for the potential $A_z(r)$. The solution is required to meet two boundary conditions at $r = a$.

Section G.3 very quickly computes this same $A_z(r)$ using Ampere's Law with the same boundary conditions and obtains the same result found in Section G.2.

Section G.4 laboriously obtains the same $A_z(r)$ result using the 2D Helmholtz integral (which in this case is really just a Laplace integral). This serves as a prototype case for dealing with such integrals, so much detail is provided. It is found that for $\mu_1 \neq \mu_2$ homogenous terms must be added to the Helmholtz integral in order to meet the boundary conditions.

Section G.5 comments on the solution for A_z at low frequencies.

G.1 Setup and Assumptions

1 = dielectric 2 = conductor

The ω -domain Helmholtz wave equation for \mathbf{A} using the King gauge is given by (1.5.4),

$$(\nabla^2 + \beta_1^2)\mathbf{A} = -\mu_2\mathbf{J}_2 \quad \beta_1^2 = \omega^2\mu_1\xi_1 \quad \xi_1 \equiv \epsilon_1 - j\sigma_1/\omega \quad (\text{G.1.1})$$

$$\text{div } \mathbf{A} = j\omega\mu_1\xi_1\phi \quad // \text{ King gauge } \quad [1 = \text{dielectric}, 2 = \text{wire}] \quad (\text{G.1.2})$$

We take a uniform prescribed current inside the wire (assume low frequency),

$$\mathbf{J}_2 = [I/(\pi a^2)] \hat{\mathbf{z}} \quad (\text{G.1.3})$$

so the Helmholtz wave equation reads

$$(\nabla^2 + \beta_1^2)\mathbf{A}(\mathbf{x}) = - [I\mu_2/(\pi a^2)] \theta(\sqrt{x^2+y^2} < a) \hat{\mathbf{z}}$$

where ∇^2 is the *vector* Laplacian and where $\theta(B) = 1$ if B is true, else 0.

In Cartesian components this says,

$$\begin{aligned} (\nabla^2 + \beta_1^2)A_x(\mathbf{x}) &= 0 \\ (\nabla^2 + \beta_1^2)A_y(\mathbf{x}) &= 0 \\ (\nabla^2 + \beta_1^2)A_z(\mathbf{x}) &= - [I\mu_2/(\pi a^2)] \theta(\sqrt{x^2+y^2} < a) \end{aligned}$$

where in *these* three equations ∇^2 is the *scalar* Laplacian. We shall seek a solution in which both A_x and A_y vanish. In this case one has,

$$\mathbf{A}(\mathbf{x}) = A_z(\mathbf{x}) \hat{\mathbf{z}} .$$

We assume a very low frequency ω for which we know any longitudinal wave that might be going down the wire has a very long wavelength. We then ignore z variations in A_z to write

$$\mathbf{A}(\mathbf{x}) = A_z(x,y) \hat{\mathbf{z}} . \quad (\text{G.1.4})$$

In this case, one finds that $\nabla^2 A_z = \nabla_{2D}^2 A_z$ and then the only equation of interest is this:

$$(\nabla_{2D}^2 + \beta_1^2) A_z(x,y) = - [\mu_2/(\pi a^2)] \theta(\sqrt{x^2+y^2} < a) . \quad // \nabla_{2D}^2 = \nabla^2 - \partial_z^2 \quad (\text{G.1.5})$$

Now take $\omega \rightarrow 0$ to get

$$\nabla_{2D}^2 A_z(x,y) = - [\mu_2/(\pi a^2)] \theta(x^2+y^2 < a^2)$$

which is just a 2D Poisson equation with a constant source limited to a region of space. At this point we are free to replace x,y with polar coordinates r,θ , so we have for r in the range $(0,\infty)$,

$$\nabla_{2D}^2 A_z(r,\theta) = - [\mu_2/(\pi a^2)] \theta(r < a) . \quad // \theta(r < a) = \text{Heaviside } \theta(a-r). \quad (\text{G.1.6})$$

From $\mathbf{B} = \text{curl } \mathbf{A}$ in cylindrical coordinates one finds that, since only A_z is non-vanishing,

$$\begin{aligned} \mathbf{B} = \text{curl } \mathbf{A} &= \hat{\mathbf{r}} [r^{-1} \partial_\theta A_z - \partial_z A_\theta] + \hat{\boldsymbol{\theta}} [\partial_z A_r - \partial_r A_z] + \hat{\mathbf{z}} [r^{-1} \partial_r (r A_\theta) - r^{-1} \partial_\theta A_r] \\ &= \hat{\mathbf{r}} [r^{-1} \partial_\theta A_z] + \hat{\boldsymbol{\theta}} [-\partial_r A_z] . \end{aligned}$$

Since we expect the magnetic field lines to be entirely in the $\hat{\boldsymbol{\theta}}$ direction, we are led to make the assumption that $\partial_\theta A_z = 0$ and then the problem is this,

$$\nabla_{2D}^2 A_z(r) = - [\mu_2/(\pi a^2)] \theta(r < a) \quad \mathbf{B} = B_\theta \hat{\boldsymbol{\theta}} \quad \text{with } B_\theta = -\partial_r A_z . \quad (\text{G.1.7})$$

If we can find a solution, then the ansatz assumptions that $A_x = A_y = 0$ and $\mathbf{B} = B_\theta \hat{\boldsymbol{\theta}}$ are justified.

G.2 Direct solution for $A_z(r)$ from the differential equation

Using ∇_{2D}^2 in polar coordinates the ODE (G.1.7) reads

$$(1/r) \partial_r (r \partial_r A_z(r)) = - [\mu_2/(\pi a^2)] \theta(r \leq a)$$

or

$$\begin{aligned} \partial_{\mathbf{r}}(r\partial_{\mathbf{r}}A_{\mathbf{z}}(r)) &= - [\mu_2/(\pi a^2)] r \theta(r \leq a) \\ \text{or} \\ r A_{\mathbf{z}}''(r) + A_{\mathbf{z}}'(r) &= - [\mu_2/(\pi a^2)] r \theta(r \leq a) . \end{aligned} \quad (\text{G.2.1})$$

The two regional differential equations are then

$$\begin{aligned} r A_{\mathbf{z}}''(r) + A_{\mathbf{z}}'(r) &= 0 & r > a & \text{region 1 (dielectric)} \\ r A_{\mathbf{z}}''(r) + A_{\mathbf{z}}'(r) &= - [\mu_2/(\pi a^2)] r & r < a & \text{region 2 (conductor)} . \end{aligned} \quad (\text{G.2.2})$$

The general-form solutions to these ODE's are,

$$\begin{aligned} A_{\mathbf{z}}(r) &= C \ln(r) + D & r > a & \text{region 1} \\ A_{\mathbf{z}}(r) &= - [\mu_2/(4\pi a^2)] r^2 + E \ln(r) + F & r < a & \text{region 2} \end{aligned} \quad (\text{G.2.3})$$

where there are 4 constants to be determined. For $r > a$ the functions 1 and $\ln r$ are the well-known atomic forms (harmonic elements) for the 2D Laplace equation for situations of azimuthal symmetry. The first term in region 2 (G.2.3) is the particular solution of region 2 (G.2.2) to which we have added a possible homogeneous solution $E \ln(r) + F$.

In order that $A_{\mathbf{z}}(r)$ be finite at $r = 0$, one must set $E = 0$.

For very large r the round wire looks like a line source and we know the solution of *that* problem. Using Ampere's Law that $2\pi r H_{\theta} = I$ we find (recall that $B_{\theta} = -\partial_{\mathbf{r}}A_{\mathbf{z}}$)

$$H_{\theta} = [I/2\pi](1/r) \quad \Rightarrow \quad B_{\theta} = \mu_1 [I/2\pi](1/r) \quad \Rightarrow \quad A_{\mathbf{z}} = - [I \mu_1/2\pi] \ln(r) + D' \quad . \quad r \gg a$$

Comparing this solution to our $r > a$ round wire solution we conclude that $D' = D$ and $C = -[\mu_1 I/2\pi]$. There are still two unknown constants D and F :

$$\begin{aligned} A_{\mathbf{z}}(r) &= -[\mu_1/2\pi] \ln(r) + D & r > a & \text{region 1} \\ A_{\mathbf{z}}(r) &= - [\mu_2/(4\pi a^2)] r^2 + F & r < a & \text{region 2} . \end{aligned} \quad (\text{G.2.4})$$

The potential $A_{\mathbf{z}}(r)$ always has an additive constant which one is free to specify and which affects nothing. We shall choose the zero point of $A_{\mathbf{z}}(r)$ by setting $D = 0$ arbitrarily. This means that $A_{\mathbf{z}}(r)$ has the simple form $K \ln(r)$ for $r > a$, and that choice implies that $A_{\mathbf{z}}(a) = - [\mu_1/2\pi] \ln(a)$, so we have in effect specified $A_{\mathbf{z}}(r)$ on the wire surface to be this value. Notice for future reference that,

$$\begin{aligned} \partial_{\mathbf{r}}A_{\mathbf{z}}(r) &= - [\mu_1/2\pi] (1/r) & r > a & \text{region 1} \\ \partial_{\mathbf{r}}A_{\mathbf{z}}(r) &= - [\mu_2/(2\pi a^2)] r & r < a & \text{region 2} . \end{aligned} \quad (\text{G.2.5})$$

Now, since our prescribed current J_2 does *not* specify a free surface current $K_{\mathbf{z}}$ on the round wire surface, which would have the form

$$J_{\mathbf{s}, \text{surface}} = K_{\mathbf{z}}^{\text{free}} \delta(a-r),$$

we conclude that there is no free surface current on the round wire surface; there is only the bulk volume current $\mathbf{J}_z = I/(\pi a^2)\theta(r < a)$. Therefore the boundary condition (1.1.46) applies (though now in polar coordinates) and we conclude that

$$(1/\mu_1) [(\partial_r A_z)(a)]^1 = (1/\mu_2) [(\partial_r A_z)(a)]^2 .$$

In addition, we shall require that A_z itself be continuous at the boundary, so here are our two boundary conditions of interest (superscript 1 means region 1 which is $r > a$),

$$\begin{aligned} [A_z(a)]^1 &= [A_z(a)]^2 . \\ (1/\mu_1) [(\partial_r A_z)(a)]^1 &= (1/\mu_2) [(\partial_r A_z)(a)]^2 . \end{aligned} \quad (G.2.6)$$

We now require that both these boundary conditions be met by the A_z expressions of (G.2.4),

$$\begin{aligned} [A_z(a)]^1 &= [A_z(a)]^2 && // (G.2.6) \text{ repeated} \\ (1/\mu_1) [(\partial_r A_z)(a)]^1 &= (1/\mu_2) [(\partial_r A_z)(a)]^2 \\ \text{or} &&& \\ -[I\mu_1/2\pi] \ln(a) &= -[I\mu_2/(4\pi a^2)] a^2 + F && // \text{insert expressions, set } r = a \\ (1/\mu_1) \{- [I\mu_1/2\pi] (1/a)\} &= (1/\mu_2) \{- [I\mu_2/(2\pi a^2)] a \} \\ \text{or} &&& \\ -[I\mu_1/2\pi] \ln(a) &= -[I\mu_2/(4\pi)] + F && // \text{simplify} \\ 1 &= 1 \end{aligned}$$

The second boundary condition is thus met automatically by our solution. The first says

$$F = [I\mu_2/(4\pi)] - [I\mu_1/2\pi] \ln(a) .$$

Finally all constants are determined, so the solution is,

$$\begin{aligned} A_z(r) &= - [I\mu_1/2\pi] \ln(r) && r > a && \text{region 1} \\ A_z(r) &= - [I\mu_2/(4\pi a^2)] r^2 + [I\mu_2/(4\pi)] - [I\mu_1/2\pi] \ln(a) && r < a && \text{region 2} \\ \text{or} &&& && \\ A_z(r) &= - [I\mu_1/2\pi] \ln(r) && r > a && \text{region 1} \\ A_z(r) &= - [I\mu_2/(4\pi a^2)] (r^2 - a^2) - [I\mu_1/2\pi] \ln(a) && r < a && \text{region 2} . \end{aligned} \quad (G.2.7)$$

This then is the complete solution to the problem for the round wire,

$$\nabla_{2D}^2 A_z(r) = - [I\mu_2/(\pi a^2)] \theta(r \leq a) \quad \mathbf{B} = B_\theta \hat{\boldsymbol{\theta}} \quad \text{with } B_\theta = - \partial_r A_z \quad (G.1.7)$$

where the potential is "pinned" by the requirement that $A_z = K \ln(r)$ for $r > a$.

One may now compute the B field from the potential solution (G.2.7),

$$\begin{aligned}
 B_{\theta} &= -\partial_r A_z = [I\mu_1/2\pi]\partial_r \ln(r) = [I\mu_1/2\pi](1/r) & r > a & \text{region 1} \\
 B_{\theta} &= -\partial_r A_z = [I\mu_2/(2\pi a^2)] r = [I\mu_2/2\pi](r/a^2) & r < a & \text{region 2} .
 \end{aligned} \tag{G.2.8}$$

Comment: Although only μ_2 appears in the differential equation (G.1.7), once the equation is properly solved with attention to boundary conditions, one finds that μ_1 appears in B_{θ} in region 1, while μ_2 appears in B_{θ} in region 2! This is the main point of this Section G.2.

G.3 Instant solution for A using Ampere's Law, and computation of J_m

For $r > a$ Ampere's law (1.1.37) (converted to ω space with $\omega = 0$) says $2\pi r H_{\theta} = I$ so

$$\begin{aligned}
 H_{\theta} &= I/(2\pi r) \quad \Rightarrow \quad B_{\theta} = \mu_1 I/(2\pi r) & [1 = \text{dielectric}] \\
 & & r > a & \text{region 1} \\
 \Rightarrow -\partial_r A_z &= \mu_1 I/(2\pi r) \quad \Rightarrow \quad A_z = -[I\mu_1/(2\pi)] \ln(r) + D .
 \end{aligned} \tag{G.3.1}$$

For $r < a$ Ampere's law says $2\pi r H_{\theta} = I(\pi r^2/\pi a^2)$ [the "current enclosed"]

$$\begin{aligned}
 H_{\theta} &= I(r^2/a^2)/(2\pi r) = I r/(2\pi a^2) \quad \Rightarrow \quad B_{\theta} = [I\mu_2/2\pi](r/a^2) & [2 = \text{wire}] \\
 & & r < a & \text{region 2} \\
 \Rightarrow -\partial_r A_z &= [I\mu_2/2\pi](r/a^2) \quad \Rightarrow \quad A_z = -[I\mu_2/4\pi](r^2/a^2) + E .
 \end{aligned} \tag{G.3.2}$$

We then set $D = 0$ to get $A_z = K \ln(r)$ for $r > 0$, as done previously, and then we must match at $r = a$:

$$-[I\mu_1/(2\pi)] \ln(a) = -[I\mu_2/4\pi] + E \quad \Rightarrow \quad E = [I\mu_2/4\pi] - [I\mu_1/(2\pi)] \ln(a)$$

so the potential solution is then,

$$\begin{aligned}
 A_z(r) &= -[I\mu_1/(2\pi)] \ln(r) & r > a \\
 A_z(r) &= -[I\mu_2/4\pi](r^2/a^2) + \{ [I\mu_2/4\pi] - [I\mu_1/(2\pi)] \ln(a) \} & r < a \\
 \text{or} \\
 A_z(r) &= -[I\mu_1/(2\pi)] \ln(r) & r > a \\
 A_z(r) &= -[I\mu_2/4\pi a^2]r^2 + [I\mu_2/4\pi] - [I\mu_1/(2\pi)] \ln(a) & r < a \\
 \text{or} \\
 A_z(r) &= -[I\mu_1/(2\pi)] \ln(r) & r > a \\
 A_z(r) &= -[I\mu_2/4\pi a^2](r^2 - a^2) - [I\mu_1/(2\pi)] \ln(a) & r < a
 \end{aligned} \tag{G.3.3}$$

This result agrees with result (G.2.7) of the previous section.

The Magnetization Current

It was mentioned in Section G.2 that there is no *free* surface current K_z^{free} at the wire surface. There is in fact a bound magnetization current on this surface and inside the wire as well. Luckily, our Helmholtz equation only "sees" conduction currents so we don't have to worry about the magnetization currents. The magnetization current density is given by $\mathbf{J}_m = \text{curl } \mathbf{M}$ where $\mathbf{M} = [\mu/\mu_0 - 1] \mathbf{H}$ as shown in (1.1.20-23).

Here then is the calculation of \mathbf{J}_m :

$$\begin{aligned} M_\theta^1 &= [\mu_1/\mu_0 - 1] H_\theta^1 = [\mu_1/\mu_0 - 1] (I/2\pi r) & r > a \\ M_\theta^2 &= [\mu_2/\mu_0 - 1] H_\theta^2 = [\mu_2/\mu_0 - 1] (Ir/2\pi a^2) & r < a \end{aligned}$$

or

$$M_\theta(r) = [\mu_1/\mu_0 - 1] (I/2\pi r) \theta(r>a) + [\mu_2/\mu_0 - 1] (Ir/2\pi a^2) \theta(r<a) \quad // \theta(r>a) = \theta(r-a)$$

$$\begin{aligned} \partial_x M_\theta &= - [\mu_1/\mu_0 - 1] (I/2\pi r^2) \theta(r>a) + [\mu_1/\mu_0 - 1] (I/2\pi r) \delta(r-a) \\ &\quad + [\mu_2/\mu_0 - 1] (I/2\pi a^2) \theta(r<a) + [\mu_2/\mu_0 - 1] (Ir/2\pi a^2) [-\delta(r-a)] \\ &= - [\mu_1/\mu_0 - 1] (I/2\pi r^2) \theta(r>a) + [\mu_2/\mu_0 - 1] (I/2\pi a^2) \theta(r<a) + [\mu_1/\mu_0 - \mu_2/\mu_0] (I/2\pi a) \delta(r-a) \end{aligned}$$

$$\begin{aligned} J_{mz} &= [\text{curl } \mathbf{M}]_z = r^{-1} \partial_x \{r M_\theta\} = r^{-1} [M_\theta + r \partial_x M_\theta] = r^{-1} M_\theta + \partial_x M_\theta \\ &= [\mu_1/\mu_0 - 1] (I/2\pi r^2) \theta(r>a) + [\mu_2/\mu_0 - 1] (I/2\pi a^2) \theta(r<a) \\ &\quad - [\mu_1/\mu_0 - 1] (I/2\pi r^2) \theta(r>a) + [\mu_2/\mu_0 - 1] (I/2\pi a^2) \theta(r<a) + [\mu_1/\mu_0 - \mu_2/\mu_0] (I/2\pi a) \delta(r-a) \\ &= [\mu_2/\mu_0 - 1] (I/\pi a^2) \theta(r<a) + [\mu_1/\mu_0 - \mu_2/\mu_0] (I/2\pi a) \delta(r-a) . \end{aligned} \tag{G.3.4}$$

constant inside wire
surface current

It is the discontinuity of $M_\theta(r)$ at the wire surface $r = a$ which creates the surface current term in J_{mz} .

The simplest possible case to consider is the boundary at $x = 0$ between two half spaces of μ_1 and μ_2 assuming there exists a uniform constant H_y field everywhere. In this case, one would have

$$\begin{aligned} M_y^1(x) &= [\mu_1/\mu_0 - 1] H_y \theta(x) & // H_y \text{ is continuous at the boundary by (1.1.42)} \\ M_y^2(x) &= [\mu_2/\mu_0 - 1] H_y \theta(-x) \end{aligned} \tag{G.3.5}$$

$$\partial_x M_y(x) = [\mu_1/\mu_0 - \mu_2/\mu_0] H_y \delta(x)$$

$$J_{mz} = [\text{curl } \mathbf{M}]_z = \partial_x M_y = [\mu_1/\mu_0 - \mu_2/\mu_0] H_y \delta(x) . \tag{G.3.6}$$

so here there is only a surface magnetization current and no bulk magnetization current on either side.

G.4 Solution for A_z using the 2D Helmholtz Integral

This method of finding A_z is technically more difficult than the first two methods shown in Section G.2 (solving the ODE and adding a homogeneous solution to meet the boundary conditions) and Section G.3 (instant Ampere's Law solution). The method is important because our entire Chapter 4 is based on using Helmholtz integrals to develop the theory of transmission lines, and this is one Helmholtz integral that we can actually compute without too much effort. An important result we find is that, when $\mu_1 \neq \mu_2$, the Helmholtz integral by itself does not supply the complete solution, and one must add in some amount of homogeneous solution of $\nabla^2_{2D} A_z(r) = 0$ to meet the required boundary conditions at $r=a$.

We really have a Laplace integral since $\beta_1^2 = 0$, but the full Helmholtz integral works the same way so we keep referring to it as a Helmholtz integral.

Recall from above:

$$\nabla^2_{2D} A_z(r) = - [I\mu_2/(\pi a^2)] \theta(r \leq a) \quad \mathbf{B} = B_\theta \hat{\theta} \quad \text{with} \quad B_\theta = - \partial_r A_z . \quad (G.1.7)$$

Using the 2D free-space Green's function (propagator) as reviewed in Appendix I equation (I.1.6),

$$g(\mathbf{x}|\mathbf{x}') = (1/2\pi) \ln(1/R) = - (1/4\pi) \ln(R^2) \quad R = |\mathbf{x} - \mathbf{x}'| , \quad (G.4.1)$$

we may write the particular solution to (G.1.7) as the following "Helmholtz integral" [see (I.1.8)]

$$\begin{aligned} -A_z^H(r) &= \int dS' [(1/4\pi) \ln(R^2)] [I\mu_2/(\pi a^2)] \theta(r \leq a) \\ &= \int_0^a r' dr' \int_{-\pi}^{\pi} d\theta' [(1/4\pi) \ln(r^2 + r'^2 - 2rr'\cos(\theta-\theta'))] [I\mu_2/(\pi a^2)] \\ &= (1/4\pi) [I\mu_2/(\pi a^2)] \int_0^a r' dr' \left[\int_{-\pi}^{\pi} d\theta' \ln(r^2 + r'^2 - 2rr'\cos(\theta-\theta')) \right] \\ &= \frac{\mu_2 I}{4\pi^2 a^2} \int_0^a r' dr' [2 Q(r',r)] \end{aligned} \quad (G.4.2)$$

where

$$\begin{aligned} Q(r',r) &\equiv (1/2) \int_{-\pi}^{\pi} d\theta' \ln(r^2 + r'^2 - 2rr'\cos(\theta-\theta')) = (1/2) \int_{-\pi}^{\pi} d\theta'' \ln(r^2 + r'^2 - 2rr'\cos(\theta'')) \\ &= \int_0^{\pi} dx \ln(r^2 + r'^2 - 2rr'\cos x) . \end{aligned} \quad (G.4.3)$$

But we have already computed this $A_z^H(r)$ in Appendix B where it was called $A_z^{(c)}(r, \theta)$, see (B.7.3) and (B.7.4). We may therefore borrow the solution (B.7.7) to obtain the results,

$$\begin{aligned}
 A_z^H(r>a) &= -\frac{\mu_2 I}{\pi a^2} \left\{ (1/2) a^2 \ln r \right\} = -\frac{\mu_2 I}{2\pi} \ln r \\
 A_z^H(r<a) &= \frac{\mu_2 I}{2\pi a^2} \left\{ (a^2 - r^2)/2 - a^2 \ln a \right\} .
 \end{aligned} \tag{G.4.4}$$

The derivatives are

$$\begin{aligned}
 \partial_r A_z^H(r>a) &= -\frac{\mu_2 I}{2\pi r} \\
 \partial_r A_z^H(r<a) &= -\frac{\mu_2 I}{2\pi a^2} r .
 \end{aligned} \tag{G.4.5}$$

Recall the two boundary conditions,

$$\begin{aligned}
 [A_z(a)]^1 &= [A_z(a)]^2 . \\
 (1/\mu_1) [(\partial_r A_z)(a)]^1 &= (1/\mu_2) [(\partial_r A_z)(a)]^2 .
 \end{aligned} \tag{G.2.6}$$

For our particular Helmholtz integral $A_z^H(r)$ we evaluate these boundary conditions to find

$$\begin{aligned}
 -\frac{\mu_2 I}{2\pi} \ln a &= \frac{\mu_2 I}{2\pi a^2} \left\{ (a^2 - a)/2 - a^2 \ln a \right\} \\
 (1/\mu_1) \left[-\frac{\mu_2 I}{2\pi a} \right] &= (1/\mu_2) \left[-\frac{\mu_2 I}{2\pi a^2} a \right]
 \end{aligned}$$

or

$$\begin{aligned}
 1 &= 1 \\
 (\mu_2/\mu_1) &= 1 .
 \end{aligned} \tag{G.4.6}$$

Thus, only in the case $\mu_1 = \mu_2$ does the Helmholtz particular solution meet both boundary conditions. If $\mu_1 \neq \mu_2$, we must add to the particular solution some amount of homogeneous solution of $\nabla_{2D}^2 A_z(r, \theta) = 0$. So we then write generally,

$$A_z(r) = A_z^H(r) + A_z^{\text{homo}}(r) \tag{G.4.7}$$

where we know that $A_z^{\text{homo}}(r)$ can only have terms $\alpha + \beta \ln r$. We then write for the two regions

$$\begin{aligned}
 A_z(r) &= -\frac{\mu_2 I}{2\pi} \ln(r) + \alpha + \beta \ln r & r > a \\
 A_z(r) &= \frac{\mu_2 I}{2\pi a^2} \left\{ (a^2 - r^2)/2 - a^2 \ln a \right\} + \alpha' + \beta' \ln r & r < a .
 \end{aligned} \tag{G.4.8}$$

As earlier, we choose the zero point for $A_z(r)$ by requiring that the large r behavior be $K \ln(r)$ without a constant added, which then means $\alpha = 0$. And for $r < a$ we must have $\beta' = 0$ to be finite at $r = 0$. So

$$\begin{aligned}
 A_z(r) &= -\frac{\mu_2 I}{2\pi} \ln(r) + \beta \ln r & r > a \\
 A_z(r) &= \frac{\mu_2 I}{2\pi a^2} \{ (a^2 - r^2)/2 - a^2 \ln a \} + \alpha' & r < a
 \end{aligned} \tag{G.4.9}$$

$$\begin{aligned}
 -\partial_r A_z(r) &= \left[\frac{\mu_2 I}{2\pi} - \beta \right] (1/r) & r > a \\
 -\partial_r A_z(r) &= \frac{\mu_2 I}{\pi a^2} (2r) & r < a
 \end{aligned} \tag{G.4.10}$$

The boundary conditions are then

$$\begin{aligned}
 [A_z(a)]^1 &= [A_z(a)]^2 \\
 (1/\mu_1) [(-\partial_r A_z)(a)]^1 &= (1/\mu_2) [(-\partial_r A_z)(a)]^2
 \end{aligned} \tag{G.2.6}$$

or

$$-\frac{\mu_2 I}{2\pi} \ln(a) + \beta \ln a = \frac{\mu_2 I}{2\pi a^2} \{ (a^2 - a^2)/2 - a^2 \ln a \} + \alpha'$$

$$(1/\mu_1) \left[\frac{\mu_2 I}{2\pi} - \beta \right] (1/a) = (1/\mu_2) \frac{\mu_2 I}{\pi a^2} (2a)$$

or

$$[-I\mu_2/(2\pi) + \beta] \ln a = -I\mu_2/(2\pi) \ln a + \alpha'$$

$$(1/\mu_1) [I\mu_2/(2\pi) - \beta] (1/a) = I/(2\pi a)$$

// simplify

or

$$\beta \ln a = \alpha'$$

$$I\mu_2/(2\pi) - \beta = \mu_1 I/(2\pi)$$

// simplify some more

so we find that

$$\beta = I/(2\pi) (\mu_2 - \mu_1)$$

$$\alpha' = I/(2\pi) (\mu_2 - \mu_1) \ln a$$

(G.4.11)

The full solution is then

$$A_z(r) = [-I\mu_2/(2\pi) + \beta] \ln r \quad r > a$$

$$A_z(r) = -I\mu_2/(\pi a^2) \{ (1/4) (r^2 - a^2) + (1/2) a^2 \ln a \} + \alpha' \quad r < a$$

or

$$A_z(r) = [-I\mu_2/(2\pi) + \{I/(2\pi) (\mu_2 - \mu_1)\}] \ln r \quad r > a$$

$$A_z(r) = -I\mu_2/(\pi a^2) \{ (1/4) (r^2 - a^2) + (1/2) a^2 \ln a \} + \{ I/(2\pi) (\mu_2 - \mu_1) \ln a \} \quad r < a$$

or

$$A_z(r) = I/(2\pi) [-\mu_2 + (\mu_2 - \mu_1)] \ln r \quad r > a$$

$$A_z(r) = -I\mu_2/(\pi a^2) (1/4) (r^2 - a^2) - I\mu_2/(\pi a^2) (1/2) a^2 \ln a + I/(2\pi) (\mu_2 - \mu_1) \ln a \quad r < a$$

or

$$A_z(r) = -[I\mu_1/2\pi] \ln r \quad r > a$$

$$A_z(r) = -[I\mu_2/(4\pi a^2)] (r^2 - a^2) - [I\mu_1/2\pi] \ln a \quad r < a \tag{G.4.12}$$

This result matches the results (G.2.7) and (G.3.3) of the previous two methods and then gives the usual B field solution,

$$\begin{aligned} B_{\theta} &= -\partial_{\mathbf{r}} A_{\mathbf{z}} = [\mu_1/2\pi] \partial_{\mathbf{r}} \ln(r) = [\mu_1/2\pi](1/r) & r > a & \text{region 1} \\ B_{\theta} &= -\partial_{\mathbf{r}} A_{\mathbf{z}} = [\mu_2/(2\pi a^2)] r = [\mu_2/2\pi](r/a^2) & r < a & \text{region 2} \end{aligned} \quad (G.2.8)$$

G.5 Comments on the low frequency solution for A_z

In Chapter 2 we compute the E and B fields inside a round wire operating at frequency ω . The results are rather complicated and involve Bessel functions (of unusual argument phase) whose real and imaginary parts are called Kelvin functions. The vector potential was not used in that Chapter. Here we consider computing A_z using the true Helmholtz integral rather than its Laplace approximation, and see how the derived results might compare with the Chapter 2 results.

Comments:

1. For sufficiently low frequencies (the transmission line limit) we imagine that the ansatz assumptions made in Section G.1 are still pretty good. The current distribution will be nearly uniform. There will likely be some small A_x and A_y fields which can be ignored, and we still assume roughly that $\mathbf{B} = B_{\theta} \hat{\theta}$ with $B_{\theta} = -\partial_{\mathbf{r}} A_{\mathbf{z}}$ and that we can ignore the z-dependence of A_z , though we know it must vary some small amount in order to have a long- λ wave passing down the wire. Therefore, our problem is basically (G.1.5) for small β_1^2 ,

$$(\nabla_{2D}^2 + \beta_1^2) A_z(r) = -[\mu_2/(\pi a^2)] \theta(r < a) \quad \mathbf{B} = B_{\theta} \hat{\theta} \quad \text{with} \quad B_{\theta} = -\partial_{\mathbf{r}} A_{\mathbf{z}} \quad (G.5.1)$$

2. Since $\nabla_{2D}^2 = (1/r)\partial_{\mathbf{r}}(r\partial_{\mathbf{r}})$, one could write out the above differential equation and repeat the work of section G.2 above. The resulting B field obtained from $B_{\theta} = -\partial_{\mathbf{r}} A_{\mathbf{z}}$ should then agree with the low frequency limit of (2.2.25) which applies inside the round wire,

$$B_{\theta}(r) = B_{\theta}(a) \frac{J_1(\beta_1 r)}{J_1(\beta_1 a)} \quad (2.2.25)$$

That low-frequency limit is

$$B_{\theta}(r) \approx B_{\theta}(a) \frac{r - \beta_1^2 r^3/8}{a - \beta_1^2 a^3/8} \quad \beta_1^2 = \omega^2 \mu \xi_1 \quad (G.5.2)$$

Certainly as $\omega \rightarrow 0$ (so $\beta_1 \rightarrow 0$) the result $B_{\theta}(r) = B_{\theta}(a)(r/a)$ agrees with (G.2.8).

3. The 2D free-space Helmholtz propagator is shown in (I.1.7) to be

$$g(\mathbf{x}|\mathbf{x}') = (j/4) H_0^{(1)}(\beta_1 R) \quad R = R = |\mathbf{x} - \mathbf{x}'|$$

where $H_0^{(1)}$ is a Hankel function. Thus, we may write the particular solution to (G.5.1) as the following Helmholtz integral [see (I.1.9)],

$$\begin{aligned} A_{\mathbf{z}}^{\mathbf{H}}(\mathbf{r}) &= \int dS' [(j/4) H_0^{(1)}(kR)] [I\mu_2/(\pi a^2)] \theta(r \leq a) \quad R = R = |\mathbf{x} - \mathbf{x}'| \\ &= [I\mu_2/(\pi a^2)] (j/4) \int_0^a r' dr' \int_{-\pi}^{\pi} d\theta' H_0^{(1)}(\beta_1 \sqrt{r^2 + r'^2 - 2rr'\cos(\theta - \theta')}) . \end{aligned} \quad (\text{G.5.3})$$

The $d\theta'$ integral is actually doable with this result (making use of GR7 p 726 6.684 1 and 2)

$$\begin{aligned} &\int_{-\pi}^{\pi} d\theta' H_0^{(1)}(\beta_1 \sqrt{r^2 + r'^2 - 2rr'\cos(\theta - \theta')}) \\ &= (1/2) \{ \pi J_0(\beta_1 r) H_0^{(1)}(\beta_1 r') \theta(r' > r) + \pi J_0(\beta_1 r') H_0^{(1)}(\beta_1 r) \theta(r' < r) \} . \end{aligned} \quad (\text{G.5.4})$$

The two dr' integrals can then be done (using GR7 p 629-630 Section 5.5) with the final result

$$\begin{aligned} A_{\mathbf{z}}^{\mathbf{H}}(\mathbf{r}) &= [I\mu_2/(\pi a^2)] (j/4) 2\pi (1/\beta_1) * \\ &\{ J_0(\beta_1 r) \theta(a > r) [a H_1^{(1)}(\beta_1 a) - r H_1^{(1)}(\beta_1 r)] + H_0^{(1)}(\beta_1 r) \begin{cases} r J_1(\beta_1 r) & r < a \\ a J_1(\beta_1 a) & r > a \end{cases} \} . \end{aligned} \quad (\text{G.5.5})$$

We leave it to the reader to determine the small β_1 limit of this result and see if the resulting $\mathbf{B}_{\theta} = -\partial_{\mathbf{x}} A_{\mathbf{z}}$ agrees with (G.5.2) after homogeneous solutions are added to match boundary conditions. Remember that we only expect this result to be meaningful for low ω since we have assumed the uniform current distribution of (G.1.3).

If one makes the small-argument approximation $H_0^{(1)}(x) \approx (2j/\pi)\ln(x)$ directly in (G.5.3), the integral replicates the Laplace result (G.4.2), so more expansion terms would be needed for this approach.

Reader Exercise: For general ω , one can use the 3D PDE $(\nabla^2 + \beta_1^2)A_{\mathbf{z}}(\mathbf{x}) = -[I\mu_2/(\pi a^2)] \theta(\sqrt{x^2 + y^2} < a)$ in place of the 2D PDE (G.1.5). Assume $e^{-j\mathbf{kz}}$ for the z dependence and use (H.1.9) to show that,

$$\begin{aligned} A_{\mathbf{z}}(\mathbf{x}) &= \int d^3x' [e^{-j\beta_1 R}/4\pi R] [I\mu_2/(\pi a^2)] \theta(\sqrt{x'^2 + y'^2} < a)] e^{-j\mathbf{kz}'} \quad R = |\mathbf{x} - \mathbf{x}'| \\ &= [I\mu_2/(\pi a^2)] \int_{-\pi}^{\pi} d\theta' \int_{-\infty}^{\infty} dz' \int_0^a r' dr' [e^{-j\beta_1 R}/4\pi R] e^{-j\mathbf{kz}'} \end{aligned} \quad (\text{G.5.6})$$

where

$$R^2 = s^2 + (z - z')^2 \quad s = \sqrt{r^2 + r'^2 - 2rr'\cos(\theta - \theta')} .$$

Complete this calculation and try to obtain a closed form result for $A_{\mathbf{z}}(\mathbf{x})$. The problem is difficult to set up in the real world since $\mathbf{J}_{\mathbf{z}}$ is non-uniform in a real wire at $\omega > 0$ (see Chapter 2), but one could imagine constructing a special round wire from insulated thin filaments in order to create a uniform $\mathbf{J}_{\mathbf{z}} = I/(\pi a^2)$.

See Section 1.5 (e).

Appendix H: Laplace and Helmholtz Propagators in 3D

Note: Appendix I deals with these propagators in 2D rather than 3D.

H.1 Overview and Meaning of Free-Space Propagators

This appendix proves the following Facts:

$$\mathbf{Fact\ 1 :} \quad -\nabla^2[1/4\pi r] = \delta(\mathbf{r}) \quad (H.2.1) \quad (H.1.1)$$

$$\mathbf{Fact\ 2 :} \quad -\nabla^2[h(r)/r] = 4\pi h(0) \delta(\mathbf{r}) - h''(r)/r \quad (H.3.1) \quad (H.1.2)$$

$$\mathbf{Fact\ 3 :} \quad -(\nabla^2+k^2) (e^{-j\mathbf{k}\cdot\mathbf{r}}/4\pi r) = \delta(\mathbf{r}) \quad (H.3.5) \quad (H.1.3)$$

Throughout, ∇^2 is the usual 3D Laplacian operator $\nabla^2 = \partial_{\mathbf{x}}^2 + \partial_{\mathbf{y}}^2 + \partial_{\mathbf{z}}^2$. In the first and last results above, if one replaces $\mathbf{r} \rightarrow \mathbf{r}-\mathbf{r}'$ (a simple translational shift of origin) ones finds

$$-\nabla^2[1/4\pi R] = \delta(\mathbf{r}-\mathbf{r}') \quad R = |\mathbf{r} - \mathbf{r}'| \quad (H.1.4)$$

$$-(\nabla^2+k^2) [e^{-j\mathbf{k}\cdot\mathbf{R}}/4\pi R] = \delta(\mathbf{r}-\mathbf{r}') \quad \delta(\mathbf{r}-\mathbf{r}') = \delta(x-x') \delta(y-y') \delta(z-z') \quad (H.1.5)$$

The quantities in brackets are known as free-space Green's Functions (Green Functions) or propagators, or as "fundamental solutions":

$$1/4\pi R = \text{the Laplace 3D free-space propagator} \quad (H.1.6)$$

$$e^{-j\mathbf{k}\cdot\mathbf{R}}/4\pi R = \text{the Helmholtz 3D free-space propagator} \quad (H.1.7)$$

The last item above is the ω -domain 3D Helmholtz propagator, where $k^2 = \omega^2\mu\epsilon$. See (A.7.4) for a discussion of the time domain version of this propagator which is the 3D wave equation propagator.

The significance of these propagators is the following:

$$\begin{aligned} -\nabla^2 f(\mathbf{x}) = s(\mathbf{x}) & \Rightarrow f(\mathbf{x}) = \int d^3x' [1/4\pi R] s(\mathbf{x}') + \text{homogeneous solutions} \\ \text{The Poisson Equation} & \quad (H.1.8) \end{aligned}$$

$$\begin{aligned} -(\nabla^2+k^2) f(\mathbf{x}) = s(\mathbf{x}) & \Rightarrow f(\mathbf{x}) = \int d^3x' [e^{-j\mathbf{k}\cdot\mathbf{R}}/4\pi R] s(\mathbf{x}') + \text{homogeneous solutions} \\ \text{The Helmholtz Equation} & \quad (H.1.9) \end{aligned}$$

The equations on the left are inhomogeneous partial differential equations driven by source function $s(\mathbf{x})$. If one is careful to include in $s(\mathbf{x})$ all source contributions (such as those on boundary surfaces), one generally does not have to add any homogeneous solutions on the right. A homogeneous solution refers to

$-\nabla^2 f_h(\mathbf{x}) = 0$, for example. The solutions shown on the right above can be instantly verified as follows:

$$f(\mathbf{x}) = \int d^3x' [1/4\pi R] s(\mathbf{x}') + f_h(\mathbf{x})$$

$$-\nabla^2 f(\mathbf{x}) = \int d^3x' (-\nabla^2 [1/4\pi R]) s(\mathbf{x}') - \nabla^2 f_h(\mathbf{x}) = \int d^3x' \delta(\mathbf{r}-\mathbf{r}') s(\mathbf{x}') - 0 = s(\mathbf{x}) \quad (\text{H.1.10})$$

and similarly for $-(\nabla^2+k^2) f = g$.

A "free space" Green's Function g_F in general is a solution of

$$L_x g_F(\mathbf{r}, \mathbf{r}') = \delta(\mathbf{r}-\mathbf{r}'), \quad g_F(\mathbf{r}, \mathbf{r}') \rightarrow 0 \text{ as } \mathbf{r} \rightarrow \infty \quad (\text{H.1.11})$$

where L_x is some differential operator. The condition on the right says g_F must vanish on the Great Sphere. More generally one can define a *full* Green's function by,

$$L_x g(\mathbf{r}, \mathbf{r}') = \delta(\mathbf{r}-\mathbf{r}'), \quad g(\mathbf{r}, \mathbf{r}') = 0 \text{ for } \mathbf{r} \text{ on some closed surface enclosing a region of interest} \quad (\text{H.1.12})$$

This non-free-space Green's function is briefly discussed in the text surrounding (1.5.11). George Green (1793-1841), by the way, was an English grain miller (his day job).

Looking at $f(\mathbf{x}) = \int d^3x' [1/4\pi R] s(\mathbf{x}') = \int g_F(\mathbf{x},\mathbf{x}') [s(\mathbf{x}') d^3x']$, one can say that the kernel Green's Function $g_F(\mathbf{x},\mathbf{x}')$ "propagates" a tiny piece of "source" $[s(\mathbf{x}')d^3x']$ from location \mathbf{x}' to location \mathbf{x} so that the solution $f(\mathbf{x})$ is then a sum of all such propagated contributions as the source ranges over the entire volume of interest, which for us is all 3D space where the source is non-vanishing. See Fig 1.6.

H.2 Derivation of Fact 1: $-\nabla^2[1/r] = 4\pi\delta(\mathbf{r})$ (H.2.1)

Proof: Let volume V be all of 3D space. Carve out from V a small spherical cavity of radius a centered at $\mathbf{r} = 0$. If we call this spherical volume V_a and then $V' = V - V_a$ is the original volume with the spherical cavity carved out:

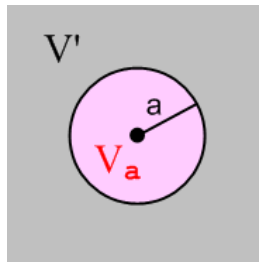


Fig H.1

In order to show that some function $g(\mathbf{r}) = \delta(\mathbf{r})$, one has to show that

$$\lim_{a \rightarrow 0} \int_{V'} dV g(\mathbf{r}) = 0 \quad (\text{H.2.2a})$$

$$\lim_{a \rightarrow 0} \int_{V_a} dV g(\mathbf{r}) = 1 \quad (\text{H.2.2b})$$

This is basically the definition of $\delta(\mathbf{r})$. Since $\delta(\mathbf{r})$ has units L^{-3} , $g(\mathbf{r}) = g(\mathbf{r})$ has units L^{-3} .

Our candidate function of interest is

$$g(\mathbf{r}) = - (1/4\pi) \nabla^2 [1/r] \quad (\text{H.2.3})$$

Using ∇^2 in spherical coordinates acting on a function of r , one finds that, since $\partial_{\mathbf{x}}(1) = 0$,

$$\nabla^2 [1/r] = (1/r^2) \partial_{\mathbf{x}} (r^2 \partial_{\mathbf{x}}) [1/r] = 0 \quad r > 0 \quad (\text{H.2.4})$$

so that

$$g(\mathbf{r}) = - (1/4\pi) \nabla^2 [1/r] = 0 \quad r > 0 \quad (\text{H.2.5})$$

Thus, condition (H.2.2a) is trivially satisfied since $r > 0$ everywhere in volume V' .

It remains to verify condition (H.2.2b). Consider the integral appearing on the left side of (H.2.2b)

$$\int_{V_a} dV g(\mathbf{r}) = - (1/4\pi) \int_{V_a} dV \nabla^2 [1/r] = - (1/4\pi) \int_{V_a} dV \nabla \cdot \nabla [1/r] \quad (\text{H.2.6})$$

The divergence theorem (1.1.30) says,

$$\int_V dV \operatorname{div} \mathbf{F} = \int_S d\mathbf{S} \cdot \mathbf{F} \quad (\text{H.2.7})$$

where V is any closed volume whose surface is S , and $d\mathbf{S}$ points out. Using

$$V = V_a \quad \text{and} \quad \mathbf{F} = \nabla [1/r] = \hat{\mathbf{r}} \partial_{\mathbf{x}} (1/r) = -r^{-2} \hat{\mathbf{r}}$$

we find that

$$\text{LHS (H.2.7)} = \int_{V_a} dV \operatorname{div} \nabla [1/r] = \int_{V_a} dV \nabla^2 [1/r] = \int_{V_a} dV [-4\pi g(\mathbf{r})] = -4\pi \int_{V_a} dV g(\mathbf{r})$$

$$\text{RHS (H.2.7)} = \int_S d\mathbf{S} \cdot \nabla [1/r] = \int d\Omega [a^2 \hat{\mathbf{r}}] \cdot \nabla [1/r]^{r=a} = \int d\Omega [a^2 \hat{\mathbf{r}}] \cdot [-a^{-2} \hat{\mathbf{r}}] = -4\pi$$

which tells us that $\int_{V_a} dV g(\mathbf{r}) = 1$ for any a . Thus,

$$\lim_{\mathbf{a} \rightarrow \mathbf{0}} \int_{\mathbf{v}_a} dV g(\mathbf{r}) = 1$$

and we have then verified (H.2.2b). Therefore we conclude that the candidate $g(\mathbf{r})$ of (H.2.3) is in fact the same as $\delta(\mathbf{r})$ so

$$-(1/4\pi)\nabla^2[1/r] = \delta(\mathbf{r}) \quad (\text{H.2.8})$$

or

$$\nabla^2[1/r] = -4\pi\delta(\mathbf{r}) \quad (\text{H.2.9})$$

which is (H.2.1).

QED

$$\mathbf{H.3 Derivation of Fact 2:} \quad \nabla^2[h(r)/r] = -4\pi h(0) \delta(\mathbf{r}) + h''(r)/r \quad (\text{H.3.1})$$

Proof: Start with this vector identity,

$$\nabla^2(\phi\psi) = \phi\nabla^2\psi + \psi\nabla^2\phi + 2 \nabla\phi \cdot \nabla\psi \quad (\text{H.3.2})$$

This identity is valid in any number of dimensions (implied sum on i from 1 to N),

$$\partial_i^2(\phi\psi) = \partial_i[(\partial_i\phi)\psi + \psi(\partial_i\phi)] = (\partial_i^2\phi)\psi + (\partial_i\phi)(\partial_i\psi) + \phi(\partial_i^2\psi) + (\partial_i\phi)(\partial_i\psi).$$

So apply (H.3.2) to the case $\phi = h$ and $\psi = r^{-1}$,

$$\begin{aligned} \nabla^2(h r^{-1}) &= h\nabla^2(r^{-1}) + r^{-1}\nabla^2h + 2 \nabla h \cdot \nabla(r^{-1}) \\ &= -h 4\pi \delta(\mathbf{r}) + r^{-1}\nabla^2h + 2 [h' \hat{\mathbf{r}} \cdot (-r^{-2}) \hat{\mathbf{r}}] \quad // \text{ using (H.2.9)} \\ &= -4\pi h(0) \delta(\mathbf{r}) + r^{-1}\nabla^2h - 2 r^{-2} h'(r) \quad (\text{H.3.3}) \end{aligned}$$

Algebra shows that, using spherical coordinates,

$$\nabla^2h = (1/r^2)\partial_{\mathbf{r}}(r^2\partial_{\mathbf{r}})h(r) = h''(r) + (2/r)h'(r) \quad (\text{H.3.4})$$

so then

$$\begin{aligned} \nabla^2(h r^{-1}) &= -4\pi h(0) \delta(\mathbf{r}) + r^{-1} [h''(r) + (2/r)h'(r)] - 2 r^{-2} h'(r) \\ &= -4\pi h(0) \delta(\mathbf{r}) + h''(r)/r \end{aligned}$$

which is the claim of (H.3.1).

QED

$$\mathbf{Fact\ 3:} \quad -(\nabla^2+k^2) (e^{-j\mathbf{k}\mathbf{x}}/4\pi r) = \delta(\mathbf{r}) \quad (\text{H.3.5})$$

This Fact is just an application of Fact 2 to the case $h(\mathbf{r}) = e^{-j\mathbf{k}\mathbf{x}}$:

$$h = e^{-j\mathbf{k}\mathbf{x}} \quad h(0) = 1 \quad h' = -j\mathbf{k} e^{-j\mathbf{k}\mathbf{x}} \quad h'' = -k^2 e^{-j\mathbf{k}\mathbf{x}}$$

$$\nabla^2[h(\mathbf{r})/r] = -4\pi h(0) \delta(\mathbf{r}) + h''(\mathbf{r})/r \quad (\text{H.3.1})$$

so

$$\begin{aligned} \nabla^2(e^{-j\mathbf{k}\mathbf{x}}/r) &= -4\pi \delta(\mathbf{r}) + [-k^2 e^{-j\mathbf{k}\mathbf{x}}] / r \\ &= -4\pi\delta(\mathbf{r}) - k^2(e^{-j\mathbf{k}\mathbf{x}}/r) \end{aligned}$$

Thus,

$$(\nabla^2+k^2) (e^{-j\mathbf{k}\mathbf{x}}/r) = -4\pi\delta(\mathbf{r})$$

or

$$-(\nabla^2+k^2) (e^{-j\mathbf{k}\mathbf{x}}/4\pi r) = \delta(\mathbf{r})$$

as claimed.

Appendix I: Laplace and Helmholtz Propagators in 2D

Note: Appendix H deals with these propagators in 3D rather than 2D. Sections I.1 and I.2 below are basically "cut, paste and edit" versions of Sections H.1 and H.2, and we have made equation numbers match. However, Section I.3 is something new since it involves a "special function".

I.1 Overview and Meaning of Free-Space Propagators

This appendix proves two Facts: ($H_0^{(1)}$ is a Hankel function)

$$\mathbf{Fact\ 1 :} \quad -\nabla^2[\ln(1/r)/2\pi] = \delta(\mathbf{r}) \quad (I.2.1) \quad (I.1.1)$$

$$\mathbf{Fact\ 2 :} \quad -(\nabla^2+k^2) [(j/4) H_0^{(1)}(kr)] = \delta(\mathbf{r}) \quad (I.3.1) \quad (I.1.2)$$

Throughout this Appendix, ∇^2 is the usual 2D Laplacian operator,

$$\nabla^2 = \partial_{\mathbf{x}}^2 + \partial_{\mathbf{y}}^2. \quad \text{and} \quad \delta(\mathbf{r}) = \delta(x) \delta(y) \quad (I.1.3)$$

In the two Facts above, if one replaces $\mathbf{r} \rightarrow \mathbf{r}-\mathbf{r}'$ (a simple translational shift of origin) ones finds

$$-\nabla^2[\ln(1/R)/2\pi] = \delta(\mathbf{r}-\mathbf{r}') \quad R = |\mathbf{r} - \mathbf{r}'| \quad (I.1.4)$$

$$-(\nabla^2+k^2) [(j/4) H_0^{(1)}(kR)] = \delta(\mathbf{r}-\mathbf{r}') \quad \delta(\mathbf{r}-\mathbf{r}') = \delta(x-x') \delta(y-y') \quad (I.1.5)$$

The quantities in brackets are known as free-space Green's Functions (Green Functions) or propagators, or as "fundamental solutions" :

$$\frac{1}{2\pi} \ln(1/R) = \text{the Laplace 2D free-space propagator} = -\ln(R)/2\pi \quad (I.1.6)$$

$$(j/4) H_0^{(1)}(kR) = \text{the Helmholtz 2D free-space propagator} \quad (I.1.7)$$

The last item above is the ω -domain 2D Helmholtz propagator, where $k^2 = \omega^2\mu\epsilon$. See (A.7.7) for a discussion of the time domain version of this propagator which is the 2D wave equation propagator.

The significance of these propagators is the following:

$$-\nabla^2 f(\mathbf{x}) = s(\mathbf{x}) \quad \Rightarrow \quad f(\mathbf{x}) = \int d^2x' [\ln(1/R)/2\pi] s(\mathbf{x}') + \text{homogeneous solutions}$$

The Poisson Equation (I.1.8)

$$-(\nabla^2+k^2) f(\mathbf{x}) = s(\mathbf{x}) \quad \Rightarrow \quad f(\mathbf{x}) = \int d^2x' [(j/4) H_0^{(1)}(kR)] s(\mathbf{x}') + \text{homogeneous solutions}$$

The Helmholtz Equation (I.1.9)

The equations on the left are inhomogeneous partial differential equations driven by source function $s(\mathbf{x})$. If one is careful to include in $s(\mathbf{x})$ all source contributions (such as those on boundary curves), one generally does not have to add any homogeneous solutions on the right. A homogeneous solution refers to $-\nabla^2 f_h(\mathbf{x}) = 0$, for example. The solutions shown on the right above can be instantly verified as follows:

$$f(\mathbf{x}) = \int d^2x' [\ln(1/R)/2\pi] s(\mathbf{x}') + f_h(\mathbf{x})$$

$$-\nabla^2 f(\mathbf{x}) = \int d^2x' (-\nabla^2 [\ln(1/R)/2\pi]) s(\mathbf{x}') - \nabla^2 f_h(\mathbf{x}) = \int d^2x' \delta(\mathbf{r}-\mathbf{r}') s(\mathbf{x}') - 0 = s(\mathbf{x}) \quad (\text{I.1.10})$$

and similarly for $-(\nabla^2+k^2) f = g$.

A "free space" Green's Function g_F in general is a solution of

$$D g_F(\mathbf{r}, \mathbf{r}') = \delta(\mathbf{r}-\mathbf{r}'), \quad g_F(\mathbf{r}, \mathbf{r}') \rightarrow 0 \text{ as } \mathbf{r} \rightarrow \infty \quad (\text{I.1.11})$$

where D is some differential operator. The condition on the right says g_F must vanish on the Great Circle. More generally one can define a *full* Green's function by,

$$D g(\mathbf{r}, \mathbf{r}') = \delta(\mathbf{r}-\mathbf{r}'), \quad g(\mathbf{r}, \mathbf{r}') = 0 \text{ for } \mathbf{r} \text{ on some closed curve enclosing a region of interest} \quad (\text{I.1.12})$$

This non-free-space Green's function is briefly discussed in the text surrounding (1.5.11).

Looking at $f(\mathbf{x}) = \int d^2x' [\ln(1/R)/2\pi] s(\mathbf{x}') = \int g_F(\mathbf{x},\mathbf{x}') [s(\mathbf{x}') d^2x']$, one can say that the kernel Green's Function $g_F(\mathbf{x},\mathbf{x}')$ "propagates" a tiny piece of "source" $[s(\mathbf{x}')d^2x']$ from location \mathbf{x}' to location \mathbf{x} so that the solution $f(\mathbf{x})$ is then a sum of all such propagated contributions as the source ranges over the entire area of interest, which for us is all 2D space where the source is non-vanishing.

I.2 Derivation of Fact 1: $\nabla^2[\ln(1/r)] = -2\pi\delta(\mathbf{r}) \quad (\text{I.2.1})$

Proof: Let area A be all of 2D space. Cut out from A a small circular hole of radius a centered at $\mathbf{r} = 0$. If we call this circular area A_a and then $A' = A - A_a$ is the original area with the circular hole cut out:

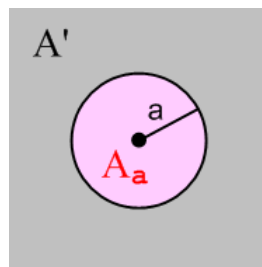


Fig I.1

In order to show that some function $g(\mathbf{r}) = \delta(\mathbf{r})$, one has to show that

$$\lim_{a \rightarrow 0} \int_{\mathbf{A}} dA g(\mathbf{r}) = 0 \quad (\text{I.2.2a})$$

$$\lim_{a \rightarrow 0} \int_{\mathbf{A}_a} dA g(\mathbf{r}) = 1 . \quad (\text{I.2.2b})$$

This is basically the definition of $\delta(\mathbf{r})$. Since $\delta(\mathbf{r})$ has units L^{-2} , $g(\mathbf{r})$ has units L^{-2} .

Comment: When any differential operator like ∇ or ∇^2 is applied to $\ln(r_0/r)$, the result is independent of r_0 so we can always take $r_0 = 1$. For example, $\partial_{\mathbf{x}} [\ln(r_0/r)] = \partial_{\mathbf{x}} [\ln r_0 + \ln(1/r)] = \partial_{\mathbf{x}} \ln(1/r)$. In what follows, $\ln(r)$ and $\ln(1/r)$ are always acted upon by differential operators, so we can interpret these objects as dimensionless quantities $\ln(r/r_0)$ and $\ln(r_0/r)$ for any r_0 . Then it is clear below that $\dim [g(\mathbf{r})] = L^{-2}$.

Our candidate function of interest is

$$g(\mathbf{r}) = - (1/2\pi) \nabla^2 [\ln(1/r)] = + (1/2\pi) \nabla^2 [\ln(r)] . \quad (\text{I.2.3})$$

Using ∇^2 in polar (cylindrical without the z) coordinates acting on a function of r , one finds that, since $\partial_{\mathbf{x}}(1) = 0$,

$$\nabla^2 [\ln(r)] = (1/r) \partial_{\mathbf{x}} (r \partial_{\mathbf{x}}) [\ln(r)] = 0 \quad r > 0 \quad (\text{I.2.4})$$

so that

$$g(\mathbf{r}) = - (1/2\pi) \nabla^2 [\ln(1/r)] = 0 \quad r > 0 . \quad (\text{I.2.5})$$

Thus, condition (I.2.2a) is trivially satisfied since $r > 0$ everywhere in area A' for any $a > 0$.

It remains to verify condition (I.2.2b). Consider the integral appearing in the left side of (I.2.2b)

$$\int_{\mathbf{A}_a} dA g(\mathbf{r}) = - (1/4\pi) \int_{\mathbf{A}_a} dA \nabla^2 [1/r] = - (1/4\pi) \int_{\mathbf{A}_a} dA \nabla \cdot \nabla [1/r] . \quad (\text{I.2.6})$$

The divergence theorem (1.1.30) says, in 2D,

$$\int_{\mathbf{A}} dA \operatorname{div} \mathbf{F} = \oint_C ds \cdot \mathbf{F} \quad (\text{I.2.7})$$

where A is any closed area whose bounding curve is C , and where $ds = ds \hat{\mathbf{n}}$ where $\hat{\mathbf{n}}$ is normal to C at any given point on C . Notice that this closed area is necessarily planar since everything is 2D here. Using

$$A = A_a = \text{disk of radius } a \quad \text{and} \quad \mathbf{F} = \nabla [\ln(1/r)] = \hat{\mathbf{r}} \partial_{\mathbf{x}} (\ln(1/r)) = - \hat{\mathbf{r}} \partial_{\mathbf{x}} (\ln r) = [-r^{-1}] \hat{\mathbf{r}}$$

we find that

$$\text{LHS (I.2.7)} = \int_{\mathbf{A}_a} dA \operatorname{div} \nabla [\ln(1/r)] = \int_{\mathbf{A}_a} dA \nabla^2 [\ln(1/r)] = \int_{\mathbf{A}_a} dA [-2\pi g(r)] = -2\pi \int_{\mathbf{A}_a} dA g(r)$$

$$\text{RHS (I.2.7)} = \int_{\mathbf{C}} ds \cdot \nabla [\ln(1/r)] = \int [ad\theta \hat{\mathbf{r}}] \cdot \nabla [\ln(1/r)]|_{r=a} = \int d\theta [a \hat{\mathbf{r}}] \cdot [-a^{-1} \hat{\mathbf{r}}] = -2\pi$$

which tells us that $\int_{\mathbf{A}_a} dA g(r) = 1$ for any a . Thus,

$$\lim_{a \rightarrow 0} \int_{\mathbf{A}_a} dA g(r) = 1$$

and we have then verified (I.2.2b). Therefore we conclude that the candidate $g(\mathbf{r})$ of (I.2.3) is in fact the same as $\delta(\mathbf{r})$ so

$$-(1/2\pi)\nabla^2 [\ln(1/r)] = \delta(\mathbf{r}) \quad (\text{I.2.8})$$

or

$$\nabla^2 [\ln(1/r)] = -2\pi\delta(\mathbf{r}) \quad (\text{I.2.9})$$

which is (I.2.1).

QED

I.3 Derivation of Fact 2: $-(\nabla^2 + k^2) [(j/4) H_0^{(1)}(kr)] = \delta(\mathbf{r}) \quad (\text{I.3.1})$

We seek the solution $E(r)$ of this equation

$$-(\nabla^2 + k^2) E(r) = \delta(\mathbf{r}) \quad \text{where } E(r \rightarrow \infty) = 0 \quad (\text{I.3.2})$$

which we write as

$$\nabla^2 E + k^2 E = -\delta(\mathbf{r}).$$

In polar coordinates this says

$$r^{-1} \partial_r (r \partial_r E) + k^2 E = -\delta(\mathbf{r})$$

or

$$E'' + r^{-1} E' + k^2 E = -\delta(\mathbf{r})$$

or

$$r^2 E''(r) + r E'(r) + r^2 k^2 E(r) = -\delta(\mathbf{r}) \quad (\text{I.3.3})$$

Writing $E(r) = F(kr)$ we get

$$r^2 k^2 F''(kr) + rk F'(kr) + r^2 k^2 F(kr) = -\delta(\mathbf{r})$$

or

$$(rk)^2 F''(kr) + (rk) F'(kr) + (rk)^2 F(kr) = -\delta(\mathbf{r})$$

or

$$z^2 F''(z) + z F'(z) + z^2 F(z) = -\delta(\mathbf{r}) \quad \text{where } z \equiv kr \quad (\text{I.3.4})$$

Away from $r = z = 0$, this is Bessel's equation of index 0 (NIST 10.2.1) so solutions are Bessel functions like these,

$$F(z) = J_0(z), Y_0(z), H_0^{(1)}(z), H_0^{(2)}(z). \quad z = kr \quad (I.3.5)$$

which are Bessel functions of the first, second and third kind. The third kind functions (the H's) are called Hankel Functions. If we assume that k has a tiny positive imaginary part (see Comments later), then of all the functions just listed, only $H_0^{(1)}(kr)$ has decaying behavior for large r (NIST 10.2.5, more on this below). We therefore put forward the following *candidate* for a delta function

$$g(\mathbf{r}) = -(\nabla^2 + k^2) C H_0^{(1)}(kr). \quad (I.3.6)$$

Recall from Section I.2 that a successful $\delta(\mathbf{r})$ candidate must satisfy these two conditions (same as in the previous section, and same figure),

$$\lim_{a \rightarrow 0} \int_{A'} dA g(\mathbf{r}) = 0 \quad (I.2.2a)$$

$$\lim_{a \rightarrow 0} \int_{A_a} dA g(\mathbf{r}) = 1 \quad (I.2.2b)$$

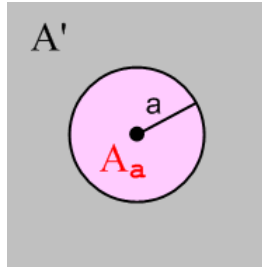


Fig I.1

Our candidate $g(\mathbf{r})$ vanishes within any region A' no matter how small the hole because $g(\mathbf{r}) = 0$ for any $r > 0$, so the first condition is already met. It remains only to show that the second condition is also met. We must then show that

$$\lim_{a \rightarrow 0} \int_{A_a} dA \{- (\nabla^2 + k^2) C H_0^{(1)}(kr)\} = 1. \quad (I.3.7)$$

Since A_a is a very small disk as we approach the limit, we may use the small argument behavior of our candidate $g(\mathbf{r})$ in studying the situation. We know that

$$H_0^{(1)}(kr) \approx (2j/\pi) \ln(kr) \quad // \text{ NIST 10.7.2} \quad (I.3.8)$$

so what we need to show is that

$$\lim_{a \rightarrow 0} \int_{\mathbf{A}_a} dA \{ -(\nabla^2 + k^2) C (2j/\pi) \ln(kr) \} = 1$$

or

$$- C (2j/\pi) \lim_{a \rightarrow 0} \int_{\mathbf{A}_a} dA \{ (\nabla^2 + k^2) \ln(kr) \} = 1$$

or

$$- C (2j/\pi) 2\pi \lim_{a \rightarrow 0} \int_0^a r dr \{ (\nabla^2 + k^2) \ln(kr) \} = 1 \quad // \int d\theta = 2\pi$$

or

$$C (4/j) \lim_{a \rightarrow 0} \int_0^a r dr \{ (\nabla^2 + k^2) \ln(kr) \} = 1 \quad (I.3.9)$$

Now consider :

$$\lim_{a \rightarrow 0} \left[\int_0^a r dr \ln(kr) \right] = \lim_{a \rightarrow 0} \left[(1/4)a^2 \{ 2\ln(ka) - 1 \} \right] = 0 \quad (I.3.10)$$

Thus, the $k^2 \ln(kr)$ term in (I.3.9) makes no contribution in the limit, so we then have to show that

$$C (4/j) \lim_{a \rightarrow 0} \int_0^a r dr \nabla^2 [\ln(kr)] = 1 \quad (I.3.11)$$

But (I.2.9) says that

$$\nabla^2 [\ln(r)] = 2\pi\delta(\mathbf{r}) \quad (I.2.9)$$

Now

$$\delta(\mathbf{r}) = \delta(x)\delta(y) = \delta(r)/2\pi r \quad (I.3.12)$$

since

$$1 = \int \int dx dy \delta(x)\delta(y) = \int r dr \int d\theta \delta(r)/2\pi r = 2\pi \int r dr \delta(r)/2\pi r = \int dr \delta(r) = 1 \quad .$$

Therefore

$$\nabla^2 [\ln(r)] = \delta(r)/r \quad (I.3.13)$$

and then

$$\nabla^2 [\ln(kr)] = \nabla^2 [\ln(k) + \ln(r)] = \nabla^2 [\ln(r)] = \delta(r)/r \quad (I.3.14)$$

Inserting this last result into (I.3.11) then gives,

$$C (4/j) \lim_{a \rightarrow 0} \int_0^a r dr \nabla^2 [\ln(kr)] = 1$$

$$C (4/j) \lim_{a \rightarrow 0} \int_0^a r dr \delta(r)/r = 1$$

$$C (4/j) \lim_{a \rightarrow 0} \int_0^a dr \delta(r) = 1$$

$$C (4/j) \lim_{a \rightarrow 0} 1 = 1$$

$$C (4/j) = 1 .$$

Thus, we have a solution if we select constant $C = (j/4)$. Therefore, the solution to (I.3.2) is

$$E(r) = C H_0^{(1)}(kr) = (j/4) H_0^{(1)}(kr) . \tag{I.3.15}$$

Stakgold Vol II page 55 (5.120) confirms this result where $\sqrt{\lambda} = k$.

Therefore we have shown that

$$-(\nabla^2 + k^2) [(j/4) H_0^{(1)}(kr)] = \delta(\mathbf{r}) \tag{I.3.16}$$

which is the Fact stated as (I.3.1).

QED

On page 54 Stakgold gives the solution to $-(\nabla^2 + k^2) E(r) = \delta(\mathbf{r})$ for $n \geq 2$ dimensions as (5.118):

$$E_n(r; \lambda) = \frac{i}{4} \left(\frac{\sqrt{\lambda}}{2\pi r} \right)^{(n-2)/2} H_{(n/2)-1}^{(1)}(\sqrt{\lambda} r), \quad n \geq 2. \tag{5.118}$$

Comments:

1. Complex Helmholtz Parameter and $H_\nu^{(1)}(z)$. Stakgold considers the Helmholtz parameter to be λ which is our k^2 . He regards λ as a complex variable which can lie anywhere in the complex λ plane. If we consider the function $k(\lambda) = \lambda^{1/2}$, we find that it has a branch point at $\lambda = 0$. If we take the branch cut to the right, then one of the two Riemann sheets in λ -space for this function maps to the upper half k -plane as shown. This is the branch of $\lambda^{1/2}$ that Stakgold selects and that is why we think of k and therefore k^2 as having a tiny positive imaginary part when k is "real". The point is that we approach the positive real k axis from above, not from below. It is this assumption that causes the large- r -decaying solution to our problem to be $H_0^{(1)}(kr)$ instead of $H_0^{(2)}(kr)$.

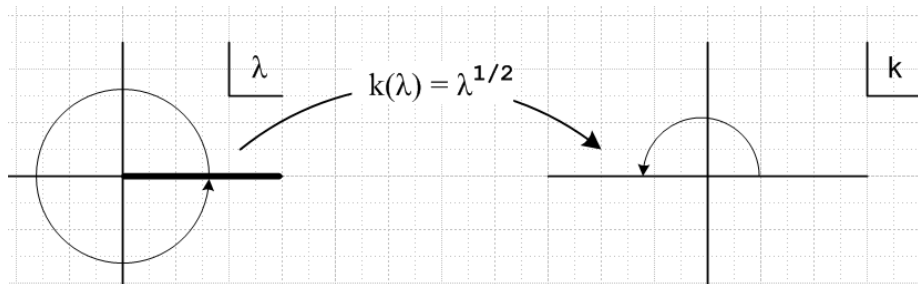


Fig I.2

As shown on NIST p 229 10.17.5,6, expansions of the Hankel functions for large argument are,

$$\begin{aligned}
 H_\nu^{(1)}(z) &\approx \sqrt{2/\pi} z^{-1/2} e^{+j(z-\nu\pi/2-\pi/4)} \sum_{k=0}^{\infty} (+j)^k a_k(\nu) z^{-k} \\
 H_\nu^{(2)}(z) &\approx \sqrt{2/\pi} z^{-1/2} e^{-j(z-\nu\pi/2-\pi/4)} \sum_{k=0}^{\infty} (-j)^k a_k(\nu) z^{-k}
 \end{aligned}$$

where $a_k(\nu)$ are some real coefficients shown in 10.17.1 which we don't care about right now. The differences are highlighted in red. Here one sees that $H_\nu^{(1)}(z) \sim e^{+jz} = e^{-\text{Im}z} e^{j\text{Re}z}$. Thus $H_\nu^{(1)}(kr) \sim e^{-\text{rIm}k} e^{j\text{rRe}k}$ and as long as k is in the upper half plane as shown in the right, $H_\nu^{(1)}(kr)$ decays exponentially (whereas $H_\nu^{(2)}(kr)$ blows up).

2. Helmholtz morphs into Laplace. We have shown that

$$-(\nabla^2+k^2) [(j/4) H_0^{(1)}(kr)] = \delta(\mathbf{r}) \quad . \quad (I.3.16)$$

In the limit that $k \ll 1$, it was shown above that

$$H_0^{(1)}(kr) \approx (2j/\pi) \ln(kr) \quad // \text{ A\&S 10.7.2} \quad (I.3.8)$$

In this limit we then have

$$-(\nabla^2+k^2) [(j/4) (2j/\pi) \ln(kr)] = \delta(\mathbf{r})$$

or

$$-(\nabla^2) [(1/2\pi) \ln(kr)] = \delta(\mathbf{r})$$

and this is in agreement with the Laplace result (I.1.1). So as the Helmholtz equation morphs into the Laplace equation as $k \rightarrow 0$, the Helmholtz propagator morphs into the Laplace propagator.

Appendix J: The 3D→2D Propagator Transition

Infinitely long transmission lines are -- in the transmission line limit of long wavelength -- basically 2D objects rather than 3D objects. We see that fact appearing in various Chapters and Appendices of this document. Here we wish to focus on this single fact.

Case 1

In Chapter 1 we presented the natural 3D view of transmission lines with equations like the following taken from (1.5.3), (1.5.4) and (1.5.23), where we used the King gauge,

$$\begin{aligned}
 (\nabla^2 + \beta_d^2)\varphi &= - (1/\epsilon) \sum_i \rho_i & \Leftrightarrow & \quad \varphi(\mathbf{x},\omega) = \frac{1}{4\pi\epsilon_d} \sum_i \int \rho_{ci}(\mathbf{x}',\omega) \frac{e^{-j\beta_d R}}{R} dV' \\
 (\nabla^2 + \beta_d^2)\mathbf{A} &= - \sum_i \mu_i \mathbf{J}_i & \Leftrightarrow & \quad \mathbf{A}(\mathbf{x},\omega) = \frac{1}{4\pi} \sum_i \int \mu_i \mathbf{J}_i(\mathbf{x}',\omega) \frac{e^{-j\beta_d R}}{R} dV' .
 \end{aligned} \tag{J.1}$$

The Helmholtz integrals on the right are particular solutions of the PDEs on the left. The equations on the right are derived from those on the left as shown in Appendix H where we had the more generic statement that

$$\begin{aligned}
 - (\nabla^2 + k^2) f(\mathbf{x}) = s(\mathbf{x}) & \quad \Rightarrow \quad f(\mathbf{x}) = \int d^3x' [e^{-jkR}/4\pi R] s(\mathbf{x}') + \text{homogeneous solutions} \\
 \text{The 3D Helmholtz Equation} & \quad \quad \quad \text{particular solution} & \quad \quad \quad (H.1.9)
 \end{aligned}$$

The object $[e^{-jkR}/4\pi R]$ is the 3D free-space Helmholtz propagator as discussed in Appendix H.

If it happens that $f(\mathbf{x}) = f(x,y)$ in this last equation, then $\partial_z^2 f = 0$ and we find ourselves looking at a 2D Helmholtz equation which has a completely different-looking particular solution, where $\nabla^2 = \nabla_{2D}^2 + \partial_z^2$,

$$\begin{aligned}
 - (\nabla_{2D}^2 + k^2) f(\mathbf{x}) = s(\mathbf{x}) & \quad \Rightarrow \quad f(\mathbf{x}) = \int d^2x' [(j/4) H_0^{(1)}(kR)] s(\mathbf{x}') + \text{homogeneous solutions} \\
 \text{The 2D Helmholtz Equation} & \quad \quad \quad \text{particular solution} & \quad \quad \quad (I.1.9)
 \end{aligned}$$

This is the most abrupt and simple way the transition from 3D to 2D can occur.

If k is small, meaning the corresponding wavelength $\lambda = 2\pi/k$ is large, one can take the small k limit of the above two particular integrals. The limit of $[e^{-jkR}/4\pi R]$ is completely obvious,

$$[e^{-jkR}/4\pi R] \rightarrow [1/4\pi R] \tag{J.2}$$

whereas the limit of the 2D propagator $[(j/4) H_0^{(1)}(kR)]$ is less obvious:

$$H_0^{(1)}(kr) \approx (2j/\pi) \ln(kr) \quad // \text{ NIST 10.7.2} \tag{I.3.8}$$

so that

$$[(j/4) H_0^{(1)}(kR)] \approx - (1/2\pi) \ln(kR) = [- (1/2\pi) \ln(R)] - (1/2\pi) \ln(k) . \quad (J.3)$$

Momentarily ignoring the inconvenient constant $- (1/2\pi) \ln(k)$, one can say that

$$\text{2D Helmholtz propagator} = [\frac{j}{4} H_0^{(1)}(kR)] \rightarrow [- \frac{1}{2\pi} \ln(R)] = [- \frac{1}{4\pi} \ln(R^2)] = [\frac{1}{2\pi} \ln(1/R)] . \quad (J.4)$$

The objects on the right of (J.2) and (J.4) and are in fact the 2D Laplace propagators which belong to this pair of PDE's and their particular solutions,

$$\begin{aligned} -\nabla^2 f(\mathbf{x}) = s(\mathbf{x}) & \Rightarrow f(\mathbf{x}) = \int d^3x' [1/4\pi R] s(\mathbf{x}') + \text{homogeneous solutions} \\ \text{The 3D Poisson Equation} & \qquad \qquad \qquad \text{particular solution} \end{aligned} \quad (H.1.8)$$

$$\begin{aligned} -\nabla_{2D}^2 f(\mathbf{x}) = s(\mathbf{x}) & \Rightarrow f(\mathbf{x}) = \int d^2x' [\ln(1/R)/2\pi] s(\mathbf{x}') + \text{homogeneous solutions} \\ \text{The 2D Poisson Equation} & \qquad \qquad \qquad \text{particular solution} \end{aligned} \quad (I.1.8)$$

Since in our applications $f(\mathbf{x})$ is always a potential like ϕ or \mathbf{A} , and since

$$\mathbf{B} = \text{curl } \mathbf{A} \qquad \mathbf{E} = - \text{grad } \phi - \partial_t \mathbf{A} \quad (I.3.1)$$

we see that a constant like $- (1/2\pi) \ln(k)$ added to a potential has no effect on the physical fields \mathbf{E} and \mathbf{B} , so we can just ignore such constants. Another way to say this is that the zero level of a potential is always arbitrary so additive constants are meaningless. In Chapter 4 we are only really concerned with the potential *difference* $V(z)$ or $W(z)$ between conductors.

We can now examine some of the 3D/2D "transitions" that occurred in other parts of the document.

Case 2

In Section 4.4 we had

$$\begin{aligned} V(z) &\equiv \phi_{12}(\mathbf{x}_1) - \phi_{12}(\mathbf{x}_2) \\ &= \frac{1}{4\pi\epsilon_d} q(z) \int_{-\infty}^{\infty} dz' \left\{ \int_{C_1} dx_1' dy_1' \alpha_1(x_1', y_1') \frac{1}{R_{11}} - \int_{C_2} dx_2' dy_2' \alpha_2(x_2', y_2') \frac{1}{R_{12}} \right\} \\ &- \frac{1}{4\pi\epsilon_d} q(z) \int_{-\infty}^{\infty} dz' \left\{ \int_{C_1} dx_1' dy_1' \alpha_1(x_1', y_1') - \int_{C_2} dx_2' dy_2' \alpha_2(x_2', y_2') \frac{1}{R_{22}} \right\} \end{aligned} \quad (4.4.1)$$

which we obtained by assuming a separated form (4.1.2) for the charge density and by assuming a small Helmholtz parameter β . The $1/4\pi R$ factors here are in fact the 3D Laplace free-space propagators. This propagator has the less glamorous name of being the electrostatic potential of a $(1/\epsilon)$ -size point charge (in "free space" of course), so by assuming the transmission line limit of small Helmholtz parameter β , we

arrive at this electrostatics Laplace propagator appearing in the integrals. These propagators are "propagating" the effect of charges on the conductor surfaces to their destinations \mathbf{x}_1 and \mathbf{x}_2 in Fig 4.2 .

We then did the dz' integral over $(-\infty, \infty)$ making use of integral (4.4.5),

$$\int_{-\infty}^{\infty} dz' \left(\frac{1}{R_{12}} - \frac{1}{R_{22}} \right) = \ln(s_{22}^2/s_{12}^2) \quad (4.4.5)$$

and arrived at

$$V(z) = q(z) \frac{1}{4\pi\epsilon_d} \left\{ \int_{C_1} dx_1' dy_1' \alpha_1(x_1', y_1') \ln(s_{21}^2/s_{11}^2) - \int_{C_2} dx_2' dy_2' \alpha_2(x_2', y_2') \ln(s_{22}^2/s_{12}^2) \right\}. \quad (4.4.6)$$

This is really four terms and one recognizes $-\frac{1}{4\pi} \ln(R^2)$ in the form $-\frac{1}{4\pi} \ln(s_{ij}^2)$ as the 2D Laplace propagator just discussed above, and the s_{ij} are the 2D transverse distances shown in Fig 4.3. So here we see a very clear example of doing the 3D → 2D transition.

Case 3

Another transition example is the "scaling boundary condition" of Section 5.3 (b). We started there with

$$\varphi_{\mathbf{t}}(\mathbf{x}) = \int_{-\infty}^{\infty} dz' \left\{ \int_{C_1} dx_1' dy_1' \alpha_1(x_1', y_1') \frac{1}{R_1} - \int_{C_2} dx_2' dy_2' \alpha_2(x_2', y_2') \frac{1}{R_2} \right\} \quad (5.1.2)$$

and we moved the observation point \mathbf{x} far away from the transmission line. The result in this limit was found to be

$$\varphi_{\mathbf{t}}(\mathbf{x}) \approx \ln(s_2^2/s_1^2) \quad // \text{ limiting form as point } \mathbf{x} = (x, y) \text{ moves far from the conductors} \quad (5.3.13)$$

In this case, we had earlier done the following separation of the full potential

$$\varphi(x, y, z) = \frac{1}{4\pi\epsilon_d} q(z) \varphi_{\mathbf{t}}(x, y) \quad (5.1.1)$$

so the limit shown for $\varphi_{\mathbf{t}}$ says

$$\varphi(x, y, z) \approx (q/\epsilon_d) \frac{1}{4\pi} \ln(s_2^2/s_1^2) = (q/\epsilon^d) \frac{1}{4\pi} \ln(s_2^2) - (q/\epsilon_d) \frac{1}{4\pi} \ln(s_1^2) \quad (J.5)$$

and we interpret this as being the sum of the 2D free-space propagations of charges $\pm q(z)dz$ to our distant point. We are so far from the transmission line that these charges appear as 2D point charges which form a little electric dipole as shown in Section 5.4 (b).

Case 4

As a third example, we consider a simple generic situation alluded to above as our "abrupt" transition. Start again with

$$-(\nabla^2+k^2) f(\mathbf{x}) = h(\mathbf{x}) \quad \Rightarrow \quad f(\mathbf{x}) = \int d^3x' [e^{-jkR}/4\pi R] h(\mathbf{x}') + \text{homogeneous solutions}$$

The Helmholtz Equation particular solution (H.1.9)

We changed the source name from $s(x)$ to $h(x)$ to avoid confusion with distance s below. Assume now that $f(\mathbf{x}) = f(x,y)$. What happens to the Helmholtz integral on the right?

$$f(\mathbf{x}) = \int d^3x' [e^{-jkR}/4\pi R] h(\mathbf{x}') = \int dx' \int dy' \int_{-\infty}^{\infty} dz' h(x',y') [e^{-jkR}/4\pi R]$$

where

$$s = \sqrt{(x-x')^2 + (y-y')^2} \quad \text{and} \quad R = \sqrt{s^2 + z'^2} .$$

Then

$$f(\mathbf{x}) = \int dx' \int dy' h(x',y') \frac{1}{4\pi} \int_{-\infty}^{\infty} dz' \frac{e^{-jkR}}{R} \quad R = \sqrt{s^2 + z'^2} .$$

The dz' integral can be done as follows:

$$R^2 = s^2 + z'^2 \quad \Rightarrow \quad RdR = z'dz'$$

so

$$\begin{aligned} \int_{-\infty}^{\infty} dz' \frac{e^{-jkR}}{R} &= \int_{-\infty}^{\infty} \frac{RdR}{z'} \frac{e^{-jkR}}{R} = \int_{-\infty}^{\infty} dR \frac{e^{-jkR}}{\sqrt{R^2-s^2}} = \int_{-\infty}^{\infty} dR \frac{\cos(kR)}{\sqrt{R^2-s^2}} \\ &= 2 \int_0^{\infty} dR \frac{\cos(kR)}{\sqrt{R^2-s^2}} . \end{aligned} \tag{J.6}$$

Take note of the following integral in GR7 3.754.2 page 435,

$$2. \quad \int_0^{\infty} \frac{\cos(ax) dx}{\sqrt{\beta^2 + x^2}} = K_0(a\beta) \quad [a > 0, \quad \text{Re } \beta > 0]$$

which then says

$$\begin{aligned} \int_{-\infty}^{\infty} dR \frac{\cos(kR)}{\sqrt{R^2-s^2}} &= K_0(k\sqrt{-s^2}) = K_0(-jks) & z = -jks & \text{phase}(z) = -\pi/2 \\ & & (ze^{\pi j/2}) = zj & = ks \end{aligned} \tag{J.7}$$

But NIST p 250 says

10.27.8

$$K_\nu(z) = \begin{cases} \frac{1}{2}\pi i e^{\nu\pi i/2} H_\nu^{(1)}(ze^{\pi i/2}), & -\pi \leq \text{ph } z \leq \frac{1}{2}\pi, \\ -\frac{1}{2}\pi i e^{-\nu\pi i/2} H_\nu^{(2)}(ze^{-\pi i/2}), & -\frac{1}{2}\pi \leq \text{ph } z \leq \pi. \end{cases}$$

so that

$$K_0(-jks) = \pi(j/2)H_0^{(1)}(ks) \quad (\text{J.8})$$

and then

$$\int_{-\infty}^{\infty} dz' \frac{e^{-j\mathbf{k}\mathbf{R}}}{R} = 2 \int_{-\infty}^{\infty} dR \frac{\cos(kR)}{\sqrt{R^2-s^2}} = j\pi H_0^{(1)}(ks). \quad (\text{J.9})$$

Finally

$$\begin{aligned} f(\mathbf{x}) &= \int dx' \int dy' h(x',y') \frac{1}{4\pi} \int_{-\infty}^{\infty} dz' \frac{e^{-j\mathbf{k}\mathbf{R}}}{R} && R = \sqrt{s^2 + z'^2} \\ &= \int dx' \int dy' h(x',y') \frac{1}{4\pi} j\pi H_0^{(1)}(ks) \\ &= \int dx' \int dy' h(x',y') [(j/4) H_0^{(1)}(ks)] && s^2 (x-x')^2 + (y-y')^2 \end{aligned}$$

and once again we have transitioned from the 3D propagator $\frac{e^{-j\mathbf{k}\mathbf{R}}}{R}$ to the 2D one $(j/4) H_0^{(1)}(ks)$.

Case 5

In the $k = 0$ limit the above Case becomes a transition from 3D propagator $\frac{1}{R}$ to 2D propagator $-\frac{1}{2\pi} \ln(s)$ as follows :

$$f(\mathbf{x}) = \int d^3x' [1/4\pi R] h(\mathbf{x}') = (1/4\pi) \int dx' \int dy' h(x',y') \int_{-\infty}^{\infty} \frac{dz'}{\sqrt{s^2 + z'^2}}.$$

But now the dz' integral is logarithmically divergent so we install a very large cutoff Λ and write

$$\begin{aligned} \int_{-\infty}^{\infty} \frac{dz'}{\sqrt{s^2 + z'^2}} &\rightarrow \int_{-\Lambda/2}^{\Lambda/2} \frac{dz'}{\sqrt{s^2 + z'^2}} = 2 \int_0^{\Lambda/2} \frac{dz'}{\sqrt{s^2 + z'^2}} = 2 \ln [z' + \sqrt{z'^2 + s^2}] \Big|_0^{\Lambda/2} \\ &= 2 \ln [\Lambda/2 + \sqrt{(\Lambda/2)^2 + s^2}] - 2 \ln s \end{aligned}$$

$$\approx 2\ln(\Lambda) - 2\ln s = -2\ln(s/\Lambda) . \quad (\text{J.10})$$

Now we apply the argument above about ignoring constants to get,

$$\int_{-\infty}^{\infty} \frac{dz'}{\sqrt{s^2 + z'^2}} = -2\ln s \quad // \text{ ignoring constants}$$

$$f(\mathbf{x}) = \int dx' \int dy' h(x',y') (1/4\pi) (-2\ln s) = \int dx' \int dy' h(x',y') \left[-\frac{1}{2\pi} \ln(s)\right]$$

and so we have transitioned in this case from the 3D Laplace propagator to the 2D propagator.

Appendix K: The Network Model: Comparison of Network and Maxwell Views

(a) The Network Model

The usual network model of a 2-conductor transmission line is an infinite repetition of differentially small R,L,C,G segments as shown here between the vertical red lines,

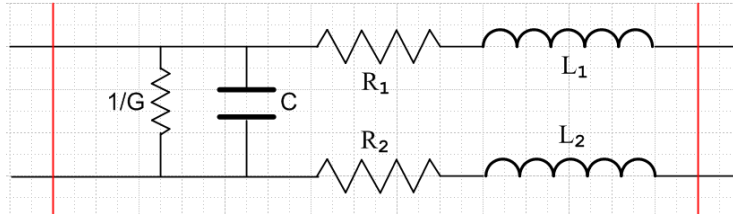


Fig K.1

If some load Z_L is put on the right end of Fig K.1, the impedance seen from the left end is unchanged if the segment circuit is replaced by the following equivalent circuit,

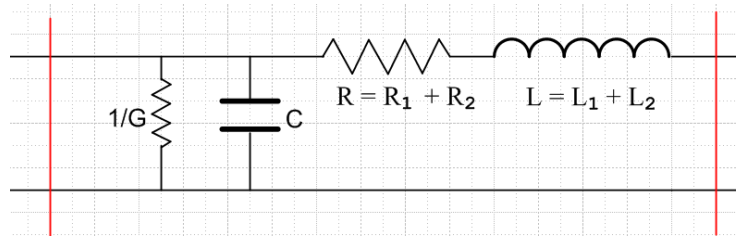


Fig K.2

where $R = R_1 + R_2$ and $L = L_1 + L_2$. In the circuit diagrams, it is implied that R,L,C,G are all quantities *per unit length* of the transmission line. Thus, if the distance between the two red lines is δ , the values of the lumped parameters in Fig K.2 are $R\delta, L\delta, C\delta, G\delta$. For example, if δ doubles, the total conductance of the segment doubles since it is a measure of current flowing between the conductors. The model implied by the picture is then the limit as $\delta \rightarrow 0$.

We wish to compare this "network model" to our Maxwell equation results. To start, we note that the impedance of a capacitor C and inductor L operating at frequency ω are determined by

$$\begin{aligned}
 Q = CV \quad \Rightarrow \quad I = \partial_t Q = C \partial_t V \quad \Rightarrow \quad I = j\omega CV \quad \Rightarrow \quad Z_C = V/I = 1/(j\omega C) \\
 V = L \partial_t I \quad \Rightarrow \quad V = j\omega LI \quad \Rightarrow \quad Z_L = V/I = j\omega L \quad . \quad (K.1)
 \end{aligned}$$

Note that the "admittance" of a capacitor is $Y_C = 1/Z_C = j\omega C$. We can then combine the G and C elements together into a single element having $y = G + j\omega C$, since parallel admittances are additive. Similarly, we combine the two series elements R and L into impedance $z = R + j\omega L$. The network picture is then,

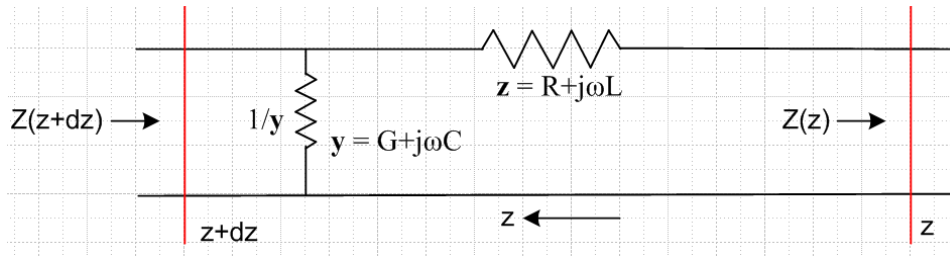


Fig K.3

We use King's bolded symbols \mathbf{y} and \mathbf{z} and of course \mathbf{z} is unrelated to distance z . Here we arbitrarily have the z axis pointing to the *left* (!), and the vertical red lines are placed at z and $z+dz$ so that $\delta = dz$. The impedance looking into the transmission line from the left is $Z(z+dz)$ at $z+dz$ and is $Z(z)$ at z .

(b) Network Model Characteristic Impedance

Since the impedance $1/\mathbf{y}$ is in parallel with the impedance $\mathbf{z} + Z(z)$ one has

$$\begin{aligned} Z(z+dz) &= (\mathbf{y}dz)^{-1} \parallel (\mathbf{z}dz + Z(z)) = \text{product over sum} = \frac{(\mathbf{y}dz)^{-1} (\mathbf{z}dz + Z(z))}{(\mathbf{y}dz)^{-1} + (\mathbf{z}dz + Z(z))} \\ &= \frac{(\mathbf{z}dz + Z(z))}{1 + (\mathbf{y}dz) (\mathbf{z}dz + Z(z))} \approx [Z(z) + \mathbf{z}dz] [1 - (\mathbf{y}dz)(\mathbf{z}dz + Z(z))] \\ &\approx [Z(z) + \mathbf{z}dz] [1 - (\mathbf{y}dz) Z(z)] \quad // \text{dropping order } (dz)^2 \\ &\approx Z(z) + [\mathbf{z} - \mathbf{y}Z^2(z)] dz \quad // \text{dropping order } (dz)^2 \text{ again} \end{aligned}$$

Therefore $Z(z)$ must solve this non-linear first order differential equation,

$$\frac{dZ(z)}{dz} = \mathbf{z} - \mathbf{y}Z^2(z) \quad \text{or} \quad \frac{dZ(z)}{dz} + \mathbf{y}Z^2(z) = \mathbf{z} \quad (\text{K.2})$$

The most general solution to this equation is

$$Z(z) = \sqrt{\frac{\mathbf{z}}{\mathbf{y}}} \operatorname{th}(\sqrt{\mathbf{z}\mathbf{y}} z + C) \quad C = \text{constant} \quad (\text{K.3})$$

since

$$\begin{aligned} \partial_z Z &= \sqrt{\frac{\mathbf{z}}{\mathbf{y}}} * \sqrt{\mathbf{z}\mathbf{y}} \operatorname{sech}^2(\sqrt{\frac{\mathbf{z}}{\mathbf{y}}} z + C) = \mathbf{z} [1 - \operatorname{th}^2(\sqrt{\frac{\mathbf{z}}{\mathbf{y}}} z + C)] \\ &= \mathbf{z} [1 - \frac{\mathbf{y}}{\mathbf{z}} Z^2(z)] = \mathbf{z} - \mathbf{y} Z^2(z) \end{aligned}$$

If the transmission line is of finite length running from $z = L$ (left end) to $z = 0$ (right end), and if the line is *terminated* at $z = 0$ by some impedance Z_t , we must have $Z(0) = Z_t$ so that

$$Z_t = Z(0) = \sqrt{\frac{z}{y}} \operatorname{th}(\sqrt{zy} \cdot 0 + C) = \sqrt{\frac{z}{y}} \operatorname{th}(C)$$

$$\Rightarrow C = \operatorname{th}^{-1}\left(\sqrt{\frac{y}{z}} Z_t\right)$$

so then the solution is

$$Z(z) = \sqrt{\frac{z}{y}} \operatorname{th}\left[\sqrt{zy} z + \operatorname{th}^{-1}\left(\sqrt{\frac{y}{z}} Z_t\right)\right]$$

and at the left end we find

$$Z(L) = \sqrt{\frac{z}{y}} \operatorname{th}\left[\sqrt{zy} L + \operatorname{th}^{-1}\left(\sqrt{\frac{y}{z}} Z_t\right)\right].$$

If we take $L \rightarrow \infty$ (line becomes infinitely long), then $\operatorname{th}[\dots] \rightarrow 1$ and we find

$$Z(\infty) = \sqrt{\frac{z}{y}},$$

so the impedance looking into the left end of the *infinite* transmission line is independent of the termination value Z_t at $z = 0$. This infinite line impedance is called the **characteristic impedance** Z_0 and we have shown then that

$$Z_0 = \sqrt{\frac{z}{y}} = \sqrt{\frac{R+j\omega L}{G+j\omega C}}. \tag{K.4}$$

Since this is the same result obtained from Maxwell's equations in (4.12.18), one is motivated to regard the network transmission line model as a *correct* model, and then the network model parameters R,L,G,C can be identified with the parameters obtained from Maxwell's equations.

Reader Exercise: Consider this purely resistive finite ladder network shorted at the right end,

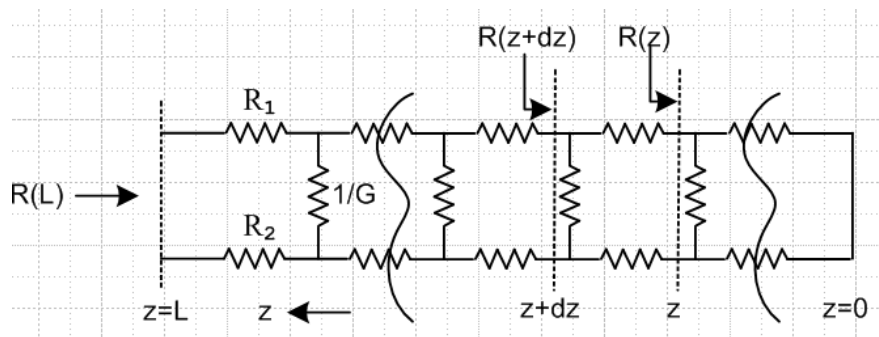


Fig K.4

(1) Using the results above, show that

$$R(L) = \sqrt{R_3/G} \tanh(\sqrt{R_3G} L) \quad \text{where } R_3 \equiv R_1 + R_2 .$$

(2) Show that

$$R(L) \approx \sqrt{R_3/G} \quad \text{if } L \gg 1/\sqrt{R_3G} .$$

Thus, for large L the fact that the line is shorted at the right end makes no difference.

(3) Show that for finite L :

$$\begin{array}{lll} R(L) \rightarrow R_3 L & \text{as } G \rightarrow 0 & \text{no conductance} \\ R(L) \rightarrow 0 & \text{as } R_3 \rightarrow 0 & \text{no wire resistance} \end{array}$$

Both limits should seem obvious.

(c) Network Model Transmission Line Equations

We now switch the z axis back to its usual direction (increasing to the right), and we label currents and voltages on our transmission line section,

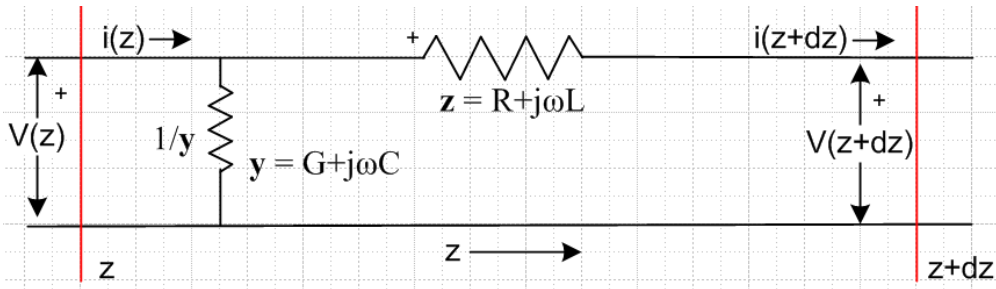


Fig K.5

Staring at the picture, it seems clear that

$$i(z) - i(z+dz) = \text{current going down through impedance } 1/(ydz) = \frac{V(z)}{1/(ydz)} = ydz V(z)$$

and therefore

$$-\frac{di(z)}{dz} = y V(z) .$$

Meanwhile, the voltage across the impedance z is V(z) - V(z+dz) so

$$V(z) - V(z+dz) = i(z) z$$

and therefore

$$-\frac{dV(z)}{dz} = \mathbf{z} i(z) .$$

Thus we have shown that

$$\begin{aligned} \frac{dV(z)}{dz} &= -\mathbf{z} i(z) & \frac{di(z)}{dz} &= -\mathbf{y} V(z) \\ \text{with} & & & \\ \mathbf{z} &= R + j\omega L & \mathbf{y} &= G + j\omega C . \end{aligned} \quad (\text{K.5})$$

Differentiating these equations with respect to z , we find that

$$\frac{d^2V(z)}{dz^2} - \mathbf{zy} V(z) = 0 \qquad \frac{d^2i(z)}{dz^2} - \mathbf{zy} i(z) = 0 \quad (\text{K.6})$$

But (K.5) and (K.6) are the same transmission line equations obtained from Maxwell's equations as shown in (4.11.15) and (4.11.17). Thus we are further encouraged in our use of the network model to represent a transmission line. Since the equations found from Maxwell's equations were qualified as being questionable at very low frequencies, the network model is also suspect at very low ω .

The solutions of equations (K.6) naturally have the same form as shown in Chapter 4, for example,

$$V(z) = V(0) e^{-j\mathbf{k}z} \qquad \mathbf{k}^2 = -\mathbf{zy} \qquad \mathbf{k} = -j\sqrt{\mathbf{zy}} = -j\sqrt{(R+j\omega L)(G+j\omega C)} \quad (\text{K.7})$$

(d) Network Model Parameters obtained from Maxwell's Equations

The main results of Chapter 4 appear in summary box (4.12.24) from which we quote in part,

$$\begin{aligned} \frac{dV(z)}{dz} &= -\mathbf{z} i(z) & \left(\frac{d^2}{dz^2} - \mathbf{zy}\right) V(z) &= 0 & \mathbf{z} &= R + j\omega L & \text{transmission line equations} \\ \frac{di(z)}{dz} &= -\mathbf{y} V(z) & \left(\frac{d^2}{dz^2} - \mathbf{zy}\right) i(z) &= 0 & \mathbf{y} &= G + j\omega C & (4.12.15,16 \text{ and } 17) \end{aligned}$$

$$\begin{aligned} \mathbf{z} &= \mathbf{Z}_{s1} + \mathbf{Z}_{s2} + j\omega L_e & (4.12.16) & & X_L &\equiv \omega L_e , & X_C &\equiv 1/(\omega C) \\ \mathbf{y} &= j\omega C' = j\omega C + (\sigma_d/\epsilon_d)C & (4.12.16) & & G &= (\sigma_d/\epsilon_d)C & (4.11.15) \end{aligned}$$

$$\begin{aligned} R &= \text{Re}(\mathbf{Z}_{s1} + \mathbf{Z}_{s2}) \\ L &= L_e + (1/\omega) \text{Im}(\mathbf{Z}_{s1} + \mathbf{Z}_{s2}) \end{aligned}$$

$$\begin{aligned} L_e &= (\mu_d/4\pi)K & (4.10.8) \text{ and } (4.12.20) \\ C &= 4\pi\epsilon_d/K & (4.4.7) \text{ and } (4.11.9a) \text{ and} \\ G &= 4\pi\sigma_d/K & \text{above and } (4.4.10) \end{aligned} \quad (\text{K.8})$$

Thus, we make the connection between the network parameters and the Maxwell calculation parameters as follows:

$$\begin{aligned}
 R &= \text{Re}(Z_{s1} + Z_{s2}) \\
 L &= L_e + (1/\omega) \text{Im}(Z_{s1} + Z_{s2}) \\
 L_e &= (\mu_d/4\pi)K \\
 G &= 4\pi\sigma_d/K \\
 C &= 4\pi\epsilon_d/K
 \end{aligned} \tag{K.9}$$

where K is the dimensionless real integral in Chapter 4, see (4.4.8). Recall that this integral requires knowledge of both the conductor geometry as well as the normalized transverse surface charge distributions on the conductors. Here ϵ_d , μ_d and σ_d are for the dielectric between the conductors. The effective σ_d appearing in G is often frequency dependent as shown in (3.3.4) [see Appendix R for an example]. The Z_{s_i} are always frequency dependent, as discussed below.

(e) Low frequency case for round conductors (no skin effect)

At low frequencies, when conductors are not extremely close together, the current densities are close to uniform (see for example Fig 6.16), so that $J_z = I/\text{area}$ for each conductor. This uniformity is exact for a conductor which is the central conductor of a coaxial cable, as studied in Chapter 2. There we found at low frequency that

$$Z_{s1}(\omega) = \frac{1}{\sigma_1\pi a^2} + j\omega \frac{\mu_1}{8\pi} \quad // \text{ low frequency limit} \tag{2.4.12}$$

$$\Rightarrow \quad \text{Re}(Z_{s1}) = \frac{1}{\sigma_1\pi a^2} \quad \text{and} \quad \text{Im}(Z_{s1}) = \omega \frac{\mu_1}{8\pi} . \tag{K.10}$$

From (K.9) we then find that for low frequencies and parallel round conductors,

$$R = \frac{1}{\sigma_1\pi a_1^2} + \frac{1}{\sigma_2\pi a_2^2} = R_{dc1} + R_{dc2} \tag{K.11}$$

$$L = L_e + \left(\frac{\mu_1}{8\pi} + \frac{\mu_2}{8\pi} \right) = L_e + (L_{i1} + L_{i2}) . \tag{K.12}$$

In this case parameter R is just the sum of the DC resistances of the conductors (per unit length), and parameter L is the sum of the external inductance L_e and the internal inductances of the two wires. Here σ_i and μ_i are for the material from which conductor C_i is constructed. The external inductance L_e can be interpreted as the inductance associated with the red wire loop below,

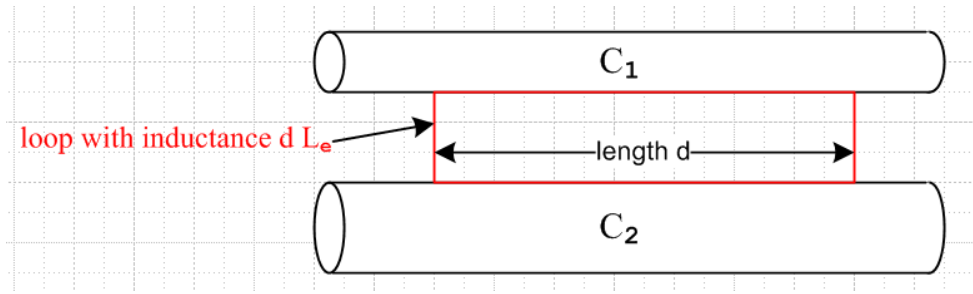


Fig K.6

The sides of the red loop make contact on any line on the conductor surfaces, though here we show it having its minimal size. The red loop may in fact be replaced by any loop, possibly non-planar, which captures all the external magnetic flux passing between the conductors. See Fig 4.11 and discussion there.

Note that L_e is *not* the self-inductance of a rectangular thin wire loop *in isolation* occupying the red outline above, but rather $L_e = (\mu_d/4\pi)K$ as in (K.9) above, where K is related to the capacitance between the conductors. If both conductors are round and very thin and separated by distance b , we know from (4.5.7) that $K = 4 \ln(b/\sqrt{a_1 a_2})$ and then $L_e = (\mu_d/\pi) \ln(b/\sqrt{a_1 a_2})$.

Although we have not formally proven it, it seems clear that for arbitrary conductor cross sections (not too closely spaced) the following equations will apply at low frequency :

$$R = \frac{1}{\sigma_1 A_1} + \frac{1}{\sigma_2 A_2} \quad A_i = \text{cross section area of } C_i \quad (\text{K.13})$$

$$L = L_e + (L_{i1} + L_{i2}) . \quad (\text{K.14})$$

Appendix C computes the DC L_i for various conductor cross section shapes. One result quoted there from the literature is that for a square conductor,

$$L_i = (\mu_i/8\pi) [0.96639] . \quad (\text{C.4.12})$$

Thus the L_i for a square cross-section conductor is barely different from that of a round conductor.

(f) High frequency case for round conductors (strong skin effect)

At high frequencies there is a pronounced skin effect. In Chapter 2 for a round conductor C_1 at high frequency (and with a symmetric current distribution) we found that

$$Z_{s1}(\omega) \approx \frac{1}{\sigma_1(2\pi a_1)\delta_1} (1+j) \quad \delta_1 \ll 4a_1 \quad (\text{2.4.16})$$

so

$$\text{Re}(Z_{s1}) = \text{Im}(Z_{s1}) = \frac{1}{\sigma_1(2\pi a_1)\delta_1} = \frac{1}{2\pi a_1} \sqrt{\frac{\mu_1 \omega}{2\sigma_1}}$$

where $\delta_1 = \sqrt{2/(\omega\mu_1\sigma_1)}$ is the skin depth and a_1 the wire radius.

From (K.9) we find that for high frequencies and round conductors,

$$R = \frac{1}{\sigma_1(2\pi a_1)\delta_1} + \frac{1}{\sigma_2(2\pi a_2)\delta_2}$$

$$L = L_e + (1/\omega) \operatorname{Im}(Z_{s1} + Z_{s2}) = L_e + (1/\omega) R \quad . \quad (\text{K.15})$$

In this case, we recognize $2\pi a_1\delta_1$ as the effective current carrying cross-sectional area of round conductor C_1 (the area of the current sheath), so the expression for R is quite intuitive. Since,

$$\delta \equiv \sqrt{2/\omega\mu\sigma} \quad \Rightarrow \quad 1/\delta_1 = \sqrt{(\omega\mu_1\sigma_1)/2} \quad \text{and} \quad 1/\omega = \mu_1\sigma_1\delta_1^2/2 \quad (\text{K.16})$$

we may write

$$L_i(\omega) = (1/\omega) \operatorname{Im}(Z_s) = (1/\omega) \frac{1}{\sigma_1(2\pi a_1)\delta_1} = (1/\omega) \frac{1}{\sigma_1(2\pi a_1)} \sqrt{(\omega\mu_1\sigma_1)/2} = \frac{1}{2\pi a_1} \sqrt{\frac{\mu_1}{2\sigma_1\omega}} \quad (\text{K.17})$$

so $L_i(\omega) \sim 1/\sqrt{\omega}$. Expressing L_i instead in terms of δ_1 we find

$$L_i(\delta_1) = (1/\omega) \operatorname{Im}(Z_s) = (1/\omega) \frac{1}{\sigma_1(2\pi a_1)\delta_1} = \mu_1\sigma_1(\delta_1^2/2) \frac{1}{\sigma_1(2\pi a_1)\delta_1} = \mu_1 (1/4\pi) (\delta_1/a_1)$$

$$= \frac{\mu_i}{8\pi} [2 (\delta_1/a_1)] \quad . \quad (\text{K.18})$$

The DC internal inductance of a thin shell of radius a and thickness d is shown in Appendix C.6 to be

$$L_i = \mu_i \frac{1}{6\pi} (d/a) = \frac{\mu_i}{8\pi} [(4/3)(d/a)] \quad \text{thin shell, valid for } d \ll a \quad (\text{C.6.8})$$

so the high frequency internal inductance of a round wire is the same as the DC internal inductance a shell of thickness $d = (3/2)\delta$ which seems fairly reasonable. The above expression (C.6.8) shows that the inductance of a thin cylindrical shell is linear in the shell thickness d , so we expect that the high frequency L_i of a round wire should be linear in δ , and thus proportional to $1/\sqrt{\omega}$.

Section 2.5 shows how to handle non-round conductors and non-symmetric current distributions by replacing $2\pi a$ by an effective active perimeter p . Chapter 4.12 (b) formalizes this notion, giving the effective perimeter in (4.12.10).

In Section D.10 and D.11 the claims made in the last two sections regarding surface impedance are vindicated when one uses the surface impedance averaged over the round wire surface: see (D.10.17) for large ω and (D.11.17) for small ω .

Appendix L: Point and Line Charges in Dielectrics

Chapter 1 states in (1.1.19) through (1.1.24) various equations concerning the magnetization of a magnetic medium. These equations are "exercised" somewhat in Section G.3 and also in Appendix B concerning how the transmission line theory is altered when the dielectric and conductors have different μ values.

Chapter 1 also states in (1.1.9) through (1.1.15) corresponding equations concerning the polarization of a dielectric medium. Although the transmission line theory assumes a dielectric between the conductors, and in fact allows for a complex dielectric constant ξ , there has been no "exercise" of the polarization equations, so in this Appendix some simple examples are provided.

The examples presented here are rarely presented in E&M texts perhaps because they are too simple. The spherical problem appears in the 2nd edition of Corson and Lorrain (p 111-113) but it got replaced by a short comment in the 3rd edition (Corson and two Lorrains) p 186.

The examples are useful to the author in that they provide a physical picture of how the potential and field of a point or line charge are affected by the presence of a dielectric medium. In Sections L.1 and L.2 the 3D problem is solved and limits are taken of the solution. Two of these limits involve a full embedding of the charge in the dielectric where dielectric charge shielding is exhibited. Sections L.3 and L.4 briefly repeat the solution in two dimensions, so the results then apply to the extruded cross section.

L.1 The potential of a point charge inside a thick dielectric spherical shell.

A positive point charge q lies at the center of a spherical shell of radii $b > a$ as follows,

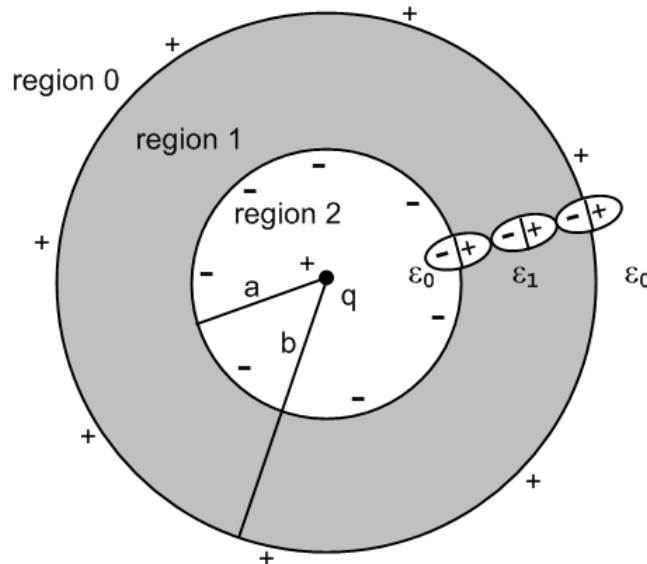


Fig L.1

Inside and outside the shell of dielectric constant ϵ_1 is empty space with ϵ_0 .

Whatever the potential ϕ is for the above picture, it is obviously spherically symmetric and is then $\phi(r)$. This in turn means that the E field is just $\mathbf{E} = E_r \hat{\mathbf{r}}$ where $E_r = -\partial_r \phi$ (in each region), so the E field is

radial. This radial E field polarizes the dielectric in the shell as suggested by the three symbolic polarized molecules shown in the figure. If the total bound charge on the $r = a$ surface is $-Q$, then the total charge on the $r = b$ surface must be $+Q$, as one would conclude imagining the entire dielectric having the form of the three molecules shown.

One implication of this fact is that for a sphere of $r > b$, the total charge enclosed is just q . Applying Gauss's law to a spherical Gaussian box of radius $r > b$

$$q = \int_V \rho \, dV = \int_S \epsilon \mathbf{E} \cdot d\mathbf{S} = \epsilon_0 \left[\int d\Omega \right] r^2 \mathbf{E} \cdot d\mathbf{\hat{r}} = \epsilon_0 4\pi r^2 E_r \quad (1.1.33)$$

$$\Rightarrow \quad E_{r0} = (1/4\pi\epsilon_0) q/r^2 .$$

The corresponding potential is

$$\varphi_0(r) = (1/4\pi\epsilon_0) q/r \quad r > b \quad \text{region 0}$$

since then $E_{r0} = -\partial_r \varphi_0(r) = (1/4\pi\epsilon_0) q/r^2$. This is a special case of the fact that any spherical distribution of charge appears outside that distribution as a point charge at the center, so $\varphi_0(r)$ is just the potential of a point charge q at the origin. We then at least know φ in one of the three regions.

In regions 1 and 2 as an ansatz we assume these forms with constants α , C and D to be determined,

$$\begin{aligned} \varphi_1(r) &= (1/4\pi\alpha) q/r + C \\ \varphi_2(r) &= (1/4\pi\epsilon_0) q/r + D . \end{aligned}$$

In a spherically symmetric geometry the Laplace equation only allows harmonics that are powers r^n and each term above is one such power times a constant. A motivation for the φ_2 form is that for r very close to $r = 0$, the potential must be that of the point charge since everything else is then relatively far away.

We now determine constants α , C and D from boundary conditions. The three potentials and fields are

$$\begin{aligned} \varphi_0(r) &= (1/4\pi\epsilon_0) q/r & E_{r0}(r) &= (1/4\pi\epsilon_0) q/r^2 & \text{region 0} \\ \varphi_1(r) &= (1/4\pi\alpha) q/r + C & E_{r1}(r) &= (1/4\pi\alpha) q/r^2 & \text{region 1} \\ \varphi_2(r) &= (1/4\pi\epsilon_0) q/r + D & E_{r2}(r) &= (1/4\pi\epsilon_0) q/r^2 & \text{region 2} . \end{aligned} \quad (L.1.1)$$

The electrostatic potential must be continuous at all values of r . Why? Consider:

$$E_r = -\partial_r \varphi \quad \int_a^b E_r dr = - \int_a^b \partial_r \varphi \, dr = - [\varphi(b) - \varphi(a)] .$$

The physical electric field at any point must have a well-defined finite single value. Then for small ϵ

$$\int_a^{a+\epsilon} E_r dr = E_r(a) \epsilon = - [\varphi(a+\epsilon) - \varphi(a)] \quad \Rightarrow \quad \varphi \text{ continuous at } a . \quad (L.1.2)$$

As $\epsilon \rightarrow 0$, we must have $\varphi(a+\epsilon) \rightarrow \varphi(a)$ so $\varphi(r)$ must be continuous at $r = a$.

Apply this rule at our two boundaries to find that,

$$\begin{aligned} (1/4\pi\epsilon_0) q/b &= (1/4\pi\alpha) q/b + C && \text{region 0/1 boundary, } r = b \\ (1/4\pi\epsilon_0) q/a + D &= (1/4\pi\alpha) q/a + C && \text{region 2/1 boundary, } r = a \end{aligned} \quad (\text{L.1.3})$$

which is two conditions on the unknown constants α, C, D .

Meanwhile, the normal electric field boundary condition from Chapter 1 is

$$[\epsilon_1 E_{n1} - \epsilon_2 E_{n2}] = \eta_{\text{free}} \quad . \quad (1.1.47)$$

Although there exists bound charge at each of our two boundaries, there is no free charge, so

$$\begin{aligned} \epsilon_0 E_{r0}(b) &= \epsilon_1 E_{r1}(b) && \text{region 0/1 boundary, } r = b \\ \epsilon_0 E_{r2}(a) &= \epsilon_1 E_{r1}(a) && \text{region 2/1 boundary, } r = a \end{aligned}$$

or

$$\begin{aligned} \epsilon_0 q / [4\pi\epsilon_0 b^2] &= \epsilon_1 (1/4\pi\alpha) q/b^2 && \Rightarrow 1 = \epsilon_1/\alpha \\ \epsilon_0 q / [4\pi\epsilon_0 a^2] &= \epsilon_1 (1/4\pi\alpha) q/a^2 && \Rightarrow 1 = \epsilon_1/\alpha \end{aligned} \quad (\text{L.1.4})$$

The right side equations are the same and tell us that $\alpha = \epsilon_0$. The boundary conditions (L.1.3) then say,

$$\begin{aligned} (1/4\pi\epsilon_0) q/b &= (1/4\pi\epsilon_1) q/b + C && \text{region 0/1 boundary, } r = b \\ (1/4\pi\epsilon_0) q/a + D &= (1/4\pi\epsilon_1) q/a + C && \text{region 2/1 boundary, } r = a \end{aligned} \quad (\text{L.1.5})$$

Subtract the first from the second to cancel the C,

$$D + (1/4\pi\epsilon_0) q(1/a-1/b) = (1/4\pi\epsilon_1) q(1/a-1/b)$$

so

$$D = (1/a-1/b)(q/4\pi)(1/\epsilon_1-1/\epsilon_0) = - (b/a-1)(q/4\pi b)(1/\epsilon_0-1/\epsilon_1) .$$

From the first of (L.1.5) we find

$$C = (q/4\pi b) (1/\epsilon_0-1/\epsilon_1) .$$

Thus the boundary conditions have determined our three constants

$$\begin{aligned} \alpha &= \epsilon_0 \\ C &= (q/4\pi b) (1/\epsilon_0-1/\epsilon_1) \\ D &= (q/4\pi b)(1/\epsilon_0-1/\epsilon_1) (1-b/a) \end{aligned} \quad (\text{L.1.6})$$

The potentials in the three regions are then

$$\begin{aligned}\varphi_0(r) &= (1/4\pi\epsilon_0) q/r \\ \varphi_1(r) &= (1/4\pi\epsilon_1) q/r + (q/4\pi b)(1/\epsilon_0 - 1/\epsilon_1) \\ \varphi_2(r) &= (1/4\pi\epsilon_0) q/r + (q/4\pi b)(1/\epsilon_0 - 1/\epsilon_1) (1-b/a)\end{aligned}\quad (\text{L.1.7})$$

while the fields are

$$\begin{aligned}E_{r0} &= (1/4\pi\epsilon_0) q/r^2 \\ E_{r1} &= (1/4\pi\epsilon_1) q/r^2 \\ E_{r2} &= (1/4\pi\epsilon_0) q/r^2\end{aligned}\quad (\text{L.1.8})$$

We know that a spherical shell of charge has no effect on E_r inside the shell, verifying the E_{r2} result. We also know that a spherical shell acts as a point charge at the origin when viewed from outside the shell, thus verifying E_{r0} which then sees a charge of $q + Q - Q = q$ at the origin.

The following Maple plots show the continuity of φ and the jumps in E_r at the boundaries

```
phi := piecewise(r >= 0 and r < a, phi2, r >= a and r < b, phi1, r >= b, phi0):
Er := piecewise(r >= 0 and r < a, Er2, r >= a and r < b, Er1, r >= b, Er0):
phi0 := q/(4*Pi*e0*r):
phi1 := q/(4*Pi*e1*r) + q/(4*Pi*b)*(1/e0-1/e1):
phi2 := q/(4*Pi*e0*r) + q/(4*Pi*b)*(1/e0-1/e1)*(1-b/a):
Er0 := q/(4*Pi*e0*r^2):
Er1 := q/(4*Pi*e1*r^2):
Er2 := q/(4*Pi*e0*r^2):
q := 1: a := 1: b := 2: e0 := 1: e1 := 2:
plot([phi, Er], r=0.5..5, color = [red, blue]);
```

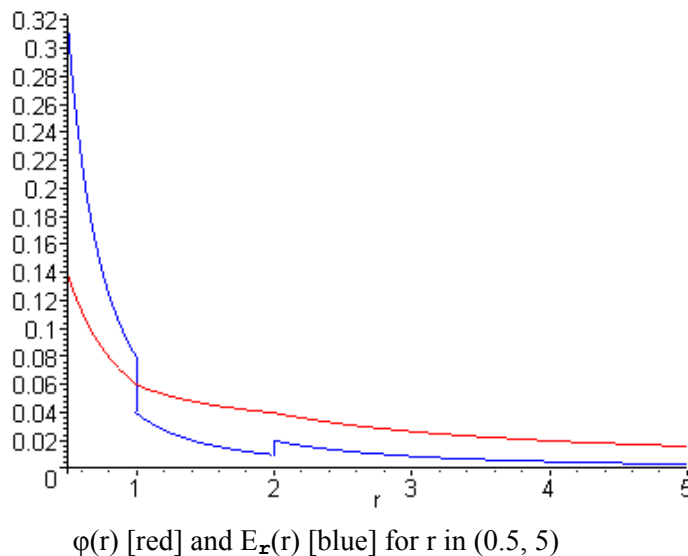


Fig L.2

What about the bound charge densities at $r = a$ and $r = b$?

One must first compute polarization \mathbf{P} , and for a region with ϵ , \mathbf{P} is given by

$$\mathbf{P} = \epsilon_0 \chi_e \mathbf{E} \quad // \text{ polarization assumed proportional to the polarizing } \mathbf{E} \text{ field} \quad (1.1.12)$$

so

$$\mathbf{P} = \epsilon_0 \chi_e E_{\mathbf{r}} \hat{\mathbf{r}} \quad \chi_e = (\epsilon/\epsilon_0 - 1) \quad \Rightarrow \quad \mathbf{P} = \epsilon_0 (\epsilon/\epsilon_0 - 1) E_{\mathbf{r}} \hat{\mathbf{r}} = (\epsilon - \epsilon_0) E_{\mathbf{r}} \hat{\mathbf{r}} .$$

Obviously $\mathbf{P} = 0$ in regions 0 and 2, while in region 1 we have

$$\mathbf{P}_{\mathbf{r}1}(r) = (\epsilon_1 - \epsilon_0) E_{\mathbf{r}1}(r) \theta(r>a) \theta(r<b) \quad . \quad // \text{ points radially outward since } \epsilon_1 > \epsilon_0 \quad (L.1.9)$$

From (1.1.11) the polarization charge density is then

$$\rho_{\mathbf{p}o1} = - \operatorname{div} \mathbf{P} \quad (1.1.11)$$

so in spherical coordinates,

$$\begin{aligned} \rho_{\mathbf{p}o1}(r) &= - [r^{-2} \partial_{\mathbf{r}}(r^2 P_{\mathbf{r}}) + [r \sin \theta]^{-1} \partial_{\theta}[\sin \theta P_{\theta}] + [r \sin \theta]^{-1} \partial_{\phi} P_{\phi}] \\ &= - r^{-2} \partial_{\mathbf{r}}(r^2 P_{\mathbf{r}1}) \\ &= - r^{-2} \partial_{\mathbf{r}}(r^2 [(\epsilon_1 - \epsilon_0) E_{\mathbf{r}1}(r) \theta(r>a) \theta(r<b)]) \quad // \text{ from (L.1.9)} \\ &= - r^{-2} \partial_{\mathbf{r}}([(\epsilon_1 - \epsilon_0)(1/4\pi\epsilon_1) q \theta(r>a) \theta(r<b)]) \quad // \text{ from (L.1.8)} \\ &= - q(\epsilon_1 - \epsilon_0)(1/4\pi\epsilon_1) r^{-2} \partial_{\mathbf{r}}([\theta(r>a) \theta(r<b)]) \end{aligned}$$

But

$$\begin{aligned} \partial_{\mathbf{r}}[\theta(r>a) \theta(r<b)] &= \partial_{\mathbf{r}}[\theta(r-a) \theta(b-r)] = \delta(r-a) \theta(b-r) + \theta(r-a) [-\delta(r-b)] \\ &= \delta(r-a) \theta(b-a) - \theta(b-a) \delta(r-b) = [\delta(r-a) - \delta(r-b)] , \end{aligned}$$

so

$$\begin{aligned} \rho_{\mathbf{p}o1}(r) &= - q(\epsilon_1 - \epsilon_0)(1/4\pi\epsilon_1) r^{-2} [\delta(r-a) - \delta(r-b)] \\ &= - q(\epsilon_1 - \epsilon_0) (1/4\pi\epsilon_1) \{ \delta(r-a)/a^2 - \delta(r-b)/b^2 \} \quad . \quad (L.1.10) \end{aligned}$$

We may then read off the bound *surface* charge densities at $r = a$ and b ,

$$\begin{aligned} \sigma_{\text{inner}} &= - (\epsilon_1 - \epsilon_0) (1/4\pi\epsilon_1)(q/a^2) \\ \sigma_{\text{outer}} &= (\epsilon_1 - \epsilon_0) (1/4\pi\epsilon_1)(q/b^2) \end{aligned} \quad (L.1.11)$$

so

$$\begin{aligned} Q_{\text{inner}} &= \int dS \sigma_{\text{inner}} = - (\epsilon_1 - \epsilon_0) (1/4\pi\epsilon_1)(q/a^2) * 4\pi a^2 = - (1 - \epsilon_0/\epsilon_1) q \\ Q_{\text{outer}} &= \int dS \sigma_{\text{outer}} = (\epsilon_1 - \epsilon_0) (1/4\pi\epsilon_1)(q/b^2) * 4\pi b^2 = (1 - \epsilon_0/\epsilon_1) q \quad . \quad (L.1.12) \end{aligned}$$

Thus the outer boundary has total charge

$$Q = (1 - \epsilon_0/\epsilon_1) q \quad // \text{ ranges from } 0 \text{ to } q \quad (\text{L.1.13})$$

and the inner boundary has $-Q$. If the dielectric were a conductor, we would replace $\epsilon_1 \rightarrow \xi_1$ as in (1.5.1c) and then a perfect conductor has $\xi_1 = \infty$ and so $Q = q$, as one would expect looking at Fig L.1.

L.2 Limits of the Previous Problem

(a) Point charge in a spherical cavity in a dielectric

Taking $b \rightarrow \infty$ in the previous problem removes outer region 0 and leaves us with this picture of a point charge at the center of a spherical hole in an infinite medium of ϵ_1 :

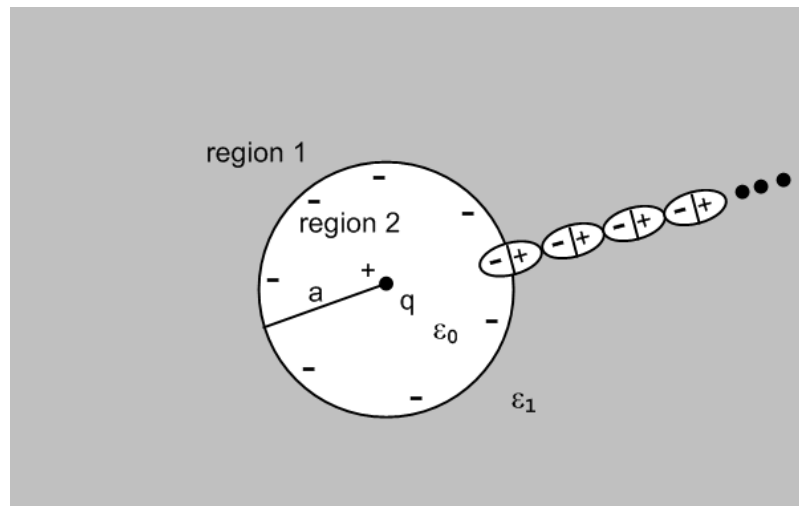


Fig L.3

The potentials and fields shown in (L.1.7) and (L.1.8) are then, taking $b \rightarrow \infty$,

$$\begin{aligned} \phi_1(r) &= (1/4\pi\epsilon_1) q/r \\ \phi_2(r) &= (1/4\pi\epsilon_0) q/r - (q/4\pi a)(1/\epsilon_0 - 1/\epsilon_1) \end{aligned} \quad (\text{L.2.1})$$

while the fields are

$$\begin{aligned} E_{r1} &= (1/4\pi\epsilon_1) q/r^2 \\ E_{r2} &= (1/4\pi\epsilon_0) q/r^2 \end{aligned} \quad (\text{L.2.2})$$

The induced bound charge density σ at $r = a$, and the total charge there, are still given by

$$\begin{aligned} \sigma &= -(\epsilon_1 - \epsilon_0) (1/4\pi\epsilon_1)(q/a^2) \\ -Q &= (1 - \epsilon_0/\epsilon_1) q \end{aligned} \quad (\text{L.2.3})$$

(b) Point charge embedded in a dielectric sphere

Here we take the limit $a \rightarrow 0$ so that region 2 of Fig L.1 goes away. Looking at (L.1.12), the total inner surface bound charge continues to be $-(1-\epsilon_0/\epsilon_1) q = -Q$ in this limit. It just crowds around the point charge and of course the surface density $\sigma_{\text{inner}} \rightarrow \infty$. Here is a suggestive drawing of a piece of region 1 in this limit:

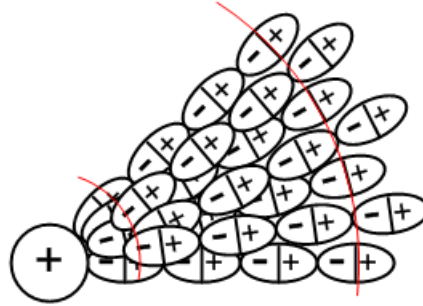


Fig L.4

The limiting picture of Fig L.1 is then the following,

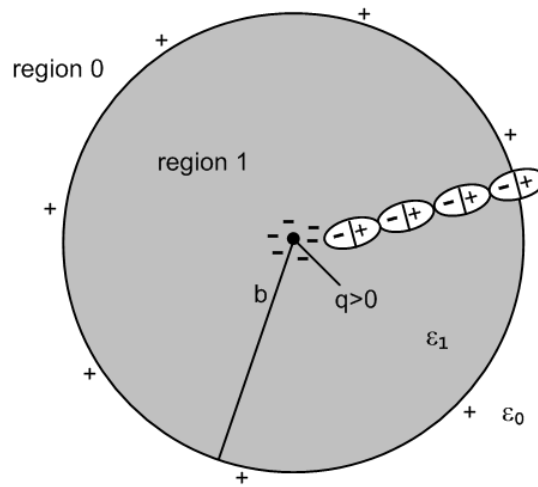


Fig L.5

The potentials and fields shown in (L.1.7) and (L.1.8) are then, taking $a \rightarrow 0$,

$$\begin{aligned} \varphi_0(r) &= (1/4\pi\epsilon_0) q/r \\ \varphi_1(r) &= (1/4\pi\epsilon_1) q/r + (q/4\pi b)(1/\epsilon_0 - 1/\epsilon_1) \end{aligned} \quad (\text{L.2.4})$$

while the fields are

$$\begin{aligned} E_{r0} &= (1/4\pi\epsilon_0) q/r^2 \\ E_{r1} &= (1/4\pi\epsilon_1) q/r^2 . \end{aligned} \quad (\text{L.2.5})$$

Inside the dielectric the E field is $E_{r1} = (1/4\pi\epsilon_1) q/r^2$ where ϵ_1 takes into account both the point charge q and the bound charge crowding around it which is $-(1-\epsilon_0/\epsilon_1) q$. One could interpret this as saying that the total charge at the origin is $q - (1-\epsilon_0/\epsilon_1) q = q(\epsilon_0/\epsilon_1)$ and then $E = (1/4\pi\epsilon_0) [q(\epsilon_0/\epsilon_1)]/r^2$. Remember from (1.1.15) that E sees both free and bound charge. In this last interpretation, the dielectric is shielding the point charge, reducing it from q to $q(\epsilon_0/\epsilon_1)$.

Outside the sphere, the E field is $E_{r1} = (1/4\pi\epsilon_0) q/r^2$, just as if the sphere were not there. The reason of course is that the surface charge at $r = b$ still cancels the crowded surface charge at $r = 0$, so outside one sees in effect just the point charge q .

(c) Point charge embedded in an infinite dielectric medium

We now take $b \rightarrow \infty$ in Fig L.5 to remove outer region 0, with this result:

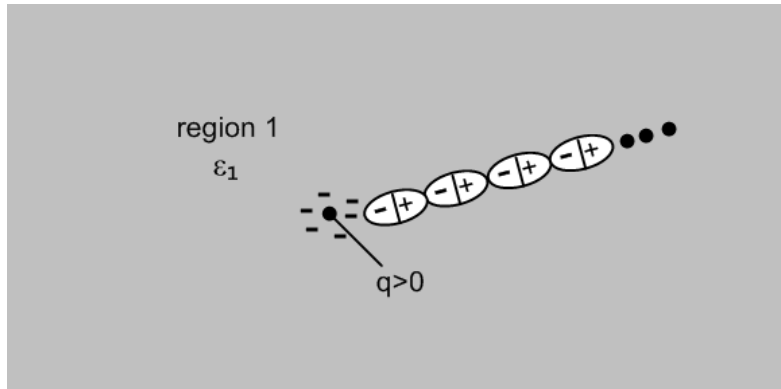


Fig L.6

There is only one region left and from (L.2.4) and (L.2.5) we get

$$\phi_1(r) = (1/4\pi\epsilon_1) q/r \quad (\text{L.2.6})$$

while the field is

$$E_{r1} = (1/4\pi\epsilon_1) q/r^2. \quad (\text{L.2.7})$$

The presence of the dielectric ϵ_1 is then completely accounted for by the $(1/4\pi\epsilon_1)$ factor. As before, one could interpret this as a shielded charge $[q(\epsilon_0/\epsilon_1)]$ and $E = (1/4\pi\epsilon_0) [q(\epsilon_0/\epsilon_1)]/r^2$. The crowded-around polarization charge is still $-Q = -(1-\epsilon_0/\epsilon_1) q$, and the positive Q that was on the $r = b$ surface is still present, but at $r = \infty$.

L.3 The potential of a line charge inside a thick dielectric cylindrical shell

In this section, we repeat everything done in Section L.1 in the 2D world instead of the 3D world. The 3D Laplace propagator $(1/4\pi\epsilon_0)(1/r)$ becomes $(1/2\pi\epsilon_0) \ln(1/r)$ as discussed in Appendix J. We reuse the same drawings, the first of which is

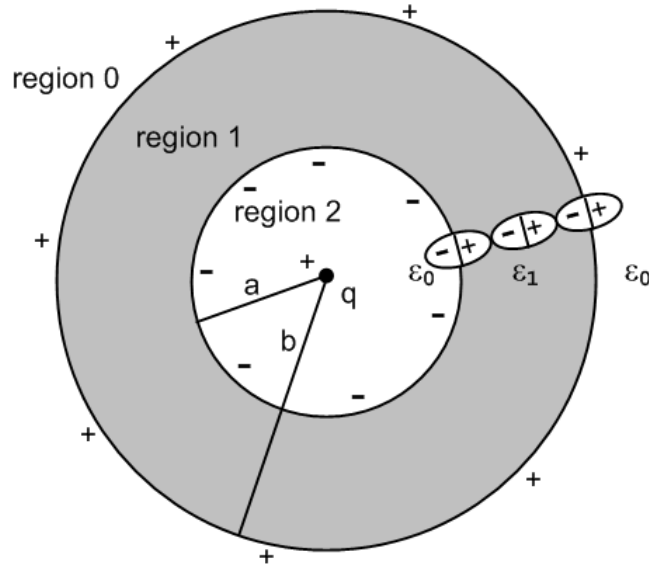


Fig L.1'

This is now a cross section of an infinite uniform cylindrical hollow dielectric pipe. Quantity q is now a linear charge density with dimensions Coulombs/m. Rather than copy, paste and edit Section L.1, here we just show the altered equations and skip most of the words. The equation numbers are those of Section L.1 with a prime added. One difference encountered is that we must take $b \rightarrow R$ (a large value) rather than $b \rightarrow \infty$. As noted in Appendix J, a constant in a potential can be ignored even if it is infinite, and such constants do not appear in the field $\mathbf{E} = -\nabla\phi$.

Ansatz potential forms: (to-be-determined constants are α , C, D)

$$\begin{array}{lll}
 \phi_0(r) = (1/2\pi\epsilon_0) q \ln(1/r) & E_{r0}(r) = (1/2\pi\epsilon_0) q/r & \text{region 0} \\
 \phi_1(r) = (1/2\pi\alpha) q \ln(1/r) + C & E_{r1}(r) = (1/2\pi\alpha) q/r & \text{region 1} \\
 \phi_2(r) = (1/2\pi\epsilon_0) q \ln(1/r) + D & E_{r2}(r) = (1/2\pi\epsilon_0) q/r & \text{region 2} \quad . \quad (L.1.1)'
 \end{array}$$

Continuity of ϕ at $r=a$ and b :

$$\begin{array}{ll}
 (1/2\pi\epsilon_0) q \ln(1/b) = (1/2\pi\alpha) q \ln(1/b) + C & \text{region 0/1 boundary, } r = b \\
 (1/2\pi\epsilon_0) q \ln(1/a) + D = (1/2\pi\alpha) q \ln(1/a) + C & \text{region 2/1 boundary, } r = a \quad . \quad (L.1.3)'
 \end{array}$$

Rule for E field normal components at a boundary:

$$\begin{array}{ll}
 \epsilon_0 E_{r0}(b) = \epsilon_1 E_{r1}(b) & \text{region 0/1 boundary, } r = b \\
 \epsilon_0 E_{r2}(a) = \epsilon_1 E_{r1}(a) & \text{region 2/1 boundary, } r = a
 \end{array}$$

or

$$\begin{aligned}\epsilon_0 q / [2\pi\epsilon_0 b] &= \epsilon_1 (1/2\pi\alpha) q/b && \Rightarrow 1 = \epsilon_1/\alpha \\ \epsilon_0 q / [2\pi\epsilon_0 a] &= \epsilon_1 (1/2\pi\alpha) q/a && \Rightarrow 1 = \epsilon_1/\alpha .\end{aligned}\tag{L.1.4}'$$

Restated continuity of ϕ with $\alpha = \epsilon_1$:

$$\begin{aligned}(1/2\pi\epsilon_0) q \ln(1/b) &= (1/2\pi\epsilon_1) q \ln(1/b) + C && \text{region 0/1 boundary, } r = b \\ (1/2\pi\epsilon_0) q \ln(1/a) + D &= (1/2\pi\epsilon_1) q \ln(1/a) + C && \text{region 2/1 boundary, } r = a .\end{aligned}\tag{L.1.5}'$$

Second equation minus first above:

$$\begin{aligned}D + (1/2\pi\epsilon_0) q (\ln(1/a) - \ln(1/b)) &= (1/2\pi\epsilon_1) q (\ln(1/a) - \ln(1/b)) \\ \Rightarrow D + (1/2\pi\epsilon_0) q \ln(b/a) &= (1/2\pi\epsilon_1) q \ln(b/a) .\end{aligned}$$

Solution for the three constants:

$$\begin{aligned}\alpha &= \epsilon \\ C &= q \ln(1/b)(1/2\pi) (1/\epsilon_0 - 1/\epsilon_1) \\ D &= q \ln(a/b)(1/2\pi) (1/\epsilon_0 - 1/\epsilon_1) .\end{aligned}\tag{L.1.6}'$$

The potentials in the three regions are then

$$\begin{aligned}\phi_0(r) &= (1/2\pi\epsilon_0) q \ln(1/r) \\ \phi_1(r) &= (1/2\pi\epsilon_1) q \ln(1/r) + (q/2\pi) \ln(1/b) (1/\epsilon_0 - 1/\epsilon_1) \\ \phi_2(r) &= (1/2\pi\epsilon_0) q \ln(1/r) + (q/2\pi) \ln(a/b) (1/\epsilon_0 - 1/\epsilon_1)\end{aligned}\tag{L.1.7}'$$

while the fields are

$$\begin{aligned}E_{r0} &= (1/2\pi\epsilon_0) q/r \\ E_{r1} &= (1/2\pi\epsilon_1) q/r \\ E_{r2} &= (1/2\pi\epsilon_0) q/r .\end{aligned}\tag{L.1.8}'$$

The following Maple plots show the continuity of ϕ and the jumps in E_r at the boundaries

```
phi := piecewise(r>=0 and r<a,phi2,r)=a and r<b,phi1,r)=b,phi0):
Er := piecewise(r>=0 and r<a,Er2,r)=a and r<b,Er1,r)=b,Er0):
phi0 := q/(2*Pi*e0)*ln(1/r):
phi1 := q/(2*Pi*e1)*ln(1/r) + q/(2*Pi)*ln(1/b)*(1/e0-1/e1):
phi2 := q/(2*Pi*e0)*ln(1/r) + q/(2*Pi)*ln(a/b)*(1/e0-1/e1):
Er0 := q/(2*Pi*e0*r):
Er1 := q/(2*Pi*e1*r):
Er2 := q/(2*Pi*e0*r):
q := 1: a := 1: b := 2: e0 := 1: e1 := 2:
plot([phi,Er], r=0.5..5, color = [red,blue]);
```

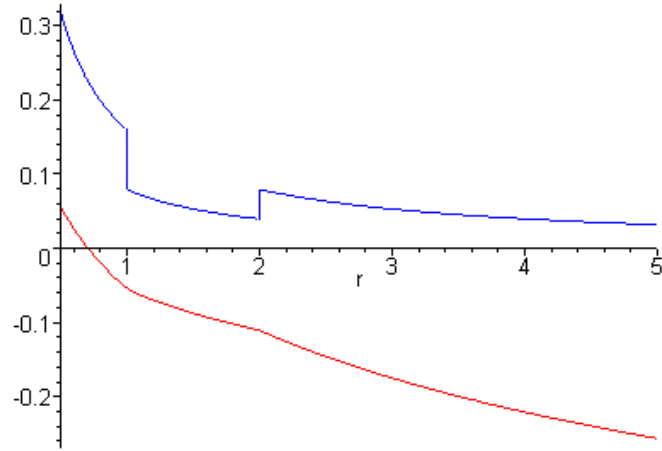


Fig L.2'

$\phi(r)$ [red] and $E_r(r)$ [blue] for r in $(0.5, 5)$

What about the (now linear) bound charge densities at $r = a$ and $r = b$?

$$\mathbf{P} = (\epsilon_1 - \epsilon_0) \mathbf{E}_r \hat{\mathbf{r}}$$

$$P_{r1}(r) = (\epsilon_1 - \epsilon_0) E_{r1}(r) \theta(r > a) \theta(r < b) \quad // \text{ points radially outward since } \epsilon_1 > \epsilon_0 \quad (\text{L.1.9})'$$

From (1.1.11) the polarization charge density is then

$$\rho_{p01} = - \text{div } \mathbf{P} \quad (1.1.11)$$

so in cylindrical coordinates,

$$\begin{aligned} \rho_{p01}(r) &= - [r^{-1} \partial_r (r P_r) + r^{-1} \partial_\theta P_\theta + \partial_z P_z] \\ &= - r^{-1} \partial_r (r P_r) \\ &= - r^{-1} \partial_r (r [(\epsilon_1 - \epsilon_0) E_{r1}(r) \theta(r > a) \theta(r < b)]) \\ &= - r^{-1} \partial_r (r [(\epsilon_1 - \epsilon_0) (1/2\pi\epsilon_1) q/r \theta(r > a) \theta(r < b)]) \quad // \text{ from (L.1.8)'} \\ &= - q(\epsilon_1 - \epsilon_0) (1/2\pi\epsilon_1) r^{-1} \partial_r [\theta(r - a) \theta(b - r)] \\ &= - q(\epsilon_1 - \epsilon_0) (1/2\pi\epsilon_1) r^{-1} [\delta(r - a) - \delta(r - b)] \quad // \text{ from above (L.1.10)} \\ &= - q(\epsilon_1 - \epsilon_0) (1/2\pi\epsilon_1) [\delta(r - a)/a - \delta(r - b)/b] \quad (\text{L.1.10})' \end{aligned}$$

We may then read off the bound *linear* charge densities at $r = a$ and b

$$\begin{aligned}\sigma_{\text{inner}} &= -(\epsilon_1 - \epsilon_0) (1/2\pi\epsilon_1)(q/a) && // \text{Coulombs/m} \\ \sigma_{\text{outer}} &= (\epsilon_1 - \epsilon_0) (1/2\pi\epsilon_1)(q/b) && \text{(L.1.11)'}\end{aligned}$$

so

$$\begin{aligned}Q_{\text{inner}} &= \oint ds \sigma_{\text{inner}} = -(\epsilon_1 - \epsilon_0) (1/2\pi\epsilon_1)(q/a) * 2\pi a = -(1 - \epsilon_0/\epsilon_1) q \\ Q_{\text{outer}} &= \oint ds \sigma_{\text{outer}} = (\epsilon_1 - \epsilon_0) (1/2\pi\epsilon_1)(q/b) * 2\pi b = (1 - \epsilon_0/\epsilon_1) q && \text{(L.1.12)'}\end{aligned}$$

$$Q = (1 - \epsilon_0/\epsilon_1) q \quad // \text{ exactly the same equation as in the 3D case} \quad \text{(L.1.13)'}$$

Here Q is the total charge/m on the outer surface of the cylindrical shell at $r = b$, and $-Q$ is the same thing at $r = a$. Recall that q is the charge/m of the central linear line charge.

L.4 Limits of the Previous Problem

(a) Line charge in an infinite cylindrical hole in a dielectric

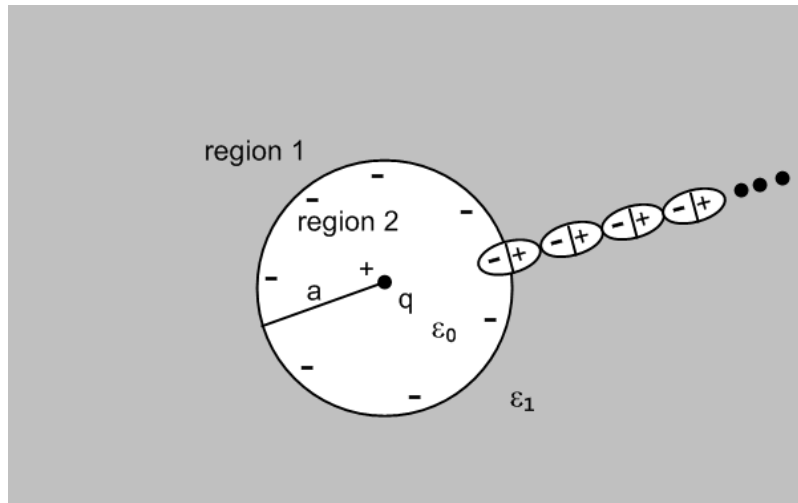


Fig L.3'

The potentials and fields shown in (L.1.7)' and (L.1.8)' are then, taking $b \rightarrow R$ (some large value)

$$\begin{aligned}\phi_1(r) &= (1/2\pi\epsilon_1) q \ln(1/r) + (q/2\pi) \ln(1/R) (1/\epsilon_0 - 1/\epsilon_1) \\ \phi_2(r) &= (1/4\pi\epsilon_0) q/r - (q/4\pi a)(1/\epsilon_0 - 1/\epsilon_1) && \text{(L.2.1)'}\end{aligned}$$

while the fields are

$$\begin{aligned}E_{r1} &= (1/2\pi\epsilon_1) q/r \\ E_{r2} &= (1/2\pi\epsilon_0) q/r && \text{(L.2.2)'}\end{aligned}$$

The induced bound charge density σ at $r = a$, and the total charge there, are still given by

$$\begin{aligned}\sigma &= -(\epsilon_1 - \epsilon_0) (1/2\pi\epsilon_1)(q/a) \\ -Q &= (1 - \epsilon_0/\epsilon_1) q && \text{(L.2.3)'}\end{aligned}$$

(b) Line charge embedded in an infinite dielectric cylinder

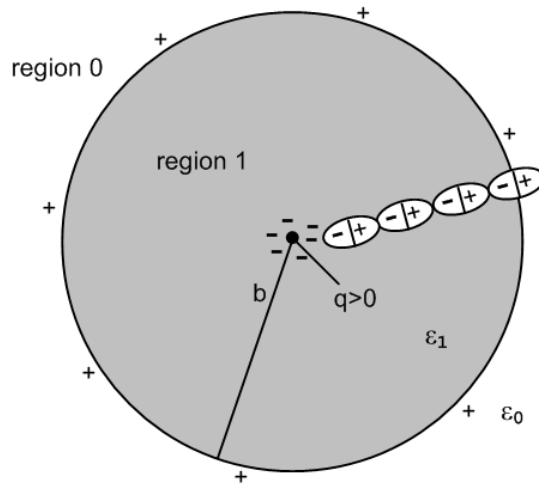


Fig L.5'

The potentials and fields shown in (L.1.7)' and (L.1.8)' are then, taking $a \rightarrow 0$

$$\begin{aligned} \varphi_0(r) &= (1/2\pi\epsilon_0) q \ln(1/r) \\ \varphi_1(r) &= (1/2\pi\epsilon_1) q \ln(1/r) + (q/2\pi) \ln(1/b) (1/\epsilon_0 - 1/\epsilon_1) \end{aligned} \tag{L.2.4}'$$

while the fields are

$$\begin{aligned} E_{r0} &= (1/2\pi\epsilon_0) q/r \\ E_{r1} &= (1/2\pi\epsilon_1) q/r = (1/2\pi\epsilon_0) [q(\epsilon_0/\epsilon_1)] / r \end{aligned} \tag{L.2.5}'$$

where the last expression shows the "shielded charge interpretation".

Outside the cylinder, the E field is $E_{r1} = (1/2\pi\epsilon_0) q/r$, just as if the cylinder were not there.

(c) Line charge embedded in an infinite dielectric medium

We now take $b \rightarrow R$ (a large value) in Fig L.5' to remove outer region 0, with this result:

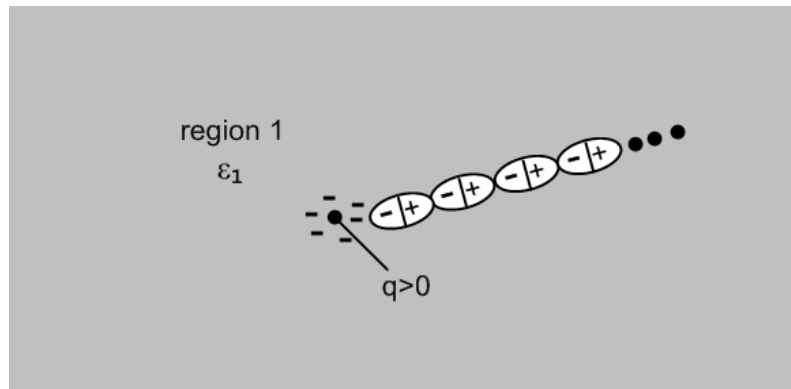


Fig L.6'

There is only one region left and from (L.2.4)' and (L.2.5') we get

$$\phi_1(r) = (1/2\pi\epsilon_1) q \ln(1/r) + (q/2\pi) \ln(1/R) (1/\epsilon_0 - 1/\epsilon_1) \quad (\text{L.2.6})'$$

while the field is

$$E_{r1} = (1/2\pi\epsilon_1) q/r = (1/2\pi\epsilon_0) [q(\epsilon_0/\epsilon_1)] / r \quad (\text{L.2.7})'$$

where the last expression shows the "shielded charge interpretation". As usual, we can ignore the infinite constant in the potential $\phi_1(r)$.

Appendix M: Why the transverse vector potential A_t is small for a transmission line

Claim: In the King gauge, the transverse vector potential A_t may be neglected for frequencies in the range 0 to 500 GHz. (M.1)

Overview: The vector potential is written below as $A_t = \int_{\text{conductors}} dx dy \mathbf{J}_t(x,y) * (\text{stuff})$.

We shall make the following claims:

- $|\mathbf{J}_t| < 10^{-3} |\mathbf{J}_z|$ for $f = 0$ to 500 GHz (which is to say: "transverse currents are small inside the conductors") *Observation 1*
- in the A_t integral there is a cancellation effect not present in the A_z integral which in effect reduces A_t by a factor of 10 (ballpark) relative to A_z . *Observation 2*
- the net ballpark result is that $|A_t| < 10^{-4} |A_z|$ for $f = 0$ to 500 GHz which is the opening claim (M.1) above. *(M.16)*

The conclusions of this Appendix are stated as three observations which we gather here:

Observation (1): The transverse currents J_x and J_θ are very small compared to J_z . *(M.6)*

Observation (2): In the Helmholtz integration (M.3) there is a large amount of cancellation. *(M.8)*

Observation (3): As ω decreases, $\partial_x A_x$ grows in size relative to $\partial_z A_z$. *(M.17)*

According to (1.5.9) one can express the King gauge vector potential at all points in space in terms of the currents in the transmission line conductors in this manner,

$$\mathbf{A}(\mathbf{x}, \omega) = \frac{1}{4\pi} \sum_i \int \mu_i \mathbf{J}_i(\mathbf{x}', \omega) \frac{e^{-j\beta_d R}}{R} dV' \quad R = |\mathbf{x} - \mathbf{x}'| \quad (1.5.9)$$

where \sum_i is a sum over all the conductors, and β_d is the wavenumber in the dielectric. Therefore, the transverse part A_t may be written as an integral of the transverse conductor currents $\mathbf{J}_{t,i}$:

$$\mathbf{A}_t(\mathbf{x}) = \frac{1}{4\pi} \sum_i \mu_i \int \mathbf{J}_{t,i}(x', y', z') \frac{e^{-j\beta_d R}}{R} dx' dy' dz' \quad (M.2)$$

Transverse refers to the x and y directions, where the infinite conductors are aligned in the z direction. The main current in a transmission line conductor is the longitudinal one J_z . When the above equation is processed in the manner of Chapter 4, and one assumes the transmission line limit, the result is

$$\mathbf{A}_t(\mathbf{x}) = -\frac{1}{4\pi} \sum_i \mu_i \int \mathbf{J}_{t,i}(x', y') \ln(s^2) dx' dy' \quad s^2 = (x-x')^2 + (y-y')^2 \quad (M.3)$$

As discussed in Section 4.3, in the transmission line limit both β_d and k are small (long wavelength), so

$e^{-j\beta_{\mathbf{d}}\mathbf{R}} \approx 1$ and $e^{-j\mathbf{k}\mathbf{R}} \approx 1$. We assume the standard wave functional form such that $\mathbf{J}_{\mathbf{t},i}(x,y,z) = e^{-j\mathbf{k}z} \mathbf{J}_{\mathbf{t},i}(x,y)$ and then set $e^{-j\mathbf{k}z} \approx 1$ for the contributing portion of the dz' integration and that integration produces $-\ln(s^2)$ as in Ch 4 or (J.10).

Meanwhile, Appendix D computes the \mathbf{E} fields inside a round conductor (radius a) for each partial wave m , and here we multiply them each by σ to get the current density components,

Current Densities in a Round Wire:	$R_{\mathbf{dc}} = \frac{1}{\sigma\pi a^2} \quad \beta'^2 = \beta^2 - k^2 \quad (D.9.37)$
$J_z(r,m) = (1/4) \sigma \eta_m \mathcal{B}(\omega a) (\beta'/k) f_m$	$f_m = \left[\frac{J_m(x)}{J_{m+1}(x_a)} - \frac{J_m(x)}{J_{m-1}(x_a)} \right] \quad x = \beta'r \quad x_a = \beta'a$
$J_r(r,m) = (j/4) \sigma \eta_m \mathcal{B}(\omega a) g_m$	$g_m = \left[\frac{J_{m+1}(x)}{J_{m+1}(x_a)} + \frac{J_{m-1}(x)}{J_{m-1}(x_a)} \right] \quad \mathcal{B} \equiv (\xi_d/\epsilon_d) CV R_{\mathbf{dc}}$
$J_\theta(r,m) = (1/4) \sigma \eta_m \mathcal{B}(\omega a) h_m$	$h_m = \left[\frac{J_{m+1}(x)}{J_{m+1}(x_a)} - \frac{J_{m-1}(x)}{J_{m-1}(x_a)} \right] \quad G \geq 0$

The currents are expressed in terms of a cylindrical coordinate system whose z axis runs down the center of the round conductor. Coefficient η_m is the "surface charge moment" of the m^{th} partial wave, and the θ -space currents are given by (D.1.3a),

$$\mathbf{J}(r,\theta) = \sum_{m=-\infty}^{\infty} \mathbf{J}(r,m) e^{jm\theta} \quad // \text{ partial wave expansion} \quad (M.4)$$

The moments η_m may be obtained by solving the transmission line "capacitor problem" as outlined in Section 6.5 (a). One finds potential ϕ , then \mathbf{E} , then surface charge $n(\theta)$, and finally η_m .

The current components are,

$$\mathbf{J} = J_z \hat{\mathbf{z}} + J_r \hat{\mathbf{r}} + J_\theta \hat{\boldsymbol{\theta}} = J_z \hat{\mathbf{z}} + \mathbf{J}_{\mathbf{t}} \quad \mathbf{J}_{\mathbf{t}} = J_r \hat{\mathbf{r}} + J_\theta \hat{\boldsymbol{\theta}} \quad (M.5)$$

Rather than study these round wire internal solutions in detail, we make two observations:

Observation (1): The transverse currents J_r and J_θ are very small compared to J_z . (M.6)

We examine this issue first for large ω , and then for small ω .

For **large ω** (skin effect regime) the partial wave fields shown above in (D.2.33) have these limiting forms:

Large ω limits of the E field solutions :	$R_{dc} = \frac{1}{\sigma\pi a^2}$	<i>(D.10.13)</i>
$E_z(r,m) = - (j/2) \eta_m \mathcal{B}(\omega a) (\beta/\beta_{d0}) \sqrt{\frac{a}{r}} e^{(1+j)(x-a)/\delta}$		$x = \beta r$
$E_r(r,m) = (j/2) \eta_m \mathcal{B}(\omega a) \sqrt{\frac{a}{r}} e^{(1+j)(x-a)/\delta}$		$x_a = \beta a$
$E_\theta(r,m) = 0$		$\mathcal{B} \equiv CV R_{dc}$

Multiplying by σ and squaring, one finds using (1.5.1a) and (1.5.1d) that

$$\left| \frac{J_r}{J_z} \right|^2 = \left| \frac{\beta_d^2}{\beta^2} \right| = \left| \frac{\mu_d \epsilon_d \omega^2}{-j\omega\mu\sigma} \right| = \frac{\mu_d \epsilon_d}{\mu\sigma} \omega \approx (\epsilon_d/\sigma) \omega .$$

If we arbitrarily require that $|J_r/J_z| < 10^{-3}$, then ω must be less than

$$\omega_{hi} \equiv \left| \frac{J_r}{J_z} \right|^2 (\sigma/\epsilon_d) = 10^{-6} (\sigma/\epsilon_d) .$$

For a copper conductor and polyethylene dielectric, we find

$$\omega_{hi} = 10^{-6} * (5.81 \times 10^7) / (2.3 * 8.85 \times 10^{-12}) = 28 \times 10^{11}$$

$$f_{hi} = \omega_{hi}/(2\pi) \approx 4.5 \times 10^{11} \sim 500 \text{ GHz}$$

Thus, for high frequencies we conclude that $|J_r/J_z| < 10^{-3}$ for $f \leq \sim 500$ GHz which is beyond the frequency used in any normal transmission line.

What about **small ω** ? In this case the limiting forms of the fields are given by

$E_z(r,m) = (1/2) \eta_m \mathcal{B}(\omega/k) (r/a)^m (m+1)$		<i>(D.11.7)</i>
$E_r(r,m) = (j/4) \eta_m \mathcal{B}(\omega a) [(r/a)^{m+1} + (r/a)^{m-1}]$		
$E_\theta(r,m) = (1/4) \eta_m \mathcal{B}(\omega a) [(r/a)^{m+1} - (r/a)^{m-1}]$		$m > 0$
$E_z(r,0) = \mathcal{B}(\omega/k)$		$\mathcal{B} \equiv (\xi_d/\epsilon_d) CV R_{dc}$
$E_r(r,0) = (j/2) \mathcal{B}(\omega r)$		
$E_\theta(r,0) = 0$		$m = 0 \quad G \geq 0$

In this low ω situation we find that, for any partial wave m ,

$$\left| \frac{J_r}{J_z} \right| \approx a |k| .$$

The wavenumber k is given by

$$k = -j\sqrt{zy} = -j\sqrt{(R+j\omega L)(G+j\omega C)} . \tag{5.3.5} \tag{K.7}$$

As $\omega \rightarrow 0$, we showed in (D.11.1) that for $G > 0$, $k \rightarrow -j\sqrt{R_{dc}G_{dc}}$, while for $G = 0$ $k \rightarrow 0$, so the worst case is the first situation where $|k| \rightarrow \sqrt{R_{dc}G_{dc}}$. But this is always a very small number, and we showed that for our Belden 8281 example $\sqrt{R_{dc}G_{dc}} \approx 10^{-8}$ and then $|J_x/J_z| \approx a|k| \approx 5 \times 10^{-12}$.

Our conclusion so far is that $|J_x/J_z| < 10^{-3}$ for both high frequencies and low frequencies. Showing this is also true in the middle frequency range requires much more work, but we appeal to the general smooth and monotonic nature of k as illustrated in Fig Q.5.7 to argue that the worst case will still be at high frequency and thus our conclusion stands for all frequencies:

Conclusion: For frequencies from 0 to 500 GHz,

$$\begin{aligned} |J_x| &< 10^{-3} |J_z| \\ |J_\theta| &< 10^{-3} |J_z| \end{aligned} \quad f = 0 \text{ to } 500 \text{ GHz} \tag{M.7}$$

The conclusion then is that the transverse currents are less than 1/1000th of the size of the longitudinal currents for the round copper conductor at all frequencies of interest below 500 GHz, and we can reasonably assume that a similar conclusion applies to a conductor of any cross sectional shape (while maintaining the transmission line limit). This then concludes our "proof" of the claim that "transverse currents are very small" inside the conductors of a transmission line.

Observation (2): In the Helmholtz integration (M.3) there is a large amount of cancellation. (M.8)

Let us consider the nature of this integration in the illustrative case of a two round conductors,

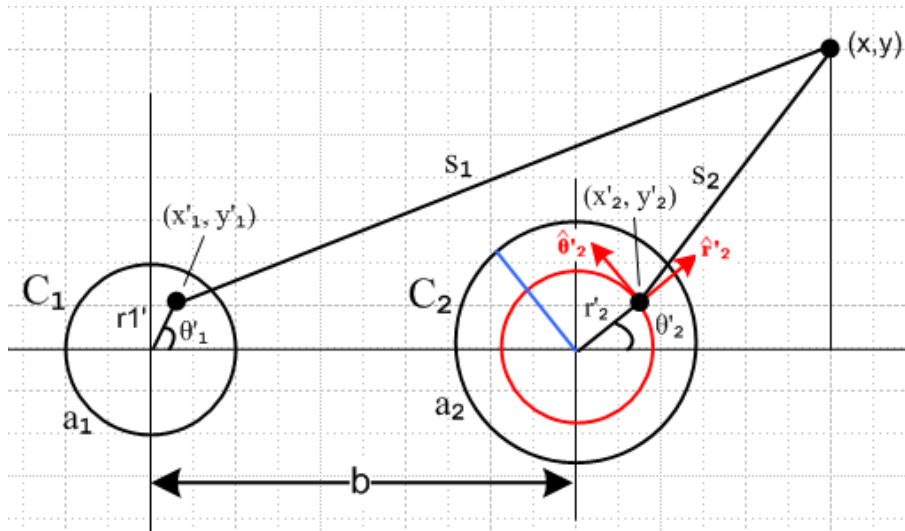


Fig M.1

Consider the contribution to the transverse vector potential component A_x from the right conductor C_2 ,

$$A_{\mathbf{x}}(\mathbf{x}) = -\frac{\mu_d}{4\pi} \int J_{\mathbf{x}}(x'_2, y'_2) \ln(s_2^2) dx'_2 dy'_2 \quad s_2^2 = (x-x'_2)^2 + (y-y'_2)^2 \quad (\text{M.9})$$

or

$$A_{\mathbf{x}}(\mathbf{x}) = -\frac{\mu_d}{4\pi} \int [J_{\mathbf{r}}(r'_2, \theta'_2) \hat{\mathbf{r}}'_2 \cdot \hat{\mathbf{x}} + J_{\theta}(r'_2, \theta'_2) \hat{\theta}'_2 \cdot \hat{\mathbf{x}}] \ln(s_2^2) [a_2 d\theta'_2] dr'_2 \quad (\text{M.10})$$

or

$$A_{\mathbf{x}}(\mathbf{x}) = -\frac{\mu_d}{4\pi} \int [J_{\mathbf{r}}(r'_2, \theta'_2) \cos\theta'_2 - J_{\theta}(r'_2, \theta'_2) \sin\theta'_2] \ln(s_2^2) [a_2 d\theta'_2] dr'_2 . \quad (\text{M.11})$$

The transverse currents in conductor C_2 have this partial wave expansion from (M.4),

$$J_{\mathbf{r}}(r'_2, \theta'_2) = \sum_{m=-\infty}^{\infty} J_{\mathbf{r}}(r'_2, m) e^{jm\theta'_2} \quad (\text{M.12})$$

and similarly for J_{θ} . Thus we get

$$A_{\mathbf{x}}(x, y) = -\frac{\mu_d}{4\pi} a_2 \sum_m \int_0^{a_2} dr'_2 J_{\mathbf{r}}(r'_2, m) \int_0^{2\pi} d\theta'_2 e^{jm\theta'_2} \cos\theta'_2 \ln(s_2^2) + \frac{\mu_d}{4\pi} a_2 \sum_m \int_0^{a_2} dr'_2 J_{\theta}(r'_2, m) \int_0^{2\pi} d\theta'_2 e^{jm\theta'_2} \sin\theta'_2 \ln(s_2^2) \quad (\text{M.13})$$

where, from (D.2.33) quoted above,

$$J_{\mathbf{r}}(r, m) = \sigma(j/4) \eta_m I R_{dc} (a\beta_d) \left[\frac{J_{m+1}(x)}{J_{m+1}(x_a)} + \frac{J_{m-1}(x)}{J_{m-1}(x_a)} \right] \quad x = \beta'r$$

$$J_{\theta}(r, m) = \sigma(1/4) \eta_m I R_{dc} (a\beta_d) \left[\frac{J_{m+1}(x)}{J_{m+1}(x_a)} - \frac{J_{m-1}(x)}{J_{m-1}(x_a)} \right] \quad x_a = \beta'a .$$

It is in theory possible to first do the $d\theta'_2$ integration in (M.13) and then do the dr'_2 integration and get an analytic result for $A_{\mathbf{x}}(x, y)$. We have dealt with similar angle integrations elsewhere in this document. Rather than attempt this task, we instead consider the portion of the 2D integration represented by the **red ring** in Fig M.1. On this ring, r'_2 is constant, and our interest is the θ'_2 integration. For any value of m (except for ± 1) the trigonometric functions like $e^{jm\theta'_2} \cos\theta'_2$ integrate to 0, for example,

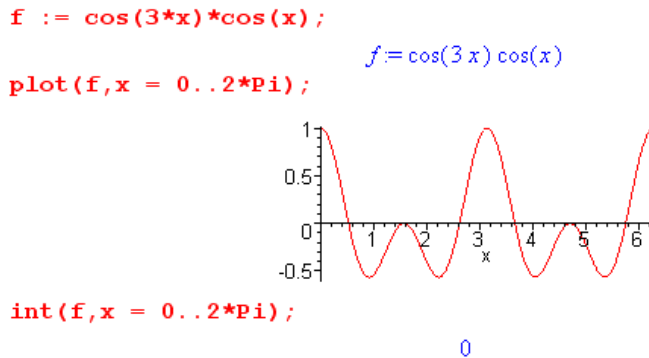


Fig M.2

For these values of m , were it not for the fact that s_2^2 varies around the red circle, $A_{\mathbf{x}}(x,y)$ would be identically 0. Although s_2^2 does vary on the red circle, $\ln(s^2)$ varies very little, and we expect to still have this strong cancellation in the θ'_2 integral so $A_{\mathbf{x}}(x,y)$ is then small. It is true that if \mathbf{x} and \mathbf{x}'_2 were to approach the conductor boundary from opposite sides, then $\ln(s^2)$ would vary a lot more and the cancellation would be less, but we ignore this detail in our qualitative argument.

For $m = \pm 1$ this smallness argument fails since for example $\cos^2(\theta'_2)$ does not average to 0 around the red ring. Ignoring the θ'_2 variation in s_2^2 we get in this case (setting $e^{\pm j\theta'_2} \sim \cos\theta'_2$)

$$\begin{aligned} A_{\mathbf{x}}(x,y) &\approx -\frac{\mu_d}{4\pi} a_2 \sum_m \int_0^{a_2} dr'_2 J_{\mathbf{x}}(r'_2, m) \ln(s_2^2) \int_0^{2\pi} d\theta'_2 \cos^2\theta'_2 \\ &\approx -\frac{\mu_d}{4\pi} a_2 \sum_m \int_0^{a_2} dr'_2 J_{\mathbf{x}}(r'_2, \pm 1) \ln(s_2^2) \pi \end{aligned} \quad (M.14)$$

Now we make a different argument which concerns the behavior of the complex Bessel functions as a function of r'_2 . As studied in Chapter 2, these functions have a dramatically oscillating phase even in the soft skin depth limit, and we expect then to get cancellation due to this phase as we integrate on the radial **blue segment** in Fig M.1, and again $\ln(s_2^2)$ varies slowly on this ray due to the nature of \ln .

The arguments made above for $A_{\mathbf{x}}(x,y)$ also apply to $A_{\mathbf{y}}(x,y)$, and it seems reasonable to assume that the arguments are generally valid for an arbitrary conductor cross section.

Admittedly our analysis here is imprecise and qualitative, but we think it is convincing that there is in fact much cancellation when the transverse currents are integrated over the conductors.

This stands in stark contrast to the longitudinal situation where $A_{\mathbf{z}}$, being the Helmholtz integral of $J_{\mathbf{z}}$, involves a generally non-cancelling integration (per conductor) over a generally large current component.

We now wish to compare the following two integrals, where we pick component $A_{\mathbf{x}}$ to represent a transverse component of \mathbf{A}_t ,

$$A_{\mathbf{x}}(\mathbf{x}) = -\frac{1}{4\pi} \sum_i \mu_i \int J_{\mathbf{x},i}(x',y') \ln(s^2) dx' dy' \quad . \quad s^2 = (x-x')^2 + (y-y')^2 \quad (M.3)$$

$$A_{\mathbf{z}}(\mathbf{x}) = -\frac{1}{4\pi} \sum_i \mu_i \int J_{\mathbf{z},i}(x',y') \ln(s^2) dx' dy' \quad . \quad s^2 = (x-x')^2 + (y-y')^2 \quad (M.15)$$

We have shown in (M.7) that $|J_{\mathbf{x}}| < 10^{-3} |J_{\mathbf{z}}|$. Without any mathematical rigor, and allowing a factor of 10 "gain" from the cancellation effect of Observation (2), we make the following *ballpark* estimate,

$$|\mathbf{A}_t| < 10^{-4} |\mathbf{A}_z| \quad f = 0 \text{ to } 500 \text{ GHz.} \quad (M.16)$$

It is assumed that as ω increases, the transmission line geometry is appropriately shrunk so the transmission line limit remains operative.

Observation (3): As ω decreases, $\partial_{\mathbf{x}}A_{\mathbf{x}}$ grows in size relative to $\partial_{\mathbf{z}}A_{\mathbf{z}}$. (M.17)

Notice that the Claim (M.1) says nothing about *derivatives* of A_t and A_z .

Observation (3) relates to the discussion of Section 7.5 and the presence of $T(z)$ in Appendix S. In Section 7.5 we present two arguments for $\partial_{\mathbf{x}}A_{\mathbf{x}}$ growing in size relative to $\partial_{\mathbf{z}}A_{\mathbf{z}}$ as ω decreases. Here we present a third argument. We imagine that at large ω , we have $|\partial_{\mathbf{z}}A_{\mathbf{z}}| \gg |\partial_{\mathbf{x}}A_{\mathbf{x}}|$ just because $|A_z|$ is so much larger than $|A_x|$. But we then argue that as ω decreases, $|\partial_{\mathbf{x}}A_{\mathbf{x}}|$ increases in size and becomes more important relative to $|\partial_{\mathbf{z}}A_{\mathbf{z}}|$.

From (M.2) we may write, using the ansatz $e^{-j\mathbf{kz}}$ behavior for $J_{zi}(x,y,z)$,

$$\begin{aligned}\partial_{\mathbf{z}}A_{\mathbf{z}}(\mathbf{x},\omega) &= \frac{1}{4\pi} \sum_i \int \mu_i J_{zi}(x',y',\omega) e^{-j\mathbf{kz}'} \partial_{\mathbf{z}} \left[\frac{e^{-j\beta_d R}}{R} \right] dV' & R = |\mathbf{x}-\mathbf{x}'| \\ \partial_{\mathbf{x}}A_{\mathbf{x}}(\mathbf{x},\omega) &= \frac{1}{4\pi} \sum_i \int \mu_i J_{xi}(x',y',\omega) e^{-j\mathbf{kz}'} \partial_{\mathbf{x}} \left[\frac{e^{-j\beta_d R}}{R} \right] dV' .\end{aligned}\tag{M.18}$$

Since $(\partial_{\mathbf{z}}R) = (z-z')/R$ and $(\partial_{\mathbf{x}}R) = (x-x')/R$ it is not hard to show that

$$\begin{aligned}\partial_{\mathbf{z}} \left[\frac{e^{-j\beta_d R}}{R} \right] &= - (z-z') (1+j\beta_d R) e^{-j\beta_d R} / R^3 \\ \partial_{\mathbf{x}} \left[\frac{e^{-j\beta_d R}}{R} \right] &= - (x-x') (1+j\beta_d R) e^{-j\beta_d R} / R^3 .\end{aligned}\tag{M.19}$$

It follows then that one can write

$$\begin{aligned}\partial_{\mathbf{z}}A_{\mathbf{z}}(\mathbf{x},\omega) &= - \frac{1}{4\pi} \sum_i \int \mu_i J_{zi}(x',y',\omega) I_1(x',y') dx' dy' \\ \partial_{\mathbf{x}}A_{\mathbf{x}}(\mathbf{x},\omega) &= - \frac{1}{4\pi} \sum_i \int \mu_i J_{xi}(x',y',\omega) I_2(x',y') (x-x') dx' dy'\end{aligned}\tag{M.20}$$

where

$$\begin{aligned}I_1 &\equiv \int_{-\infty}^{\infty} dz' e^{-j\mathbf{kz}'} e^{-j\beta_d R} (1+j\beta_d R) / R^3 * (z-z') \\ I_2 &\equiv \int_{-\infty}^{\infty} dz' e^{-j\mathbf{kz}'} e^{-j\beta_d R} (1+j\beta_d R) / R^3 .\end{aligned}\tag{M.21}$$

Writing $z'' = z-z'$ and then replacing $e^{+j\mathbf{kz}''} = \cos(kz'') + j\sin(kz'')$ and noting that $R^2 = s^2 + z''^2$ which is even in z'' , one finds that

$$I_1 = -j e^{-j\mathbf{kz}} \int_{-\infty}^{\infty} dz'' [z'' \sin(kz'')] (1+j\beta_{\mathbf{a}}R) e^{-j\beta_{\mathbf{a}}R}/R^3 \quad R^2 = (x-x')^2 + (y-y')^2 + z''^2$$

$$I_2 = e^{-j\mathbf{kz}} \int_{-\infty}^{\infty} dz'' [\cos(kz'')] (1+j\beta_{\mathbf{a}}R) e^{-j\beta_{\mathbf{a}}R}/R^3 \quad . \quad (\text{M.22})$$

One could evaluate these integrals, but we just make the following observations. We expect both integrals to be dominated by the region near $z'' = 0$ since R is smallest at that point. In that region, the factor $z'' \sin(kz'')$ is small if $k \approx 0$ or if k is large, so I_1 is not very sensitive to the value of k . But I_2 is sensitive to k . For large ω , meaning large k , the I_2 integrand is chopped up by $\cos(kz'')$ and I_2 is small. As $\omega \rightarrow 0$ and $k \rightarrow 0$ or some very small value, $\cos(kz'') \approx 1$ so I_2 is large. Thus, we argue that the size of I_2 relative to I_1 increases as $\omega \rightarrow 0$, and this then suggests that the size of $\partial_{\mathbf{x}}A_{\mathbf{x}}$ increases relative to $\partial_{\mathbf{z}}A_{\mathbf{z}}$.

Appendix N: Drude, Magnetic Ohm's Law, Regular Hall Effect, Radial Hall Effect

The first sections of this Appendix follow the general outline of notes prepared by Pengra *et. al.* for a Laboratory Class at the University of Washington.

N.1 The Drude Model of Conduction

The current due to carriers of charge q and density n with drift velocity \mathbf{v} is easily shown to be

$$\mathbf{J} = nq\mathbf{v} . \quad \dim \text{RHS} = \text{m}^{-3} * \text{Coul} * \text{m/sec} = \text{amp/m}^2 \quad (\text{N.1.1})$$

In the classical 1900 Drude/Lorentz model (which of course predates quantum mechanics), the charges are assumed to be electrons with charge $q = -|e|$ and mass $m = m_e$. At this time there was no band-gap theory, no holes, no effective mass, none of that good stuff. The density n is one electron per atom for a metal like copper. Here are some basic numbers :

$$n = 8.5 \times 10^{28} \text{ electrons/m}^3 \quad // \text{ for copper}$$

$$|e| = 1.6 \times 10^{-19} \text{ Coul} . \quad (\text{N.1.2})$$

If a relatively large current of 1000 Amps flows through a wire of 1 cm^2 cross sectional area, one has

$$J = 1000 \text{ amps} / 10^{-4} \text{m}^2 = 10^7 \text{ amp/m}^2 .$$

The drift velocity is then

$$v = J/(nq) = \frac{1000}{1.6 * 8.5} \times 10^{4+19-28} = 7.4 \times 10^{-4} \text{ m/sec} = 0.74 \text{ mm/sec} \approx 1 \text{ mm/sec} .$$

In this same classical vein, if the electron has thermal energy $(1/2) m v_{\text{th}}^2 = (3/2) kT$, one can solve for the thermal electron velocity at room temperature,

$$v_{\text{th}} \sim 100,000 \text{ m/sec} .$$

Although this number is wrong from a quantum view, the fact that it is very much larger than the drift velocity is correct. In the Drude theory, these fast-moving electrons are colliding with copper ions at a high rate, and every collision results in a complete redirection of the electron. In copper the effective **mean collision time** is on the order of $\tau = 10^{-14}$ sec. It is only between these closely spaced collisions that the electrons have time to drift a little in the presence of an electric field. Since $\mathbf{F} = q\mathbf{E} = d\mathbf{p}/dt$, one concludes that $\Delta\mathbf{p} = q\mathbf{E}\Delta t$ or just $\mathbf{p} = q\mathbf{E}\tau$ where \mathbf{p} is the amount of drift momentum an electron picks up between collisions. Since on average an electron on each collision dumps this momentum into the lattice, the lattice can be regarded as a frictional or drag force acting against the electron's flow, and that force is $-\Delta\mathbf{p}/\Delta t = -\mathbf{p}/\tau$. So,

$$\mathbf{F}_{\text{f}} = -\mathbf{p}/\tau = -(m/\tau) \mathbf{v} . \quad (\text{N.1.3})$$

This frictional force is proportional to velocity, as is typical for low-velocity fluid drag, and is naturally in a direction opposite the velocity. When combined with the Lorentz force,

$$\mathbf{F} = q\mathbf{E} + q\mathbf{v}\times\mathbf{B} \quad (\text{N.1.4})$$

and $\mathbf{F} = m\mathbf{a}$, one obtains a fairly reasonable equation describing the motion of a conduction electron,

$$m\frac{d\mathbf{v}}{dt} = q\mathbf{E} + q\mathbf{v}\times\mathbf{B} - (m/\tau)\mathbf{v} . \quad (\text{N.1.5})$$

If $\mathbf{B} = 0$ and the conduction is in steady-state, this says

$$\begin{aligned} 0 &= q\mathbf{E} - (m/\tau)\mathbf{v} \\ \text{or} \\ \mathbf{v} &= (q\tau/m)\mathbf{E} . \end{aligned} \quad (\text{N.1.6})$$

The constant appearing here is called the carrier **mobility** μ , so then

$$\mathbf{v} = \mu\mathbf{E} \quad \mu = (q\tau/m) . \quad // \text{ units of } \mu \text{ are } \text{tesla}^{-1} \quad (\text{N.1.7})$$

Officially mobility is $(|q|\tau/m) > 0$, but we shall use the signed mobility shown above.

Warning: μ is the same symbol used for magnetic permeability.

If one now installs the drift velocity (N.1.6) into (N.1.1), one gets

$$\mathbf{J} = nq\mathbf{v} = (nq^2\tau/m)\mathbf{E} = \sigma\mathbf{E} . \quad \sigma = \text{conductivity} \quad (\text{N.1.8})$$

The coefficient appearing in (N.1.8) is known as the **conductivity** of the medium, as we well know by now, so the classical Drude theory is predicting that

$$\sigma = (nq^2\tau/m) . \quad // \sigma = n q \mu \quad (\text{N.1.9})$$

If one measures σ for copper, one can deduce the value of τ for the Drude model of conduction:

$$\tau = m\sigma/(nq^2) \quad (\text{N.1.10})$$

We know that

$$\begin{aligned} m &= 9.109 \times 10^{-31} \text{ kg} && // \text{ electron mass} \\ \sigma &= 5.81 \times 10^7 \text{ mho/m} && // \text{ conductivity of copper} \end{aligned} \quad (\text{N.1.11})$$

so that, along with the numbers stated earlier in (N.1.2),

$$\tau = m\sigma/(nq^2) = 2.43 \times 10^{-14} \sim 10^{-14} \quad (\text{N.1.12})$$

as claimed earlier.

If the electrons are moving with time dependence $e^{j\omega t}$, the left side of the equation of motion (N.1.5) becomes $j\omega m \mathbf{v}$. We then get

$$j\omega m \mathbf{v} = q\mathbf{E} - (m/\tau) \mathbf{v}$$

$$(m/\tau)(1+j\omega\tau) \mathbf{v} = q\mathbf{E}$$

$$\mathbf{v} = \frac{1}{1+j\omega\tau} (q\tau/m)\mathbf{E} \qquad \mu_{ac} = \frac{1}{1+j\omega\tau} \mu \qquad (N.1.13)$$

$$\mathbf{J} = nq\mathbf{v} = \frac{1}{1+j\omega\tau} (nq^2\tau/m)\mathbf{E} = \sigma_{ac}\mathbf{E} \qquad \sigma_{ac} = \frac{1}{1+j\omega\tau} \sigma \ . \qquad (N.1.14)$$

In our analysis of transmission lines, $\omega\tau \ll 1$, so we may neglect this AC adjustment of the mobility and conductivity. Roughly $\omega\tau \approx 1$ when

$$\omega = 2\pi f = 1/\tau = 10^{14} \qquad \Rightarrow \qquad f \approx 16,000 \text{ GHz} \qquad (N.1.15)$$

so for $f < 160$ GHz there will be $< 1\%$ change in μ or σ in the Drude Model.

N.2 A Theory of the Hall Effect

All theories and models are deficient in some way but might still deliver a reasonable result. The Drude model above is generally "reasonable" in this regard, though it fails to match reality in various ways. Here we present an instant theory of the Hall Effect which correctly predicts the main result to within about 30%, but has an annoying theoretical defect noted at the end of the section.

Using the traditional directions x , y , and z , here is the classical Hall Effect picture, where we put the origin at the center of a rectangular sample block,

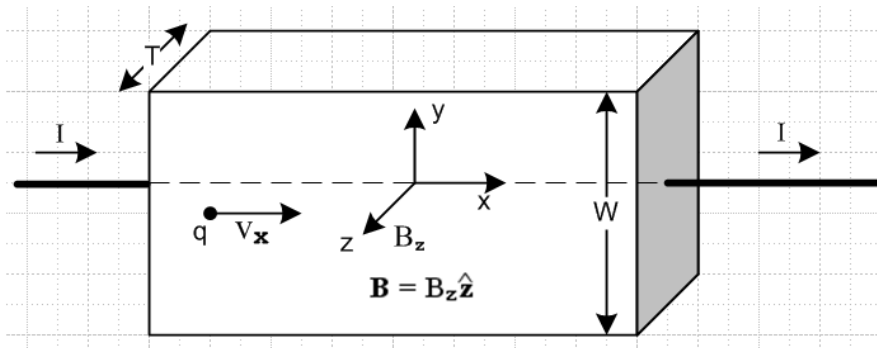


Fig N.1

The idea is that current flows through a sample in the presence of an externally applied uniform transverse magnetic field which in this case is $\mathbf{B} = B_z \hat{z}$ with $B_z > 0$. Semiconductors have much lower carrier densities than copper, and one can imagine for a semiconductor sample that the block above is placed between two copper plates (gray on right) to cause the applied current to be spread out evenly in

the sample. This is one of several technical details we shall ignore, and we just assume the current is spread out evenly. Typically the thickness T is made very small because this boosts the Hall voltage as we shall see below in (N.2.6).

We imagine the two wires from the sample being connected to a battery with + on the left and - on the right, so that $I > 0$, but we allow the charge carriers q to have either sign. Since the apparatus forces $I > 0$, we must have $\text{sign}(v_x) = \text{sign}(q)$ so $qv_x > 0$.

The Lorentz force acting on a carrier of charge q , along with the friction term, was shown in (N.1.5),

$$\mathbf{F} = q \mathbf{E} + q \mathbf{v} \times \mathbf{B} - (m/\tau) \mathbf{v} \quad . \quad (N.1.5)$$

Applying this to the Hall apparatus of Fig N.1 one finds that.

$$\mathbf{F} = q \mathbf{E} + q [v_x \hat{x}] \times [B_z \hat{z}] - (m/\tau) [v_x \hat{x}] = q \mathbf{E} - (qv_x) B_z \hat{y} - (m/\tau) [v_x \hat{x}] \quad (N.2.1)$$

Since $qv_x > 0$, the carriers are deflected downward regardless of their sign. After a short while, this vertical carrier deflection causes equal and opposite surface charges to pile up on the upper and lower plates, and this in turn creates an electric field E_y which neutralizes the deflecting force and then the carriers move only horizontally. In (N.2.1) one then must have $\mathbf{E} = + v_x B_z \hat{y}$ so then only the horizontal drag force is left and $\mathbf{F} = - (m/\tau) [v_x \hat{x}]$. Therefore,

$$E_y = v_x B_z \quad . \quad // \text{ the Hall field} \quad (N.2.2)$$

If $q > 0$, then $v_x > 0$ and the E_y field points up, indicating positive charge on the lower plate.

If $q < 0$, then $v_x < 0$ and the E_y field points down, indicating positive charge on the upper plate.

From (N.1.1) we have $J_x = nqv_x$ and also $J_x = I/(WT)$ so

$$v_x = \frac{I}{nqWT} \quad \text{and then} \quad E_y = \frac{IB_z}{nqWT} \quad . \quad (N.2.3)$$

One usually then defines

$$R_H \equiv \frac{1}{nq} \quad // \text{ the Hall coefficient} \quad (N.2.4)$$

so (N.2.3) becomes

$$v_x = R_H \frac{I}{WT} \quad \text{and} \quad E_y = R_H \frac{IB_z}{WT} \quad // \text{ the Hall field} \quad (N.2.5)$$

Note that $\text{sign}(R_H) = \text{sign}(q)$. The E_y field produces a potential (a voltage) between the top and bottom faces, and since $\mathbf{E} = -\nabla V$,

$$V_H = V_{top} - V_{bot} = V(W) - V(0) = \int_0^W \frac{dV}{dy} dy = - \int_0^W E_y dy = - E_y W = - R_H \frac{IB_z}{WT} * W$$

so

$$V_H = - R_H * \frac{IB_z}{T} \quad // \text{ the Hall voltage} \quad (N.2.6)$$

Fact: The sign of the Hall voltage V_H indicates the sign of R_H and thus the sign of the charge carriers! If for some metal the carriers are holes (in the quantum theory of metals), R_H will be positive. Pre-quantum researchers were indeed surprised when they found different signs of R_H for different metals.

Using the numbers in (N.1.2), the Drude theory for copper predicts that

$$R_H \approx \frac{1}{n(-|e|)} = -.73 \times 10^{-10} \quad // \text{ Drude theory} \quad (N.2.7)$$

as shown by this Maple calculation where we have included units,

```

RH := 1/(n*q);
RH := 1
      n q
n := 8.5e28*m^(-3);
q := -1.6e-19*cou;
RH;
-7352941175 10^-10 m^3
              cou
    
```

This is not too far from the measured and quantum-correct value of -0.55×10^{-10} (though the literature seems a bit unsure of this number). This is an impressive success of the *classical* Drude theory.

As claimed earlier, and as seen in (N.2.6), making thickness T very small makes V_H larger so it can be measured with a voltmeter one can afford to place in a student lab. Typical numbers for a student lab experiment might be

$$\begin{aligned} T &= 18 \text{ microns} = 18 \times 10^{-6} \text{ m} && // \text{ a thin film of copper} \\ W &= 1 \text{ cm} = 1 \times 10^{-2} \text{ m} \\ B_z &= 5000 \text{ gauss} = 0.5 \text{ T} \\ I &= 10 \text{ amps} \end{aligned} \quad (N.2.8)$$

so that, according to the Drude theory,

```

T := 18e-6*m;
      T := .000018 m
W := 1e-2*m;
      W := .01 m
Bz := 0.5*tes;
      Bz := .5 tes
I := 10*amp;
      I := 10 amp
amp := cou/sec:
tes := volt*sec/m^2:
Ey := RH*I*Bz/(W*T);
      Ey := -.002042483660  $\frac{\text{volt}}{\text{m}}$ 
VH := -Ey*W;
      VH := .00002042483660 volt
vx := RH/(W*T);
      vx := -.0004084967319  $\frac{\text{m}}{\text{cou}}$ 

```

so we end up for this experiment with

$E_y = -2 \text{ mV/m}$	Hall field	
$V_H = 20 \text{ } \mu\text{V}$	Hall voltage	
$v_x = -0.4 \text{ mm/sec}$	drift velocity	(N.2.9)

Recall that $R_H = \frac{1}{nq}$. Since the carrier density n in a semiconductor is much smaller than in a metal, R_H and V_H are much larger, so practical Hall devices become more feasible. But our theory has to first be generalized to two types of carriers (electrons and holes), and this is done in Section N.6 below.

A Hall effect sensor exists in almost every fan in every personal computer in the world. Since the fan has some rotating permanent magnets, the Hall sensor can detect the rotational position and speed of the blades and most importantly detects when the fan has stopped rotating altogether (pulses stop). In general, Hall sensors are used to measure magnetic fields, and can be used as simple magnetic switches.

And now comes the "theoretical defect" of our Hall effect analysis. Assuming that Ohm's Law $\mathbf{J} = \sigma \mathbf{E}$ is operative in the Hall sample, and since there is an internal field E_y in the sample, there should be a corresponding and uniform current density $J_y = \sigma E_y$ in the sample. Unfortunately, at the top face (for example) this current has no place to go, so something is wrong. This problem will be dealt with in Section N.5 below.

N.3 The Cyclotron Frequency

When a charged particle travels through an empty region of space having a uniform \mathbf{B} field and no \mathbf{E} field, the equation of motion (N.1.5) becomes (dot means time derivative),

$$m\dot{\mathbf{v}} = q \mathbf{v} \times \mathbf{B} . \quad (N.1.5)$$

Assume that $\mathbf{B} = B\hat{\mathbf{z}}$ so then

$$q \mathbf{v} \times \mathbf{B} = [v_x\hat{\mathbf{x}} + v_y\hat{\mathbf{y}} + v_z\hat{\mathbf{z}}] \times [qB\hat{\mathbf{z}}] = -v_xqB\hat{\mathbf{y}} + v_yqB\hat{\mathbf{x}}$$

so

$$\begin{aligned} m\dot{v}_x &= v_yqB & \Rightarrow & \dot{v}_x = \omega_c v_y & \Rightarrow & \ddot{v}_x = -\omega_c^2 v_x \\ m\dot{v}_y &= -v_xqB & & \dot{v}_y = -\omega_c v_x & & \ddot{v}_y = -\omega_c^2 v_y \\ m\dot{v}_z &= 0 & & \dot{v}_z = 0 & & \text{where } \omega_c \equiv (qB/m) . \end{aligned} \quad (N.3.1)$$

Looking at the 2nd order ODE for v_x we may write the general solution for v_x in terms of two constants R and ϕ in this way

$$v_x = -R\omega_c \sin(\omega_c t + \phi) \quad \Rightarrow \quad v_y = (1/\omega_c) \dot{v}_x = -R\omega_c \cos(\omega_c t + \phi)$$

so that

$$v = \sqrt{v_x^2 + v_y^2} = R\omega_c = (RqB/m) \quad (N.3.2)$$

$$\begin{aligned} v_x &= -R\omega_c \sin(\omega_c t + \phi) & \Rightarrow & x = R \cos(\omega_c t + \phi) + x_1 \\ v_y &= -R\omega_c \cos(\omega_c t + \phi) & \Rightarrow & y = -R \sin(\omega_c t + \phi) + y_1 \\ v_z &= v_z & \Rightarrow & z = v_z t + z_0 \end{aligned} \quad (N.3.3)$$

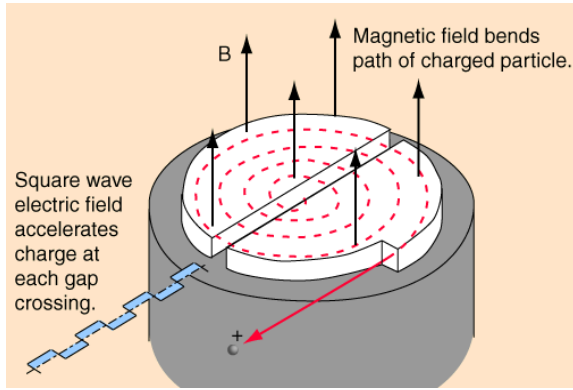
so

$$\begin{aligned} (x-x_1) &= R \cos(\omega_c t + \phi) \\ (y-y_1) &= -R \sin(\omega_c t + \phi) & \Rightarrow & (x-x_1)^2 + (y-y_1)^2 = R^2 \\ (z-z_0) &= v_z t . \end{aligned} \quad (N.3.4)$$

In the x,y dimension the particle goes around in a circle of radius R at rate ω_c (clockwise if $\omega_c > 0$), while in the z direction of \mathbf{B} it moves at some constant velocity, resulting in a circular or slinky spiral trajectory.

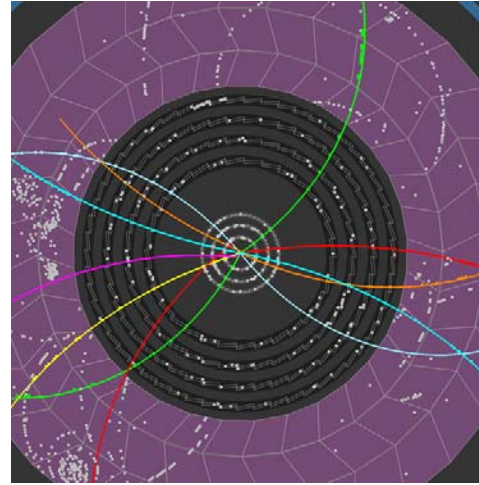
The angular frequency ω_c is known as the cyclotron frequency, named after a charged-particle accelerator invented in 1932 by Lawrence known as a cyclotron, see wiki and left drawing below. In this machine particles traverse an outward-going spiral (different from the one just mentioned) because they are accelerated by an AC electric field driving two hollow D-shaped conductors of a capacitor enclosing the particle beam. As v increases, R must increase as shown above in (N.3.2). The capacitor is driven at the cyclotron frequency ω_c so the accelerating \mathbf{E} field is in sync with the circular particle motion. Since $\omega_c \equiv (qB/m)$, this frequency has to be reduced if the charged particle bunch being accelerated reaches relativistic speeds and m increases.

The circular motion of charged particles in a uniform B field is also used to identify particles produced in high energy collisions inside particle accelerator detectors. Since $v = RqB/m$ from (N.3.2), if the particle m and q is known, the speed v and hence energy can be determined from R, and the sign of q can be found from the CW or CCW nature of the particle path. Alternatively, if the energy and speed are known from "calorimetry" and a charge q is assumed, the mass m of the particle can be found from R.



<http://hyperphysics.phy-astr.gsu.edu/hbase/magnetic/cyclot.html>

The Cyclotron



CERN

Particle Tracks (B field out of paper) Fig N.2

N.4 Steady-state Electron Motion with E and B fields: Magnetic Ohm's Law

We start again with the motion equation for an electron in copper,

$$m \frac{d\mathbf{v}}{dt} = q\mathbf{E} + q\mathbf{v} \times \mathbf{B} - (m/\tau) \mathbf{v} . \quad (N.1.5)$$

We now seek a steady-state solution, so the equation becomes

$$(m/\tau) \mathbf{v} = q\mathbf{E} + q\mathbf{v} \times \mathbf{B} . \quad (N.4.1)$$

Making use of the signed mobility $\mu = q\tau/m$ shown in (N.1.7), we can write (N.4.1) as

$$\mathbf{v} = \mu\mathbf{E} + \mu\mathbf{v} \times \mathbf{B}$$

or

$$\mathbf{v} - \mu\mathbf{v} \times \mathbf{B} = \mu\mathbf{E} . \quad (N.4.2)$$

The plan is to solve this equation for \mathbf{v} and then to obtain the current density using $\mathbf{J} = nq\mathbf{v}$ from (N.1.1). Recall that Ohm's Law says $\mathbf{J} = \sigma \mathbf{E}$, but with \mathbf{B} present, Ohm's Law will be different. For simplicity, we again assume $\mathbf{B} = B \hat{\mathbf{z}}$. Then

$$\mu \mathbf{v} \times \mathbf{B} = [v_x \hat{\mathbf{x}} + v_y \hat{\mathbf{y}} + v_z \hat{\mathbf{z}}] \times [\mu B \hat{\mathbf{z}}] = -v_x \mu B \hat{\mathbf{y}} + v_y \mu B \hat{\mathbf{x}}$$

so that (N.4.2) becomes

$$[v_x \hat{x} + v_y \hat{y} + v_z \hat{z}] - [-v_x \mu B \hat{y} + v_y \mu B \hat{x}] = [\mu E_x \hat{x} + \mu E_y \hat{y} + \mu E_z \hat{z}]$$

which may be decomposed into the following three equations,

$$\begin{aligned} v_x - \mu B v_y &= \mu E_x \\ v_y + \mu B v_x &= \mu E_y \\ v_z &= \mu E_z \end{aligned} \quad (N.4.3)$$

The first two equations may be expressed in matrix form

$$\begin{pmatrix} 1 & -\mu B \\ \mu B & 1 \end{pmatrix} \begin{pmatrix} v_x \\ v_y \end{pmatrix} = \mu \begin{pmatrix} E_x \\ E_y \end{pmatrix} \quad (N.4.4)$$

and then

$$\begin{pmatrix} v_x \\ v_y \end{pmatrix} = \mu \begin{pmatrix} 1 & -\mu B \\ \mu B & 1 \end{pmatrix}^{-1} \begin{pmatrix} E_x \\ E_y \end{pmatrix} \quad (N.4.5)$$

Maple tells us

```
M := matrix(2,2,[1,-mu*B,mu*B,1]);
```

$$M := \begin{bmatrix} 1 & -\mu B \\ \mu B & 1 \end{bmatrix}$$

```
inverse(M);
```

$$\begin{bmatrix} \frac{1}{1+\mu^2 B^2} & \frac{\mu B}{1+\mu^2 B^2} \\ -\frac{\mu B}{1+\mu^2 B^2} & \frac{1}{1+\mu^2 B^2} \end{bmatrix}$$

so then

$$\begin{pmatrix} v_x \\ v_y \end{pmatrix} = \frac{\mu}{1+(\mu B)^2} \begin{pmatrix} 1 & \mu B \\ -\mu B & 1 \end{pmatrix} \begin{pmatrix} E_x \\ E_y \end{pmatrix} = \frac{\mu}{1+(\mu B)^2} \begin{pmatrix} E_x + \mu B E_y \\ E_y - \mu B E_x \end{pmatrix} \quad (N.4.6)$$

But using (N.3.1) that $\omega_c \equiv (qB/m)$ one finds that

$$\mu B = (q\tau/m)B = (qB/m)\tau = \omega_c \tau \quad (N.4.7)$$

so the solutions above, combined with the known third solution $v_z = \mu E_z$, become

$$\begin{aligned}
 v_x &= \mu (E_x + \omega_c \tau E_y) \frac{1}{1 + (\omega_c \tau)^2} \\
 v_y &= \mu (E_y - \omega_c \tau E_x) \frac{1}{1 + (\omega_c \tau)^2} \\
 v_z &= \mu E_z .
 \end{aligned} \tag{N.4.8}$$

We have found our solution for \mathbf{v} ! To find \mathbf{J} , use (N.1.1) that $\mathbf{J} = nq\mathbf{v}$ and the fact that

$$nq\mu = nq(q\tau/m) = (nq^2\tau/m) = \sigma \quad // \text{ from (N.1.7) and (N.1.9)} \tag{N.4.9}$$

to find that (in agreement with (10) of Pengra),

$$\begin{aligned}
 J_x &= \sigma (E_x + \omega_c \tau E_y) \frac{1}{1 + (\omega_c \tau)^2} & \omega_c &\equiv (qB/m) \\
 J_y &= \sigma (E_y - \omega_c \tau E_x) \frac{1}{1 + (\omega_c \tau)^2} & \mathbf{B} &= B \hat{\mathbf{z}} \\
 J_z &= \sigma E_z . & \sigma &= (nq^2\tau/m)
 \end{aligned} \tag{N.4.10}$$

This is the "Magnetic Ohm's Law" which, in the presence of $\mathbf{B} = B \hat{\mathbf{z}}$, replaces the usual Ohm's Law,

$$\begin{aligned}
 J_x &= \sigma E_x \\
 J_y &= \sigma E_y \\
 J_z &= \sigma E_z
 \end{aligned} \tag{1.1.7}$$

In matrix notation one can express (N.4.10) as

$$\begin{pmatrix} J_x \\ J_y \\ J_z \end{pmatrix} = \begin{pmatrix} \sigma c & \sigma c \omega_c \tau & 0 \\ -\sigma c \omega_c \tau & \sigma & 0 \\ 0 & 0 & \sigma \end{pmatrix} \begin{pmatrix} E_x \\ E_y \\ E_z \end{pmatrix} \quad \text{where } c = \frac{1}{1 + (\omega_c \tau)^2} \tag{N.4.11}$$

or

$$\mathbf{J} = \Sigma \mathbf{E} \quad \Sigma = \begin{pmatrix} \sigma c & \sigma c \omega_c \tau & 0 \\ -\sigma c \omega_c \tau & \sigma & 0 \\ 0 & 0 & \sigma \end{pmatrix} \tag{N.4.12}$$

Since \mathbf{J} and \mathbf{E} are 3-vectors, the matrix Σ is a rank-2 tensor under rotations.

Fortunately, as will be shown below, the magnetic field strength in a transmission line is small enough so that $\omega_c \tau \ll 1$, which means that the normal Ohm's Law is justified despite the presence of B fields.

N.5 Theory of the Hall Effect Revisited

We replicate the Hall geometry from above, where recall that $\mathbf{B} = B_z \hat{\mathbf{z}}$:

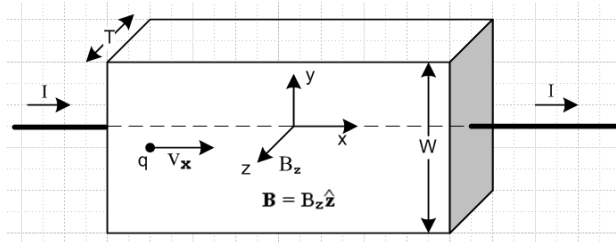


Fig N.1

Looking at the drawing, and recalling the small "defect" in the theory of Section N.3, and staring at the Magnetic Ohm's Law (N.4.10), we insist that $J_y = 0$ at least at the top and bottom faces, since as noted earlier, this current "has nowhere to go" in the steady state. Since things are generally uniform in this slab of material, we make the ansatz that $J_y \equiv 0$ everywhere in the sample. The second equation of (N.4.10) then says

$$E_y - \omega_c \tau E_x = 0 \quad \Rightarrow \quad E_y = \omega_c \tau E_x \quad (\text{N.5.1})$$

When this is inserted into the first equation we find, along with the other two equations of (N.4.10),

$$\begin{aligned} J_x &= \sigma (E_x + \omega_c \tau [\omega_c \tau E_x]) \frac{1}{1 + (\omega_c \tau)^2} = \sigma E_x \\ J_y &= 0 \\ J_z &= \sigma E_z \end{aligned} \quad (\text{N.5.2})$$

There is no reason to have $E_z \neq 0$ since the electrons are only deflected up and down. Moreover, we would like to have $J_z = 0$ on the front and back face, so $E_z \equiv 0$ is the obvious choice.

Then from (N.5.1) we must have (the last three factors on the line below are each unity),

$$\begin{aligned} E_y &= \omega_c \tau E_x = \omega_c \tau [J_x / \sigma] = \frac{\omega_c \tau J_x}{\sigma} * \frac{I}{J_x T W} * \frac{q B_z / m}{\omega_c} * \frac{\sigma}{n q^2 \tau / m} \\ &= \frac{1}{n q} * \frac{I B_z}{T W} \end{aligned} \quad (\text{N.5.3})$$

This is the Hall field ! The Hall voltage is then

$$V_H = -E_y W = \frac{1}{n q} * \frac{I B_z}{T} = -R_H \frac{I B_z}{T} \quad R_H = \frac{1}{n q} \quad (\text{N.5.4})$$

This is the same as the Hall field and voltage obtained in our previous derivation, as shown in (N.2.5) and (N.2.6). But now we end up with $J_y = 0$ so there is no vertical current having nowhere to go, nor is there front-back current, and we also have J_x doing the regular Ohm's Law as shown in (N.5.2)

$$\begin{aligned} J_x &= \sigma E_x \\ J_y &= 0 \\ J_z &= 0 . \end{aligned} \tag{N.5.5}$$

This seems a more complete solution to the Hall problem than that of Section N.2.

N.6 Theory of the Hall Effect with Multiple Carrier Types

Let index i label the types of carriers. The developments of Sections N.1 through Section N.4 carry through as is, but everything now has an i index. For example, we now have

$$\mathbf{J} = \sum_i n_i q_i \mathbf{v}_i \tag{N.1.1} \tag{N.6.1}$$

$$\mathbf{v}_i = (q_i \tau_i / m_i) \mathbf{E} = \mu_i \mathbf{E} \quad \mu_i = (q_i \tau_i / m_i) = \text{signed mobility} \tag{N.1.7} \tag{N.6.2}$$

$$\sigma_i = n_i q_i \mu_i = n_i q (q_i \tau_i / m_i) = (n_i q_i^2 \tau_i / m_i) \tag{N.1.9} \tag{N.6.3}$$

$$\mathbf{v}_i - \mu_i \mathbf{v}_i \times \mathbf{B} = \mu_i \mathbf{E} . \tag{N.4.2} \tag{N.6.4}$$

This leads to solutions for velocities \mathbf{v}_i ,

$$\begin{aligned} v_{xi} &= \mu_i (E_x + \omega_{ci} \tau_i E_y) \frac{1}{1 + (\omega_{ci} \tau_i)^2} & \omega_{ci} &\equiv (q_i B / m_i) \\ v_{yi} &= \mu_i (E_y - \omega_{ci} \tau_i E_x) \frac{1}{1 + (\omega_{ci} \tau_i)^2} & \mu_i &= (q_i \tau_i / m_i) \\ v_{zi} &= \mu_i E_z \end{aligned} \tag{N.4.8} \tag{N.6.5}$$

and we can define the total conductivity as

$$\sigma \equiv \sum_i \sigma_i . \tag{N.6.6}$$

The current densities from (N.6.1) and (N.6.5) are then, using also (N.6.3) that $\sigma_i = n_i q_i \mu_i$,

$$\begin{aligned} J_x &= \sum_i \sigma_i [(E_x + \omega_{ci} \tau_i E_y) \frac{1}{1 + (\omega_{ci} \tau_i)^2}] & \omega_{ci} &\equiv (q_i B / m_i) \\ J_y &= \sum_i \sigma_i [(E_y - \omega_{ci} \tau_i E_x) \frac{1}{1 + (\omega_{ci} \tau_i)^2}] & \omega_{ci} \tau_i &= (q_i \tau_i B / m_i) = B \mu_i \\ J_z &= \sum_i \sigma_i E_z = E_z \sum_i \sigma_i = E_z \sigma . \end{aligned} \tag{N.6.7}$$

At this point it is useful to define objects α and β having the dimensions of conductivity, and a third object which is $\gamma = \beta/B$:

$$\begin{aligned}\alpha &\equiv \sum_i \sigma_i \frac{1}{1+(\omega_{ci}\tau_i)^2} \\ \beta &\equiv \sum_i \sigma_i \frac{\omega_{ci}\tau_i}{1+(\omega_{ci}\tau_i)^2} = B \sum_i \sigma_i \frac{\mu_i}{1+(\omega_{ci}\tau_i)^2} \\ &= B \gamma \quad \gamma \equiv \sum_i \sigma_i \frac{\mu_i}{1+(\omega_{ci}\tau_i)^2} .\end{aligned}\tag{N.6.8}$$

In terms of α and β we rewrite (N.6.7) as

$$\begin{aligned}J_x &= \alpha E_x + \beta E_y \\ J_y &= \alpha E_y - \beta E_x \\ J_z &= E_z (\sum_i \sigma_i) = E_z \sigma .\end{aligned}\tag{N.6.9}$$

Our Hall effect geometry again requires that $J_y = 0$ and that $J_z = 0$ ("nowhere to go") ,

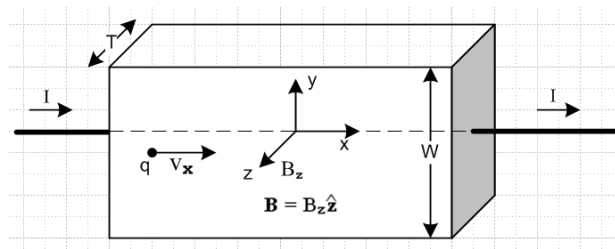


Fig N.1

so the second equation of (N.6.9) says

$$\begin{aligned}\alpha E_y &= \beta E_x \\ \text{or} \\ E_y &= (\beta/\alpha) E_x \quad // = \text{the Hall field}\end{aligned}\tag{N.6.10}$$

and this E_y is the Hall-effect electric field in the case of multiple carrier types. Inserting this into the first equation of (N.6.9) gives

$$J_x = \alpha E_x + \beta E_y = \alpha E_x + \beta (\beta/\alpha) E_x = [\alpha + \beta^2/\alpha] E_x\tag{N.6.11}$$

so our triplet of current densities is now

$$\begin{aligned}J_x &= [\alpha + \beta^2/\alpha] E_x \\ J_y &= 0 \\ J_z &= 0 .\end{aligned}\tag{N.6.12}$$

The conductivity appearing in the J_x equation we define as σ_{mx} so that

$$J_x = \sigma_{mx} E_x \quad \sigma_{mx} = \alpha + \beta^2/\alpha = \alpha(B) + B^2 \gamma(B)^2/\alpha(B)\tag{N.6.13}$$

where we must remember that α , β and γ all depend on B through each $\omega_{ci}\tau_i = B\mu_i$. In general, we have $\sigma_{mx} \neq \sigma$, so the Hall sample has a conductivity in the main current direction x which depends in a complicated manner on field B. This effect is called **magnetoresistance**. However, if there is only one carrier type, one finds that $\sigma_{mx} = \sigma$ (see below) and there is then no magnetoresistance effect, as we already saw in the first equation of (N.5.2).

The Hall field can be written

$$\begin{aligned} E_y &= (\beta/\alpha) E_x = (\beta/\alpha) [\alpha + \beta^2/\alpha]^{-1} J_x = (\beta/\alpha) [\alpha + \beta^2/\alpha]^{-1} I / (WT) \\ &= \frac{\beta}{\alpha^2 + \beta^2} I / (WT) = \frac{B\gamma}{\alpha^2 + B\gamma^2} I / (WT) = \frac{\gamma}{\alpha^2 + B\gamma^2} B I / (WT) \end{aligned} \quad (N.6.14)$$

and then the Hall voltage is

$$V_H = -E_y W = -\frac{\gamma}{\alpha^2 + B\gamma^2} B I / T \quad (N.6.15)$$

and the Hall coefficient is

$$R_H = \frac{\gamma}{\alpha^2 + \beta^2} = \frac{\gamma(B)}{[\alpha(B)]^2 + [\beta(B)]^2} . \quad (N.6.16)$$

Unlike the single-carrier case, R_H now depends on B in a complicated manner. Just to verify the single carrier case we evaluate:

$$\begin{aligned} \alpha &= \sigma \frac{1}{1 + (\omega_c \tau)^2} & \beta &= \sigma \frac{\omega_c \tau}{1 + (\omega_c \tau)^2} \gamma = \sigma \mu \frac{1}{1 + (\omega_c \tau)^2} \\ \alpha^2 + \beta^2 &= \sigma^2 \frac{1}{1 + (\omega_c \tau)^2} & R_H &= \frac{\gamma}{\alpha^2 + \beta^2} = \frac{\sigma \mu}{\sigma^2} = \mu / \sigma = (q\tau/m) / (nq^2\tau/m) = 1/(nq) \\ \sigma_{mx} &= \alpha + \beta^2/\alpha = (1/\alpha)(\alpha^2 + \beta^2) = \sigma^2/\sigma = \sigma . & & // \text{ no magnetoresistance} \end{aligned} \quad (N.6.17)$$

If we take the magnetic field B small enough so that $\omega_{ci}\tau_i \ll 1$ for all carrier types (a normal situation), where recall that $\omega_{ci} \equiv (q_i B/m_i)$, there is considerable simplification. One finds that,

$$\begin{aligned} \alpha &\equiv \sum_i \sigma_i \frac{1}{1 + (\omega_{ci}\tau_i)^2} \approx \sum_i \sigma_i = \sigma \\ \beta &= \sum_i \sigma_i \frac{\omega_{ci}\tau_i}{1 + (\omega_{ci}\tau_i)^2} \approx \sum_i \sigma_i \frac{\omega_{ci}\tau_i}{1} \ll \sum_i \sigma_i \cdot 1 \ll \sigma \\ \alpha^2 + \beta^2 &\approx \alpha^2 \approx \sigma^2 \\ \gamma &= \sum_i \sigma_i \frac{\mu_i}{1 + (\omega_{ci}\tau_i)^2} \approx \sum_i \sigma_i \mu_i . & & // \text{ signed mobilities !} \end{aligned} \quad (N.6.18)$$

Then,

$$R_H = \frac{\gamma}{\alpha^2 + \beta^2} \approx \frac{\sum_i \sigma_i \mu_i}{\sigma^2} = \frac{\sum_i \sigma_i \mu_i}{(\sum_i \sigma_i)^2} \quad (N.6.19)$$

For two charge carrier types this gives [recall (N.6.3) that $\sigma_i = n_i q_i \mu_i$],

$$R_H = \frac{\sigma_1 \mu_1 + \sigma_2 \mu_2}{(\sigma_1 + \sigma_2)^2} = \frac{n_1 q_1 \mu_1 \mu_1 + n_2 q_2 \mu_2 \mu_2}{(n_1 q_1 \mu_1 + n_2 q_2 \mu_2)^2} \quad (N.6.20)$$

Now suppose 1 = hole and 2 = electron so $q_1 = -q_2 = |e|$. Then,

$$R_H = \frac{1}{|e|} \frac{n_1 \mu_1^2 - n_2 \mu_2^2}{(n_1 \mu_1 - n_2 \mu_2)^2} \quad // \text{ signed mobilities } \mu = (q\tau/m), \text{ weak B field} \quad (N.6.21)$$

or

$$R_H = \frac{1}{|e|} \frac{n_1 \mu_1^2 - n_2 \mu_2^2}{(n_1 \mu_1 + n_2 \mu_2)^2} \quad // \text{ unsigned mobilities, } \mu = (|q|\tau/m), \text{ weak B field} \quad (N.6.22)$$

The last result is in agreement with Eq. (13) of our Pengra *et. al.* reference. The Hall coefficient could have either sign!

N.7 The Radial Hall Effect in a Round Wire

The author has had difficulty finding a treatment of this subject, but it must exist somewhere.

Consider an "isolated" infinitely long round wire of radius a carrying static current I . We use cylindrical coordinates r, θ, z with the symmetry axis along the wire center line. It is often casually claimed that the current density J_z in such a wire is uniform throughout the cross section and that there is no charge density on the surface. Here we wish to explore these claims.

In cross section, the situation is as follows:

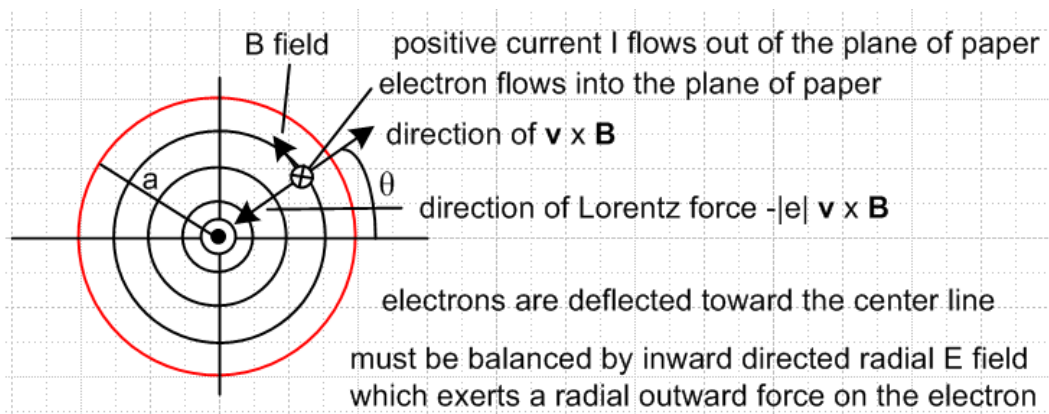


Fig N.2

Each electron sees the magnetic field \mathbf{B} created by all the other flowing electrons. At any azimuthal location θ , the electrons are deflected toward the center line by this \mathbf{B} field, causing a free charge

distribution inside the wire which results in a radial field component E_r . This radial Hall field then offsets the deflection resulting in all electrons flowing exactly in the z direction.

This problem differs from the regular Hall effect problem studied in Sections N.2 and N.5 in two major ways: (1) The magnetic field is generated *by* the flowing current under study, it is not externally applied; (2) the magnetic field is non-uniform and in fact is a function of r .

We shall use the method of Section N.5 to determine the E_r field and the associated charge distribution. The three unit vectors \hat{x} , \hat{y} , \hat{z} of that section can be replaced by the cylindrical unit vectors \hat{r} , $\hat{\theta}$, \hat{z} where the usual cyclic sense of unit vector cross products is then maintained. In a cross section of the round wire, r and θ are then "the usual" polar coordinates, while the z axis comes out of the plane of paper.

Since the situation is static, one must have $\text{curl } \mathbf{E} = 0$. But in cylindrical coordinates,

$$\text{curl } \mathbf{E} = \hat{r} [\underset{1}{r^{-1}\partial_{\theta}E_z} - \underset{2}{\partial_z E_{\theta}}] + \hat{\theta} [\underset{3}{\partial_z E_r} - \underset{4}{\partial_r E_z}] + \hat{z} [\underset{5}{r^{-1}\partial_r(rE_{\theta})} - \underset{6}{r^{-1}\partial_{\theta}E_r}] .$$

We certainly expect to have $E_{\theta} = 0$ at $r = a$ since the round wire surface should be an electrostatic equipotential, and it seems reasonable to have $E_{\theta} = 0$ everywhere inside the wire, so we set $E_{\theta} = 0$ as an ansatz in a search for a Maxwell-Equations solution, and this knocks out terms 2 and 5. Any term with ∂_z must also vanish since the wire is static and infinite in length, killing off terms 2 and 3. Since the wire is in isolation, the field pattern must be azimuthally symmetric, so ∂_{θ} terms vanish, killing off 1 and 6. Having thus removed terms 1,2,3,5,6, we are left only with term 4 so

$$\text{curl } \mathbf{E} = \hat{\theta} [-\partial_r E_z] . \quad (\text{N.7.1})$$

Since the static situation requires $\text{curl } \mathbf{E} = 0$, we end up with

$$\partial_r E_z(r, \theta, z) = \partial_r E_z(r) = 0 \quad \Rightarrow \quad E_z(r) = \text{constant} . \quad (\text{N.7.2})$$

Recalling from Section N.4 that Ohm's Law can be affected by magnetic fields, we now make a second ansatz which is that the regular Ohm's Law applies in the z direction. We then obtain

$$\mathbf{J}_z(r) = \sigma E_z(r) = \text{constant} \quad \mathbf{J}_z = \text{uniform} \quad (\text{N.7.3})$$

and in this way we arrive at a uniform \mathbf{J}_z in the wire, but we need to verify that our assumptions made so far are consistent with other requirements. Given then that \mathbf{J}_z is constant in r and θ , we can compute the magnetic field inside the wire from Ampere's Law in the usual fashion,

$$2\pi r H(r) = \frac{\pi r^2}{\pi a^2} I \quad \Rightarrow \quad H(r) = \frac{I}{2\pi a} (r/a) \quad \Rightarrow \quad \mathbf{B}(r) = \frac{\mu_0 I}{2\pi a} (r/a) \hat{\theta} = B(r) \hat{\theta} \quad (\text{N.7.4})$$

Here we make a third ansatz that the other two \mathbf{B} field components are 0. Note that μ_0 is magnetic permeability, while μ to appear below is the (signed) electron mobility.

At this point, we recall the static equation (N.4.2) arising from the Lorentz force and collision friction,

$$\mathbf{v} - \mu \mathbf{v} \times \mathbf{B} = \mu \mathbf{E} \quad (N.4.2) \quad (N.7.5)$$

and we solve for \mathbf{v} using the method of Section N.4. First,

$$\mu \mathbf{v} \times \mathbf{B} = [v_x \hat{\mathbf{r}} + v_\theta \hat{\boldsymbol{\theta}} + v_z \hat{\mathbf{z}}] \times [\mu B \hat{\boldsymbol{\theta}}] = v_x \mu B \hat{\mathbf{z}} - v_z \mu B \hat{\mathbf{r}}$$

$$\mathbf{v} = v_x \hat{\mathbf{r}} + v_\theta \hat{\boldsymbol{\theta}} + v_z \hat{\mathbf{z}}$$

Then (N.7.5) becomes

$$[v_x \hat{\mathbf{r}} + v_\theta \hat{\boldsymbol{\theta}} + v_z \hat{\mathbf{z}}] - [v_x \mu B \hat{\mathbf{z}} - v_z \mu B \hat{\mathbf{r}}] = \mu E_x \hat{\mathbf{r}} + \mu E_\theta \hat{\boldsymbol{\theta}} + \mu E_z \hat{\mathbf{z}}$$

which may be decomposed into the following three equations (here in z,r,\theta order),

$$\begin{aligned} v_z - \mu B v_x &= \mu E_z \\ v_x + \mu B v_z &= \mu E_x \\ v_\theta &= \mu E_\theta \end{aligned} \quad (N.7.6)$$

We note that the first two equations of (N.7.6) have the same form as the first two equations in (N.4.3) which were

$$\begin{aligned} v_x - \mu B v_y &= \mu E_x \\ v_y + \mu B v_x &= \mu E_y \end{aligned} \quad (N.4.3)$$

Taking then the previous solution with $(x,y) \rightarrow (z,r)$ we find from (N.4.8) that

$$\begin{aligned} v_z &= \mu (E_z + \omega_c \tau E_x) \frac{1}{1 + (\omega_c \tau)^2} \\ v_x &= \mu (E_x - \omega_c \tau E_z) \frac{1}{1 + (\omega_c \tau)^2} \\ v_\theta &= \mu E_\theta \end{aligned} \quad (N.7.7)$$

where we have carried down the third equation from above. Recall that the cyclotron frequency ω_c enters the picture since $\mu B = \omega_c \tau$ as shown in (N.4.7). However, now since $B = B(r)$, we have $\omega_c = \omega_c(r) = qB(r)/m$. Nothing in the development of Section N.4 precluded the B field from having spatial dependence because no spatial derivatives (like curl or div) were involved.

The next step is to use (N.1.1) that $\mathbf{J} = nq\mathbf{v}$ and the fact (N.4.9) that $nq\mu = \sigma$ to obtain,

$$\begin{aligned} \mathbf{J}_z &= \sigma (E_z + \omega_c \tau E_x) \frac{1}{1 + (\omega_c \tau)^2} & \omega_c &\equiv (qB/m) \\ \mathbf{J}_x &= \sigma (E_x - \omega_c \tau E_z) \frac{1}{1 + (\omega_c \tau)^2} & \mathbf{B} &= B \hat{\boldsymbol{\theta}} \\ \mathbf{J}_\theta &= \sigma E_\theta & \sigma &= (nq^2 \tau / m) \end{aligned} \quad (N.7.8)$$

Since the radial current at the surface "has nowhere to go" we set $J_r = 0$ just as we set $J_y = 0$ in the Hall effect analysis of Section N.5. One then finds

$$E_r = \omega_c \tau E_z \quad (\text{N.7.9})$$

where E_r is a radial Hall field. Insertion of (N.7.9) into the first line of (N.7.8) gives

$$J_z = \sigma (E_z + \omega_c \tau [\omega_c \tau E_z]) \frac{1}{1 + (\omega_c \tau)^2} = \sigma E_z \quad (\text{N.7.10})$$

and then our current components are

$$\begin{aligned} J_z &= \sigma E_z \\ J_r &= 0 \\ J_\theta &= 0 \end{aligned} \quad (\text{N.7.11})$$

where in the last line we have applied our ansatz that $E_\theta = 0$. Our earlier assumption that the regular Ohm's Law applies in the z direction is now self-consistently born out.

The radial Hall field from (N.7.9) is

$$E_r(r) = \omega_c(r) \tau E_z = (qB(r)/m) \tau E_z = (q\tau/m) B(r) E_z = \mu B(r) E_z \quad // \text{ (N.1.7) for } \mu$$

$$= \mu * \frac{\mu_0 I}{2\pi a} (r/a) * \frac{J_z}{\sigma} \quad // \text{ (N.7.4) for } B(r) \text{ and (N.7.11) for } E_z$$

$$= \frac{\mu}{\sigma} * \frac{\mu_0 I}{2\pi a} (r/a) * \frac{I}{\pi a^2} = \frac{1}{nq} * \frac{\mu_0 I^2}{2\pi^2 a^3} (r/a) \quad // \text{ (N.1.9) for } \mu/\sigma$$

$$= \frac{\mu_0 I^2}{2\pi^2 a^3 nq} (r/a) \equiv E_s (r/a) \quad (\text{N.7.12})$$

where

$$E_s \equiv E_r(a) = \frac{\mu_0 I^2}{2\pi^2 a^3 nq} \text{ volts/m} . \quad // E_s < 0 \text{ since } q = -|e| \quad (\text{N.7.13})$$

The three electric field components are then

$$\begin{aligned} E_z &= I / (\pi a^2) \\ E_r &= E_s (r/a) \\ E_\theta &= 0 . \end{aligned} \quad (\text{N.7.14})$$

We may then compute $\text{div } \mathbf{E}$,

$$\begin{aligned}\operatorname{div} \mathbf{E} &= r^{-1} \partial_{\mathbf{r}}(r E_{\mathbf{r}}) + r^{-1} \partial_{\theta} E_{\theta} + \partial_{\mathbf{z}} E_{\mathbf{z}} = r^{-1} \partial_{\mathbf{r}}(r E_{\mathbf{r}}) \\ &= r^{-1} \partial_{\mathbf{r}}(r [E_{\mathbf{s}}(r/a)]) = (E_{\mathbf{s}}/a) r^{-1} \partial_{\mathbf{r}}(r^2) = (E_{\mathbf{s}}/a) r^{-1} 2r = (2E_{\mathbf{s}}/a)\end{aligned}\quad (\text{N.7.15})$$

Since $\operatorname{div} \mathbf{E} = \rho/\epsilon_0$, we conclude that there must be a constant free charge density inside the wire,

$$\rho = \epsilon_0(2E_{\mathbf{s}}/a) . \quad (\text{N.7.16})$$

In a slice of the round wire of length dz , the total internal charge is

$$Q = \rho * (\text{area}) * dz = \rho \pi a^2 dz = \epsilon_0(2E_{\mathbf{s}}/a) \pi a^2 dz = \epsilon_0(2\pi a E_{\mathbf{s}}) dz . \quad (\text{N.7.17})$$

Since this charge had to come from somewhere, we conclude that the outer surface of the wire slice has charge - Q and surface charge density $n_{\mathbf{s}}$

$$n_{\mathbf{s}} = -Q/(2\pi a dz) = -\epsilon_0(2\pi a E_{\mathbf{s}}) dz / (2\pi a dz) = -\epsilon_0 E_{\mathbf{s}} , \quad (\text{N.7.18})$$

a result one could also obtain from a gaussian box at the surface. Outside the wire, each charge density acts as a line charge at the wire center and they cancel out, so there is no external Hall field.

There exists a Hall voltage between the wire surface and the wire's center line,

$$\begin{aligned}V_{\mathbf{H}} &= V(a) - V(0) = \int_0^a \frac{dV}{dr} dr = - \int_0^a E_{\mathbf{r}}(r) dr = -(E_{\mathbf{s}}/a) \int_0^a r dr \\ &= -(a/2)E_{\mathbf{s}} = -(a/2) \frac{\mu_0 I^2}{2\pi^2 a^3 nq} = -\frac{1}{nq} * \frac{\mu_0 I}{2\pi a} * \frac{I}{2\pi a} = -\frac{1}{nq} * B_{\theta}(a) * \frac{I}{2\pi a}\end{aligned}\quad (\text{N.7.19})$$

so

$$V_{\mathbf{H}} = -R_{\mathbf{H}} [B_{\theta}(a)/2\pi] I / a \quad R_{\mathbf{H}} = \frac{1}{nq} \quad (\text{N.7.20})$$

which we compare to the normal Hall effect result (N.2.6)

$$V_{\mathbf{H}} = -R_{\mathbf{H}} B_{\mathbf{z}} I / T . \quad // \text{ the Hall voltage} \quad (\text{N.2.5})$$

The $R_{\mathbf{H}}$ is the same in both geometries, but the thickness T is replaced by radius a , and the uniform Hall B field is replaced by $B_{\theta}(a)/2\pi$. We make this arbitrary partitioning of the factors since radius a seems the distance that most corresponds to thickness T of the normal Hall effect.

It is certainly unclear how one would measure this radial Hall voltage, since it is rather difficult to place one of the voltmeter probes on the center line of a round copper wire, but doubtless this could be managed in some manner.

Radial Hall Effect Hypothetical Experiment

We have shown in (N.7.19) that

$$V_H = -(a/2)E_s = -(a/2)\frac{\mu_0 I^2}{2\pi^2 a^3 n q} = -\frac{\mu_0 I^2}{4\pi^2 a^2 n q} = -\frac{\mu_0}{4\pi^2 n q} (I/a)^2. \quad (\text{N.7.21})$$

We would like to maximize I/a in order to maximize V_H , but we don't want our wire to melt. According to <http://www.powerstream.com/wire-fusing-currents.htm>, a fairly large I/a ratio of 45 (SI) is provided by an AWG #16 copper wire having a diameter $d = 1.29$ mm and a fusing current of 117 amps, so we shall run this lab experiment optimistically with $I = 100$ amps. What voltage V_H might one observe? We have Maple evaluate these quantities:

$$E_s = \frac{\mu_0 I^2}{2\pi^2 a^3 n q} \text{ volts/m}$$

$$V_H = -(a/2)E_s \text{ volts}$$

$$v_z = J_z/nq = (I/\pi a^2)(1/nq) = I/(\pi a^2 n q) \text{ m/sec}$$

```

Es := u0*I^2/(2*Pi^2*a^3*n*q);      I := 100*amp:
Es = 1/2 * u0 I^2 / (pi^2 a^3 n q)  a := (1/2)*1.29e-3*m:
                                     evalf(Es);
                                     -0.001744464238 volt/m
hen := volt*sec/amp:                VH := evalf(-Es*a/2);
amp := cou/sec:                     VH = .5625897169 10-7 volt
far := cou/volt:                    vx := I/(Pi*a^2*n*q);
n := 8.5e28*m^(-3):                 vx = -.01767427721 m/sec pi
q := -1.6e-19*cou:
u0 := 4*Pi*1e-7*hen/m:
e0 := 8.85e-12*far/m:

```

The results are then

$$E_r(a-\epsilon) = E_s = -0.17 \text{ mV/m}$$

$$V_H = 56 \text{ nV}$$

$$v_x = -18 \text{ mm/sec}$$

(N.7.22)

which can be compared with the results of our "regular" Hall effect experiment shown in (N.2.9). The Hall field is about 10x smaller, the Hall voltage about 350x smaller, and the drift velocity 45x larger.

The Hall field just below the surface is $E_r(a) = E_s = -174 \mu\text{V/m}$ and decreases linearly to 0 at the wire center. Just outside the surface the field is zero since it is cancelled by the surface charge.

The internal charge density ρ and the surface charge density n are then,

<pre>rho := evalf(e0*2*Es/a); rho = -.4787134420 10⁻¹¹ $\frac{Coul}{m^3}$ rho/q; .2991959013 10⁸ $\frac{1}{m^3}$ (rho/q)/n; .3519951780 10⁻²¹</pre>	<pre>ns := evalf(-e0*Es); ns = .1543850850 10⁻¹⁴ $\frac{Coul}{m^2}$ ns/q; -9649.067813 $\frac{1}{m^2}$ Ba := u0*I/(2*Pi*a); Ba = .03100775194 $\frac{volt\ sec}{m^2}$</pre>
--	---

The internal constant negative charge density ρ is very small and represents an excess of about 1 electron for every 10^{21} conduction electrons. The positive surface charge n_s is also tiny, being a deficiency of only 10,000 electrons per square meter.

One reason the radial Hall effect is small is that the self-created B field is relatively small. On the right above Maple shows our lab example field is $B_\theta(a) = .03T = 300$ gauss, whereas in the Section N.2 the external B field was assumed to be $0.5 T = 5000$ gauss.

So why were we allowed to ignore the self-generated B field in the regular Hall effect of Fig N.1? Presumably the "radial" Hall effect due to the (not shown) self-generated B field will create an internal and surface charge distribution pattern (and an internal Hall field) in Fig N.1 that is mirror-symmetric in the $y = 0$ plane. Thus, the regular Hall field E_y gets equal and opposite radial Hall effect contributions above and below this plane and is therefore not affected by superposing the two problems.

Reader Exercise: Calculate the "radial Hall effect" for a rectangular wire like that in Fig N.1

Conclusions. In the above analysis, we made certain assumptions ($E_\theta = 0$, $J_z = \sigma E_z$, and $\mathbf{B} = B\hat{\theta}$) in seeking a solution for the E and B fields of an isolated, axially symmetric infinite round wire carrying static current I. We found a solution which satisfies all four Maxwell equations, and since solutions are unique, that is *the* solution to the problem. The characteristics of this solution are:

1. There exist no radial or azimuthal current densities inside the wire, $J_r = J_\theta = 0$. The only current density is J_z .
2. This current density J_z is uniform over the wire cross section, so $J_z = I/(\pi a^2)$.
3. The regular Ohm's Law applies to J_z , so that $J_z = \sigma E_z$.
4. The magnetic field inside the wire is given by $\mathbf{B}(r) = \frac{\mu_0 I}{2\pi a} (r/a) \hat{\theta}$.
5. In order to balance internal radial Lorentz deflections of the current-carrying electrons, a very small internal radial E_r Hall field exists inside the wire which is directed toward the center line and has the form

$$E_r(r) = E_s (r/a) \quad \text{where } E_s = - \frac{\mu_0 I^2}{2\pi^2 a^3 n|e|} \quad (N.7.12)$$

6. Associated with this radial Hall field is a very small, negative, constant free charge distribution inside the wire which is given by

$$\rho = \epsilon_0(2E_s/a) \qquad Q = \rho \pi a^2 dz = \epsilon_0(2\pi a E_s)dz$$

7. This fact contradicts (but in a very small way) the claim of Section 3.1 that there can be no free charge inside a conductor. That section did not include the possible effect of magnetic fields.

8. This negative volume charge is extracted from the wire surface which then has a positive surface charge which is equal and opposite to Q shown above. Observed from outside the wire, the electric fields of these two charge distributions exactly cancel, resulting in no external radial E field.

9. We refer to the last items 5,6,7,8 above as "the radial Hall effect", for want of a better term.

10. It is hard to imagine how would might measure this effect.

N.8 Magnetic Ohm's Law for Arbitrary B

Section N.4 developed a Magnetic Ohm's Law for $\mathbf{B} = B\hat{z}$. Now allow $\mathbf{B}(\mathbf{x})$ to point in a general direction with components B_1 , B_2 and B_3 and consider a DC static situation. Equation (N.4.2) then says,

$$\kappa \mathbf{v} = \mathbf{E} + \mathbf{v} \times \mathbf{B} \quad \text{where} \quad \kappa \equiv 1/\mu \qquad // \mu = (q\tau/m) \text{ from (N.1.7)} \qquad \text{(N.8.1)}$$

or

$$\begin{aligned} \kappa v_1 &= E_1 + v_2 B_3 - v_3 B_2 \\ \kappa v_2 &= E_2 + v_3 B_1 - v_1 B_3 \\ \kappa v_3 &= E_3 + v_1 B_2 - v_2 B_1 \end{aligned} \qquad \text{(N.8.2)}$$

Notice that $\dim(\kappa) = \dim(B) = \text{Tesla}$. Maple solves this vector equation for the velocity components v_i :

```

[ > eq1 := kappa*v1 - B3*v2 + B2*v3 = E1;
  eq1 := kappa*v1 - B3*v2 + B2*v3 = E1
[ > eq2 := kappa*v2 - B1*v3 + B3*v1 = E2;
  eq2 := kappa*v2 - B1*v3 + B3*v1 = E2
[ > eq3 := kappa*v3 - B2*v1 + B1*v2 = E3;
  eq3 := kappa*v3 - B2*v1 + B1*v2 = E3
[ > f := solve({eq1,eq2,eq3},{v1,v2,v3});
  f := {
    v2 = (B2*B3*E3 - E1*B3*kappa + kappa^2*E2 + kappa*B1*E3 + E2*B2^2 + B1*B2*E1) /
          (kappa*(B2^2 + B1^2 + kappa^2 + B3^2)),
    v3 = (B2*kappa*E1 - B1*kappa*E2 + B1*B3*E1 + B2*E2*B3 + E3*kappa^2 + E3*B3^2) /
          (kappa*(B2^2 + B1^2 + kappa^2 + B3^2)),
    v1 = (-kappa*B2*E3 + kappa^2*E1 + B1^2*E1 + B1*B2*E2 + B1*E3*B3 + kappa*E2*B3) /
          (kappa*(B2^2 + B1^2 + kappa^2 + B3^2))
  }

```

From (N.1.8) and (N.1.9) we know that $\mathbf{J} = nq\mathbf{v} = (\sigma/\mu)\mathbf{v} = \kappa\sigma \mathbf{v}$. Extracting the v_i from the above Maple solution and multiplying by $\kappa\sigma$ we get

$$J1 := \kappa\sigma v1;$$

$$J1 = \frac{\sigma(-\kappa B2 E3 + \kappa^2 E1 + B1^2 E1 + B1 B2 E2 + B1 E3 B3 + \kappa E2 B3)}{B2^2 + B1^2 + \kappa^2 + B3^2}$$

$$J2 := \kappa\sigma v2;$$

$$J2 = \frac{\sigma(B2 B3 E3 - E1 B3 \kappa + \kappa^2 E2 + \kappa B1 E3 + E2 B2^2 + B1 B2 E1)}{B2^2 + B1^2 + \kappa^2 + B3^2}$$

$$J3 := \kappa\sigma v3;$$

$$J3 = \frac{\sigma(B2 \kappa E1 - B1 \kappa E2 + B1 B3 E1 + B2 E2 B3 + E3 \kappa^2 + E3 B3^2)}{B2^2 + B1^2 + \kappa^2 + B3^2}$$

(N.8.3)

which is our new and very complicated tensor Magnetic Ohm's Law in the presence of an arbitrary \mathbf{E} and \mathbf{B} field. That is to say, we have $\mathbf{J} = \Sigma \mathbf{E}$ where Σ is a 3x3 matrix which is a function of the B_i . If we could ignore the three B_i components (set them to zero in the above equations), the equations would reduce to the regular Ohm's Law $J_i = \sigma E_i$. This is in effect the case if $|B_i| \ll |\kappa|$ for all three components of \mathbf{B} . So a condition for the tensor Ohm's Law reducing to the regular Ohm's law is this,

$$|B_i| \ll |\kappa| \quad \kappa = 1/\mu \quad \mu = (q\tau/m) \quad \kappa = (m/q\tau) , \quad (N.8.4)$$

so we need then

$$|B_i| \ll (m/q\tau) . \quad // \text{ same as } |\omega_{c,i}\tau| \ll 1 \text{ where } (\omega_{c,i}\tau) \equiv (qB_i/m) \quad (N.8.5)$$

For copper, we compute $\kappa = m/q\tau$ using numbers from Section N.1,

$$me := 9.109e-31 * kg;$$

$$me = .9109 \cdot 10^{-30} \text{ kg}$$

$$\tau := 1e-14 * sec;$$

$$\tau = .1 \cdot 10^{-13} \text{ sec}$$

$$kg := cou * volt * sec^2 * m^2;$$

$$kg = cou \text{ volt sec}^2 \text{ m}^2$$

$$\kappa := me / (q * \tau);$$

$$\kappa = -569.3125000 \text{ volt sec m}^2$$

Our conclusion is that "regular Ohm's Law" is applicable as long as $|B_i| \ll 569$ Tesla. Even the largest practical B fields are far below this number. From wiki:

Examples [\[edit\]](#)

Main article: Orders of magnitude (magnetic field)

- 31.869 μT (3.1×10^{-5} T) – strength of Earth's magnetic field at 0° latitude, 0° longitude
- 5 mT – the strength of a typical [refrigerator magnet](#)
- 0.3 T – the strength of solar sunspots
- 1.25 T – magnetic field intensity at the surface of a [neodymium magnet](#)
- 1 T to 2.4 T – coil gap of a typical loudspeaker magnet
- 1.5 T to 3 T – strength of medical magnetic resonance imaging systems in practice, experimentally up to 17 T^[9]
- 4 T – strength of the [superconducting](#) magnet built around the [CMS detector](#) at [CERN](#)^[10]
- 8 T – the strength of [LHC](#) magnets.
- 11.75 T – the strength of INUMAC magnets, largest MRI scanner.^[11]
- 13 T – strength of the superconducting [ITER](#) magnet system ^[12]
- 16 T – magnetic field strength required to levitate a frog,^[13] according to the 2000 [Ig Nobel Prize](#) in Physics.^[14]

So even the Large Hadron Collider designers and frog levitators can use regular Ohm's Law (along with the writer of Chapter 1 and Appendix D of this document).

So why do we need to use the Magnetic Ohm's Law when dealing with the Hall Effect which has a relatively small B field? Recall (N.4.10),

$$\begin{aligned} J_x &= \sigma (E_x + \omega_c \tau E_y) \frac{1}{1 + (\omega_c \tau)^2} & \omega_c &\equiv (qB/m) \\ J_y &= \sigma (E_y - \omega_c \tau E_x) \frac{1}{1 + (\omega_c \tau)^2} & \mathbf{B} &= B \hat{z} \\ J_z &= \sigma E_z & \sigma &= (nq^2 \tau / m) \end{aligned} \quad (N.4.10)$$

In the Hall experiment of Fig N.1 we must have $J_y = 0$ and that means we cannot ignore the second term in the J_y expression above, which implies $E_y = \omega_c \tau E_x$ as in (N.5.3). Were we to prematurely set $\omega_c \tau = 0$, the Hall effect would go away since then $E_y = 0$. Although $\omega_c \tau \ll 1$, E_y is still a finite value, albeit a very small finite value.

One can repeat the above analysis to get a tensor Magnetic Ohm's Law for a monochromatic AC situation by replacing $\kappa \rightarrow \kappa [1 + j\omega\tau]$ in (N.8.1), based on (N.1.5) with $\partial_t \rightarrow j\omega$. As shown at the end of Section N.1, for copper $\omega\tau \ll 1$ for $f \ll 16,000$ GHz, so this κ replacement has a miniscule effect and our conclusions above still apply.

Appendix O: How to plot 2D magnetic field lines

Maple 18 and earlier versions can plot field lines (flow lines) given a function and a starting point using a certain vector calculus library package. Here we review the theory of such plots and show how the plots can be made directly. The methods given here can easily be generalized to make 3D plots.

(a) Statement of the Problem

One is given two functions $H_x(x,y)$ and $H_y(x,y)$ which describe a 2D vector field $\mathbf{H}(x,y)$. This field can be directly plotted in Maple in terms of little arrows as shown for example in Fig C.2 (code shown there) using the Maple fieldplot command (this is for a rectangular conductor with a uniform current density),

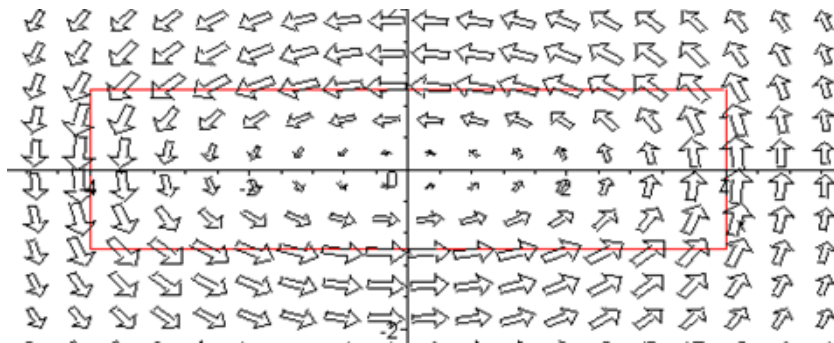


Fig O.1

But we want field *lines*, not field *arrows*. One can vaguely deduce the field lines from the above picture, but we want a precise plot.

(b) The Brute Force Method

To track a field line, one can write a small spatial displacement $d\mathbf{r}$ in the direction of \mathbf{H} ,

$$d\mathbf{r} = ds \mathbf{H}(\mathbf{r}) . \quad (\text{O.1})$$

The field line plotting code is then (pseudo Maple syntax)

```
ds = .01           // some small number relative to the problem at hand
r[1] = r1         // pick some starting point of interest for a field line
for n from 1 to 100 do
  dr = ds * H(r[n]) // compute a small displacement in the direction of H
  r[n+1] = r[n] + dr // update position for use in next iteration
od
plot the list of points r[n] // this is then a field line (listplot, pointplot, etc) (O.2)
```

One might gussy up the code to prevent wasted computation in locations where \mathbf{H} is very small, perhaps computing $\hat{\mathbf{H}} = \mathbf{H} / |\mathbf{H}|$ in each iteration then doing $d\mathbf{r} = ds * \hat{\mathbf{H}}$. A different kind of improvement would be to use some kind of quadratic Simpson's Rule affair.

The code above works fine, but error can build up for any finite ds . When a field line is a closed curve, the error can become visible where the line returns to its starting point, as in the drawing below which shows some brute-force-method \mathbf{H} fields lines corresponding to Fig O.1 above,

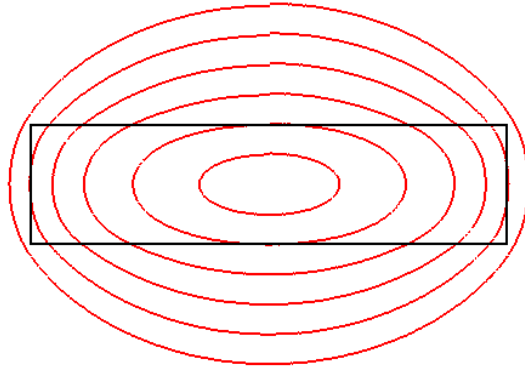


Fig O.2

The field lines may seem a little surprising given the look of Fig O.1, but here is a superposition with the rectangles lined up,

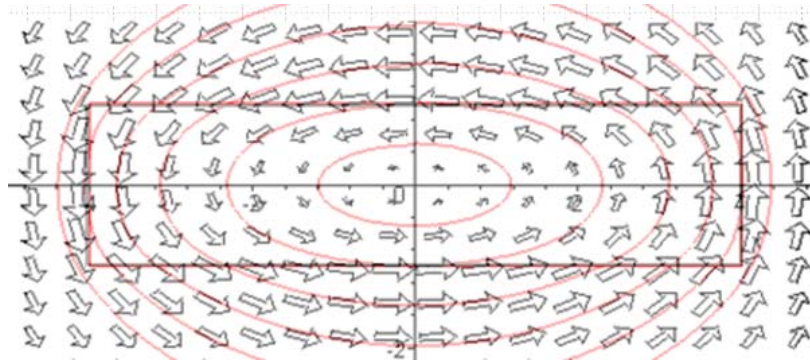


Fig O.3

(c) The ODE Method

We outline now an alternate (and doubtless well-known) method of plotting field lines. We imagine that the description of our field \mathbf{H} can be described by a pair of parametric equations (not yet known),

$$\begin{aligned} x &= X(s) \\ y &= Y(s) \end{aligned} \tag{O.3}$$

where s is a real parameter. It follows that

$$\begin{aligned} dx &= (dX/ds)ds & d\mathbf{r} &= (dX/ds)ds \hat{\mathbf{x}} + (dY/ds)ds \hat{\mathbf{y}} \\ dy &= (dY/ds)ds \end{aligned} \tag{O.4}$$

We alter (O.1) by adding a "speed function" $\alpha(s)$ just because this might simplify calculations later. This function α is an arbitrary positive-definite function of parameter s . So,

$$d\mathbf{r} = \alpha(s) ds \mathbf{H} . \tag{O.5}$$

Then (O.4) and (O.5) give

$$\alpha(s) ds \mathbf{H} = (dX/ds)ds \hat{\mathbf{x}} + (dY/ds)ds \hat{\mathbf{y}}$$

$$\alpha(s) ds [H_x(x,y) \hat{\mathbf{x}} + H_y(x,y) \hat{\mathbf{y}}] = (dX/ds)ds \hat{\mathbf{x}} + (dY/ds)ds \hat{\mathbf{y}}$$

$$\alpha(s) H_x(x,y) = (dX/ds)$$

$$\alpha(s) H_y(x,y) = (dY/ds) \quad // \text{ component equations}$$

$$(dX/ds) = \alpha(s) H_x(X(s),Y(s))$$

$$(dY/ds) = \alpha(s) H_y(X(s),Y(s)) . \tag{O.6} \quad // \text{ using (O.3)}$$

This is a pair of coupled, non-linear, first order differential equations. Conveniently, Maple knows how to numerically (and quickly) solve such a set of equations using its dsolve command (NDSolve in Mathematica). Given the solutions X(s) and Y(s), it is then a simple matter to plot the field lines. This is done in the following example.

Example: Magnetic field lines for a two-cylinder transmission line

In this example we assume that the current density in each conductor is uniform over the conductor cross section. This assumption is incorrect for a properly terminated transmission line as shown in Section 6.5, but is valid at DC and low ω for a finite-length pair of parallel wires perhaps shorted at one end to form a closed circuit. Nevertheless, we make the uniform current density approximation for a transmission line just to have a simple plotting example.

Our first task is to derive expressions for the magnetic field components H_x and H_y . Consider this drawing of the transmission line cross section (radii are a_1 and a_2 , center separation b) :

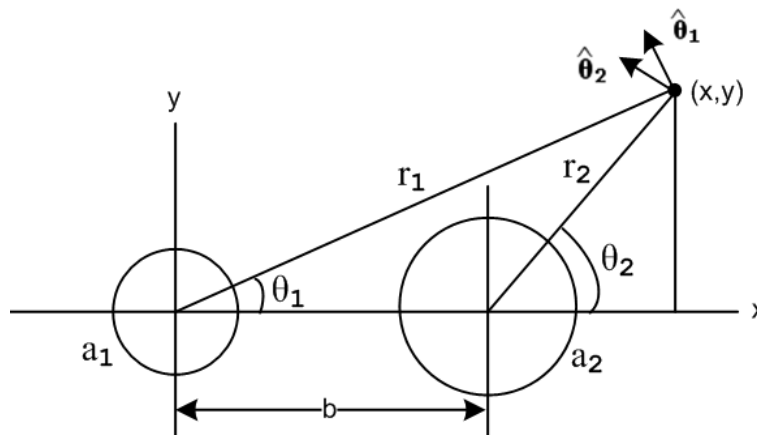


Fig O.4

Current I flows into the plane of paper for the left conductor, and out of the plane for the right. We must do a vector addition of the two magnetic fields,

$$\mathbf{H} = H_1(r_1) \hat{\boldsymbol{\theta}}_1 + H_2(r_2) \hat{\boldsymbol{\theta}}_2 \quad (\text{O.7})$$

where

$$\begin{aligned} \hat{\boldsymbol{\theta}}_1 &= -\sin\theta_1 \hat{\mathbf{x}} + \cos\theta_1 \hat{\mathbf{y}} \\ \hat{\boldsymbol{\theta}}_2 &= -\sin\theta_2 \hat{\mathbf{x}} + \cos\theta_2 \hat{\mathbf{y}} . \end{aligned} \quad (\text{O.8})$$

From Ampere's Law for each conductor, as shown in (B.4.1) and (B.4.2), the field magnitudes are

$$\begin{aligned} H_1(r_1) &= (I/2\pi) [\theta(r_1 > a_1) (1/r_1) + \theta(a_1 > r_1) (r_1/a_1^2)] \\ H_2(r_2) &= -(I/2\pi) [\theta(r_2 > a_2) (1/r_2) + \theta(a_2 > r_2) (r_2/a_2^2)] \end{aligned} \quad (\text{O.9})$$

where $\theta(x > y) = H(x-y)$, the Heaviside step function. One then has from (O.7),

$$\begin{aligned} \mathbf{H} &= H_1(r_1) [-\sin\theta_1 \hat{\mathbf{x}} + \cos\theta_1 \hat{\mathbf{y}}] + H_2(r_2) [-\sin\theta_2 \hat{\mathbf{x}} + \cos\theta_2 \hat{\mathbf{y}}] \\ &= [-\sin\theta_1 H_1(r_1) - \sin\theta_2 H_2(r_2)] \hat{\mathbf{x}} + [\cos\theta_1 H_1(r_1) + \cos\theta_2 H_2(r_2)] \hat{\mathbf{y}} . \end{aligned}$$

But

$$\begin{aligned} \cos\theta_1 &= (x/r_1) & \sin\theta_1 &= (y/r_1) \\ \cos\theta_2 &= ((x-b)/r_2) & \sin\theta_2 &= (y/r_2) \end{aligned} \quad (\text{O.10})$$

so

$$\mathbf{H} = [- (y/r_1) H_1(r_1) - (y/r_2) H_2(r_2)] \hat{\mathbf{x}} + [(x/r_1) H_1(r_1) + ((x-b)/r_2) H_2(r_2)] \hat{\mathbf{y}}$$

and the magnetic component fields are then

$$\begin{aligned} H_{\mathbf{x}} &= - (y/r_1) H_1(r_1) - (y/r_2) H_2(r_2) & r_1^2 &= x^2 + y^2 \\ H_{\mathbf{y}} &= (x/r_1) H_1(r_1) + ((x-b)/r_2) H_2(r_2) & r_2^2 &= (x-b)^2 + y^2 . \end{aligned} \quad (\text{O.11})$$

We now enter the expressions (O.11) and (O.9) for the field components into Maple, setting the current arbitrarily to $I = 2\pi$ units. Both conductor radii are set to 0.5 unit with center separation 1.25 units :

```
restart; alias(I=I, j=sqrt(-1)): with(plots):with(plottools):
K := I/(2*Pi):
I := 2*Pi:
Hx := - (y/r1)*H1 - (y/r2)*H2:
Hy := (x/r1)*H1 + ((x-b)/r2)*H2:
H1 := K*(Heaviside(r1-a1)*(1/r1) + Heaviside(a1-r1)*(r1/a1^2)):
H2 := -K*(Heaviside(r2-a2)*(1/r2) + Heaviside(a2-r2)*(r2/a2^2)):
r1 := sqrt(x^2+y^2):
r2 := sqrt((x-b)^2+y^2):
b := 1.25: a1 := 0.5: a2 := 0.5:
```

The conventional Maple "field plot" can then be done this way :

```

c1 := circle([0,0],a1,color=red):
c2 := circle([b,0],a2,color=red):
p := fieldplot([Hx,Hy],x=-1..2,y=-1..1,arrows = THICK,scaling=constrained,grid
= [30,30]):
display(p,c1,c2):

```

where the two red circles show the conductor surfaces,

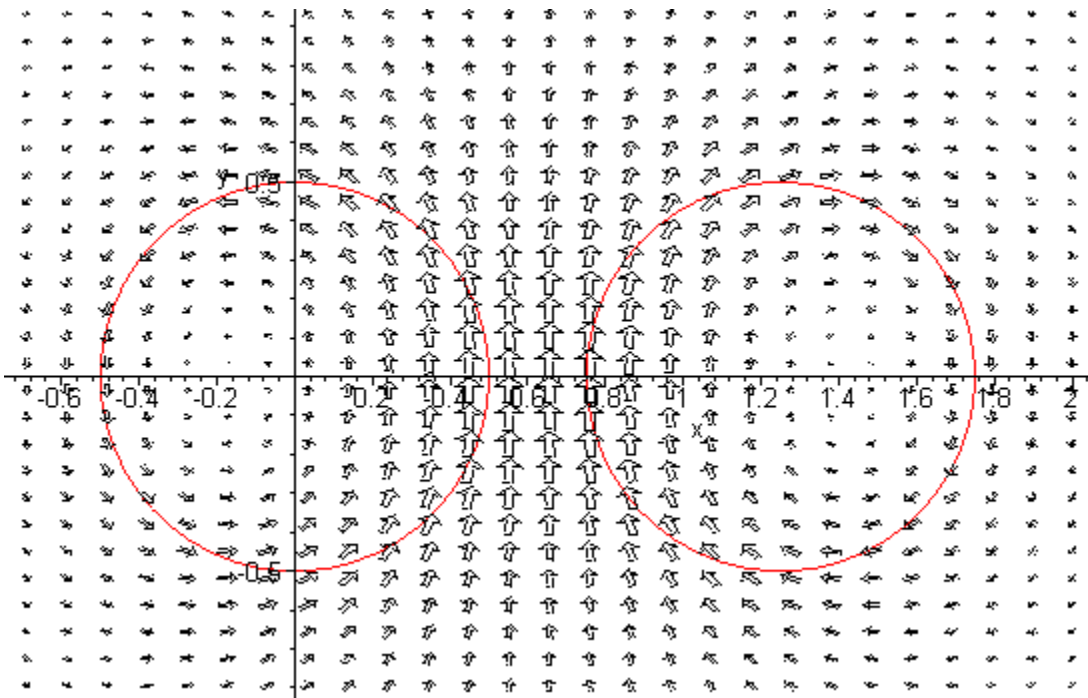


Fig O.5

Again, we get a vague feel for what the field *lines* might look like. We now compute these field lines using the ODE method. So after the first block of code shown above we add instead the following:

```

Hx_ := unapply(Hx,x,y):
Hy_ := unapply(Hy,x,y):
eq1 := diff(X(s),s) = Hx_(X(s),Y(s)):
eq2 := diff(Y(s),s) = Hy_(X(s),Y(s)):
# set Ncurves to plot
Ncurves := 16:
for J from 1 to Ncurves do
  print("starting curve J = ",J);
  # find parametric curve described by x=X(s) and y=Y(s)
  ff := dsolve({eq1,eq2,X(0)=J*b/(Ncurves+1)+.0001,Y(0)=0},{X(s),Y(s)},
type=numeric, method=gear, output=listprocedure):
  Y_ := subs(ff,Y(s)); #needed to directly access the Y(s) data
  # find range for parameter s so each curve just closes with no overlap
  S := 0;
  # closure goes too high
  while (Y_(S) >= 0) and (Y_(S) < b) do
    S := S +.1;
  od:
  p[J] := odeplot(ff, [X(s),Y(s)],-S...S,scaling=constrained,numpoints=140):
od:

p2 := PLOT(CURVES([[a,b],[a,-b],[-a,-b],[-a,b],[a,b]],COLOR(RGB,0,0,0))):
display(p2,seq(p[i],i=1..Ncurves),axes=boxed,scaling = constrained, axes =
none,thickness = 2);

```

The two unapply commands formally make $Hx_$ and $Hy_$ functions of variables x and y .

The two equation lines define ODE's eq1 and eq2 which are none other than (O.6) with $\alpha(s) = 1$.

We decide to plot $Ncurves = 16$ field lines indexed by J .

The Maple dsolve command numerically solves the ODE's with $x_0 = J*b/(Ncurves+1)$ and $y_0 = 0$ as the starting point for the curve J . Maple returns its solution as two numerically interpolated functions $X(s)$ and $Y(s)$ which are just those functions we assumed we had in (O.3).

Special code finds an appropriate range for parameter s so curves just close on themselves, or get truncated if they go beyond a set range.

Finally, the odeplot command plots the parametric functions $X(s)$ and $Y(s)$ to create the field lines in certain display data structures called $p[J]$ for $J = 1$ to 16. The PLOT command makes the rectangle in $p2$ and finally the display command shows the results.

Even on an ancient PC, this code runs in about 15 seconds.

Here is the resulting plot where we have made the conductor perimeters black and the field lines red:

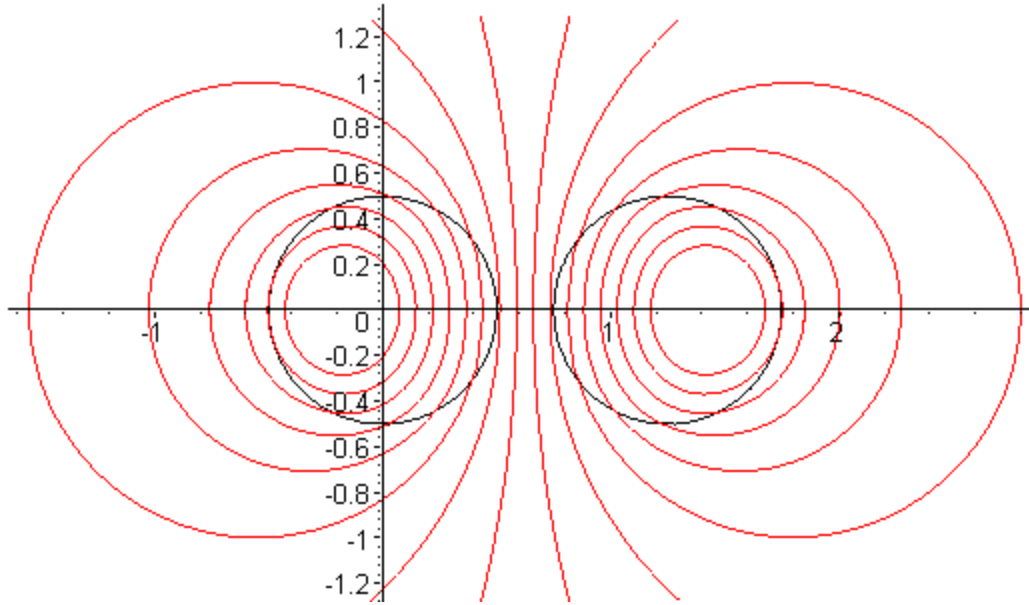


Fig O.6

Outside both conductors, the magnetic field is the same as it would be for conductors of a tiny radius, as the reader can verify by staring at (O.9). Here is the same plot with $a_1 = a_2 = .01$:

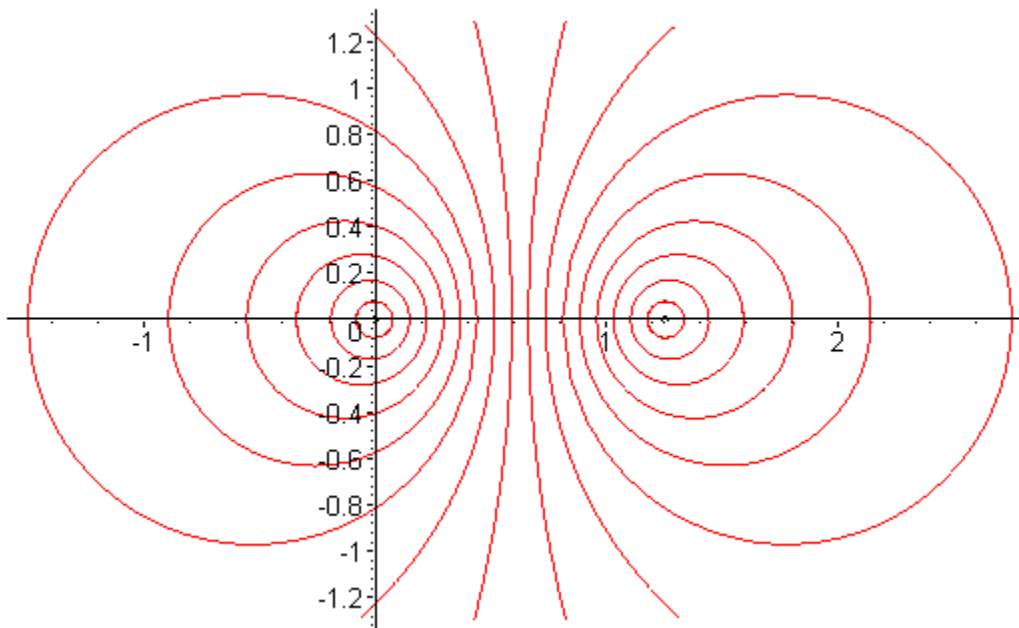


Fig O.7

Reader Exercise: Use $\mathbf{H}(x,y)$ as stated in (C.4.7), with F in (C.4.6), to plot field lines using the ODE method. Compare with the brute force method results shown in Fig O.2.

(d) The Analytic Method

The reader may notice a striking similarity between the last plot above and Fig 6.2 which displays some Circles of Apollonius. The magnetic field lines of two parallel thin wires are indeed such circles, and this can be shown using the following third method of plotting field lines.

From (O.5) that $d\mathbf{r} = \alpha(s) ds \mathbf{H}$ we may write

$$\begin{aligned} dy &= \alpha(s) ds H_y \\ dx &= \alpha(s) ds H_x \end{aligned} \quad (\text{O.12})$$

so

$$\frac{dy}{dx} = H_y/H_x \quad // \text{ right side is ratio "rat" in the code below} \quad (\text{O.13})$$

or

$$H_x(x,y) \frac{dy}{dx} = H_y(x,y). \quad (\text{O.14})$$

This is a first-order non-linear ODE for which Maple (or the reader) may be able to solve analytically for the solution $y(x)$ which is then an analytic expression for the field line. For two thin wires, here is Maple's analytic solution using the `dsolve` command in its default analytic mode,

```
restart; alias(I=I, j=sqrt(-1)): with(plots):with(plottools):
K := I/(2*Pi):
I := 2*Pi:
Hx := - (y/r1)*H1 - (y/r2)*H2:
Hy := (x/r1)*H1 + ((x-b)/r2)*H2:
H1 := K*(1/r1):
H2 := -K*(1/r2):
r1 := sqrt(x^2+y^2):
r2 := sqrt((x-b)^2+y^2):
Hx_ := unapply(Hx,x,y):
Hy_ := unapply(Hy,x,y):
rat := simplify(Hy/Hx):
```

$$rat := -\frac{x^2 - x b - y^2}{y(2x - b)}$$

```
rat1 :=subs(y = y(x),rat):
```

$$rat1 := -\frac{x^2 - x b - y(x)^2}{y(x)(2x - b)}$$

```
ode := diff(y(x),x) = rat1:
```

$$ode = \frac{\partial}{\partial x} y(x) = -\frac{x^2 - x b - y(x)^2}{y(x)(2x - b)}$$

```
s := dsolve(ode):
```

$$s := y(x) = \frac{1}{2} \sqrt{8_C1 x + 2 x b - 4_C1 b - 4 x^2 - b^2}, y(x) = -\frac{1}{2} \sqrt{8_C1 x + 2 x b - 4_C1 b - 4 x^2 - b^2}$$

Renaming the constant `_C1` to be "c", and squaring the solutions shown above, one finds that

$$(x-x_c)^2 + y^2 = r^2$$

$$x_c = b/4+c \quad r^2 = c^2 - bc/2 - 3(b/4)^2 \quad (\text{O.15})$$

where recall that b is the separation of the two thin wires. Thus, the field lines are in fact circles with centers on the x axis.

Reader Exercise :

1. Using the data presented in *Bipolar Coordinates and the Two-Cylinder Capacitor* , show that the set of circles found above are Apollonian circles with these Apollonian parameters,

$$\begin{aligned} a &= b/2 \\ \xi &= \text{ch}^{-1}[(b/4+c)/(c^2 - bc/2 - 3(b/4)^2)] \end{aligned} \quad (\text{O.16})$$

2. Why might one expect Apollonian Circles for the B field lines in this magnetostatics problem, knowing that such circles also describe the potential contours of the electrostatics problem of two cylinders?

[Hint: See (5.3.10) and (5.3.11) with $\beta^2 = k^2$ and (3.7.19) concerning the relation between A_z and the B field lines.]

Appendix P: Eddy Currents and the Proximity Effect

The Maxwell curl E equation (1.1.2) and its integral form are,

$$\text{curl } \mathbf{E} = -\partial_t \mathbf{B} \quad \Leftrightarrow \quad \oint_C \mathbf{E} \cdot d\mathbf{s} = -\partial_t \left[\int_S \mathbf{B} \cdot d\mathbf{S} \right] \quad . \quad (1.1.36)$$

The integral form is often written as $\mathcal{E}_{\text{emf}} = -\partial_t[\text{magnetic flux}]$ and one says that a changing magnetic flux through a loop induces a voltage \mathcal{E}_{emf} (an "electro motive force") in that loop which then drives a current around the loop if the loop lies in a conducting medium. This is Faraday's Law of Induction and the loop of interest is usually a thin wire or coil of such wires inside, say, an electric generator. The wire or coil of wires is attached to some R_{load} and some current I flows through the loop and load. There is Ohmic loss $I^2 R_{\text{loop}}$ in the generating loop(s), but if $R_{\text{load}} \gg R_{\text{loop}}$ this loss is minimal in the context of the generator.

When the loop lies inside an open conducting medium, things become more complicated and the currents which are then driven around mathematical loops in that medium are called eddy currents. The word eddy suggests the way water swirls around in a constrained environment when driven by wind or water currents (see Fig P.4 below). Just as the water flow velocity can have no normal component at a boundary (a steep river bank for example), an electrical eddy current generally has no normal component at a boundary of the conductor. An exception to this rule occurs if the eddy current is feeding a charge density on the outer surface of that boundary, and this exception would apply to water flow as well if a bank were shallow and could act as a temporary reservoir of water. The analogy is not exact, but the word eddy is apt.

In practical terms, eddy currents are normally seen as undesirable, as in a transformer core, since they represent Ohmic loss which results in power waste and heating of the core ($R_{\text{load}} = 0$). Sometimes, however, eddy currents are useful, such as in non-destructive testing for internal cracks in metal parts, as noted below. Other eddy current applications include induction heating, object movement and levitation, and braking.

There are whole books on the subject of eddy currents, and the web reveals a plethora of papers and theses on eddy current applications. However, simple analytic examples of eddy current problems are hard to find. The general theory is quite complicated, and we present below a simplified approach which suits are limited purposes.

In this Appendix we explore the nature of eddy currents and compute these currents for some simple situations. We then show how one can interpret both the skin effect and the proximity effect (non-uniform current densities in nearby conductors) in terms of eddy currents.

P.1 Eddy Current Analysis

Consider this drawing,

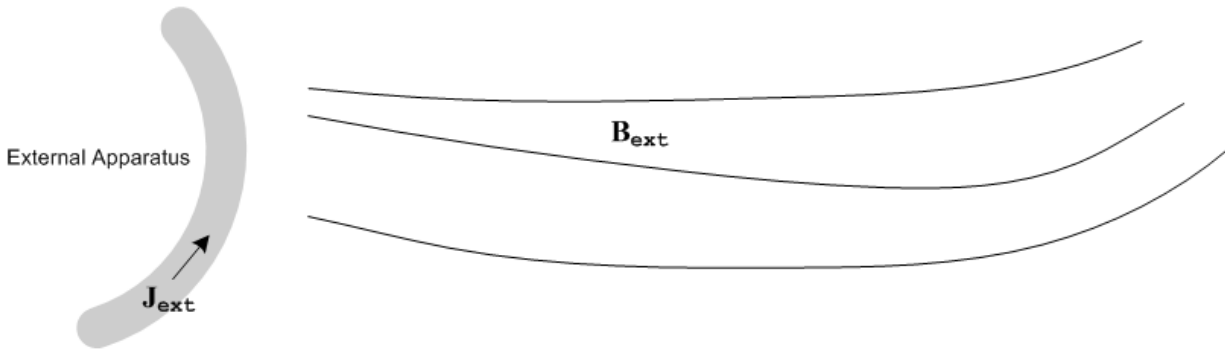


Fig P.1

An external apparatus has time-varying current density \mathbf{J}_{ext} flowing in some wires and creates a time-varying magnetic field \mathbf{B}_{ext} .

We now bring in a **Device Under Test (DUT)** to obtain a new picture:

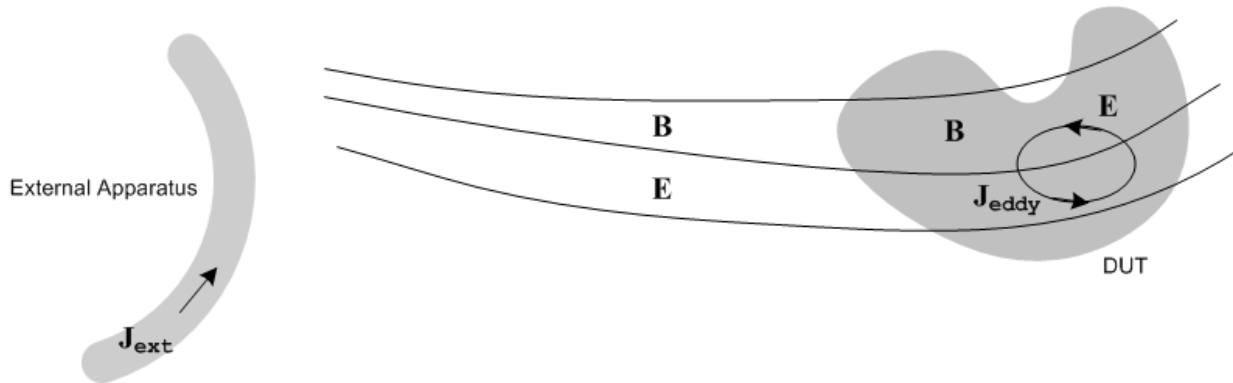


Fig P.2

For simplicity we assume that the DUT is non-magnetic ($\mu = \mu_0$) and is a good conductor with conductivity σ . We therefore ignore displacement currents inside the DUT, in accordance with the discussion below (2.2.2). Permeability ϵ applies to the region outside the DUT.

Iterative Interpretation

We now imagine the analysis of the \mathbf{E} and \mathbf{B} fields to take place in the following iterative sense, where we alternately consider the two Maxwell curl equations:

$$\mathbf{E}^{(0)} = 0$$

$$\text{curl } \mathbf{B}_{ext} = 0$$

we assume no zeroth order electric field anywhere because $\mathbf{J}_{ext} = 0$ outside the external apparatus

$$\begin{aligned}\text{curl } \mathbf{E}^{(1)} &= -j\omega \mathbf{B}_{\text{ext}} \\ \mathbf{E} &= \mathbf{E}^{(0)} + \mathbf{E}^{(1)} = \mathbf{E}^{(1)}\end{aligned}$$

time-changing \mathbf{B}_{ext} creates $\mathbf{E}^{(1)}$ everywhere (Faraday)
which is superposed onto the existing $\mathbf{E}^{(0)} = 0$

$$\begin{aligned}\mathbf{J}_{\text{eddy}}^{(1)} &= \sigma \mathbf{E}^{(1)} \\ \text{curl } \mathbf{B}_{\text{eddy}}^{(1)} &= \mu \mathbf{J}_{\text{eddy}}^{(1)} \\ \text{curl } \mathbf{B}_{\text{eddy}}^{(1)} &= j\omega \varepsilon \mathbf{E}^{(1)} \\ \mathbf{B} &= \mathbf{B}_{\text{ext}} + \mathbf{B}_{\text{eddy}}^{(1)}\end{aligned}$$

$\mathbf{E}^{(1)}$ inside the DUT creates $\mathbf{J}_{\text{eddy}}^{(1)}$ in the DUT
 $\mathbf{J}_{\text{eddy}}^{(1)}$ in the DUT creates $\mathbf{B}_{\text{eddy}}^{(1)}$ in the DUT (Ampere)
and $\mathbf{B}_{\text{eddy}}^{(1)}$ also exists outside the DUT where $\mathbf{J}_{\text{eddy}} = 0$.
This new $\mathbf{B}_{\text{eddy}}^{(1)}$ is superposed onto the original \mathbf{B}_{ext}

$$\begin{aligned}\text{curl } \mathbf{E}^{(2)} &= -j\omega \mathbf{B}_{\text{eddy}}^{(1)} \\ \mathbf{E} &= \mathbf{E}^{(1)} + \mathbf{E}^{(2)}\end{aligned}$$

$\mathbf{B}_{\text{eddy}}^{(1)}$ in turn results in a further adjustment to \mathbf{E} (Faraday)
which is then superposed onto the existing \mathbf{E}

$$\begin{aligned}\mathbf{J}_{\text{eddy}}^{(2)} &= \sigma \mathbf{E}^{(2)} \\ \text{curl } \mathbf{B}_{\text{eddy}}^{(2)} &= \mu \mathbf{J}_{\text{eddy}}^{(2)} \\ \text{curl } \mathbf{B}_{\text{eddy}}^{(2)} &= j\omega \varepsilon \mathbf{E}^{(2)} \\ \mathbf{B}_1 &= \mathbf{B}_{\text{ext}} + \mathbf{B}_{\text{eddy}}^{(1)} + \mathbf{B}_{\text{eddy}}^{(2)}\end{aligned}$$

This new adjustment to \mathbf{E} causes an adjustment in \mathbf{J}_{eddy}
This in turn causes an adjustment to \mathbf{B}_{eddy} in the DUT
and outside the DUT
which is then superposed onto the existing \mathbf{B} field.

and so on.

(P.1.1)

Eventually we arrive at this situation inside the DUT :

$$\text{curl } (\mathbf{E}^{(1)} + \mathbf{E}^{(2)} + \dots) = -j\omega (\mathbf{B}_{\text{ext}} + \mathbf{B}_{\text{eddy}}^{(1)} + \mathbf{B}_{\text{eddy}}^{(2)} + \dots)$$

$$\begin{aligned}\text{curl } (\mathbf{B}_{\text{ext}} + \mathbf{B}_{\text{eddy}}^{(1)} + \mathbf{B}_{\text{eddy}}^{(2)} + \dots) &= \mu \sigma (\mathbf{E}^{(1)} + \mathbf{E}^{(2)} + \dots) \\ &= \mu (\mathbf{J}_{\text{eddy}}^{(1)} + \mathbf{J}_{\text{eddy}}^{(2)} + \dots)\end{aligned}\quad (\text{P.1.2})$$

which, when all is said and done, is just an iterative interpretation of Maxwell's curl equations inside the DUT,

$$\begin{aligned}\text{curl } \mathbf{E} &= -j\omega \mathbf{B} \\ \text{curl } \mathbf{B} &= \mu \mathbf{J} = \mu(\sigma \mathbf{E})\end{aligned}\quad (\text{P.1.3})$$

$$\begin{aligned}\mathbf{B} &= \mathbf{B}_{\text{ext}} + \mathbf{B}_{\text{eddy}}^{(1)} + \mathbf{B}_{\text{eddy}}^{(2)} + \dots \\ \mathbf{E} &= \mathbf{E}^{(1)} + \mathbf{E}^{(2)} + \dots \\ \mathbf{J} &= \mathbf{J}_{\text{eddy}}^{(1)} + \mathbf{J}_{\text{eddy}}^{(2)} + \dots\end{aligned}\quad (\text{P.1.4})$$

One hidden assumption above is that \mathbf{J}_{ext} is not affected by the eddy currents and their fields, and we imagine this is implemented by some kind of current source control in the external apparatus.

Writing the solution of Maxwell's equations iteratively of course does not resolve the inherent complexity of the problem. For example, in the step above where we imagine computing $\mathbf{B}_{\text{eddy}}^{(1)}$, we have to compute $\mathbf{B}_{\text{eddy}}^{(1)}$ inside the DUT using $\text{curl } \mathbf{B}_{\text{eddy}}^{(1)} = \mu \mathbf{J}_{\text{eddy}}^{(1)}$ and then we have to compute $\mathbf{B}_{\text{eddy}}^{(1)}$ outside the DUT using $\text{curl } \mathbf{B}_{\text{eddy}}^{(1)} = j\omega \varepsilon \mathbf{E}^{(1)}$, and then we have to match the values of $\mathbf{B}_{\text{eddy}}^{(1)}$ on the DUT boundary. This is a full-blown boundary problem that requires much effort to solve for a general DUT and is further complicated if the DUT is made of magnetic material.

Small ω

Looking at the above series of iterative steps, it would appear that if ω is in some sense "small", the series shown above for \mathbf{B} , \mathbf{E} and \mathbf{J} are highly convergent and can be well approximated by the first one or two terms. In this situation, we have in essence a perturbation theory solution where ω is the smallness parameter. For very low frequencies, the key steps in the above iterative sequence are these:

$$\begin{aligned} \text{curl } \mathbf{E}^{(1)} &= -j\omega \mathbf{B}_{\text{ext}} \\ \mathbf{J}_{\text{eddy}}^{(1)} &= \sigma \mathbf{E}^{(1)} \end{aligned} \quad (\text{P.1.5})$$

which we combine to get

$$\text{curl } \mathbf{J}_{\text{eddy}}^{(1)} = -j\omega\sigma \mathbf{B}_{\text{ext}} \quad (\text{P.1.6})$$

and this will be the basis for the quantitative calculations of our first two examples below. Since ω is small, $\mathbf{J}_{\text{eddy}}^{(1)}$ is small. The next iterative step

$$\text{curl } \mathbf{B}_{\text{eddy}}^{(1)} = \mu \mathbf{J}_{\text{eddy}}^{(1)} \quad (\text{P.1.7})$$

then results in a small $\mathbf{B}_{\text{eddy}}^{(1)}$, and then

$$|\mathbf{B}_{\text{eddy}}^{(1)}| \ll |\mathbf{B}_{\text{ext}}| \quad (\text{P.1.8})$$

Although we present no formal proof, it seems likely that our simple perturbative eddy current analysis can only be viable at a frequency low enough that the skin depth δ is large compared to the dimensions of the DUT.

Larger ω

If ω is not small, we can still write (P.1.3) as

$$\begin{aligned} \text{curl } \mathbf{E} &= -j\omega(\mathbf{B}_{\text{ext}} + \mathbf{B}_{\text{eddy}}) \\ \text{curl } (\mathbf{B}_{\text{ext}} + \mathbf{B}_{\text{eddy}}) &= \mu \mathbf{J}_{\text{eddy}} = \mu\sigma \mathbf{E} \end{aligned} \quad (\text{P.1.9})$$

but the perturbation series interpretations of \mathbf{B}_{eddy} , \mathbf{J}_{eddy} and \mathbf{E} are not meaningful since they (probably) don't converge. In this case, we have a single monolithic problem that must be solved all at once by some method other than our simple iterative eddy current analysis starting with (P.1.6). What happens at higher frequencies is this: the external field \mathbf{B}_{ext} still creates eddy currents in the DUT, but these currents in turn generate \mathbf{B}_{eddy} fields which are large enough that they significantly alter \mathbf{B}_{ext} within the DUT and one must then deal with $\mathbf{B} \equiv \mathbf{B}_{\text{ext}} + \mathbf{B}_{\text{eddy}}$ as the true field which is causing those eddy currents. In this case, one can combine the two Maxwell curl equations into a wave / Helmholtz equation as we have done in (1.2.2) and later in (1.5.27) and (1.5.32), and then one must solve that Helmholtz equation subject to appropriate boundary conditions, both inside and outside the DUT. In effect we did this for an isolated round wire in Chapter 2 and the solution there involved rather complicated \mathbf{E} and \mathbf{B} fields (recall the Kelvin functions) exhibiting skin effect and a rapidly winding phase as shown in Figure 2.9.

Despite the difficulty of the solution for larger ω , we know a solution exists, and we can make qualitative observations about that solution based on the results of our simple low- ω example solutions. We shall do this below to provide an eddy current interpretation of both the skin effect in a round wire, and the proximity effect in a transmission line.

ECT Application

In typical **Eddy Current Testing** (ECT) systems, the frequency used might range from 10Hz to 1500 Hz. The idea of an ECT system is to try to detect \mathbf{B}_{eddy} using a sensitive Hall Effect or SQUID device, and take note of the field pattern produced by a DUT which is "known good" (has no internal cracks in the metal). An internal crack in a bad DUT will alter \mathbf{J}_{eddy} in some way, which in turn causes an alteration in \mathbf{B}_{eddy} which can hopefully be detected. Due to the skin depth penetration issue, the useful depth of such non-destructive testing systems might be up to 15 mm (ballpark). Higher ω generates a larger signal, gives more accuracy on the defect size and location, but penetration depth is less, so there is always a tradeoff. Often scans at different ω values are optimal for different depths of the defect. ECT is a subject of much current interest and many papers have been and are being written.

P.2 Eddy currents in a thin round plate in a uniform B field

To reduce symbol clutter, in this section we use the following notation in relation to Section P.1 :

$$\mathbf{B} \equiv \mathbf{B}_{\text{ext}} \quad \mathbf{J} \equiv \mathbf{J}_{\text{eddy}}^{(1)} \quad (\text{P.2.1})$$

A thin round plate of radius a and thickness h lies centered in the $z = 0$ plane of a cylindrical coordinate system. This plate is the Device Under Test (DUT) for this problem. An unseen external apparatus creates a time-varying and spatially uniform magnetic field $\mathbf{B} = B \hat{\mathbf{z}}$ perpendicular to the plate. The problem is to compute the electric field \mathbf{E} in the plate, and the corresponding eddy currents $\mathbf{J} = \sigma \mathbf{E}$. The region surrounding the plate is assumed non-conducting, perhaps it is air.

Faraday's Law and symmetry imply circular closed electric field lines in the plate. We are perhaps more used to magnetic field lines being closed since $\text{div } \mathbf{B} = 0$, but here we have closed electric field lines since $\text{div } \mathbf{E} = 0$ inside the plate (since there is no free charge inside the plate, see Section 3.1). We assume sufficiently low ω so skin depth $\delta \gg h$ (recall $\delta \equiv \sqrt{2/(\omega\mu\sigma)}$) so the E field lines are uniform in the z direction of the plate thickness. This is the implication of the word "thin" in discussing a "thin plate". In this drawing, the plate is gray, and some of the circular closed E field lines are shown in red,

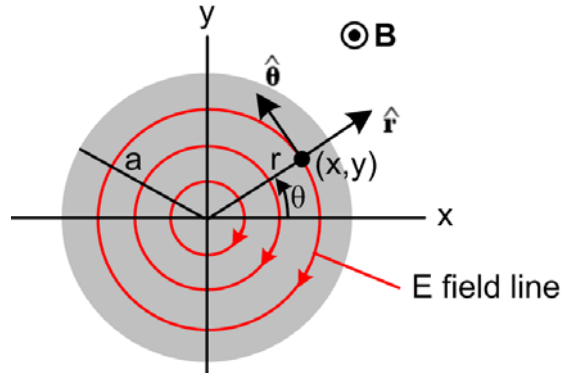


Fig P.3

The magnitude of the E field is constant on each circle due to symmetry. The field lines are drawn clockwise since we know by Lenz's Law that the associated eddy currents produce a B field opposed to the applied B field.

Since ω is small, we may use our first perturbation theory expansion term (P.1.6),

$$\text{curl } \mathbf{J}_{\text{eddy}}^{(1)} = -j\omega\sigma\mathbf{B}_{\text{ext}} \quad (\text{P.1.6})$$

Setting $\mathbf{J} \equiv \mathbf{J}_{\text{eddy}}^{(1)}$, $\mathbf{B} \equiv \mathbf{B}_{\text{ext}}$, $\mathbf{J} = \sigma\mathbf{E}$, and $j\omega \rightarrow \partial_t$, this says,

$$\text{curl } \mathbf{E} = -\partial_t\mathbf{B} \quad \Leftrightarrow \quad \oint_C \mathbf{E} \cdot d\mathbf{s} = -\partial_t \left[\int_S \mathbf{B} \cdot d\mathbf{S} \right] \quad (\text{P.2.2})$$

which we recognize as the Maxwell curl E equation and its integral form as shown in (1.1.36). Section P.1 has provided a context and an interpretation of the symbols \mathbf{B} , \mathbf{E} and $\mathbf{J} = \sigma\mathbf{E}$ appearing in (P.2.2).

Note: The last paragraphs of Appendix N explain why Ohm's Law is still valid despite the presence of magnetic fields. We assume in Fig P.3 that $B \ll 569$ tesla.

Consider now a circle at radius r . We then have from the right equation of (P.2.2),

$$E_\theta * 2\pi r = -\dot{B} \pi r^2 \quad \Rightarrow \quad E_\theta(r) = -\dot{B} \pi r^2 / 2\pi r = (-\dot{B} / 2) r \quad (\text{P.2.3})$$

The E field is linear in r , and is reminiscent of the result for the H field inside a round wire which carries a DC current I ,

$$H * 2\pi r = I \pi r^2 / \pi a^2 \quad \Rightarrow \quad H(r) = I r^2 / a^2 / 2\pi r = (I / 2\pi a^2) r \quad (\text{C.3.9})$$

Notice that the E field-line circles continue outside the plate and under and over it, but there will only be current in the plate. Here then is our result for \mathbf{E} and \mathbf{J} inside the plate:

$$\mathbf{E}(\mathbf{r}) = E_\theta(r) \hat{\theta} \quad E_\theta(r) = (-\dot{B} / 2) r \quad \mathbf{J}_\theta(r) = \sigma (-\dot{B} / 2) r \quad (\text{P.2.4})$$

We digress momentarily to study the heat loss generated in the plate. Consider a thin cylindrical shell of height dz and radius r and thickness dr . Think of this as a circular wire of rectangular cross section $dA = dzdr$. The current in this wire is given by,

$$dI = J_{\theta} dA = J_{\theta} dzdr \quad . \quad (P.2.5)$$

The resistance of the wire is $dR = \rho L/dA = \rho 2\pi r/(dzdr)$ where $\rho = 1/\sigma$. The power burned from $P = I^2R$ is

$$\begin{aligned} dP &= (dI)^2 dR = [J_{\theta} dzdr]^2 * \rho 2\pi r/(dzdr) = J_{\theta}^2 [dzdr] * \rho 2\pi r \\ &= J_{\theta}^2 2\pi r \rho dr dz = [\sigma (-\dot{B}_z/2) r]^2 2\pi r \rho dr dz = (\pi/2)\sigma \dot{B}_z^2 r^3 dr dz \quad . \end{aligned} \quad (P.2.6)$$

Now integrate over the plate thickness h to replace dz by h . Then integrate r from 0 to a to get

$$P = (\pi/2)\sigma \dot{B}_z^2 h(a^4/4) = (\pi/8)\sigma \dot{B}_z^2 a^4 h \quad . \quad (P.2.7)$$

Dimensions:

$$\text{RHS} = [\text{ohm}^{-1} \text{m}^{-1}] \text{sec}^{-2} [\text{volt-sec/m}^2]^2 \text{m}^5 = \text{ohm}^{-1} \text{sec}^{-2} [\text{volt-sec}]^2 = \text{volt}^2/\text{ohm} = \text{watts}$$

The total current going around the plate as observed through any azimuthal slice $\theta = \theta_1$ is,

$$I = h \int_0^a dr J_{\theta}(r) = h \sigma (-\dot{B}_z/2) \int_0^a r dr = h \sigma (-\dot{B}_z/4)a^2 = -(1/4) h \sigma a^2 \dot{B}_z \quad . \quad (P.2.8)$$

To summarize our conclusions for eddy currents in the thin round plate of radius a , thickness h and conductivity σ ,

$$J_{\theta}(r) = -(1/2)\sigma \dot{B} r \quad (P.2.4) \quad // \text{ the eddy current density}$$

$$I = -(1/4) \sigma h a^2 \dot{B} \quad (P.2.8)$$

$$P = (\pi/8) \sigma h a^4 \dot{B}^2 \quad (P.2.7) \quad (P.2.9)$$

These results are in agreement with equations (36), (37) and (38) of Siakavellas. Since $\dot{B} \rightarrow j\omega B$, the power loss is proportional to the square of the frequency of the external B field, and it is proportional to the conductivity of the plate and its thickness. [Siakavellas also treats thin plates with polygonal boundaries.]

It is a simple matter now to plot the eddy current vector inside the plate:

$$\begin{aligned} J_x &= J_{\theta} \hat{\theta} \cdot \hat{x} = -J_{\theta} \sin\theta = -J_{\theta} (y/r) = +(1/2) \dot{B} \sigma y \equiv ky \theta(r < a) & k &= (1/2) \dot{B} \sigma \\ J_y &= J_{\theta} \hat{\theta} \cdot \hat{y} = J_{\theta} \cos\theta = J_{\theta} (x/r) = -(1/2) \dot{B} \sigma x \equiv -kx \theta(r < a) \quad . \end{aligned} \quad (P.2.10)$$

With $k = 1$ and $a = 1$ Maple produces the following plot of the eddy currents inside the plate:

```

restart;with(plots):with(plottools):
k := 1:
a := 1:
Jx := k*y*Heaviside(a-r):
Jy := -k*x*Heaviside(a-r):
r := sqrt(x^2+y^2):
p1 := circle([0,0],a,color=red):
p2 := fieldplot([Jx,Jy], x=-a..a, y = -a..a, scaling=constrained, arrows=thick):
display(p1,p2);

```

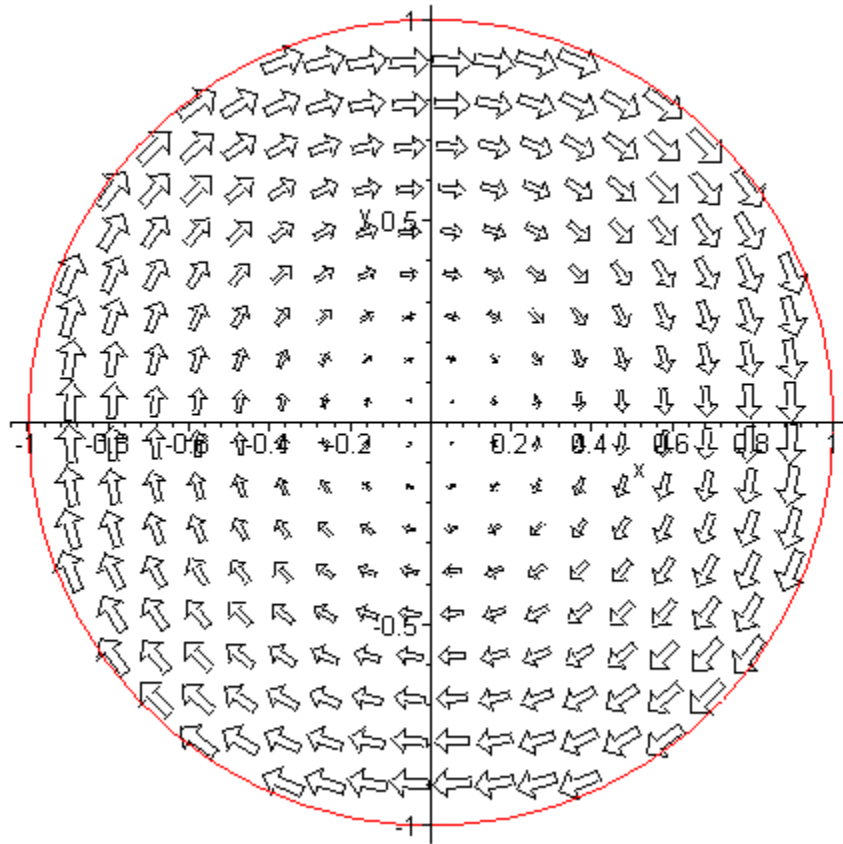


Fig P.4

With $k = 1$ we have assumed that $\dot{\mathbf{B}} > 0$ (out of plane of paper), and according to Lenz's Law, the eddy current creates a B field whose flux cancels some of the applied B flux, hence the clockwise direction.

Why is the eddy current larger at a larger radius? The circular path over which \mathcal{E}_{emf} is generated is proportional to r (being $2\pi r$), but the encircled magnetic flux is proportional to r^2 (being $\pi r^2 B$), so we expect E_θ to be proportional to r , which (P.2.4) confirms. [$E_\theta(2\pi r) = \mathcal{E}_{\text{emf}} = -j\omega (\pi r^2 B)$.]

Reader Exercise: Notice that the \mathbf{E}_{eddy} current arrows are largest near the edge of the plate according to (P.2.4) which says $E_\theta(r) = \text{constant} * r$. Is it correct to interpret this as a 2D skin effect of the type encountered in Chapter 2? In terms of the external \mathbf{B} field penetrating the disk, since the disk is thin we have assumed no skin effect in the z dimension and that \mathbf{B} field penetrates fully and $\delta \gg h$.

P.3 Eddy currents in a thin round plate in a *non-uniform* B field

This example is the same as that of the previous section, *except* the B field is no longer spatially uniform and for simplicity we assume it has the following simple linear form,

$$B(x) = B_0 - \alpha x . \quad \alpha > 0 \quad // \text{ B(x) larger for } x < 0 \text{ (on the left)} \quad (\text{P.3.1})$$

This is then a simple case where $\mathbf{B}_{\text{ext}}(\mathbf{x}) = \mathbf{B}(\mathbf{x})$ has a *gradient* over the plate.

Even with this simple form, the problem is considerably more complicated than the previous problem since we can no longer make use of azimuthal symmetry. First consider (P.2.2) now in the frequency domain, where as before $\mathbf{B} \equiv \mathbf{B}_{\text{ext}}$ and $\mathbf{E} = \mathbf{J}_{\text{eddy}}/\sigma$. (This equation is really (P.1.6) of Section P.1.)

$$\text{curl } \mathbf{E} = -j\omega \mathbf{B} . \quad (\text{P.2.2}) \quad (\text{P.3.2})$$

In cylindrical coordinates this says

$$\hat{\mathbf{r}} [r^{-1} \partial_{\theta} E_z - \partial_z E_{\theta}] + \hat{\boldsymbol{\theta}} [\partial_z E_r - \partial_r E_z] + \hat{\mathbf{z}} [r^{-1} \partial_r (r E_{\theta}) - r^{-1} \partial_{\theta} E_r] = -j\omega B \hat{\mathbf{z}} . \quad (\text{P.3.3})$$

As in the previous example, we assume the plate is very thin and ω is very small so $\delta \gg h$, so fields are constant in the z direction allowing us to replace $\partial_z \rightarrow 0$. At the same time, we assume $E_z = 0$ since E_z has no apparent source (and J_z has nowhere to flow). Then the above vector curl equation boils down to this scalar equation for the z component,

$$\begin{aligned} r^{-1} \partial_r (r E_{\theta}) - r^{-1} \partial_{\theta} E_r &= -j\omega [B_0 - \alpha x] \\ \text{or} \\ \partial_r (r E_{\theta}) - \partial_{\theta} E_r &= -j\omega [B_0 - \alpha r \cos\theta] r \end{aligned} \quad (\text{P.3.4})$$

since $x = r \cos\theta$. Since there is no charge inside the plate (as before), we know $\text{div } \mathbf{E} = 0$, or

$$\text{div } \mathbf{E} = r^{-1} \partial_r (r E_r) + r^{-1} \partial_{\theta} E_{\theta} + \partial_z E_z = 0 . \quad (\text{P.3.5})$$

Again we set $E_z = 0$ (or $\partial_z \rightarrow 0$) which kills off the last term. Then (P.3.4) and (P.3.5) may be written

$$\begin{aligned} \partial_r (r E_{\theta}) - \partial_{\theta} E_r &= -j\omega [B_0 - \alpha r \cos\theta] r \\ \partial_r (r E_r) + \partial_{\theta} E_{\theta} &= 0 . \end{aligned} \quad (\text{P.3.6})$$

These equations form a system of coupled first-order linear PDE's in variables r and θ for functions $E_r(r, \theta)$ and $E_{\theta}(r, \theta)$. There is no z argument since we assumed $\partial_z \rightarrow 0$ above, so basically we have a 2D problem in polar coordinates. The first equation is inhomogeneous (has a driving term) while the second is homogeneous.

We wish to emphasize how the addition of a simple linear external B field variation has converted the trivial problem of Section P.2 to a non-trivial problem involving coupled partial differential equations. There are of course associated boundary conditions, such as $E_r(a, \theta) = 0$ since J_r can have no normal

component at the rim of the plate. This complexity is typical of "eddy current problems". Below we shall solve this problem using a potential method, and one can then show that the solutions so obtained do in fact satisfy (P.3.6).

(a) The stream function method in Cartesian Coordinates

In our treatment of transmission lines in Chapter 4, we used the fact that $\text{div } \mathbf{B} = 0$ to describe the magnetic field in terms of a magnetic vector potential \mathbf{A} , where $\mathbf{B} = \text{curl } \mathbf{A}$ (since $\text{div curl } \mathbf{A} = 0$ for any \mathbf{A}). Under suitable conditions, it was then possible to ignore the "transverse" components of \mathbf{A} and deal only with the z component A_z . This then replaced the complexity of three fields B_i with one field A_z .

In our current context of dealing with electric fields inside a conductor (where $\rho = 0$) we have $\text{div } \mathbf{E} = 0$ and therefore $\text{div } \mathbf{J} = 0$ since $\mathbf{J} = \sigma \mathbf{E}$. We can then describe the current \mathbf{J} in terms of a *current* vector potential \mathbf{T} , where $\mathbf{J} = \text{curl } \mathbf{T}$ (since $\text{div curl } \mathbf{T} = 0$ for any \mathbf{T}). For a thin plate at low frequency ω , we will argue that the transverse components of \mathbf{T} may be neglected, and then the complexity of three fields J_i is replaced by one field T_z . This field is known in incompressible fluid dynamics as a **stream function** where $\mathbf{J} = \text{nev}$ is essentially the fluid flow velocity field \mathbf{v} .

Here then is the stream function method presented in Cartesian coordinates. First,

$$\begin{aligned} \mathbf{J} = \text{curl } \mathbf{T} &= \hat{\mathbf{x}} (\partial_y T_z - \partial_z T_y) + \hat{\mathbf{y}} (\partial_z T_x - \partial_x T_z) + \hat{\mathbf{z}} (\partial_x T_y - \partial_y T_x) \\ J_x &= \partial_y T_z - \partial_z T_y \\ J_y &= \partial_z T_x - \partial_x T_z \\ J_z &= \partial_x T_y - \partial_y T_x \quad . \quad // \text{ components of the above} \end{aligned} \quad (\text{P.3.7})$$

The \mathbf{J} we have in mind is $\mathbf{J}_{\text{eddy}}^{(1)}$ appearing in (P.1.6). Using the symbols of (P.2.1), we have

$$\text{curl } \mathbf{J} = -j\omega\sigma \mathbf{B} \quad (\text{P.1.6}) \quad (\text{P.3.8})$$

where $\mathbf{B} = B_z \hat{\mathbf{z}}$ [$= \mathbf{B}_{\text{ext}}$]. Using a standard vector identity we find then that

$$\text{curl } \mathbf{J} = \text{curl curl } \mathbf{T} = \text{grad}(\text{div } \mathbf{T}) - \nabla^2 \mathbf{T} \quad (\text{P.3.9})$$

Just as we are allowed to work in the "Coulomb gauge" $\text{div } \mathbf{A} = 0$ with the magnetic vector potential (see Appendix A), here we can work in the $\text{div } \mathbf{T} = 0$ gauge for the current vector potential. In this gauge, we combine (P.3.8) and (P.3.9) to get

$$\nabla^2 \mathbf{T} = j\omega\sigma \mathbf{B} \quad (\text{P.3.10})$$

where ∇^2 is the vector Laplacian operator. This equation can be compared with $\nabla^2 \mathbf{A} = -\mu \mathbf{J}$ which is (1.3.5) for a magnetostatic situation where \mathbf{A} has no time dependence. As shown in (H.1.9), equation (P.3.10) has the solution

$$\mathbf{T}(\mathbf{x}) = -\int d^3x' [1/4\pi R][j\omega\sigma \mathbf{B}] + \text{possible homogeneous solutions} \quad R = |\mathbf{x} - \mathbf{x}'| \quad (\text{P.3.11})$$

where the integral is the "particular solution" of (P.3.10). Since $\mathbf{B} = \mathbf{B}_{\text{ext}} = B_z(\mathbf{x}) \hat{\mathbf{z}}$, the particular solution is entirely in the z direction. There may be some homogeneous adder solutions which create transverse components T_x and T_y , but we make the ansatz that

$$T_x, T_y \ll T_z \quad . \quad (\text{P.3.12})$$

One motivation for this assumption is that then $J_z = \partial_x T_y - \partial_y T_x$ of (P.3.7) will be very small as we expect for a "thin" plate (we already assumed $E_z = 0$ above). Bypassing a detailed analysis of this issue, we shall assume that $T_x = T_y = 0$ and only T_z is significant. Then (P.3.7) becomes

$$\begin{aligned} J_x &= \partial_y T_z \\ J_y &= -\partial_x T_z \\ J_z &= 0 \quad . \end{aligned} \quad (\text{P.3.13})$$

Furthermore, we assume that $T_z = T_z(x,y)$ with no z dependence, since then (P.3.13) will lead to currents J_x and J_y which have no z dependence. With all these assumptions, (P.3.10) becomes a scalar equation

$$\nabla_{2D}^2 T_z(x,y) = j\omega\sigma B_z(x,y) \quad (\text{P.3.14})$$

where $\nabla_{2D}^2 \equiv \nabla^2 - \partial_z^2$ is the transverse component of the 3D scalar Laplacian.

Equation (P.3.14) is just the 2D Poisson equation of 2D potential theory [see (A.0.1) for the normal Poisson equation in 3D]. Many tools are available for solving this equation, and we shall use some of these tools below in our solution of the thin plate problem.

(b) The stream function method in Cylindrical Coordinates

In cylindrical coordinates (really polar coordinates) one writes

$$\nabla_{2D}^2 T_z = r^{-1} \partial_r (r \partial_r T_z) + r^{-2} \partial_\theta^2 T_z$$

so (P.3.14) becomes

$$r^{-1} \partial_r [r \partial_r T_z(r,\theta)] + r^{-2} \partial_\theta^2 T_z(r,\theta) = j\omega\sigma B_z(r,\theta) \quad . \quad (\text{P.3.15})$$

The ansatz (P.3.12) becomes

$$T_r, T_\theta \ll T_z \quad . \quad (\text{P.3.16})$$

The cylindrical replacement for (P.3.7) is

$$\mathbf{J} = \text{curl } \mathbf{T} = \hat{\mathbf{r}} [r^{-1}\partial_{\theta}T_z - \partial_zT_{\theta}] + \hat{\boldsymbol{\theta}} [\partial_zT_r - \partial_rT_z] + \hat{\mathbf{z}} [r^{-1}\partial_r(rT_{\theta}) - r^{-1}\partial_{\theta}T_r]$$

$$J_r = r^{-1}\partial_{\theta}T_z - \partial_zT_{\theta}$$

$$J_{\theta} = \partial_zT_r - \partial_rT_z$$

$$J_z = r^{-1}\partial_r(rT_{\theta}) - r^{-1}\partial_{\theta}T_r \quad // \text{ components of the above} \quad (\text{P.3.17})$$

which, using (P.3.16), we approximate as

$$J_r = r^{-1}\partial_{\theta}T_z$$

$$J_{\theta} = -\partial_rT_z$$

$$J_z = 0 \quad (\text{P.3.18})$$

(c) Using the stream function method to solve the plate problem

From (P.3.1) we have $B_z(\mathbf{x}) = B_0 - \alpha x = B_0 - \alpha r \cos\theta$, so (P.3.15) states that

$$\partial_r[r\partial_rT_z(r,\theta)] + r^{-1}\partial_{\theta}^2T_z(r,\theta) = j\omega\sigma [B_0 - \alpha r \cos\theta] r \quad (\text{P.3.19})$$

Here we have a single second-order PDE in r,θ for a single function $T_z(r,\theta)$ [the stream function]. One can compare this with the pair of coupled first-order PDE's found earlier in (P.3.6).

Since the angle θ has the full range $(0,2\pi)$ we can expand the various functions into "partial waves" as shown in (D.1.5) for a scalar function, so

$$T_z(r,\theta) = \sum_{m=-\infty}^{\infty} T_z(r,m) e^{jm\theta} \quad (\text{D.1.5a})$$

$$T_z(r,m) = (1/2\pi) \int_{-\pi}^{\pi} d\theta T_z(r,\theta) e^{-jm\theta} \quad (\text{D.1.5b}) \quad (\text{P.3.20})$$

where we use our usual overloaded notation for T_z . Then (P.3.15) becomes, using $\partial_{\theta} \rightarrow +jm$,

$$\partial_r[r\partial_rT_z(r,m)] - r^{-1}m^2T_z(r,m) = j\omega\sigma B_z(r,m) r \quad (\text{P.3.21})$$

where

$$\begin{aligned} B_z(r,m) &= (1/2\pi) \int_{-\pi}^{\pi} d\theta B_z(r,\theta) e^{-jm\theta} = (1/2\pi) \int_{-\pi}^{\pi} d\theta [B_0 - \alpha r \cos\theta] e^{-jm\theta} \\ &= B_0 (1/2\pi) \int_{-\pi}^{\pi} d\theta e^{-jm\theta} - \alpha r (1/2\pi) \int_{-\pi}^{\pi} d\theta \cos\theta e^{-jm\theta} \\ &= B_0 (1/2\pi) \int_{-\pi}^{\pi} d\theta \cos(m\theta) - \alpha r (1/2\pi) \int_{-\pi}^{\pi} d\theta \cos\theta \cos(m\theta) \end{aligned}$$

$$\begin{aligned}
 &= B_0 (1/\pi) \int_0^\pi d\theta \cos(m\theta) - \alpha r (1/\pi) \int_0^\pi d\theta \cos\theta \cos(m\theta) \\
 &= \delta_{m,0} B_0 (1/\pi) \pi - \alpha r (1/\pi) \delta_{m,\pm 1} \pi/2 \\
 &= \delta_{m,0} B_0 - (\alpha/2) r \delta_{m,\pm 1}
 \end{aligned} \tag{P.3.22}$$

where we use the following integral for integers m and n,

$$\int_0^\pi d\theta \cos(m\theta)\cos(n\theta) = \begin{cases} 0 & m \neq n \\ \pi/2 & m = n \neq 0 \\ \pi & m = n = 0 \end{cases} . \quad // \text{ Spiegel p 96 15.27}$$

Equations (P.3.21) become

$$\partial_{\mathbf{r}}(r\partial_{\mathbf{r}}T_{\mathbf{z}}(r,0)) = j\omega\sigma B_0 r \quad m = 0 \tag{P.3.23}$$

$$\partial_{\mathbf{r}}(r\partial_{\mathbf{r}}T_{\mathbf{z}}(r,\pm 1)) - r^{-1}T_{\mathbf{z}}(r,\pm 1) = -j\omega\sigma (\alpha/2) r^2 \quad m = \pm 1 \tag{P.3.24}$$

$$\partial_{\mathbf{r}}(r\partial_{\mathbf{r}}T_{\mathbf{z}}(r,m)) - r^{-1}m^2T_{\mathbf{z}}(r,m) = 0 \quad m = \text{other integers} \tag{P.3.25}$$

We assume the relevant solution to (P.3.25) is $T_{\mathbf{z}}(r,m) = 0$. Maple tells us the general solutions to the first two equations,

```

restart: alias(I=I,j=sqrt(-1));
eq1 := diff(r*diff(Tz(r),r),r) = j*omega*sigma*B0*r;
      eq1 := (∂/∂r Tz(r)) + r (∂²/∂r² Tz(r)) = j ω σ B0 r
dsolve(eq1);
      Tz(r) = 1/4 j ω σ B0 r² + _C1 + _C2 ln(r)
eq2 := diff(r*diff(Tz(r),r),r) - (1/r)*Tz(r) = -(alpha/2)*j*omega*sigma*r^2;
      eq2 := (∂/∂r Tz(r)) + r (∂²/∂r² Tz(r)) - Tz(r)/r = -1/2 j α ω σ r²
dsolve(eq2): simplify(%): expand(%);
      Tz(r) = -1/16 j α ω σ r³ + r_C1 + C1/r + r_C2 - C2/r
    
```

We rename the constants to write these solutions as,

$$\begin{aligned}
 T_{\mathbf{z}}(r,0) &= j\omega\sigma B_0 (1/4)r^2 + C_1 \ln(r) + C_2 \\
 T_{\mathbf{z}}(r,\pm 1) &= - (1/8) j\omega\sigma (\alpha/2) r^3 + D_1(r-1/r) + D_2(r+1/r) .
 \end{aligned} \tag{P.3.26}$$

To have $T_z(r,0)$ finite at $r = 0$ we must have $C_1 = 0$.

To have $T_z(r,\pm 1)$ finite at $r = 0$ we must have $D_1 = D_2$. The solution forms are then

$$\begin{aligned} T_z(r,0) &= j\omega\sigma B_0 (1/4) r^2 + C_2 \\ T_z(r,\pm 1) &= - (1/8) j\omega\sigma (\alpha/2) r^3 + 2D_1 r . \end{aligned} \quad (P.3.27)$$

Inserting these partial wave amplitudes into (P.3.20) gives

$$\begin{aligned} T_z(r,\theta) &= T_z(r,0) + T(r,+1)e^{j\theta} + T(r,-1)e^{-j\theta} = T_z(r,0) + T(r,+1) 2 \cos\theta \\ &= [j\omega\sigma B_0 (1/4) r^2 + C_2] + 2 \cos\theta [- (1/8) j\omega\sigma (\alpha/2) r^3 + 2D_1 r] \\ &= [j\omega\sigma B_0 (1/4) r^2 + C_2] - \cos\theta r [(1/8) j\omega\sigma \alpha r^2 - 4D_1] . \end{aligned} \quad (P.3.28)$$

At the origin point $r = 0$ we arbitrarily set the potential $T_z(0,\theta) = 0$ so $C_2 = 0$. One always has this freedom with a potential: since $\mathbf{J} = \text{curl } \mathbf{T}$, constants in \mathbf{T} don't affect \mathbf{J} . We then compute J_x as shown in (P.3.18) to obtain

$$J_x(r,\theta) = r^{-1} \partial_\theta T_z = \sin\theta [(1/8) j\omega\sigma \alpha r^2 - 4D_1] . \quad (P.3.29)$$

But at $r = a$, we must have $J_x(a,\theta) = 0$ since there can be only tangential currents at the rim of our circular plate, and this determines D_1 giving this final result for the stream function T_z ,

$$\begin{aligned} T_z(r,\theta) &= j\omega\sigma B_0 (1/4) r^2 - (1/8) \cos\theta r j\omega\sigma \alpha (r^2 - a^2) \\ &= j\omega\sigma [(1/4)B_0 r^2 - (\alpha/8) \cos\theta (r^3 - a^2 r)] . \end{aligned} \quad (P.3.30)$$

The eddy current components are then, again from (P.3.18),

$$\begin{aligned} J_x(r,\theta) &= r^{-1} \partial_\theta T_z = r^{-1} j\omega\sigma (\alpha/8) \sin\theta (r^3 - a^2 r) = j\omega\sigma [(\alpha/8) \sin\theta (r^2 - a^2)] \\ J_\theta(r,\theta) &= - \partial_r T_z = j\omega\sigma [- (1/2)B_0 r + (\alpha/8) \cos\theta (3r^2 - a^2)] . \end{aligned} \quad (P.3.31)$$

Here then is a **summary** of the solution for a circular plate of radius r and conductivity σ in the presence of an external magnetic field $B(x) = B_0 - \alpha x$:

$$\begin{aligned} T_z(r,\theta) &= j\omega\sigma [(1/4)B_0 r^2 - (\alpha/8) \cos\theta r (r^2 - a^2)] \\ J_x(r,\theta) &= j\omega\sigma [(\alpha/8) \sin\theta (r^2 - a^2)] \\ J_\theta(r,\theta) &= j\omega\sigma [- (1/2)B_0 r + (\alpha/8) \cos\theta (3r^2 - a^2)] \\ E_x(r,\theta) &= j\omega [(\alpha/8) \sin\theta (r^2 - a^2)] \\ E_\theta(r,\theta) &= j\omega [- (1/2)B_0 r + (\alpha/8) \cos\theta (3r^2 - a^2)] . \end{aligned} \quad (P.3.32)$$

The eddy currents J_x and J_θ are proportional to ω as expected from (P.1.6). Current J_x vanishes at the edge of the plate. When $\alpha = 0$, we find $J_x(r, \theta) = 0$ and $J_\theta(r, \theta) = j\omega\sigma [- (1/2)B_0 r]$ which replicates our uniform-B solution (P.2.4) which was $J_\theta(r) = \sigma (-\dot{B}/2) r$.

We have verified using Maple that the stream function $T_z(r, \theta)$ shown in (P.3.32) satisfies (P.3.19) and that the electric fields $E_x(r, \theta)$ and $E_\theta(r, \theta)$ satisfy (P.3.6).

Finally, Maple will plot the resulting eddy currents. First write,

$$\begin{aligned} J_x &= J_x \hat{r} \cdot \hat{x} + J_\theta \hat{\theta} \cdot \hat{x} = J_x \cos\theta - J_\theta \sin\theta \\ J_y &= J_x \hat{r} \cdot \hat{y} + J_\theta \hat{\theta} \cdot \hat{y} = J_x \sin\theta + J_\theta \cos\theta \end{aligned} \quad (P.3.33)$$

For plotting we set $j\omega\sigma = 1$, $a = 1$, $B_0 = 1$, and $\alpha = 1$. Here is the plotting code,

```
Jr := (alpha/8)*(r^2-a^2)*sin(theta);
      Jr := 1/8 alpha (r^2 - a^2) sin(theta)
Jth := (-B0*r/2 + (alpha/8)*cos(theta)*(3*r^2-a^2));
      Jth := -1/2 B0 r + 1/8 alpha cos(theta) (3 r^2 - a^2)
Jx := Jr*cos(theta)-Jth*sin(theta);
Jy := Jr*sin(theta)+Jth*cos(theta);
Jx1 := subs([sin(theta)=y/r,cos(theta)=x/r],Jx);
Jy1 := subs([sin(theta)=y/r,cos(theta)=x/r],Jy);
a := 1: B0 := 1: alpha := 1:
r := sqrt(x^2+y^2):
Jx2 := Jx1*Heaviside(a-r):
Jy2 := Jy1*Heaviside(a-r):
p1 := circle([0,0],a,color=red):
p2 := fieldplot([Jx2,Jy2],
x=-a..a,y=-a..a,scaling=constrained,arrows=thick):
display(p1,p2);
```

and here is the resulting plot,

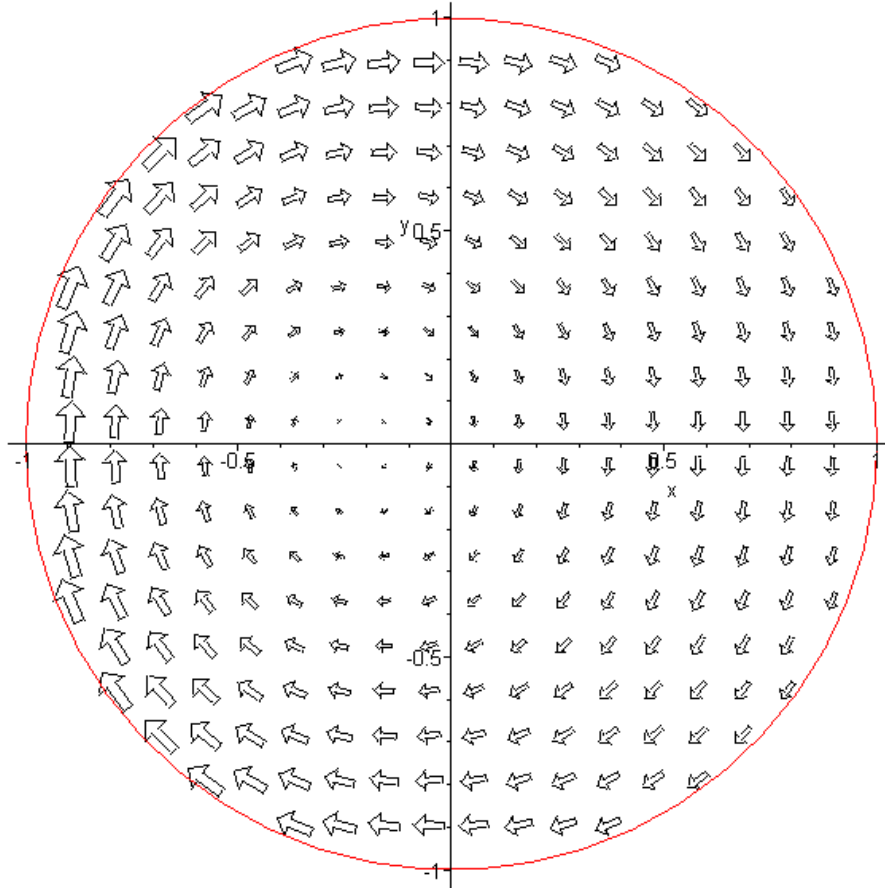


Fig P.5

which one can compare with the no-gradient plot of Fig P.4. As expected, the eddy currents are larger on the left side because the external B field is larger there. One can imagine the E field lines being a set of distorted circles which shrink down about a point to the left of the origin.

The main point of this example is to demonstrate the fact that a gradient in the external B field results in an *asymmetry* in the eddy current distribution such that the larger eddy current vectors are in the region in which the external B field is largest. We shall see below in a different geometry how this fact accounts for the so-called proximity effect in a transmission line.

Reader Exercise: Use one of the methods of Appendix O to plot the E field lines for Fig P.5.

P.4 Self-induced eddy currents in a round wire

We now reconsider our well-studied axially symmetric radius- a round wire of Chapter 2. In this eddy current example, the "external apparatus" and the "device under test" (DUT) are one in the same! In the zeroth order of the Section P.1 perturbation theory (very low ω), the current density in the wire is $\mathbf{J}_{\text{ext}}(\mathbf{x}, \omega)$ which is perfectly uniform across the wire cross section and flows in the $\hat{\mathbf{z}}$ direction. This current density creates a magnetic field \mathbf{B}_{ext} in the $\hat{\boldsymbol{\theta}}$ direction which is obtained from Ampere's Law,

$$2\pi r B_{\text{ext}}(r) = \frac{\pi r^2}{\pi a^2} \mu I_{\text{enc}} = \frac{\pi r^2}{\pi a^2} \mu J_{\text{ext}} \pi a^2 = \pi r^2 \mu J_{\text{ext}}$$

$$\Rightarrow \mathbf{B}_{\text{ext}}(r) = (1/2) \mu r \mathbf{J}_{\text{ext}} . \quad (\text{P.4.1})$$

In this problem the "external" current density \mathbf{J}_{ext} is generated by the round wire itself, as if it were somehow its own "external apparatus". A better notation would be \mathbf{J}_{dc} since this is the $\omega = 0$ current distribution, but we continue to use \mathbf{J}_{ext} to maintain contact with the Section P.1. Similarly, $\mathbf{B}_{\text{ext}} = \mathbf{B}_{\text{dc}}$.

If the skin depth δ is large compared to the wire radius a , we expect the perturbation eddy current analysis of Section P.1 to be viable, and we write (P.1.6) as

$$\text{curl } \mathbf{J}_{\text{eddy}} \approx -j\omega\sigma \mathbf{B}_{\text{ext}} \quad \text{where } \mathbf{B}_{\text{ext}} = (1/2) \mu r \mathbf{J}_{\text{ext}} \hat{\boldsymbol{\theta}} = \mathbf{B}_{\text{ext}}(r) \hat{\boldsymbol{\theta}} . \quad (\text{P.4.2})$$

In cylindrical coordinates one writes for an arbitrary vector field \mathbf{F} ,

$$\text{curl } \mathbf{F} = \hat{\mathbf{r}} [r^{-1} \partial_{\theta} F_z - \partial_z F_{\theta}] + \hat{\boldsymbol{\theta}} [\partial_z F_r - \partial_r F_z] + \hat{\mathbf{z}} [r^{-1} \partial_r (r F_{\theta}) - r^{-1} \partial_{\theta} F_r] . \quad (\text{P.4.3})$$

For a vector field \mathbf{F} which is a function only of r this reduces to,

$$\text{curl } \mathbf{F} = \hat{\boldsymbol{\theta}} [- \partial_r F_z] + \hat{\mathbf{z}} [r^{-1} \partial_r (r F_{\theta})] . \quad (\text{P.4.4})$$

Thus (P.4.2) becomes these two equations,

$$\begin{aligned} r^{-1} \partial_r [r (J_{\text{eddy}})_{\theta}] &= 0 \\ - \partial_r (J_{\text{eddy}})_z &= -j\omega\sigma \mathbf{B}_{\text{ext}}(r) = -j\omega\sigma (1/2) \mu r \mathbf{J}_{\text{ext}} . \end{aligned} \quad (\text{P.4.5})$$

The first equation of (P.4.5) may be written as

$$\begin{aligned} \partial_r [r (J_{\text{eddy}})_{\theta}] &= 0 \\ \text{or} \\ [r (J_{\text{eddy}})_{\theta}] &= C_1 \\ \text{or} \\ (J_{\text{eddy}})_{\theta}(r) &= C_1/r \end{aligned}$$

from which we must conclude that $C_1 = 0$ and then $(J_{\text{eddy}})_{\theta}(r) = 0$, so there is no azimuthal eddy current in the wire.

The second equation of (P.4.5) may be integrated from $r=0$ to $r=r$ to obtain

$$(J_{\text{eddy}})_z(r) - (J_{\text{eddy}})_z(0) = j\omega\sigma (1/2) \mu \mathbf{J}_{\text{ext}} \int_0^r dr' r' = j\omega\sigma (1/4) \mu \mathbf{J}_{\text{ext}} r^2 . \quad (\text{P.4.6})$$

Thus, the total current density in the wire obtained from eddy current analysis is in the z direction and is given by

$$\begin{aligned}
 J_z &= J_{\text{ext}} + (J_{\text{eddy}})_z = J_{\text{ext}} + (J_{\text{eddy}})_z(0) + j\omega\sigma (1/4) \mu J_{\text{ext}} r^2 \\
 &= J_{\text{ext}} \left[1 + \frac{(J_{\text{eddy}})_z(0)}{J_{\text{ext}}} + j\omega\mu\sigma (1/4) r^2 \right] \\
 &\approx J_{\text{ext}} \left[1 + j\omega\mu\sigma (1/4) r^2 \right]. \quad // \text{ since } |(J_{\text{eddy}})_z(0)| \ll |J_{\text{ext}}| \text{ at low } \omega
 \end{aligned} \tag{P.4.7}$$

Recall from (2.2.20) and (2.2.21) that

$$j\beta^2 = \omega\mu\sigma = 2/\delta^2 = |\beta^2| \quad // \quad j\omega\mu\sigma = -\beta^2 \tag{P.4.8}$$

where β is the complex Helmholtz parameter of (1.5.1c). Therefore we have shown that

$$J_z = J_{\text{ext}} \left[1 + j\omega\mu\sigma (1/4) r^2 \right] = J_{\text{ext}} \left[1 - \beta^2(1/4) r^2 \right]. \tag{P.4.9}$$

Notice that the eddy current contribution is $\pi/2$ out of phase with J_{ext} . Since we have assumed $\delta \gg a$, it follows that

$$|\beta a| = (\sqrt{2}/\delta) a = \sqrt{2} (a/\delta) \ll 1 \tag{P.4.10}$$

so then $|\beta r| \ll 1$ and the eddy current contribution is very small, as required to use the first term in the perturbation expansion of Section P.1 as we have done. Defining

$$\begin{aligned}
 \kappa &\equiv \omega\sigma\mu (1/4)r^2 = (j\beta^2) (1/4) r^2 = |\beta^2| (1/4)r^2 \ll 1 \\
 j\kappa &= j\omega\sigma\mu (1/4)r^2 = -\beta^2(1/4) r^2
 \end{aligned} \tag{P.4.11}$$

one finds

$$\begin{aligned}
 J_z &= J_{\text{ext}} \left[1 - (\beta^2/4)r^2 \right] = J_{\text{ext}} \left[1 + j\kappa \right] \\
 |J_z|^2 &= |J_{\text{ext}}|^2 (1+j\kappa)(1-j\kappa) \\
 |J_z| &= |J_{\text{ext}}| \sqrt{(1+j\kappa)(1-j\kappa)} = |J_{\text{ext}}| \sqrt{1 + \kappa^2} \approx |J_{\text{ext}}| \left[1 + (1/2)\kappa^2 \right]
 \end{aligned} \tag{P.4.12}$$

so that

$$\begin{aligned}
 \frac{|J_z|}{|J_{\text{ext}}|} &= \left[1 + (1/2)\kappa^2 \right] = \left[1 + (1/2) \{ |\beta^2| (1/4)r^2 \}^2 \right] \\
 &= 1 + \frac{1}{2} \{ (2/\delta^2) (1/4)r^2 \}^2 = 1 + \frac{1}{2} \{ (1/\delta^2) (1/2)r^2 \}^2 \\
 &= 1 + \frac{1}{8} (r/\delta)^4
 \end{aligned} \tag{P.4.13}$$

which then exhibits a very slight skin effect and has the same r dependence as (2.3.10), see Fig 2.7.

In Chapter 2 we found in (2.2.30) the following exact result for J_z in a round wire operating at ω ,

$$J_z(r) = \frac{I}{2\pi a} \frac{J_0(\beta r)}{J_1(\beta a)} \beta \quad (2.2.30)$$

For small ω , since $|\beta r| \ll 1$, one has for small arguments [Spiegel 24.5 and 24.6]

$$J_0(x) \approx 1 - x^2/4$$

$$J_1(x) \approx (x/2)(1 - x^2/8) \quad \Rightarrow \quad 1/J_1(x) \approx (2/x) (1 + x^2/8) \approx (2/x) \quad (P.4.14)$$

so

$$\frac{J_0(\beta r)}{J_1(\beta a)} \approx (2/\beta a) (1 - \beta^2 r^2/4) \quad (P.4.15)$$

and then

$$\begin{aligned} J_z(r) &= \frac{I}{2\pi a} [(2/\beta a) (1 - \beta^2 r^2/4)] \beta = \frac{I}{2\pi a} [(2/a) (1 - \beta^2 r^2/4)] = \frac{I}{\pi a^2} [(1 - \beta^2 r^2/4)] \\ &= J_{\text{ext}} (1 - \beta^2 r^2/4) \end{aligned} \quad (P.4.16)$$

in agreement with our eddy current analysis result (P.4.9).

At higher frequencies where we no longer have $\delta \gg a$, the eddy current perturbation expansion diverges and becomes meaningless and one must instead solve the Helmholtz equation stated at the end of Section P.1. In Chapter 2 this task was in essence carried out and the skin effect was observed. One can then interpret the skin effect by saying that the eddy currents cancel the DC current density in the interior of the round wire, allowing a net current to exist only at the periphery. In other words, the skin effect is *caused* by eddy currents. But this is just a manner of speaking, and is like saying that the skin effect is "caused by Maxwell's Equations", which it is.

For a moderate skin effect, we can illustrate the eddy currents in a round wire by crudely plotting them just in the central gray plane of the following drawing :

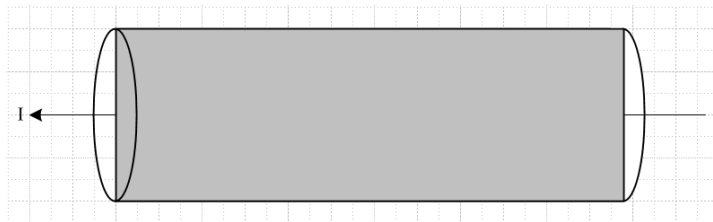


Fig P.6

Theses qualitative-only plots are for some particular instant in time. We know that the phase of J varies as shown in Fig 2.8, so we attempt to illustrate only the real part of the currents:

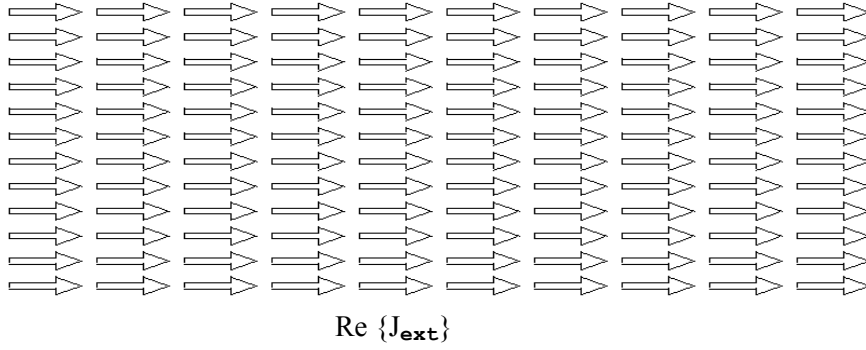


Fig P.7 (a)

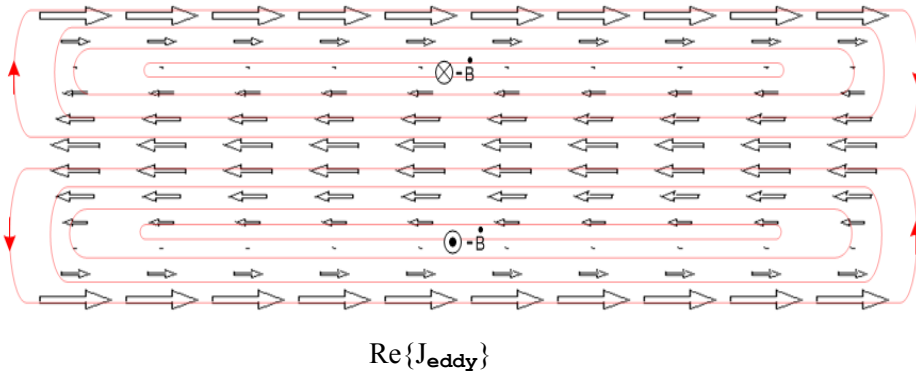


Fig P.7 (b)

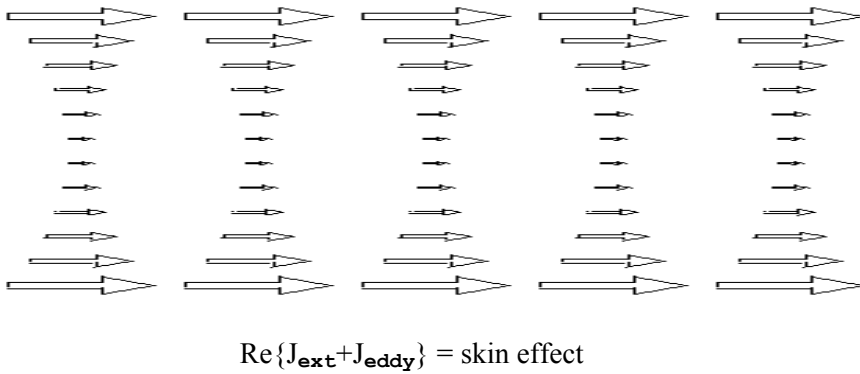


Fig P.7 (c)

The closed red curves in Fig P.7 (b) represent the J_{eddy} field lines, and these then represent the actual induced "eddies" of current. One could write $J_{\text{eddy}} = \sigma E_{\text{eddy}}$ and then they are electric field lines. The lines close on themselves because they have no sources: inside the wire $\rho = 0$ so $\text{div } J_{\text{eddy}} = 0$ and $\text{div } E_{\text{eddy}} = 0$. Recall that a field in general does not have a constant magnitude along a field line. In the geometry of a round wire, the field lines in fact loop around at the ends of the wire.

P.5 Eddy currents induced in a quiet round-wire by an external B field

Uniform B_{ext}

In this example, we start with our Device Under Test (DUT) which is a straight round wire which carries no current. Some "external apparatus" creates a time-changing magnetic field $\mathbf{B}_{ext} = B_{ext}\hat{y}$ as shown in the figure below, where $B_{ext}(x,\omega)$ is for the moment constant in space. At the instant in time shown, the time-domain field $\mathbf{B}_{ext}(x,t)$ is increasing in the $-\hat{y}$ direction so that $-\dot{\mathbf{B}}_{ext}(x,t)$ points in the $+\hat{y}$ direction, out of the plane of paper.

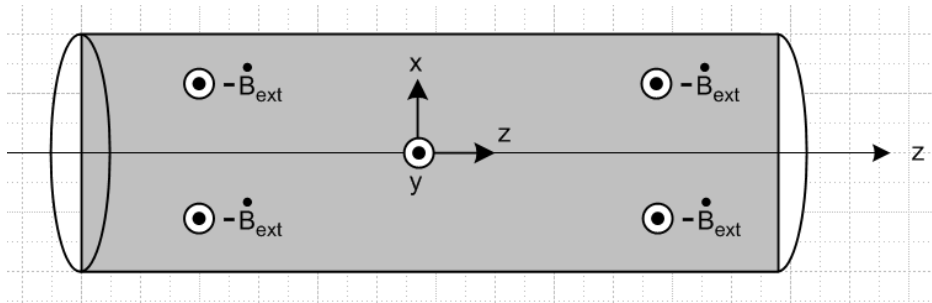


Fig P.8

The time-domain eddy current equation (P.1.6) (we assume small ω) and its integral form are

$$\text{curl } \mathbf{J}_{eddy} = \sigma [-\dot{\mathbf{B}}_{ext}] \quad \Leftrightarrow \quad \oint_C \mathbf{J}_{eddy} \cdot d\mathbf{s} = \sigma \int_S [-\dot{\mathbf{B}}_{ext}] \cdot d\mathbf{S} \quad . \quad (P.5.1)$$

The integral form implies that the flux change through any math loop in the gray rectangle is positive at our time instant, so according to the right hand rule, the eddy currents in the gray rectangle have the following general shape,

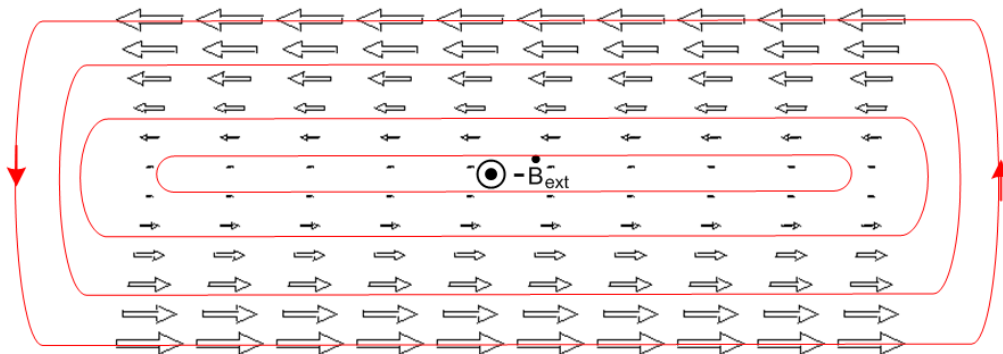


Fig P.9

This figure is analogous to Fig P.4 above which shows the eddy current in a thin round plate for a uniform external B field.

To justify the linear variation with x (vertical), if we assume that away from the ends of the wire nothing varies with z, and if we write \mathbf{J}_{eddy} as \mathbf{J} , we find that

$$\text{curl } \mathbf{J} = \hat{\mathbf{x}} (\partial_y J_z - \partial_z J_y) + \hat{\mathbf{y}} (\partial_z J_x - \partial_x J_z) + \hat{\mathbf{z}} (\partial_x J_y - \partial_y J_x) = -\sigma \dot{\mathbf{B}}_{\text{ext}} \hat{\mathbf{y}}$$

or

$$\hat{\mathbf{x}} (\partial_y J_z) + \hat{\mathbf{y}} (-\partial_x J_z) + \hat{\mathbf{z}} (\partial_x J_y - \partial_y J_x) = -\sigma \dot{\mathbf{B}}_{\text{ext}} \hat{\mathbf{y}} \quad (\text{P.5.2})$$

which produces the three equations

$$\begin{aligned} \partial_x J_z &= \sigma \dot{\mathbf{B}}_{\text{ext}} & \Rightarrow J_z(x) &= \sigma \dot{\mathbf{B}}_{\text{ext}} x & // \text{ linear in } x \\ \partial_y J_z &= 0 & \Rightarrow J_z &= J_z(x) \text{ only} \\ \partial_x J_y - \partial_y J_x &= 0 & \text{satisfied if } J_x \text{ and } J_y &= 0 \end{aligned} \quad (\text{P.5.3})$$

The eddy pattern in the round wire would have the same general appearance in any slice of the wire parallel to the slice shown as the gray rectangle in Fig P.8. The current of course drops to 0 at the wire surface since we assume the wire is surrounded by an insulating medium. Conversely, in any planar slice of the wire which is perpendicular to the gray plane (and still parallel to the z axis), there are no eddy currents because any math loop in such a plane sees no flux.

Non-uniform \mathbf{B}_{ext}

Suppose now that the field \mathbf{B}_{ext} has a positive linear gradient in the x direction. We can write,

$$j\omega \mathbf{B}_{\text{ext}}(\mathbf{x},\omega) = j\omega [\mathbf{B}_{\text{ext}0} + \alpha x] \quad \Rightarrow \quad \dot{\mathbf{B}}_{\text{ext}}(\mathbf{x},t) = \dot{\mathbf{B}}_{\text{ext}0} + \dot{\alpha} x \quad (\text{P.5.4})$$

Then,

$$\dot{\mathbf{B}}_{\text{ext}}(\mathbf{x},t) = \dot{\mathbf{B}}_{\text{ext}}(t) + \dot{\alpha}(t) x = j\omega e^{j\omega t} [\mathbf{B}_{\text{ext}}(0) + \alpha(0) x] \quad (\text{P.5.5})$$

We assume $\alpha(0) > 0$ so the B field magnitude is larger at the top of Fig P.8 than at the bottom at $t = 0$.

Below we shall assume a time such that $e^{j\omega t} = -1$ so then both $\dot{\mathbf{B}}_{\text{ext}}(t)$ and $\dot{\alpha}(t)$ are negative. Then the first equation of (P.5.3) becomes,

$$\partial_x J_z = \sigma \dot{\mathbf{B}}_{\text{ext}} = \sigma [\dot{\mathbf{B}}_{\text{ext}0} + \dot{\alpha} x] \quad \Rightarrow \quad J_z(x) = \sigma [\dot{\mathbf{B}}_{\text{ext}0} x + (1/2) \dot{\alpha} x^2 - (1/6) \dot{\alpha}]$$

or

$$J_z(x) = -\sigma [| \dot{\mathbf{B}}_{\text{ext}0} | x + (1/2) | \dot{\alpha} | x^2 - (1/6) | \dot{\alpha} |] \quad // \text{ for our time of interest} \quad (\text{P.5.6})$$

where we have added a constant such that $\int_{-1}^1 dx J_z(x) = 0$ for a wire of radius $a = 1$. $J_{\text{eddy}} = J_z$ is now larger in the upper half of the gray rectangle than in the lower half, and we would expect then a pattern having this general shape,

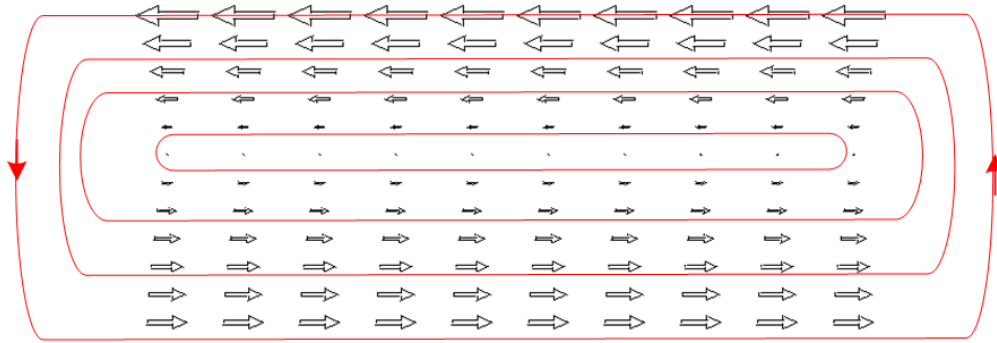


Fig P.10

The eddy currents are now larger on the side of the wire where the external field B_{ext} is larger. In addition, one sees the eddy current in general to be larger near the surface of the wire and small in the interior. Figure P.10 is analogous to Fig P.5 above which shows the eddy current in a thin round plate for a non-uniform external B field.

P.6 Eddy currents induced in an current-carrying wire by an external B field

We start with the self-induced eddy current pattern in a round wire shown in Fig P.7 (b),

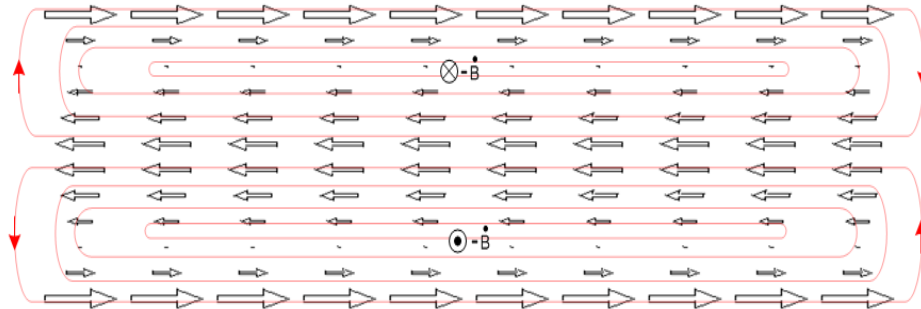


Fig P.7 (b)

We then turn on a uniform external B field which induces an additional eddy current pattern in the same round wire, as shown in Fig P.9,

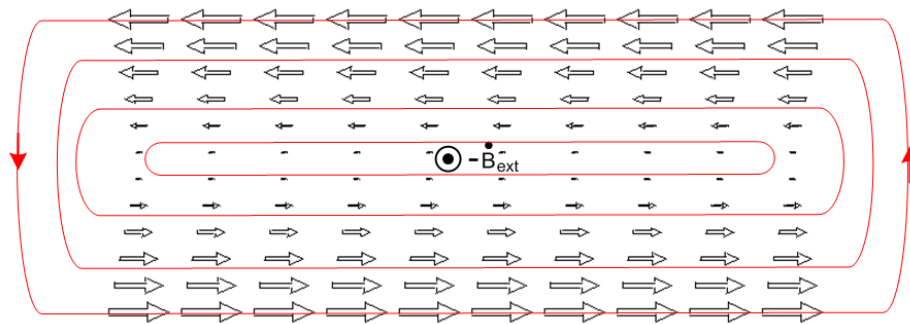


Fig P.9

We assume the external B field has the proper phase relative to the current in the wire such that the patterns look as shown above. When a small amount of the lower pattern is superposed on the upper pattern, there is partial cancellation on the top edge, and reinforcement on the lower edge, resulting in the following eddy current pattern,

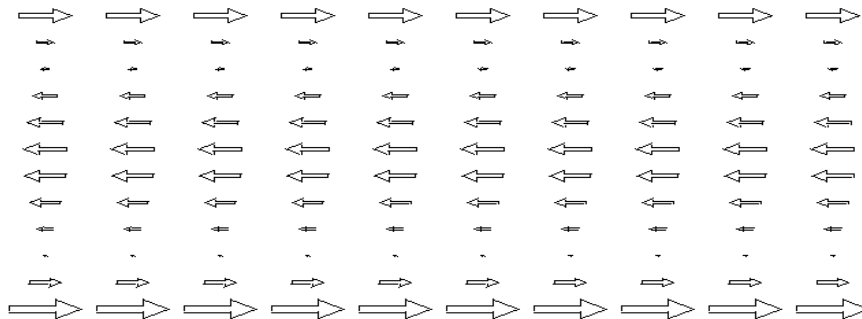


Fig P.11

Thus we arrive at another mechanism for the eddy current to be larger on one side of a wire than on the other side. Notice that B_{ext} has no gradient in this example, and also that we are not showing the underlying DC uniform current pattern of Fig P.7 (a).

P.7 Summary of Round Wire Examples

1. The eddy currents which a current-carrying round wire induces into itself vary with radius inside the wire, but are azimuthally symmetric. These eddy currents are interpreted as causing the skin effect. This situation is depicted in Fig P.7 (c).
2. A *quiet* round wire in the presence of a spatially-uniform external B field will have induced eddy currents which are oppositely directed on the two sides of the wire, but the absolute value of the current is symmetric on the two sides, as in Fig P.9.
3. If this *quiet* wire is placed in an external B_{ext} field which has a *gradient*, then the absolute value of the current density will be larger on the side of the wire where B_{ext} is larger, as shown in Fig P.10.
4. When a *current-carrying* round wire is placed in a uniform external B_{ext} field, even though that field is uniform, the absolute value of the current density is larger on one side of the wire compared to the other side, as shown in Fig P.11.
5. When a *current-carrying* round wire is placed in a external B_{ext} field which has a gradient, we again expect to have a side-to-side eddy current asymmetry which is a combination of the effects of items 3 and 4 above. The asymmetry will depend on the direction of the current in the wire and on the size and polarity of B_{ext} .

P.8 Eddy currents in Transmission Lines: The Proximity Effect

We consider a transmission line composed of two round wires and focus our attention on wire #1 as our Device Under Test. If wire #2 is far away, as in a wide-spaced twin-line, then B_{ext} created by wire #2 is roughly uniform at the location of wire #1, and we then have the current asymmetry of Case 4 above. If wire #2 is close to wire #1, then B_{ext} created by wire #2 will have a gradient over wire #1, and then we have the asymmetry combination Case 5 above where both effects must be considered. In the following drawing, we show in cross section two round wires both of which carry current I in the **same direction**, out of the plane of paper :

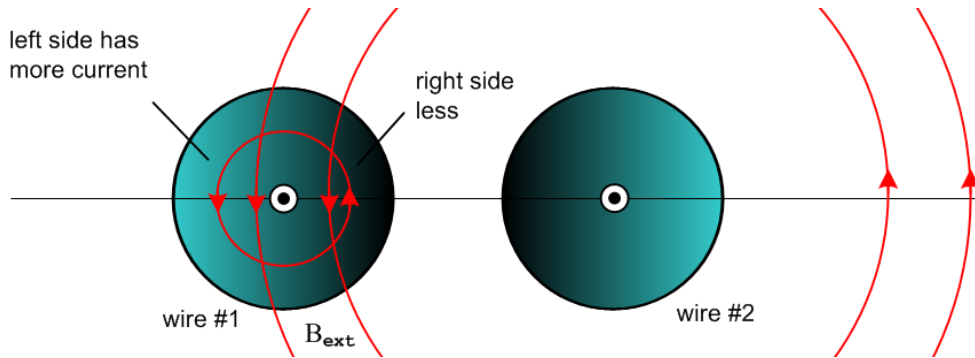


Fig P.12

The field B_{ext} created by wire #2 is slightly stronger on the right side of wire #1 than on the left side, which of itself would argue for more eddy current on the right side of wire #1. However this effect is swamped by the Case 4 effect where we have cancellation of B fields on the right side of wire #1 and addition on the left side, so the total B field is stronger on the left side of wire #1 and thus the eddy current (and hence the total current density) is larger there, as indicated by the lighter coloration. The current asymmetry increases as the two conductors get closer together because both the B field cancellation and reinforcement are enhanced as B_{ext} becomes larger and more comparable to the internal B field. The asymmetry also increases as ω increases, since the eddy currents increase, and at $\omega = 0$ there is no asymmetry because there are no eddy currents.

If we imagine positive charge carriers coming out of the plane of paper in wire #1, the ones on the left side of wire #1 feel a Lorentz force $q \mathbf{v} \times \mathbf{B}$ pushing them to the right, while those on right side of wire #1 feel an oppositely directed force pushing them to the left. This is so because the net \mathbf{B} in general points down on the left side of the center line of wire #1, and up on the right side (see Fig P.16 below). But the charge carriers on the right are in a smaller B field *and* travel at a smaller velocity v since $J_z = nqv$ is smaller (although at $\omega = 0$ this second fact is not true). The net effect is that for any $\omega \geq 0$ the charge carriers in wire #1 feel an overall force to the right and this force is transferred to the conductor ion lattice to maintain $\rho = 0$ causing the entire wire #1 to be pushed to the right. The opposite happens inside wire #2 and the result is that wires with currents in the same direction attract each other for any $\omega \geq 0$.

The fact that (for $\omega > 0$) the current distribution in each wire is skewed away from the other wire is sometimes called the **proximity effect**, or **current crowding**. One effect of having a non-uniform J_z distribution is that the wires have resistance larger than their DC values (see Section P.10 below). If the

above two wires were two strands of a power transmission line cable carrying current in the same direction, the Ohmic loss in the strands is enhanced by this crowding effect.

The coloration patterns in Fig P.12 don't really illustrate the skin effect which is of course always present at any $\omega > 0$, more strongly of course when $\delta < a$ (see Fig 6.12.). Even in power lines at 60 Hz where $\delta \sim 1$ cm the skin effect does cause a waste of the wire interior since less current flows there. If a large round conductor is replaced by a set of smaller insulated round wires, this waste is reduced since the smaller wires each have more uniform current (see Litz wire).

In a transmission line the currents are of course **oppositely directed** and the picture is different:

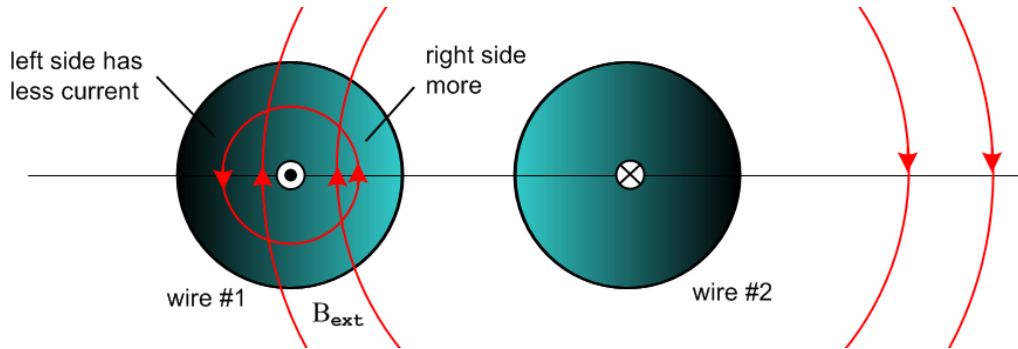


Fig P.13

Now the B field is larger on the right side of wire #1 so the eddy current is larger there causing the total current density J_z to be larger there compared to the left side. The currents are now crowded on the side of each wire facing the other wire ($\omega > 0$). The Lorentz force now causes the two wires to repel each other, reversing the argument given above ($\omega \geq 0$). There is still extra Ohmic loss compared to DC since J_z is non-uniform. Closer wire spacing again results in increased asymmetry.

Companies like "Monster Cables" advocate using their low-ohm expensive cables for driving audio speakers in order to offset the resistance increase due to both proximity and skin effects.

As support for the comments above concerning the strength of the B fields at various locations, here are plots of the DC B field along the horizontal line shown in Fig P.12 and Fig P.13. In these plots we show $|B_y(x,y=0)|$ (red) as a function of x in the $y = 0$ plane. The wires have radius $1/2$ unit and center separation 3 units (the straight-looking red curve segments are not exactly straight). The math for these plots appears in the Example in Appendix O (c), where J_z is uniform in each conductor.

Currents in same direction: [horizontal line in Fig P.12]

$|B_y(x,y=0)|$

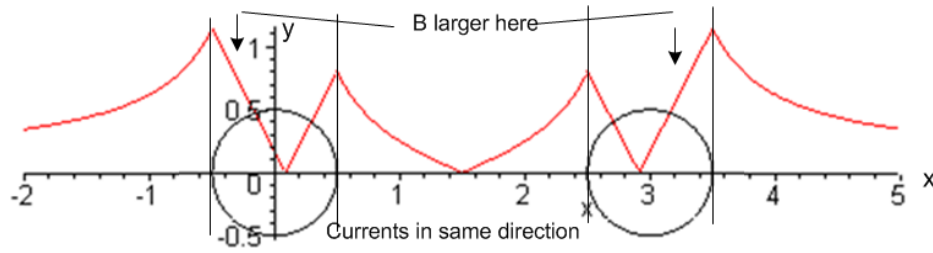


Fig P.14

Currents in opposite direction: [horizontal line in Fig P.13]

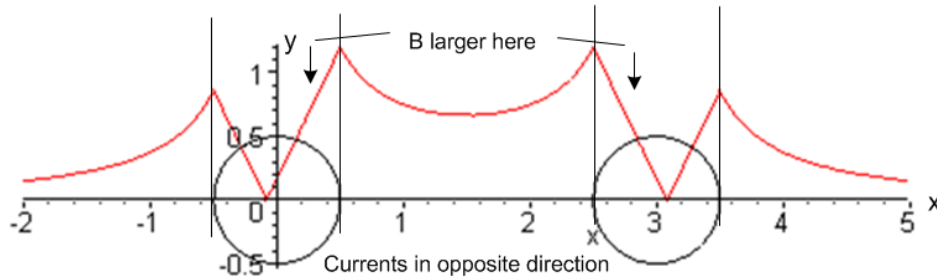


Fig P.15

If we plot $B_y(x,y=0)$ instead of $|B_y(x,y=0)|$, these plots have the following form,

Currents in same direction: [horizontal line in Fig P.12]

$B_y(x,y=0)$

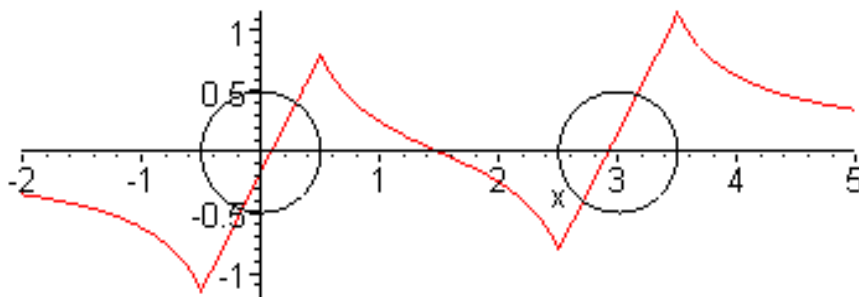


Fig P.16

Currents in opposite direction: [horizontal line in Fig P.13]

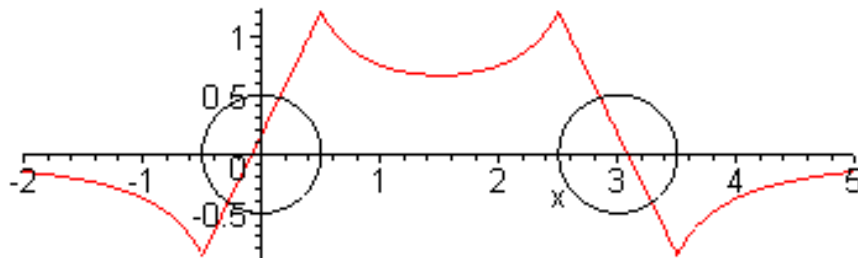


Fig P.17

The figure below shows the total **eddy currents** in the two conductors of a transmission line (oppositely directed currents as in Fig P.13) as seen on a certain slicing plane through the conductors. The arrow patterns come from Fig P.11 making use of the B field strengths shown in Fig P.15 (that is, B fields are stronger on each conductor side closest to the other conductor).

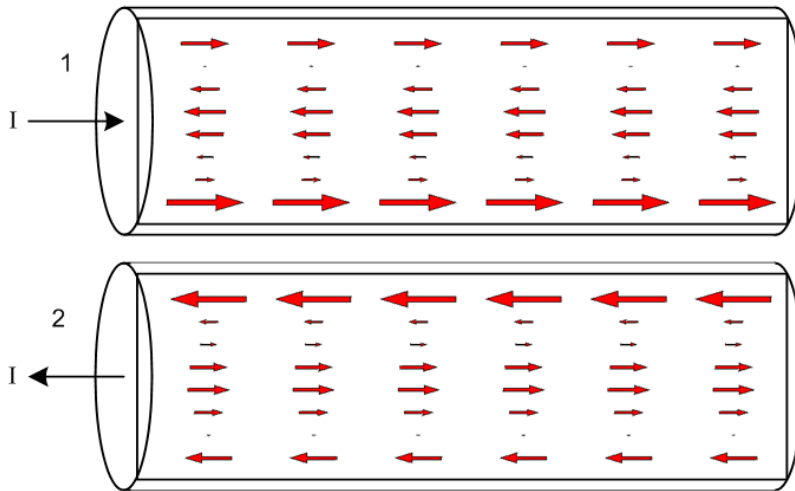


Fig P.18

When the eddy current patterns of Fig P.18 are added to the DC uniform current pattern of Fig P.7a, one obtains the expected pattern of **total current** distribution in a transmission line :

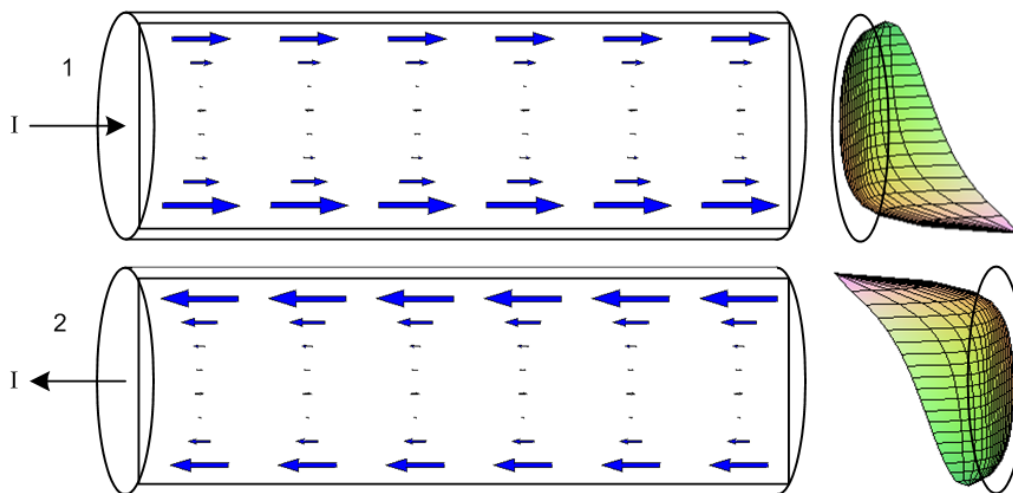


Fig P.19

Both the skin effect and the proximity effect are visible in the current density arrow patterns. The 3D graphs on the right are from Fig 6.12 showing a computed current distribution on each wire cross section.

The reader is reminded that all the arrow drawings in this Section are crude *qualitative* representations and are not the result of any true calculation.

P.9 Quantitative Evaluation of Eddy Currents and The Proximity Effect

Our round-wire discussion above has all been qualitative, and no method was given for computing the actual size of the eddy currents and thus of the proximity effect for two parallel round wires. G. Smith presents the following intriguing graph showing the strength of the proximity effect versus conductor separation for currents in the same direction. In his case $c/a = 1.0$ the conductors are just touching.

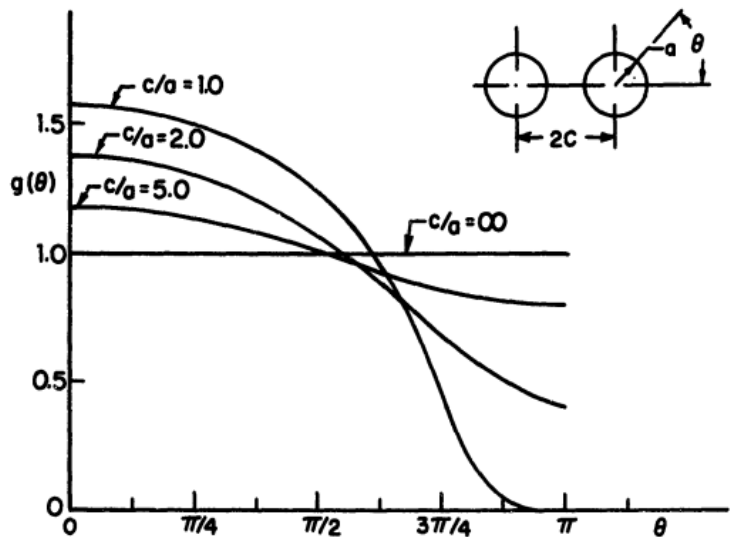


FIG. 1-3 THE NORMALIZED SURFACE CURRENT DISTRIBUTION ON TWO WIRES VARIOUS WIRE SPACINGS c/a

Fig P.20

Presumably ω is high enough to put the conductors into the skin effect regime so all currents are surface currents of thickness $\delta \ll a$.

We present in Section 6.5 a quantitative treatment of the skin and proximity effects for an infinite (or properly terminated) transmission line consisting of parallel round wires, and the results are similar to those of the above graph with $\theta \rightarrow \pi - \theta$. Our treatment, however, is not based on "eddy current analysis", but rather on the charge distribution on the conductor surfaces (think capacitance) and the radial charge pumping boundary condition (D.2.25) which causes internal currents to be larger where the time-changing surface charge is larger. In Section 6.5 (g) we comment on how our methods might be applied to currents flowing in the same direction. As shown in Chapter 7, our general theory is not valid at very low frequencies, and for such the reader is referred to the book of Rodrigues and Valli .

P.10 Influence of Proximity and Skin Effects on Wire Resistance

Consider a small differential volume $rd\theta dr dz$ in a round wire (relative to a cylindrical coordinate system for that wire). Its cross sectional area is $dA = rd\theta dr$. This volume has resistance

$$dR = \rho L/A = \rho dz / dA \quad (\text{P.10.1})$$

and the current through this resistor will be

$$dI = J_z(r,\theta) dA . \quad (\text{P.10.2})$$

The Ohmic power generated in this tiny resistor is, from $P = I^2 R$,

$$dP = (dI)^2 (dR) = [J_z(r,\theta) dA]^2 \rho dz / dA = \rho J_z(r,\theta)^2 dA dz . \quad (\text{P.10.3})$$

For the coin-shaped resistor consisting of length dz of the entire round wire cross section we find then that

$$P = \int dP = dz \int dA \rho J_z(r,\theta)^2 . \quad (\text{P.10.4})$$

The total current in the wire is

$$I = \int dA J_z(r,\theta) \quad (\text{P.10.5})$$

and then from $P = I^2 R$ the effective wire resistance of a cross sectional slice of wire of length dz is,

$$R = \frac{P}{I^2} = \rho dz \frac{\int dA [J_z(r,\theta)]^2}{[\int dA J_z(r,\theta)]^2} \quad \int dA [...] = \int_0^a dr r \int_{-\pi}^{\pi} d\theta [...] \quad (\text{P.10.6})$$

Adding some cancelling factors of $A = \pi a^2$ we get,

$$\mathcal{R} = R/dz = [\rho/A] \frac{\int dA [J_z(r,\theta)]^2/A}{[\int dA J_z(r,\theta)/A]^2} = \mathcal{R}_{dc} \frac{\langle J_z^2 \rangle}{\langle J_z \rangle^2} = \mathcal{R}_{dc} \frac{E(J_z^2)}{[E(J_z)]^2} \quad (\text{P.10.7})$$

where \mathcal{R}_{dc} is the DC resistance per unit length of the wire. Our notations $\langle \rangle$ and $E()$ mean "expected value". In elementary probability theory one writes

$$\begin{aligned} \mu_x &= E(X) && // \text{ mean} \\ \sigma_x^2 &\equiv \text{var}_x = E(X^2) - E(X)^2 = E(X^2) - \mu_x^2 && // \text{ variance; } \sigma_x = \text{standard deviation} \end{aligned}$$

so that

$$\frac{E(X^2)}{[E(X)]^2} = \frac{\sigma_x^2 + \mu_x^2}{\mu_x^2} = 1 + \frac{\sigma_x^2}{\mu_x^2} . \quad (\text{P.10.8})$$

Thus, taking $X = J_z$ we find this result for the round wire AC resistance per unit length [$P = I^2 \mathcal{R}$]

$$\mathcal{R} = \mathcal{R}_{\text{dc}} \left(1 + \frac{\sigma_{J_z}^2}{\mu_{J_z}^2} \right) \quad \frac{\mathcal{R}}{\mathcal{R}_{\text{dc}}} = 1 + \frac{\sigma_{J_z}^2}{\mu_{J_z}^2} \quad \frac{P}{P_{\text{dc}}} = \left[1 + \frac{\sigma_{J_z}^2}{\mu_{J_z}^2} \right] \quad // \text{ loss} \quad (\text{P.10.9})$$

At DC, J_z is constant across the wire cross section so its variance is 0 and the above says $\mathcal{R} = \mathcal{R}_{\text{dc}}$. For *any other* function $J_z(r, \theta) \neq \text{constant}$, one will have some variance $\sigma_{J_z}^2 > 0$ and then $\mathcal{R} > \mathcal{R}_{\text{dc}}$. This discussion presented for a round wire of course applies to a wire of any constant cross sectional shape.

Thus, the proximity and skin effects increase the effective resistance of the wires in Fig P.12 or P.13, causing an increase in the Ohmic loss. Notice that the percentage proximity/skin-effect loss is independent of the current I.

Appendix Q: Properties of the functions $k(\omega)$ and $Z_0(\omega)$; plots for Belden 8281 cable

The two functions of interest are,

	<u>physics model</u>	<u>network model</u>
$k(\omega) = -j\sqrt{zy} = -j\sqrt{(R+j\omega L)(G+j\omega C)}$	(5.3.5)	(K.7)
$Z_0(\omega) = \sqrt{\frac{z}{y}} = \sqrt{\frac{R + j\omega L}{G + j\omega C}}$	(4.12.18)	(K.4)

These expressions for $k(\omega)$ and $Z_0(\omega)$ were derived from both the "physics model" of Chapters 4 and 5 and the network model of Appendix K, with equations numbers shown above. The expressions are valid for all ω in the network model, but in the physics model they were derived only in the skin effect regime, though we might have some expectation that the expressions are approximately valid for low ω . We ignore this issue and just treat $k(\omega)$ and $Z_0(\omega)$ as abstract functions valid for $0 \leq \omega < \infty$.

The four parameters R,L,G and C are by definition all real numbers. For example, in the physics model R is defined to be the real part of z , and ωL the imaginary part of z . In the k and Z_0 sections below, our first task shall be to compute the real and imaginary parts of k and Z_0 . We shall then be interested in the large and small ω limits of these expressions. In order to compute these limits properly, we must remember that the four real parameters R,L,G and C are in general functions of ω and cannot be treated as constants. This requires that we construct a model for these parameters as functions of ω , and that is the task of the first Section Q.1.

This Appendix shows all the Maple calculations required to obtain the large and small ω limits for small $\tan\delta$, and is therefore rather long and opaque. Here is the simple outline to serve as a guide:

- Q.1 A Simple Model for R, L, G and C.**
- Q.2 Real and Imaginary parts of $k(\omega)$
- Q.3 Large ω limit of $k(\omega)$
- Q.4 Small ω limit of $k(\omega)$
- Q.5 The general appearance of $Re(k)$ and $Im(k)$ for Belden 8281 cable.**
- Q.6 Real and Imaginary parts of $Z_0(\omega)$
- Q.7 Large ω limit of $Z_0(\omega)$
- Q.8 Small ω limit of $Z_0(\omega)$
- Q.9 The general appearance of $Re(Z_0)$ and $Im(Z_0)$ for Belden 8281 cable .**

Q.1 A Simple Model for R, L, G and C

The model considered here is just an *ad hoc* "reasonable" model which is accurate at high and low frequencies and which bridges the gap in a crude manner just so we have something to work with. We shall assume that C and L_e are the constants appearing in box (4.12.24), namely

$$\begin{aligned} C &= 4\pi\epsilon_d/K && \text{capacitance per meter} \\ L_e &= \frac{\mu_d}{4\pi} K && \text{external inductance per meter} \\ G_{dc} &= 4\pi\sigma_d/K && \text{DC conductance per meter} \end{aligned}$$

where K is the constant defined also in (4.12.24). The conductance has a dc subscript because σ_d is the DC conductivity of the transmission line dielectric.

Model for C

We assume C to be the constant value shown above, so

$$C(\omega) = C = 4\pi\epsilon_d/K = \text{independent of } \omega \quad (\text{Q.1.1})$$

Model for G

Recall first from (3.3.2) and (3.3.4) that

$$\sigma_{eff} = (\sigma_d + \omega\epsilon'_d \tan_{\mathcal{L}}) \quad \text{where} \quad \tan_{\mathcal{L}} \equiv (\epsilon''_d/\epsilon'_d) \quad \text{and} \quad \epsilon_d = \epsilon'_d - j\epsilon''_d .$$

This σ_{eff} is the effective conductivity of a dielectric whose dielectric constant has an imaginary part. The dielectric burns energy just as if the loss were all simple ohmic loss. From (4.12.24) we then have

$$\begin{aligned} G &= (\sigma_{eff}/\epsilon_d)C = (\sigma_d + \omega\epsilon'_d \tan_{\mathcal{L}})C/\epsilon_d = (\sigma_d/\epsilon_d)C + (\epsilon'_d/\epsilon_d) \tan_{\mathcal{L}} \omega C \\ &= G_{dc} + (\epsilon'_d/\epsilon_d) \tan_{\mathcal{L}} \omega C \end{aligned}$$

where recall that $\tan_{\mathcal{L}}$ is the loss-tangent or dissipation factor of the dielectric. Clearly G has a strong dependence on ω , being a linear function of ω . Normally $(\epsilon'_d/\epsilon_d) \approx 1$ since ϵ''_d and $\tan_{\mathcal{L}}$ are typically very small. Rather than set $(\epsilon'_d/\epsilon_d) = 1$, we just absorb this factor into the definition of $\tan_{\mathcal{L}}$ and then write $G(\omega)$ in this simpler form,

$$G(\omega) = G_{dc} + (C \tan_{\mathcal{L}}) \omega \quad \text{where} \quad G_{dc} = (\sigma_d/\epsilon_d)C . \quad (\text{Q.1.2})$$

Since (σ_d/ϵ_d) has the dimensions sec^{-1} it is convenient to rewrite the above $G(\omega)$ as

$$G(\omega) = C (\omega_d + \tan_{\mathcal{L}} \omega) \quad \omega_d \equiv (\sigma_d/\epsilon_d) \quad G_{dc} = \omega_d C . \quad (\text{Q.1.3})$$

This then is our working model for the frequency-dependent real parameter $G(\omega)$. The interpretation of ω_d is straightforward. If one constructs a parallel plate capacitor with area A , separation s , dielectric constant ϵ_d and dielectric conductivity σ_d , one finds that $R = s/(\sigma_d A)$ and $C = A\epsilon_d/s$ so that $RC = \epsilon_d/\sigma_d$ which is the discharge time constant τ_d for such a capacitor. Then $\omega_d = 1/\tau_d$. In the transmission line context, R is really $1/G_{dc}$, the DC resistance per unit length between the conductors, while C is the capacitance per unit length, and then $\tau_d = RC = C/G_{dc}$ [dim = (far/m)/(mho/m) = far-ohm = sec]. Inversely, $\omega_d = G_{dc}/C$.

Examples:

1. A perfect vacuum dielectric has $\sigma_d = 0$ so both $\omega_d = (\sigma_d/\epsilon_d) = 0$ and $\tan_{\mathbf{L}} = 0$, resulting in $G(\omega) = 0$. This situation with $\omega_d = 0$ presents special problems noted below.

2. As excellent low-conductivity dielectrics, both polyethylene and air have $\sigma_d \sim 10^{-15}$ mho/m. For such dielectrics one finds that

$$\begin{aligned}\omega_d &= \sigma_d/\epsilon_d \approx 10^{-15}/8.85 \times 10^{-12} = 10^{-3}/8.85 = (10/8.85) \times 10^{-4} = 1.13 \times 10^{-4} \text{ sec}^{-1} \\ \tau_d &= 8850 \text{ sec} = 2.5 \text{ hours}\end{aligned}$$

As will be seen below, our low- ω limits are only valid for $\omega < \omega_d$ and are thus in fact "very low ω " limits. This is fine, since we are interested in what happens as $\omega \rightarrow 0$.

3. The loss tangent for the polyethylene used in Belden 8281 coaxial cable has $\tan_{\mathbf{L}} \approx .0005$ and this can be regarded as a typical value for $\tan_{\mathbf{L}}$.

Model for L and R

Recall from Chapter 2 these expressions for the high-frequency resistance and internal inductance of a round wire of radius a_1 ,

$$R_1 = \frac{1}{\sigma(2\pi a_1)\delta} \quad \delta \equiv \sqrt{2/\omega\mu\sigma} \quad (2.4.18)$$

$$L_{1i} = (1/\omega) R_1 = \frac{1}{\omega\sigma(2\pi a_1)\delta} = \frac{1}{\omega\sigma(2\pi a_1)\sqrt{2/\omega\mu\sigma}} = \frac{1}{2\pi a_1} \sqrt{\frac{\mu}{2\sigma\omega}} \quad (2.4.19)$$

These are for conductor C_1 and similar expressions apply to conductor C_2 for a transmission line of the type considered in Chapter 6. Note that σ and μ are parameters of the conductor, not the dielectric. We can rewrite the above equations in this manner

$$\begin{aligned}L_{1i} &= \frac{1}{2\pi a_1} \sqrt{\frac{\mu}{2\sigma}} \omega^{-1/2} && \text{decreases with } \omega \\ R_1 &= \frac{1}{2\pi a_1} \sqrt{\frac{\mu}{2\sigma}} \omega^{+1/2} = \omega L_{1i} && \text{increases with } \omega\end{aligned} \quad (Q.1.4)$$

We now generalize these results for an arbitrary conductor C_1 as follows

$$\begin{aligned}
 L_{1i} &= \frac{1}{p_1} \sqrt{\frac{\mu}{2\sigma}} \omega^{-1/2} && \text{decreases with } \omega \\
 R_1 = \omega L_{1i} &= \frac{1}{p_1} \sqrt{\frac{\mu}{2\sigma}} \omega^{+1/2} && \text{increases with } \omega
 \end{aligned} \tag{Q.1.5}$$

where p_1 is the "active perimeter" distance around the cross section of the conductor, as mentioned in (4.12.10). Recall that surface impedance $Z_{s1}(\theta) = R_1(\theta) + \omega L_{1i}(\theta)$ but we average these quantities over θ to get the above results, as discussed in Section 4.12 (b). For widely spaced thin wires (or a centered coaxial cable), the active perimeter of a round wire is the full perimeter so $p_1 = 2\pi a_1$, but the active perimeter is much less than the total perimeter for a pair of closely spaced conductors such as shown in Fig 4.13. We regard the generalization (Q.1.5) as being "reasonable" if not precise. Summing over the two conductors of our transmission line, we then find for large ω that

$$\begin{aligned}
 L_i &= \left(\frac{1}{p_1} + \frac{1}{p_2}\right) \sqrt{\frac{\mu}{2\sigma}} \omega^{-1/2} \equiv \kappa \omega^{-1/2} && \kappa \equiv \left(\frac{1}{p_1} + \frac{1}{p_2}\right) \sqrt{\frac{\mu}{2\sigma}} \\
 R &= \left(\frac{1}{p_1} + \frac{1}{p_2}\right) \sqrt{\frac{\mu}{2\sigma}} \omega^{+1/2} \equiv \kappa \omega^{+1/2} . && \dim(\kappa) = \text{ohm/m} * \text{sec}^{1/2}
 \end{aligned} \tag{Q.1.6}$$

In order to crudely blend these expressions down into the low ω region, we write

$$\begin{aligned}
 R(\omega) &= R_{dc} \theta(\omega < \omega_R) + (\kappa \sqrt{\omega}) \theta(\omega \geq \omega_R) && \omega_R \equiv (R_{dc}/\kappa)^2 \\
 L_i(\omega) &= L_{i,dc} \theta(\omega < \omega_L) + (\kappa/\sqrt{\omega}) \theta(\omega \geq \omega_L) && \omega_L \equiv (\kappa/L_{i,dc})^2
 \end{aligned} \tag{Q.1.7}$$

where $\theta(\text{bool}) = 1$ if $\text{bool} = \text{true}$, else 0. The values of ω_R and ω_L cause the two functions to match at the boundaries $\omega = \omega_R$ and $\omega = \omega_L$. Here $R_{dc} = 1/(\sigma A_1) + 1/(\sigma A_2)$ is the total DC resistance of the two conductors of cross sectional area A_i , while $L_{i,dc}$ is the total DC internal inductance. Examples of computing the latter appear in Appendix C. For a round wire, $L_i = \mu/8\pi$, so for a pair of same, $L_{i,dc} = \mu/4\pi$ henry/m.

Using parameters shown in Appendix R for **Belden 8281** coaxial cable, we may plot $R(\omega)$ and $L_i(\omega)$ for our crude model. First, the two expressions are entered into Maple (using w for ω),

```

restart; with(plots): unprotect('Li');
R := Rdc*Heaviside(wR-w) + (kappa*sqrt(w))*Heaviside(w-wR);
      R := Rdc Heaviside(wR - w) + kappa*sqrt(w) Heaviside(w - wR)
Li := Lidc*Heaviside(wL-w) + (kappa/sqrt(w))*Heaviside(w-wL);
      Li := Lidc Heaviside(wL - w) + (kappa Heaviside(w - wL)) / sqrt(w)
kappa := (1/p1 + 1/p2)*sqrt(mu0/(2*sigma));
    
```

followed by parameters for the Belden cable obtained in Appendix R,

```

pi := evalf(Pi):
mu0 := 4*pi*1e-7:
sigma := 5.81e7:
a1 := (1/2)*0.7874e-3:
a2 := ((1/2)*5020.2 + 11.5) * 1e-6:
p1 := 2*pi*a1: p2 := 2*pi*a2:
R2DC := 3.6091e-3:
R1DC := 32.4819e-3:
Rdc := R2DC + R1DC:
Lidc := .58e-7:
evalf(kappa);

.00004860306321
    
```

The two blending frequencies are computed,

```

wR := (Rdc/kappa)^2;
wL := (kappa/Lidc)^2;
    
```

$wR = 551404.8070$
 $wL = 702216.9304$

and are seen to be in the 1 MHz range. Finally, here are plots for R and L_i versus ω for a very wide range of ω : $\omega = 1$ to $\omega = 10^{10}$,

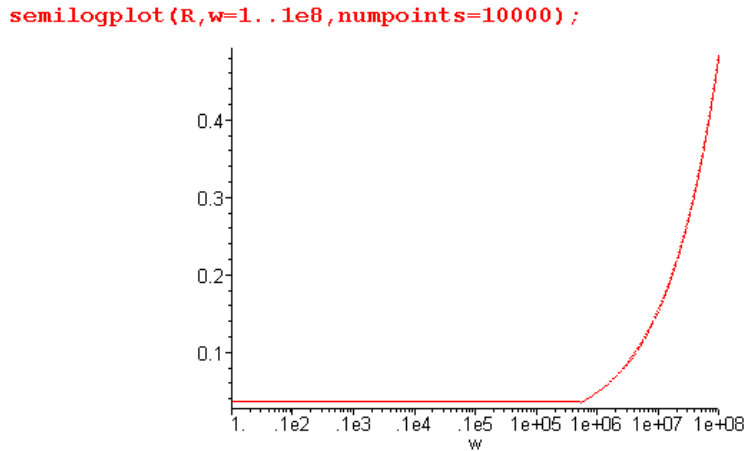


Fig Q.1.1

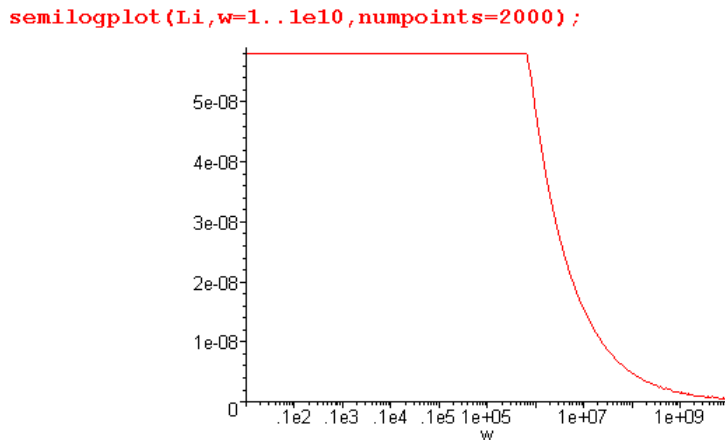


Fig Q.1.2

These plots duly show the resistance increasing as $\sqrt{\omega}$ and internal inductance decreasing as $1/\sqrt{\omega}$ for large ω . It would not be difficult to provide a smooth blending function to remove the sharp corners from these plots, but since our main interest is in very large and very small ω , we leave things as is (but see below).

The final step is to add in the external inductance L_e so our model for $R(\omega)$ and $L(\omega)$ is then

$$\begin{aligned}
 R(\omega) &= R_{dc} \theta(\omega < \omega_R) + (\kappa \sqrt{\omega}) \theta(\omega \geq \omega_R) & \omega_R &\equiv (R_{dc}/\kappa)^2 \\
 L(\omega) &= L_e + L_{i,dc} \theta(\omega < \omega_L) + (\kappa/\sqrt{\omega}) \theta(\omega \geq \omega_L) & \omega_L &\equiv (\kappa/L_{i,DC})^2 .
 \end{aligned}
 \tag{Q.1.8}$$

For the Belden cable example $L_e = 0.37 \mu\text{H/m} = 3.7 \times 10^{-7} \text{ H/m}$, giving this plot for $L(\omega)$ versus ω :

```
semilogplot([L,Le],w=1..1e10,numpoints=2000,view=[1..1e10,0..1.5*Le],color=[red,black]);
```

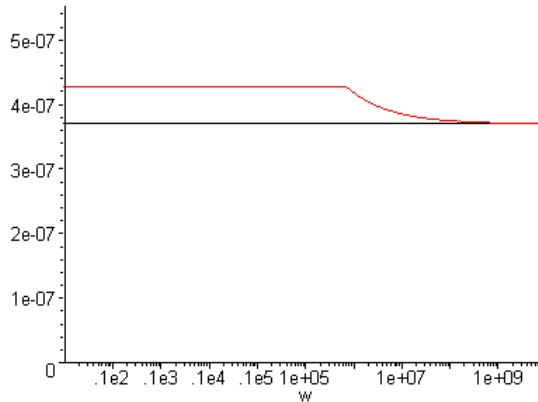


Fig Q.1.3

$L(\omega)$ is shown in red, while L_e is shown in black. This last plot shows that L_e is really the dominant term in $L(\omega)$ at all ω . More magnetic energy is stored in the dielectric than inside the conductors. So:

Simple Transmission Line Parameter Model		(Q.1.9)
$C(\omega) = C = \text{independent of } \omega$		$\kappa \equiv \left(\frac{1}{p_1} + \frac{1}{p_2}\right) \sqrt{\frac{\mu}{2\sigma}}$
$G(\omega) = C (\omega_d + \tan_L \omega)$		$\omega_d \equiv (\sigma_d/\epsilon_d) \quad G_{dc} \equiv \omega_d C$
$R(\omega) = R_{dc} \theta(\omega < \omega_R) + (\kappa \sqrt{\omega}) \theta(\omega \geq \omega_R)$		$\omega_R \equiv (R_{dc}/\kappa)^2$
$L(\omega) = L_e + L_{i,dc} \theta(\omega < \omega_L) + (\kappa/\sqrt{\omega}) \theta(\omega \geq \omega_L)$		$\omega_L \equiv (\kappa/L_{i,dc})^2$
$L_e C = \mu_d \epsilon_d = 1/v_d^2 \quad (4.12.24)$		$L_{dc} \equiv L_e + L_{i,dc}$

The last line shows that L_e has a simple relation to C in terms of the dielectric speed of light v_d . The two p_i are the active perimeters of the conductors, μ and σ are for the conductors, and σ_d , ϵ_d and μ_d are for the dielectric. R_{dc} and L_{idc} are the DC resistance and internal inductance total for the two conductors.

How Good is this Crude Model?

Recall that R and ωL_i are the real and imaginary parts of the total (mean) *surface* impedance Z_i of the two transmission line conductors. For the Belden coaxial cable example, the central conductor is in a symmetric environment and for that situation we have an exact expression for Z_i from (2.4.6),

$$Z_s(\omega) = \frac{-j\omega\mu}{2\pi a\beta} \frac{J_0(\beta a)}{J_1(\beta a)} \quad \beta^2 = -j\omega\mu\sigma \quad (2.4.6)$$

We do not have an exact expression for the surface impedance of the shield, but based on the high and low ω numbers shown in Appendix R, we can roughly account for the shield by adding 15% to the above central conductor function, resulting in a function for the total $Z_i(\omega)$ which is a smooth function of ω . We can then plot this function and compare it with our simple Heaviside model presented above, again for the Belden 8281 example. First, here is the "smooth 115% model" followed by the "crude Heaviside model",

```
restart; with(plots): unprotect('Li');
alias(I=I,j=sqrt(-1), J = BesselJ); pi := evalf(Pi):
```

The smooth 115% model

```
Zs1 := (-j*omega*mu0/(2*pi*a1*beta))*J(0,beta*a1)/J(1,beta*a1);
```

$$Z_{s1} := -0.1591549431 \frac{j \omega \mu_0 J(0, \beta a_1)}{a_1 \beta J(1, \beta a_1)}$$

```
beta := sqrt(-j*omega*mu0*sigma):
```

```
mu0 := 4*pi*1e-7: sigma := 5.81e7:
```

```
a1 := (1/2)*0.7874e-3: a2 := ((1/2)*5020.2 + 11.5) * 1e-6:
```

```
R := 1.15*Re(Zs1):
```

```
Li := 1.15*Im(Zs1)/omega:
```

The crude Heaviside model

```
R_ := Rdc*Heaviside(wR-omega) + (kappa*sqrt(omega))*Heaviside(omega-wR);
```

$$R_ := R_{dc} \text{Heaviside}(wR - \omega) + \kappa \sqrt{\omega} \text{Heaviside}(\omega - wR)$$

```
Li_ := Lidc*Heaviside(wL-omega) + (kappa/sqrt(omega))*Heaviside(omega-wL);
```

$$Li_ := L_{dc} \text{Heaviside}(wL - \omega) + \frac{\kappa \text{Heaviside}(\omega - wL)}{\sqrt{\omega}}$$

```
kappa := (1/p1 + 1/p2)*sqrt(mu0/(2*sigma)):
```

```
p1 := 2*pi*a1: p2 := 2*pi*a2:
```

```
Rdc := .360910e-1: Lidc := .58e-7:
```

```
wR := (Rdc/kappa)^2: wL := (kappa/Lidc)^2:
```

And here are "side by side" plots of R and L_i for the two models for $\omega = 10^4$ to 10^8 ,

```
wlo := 1e4: whi := 1e8:
```

```
semilogplot([R_,R],omega = wlo..whi, view = [wlo..whi,  
0..6e-1],numpoints=800,thickness=2, color = [red,black]);
```

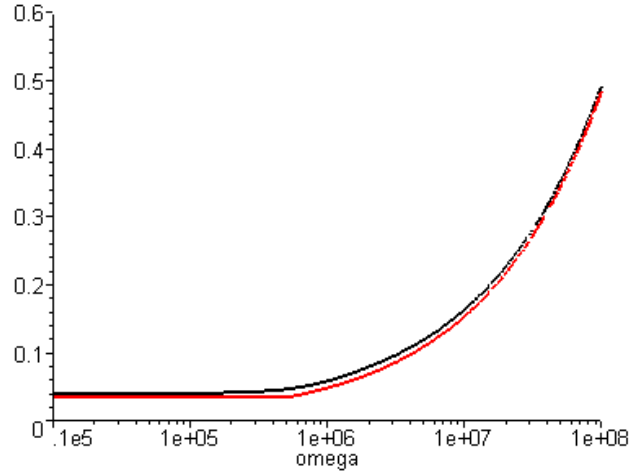


Fig Q.1.4

```
semilogplot([Li_,Li],omega = wlo..whi, view = [wlo..whi,  
0..6e-8],numpoints=800,thickness=2, color = [red,black]);
```

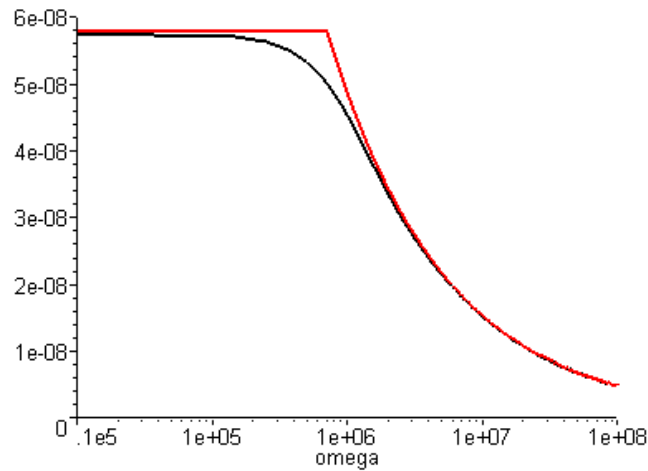


Fig Q.1.5

Below $\omega = 10^4$ and above $\omega = 10^8$ the two models are in very close agreement, and the smooth model (black) then shows what the correct interpolation of the crude Heaviside model (red) might look like. The Heaviside model we think gives the essence of the behavior of R and L_i versus ω .

Reader Exercise: Using the methods of Chapter 2, develop an expression for Z_i (like (2.4.6) quoted just above) which applies to the sheath of a coaxial cable. Verify against data presented in Appendix R. The DC limit should agree with (C.6.6) and the large- ω limit with (Q.1.5). Perhaps assume $t \ll a_2$.

Q.2 Real and Imaginary parts of $k(\omega)$

Fact 1: The real and imaginary decomposition of k is given by (Q.2.1)

$$\begin{aligned}
 k &= \sqrt{\frac{a^2-c}{2}} - j \sqrt{\frac{a^2+c}{2}} & k &\equiv -j \sqrt{(R+j\omega L)(G+j\omega C)} \\
 jk &= \sqrt{\frac{a^2+c}{2}} + j \sqrt{\frac{a^2-c}{2}} & jk &= \sqrt{zy} = \sqrt{(R+j\omega L)(G+j\omega C)}
 \end{aligned}$$

where

$$a \equiv [(R^2 + \omega^2 L^2)(G^2 + \omega^2 C^2)]^{1/4} = |k| \quad \dim(a) = 1/m \quad a > 0$$

$$c \equiv RG - \omega^2 LC \quad \dim(c) = 1/m^2 \quad c = \text{real}, \quad |c| < a^2$$

Proof of Fact 1: Let

$$q \equiv zy = (R+j\omega L)(G+j\omega C) = (RG - \omega^2 LC) + j\omega(LG+RC) = c + j\omega(LG+RC) = |q| e^{j\theta}$$

$$\Rightarrow |q|^2 = |(R+j\omega L)(G+j\omega C)|^2 = |(R+j\omega L)|^2 |(G+j\omega C)|^2 = (R^2 + \omega^2 L^2)(G^2 + \omega^2 C^2) \equiv a^4$$

$$|q| = a^2$$

$$\cos\theta = \text{Re}(q) / |q| = c/a^2$$

Now write

$$s \equiv \sqrt{zy} = \sqrt{(R+j\omega L)(G+j\omega C)} = \sqrt{q} = |s| e^{i\phi} \quad |s| = \sqrt{|q|} = a \quad \phi = \theta/2$$

$$\text{Re}(s) = |s| \cos\phi = a \cos(\theta/2) = a \sqrt{(1+\cos\theta)/2} = (a/\sqrt{2}) \sqrt{1+c/a^2} = \sqrt{\frac{a^2+c}{2}}$$

$$\text{Im}(s) = |s| \sin\phi = a \sin(\theta/2) = a \sqrt{(1-\cos\theta)/2} = (a/\sqrt{2}) \sqrt{1-c/a^2} = \sqrt{\frac{a^2-c}{2}}$$

$$s = \sqrt{zy} = \sqrt{\frac{a^2+c}{2}} + j \sqrt{\frac{a^2-c}{2}}$$

$$k = -j\sqrt{zy} = -js = \sqrt{\frac{a^2-c}{2}} - j \sqrt{\frac{a^2+c}{2}} \quad \text{QED}$$

Maple verification:

```

restart; alias(I=I,j=sqrt(-1));
assume(R>0,L>0,G>0,C>0,omega>0);
k := (-j)*sqrt((R+j*omega*L)*(G+j*omega*C));
                                     k = -j*sqrt((R+j*omega*L)*(G+j*omega*C))
asq_ := ((R^2+omega^2*L^2)*(G^2+omega^2*C^2))^(1/2); # a^2
                                     asq_ = sqrt((R^2+omega^2*L^2)*(G^2+omega^2*C^2))
c_ := R*G - omega^2*L*C;
                                     c_ = R*G - omega^2*L*C
k := factor(evalc(k));
                                     k = 1/2*sqrt(2*sqrt((R^2+omega^2*L^2)*(G^2+omega^2*C^2)) - 2*R*G + 2*omega^2*L*C) - 1/2*j*sqrt(-2*omega^2*L*C + 2*R*G + 2*sqrt((R^2+omega^2*L^2)*(G^2+omega^2*C^2)))
k := subs(asq_ = a^2,k);
                                     k = 1/2*sqrt(2*a^2 - 2*R*G + 2*omega^2*L*C) - 1/2*j*sqrt(-2*omega^2*L*C + 2*R*G + 2*a^2)
k := subs(R*G = c + omega^2*L*C,k);
                                     k = 1/2*sqrt(2*a^2 - 2*c) - 1/2*j*sqrt(2*c + 2*a^2)
factor(expand(asq_^2 - c_^2)); # to show that a^2 > |c|
                                     omega^2*(R*C + L*G)^2
    
```

Q.3 Large ω limit of $k(\omega)$

The model of box (Q.1.9) at large ω indicates, using $L_e = 1/(Cv_d^2)$,

$$\begin{aligned}
 G(\omega) &= C(\omega_d + \tan_{\mathbf{r}} \omega) & \omega_d &\equiv (\sigma_d/\varepsilon_d) \\
 R(\omega) &= \kappa\sqrt{\omega} \\
 L(\omega) &= 1/(Cv_d^2) + (\kappa/\sqrt{\omega}) \quad . & \kappa &\equiv \left(\frac{1}{p_1} + \frac{1}{p_2}\right)\sqrt{\frac{\mu}{2\sigma}}
 \end{aligned} \tag{Q.3.1}$$

Defining $t \equiv \tan_{\mathbf{r}}$ these expressions are,

$$G = C(\omega_d + t \omega) \quad R = \kappa\sqrt{\omega} \quad L = 1/(Cv_d^2) + \kappa/\sqrt{\omega} \quad . \tag{Q.3.2}$$

We duly enter the expressions into Maple (using w for ω)

```

G := C*(wd + t*w);
                                     G = C*(wd + t*w)
R := kappa*sqrt(w);
                                     R = kappa*sqrt(w)
L := 1/(vd^2*C) + kappa/sqrt(w);
                                     L = 1/(vd^2*C) + kappa/sqrt(w)
    
```

followed by the intermediate variables a and c from box (Q.2.1),

$$a := ((R^2 + w^2 * L^2) * (G^2 + w^2 * C^2))^{(1/4)};$$

$$a := \left(\left(\kappa^2 w + w^2 \left(\frac{1}{v d^2 C} + \frac{\kappa}{\sqrt{w}} \right)^2 \right) (C^2 (w d + t w)^2 + w^2 C^2) \right)^{\left(\frac{1}{4} \right)}$$

$$c := R * G - w^2 * L * C;$$

$$c := \kappa \sqrt{w} C (w d + t w) - w^2 \left(\frac{1}{v d^2 C} + \frac{\kappa}{\sqrt{w}} \right) C$$

The real part of $k(\omega)$ is then given from (Q.2.1) as follows:

$$> \text{Rek} := \text{sqrt}((a^2 - c)/2);$$

Rek :=

$$\frac{1}{2} \sqrt{2 \sqrt{\left(\kappa^2 w + w^2 \left(\frac{1}{v d^2 C} + \frac{\kappa}{\sqrt{w}} \right)^2 \right) (C^2 (w d + t w)^2 + w^2 C^2) - 2 \kappa \sqrt{w} C (w d + t w) + 2 w^2 \left(\frac{1}{v d^2 C} + \frac{\kappa}{\sqrt{w}} \right) C}}$$

The asymptotic expansion of $\text{Re}(k)$ for large ω is then found to be,

$$> \text{series}(\text{Rek}, w = \text{infinity}, 1): \text{Rek1} := \text{collect}(\%, w);$$

$$\text{Rek1} = \frac{1}{2} \sqrt{2 \frac{\sqrt{C^2 t^2 + C^2}}{v d^2 C} + 2 \frac{1}{v d^2} w} + \frac{1}{4} \frac{2 \sqrt{C^2 t^2 + C^2} \kappa + 2 \kappa C - 2 \kappa C t}{\sqrt{2 \frac{\sqrt{C^2 t^2 + C^2}}{v d^2 C} + 2 \frac{1}{v d^2} w} \sqrt{\frac{1}{w}}}$$

which has the form $A\omega + B\sqrt{\omega} + C + D/\sqrt{\omega} + O(1/\omega)$, but we have not displayed the C and D terms since they are quite complicated. Maple next processes the terms by first simplifying them, then expanding them in small parameter t . That is, we now regard $t \equiv \tan_{\underline{L}} \ll 1$. The results are shown below.

Maple notes: (1) The n th term in the Rek1 series can be accessed as $\text{op}(n, \text{Rek1})$; (2) Maple displays the output of a command terminated by a semicolon, but suppresses the output if terminated by a colon; (3) in the series command, the second argument gives the variable and point of expansion, the third the number of terms; (4) symbol $\%$ always refers to the last thing computed.

`op(1,Rek1); simplify(%): series(%,t=0,3);`

$$\frac{1}{2} \sqrt{2 \frac{\sqrt{C^2 t^2 + C^2}}{vd^2 C} + 2 \frac{1}{vd^2} w}$$

$$\frac{w}{vd} + \frac{1}{8} \frac{w}{vd} t^2 + O(t^4)$$

`op(2,Rek1); simplify(%): series(%,t=0,2);`

$$\frac{1}{4} \frac{2 \sqrt{C^2 t^2 + C^2} \kappa + 2 \kappa C - 2 \kappa C t}{\sqrt{2 \frac{\sqrt{C^2 t^2 + C^2}}{vd^2 C} + 2 \frac{1}{vd^2} \sqrt{\frac{1}{w}}}}$$

$$\frac{1}{2} vd \kappa C \sqrt{w} - \frac{1}{4} vd \kappa C \sqrt{w} t + O(t^2)$$

`op(3,Rek1); simplify(%): series(%,t=0,3); simplify(%);`

$$\frac{1}{8} \frac{vd^4 C^2 \kappa^2 + 2 wd}{vd} t + O(t^3)$$

`op(4,Rek1); simplify(%): series(%,t=0,2); simplify(%);`

$$-\frac{1}{8} \frac{vd \kappa C (vd^4 C^2 \kappa^2 + 2 wd)}{\sqrt{w}} - \frac{1}{16} \frac{vd \kappa C (vd^4 C^2 \kappa^2 - 2 wd)}{\sqrt{w}} t + O(t^2)$$

Although we have suppressed the last two "op" expressions, we did verify that they were the correct terms in the series. Maple sometimes orders series in strange ways but here the ordering was as expected.

Collecting the results and keeping only the leading terms in $t = \tan_{\mathbf{L}}$, the resulting large ω limit for $\text{Re}(k)$ is seen to be,

$$\text{Re}(k) \approx (\omega/v_d) + (1/2)v_d \kappa C \sqrt{\omega} + (1/8v_d)(v_d^4 C^2 \kappa^2 + 2\omega_d) \tan_{\mathbf{L}} + O(1/\sqrt{\omega}) \quad (\text{Q.3.3})$$

where we have ignored the details of the $O(1/\sqrt{\omega})$ term.

Treating $\text{Im}(k)$ in the same manner one finds,

`Imk := - sqrt((a^2+c)/2);`

$$\text{Imk} := -\frac{1}{2} \sqrt{2 \sqrt{\left(\kappa^2 w + w^2 \left(\frac{1}{vd^2 C} + \frac{\kappa}{\sqrt{w}} \right)^2 \right) (C^2 (wd + tw)^2 + w^2 C^2) + 2 \kappa \sqrt{w} C (wd + tw) - 2 w^2 \left(\frac{1}{vd^2 C} + \frac{\kappa}{\sqrt{w}} \right) C}}$$

`> series(Imk,w=infinity,1): Imk1 :=collect(%,w);`

$$\text{Imk1} := -\frac{1}{2} \sqrt{2 \frac{\sqrt{C^2 t^2 + C^2}}{vd^2 C} - 2 \frac{1}{vd^2} w} - \frac{1}{4} \frac{2 \sqrt{C^2 t^2 + C^2} \kappa - 2 \kappa C + 2 \kappa C t}{\sqrt{2 \frac{\sqrt{C^2 t^2 + C^2}}{vd^2 C} - 2 \frac{1}{vd^2} \sqrt{\frac{1}{w}}}}$$

Once again the series has the form $A\omega + B\sqrt{\omega} + C + D/\sqrt{\omega} + O(1/\omega)$, but we have not displayed the C and D terms since they are complicated. Expanding each series term for small t gives

`op(1,Imk1); simplify(%): series(%,t=0,4);`

$$-\frac{1}{2} \sqrt{2 \frac{\sqrt{C^2 t^2 + C^2}}{v_d^2 C} - 2 \frac{1}{v_d^2} \omega} - \frac{1}{2} \frac{\omega}{v_d} t + \frac{1}{16} \frac{\omega}{v_d} t^3 + O(t^5)$$

`op(2,Imk1); simplify(%): series(%,t=0,4);`

$$-\frac{1}{4} \frac{2 \sqrt{C^2 t^2 + C^2} \kappa - 2 \kappa C + 2 \kappa C t}{\sqrt{2 \frac{\sqrt{C^2 t^2 + C^2}}{v_d^2 C} - 2 \frac{1}{v_d^2} \omega} \sqrt{\frac{1}{\omega}}} - \frac{1}{2} v_d \kappa C \sqrt{\omega} - \frac{1}{4} v_d \kappa C \sqrt{\omega} t - \frac{1}{16} v_d \kappa C \sqrt{\omega} t^2 + O(t^3)$$

`op(3,Imk1); simplify(%): series(%,t=0,6);`

$$-\frac{1}{2} \frac{\omega d - \frac{1}{2} v_d^4 C^2 \kappa^2}{v_d} + \left(\frac{1}{16} \frac{\omega d - \frac{1}{2} v_d^4 C^2 \kappa^2}{v_d} - \frac{1}{2} \frac{-\frac{1}{4} \omega d - \frac{1}{8} v_d^4 C^2 \kappa^2}{v_d} \right) t^2 + O(t^4)$$

`op(4,Imk1); simplify(%): series(%,t=0,7);`

$$-\frac{1}{2} \frac{v_d \kappa C \left(\frac{1}{2} \omega d + \frac{1}{4} v_d^4 C^2 \kappa^2 \right)}{\sqrt{\omega}} - \frac{1}{2} \frac{v_d \kappa C \left(\frac{1}{4} \omega d - \frac{1}{8} v_d^4 C^2 \kappa^2 \right)}{\sqrt{\omega}} t + O(t^2)$$

Collecting the results and keeping only the leading terms in $t = \tan_{\mathbf{L}}$, the resulting large ω limit for $\text{Im}(k)$ is seen to be,

$$\text{Im}(k) \approx -(\omega/v_d) \tan_{\mathbf{L}}/2 - (v_d \kappa C/2) \sqrt{\omega} - (1/2 v_d)(\omega_d - v_d^4 C^2 \kappa^2/2) + O(1/\sqrt{\omega}) \quad (\text{Q.3.4})$$

where we have again ignored the details of the $O(1/\sqrt{\omega})$ term. We now summarize these results :

Fact 2: The large ω asymptotic expansion for $k(\omega)$, assuming $\tan_{\mathbf{L}} \ll 1$, is given by (Q.3.5)

$$\begin{aligned} \text{Re}(k) &\approx (\omega/v_d) + (v_d \kappa C/2) \sqrt{\omega} + (1/4 v_d)(\omega_d + v_d^4 C^2 \kappa^2/2) \tan_{\mathbf{L}} + O(1/\sqrt{\omega}) \\ \text{Im}(k) &\approx -(\omega/v_d) \tan_{\mathbf{L}}/2 - (v_d \kappa C/2) \sqrt{\omega} - (1/2 v_d)(\omega_d - v_d^4 C^2 \kappa^2/2) + O(1/\sqrt{\omega}) \end{aligned}$$

$$\text{where } \kappa \equiv \left(\frac{1}{p_1} + \frac{1}{p_2} \right) \sqrt{\frac{\mu}{2\sigma}} \quad \text{and } \omega_d \equiv (\sigma_d/\epsilon_d)$$

Keeping only the leading terms for large ω ,

$$\begin{aligned} \text{Re}(k) &\approx (\omega/v_d) & v_d &= 1/\sqrt{L_e C} \approx 1/\sqrt{LC} \\ \text{Im}(k) &\approx -\omega \tan_{\mathbf{L}}/(2v_d) \end{aligned}$$

The leading term $\text{Re}(k) = \omega/v_d$ is the usual result obtained from taking the large ω limit of the expression $k = -j\sqrt{(R+j\omega L)(G+j\omega C)}$ when the four parameters are treated as constants in ω ,

$$k = -j\sqrt{(R+j\omega L)(G+j\omega C)} \approx -j\sqrt{(j\omega L)(j\omega C)} = (-j)(j)\omega\sqrt{LC} = \omega\sqrt{LC} \approx \omega\sqrt{L_e C} = \omega/v_d .$$

This fact is obvious from the large- ω model stated in (Q.3.1) which we repeat here:

$$\begin{aligned} G(\omega) &= C (\omega_d + \tan_{\mathbf{L}} \omega) & \omega_d &\equiv (\sigma_d/\epsilon_d) \\ R(\omega) &= \kappa\sqrt{\omega} \\ L(\omega) &= 1/(Cv_d^2) + (\kappa/\sqrt{\omega}) \quad . & \kappa &\equiv \left(\frac{1}{p_1} + \frac{1}{p_2}\right)\sqrt{\frac{\mu}{2\sigma}} \end{aligned} \quad (Q.3.1)$$

Since $\tan_{\mathbf{L}} \ll 1$ one has for large ω ,

$$\begin{aligned} G + j\omega C &= C (\omega_d + \tan_{\mathbf{L}} \omega) + j\omega C = C \omega_d + \omega C (\tan_{\mathbf{L}} + j) \approx \omega C j = j\omega C \\ R + j\omega L &= \kappa\sqrt{\omega} + j\omega [L_e + (\kappa/\sqrt{\omega})] \approx j\omega L_e \approx j\omega L \end{aligned}$$

so

$$k = -j\sqrt{(R+j\omega L)(G+j\omega C)} = -j\sqrt{(j\omega L)(j\omega C)} = \omega\sqrt{LC} \approx \omega\sqrt{L_e C} = \omega/v_d$$

The leading term $\text{Im}(k) = -\omega \tan_{\mathbf{L}} / (2v_d)$ indicates the presence of loss due to the aptly named loss tangent $\tan_{\mathbf{L}}$. The quantity $\text{Re}(k) = \omega/v_d$ is called β_{d0} in (1.5.1b) [since $v_d = 1/\sqrt{\mu_d \epsilon_d}$] and is the wavenumber that an electromagnetic plane wave would have traveling through an infinite dielectric.

Q.4 Small ω limit of $k(\omega)$

If the DC conductance $G_d = \omega_d C$ is non-vanishing (because $\sigma_d > 0$) we find one set of results, but if the dielectric is a perfect vacuum with $\sigma_d = 0$, we get a different set of results. The two cases are treated separately below with an explanation.

Small ω limit of $k(\omega)$ for $\omega_d > 0$

The model of box (Q.1.9) at small ω reads,

$$\begin{aligned} G(\omega) &= C (\omega_d + \tan_{\mathbf{L}} \omega) & \omega_d &\equiv (\sigma_d/\epsilon_d) \\ R(\omega) &= R_{dc} \\ L(\omega) &= L_e + L_{idc} \equiv L_{dc} \quad . \end{aligned} \quad (Q.4.1)$$

With $t \equiv \tan_{\mathbf{L}}$ these expressions are,

$$G = C(\omega_d + t \omega) \quad R = R_{dc} \quad L = L_{dc} . \quad (Q.4.2)$$

Enter the expressions into Maple (using w for ω)

$$G := C*(wd + t*w);$$

$$G = C (wd + t w)$$

$$R := Rdc;$$

$$R = Rdc$$

$$L := Ldc;$$

$$L = Ldc$$

followed by the intermediate variables a and c from box (Q.2.1),

$$a := ((R^2 + w^2 * L^2) * (G^2 + w^2 * C^2))^{(1/4)};$$

$$a = ((Rdc^2 + w^2 Ldc^2) (C^2 (wd + t w)^2 + w^2 C^2))^{(1/4)}$$

$$c := R * G - w^2 * L * C;$$

$$c = Rdc C (wd + t w) - w^2 Ldc C$$

The real part of $k(\omega)$ is given from (Q.2.1) as follows:

$$Rek := \text{sqrt}((a^2 - c)/2);$$

$$Rek = \frac{1}{2} \sqrt{2 \sqrt{(Rdc^2 + w^2 Ldc^2) (C^2 (wd + t w)^2 + w^2 C^2)} - 2 Rdc C (wd + t w) + 2 w^2 Ldc C}$$

The expansion of $Re(k)$ for small ω is found to be,

$$> \text{series}(Rek, w=0, 4): Rekl := \text{simplify}(\text{collect}(\%, w));$$

$$Rekl = \frac{1}{2} \frac{\sqrt{C} (Rdc + Ldc wd)}{\sqrt{Rdc} \sqrt{wd}} w - \frac{1}{4} \frac{(Rdc - Ldc wd) t \sqrt{C}}{wd \sqrt{Rdc}} w^2 + \frac{1}{16} \frac{\sqrt{C} (-Rdc^3 + 3 Rdc^3 t^2 - Rdc^2 t^2 Ldc wd + Rdc^2 Ldc wd + Ldc^2 wd^2 Rdc - Ldc^3 wd^3)}{Rdc \left(\frac{5}{2}\right) wd \left(\frac{5}{2}\right)} w^3 + O(w^4)$$

We show several terms to illustrate that the general form of this series is

$$Re(k) = \sqrt{\omega_d} \sum_{n=1}^{\infty} A_n(R_{dc}, L_{dc}, \omega_d) (\omega/\omega_d)^n. \quad (Q.4.3)$$

The coefficients A_n do not vanish as $\omega_d \rightarrow 0$, so we infer that the power series converges only for $\omega < \omega_d$, which is a very low frequency as noted earlier ($\omega_d = 10^{-4}$ for Belden 8281 cable). If one attempts to take the limit $\omega_d \rightarrow 0$ of the above series, the function $Re(k)$ has a branch point in the complex ω plane at $\omega = \omega_d$ which impinges on the origin as $\omega_d \rightarrow 0$, causing the series's radius of convergence to shrink down to nothing, and the series then diverges and is meaningless. That is why $\omega_d = 0$ is treated separately below.

Keeping only the first term of the expansion above, we find

```
series(Rek,w=0,2): Rekl := simplify(collect(%,w));
```

$$Rekl = \frac{1}{2} \frac{\sqrt{C} (R_{dc} + L_{dc} \omega d)}{\sqrt{R_{dc}} \sqrt{\omega d}} \omega + O(\omega^2)$$

so that

$$\text{Re}(k) \approx (\omega/2) (R_{dc} + \omega_d L_{dc}) \sqrt{C/(\omega_d R_{dc})} + O(\omega^2) \quad (\text{Q.4.4})$$

Treating $\text{Im}(k)$ in the same manner one finds,

```
Imk := - sqrt((a^2+c)/2);
```

$$Imk = -\frac{1}{2} \sqrt{2 \sqrt{(R_{dc}^2 + \omega^2 L_{dc}^2) (C^2 (\omega d + t \omega)^2 + \omega^2 C^2) + 2 R_{dc} C (\omega d + t \omega) - 2 \omega^2 L_{dc} C}}$$

```
series(Imk,w=0,2): Imkl := collect(%,w);
```

$$Imkl = -\sqrt{R_{dc} C \omega d} - \frac{1}{2} \frac{\sqrt{R_{dc} C \omega d} t}{\omega d} \omega + O(\omega^2)$$

so that

$$\text{Im}(k) \approx -\sqrt{R_{dc} C \omega_d} [1 + (1/2) \tan_{\mathbf{L}}(\omega/\omega_d)] + O(\omega^2) \quad (\text{Q.4.5})$$

To summarize:

Fact 3: The small ω limit for $k(\omega)$, assuming $\omega_d > 0$, is given by (Q.4.6)

$$\begin{aligned} \text{Re}(k) &\approx (\omega/2) (R_{dc} + \omega_d L_{dc}) \sqrt{C/(\omega_d R_{dc})} + O(\omega^2) & \omega < \omega_d = (\sigma_d/\epsilon_d) \\ \text{Im}(k) &\approx -\sqrt{R_{dc} C \omega_d} [1 + (\tan_{\mathbf{L}}/2) (\omega/\omega_d)] + O(\omega^2) & G_{dc} = C \omega_d \end{aligned}$$

Notice that $\text{Im}(k) \rightarrow -\sqrt{R_{dc} G_{dc}} > 0$ as $\omega \rightarrow 0$, indicating the presence of loss at DC. This loss is just the ohmic loss in the dielectric due to $\sigma_d > 0$, and associated loss in the conductors due to $R_{dc} > 0$. This limiting situation is shown in the network model of Fig K.4.

Small ω limit of $k(\omega)$ for $\omega_a = 0$

Here we rerun the Maple code shown above setting $\omega_a = 0$ at the start. For $\text{Re}(k)$ we find,

Rek := sqrt((a^2-c)/2);

$$\text{Rek} := \frac{1}{2} \sqrt{2 \sqrt{(Rdc^2 + w^2 Ldc^2) (C^2 t^2 w^2 + w^2 C^2) - 2 Rdc C t w + 2 w^2 Ldc C}}$$

series(Rek, w=0, 2);

$$\frac{1}{2} \sqrt{2 Rdc \sqrt{C^2 t^2 + C^2} - 2 t C Rdc} \sqrt{w} + \frac{1}{2} \frac{Ldc C w^{\left(\frac{3}{2}\right)}}{\sqrt{2 Rdc \sqrt{C^2 t^2 + C^2} - 2 t C Rdc}} + O\left(w^{\left(\frac{5}{2}\right)}\right)$$

Expanding each coefficient for small t gives

op(1,Rek1); series(%, t=0, 2);

$$\frac{1}{2} \sqrt{2 Rdc \sqrt{C^2 t^2 + C^2} - 2 t C Rdc} \sqrt{w}$$

$$\frac{1}{2} \sqrt{2} \sqrt{Rdc C} \sqrt{w} - \frac{1}{4} \sqrt{2} \sqrt{Rdc C} \sqrt{w} t + O(t^2)$$

op(2,Rek1); series(%, t=0, 2);

$$\frac{1}{2} \frac{Ldc C w^{\left(\frac{3}{2}\right)}}{\sqrt{2 Rdc \sqrt{C^2 t^2 + C^2} - 2 t C Rdc}}$$

$$\frac{1}{4} \frac{\sqrt{2} Ldc C w^{\left(\frac{3}{2}\right)}}{\sqrt{Rdc C}} + \frac{1}{8} \frac{\sqrt{2} Ldc C w^{\left(\frac{3}{2}\right)}}{\sqrt{Rdc C}} t + O(t^2)$$

Keeping only the first term in the ω expansion, we have shown that

$$\text{Re}(k) \approx \sqrt{Rdc C / 2} \sqrt{\omega} (1 - \tan_{\mathbf{I}}/2) + O(\omega^{3/2}) . \quad (\text{Q.4.7})$$

Treating $\text{Im}(k)$ in the same manner one finds:

`Imk := - sqrt((a^2+c)/2);`

$$Imk = -\frac{1}{2}\sqrt{2\sqrt{(Rdc^2 + w^2 Ldc^2)(C^2 t^2 w^2 + w^2 C^2) + 2 Rdc C t w - 2 w^2 Ldc C}}$$

`series(Imk,w=0,2): Imk1 :=collect(%,w);`

$$Imk1 = -\frac{1}{2}\sqrt{2 Rdc \sqrt{C^2 t^2 + C^2} + 2 t C Rdc} \sqrt{w} + \frac{1}{2} \frac{Ldc C w^{\left(\frac{3}{2}\right)}}{\sqrt{2 Rdc \sqrt{C^2 t^2 + C^2} + 2 t C Rdc}} + O\left(w^{\left(\frac{5}{2}\right)}\right)$$

`op(1,Imk1); simplify(%): series(%,t=0,2);`

$$-\frac{1}{2}\sqrt{2 Rdc \sqrt{C^2 t^2 + C^2} + 2 t C Rdc} \sqrt{w} - \frac{1}{2}\sqrt{2} \sqrt{Rdc} \sqrt{C} \sqrt{w} - \frac{1}{4}\sqrt{2} \sqrt{Rdc} \sqrt{C} \sqrt{w} t + O(t^2)$$

`op(2,Imk1); simplify(%): series(%,t=0,2);`

$$\frac{1}{2} \frac{Ldc C w^{\left(\frac{3}{2}\right)}}{\sqrt{2 Rdc \sqrt{C^2 t^2 + C^2} + 2 t C Rdc}} - \frac{1}{4} \frac{\sqrt{2} \sqrt{C} Ldc w^{\left(\frac{3}{2}\right)}}{\sqrt{Rdc}} + \frac{1}{8} \frac{\sqrt{2} \sqrt{C} Ldc w^{\left(\frac{3}{2}\right)}}{\sqrt{Rdc}} t + O(t^2)$$

from which we read off the leading term,

$$Im(k) \approx -\sqrt{R_{dc}C/2} \sqrt{\omega} (1 + \tan_L/2) + O(\omega^{3/2}). \quad (Q.4.8)$$

To summarize:

Fact 4: The small ω limit for $k(\omega)$, assuming $\omega_d = 0$, is given by (Q.4.9)

$$Re(k) \approx +\sqrt{R_{dc}C/2} \sqrt{\omega} (1 - \tan_L/2) + O(\omega^{3/2})$$

$$Im(k) \approx -\sqrt{R_{dc}C/2} \sqrt{\omega} (1 + \tan_L/2) + O(\omega^{3/2})$$

In this case, $Im(k) \rightarrow 0$ as $\omega \rightarrow 0$ so there is no DC loss in the dielectric. This is as expected with $\sigma_d = 0$ which implies $Z_0 = \infty$ and $I = 0$ for an infinite transmission line. See Fig K.4 with no ladder rungs.

Q.5 The general appearance of $\text{Re}(k)$ and $\text{Im}(k)$ for Belden 8281 cable

Here we are interested in viewing the real and imaginary parts of $\text{Re}(k)$ over the full frequency range, not just at the extremes of small ω and large ω . The expressions shown in (Q.2.1) are,

Rek ;

$$\frac{1}{2} \sqrt{2 \sqrt{(R^2 + \omega^2 L^2)(G^2 + \omega^2 C^2) - 2RG + 2\omega^2 LC}}$$

Imk ;

$$-\frac{1}{2} \sqrt{2 \sqrt{(R^2 + \omega^2 L^2)(G^2 + \omega^2 C^2) + 2RG - 2\omega^2 LC}}$$

(Q.5.1)

For frequencies below ω_L and ω_R of the parameter model of Section Q.1, the above expressions become

Rek ;

$$\frac{1}{2} \sqrt{2 \sqrt{(R_{dc}^2 + \omega^2 (L_e + L_{idc})^2)(C^2 (\omega d + \tan L \omega)^2 + \omega^2 C^2) - 2 R_{dc} C (\omega d + \tan L \omega) + 2 \omega^2 (L_e + L_{idc}) C}}$$

Imk ;

$$-\frac{1}{2} \sqrt{2 \sqrt{(R_{dc}^2 + \omega^2 (L_e + L_{idc})^2)(C^2 (\omega d + \tan L \omega)^2 + \omega^2 C^2) + 2 R_{dc} C (\omega d + \tan L \omega) - 2 \omega^2 (L_e + L_{idc}) C}}$$

(Q.5.2)

Each expression depends on ω in five places, and is also a function of R_{dc} , L_e , L_{idc} , C , ωd , and $\tan L$. For this reason, it is difficult to make generalizations about the ω dependence of $\text{Re}(k)$ and $\text{Im}(k)$ which would apply to all possible transmission lines. We shall consider the Belden 8281 cable of Appendix R to be a "typical" transmission line with regard to the relative sizes of the parameters just listed, and we shall create plots of $\text{Re}k$ and $\text{Im}k$ for that specific system. For this cable, $\omega_R \approx 550,000$ and $\omega_L \approx 700,000$ so the above expressions for $\text{Re}k$ and $\text{Im}k$ would apply for $\omega < 500,000$ as used in the plots below.

First of all, recall from (Q.2.1) that

$$\text{Re}k = \sqrt{\frac{a^2 - c}{2}} \quad -\text{Im}k = \sqrt{\frac{a^2 + c}{2}} \quad (Q.5.3)$$

We use the expressions for a and c shown in (Q.2.1), along with the expressions for R, G, C, L given in the model (Q.1.9), and data for C , σ_d , ϵ_d , R_{dc} , L_e and L_{idc} taken from the Belden Appendix R.

$$\begin{array}{ll} C = 69 \text{ pF/m} & L_e = 361.4 \text{ } \mu\text{H/m} \\ R_{dc} = .0360910 \text{ ohms/m} & L_{idc} = 58 \text{ nH/m} \\ \epsilon_d = 2.3 \epsilon_0 & \sigma_d = 10^{-15} \text{ mho/m} \quad \Rightarrow \quad \omega_d = 4.8 \times 10^{-5} \text{ sec}^{-1} > 0 \\ a_1 = (1/2) * 787.4 \text{ } \mu & p_1 = 2\pi a_1 \\ a_2 = ((1/2) * 5020.2 + 11.5) \text{ } \mu & p_2 = 2\pi a_2 \end{array} \quad (Q.5.4)$$

Here is a plot of the ratio c/a^2 ,

```
semilogplot(c/a^2,omega = 1e0..5e5,thickness=2,numpoints = 2000);
```

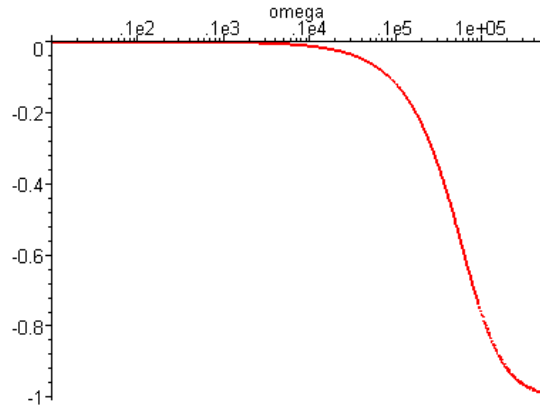


Fig Q.5.1

This shows that $c \ll a^2$ on the left side of the graph, so for that range we would expect to find that $\text{Re}k$ and $\text{Im}k$ are about the same. That fact is born out in this plot of $\text{Re}k$ and $-\text{Im}k$ for ω in (10,500,000):

```
loglogplot([Rek,-Imk],omega = 1e1..5e5,numpoints=2000,thickness=2, color = [red,black],scaling = constrained);
```

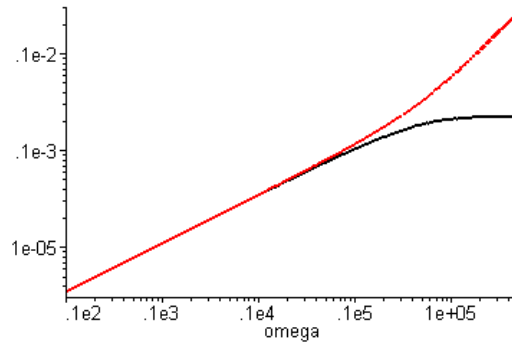


Fig Q.5.2

The red curve is $\text{Re}k$, while the black curve is $-\text{Im}k$. This plot then gives a good view of $\text{Re}k$ and $\text{Im}k$ for what one would normally call "the low frequency range" of this Belden cable, roughly below 1 MHz.

However, this is not the low frequency range for which (Q.4.6) applies. Recall that (Q.4.6) only applies for $\omega < \omega_d$ and $\omega_d = \sigma_d/\epsilon_d \approx 5 \times 10^{-5}$ for the Belden 8281 cable, so $\omega < \omega_d$ is what we might call the "ultra low frequency range". We can redo the above plot in the ultra-low range $\omega = 10^{-7}$ to 10^{-2} sec^{-1} :

```
loglogplot([Rek, -Imk], omega = 1e-7..1e-2, numpoints=2000, thickness=2,
color = [red, black], scaling = constrained);
```

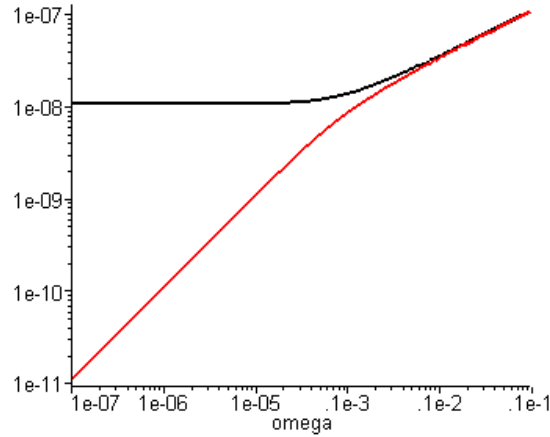


Fig Q.5.3

This shows what happens as we go off the left edge of the previous graph. We find that $-Imk$ goes to a constant, while Rek has slope 1 so is proportional to ω . This is consistent with the low ω limit (Q.4.6),

$$\begin{aligned} Re(k) &\approx (\omega/2) (R_{dc} + \omega_d L_{dc}) \sqrt{C/(\omega_d R_{dc})} + O(\omega^2) & \omega < \omega_d = (\sigma_d/\epsilon_d) & \quad (Q.4.6) \\ Im(k) &\approx -\sqrt{R_{dc} C \omega_d} [1 + (\tan \tau_L/2) (\omega/\omega_d)] + O(\omega^2) \end{aligned}$$

Specifically, $\sqrt{R_{dc} C \omega_d} = \sqrt{R_{dc} G_{dc}} = \sqrt{.036 * .34 * 10^{-14}} = 1.1 * 10^{-8}$ as the plot shows.

Having dealt with low and ultra-low frequencies, we turn now to higher frequencies, and for this purpose we reinstall the full Heaviside model into our Maple code and then continue to make plots. For ω in the range 10^3 to 10^7 one finds,

```
loglogplot([Rek, -Imk], omega = 1e3..1e7, numpoints=2000, thickness=2,
color = [red, black], scaling = constrained);
```

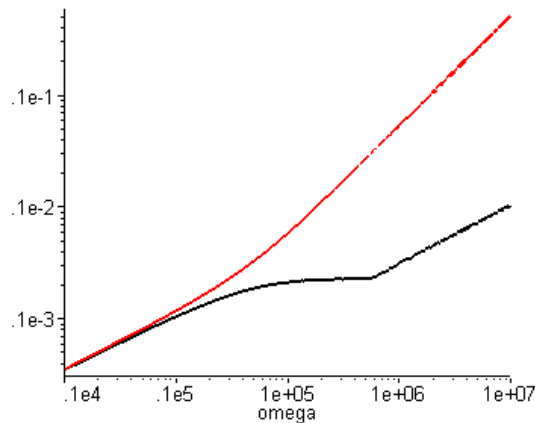


Fig Q.5.4

which shows what happens off the right end of Fig Q.5.2. For ω range 10^3 to 10^{10} the plot is,

```
loglogplot([Rek, -Imk], omega = 1e3..1e10, numpoints=2000, thickness=2,
color = [red, black], scaling = constrained);
```

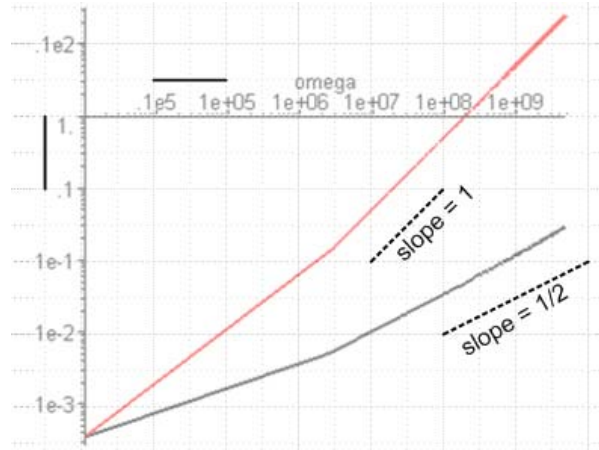


Fig Q.5.5

where we have used a transparent overlay to show the slopes of $\text{Re}k$ and $\text{Im}k$. Certainly $\omega = 10^{10}$ corresponding to $f = 1.6$ GHz is getting near the high end of the usefulness of Belden 8281 cable, but the slope of $\text{Im}k$ (on this log log plot) is still $1/2$, indicating that $\text{Im}k \sim \sqrt{\omega}$. Thus we have not yet reached the true high frequency limit for $\text{Im}(k)$ which (Q.3.5) says is this,

$$\begin{aligned} \text{Re}(k) &\approx (\omega/v_d) + (v_d\kappa C/2)\sqrt{\omega} + (1/4v_d)(\omega_d + v_d^4 C^2 \kappa^2/2) \tan_L + O(1/\sqrt{\omega}) \\ \text{Im}(k) &\approx -(\omega/v_d) \tan_L/2 - (v_d\kappa C/2)\sqrt{\omega} - (1/2v_d)(\omega_d - v_d^4 C^2 \kappa^2/2) + O(1/\sqrt{\omega}). \end{aligned} \quad (Q.3.5)$$

It is the smallness of $\tan_L/(2v_d)$ which causes $-(v_d\kappa C/2)\sqrt{\omega}$ to still be the leading term. Finally, we take ω even higher to get this final plot for ω in 10^8 to 10^{13} (1600 GHz),

```
loglogplot([Rek, -Imk], omega = 1e8..5e13, numpoints=4000, thickness=2,
color = [red, black], scaling = constrained);
```

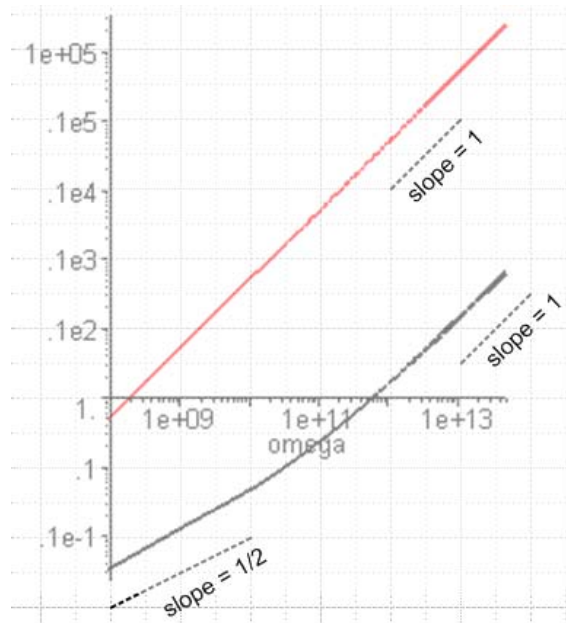


Fig Q.5.6

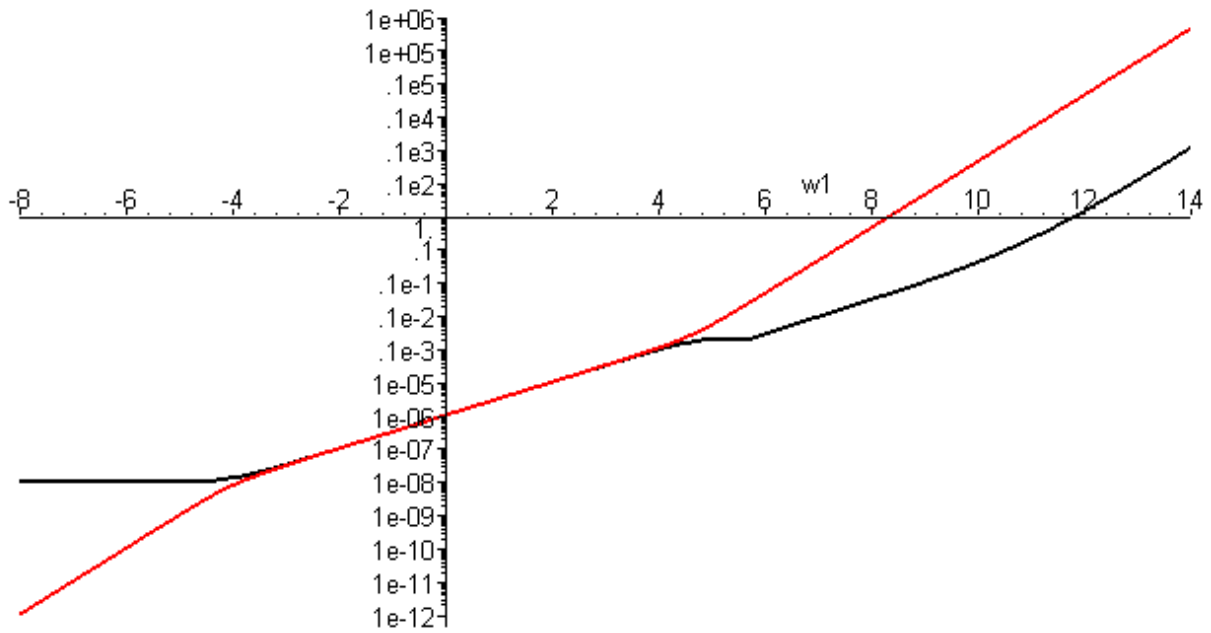
and finally the slope of $\text{Im}k$ is 1 showing that the first term in (Q.3.5) is now dominant. Of course at this value of 1600 GHz ($\omega=10^{13}$) one sees that $-\text{Im}(k) \approx .1e3 = 100$ which means the cable is good for a length of about 1 cm ($e^{jkz} \sim e^{-\text{Im}(k)z}$).

Finally, we can combine all the above onto a single graph, where the horizontal axis shows $\log_{10}(\omega)$:

`omega := 10^w1;`

$\omega = 10^{w1}$

`logplot([Rek, -Imk], w1 = -8..14, thickness=2, color = [red, black]);`



vertical: Red = $\text{Re}[k(\omega)]$ horizontal: $\log_{10}(\omega)$
 Black = $-\text{Im}[k(\omega)]$

Fig Q.5.7

The origin represents ($\omega = 10^0 = 1 \text{ sec}^{-1}$, value = 1 m^{-1}). Note that all plotted values are positive, and that the functions plotted are $\text{Re}(k)$ and $-\text{Im}(k)$. The plots are for the simple model presented in Section Q.1. Function $\text{Re}(k)$ (red) is the lower function on the left and the upper function on the right.

We now clutter up the above figure by adding two more functions $\beta_a = \omega/v_a$ (green) and $|k|$ (blue) :

```

betad := omega/vd:
absk := sqrt(Rek^2 + Imk^2):
logplot([Rek, -Imk, 1/2*betad, 2*absk], w1 = -8..14, thickness=2, color =
[red, black, green, blue]);
    
```

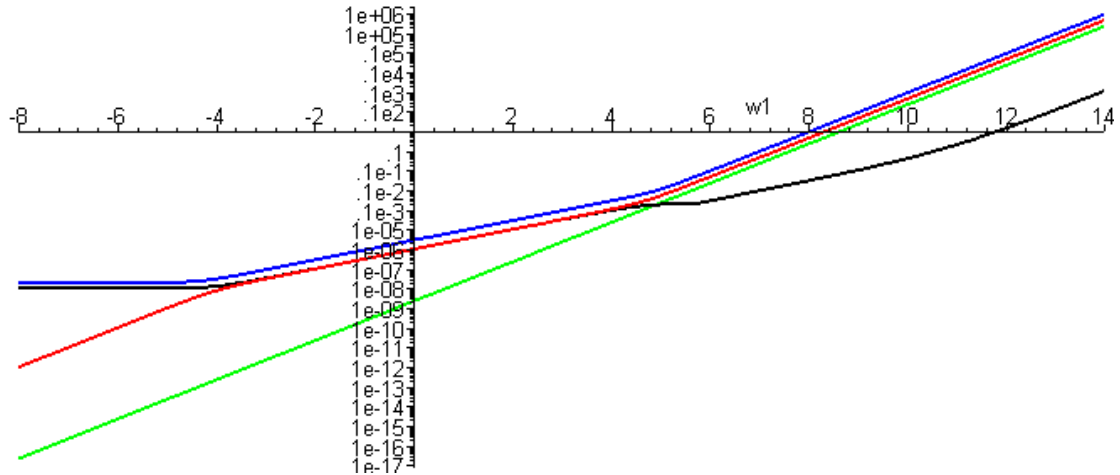


Fig Q.5.8

The green function β_a is a straight line and it just lies underneath the red line on the right.

The blue function $|k|$ lies just above the uppermost of the red or black curve at any point.

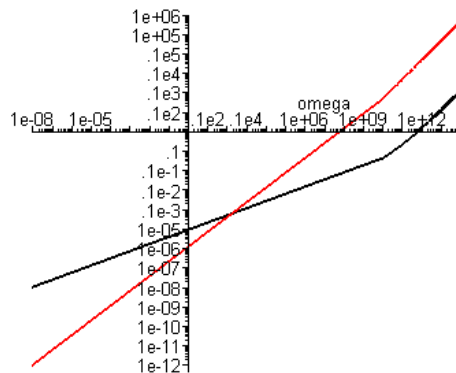
Notice that $|k| \geq \beta_a$ (blue \geq green) for all ω and $|k| \approx \beta_a$ at high frequencies.

The close lines really overlap, so we have artificially added a factor of 1/2 and 2 in the logplot call to pull them apart just to make them visible.

Note on Log Plots: We are using ancient Maple V which has a bug in its distribution of sample points for the semilogplot and loglogplot functions. For this reason, these plotting calls are inaccurate if the ω domain is more than a few decades wide. This bug has no doubt been fixed in later Maple releases. As a workaround, we use the method shown above to force an equal spacing of points per decade. Just for the record, here is what Maple V shows for the plot of Fig Q.5.7 even with 10,000 plotting points

```

loglogplot([Rek, -Imk], omega = 1e-8..1e14, numpoints=10000, thickness=2,
color = [red, black], scaling = constrained);
    
```



// Bad Plot !

Q.6 Real and Imaginary parts of $Z_0(\omega)$

Fact 5: The real and imaginary decomposition of Z_0 is given by (Q.6.1)

$$Z_0 = \sqrt{\frac{R+j\omega L}{G+j\omega C}} = \sqrt{\frac{z}{y}} = (b/\sqrt{2}) [\sqrt{1+(d/a^2)} - jS\sqrt{1-(d/a^2)}]$$

where $b = \left(\frac{R^2+\omega^2 L^2}{G^2+\omega^2 C^2}\right)^{1/4} = |Z_0|$ $a = [(R^2+\omega^2 L^2)(G^2+\omega^2 C^2)]^{1/4}$ as in (Q.2.1)
 $S = \text{sign}(RC-LG)$ $d = RG + \omega^2 LC$

Proof of Fact 5: The proof is similar to that of Fact 1, (Q.2.1). Let

$$q = \frac{z}{y} = \frac{R+j\omega L}{G+j\omega C} = |q| e^{j\theta} \quad -\pi < \theta < \pi \text{ (but see few lines below) .}$$

Then

$$|q|^2 = \left| \frac{R+j\omega L}{G+j\omega C} \right|^2 = \frac{R^2+\omega^2 L^2}{G^2+\omega^2 C^2} \equiv b^4 \quad \Rightarrow \quad |q| = \sqrt{\frac{R^2+\omega^2 L^2}{G^2+\omega^2 C^2}} = b^2 .$$

Next,

$$q = \frac{R+j\omega L}{G+j\omega C} = \frac{R+j\omega L}{G+j\omega C} \frac{G-j\omega C}{G-j\omega C} = \frac{(R+j\omega L)(G-j\omega C)}{G^2+\omega^2 C^2} = \frac{RG+j\omega(LG-RC) + \omega^2 LC}{G^2+\omega^2 C^2}$$

so

$$\text{Re}(q) = \frac{RG + \omega^2 LC}{G^2 + \omega^2 C^2} > 0 \quad \Rightarrow \quad -\pi/2 < \theta < \pi/2$$

$$\text{Im}(q) = \frac{\omega(LG-RC)}{G^2 + \omega^2 C^2} \quad \text{sign}[\text{Im}(q)] = \text{sign}(LG-RC) = \text{sign}(\theta) \equiv -S .$$

Then

$$\cos\theta = \text{Re}(q)/|q| = \frac{(RG + \omega^2 LC)}{G^2 + \omega^2 C^2} \sqrt{\frac{G^2 + \omega^2 C^2}{R^2 + \omega^2 L^2}} = \frac{RG + \omega^2 LC}{\sqrt{(G^2 + \omega^2 C^2)(R^2 + \omega^2 L^2)}}$$

$$\equiv d/a^2 \quad \text{where } a = [(R^2 + \omega^2 L^2)(G^2 + \omega^2 C^2)]^{1/4} \quad \text{and} \quad d \equiv RG + \omega^2 LC .$$

Now write

$$s \equiv \sqrt{\frac{z}{y}} = \sqrt{q} = |s| e^{i\phi} \quad |s| = \sqrt{|q|} = b = |Z_0| \quad \phi = \theta/2 \quad -\pi/4 < \phi < \pi/4$$

$$\begin{aligned} \operatorname{Re}(s) &= |s| \cos\phi = b \cos(\theta/2) = b \sqrt{(1+\cos\theta)/2} = (b/\sqrt{2})\sqrt{1+d/a^2} \\ \operatorname{Im}(s) &= |s| \sin\phi = b \sin(\theta/2) = -\sigma b \sqrt{(1-\cos\theta)/2} = -\sigma (b/\sqrt{2})\sqrt{1-d/a^2} \end{aligned}$$

giving the result

$$s = (b/\sqrt{2}) [\sqrt{1+d/a^2} - jS \sqrt{1-d/a^2}]$$

$$\begin{aligned} \text{where } b &= \left(\frac{R^2 + \omega^2 L^2}{G^2 + \omega^2 C^2} \right)^{1/4} = |Z_0| & a &= [(R^2 + \omega^2 L^2)(G^2 + \omega^2 C^2)]^{1/4} \\ S &= \operatorname{sign}(RC - LG) & d &\equiv RG + \omega^2 LC. \end{aligned}$$

Our Maple verification of this result is a bit ugly so we omit the code.

An alternate geometric derivation giving the same results begins as follows, where $z = j\omega$

$$Z_0 = \sqrt{\frac{R+zL}{G+zC}} = \sqrt{\frac{L}{C}} \sqrt{\frac{z+(R/L)}{z+(G/C)}} = \sqrt{\frac{L}{C}} \sqrt{\frac{z+r}{z+g}} \quad \text{where } r = (R/L) \text{ and } g = (G/C).$$

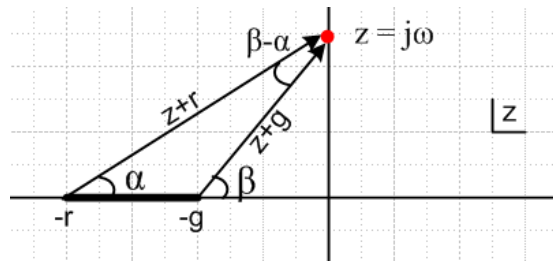


Fig Q.6.1

The drawing shows the complex z plane for the function $Z_0(z) = \sqrt{\frac{L}{C}} \sqrt{\frac{z+r}{z+g}}$ in the particular case that $r > g$, where the z -plane has a branch cut from $-r$ to $-g$. The z values of interest are only those on the positive imaginary axis where $z = j\omega$.

Reader Exercise: Finish this derivation and obtain the results shown in (Q.6.1).

Hint: $\cos(\beta-\alpha) = (rg+\omega^2)/(AB)$ and $\sin(\beta-\alpha) = \omega(r-g)/(AB)$ where $A = \sqrt{\omega^2+r^2}$ and $B = \sqrt{\omega^2+g^2}$.

Q.7 Large ω limit of $Z_0(\omega)$

For large ω , our models for G,R,L were found to be

$$G = C(\omega_d + t \omega) \quad R = \kappa \sqrt{\omega} \quad L = 1/(Cv_d^2) + \kappa/\sqrt{\omega} . \quad (Q.3.2)$$

These expressions are entered into Maple as in Section Q.3 above. Next, enter the intermediate variables a, b, and d from box (Q.6.1)

$$a := ((R^2 + w^2 * L^2) * (G^2 + w^2 * C^2))^{(1/4)};$$

$$a = \left(\left(\kappa^2 w + w^2 \left(\frac{1}{vd^2 C} + \frac{\kappa}{\sqrt{w}} \right)^2 \right) (C^2 (wd + tw)^2 + w^2 C^2) \right)^{\left(\frac{1}{4}\right)}$$

$$b := ((R^2 + w^2 * L^2) / (G^2 + w^2 * C^2))^{(1/4)};$$

$$b = \left(\frac{\kappa^2 w + w^2 \left(\frac{1}{vd^2 C} + \frac{\kappa}{\sqrt{w}} \right)^2}{C^2 (wd + tw)^2 + w^2 C^2} \right)^{\left(\frac{1}{4}\right)}$$

$$d := R * G + w^2 * L * C;$$

$$d = \kappa \sqrt{w} C (wd + tw) + w^2 \left(\frac{1}{vd^2 C} + \frac{\kappa}{\sqrt{w}} \right) C$$

The real part of $Z_0(\omega)$ is then given from (Q.6.1) as follows:

$$> \text{ReZ} := (b/\text{sqrt}(2)) * \text{sqrt}(1 + (d/a^2));$$

ReZ :=

$$\frac{1}{2} \left(\frac{\kappa^2 w + w^2 \left(\frac{1}{vd^2 C} + \frac{\kappa}{\sqrt{w}} \right)^2}{C^2 (wd + tw)^2 + w^2 C^2} \right)^{\left(\frac{1}{4}\right)} \sqrt{2} \sqrt{1 + \frac{\kappa \sqrt{w} C (wd + tw) + w^2 \left(\frac{1}{vd^2 C} + \frac{\kappa}{\sqrt{w}} \right) C}{\sqrt{\left(\kappa^2 w + w^2 \left(\frac{1}{vd^2 C} + \frac{\kappa}{\sqrt{w}} \right)^2 \right) (C^2 (wd + tw)^2 + w^2 C^2)}}}$$

The asymptotic expansion of $\text{Re}(Z_0)$ for large ω is then found to be,

$$> \text{series}(\text{ReZ}, w = \text{infinity}, 3): \text{ReZ1} := \text{collect}(\%, w);$$

$$\text{ReZ1} = \frac{1}{2} \left(\frac{1}{vd^4 C^2 (C^2 t^2 + C^2)} \right)^{\left(\frac{1}{4}\right)} \sqrt{2} \sqrt{1 + \frac{C}{\sqrt{C^2 t^2 + C^2}}}$$

This expansion has the form $A + B/\sqrt{\omega} + C/\omega + O(\omega^{-3/2})$ but above we only display term A because the other expressions are large and uninspiring. As before, we pick off each term, simplify it, then expand it for small t:

`op(1,ReZ1); simplify(%): series(% ,t=0,3);`

$$\frac{1}{2} \left(\frac{1}{v_d^4 C^2 (C^2 t^2 + C^2)} \right)^{\left(\frac{1}{4}\right)} \sqrt{2} \sqrt{1 + \frac{C}{\sqrt{C^2 t^2 + C^2}}} \\ \frac{1}{v_d C} - \frac{3}{8} \frac{1}{v_d C} t^2 + O(t^4)$$

`op(2,ReZ1); simplify(%): series(% ,t=0,3);`

$$\frac{1}{2} \frac{v_d \kappa}{\sqrt{w}} + \frac{1}{4} \frac{v_d \kappa}{\sqrt{w}} t - \frac{3}{16} \frac{v_d \kappa}{\sqrt{w}} t^2 + O(t^3)$$

`op(3,ReZ1); simplify(%): series(% ,t=0,3):simplify(%);`

$$-\frac{1}{8} \frac{6 w d + \kappa^2 v_d^4 C^2}{w C v_d} t + O(t^3)$$

Collecting the results and keeping only the leading terms in $t = \tan_L$, the resulting large ω limit for $\text{Re}(k)$ is seen to be,

$$\text{Re}(Z_0) \approx 1/(v_d C) + (v_d \kappa/2) 1/\sqrt{\omega} + O(1/\omega) \quad (\text{Q.7.1})$$

where we have ignored the details of the $O(1/\omega)$ term.

Treating $\text{Im}(Z_0)$ in the same manner one finds,

`ImZ := - S*(b/sqrt(2))*sqrt(1-(d/a^2));`

$$\text{ImZ} = -\frac{1}{2} S \left(\frac{\kappa^2 w + w^2 \left(\frac{1}{v_d^2 C} + \frac{\kappa}{\sqrt{w}} \right)^2}{C^2 (w d + t w)^2 + w^2 C^2} \right)^{\left(\frac{1}{4}\right)} \sqrt{2} \sqrt{1 - \frac{\kappa \sqrt{w} C (w d + t w) + w^2 \left(\frac{1}{v_d^2 C} + \frac{\kappa}{\sqrt{w}} \right) C}{\sqrt{\left(\kappa^2 w + w^2 \left(\frac{1}{v_d^2 C} + \frac{\kappa}{\sqrt{w}} \right)^2 \right) (C^2 (w d + t w)^2 + w^2 C^2)}}$$

`series(ImZ,w=infinity,3): ImZ1 := collect(% ,w);`

$$\text{ImZ1} = -\frac{1}{2} S \left(\frac{1}{v_d^4 C^2 (C^2 t^2 + C^2)} \right)^{\left(\frac{1}{4}\right)} \sqrt{2} \sqrt{1 - \frac{C}{\sqrt{C^2 t^2 + C^2}}}$$

Again this expansion has the form $A + B/\sqrt{\omega} + C/\omega + O(\omega^{-3/2})$ but we only display term A because expressions are clumsy. As before, we pick off each term, simplify it, then expand it for small t:

```
op(1,ImZ1): simplify(%): series(%,t=0,4);
```

$$-\frac{1}{2}S \left(\frac{1}{v_d^4 C^2 (C^2 t^2 + C^2)} \right)^{\left(\frac{1}{4}\right)} \sqrt{2} \sqrt{1 - \frac{C}{\sqrt{C^2 t^2 + C^2}}} - \frac{1}{2} \frac{S}{v_d C} t + \frac{5}{16} \frac{S}{v_d C} t^3 + O(t^5)$$

```
op(2,ImZ1): simplify(%): series(%,t=0,4);
```

$$-\frac{1}{4} \frac{S \sqrt{2} v_d \kappa (-t - 1 + \sqrt{t^2 + 1})}{\sqrt{t^2 + 1} \sqrt{-1 + \sqrt{t^2 + 1}} \sqrt{w}} - \frac{1}{2} \frac{S v_d \kappa}{\sqrt{w}} - \frac{1}{4} \frac{S v_d \kappa}{\sqrt{w}} t - \frac{3}{16} \frac{S v_d \kappa}{\sqrt{w}} t^2 + O(t^3)$$

```
op(3,ImZ1): simplify(%): series(%,t=0,6);
```

$$S \left(\frac{1}{4} \kappa^2 v_d^4 C^2 + \frac{1}{2} w d \right) - \frac{1}{v_d C w} + O(t^2)$$

Collecting the results and keeping only the leading terms in $t = \tan_{\mathbf{L}}$, the resulting large ω limit for $\text{Im}(k)$ is seen to be,

$$\text{Im}(Z_0) \approx -S \tan_{\mathbf{L}} / (2v_d C) + S (v_d \kappa / 2) 1/\sqrt{\omega} + O(1/\omega) \quad (\text{Q.7.2})$$

where we have again ignored the details of the $O(1/\omega)$ term.

Finally, S is the *sign* of expression RC-LG,

```
e := expand(R*C-L*G,w);
```

$$e = \kappa \sqrt{w} C - \frac{w d}{v_d^2} - \frac{t w}{v_d^2} - \frac{C \kappa w d}{\sqrt{w}} - C \kappa \sqrt{w} t$$

```
series(e,w=infinity,1): e1 := collect(%,u);
```

$$e1 = -\frac{t w}{v_d^2} + \frac{\kappa C - \kappa C t}{\sqrt{\frac{1}{w}}} - \frac{w d}{v_d^2} - C \kappa w d \sqrt{\frac{1}{w}}$$

so for large ω and small $t = \tan_{\mathbf{L}}$ we have

$$S = \text{sign} \left[-(\tan_{\mathbf{L}} / v_d^2) \omega + \kappa C \sqrt{\omega} - \omega d / v_d^2 \right] \quad (\text{Q.7.3})$$

which then gives $S = -1$ for very large ω . We now summarize these results :

Fact 6: The large ω asymptotic expansion for $Z_0(\omega)$, assuming $\tan_{\mathbf{r}} \ll 1$, is given by (Q.7.4)

$$\operatorname{Re}(Z_0) \approx [1/(v_{\mathbf{d}}C)] + (v_{\mathbf{d}}\kappa/2)/\sqrt{\omega} + O(1/\omega)$$

$$\operatorname{Im}(Z_0) \approx [1/(v_{\mathbf{d}}C)] \tan_{\mathbf{r}}/2 - (v_{\mathbf{d}}\kappa/2)/\sqrt{\omega} + O(1/\omega)$$

$$\text{where } \kappa \equiv \left(\frac{1}{p_1} + \frac{1}{p_2} \right) \sqrt{\frac{\mu}{2\sigma}}$$

Keeping only the leading terms for large ω ,

$$\operatorname{Re}(Z_0) \approx 1/(v_{\mathbf{d}}C) = \sqrt{L_{\mathbf{e}}/C} \approx \sqrt{L/C}$$

$$v_{\mathbf{d}} = 1/\sqrt{L_{\mathbf{e}}C} \approx 1/\sqrt{LC}$$

$$\operatorname{Im}(Z_0) \approx + \tan_{\mathbf{r}}/(2v_{\mathbf{d}}C) = (1/2) \tan_{\mathbf{r}} \sqrt{L_{\mathbf{e}}/C}$$

$$S = -1$$

The leading term $\operatorname{Re}(Z_0) \approx \sqrt{L/C}$ is the usual result obtained from taking the large ω limit of the expression $Z_0 = \sqrt{\frac{R + j\omega L}{G + j\omega C}}$ when the four parameters are treated as constants in ω . This fact is obvious from the large- ω model stated in (Q.3.1) which we repeat here:

$$G(\omega) = C(\omega_{\mathbf{d}} + \tan_{\mathbf{r}} \omega)$$

$$\omega_{\mathbf{d}} \equiv (\sigma_{\mathbf{d}}/\varepsilon_{\mathbf{d}})$$

$$R(\omega) = \kappa \sqrt{\omega}$$

$$L(\omega) = 1/(Cv_{\mathbf{d}}^2) + (\kappa/\sqrt{\omega}) \quad \kappa \equiv \left(\frac{1}{p_1} + \frac{1}{p_2} \right) \sqrt{\frac{\mu}{2\sigma}} \quad (Q.3.1)$$

Since $\tan_{\mathbf{r}} \ll 1$ one has

$$G + j\omega C = C(\omega_{\mathbf{d}} + \tan_{\mathbf{r}} \omega) + j\omega C = C\omega_{\mathbf{d}} + \omega C(\tan_{\mathbf{r}} + j) \approx \omega Cj = j\omega C$$

$$R + j\omega L = \kappa \sqrt{\omega} + j\omega [1/(Cv_{\mathbf{d}}^2) + (\kappa/\sqrt{\omega})] \approx j\omega L_{\mathbf{e}} \approx j\omega L$$

so

$$Z_0 = \sqrt{j\omega L/j\omega C} = \sqrt{L/C}.$$

Q.8 Small ω limit of $Z_0(\omega)$

The same partition into $\omega_d > 0$ and $\omega_d = 0$ occurs here as in Section Q.4.

Small ω limit of $Z_0(\omega)$ for $\omega_d > 0$

For small ω the parameter model is that stated in (Q.4.2.)

$$G = C(\omega_d + t \omega) \quad R = R_{dc} \quad L = L_{dc} . \quad (Q.4.2)$$

These expressions are entered into Maple as in Section Q.4 followed by expressions for the intermediate parameters of (Q.6.1),

$$a := ((R^2 + \omega^2 L^2) * (G^2 + \omega^2 C^2))^{1/4};$$

$$a := ((R_{dc}^2 + \omega^2 L_{dc}^2) (C^2 (\omega d + t \omega)^2 + \omega^2 C^2))^{1/4};$$

$$b := ((R^2 + \omega^2 L^2) / (G^2 + \omega^2 C^2))^{1/4};$$

$$b := \left(\frac{R_{dc}^2 + \omega^2 L_{dc}^2}{C^2 (\omega d + t \omega)^2 + \omega^2 C^2} \right)^{1/4};$$

$$d := R * G + \omega^2 * L * C;$$

$$d := R_{dc} C (\omega d + t \omega) + \omega^2 L_{dc} C$$

The real part of $Z_0(\omega)$ is then given from (Q.6.1) as follows:

$$ReZ := (b / \sqrt{2}) * \sqrt{1 + (d / a^2)};$$

$$ReZ := \frac{1}{2} \left(\frac{R_{dc}^2 + \omega^2 L_{dc}^2}{C^2 (\omega d + t \omega)^2 + \omega^2 C^2} \right)^{1/4} \sqrt{2} \sqrt{1 + \frac{R_{dc} C (\omega d + t \omega) + \omega^2 L_{dc} C}{\sqrt{(R_{dc}^2 + \omega^2 L_{dc}^2) (C^2 (\omega d + t \omega)^2 + \omega^2 C^2)}}}$$

The expansion of $Re(Z_0)$ for small ω is found to be,

$$series(ReZ, \omega=0, 2): ReZ1 := collect(%, \omega);$$

$$ReZ1 := \left(\frac{R_{dc}^2}{C^2 \omega d^2} \right)^{1/4} - \frac{1}{2} \left(\frac{R_{dc}^2}{C^2 \omega d^2} \right)^{1/4} \frac{t}{\omega} + O(\omega^2)$$

We thus find that, for small ω ,

$$\operatorname{Re}(Z_0) \approx \sqrt{R_{dc}/(C\omega_d)} - \sqrt{R_{dc}/(C\omega_d)} \tan_{\mathbf{L}}/2 (\omega/\omega_d) + O(\omega^2). \quad (\text{Q.8.1})$$

Treating $\operatorname{Im}(k)$ in the same manner one finds,

$$\mathbf{ImZ} := - \mathbf{S*(b/sqrt(2))*sqrt(1-(d/a^2))};$$

$$\operatorname{Im}Z = -\frac{1}{2} S \left(\frac{R_{dc}^2 + \omega^2 L_{dc}^2}{C^2 (\omega d + t \omega)^2 + \omega^2 C^2} \right)^{\left(\frac{1}{4}\right)} \sqrt{2} \sqrt{1 - \frac{R_{dc} C (\omega d + t \omega) + \omega^2 L_{dc} C}{\sqrt{(R_{dc}^2 + \omega^2 L_{dc}^2) (C^2 (\omega d + t \omega)^2 + \omega^2 C^2)}}}$$

The expansion of $\operatorname{Im}(Z_0)$ for small ω is then found to be,

$$\mathbf{series(ImZ,w=0,2): ImZ1 :=simplify(collect(%,w))};$$

$$\operatorname{Im}Z1 = -\frac{1}{2} \frac{S \operatorname{signum}(R_{dc} - L_{dc} \omega d) (R_{dc} - L_{dc} \omega d)}{\sqrt{R_{dc}} \sqrt{C} \omega d} \omega + O(\omega^2)$$

We thus find that, for small ω ,

$$\operatorname{Im}(Z_0) \approx - (1/2) S |R_{dc} - \omega_d L_{dc}| (\omega/\omega_d) / \sqrt{R_{dc} C \omega_d} + O(\omega^2). \quad (\text{Q.8.2})$$

Finally, S is the sign of expression RC-LG,

$$\mathbf{e := collect(R*C -L*G,w)};$$

$$e = -L_{dc} C t \omega + R_{dc} C - L_{dc} C \omega d$$

Then for small ω , $\text{RC-LG} = C(R_{dc} - \omega_d L_{dc})$, so $S = \operatorname{sign}(R_{dc} - \omega_d L_{dc})$. Thus

$$\operatorname{Im}(Z_0) \approx - (1/2) (R_{dc} - \omega_d L_{dc}) (\omega/\omega_d) / \sqrt{R_{dc} C \omega_d} + O(\omega^2).$$

To summarize:

Fact 7: The small ω limit for $Z_0(\omega)$, assuming $\omega_d > 0$, is given by (Q.8.3)

$$\begin{aligned} \operatorname{Re}(Z_0) &\approx \sqrt{R_{dc}/(C\omega_d)} - \sqrt{R_{dc}/(C\omega_d)} \tan_{\mathbf{L}}/2 (\omega/\omega_d) + O(\omega^2) \\ \operatorname{Im}(Z_0) &\approx - (1/2) (R_{dc} - \omega_d L_{dc}) (\omega/\omega_d) / \sqrt{R_{dc} C \omega_d} + O(\omega^2) \end{aligned} \quad \omega < \omega_d \equiv (\sigma_d/\varepsilon_d)$$

As $\omega \rightarrow 0$, we find that $Z_0 \rightarrow \sqrt{R_{dc}/(C\omega_d)} = \sqrt{R_{dc}/G_{dc}}$, in agreement with result (2) of the Reader Exercise below Fig K.4.

Small ω limit of $Z_0(\omega)$ for $\omega_d = 0$

We rerun the Maple code shown above setting $\omega_d = 0$ at the start. For $\text{Re}(Z_0)$ one finds,

$$\begin{aligned} & \text{ReZ} := (b/\text{sqrt}(2)) * \text{sqrt}(1 + (d/a^2)); \\ & \text{ReZ} = \frac{1}{2} \left(\frac{Rdc^2 + w^2 Ldc^2}{C^2 t^2 w^2 + w^2 C^2} \right)^{\left(\frac{1}{4}\right)} \sqrt{2} \sqrt{1 + \frac{Rdc C t w + w^2 Ldc C}{\sqrt{(Rdc^2 + w^2 Ldc^2)} (C^2 t^2 w^2 + w^2 C^2)}} \\ & \text{series}(\text{ReZ}, w=0, 2): \text{ReZ1} := \text{collect}(\%, w); \\ & \text{ReZ1} = \frac{1}{2} \frac{\left(\frac{Rdc^2}{C^2 t^2 + C^2} \right)^{\left(\frac{1}{4}\right)} \sqrt{2} \sqrt{1 + \frac{C t}{\sqrt{C^2 t^2 + C^2}}}}{\sqrt{w}} + \frac{1}{4} \frac{\left(\frac{Rdc^2}{C^2 t^2 + C^2} \right)^{\left(\frac{1}{4}\right)} \sqrt{2} Ldc C \sqrt{w}}{\sqrt{1 + \frac{C t}{\sqrt{C^2 t^2 + C^2}}} Rdc \sqrt{C^2 t^2 + C^2}} + O\left(w^{\left(\frac{3}{2}\right)}\right) \end{aligned}$$

Expanding each coefficient for small t gives,

$$\begin{aligned} & \text{op}(1, \text{ReZ1}): \text{simplify}(\%): \text{series}(\%, t=0, 2); \\ & \frac{1}{2} \frac{\sqrt{Rdc} \sqrt{2}}{\sqrt{C} \sqrt{w}} + \frac{1}{4} \frac{\sqrt{Rdc} \sqrt{2}}{\sqrt{C} \sqrt{w}} t + O(t^2) \\ & \text{op}(2, \text{ReZ1}): \text{simplify}(\%): \text{series}(\%, t=0, 2); \\ & \frac{1}{4} \frac{\sqrt{2} Ldc \sqrt{w}}{\sqrt{Rdc} \sqrt{C}} - \frac{1}{8} \frac{\sqrt{2} Ldc \sqrt{w}}{\sqrt{Rdc} \sqrt{C}} t + O(t^2) \end{aligned}$$

Thus the small ω expansion for $\text{Re}(Z_0)$ is

$$\text{Re}(Z_0) \approx \sqrt{R_{dc}/(2C)} \frac{1}{\sqrt{\omega}} + (1/2) [L_{dc}/\sqrt{2R_{dc}C}] \sqrt{\omega} + O(\omega^{3/2}) \quad (\text{Q.8.4})$$

Treating $\text{Im}(Z_0)$ in the same manner one finds,

`ImZ := - S*(b/sqrt(2))*sqrt(1-(d/a^2));`

$$\text{ImZ} = -\frac{1}{2} S \left(\frac{Rdc^2 + w^2 Ldc^2}{C^2 t^2 w^2 + w^2 C^2} \right)^{\left(\frac{1}{4}\right)} \sqrt{2} \sqrt{1 - \frac{Rdc C t w + w^2 Ldc C}{\sqrt{(Rdc^2 + w^2 Ldc^2)(C^2 t^2 w^2 + w^2 C^2)}}}$$

`series(ImZ,w=0,2): ImZ1 := collect(%,w);`

$$\text{ImZ1} = -\frac{1}{2} \frac{S \left(\frac{Rdc^2}{C^2 t^2 + C^2} \right)^{\left(\frac{1}{4}\right)} \sqrt{2} \sqrt{1 - \frac{C t}{\sqrt{C^2 t^2 + C^2}}}}{\sqrt{w}} + \frac{1}{4} \frac{S \left(\frac{Rdc^2}{C^2 t^2 + C^2} \right)^{\left(\frac{1}{4}\right)} \sqrt{2} Ldc C \sqrt{w}}{\sqrt{1 - \frac{C t}{\sqrt{C^2 t^2 + C^2}}} Rdc \sqrt{C^2 t^2 + C^2}} + O\left(w^{\left(\frac{3}{2}\right)}\right)$$

Expanding each coefficient for small t gives,

`op(1,ImZ1): simplify(%): series(%,t=0,2);`

$$-\frac{1}{2} \frac{S \sqrt{Rdc} \sqrt{2}}{\sqrt{C} \sqrt{w}} + \frac{1}{4} \frac{S \sqrt{Rdc} \sqrt{2}}{\sqrt{C} \sqrt{w}} t + O(t^2)$$

`op(2,ImZ1): simplify(%): series(%,t=0,2);`

$$\frac{1}{4} \frac{S \sqrt{2} Ldc \sqrt{w}}{\sqrt{Rdc} \sqrt{C}} + \frac{1}{8} \frac{S \sqrt{2} Ldc \sqrt{w}}{\sqrt{Rdc} \sqrt{C}} t + O(t^2)$$

from which we can write the small ω , small t expansion of $\text{Im}(Z_0)$,

$$\text{Im}(Z_0) \approx -S \sqrt{R_{dc}/(2C)} \frac{1}{\sqrt{\omega}} + (1/2) S [L_{dc}/\sqrt{2R_{dc}C}] \sqrt{\omega} + O(\omega^{3/2}) \quad (\text{Q.8.5})$$

Since S is the sign of (RC-LG) and since

`e := R*C -L*G;`

$$e = Rdc C - Ldc C t w$$

we conclude that for small ω , $S = +1$. To summarize:

Fact 8: The small ω limit for $Z_0(\omega)$, assuming $\omega_d = 0$, is given by (Q.8.6)

$$\text{Re}(Z_0) \approx \sqrt{R_{dc}/(2C)} \frac{1}{\sqrt{\omega}} + (1/2) [L_{dc}/\sqrt{2R_{dc}C}] \sqrt{\omega} + O(\omega^{3/2})$$

$$\text{Im}(Z_0) \approx -\sqrt{R_{dc}/(2C)} \frac{1}{\sqrt{\omega}} + (1/2) [L_{dc}/\sqrt{2R_{dc}C}] \sqrt{\omega} + O(\omega^{3/2})$$

We can quickly verify the leading terms:

$$Z_0 = \sqrt{\frac{R + j\omega L}{G + j\omega C}} = \sqrt{\frac{R_{dc} + j\omega L_{dc}}{(C \tan_L) \omega + j\omega C}} \approx \sqrt{\frac{R_{dc}}{j\omega C}} = \sqrt{\frac{R_{dc}}{\omega C}} \sqrt{-j} = \sqrt{\frac{R_{dc}}{\omega C}} (1-j)/\sqrt{2}$$

$$= \sqrt{\frac{R_{dc}}{2C}} \frac{1}{\sqrt{\omega}} (1 - j) .$$

As suggested by the network model for $\omega_d = 0$ and $\omega = 0$,

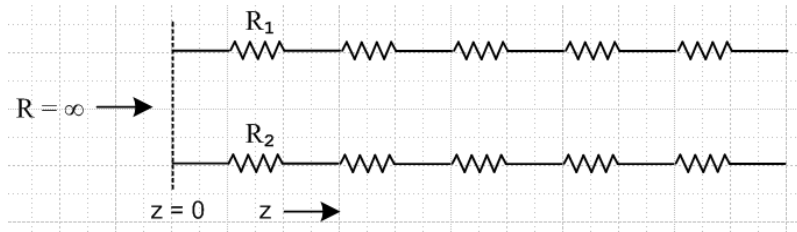


Fig D.8

it is not surprising that $Z_0 \rightarrow \infty$ as $\omega \rightarrow 0$. The phase is perhaps unexpected.

Q.9 The general appearance of $Re(Z_0)$ and $Im(Z_0)$ for Belden 8281 cable

This section is very similar to Section Q.5 above concerning the appearance of $k(\omega)$. We are interested in viewing the real and imaginary parts of $Re(Z_0)$ over the full frequency range, not just at the extremes of small ω and large ω . The expressions shown in (Q.6.1) are,

$ReZ_0 := (b/\sqrt{2}) * \sqrt{1 + (d/a^2)} ;$

$$ReZ_0 := \frac{1}{2} \left(\frac{R^2 + \omega^2 L^2}{G^2 + \omega^2 C^2} \right)^{\left(\frac{1}{4}\right)} \sqrt{2} \sqrt{1 + \frac{RG + \omega^2 LC}{\sqrt{(R^2 + \omega^2 L^2)(G^2 + \omega^2 C^2)}}}$$

$ImZ_0 := -S * (b/\sqrt{2}) * \sqrt{1 - (d/a^2)} ;$

$$ImZ_0 := -\frac{1}{2} S \left(\frac{R^2 + \omega^2 L^2}{G^2 + \omega^2 C^2} \right)^{\left(\frac{1}{4}\right)} \sqrt{2} \sqrt{1 - \frac{RG + \omega^2 LC}{\sqrt{(R^2 + \omega^2 L^2)(G^2 + \omega^2 C^2)}}}$$

(Q.9.1)

When the full Heaviside model of Section Q.1 is inserted for the parameters R,L and G, one can see that ReZ_0 and ImZ_0 are complicated functions of ω . Rather than attempt to deal with generic special cases (such as small G), we shall again consider the Belden 8281 cable of Appendix R to be a "typical" transmission line with regard to the relative sizes of the parameters R_{dc} , L_e , L_{idc} , C, ω_d , and \tan_L . In our model the "low frequency" range will be taken to be $\omega = 1$ to 500,000.

A new feature not present in the $k(\omega)$ case is the sign S which from (Q.6.1) is $S = \text{sign}(RC-LG)$. Here are plots of $RC-LG$ and $S = \text{sign}(RC-LG)$ for the Belden cable, using the same wide-range ω plotting trick mentioned at the end of Section Q.5 (horizontal axis labeled by $\log_{10}(\omega)$):

```
omega := 10^w1:
plot((R*C-L*G),w1 = -8..11):
plot(S,w1 = -8..14);
```

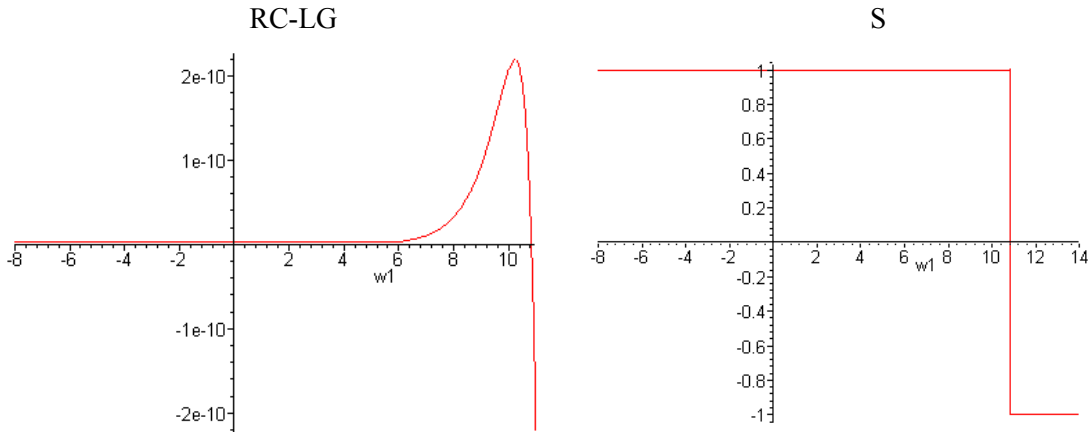


Fig Q.9.1

Basically $S = +1$ up to about $\omega = 10^{11}$ then it becomes -1 .

Now recall from (Q.6.1) that

$$\text{Re}k = (b/\sqrt{2}) [\sqrt{1+(d/a^2)}] \quad -\text{Im}k = S (b/\sqrt{2}) [\sqrt{1-(d/a^2)}] \quad . \quad (\text{Q.9.2})$$

We use the expressions for a,b,d,S shown in (Q.6.1), along with the expressions for R,G,C,L given in the model (Q.1.9), and Belden cable data for $C, \sigma_d, \epsilon_d, R_{dc}, L_e$ and L_{idc} as shown in (Q.5.4).

Here is a plot of the ratio d/a^2 (using our model and the Belden parameters) only up to $\omega = 500,000$:

```
semilogplot(d/a^2,omega = 1e0..5e5,thickness=2,numpoints = 2000);
```

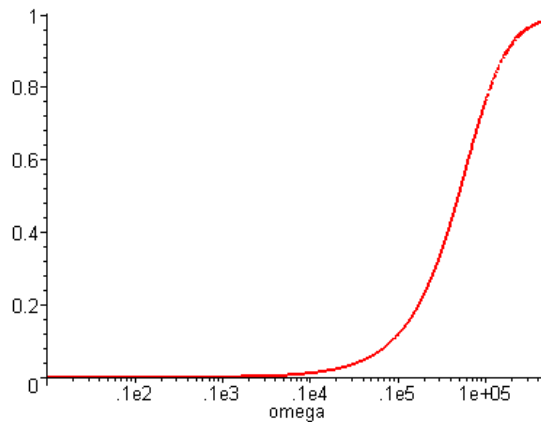


Fig Q.9.2

This shows that $d \ll a^2$ on the left side of the graph, so for that range we would expect to find that $\text{Re}Z_0$ and $-\text{Im}Z_0$ are about the same. That fact is born out in this plot of $\text{Re}Z_0$ and $-\text{Im}Z_0$ for ω in (10,500,000):

```
loglogplot([ReZ0,-ImZ0],omega = 1e1..5e5,numpoints=2000,thickness=2, color =
[red,black],scaling = constrained);
```

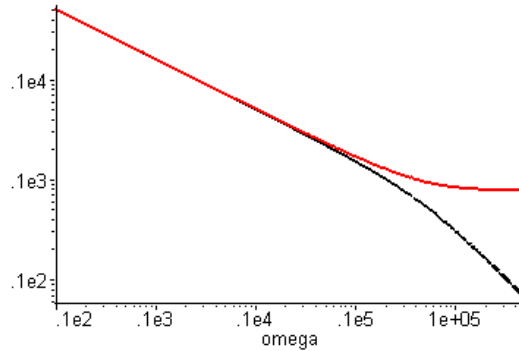


Fig Q.9.3

The red curve is $\text{Re}Z_0$, while the black curve is $-\text{Im}Z_0$. This plot then gives a good view of $\text{Re}Z_0$ and $\text{Im}Z_0$ for what one would normally call "the low frequency range" of this Belden cable, roughly below 1 MHz. However, this is not the low frequency range for which (Q.8.3) applies. Recall that (Q.8.3) only applies for $\omega < \omega_d$ (and $\omega_d = \sigma_d/\epsilon_d \approx 5 \times 10^{-5}$ for the Belden 8281 cable), which we call "ultra low frequencies". We can redo the above plot in the ultra-low range $\omega = 10^{-7}$ to 10^{-2} sec^{-1} :

```
loglogplot([ReZ0,-ImZ0],omega = 1e-7..1e-2,numpoints=2000,thickness=2, color
= [red,black],scaling = constrained);
```

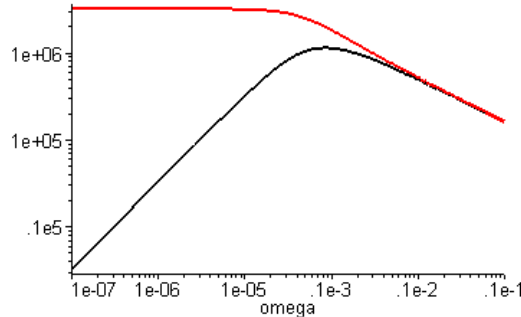


Fig Q.9.4

This shows what happens going off the left edge of the previous graph. One sees that $\text{Re}Z_0$ goes to a constant, while $-\text{Im}Z_0$ has slope 1 so is proportional to ω . This is consistent with the low ω limit (Q.8.3),

$$\begin{aligned} \text{Re}(Z_0) &\approx \sqrt{R_{dc}/(C\omega_d)} - \sqrt{R_{dc}/(C\omega_d)} \tan_{\mathbf{L}}/2 (\omega/\omega_d) + O(\omega^2) \\ \text{Im}(Z_0) &\approx -(1/2) (R_{dc} - \omega_d L_{dc}) (\omega/\omega_d) / \sqrt{R_{dc}C \omega_d} + O(\omega^2) \end{aligned} \quad \omega < \omega_d \equiv (\sigma_d/\epsilon_d) \quad (Q.8.3)$$

Specifically, $\sqrt{R_{dc}/(C\omega_d)} = \sqrt{R_{dc}/G_{dc}} = \sqrt{.036 / .34 \times 10^{-14}} = 3.25 \times 10^6$ as the plot shows.

Having dealt with low and ultra-low frequencies, we turn now to higher frequencies. For ω in the range 10^3 to 10^{10} one finds,

```
logplot([ReZ0,-Re(ImZ0)],w1 = 3..10,thickness=2, color = [red,black],scaling = constrained);
```

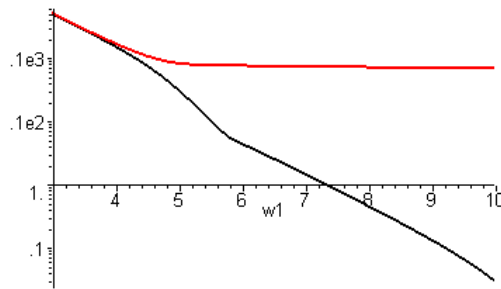


Fig Q.9.5

Recall that $\text{Im}Z_0$ experiences a sign change in the region of $\omega = 10^{11}$ (sign S goes from +1 to -1) as shown in this non-log plot of just $-\text{Im}Z_0$ for $\omega=10^9$ to 10^{18} :

```
plot(-ImZ0,w1 = 9..18,thickness=2, color = [red,black]);
```

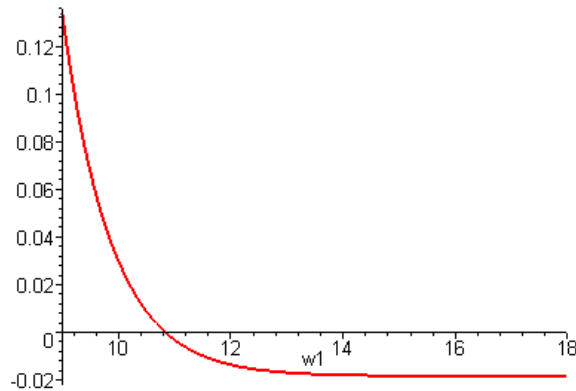


Fig Q.9.6

In fact, $-\text{Im}Z_0$ approaches the constant value indicated in the large ω limit given in (Q.7.4),

$$\begin{aligned} \text{Re}(Z_0) &\approx [1/(v_d C)] + (v_d \kappa / 2) / \sqrt{\omega} + O(1/\omega) \\ \text{Im}(Z_0) &\approx [1/(v_d C)] \tan_{\text{r}} / 2 - (v_d \kappa / 2) / \sqrt{\omega} + O(1/\omega) \end{aligned} \tag{Q.7.4}$$

where $\kappa \equiv \left(\frac{1}{p_1} + \frac{1}{p_2}\right) \sqrt{\frac{\mu}{2\sigma}}$

that value being about

$$\text{Im}Z_0 \rightarrow [1/(v_d C)] \tan_{\text{r}} / 2 = [\sqrt{\epsilon_d / \epsilon_0} / (cC)] \tan_{\text{r}} / 2 = [\sqrt{2.3} / (3 \times 10^8 \times 69 \times 10^{-12})] \cdot 0.0005 / 2$$

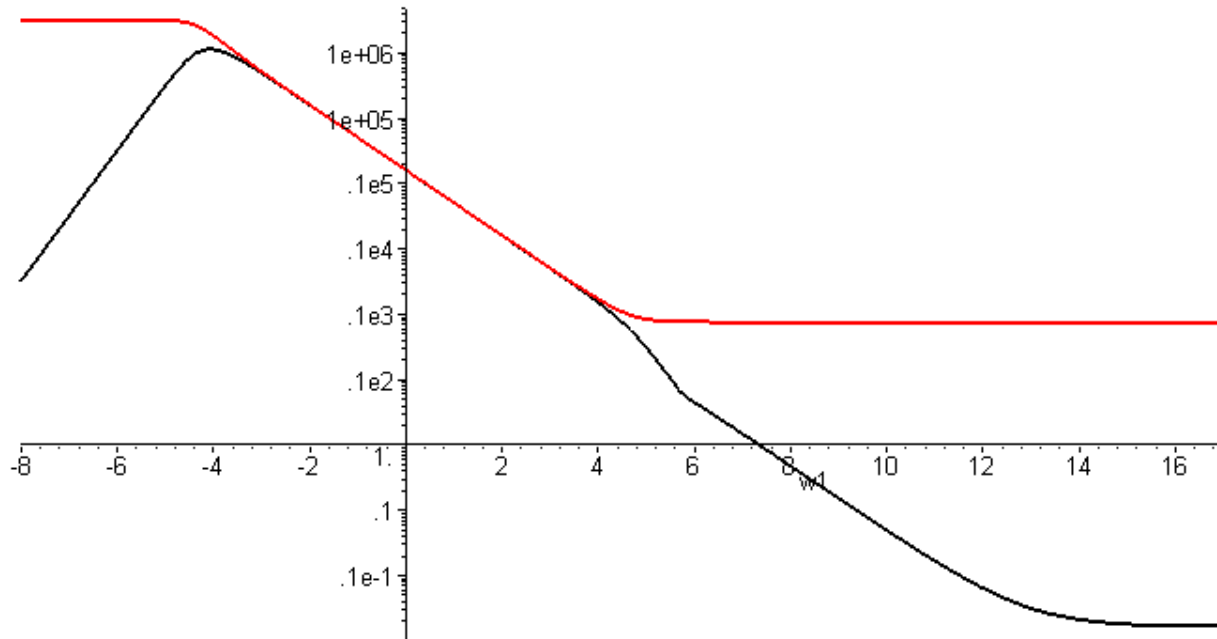
```
(sqrt(2.3)/(3e8*69e-12))*0.0005/2;  
.01831612427
```

in agreement with the above plot.

Because $-\text{Im}Z_0$ goes negative, we cannot do a full log plot of $-\text{Im}Z_0$ without adding a small positive offset. This problem did not arise when dealing with $k(\omega)$ in Section Q.5 because $\text{Im}k$ must always be negative to insure a loss (and not a gain!) at any ω .

Adding an offset of .02, we then make our plot over a full range of ω :

```
logplot([ReZ0, -ImZ0 + .02], w1 = -8..17, thickness=2, color =
[red, black], numpoints=200);
```



Red = $\text{Re}(Z_0)$ Black = $-\text{Im}(Z_0) + 0.02$

Fig Q.9.7

We have just shown that, for large ω , $\text{Im}Z_0$ approaches the constant -0.18Ω shown in (Q.7.4). We now see that $\text{Re}Z_0$ also approaches a constant value $[1/(v_d C)] = [\sqrt{\epsilon_d/\epsilon_0}/(cC)]$ which is

```
(sqrt(2.3)/(3e8*69e-12));
```

73.26449705

This value of 73.26Ω is slightly less than the nominal cable impedance of 75Ω . The following plot shows $\text{Re}Z_0$ (red) and $-\text{Im}Z_0$ (black) for 10 KHz to 100 KHz on the left, and 100 KHz to 1 GHz on the right :

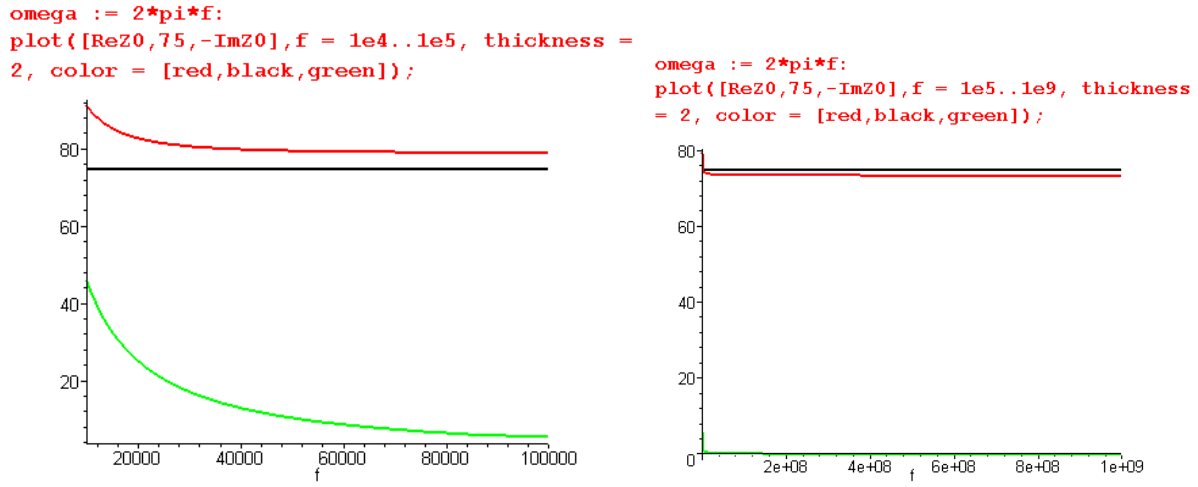


Fig Q.9.8

Above 100 KHz $-\text{Im}Z_0$ can be neglected, but at 10KHz it jumps up to 45Ω .

Appendix R: Belden 8281 Coaxial Cable, a Case Study

Here we gradually work our way through Belden's data sheet for its "8281" coaxial cable, correlating the data presented there with the general theory of this document. The data sheet is available here,

www.belden.com/techdatas/metric/8281.pdf

but we will be quoting most of it below. We note that over the decades, the parameters on this data sheet have changed slightly. At its market introduction more than 50 years ago, this RG-59 75 Ω coaxial cable was pretty much top of the line for general purpose RF use, and it is still available today. It is often used to carry uncompressed analog video signals. Today Belden offers more advanced coaxial cables for use with high bandwidth digital video signals. Such cables often have a foam dielectric to reduce attenuation, while the 8281 cable has a solid polyethylene dielectric.

Below we use various equations from our main document to construct a "model" of the Belden cable, but this model is limited to "high frequency" meaning here roughly $f > 1$ MHz. A more careful analysis would also produce a "low frequency" model for frequencies from DC to 1 MHz, and would then blend these two models at the boundary in some smooth manner.

Of the four transmission line parameters R,L,G,C, only C is treated below as a constant in frequency, although L is roughly constant in our frequency range of interest. Often in textbook treatments, all four parameters are considered constants when expressions like $k(\omega)$ and $Z_0(\omega)$ are plotted (see below).

(a) Geometry of the cable

We start with this data from the Belden specification,

Physical Characteristics (Overall)

Conductor

AWG:

# Coax	AWG	Stranding	Conductor Material	Dia. (mm)
1	20	Solid	BC - Bare Copper	0.7874

Total Number of Conductors:

Insulation

Insulation Material:

Insulation Material	Dia. (mm)
PE - Polyethylene	5.0292

Outer Shield

Outer Shield Material:

Layer #	Type	Outer Shield Material	Coverage (%)
1	Braid	TC - Tinned Copper	95.000
2	Braid	TC - Tinned Copper	95.000



The center wire is solid copper with a specified diameter of 0.7874 mm, so $a_1 = .7874/2 \text{ mm} = 0.3937 \text{ mm} = 393.7 \mu$. The diameter of the PE core is specified as 5.0202 mm so the radius is $5.0202/2 = 2.5101 \text{ mm} = 2510.1 \mu$. This core is surrounded by a tinned double copper braid. One sometimes adds the radius (80 μ) of the fine braiding wire to the effective outer cable radius, but we shall add 11.5 μ to the radius since this makes C match the Belden data sheet value if $\epsilon_d/\epsilon_0 = 2.3000$. So $a_2 = 2510.1 + 11.5 = 2521.6 \mu$. We then have,

$$\begin{array}{ll} a_1 = 393.7 \mu & \text{inner wire radius} \\ a_2 = 2521.6 \mu & \text{inside radius of the shield} \end{array}$$

Obviously the 2.3000 number is not exact. We are just building a reasonable model here to try and replicate the Belden claimed cable parameters, and some parameters have to be tuned to get consistency. The double braid is not exactly the same as a solid cylindrical shell of copper, so things are approximate.

As we go along here, the corresponding Maple code will be displayed. So far then,

```
a1 := (1/2)*0.7874e-3;
a2 := ((1/2)*5020.2 + 11.5) * 1e-6;
a1 := .0003937000000
a2 := .002521600000
```

where all quantities are stated in the usual SI units (meters for a_1 and a_2). From these radii one computes K from (4.6.3),

$$K = 2 \ln(a_2/a_1), \quad (4.6.3)$$

to get $K = 3.7141$,

```
K := 2*ln(a2/a1);
K := 3.714119404
```

(b) Capacitance C

Assuming $\epsilon_d/\epsilon_0 = 2.3000$, one uses (4.4.17)

$$C = 4\pi\epsilon_d/K \quad \text{capacitance per unit length} \quad (4.4.17)$$

to get

```
e0 := 8.8541877e-12;
ed := 2.3*e0;
C := 4*pi*ed/K;
e0 := .88541877 10^-11
ed := .2036463171 10^-10
C := .6890179924 10^-10
```

The Belden data sheet quotes $C = 68.901$ pF/m.

Nom. Capacitance Conductor to Shield:

Capacitance (pF/m)
68.901

in agreement with our calculation. We regard C as a constant independent of ω .

(c) Conductance G

The DC conductance G of the dielectric is related to the capacitance according to

$$G_{dc} = (\sigma_{dc}/\epsilon_d) C \quad (4.11.15)$$

where σ_{dc} is the DC dielectric conductivity. Recall now (3.3.4),

$$\sigma_{eff} = (\sigma_{dc} + \omega \epsilon'_d \tan_L) \quad (3.3.4)$$

which gives the effective conductivity of the dielectric in terms of the DC conductivity σ_d , the real part of ϵ_d called ϵ'_d and the loss tangent factor. For PE we know that $\sigma_{dc} \sim 10^{-15}$ so we neglect that term. We shall be using $\tan_L = .0005$ below, and since this is small, $\epsilon'_d \approx \epsilon_d$. Finally, to reduce symbol clutter we rename σ_{eff} to be σ_d so the above equation becomes

$$\sigma_d = \epsilon_d \tan_L \omega \quad \Rightarrow \quad (\sigma_d/\epsilon_d) = \tan_L \omega$$

and then

$$G = \tan_L \omega C = \tan_L 2\pi f C. \quad (R.1)$$

Although Fig 3.1 mentions $\tan_L = .0002$ for a high quality sample of polyethylene, our experience has shown that for the bulk low-cost PE product used in coaxial cables, $\tan_L \approx .0005$. The larger loss is due to many effects including milling, aging (oxidation), water absorption ("treering") and additives intended to reduce these loss effects. Very poor quality PE can have a loss tangent ($\tan_L = \tan\delta =$ dissipation factor) of .0075. For more accuracy, one can develop frequency dependent models for \tan_L .

The corresponding Maple expressions are duly entered,

```

tanL := .0005;
G := f -> tanL*2*pi*f*C;

```

$\tan_L = .0005$
 $G = f \rightarrow 2 \tan_L \pi f C$

where the last notation indicates that $G(f)$ is a function of frequency f .

In either the Z_0 or attenuation calculations below, the quantity $G + j\omega C$ ($= y$) always appears as a grouping, and we have determined that

$$G + j\omega C = \tan_{\alpha} \omega C + j\omega C = (-j \tan_{\alpha} + 1) j\omega C = (1 - 0.0005j) j\omega C \quad . \quad (R.2)$$

Based on this grouping, one sees that our model is not very sensitive to the value of \tan_{α} as long as it is a relatively small value.

(d) External inductance L_e

Using the numbers developed so far, one computes L_e from $L_e = \frac{\mu_0}{4\pi} K$ in (4.12.24) :

$$\mu_0 := 4 * \pi * 1e-7 ;$$

$$\mu_0 := .1256637062 \cdot 10^{-5}$$

$$K := 2 * \ln(a_2/a_1) ;$$

$$K := 3.714119404$$

$$L_e := \mu_0 * K / (4 * \pi) ;$$

$$L_e := .3714119405 \cdot 10^{-6}$$

which is $L_e = 371.41$ nH/m.

(e) Total DC Inductance

From (C.3.10) we know that the center wire DC internal inductance is given by

$$L_i(\text{center}) = \frac{\mu_0}{8\pi} = 50 \text{ nH/m} \quad . \quad \text{DC} \quad (C.3.10)$$

Assuming the shield has a thickness t , (C.6.8) indicates that

$$L_i(\text{shield}) = \frac{\mu_0}{8\pi} \left[\frac{4}{3} \left(\frac{t}{a_2} \right) \right] \quad . \quad \text{DC} \quad \text{thin shell, valid for } t \ll a_2 \quad . \quad (C.6.8)$$

We can compute an effective shield thickness t by making use of its DC resistance R_{2DC} :

$$R_{2DC} = \rho/A = 1/(\sigma A) = 1/(\sigma 2\pi a_2 t)$$

$$\Rightarrow t = 1/(\sigma 2\pi a_2 R_{2DC}) \quad (R.3)$$

Then

$$L_i(\text{shield}) = \frac{\mu_0}{8\pi} \left[\frac{4}{3} \frac{1}{\sigma 2\pi a_2^2 R_{2DC}} \right] \quad . \quad (R.4)$$

The value of R_{2DC} is specified as 3.6091 ohms/km,

Nominal Outer Shield DC Resistance:

DCR @ 20°C (Ohm/km)
3.6091

Here then are some calculations leading to a total DC inductance for the cable,

```

mu0 := 4*pi*1e-7;
Le := mu0*K/(4*pi);
sigma := 5.81e7;
R2DC := 3.6091e-3;
t := 1/(sigma*2*pi*a2*R2DC);
Li_shield_DC := (mu0/(8*pi))*(4/3)* 1/(sigma*2*pi*a2^2*R2DC);
Li_center_DC := 50e-9;
Li_DC := Li_shield_DC + Li_center_DC;
L_DC := Li_DC + Le;

```

$$\mu_0 = .1256637062 \cdot 10^{-5}$$

$$L_e = .3714119405 \cdot 10^{-6}$$

$$\sigma = .581 \cdot 10^8$$

$$R_{2DC} = .0036091$$

$$t = .0003010016581$$

$$L_{i_shield_DC} = .7957954160 \cdot 10^{-8}$$

$$L_{i_center_DC} = .50 \cdot 10^{-7}$$

$$L_{i_DC} = .5795795416 \cdot 10^{-7}$$

$$L_{DC} = .4293698947 \cdot 10^{-6}$$

The center wire contributes 50.00 nH/m to the DC internal inductance, while the shield contributes another 7.96 nH/m giving a total of 57.96 nH/m for the total cable internal DC inductance. When this is added to the external inductance L_e of 371.41 nH/m, the total is seen to be 429.37 nH/m. The Belden data sheet quotes 429.811 nH/m giving a small discrepancy of 1/10th of 1% compared to our calculation,

Nom. Inductance:

Inductance (μH/m)
0.429811

We see that Belden's "nominal inductance" is the total DC inductance of the cable $L_e + L_i$.

(f) High Frequency Inductance and Resistance

At high ω where the skin effect dominates, one thinks of the current being restricted to a sheath of approximate thickness δ (skin depth). In Chapter 2 we showed that, for the center conductor of radius a_1 , the high frequency resistance and internal inductance (per unit length) are given by,

$$R_1 = \frac{1}{\sigma(2\pi a_1)\delta} \quad (2.4.18)$$

$$L_{1i} = (1/\omega) R_1 = \frac{1}{\omega\sigma(2\pi a_1)\delta} = \frac{1}{\omega\sigma(2\pi a_1)\sqrt{2/\omega\mu_0\sigma}} = \frac{1}{2\pi a_1} \sqrt{\frac{\mu_0}{2\sigma\omega}} \quad (2.4.19)$$

It was noted that R_1 has the simple interpretation of being the resistance of a shell of radius a_1 and thickness δ .

Since this same kind of thin skin-effect sheath also exists on the inner surface of the outer conductor, we shall assume that the corresponding parameters for the outer conductor are obtained by replacing a_1 by a_2 in the above, so

$$R_2 = \frac{1}{\sigma(2\pi a_2)\delta}$$

$$L_{2i} = \frac{1}{\omega\sigma(2\pi a_2)\delta} = \frac{1}{\omega\sigma(2\pi a_2)\sqrt{2/\omega\mu_0\sigma}} = \frac{1}{2\pi a_2} \sqrt{\frac{\mu_0}{2\sigma\omega}} \quad (R.5)$$

We have assumed that the shield and center conductor are made of the same metal (copper) with σ and δ . For other cables, the shield might be aluminum foil, and one would then adjust the above equations.

Adding, we then arrive at these expressions for high frequency resistance and internal inductance:

$$R = \frac{1}{\sigma(2\pi)\delta} \left[\frac{1}{a_1} + \frac{1}{a_2} \right]$$

$$L_i = \frac{R}{\omega} = \frac{1}{\omega\sigma(2\pi)\delta} \left[\frac{1}{a_1} + \frac{1}{a_2} \right] = \frac{1}{f\sigma(2\pi)^2\delta} \left[\frac{1}{a_1} + \frac{1}{a_2} \right] \quad (R.6)$$

At 1 MHz (2.3.9) says $\delta = 66\mu$. Since the center conductor has $a_1 =$ radius 394μ and the shield has thickness $t = 301\mu$, we shall restrict our model to apply only to frequencies over 1 MHz (ballpark).

For the Belden 8281 cable, the first term in $\left[\frac{1}{a_1} + \frac{1}{a_2} \right]$ is 6.4 times larger than the second term

$$(1/a_1)/(1/a_2) ;$$

$$6.404876810$$

so most of the R and L_i at high frequency come from the inner conductor, not the shield.

(g) The Tinning Correction

A model complication is that the 160 μ diameter copper braid wires (34 gauge) of the shield are coated with tin of thickness 1.3 μ (50 micro-inches). This coating is added to prevent the copper shield from oxidizing. At 1 GHz (2.3.9) gives $\delta_{\text{copper}} = 2.09\mu$. Since tin has about 6.3 times more resistance than copper, and since $\delta = \sqrt{2/\omega\mu\sigma}$, one finds that $\delta_{\text{tin}} = 5.24\mu$ at 1 GHz. As the frequency increases, one has to somehow gradually replace the copper δ with the tin δ in the second term of the R and L_i expressions above. An analytic solution to this problem can be found by applying the Helmholtz equation $[\nabla^2 + \beta^2]\mathbf{E} = 0$ to a simple one-dimensional model of the tin/copper interface. We have done this and then obtained the following "phenomenological" model to handle the tinning correction:

$$R = \frac{1}{\sigma(2\pi)\delta} \left[\frac{1}{a_1} + \frac{1}{a_2} * tf \right]$$

$$L_i = \frac{1}{f\sigma(2\pi)^2\delta} \left[\frac{1}{a_1} + \frac{1}{a_2} * tf \right] \quad L_i = R / (2\pi f)$$

$$tf = 1.765 + 0.8 \tanh(\sqrt{f(\text{GHz})} - 1.9) \quad \text{" tinning factor" } \quad (\text{R.7})$$

Here is a plot of this tinning factor for f ranging from 10 KHz to 1 GHz,

```
semilogplot(tf(f), f=1e4..1e9, numpoints = 500);
```

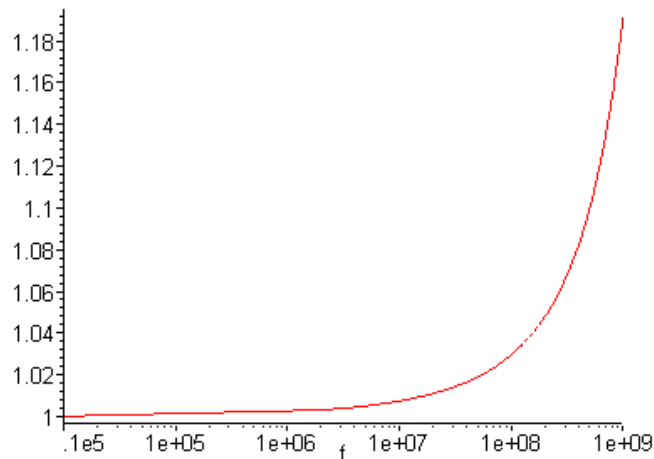


Fig R.1

Tinning Factor versus Frequency

It was shown above that $\frac{1}{a_1}$ is 6.4 times larger than $\frac{1}{a_2}$, so the tinning factor correction is fairly small at frequencies below 1 GHz (our region of interest). Even at 1 GHz we have

$$\frac{R_{\text{corrected}}}{R_{\text{uncorrected}}} = \frac{\frac{1}{a_1} + \frac{1}{a_2} * tf}{\frac{1}{a_1} + \frac{1}{a_2}} = 1.026$$

$$((1/a1)+(1/a2)*tf(1e9))/((1/a1)+(1/a2));$$

$$1.025923686$$

so the tinning factor increases R and L_i by about 2.6% at 1 GHz, and less below 1 GHz. Although small, we shall include this tinning correction in our calculations below.

Here then are the Maple entries for high-frequency R and L_i , where $\delta = \sqrt{2/(\omega\mu\sigma)} = \sqrt{1/(\pi f\mu\sigma)}$:

$$\text{delta} := f \rightarrow \sqrt{1/(\pi * f * \mu_0 * \sigma)};$$

$$\delta = f \rightarrow \sqrt{\frac{1}{\pi f \mu_0 \sigma}}$$

$$R := f \rightarrow 1/(2 * \pi * \sigma * \text{delta}(f)) * ((1/a1)+(1/a2)*tf(f));$$

$$R = f \rightarrow \frac{1}{2} \frac{\frac{1}{a1} + \frac{tf(f)}{a2}}{\pi \sigma \delta(f)}$$

$$Li := f \rightarrow R(f)/(2 * \pi * f);$$

$$Li = f \rightarrow \frac{1}{2} \frac{R(f)}{\pi f}$$

$$L := f \rightarrow Li(f) + Le;$$

$$L = f \rightarrow Li(f) + Le$$

Since $\delta \sim 1/\sqrt{f}$ and $L_i \sim 1/(\delta f) \sim 1/\sqrt{f}$, the internal inductance L_i drops off rapidly at high frequencies and is in general much smaller than L_e . This is due to the fact shown in (C.6.8) that the internal inductance of an annular shell goes to zero as that shell (thickness δ) becomes thinner. Here is a plot of L_i (red), $L_e = 371.4$ nH (black), and $L = L_i + L_e$ (green) for f in the range 1 MHz to 1 GHz,


```
semilogplot([Li(f),Le,L(f)], f=1e6..1e9, color = [red,black,green]);
```

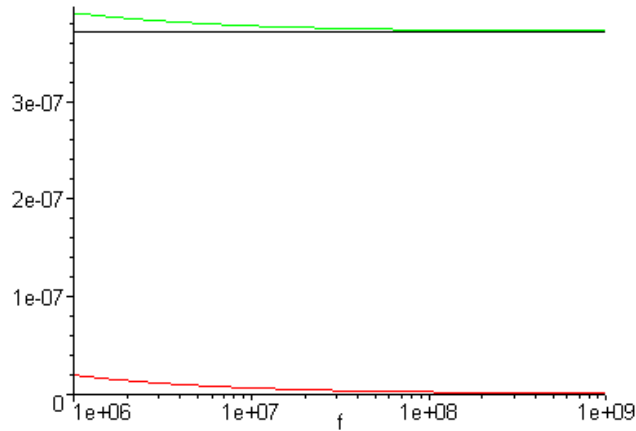


Fig R.2

Thus, for our range of interest, L is dominated by L_e .
The corresponding plot of resistance R is the following,

```
semilogplot(R(f), f=1e6..1e9,numpoints = 400);
```

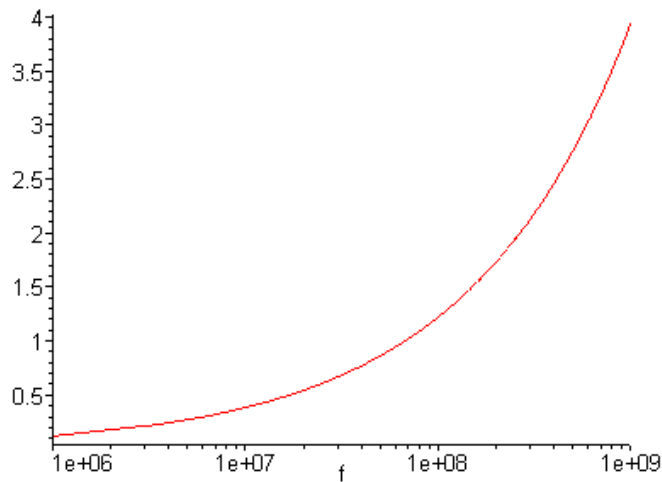


Fig R.3

Notice that this plotted R is in ohms/m, whereas the DC resistances of the center wire and shield are stated in ohms/km,

Nom. Conductor DC Resistance:

DCR @ 20°C (Ohm/km)
32.4819

Nominal Outer Shield DC Resistance:

DCR @ 20°C (Ohm/km)
3.6091

Compared to these DC resistances, resistance R is quite large, and of course this is due to the skin effect.

(h) Characteristic Impedance

Although the cable has a nominal Z_0 of 75Ω ,

Nom. Characteristic Impedance:

Impedance (Ohm)
75

the actual Z_0 is a slow function of frequency and can vary slightly ($\sim 1.5\Omega$) from the advertised nominal value. Recall from Chapter 4 that

$$Z_0 \equiv V(z)/i(z) = \sqrt{\frac{z}{y}} = \sqrt{\frac{R + j\omega L}{G + j\omega C}} \quad (4.12.18)$$

which is in general complex. We enter this into Maple,

```
Z0 := f -> sqrt((R(f)+j*2*pi*f*L(f))/(G(f) + j*2*pi*f*C));
```

$$Z_0 = f \rightarrow \sqrt{\frac{R(f) + 2j\pi f L(f)}{G(f) + 2j\pi f C}}$$

where the functions $R(f)$, $L(f)$ and $G(f)$ have been stated above. We then plot $\text{Re}\{Z_0\}$ for f ranging from 1MHz to 10 GHz,

```
semilogplot([Re(Z0(f)),75], f = 1e6..1e10, color=[red,black], numpoints = 1000);
```

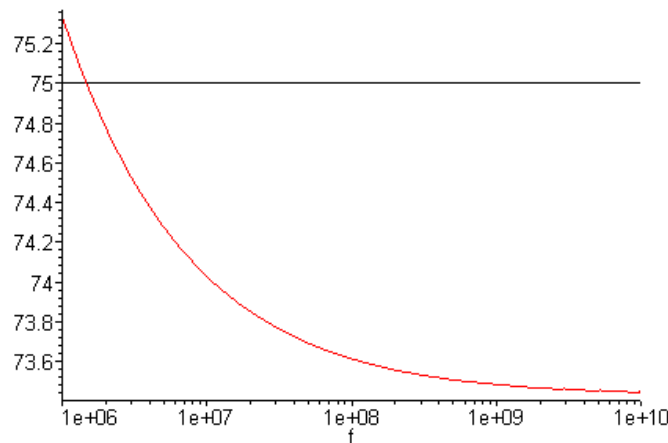


Fig R.4

Recall that our cable model using high frequency expressions for L_i and R is only valid above 1 MHz more or less. The plot shows that the cable has $Z_0 = 75\Omega$ near $f = 2$ MHz, but drops to 73.48Ω at 1 GHz, and is a little larger than 75Ω below 2 MHz.

The imaginary part of Z_0 over this same frequency range is on the order of -1Ω :

```
semilogplot(Im(Z0(f)), f = 1e6..1e10,numpoints = 1000);
```

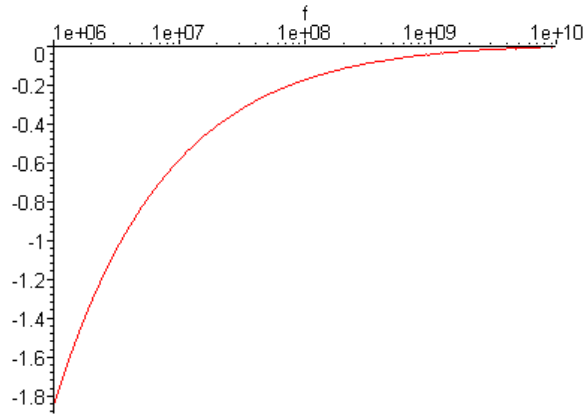


Fig R.5

A proper no-reflections termination of the cable thus requires both a resistance on the order of 75Ω and a small reactive component.

Since the imaginary part is so small, there is little distinction between $\text{Re}(Z_0)$ and $|Z_0|$. This is illustrated in the following plot,

```
magZ0 := f -> sqrt(Re(Z0(f))^2 + Im(Z0(f))^2);
```

$$\text{magZ0} = f \rightarrow \sqrt{\Re(Z_0(f))^2 + \Im(Z_0(f))^2}$$

```
semilogplot([Re(Z0(f)), magZ0(f), 75], f = 1e6..1e10,numpoints = 1000, color = [red, green, black]);
```

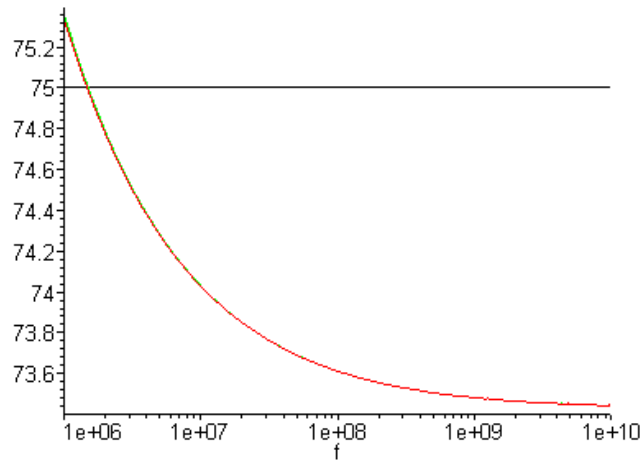


Fig R.6

where the red ($\text{Re}(Z_0)$) and green ($|Z_0|$) curves lie right on top of each other.

At large ω , we expect Z_0 to approach a limiting value of 73.42Ω ,

$$Z_0 = \sqrt{L/C} \rightarrow \sqrt{L_e/C}$$

```

Z0_limit := sqrt(Le/C);
Z0_limit := 73.41970742
Z0_limit := (1/(4*pi))*K*sqrt(mu0/ed); # see (4.4.14)
Z0_limit := 73.41970738

```

in agreement with Fig R.4 above.

At very low ω , we have instead that $Z_0 = \sqrt{R/G}$. One can use $R = .036 \Omega/\text{m}$ by adding the DC resistances of the shield and center conductor. However, G is miniscule at DC since polyethylene is such a good insulator, so Z_0 is in the $3 \text{ M}\Omega$ range,

```

R2DC := 3.6091e-3;
R2DC = .0036091
R1DC := 32.4819e-3;
R1DC = .0324819
RDC := R2DC + R1DC;
RDC = .0360910
sigmad := 1e-15; #DC conductivity of PE
sigmad = .1 10^-14
GDC := (sigmad/ed) * C; # see in box (4.11.34)
GDC = .3383405123 10^-14
Z0DC := sqrt(RDC/GDC);
Z0DC = .3266047198 10^7

```

Here we have assumed $\sigma_d \sim 10^{-15}$ mho/m, though this could be much larger for the kind of PE that is used in Belden cables, resulting in a somewhat smaller Z_{0DC} .

Our model does not account for micro detail involving the mesh shield and manufacturing variations, and one finds with a network analyzer (and an actual piece of Belden 8281 cable) that there is "noise" superimposed on our idealized plot of Z_0 versus f which has an RMS value on the order of 1 ohm, see the work of Van Der Burgt. He argues that due to this "noise", it makes little sense to try to pin down a Z_0 tolerance beyond current values, although cable makers still try to do it as part of their marketing specmanship wars.

(i) Phase Velocity and Attenuation

Recall (5.3.6) which we apply to the voltage on a transmission line whose left end is at $z = 0$:

$$V(z) = V(0) e^{-jkz} = V(0) e^{-az} e^{-jbz} \quad jk = a + jb = \sqrt{zy} = \sqrt{(R+j\omega L)(G+j\omega C)}$$

$$a \equiv \text{Re}(\sqrt{zy}) = \text{Re}[\sqrt{(R+j\omega L)(G+j\omega C)}] = -\text{Im}(k) \quad // \text{attenuation per distance of } F(z)$$

$$b \equiv \text{Im}(\sqrt{zy}) = \text{Im}[\sqrt{(R+j\omega L)(G+j\omega C)}] = \text{Re}(k) \quad // \text{phase of } F(z) \quad (5.3.6)$$

Conventional symbols for the attenuation and phase constants are α and β , but here we call them a and b .

Phase Velocity

One can see that, for large ω ,

$$b = \text{Im}[\sqrt{(R+j\omega L)(G+j\omega C)}] = \text{Im}[\sqrt{(j\omega L)(j\omega C)}] = \omega \text{Im}[\sqrt{-LC}] = \omega \sqrt{LC}$$

and therefore the cable phase velocity is given by

$$v_{\text{phase}} = \omega/\text{Re}(k) = \omega/b = 1/\sqrt{LC} \quad // \text{ large } \omega$$

Since $L \approx L_e$ in our frequency range of interest, and since the speed of light in the dielectric is determined by $v_d = 1/\sqrt{L_e C} = 1/\sqrt{\mu_d \epsilon_d}$ [see (4.12.19)], we conclude that

$$v_{\text{phase}} = v_d = 1/\sqrt{L_e C} = 1/\sqrt{\mu_d \epsilon_d} \quad // \text{ large } \omega$$

and we can compute this two different ways, knowing that the result must be the same,

```
vphase_over_c := (1/sqrt(Le*C))/c;
vphase = .6589243140
vd_over_c := (1/sqrt(mu0*ed))/c;
vd_over_c = .6589243140
```

This is in agreement with the Belden claim,

Nominal Velocity of Propagation:

VP (%)
66

The time for a phase front to move 1 meter is given by $1/v_d$,

```
delay := 1/(c * vd_over_c);
delay = .5058749939 10^-8
```

which is 5.059 nsec. Belden gives

Nominal Delay:

Delay (ns/m)
5.05274

which is within 1/10th a 1% of our computed value.

Reader Exercise: Derive an expression for group velocity v_g in the presence of attenuation (k is complex). How does your result compare with the classical expression $1/v_g = \partial k / \partial \omega$ or $v_g = \partial \omega / \partial k$? Using expressions of the model above, compute v_g as a function of frequency. Since v_g varies with f , the

cable exhibits dispersion -- pulses spread out as they are attenuated. Determine the group delay for a narrow pulse to travel 1 m down the Belden cable. How does this delay compare with the phase delay noted above? What is the effect of the tinning correction on group delay?

Attenuation

It is traditional to express attenuation in "voltage decibels" defined in this manner,

$$\begin{aligned} \text{dB}(z) &= -20 \log_{10}(\text{voltage attenuation over distance } z) && \text{"decibels"} \\ &= -20 \log_{10}(e^{-az}) = 20 az \log_{10}(e) = [20 \log_{10}(e)] az = 8.686 az \end{aligned} \quad (\text{R.8})$$

```
evalf(20*log10(exp(1)));
                        8.685889638
```

Belden provides attenuation data for $z = 100$ m of cable, so we just write (see above, $a = -\text{Im}(k)$)

$$\text{dB} = 868.6 a = 868.6 [-\text{Im}(k)] > 0 . \quad (\text{R.9})$$

Here then is a plot of attenuation for frequency f in the range 1 MHz to 1 GHz :

```
k := f -> -j*sqrt((R(f)+j*2*pi*f*L(f))*(G(f)+j*2*pi*f*C));
                        k:=f→-j√(R(f)+2jπfL(f))(G(f)+2jπfC)
a := f -> -Im(k(f));
                        a:=f→-ℑ(k(f))
dB := f -> 868.5*a(f);
                        dB:=f→868.5a(f)
semilogplot(dB(f), f = 1e6..1e9, numpoints=200);
```

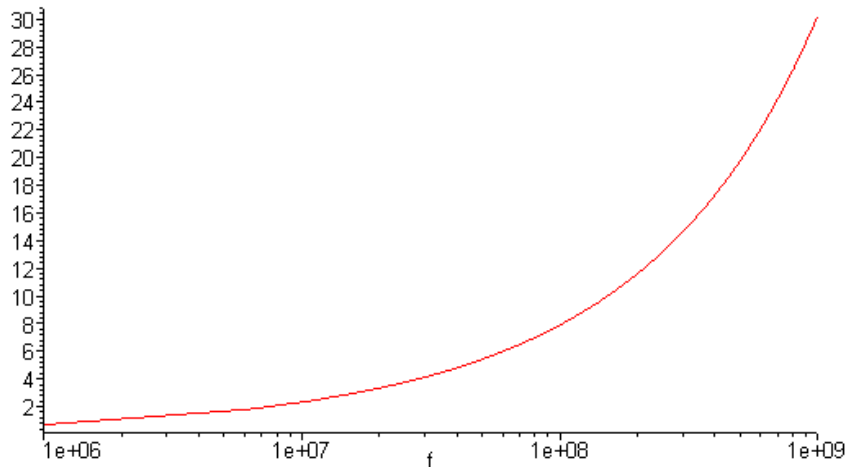


Fig R.7

In order to compare this theoretical attenuation prediction with Belden's provided data, we first evaluate our attenuation at the frequencies listed on the Belden data sheet,

```
for f in [1,3.6,10,71.5,135,270,360,540,720,750,1000,2000]*1e6 do
  printf("    f = %8.1f MHz  dB(f) = %4.2f \n", f/1e6,dB(f));
od;
```

```
f =      1.0 MHz  dB(f) =   .71
f =      3.6 MHz  dB(f) =   1.37
f =     10.0 MHz  dB(f) =   2.33
f =     71.5 MHz  dB(f) =   6.59
f =    135.0 MHz  dB(f) =   9.33
f =    270.0 MHz  dB(f) =  13.78
f =    360.0 MHz  dB(f) =  16.28
f =    540.0 MHz  dB(f) =  20.70
f =    720.0 MHz  dB(f) =  24.65
f =    750.0 MHz  dB(f) =  25.28
f =   1000.0 MHz  dB(f) =  30.26
f =   2000.0 MHz  dB(f) =  47.77
```

Freq. (MHz)	Attenuation (dB/100m)
1	0.9843
3.6	1.6405
10.0	2.6248
71.5	6.8901
135	9.843
270	14.1083
360	16.7331
540	20.6703
720	24.2794
750	24.9356
1000	30.1852

Model Calculation of Attenuation

Belden's Datasheet Attenuation

The following spreadsheet then compares Belden's decibel attenuation data with our model prediction,

MHz	Belden	Model	Model no Tin	Error	(Belden-Model)/Belden
1	0.9843	0.71	0.71	28%	
3.6	1.6405	1.37	1.37	16%	
10	2.6248	2.33	2.33	11%	
71.5	6.8901	6.59	6.57	4%	
135	9.843	9.33	9.29	5%	
270	14.1083	13.78	13.69	2%	
360	16.7331	16.28	16.14	3%	
540	20.6703	20.7	20.46	0%	
720	24.2795	24.65	24.29	-2%	
750	24.9365	25.28	24.9	-1%	
1000	30.1852	30.26	29.67	0%	
2000		47.77	46.02		

As shown, the error goes down as one moves away from the lower part of the frequency range where the model is least applicable.

Here is a plot of the results :

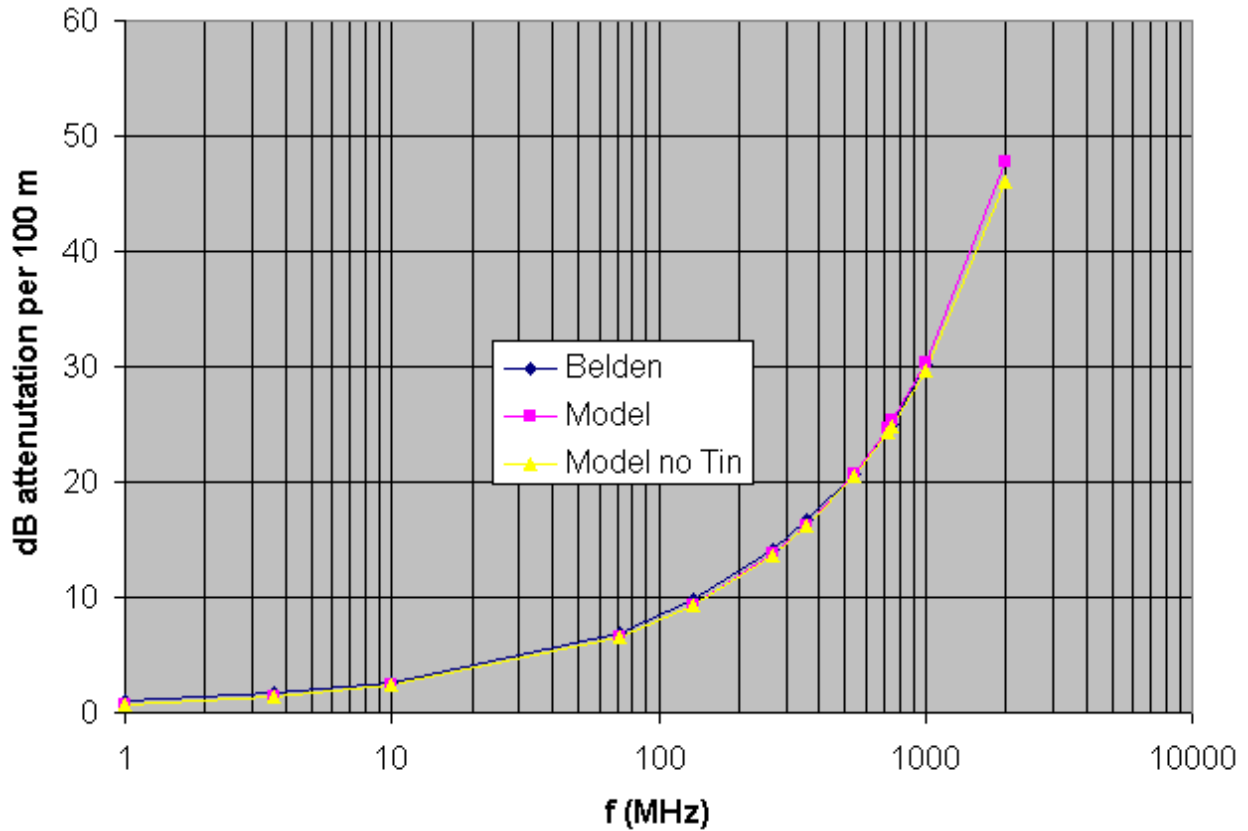


Fig R.8

We have included in the spreadsheet a model column which ignores the tinning correction (yellow triangles). This column was obtained by setting $tf(f) = 1$ in the Maple code. We added a point at 2 GHz for which Belden gives no data, and at that point one sees that the tinning correction starts to become a little more visible. Tinning increases attenuation at high frequencies.

At one time we measured the attenuation of 100 m of Belden 8281 cable using a network analyzer and found that the above model (with tinning correction) reasonably represents the cable up to 100 GHz.

Appendix S: Details of the Chapter 4 Averaging Procedure

Here we review the averaging process outlined in Section 4.12 (b) in more detail, *and* we maintain the transverse derivatives of the vector potential which were neglected in that Section. Since the process is explained there, here we just show what happens to the various equations. Corresponding equation numbers from Chapter 4 are shown in italics. The function arguments suppressed in Chapter 4 for points \mathbf{x}_1 and \mathbf{x}_2 are shown in red as $(\mathbf{x}_1, \mathbf{x}_2)$. New terms arising from the previously neglected transverse vector potential derivatives are shown in blue.

The potential difference between two conductors in the transmission line limit is given by

$$\begin{aligned} V(\mathbf{x}_1, \mathbf{x}_2) &\equiv \phi_{12}(\mathbf{x}_1) - \phi_{12}(\mathbf{x}_2) \\ &= \frac{1}{4\pi\epsilon_d} q(z) \int_{-\infty}^{\infty} dz' \left\{ \int_{C_1} dx_1' dy_1' \alpha_1(x_1', y_1') \frac{1}{R_{11}} - \int_{C_2} dx_2' dy_2' \alpha_2(x_2', y_2') \frac{1}{R_{12}} \right\} \\ &\quad - \frac{1}{4\pi\epsilon_d} q(z) \int_{-\infty}^{\infty} dz' \left\{ \int_{C_1} dx_1' dy_1' \alpha_1(x_1', y_1') \frac{1}{R_{21}} - \int_{C_2} dx_2' dy_2' \alpha_2(x_2', y_2') \frac{1}{R_{22}} \right\} \end{aligned} \quad (4.4.1) \quad (S.1)$$

and later

$$\begin{aligned} V(\mathbf{x}_1, \mathbf{x}_2) &= q(z) \frac{1}{4\pi\epsilon_d} \left\{ \int_{C_1} dx_1' dy_1' \alpha_1(x_1', y_1') \ln(s_{21}^2/s_{11}^2) - \int_{C_2} dx_2' dy_2' \alpha_2(x_2', y_2') \ln(s_{22}^2/s_{12}^2) \right\} \\ s_{21}^2 &= (x_2 - x_1')^2 + (y_2 - y_1')^2 & s_{22}^2 &= (x_2 - x_2')^2 + (y_2 - y_2')^2 & (4.4.6) \\ s_{11}^2 &= (x_1 - x_1')^2 + (y_1 - y_1')^2 & s_{12}^2 &= (x_1 - x_2')^2 + (y_1 - y_2')^2 . & (S.2) \end{aligned}$$

Then

$$\begin{aligned} \frac{1}{C'(\mathbf{x}_1, \mathbf{x}_2)} &= \frac{V(\mathbf{x}_1, \mathbf{x}_2)}{q(z)} & (S.3) \\ &= \frac{1}{4\pi\epsilon_d} \left\{ \int_{C_1} dx_1' dy_1' \alpha_1(x_1', y_1') \ln(s_{21}^2/s_{11}^2) - \int_{C_2} dx_2' dy_2' \alpha_2(x_2', y_2') \ln(s_{22}^2/s_{12}^2) \right\} \\ &= \frac{1}{4\pi\epsilon_d} K(\mathbf{x}_1, \mathbf{x}_2) \text{ and } V(\mathbf{x}_1, \mathbf{x}_2) = q(z) \frac{1}{4\pi\epsilon_d} K(\mathbf{x}_1, \mathbf{x}_2) \end{aligned} \quad (4.4.7)$$

where

$$K(\mathbf{x}_1, \mathbf{x}_2) = \frac{1}{4\pi\epsilon_d} \left\{ \int_{C_1} dx_1' dy_1' \alpha_1(x_1', y_1') \ln(s_{21}^2/s_{11}^2) - \int_{C_2} dx_2' dy_2' \alpha_2(x_2', y_2') \ln(s_{22}^2/s_{12}^2) \right\} . \quad (4.4.8) \quad (S.4)$$

Continuing along,

$$L_e(\mathbf{x}_1, \mathbf{x}_2) = (\mu_d/4\pi) K(\mathbf{x}_1, \mathbf{x}_2) \quad (4.4.11) \quad (S.5)$$

$$Z_0(\mathbf{x}_1, \mathbf{x}_2) = (1/4\pi) K(\mathbf{x}_1, \mathbf{x}_2) \sqrt{\mu_d/\epsilon_d} . \quad (4.4.14) \quad (S.6)$$

We then move from the V section to the W section which is Section 4.10 :

$$W(\mathbf{x}_1, \mathbf{x}_2) = i(z) \frac{\mu_d}{4\pi} \left\{ \int_{C_1} dx_1' dy_1' b_1(x_1', y_1') \ln(s_{21}^2/s_{11}^2) - \int_{C_2} dx_2' dy_2' b_2(x_2', y_2') \ln(s_{22}^2/s_{12}^2) \right\} \quad (4.10.4) \quad (S.7)$$

$$W(\mathbf{x}_1, \mathbf{x}_2) = L_e(\mathbf{x}_1, \mathbf{x}_2) i(z) . \quad (4.10.7) \quad (S.8)$$

$$L_e(\mathbf{x}_1, \mathbf{x}_2) = \frac{W(\mathbf{x}_1, \mathbf{x}_2)}{i(z)} = \frac{\mu_d}{4\pi} K_L(\mathbf{x}_1, \mathbf{x}_2) \quad (4.10.8) \quad (S.9)$$

where K_L is a dimensionless function we can compare to K ,

$$K_L(\mathbf{x}_1, \mathbf{x}_2) \equiv \int_{C_1} dx_1' dy_1' b_1(x_1', y_1') \ln(s_{21}^2/s_{11}^2) - \int_{C_2} dx_2' dy_2' b_2(x_2', y_2') \ln(s_{22}^2/s_{12}^2) . \quad (4.10.9) \quad (S.10)$$

$$K(\mathbf{x}_1, \mathbf{x}_2) \equiv \int_{C_1} dx_1' dy_1' \alpha_1(x_1', y_1') \ln(s_{21}^2/s_{11}^2) - \int_{C_2} dx_2' dy_2' \alpha_2(x_2', y_2') \ln(s_{22}^2/s_{12}^2) . \quad (4.4.8)$$

Moving along to Section 4.12 (a) we find (evaluated at some point \mathbf{x})

$$\mathbf{E} = -\text{grad } \varphi - \partial_t \mathbf{A} \quad (1.3.1)$$

$$\text{div } \mathbf{A} = -\mu_d \varepsilon_d \partial_t \varphi - \mu \sigma \varphi . \quad // \text{ the King gauge} \quad (1.3.18) \quad (S.11)$$

Both the above equations are exact and can be rewritten as:

$$\begin{aligned} E_z(\mathbf{x}) &= -\partial_z \varphi(\mathbf{x}) - j\omega A_z(\mathbf{x}) \\ \partial_z A_z(\mathbf{x}) + (\partial_x A_x + \partial_y A_y) &= -j(\beta_d^2/\omega) \varphi(\mathbf{x}) . \end{aligned} \quad (4.12.3) \quad (S.12)$$

where the blue term $(\partial_x A_x + \partial_y A_y)$ was assumed to vanish in Chapter 4, but now we maintain it in what follows, continuing through the development of Section 4.12. Taking into account both conductors gives

$$E_z(\mathbf{x}) = -\partial_z \varphi_{12}(\mathbf{x}) - j\omega A_{z12}(\mathbf{x}) \quad (4.12.4a)$$

$$\partial_z A_{z12}(\mathbf{x}) + (\partial_x A_{x12}(\mathbf{x}) + \partial_y A_{y12}(\mathbf{x})) = -j(\beta_d^2/\omega) \varphi_{12}(\mathbf{x}) . \quad (4.12.4b) \quad (S.13)$$

Then evaluate at \mathbf{x}_1 and \mathbf{x}_2 and subtract to get

$$E_z(\mathbf{x}_1) - E_z(\mathbf{x}_2) = -\partial_z [\varphi_{12}(\mathbf{x}_1) - \varphi_{12}(\mathbf{x}_2)] - j\omega [A_{z12}(\mathbf{x}_1) - A_{z12}(\mathbf{x}_2)] \quad (4.12.5a)$$

$$\begin{aligned} \partial_z [A_{z12}(\mathbf{x}_1) - A_{z12}(\mathbf{x}_2)] + (\partial_x A_{x12}(\mathbf{x}_1) - \partial_x A_{x12}(\mathbf{x}_2)) + (\partial_y A_{y12}(\mathbf{x}_1) - \partial_y A_{y12}(\mathbf{x}_2)) \\ = -j(\beta_d^2/\omega) [\varphi_{12}(\mathbf{x}_1) - \varphi_{12}(\mathbf{x}_2)] . \end{aligned} \quad (4.12.5b) \quad (S.14)$$

We then define

$$V(\mathbf{x}_1, \mathbf{x}_2) \equiv \varphi_{12}(\mathbf{x}_1) - \varphi_{12}(\mathbf{x}_2) \quad (4.4.1)$$

$$W(\mathbf{x}_1, \mathbf{x}_2) \equiv A_{z12}(\mathbf{x}_1) - A_{z12}(\mathbf{x}_2) \quad (4.10.1) \quad (S.15)$$

and rewrite the previous equation pair as

$$E_z(\mathbf{x}_1) - E_z(\mathbf{x}_2) = -\partial_z V(\mathbf{x}_1, \mathbf{x}_2) - j\omega W(\mathbf{x}_1, \mathbf{x}_2) \quad (4.12.6a) \quad (S.16)$$

$$\partial_z W(\mathbf{x}_1, \mathbf{x}_2) = (\partial_x A_{x12}(\mathbf{x}_1) - \partial_x A_{x12}(\mathbf{x}_2)) + (\partial_y A_{y12}(\mathbf{x}_1) - \partial_y A_{y12}(\mathbf{x}_2)) - j(\beta_d^2/\omega) V(\mathbf{x}_1, \mathbf{x}_2). \quad (4.12.6b)$$

Then define function T to represent the Transverse derivatives.

$$T(\mathbf{x}_1, \mathbf{x}_2) \equiv (\partial_x A_{x12}(\mathbf{x}_1) - \partial_x A_{x12}(\mathbf{x}_2)) + (\partial_y A_{y12}(\mathbf{x}_1) - \partial_y A_{y12}(\mathbf{x}_2)) \quad // \dim(T) = \text{tesla} \quad (S.17)$$

We can then "double average" V, W and T as demonstrated in (4.12.13) to obtain from (S.16) 2nd line,

$$\partial_z W(z) = T(z) - j(\beta_d^2/\omega) V(z) \quad (S.18)$$

where

$$W(z) \equiv \langle W(\mathbf{x}_1, \mathbf{x}_2) \rangle_{c1, c2} \quad (4.12.7)$$

$$V(z) \equiv \langle V(\mathbf{x}_1, \mathbf{x}_2) \rangle_{c1, c2} \quad (4.12.7)$$

$$T(z) \equiv \langle T(\mathbf{x}_1, \mathbf{x}_2) \rangle_{c1, c2} \quad (S.19)$$

The first line in (S.16) is then double-averaged to give

$$[E_{z1}(z) - E_{z2}(z)] = -\partial_z V(z) - j\omega W(z) \quad (4.12.6a) \quad (S.20)$$

where for example,

$$\begin{aligned} E_{z1}(z) &\equiv \langle E_{z1}(\mathbf{x}_1) \rangle_{c1, c2} = (1/P_1) \int_{c1} ds_1 (1/P_2) \int_{c2} ds_2 E_{z1}(\mathbf{x}_1) = (1/P_1) \int_{c1} ds_1 E_{z1}(\mathbf{x}_1) \\ &= \langle E_{z1}(\mathbf{x}_1) \rangle_{c1} \end{aligned} \quad (S.21)$$

Then $E_{z1}(\mathbf{x}_1) = Z_{s1}(\mathbf{x}_1) i_1(z)$ gets double-averaged in the same way to define Z_{s1} . At this point we have

$$\begin{aligned} [Z_{s1} + Z_{s2}] i(z) &= -\partial_z V(z) - j\omega W(z) \\ \partial_z W(z) &= -j(\beta_d^2/\omega) V(z) + T(z) \end{aligned} \quad (4.12.11) \quad (S.22)$$

where T(z) was not present in (4.12.11). From (S.9) we write the L_e equation then double-average it,

$$L_e(\mathbf{x}_1, \mathbf{x}_2) = \frac{W(\mathbf{x}_1, \mathbf{x}_2)}{i(z)} \quad \rightarrow \quad L_e = \frac{W(z)}{i(z)} \quad (4.10.8) \quad (S.23)$$

Since then $W(z) = L_e i(z)$, the equation pair (S.22) maybe be rewritten,

$$\begin{aligned} [Z_{s1} + Z_{s2}] i(z) &= -\partial_z V(z) - j\omega W(z) \\ L_e \partial_z i(z) &= -j(\beta_d^2/\omega) V(z) + T(z) \end{aligned} \quad (S.24)$$

or

$$\begin{aligned} \partial_z V(z) &= -[Z_{s1} + Z_{s2} + j\omega L_e] i(z) \\ \partial_z i(z) &= -[j\beta_d^2/(\omega L_e)] V(z) + T(z)/L_e \end{aligned} \quad (4.12.14) \quad (S.25)$$

These are the classical **transmission line equations**, usually written as

$$\frac{dV(z)}{dz} = -z i(z) \quad \frac{di(z)}{dz} = -y V(z) + T(z)/L_e \quad (4.12.15) \quad (S.26)$$

where

$$z = Z_{s1} + Z_{s2} + j\omega L_e = R + j\omega L \quad // z \text{ and } R \text{ are ohms/m} \quad (S.27)$$

$$y = j\beta_d^2/(\omega L_e) = G + j\omega C = j\omega C' \quad // y \text{ and } G \text{ are mhos/m} \quad (4.12.16) \quad (S.28)$$

but now we have an extra term $T(z)/L_e$ in the $\partial_z i$ equation. Applying ∂_z to the transmission line equations (S.26) then re-using them results in the following second order transmission line equations:

$$\frac{d^2 V(z)}{dz^2} - zy V(z) = (-z/L_e)T(z) \quad \frac{d^2 i(z)}{dz^2} - zy i(z) = (1/L_e) \partial_z T(z) \quad (4.12.17) \quad (S.29)$$

which are now inhomogeneous differential equations due to $T(z) \neq 0$.

In the z equation (S.27) both R and L can be represented as double averages,

$$\begin{aligned} R &= \langle \text{Re}(z) \rangle_{c1, c2} = \langle \text{Re}[Z_{s1}(\mathbf{x}_1) + Z_{s2}(\mathbf{x}_2) + j\omega L_e(\mathbf{x}_1, \mathbf{x}_2)] \rangle_{c1, c2} \\ j\omega L &= \langle \text{Im}(z) \rangle_{c1, c2} = \langle \text{Im}[Z_{s1}(\mathbf{x}_1) + Z_{s2}(\mathbf{x}_2) + j\omega L_e(\mathbf{x}_1, \mathbf{x}_2)] \rangle_{c1, c2} \end{aligned} \quad (S.30)$$

However, in the y equation (S.28) this cannot be done because the number $L_e \equiv \langle L_e(\mathbf{x}_1, \mathbf{x}_2) \rangle_{c1, c2}$ is in the denominator instead of the numerator. Thus we must regard the numbers G, C and C' in (S.28) as being defined by the quantity $j\beta_d^2/(\omega L_e)$. However, we can invert both sides of the y equation to get

$$1/y = \omega L_e / (j\beta_d^2) = (1/C') / (j\omega) \quad (S.31)$$

which can be interpreted as

$$\omega / (j\beta_d^2) * \langle L_e(\mathbf{x}_1, \mathbf{x}_2) \rangle_{c1, c2} = (1/j\omega) * \langle \frac{1}{C'(\mathbf{x}_1, \mathbf{x}_2)} \rangle_{c1, c2} \quad (S.32)$$

or

$$\omega L_e / (j\beta_d^2) = \langle \frac{1}{C'} \rangle / (j\omega) \quad (S.33)$$

or

$$L_e \langle \frac{1}{C'} \rangle^{-1} = (\beta_d^2/\omega^2) = \mu_d \xi_d \quad // \text{ using (1.5.1a)} \quad (4.12.19) \quad (S.34)$$

Comparing (S.33) with (S.31) shows that the number C' appearing in (S.31) and (S.28) can be interpreted in this manner,

$$C' = \langle \frac{1}{C'} \rangle^{-1} . \tag{S.35}$$

Going back a bit, we had

$$\frac{1}{C'(\mathbf{x}_1, \mathbf{x}_2)} = V(\mathbf{x}_1, \mathbf{x}_2)/q(z) = \frac{1}{4\pi\zeta_d} K(\mathbf{x}_1, \mathbf{x}_2) \tag{4.4.7} \tag{S.3}$$

$$L_e(\mathbf{x}_1, \mathbf{x}_2) = \frac{W(\mathbf{x}_1, \mathbf{x}_2)}{i(z)} = \frac{\mu_d}{4\pi} K_L(\mathbf{x}_1, \mathbf{x}_2) \tag{4.10.8} \tag{S.9}$$

which can be double averaged to get

$$\langle \frac{1}{C'} \rangle = V(z)/q(z) = \frac{1}{4\pi\zeta_d} K \tag{S.36}$$

$$L_e = \frac{W(z)}{i(z)} = \frac{\mu_d}{4\pi} K_L . \tag{S.37}$$

Inserting these last expressions into (S.34) gives,

$$L_e \langle \frac{1}{C'} \rangle^{-1} = \mu_d \zeta_d$$

Substituting from (S.37) and (S.36) one then finds,

$$\left[\frac{\mu_d}{4\pi} K_L \right] \left[4\pi\zeta_d/K \right] = \mu_d \zeta_d$$

or

$$K_L = K . \tag{4.12.20} \tag{S.38}$$

This equality has thus survived the double averaging procedure.

References

References are in alphabetical order by the last name of the (first) author. For broken links, the referenced item can usually be found by a quick web search on the item title. [all links verified 19 Oct 2014].

B.I. Bleaney and B. Bleaney, *Electricity and Magnetism, 3rd Ed.* (Oxford University Press, London, 1976). That would be Brevis Bleaney and wife Betty Isabelle. Brevis pioneered electron spin resonance independently with Russian Yevgeny Zavoisky in 1944. This book was reissued in 2013 as a two-volume paperback set. Chapter 10 on dielectrics is the first chapter of the second volume.

R.F. Eaton and C.J. Kmiec, "Electrical Losses in Coaxial Cable" (Proceedings of the 57th International Wire and Cable Symposium, Nov. 2008), http://iwcs.omnibooksonline.com/data/papers/2008/14_2.pdf

[GR7] I.S. Gradshteyn and I.M. Ryzhik, *Table of Integrals, Series, and Products, 7th Ed.* (Academic Press, New York, 2007). Editor Dan Zwillinger has been collecting errata. A PDF version exists.

H.A. Haus and J.R. Melcher, *Electromagnetic Fields and Energy* (Prentice-Hall, New Jersey, 1989). Though out of print and hard to get, this very detailed and practical book is alive and well on the MIT OpenCourseWare website where all chapters can be read and downloaded. Two of the instructors are the authors. <http://ocw.mit.edu/resources/res-6-001-electromagnetic-fields-and-energy-spring-2008/>

C.L. Holloway and E.F. Kuester, "DC Internal Inductance for a Conductor of Rectangular Cross Section", IEEE Transactions on Electromagnetic Compatibility, Vol. 51, No. 2, pp. 338-344, May 2009.

J.D. Jackson, *Classical Electrodynamics, 3rd Ed.* (John Wiley & Sons, New York, 1998). The author was fortunate to have learned his E&M from Dave Jackson circa 1971 (green 1st edition).

R.W.P. King, *Electromagnetic Engineering* (McGraw-Hill, New York, 1945). This is the first of twelve books that Ronold King wrote or co-authored. His last was an antenna book (his specialty) published in 2002; he died in 2006 at age 100. It happens that the author did an "independent study" with Prof. King circa 1969, but regrettably knew so little that Prof. King could only smile and be encouraging.

[TLT] R.W.P. King, *Transmission Line Theory* (Dover, 1965). Another of the twelve books.

C. Kittel, *Introduction to Solid State Physics, 4th Ed.* (John Wiley & Son, New York, 1971) .

P. Lorrain, D.R Corson, F. Lorrain, *Electromagnetic Fields and Waves, 3rd Ed.* (W.H. Freeman & Co., New York, 1988). The first and second editions (without the third author) were published in 1962 and 1970. These authors have written various other books on related topics at least through 2006.

P. Lucht, *Bipolar Coordinates and the Two-Cylinder Capacitor* (2014). This document and the one you are reading are downloadable at <http://user.xmission.com/~rimrock>. If not there, search on "Phil Lucht Documents" or the document title.

P. Lucht, *Tensor Analysis and Curvilinear Coordinates* (2012). See previous reference.

P. Moon and D.E. Spencer, *Field Theory Handbook, Including Coordinate Systems, Differential Equations and their Solutions* (Springer-Verlag, Berlin, 1961). This book is not about quantum field theory or anything like that, it is about curvilinear coordinate systems, how the Laplace and Helmholtz equations appear in each system, and what the solutions of these equations look like. This husband and wife team wrote several excellent books. Long ago they were strangely involved in an accident involving a test of general relativity.

P.M. Morse and H. Feshbach, *Methods of Theoretical Physics* (McGraw-Hill, New York, 1953). This 2000 page 2-volume classic behemoth is simply amazing.

R. Nevels and C-S Shin, "Lorenz, Lorentz, and the Gauge", *IEEE Antennas and Propagation Magazine*, Vol 43, No 3, June 2001, pp 70-71.

See www.engr.mun.ca/~egill/index_files/7811_w10/lorenz_gauge.pdf and elsewhere.

[NIST] F.W.J. Olver, D.W. Lozier, R.F. Boisvert and C.W. Clark, *NIST Handbook of Mathematical Functions* (Cambridge University Press, 2010). NIST is the U.S. National Institute of Standards and Technology which published the world-famous earlier edition in 1964 with editors Abramowitz and Stegun, known affectionately as "A&S". The greatly expanded 2010 edition (968 p) can be accessed online at dlmf.nist.gov which also has errata. The book (\geq \$17) comes with a CD containing a bookmarked PDF file which of course has been bootlegged onto the web. Olver died in 2013.

K.E. Oughstun, "EE 141 Lecture Notes Topic 15" (School of Engineering, University of Vermont, 2012).

See [http://www.emba.uvm.edu/~keoughst/LectureNotes141/Topic_15_\(Capacitance\).pdf](http://www.emba.uvm.edu/~keoughst/LectureNotes141/Topic_15_(Capacitance).pdf)

W.K.H. Panofsky and M. Phillips, *Classical Electricity and Magnetism, 2nd Ed.* (Addison-Wesley, Reading MA, 1962), reissued as a Dover paperback in 2005. Some of the fascinating history of Prof. Wolfgang "Pief" Panofsky appears in Dave Jackson's Jan 2009 *Physics Today* article "Panofsky agonistes" which can be found at http://www-theory.lbl.gov/jdj/PT_article.pdf.

H. Pender and W.A. Del Mar Editors, *Handbook for Electrical Engineers, 2nd Ed* (John Wiley & Sons, New York, 1922).

D.B. Pengra, J. Stoltenberg, R. Van Dyck, O. Vilches, "The Hall Effect" (University of Washington, Dept of Physics, 2007). http://courses.washington.edu/phys431/hall_effect/hall_effect.pdf.

A.D. Polyanin, *Handbook of Linear Partial Differential Equations for Engineers and Scientists* (Taylor & Francis, CRC Press, 2001). Polyanin and his Russian friends have recently published a whole bookshelf of fat and excellent handbooks. One deals with non-linear PDEs, another with integral equations. Search for him at <http://www.taylorandfrancis.com/search/> and on the web.

A.M. Portis, *Electromagnetic Fields: Sources and Media* (John Wiley & Sons, New York, 1978).

D.M. Pozar, *Microwave Engineering, 4th Ed.* (John Wiley & Sons, New York, 2012). Chapters 2 and 3 concern transmission lines.

- C. Quigley, "On the Origins of Gauge Theory" (2003), www.math.toronto.edu/~colliand/426_03/Papers03/C_Quigley.pdf.
- R.K. Rajput, *Power System Engineering* (Laxmi Publications, 2006), see Google books.
- A.A. Rodrigues and A. Valli, *Eddy Current Approximation of Maxwell's Equations* (Springer, Heidelberg, 2010).
- N.J. Siakavellas, "Two Simple Models for Analytical Calculation of Eddy Currents in Thin Conducting Plates", IEEE Trans. on Magnetics, Vol 33, No. 3, May 1997, pp 2245-2257.
- G. Smith, "The Proximity Effect in Systems of Parallel Conductors and Electrically Small Multiturn Loop Antennas" (Harvard University Division of Engineering and Applied Physics, Technical Report No. 642, Dec 1971) see www.dtic.mil/dtic/tr/fulltext/u2/736984.pdf. This document contains a long list of references. See also the search engine at www.dtic.mil/dtic.
- W.R. Smythe, *Static and Dynamic Electricity, 2nd Ed.* (McGraw-Hill, New York, 1950).
- M. Spiegel, S. Lipschutz, and J. Liu, *Schaum's Outlines: Mathematical Handbook of Formulas and Tables (4th Ed.)*, (McGraw-Hill, 2012). The excellent original 1968 edition by Murray Spiegel has been a dog-eared reliable friend for many years. John Liu was added for the 1999 2nd Ed, and Seymour Lipschutz joined for the 2008 3rd Ed. Not to be confused with a watered-down "Easy Outline" version. This low-cost paperback is an excellent fast reference for well-known mathematical facts. Our equation numbers refer to the 1968 edition.
- I. Stakgold, *Boundary Value Problems of Mathematical Physics*, Volumes 1 and 2 (MacMillan, London, 1967). These are astoundingly good books, but the high level of detail (the subject *is* intrinsically complex) makes them hard to use in a normal "course", which is why the author later put out a condensed single-volume version *Green's Functions and Boundary Value Problems*, now in a third edition. The original two volumes were reprinted with some corrections in 2000 (SIAM, Philadelphia). P. Lucht has a short list of errata on line.
- W.T. Thomson (aka Lord Kelvin), "*Ether, Electricity and Ponderable Matter*", The Proceedings of the Institution of Electrical Engineers (founded 1871), Volume 18 (1889), No 77, pp 4-37. The Appendix with ber and bei begins on page 35. Google Books has an unrestricted scan of a Harvard library copy of Vol. 18 which can be downloaded in PDF format: <http://books.google.com/books?id=Wy89AAAAYAAJ>
- [RDE] M.E.V. Valkenburg and W.M. Middleton (editors), *Reference Data for Engineers: Radio, Electronics, Computers and Communications, 9th Ed.* (Newness/Elsevier, Boston, 2001). Some of this document exists in Google book preview form.
- M. J. Van Der Burgt, "*Precision Video Cables Part 1: Impedance*" (Belden Electronics Division, 2002). <http://www.belden.com/docs/upload/Precision-Video-Cables-Part-1.pdf> . Part 2 is about return loss.